L SHELL IONISATION AND X-RAY PRODUCTION CROSS SECTION MEASUREMENTS FOR ASYMMETRIC ION-ATOM COLLISIONS

BY

RANJEET SINGH SOKHI

A thesis submitted to The University of Aston in Birmingham for the degree of Doctor of Philosophy

DEPARTMENT OF MATHEMATICS AND PHYSICS

MAY 1984

DEDICATED TO THE

MEMORY OF MY

BELOVED FATHER

DALIP SINGH SOKHI

THE UNIVERSITY OF ASTON IN BIRMINGHAM

L SHELL IONISATION AND X-RAY PRODUCTION CROSS SECTION MEASUREMENTS FOR AYSMMETRIC ION-ATOM COLLISIONS

Submitted for the degree of Doctor of Philosophy

Ranjeet Singh Sokhi

May 1984

SUMMARY

L shell ionisation and x-ray production cross sections have been measured for Dy, Yb, W, Au, Pb, Bi, Th, and U in the form of carbon backed thin targets. Incident protons, deuterons and alpha particles of energy 1 to 3 MeV were employed to ionise the L shell and the resulting L x-rays were detected with an energy-dispersive Si(Li) x-ray system. The individual $2_{s\frac{1}{2}}$, $2_{p\frac{1}{2}}$ and $2_{p\frac{3}{2}}$ state ionisation cross sections were deduced from the measured x-ray production cross sections with the aid of a spectrum fitting programme specifically written for this purpose in Fortran 77. The efficiency of the Si(Li) x-ray detector and the target thicknesses were determined experimentally.

The measured L shell ionisation and x-ray production cross sections, and their ratios, have been compared with the predictions of the plane-wave Born approximation and the ECPSSR theory proposed by Brandt and Lapicki (1981). Comparisons have also been made with the available data of other authors. These comparisons have revealed significant discrepencies between the ECPSSR theory and the measured data for all three subshells. These discrepencies have been found to be particularly large for the $2_{p\frac{1}{2}}$ state ionised by incident alpha particles. Possible reasons for theses disagreements are discussed and suggestions are made for future work.

To assess the extent of progress made in this field with regard to proton impact, a comprehensive tabulation of L shell ionisation and x-ray production cross sections, and the pertinent experimental details, has been compiled.

Key words: L shell ionisation, particle induced x-rays, inner-shell x-ray production, cross sections.

ACKNOWLEDGEMENTS

It is with great respect and admiration that I acknowledge Dr D. Crumpton for his guidance and encouragement throughout the duration of this study. The head of department, Professor E. Neal, and Emeritus Professor S.E. Hunt are thanked for their interest in the present work. The assistance of Dr W. Cox is appreciated regarding some mathematical aspects.

Thanks are due to Mr T. Kennedy and J. Phull for their help and friendship. The assistance offered by the staff at the Physics Workshop and at the Birmingham Radiation Centre is gratefully appreciated. I am much indebted to the members of the applied nuclear physics group for their friendship and for making the research period a very enjoyable one.

The Science and Engineering Research Council is acknowledged for funding this study.

I would like to express my gratitude to Mrs S. Puar for typing the thesis and to Miss E. Taylor and Miss P. Blower for labelling the diagrams.

The encouragement and understanding shown by my family is deeply appreciated. In particular, I am indebted to my mother since it is her patience and her unending sacrifices which have provided me with the opportunity to study for this degree.

R.S. Sokhi

May 1984

TABLE OF CONTENTS

Page

Page

Page

Page

Page

LIST OF FIGURES

Page

Page

LIST OF TABLES

CHAPTER 1

INTRODUCTION

General interest in inner-shell ionisation by light charged particles was initially stimulated by the publication of Merzbacher and Lewis's (1958) review article which provided a comprehensive theoretical description of this phenomenon in terms of the plane-wave Born approximation (PWBA). Comparable theoretical explanations were offered by Bang and Hansteen (1959) and more recently by Garcia et al (1973) who employed the semi-classical (SCA) and the binary-encounter (BEA) approximations respectively. As a direct consequence of these works there was an upsurge of experimental activity in the area of K-shell ionisation by light ions in order to test the above theoretical predictions. The large amount of data that resulted has been tabulated by Gardner and Gray (1978).

Because of the widespread availability of low MeV charged particle accelerators much of the measurements were restricted to particle energies < 4MeV. Comparison of the measured data with the proposed theories revealed large discrepencies, particularly at low impact energies where the theories tended to overpredict the data. Although some improvements have been suggested for the SCA and BEA theories, a much more methodical approach was adopted by Brandt and his colleagues to explain these disagreements by incorporating certain corrections to the first order PWBA model. Over a period of several years their work culminated into the ECPSSR theory (Brandt and Lapiciki 1979 and 1981) to explain K and L shell ionisation by simple projectiles. The ECPSSR theory takes into account the energy loss (E), Coulomb deflection (C), perturbed-stationary-state (PSS) and relativistic (R) effects.

As a result of the developments in the PWBA, SCA and BEA theories there has been considerable recent interest in K shell ionisation (Badica et al 1977, Khan et al 1977, Bauer et al 1978, Badica et al 1979, Benka and Geretschlager 1980, Lopes et al 1980 and Barfoot et al 1980).

Paul (1982) has conducted a detailed comparison of proton-induced K shell ionisation cross sections with the ECPSSR theory and has observed reasonable qualitative and quatitative agreement at intermediate and high impact velocities. At lower proton velocities, however, a modified Coulomb deflection factor has been proposed by Paul (1982) to account for the deviations between theory and experiment.

The amount of L shell x-ray production and ionisation cross section data is not as comprehensive as for the K shell. To estimate the progress achieved in the field of L shell ionisation by proton bombardment of a major compilation containing all the available measured L shell x-ray production and ionisation cross sections, and the associated experimental details, from 1975 to November 1982 has been prepared (Sokhi and Crumpton 1984). This compilation, which is presented in apprendix E, clearly illustrates the need for further data, in particular with regard to ionisation cross sections. In the case of deuteron impact, measurements are very scarce and only a few published values are available for incident alpha particles.

The major purpose of this study is to provide a comprehensive set of L shell data for protons, deuterons and alpha particles incident on medium to high atomic number elements and to perform a detailed comparison with the ECPSSR theory, with the intention of highlighting any significant discrepencies between the data and theory. Measurements have been made between projectile energies of 1 to 3 MeV at steps of 200 keV to establish the energy dependence of the cross sections. To study the dependence of the ionisation cross sections on the target atomic number (Z_2), several targets were selected between the range $66 \leq Z_2 \leq 92$. Recently Cohen (1983) has measured L shell ionisation cross sections for 1 to 3 MeV protons and alpha particles incident on some heavy elements. Cohen (1983) has compared his data with the ECPSSR model and has noticed serious disagreements. The present work provides an independent check on the conclusions reached by Cohen (1983). An additional reason for carrying out this work is to make L shell x-ray production cross sections for experimentalists involved in particle induced x-ray emission analysis (PIXE). This technique has developed over the past decade into a highly versatile analytical tool for solving problems regarding trace elements (Khan and Crumpton 1981). Wherever high Z_2 trace elements are involved L x-rays are employed and thus a reliable data base of particle induced L shell x-ray production cross sections is vital.

Each chapter of this thesis begins with an introduction which explain the underlying philosophy adopted in the chapter. The remaining part of this main introduction outlines the contents of each chapter and discusses the overall philosophy behind this investigation.

The atomic processes which occur once an atom has been ionised by an external purterbation in one of its inner-shells are discussed in chapter 2. For completeness the chapter also discusses processes which are allied to this study. Chapter 3 outlines the principles of nuclear backscattering spectrometery, which is employed in the present work to determine target thicknesses.

The concepts of the ECPSSR theory, and its underlying assumptions, are considered in chapter 4. The SCA and the BEA models are discussed in appendix A for completness.. Chapter 5 contains details regarding the apparatus and procedure employed for measuring the L shell ionisation and x-ray production cross sections. This chapter also deals with the method for calculating theoretical cross sections for comparison with the present data.

Detailed comparisons of the measured data in this work with the PWBA and the ECPSSR theories, and with other measured values, are presented in chapter 6. Results of each element are discussed in order of atomic number before highlighting common trends revealed by the individual comparisons. The final conclusions of the present work are outlined in chapter 7.

CHAPTER 2

FUNDAMENTALS OF CHARGED PARTICLE INDUCED X-RAY EMISSION

CONTENTS

2.1 INTRODUCTION

Physical concepts necessary for understanding the major features of an x-ray spectrum are reviewed in this chapter. The chapter concentrates on the atomic processes which occur once an inner-shell vacancy has been created, by light positively charged particles in the present case, although processes which are peripheral to this study have been mentioned for completeness. These include phenomena more closely associated with impact by very energetic or heavy charged particles.

The mechanisms by which the projectile produces bremsstrahlung, directly and indirectly, as it traverses matter are also examined. Finally, the main interactions of x-rays with matter, which leads to their attenuation, are mentioned.

Throughout this chapter the underlying philosophy has been to highlight contemporary ideas regarding the relevant atomic processes. Consequently a determined attempt has been made to cite references that are fully representative of the current views held on these areas. Where appropriate, recent noteworthy advances in the fields discussed in this chapter have been indicated.

2.2 NOMENCLATURE

The electronic states of an atom are characterised by four basic quantum numbers. These are the principal quantum number, n, the orbital quantum number, ℓ, the total angular quantum number, j, and the magnetic quantum number, m. n can have positive integer values 1, 2, 3 ... or in the x-ray notation K, L, M... and so on. ℓ can taken any integer value from 0 to n -1, m can assume any integral value from $-\ell$ to $+\ell$ including zero and j can adopt the values $\ell \pm \frac{1}{2}$ where $\pm\frac{1}{2}$ represents the two possible values of the electron spin, s.

In the spectroscopic notation different values of ℓ can be denoted by the letters s,p,d.... corresponding numerically to 0, 1, 2, ..., n -1. Derivation of these numbers can be found in any standard text book on quantum mechanics such as Schiff (1968) and Landau and Liftshitz (1977). The three L subshells can be represented by L_1, L_2, L_3 in the x-ray notation or equivalently by $2s_{\frac{1}{2}}$, $2p_{\frac{1}{2}}$ and $2p_{3/2}$ in the spectroscopic notation. Both of these notations are employed in the present work.

2.3 ATOMIC TRANSITIONS

When an atom experiences a perturbation, such as an encounter with a charged particle, there is a finite probability that an inner-shell electron may be ejected into the continuum or into a higher shell leaving a vacancy in the inner-shell. The excited atom has then several channels open to it through which it may deexcite. These modes of relaxation manifest themselves as characteristic features in an x-ray spectrum.

To understand the mechanisms by which the excited atom deexcites the atom should strictly be treated as a many-body problem. This, however, is extremely difficult even for the simplest atoms. To avoid the complex nature of the many-body problem and to facilitate the discussion the following simplifying assumptions can be made.

(i) the perturbation experienced by the atom creates a single vacancy in an inner-shell and leaves the other orbitals unaffected or 'frozen' - the sudden or the frozen - orbital model (Koopmans 1933),

(ii) the electrons are considered to be approximately free in relation to the atomic nucleus, and

(iii) any individual electron is considered to be independent of the position of any other electron at any particular moment (Rooke 1974).

These assumptions, although crude, enable the gross features of an x-ray spectrum to be explained. In light of these assumptions the major relaxation mechanisms relevant to this study are discussed below. A more thorough treatment, however, has been given by Azaroff (1974).

2.3.1 X-Ray Emission

Consider an electron transition from an initial higher atomic state q to a final lower state q^1 where q and q^1 represent sets of quantum numbers

n, ℓ, s, m and n^1, ℓ^1, s^1, m^1 respectively. The transition probability per unit time for this transition, resulting in the emission of a photon with energy $\hbar\omega$ and momentum $\underline{p} = \hbar\underline{k}$, is proportional to the square of the transition matrix element, M_{qq^1}, given by (Merzbacher 1970)

$$|M_{qq^1}|^2 = | < q| \underline{\varepsilon}.\underline{p} \exp (i\underline{k}.\underline{r}) | q^1 > |^2 \qquad 2.1$$

where $\hbar$ is the Planck's constant, h, divided by 2π, ω is the angular frequency of the emitted radiation, $\underline{k}$ is the propagation vector, $\underline{r}$ is the electron position vector and $\underline{\varepsilon}$ is the polarisation vector of the emitted photon.

When calculating the transition probability for photon emission it is found that by approximating the exponential term in equation 2.1 by unity much of the emitted radiation can be explained (Rooke 1974). This approximation is referred to as the 'electric dipole approximation' and the transitions for which the probability can be calculated, by making use of this simplification, are known as 'electric dipole transitions'.

These transitions are governed by certain 'selection rules' which decide whether the transition is allowed or forbidden. These rules originate from the so-called 'recurrence relations' which arise in the quantum mechanical treatment of radiative transition probabilities (Tralli and Pomilla 1969 and Rooke 1974). The selection rules are basically restrictions on the magnitude by which the quantum numbers representing the atomic states can change when a transition takes place from one state to another. These rules ensure that the electric dipole matrix element does not vanish (Schiff 1968). For this to be the case the changes in the quantum numbers, during a transition, must be limited to

$$m - m^1 = \Delta m = 0, \pm 1; \quad j - j^1 = \Delta j = 0, \pm 1$$
$$\ell - \ell^1 = \Delta\ell = \pm 1 \; ; \; s - s^1 = \Delta s = 0 \qquad 2.2$$

The change in the principal quantum number, n, is not restricted.

A large number of observed transitions obey these rules and are called 'allowed' transitions while the relatively few that do not are termed 'forbidden' transitions. Some of these are explained by including the second term in the power series expansion of exp($i\underline{k}.\underline{r}$) in equation 2.1 (electric quadrupole approximation). Such transitions, however, only have a probability of the order of 10^{-8} relative to the dipole transitions (Tralli and Pomilla 1969) which makes them insignificant in relation to the present study.

When a radiative dipole transition takes place in an excited atom the emitted photon has a discrete energy value given by

$$\hbar\omega = E_f - E_i \qquad 2.3$$

where E_i is the energy of the initial level where the vacancy is created and E_f the energy of the final level where the vacancy is transferred to as a result of the transition.Figure 2.1 shows schematically the allowed x-ray transitions to the L-shell. Although individual 'diagram' lines are shown in figure 2.1 the resolution of the present-day lithuim drifted silicon detectors, such as the one employed in this study, allow only groups of lines to be observed. L_α, L_β and L_γ transitions, occuring as a result of vacancies in the L-shell, are such groups.

2.3.2 Non-radiative Processes

In the event of inner-shell ionisation by charged particles electrons are emitted by two successive processes (Stolterfoht 1978). Firstly, electrons which exhibit a continuous energy distribution are ejected as a result of ionisation and secondly, electrons with discrete energies are emitted as a result of Auger transitions which fill the vaciencies (Auger 1925). The latter process, which is another mode of deexcitation and competes with x-ray emission, is treated in terms of a direct interaction between the 'active' atomic electrons (Wentzel 1927). This model is based on the assumption that the electrons taking part in the interaction are

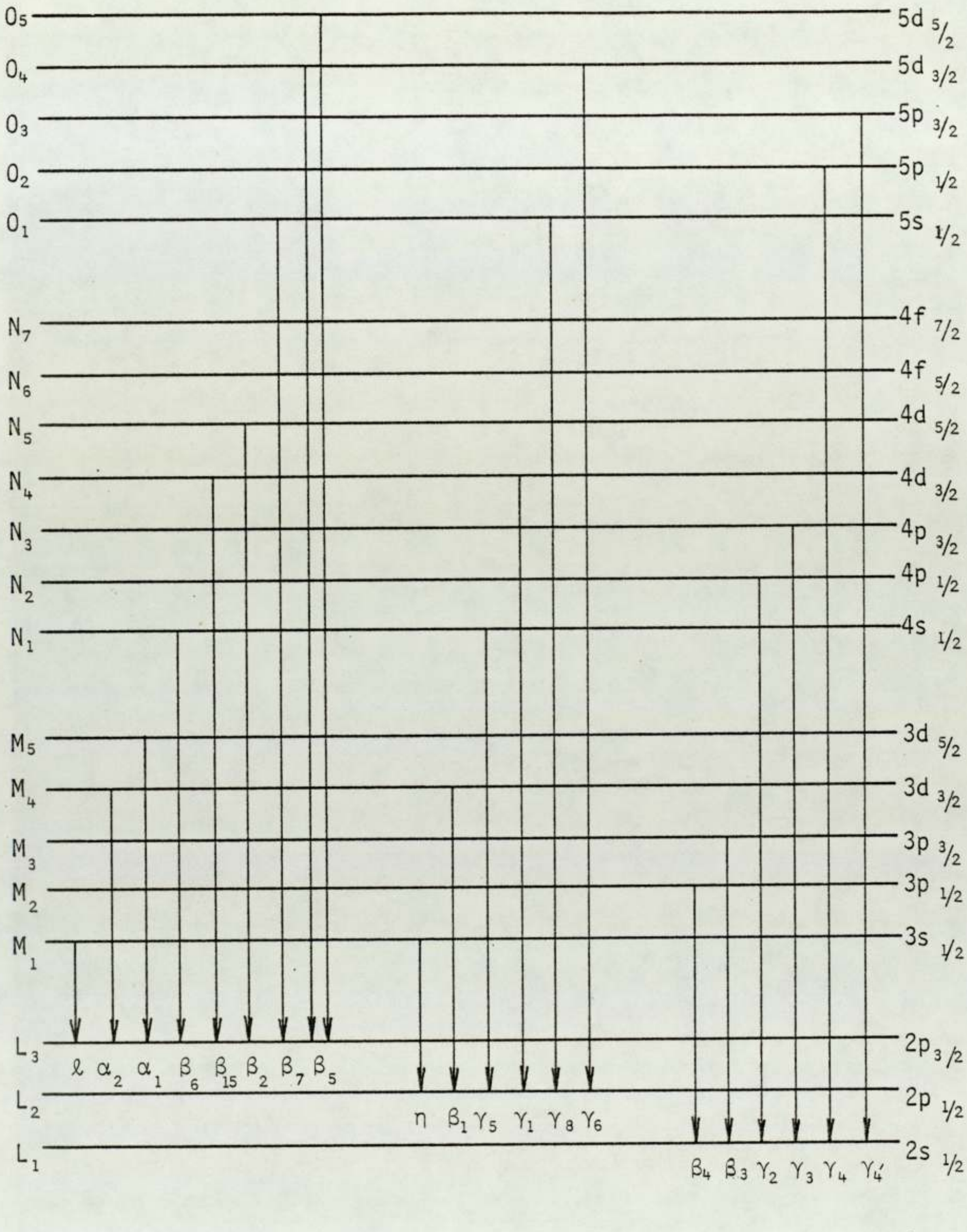

Figure 2.1 Schematic diagram of L shell x-ray transitions (Gray 1974).

non-relativistic. This is a valid assumption for light elements.

The Auger transition is effected by a perturbation arising from the Coulomb interaction between the neighbouring electrons, that is, the ejected and the emitted Auger electron (Burhop 1952). The general theory of the Auger effect is most successfully explained by the Lorentz-covariant theory of quantum electrodynamics discussed by Chattarji (1976). According to this theory the non-radiative Auger transition is caused by the retarded electromagnetic interaction between two bound-state electrons described by Dirac wave functions. The electromagnetic interaction consists of a charge-charge (Coulomb) interaction and a current-current (magnetic) interaction. For non-relativistic cases the interaction reduces to one that is purely Coulombic. A thorough treatment of the Auger effect has also been provided by McGuire (1975).

The energy of the Auger electron, E_A, is given by (McGuire 1975)

$$E_A = E_a - E_{b_1 b_2} \qquad 2.4$$

where E_a is the energy of the subshell, a, with the primary vacancy and $E_{b_1 b_2}$ is the energy associated with subshells b_1 and b_2 in which holes are produced as a result of the Auger transition. Since Auger electrons have discrete energies their study provides a very informative method for investigating inner-shell excitation by charged particles (Stolterfoht 1978). This avenue is being explored not only to understand the collision process (Kojima et al 1979, Schneider and Stolterfoht 1981) but also the mechanism by which Auger electrons are emitted as a consequence of the collision (Schmidt et al 1981, Baragiola et al 1982 and Bastasz and Felter 1982). A recent review article by Weightman (1982) discusses different aspects of x-ray-excited Auger spectroscopy.

If the primary vacancy is created in a shell other than the K, then Coster-Kronig transitions (Coster and Kronig 1935) may compete with the x-ray and the Auger transitions. Essentially these transitions are Auger transitions which occur in the subshells of the shell which initially suffers the creation of the primary vacancy. Thus a vacancy in the $2s_{\frac{1}{2}}$ subshell for example, may be filled by an electron from a higher subshell of the same shell, L in this case. The mechanism is similar to that of Auger transitions and is based on a Coulomb interaction of the electrons involved. Via this mechanism a vacancy initially in the $2s_{\frac{1}{2}}$ may be transferred to a higher subshell ($2p_{\frac{1}{2}}$ or $2p_{3/2}$) before taking part in a radiative transition. For obvious reasons if a vacancy is created in the highest subshell of any given shell Coster-Kronig transitions are absent. Once the electron redistribution is complete in the subshell an electron in a higher shell may be ejected, again by Coulomb interaction. Coster-Kronig transitions explain why for many elements diagram lines such as L_{β_3} ($L_1 \rightarrow M_3$) and L_{β_4}($L_1 \rightarrow M_2$) are absent or abnormally weak and transitions originating in $2p_{\frac{1}{2}}$ and $2p_{3/2}$ subshells appear with considerable intensity (Chattarji 1976). Coster-Kronig transitions are only energetically favourable for certain regions of atomic number (Z_2) and thus exhibit sharp cut-offs at critical Z_2 values (McGuire 1975 and Doyle and Shafroth 1979).

Transitions in which both the final vacancies occur in the same shell as the initial vacancy but in a different subshell also take place, but with a small probability. These transitions have been termed 'Super Coster-Kronig' transitions by McGuire (1972). There is a small but finite probability that Coster-Kronig transitions may be radiative. This has been confirmed by Karttunen et al (1971) for the L_1 to L_3 transition.

2.3.3 Atomic Parameters

When calculating x-ray yields account must be taken of the other relaxation mechanisms discussed in subsection 2.3.2, because of their competitive nature. To do this, information on the atomic yields for each of these processes is required. Definitions of these yields are stated below. Although the definitions are similar for all the shells, the subscripts apply specifically to the L subshells. The fluorescence yield, ω_i, (i = 1, 2, 3) is the number of characteristic L x-ray photons per L_i

vacancy. The Auger yield, a_i, is the number of Auger electrons per L_i vacancy and similarly the Coster-Kronig yield, f_{ij}, $(i < j)$ is the number of transitions transferring vacancies from the L_i subshell to the higher L_j subshell per L_i vacancy. As mentioned in subsection 2.3.2 Coster-Kronig transitions may be radiative and the total Coster-Kronig yield, f_{ij}^T, can be expressed as

$$f_{ij}^T = f_{ij} + f'_{ij} \qquad 2.5$$

where f_{ij} and f'_{ij} denote the radiative and non-radiative parts. For high atomic number elements the radiative transition from L_1 to L_3 subshell becomes important and has to be taken into account. This is illustrated in figure 2.2 which shows the variation of the radiative Coster-Kronig yield (f'_{13}) for this transition, expressed as a percentage of its non-radiative counterpart (f_{13}), with atomic number. Since the total decay probability for an atom with a vacancy in a shell, L in this case, is unity we can write

$$\omega_i + a_i + \sum_{j=2,3} f_{ij}^T = 1 \qquad 2.6$$

The definition of ω_i, as stated earlier, is subject to the condition that the primary vacancy distribution of subshell i does not change before the vacancies are filled. However, the presence of the Coster-Kronig transitions between the subshells alter the primary vacancy distribution and to determine the average or the effective fluorescence yields of the subshells the effects of the Coster-Kronig transitions, therefore, have to be incorporated. The average fluorescence yield (ν_i) for the i^{th} L subshell can be defined as the number of characteristic L-shell x-rays (not necessarily from transitions to the same subshell L_i) that are emitted per primary vacancy created in the L_i subshell (Rao 1975). Thus, ν_i is the number of L x-rays emitted including those emitted after rearrangement of vacancies by the Coster-Kronig transitions. The expressions for ν_i $(i = 1, 2, 3)$ for

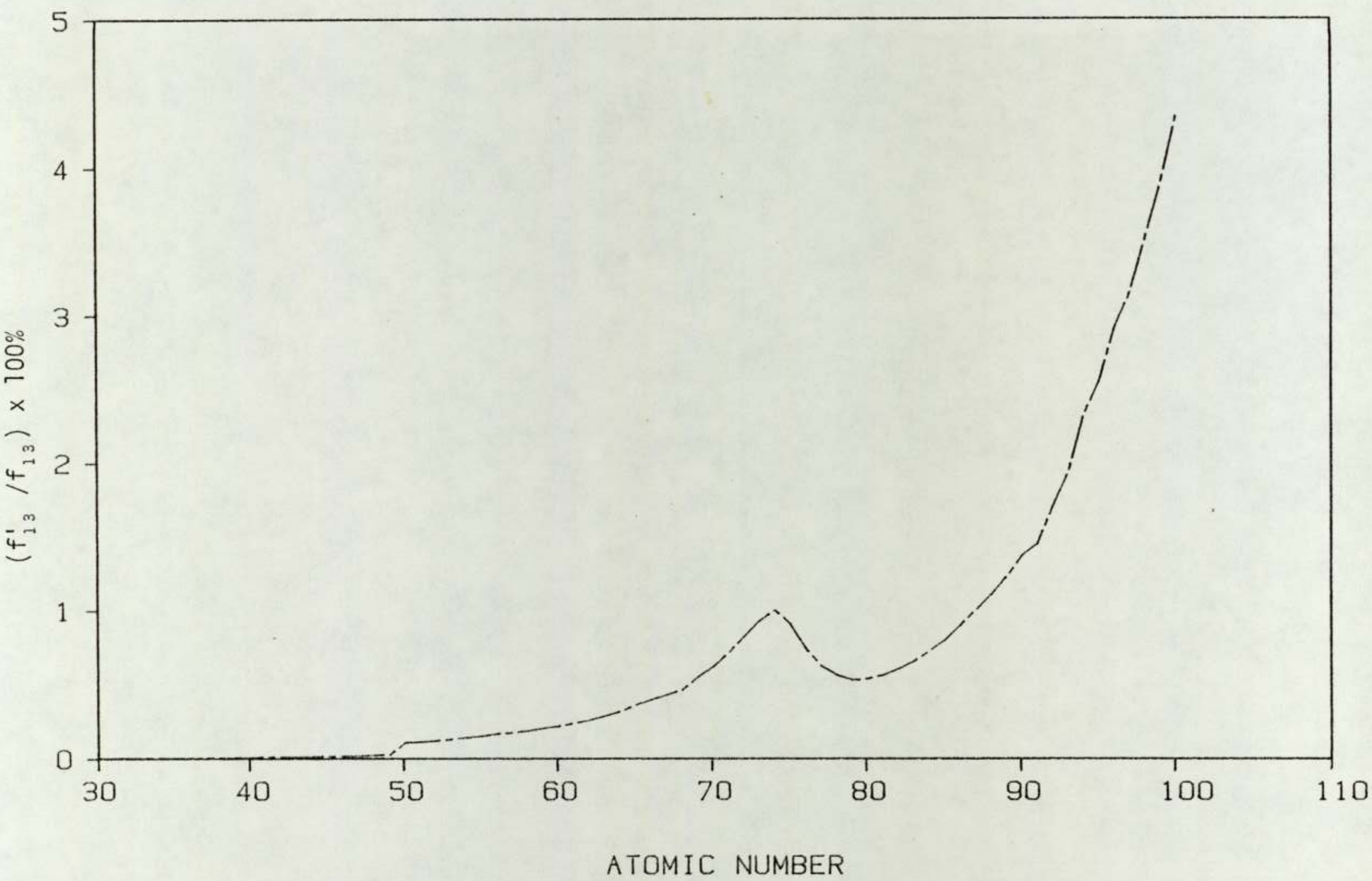

Figure 2.2 Importance of the radiative Coster-Kronig yield (f'_{13}) relative to its non-radiative counterpart (f_{13}) with atomic number. Values taken from Krause (1979).

the L subshells interms of ω_i and f_{ij} are

$$\nu_1 = \omega_1 + f_{12}\omega_2 + (f_{12}f_{23} + f_{13} + f'_{13})\omega_3$$
$$\nu_2 = \omega_2 + f_{23}\omega_3 \qquad 2.7$$
$$\nu_3 = \omega_3$$

Only limited work has been performed to determine the atomic parameters experimentally and theoretically despite their considerable importance in x-ray analytical techniques (McGuire 1971 and Bambynek et al 1972). An internally consistent set of values for the atomic yields has been produced by Krause (1979). Values have been supplied by Krause (1979) for K and L-shell yields and in the case of the L-shell atomic number from 12 upwards have been covered. This tabulation has been used to show the variations of the atomic yields with atomic number. Figure 2.3 shows the variation of the Coster-Kronig yields for the L_1 subshell with atomic number. It illustrates clearly the regions of atomic number where the L_1 Coster-Kronig yields are energetically unfavourable. The three major L_1 subshell atomic yields, that is, the total non-radiative Coster-Kronig yield ($f_1 = f_{12} + f_{13}$), the fluorescence yield (ω_1) and the Auger yield (a_1) are shown in figure 2.4. It shows the dominance of the nonradiative processes throughout the relevant range of atomic numbers for the L_1 subshell. Another interesting feature highlighted by figure 2.4 is the range of atomic numbers, 50 to 76, where the Coster-Kronig process looses its importance and being competive, the Auger process becomes equally probable. The atomic yields for the L_2 subshell are illustrated in figure 2.5. In this case the Coster-Kronig transitions play a relatively minor role for high atomic number elements. The Auger process dominates the mode of decay for most of the elements and becomes less probable than x-ray emission only for the heaviest elements. The situation is very similar for the L_3 Auger and fluorescence yields as shown in figure 2.6. The Coster-Kronig process is obviously absent for the L_3 shell. Using the expressions 2.7 the average

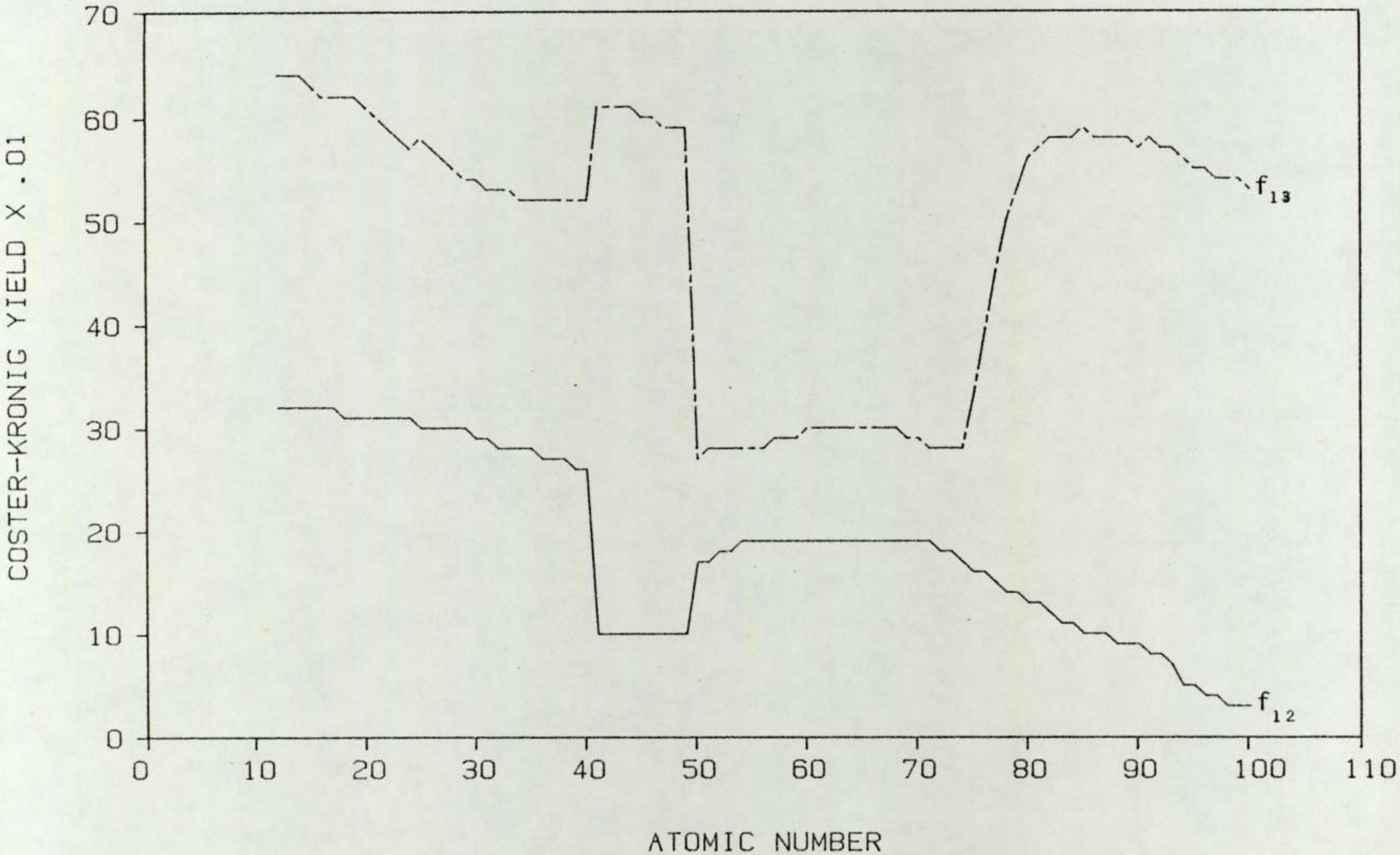

Figure 2.3 Variation of the L_1 subshell nonradiative Coster-Kronig yields with atomic number. Values taken from Krause (1979).

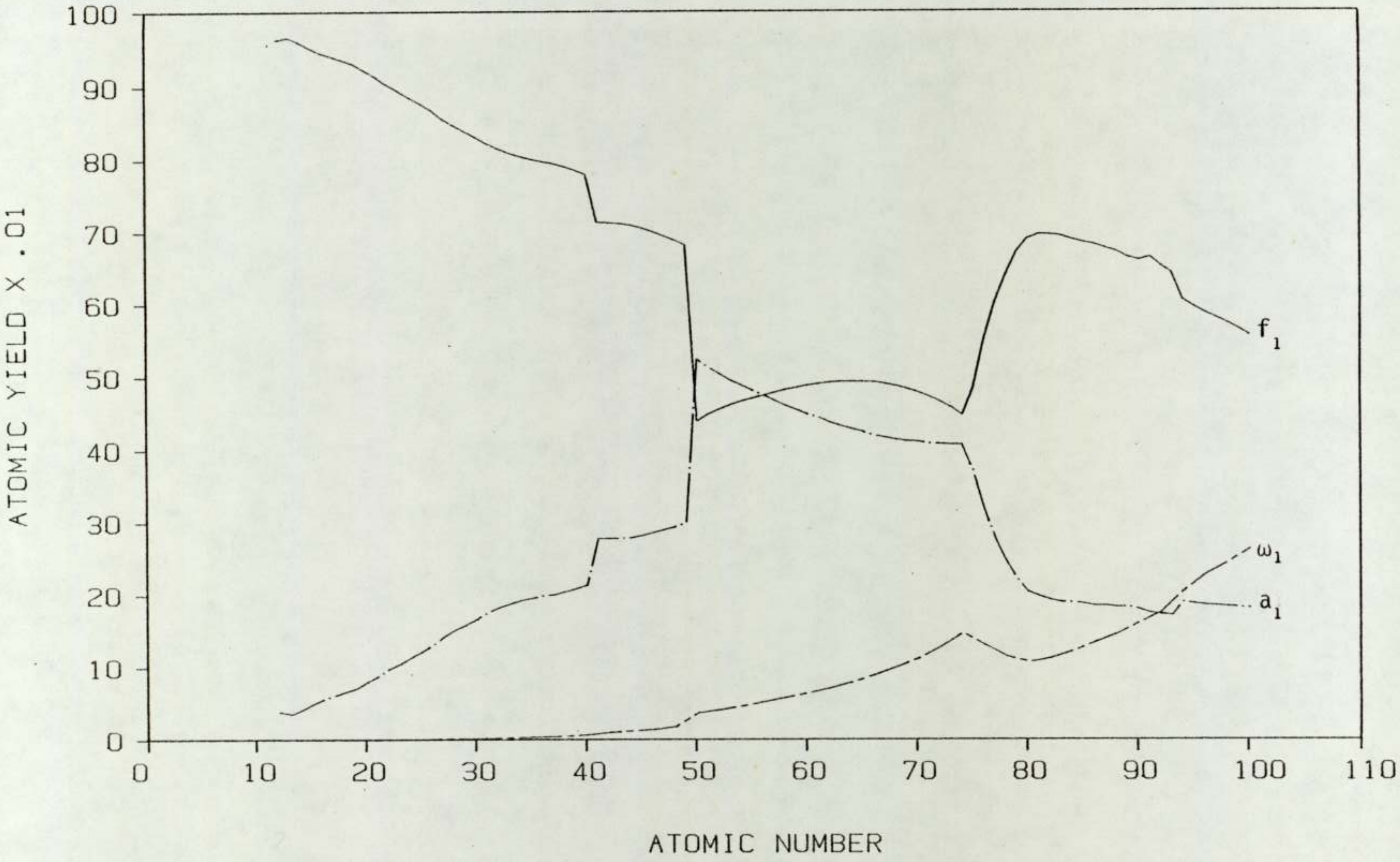

Figure 2.4 Variation of the L_1 subshell atomic yields with atomic number. Values taken from Krause (1979).

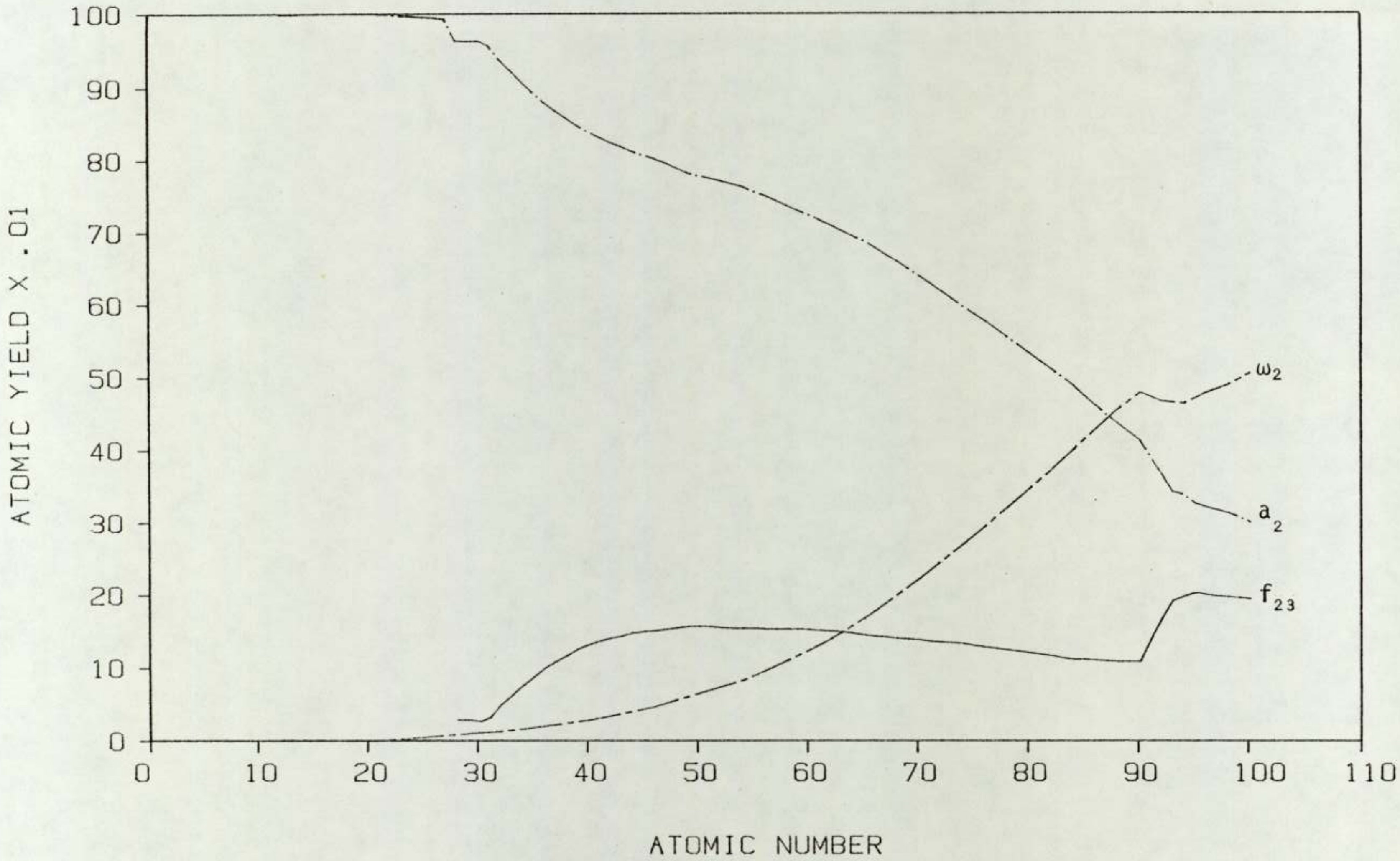

Figure 2.5 Variation of the L_2 subshell atomic yields with atomic number. Values taken from Krause (1979).

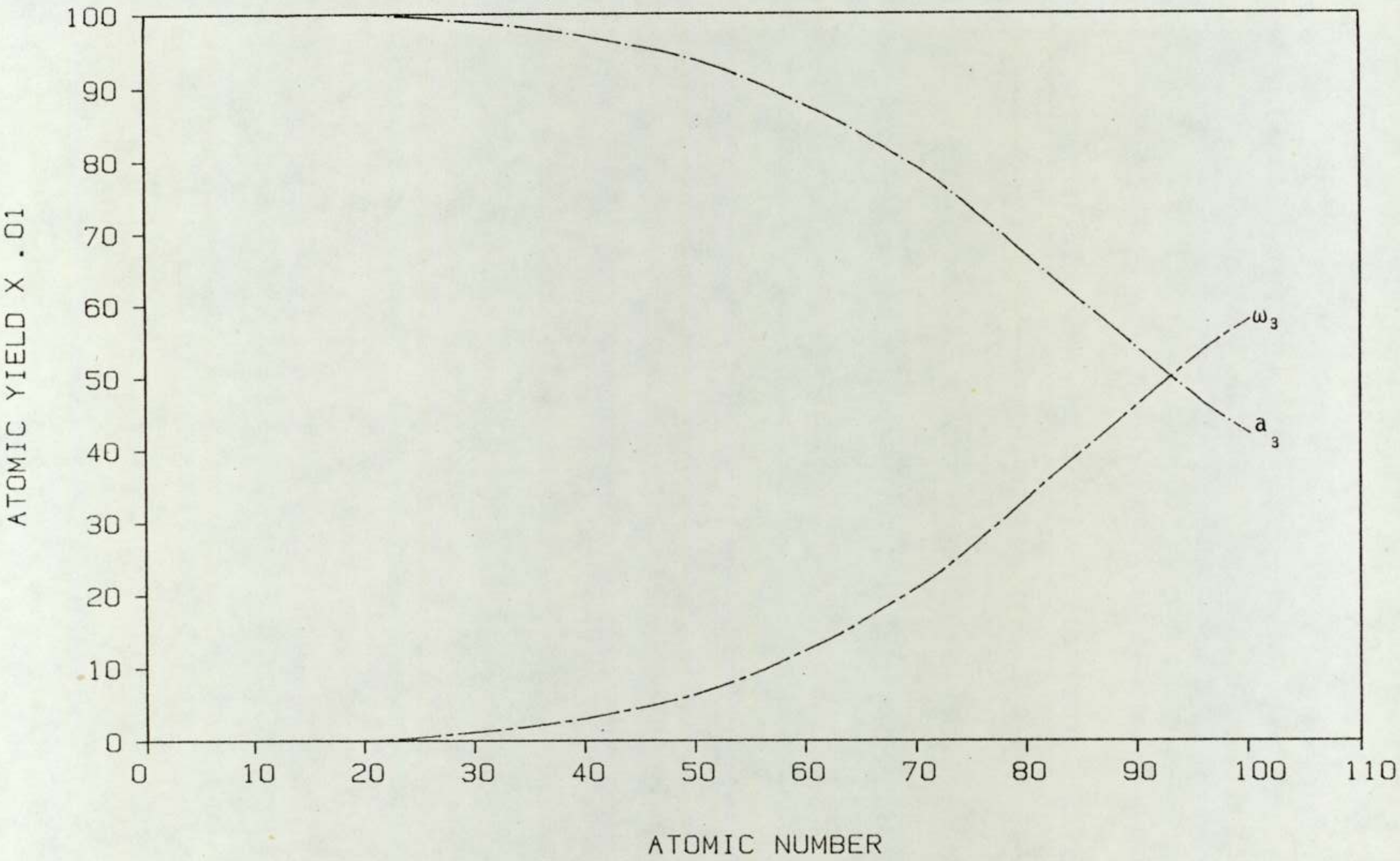

Figure 2.6 Variation of the L_3 subshell atomic yields with atomic number. Values taken from Krause (1979).

fluorescence yields were calculated for the L_1 and L_2 subshells and are illustrated in figure 2.7. As shown in this figure ν_1 and ν_2 have comparable values for all the elements.

For elements of interest in this study Krause (1979) has quoted uncertainties of upto 10% in their ω_i values and upto 50% in f_{ij}. The small number of measurements, or the lack of them, has been emphasised by Krause (1979) as being one of the major factors contributing to these large uncertainties. Recent measurements by Kodre et al (1981) of ω_i for Pb show similar large uncertainties. 25% in ω_1 and ω_2 have been quoted, although ω_3 is much more reliable. The experimental and theoretical values given in the review article by Bambynek (1972) are no more reliable. Comparison of these values and those of Krause (1979) show significant discrepancies between the two, especially for f_{ij} and this further casts doubt on the reliability of the availalbe data regarding atomic parameters. In theoretical calculations the precision of these parameters is hampered by the lack or scarity of knowledge of the influence of multiple vacancies and many-body effects (Krause 1979). Experimental problems such as isolating vacancies in the subshells have been discussed by Rao (1975).

A vacancy in a state has a finite life time (τ) and is related to the natural width (Γ) of that state by the uncertainty principle, that is,

$$\Gamma = \frac{\hbar}{\tau} \qquad 2.8$$

The total width of a state is given by the sum of the radiative (R), Auger (A) and Coster-Kronig (CK) partial widths.

$$\Gamma = \Gamma_R + \Gamma_A + \Gamma_{CK} \qquad 2.9$$

Γ_k (k = R, A, CK) is proportional to the transition rate (S_k) of the particular mode of decay (Parratt 1959, McGuire 1970 and Kostroun et al 1971) which is defined as

$$S_k = \frac{\Gamma_k}{\hbar} \qquad 2.10$$

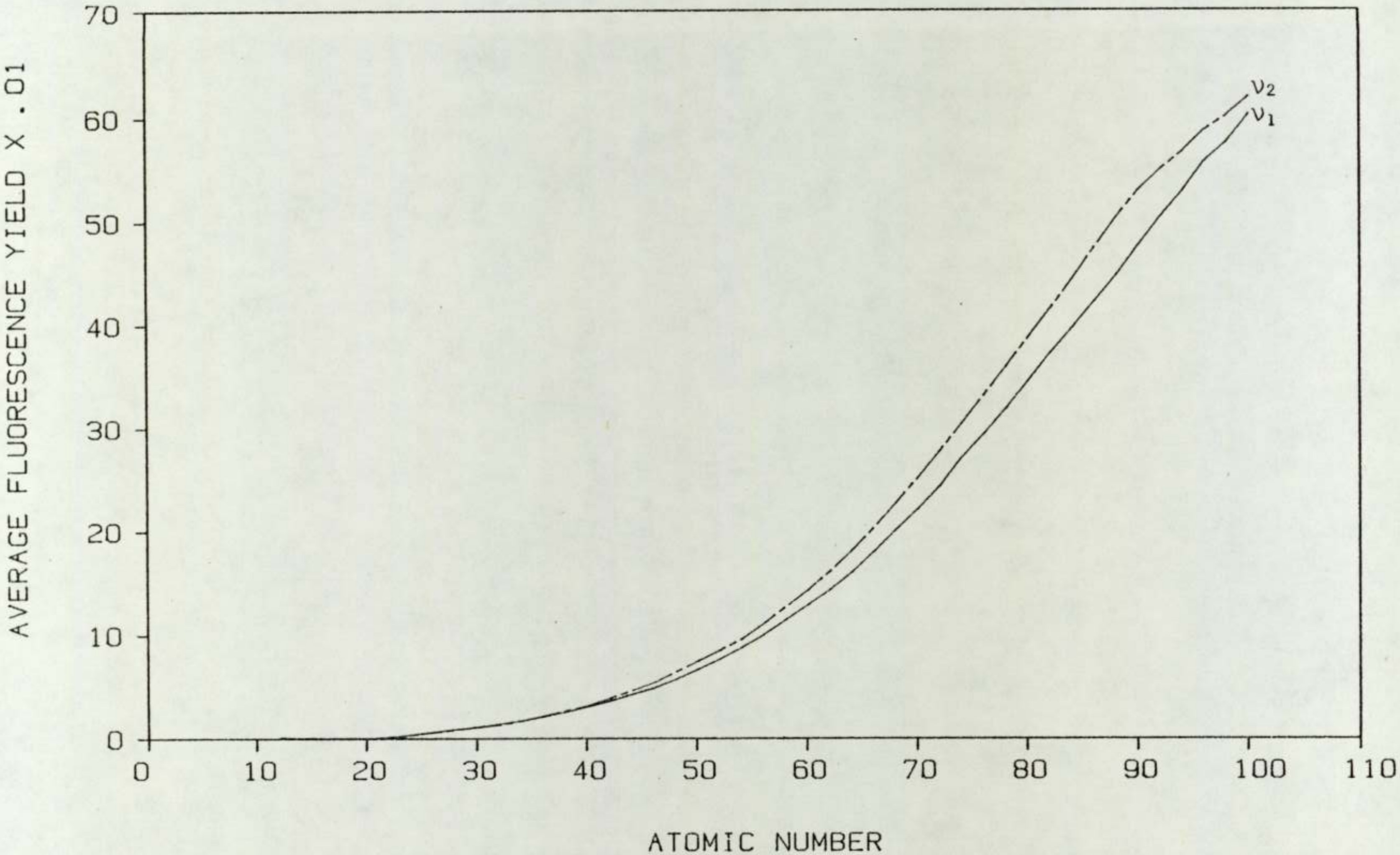

Figure 2.7 Variation of the average fluorescence yields (ν_i) for the L_1 and L_2 subshells with atomic number. ν_i calculated using equation 2.7 and atomic parameters taken from Krause (1979).

and as a counterpart to equation 2.9 we have

$$S = S_R + S_A + S_{CK} \qquad 2.11$$

Theoretical values for the radiative rates have been reported by McGuire (1971) for selected elements up to an atomic number of 90 and by Scofield (1974a) for atomic numbers upto 94. Scofield (1974b) has presented theoretical values for all elements. Keski-Rahkonen and Krause (1974) have provided a graphically representation of the radiative rates with atomic number up to 120. Theoretical electric dipole x-ray transition rates for all elements have been calculated by Manson and Kennedy (1974). The most probable values for K and L-shell radiative rates have been determined by Salem et al (1974) by fitting a curve to the available experimental data. These authors have presented their values numerically and graphically. A comperhensive list of the atomic parameters, determined experimentally or theoretically between 1972 and 1977 has been provided by Krause (1979).

Typical uncertainties in radiative rates, determined experimentally, range from about 10-20% (Salem and Lee 1974). These values show systematic discrepencies of the order of 10% from theoretical results (Scofield 1974b). Theoretical calculations may themselves be uncertain by several percent. Scofied (1975) does, however, point out in his theoretical discussion of radiative rates that uncertainties are greatest for low atomic number elements and outer-shell electrons.

2.3.4 Multiple Ionisation Phenomena

Double or multiple vacancies may be produced in an atom by (Nagel and Baun 1974)

(i) ejection of an electron by non radiative transitions (already discussed in section 2.3.2),

(ii) the 'shake-off' process (internal ionisation),

(iii) direct ejection of more than one electron, for example by heavy charge particles.

In the electron 'shake-off' process an outer-shell electron is ejected as a result of an impulsive perturbation produced by the sudden loss of a core-level electron which partially screens the outer electrons from the nucleus. For charged particle ionisation at very high energies this is the dominant process for producing double vacancies (Nagel and Baun 1974). Ionisation by heavy charged particles can also lead to multiple vacancies (Madison and Merzbacher 1975) by Coulomb interaction with the target atom. Double vacancies can also be produced by light particles such as protons and alpha particles (Knudsen et al 1973, Madison and Merzbacher 1975 and Mokler and Folkmann 1978). Evidence for these effects is seen in x-ray and Auger spectra which reveal the presence of 'satellite' lines with energy higher than the diagram lines (McGuire 1975, Richard 1975, Dyall and Larkins 1982 and Tawara and Richard 1983). Satellite lines on both sides of the main lines due to heavy particle collision have also been studied (Burhop 1979). When multiple vacancies are confined to the inner shells 'hypersatellite' lines originate (Stoller et al 1977).

The radiative counterpart of the radiationless Auger process was discovered by Aberg and Utriainen (1969) giving rise to a simultaneous emission of an electon and a photon with energy lower than that of the main emission line. This effect has been called the 'radiative' or the 'semi-Auger' effect. In this case the Auger electon emitted, when a vacancy is filled, is excited to a higher boundstate by the 'shake-up' processes instead of being ejected into the continuum as in the normal Auger effect (Cooper and La Villa 1970, Burhop and Asaad 1972 and Aberg 1975). Discrete structure as a result of this radiative electon rearrangement has been observerd by Jamison and Richard (1977) for heavy particle impact. Afrosimov et al (1976) observed a variation of this effect where a third electon is emitted instead of a photon for low energy Ar^- and Cl^+ particles. For highly energetic and highly stripped heavy ions a broad structure on the high energy side of the emission spectrum is observed due to radiation being emitted when target electrons, bound or free, are captured by the projectile (Schnopper et al

1972 and Kienle et al 1973). This 'radiative electron capture' is important at high projectile energies where the particle velocity is comparable to the velocity of the bound target electron (Burhop 1979).

It is clear from above that the degree of inner-shell ionisation will have significant effect on the different modes of decay and consequently makes the mean fluorescence yield dependent on parameters such as the energy and the charge state of the projectile (Burhop 1979). However, with the advent of Synchrotron radiation sources x-rays of specific energies can be used to study x-ray spectra free from the complications of multiple ionisation (Madden 1974 and Chevallier 1978).

2.4 PRODUCTION OF BREMSSTRAHLUNG

In the previous section the mechanism by which characteristic x-rays are produced after the creation of an inner-shell vacancy by an incident charged particle was elucidated in some detail. A major feature of an x-ray spectrum is the background continuum on which these characteristic x-rays are superimposed. The exact nature of this 'bremsstrahlung' is influenced to a large extent by the energy of the projectile and the degree of asymmetry of the ion-atom collision system. Although the term 'bremsstrahlung' refers to the continuum as a whole, in reality several distinct processes, which give rise to this continuum, take place. This section is devoted to the discussion of these processes.

2.4.1 Projectile Bremsstrahlung

In an ion-atom collision as the charged particle approaches an atomic nucleus of a target atom, it will suffer a change of velocity, the extent of which is determined by the proximity of the encounter. This change of velocity is caused by the Coulomb field of the nucleus which also changes the particles direction. This results in the emission of electromagnetic radiation and hence in a decrease in the particles kinetic energy. This contributes to the general stopping of the ions in matter. The electrodynamical theory for this process has been provided by Jackson (1975). The energy of the projectile bremsstrahlung extends from zero upto the projectile energy (E). Electric dipole radiation is the major contributor to this bremsstrahlung, the cross section of which has been derived by Jakubassa (1975) and Reinhardt et al (1976) in the restraints of the Born approximation. The cross section is approximately proportional to $Z_1^4 Z_2^2/M_1^2$ (Alder 1956 and Read 1980), where Z_1 is the projectile atomic number, Z_2 is the target atomic number and M_1 is the mass of the projectile. This process is therefore, most important, for incident particles of small mass. Protons, for example, give rise to bremsstrahlung a factor of $3X10^6$ smaller in intensity than electrons of the same velocity, and thus offer obvious advantages for trace elemental analysis by proton impact (Folkmann et al 1974a and Johansson and Johansson 1976). The bremstrahlung cross section decreases slowly with increasing projectile energy as E^{-1}. (Folkmann et al 1974a and Mokler and Folkmann 1978), This is illustrated in figure 2.8 which shows the variation of the cross section, $d\sigma/dE_r$, with the energy of the radiation E_r in relation to the other major source of bremsstralung (subsection 2.4.2). It is clear from this figure that although projectile bremsstrahlung decreases slowly with E_r, its contribution to the total background at the higher energy side of the x-ray spectrum gains importance. It is interesting to note that for a collision system consisting of interacting 'partners' with the same charge-to-mass ratio the electric dipole radiation component vanishes (Folkmann et al 1974a). This is due to the fact that the intensity is proportional to the acceleration of the centre of mass of the collision system, which for a symmetrical system moves uniformly (Landau and Liftshitz 1972). For most targets which have a charge-to-mass ratio close to a half bombarded by say, alpha particles ($Z_1/M_1 = \frac{1}{2}$) the projectile bremsstrahlung is negligible and consists of higher multipolarity contributions. This fact has been experimentally verified by Watson et al (1975). The anisotropy of projectile bremsstrahlung has been pointed out to be insignificant for practical situations (Folkmann et al 1974a).

2.4.2 Secondary Electron Bremsstrahlung

The secondary electrons ejected in ion-atom collisions undergo strong accelerations in the nuclear electric fields of target atoms and radiate bremsstrahlung (Ogier et al 1966) the energy of which may range from zero to the full kinetic energy of the secondary electrons. Intensity of this secondary electron bremsstrahlung (SEB) decreases rapidly at x-rays energies (E_X) above $T_m = (4m/M_1)E$ which is the maximum energy transferable to a free electron of mass, m, by a projectile with energy, E, and mass, M_1, (Merzbacher and Lewis 1958). SEB is the dominant process by which bremsstrahlung is produced at low x-ray energies ($E_X < T_m$). Detailed calculations regarding this process have been performed by Folkmann et al (1974a) for proton impact. The cross section for this process as a function of the emitted radiation energy (E_r) is shown in figure 2.8 in comparison with projectile bremsstrahlung. For E_X upto about 20keV SEB falls approximately as E_r^{-10} (Folkmann et al 1974b). For $E_X < T_m$ Tawara et al (1976) have pointed out that outer-shell electrons play the dominant role in the SEB process where as inner-shell electrons are the major contributors for $E_X > T_m$. In experimental situations we must note that for thin targets SEB is less prominant than for thick targets because the secondary electrons will have a greater probability of escaping from the target surface without producing any bremsstrahlung - a meritorious point in favour of thin target measurements (Johansson and Johansson 1976 and Yamadera et al 1981a).

The angular distribution of SEB is peaked at 90^0 to the incident particle direction and the intensity may change by as much as a factor of two with angle (Folkmann 1976, Ishii et al 1976, Tawara et al 1976 and Kaji et al 1977). Theoretical description of SEB is made difficult by the fact that the electrons may suffer severe deflections before radiating bremsstrahlung. Tawara et al (1976) have, however, compared measured data for protons and helium-3 impact on Al target with theoretical predictions based on the

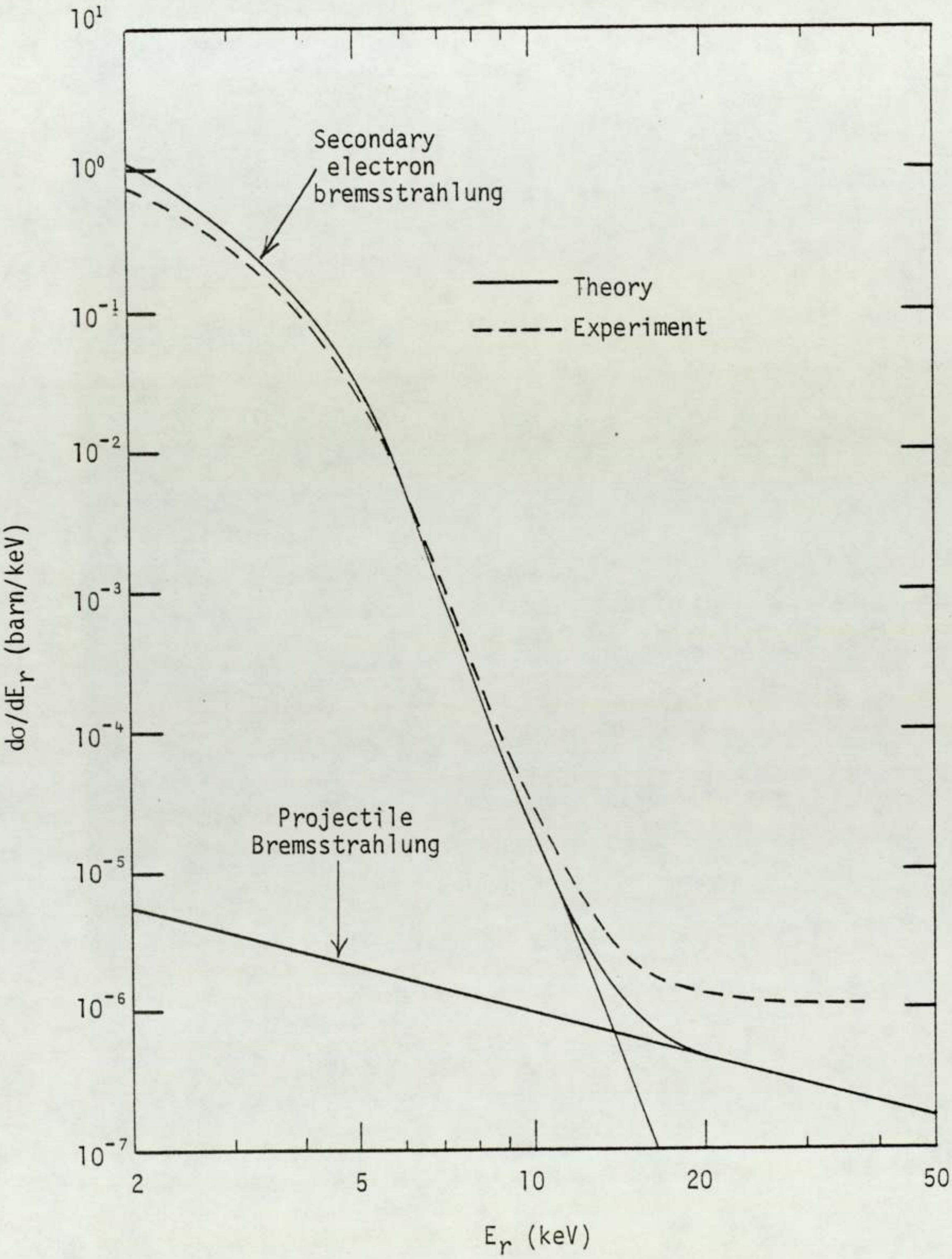

Figure 2.8 Experimental and theoretical background radiation cross sections for 3MeV protons on thin carbon foil. Detector at 90^0 to the beam (Folkmann et al 1974a)

binary encounter approximation model of Bonsen and Vriens (1970) and have obtained reasonable qualitative agreement.

Past and future interest in SEB stems from the fact that it is the major source of bremsstrahlung at low x-ray energies, precisely the region which is of fundamental concern to expermenters involved in trace elemental analysis by charged particle impact (Folkmann 1975, Johansson and Johansson 1976, Renan 1980, Khan and Crumpton 1981). It may also be relevant to the understanding of ion-atom collision mechanisms (Tawara et al 1976 and Mokler and Folkmann 1978).

2.4.3 Compton Scattering of Gamma-Rays

If a charged particle has sufficient energy to overcome the Coulomb potential barrier surrounding the target nucleus, it may undergo an inelastic interaction with the nucleaus. At low MeV energies the interaction is most likely with the nucleus as a whole leading to its excitation. The excited nucleus may then deexcite by releasing its excess energy in the form of gamma (γ) - rays (Lapp and Andrews 1972 and Burcham 1973). These γ-rays Compton scatter (see subsection 2.5.2) from the surroundings and in the detector producing a continuous background in the low keV x-ray region. This form of background is not 'bremsstrahlung' in the strictest sense since bremsstrahlung describes electromagnetic radiation emitted while charged particles are accelerated in an electric field. It is however, discussed in this section because of its direct relevance to the total continuum seen in an x-ray spectrum produced by charged particle impact.

Background due to Compton scattering of γ-rays is only acute for target elements which have high excitation cross sections or exhibit large resonances at low MeV energies. Elements such as ^{19}F, $^{23}N_a$, ^{27}Al, ^{12}C and ^{16}O are particularly prone to this problem causing the background from this source to be comparable, if not more important than the projectile bremmstrahlung at the high energy region of the x-ray spectrum (Folkmann et al 1974a). The discrepency between theory and experiment in figure 2.8 is explained by the contribution of Compton scattering to the total bremmsstrahlung (Renan 1980).

For the same energy, alpha particles are less susceptible than protons and deuterons to nuclear reactions leading to the emission of γ-rays. Deuterons can undergo 'stipping' and 'pick-up' reactions making them a less attractive choice of bombarding particles for trace-elemental analysis. The significance of Compton scattering to the afore-mentioned analytical technique has been discussed by Folkmann et al (1974b), Folkmann (1975), Johansson and Johansson (1976), Ahlberg and Adams (1978) and Khan and Crumpton (1981).

2.4.4 Quasi-Free Electron Bremsstrahlung

Bremsstrahlung can result from the direct interaction of a charged particle with the orbital electrons of a target atom. This type of bremsstrahlung has been called 'quasi-free electron bremsstrahlung' (QFEB) by Yamadera et al (1981b). It was, however, initially observed by Schnopper et al (1974) who named it 'primary bremsstrahlung'. Jakubassa and Kleber (1975) who developed a theory explaining this phenomenon referred to it as 'radiative ionisation'. In this process when the electric fields of the incident particle and the atomic electron interact, the electron is ejected and experiences an acceleration and thereby emits electromagnetic radiation (Anholt and Saylor 1976). Assuming the projectile velocity (v) is large compared to the orbital electron velocity the electron may be considered to be quasi-free. The resulting bremsstrahlung is characterised by the relative kinetic energy (T_r) which is equal to $\frac{1}{2}mv^2$, where m is the electron mass (Yamadera et al 1981b). QFEB should not be confused with SEB where the radiation is emitted as a result of a two-step process since the electron is first ejected and then suffers a deviation as it interacts with the electric fields of other target atoms. However, like SEB, this process is important for light-ion impact (Chu et al 1981). For heavier targets (Z_2 increasing) QFEB depends increasingly on the velocity of the orbital electrons and the intensity decreases less steeply in the vicinity of the high-energy limit T_r (Yamadera et al 1981b).

2.4.5 Discharge Electron Bremsstrahlung

Surfaces of targets, which are good insulators, can charge-up to a high voltage (several tens of volts) when bombarded continuously by positively charge particles. The target discharges by attracting free electrons in the vicinity of the target causing their acceleration. As a result an intense bremsstrahlung of energy upto several tens of keV is emitted by the electrons (Ahlberg et al 1975 and Renan 1980). This discharge electron bremsstrahlung (DEB) is particularly severe for thick insulating targets. Several solutions for eliminating this source of background have been proposed. Shabason et al (1973) suggests that the target should be neutralised by placing a hot filament a short distance away from the target. Evaporating a thin layer of carbon on the target to avoid charge build-up has been proposed by Papper et al (1978). Mingay and Barnard (1978) have employed a magnetic field to deflect the secondary electrons onto the target. The tertiary electrons generated as a result discharge the target. Huda (1979) has irradiated his targets in air to eliminate DEB.

2.4.6 Transition Radiation

This name is given to the radiation emitted when a charged particle suddenly crosses a boundary between two media with different dielectric constants. (Ginsburg and Frank 1946 and Garibyan 1958). When the particle passes through the interface its electric field, which is characteristic of its motion and the medium, adapts to the properties of the second medium. As the field reorganises itself transition radiation is emitted (Jackson 1975). The wavelength of this radiation may range from the optical to the x-ray region of the electromagnetic spectrum depending on the energy of the incident particle. Gibb et al (1977) indicated that this radiation, when in the x-ray region, may contribute to the bremsstrahlung normally associated with particle-induced x-ray experiments. Ramsay and Mckee (1978) have confirmed, however, that the contribution would be negligible even for high energy protons and would not pose any significant problem.

2.4.7 Heavy-Ion Effects

Highly stripped heavy ions can capture electrons from target atoms into their vacant states and may directly radiate the excess energy gained through this transition (Mokler and Folkmann 1978 and see subsection 2.3.4). The outer target atomic electrons are normally the participants in this 'radiative electron capture' (REC) and consequently give rise to a peak-like continuum centred above the binding energy of the projectile. The width of this continuum increases with atomic number of the target. Inner-shell electrons may also be captured by the incoming heavy ion but instead of a distinct peak a continuum ranging to high energies is observed. For light charged particles ($Z_1 << Z_2$) REC is not significantly important in relation to the total bremsstrahlung (Schnopper et al 1974). REC has also been studied by Kleber and Jakubassa (1975), Sohval et al (1976) and Spindler et al (1977).

Another process, which is only significant for heavy ions and gives rise to non-characteristic x-rays is that of quasimolecular x-ray emission (Saris et al 1972). In this case a broad non-characteristic band is observed as well as the individual characteristic x-rays of the projectile and the target. The electron shells of the ion and the target atom interpenetrate and form a transient quasimolecule. The non-characteristic band is due to radiative transitions between the quasimolecular orbital (Kraft et al 1974, Greenberg et al 1974 and Thoe et al 1975). In solid targets x-rays due to one- and two- collisions are emitted and the quasimolecular x-ray yield has been shown to be strongly dependent on the target density and the projectile velocity by Stoller et al (1981).

2.5 ATTENUATION OF X-RAYS

The attenuation of a narrow parallel beam of photons with intensity, I_0, passing through a thin homogeneous absorber of thickness, x, is described by Bouguer-Lambert-Beer exponential absorption law:

$$I = I_0 \exp(-\sigma n x) \qquad 2.12$$

where I is the photon beam intensity after attenuation, σ is the attenuation cross section and n is the number of absorber atoms per unit volume. The term σn is called the linear attenuation coefficient (μ) and is the attenuation of the photon beam per unit length. That is

$$\mu = \sigma n = \sigma \frac{N_0 \rho}{A_2} \qquad 2.13$$

where N_0 is the Avogardro's number, ρ is the absorber density and A_2 is the absorber atomic weight. Since the interaction cross-section (σ) is dependent on the absorber density, it is more convenient to use the mass attenuation coefficient, μ/ρ, which is independent of the mass density. Thus

$$\frac{\mu}{\rho} = \frac{\sigma N_0}{A_2} \qquad 2.14$$

For a mixture or a chemical compound the mass attenuation coefficient, $(\mu/\rho)_{mix}$, can be evaluated from the mass attenuation coefficients, $(\mu/\rho)_i$, of the constituent elements using the mixute rule

$$\left(\frac{\mu}{\rho}\right)_{mix} = \sum_i w_i \left(\frac{\mu}{\rho}\right)_i \qquad 2.15$$

where w_i is the proportion by weight of the i^{th} constituent element.

The different interaction mechanisms by which the incoming photon can be completely absorbed or scattered depend on the photon energy and the atomic number of the absorbing material. The major mechanisms pertinent to this study are mentioned below.

2.5.1 Photoelectric Absorption

In this process an incoming photon interacts with an absorber atom as a whole and is completely absorbed. The perturbation on the atom causes a bound electron to be ejected from the atom, as a result of which, the atom recoils.. Photoelectric absorption occurs most readily when the energy of the photon (E_X) is just larger than the binding energy of the shell from which the electron is ejected. For photons with energy less than 100keV this type of interaction is the most probable. The photoelectric interaction cross section increases rapidly with absorber atomic number (Z_2^{4-5})

and decreases with photon energy approximately as $E_X^{-3.5}$ (Knoll 1979).

The photoelectric effect has been discussed theoretically be Hall (1936), Pratt et al (1964), Rakavy and Ron (1967), Pratt et al (1973) and Park (1974). Experimental measurements of the photoelectric mass absorption coefficient, $(\mu/\rho)_{PE}$, have also continued in the past decade (Millar and Greening 1974 a, b, Lawrence 1979, Berry and Lawrence 1979) and more recently measurements have been reported by Sarma et al (1982). A detailed comparison of theoretical and experimental data in the photon energy range 0.1 keV to 1.5 MeV has been given by Hubbell and Veigele (1976). Hubbell (1977a) has presented $(\mu/\rho)_{PE}$ for light elements and some mixtures deduced from experimental and theoretical data. Parametric expressions for calculating $(\mu/\rho)_{PE}$ have been derived by Jackson and Hawkes (1981) starting from the fundamental theory of photon-electron interaction. Cross sections for the emission of an inner-shell electron derived using the Born approximation (Bethe and Salpeter 1957) were used and excellent agreement with other published work was acheived (Hawkes and Jackson 1980).

2.5.2 Incoherent Scattering

This process involves an incoherent interaction between a photon and an atomic electron assumed to be free. The electron may be excited to a higher shell or ejected into the continuum. This effect, named after Compton (1923) causes an increase in the wavelength of the incident photon. Compton scattering occurs impulsively and only when the energy transfer to the atomic electron is greater than its binding energy (Jauncey 1925).

The Compton scattering cross section increases linearly with Z_2 and decreases gradually with increasing E_X (Knoll 1979). However, for high Z_2, the cross section looses importance in favour of the photoelectric effect.

The fundamental theory for calculating scattering cross sections is that of Klein and Nishina (1929). The basic assumption of this theory is that the electron involved is free and stationary. This is a reasonable approximation for high energy photons and outer-shell electrons or electrons of light elements. However, for low energy photons or for inner-shell electrons of medium and heavy atoms relativistic and binding effects have to be allowed for. The binding effects are estimated by the incoherent scattering factor, which is the probability for excitation or ionisation of an atom when it undergoes an incoherent interaction (Raghava Rao et al 1982). The theoretical calculation of this functions has been discussed in detail by Hubbell et al (1975) who have made detailed comparisons with experimental data. Raghava Rao et al (1982) have reported experimental measurements of this factor exclusively for the K-shell which show marked discrepancies when compared with theoretical data of Hubbell et al (1975), highlighting the need for further work in this area. Hawkes and Jackson (1980) have modified the Klein-Nishna cross sections and have formulated parametric expressions for the Compton scattering cross sections. The contribution by Compton scattering to the mass attenuation coefficient of Mg and Ag have been estimated by Lawrence (1979).

Compton scattering has been successfully employed in the study of electron momentum distributions (Cooper 1971) and is thus proving invaluable for studying solid-state properties. Progress in this field, experimental and theoretical, has been surveyed by Williams (1977). Recent work includes that of Pattison and Weyrich (1979), Rindby et al (1982) and Pattison et al (1982).

2.5.3 Coherent Scattering

When bound electrons participate in the photon-atom interaction, there is a finite probability that the electrons will not be transferred to higher atomic states or ejected into the continuum. Scattering in this case is coherent (Rayleigh) and takes place with the atom as a whole, causing the electron to oscillate at the frequency of the incident radiation. The electrons then relax by radiating electromagnetic energy without any change in the frequency, which appears as scattered radiation concentrated in the forward direction. The scattering cross section increases as $Z_2^{2.5-2.7}$ and decreases with photon energy as E_X^{-2} (Dyson 1973). Consequently, this process is important at low photon energies and for heavy absorber elements.

When the interaction takes place with a single electron, assumed to be free, we then have Thomson scattering (Jackson 1975 and Read 1980). Thomson scattering occurs only at low energies where the momentum of the incident photon can be ignored. At higher frequencies the Compton effect comes into operation. Thomson scattering is, therefore, the low frequency limit of the Compton effect (Davisson 1965). Thomson scattering is independent of the photon energy, in the energy region where it takes place, and is approximately proportional to Z_2 (Davisson 1965). A parametrized approach for calculating coherent scattering has been provided by Hawkes and Jackson (1980). The atomic form factors, the square of which gives the probability that the Z_2 electrons of an atom take up a certain recoil momentum without absorbing any energy (Hubbell 1969), required for calculating interaction cross sections for this process have been tabulated by Hubbell (1975).

2.5.4 Tabulations of Mass Attenuation Coefficients

The total mass attenuation coefficient, μ/ρ, is obtained by summing the individual contributions. Using equation 2.14 we get,

$$\frac{\mu}{\rho} = (\sigma_{PE} + \sigma_{INC} + \sigma_{COH}) \frac{N_0}{A_2} \qquad 2.16$$

where σ_{PH}, σ_{INC} and σ_{COH} are the interaction cross sections for the photoelectric absorption, incoherent scattering and coherent scattering respectively.

Considerable activity has been directed to the specific task of compiling an internally consistent and reliable set of data for these quantities. Hubbell (1969) has published tabulated data for mass attenuation coefficients and interaction cross sections for 23 elements and 13 compounds and mixtures, covering a photon energy range of 10keV to 100GeV. For the low energy region uncertainties upto 10% in these quantities are quoted depending on Z_2, low Z_2 elements having larger uncertainties. The experimental and theoretical data have been comprehensively reviewed by Hubbell (1969, 1971). The very popular tabulation of theoretical cross section values of Storm and Israel (1970) covers all elements up to Z_2 = 100 and an energy range of 1kev to 100MeV. These authors have quoted uncertainties ranging from 3 to 10% depending on the photon energy, higher uncertainties applying to energies less than 6keV. Storm and Israel (1970) include a comparison of experimental and theoretical values and relative shell contributions to the photo-electric cross section. To facilitate the use of this tabulation Montenegro et al (1978) have fitted logarithmic polynomials to the values of Storm and Israel (1970) and have tabulated mass attentuation coefficients for elements with $6 \leq Z_2 \leq 33$ for characteristic K and L x-rays of elements with $17 \leq Z_2 \leq 94$. Semi-experical expressions have been utilised by Gerward (1980) to fit the data of Hubbell et al (1974). An energy range of 5 to 100 keV and elements with $2 \leq Z_2 \leq 92$ have been covered. However, the author has admitted in his article that logarithmic expressions, such as those employed by Montenagro et al (1978) would provide better fits. Hubbell (1982) has published theoretical values of the total mass attentuation coefficients for photon energies 1 keV to 20MeV for 40 elements ranging from $1 \leq Z_2 \leq 92$ and 45 mixtures and compounds.

From above it is clear that the low x-ray energy region, which is important for most x-ray analytical techniques, photon attenuation coefficients are uncertain by about 10%. At energies around or below 1 keV the uncertainty can be as high as 20% or even greater (Hubbell 1977b). Recognising the necessity of reliable mass attenuation data it was decided at the International Union of Crystallography Congress, held in Warsaw 1978, to set up a committee to organise an evaluation of the experimental techniques adopted for measuring x-ray attenuation coefficients. Further details can be found in the Journal of Applied Crystallography Volume 13 (1980) pp199-200.

CHAPTER 3

CONCEPTS OF NUCLEAR BACKSCATTERING

CONTENTS

3.1 INTRODUCTION

The atomic processes which reveal themselves through characteristic features in an x-ray spectrum were examined in the preceeding chapter. In the present chapter, concepts which are closely related to a nuclear backscattering spectrum have been addressed. Energy loss and straggling of charged particles passing through matter have been considered qualitatively and contemporary problems in both these areas are highlighted.

Nuclear backscattering spectrometry has been dealt with from the view point of measuring thin film thicknesses and the analytical capabilities of this technique are mentioned only briefly. However, references which consider the analytical aspects in greater detail have been quoted. Fundamental formulae required for determining thin film thicknesses have been stated and corrections to the Coulombic scattering cross section, including recent contributions, are discussed. Throughout this chapter cgs units have been employed in order to be consistent with the published literature on this subject.

3.2 ENERGY LOSS AND STRAGGLING OF CHARGED PARTICLES

The study of energy loss and straggling processes of charged particles is important not only for understanding the process mechanisms themselves, but also for the correct interpretation of quantitative information obtained from charged particle based analytical techniques. Two such major techniques are nuclear backscattering spectroscopy (Chu et al 1978) and particle induced x-ray emission analysis (Johansson 1981). The former technique is based on the actual physical laws governing the energy loss of a charged particle as it traverses matter and the latter requires energy loss data for the purpose of applying corrections to quantitative results obtained from thick and semi-thick targets. Although a particle traversing matter loses its energy through collision and radiative processes, only the former is discussed in this section. Radiative losses have been dealt with in Chapter 2.(section 2.4) in the context of bremsstrahlung emission.

3.2.1 Energy Loss by Collision

As a charged particle travels through a medium it loses its energy to the atomic electrons (electronic stopping) and to the atomic nuclei (nuclear stopping) by electrostatic interaction (Bohr 1913). Nuclear stopping is due to elastic collisions with the target nucleus and predominates when $v << v_0$, where v is the particle velocity and v_0 is the Bohr velocity. At particle energies above 200keV/amu it is typically around 1% of the electronic stopping (Ziegler 1980). At higher energies nuclear stopping becomes even more insignificant and the interaction of the projectile with the target nucleus changes from elastic to inelastic. The relative contributions of electronic and nuclear stopping are shown in figure 3.1. At projectile velocities, $v < v_0 Z_1^{2/3}$, electronic stopping is proportional to the particle velocity (Linhard and Scharff 1981) where Z is the projectile charge and $v_0 Z_1^{2/3}$ is the mean velocity of the bound projectile electrons. It reaches a maximum when v approaches $v_0 Z_1^{2/3}$ beyond which it falls as $\ln v^2/v^2$.

The proximity of the ion to the atomic electrons determines whether electronic stopping is through excitation or ionisation of the atom. Excitation is predominant for distant collisions and ionisation for close ones. Ionisation contributions to the energy loss of the ion originate in two ways. Firstly, they arise through primary collisions with atomic electrons. The most probable collisions are where the energy transfers in each collision are small, thus resulting in the ejection of low energy secondary electrons (Segre 1953). A small fraction of ionising collisions (close) may produce energetic secondary electrons (delta rays) with a maximum kinetic enegy of $(4m/M_1)E$. This is the maximum energy that an ion of mass, M_1, and energy, E, can transfer to a free electron of mass, m, in a direct collision and corresponds to the electron having a velocity twice that of the incident ion. Secondly, the contribution may come from ionisation by

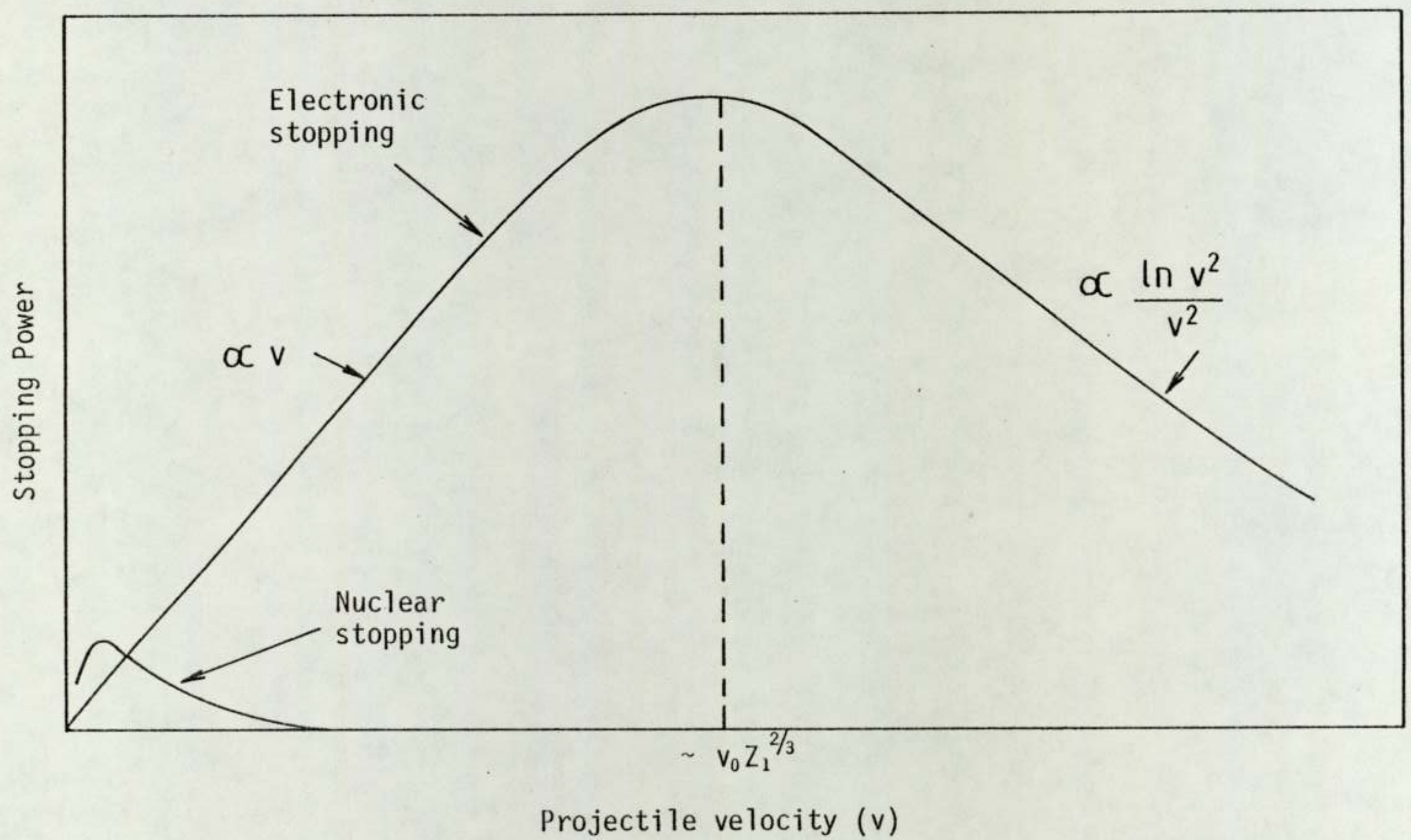

Figure 3.1 Comparison of electronic and nuclear stopping of charged particles in matter (Datz 1978).

indirect interaction with the atomic electrons. This can occur either by the energetic delta rays causing further ionisation or a target atom recoiling as a result of the primary collision and causing ionisation of other atoms (Holmen et al 1979). The direct relationship between secondary electron emission and the electronic stopping of the ion was formulated by Sternglass (1957). The investigation of secondary electron emission as a result of ion impact has been pursued vigorously in recent years, not only for academic interest but also for its direct relevance in stopping power and thermonuclear fusion studies (Stolterfohr 1978, Veje 1982, Svenson and Holmen 1982 and Bell et al 1982).

The behaviour of the rate of energy loss with distances, x, travelled by a fully stripped ion with charge Z_1e in a medium with atomic number Z_2, and atomic density, n, is described by the fundamental Bethe formula based on a relativistic quantum mechanical treatment (Bethe and Ashkin 1953 and Fano 1963)

$$-\frac{dE}{dx} = \frac{4\pi(Z_1e^2)^2 Z_2}{mv^2} n B$$

$$\text{and } B = \left[\ln\left(\frac{2mv^2}{I}\right) - \ln(1-\beta^2) - \beta^2 - \frac{C_i}{Z_2}\right] \qquad 3.1$$

where m is the electron rest mass, v is the projectile velocity, e is the electronic charge, β is v/c ratio, c being the velocity of light, I is the mean excitation potential of the stopping medium, C_i/Z_2 is the ith shell correction and B is the stopping number. This equation assumes that there are no radiative energy losses. We should note that the stopping power, dE/dx, shows a simple Z_1^2 dependence assuming that the stopping number is a function of v and Z_2 only. A further important point to note is that this equation is valid only for high energies (>1MeV/amu), that is, beyond the stopping power maximum (figure 3.1). The mean excitation potential, I, is independent of the ion velocity and is defined theoretically, as (Bethe 1930)

$$\ln (I) = \sum_n f_n \ln (E_n) \qquad 3.2$$

where E_n are all possible energy transitions of the target atoms and f_n are the corresponding dipole oscillator strengths. Except for the simplest atoms the complexity of this equation is overwhelming (Anderson and Ziegler 1977a) and for practical purposes values for I are usually extracted from experimental data (Chu and Powers 1972). For recent progress in this area the reader is referred to Inokuti (1981). The energy dependent shell corrections, C_i/Z_2, allow for the lack of participation of the inner most electrons in the stopping process (Walske 1956 and Sorensen and Anderson 1973). Without these corrections equation 3.1 is only valid when v is much greater than the orbital velocity of the Z_2 bound electrons. When this is not the case, as for inner-shell electrons of heavy elements, these corrections are necessary (Walske 1956). Such corrections have been formulated by Walske (1952 and 1956) and Brandt (1975), and Andersen and Ziegler 1977a).

Experimental energy loss data that has accumulated over the past years have revealed the need for high order charge-dependent corrections to Bethe's formula (Andersen et al 1969, Lindhard 1976, Andersen et al 1977 and Anthony and Lanford 1981). A Z_1^3 term takes into account polarisation effects at low velocities. It explains observed differences between stopping powers of particles and their antiparticles, originally noticed by Barkas et al (1963) and thus called the Barkas effect by Lindhard (1976) (Ashley et al 1972, Jackson and McCarthy 1972 and Hill and Merzbacher 1974). Lindhard (1976) obtained a correction twice that of Ashley et al (1972) which was confirmed by Andersen et al (1977). At high energies deviations from the Rutherford formula introduces higher order Z_1 terms known as the Mott correction (Morgan and Eby 1973). An expression for this term to order Z_1^7 has been derived by Ahlen (1978). At the two velocity extremes a Bloch's correction of Z_1^{2n} (n = 2, 3...) is required (Bloch 1933). Recent work on Z_1^3 and Z_1^4 corrections has been published by Porter and Bryan (1980). Measurements performed by Salaman et al (1981) have revealed a need for a further correction for relativistic heavy ions. Such a correction has been confirmed and derived by Ahlen (1982).

At low velocities ($v \sim v_0$) the electronic stopping was found to depend in an oscillatory fashion on Z_1 by Bottiger and Bosson (1969). Theoretical explanations for this behaviour has been given by Briggs and Pathak (1974). Also at low velocities stopping power for a given ion (Z_1 fixed) shows similar oscillatory dependence on the stopping medium (Z_2). This is true for light ions (Ziegler and Chu 1974 and Gertner et al 1980) and for heavy ions (Pietsch et al 1976 and Land et al 1980). Kreussler et al (1981) have shown experimentally that these pronounced target effects diminish with increasing velocity and beyond the stopping power maximum show a smooth Z_2 dependence (Mann and Brandt 1981). At low particle velocities stopping power is determined by the properties of the valance electrons in the medium and not the inner-shell electrons which remain relatively inactive implying that these fluctuations are most likely to be a consequence of the valance-electron configuration of the elements (Brandt 1981).

The energy loss process for heavy ions is further complicated by the fact that the charge state of the ions changes with penetration. This has been recognised as one of the most fundamental problems in stopping theory (Andersen and Ziegler 1977b). As the ion penetrates matter its charge changes either by electron loss to the medium or by electron capture from the medium. This effect produces discrepencies in the Z_1^2 scaling law unless the effective charge state of the ion is known (Andersen and Ziegler 1977b). At high velocities ($v \gg v_0 Z_1$, where $v_0 Z_1$ is the velocity of the K-shell electron) the ion can be assumed to be completely stripped of its electrons but if $v \lesssim v_0 Z_1^{2/3}$ the ion is only partially stripped (Brandt 1981). Using the Thomas-Fermi model of the atom, Ziegler (1977) has derived an empirical expression for the effective charge of ions. An empirical expression has also been derived by Andersen and Ziegler (1977b) based on the work of Northcliffe (1963) and Forster et al (1976) for scaling proton stopping powers to obtain values for heavy ions. This problem has been tackled theoretically by Brandt (1981) and Wietschorke and Soff (1981) and experimentally by Schulz and Brandt (1981) and Anthony and Lanford (1982). Other notable references in the field of energy loss of charged particles include Mayer and Ziegler (1973), Saris and Van der Weg (1976), Andersen et al (1980) and Bird and Clark (1981). Recent measurements have been made by Fukuda (1981) and Santry and Werner (1981) and Ahlen (1980) has recently published a review article on the subject.

Despite the difficulties in explaining the energy loss process theoretically, experimental work on this subject has been unceasing. A comprehensive bibliography has been presented by Andersen (1977) on the subject. Recent tabulations of stopping powers have been published by Andersen and Ziegler (1977a,b) for protons and alpha particles passing through all elements. A more recent tabulation by Ziegler (1980) gives the stopping powers of all ions in all elemental absorbers. The values in these tabulations were obtained by combining experimental and theoretical results. The latter were used to determine stopping powers of ions in elements for which experimental values were unavailable. The projectile energy range covered is 1 - 10^5keV and empirical formulae fitted to the experimental data are also presented by these authors. These fits are reported to be accurate to 1% and the interpolated values are reliable to 0.5% (Andersen and Ziegler 1977a).

3.2.2 Energy Straggling

The energy loss process mainly involves a large number of independent interactions between the ion and the atomic electrons of the absorber which are subject to statistical fluctuations (Bohr 1915). This stochastic nature of energy loss of ions causes the delta distributions of a mono-energetic ion beam, of identical particles, to broaden considerably after passing through an absorber. The fluctuations in the energy loss of the particles is known as energy straggling. This is closely related to range straggling (Lewis 1952). The upsurge of interest in this phenomenon in recent years can be attributed to the successful application of ion beam analysis techniques which require a detailed knowledge of energy straggling (Mayer and Ziegler 1973, Saris and Van Der Weg 1976, Andersen et al (1980), and Bird and Clark 1981). In nuclear backscattering spectroscopy, for instance (section 3.3), energy straggling is one of the major factors which limit depth resolution studies (Friedland 1978) and, therefore, it is essential that its effect is quantified.

The original theory formulated by Bohr (1915) predicts that the energy straggling is independent of the particle energy and that the root-mean-square (rms) value of the energy variation increases with the square root of the electron density per unit area ($n Z_2 t$) in the target, that is,

$$\Omega^2_B = 4\pi(Z_1e^2)^2nZ_2t \qquad 3.3$$

where Ω^2_B (keV^2) is the variance of the energy loss distributions, Z_1 is the projectile atomic number, Z_2 is the targets atomic number, t is the target thickness and n is the number of target atoms per unit volume. The above expression is based on the assumption that the individual energy transfers takes place between a free electron at rest and a fully ionised projectile. Therefore, it is only applicable beyond the stopping power maximum. Lindhard and Scharff (1953) have refined Bohr's theory to extend the range of applicability to below and in the vicinity of the stopping power maximum. Bonderup and Hvelplund (1971) added further improvement to take into account the oscillatory dependence of energy straggling on Z_2, a situation similar to that found for stopping power. Chu (1976) by incorporating Hartree-Foch-Slater atomic wave functions into the theory of Bonderup and Hvelplund (1971), explained these material dependences. Contrary to Bohr's theory (Bohr 1915), energy straggling measurements reported by Harris and Nicolet (1975) revealed a weak dependence on the projectile energy which is in qualitative agreement with the other formulations by Lindhard and Scharff (1953), Bonderup and Hvelplund (1971) and Chu (1976). Bohr's theory further predicts a Gaussian energy loss distribution. This, however, has been found to be true only for low velocity projectiles (Wilken and Fritz 1976) and in general is only an approximation. A realistic distribution is asymmetrical and shows significant skewness as shown by Landau (1944), Tschalar (1968) and Bichsel and Saxon (1975). However, in the low MeV energy region for ligh ions the energy resolution of conventional solid-state detectors is not fine enough to show the non-Gaussian shape and the assumption of a Gaussian distribution is acceptable for practical purposes. If the particle has enough energy to completely penetrate through the detector's sensitive volume considerable dispersion is observed in the distribution (Wilken and Fritz 1976).

Experimental investigation of energy straggling has inherent difficulties since the true straggling is hidden within instrumental (Wilken and Fritz 1976) and target inhomogeniety effects (Stoquert et al 1981a). Despite these hindrances interest has continued (Friedland and Kotze 1981 and Molherbe and Alberts 1982).

An important contribution to energy straggling concerns the fluctuations in energy loss caused by charge-exchange effects as the particle passes through matter (Vollmer 1974). This effect is particularly important at the vicinity of the stopping power maximum where the probability of charge exchange is high (Cuevas et al 1964). Sofield et al (1981) has explained discrepencies of upto a factor of two between experimental measurements and theoretical predictions in terms of charge exchange effects. The importance of these effects to the energy loss and straggling processes accompnaying the passage of ions through matter is self-evident from the above discussion and makes the continued pursuance of experimental and theoretical investigations in this area vital.

3.3 NUCLEAR BACKSCATTERING SPECTROMETRY

Although the pioneering work of Rutherford (1911) and Geiger and Marsden (1913) gave birth to nuclear backscattering spectrometry it is only in the last two decades that is has established a firm foothold as one of the major surface analystical techniques (Chu et al 1978). This development was primarily a consequence of the advent of fast-response solid-state detectors which offered good resolution and good linearity over a wide range of energies and to the improvements acheived in the electronic systems required for data handling and processing (Chu et al 1978).

The physical concepts of nuclear backscattering spectrometry have been considered only briefly here, simply because as a result of its generally wide acceptance and its high level of development a prodigious amount of literature is now available which covers its concepts and applications in great depth (Mayer and Ziegler 1973, Ziegler 1975, Foti et al 1977, Chu et al 1978, Gyulai 1980, Bird and Clark 1981, Gyulai 1981 and Simons et al 1982).

3.3.1 Kinematic Factor

When a light charged particle of mass, M_1, impinges on a target there is a finite probability that it will experience a Coulombic interaction with a target nucleus of mass, M_2. As a result of this interaction the particle transfers momentum to the target nucleus causing it to recoil and is, itself, deflected at an angle, θ. A minority of the impinging particles may suffer close 'billiard ball' type encounters with the nucleus and be deflected by obtuse angles as shown in figure 3.2. Provided that the incident projectile energy is below the threshold of nuclear reactions and greater than the binding energy of the target atom (Chu et al 1978) the collision may be considered as an elastic one and using the conservation laws the kinematic factor, K, defined as the ratio of the projectile energy after (E_1) and before (E) the collision can be calculated. For the non-relativistic case in the laboratory frame and provided $M_1 < M_2$ we have

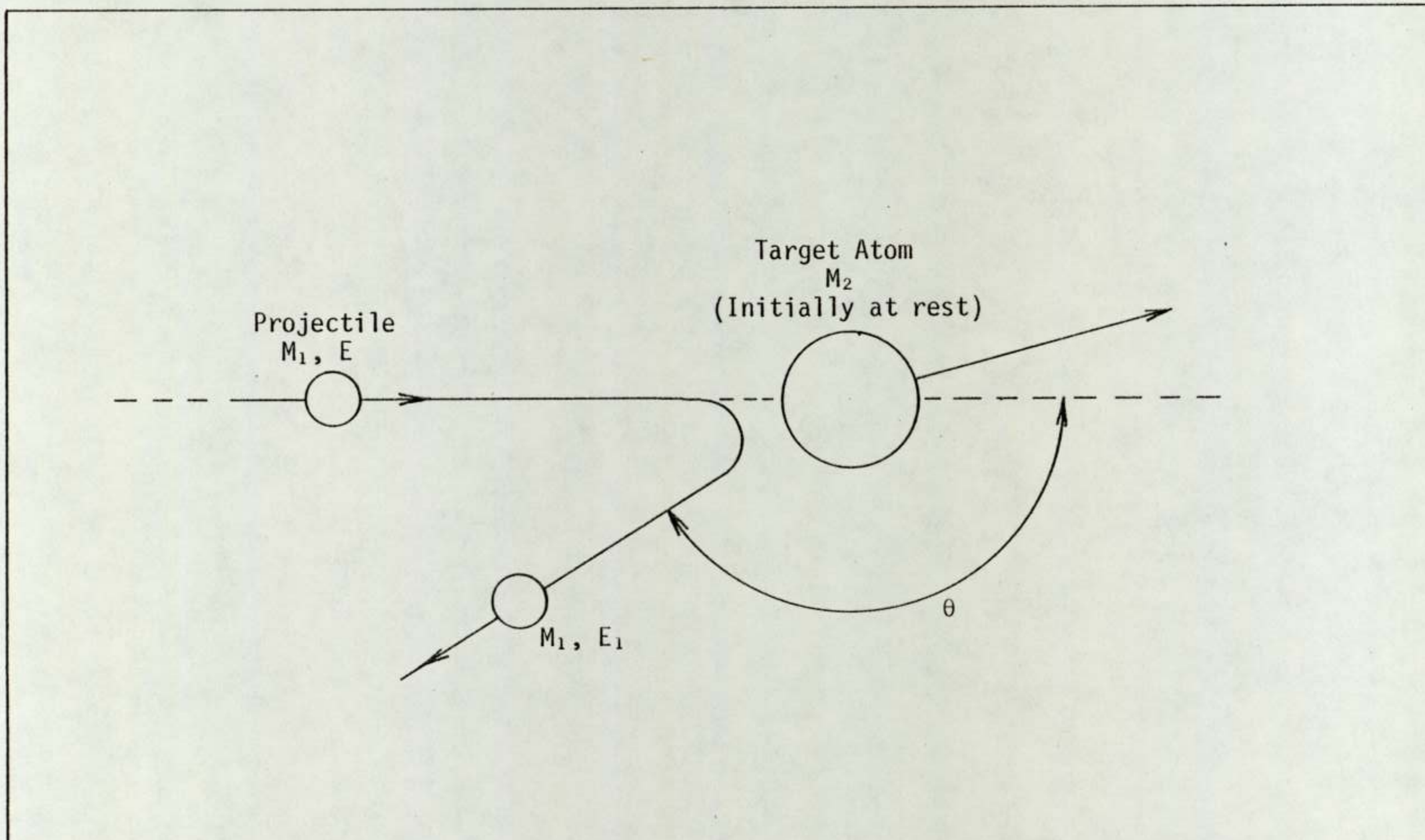

Figure 3.2 Schematic representation of the collision system in the laboratory frame of reference.

$$K = \frac{E_1}{E} \qquad 3.4$$

$$= \left[\frac{(M_2^2 - M_1^2 \ Sin^2\theta)^{\frac{1}{2}} + M_1 Cos\theta}{M_2 + M_1}\right]^2 \qquad 3.5$$

$$= \left[\frac{(1 - (M_1/M_2)^2 Sin^2\theta)^{\frac{1}{2}} + (M_1/M_2) Cos\theta}{1 + (M_1/M_2)}\right]^2 \qquad 3.6$$

The kinematic factor, therefore, depends on the ratio of M_1 and M_2 and for fixed M_1 and E it facilitates mass discrimination by nuclear back-scattering spectrometry.

In practice the mass difference, ΔM_2, between two elements of interest in a target must produce as large an energy change, ΔE_1, as possible after collision. For fixed M_1 and $\dot{E}$, ΔM_2 will induce the largest change in K at a scattering angle of 180^{o}. Consequently, to achieve the maximum mass resolution θ is chosen to be as close as possible to 180^{o} as the experimental set-up will allow. Quatitatively ΔE_1 can be expressed as (Chu et al 1978)

$$\Delta E_1 = E\left(\frac{dK}{dM_2}\right)\Delta M_2 \qquad 3.7$$

dK/dM_2 can be readily obtained from equation 3.5 and

$$\frac{dK}{dM_2} \simeq \frac{-4M_1}{M_2^2} Cos\theta \qquad 3.8$$

If θ is different from π by δ, where δ is small, equation 3.8 can be written as

$$\frac{dK}{dM_2} \simeq (4 - 2\delta^2)\ \frac{M_1}{M_2^2} \qquad 3.9$$

Substituting 3.9 into 3.7 we arrive at

$$\Delta E_1 = E\ (4 - 2\delta^2)\ \frac{M_1}{M_2^2}\Delta M_2 \qquad 3.10$$

From equation 3.10 we can deduce that the mass resolution can be optimised by

(i) increasing E

(ii) using heavy ions (increase M_1 provided $M_1 < M_2$)

(iii) measuring at scattering angle as close as possible to 180^0 so that $\delta \to 0$, and

(iv) analysing light elements (small M_2)

The possibility of employing heavy ions for backscattering spectrometry has been explored rigorously by many workers (Peterson et al 1973, Miller and Ischenko 1976, Thomas et al 1976 and Sullins et al 1981). The main disadvantage of adopting heavy ions such as ^{12}C and ^{16}O as projectiles instead of ^1H and ^4H_e is the worsening of the detector resolution that results and which dampens considerably the advantages. However, despte this problem Petersson et al (1973) have attained improvements in the mass resolution of upto a factor of four. Thomas et al (1976) used Lithuim ions of energy upto 3MeV and obtained improvements while still maintaining the detector resolution. Sullins et al (1981) have compared high energy ^{16}O, ^{20}Ne and ^{40}Ar ions and have highlighted the potential capabilities of heavy-ion nuclear backscattering spectrometry for resolving neighbouring masses for elements with $50 < M_2 < 100$. A mass resolution of better than 1 amu has been achieved by Chevarier et al (1981) with ^{14}N and ^{40}Ar ions by using a time-of-flight spectrometer.

The choice of E and the inherent advantage of analysing light elements cannot be discussed in isolation and are subject to compromises imposed by the scattering cross section considered below.

3.3.2 Scattering Cross Section

The concept of the differential scattering cross section, $d\sigma_R/d\Omega$, allows quantitative analysis by backscattering spectrometry. $d\sigma_R/d\Omega$ is a measure of the probability of a scattering event occuring due to a Coulomb interaction. This can be derived classically (Rutherford 1911) or quantum mechanically (Tralli and Pomilla 1969) and in laboratory co-ordinates is given by

$$\frac{d\sigma_R}{d\Omega} = \left(\frac{Z_1 Z_2 e^2}{4E}\right)^2 \frac{4}{\sin^4\theta} \quad \frac{[(1 - (M_1/M_2)^2 \operatorname{Sin}^2\theta)^{\frac{1}{2}} + \operatorname{Cos}\theta]^2}{[1 - (M_1/M_2)^2 \operatorname{Sin}^2\theta]^{\frac{1}{2}}} \qquad 3.11$$

This is the Rutherford forumla and gives the differential scattering cross-section with respect to the detector solid angle, Ω, for a projectile with incident energy, E, charge, Z_1e, and atomic mass, M_1, scattered by a target nucleus of atomic number, Z_2, and mass, M_2, at an angle, θ. Equation 3.11 assumes that the force between the two nuclei is Coulombic. This is a valid assumption provided that the distance of closest approach is much greater than the nuclear dimensions but smaller than the Bohr radius. For very small solid angles θ is well defined and the absolute scattering cross section (σ_R) can be approximated by $d\sigma_R/d\Omega$ (Chu et al 1978).

The following points are worth noting, that, $d\sigma_R/d\Omega$ is

(i) proportional to Z_1^2 giving an alpha particle backscattered yield four times that of protons or deutrons.

(ii) proportional to Z_2^2 making nuclear backscattering much more sensitive to heavy elements than to light ions,

(iii) proportional to E^{-2} and, therefore, the backscattering yield increases rapidly with diminishing projectile energy,

(iv) a function of θ and, therefore, is axially symmetrical with respect to the axis of the incident beam, and

(v) approximately proportional to $\operatorname{cosec}^4\theta$ and as a result the backscattering yield decreases rapidly with increasing θ.

Although the mass resolution is improved by increasing E, the fact that the scattered yield diminishes as E^{-2} for a given projectile has to be taken into account. Using light charged particles such as alpha particles, at about 2MeV is usually a good compromise. The inherent advantage of high mass resolution for light elements, mentioned in sub-section 3.3.1, has to be weighed with the disadvantage of the backscattering yield being less sensitive to light elements. These points illustrate that the exact experimental conditions depend on the nature of the analytic problem.

3.3.3 Corrections to the Scattering Cross Section

As the incoming projectile approaches a target nucleus it experiences and responds to the Coulomb potential of this nucleus which is itself screened by its atomic electrons. When scattering takes place in the vicinity of the atomic electron 'cloud' significant deviations from the Rutherford formula (equation 3.15) arise, as pointed out by Wenzel and Whaling (1952). This is because the Rutherford formula corresponds to the case where the target nucleus is unscreened. These deviations remain significant even when the scattering takes place close to the nucleus, that is within the K-shell radius, since in a screened atomic nucleus the particle is affected by the repulsive nuclear force only after it has penetrated the electron 'cloud' unlike the Rutherford case where the repulsive force is present even at large distances (L'Ecuyer et al 1979). Deviation of up to 4% for 1MeV He ion incident on a Bi target have been observed by L'Ecuyer et al (1979).

While determining stopping powers of low energy protons and deuterons in D_2O ice Wenzel and Whaling (1952) formulated a correction to the Rutherford cross section, σ_R, that is,

$$\frac{\sigma - \sigma_R}{\sigma_R} = \frac{-\Delta}{E_{CM}} \qquad 3.12$$

or

$$\sigma = \left(1 - \frac{\Delta}{E_{CM}}\right) \sigma_R \qquad 3.13$$

Where σ is the corrected cross section, E_{CM} is the projectile energy (keV) in the centre-of-mass frame, given by $E_{CM} = EM_2/(M_1 + M_2)$, assuming M_2 is initially at rest, and Δ is the absolute value of the electrostatic potential at the atomic nucleus. Δ has been derived by Foldy (1951) using a Hartree model of the atom and employed by Wenzel and Whaling (1952), where

$$\Delta = \frac{12}{5} R_{\infty} Z_1 Z_2^{7/5} \qquad 3.14$$

and since the Rydberg (R_{∞}) has the value 13.6eV,

$$\Delta = 0.0326 Z_1 Z_2^{7/5} \text{ keV} \qquad 3.15$$

By substituting equation 3.15 into 3.13, we arrive at the correction factor, F, used by Wenzel and Whaling (1952),

$$F = 1 - \frac{0.0326 Z_1 Z_2^{7/5}}{E_{CM}} \qquad 3.16$$

L'Ecuyer et al (1979) utilised a classical approach by assuming that the distance of closest approach is greater than the de Broglie wavelength (Bohr 1948) and have derived F where

$$F = 1 - \frac{0.049 Z_1 Z_2^{4/3}}{E_{CM}} \qquad 3.17$$

From equations 3.16 and 3.17 the increasing importance of the correction at low incident energies and for heavy targets is clearly apparant. L'Ecuyer et al (1979) have achieved good agreement with experimental results.

Hautala and Luomajarvi (1980) have given a more accurate treatment using Dirac-Fock electron distributions (Desclaux 1975). They, like L'Ecuyer et al (1979), have found the correction factor to be a function of $Z_1 Z_2^{4/3}/E_{CM}$. However, the older correction given by Wenzel and Whaling (1952) have yielded closer agreement with their calculated results, except at high Z_2 where good agreement was found by applying the correction derived by L'Ecuyer et al (1979). Hautala and Luomajarvi (1980) have also investigated the angular dependence of the correction factor and have noticed a weak dependence at backward angles in accordance with the above correction formulae.

From the foregoing discussion it is clear that the calculated scattering cross section may be employed reliably in quatitative work provided that the appropriate correction is made.

3.3.4 Determination of Thin Film Thicknesses

A target in the form of a film is considered to be 'thin' when the energy loss suffered by a projectile passing through it produces no significant variation in the interaction cross section. This criterion is discussed further in Chapter 5 while considering the choice of target thickness employed in the present study. It is shown that if a target is thin in relation to inner-shell ionisation cross section then it is also thin in relation to the Rutherford scattering cross section.

Unlike thick targets, both the front and the back surface features of thin targets are identifiable in a backscattering spectrum. Ideally, this spectrum would be rectangular in shape with a constant width, ΔE, which is the sum of the energy loss suffered by the ingoing particle and the outgoing particle scattered from the back surface. In reality, however, this shape is superimposed by instrumental and energy straggling effects (Stoquert 1981b). Whereas the former effect contributes to both sides of the spectrum the latter appears only on the low energy side giving the spectrum a slightly skewed-Gaussian appearance, but as mentioned in subsection 3.2.2, for thin targets the skewness is minimal and is not noticed significantly by the present-day surface-barrier detectors. The experimental measurement of the full-width-at-half maximum (FWHM) or ΔE, affords a means by which the target thickness can be determined (Chu et al 1978). Although ΔE decreases as the target thickness decreases, for a given set of experimental conditions a natural delimitation is imposed on the FWHM of the Gaussian peak by the instrumental effects, namely the detector resolution and the noise of the electronics. This fact makes the use of ΔE for calculating very thin target thickness unreliable. For such targets the thickness may be determined from their backscattering yield, Y_B, which is related to the thickness, t, of the target by the expression

$$Y_B = N_p \sigma \Omega n t \qquad 3.18$$

where N_p is the total number of particles to which the target has been exposed, σ is the nuclear elastic scattering cross section at a particular scattering angle, Ω is the detector solid angle and n is the number of target atoms per unit volume. Expression 3.18 relies on the assumptions that the projectile energy loss in the target is negligible. Furthermore, the thin film density is assumed to be equivalent to the bulk density.

In the cases where the energy loss of the projectile in the target, although small, is not negligible a correction is required to account for the variation of the nuclear scattering cross section in the target. A simple correction can be derived by assuming that the energy loss varies linearly with projectile energy and can be incorporated in equation 3.18 giving (Foti et al 1977 and Chu et al 1978)

$$Y_B = N_p \sigma \Omega n t \, C_F \qquad 3.19$$

and

$$C_F = \left(1 - \frac{nt\varepsilon(\bar{E}_{in})}{E}\right)^{-1} \qquad 3.20$$

where C_F is the correction factor, $\varepsilon(\bar{E}_{in})$ is the stopping power of the projectile in the film and is defined as

$$\varepsilon(\bar{E}_{in}) = \frac{-1}{n}\frac{dE}{dx}\bigg|_{\bar{E}_{in}} \qquad 3.21$$

$\bar{E}_{in}$ is the mean energy in the target of the incident projectile of energy E and can be estimated by E - (ΔE /4) or simply by E (Chu 1975 and Chu et al 1978). $\varepsilon(\bar{E}_{in})$ may be obtained from the tables of Andersen and Ziegler (1977a,b). It is worthwhile remarking that $\varepsilon(\bar{E}_{in})$ appears only as a correction in the yield equation (3.19) and the uncertainty in $\varepsilon(\bar{E}_{in})$, therefore, does not play a major part in the thickness measurement. t can be isolated from equations 3.19 and 3.20 to give

$$t = \frac{Y_B}{n\left(N_p\sigma\Omega + Y_B\,\frac{\varepsilon(E_{in})}{E}\right)} \qquad 3.22$$

The above approach has been used to determine target thicknesses in the present study. The uncertainties in the experimentally measured quantities, Y_B, N_p and Ω determine the precision of t and are discussed in Chapter 5 along with the experimental procedure. The reliability of the calculated elastic nuclear scattering cross section σ, via equations 3.11 and 3.17, has already been referred to in subsection 3.3.3. The stopping power $\varepsilon(\bar{E}_{in})$ was determined at $\bar{E}_{in} = E$ since the energy lost by the charge particles in thin elemental targets of interest in this work is only a few keV at an incident energy of 1MeV and less at higher energies.

CHAPTER 4

THEORETICAL DESCRIPTION OF INNER-SHELL IONISATION BY LIGHT CHARGED PARTICLES

CONTENTS

4.1 INTRODUCTION

The plane-wave Born approximation (PWBA) and its recent improvements by Brandt and Lapicki (1979, 1981), known as the ECPSSR theory, are discussed in this chapter. The other major theoretical models for describing inner-shell ionisation are the semi-classical approximation (SCA) and the binary-encounter approximation (BEA). The ECPSSR theory has been chosen for comparison with the measured L-shell ionisation and x-ray production cross sections in this study (Chapter 6) instead of the SCA and the BEA. This approach has been followed because the ECPSSR model has been developed to a sufficient degree to allow detailed quantitative as well as qualitative comparison with the experimental data. The formulation of this theory by Brandt and Lapicki (1981) permits the major corrections to be included in the PWBA. In the case of the SCA and the BEA an equivalent readily accessible formulation to improve the calculated cross sections does not exist. However, both of these theories are reviewed in appendix A, not only for completeness but also because they can be closely related to the PWBA (Madison and Merzbacher 1975).

For the sake of brevity emphasis is placed on the discussion of the underlying assumptions on which the PWBA is based and the mathematical details have been omitted. References are, however, quoted which deal with the latter in great depth.

To explain exactly the mechanism of inelastic collisions between charged particles and atoms is a formidable task even for the simplest case and consequently the above-mentioned theories were introduced, which rely on substantial simplifications. The following two assumptions are common to these theoretical descriptions.

(i) The dynamics of the inner-shell ionisation process can be adequately treated in terms of an independent-electron model. The projectile and an independent inner-shell electron experience a Coulombic interaction, the result of which is to cause a transition to the continuum. This inner-shell electron, therefore, plays the 'active' role with the projectile, while the other electrons of the target atom are mere 'spectators' of the collision. This assumption is consistent with most of the x-ray phenomena discussed in Chapter 2.

(ii) The collision which creates the single inner-shell vacancy is assumed to take place in a short time compared with the time taken for the occurrence of the subsequent atomic transition ($\simeq 10^{-8}$ s) (Madison and Merzbacher 1975).

Protons, deuterons and alpha particles as projectiles with velocities less than the velocity of the inner-shell electron are considered in the present work.. In this collision regime, effects such as electron capture by the projectile and target-orbital contractions can be neglected (Brandt and Lapicki 1981 and McDaniel 1983).

In order to maintain consistency with the published literature cgs and atomic units are used throughout this chapter.

4.2 PLANE-WAVE BORN APPROXIMATION

The first quantum mechanical treatment of inner-shell ionisation by charged particles was based on the Born approximation (Born 1926). The interaction between the projectile and an inner-shell electron, which causes the electron to be ejected into the continuum, is Coulombic in nature and is treated in terms of the first order time-independent perturbation theory. The validity of such an approach is only ensured when the perturbing potential is small and since the magnitude of this potential depends on the charge of the projectile (Z_1), incident particles with low atomic numbers such as protons and alpha particles are the most suitable for testing the predictions of this theory (Sarkadi 1983). The theory, therefore, holds for $Z_1 << Z_2$ where Z_2 is the atomic number of the target atom. This is the region of direct Coulomb ionisation (Madison and

Merzbacher 1975).

In the Born approximation the distortion of the wave function of the incoming particle by the inner-shell electron involved in the inelastic collision is assumed to be negligible and is, therefore, ignored. This is the primary assumption in the Born approximation (Madison and Merzbacher 1975). For an asymmetric collision between an incident partice of charge Z_1e and velocity v_1 and a target atom with a nuclear charge of Z_2e the validity condition for the Born approximation is given by (Williams 1945 and Bohr 1948).

$$\frac{Z_1 Z_2 e^2}{\hbar\, v_1} \ll 1 \qquad 4.1$$

This condition can be interpreted as the de Broglie wavelength being larger than the dimensions of the scattering field (Williams 1945).

The ionisation of the K-shell by light charged particle impact was treated non-relativistically by Henneberg (1933) who based his theoretical approach on the Born approximation. Henneberg (1933) replaced the initial and final wave functions of the incident particle by the product of two plane waves, that is

$$\exp\,(i\ (\underline{k}_i - \underline{k}_f).\ \underline{R}) \qquad 4.2$$

and $\underline{k} = \frac{2\pi}{\lambda}$

where $\hbar\underline{k}_i$ and $\hbar\underline{k}_f$ are the initial and final momenta of the incident particle with a position vector $\underline{R}$ and a wavelength λ. The momentum change suffered by the particle is then $\hbar(\underline{k}_i - \underline{k}_f)$ or $\hbar\underline{q}$ where $\underline{q} = \underline{k}_i - \underline{k}_f$. Plane waves can be used provided that the radii of the inner-shell electron orbits are large compared to the classical distance of closest approach for the projectile (Henneberg 1933). This approximation is known as the plane-wave Born approximation (PWBA) (Merzbacher and Lewis 1958 and Inokuti 1971). The assumption that the plane wave is not distorted by the inner-shell electron during the collision is justified if the inequality 4.1 is satisfied (Merzbacher and Lewis 1958).

During an inelastic collision between a charged particle and an heavy target atom an inner-shell vacancy can be created even at very low incident energies. However, atomic transitions caused by the collision are not detectable unless the relative energy of the collision partners is much greater than the electronic binding energies of the inner-shells involved (Madison and Merzbacher 1975). A lower limit to the velocity of the incident particle is set by the inequality 4.1. For direct collisions in the region of a few MeV the velocity of the projectile is less than or comparable to the velocity of the inner-shell orbital electron (Madison and Merzbacher 1975). The present work deals with collisions in this 'near-adiabatic' region. It is convenient to employ the maximum energy transferrable (T_m) to a free electron of mass, m, by a projectile of mass, M_1, and energy, E, that is

$$T_m \simeq \frac{4m}{M_1} E \qquad 4.3$$

to compare with the binding energy of the inner-shell electron (I)(Merzbacher and Lewis 1958). As the collision becomes less adiabatic and T_m approaches I, inner-shell ionisation becomes increasingly probable and reaches a maximum when T_m is comparable to I.

The problem of representing the inner-shell electron, involved in the collision, by a suitable wave function is considered below. Initially this electron is in its ground state, 2s or 2p in the present context. The electron may undergo a transition into one of the continuum states if the inner-shell is ionised. The final state, therefore, represents the vacancy in the inner-shell and the electron emitted into the continuum. Provided that $Z_1 \ll Z_2$ and that the charge on the incident particle is comparable to the value of the electronic charge (e) the inner-shell orbits are not polarised to any great extent, allowing the use of atomic wave functions of the unperturbed atom for the 'active' electron (Mott 1931 and Merzbacher and Lewis 1958).

Most of the calculations of inner-shell ionisation by charged particles have employed non-relativistic hydrogenic wave functions (Mott and Massey 1965) for the electron in its initial and final states (Henneberg 1933, Merzbacher and Lewis 1958, Khandelwal et al 1969, Choi et al 1973, Rice et al 1977, Benka and Kropf 1978 and Johnson et al 1979). These wave functions approximate the more realistic atomic wave functions such as the Hartree-Fock type (Madison and Merzbacher 1975). This approximation may be applied successfully provided that the 'screening' effects of the target atomic electrons are accounted for (Taulbjerg 1976). In multi-electron atoms, the nuclear charge experienced by the active electron is reduced by the presence of other inner-shell electrons. A further effect of screening is the reduction of the binding energy of the inner-shell electrons caused by the presence of the less-tightly bound outer electrons. These two effects can be taken into account approximately by introducing simple modifications (Livingston and Bethe 1937). The 'inner' screening of the full nuclear charge (Z_2e) may be accounted for by reducing Z_2 by an appropriate amount calculated by Slater (1930). For the complete L-shell the Slater value is 4.15, giving the effective nuclear charge (Z_{2L}) felt by an L-shell electron as

$$Z_{2_L} = Z_2 - 4.15 \qquad 4.4$$

The 'outer' screening shifts the binding energy of the inner-shell without changing the wave function significantly in the vicinity of the inner-shell. This is taken into account by introducing a dimensionless quantity θ_{Li} (i = 1, 2, 3 and refers to the three L-subshells) known as the 'screening number' or the 'scaled binding energy'. It expresses the actual binding energy I_{Li}, in terms of the hydrogenic binding energy, E_{Li}, which is free from the effects of outer screening, that is,

$$\theta_{Li} = \frac{I_{Li}}{E_{Li}} \qquad 4.5$$

Since

$$E_{2L} = Z_{2L}^2 R_\infty / n_L^2$$

$$\theta_{Li} = \frac{n_L^2 \; I_{Li}}{Z_{2L}^2 \; R_\infty} \qquad 4.6$$

where $n_L = 2$ is the principal quantum number for the L-shell and R_∞ is the K-shell ionisation energy of hydrogen (Rydberg) and has the value 13.6eV. θ_{Li}, therefore, is a measure of the nonhydrogenic aspect of I_{Li}. Figure 4.1 shows the variation of θ_{Li} with Z_2. θ_{Li} was calculated from equation 4.6 and employing I_{Li} from Storm and Israel (1971). For the elements of interest in this study θ_{Li} lies between 0.4 - 0.8.

The use of the PWBA, based on the above assumptions, for evaluating inner-shell ionisation cross sections for light positively charged particles has been discussed comprehensively by Merzbacher and Lewis (1958), Madison and Merzbacher (1975) and Briggs and Taulbjerg (1978). Here only the final results are quoted.

The L-shell ionisation cross section is expressed in terms of the dimensionless quantities, W, k and Q defined by

$$W = \frac{\varepsilon}{Z_{2L}^2 R_\infty} \; ; \; k = a_2 K; \; Q = a_2^2 q^2 \qquad 4.7$$

where ε is the energy transferred to the target atom as a result of the inelastic collision, $a_2 = a_0/Z_{2L}$ is the K-shell radius of the target atom, a_0 being the Bohr radius of hydrogen, K is the wave number of the hydrogenic wave function and q is the momentum transferred to the atom in units of $\hbar$. The energy transferred to the atom is

$$\varepsilon = T + I_{Li} \qquad 4.8$$

where T is the kinetic energy of the electron of mass, m, at infinity and equals $\hbar^2 K^2/2m + V_{Li}$. The potential, V_{Li}, represents the reduction in the binding energy of the L-shell electron due to the effects of outer screening and is given by

$$V_{Li} = E_{Li} - I_{Li}$$

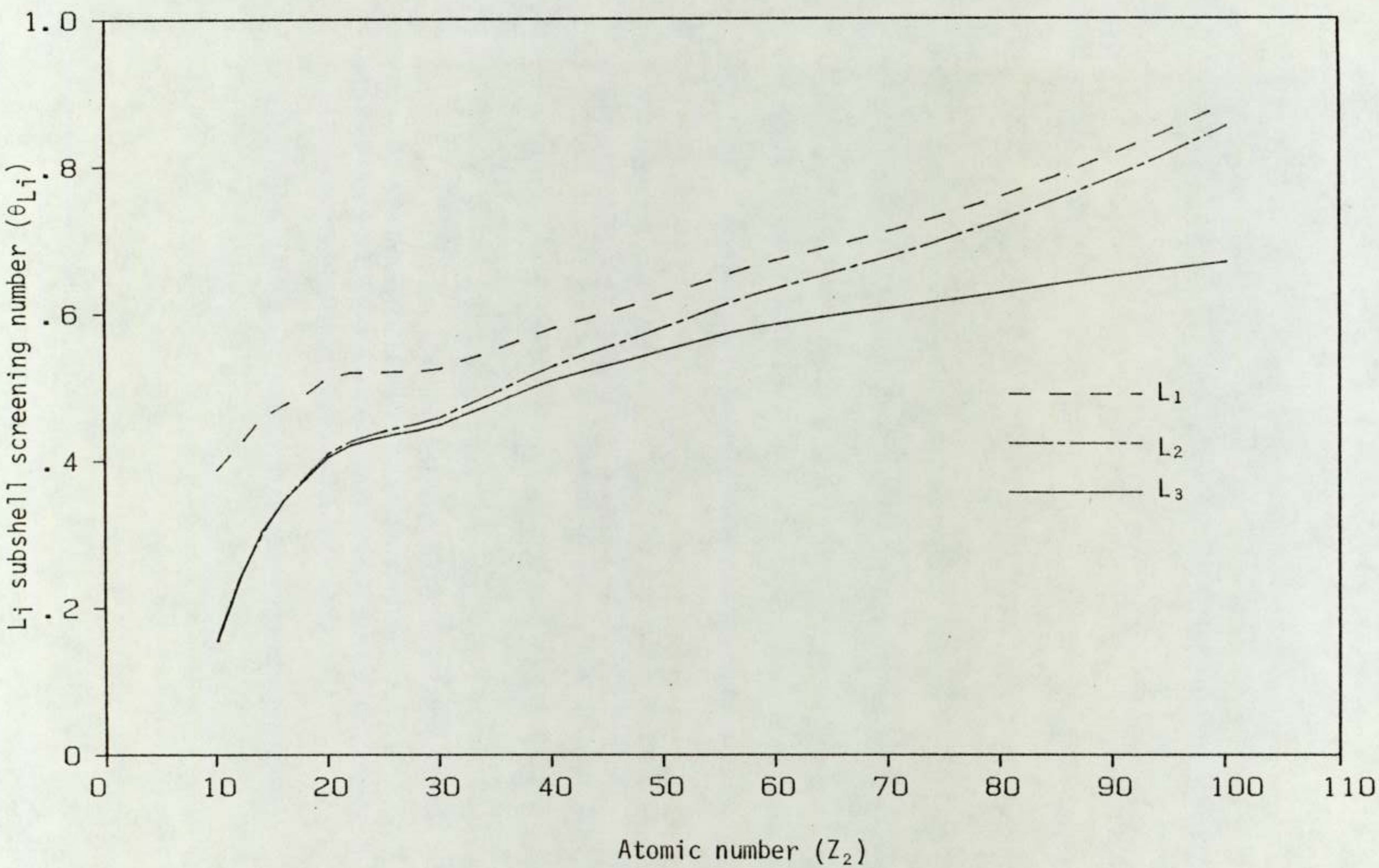

Figure 4.1 Screening number, θ_{Li}, as a function of atomic number (Z_2). Values were calculated using equation 4.6 and tables of Storm and Israel (1970) for the binding energies.

$$= \frac{Z_{2L}^2 R_\infty}{n_L^2} - I_{Li} \qquad 4.9$$

Substituting equation 4.9 into 4.8 gives

$$\varepsilon = \frac{\hbar^2 K^2}{2m} + \frac{Z_{2L}^2 R_\infty}{n_L^2} \qquad 4.10$$

Using equation 4.7 W can be expressed as

$$W = k^2 + \frac{1}{n_L^2} \qquad 4.11$$

In terms of the quantities defined by equation 4.7 the PWBA L_i-subshell ionisation cross section, σ_{Li}, in the centre-of-mass system, for an electronic transition from an initially filled Li-subshell to a final state with an energy transfer ε can be expressed as (Merzbacher and Lewis 1958).

$$\sigma_{Li} = 8\pi Z_1^2 \left(\frac{e^2}{\hbar v}\right)^2 \frac{a_0^2}{Z_{2L}^2} \int_{W_{min}}^{W_{max}} dW \int_{Q_{min}}^{Q_{max}} \frac{dQ}{Q^2} |F_{W_{Li}} (Q)|^2 \qquad 4.12$$

where v is the relative velocity of incidence and $F_{W_{Li}}(Q)$ is known as the inelastic form factor for the collision. Expressions for $F_{W_{Li}}(Q)$ can be found in Merzbacher and Lewis (1958), Choi et al (1973) and Benka and Kropf (1978). The velocity of the projectile (v_1) can be expressed in terms of the velocity of the inner-shell electron (v_{2L}) through the reduced or the scaled energy parameters, η_L,

$$\eta_L = \left(\frac{v_1}{n_L v_{2L}}\right)^2 = \frac{1}{Z_{2L}^2} \left(\frac{\hbar v_1}{e^2}\right)^2 \qquad 4.13$$

since $v_{2L} = Z_{2L}e^2/n_L\hbar$. Through η_L, sometimes referred to as the adiabaticity parameter, the energy of the projectile (E) in the laboratory frame enters the cross section calculations, that is,

$$\eta_L = \frac{m E}{M_1 Z_{2L}^2 R_\infty} \qquad 4.14$$

using $v_1^2 = 2E/M_1$ and $R_\infty = e^4 m/2\hbar^2$, where m is the mass of the electron. Employing η_L the ionisation cross section can be stated as (Choi et al 1973),

$$\sigma_{Li} = \frac{8\pi Z_1^2 a_0{}^2}{Z_{2L}^4 \eta_L} f_{Li} (\eta_L, \theta_{Li}) \qquad 4.15$$

where

$$f_{Li}\ (\eta_L, \theta_{Li}) = \int_{W_{min}}^{W_{max}} dW \int_{Q_{min}}^{Q_{max}} |F_{W_{Li}}\ (Q)|^2 \frac{dQ}{Q^2} \qquad 4.16$$

The L_i-subshell cross section can be obtained by evaluating the interals in equation 4.16 over the variables W and Q. These calculations have been performed for the L-shell by Choi et al (1973) and Benka and Kropf (1978). Choi et al (1973) have tabulated $f_{Li}\ (\eta_L, \theta_{Li})$ for bare charged particles such as protons and alpha particles and have restricted their calculations to $0.0018 < \eta_L < 7.0$ and $0.24 < \theta_{Li} < 0.78$. Benka and Kropf (1978), on the other hand, have concentrated on proton impact only and have extended their calculations to cover a larger range of proton energies and target elements. Their format is, however, slightly different to that of Choi et al (1973) and they have tabulated the 'reduced universal cross section', $F_{Li}\ (\eta_L/\theta_{Li}^2, \theta_{Li})$, defined by

$$\sigma_{Li} = \frac{8\pi Z_1^2\ a_0^2}{Z_{2L}^4\ \theta_{Li}}\ F_{Li}\ (\eta_L/\theta_{Li}^2, \theta_{Li}) \qquad 4.17$$

where

$$F_{Li} = \left(\frac{\theta_{Li}}{\eta_L}\right) f_{Li}\ (\eta_L, \theta_{Li}) \qquad 4.18$$

Their calculations cover $10^{-4} \leq \eta_L/\theta^2_{Li} < 10^2$ and $0.2 \leq \theta_{Li} < 2.7$. In terms of Z_2 and E their tabulation covers all values with $Z_2 \geq 10$ and proton energies of the order of 10^{-6} to 10^4MeV.

The more pronounced difference between the two tabulations concerns the integration limits of equation 4.16. These limits are obtained from the conservation of energy and momentum relations (Merbacher and Lewis 1958). Both the tabulations have used

$$W_{min} = \frac{\theta_{Li}}{\eta_L^2} \qquad 4.19$$

which is arrived at by substituting the minimum energy transfer $\varepsilon_{min} = I_{Li}$, obtained by setting T = 0 in equation 4.8, into equation 4.7. Choi et al

(1973) have approximated W_{max}, which corresponds to the maximum energy transferrable to the atom, by

$$W_{max} = \infty \qquad 4.20$$

Benka and Kropf (1978) have replaced this by the exact integration limit

$$W_{max} = \frac{M_1}{m}\eta_L \qquad 4.21$$

Limit 4.21 is obtained by setting ε_{max} equal to the maximum energy available for transfer to the target atom, which simply is the projectile energy before collision, E. This makes W_{max} dependent on the projectile mass, M_1, unlike the approximation used by Choi et al (1973) which clearly is independent of M_1 (equation 4.20). The expression for Q_{min} can be derived from

$$\hbar q_{min} = \hbar k_i - \hbar k_f = [2M_1 E]^{\frac{1}{2}} - [2M_1(E - \varepsilon)]^{\frac{1}{2}} \qquad 4.22$$

$$\hbar^2 q^2{}_{min} = 2M_1\ [E^{\frac{1}{2}} - (E - \varepsilon)^{\frac{1}{2}}]^2$$

$$= 2M_1 E\ \left[1 - \left(1 - \frac{\varepsilon}{E}\right)^{\frac{1}{2}}\right]^2 \qquad 4.23$$

Using the binomial theorem 4.23 can be written as

$$\hbar^2 q^2{}_{min} \simeq \frac{M_1\varepsilon^2}{2E}\left(1 + \frac{\varepsilon}{2E}\right)$$

and if the energy loss, ε, of the projectile is smaller than the projectile energy, E, that is, $\varepsilon \ll E$,

$$\hbar^2 q^2{}_{min} \simeq \frac{M_1\varepsilon^2}{2E} = \frac{\varepsilon^2}{V_1{}^2} \qquad 4.24$$

In terms of the dimensionless quantities Q, W, and η_L the minimum momentum transfer may be expressed as

$$Q_{min} = \frac{W^2}{4\eta_L} \qquad 4.25$$

This expression for Q_{min} has been employed by Choi et al (1973) for their calculations. Benka and Kropf (1978) have retained the exact expression 4.23 in their calculations, which can be rearranged to

$$Q_{min} = \left(\frac{M_1}{m}\right)^2 \eta_L \left[1 - \left(1 - \frac{m\ W}{M_1 \eta_L}\right)\ \right]^2 \qquad 4.26$$

For the maximum momentum transfer we have

$$\hbar q_{max} = \hbar k_i + \hbar k_f$$

$$= [2M_1E]^{\frac{1}{2}} + [2M_1(E - \varepsilon)]^{\frac{1}{2}} \qquad 4.27$$

$$\hbar^2 q^2_{max} = 2M_1E \left[1 + \left(1 - \frac{\varepsilon}{E}\right)^{\frac{1}{2}}\right]^2 \qquad 4.28$$

Expanding the bracket term and since $\varepsilon << E$ equation 4.28 can be approximated to

$$\hbar^2 q^2_{max} \simeq 8M_1E \qquad 4.29$$

Merzbacher and Lewis (1958) have approximated $q_{max} \simeq \infty$, which they point out introduces no serious errors. Choi et al (1973) have also used this limit for Q_{max}, that is

$$Q_{max} = \infty \qquad 4.30$$

Benka and Kropf (1978), however, have used the exact expression 4.28 for the maximum momentum transfer leading to

$$Q_{max} = \left(\frac{M_1}{m}\right)^2 \eta_L \left[1 + \left(1 - \frac{m\,W}{M_1\eta_L}\right)^{\frac{1}{2}}\right]^2 \qquad 4.31$$

As a result of using the exact integration limits the cross section values for incident protons at low energies calculated by Benka and Kropf (1978) are considerably smaller than those of Choi et al (1973). For intermediate and high energies, $\eta_L > 0.1$, the cross sections agree to within 1% for all targets (Benka and Kropf 1978). In the present study, however, η_L is typically 10^{-2} for protons and significant differences between the two tabulations exist at these energies. In the case of Au ($Z_2 = 79$), for example, bombarded by 1.6MeV protons ($\eta_L = 0.011$) the L_1 ionisation cross sections differ by about 7%.

Benka and Kropf (1978) have used the exact integration limits and as a result their tabulation has been employed in the present study to generate the cross sections for proton impact in preference to that of Choi et al (1973). For deutrons and alpha particles on the other hand, the latter tabulation was adopted since the values of Benka and Kropf (1978) are valid only for proton impact.

In pertinance to the expression 4.17 for the PWBA L-shell ionisation cross section several notable points can be made.

(i) The form factor $Fw_{Li}(Q)$ is explicitly independent of the target charge Z_2 (Madison and Merzbacher 1975) and consequently the cross section exhibits a universal behaviour for all targets and projectiles when expressed in the form

$$\frac{\theta_{Li}}{8\pi}\left(\frac{Z_{2L}^2}{Z_1}\right)^2\frac{\sigma_{Li}}{a_0^2} = F_{Li}\left(\eta_L/\theta_{Li}^2,\ \theta_{Li}\right) \qquad 4.32$$

The form factor, for a given atomic transition, has large values for $Q \simeq 1$ and then decreases rapidly as Q increases(Inokuti 1971). According to equation 4.25 Q_{min} is large at low projectile velocities, and the dominant contribution to the cross section arises, therefore, from the lowest momentum transfers. The universal behaviour observed by plotting $(\theta_{Li}\ Z_{2L}^4\ \sigma_{Li})/(8\pi Z_1^2 a_0{}^2)$ versus η_L/θ_{Li}^2 is thus limited to the low velocity region where the projectile velocity is smaller than the inner-shell electron velocity, $v_1 < v_{2_L}$. Expression 4.32 also exhibits Z_1^2 scaling and thus permits cross sections to be determined for different projectiles (Z_1) for given Z_2 and E provided that σ_{Li} is known for a certain projectile. The validity of the universal property and that of $Z_1{}^2$ scaling has attracted considerable experimental scrutiny (Madison and Merzbacher 1975, Chaturvedi et al 1975, Khan 1975, Button et al 1979 and Bhattacharya et al 1980) and reasonable qualitative agreement has been established.

(ii) The inner-shell ionisation cross section for charged particles rises to a broad maximum at around $\eta_L/\theta_{Li}^2 \simeq 1$ or $v_1 \simeq v_{2_L}$ for the L-shell. Beyond this 'velocity matching' peak the cross section falls off.

(iii) Any divergence from the universal behaviour may be indicative of the inadequacies of the PWBA model. These might include the unsuitability of the unperturbed hydrogenic wave functions, the single-independent electron assumption or more seriously the approximate nature of the Born model itself (Madison and Merzbacher 1975, McGuire and Macdonald 1975 and Chen et al 1982). Improvements of the PWBA theory are discussed in the next section.

(iv) At low projectile velocities the contribution to the ionisation cross section is predominantly from collisions which transfer energies close to zero to the electron. The cross section is sensitive to the high-momentum tail of the momentum distribution of the initial-state wave functions. In other words, the ionisation of the inner-shell occurs most probably when the particle penetrates deep inside the shell (Madison and Merzbacher 1975 and Montenegro and de Pinho 1982a). At low projectile velocities, therefore, the ionisation cross section for the 2p states rises smoothly with increasing collision energy in qualitative agreement with the momentum wave functions associated with these states. The ionisation cross section for the 2s state on the other hand displays a pronounced 'knee' in the neighbourhood of $\eta_L/\theta^2_{2Li} \simeq 0.01$, a feature which is a consequence of the radial node in the wave function of this state, either in the coordinate or the momentum representation.

(v) Provided that the target atoms are not light or highly ionised before collision, the contribution of the excitation of inner-shell electrons to unoccupied discrete bound levels, as a result of a heavy charged particle impact, to the total vacancy production cross section is negligible and may be ignored (Madison and Merzbacher 1975).

(vi) The validity condition for the PWBA, expressed in the form of the inequality 4.1, has been recognised to be over-restrictive for many ion-atom collisions (Merzbacher and Lewis 1958 and Briggs and Taulbjerg 1978), particularly in the case of total ionisation cross section. The Born approximation applied to the inner electron-projectile interaction may still be valid in certain regions where 4.1 is violated. This arises in slow collisions but provided $Z_1 << Z_2$ the effect of the incident particle may be treated as a small perturbation, authenticating the use of the plane-wave Born approximation. The validity of the perturbation theory, therefore, critically depends on the magnitudes of the nuclear charges of the projectile and of the target atom (Briggs and Taulbjerg 1978).

4.3 CORRECTIONS TO THE PLANE-WAVE BORN APPROXIMATION - THE ECPSSR THEORY

The plane-wave Born approximation has been exceedingly successful in describing the qualitative behaviour of inner-shell ionisation cross sections with respect to the incident particle energy. As far as predicting the numerical values of the cross sections or the projectile velocity dependence of the cross sections the PWBA model falls far short and consistently over estimates in the $v_1 < v_{2_L}$ region (Brandt and Lapicki 1974). This has been substantiated by the significant amount of experimental cross section measurements performed at various laboratores (Busch et al 1973, Datz et al 1974, Gray et al 1975, Chen 1977, Khan et al 1978, Button et al 1979, Bhattacharya et al 1980, Sokhi and Crumpton 1981, Cohen 1981 and Bhattacharya 1982). However, it is not surprising that this is the case since the PWBA is only the first step of a perturbation expansion using plane waves and unperturbed initial-state hydrogenic wave functions to describe the projectile and the inner-shell electron respectively. The obvious improvement of expanding the Born series to the second order term is usually avoided because of the mathematical complexity (Madison and Merabacher 1975). Some work has been done using more sophisticated atomic wave functions such as the Dirac -Hartree-Slater wave functions and agreement with experimental data has been improved (Chen et al 1982). Brandt and his co-workers have followed a phenomenological approach to the collision problem and have developed the ECPSSR theory in an attempt to explain the large descrepenceis between the PWBA predictions and experiment.

The ECPSSR theory is a result of many noteworthy contributions made to the theory of inner-shell ionisation by charged particles by Brandt and his collaborators over the past decade (Brandt et al 1966, Basbas et al 1973a, Basbas et al 1973b, Brandt and Lapicki 1974, Basbas et al 1978, Brandt and Lapicki 1979 and Brandt and Lapicki 1981). The theory accounts for the effects of the kinetic energy loss (E) of the incident particle in the ionisation process, the Coulomb deflection (C) of the projectile in the field of the target nucleus, the influence of the projectile on the inner-shell electron orbits (the binding energy and polarisation effects) in terms of the perturbed stationary states (PSS) and the relativistic effects (R) of the inner-shell electrons of high Z_2 elements on the probability of inner-shell ionisation by non-relativistic charged particles. Each of these effects and the expressions derived by Brandt and Lapicki (1979) for including these effects in the PWBA are now considered.

4.3.1 Relativistic Effect

A relativistic description of the inner-shell electrons of heavy elements is required instead of the simple hydrogenic picture because (Choi 1971)

(i) in the vicinity of the atomic nucleus the relativistic bound-state wave functions are larger in magnitude than the non-relativistics, and

(ii) the spin-orbit slitting of the inner electronic states, such as the splitting of the 2p state into $2p_{1/2}$ and $2p_{3/2}$, becomes significantly large for heavy elements, and the difference in the binding energies of these subshells has a non-trivial affect on the calculations of inner-shell ionisation cross sections.

Qualitatively this effect may be understood by recognising that at relativistic velocities the electron mass increases and as a result the maximum energy transfer to an electron increases making ionisation more probable (Paul 1980).

Jamnik and Zupancic (1957) applied hydrogenic Dirac wave functions for K-shell ionisation in the Born approximation. Similar calculations were carried out by Choi (1971) for the L-shell and highlighted the necessity of relativistic corrections for medium-heavy and heavy target elements. Mukoyama and Sarkadi (1981, 1982a) have employed an analogous relativistic procedure to that adopted by Choi (1981) for L-shell ionisation by slow protons (Mukoyama and Sarkadi 1983a) and alpha particles (Mukoyama and Sarkadi 1983b) and in addition have applied Coulomb and binding energy correction as developed by Brandt and Lapicki (1974). After comparison with experimental data they emphasise the need of relativistic corrections for low-energy projectiles ionising heavy target elements. Such calculations are complicated however, and other methods have been proposed which are less involved numerically. Merzbacher and Lewis (1958), for instance, followed the method of Honl (1933) and proposed that non-relativistic screened hydrogenic wave functions may still be used for calculating the cross section but taking into account the fact that the relativistic ideal ionisation potential without outer screening (E_{Li} for the L-shell) is larger than the non-relativistic potential, thus reducing θ_{Li} (equation 4.5 and 4.6). Hardt and Watson (1973) have suggested that the velocity of the inner-shell electron should be reduced and Berinde et al (1978) studying K-shell ionisation by protons have modified the K-shell radius to correct for the relativistic effects. Brandt and Lapicki (1979) have, however, pointed out that these approaches only explain experimental measurements when the incident projectile and the electron velocity are comparable. These approaches and that of Brandt and Lapicki (1979), which will be discussed below, entail using either relativistic wave functions or modifying parameters used in the PWBA and as a consequence yield cross sections which do not exhibit the scaling behaviour predicted by the non-relativistic treatement (Madison and Merzbacher 1975 and Mukoyama and Sarkadi 1982b). For low energy charged particles (below 1MeV for protons) Mukoyama and Sarkadi (1982b) have derived an approximate relativistic correction for L-shell ionisation following a method developed by Amundsen et al (1976) for K-shell ionisation. The relativistic cross section is simply obtained by multiplying this correction factor to the non-relativistic PWBA cross section and as a result the scaling behaviour is retained.

Before discussing Brandt and Lapicki's (1979) approach the central parameters in their theory are first defined. Consider an inelastic collision in whch a target atom of mass, M_2, is ionised in its L-shell by a projectile of mass, M_1, and velocity, v_1. The minimum momentum transfer hq_{min} is given by equation 4.24. For collisions where the projectile energy E is much larger than the binding energy $\hbar\omega_{2L}$ then

$$q_{min} \simeq \frac{\omega_{2L}}{v_1} \qquad 4.3$$

Impact parameters which contribute most to the ionisation have values $\simeq q_{min}^{-1}$ (or v_1/ω_{2L}) (Bang and Hansteen 1959). The condition for deep penetration of the inner-shell (L-shell in this case) is

$$q_{min}^{-1} << a_{2L}$$

$$\text{or} \qquad v_1 << \omega_{2L} a_{2L} \qquad 4.34$$

or in terms of θ_{Li} and using atomic units,

$$v_1 << \tfrac{1}{2}\theta_{Li}\, v_{2L} \qquad 4.35$$

A useful way of distinguishing slow and fast collisions is to compare the time it takes for the projectile to transverse the target L-shell (characteristic collision time) $\simeq a_{2L}/v_1$ with the characteristic time of the target L-shell electron n_L/ω_{2L}. The condition $a_{2L}/v_1 >> n_L/\omega_{2L}$ or $q_{min}^{-1} << a_{2L}/n_L$ defines slow collisions and leads to the central dimensionless parameter of the theory, ξ_{Li}, known as the 'reduced velocity parameter' (Brandt and Lapicki 1979)

$$\xi_{Li} = \frac{n_L}{q_{min} a_{2L}} \qquad 4.36$$

Since, in atomic units $a_{2L} = n_L{}^2/Z_{2L}$ and the velocity of the L-shell electron $v_{2L} = Z_{2L}/n_L$,

then
$$q_{min} \simeq \frac{\theta_{Li}\ v_{2L}}{2v_1} \qquad 4.37$$

and ξ_{Li} can be written as

$$\xi_{Li} = \frac{v_1}{\frac{1}{2}\theta_{Li} v_{2L}} \qquad 4.38$$

This variable differentiates between slow collisions, where $\xi_{Li} < 1$ and fast collisions, where $\xi_{Li} > 1$. The velocity of the projectile v_1 can be expressed as

$$v_1 = (Z_{2L} n_L)^{\frac{1}{2}} \qquad 4.39$$

In the low velocity region, $\xi_{Li} \ll 1$, the ionisation cross section is proportional to the fourth power of

$$T_m = 2mv_1{}^2 = m\theta_{Li}\omega_{2L}\ \xi^2_{Li} \qquad 4.40$$

(using equation 4.38 and substituting for $v_{2L} = Z_{2L}/n_L$)(Huus et al 1956). Instead of setting m to unity, Brandt and Lapicki (1979) have introduced a relativistic electron mass, $m^R_{Li}\ (\xi_{Li})$, using the virial theorem (Rose and Welton 1952) for a relativistic electron in a central potential of the form Z_{2L}/r at a distance r from the target nucleus and is given by

$$m^R_{Li}\ (\xi_{Li}) \simeq (1 + 1.1y^2_{Li})^{\frac{1}{2}} + y_{Li} \qquad 4.41$$

where

$$y_{L_1} = \frac{0.40(Z_{2L}/c)^2}{n_L \xi_{Li}}$$

and 4.42

$$y_{L_{2,3}} = \frac{0.15\ (Z_{2L}/c)^2}{\xi_{L_{2,3}}}$$

In accordance with equation 4.40 ξ_{Li} has to be transformed to $\left[m_{Li}^R\left\{\xi_{Li}\right\}\right]^{\frac{1}{2}} \xi_{Li}$. η_L may be expressed in terms of θ_{Li} and ξ_{Li}

$$\eta_L = \left(\frac{\theta_{Li}\xi_{Li}}{2n_L}\right)^2 \tag{4.43}$$

and substituting the relativistic ξ_{Li} into 4,43 allows η_L/θ_{Li}^2 to be transformed to its relativistic counterpart,

$$(\eta_L/\theta_{Li}^2)^R = \left[\frac{((M_{Li}^R(\xi_{Li}))^{\frac{1}{2}}\ \xi_{Li}}{2n_L}\right]^2 \tag{4.44}$$

where $n_L = 2$ (for the L-shell). The relativistic PWBA L-subshell ionisation cross section, σ_{Li}^{PWBAR}, can now be calculated from

$$\sigma_{Li}^{PWBAR} = \sigma_{Li}^{PWBAR}\left(\left(\frac{\eta_L}{\theta_{Li}^2}\right)^R,\ \theta_{Li}\right) \tag{4.45}$$

using equation 4.17 or from

$$\sigma_{Li}^{PWBAR} = \sigma_{Li}^{PWBA}\ (\eta_L^R,\ \theta_{Li}) \tag{4.46}$$

where

$$\eta_L^R = m_{Li}^R\ (\xi_{Li})\ \eta_L \tag{4.47}$$

and using equation 4.15. Cross sections calculated from these expressions agree closely with those obtained by using relativistic wave functions (Choi 1971).

The effect of the relativistic correction may be illustrated by plotting $\sigma_{Li}^{PWBAR}/\sigma_{Li}^{PWBA}$ ratio versus the projectile energy. This has been done for proton impact on gold and is shown in figure 4.2. The ionisation cross sections were calculated for expressions 4.17 and 4.45 and using the tables of Benka and Kropf (1978). The relativistic correction affects the L_1 subshell more than the L_2 and L_3. This is because for heavy elements (Z_2) the relativistic bound-state wave functions are larger near the atomic nucleus than the non-relativistic ones and consequently the $2s_{\frac{1}{2}}$ state is influenced much more than the $2p_{\frac{1}{2}}$ and the $2p_{3/2}$ (Justiniano et al 1980). In the low velocity region the presence of the radial node in the 2s wave functions increases the L_1 ionisation cross section and thus

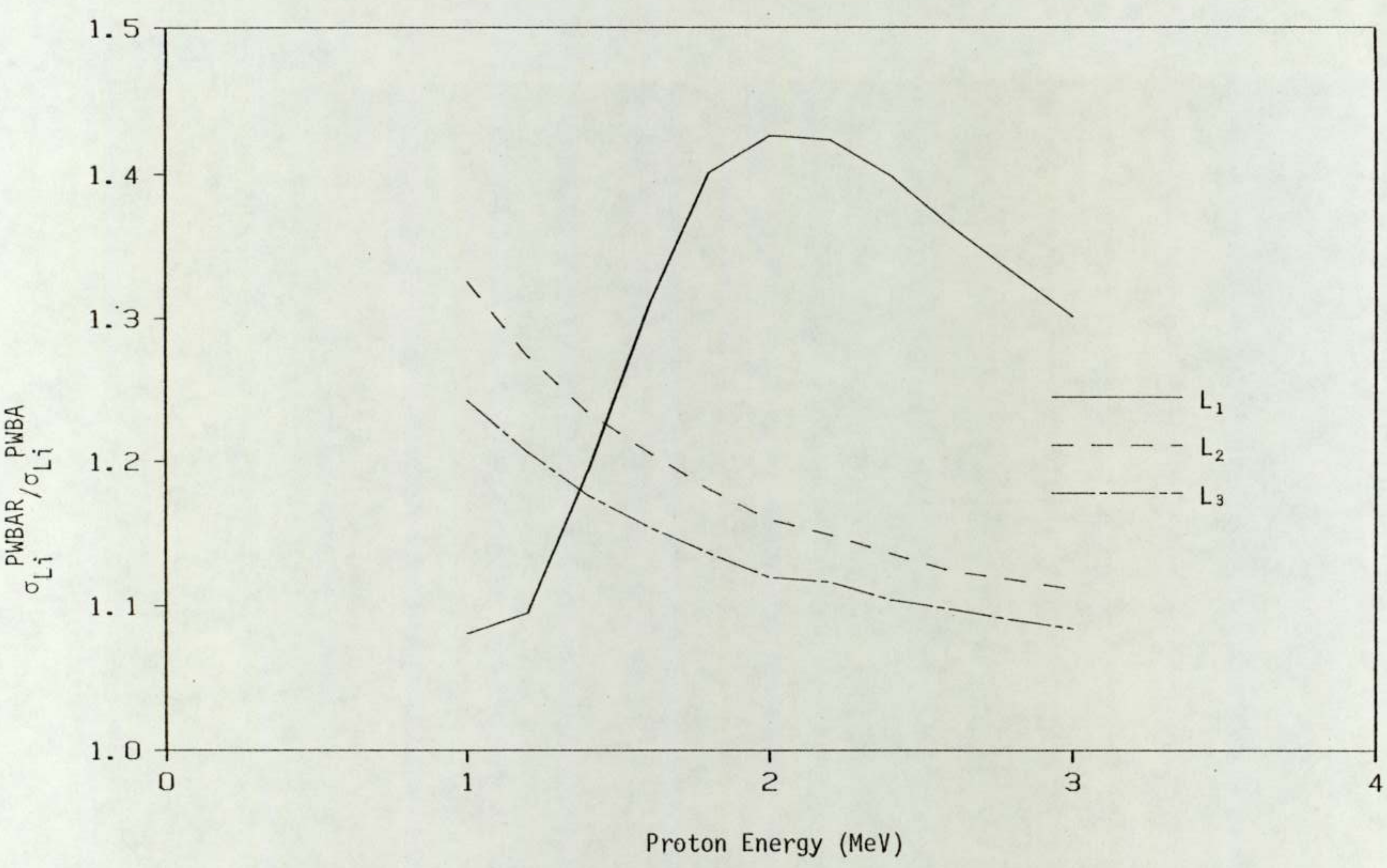

Figure 4.2 Relativistic effect for gold (Z_2 = 79) bombarded by protons. The L_i subshell ionisation cross sections were calculated using equations 4.17 and 4.45 and tables of Benka and Kropf (1978).

complicates the shape of the ratio (figure 4.2).

4.3.2 Polarisation and Binding Energy Effects

The inner-electron states experience perturbations caused by the presence of the charged particle. These perturbations affect the ionisation probability in a manner which depends on whether the impact parameter is less or greater than the inner-shell radius (a_{2L} for the L-shell). In the regime where $v_1 \ll v_{2L}$, at impact parameters less than a_{2L}, the ionisation cross section is reduced since the binding energy of the target electron is increased. At intermediate and high particle velocities impact parameters larger than the inner-shell radius contribute the most to the ionisation cross section. When the projectile is traversing 'outside' the shell, it polarises the shell, thus, reducing the binding energy of the electron (Brandt and Lapicki 1979). Both these effects have been accounted for in terms of the perturbed-stationary-state (PSS) theory (Basbas et al 1973b and Brandt and Lapicki 1979). The polarisation factor for the L-shell, calculated by Brandt and Lapicki (1979), is given by

$$\varepsilon^P_{Li} = 1 - \left(\frac{2Z_1}{Z_{2L}\theta_{Li}}\right) h_{Li}\ (\xi_{Li}, C_{Li}) \qquad 4.48$$

with

$$h_{Li}(\xi_{Li}; C_{Li}) = \left(\frac{2n_L}{\theta_{Li}\xi^3_{Li}}\right) I \left(\frac{C_{Li}n_L}{\xi_{Li}}\right) \qquad 4.49$$

where $C_{L_1} = 3/2$ and $C_{L_{2,3}} = 5/4$ and the polarisation function $I(C_{Li}n_L/\xi_{Li})$ is given by (Basbas et al 1978)

$$I(x) = \frac{3\pi}{4}\left(\ln\frac{1}{x^2} - 1\right) \text{ for } 0 < x \le 0.035$$

$$\text{and} \quad I(x) = e^{-2x}\left(0.031 + 0.210x^{\frac{1}{2}} + 0.005x - 0.069x^{3/2} + 0.324x^2\right)^{-1} \qquad 4.50$$

$$\text{for } 0.035 < x \le 3.1$$

where $x = C_{Li}n_L/\xi_{Li}$. For $x > 3.1$ the polarisation function may be neglected. The binding energy factor, accounting for the increased binding energy of the inner-shell electron is given by

$$\varepsilon_{Li}^{B} = 1 + \left(\frac{2Z_1}{Z_{2L}\theta_{Li}}\right) g_{Li}\ (\xi_{Li};\ C_{Li}) \qquad 4.51$$

The rather lengthy expressions for $g_{Li}\ (\xi_{Li};\ C_{Li})$ have been stated by Brandt and Lapicki (1979). The polarisation and the binding energy factors may be combined to give a perturbed-stationary-state factor ζ_{Li} for θ_{Li} which takes into account the polarisation and the binding energy effects on the ionisation cross section, that is,

$$\zeta_{Li} = 1 + \left(\frac{2Z_1}{Z_{2L}\theta_{Li}}\right)\left[g_{Li}\ (\xi_{Li};\ C_{Li}) - h_{Li}\ (\xi_{Li};\ C_{Li})\right] \qquad 4.52$$

The PSS cross section for direct ionisation in terms of the PWBA can be obtained by transforming θ_{Li} to $\zeta_{Li}\theta_{Li}$ and η_L/θ_{Li}^2 to $(\xi_{Li}/2n_L\zeta_{Li})^2$, thus,

$$\sigma_{Li}^{PSS} = \sigma_{Li}^{PWBA}\ ((\xi_{Li}/2n_L\zeta_{Li})^2;\ \zeta_{Li}\theta_{Li}) \qquad 4.53$$

In the collision regimes under study in this work the polarisation effect does not play a significant role and the PSS factor is dominated by the contribution of the binding energy effect.

The PSS effect is very similar for the L_2 and L_3 subshells and is demonstrated in figure 4.3 which shows the ratio, $\sigma_{Li}^{PSS}/\sigma_{Li}^{PWBA}$, as a function of proton energy for gold. The σ_{Li}^{PSS} cross sections were evaluated using equation 4.53 and the tabulation of Benka and Kropf (1978). The L_1 ionisation cross sections for protons increases in the low velocity region exhibiting a 'knee' as mentioned in section 4.2, and is less sensitive to the PSS effect. This behaviour is analogous to that shown in figure 4.2 which illustrated the relativistic effect.

The relativistic correction can be incorporated by introducing ξ_{Li}/ζ_{Li} into equation 4.41 and 4.42 to yield the relativistic reduced velocity, that is,

$$\xi_{Li}^{R} = \left[m_{Li}^{R}\ (\xi_{Li}/\zeta_{Li})\right]^{\frac{1}{2}}\ \xi_{Li} \qquad 4.54$$

To obtain the PSS cross section with relativistic correction (σ_{Li}^{PSSR}) η_L/θ_{Li}^2 in equation 4.17 has to be replaced by $(\xi_{Li}^{R}/2n_L\zeta_{Li})^2$, thus,

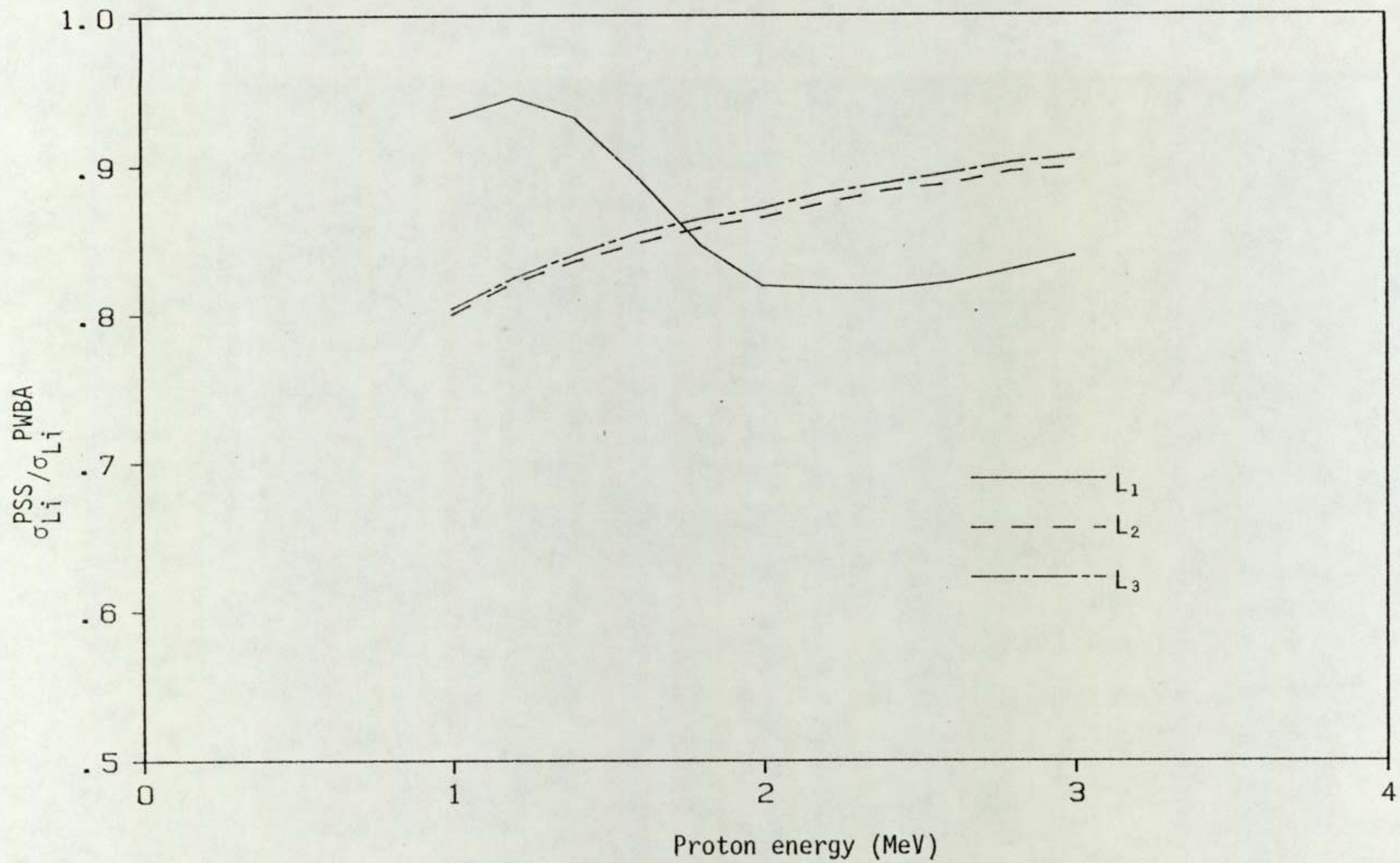

Figure 4.3 The perturbed stationary-state effect for proton impact on gold (Z_2 = 79). The L_i subshell ionisation cross sections were calculated using equations 4.17 and 4.53 and tables of Benka and Kropf (1978).

$$\sigma_{Li}^{PSSR} = \sigma_{Li}^{PWBA} ((\xi_{Li}^{R}/2n_L\zeta_{Li})^2, \zeta_{Li}\ \theta_{Li}) \quad 4.55$$

or η_L in equation 4.15 has to be replaced by η_L^R/ζ_{Li}^2, thus

$$\sigma_{Li}^{PSSR} = \sigma_{Li}^{PWBA} (\eta_L^R/\zeta_{Li}^{\ 2}, \zeta_{Li}\theta_{Li}) \quad 4.56$$

4.3.3 Coulomb Deflection Effect

The PWBA description neglects the effects of the Coulomb field of the target nucleus on the incoming bare nucleus. The projectile suffers a deviation from its incident path and retardation because of the internuclear repulsion. Both of these effects are collectively referred to as the Coulomb deflection effect (Brandt and Lapicki 1979) and reduce the ionisation cross section. The PWBA predicts that the inner-shell ionisation cross section for incident isotopes, such as protons and deutrons, of the same velocity are numerically equal. Brandt et al (1966) and Shima et al (1971) have, however, demonstrated experimentally to the contrary that the cross sections infact disagree markedly, especially at low projectile velocities. This 'isotope effect' arises because of the Coulomb deflection of the projectile and is explained by the fact that the degree of deflection is dependent on the projectile mass. (Bang and Hansteen 1959 and Brandt et al 1966). A simple multiplicative Coulomb factor has been derived by Brandt et al (1974, 1979), which, in terms of the half-distance of closest approach in a head-on collision,

$d = Z_1Z_2/Mv_1^2$ with the reduced mass $M = (M_1^{-1} + M_2^{-1})^{-1}$, q_{min} and ζ_{Li} is given by

$$C_{Li}\ (dq_{min}\zeta_{Li}) = \frac{\exp(-\pi dq_{min}\ \zeta_{Li})}{1 + \pi dq_{min}\zeta_{Li}/(9 + 2\ell)} \quad 4.57$$

where M_1 and M_2 are the masses of the projectile and the target nucleus respectively, q_{min} is evaluated using equations 4.37 and 4.39, the PSS factor ζ_{Li} is determined from equation 4.52 and ℓ is the orbital quantum number and has the values, $\ell = 0$ for L_1 and $\ell = 1$ for L_2 and L_3 subshells.

This Coulomb factor has been extracted from the formulae of Bang and Hansteen (1959), who employed the semi-classical approximation (see Appendix A) with straight-line and hyperbolic trajectories, by Brandt and his co-workers following the analytical approach of Amundsen (1977a). A fully quantum-mechanical treatment using Coulomb wave functions in the framework of the Born approximation has been given by Lapicki and Losonsky (1979). The Coulomb factor is defined as the ratio of the Coulomb to plane-wave Born cross sections and is derived for any inelastic collision in which the particle moves with a low velocity and suffers relatively small loss of its incident energy. Lapicki and Losonsky (1979) have, however, indicated that for slow collisions which occur at impact parameters comparable to d equation 4.57 is adequate for determining the correction factor. The L-subshell ionisation cross section corrected for Coulomb deflection, PSS, and relativistic effects, σ_{Li}^{CPSSR} is given by

$$\sigma_{Li}^{CPSSR} = C_{Li}(dq_{min}\xi_{Li})\sigma_{Li}^{PSSR} \qquad 4.58$$

σ_{Li}^{PSSR} may be evaluated using equation 4.55 or 4.56.

4.3.4 Energy Loss Effect

A comparison of the CPSSR theory with the published K and L-shell experimental data for protons and deuterons was performed by Brandt and Lapicki (1979) who found that on average the agreement was to within 30% which is comparable to the uncertainties associated with experiment measurements. Further analysis by the same authors showed a statistically significant disagreement between the theory and experiment at low projectile velocities ($\xi < 1$). The extent to which this discrepency may be explained by the finite energy loss suffered by the projectiles in the event of inner-shell ionisation has been investigated analytically by Brandt and Lapicki (1981). These authors have incorporated the minimum fractional energy loss of the projectile during inner-shell ionisation, L-shell in the present case and denoted by Δ_{Li}, in the minimum and the maximum momentum transfers (see expressions 4.23 and 4.28 where the energy loss is denoted by ε). A multiplicative factor $f_{Li}(Z_{Li})$ defined by

$$\sigma_{Li}^{EPWBA} = f_{Li}(Z_{Li})\sigma_{Li}^{PWBA} \qquad 4.59$$

has been derived by Brandt and Lapicki (1981) where σ_{Li}^{EPWBA} is the PWBA cross section corrected for the projectile energy loss. The energy loss correction is given by

$$f_{Li}(Z_{Li}) = 2^{-\nu}(\nu - 1)^{-1}\Big[(\nu Z_{Li} - 1)(1 + Z_{Li})^{\nu} + (\nu Z_{Li} + 1)(1 - Z_{Li})^{\nu}\Big] \qquad 4.60$$

where the argument Z_{Li} is

$$Z_{Li} = (1 - \Delta_{Li})^{\frac{1}{2}} \qquad 4.61$$

and $\nu = 9$ for L_1 and $\nu = 11$ for L_2 and L_3 subshells.

The energy loss correction varies smoothly with increasing projectile energy and ranges from about 5% at low energies to less than 2% at high energies for the collision systems under study.

The argument of the Coulomb deflection factor (equation 4.57) in the presence of projectile energy loss must be modified to take into account the energy loss effect. The Coulomb deflection factor is now given by

$$C_{Li}(x_{Li}) = \frac{\exp(-\pi x_{Li})}{1 + \pi x_{Li}/(9 + 2\ell)} \qquad 4.62$$

with $$x_{Li} = \frac{2dq_{min}\zeta_{Li}}{Z_{Li}(1 + Z_{Li})} \qquad 4.63$$

The Coulomb deflection factor, $C_{Li}(x_{Li})$, is illustrated in figure 4.4 for protons, deutrons and alpha particle impact on gold. $C_{Li}(x_{Li})$ was calculated using equation 4.62. The figure shows the deflection factor for the L_1 and L_3 subshells. The behaviour of $C_{Li}(x_{Li})$ for the L_2 subshell is very similar to that of L_3 and thus has been omitted from figure 4.4 for clarity. The importance of this correction at low impact energies and for

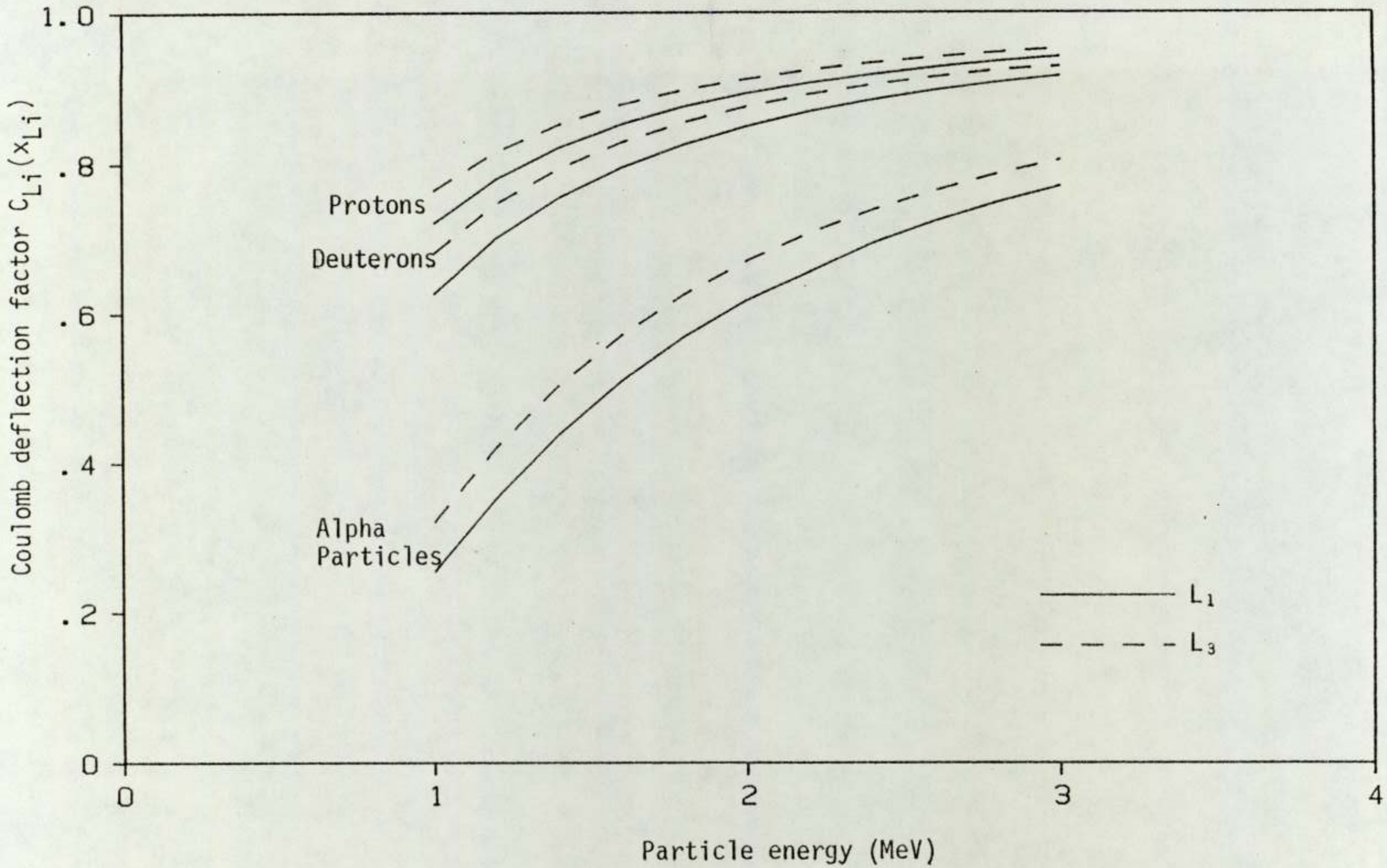

Figure 4.4 Coulomb deflection factor for protons, deuterons and alpha particles incident on gold (Z_2 = 79). $C_{Li}(x_{Li})$ was calculated using equation 4.62.

heavier charged particles is clearly evident from this figure.

Incorporating the PSS factor ζ_{Li} into the argument of the energy loss function, Z_{Li} can now be defined as

$$Z_{Li}^2 = 1 - \zeta_{Li}\Delta_{Li}$$
$$= 1 - \frac{4}{M\zeta_{Li}\theta_{Li}}\left(\frac{\zeta_{Li}}{\xi_{Li}}\right)^2 \qquad 4.64$$

where M is the reduced mass. The ionisation cross section predicted by the ECPSSR theory (E denoting the energy loss effect) is calculated from

$$\sigma_{Li}^{ECPSSR} = C_{Li}\left[\frac{2dq_{min}\zeta_{Li}}{Z_{Li}(1 + Z_{Li})}\right] f_{Li}\ (Z_{Li})\ \sigma_{Li}^{PSSR} \qquad 4.65$$

The L_2 and L_3 subshells are affected the most by incorporating the total ECPSSR effect into the PWBA cross sections. This is demonstrated in figure 4.5 which shows a plot of $\sigma_{Li}^{ECPSSR}/\sigma_{Li}^{PWBA}$ ratio for proton impact on gold. The ECPSSR ionisation cross sections were calculated using equation 4.65 and tables of Benka and Kropf (1978). In the case of the L_1 state the relativistic effect compensates to a certain extent the PSS and the Coulomb deflection effects and as a result the total ECPSSR affect on L_1 is somewhat reduced.

A systematic comparison between the predictions of the ECPSSR theory and experimental K-shell ionisation cross sections for proton impact has been made by Brandt and Lapicki (1981). An agreement to within 10% has been achieved between the theory and experiment. A detailed comparison with L-shell data, however, has yet to be performed in any substantial way. Nevertheless, at these levels of correlation it would now be possible to detect inadequacies of the atomic wave functions employed in the theoretical treatment and whether significant improvements can be achieved by using more realistic atomic wave functions (Brandt and Lapicki 1981). One of the aims of this study is to make a detailed comparison of experimentally determined Li-subshell ionisation and x-ray production cross sections for protons, deutrons and alpha particles incident on medium and high Z_2 elements with

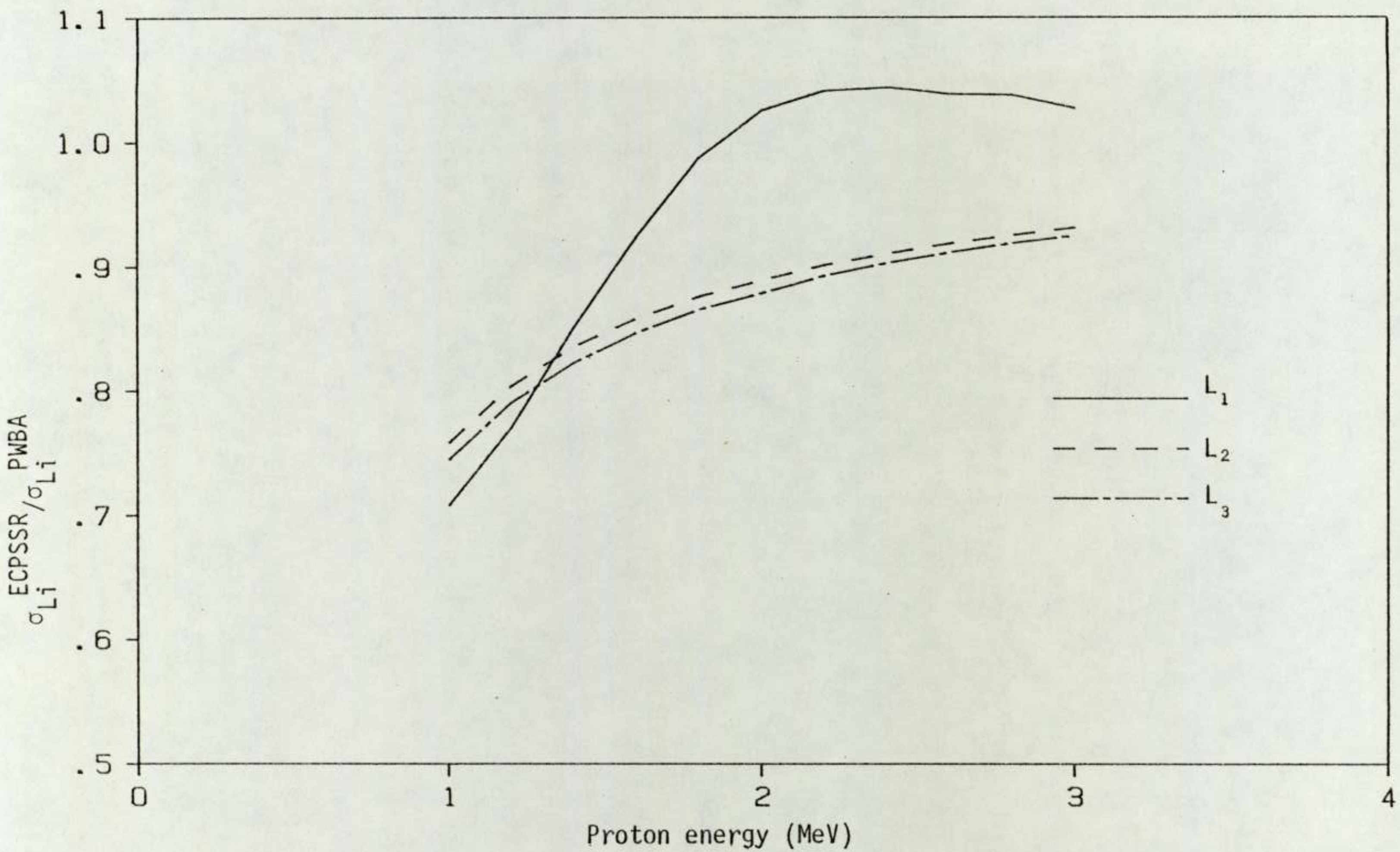

Figure 4.5 The ECPSSR effect for proton impact on gold (Z_2 = 79). The L_i subshell ionisation cross sections were calculated using equations 4.17 and 4.65 and tables of Benka and Kropf (1978).

the ECPSSR predictions.

4.4 INNER-SHELL ALIGNMENT BY CHARGED PARTICLE IMPACT

Emission of collisionally induced inner-shell x-rays have been shown to be non-isotropic for transitions to subshells with total angular momentum $j > \frac{1}{2}$ (Mehlhorn 1968). In the case of L-shell ionisations the anisotropy of x-rays resulting from transitions to the L_3 ($2p_{3/2}$) subshell has been demonstrated by Jitschin et al (1979) for proton impact on heavy atoms. This is due to the alignment of inner-shell vacancies created when an unpolarised beam of charged particles impinges upon unpolarised target atoms. The vacancies retain information regarding the incident direction of the beam and consequently the x-rays are emitted at an angle which reflects the degree of alignment of the inner-subshell. The alignment effect is understood in terms of the magnetic substates associated with the inner-shells. Alignment of an inner-subshell such as the L_3, reflects the different vacancy population of the magnetic substates (Jitschin et al 1979). Experimental measurement of inner-shell ionisation cross sections, however, involve an incoherent sum of magnetic substate populations (Rosel et al 1982). Study of alignment effects, therefore, provides complementary information to the cross section measurements for testing inner-shell theories (Sarkadi 1983). This fact has instigated the considerable work being done in this area (Jitschin et al 1979, Palinkas et al 1981, Barros Leite et al 1982, Jitschin et al 1982b and Rosel et al 1982). Cleff (1982) has provided a comprehensive review of the subject.

The anisotropy of the emitted x-rays can be studied by measuring the x-ray yield at different angles from the incident beam axis. From these measurements the degree of polarisation (P) of the x-rays can be determined. P is defined by the expression (Berezhko and Kabachnik 1977)

$$I(\theta) = I(90^o)\ (1 - P\cos^2\theta) \qquad 4.66$$

where $I(\theta)$ is the intensity of the dipole characteristic radiation at angle

θ to the direction of the beam. Energy dependence of the polarisation of emitted x-rays, resulting from vacancies in the L_3 subshell, has been established by Jitschin et al (1979) for proton impact and by Palinkas et al (1980) for helium impact.

Of all the transitions to the L_3 subshell the $L\ell$ x-rays exhibit the most anisotropy, P = +7% for 1MeV protons impact on Dy(Z_2 = 66)(Jitschin et al 1979). The other major x-ray transitions, the $L\alpha_{1,2}$ and $L\beta_{2,15}$ show relatively small anisotropy (Jitschin et al 1979 and 1982a). This alignment phenomenon explains why some experimentalists have obtained x-ray production cross section ratios of $L\alpha$ and $L\ell$ transitions for charged particle impact which are energy-dependent (Busch et al 1973, Tawara et al 1974, Tawara et al 1975 and Kamiya et al 1979). This is in contradiction to the prediction of the PWBA dicussed in section 4.2 which does not take into account the alignment of the subshells and, therefore, predicts a constant value of the ratio.

CHAPTER 5

EXPERIMENTAL APPARATUS AND PROCEDURE

CONTENTS

5.1 INTRODUCTION

The various aspects of the aparatus and the measuring techniques, employed for determining L shell x-ray production and ionisation cross sections, are explained in this chapter. Major features of the experimental arrangement for L x-ray yield measurements are described. Further details are, however, contained in Khan (1975) and Saied (1981). Procedure and results of the x-ray detector efficiency and target thickness measurements are presented. The chapter also discusses the experimental precision of the measured cross section values. The final section is addressed to the method employed for calculating theoretical ECPSSR cross sections required for comparison with the experimental data.

5.2 EXPERIMENTAL APPARATUS

The main components of the experimental arrangement employed in this study, are described in this section in such a way so as to trace the path of the particle beam from the accelerator right down into the scattering chamber where it encounters a fixed target. With this in mind the experimental apparatus may be broadly classified into the following:

(i) The Dynamitron.

(ii) Beam transport and experimental line.

(iii) Scattering chamber.

(iv) Target assembly.

Important features of each of these, pertinent to the experimental work, are highlighted in the forthcoming sub-sections.

5.2.1 The Dynamitron

The charged particles under study were accelerated to energies in the range 1-3 MeV using the Dynamitron accelerator situated at the Radiation Centre, University of Birmingham. The accelerator is a variable-energy potential-drop machine capable of terminal potentials from about 0.6 to 3MV. It is powered by a radiofrequency oscillator operating at 130 kHz. Sixty-four rectifier modules, arranged in a vertical chain from the base of the machine to the terminal, rectify the radiofrequency and produce the d.c. potential at the terminal.

The Dynamitron can be operated in a negative mode to accelerate electrons or in a positive mode to accelerate singly charged positive light ions, as in the present case. In the positive mode beam currents from about 1nA to 2mA are available.

The positive ions, employed in the collision experiments, are produced in a duoplasmatron ion source (Radiation Dynamics, Inc, 1967). Hydrogen, deuteruim and helium gases are used for producing protons, deuterons and helium (He^+) particles respectively. Ions of mass-one, two and three (protons only) are available and particles of the required mass may be selected by adjusting the potential needed to extract the ion from the source. Mass one ions were employed in the present investigation. With regard to the He^+ particle the single remaining electron can be assumed to be stripped off the ion and lost to the target medium immediately after striking the target. This assumption is valid provided that the velocity of the projectile is greater than the mean velocity of its bound electrons (Brandt 1981 and see section 3.2). In the impact energy range of interest this assumption holds true and the incident He^+ ion may be treated as an alpha (He^{2+}) particle in the context of inner-shell ionisation. As a result the helium ion is simply referred to as an alpha particle in this thesis.

The output voltage at the terminal is measured on a digital voltmeter (DVM) by drawing d.c. current through a high voltage potential divider resistor board with a total resistance of $10^{10}\Omega$. The output voltage is stabilised by an auto-regulator which compares the potential divider output with a variable reference voltage and compensates for any change in the terminal voltage (Radiation Dynamics, Inc 1967). The DVM readings can be translated into beam energy by calibrating the DVM with well-known nuclear reactions (Weaver 1976). A polynomial of the form

$$V = \sum_{i=0}^{3} a_i E^i \qquad 5.1$$

where V is the DVM reading, a_i are constants and E is the particle energy, is fitted to the measured data. The precision of the measurements range from 0.7% at 1MeV to 0.3% at 3MeV. Since the inner-shell ionisation cross sections are approximately proportional to E^4 (Merzbacher and Lewis 1958) the effect of these uncertainties is to make the measured ionisation cross sections uncertain by about 1.2% to 2.8%. Duration of x-ray yield measurements at a particular beam energy lasted upto 30 minutes. Variation of the beam energy during this time was less than 1keV producing only a nominal change in the ionisation cross section. Machine calibrations are performed regularly to ensure the reliability of the beam energy (Weaver 1976).

The accelerator has to be 'conditioned' before using beams of high energies inorder to ensure stability of the beam energy. Conditioning was performed each time prior to conducting the experiments. The 'conditioning point' tends to fall with time and to avoid any adverse affects on the beam energy, measurements were performed from 3MeV down to 1MeV, reducing the energy in steps of 200keV to establish the energy dependence of the x-ray production and ionisation cross sections.

5.2.2. Beam Transport and Experimental Line

The extracted mass one ions were subjected to a magnetic field in the top terminal causing them to be deflected into the line of the accelerator. After acceleration the particle beam can be directed into five experimental beam lines, each of which is based in an individual scattering room. For the present experimental work the ion beam was bent twice through 45^0 in succession by two magnets and transported into a horizonatal line, constructed of stainless steel components, leading to the scattering chamber. Beam focussing was achieved by means of a pair of quadrupole electromagnets.

A schematic diagram of the essential components of the experimental beam line and the scattering chamber employed in the collision experiments is shown in figure 5.1. Before the beam enters the scattering chamber the size of the beam is defined by two tantalum collimators, C_1 and C_2, 30cm apart and with diameters 2mm and 1.5mm respectively. C_2 defines the final beam diameter as it enters the scattering chamber. The collimators were tapered to reduce scattering of the charged particles and insulated from the rest of the line and the chamber with polytetrafluorethylene (PTFE) rings, which allows the current to be monitored on C_1 and C_2 as the beam travels down the line. This aided the machine operators considerably to direct the ion beam into the target chamber.

Alignment of the experimental line was achieved by passing a fine horizontal laser beam through the line after removing the target assembly and the Faraday cup (figure 5.1). The individual components of the line were adjusted until the laser beam passed through the collimators without hindrance and produced an intense spot on a reference mark, R_1, on the wall beyond the scattering chamber (figure 5.1). By placing a plane mirror at 45^0 to the beam axis inside the chamber and in the path of the laser, it was ensured that the reflected laser beam also produced an intense spot on a second reference mark, R_2, on the adjacent wall, as shown figure 5.1. The lithuim drifted silicon

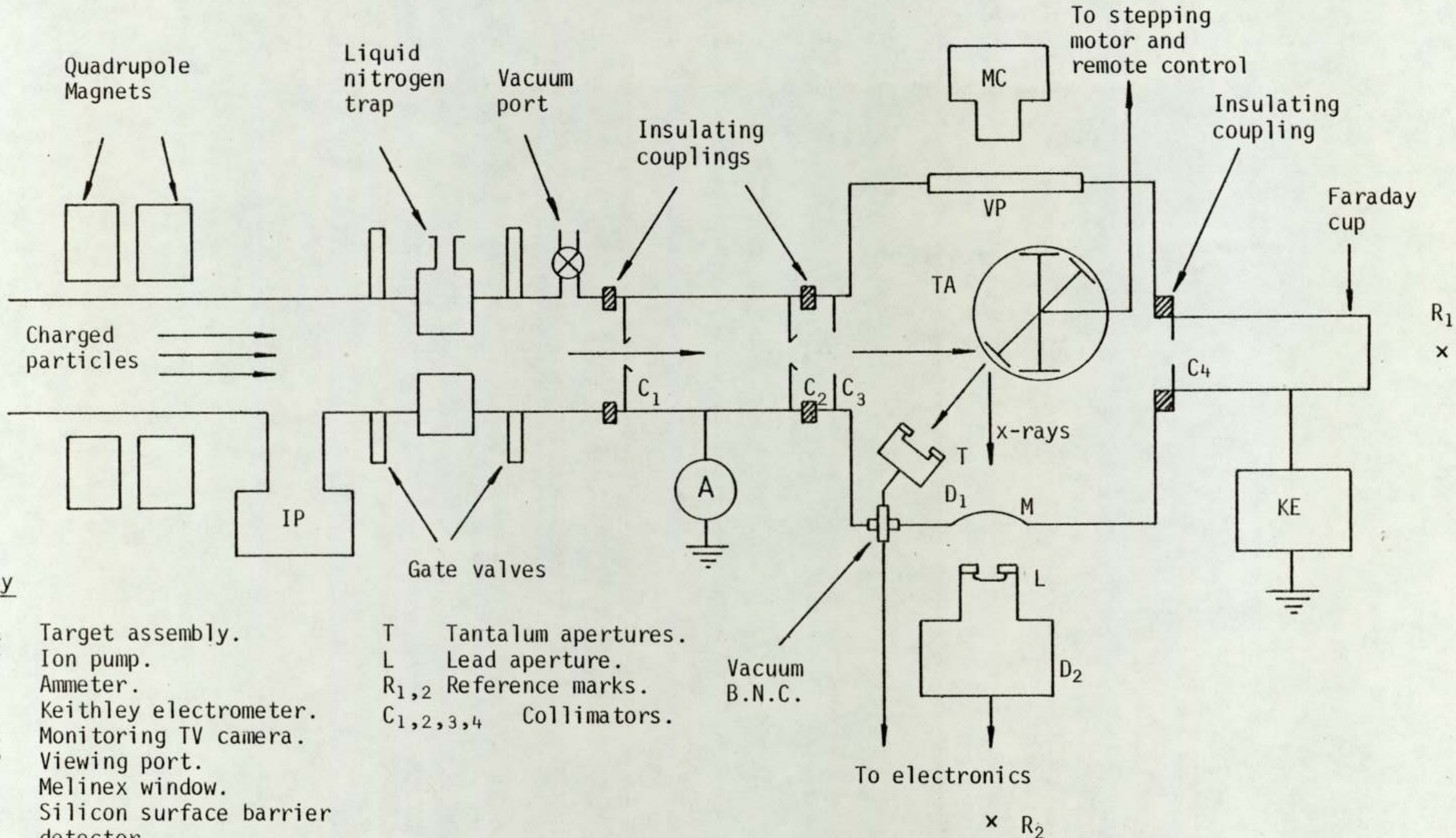

Key

TA Target assembly.
IP Ion pump.
A Ammeter.
KE Keithley electrometer.
MC Monitoring TV camera.
VP Viewing port.
M Melinex window.
D_1 Silicon surface barrier detector.
D_2 Lithium drifted silicon detector.

T Tantalum apertures.
L Lead aperture.
$R_{1,2}$ Reference marks.
$C_{1,2,3,4}$ Collimators.

Figure 5.1. Schematic diagram of the experimental line and the scattering chamber.

(Si(Li)) detector, employed for the x-ray measurements, was positioned at 90^0 to the beam axis using the reflected laser beam. The position of the silicon surface barrier (SSB) detector, required for detecting backscattered particles, was similarly checked. Positions of both of these detectors were verified each time before beginning the measurements. With the aid of R_1 and R_2 the positions of the target holders were adjusted until the laser beam created a spot on the centre of the targets when placed at 45^0 to the beam line.

A rotary pump was used to evacuate the experimental line and the scattering chamber to an initial pressure of 10^{-1} torr and then a diffusion pump to attain a working pressure of less than 10^{-5} torr. A clean system was maintained throughout the duration of the experiments by means of an ion pump and a liquid nitrogen trap illustrated in figure 5.1.

5.2.3. Scattering Chamber

After being collimated by aperatures C_1 and C_2 the particle beam enters a rectangular scattering chamber constructed of 1 cm stainless steel plates (figure 5.1). The inside dimensions of the chamber are approximately 12 x 15 cm. The chamber was electrically insulated from the beam line by teflon and PTFE insulating couplings. One of the sides of the chamber, parallel to the beam line, incorporates a viewing port made of 1.25 cm thick glass plate. The opposite side houses a 50 μm melinex window of about 5 cm diameter. The x-rays produced by the particles impinging on the target pass through this window before being measured by the Si(Li) detector.

An aluminium aperature, C_3, of 1.5 cm in diameter was placed in the entrance port of the chamber (figure 5.1). The purpose of C_3 was to 'catch' the energetic secondary electrons emitted from the target when bombarded by charged particles and thus prevents the electrons from reaching C_2 and vitiating the beam current measurements.

To measure the backscattered particles a silicon surfact barrier (SSB) detector was mounted from the 1.25 cm thick stainless steel coverplate. The backscattering angle was defined by two tantalum apertures (T in figure 5.1) attached to the front of the SSB and placed 5 mm apart. Both of the aperatures were reamed to avoid any scattering at the edges. The diameters of the aperatures were measured with a 'Universal Measuring Machine' (model MU214B) and were determined to be 2.531 ± 0.003mm. The aperatures also ensured that the collimated backscattered beam struck the centre of the active area of the SSB detector and avoided any 'edge' effects.

A Faraday cup constructed of a 40 cm long stainless steel tube was attached to the end of the chamber (figure 5.1) to collect the charged particles after interacting with the thin targets. The Faraday cup was insulated from the chamber by PTFE and teflon couplings. A tantalum aperature (C_4) of 1.5 cm diameter, attached to the entrance of the Faraday cup, prevented secondary electrons escaping from the cup into the chamber and causing 'leakage' of current. The opening of the Faraday cup was about 15 cm from the target position.

5.2.4 Target Assembly

The target assembly consisted of four aluminium mounts fixed vertically to the outer edges of a horizontal disc, also made of aluminium. The whole assembly was suspended from the chamber cover-plate by a stainless steel shaft. The target mounts were simply two columns with groves which held the targets securely in place.

Targets backed by nuclepore (1mg/cm^2) and carbon (40µg/cm^2) were employed in this work. Both types of targets were commercially obtained from MicroMatter and Co. The carbon backed targets were obtained ready-mounted on pieces of aluminium 1.5 x 1.5 cm and 0.5 mm thick with a 1 cm circular aperture. Targets backed by nuclepore were fixed onto aluminium frames 1.5 x 2.0 cm and 2 mm thick with a 1.5 cm diameter hole by means of an aluminium ring pressed into the hole. These targets were simply slotted into the mountings and the carbon backed targets were secured into the mounts with the aid of aluminiun circlips. The target assembly as a whole could be moved vertically and the target mcuntings laterally, permitting precise alignment with the laser (section 5.2.2).

The position of the targets was controlled remotely by means of a high resolution stepping motor attached to the shaft suspending the target assembly and connected to a remote control unit. This has been described in details by Saied (1981). Targets could be positioned at the required angle in increments of 0.9^{o} without breaking the vacuum. A T.V. camera was used to monitor the target assembly throughout the experiments.

5.3 CHOICE OF TARGETS

To study the dependence of L shell x-ray production and ionisation cross sections on target atomic number (Z_2), 10 solid targets spanning $46 \leq Z_2 \leq 92$ were employed for the L shell cross section measurements. Table 5.1 lists the targets, together with the form of the target, type of backing, the projectiles incident on the target and type of cross section measured. Targets of sufficiently high melting points were chosen to avoid any possibility of evaporation during bombardment by the charged particles.

All the experimental cross section measurements in this study were performed with thin targets. The criterion usually adopted to decide whether a target is 'thin' is that the interaction cross section must not be affected significantly by the energy loss suffered by the projectile as it passes through the target. In the present context

Table 5.1. Targets employed for cross section measurements.

Target (Z_2)	Target form	Type of backing	Projectiles[a]	Cross sections[b] measured
Pd (46)	Elemental	Nuclepore	p	X
Te (52)	Elemental	Nuclepore	p	X
Dy (66)	Elemental	Nuclepore	p	X
	DyF_3	Carbon	p, d	X, I
Yb (70)	YbF_3	Carbon	p, d, α	X, I
W (74)	WO_3	Carbon	p, d, α	X, I
Au (79)	Elemental	Nuclepore	p	X
		Carbon	p, d, α	X, I
Pb (82)	Elemental	Nuclepore	p	X
		Carbon	p, d, α	X, I
Bi (83)	Elemental	Carbon	p, d, α	X, I
Th (90)	ThF_4	Carbon	p	X, I
U (92)	UF_4	Carbon	p	X, I

(a) p = Protons, d = Deuterons, α = Alpha particles. (b) X = L x ray production cross sections
I = L shell ionisation cross sections

the affect on the elastic scattering and x-ray production cross sections must be minimal. The former varies with projectile energy as E^{-2} (equation 3.11) and the latter as E^4 (Merzbacher and Lewis 1958). X-ray production cross section is, therefore, more sensitive to the projectile energy loss and if this effect is small then it is also small for the nuclear elastic scattering cross section. Targets with typical thicknesses of about 50μg/cm were used for the experimental work and to estimate the effect on the x-ray production cross section of the projectile energy loss in such a target a multiplicative correction, C_x, to the x-ray production cross section was derived and is given by

$$C_x = \left[1 - \frac{at\ n\varepsilon(E)}{2E}\right]^{-1} \qquad 5.2$$

where t is the target thickness and n is the target atomic density. Equation 5.2 assumes that the stopping, $\varepsilon(E)$, varies linearly with projectile energy and that the x-ray production cross section varies as E^a. a was determined by fitting a function of the form $\sigma = \sigma_0 E^a$ to the ECPSSR cross sections in the vicinity of the incident particle energy, where σ_0 is a constant. $\varepsilon(E)$ was extracted from the tables of Andersen and Ziegler (1977b). Using equation 5.2 corrections were found to be negligible for proton and deuteron impact, even at low energies. In the case of alpha particles a correction of about 3% was necessary at low incident energies.

Since the stopping power appears only in the correction it does not introduce any significant uncertainties in the measured cross sections. In comparison, for thick target measurements $\varepsilon(E)$ enters directly into the cross section calculations. As a consequence the precision of the cross sections obtained from thick target data is determined to a large extent by the precision of $\varepsilon(E)$. Furthermore the derivative of the yield excitation function is required when using thick targets. This is usually obtained by fitting polynomials to the yield curves or simply by graphical means (Khan and Crumpton 1978). Apart from introducing futher uncertainties in the cross sections this procedure obviously entails complications. Corrections must also be made for the self-absorption suffered by the particle induced x-rays in the thick targets. This leads to an additional criterion for characterising the thickness of a target. If self-absorption can be ignored then the target is considered 'thin'. In relation to metallic targets if the x-ray production cross section criterion is fulfilled then the target is sufficiently thin to make self-absorption insignificant.

In the case of thin target measurements the calculation procedure is relatively straightforward. The problem of determining precisely the target thickness, however, does arise and is discussed in section 5.6. This difficulty is clearly absent for thick target experiments.

Thin and thick target techniques for obtaining x-ray production cross sections by light charged particle bombardment have been compared by McKnight et al (1975) and more recently by Khan and Crumpton (1978) and Barfoot et al (1980). There is a general concensus that although the uncertainties of the cross sections obtained from the two techniques are comparable, the thin target method is slightly more precise. For the aforementioned reasons present measurements were performed with thin targets only.

As mentioned in subsection 5.4.2 targets on $1 mg/cm^2$ nuclepore and $40 \mu g/cm^2$ backings were studied. Initial measurements of proton induced L shell x-ray production cross sections were conducted with nuclepore backed targets because they can be handled without difficulty and their thicknesses are known to within 5% (MicroMatter and Co.). A severe limitation of this type of target, however, is that it cannot withstand high beam currents because of the non-conducting backing material and beam currents of only a few nanoamperes can be used. As a direct consequence counting statistics, although adequate for x-ray production measurements, were poor for the purposes of deducing ionisation cross sections. To overcome this difficult targets bakced by 40μg/cm² carbon were adopted for ionisation cross section measurements. These targets can sustain beam currents of several hundred nanoamperes for a few hours without undergoing any serious deterioration. Currents of upto 100nA were employed in the measurements reported in this thesis while keeping count-rates below $500s^{-1}$ to avoid pulse pile-up. An inherent disadvantage with this type of backing is their fragile nature and its primarily because of this fact that backings of 40μg/cm² were used in favour of the initially adopted backings of 20μg/cm².

5.4 DATA AQUISITION

L x-ray production cross sections were deduced from the measured x-ray yields and the appropriate target charge. The procedures adopted for determining both of these fundamental experimental quantities are described in this section. Details are also given of the calibration of the x-ray detection system.

5.4.1 Determination of Target Charge

The total charge to which the target is exposed during irradiation by charged particles was determined by feeding the charge collected in the Faraday cup to a Keithly electrometer (model 600B), shown in figure 5.2. The electrometer integrates the beam current and outputs a voltage signal whose level is proportional to the meter deflection. By varying the input resistence the electrometer supplies a 1V signal for a fullscale-deflection (FSD). The precision of the Keithley electrometer at FSD is around 1%. The output voltage signal is fed

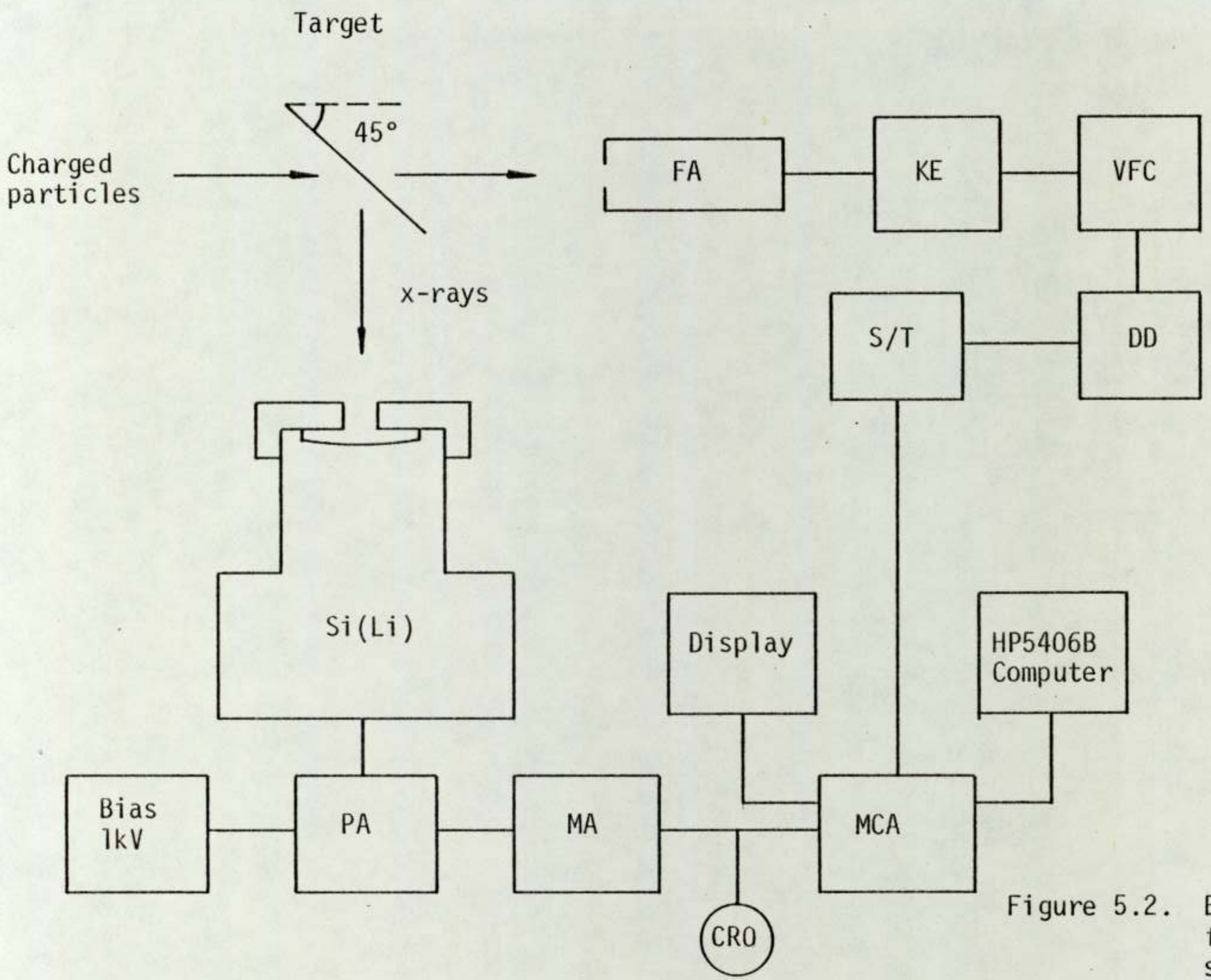

Key

FA	Faraday cup.
KE	Keithley electrometer.
VFC	Voltage-to-frequency convertor.
S/T	Scaler/Timer.
PA	Preamplifier.
MA	X-ray spectroscopy amplifier.
MCA	Multichannel analyser.
CRO	Cathode ray oscilloscope.
DD	Decade divider unit.

Figure 5.2. Block diagram of the electronics for the x-ray and current integration systems.

into a voltage-to-frequency converter (VFC) which outputs a chain of pulses with frequency proportional to the input. For an input of 1V the frequency is 10^5Hz. The pulse chain is fed into a decade divider unit which scales the pulses for counting with a scalar/timer device. Counting for a fixed number of these pulses is equivalent to counting for a fixed target charge. An automatic stop unit, linked to the scalar/timer, ceases the accumulation of data once a preset count on the scalar has been achieved. X-ray spectra of sufficient statistical precision were obtained for a specific total charge. The number of charged particles to which the target is exposed is simply obtained by dividing the integrated charge by the electronic charge (e).

Under this experimental arrangement reproducibility of K x-ray yields of low to medium Z_2 nuclepore backed targets bombarded by 2.5MeV protons was investigated in collaboration with Saied (1981). The yields were found to be irreproducible when measurements were performed at different times. This was attributed to

(i) charge leakage caused by secondary electrons escaping from the Faraday cup into the chamber and

(ii) since the Keithley electrometer is a high impedence instrument there is the possibility of direct leakage of current between the chamber and the Faraday cup.

To eliminate these causes the chamber, which was initially earthed, was electrically connected to the Faraday tube thus combining the two into one Faraday cup. With this new arrangement reproducible x-ray yields were obtained within statistical deviations. The results of these investigations have been discussed extensively by Saied (1981). During the L shell x-ray measurements reprocibility of the system was checked everytime an experiment was performed by repeating a few measurements on a target which had been studied previously.

As an alternative to utilising a current integrator the number of incident particles can also be determined by measuring the backscattered yield, accumulated over the duration of the x-ray experiment, and employing equation 3.19. This would then avoid the difficulties associated with charge collections discussed above. An additional advantage is that the target thickness, common to backscattered and x-ray yields, may be eliminated in the cross section calculations. This method was initially adopted but since the nuclear scattering cross section varies as E^{-2}, at low impact energies the enormous backscattered yield caused pulse pile-up problems. By using low beam currents this difficulty can be reduced but then the x-ray yield diminishes and accumulation times can become impracticable. An alternative is to use variable aperatures for the SSB detector, however, the present experimental set-up made this unfeasible. As a consequence the backscattering system was employed solely for measuring target thickness.

5.4.2 X-Ray Detection System

After passing through a 50μm melinex window the charged particle induced x-rays travel through 2.5 cm of air before being measured by a Si(Li) detector placed at 90^{o} to the beam axis. To ensure that the x-rays impinge only on the central area of the silicon crystal and thus avoid any complications of 'edge' effects (section 5.5) a lead aperture, denoted in figure 5.1 by L, of 3.97 mm and 4.18 mm thick was attached to the front of the detector. The solid angle subtended by the Si(Li) detector was measured with an aid of vernier calipers and value of $(1.67 \pm 0.03) \times 10^{-3}$ steradians was obtained.

A Kevex-ray Si(Li) detector (model number 3201) with a crystal of area 30 mm^2 and thickness 3 mm, cooled with liquid nitrogen, was employed for the cross section measurements. A Si(Li) detector is commonly used for such measurements because it offers good resolution, 164 ± 7eV at 5.898keV for the above detector, and high efficiency at the x-ray energies of interest. Another common photon detector is the lithuim drifted germanium , Ge(Li), detector. Although it has superior resolution to that of the Si(Li), it suffers from markedly lower detection efficiencies and would increase greatly data accumulation times. A further advantage over the Ge(Li) detector is that the Si(Li) requires less frequent replenishment of liquid nitrogen for a given dewer size, and can even be temperature cycled many times without damaging the crystal. Economically Si(Li) is also favoured to the Ge(Li) detector. Thallium activated sodium iodide, NaI(Tl), detectors are also employed for detecting photons but their poor resolution (50% at 5.898keV) makes their use in the present context inappropriate.

The operation of the Si(Li) detector is covered extensively in the literature (Gedcke 1972 and Knoll 1979) and only brief details are presented below.

The silicon crystal has an approximately 200Å thick gold layer on both sides which acts as electrical contacts. The photons also have to pass through approximately 0.1μm of silicon deadlayer before reaching the active region of the crystal. Electron-hole pairs are produced in this region by the photons interacting primarily through the photoelectric effect (section 2.5). The number of charge carriers produced are directly proportional to the x-ray energy since the average energy required to create an electron-hole pair in silicon, cooled to liquid nitrogen temperature, is a constant value of 3.8eV. The charges were collected by applying a voltage of 1kV across the crystal and converted into voltage pulses by a charge-sensitive pulse optical feedback preamplifier (model 2002) while retaining the charge-energy proportionality. The electronics adopted for the x-ray measurements are schematically shown in figure 5.2. The Si crystal and the field effect transistor, which forms the first stage of the preamplifier, are cooled by liquid nitrogen to prevent lithium diffusing through the crystal and to minimise electrical noise caused by thermally excited charge carriers in the crystal. The crystal is housed in a vacuum protected by 13μm thick berylluim window, which also acts as an optical shield.

The pulses from the preamplifier were processed and amplified by a Kevex spectroscopy amplifier (model 4500P) to make them compalible with the requirements of a 200MHz analogue-to-digital converter (ADC) forming a part of the multichannel analyser (MCA). The x-ray spectrum was displayed over 2048 channels and the pulses from the amplifier were monitored on a cathode ray oscilloscope (figure 5.2).

Deterioration of the Si(Li) detector resolution by external environmental noise, known as microphonics, has been demonstrated by Khan et al (1979). In view of this care was exercised to avoid all unnecessary mechanical noise and vibration while conducting the x-ray measurements and effects of microphonics, as a result, were not noticable.

A Hewlett-Packard 5406B computer system was available for fast storage and retrieval of data (Weaver 1976). The several ADC's offered by the sytem may be used in combination for multi-parameter or multiplex experiments. The feasibility experiments regarding the determination of the total target charge by measuring the backscattered yield, mentioned in subsection 5.4.1 were performed with two ADC's in multiplex mode. In the subsequent work one ADC was used. The MCA is directly linked to the computer allowing storage of the accumulated x-ray spectra onto a magnetic hard disc for immediate and on magnetic tape for future analysis. Various software packages are available for spectral analysis and may be initiated via a terminal. Typical L shell x-ray spectra, obtained with the aforementioned x-ray system, are shown in figure 5.3 and 5.4 for ytterbüim (Z_2 = 70) bombarded by 3MeV alpha particles and bismuth (Z_2 = 83) bombarded by 3MeV protons respectively. During the x-ray measurements $L\ell$ transition yield was monitored and x-ray spectra were accumulated until the $L\ell$ yield was greater than 500 counts to obtain reasonable counting statistics for the other peaks. Continuous monitoring of the $L\ell$ peak also allowed any significant variations in the beam current or damage to the target to be detected. Typical accumulation times ranged from about 5 to 30 minutes.

5.4.3. X-Ray Energy Calibration

The direct proportionality between x-ray energy and the number of electron-hole pairs produced in the Si crystal, referred to in the previous subsection, may be checked by performing an energy calibration of the Si(Li) detector. This may be achieved by measuring the pulse heights or the x-ray peak centroids at different energies. Such a detector response is also necessary for identifying x-ray peaks of interest.

A variable x-ray energy source, consisting of a 10mCi ^{241}Am primary source and six fluorescent targets, in the range $29 \leq Z_2 \leq 65$, together with the targets used for reproducibility studies, were employed to calibrate the x-ray detection system. A software package, available on the computer system for fitting a single Gaussian distribution to an x-ray peak, was used to determine the peak centroids and the standard deviations. The package assumes a linear background on which the x-ray peak is superimposed. A linear relationship between x-ray energy and peak centroid was obtained, validating the charge-energy proportionality. The following equation was obtained by fitting

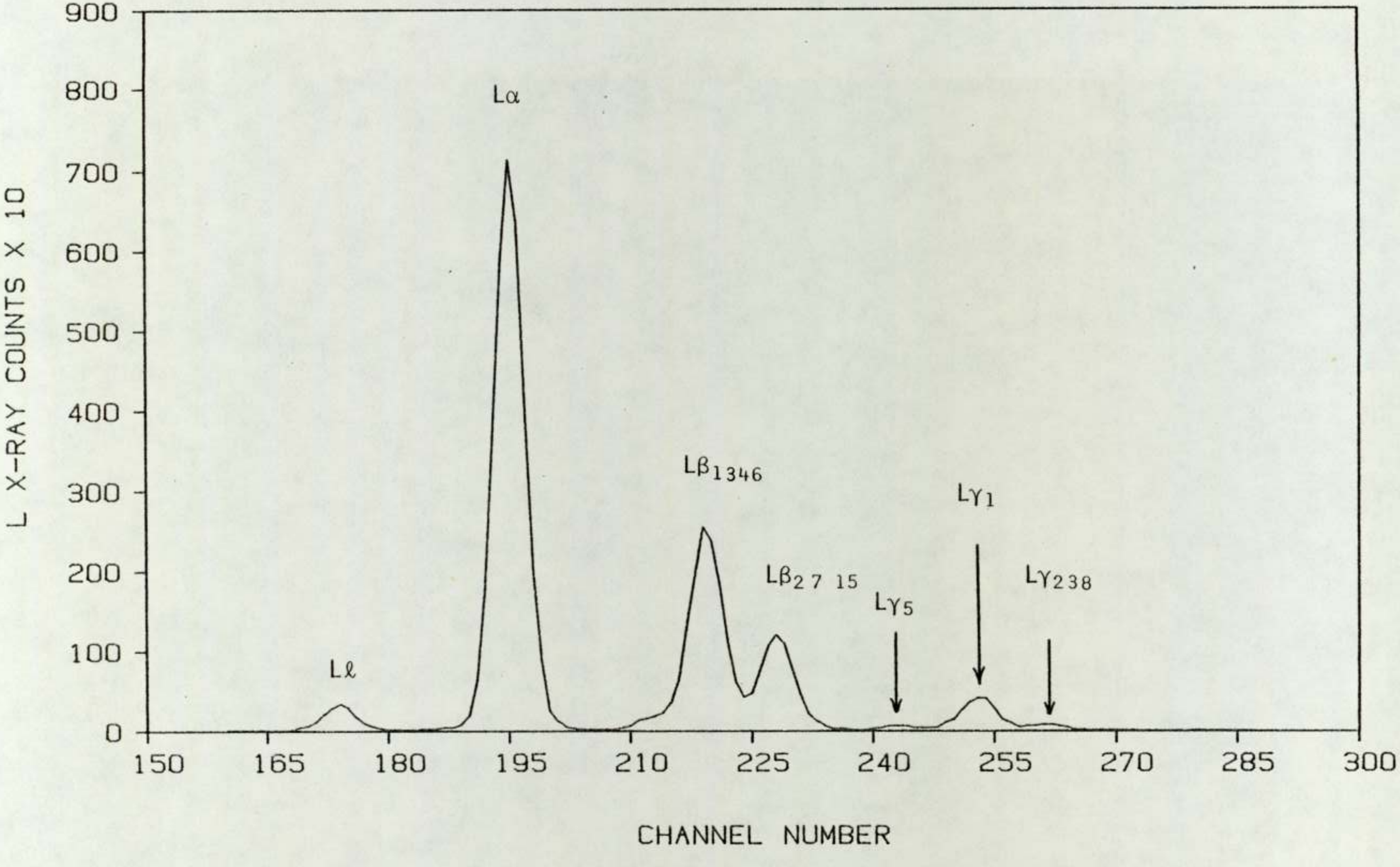

Figure 5.3. L x-ray spectrum for ytterbuim (Z_2 = 70) obtained by 3 MeV alpha particle impact.

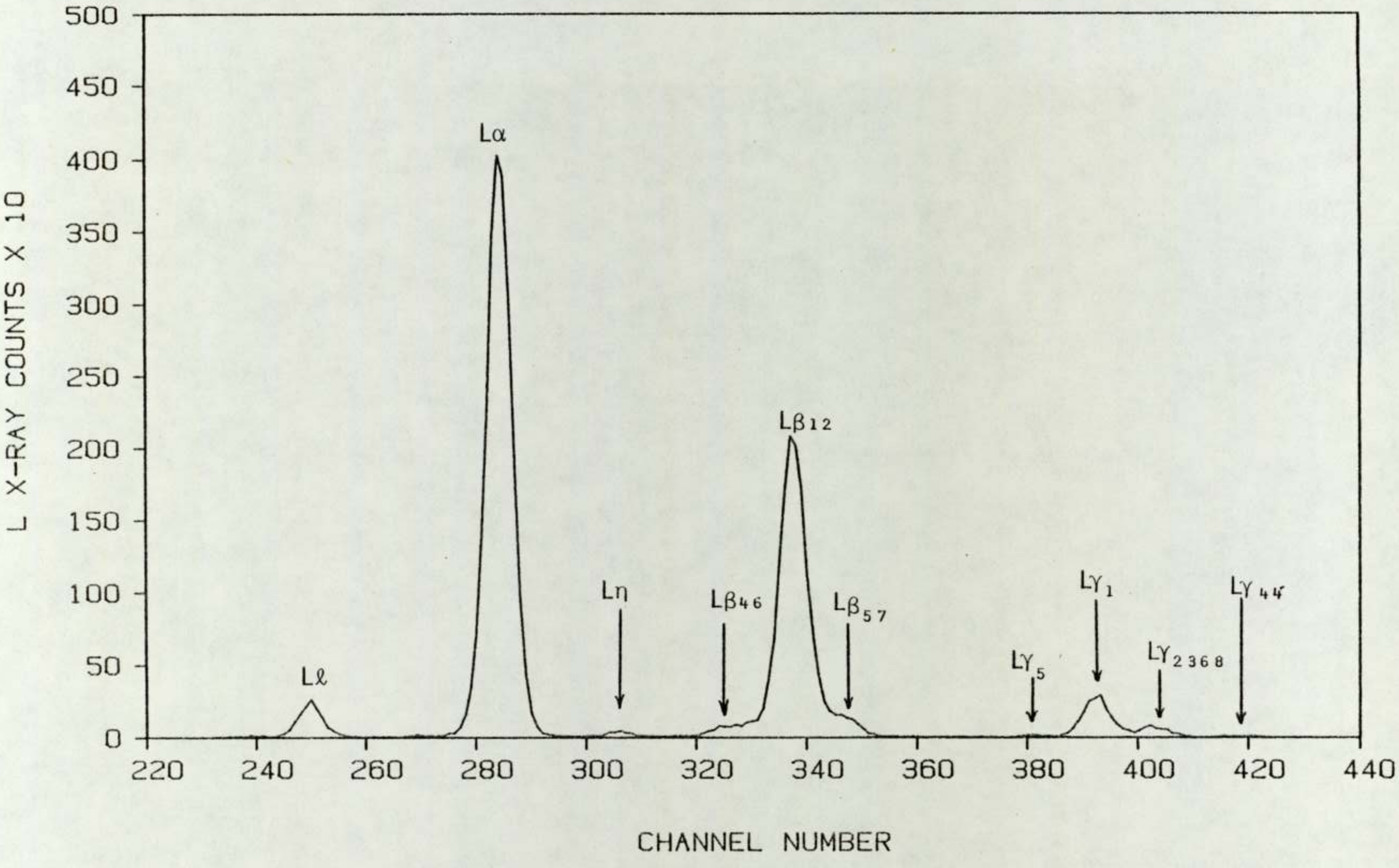

Figure 5.4. L x-ray spectrum for bismuth (Z_2 = 83) obtained by 3MeV proton impact.

a linear model to the data with the least square method

$$E_x(\text{keV}) = -0.5846 + 0.0408c \qquad 5.3$$

where E_x is the x-ray energy and c is the centroid of the x-ray peak. The correlation coefficient, R , which measures the proportion of total variation about the mean $\bar{Y}$ explained by the regression (Draper and Smith 1981), may be calculated to estimate the goodness of fit. R^2 is defined as

$$R^2 = \frac{\sum_{i=1}^{n}(\hat{Y}_i - \bar{Y})^2}{\sum_{i=1}^{n}(Y_i - \bar{Y})^2} \qquad 5.4$$

where Y_i is the observed value, x-ray energy in the above context, $\hat{Y}_i$ is the least square predictions of Y_i and n is the number of data values. A value of 0.9999 was obtained for equation 5.3. A perfect fit would yield a value of 1.0. The resolution response of the Si(Li) detector varies according to the relation

$$\sigma^2 = \sigma^2_{noise} + \varepsilon F E_x \qquad 5.5$$

where σ^2 is resultant variance of the measured x-ray peak, σ^2_{noise} is the contribution from the preamplifier noise, $\varepsilon F E_x$ is the contribution from the Si(Li) diode due to the ionisation statistics, ε is the energy required to create a single electron-hole pair (ε = 3.8eV for cooled Si) and F is the Fano factor. The variation of σ^2 with E_x has been studied by Saied (1981) for the detector employed in this work. A linear relationship between σ^2 and E_x, as predicted by equation 5.5, was demonstrated. A least square equation

$$\sigma^2 = 1.5339 + 0.4446E_x \qquad 5.6$$

was fitted to the data and a value of 0.99 for R^2 was calculated. The gradient of equation 5.6 offers a convenient method for evaluating F for the detector. A value of F = 0.117 ± 0.003 was obtained by Saied (1981). From the intercept σ_{noise} was determined to be 50.5eV.

5.5 Si(Li) DETECTOR EFFICIENCY

The reliability of the measured cross section values depends, among other factors (see subsection 5.7.4), on the precision of the x-ray detector efficiency. Much evidence has been brought to light that suggests that the detector efficiency should be determined experimentally (Gallagher and Cipolla 1974). This section is addressed to this problem.

For a well collimated and parrallel x-ray beam striking normally on the silicon crystal the efficiency of the Si(Li) detector, ε, may be calculated from

$$\varepsilon = C_{Be}\left[1 - \exp(-\mu_{si}x_{si})\right] \qquad 5.7$$

where C_{Be} represents the absorption correction for the beryllium detector window, μ_{si} is the linear absorption coefficient for Si and x_{si} is the thickness of the crystal. In practice, however, the situation is not so straightforward. Complications arise due to the possibility of the detector specifications, quoted by the manufacturers, being erroneous (Gallagher and Cipolla 1974). The main factors which are required to calculate the efficiency reliably are

(i) beryllium window thickness (12μm),

(ii) dimensions of the Si crystal (3mm x $30mm^2$),

(iii) Si dead layer thickness (0.1μm),

(iv) gold contact layer thickness (0.02μm),

(v) depletion layer thickness, and

(vi) charge collection efficiency.

The values in parenthesis refer to the manufactuer specifications for the Si(Li) detector employed in this study. Although some of these factors are quantified by the manufactors they may be unreliable or may even alter with time deteriorating the efficiency. Cohen (1982) has highlighted the deteriorating effects of ice build-up on the front face of the Si crystal at low x-ray energies. Consequently the necessity for determining the detector efficiency experimentally has been stressed by many workers (Routti and Prussin 1969, Hansen et al 1973, Gallagher and Cipolla 1974 and Johnson et al 1978).

5.5.1 Measuring Techniques

Two basic techniques are usually employed for measuring x-ray detector efficiencies. These are the 'absolute' and the 'comparison' techniques (Johnson et al 1978). The first method relies on calibrated radioactive sources with known activities, to which the x-ray detector is exposed. The efficiency is simply given by the ratio of the observed and the calculated photon fluxes. This method has been adopted recently by Dias and Renner (1982). There are, however, several drawbacks to this technique. Apart from the economic costs of obtaining the several sources that would be required to measure the efficiency at different x-ray energies, serious difficulties are encountered in determining accurate activities and acquiring knowledge of decay schemes (Hansen et al 1973 and Cipolla and Hewitt 1976). Considerable self-absorption in the radioactive source causes further complications (Johnson et al 1978 and Palinkas and Schlank 1980). Also there are relatively few sources avaiable that have convenient half lives in the x-ray region of interest (Johnson et al 1978).

These difficulties may be avoided by adopting the 'comparison' technqiue. This involves the comparison of the Si(Li) detector response with that of another detector whose efficiency is predetermined. The main advantage of this method is that the incident flux does not have to be known absolutely. The extent of the advantages depends on the way the incident fluxes are produced. Different methods for generating the test photon flux have been discussed by Johnson et al (1978). Basically the test photons may be emitted directly by radionuclides or indirectly by fluorescing a series of appropriate targets. The first method suffers from the disadvantages listed for the 'absolute' method. Johnson et al (1978) have used the second method and utilise the x-rays emitted when targets are fluoresced by a mono-energetic source. Shima (1979) and more recently Tolson and Spyrou (1982) have generated the test flux by bombarding selected targets by energetic protons and have used a proportional counter to compare the response of their Si(Li) detector. Cohen (1982) has compared the ratio of the M to L shell x-rays, produced by He^+ impact of high Z_2 elements, with the ratios predicted by the plane-wave Born approximation to calculate the Si(Li) detector efficiency.

In the present work a variation of the method used by Johnson et al (1978) is adopted for measuring the detector efficiency, while retaining the advantages of the 'comparison' technique.

5.5.2 Procedure and Results

A standard variable x-ray energy souce, consisting of Cu, Rb, Mo, Ag, Ba and Tb targets fluoresced by 60 keV γ-rays from a 10m Ci^{241}Am source, was used to provide the test photons. A 0.1mCi^{55}Fe source encased in lead for safety, was also used to extend the energy range down to 5.959keV. In addition, Ag x-rays from the variable x-ray energy source were employed to fluoresce thick targets of Ni and Zn. The efficiency was thus determined over the energy range 5.959 - 45.5keV. The sources employed here are inexpensive and readily available and thus makes the method particularly attractive. Table 5.2 lists the sources and the energies of the characteristic x-rays. The energies quoted are the weighted K x-ray energies from Storm and Israel (1970) instead of the individual K_α and K_β energies. The reason for this is that all the fluorescent targets are thick and self absorption is obviously considerable. Furthermore, self-absorption

Table 5.2. List of sources and x-ray energies employed for Si(Li) detector efficiency measurements.

Sources	Weighted K x-ray energy* (keV)
^{55}Fe	5.959
Ni[(a)]	7.558
Cu[(b)]	8.136
Zn[(a)]	8.735
Rb[(b)]	13.596
Mo[(b)]	17.781
Ag[(b)]	22.581
Ba[(b)]	32.89
Tb[(b)]	45.469

* Storm and Israel (1970).

(a) Fluoresced by Ag K x-rays.

(b) Variable x-ray energy source.

of K_α and K_β x-rays is different and as a result the K_α/K_β ratio of the emergent x-rays is unknown.

A thallium activated sodium iodide, NaI(Tl), detector (Harshaw 6SHA 6M/2A) with a 6 mm thick and 4 cm diameter crystal was used for the comparison. NaI(Tl) was used as the reference detector because its efficiency is 100% for the energies of interest. To avoid correcting for absorption in the 25.4μm thick aluminium window, of the NaI(Tl) detector an identical window was obtained from the manufacturers and placed in front of the Si(Li) detector while performing the measurements. This was done to eliminate any doubt in the manufacturers specification of the aluminium window thickness.

The geometrical arrangement and the electronics are shown in figure 5.5 for the variable x-ray energy and ^{55}Fe sources. Both of the detectors were exposed to the sources for a sufficient time to obtain satisfactory counting statistics. To eliminate pulse pile-up countrates were restricted to less than $500s^{-1}$. The Si(Li) detector was apertured with the same lead collimator as used in the cross section measurements. The NaI(Tl) detector was apertured by 1 cm thick lead with a 0.5 cm diameter hole to ensure that the photons avoid the edges and strike the crystal normally. The scintillation pulses from the NaI(Tl) detector, powered by a 1.1kV bias, were processed and amplified by a Harshaw MB11 preamplifier and a 472A Ortec amplifier. These pulses and those from the Si(Li) detector were monitored on a cathode ray oscilliscope and fed into a Canberra (series 35) multichannel analyser (figure 5.5). The data aquisition system allows storage of spectra on magnetic tape and offers plotting and printing facilities.

Thick Ni and Zn targets were placed at 45^0 to the detector axis and fluoresced by Ag K x-rays from the variable x-ray energy source placed at 90^0 to the detector (figure 5.5iii). Although Rb and Mo

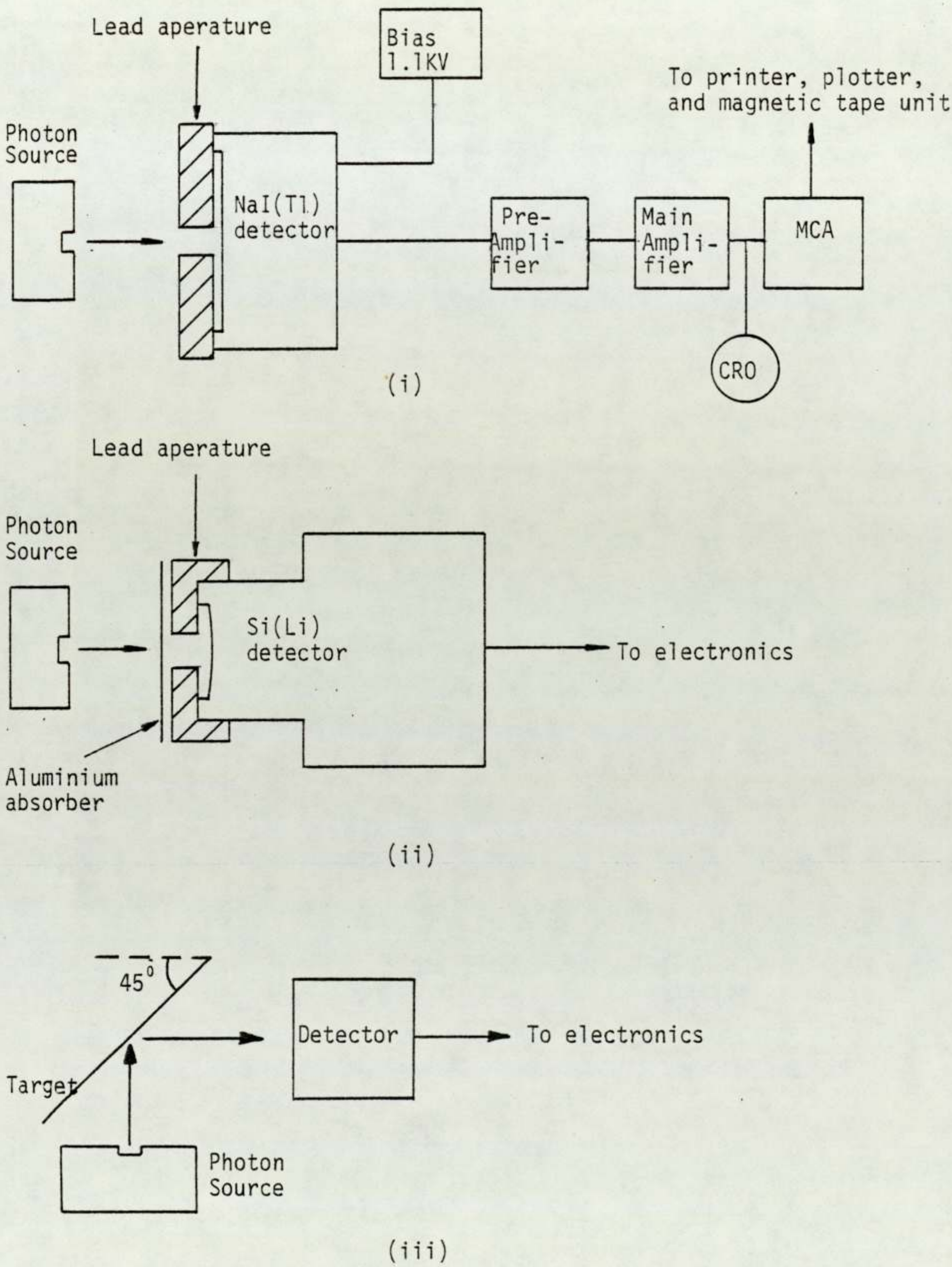

Figure 5.5. Schematic representation of the electronics for Si(Li) detector efficiency measurements.

K x-rays were also available and have energies closer to the K absorption edge of Ni and Zn and thus would ideally be chosen for fluorescing these elements, their intensities were low and consequently were not used. Source to detector distances were typically 1.5 cm.

Figures 5.6 and 5.7(i) show Mo K x-rays detected by Si(Li) and NaI(Tℓ) detectors respectively. As the figures show the NaI(Tl) spectrum is complicated compared to the Si(Li) spectrum. In the letter case the detected number of x-rays for a given collection time were simply obtained by summing the counts under the characteristic peaks and subtracting the appropriate background, assumed linear.

The procedure is somewhat more complicated in the case of NaI(Tl) spectrum. The K_α and K_β components of the Mo K x-rays are not resolved by the NaI(Tl) detector, as shown in figure 5.7(i). The characteristic K x-ray peak rests on a prominent continuum which originates from different physical processes. The high energy distribution consists of a 60 keV gamma-ray peak from the ^{241}Am variable x-ray energy source which also undergoes Compton scattering in the source and produces a peak of approximately 50 keV energy. The continuum is enhanced further by Compton scattering in the source and the detector. Both these peaks produce their associated iodine escape peaks at about 21 keV and 11 kev respectively which lie under the Mo k x-ray peak. These escape peaks make it difficult to obtain the area under the Mo x-ray peak in the same manner as described for the Si(Li) spectrum. For this reason the escape peak contributions have to be extracted before the area can be found. The following method was adopted for achieving this. A background spectrum was generated for each of the test photons from the variable x-ray energy source and for Ni and Zn which were fluoresced by this source. The characteristic x-rays of elements Ni and Mo were absorbed with Al of thickness upto 6 mm and of Ag and Ba with Ti

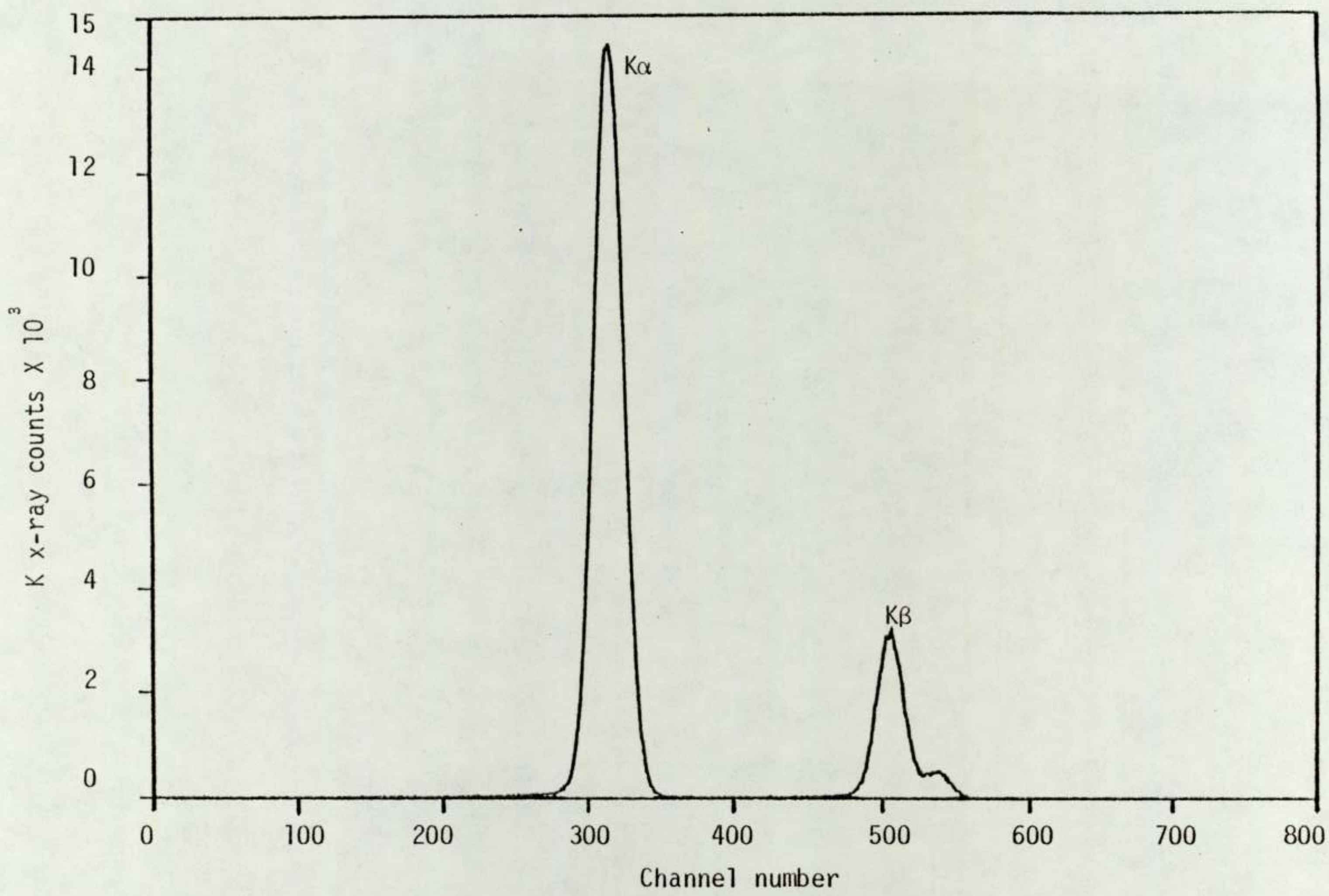

Figure 5.6. Molybdenum K x-rays detected with a Si(Li) detector.

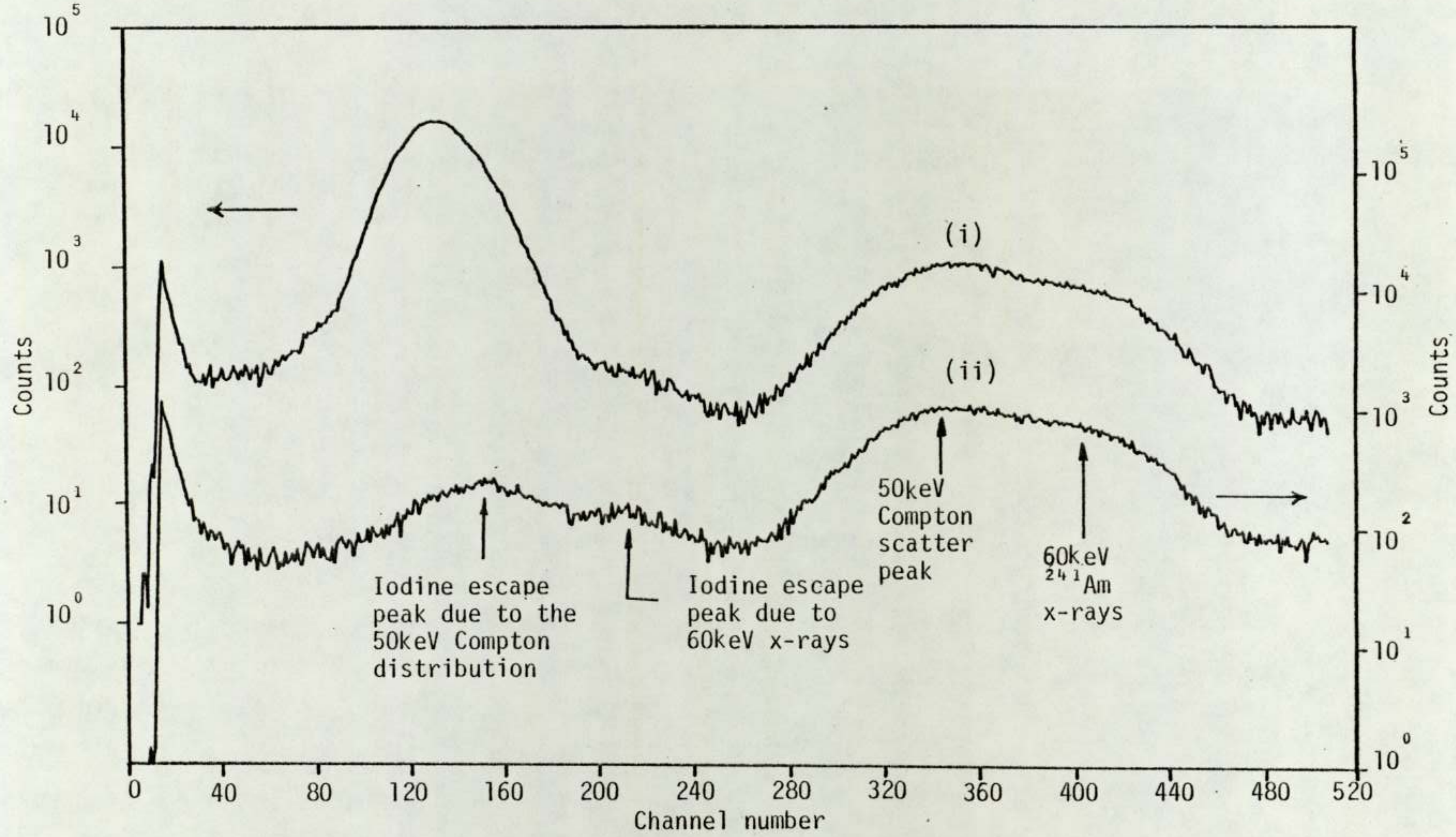

Figure 5.7. (i) Molybdenum K x-rays detected with a NaI(Tl) detector. (ii) 'Background' spectrum for Mo showing the iodine escape peak, the 60 keV x-ray peak and its associated Compton distribution.

of thickness upto 5 mm. The resulting background spectrum was accumulated until the area under the Compton + 60 keV distribution was equal to the area under the same distribution in the initial composite spectrum. Subtracting the background spectrum from the composite spectrum gives the characteristic peak and the area can be obtained readily by summing the counts. Figure 5.7(i), (ii) shows the total and the background spectrum for Mo x-rays and figure 5.8 shows the resultant x-ray peak obtained after subtraction. The Compton + 60 keV γ-ray distribution becomes less important as the target element atomic number (Z_2) increases. This is because the 60 keV γ-rays increasingly undergo photoelectric interactions (section 2.5) producing characteristic x-rays as Z_2 increases. This is clearly demonstrated by figures 5.9 and 5.10 which show Cu(Z_2 = 29) and Ag(Z_2 = 47) spectra. For Tb(Z_2 = 65) this distribution was negligible and the iodine escape peaks produced by the Tb x-rays do not interfere with the characteristic peak (figure 5.11). As a result the peak area was determined directly from the spectrum. The x-rays from the ^{55}Fe source lie on a flat distribution and do not pose any problems.

Counting times of upto 30 minutes were adequate to ensure that the statistical uncertainties for x-rays emitted from the variable energy source were insignificant for both detectors. For the ^{55}Fe source times upto 2.5 hours were necessary. In the case of Ni and Zn statistical uncertainties of less than 1.5% were achieved after accumulation times of upto 4 hours. It is difficult to quantify exactly the uncertainties caused by the stripping procedure adopted for NaI(Tℓ) spectra. This is because the Aℓ and Ti absorbers differentially attenuate the 50keV Compton and 60keV γ- ray peaks. This alters the relative intensities of their associated iodine escape peaks. Consequently the contribution of these escape peaks, approximately

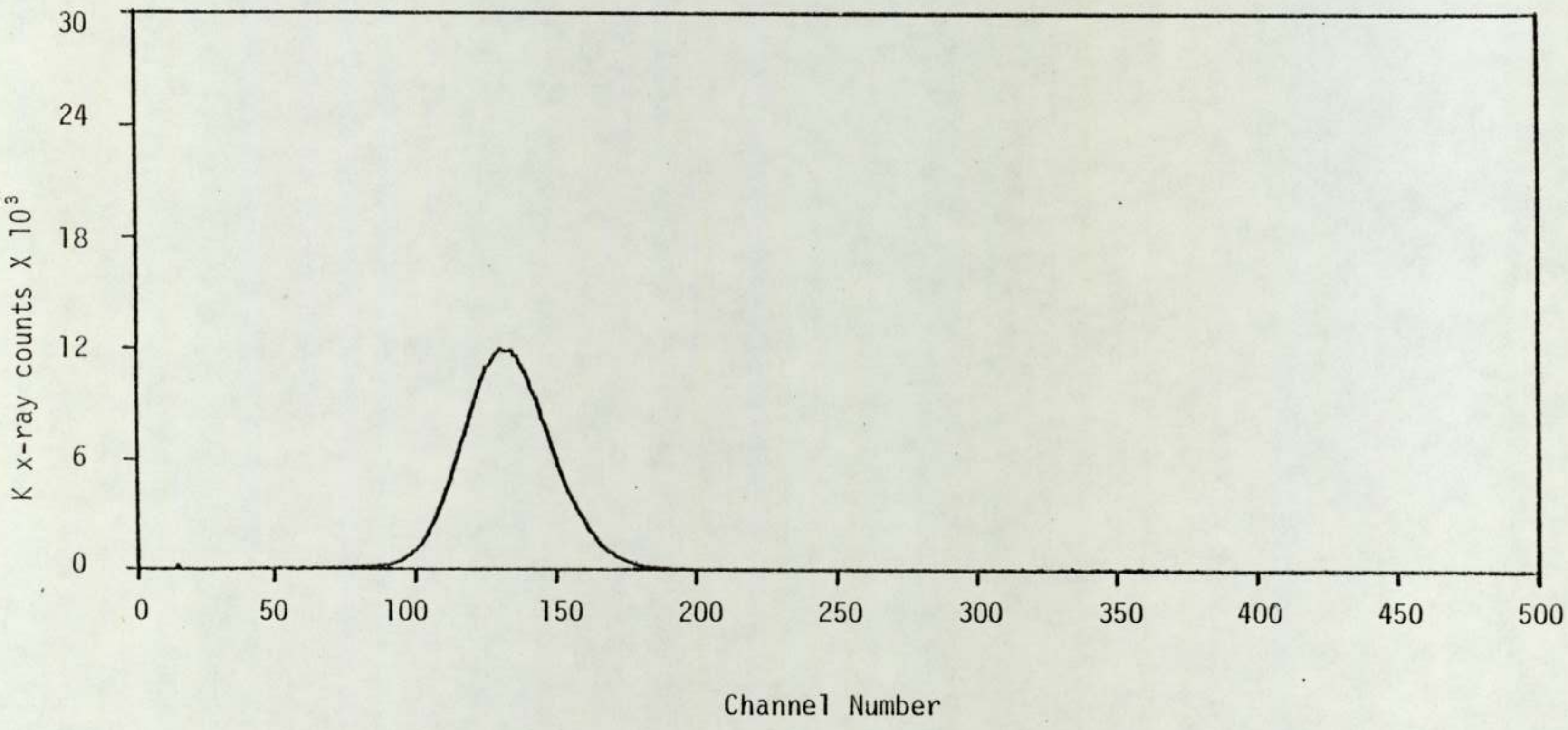

Figure 5.8. The resultant K x-ray spectrum of Mo after substracting 5.7(ii) from 5.7(i).

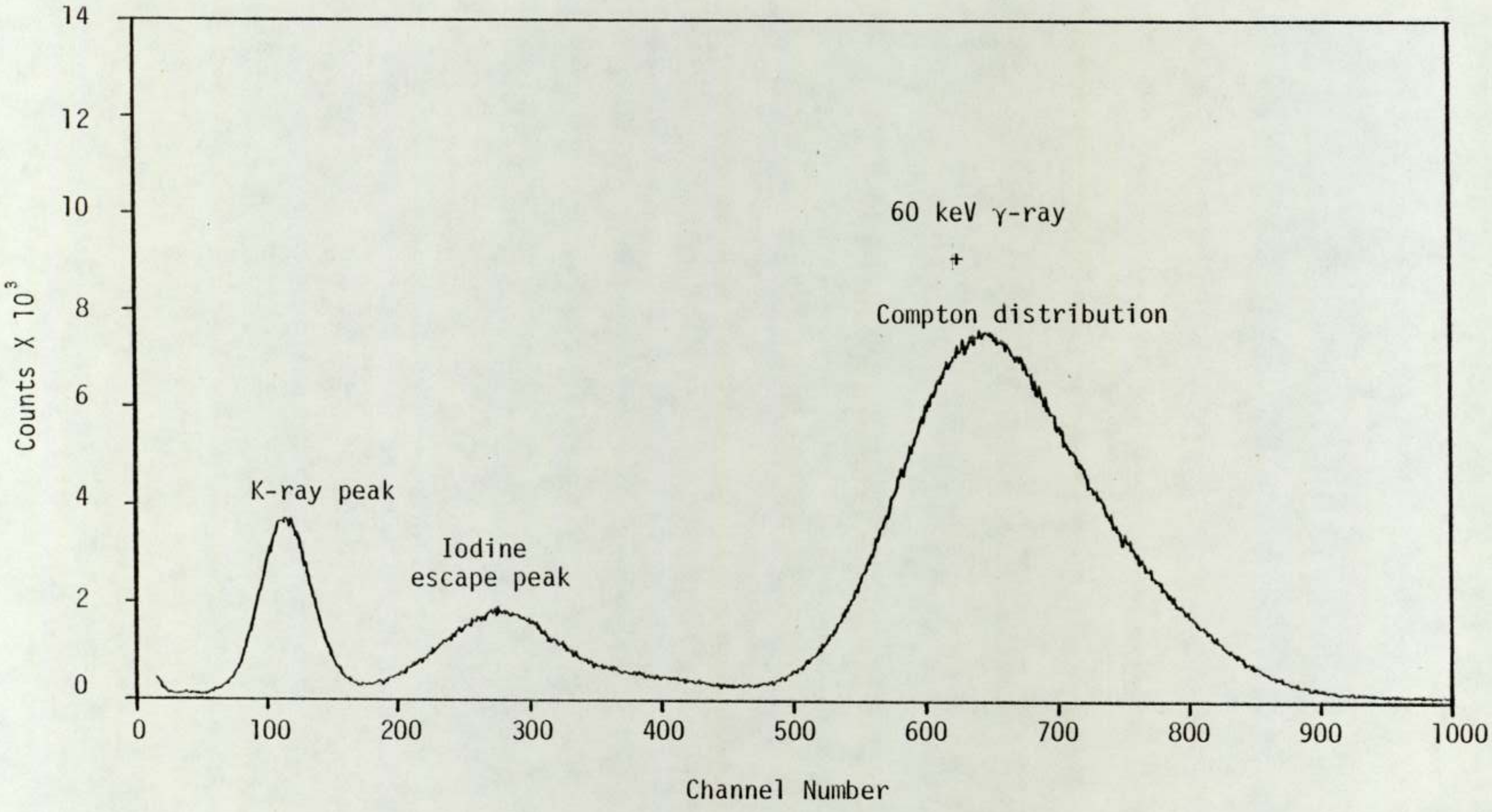

Figure 5.9. Copper K x-rays detected with a NaI(Tl) detector.

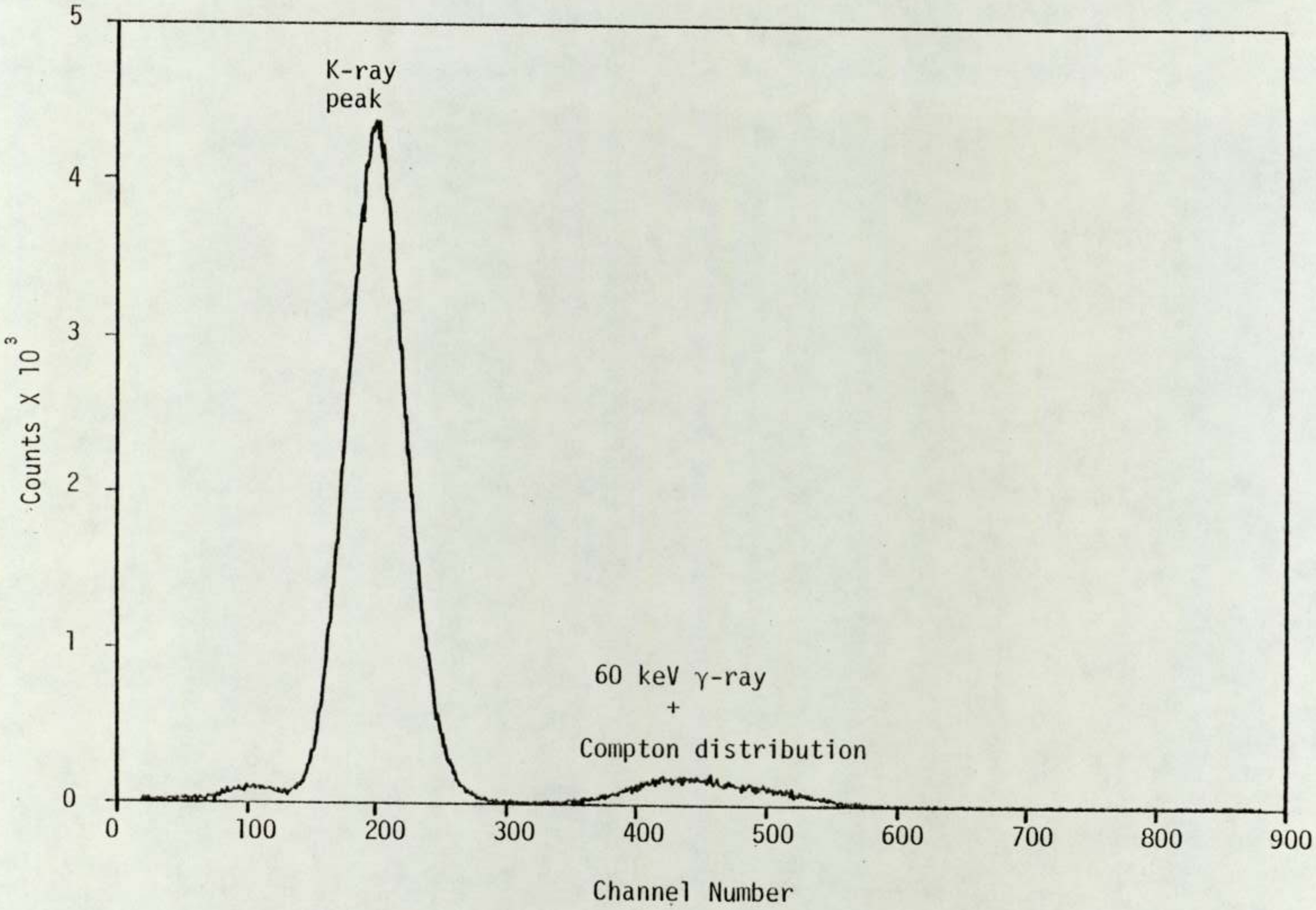

Figure 5.10. Silver K x-rays detected with a NaI(Tl) detector.

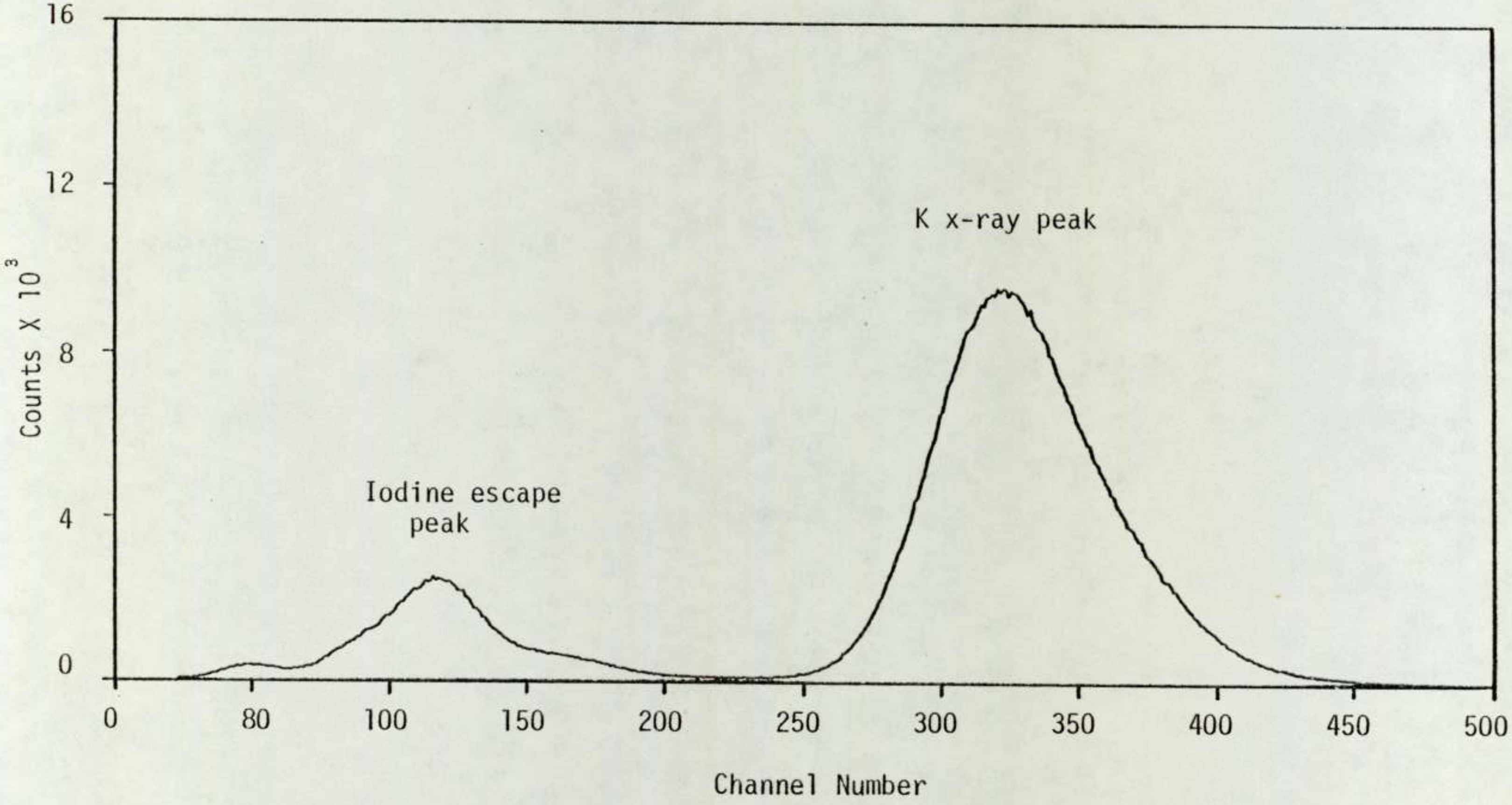

Figure 5.11. Terbium K x-rays detected with a NaI(Tl) detector.

upto 20% of the photopeak, cannot be removed completely from the observed spectra. However, it is expected that most of the contribution is removed and the remaining should be negligible. This situation only applies in the case of Mo where the photopeak rests on top of the escape peaks (figure 5.7). In the case of the other elements the photopeaks either only partially or completely separated from the iodine escape peaks. Changing the region of interest, over which the Compton + 60keV distribution was normalised, caused a variation of less than 2% in the photopeaks of Ni and Zn and less than 1% in the case of other elements. The uncertainties in the detector solid angles were typically 1.5%.

The efficiency of the Si(Li) detector, ε_{si}, can be determined from the expression

$$\varepsilon_{si} = \frac{Y_{si} \exp\left(-\frac{\mu}{\rho}(\rho t)\right)_{air}^{NaI} \Omega_{NaI}}{Y_{NaI} \exp\left(-\frac{\mu}{\rho}(\rho t)\right)_{air}^{Si} \Omega_{Si}} \qquad 5.8$$

where Y_{si} and Y_{NaI} are the photon fluxes detected by the Si(Li) and the NaI(Tℓ) detectors respectively, the exponential terms represent the air correction for both the detectors, t is the air gap and Ω_{Si} and Ω_{NaI} are the solid angles subtended by the two detectors. To evaluate the air absorption correction, mass absorption coefficients were extracted from Storm and Israel (1970). Polynomials were fitted to this data (subsection 5.7.1) and employed to facilitate the calculations for the individual target elements. The uncertainties quoted by Storm and Israel (1970) in their mass absorption coefficient data are 10% for x-ray energies less than 6 keV and 3% for energies greater than 6 keV. For the elements of interest the larger uncertainty applies only to the ^{55}Fe measurements. The air gap, t, was measured precisely using vernier calipers to an uncertainty of less than 0.5%. The total uncertainty in the efficiency calculations were in the range 2 to 3.5%.

Table 5.3 shows the numerical values of ε_{Si} for the elements. A logarithmic polynomial to power 5 was fitted to the experimental data, that is

$$\varepsilon_{Si} = \exp(-15.5404 + 32.077 \ln E_x - 26.4129(\ln E_x)^2 + 10.5938(\ln E_x)^3 - 2.0478 (\ln E_x)^4 + 0.15(\ln E_x)^5 \qquad 5.9$$

Correlation coefficient for the fit is $R^2 = 0.9998$. The fit is shown in figure 5.12 together with the experimental data and the calculated efficiency using expression 5.7 and the manufacturers specifications for the Be window. The discrepencies between experimental data and calculated efficiences is striking. It is only at the higher energies where the two curves tend to converge. The experimental values differ by up to 35% from the calculated values. In the x-ray energy range of interest the absorption in the 200Å gold layer is at most 2% and in the 0.1 μm silicon dead layer it can be ignored. However, as pointed out by Gallagher and Cipolla (1974) the depth of the dead layer may increase with time and may explain some of the discrepencies. An accumulation of dust particles was noticed on the Be window. This will absorb the low energy x-rays reducing the detector efficiency. Cohen (1982) has shown that ice build-up on the front face of the Si crystal reduces considerably the detection efficiency of low energy x-rays. The detector in question is nearly 13 years old and all the above effects are likely to be important and collectively may explain the large differences between theory and experimental data.

Preliminary measurements of L-shell x-ray production cross sections, employing nuclepore backed targets, were corrected only by the calculated detector efficiency (Appendix E). The cross section measurements using carbon backed targets, on which this thesis is mainly base, have been corrected by the experimentally determined efficiency and figure 5.12 highlights the need for doing so. The time difference between the two

Table 5.3. Measured Si(Li) detector efficiency.

X-ray energy* (KeV)	Efficiency
5.959	0.767 ± 0.027
7.558	0.771 ± 0.023
8.136	0.793 ± 0.016
8.735	0.769 ± 0.027
13.596	0.779 ± 0.016
17.781	0.707 ± 0.014
22.581	0.591 ± 0.012
32.89	0.322 ± 0.006
45.469	0.141 ± 0.003

* Weighted x-ray energies from Storm and Israel (1970).

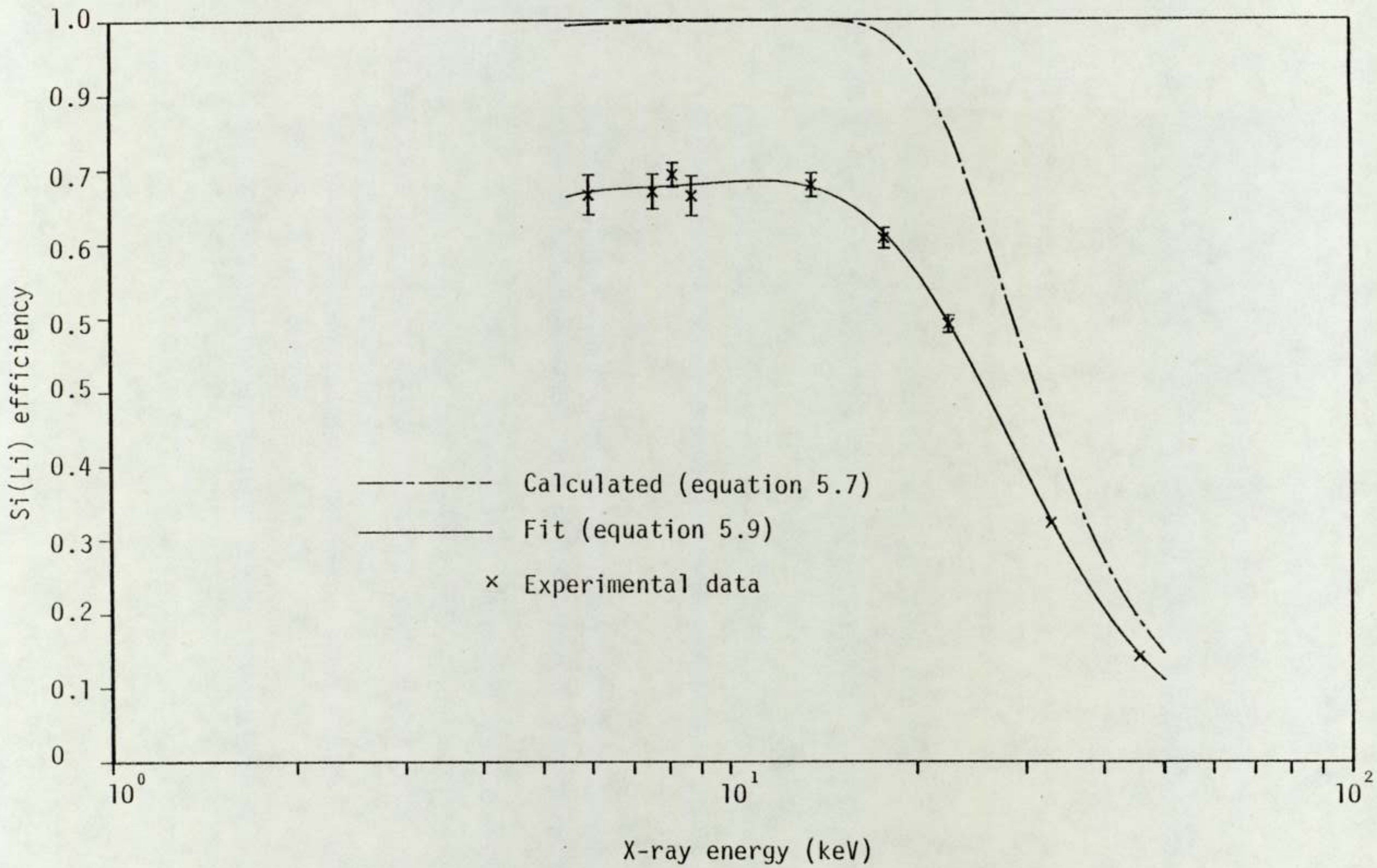

Figure 5.12. Si(Li) detector efficiency as a function of x-ray energy.

sets of cross section measurements was nearly 2.5 years and some deterioration of the detection efficiency would be expected. The efficiency measurements reported in this section were conducted immediately after the x-ray yield experiments for the carbon backed targets had been performed. This avoided the possibility of any further degeneration of the efficiency.

The energy of the Dy $L\ell$ x-rays (5.744 keV) lie just outside the lower energy limit of the efficiency measurements (5.959 keV, see table 5.3). The limited time available for performing the efficiency experiments made it impracticable to extend the measurements to lower x-ray energies. Consequently the efficiency for detecting the Dy $L\ell$ x-rays was obtained by extrapolating equation 5.9.

5.6 TARGET AREAL DENSITY MEASUREMENTS

The uncertainties in the areal densities of the carbon backed targets, quoted by MicroMatter Co, are greater than 25%. Since the precision of the target areal densities will also influence the uncertainty of the cross sections the areal densities have to be determined as reliably as possible. To measure this quantity the nuclear backscattering technique was adopted. The physical concepts on which this method is based were discussed in chapter 3 and this section deals with the procedure and the results of the experiments.

A schematic representation of the electronics employed for measuring target and areal densities is illustrated in figure 5.13. The backscattered particles were measured with a silicon surface barrier (SSB) detector with an active area of 75 mm and thickness of 190 μm and required a 12V power supply. The detector was placed at a backward angle as close as possible to 180^o to the beam axis as the experimental arrangement allowed. The angle was measured geometrically with an aid of a variable height gauge and checked with a Nikon 1354 type shadow

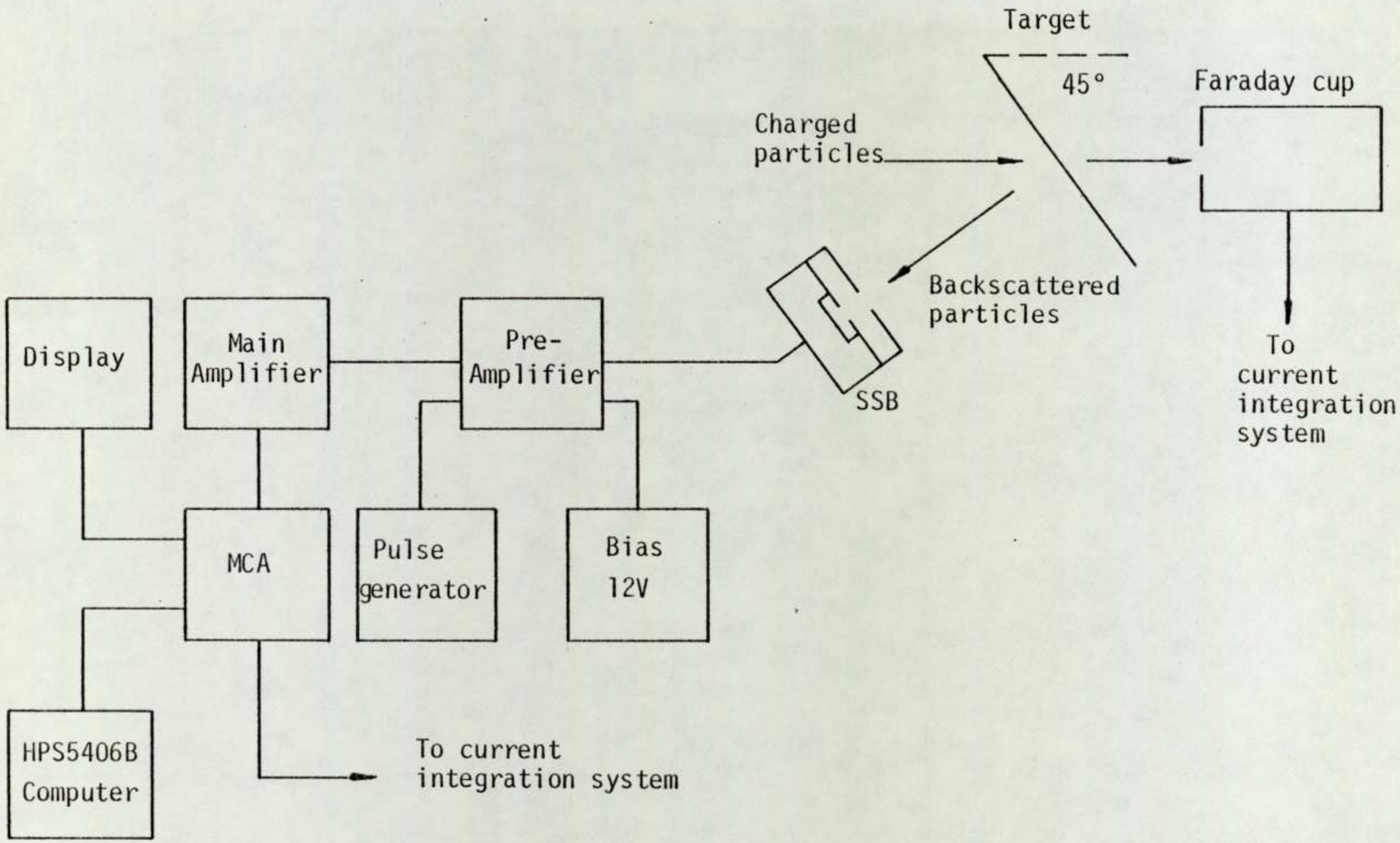

Figure 5.13. Schematic representation of the target thickness measurement system.

graph projector. A value of $144.92^{o} \pm 0.02^{o}$ was obtained. The effect of the uncertainty in the angle on the elastic scattering cross section in minimal and can be neglected. The SSB was aperatured by two tantalum collimators, 5 mm apart and 2.5 mm in diameter, to ensure that a collimated backscattered beam strikes the centre of the active region of the detector. Pulses from the SSB were processed by a preamplifier and a 472A Ortec main amplifier and then fed into an MCA of the HP5406B data aquisition system (subsection 5.4.2). The charge collection procedure is identical to that described in subsection 5.4.1. To eliminate pulse pile-up counting rates were kept below $500s^{-1}$ while maintaining good statistics (< 3%). In many cases the statistical uncertainties were negligible. Performance of the electron system was monitored by feeding test pulses of the same characteristics as the pulses due to the scattered particles into the preamplifier. Employing equation 3.22 the areal densities of the thin targets can be determined from the measured backscattered yield. Expression 3.22 however, has to be modified since the target were positioned at 45^{o} to the beam axis, that is,

$$(\rho t) = \frac{A_2 \, Y_B}{N_0\sqrt{2}\left(N_p\Omega\sigma + Y_B\,\frac{\varepsilon(E)}{E}\right)} \qquad 5.10$$

where (ρt) denotes the target areal density, ρ is the mass density of the target with atomic mass A_2, Y_B is the experimentally measured backscattered yield, Ω is the SSB solid angle, N_p is the number of incident particles with energy E, σ is the Rutherford scattering cross section, $\varepsilon(E)$ is the stopping power of the particles at energy E in the target and N_0 is the Avogadro's number.

X-ray fluorescence calibration targets, backed on nucelpore ($1mg/cm^2$), and used for the initial L x-ray production cross sections

(Appendix E), were utilised to verify the integrity of the thickness measuring system. Thicknesses of these thin targets were quoted by the manufactureres to within 5% and thus are ideally suited for testing the system. Thicknesses of Pd, Te, Dy, Au and Pb targets were measured with incident proton and alpha particles at selected impact energies. Backscatter spectra for 2.5 MeV protons and alpha particles impiring on Au are illustrated in figures 5.14 and 5.15. The figures show the carbon and oxygen 'edges', due to the polycarbonate backing, as well as the Au and pulser peaks. The position of the Te peak centroid, or more strickly the high energy edge of the peak, corresponds to a particle energy (E_1) of KE, where K is the kinematic factor for the collision system and E is the incident projectile energy (see section 3.3). Energy calibration of the system was performed by noting the peak positions and a linear relationship, as expected, between the peak positions and incident particle energy was established. Calibration was checked everytime prior to conducting each experiment. A typical least square fit to the calibration data for incident alpha particles is

$$E_1 = 0.160 + 0.01212c \qquad 5.11$$

where c is the channel number corresponding to the high energy edge of the peak. The corresponding correlation coefficient is $R^2 = 0.9996$. Although energy calibration of the system is not of primary importance in the context of target thickness measurement, it does, however, serve the purpose of testing the system response and give confidence in the measuring technique.

Low beam currents of about 3nA were used to reduce the possibility of target damage and as a result count rates were low enough to exclude the problem of pulse pile-up. Accumulation times of the order of a few minutes sufficed to reduce counting statistics to less than 3% for

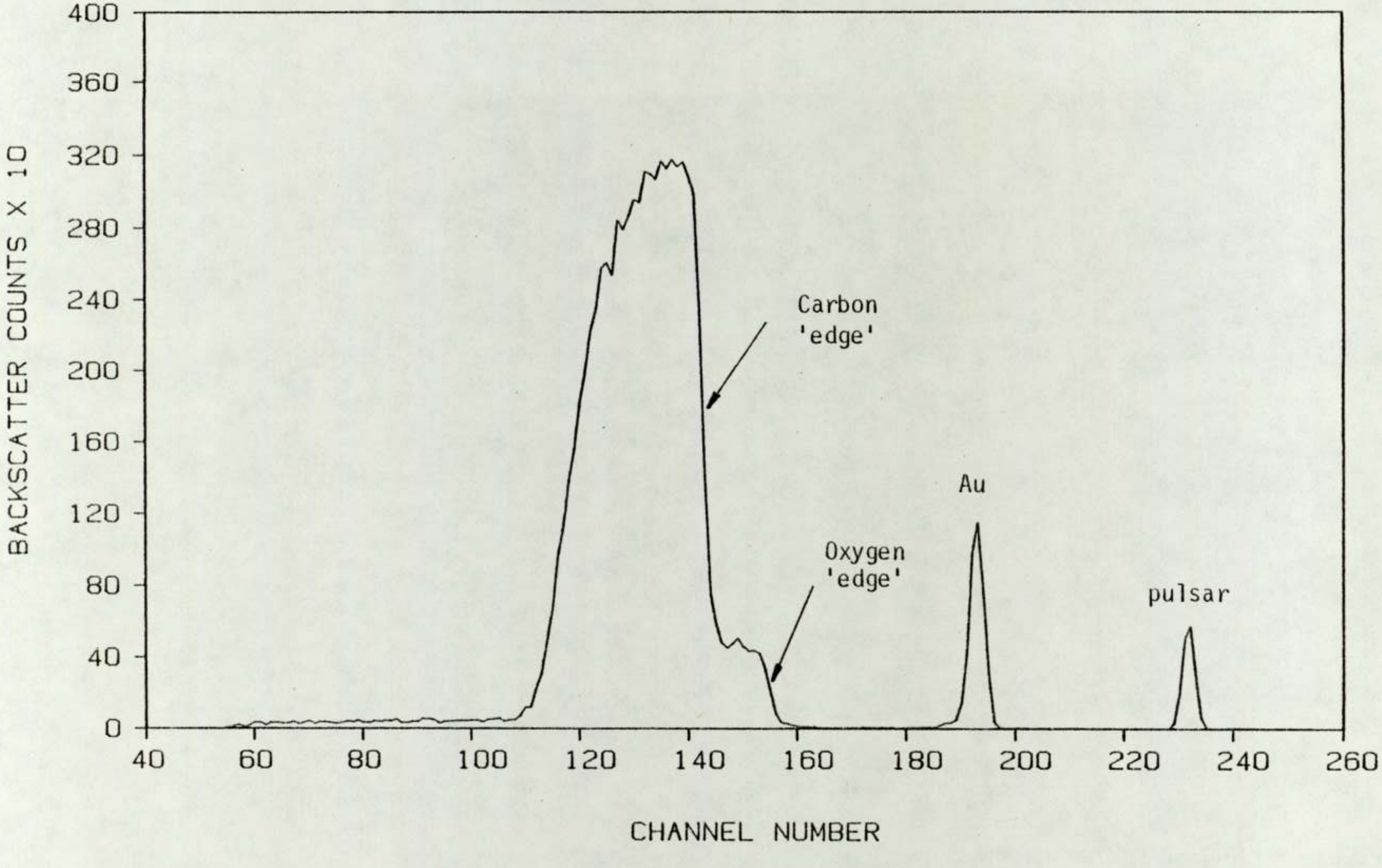

Figure 5.14. A backscattering spectrum of Au(1mg/cm^2 nuclepore backing) bombarded by 2.5 MeV protons.

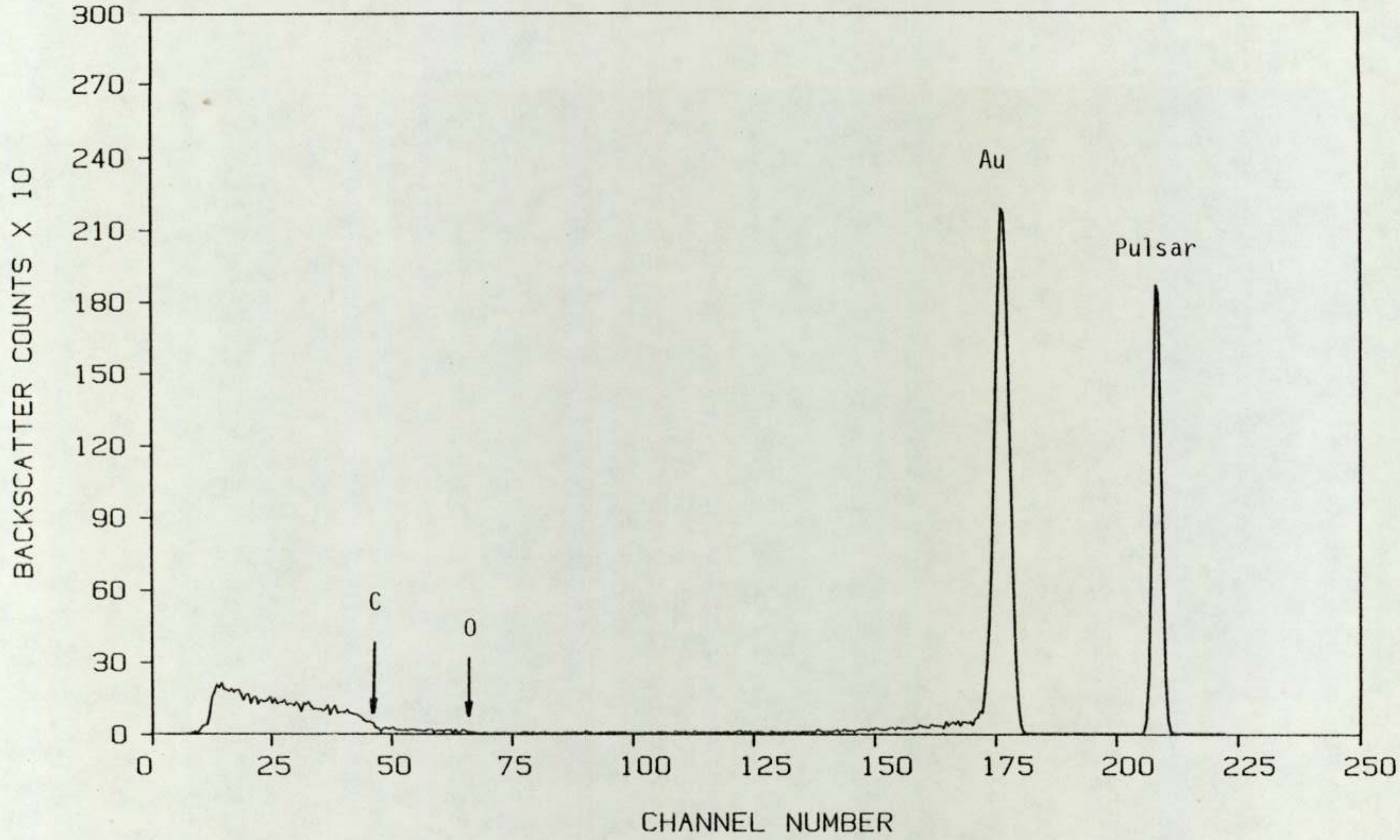

Figure 5.15. A backscattering spectrum of Au (nuclepore backing) bombarded by 2.5 MeV alpha particles.

proton impact and make them unimportant for alpha particle impact. An interactive software routine, which formed a part of the Hewlett-Packard data manipulation package, was used to determine the peak areas. The routine employs a linear model for the background over a region of interest defined by the user. Relatively small changes in the region of interest have only a minimal affect on the peak areas. Corrections for the variation of the Rutherford scattering cross section in the target was insignificant for protons and less than 2% for alpha particles.

In the case of carbon backed targets beam currents of up to 100 nA were employed which allowed yields of considerable precision to be accumulated within a few minutes while exercising due care to avoid problems of pulse pile-up. Since the target and the backing are thin the backscattering spectrum consists of peaks, as is clearly illustrated in figures 5.16 and 5.17 for Au bombarded by 2.4 MeV protons and alpha particles respectively. Comparison of the figures demonstrate how the relative intensities of low and high Z_2 elements change with projectile atomic number. For DyF_3, YbF_3, ThF_4 and UF_4 targets proton impact was avoided and measurements were performed only with alpha particles in order to minimise the possibility of nuclear reactions which would complicate backscattering spectra. To determine the stopping power of the alpha particles in these targets and WO_3, individual $\varepsilon(E)$, weighted according to their atomic masses, were summed. Effect of variation of σ in the target for incident alpha particles on the areal densities was about 2% at low energies and decreases as E increases.

The main factors which determine the precision of the measured areal densities are

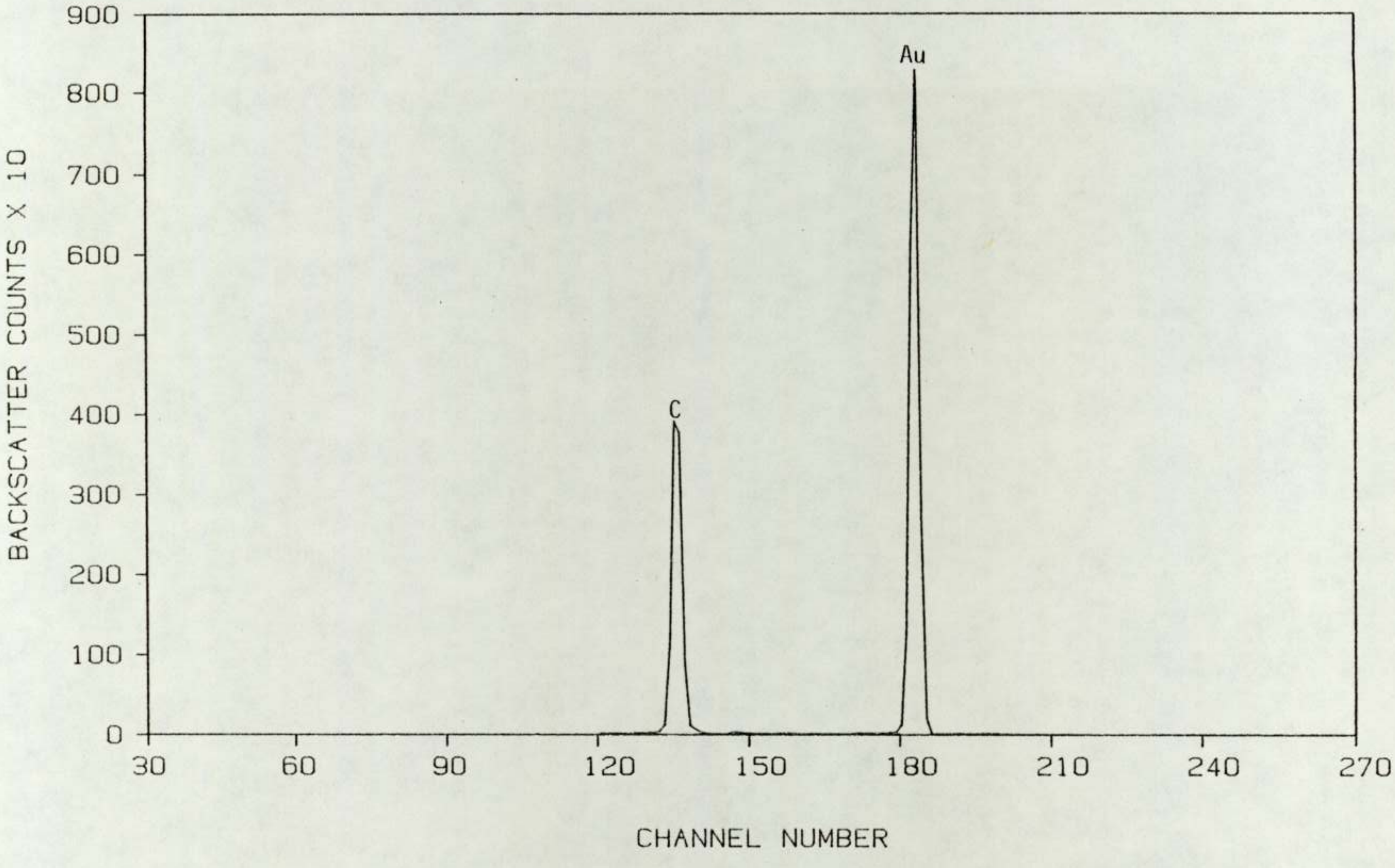

Figure 5.16. A backscattering spectrum of Au(40μg/cm^2 carbon backing) bombarded by 2.4MeV protons.

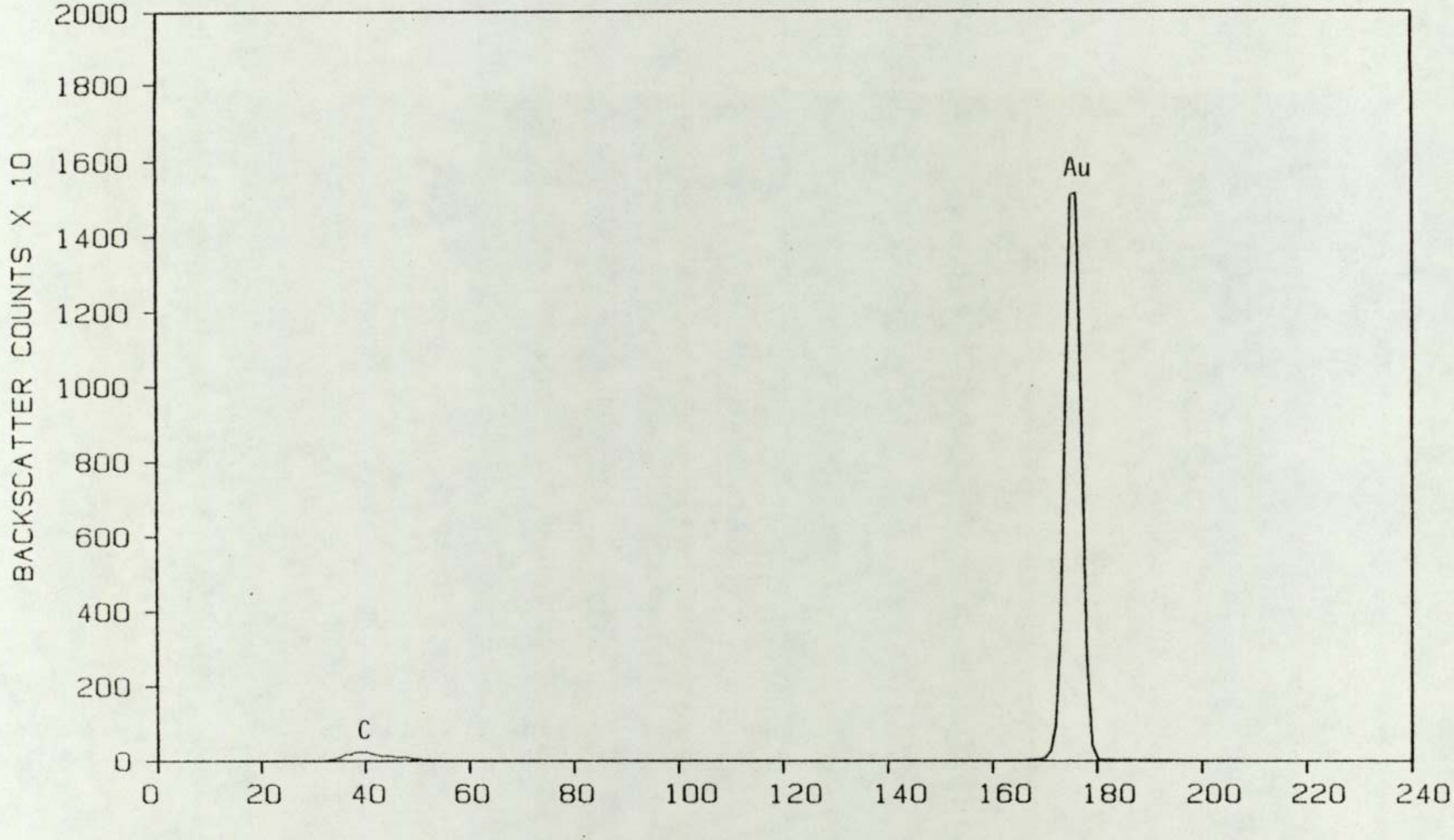

Figure 5.17. A backscattering spectrum of Au ($40\mu g/cm^2$ carbon backing) bombarded by 2.4MeV alpha particles.

(i) counting statistics <3%

(ii) beam current measurement 1%

(iii) SSB solid angle 1.5%

(iv) Rutherford scattering cross section <1.4%

The uncertainty in the Rutherford scattering cross section, which is proportional to E^{-2}, is due to E being uncertain by up to 0.7% (subsection 5.2.1). Uncertainties of the experimentally determined stopping powers range typically 5 - 10% in the literature. However, since $\varepsilon(E)$ appers only in the correction (equation 5.10) the uncertainty in $\varepsilon(E)$ has a negligible affect on the final precision of (ρt). The total uncertainty in (ρt) is obtained by combining the individual percentage errors quadratically and ranges from 2 - 4%.

The measured areal densities, and their values quoted by Micro-Matter and Co., are tabulated in tables 5.4 and 5.5. Values for all targets backed by nuclepore (table 5.4) agree within the precision quoted by the manufacturers (± 5%). Agreement is very good not only between the values at different energies but also between the proton and alpha particle data. In the case of targets backed by carbon the internal consistency of the data is very good(table 5.5). Although the measured areal densities differ markedly from those quoted by the manufacturers for some elements they do however, agree within the uncertainty specified by MicroMatter and Co (25%). Weighted means of the areal densities, measured by proton and alpha particle impact, were used in the calculations of experimental cross sections and are listed in table 5.5. The uncertainties in the means were less than 1.5%.

5.7 DETERMINATION OF EXPERIMENTAL CROSS SECTIONS

The procedure adopted for evaluating L shell x-ray production and ionisation cross sections from the measured x-ray yield is outlined in this section.

Table 5.4. Measured areal densities for nuclepore backed targets.

Target	Proton energy MeV	$(\rho t)^E$ $\mu g/am^2$	Alpha particle energy MeV	$(\rho t)^E_2$ $\mu g/cm$	$(\rho t)^M$ $\mu g/cm^2$
Pd	2.0	50.7 ± 1.5	1.5	49.3 ± 1.0	49.0 ± 2.5
	2.5	51.4 ± 1.5	2.0	49.0 ± 1.0	
	3.0	49 ± 2			
Te	2.5	50.1 ± 1.5	2.0	48.6 ± 1.0	50.0 ± 2.5
	3.0	49 ± 2	2.5	50.3 ± 1.0	
Dy	2.0	49.7 ± 1.3	1.5	48.6 ± 1.0	52.0 ± 2.6
	2.5	48.5 ± 2.0	2.0	49.0 ± 1.0	
	3.0	50 ± 2	2.5	50.0 ± 1.0	
Au	2.0	35.5 ± 0.9	1.5	36.1 ± 0.7	35.0 ± 1.8
	2.5	34.1 ± 1.0	2.0	34.9 ± 0.7	
	3.0	34.6 ± 1.4	2.5	35.2 ± 0.7	
Pb	2.6	40.9 ± 1.2	2.0	39.9 ± 0.8	39.0 ± 2.0
	3.0	41.8 ± 1.7	2.5	40.1 ± 0.8	

E = Experimental values M = Values quoted by MicroMatter and Co.

Table 5.5. Measured areal densities of carbon backed targets.

Target	Element of interest	Proton energy (MeV)	$(\rho t)^E_2$ ($\mu g/cm^2$)	Alpha particle energy (MeV)	$(\rho t)^E_2$ ($\mu g/cm^2$)	Mean $(\rho t)^E_2$ ($\mu g/cm^2$)	$(\rho t)^M$ ($\mu g/cm^2$)
DyF_3	Dy	-	-	2.4	32.4 ± 0.6	32.8 ± 0.5	28 ± 7
				3.0	33.3 ± 0.7		
YbF_3	Yb	-	-	2.0	36.7 ± 0.7	36.5 ± 0.4	35 ± 9
				2.4	35.9 ± 0.7		
				3.0	36.8 ± 0.7		
WO_3	W	2.0	45.7 ± 1.1	2.0	44.9 ± 0.9	45.5 ± 0.4	37 ± 9
		2.4	46.9 ± 1.2	2.4	45.1 ± 0.9		
		3.0	44.9 ± 1.8	2.9	45.7 ± 0.9		
Au	Au	2.0	57.5 ± 1.2	2.0	55.4 ± 1.1	56.9 ± 0.5	52 ± 13
		2.4	56.9 ± 1.1	2.4	57.3 ± 1.1		
		3.0	56 ± 2	2.9	55.2 ± 1.1		
Pb	Pb	2.0	62.1 ± 1.9	2.6	61.6 ± 1.2	61.9 ± 0.7	57 ± 14
		2.6	60.8 ± 1.8	3.0	62.4 ± 1.2		
		3.0	63.1 ± 25				
Bi	Bi	2.0	60.2 ± 1.8	2.2	59.1 ± 1.2	60.0 ± 0.6	50 ± 13
		2.6	61.5 ± 1.8	2.6	60.3 ± 1.2		
		3.0	60 ± 2	3.0	59.8 ± 1.2		
ThF_4	Th	-	-	2.0	33.7 ± 0.7	34.3 ± 0. 5	30 ± 8
				2.6	34.8 ± 0.7		
UF_4	U	-	-	2.4	41.0 ± 0.8	41.3 ± 0.6	42 ± 11
				3.0	41.5 ± 0.8		

E = Experimental values   M = Values quoted by MicroMatter and Co.

5.7.1 L shell X-Ray Production Cross Sections

For a thin elemental target (Z_2) of thickness, t, and atomic density, n, the L x-ray yield, Y_{L_j} produced by N_p charged particles (Z_1) impinging normally on the target at a given energy (E), is related to the appropriate L_j x-ray production cross section, $\sigma_{L_j}^X$, and is given by

$$Y_{L_j} = N_p n\ t\ \sigma_{L_j}^X \qquad 5.12$$

where j represents an L x-ray group transition, α, β or γ, or an individual transition such as ℓ. Expression 5.12 assumes that the x-rays are emitted isotropically and the target is thin enough to ensure that self-absorption of the x-rays and variation of σ_{L_j} in the target is negligible. In the present experimental arrangement the target is at 45° to the beam axis (subsection 5.2.4) and the number of x-rays detected are limited by the detector solid angle, Ω, and thus equation 5.12 becomes

$$Y_{L_j} = N_p\ n\ t\ \sigma_{L_j}^X\ \frac{\Omega}{4\pi}\sqrt{2} \qquad 5.13$$

Since $n = N_0\rho/A_2$

$$Y_{L_j} = \frac{N_p\ N_0\ \rho\, t\ \sigma_{L_j}^X\ \Omega\ \sqrt{2}}{A_2\ 4\pi} \qquad 5.14$$

where N_0 is the Avogadro's number and A_2 is the target atomic mass. The term ρt is usually referred to as the areal density of the target.

Euqation 5.14 has to be corrected for the attenuation suffered by the x-rays in the 50 μm melinex chamber exit window and 2.5 cm of air before reaching the Si(Li) detector and for the Si(Li) detector efficiency, thus

$$Y_{L_j} = \frac{N_p\ N_0\ \rho t\ \sigma_{L_j}^X\ \Omega}{A_2 4\pi}\sqrt{2}\quad \varepsilon_j\ C_{L_j} \qquad 5.15$$

where ε_{L_j} and C_{L_j} are the detector efficiency and the total absorption correction for the L_j x-rays. By rearranging 5.15 $\sigma^x_{L_j}$ can be isolated,

$$\sigma^x_{L_j} = \frac{Y_{L_j} A_2 4\pi}{N_p N_0 \rho t \Omega \sqrt{2} \varepsilon_{L_j} C_{L_j}} \qquad 5.16$$

The importance of correcting for the variation of the x-ray production cross section in the target for low energy α-particles was indicated in section 5.3. Applying this correction given by equations 5.2 to 5.16 we arrive at

$$\sigma^x_{L_j} = \frac{Y_{L_j} \ A_2 \ 4\pi}{N_p N_0 (\rho t) \Omega \sqrt{2} \varepsilon_{L_j} \ C_{L_j}} \left[1 - \frac{atn\varepsilon(E)}{2E}\right]^{-1} \qquad 5.17$$

L shell x-ray production cross section were evaluated from the above equation. Y_{L_j} were determined with the aid of a spectrum fitting programme, discussed in subsection 5.7.3. The determination of N_p, ρt and ε_{L_j} has already been addressed in sections 5.4, 5.6, and 5.5 respectively and the measurement of Ω and the airpath in subsection 5.4.2. The atomic parameters, A_2 and N_0 and the mass densities, ρ, were obtained from Tennet (1978). The total x-ray absorption correction, C_{L_j}, is given by

$$C_{L_j} = \exp\left[-\left(\frac{\mu}{\rho}\right)_{air} (\rho t)_{air} - \left(\frac{\mu}{\rho}\right)_M (\rho t)_M\right] \qquad 5.18$$

where M represents the melinex window. The mass absorption coefficients, μ/ρ, for melinex and air were calculated using the mixture rule (equation 2.15). μ/ρ values for the individual constituents of air and melinex were extracted from Storm and Israel (1970). To facilitate calculation of $\sigma^x_{L_j}$ logarithmic polynomials of the form

$$\ln\left(\frac{\mu}{\rho}\right) = \sum_{i=0}^{5} a_i \left[\ln(E_X)\right]^i \qquad 5.19$$

were fitted to the values of μ/ρ for x-ray energies (E_X) between 3 - 30keV employing the linear least square method. a_i represents the least square coefficients and are listed in table 5.6 for melinex and air along with the values of the regression correlation coefficient R^2

Table 5.6. Least square coefficents, a_i, for polynominal fits to mass absorption coefficients of melinex and air (equation 5.19).

Coefficients	Melinex	Air
a_0	13.1642	5.2206
a_1	-16.7939	3.7207
a_2	14.4835	-5.3016
a_3	-7.2330	2.0064
a_4	1.7124	-0.3713
a_5	-0.1551	0.0268
R^2 (+)	0.9999	0.9999

+ R^2 = Coefficient of regression (equation 5.4).

(equation 5.4). The fact that the values of R^2 are very nearly unity indicates the excellent correlation between the regression model (equation 5.19) and the mass absorption coefficient data. Discussion of experimental x-ray production cross sections and their comparison with the ECPSSR theory is contained in chapter 6. The x-ray transitions, for which the cross sections were measured, for each target will also be indicated in that chapter. The uncertainties in σ_{Li}^{x} are discussed in subsection 5.7.4.

5.7.2 L shell Ionisation Cross Sections

L shell x-ray production cross sections can be related to the individual L subshell ionisation cross sections, σ_{Li} (i = 1, 2, 3), in terms of the atomic parameters discussed in chapter 2. Relationships for the major L shell x-ray transitions are

$$\sigma_{L\ell}^{x} = \omega_3 \left[\sigma_{L_1}(f_{12}f_{23} + f_{13} + f'_{13}) + \sigma_{L_2} f_{23} + \sigma_{L_3}\right] \frac{S_{3\ell}}{S_3} \qquad 5.20$$

$$\sigma_{L\alpha}^{x} = \omega_3 \left[\sigma_{L_1}(f_{12}f_{23} + f_{13} + f'_{13}) + \sigma_{L_2} f_{23} + \sigma_{L_3}\right] \frac{S_{3\alpha}}{S_3} \qquad 5.21$$

$$\sigma_{L\beta}^{x} = \omega_1 \quad \sigma_{L_1} \frac{S_{1\beta}}{S_1} + \omega_2 \left[\sigma_{L_1} f_{12} + \sigma_{L_2}\right] \frac{S_{2\beta}}{S_2}$$

$$+ \omega_3 \left[\sigma_{L_1} (f_{12}f_{23} + f_{13} + f'_{13}) + \sigma_{L_2} f_{23} + \sigma_{L_3}\right]\frac{S_{3\beta}}{S_3} \qquad 5.22$$

$$\sigma_{L\gamma}^{x} = \omega_1\sigma_{L_1} \frac{S_{1\gamma}}{S_1} + \omega_2 \left[\sigma_{L_1} f_{12} + \sigma_{L_2}\right] \frac{S_{2\gamma}}{S_2} \qquad 5.23$$

where ω_i (i = 1, 2, 3) is the fluorescence yield for subshell L_i, f_{ik} are the Coster-Kronig nonradiative transitions, f'_{13} is the radiative Coster-Kronig transition, S_i is the total emission rate for subshell L_i and S_{ij} is the emission rate for x-ray transition or group of transitions, denoted by j, to subshell L_i. The major L shell x-ray transitions pertinent to the ongoing discussion, previously shown schematically in figure 2.1, are illustrated again in figure 5.18. It would appear that by substituting the experimental L_j x-ray production

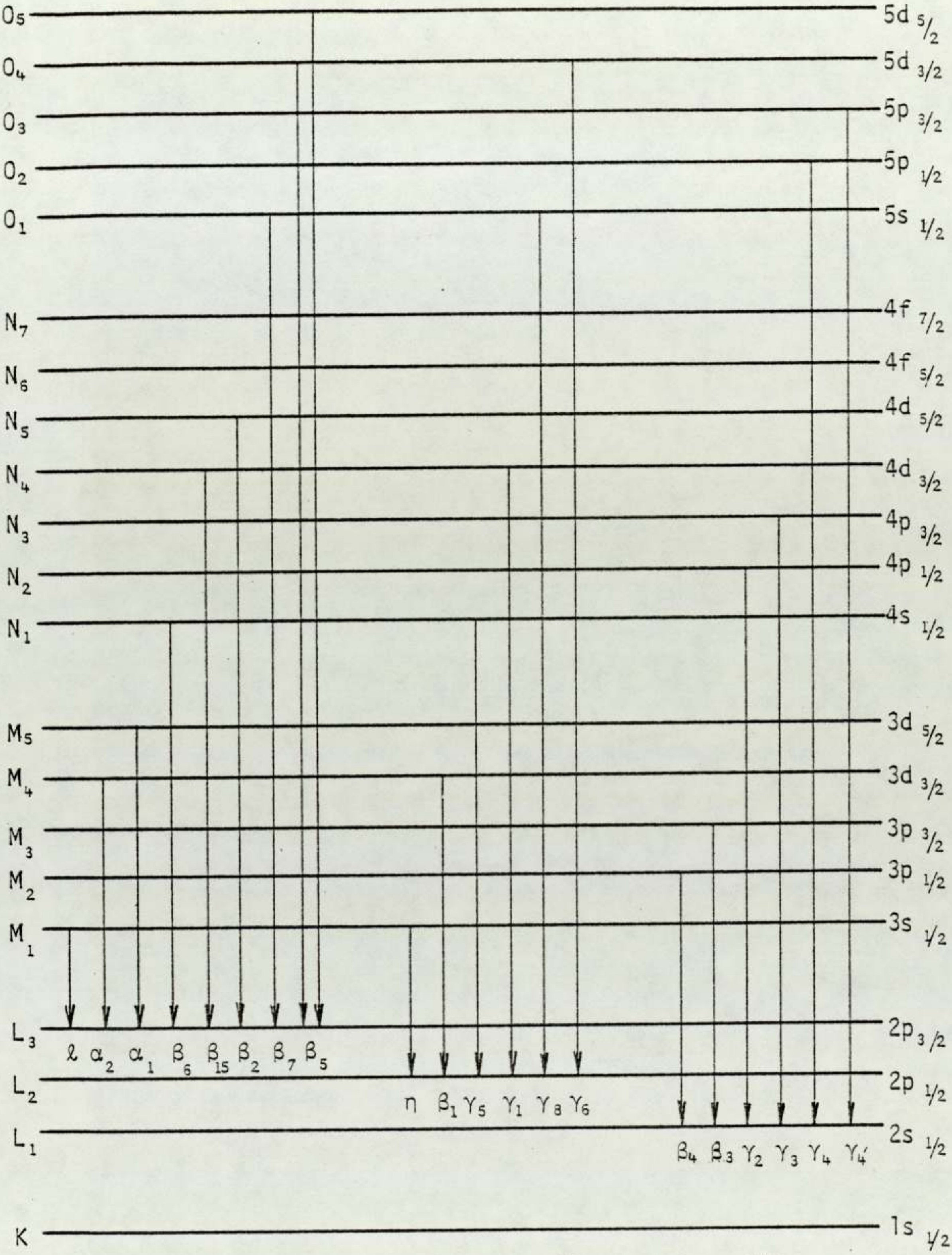

Figure 5.18. Schematic diagram of L shell x-ray transitions (Gray 1974).

cross sections, $\sigma^x_{L_j}$, into the above relations σ_{Li} may be determined by solving them. These equations, however, are not linearly independent and thus are illconditioned. Depending on the degree of illconditioning relatively small changes in $\sigma^x_{L_j}$ can yield disproportionately different values of σ_{Li} and may even lead to unphysical solutions (Madison et al 1974, Cohen 1980 and Sokhi and Crumpton 1982). In order to evaluate σ_{Li}, therefore, expressions have to be developed which are well conditioned and yield stable soltuions. Cohen (1980) has used expressions, involving L subshell x-ray production cross sections in terms of the effective fluorescence yield for the L shell and the total ionisation cross section, to determine σ_{Li}. His approach entails the use of the L_η and L_ℓ x-ray yields which are relatively weak, the former being the weaker transition, and thus involve large statistical uncertainties. An alternative is to extract from the partially resolved L_γ group the L_{γ_1} and $L_{\gamma_{23}}$ components with the aid of a spectrum fitting program. Since the $L_{\gamma_{23}}$ transitions are to the L_1 subshell contributions from the other subshells, through Coster-Kronig transitions, obviously do not arise and thus $\sigma_{L\gamma_{23}}$ can be directly related to σ_{L_1} through the simple relation

$$\sigma_{L\gamma_{23}} = \omega_1 \ \sigma_{L_1} \ \frac{S_{1\gamma_{23}}}{S_1} \qquad 5.24$$

Employing tabulated values for the fluorescent yields (Krause 1979) and emission rates (Scofied 1974b) σ_{L_1} can be determined from 5.24. The L_{γ_1} yield can now be used to evaluate σ_{L_2}. L_{γ_1} is contaminated on the low energy side by the L_{γ_1} transition, also to the L_{γ_5} subshell. The $L_{\gamma_5}/L_{\gamma_1}$ ratio is typically around 3.5% (Scofield 1974b) and has to be accounted for. The expression for $L_{\gamma_{15}}$ in terms of σ_{L_1} and σ_{L_2} is

$$\sigma^x_{L_{\gamma_{15}}} = \omega_2 \ (\sigma_{L_1} f_{12} + \sigma_{L_2}) \ \frac{S_{2\gamma_{15}}}{S_2} \qquad 5.25$$

These values for σ_{L_1} and σ_{L_2} can then be substituted into equation 5.21 to extract σ_{L_3}.

Experimental L subshell ionisation cross sections reported in this thesis have been evaluated with this approach. This approach, however, requires some qualifying remarks. Firstly, $L_{\gamma_{23}}$ and L_{γ_1} transitions are relatively weak transitions and counting times have to be sufficiently long to ensure reasonable statistical precision. It is for this reason that carbon backed targets, which can sustain high beam currents for relatively long periods, were employed. These targets yielded precisions of better than 5% for $L_{\gamma_{23}}$ group even at low particle energies. The statistics are slightly improved by including the yield of the $L_{\gamma_{44'}}$ transitions, also to the L_1 subshell. Secondly,

a complication arises in that the $L_{\gamma_{23}}$ is contaminated by contributions from the L_{γ_8} transition and, for $Z_2 \geq 71$, by the L_{γ_6} transition. The importance of these transitions is made clear by considering, for example, Au bombarded by 3 MeV protons where $\sigma^{ECPSSR}_{L\gamma_6}/\sigma^{ECPSSR}_{L\gamma_{23}} = 50\%$ and $\sigma^{ECPSSR}_{L\gamma_8}/\sigma^{ECPSSR}_{L\gamma_{23}} = 3.7\%$. These contributions may be estimated by comparing it with the $L\gamma_{15}$ group and employing theoretical radiative rates. The $L\gamma_{23}$ contribution is thus obtained from

$$L\gamma_{23} = L\gamma_{2368} - L\gamma_{15}\,\frac{S_2\gamma_{68}}{S_2\gamma_{15}} \qquad 5.26$$

Datz et al (1974) considered only the $L\gamma_6$ contribution to the $L\gamma_{23}$ peak and obtained it magnitude from the $L\gamma_1$ transition. The obtained an experimental value of 0.125 ± 0.01 for the ratio $S_2\gamma_6/S_2\gamma_1$ for proton impact on Au by comparing the response of $L\gamma_{236}/L\gamma_1$ and $L\gamma_{44'}/L\gamma_1$ at different proton energies. This was not possible in the present study since the $L\gamma_{44'}$ statistics were poor. Instead the theoretical values for the ratio from Scofield 1974b were employed. In the case of Au Scofield's value of $S_2\gamma_6/S_2\gamma_1$ is 0.094 which compares favourable with the value obtained by Datz et al (1974). Taking into account $L\gamma_8$ and $L\gamma_5$ transition the value of the ratio $S_{2\gamma_{68}}/S_{2\gamma_{15}}$ becomes 0.098. The expressions employed for determining the experimental values of σ_{L_i} are summarised below:

$$\sigma_{L_1} = \frac{S_1}{S_{1\gamma_{2344'}}} \frac{\sigma_{L\gamma_{2344'}}}{\omega_1} \qquad 5.27$$

$$\sigma_{L_2} = \frac{S_2}{S_{2\gamma_{15}}} \frac{\sigma_{L\gamma_{15}}}{\omega_2} - f_{12}\sigma_{L_1} \qquad 5.28$$

$$\sigma_{L_3} = \frac{S_3}{S_{3\alpha}} \frac{\sigma_{L\alpha}}{\omega_3} - (f_{13} + f'_{13} + f_{12}f_{23})\sigma_{L_1} - f_{23}\sigma_{L_2} \qquad 5.29$$

The method adopted for extracting the semi-resolved components of the $L\gamma$ group is described in detail in subsection 5.7.3. The values of σ_{L_i}, obtained from the above relations, for the target - projectile combinations of interest are discussed in chapter 6 and the uncertainties are dealt with in subsection 5.7.4.

5.7.3. Spectrum Fitting

Contemporary Si(Li) x-ray detectors are unable to resolve all the individual x-ray transitions to the L-shell. The energy resolution is typically 170eV at 5.898 keV and consequently, groups of several x-ray lines are observed in spectra obtained with these detectors. Figures 5.3 and 5.4 illustrate the L_α, L_β and $L\gamma$ groups for Yb and Bi obtained with 3 MeV alpha and proton impact respectively. In the L_α peak the individual components, L_{α_1} and L_{α_2}, cannot be resolved whereas the components of the L_β and L_γ group may be partially resolved depending on the atomic number of the target. The importance of the individual $L\gamma$ components, required for determining L subshell ionisation cross sections was highlighted in subsection 5.7.2. These components may be resolved sufficiently by adopting a wavelength dispersive detection system which employs a crystal spectrometer. A severe limitation with this approach is the very low detection efficiency relative to the Si(Li) detector. The comparatively high cost further outweighs the advantages offered by such a system.

The usual procedure for extracting the required components of a partially resolved x-ray group is to mathematically 'fit' suitable functions which approximate the Si(Li) detector response. Ideally, the response of a Si(Li) detector to a monoenergetic x-ray would be a delta function. In practice the effects of incomplete charge collection, bulk trapping and detector resolution produces an output which can be described approximately by a Gaussian distribution with a certain amount of skewness (Jenkins et al 1981). In the case of inner-shell x-rays the peak is further broadened by the fact that these x-rays may consist of bi or polyenergetic lines of similar energies, however, the essentially Gaussian profile still applies. The x-ray peak rests on a background which can be adequately described by a straight line function in the x-ray energy range of interest.

Detail studies of fitting non-linear mathematical functions to the response of energy dispersive detectors have been conducted by Gunnink and Niday (1971), Gunnink (1975), McNelles and Campbell (1975), Phillips and Marlow (1976), Horch and Campbell (1977) and Campbell and Jorch (1979). Exponential tailing and stepping functions are usually adopted to simulate the low energy electronic distortions of the main Gaussion. Such a description can be extended to L x-ray spectra containing several fully or partially resolved peaks from which areas of individual peaks can be extracted. As an alternative to the Gaussian description Ingamells and Fox (1979) have utilised Poisson probability functions to determine individual components of composite peaks. With regard to the present study corrections for the distortion of the L x-ray peaks were not found to be necessary. The L x-ray spectra are, therefore, approximated solely by Gaussian distributions super-imposed essentially on a linear bremsstrahlung. The remaining part of this subsection deals with the fitting procedure adopted in this work and based on the nonlinear least square method. Mathematical principles, on which this method relies, are well established and thus have been omitted. The reader interested in the theory of nonlinear regression, however, is referred to Bevington (1969) and Draper and Smith (1981).

An x-ray spectrum of m channels consisting of q Gaussian peaks, resting on a linear background, may be described by the nonlinear analystic function $f(\underline{x}_j, \underline{b})$,

$$f(\underline{x}_j, \underline{b}) = b_1 + b_2 x_j + \sum_{i=1}^{q} b_{2+i} \exp\left[\frac{-(x_j - b_{3+i})^2}{b_{4+i}}\right] \quad 5.30$$

$$(j = 1, 2, \ldots, m)$$

where the independent variable, x_j, represents the j^{th} channel number and b_u ($u = 1, 2, \ldots, p$ where $p = 3q + 2$) are the regression parameters. Thus $f(\underline{x}_j, \underline{b})$ is the fitted value of the actual number of x-ray counts in channel x_j denoted by Y_j. In the exponential term in equation 5.30 b_{2+i} represents the amplitude of the peak, b_{3+i} denotes the peak centroid and b_{4+i} equals $2\sigma_i^2$ where σ_i is the standard deviation of peak i. The regression problem entails computing estimates of the parameters b_u which will minimise the weighted sum of the squares of residuals, known as 'chi square',

$$\chi^2 = \sum_{j=1}^{m} \frac{[Y_j - f(\underline{x}_j m\ \underline{b})]^2}{\sigma_j^2} \quad 5.31$$

where the residuals are weighted by the variances, σ_j^2, associated with each data point. Since x-ray counting experiments follow a Poisson distribution σ_j^2 can be estimated simply by the counts in channel j, denoted by Y_j. Normalising 5.31 by the number of degrees of freedom ν, gives the reduced chi-square, χ_r^2

$$\chi_r^2 = \frac{\chi^2}{\nu} \quad 5.32$$

ν is obtained by subtracting the number of free parameters from the number of data channels (m). Since the height, H_i, of a Gaussian distribution depends on its standard deviation, σ_i, through the relation

$$H_i = \frac{A_i}{\sigma_i(2\pi)^{\frac{1}{2}}} \qquad 5.33$$

where A_i is the i^{th} peak area and is equivalent to Y_{L_j} in equation 5.17, there are 2 free parameters per Gaussian peak (Bevington 1969). The total number of free parameters is, therefore, 2(background) + 2q (q = number of Gaussian peaks) and thus $\nu = m - 2 - 2q$. If the regression function, $f(\underline{x}_j, \underline{b})$, is a good approximation to the measured data then χ_r^2 has a vlaue of unity or near unity. The larger the value of χ_r^2 the less appropriate is the fitting function. A χ_r^2 value of less than one does not indicate an improvement of the fit, it is merely a consequence of the finite uncertainty in the determination of the variance of the fit (Bevington 1969).

To find the least square estimate of $\underline{b}$ equation 5.30 needs to be differentiated and set to zero, giving the minimum value of χ^2;

$$\frac{\partial \chi^2}{\partial \underline{b}} = \sum_{j=1}^{m} \frac{[Y_j - f(\underline{x}_j, \underline{b})]}{\sigma_j^2} \left[\frac{\partial f(\underline{x}_j, \underline{b})}{\partial b_u}\right] = 0 \qquad 5.34$$

Equation 5.34 provides p nonlinear normal equations which have to be solved for $\underline{b}$. This, however, is complicated and it is very difficult to obtain the solution directly. Instead, iterative techniques have to be employed, either to 'search' for the minimum value of χ^2 or to solve the equations analytically.

Chi-square is considered a continuous function of the nonlinear parameters b_u and describes a hypersurface in q-dimensional space (Bevington 1969). χ^2 is minimum at the point defined by the least square estimates. For a linear model the contours of χ^2 in parameter - space, $\underline{b}$-space, consist of concentric ellipses, where as for a non linear model, such as described by equation 5.30, the contours may become distorted and often highly elongated (Draper and Smith 1981). There are several methods with varying degrees of sophistication which can be used for searching for the minimum value of χ^2 in parameter space. Details of these methods can be found in Draper and Smith (1981), Bevington (1969) and Schamber (1981). The main disadvantage of these methods is that the solution converges very slowly when the search approaches the χ^2 minimum particularly when χ^2 contours are attenuated (Draper and Smith 1981).

As an alternative to the 'search' method analytical techniques may be employed to compute the least square parameters. A major technique, known as the 'linearisation' or 'Taylor series' method improves initial estimates of the parameters, denoted by $\underline{b}_0 = (b_{10}, b_{20}, \ldots, bp_0)'$, in successive iterations by using the results of linear least squares. This method has been found to be superior to those which involve searching for the minimum value of χ^2 regarding speed of convergence and reliability of the final solutions (Draper and Smith 1981, Bevington 1969 and Schamber 1981). Consequently this method has been adopted for the fitting of L shell x-ray spectra in this study.

In order to determine the least square values of the nonlinear parameters $\underline{b}$, initial estimtes, $\underline{b}_0$, for these parameters are required. Initial values for the peak centroids and variances were estimated from equation 5.3 and 5.6. Inputing these values into the regression function (equation 5.30) transforms it into a linear form. The remaining unknown parameters, namely those for the background and the peak heights, were determined with the normal linear least square method.

Expanding $f(\underline{x}_j, \underline{b})$ in terms of a Taylor series to first order about the point $\underline{b}_0$, when b is close to $\underline{b}_0$, we have

$$f(\underline{x}_j, \underline{b}) = f(\underline{x}_j, \underline{b}_0) + \sum_{u=1}^{p}\left[\frac{\partial f(\underline{x}_j, \underline{b})}{\partial b_u}\right]_{b = b_0} (b_u - b_{u0}) \qquad 5.35$$

Adopting the following notation

$$f_j^0 = f(x_j, b_0)$$

$$\delta b_u^0 = b_u - b_{u0} \qquad 5.36$$

$$Z_{uj}^0 = \left[\frac{\partial f(\underline{x}_j, \underline{b})}{\partial b_u}\right]_{b = b_0}$$

the regression model may be written approximately as

$$Y_j - f_j^0 = \sum_{u=1}^{p} \delta b_u^0 \, Z_{uj}^0 + e_j \qquad 5.37$$

where e_j is the 'error' and is the deviation of Y_j from the regression curve. It is noted that the model is of a linear form in δb_u^0, the validity of which is true only for the selected first order approximation. Chi-square for the model is given by

$$\chi^2 = \sum_{j=1}^{m} \frac{1}{\sigma_j^2} [Y_j - f_j^0 - \sum_{u=1}^{p} Z_{uj}^0 \, \delta b_u^0]^2 \qquad 5.38$$

Applying linear least square theory χ^2 is minimised with respect to δb_u^0 and the p normal equations required for determining $\delta \underline{b}^0$ in matrix notation are

$$\underline{C}^0 \delta \underline{b}^0 = \underline{B}^0 \qquad 5.39$$

where

$$C^0 = \left[\sum_{j=1}^{m} \frac{1}{\sigma_j^2} Z_{uj}^0 \, Z_{uj}^{0\prime}\right] \delta b_u^0, \quad \text{and}$$

$$B^0 = \sum_{j=1}^{m} \frac{1}{\sigma_j^2} Z_{uj}^{0\prime} (Y_j - f_j^0) \qquad 5.40$$

where prime denote the transpose and u = 1, 2, ..., p. $\underline{C}^0$ is known as the 'curvature' matrix. The partial derivatives were evaluated using the 'centred difference' approximation (Himmelblau 1972),

$$\left[\frac{\partial f(\underline{x}_j, \underline{b})}{\partial b_u}\right]_{b = b_0} = \frac{f(x_j, b_u + \Delta b_u) - f(x_j, b_u - \Delta b_u)}{2\Delta b_u} \qquad 5.41$$

where Δb_u is a small increment. A value of $0.002b_u$ yields derivatives of sufficient precision and was adopted in the calculations. The improvements, δb_u^0, of the initial parameters are arrived at by solving the normal equations. The revised estimates after s iterations are given by

$$b_{us+1} = b_{us} + \delta b_u^s \qquad 5.42$$

where s = o for the initial parameters. From the revised estimates, b_{u1} (s = o for the first iteration), f_j^1 and Z_{uj}^1 are generated and substituted into equation 5.39 to determine δb_u^1 lead to the next revised estimates b_{u2} and so on. Chi-square is calculated for each set of parameters at the end of every iteration. The improvements of the least square estimates after each iteration is indicated by the convergence of χ^2 ; eventually to its minimum value.

Provided that the initial estimates and the subsequent value after each iteration lie inside a region where the χ^2 hypersurface is approximately parabolic the linearisation method coverges quite rapidly to the minimum χ^2 value. On the other hand if the estimates lie far from the least square values the method may not converge at all, indeed, it may even diverge (Draper and Smith 1981, Bevington 1969) implying that the χ^2 surface is so poorly approximated that the linear approximation breaks down (Schamber 1981). However, it is not always possible to arrive at good initial estimates and to reduce the possibility of divergence two modification have to be introduced into the iterative procedure.

(i) The improvements, δb_u^s, calculated after each iterations are 'damped' by an appropriate amount (Marquardt et al 1961), that is, δb_u^2 is multiplied by a factor $\kappa^2 \leq 1$ from which the new estimates are determined.

$$b_{us+1} = b_{us} + \kappa^s \delta b_u^s \qquad 5.43$$

A numerical value for κ^s is chosen which ensures covergence, that is,

$$\chi^2(s + 1) < \chi^2(s) \qquad 5.44$$

and as convergence is approached, κ^s is increased until $\kappa^s \simeq 1$, expediting the iterative procedure. An initial value of 0.4 has been suggested by Schamber (1981). In the present work, however, this value was found to be too large to initiated convergence and a much smaller value of 0.001 was adopted for the first iteration. The value is increased by this amount for successive iterations until convergence seems assured. 10 iterations seemed sufficient for the problems encounted in this study. Byond this iteration κ^s is increased by larger amounts determined from the simple empirical expression

$$\kappa^{s+1} = \kappa^s + 0.01(s - 10) \qquad 5.45$$

until $\kappa^s = 1$.

(ii) In practice failure to converge is not completely eliminated by introducing 'damping' into the fitting technique (Marquardt 1963). To reduce futher the likelihood of divergence Marquardt (1963) proposed an algorithm which greatly enlarges the number of problems that can be successfully solved by nonlinear estimation (Draper and Smith 1981). Marquardt (1963) formulated the required algorithm by combining the properties of the gradient-search and the linearisation methods. In the first method all the parameters in the proposed model are simultaneously incremented by an amount that is adjusted to ensure that the method travels along a 'direction of steepest desent'. Although this method does not converge rapidly when in the immediate vicinity of the χ^2 minimum it is, however, able to approach the minimum when the estimates are far from their least square values. The linearisation method on the other hand, coverges quite rapidly but only when the parameters are not distant from their least square estimates. Marquardt (1963) was able to reach a compromise between the two methods in his algorithm. The algorithm causes the convergence of the iterative procedure by increasing the magnitude of the diagonal terms of the curvature matrix by an amount λ^s,

$$(\underline{C}^s + \lambda^s I)\delta\underline{b}^s = \underline{B}^s \qquad 5.46$$

here I is the identity matrix. Solving for $\delta\underline{b}^s$ and using equation 5.43 the improved estimates are determined. λ^s is selected so as to ensure the validity of the inequality 5.44. The magnitude of λ^s should be small enough to allow rapid convergence when in the neighbourhood of χ^2 minimum and large enough to initiate converge successfully even when distant from the least square values. The algorithm consists of several logical statements that compare the sum of residual, Φ, defined by

$$\Phi = \sum_{j=1}^{m} [Y_j - f(\underline{x}_j, \underline{b})]^2 \qquad 5.47$$

for iteration s and s+1. In the present study the fitting procedure is weighted according to the variance σ_j^2 and as a result χ^2 are incorporated into Marquardt's (1963) algorithm. A modification of the algorithm concerns the initial value of λ^0 (s = 0). A value of 10^{-2} has been suggested by Marquardt (1963). This value was found to be unnecessarily large and was reduced to 10^{-5}. The algorithm as applied to this work is stated below:

1. Let $\lambda^0 = 10^{-5}$
2. Compute $\chi_1^2(s)$ for λ^{s-1} and $\chi_2^2(s)$ for $\lambda^{s-1}/10$ with corresponding $\underline{b}$ and $\underline{b}'$ respectively.
3. If $\chi_2^2(s) \leq \chi^2(s-1)$ let $\lambda^s = \lambda^{s-1}/10$ with b' as the improved estimates where $\chi^2(s-1)$ is chi-square of the previous iteration

4. If $\chi_2^2(s) > \chi^2(s-1)$ and $\chi_1^2(s) \le \chi^2(s-1)$ let $\lambda^S = \lambda^{S-1}$ with b as the improved estimates.

5. If $\chi_2^2(s) > \chi^2(s-1)$ and $\chi_1^2(s) > \chi^2(s-1)$ increase λ^{S-1} by succesive multiplication by 10^ω with $\omega = 2$ (Marquardt (1963) suggests $\omega = 1$) and $\kappa = \kappa/10$ until $\chi_3^2(s) \le \chi^2(s-1)$ where χ_3^2 is chi-square for increased λ^{S-1} and decreased κ adopting improved estimates for the smallest ω.

6. Let $\lambda^S = \lambda^{S-1}.\ 10^\omega$.

Condition 5 was seldom encountered and only at the final stages of the iterative procedure. Iterations were terminated when

$$\chi^2(s+1) - \chi^2(s) \le \psi \qquad 5.48$$

A value for $\psi = 0.0001$ was adequate to stabilise the least square estimates.

A software package was written in Fortran 77 as a part of this study using the University's Harris 800 mainframe computer for fitting the accumulated L shell x-ray spectra. The package entitled 'SPECTRUM' is based on the damped linearisation technique described above and incorporates Marquardt's algorithm. Two routines, entitled 'GAUSS' and 'REFINE' are included in the package and are utilised by SPECTRUM to solve the least square normal equations. GAUSS initially solves the equations using Gaussian elimination with pivotal condensation and REFINE corrects these solutions for rounding-off errors by iterative refinement (Buckingham 1962 and Gerald 1978). A hard copy of the package is presented in appendix D. SPECTRUM is capable of fitting simultaneously 20 Gaussian peaks, superimposed on a linear or a higher order background, contained in a region of 300 channels. The number of peaks and the spectra region were restricted by the allocated computer memory. Complete L x-ray spectra were fitted in one execution of the program. Figure 5.19 illustrates a typical fit to W L x-ray spectrum obtained by 2.9MeV alpha impact. Less than 30 iterations

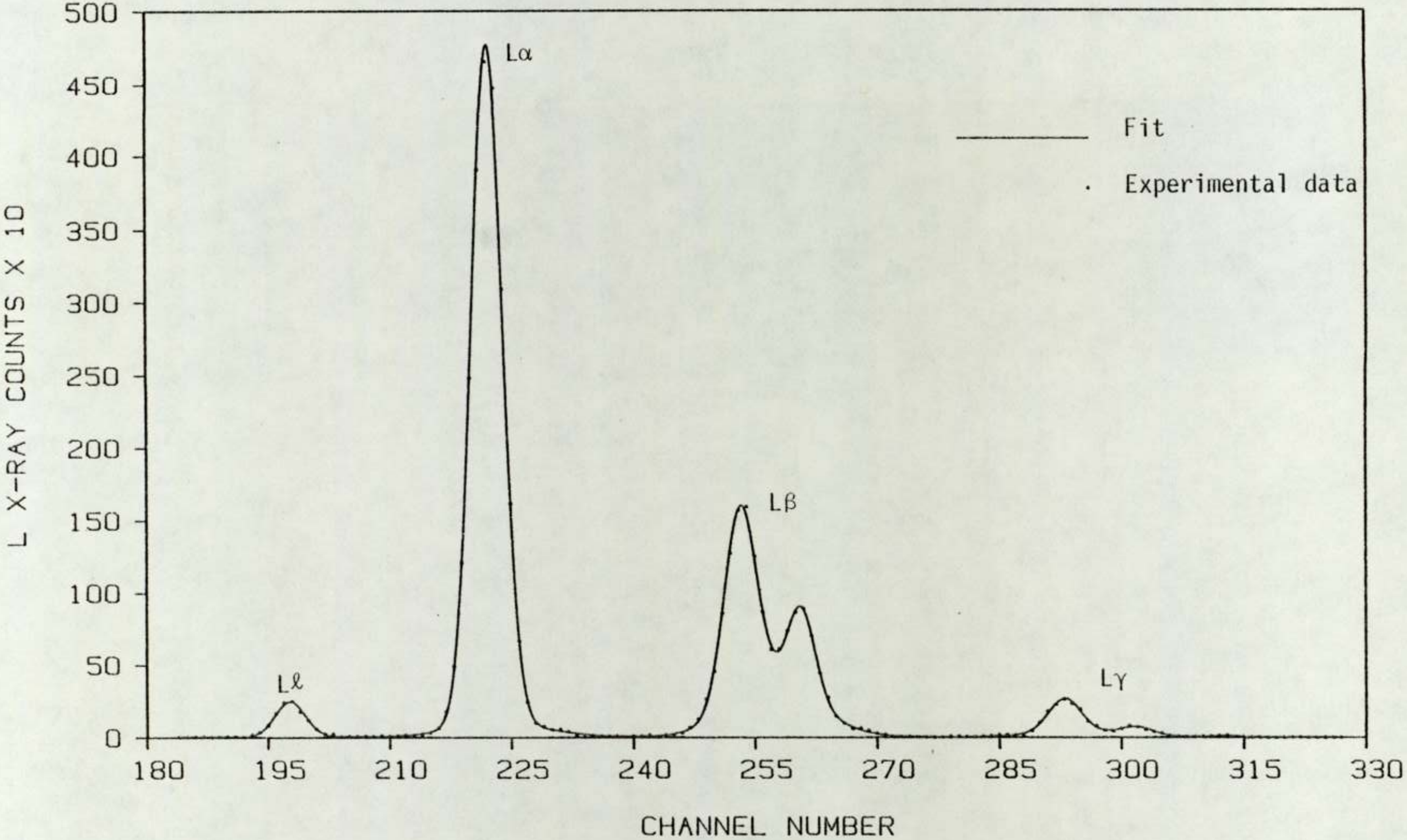

Figure 5.19. A nonlinear fit to a typical tungsten L x-ray spectrum obtained by 2.9MeV alpha particle impact (χ_r^2 = 1.05).

were required to obtain the least square values of the regression parameters. Chi square values of around and often less than 1.5 were achieved. Peak areas obtained by fitting composite spectra using equation 5.33 were checked by fitting individual L x-ray groups and agreement of less than 1%, even for the relatively weak L_ℓ and L_γ transitions, was attained. A fit to the L_γ group of Pb bombarded by 3.0 MeV protons, presented in figure 5.20 shows the individual L_γ components. As mentioned previously in subsection 5.7.2. statistics for L_{γ_5} and $L_{\gamma_{44'}}$ are poor making their yields, obtained by fitting the L_γ group, unreliable. Consequently the L_{γ_5} and $L_{\gamma_{44'}}$, were appropriate, were summed with the L_{γ_1} and $L_{\gamma_{23}}$ components respectively.

The performance of SPECTRUM is demonstrated by figures 5.21 and 5.22 which show the improvement of the peak parameters and the reduction of χ_r^2 with iteration for the Bi L_ℓ peak obtained by impact of 3MeV deuterons. Figure 5.23 shows the fit obtained with the initial estimates of $\underline{b}$, its improvement at an itermediate stage of the iterative procedure and the final fit obtained at χ_r^2 minimum for the L_ℓ peak.

Uncertainty in the actual area, A_i, of the ith peak is simply given by σ_i which can be estimated by $Ai^{\frac{1}{2}}$. σ_i, however, reflects the uncertainty of the measured data as a sample of the parent distribution and does not include the additional uncertainty in A_i introduced by the regression procedure. For $\chi_r^2 \lesssim 1$, as was invariably the case, the uncertainty in A_i is essentially that of the parent distribution since the effect of the fit on σ_i is minimal (Bevington 1969). On the other hand, for cases where $\chi_r^2 > 1$ the uncertainty due to the fitting procedure is not negligibel and has to be included in σ_i. The uncertainty introduced by the regression is of the order of χ_r^2 and the total uncertain in Ai can be estimated, according to Bevington (1969), by

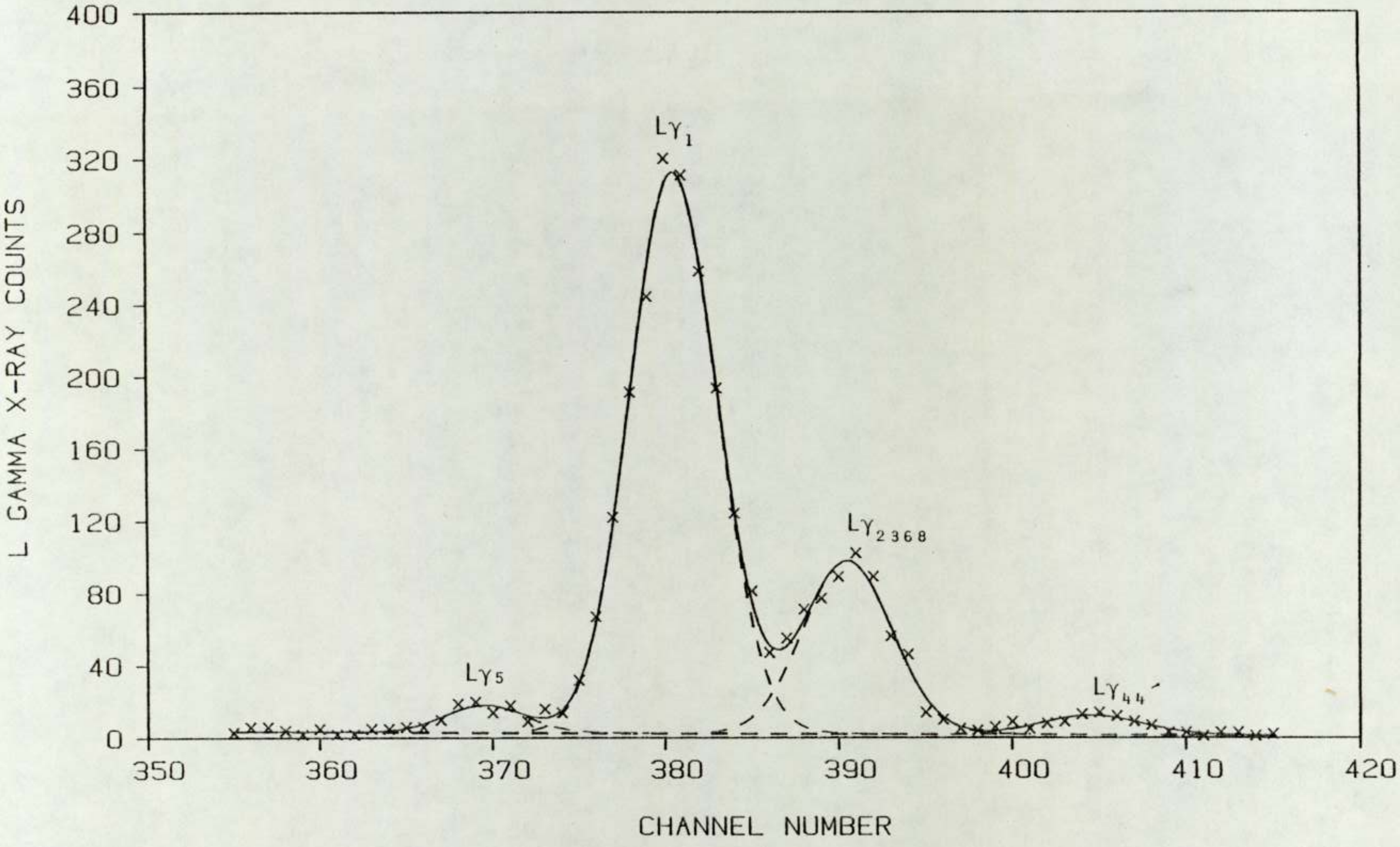

Figure 5.20. A nonlinear fit to lead Lγ x-rays obtained by 3.0 MeV proton impact (χ_r^2 = 0.79). The solid curve represents the fit to the whole Lγ group and the dashed curve indicates the individual components.

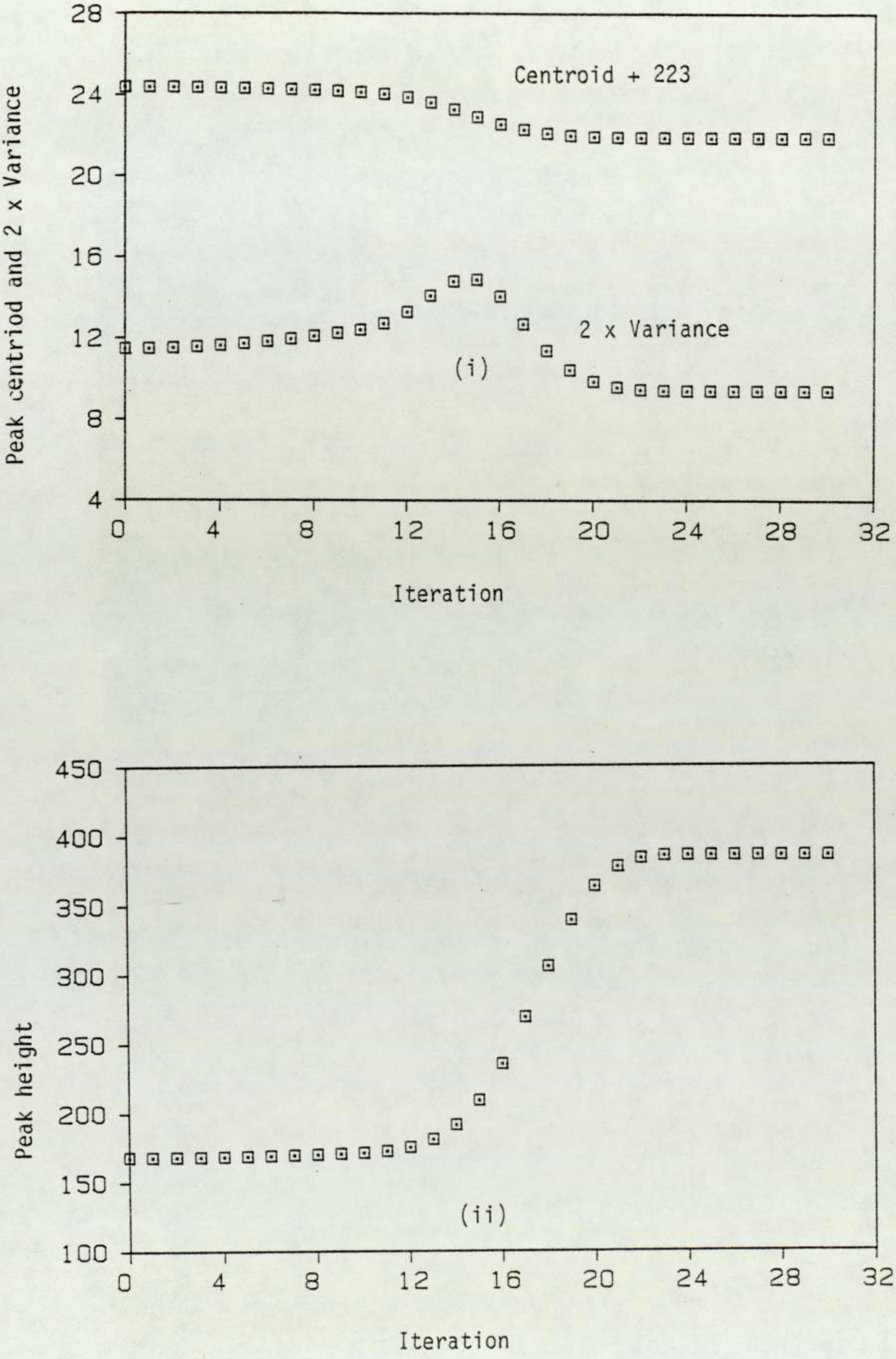

Figure 5.21. Improvement of Bi Lℓ peak fitting parameters with iteration.

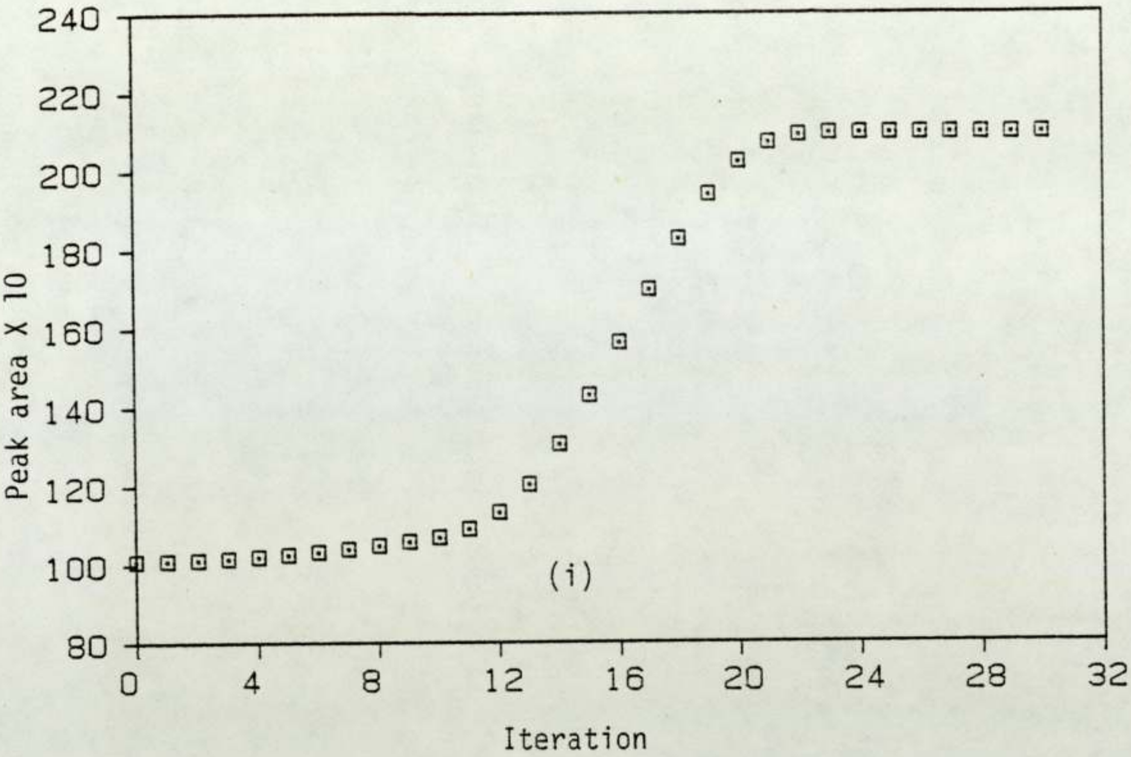

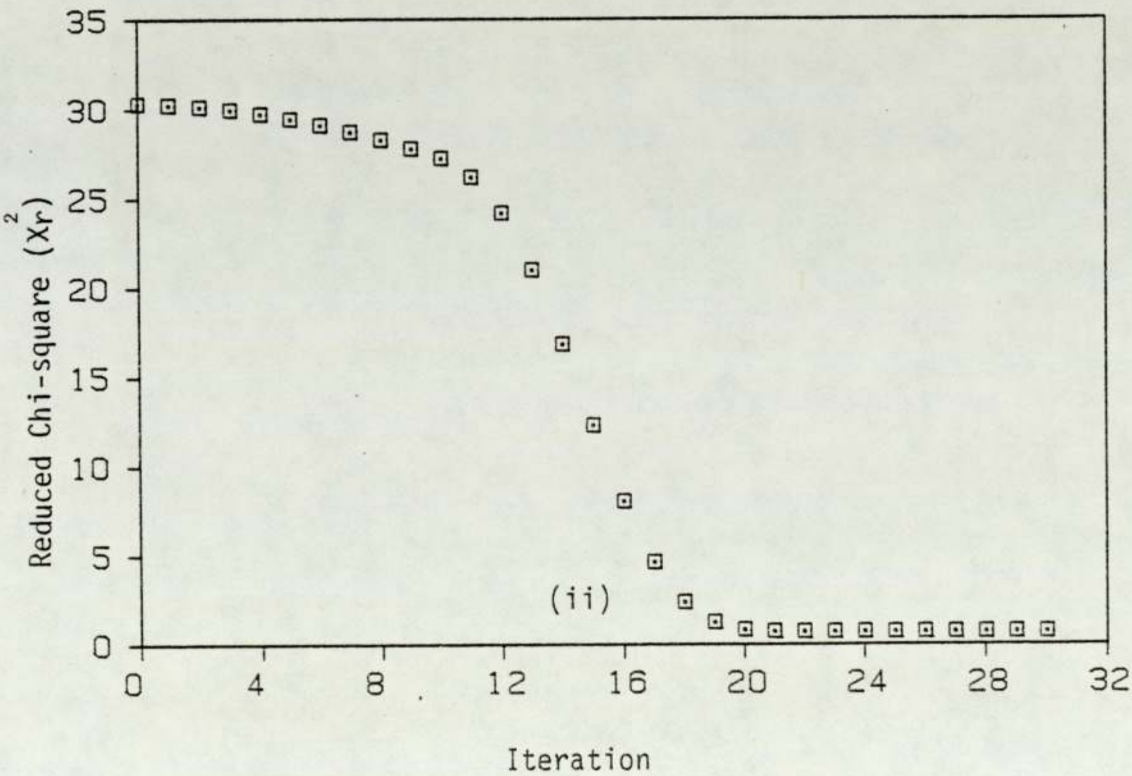

Figure 5.22. Improvement of the area under the Bi Lℓ fitted peak and the associated χ_r^2 with iteration.

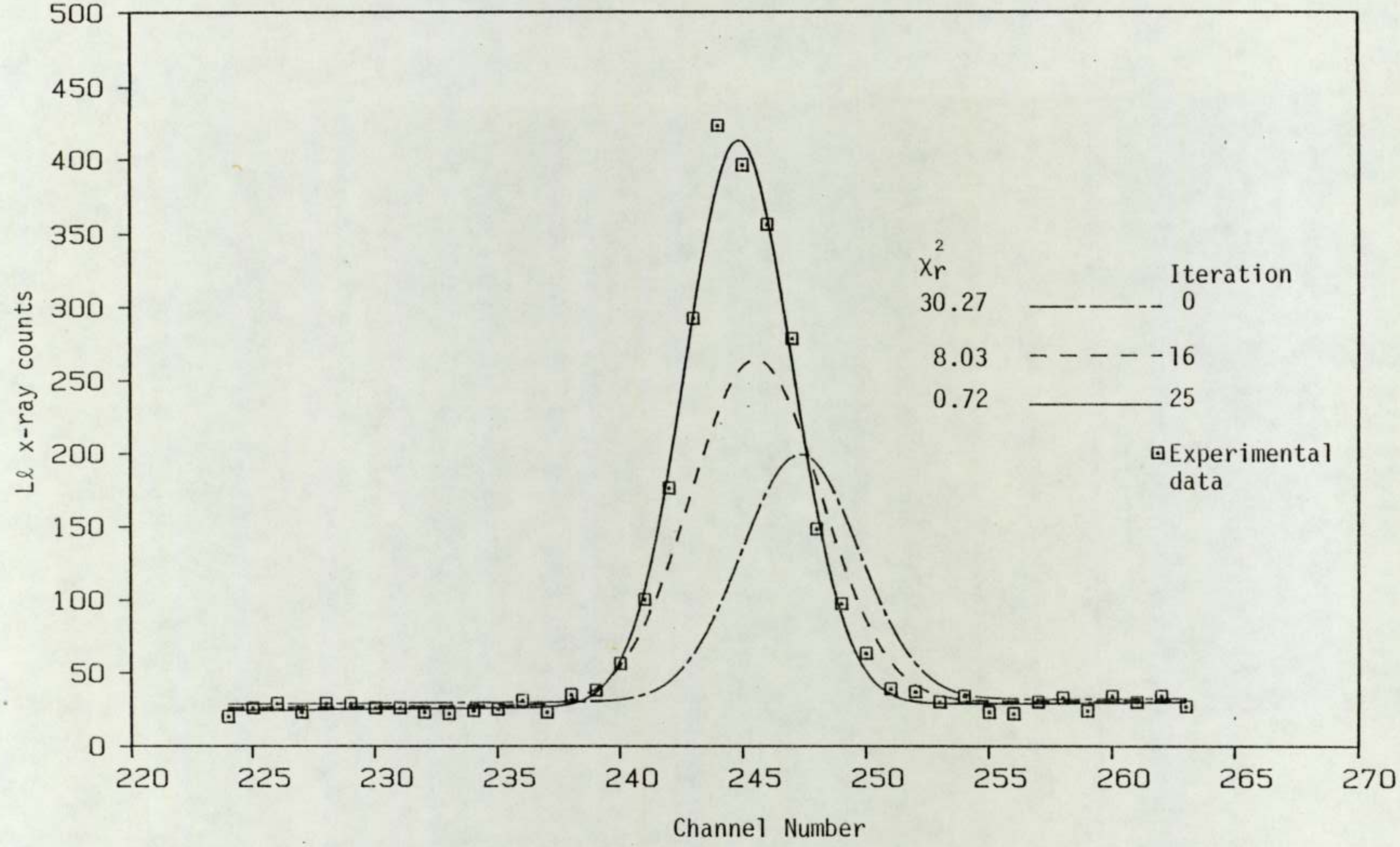

Figure 5.23. Spectrum fitting of Bi Lℓ peak obtained by 3MeV deuteron impact. Fits at different stages of the iterative procedure are illustrated.

$\sigma_i \chi_r^2$. χ_r^2 in the present work was seldom greater than 1.5 and so at worst, the uncertainty in A_i is increased by a factor between 1.5 - 2.0.

5.7.4 Uncertainties in the Measured Cross Sections

The major sources of uncertainties in the cross section measurements employing carbon backed targets are quantified and summarised below:

(i) Projectile energy (E)	1.2 - 2.8%
(ii) Charge collection (M_p)	1%
(iii) Target areal density (ρt)	≤1.5%
(iv) Si(Li) detector efficiency (E_{L_j})	2 - 3.5%
(v) X-ray absorption correction (C_{L_j})	1 - 5%
(vi) Si(Li) detector solid angle (Ω)	1.8%
(vii) Counting statistics including the effects of fitting (Y_{L_j})	≤10%

The effect of the uncertainties in the stopping power, $\varepsilon(E)$, is negligible on the measured x-ray production cross sections, $\sigma_{L_j}^X$, since it appears only in the correction factor (equation 5.17). The uncertainty in C_{L_j} depends on the x-ray energy. The values of the mass absorption coefficients in the tabulation of Storm and Israel (1970), which were used to evaluate C_{L_j}, are uncertain by 10% when the x-ray energy is less than 6keV and by 3% for higher energies. To determine the resultant uncertainty in $\sigma_{L_j}^X$ the individual uncertainties, listed above, were combined quadratically. This yields uncertainties in $\sigma_{L_j}^X$ in the range of 4 - 12%. Uncertainty of each value of $\sigma_{L_j}^X$ are listed together with the absolute cross section values in appendix B.

Uncertainties, (i) - (iii) and (iv), which appear systematically in the $\sigma_{L_j}^X$ calculations, disappear when considering ratios of x-ray production cross sections. Since the ratios are free from the systematic uncertainties their comparison with theory is usually more informative than the comparison with absolute cross sections. Uncertainties in the ratios range from about 7% to 16% depending on the x-ray transitions and particle energy.

In the case of L subshell ionisation cross sections, σ_{Li}, the situation is complicated by the presence of ω_i, S_{ij} and f_{ik} (subsection 5.7.2). These parameters introduce systematic uncertainties in σ_{Li}. For the targets under consideration, uncertainty in ω_i, f_{ik} and S_{ij} may be up to 20%, 50% (Krause 1979) and 10% (Scofield 1974b) respectively. The philosophy adopted in this work is to recognise the existence of these uncertainties but to consider only those uncertainties which arise from the adopted experimental technique. Thus the uncertainties in σ_{Li} reflect purely the experimental precision of the measurements. This philosophy is also usually adopted in the literature relevant to this work. The final uncertainties in σ_{Li} range up to 12% for σ_{Li}, 10% for σ_2 and 9% for σ_{L_3}. These result in uncertainties of up to 16% in $\sigma_{L_1}/\sigma_{L_2}$ and $\sigma_{L_1}/\sigma_{L_3}$ and 13% in $\sigma_{L_2}/\sigma_{L_3}$. Uncertainties are quoted for each σ_{Li} value in appendix B.

5.8 CALCULATION OF THEORETICAL CROSS SECTIONS

Tabulations compiled by Choi et al (1973) and Benka and Kropf (1978) have been employed in the present work to calculate L shell ionisation cross sections. Benka and Kropf (1978) have provided an interpolation formula to evalute the cross section value for any θ_{Li} and η_L/θ_{Li}^2, which lie inside the range of the tables. However, despite this, it is very tedious to calculate the cross sections since a large amount of interaction is required on the part of the user. The situation is worse in the case of the tables by Choi et al (1973) since an appropriate method for interpolation has not been suggested by the authors.

For these reasons polynomials were fitted to the data contained in both the tables. In the case of the tabulation of Benk and Kropf (1978) the data was transformed from the $f(\eta_L/\theta_{Li}, \theta_{Li})$ format to the $f(\eta_L/\theta_{Li}, \theta_{Li})$ form. This was necessary to obtain fits of adquate accuracy. A multiple regression polynomial of the form

$$\ln[f(\eta_L, \theta_{Li})] = a_0 + \sum_{i=1}^{n} a_i \left[\ln(\eta_L)\right]^i + \sum_{j=1}^{m} a_{j+n} \left[\ln \theta_{Li}\right]^j \qquad 5.49$$

was fitted to $f(\eta_L, \theta_{Li})$. Several fits had to be performed to the data in order to deduce the ionisation cross section for the collision regimes under study. Typically $n = m = 3$ and agreement to within 0.1% was attained with the values of Benka and Kropf (1978). Values for R were practically unity for the fits. The agreement obviously compares well with the interpolation formula quoted by Benka and Kropf (1978) which reproduced their data to within 2%. Cross sections obtained by their interpolation formula and by fits of the form 5.49 were compared for proton impact of Dy and agreement to within 2.5% was observed. The situation was more complicated in the case of the tables by Choi et al (1973). Fits of the form 5.49 were inadequate and the strategy adopted was as follows. Polynomials of the form

$$\ln\left[f(\eta_L)\right] = \sum_{i=0}^{n} a_i \left[\ln(\eta_L)\right]^i \qquad 5.50$$

were fitted to the tabulated data for several θ_{Li} values. n depended on the number of data points and ranged between 2 - 5. Agreement with the tabulated values to less than 0.5% was achieved and typically $R^2 = 0.9999$. These fits were incorporated into the computer programme written in basic for calculating the ECPSSR cross sections. The programme substitutes the appropriate η_L value into the polynomials and calculates $f(\eta_L)$ for the fixed θ_{Li} values. A least square regression routine was appended to the main programme which fitted a polynomial of the same form as 5.50, except that η_L is replaced by θ_{Li}, to the $f(\theta_{Li})$ values, η_L being fixed in this instance. The required $f(\eta_L, \theta_{Li})$ was calculated from this resulting polynomial.

Wherever possible the compilation of Choi et al (1973) was used to evaluate cross sections for deuteron and alpha impact. For elements heavier than Au, however, the main parameters, η_L and θ_{Li}, fall outside the ranges addressed by those authors for alpha impact. At this stage the choice available is either to omit comparison with theory or to somehow estimate the ECPSSR cross sections. In order to gain some insight at least into the theoretical descriptions of ionisation by alpha particles for heavy elements an attempt was made to determine approximate ECPSSR cross section values. To do this the tables of Benka and Kropf (1978) were employed. Although these authors caution against the use of their tables for any other projectile except protons, as noted in chapter 4 (section 4.2), it is hoped that the cross section values will approximate the 'true' ECPSSR values to a degree comparable to that of the experimental uncertainties. Values derived by this procedure for alpha particle bombardment of elements for which this problem does not arise, were compared with the values calculated from the tables of Choi et al (1973). The values obtained from the tables of Benka and Kropf (1978) were found to be smaller than those of Choi et al (1973) by about 10% at 1MeV and by about 3% at energies approximately 3MeV. These difference are indeed comparable to experimental uncertainties and imply that these value may be used to estimate the ECPSSR cross sections. It should be noted that the values of Benk and Kropf (1978) for proton impact are generally less than those of Choi et al (1973) by two percent especially at lower impact energies. This fact was highlighted in chapter 4(Section 4.2) and may explain some of the observed differences for alpha particle impact.

This approach has also been adopted by Braziewicz et al (1984) who have encounted the same difficulties. Cohen (1981) has also extracted the ionisation cross sections for alpha particle bombardment of heavy elements from the tables of Benka and Kropf (1978) but has not justified this approach.

The L x-ray production cross sections were obtained by substituting the ionisation cross sections for the appropriate collison regime into equations 5.20 - 5.23 stated previously in subsection 5.7.2. Theoretical L shell x-ray production and ionisation cross sections for the targets and projectiles under investigation are tabulated in appendix C.

CHAPTER 6

RESULTS AND DISCUSSION

CONTENTS

Page

Page

6.1 INTRODUCTION

This chapter discusses the L shell x-ray production and ionisation cross sections measured in the present study. The measured cross sections are compared with the PWBA and the ECPSSR theories (Brandt and Lapicki 1981 and see chapter 4). Comparison is also made with recent measurements reported by other authors. It must be noted, however, that there appears to be a complete lack of published deuteron impact data peritent to this study. Consequently comparison of the present deuteron measurements is made only with the theories. With regard to incident alpha particles there are a few published measurements for the elements of interest and comparison has been made whenever the data was available in tabular form. Sokhi and Crumpton (1984)(appendix E) have published a tabulation of recent experimental L shell x-ray production and ionisation cross sections for proton impact with allows comparison to be made conveniently. However, even for protons there is a significant lack of relevant data.

The cross sections measured in the present work are presented graphically in this chapter while tabulated values are contained in appendix B. To facilitate the discussion ionisation cross section are considered before proceeding with the x-ray prodcution cross sections. This approach is adopted because the latter may be understood in terms of the Li subshell ionisation cross sections. Finally, common features highlighted by measurements for the individual elements are discussed.

6.2 DYSPROSIUM (Z_2 = 66)

For dysprosium (Dy) $L\ell$, $L_{\alpha+\eta}$, $L\beta_{1346}$, $L\beta_{2715}$, $L\gamma_{15}$ and $L\gamma_{23844'}$ transitions were measured for proton and deuteron impact. The Li subshell ionisation cross sections were deduced from $L_{\alpha+\eta}$, $L\gamma_{15}$ and $L\gamma_{23844'}$ x-ray transitions as outlined in section 5.7.2. It should be noted here that the L_α and L_η transitions could not be resolved with the experimental set-up employed in this study and consequently the $L\eta$ contribution had to be accounted for in expression 5.29.

6.2.1 Proton Impact Measurements

Total and individual Li subshell ionisation cross section, σ_{Lt} and σ_{Li} respectively, are illustrated in figure 6.1 with the PWBA and ECPSSR predictions. For both the L_2 and L_3 subshells the data and the ECPSSR theory shows reasonable agreement only at high energies. As the proton enegy (E_p) decreases discrepencies increase upto 35%, which is about five times the experimental uncertainties in the measured cross sections, and the data converges towards the PWBA predictions. Figure 6.1 clearly demonstrates that the variation of σ_{L_2} and σ_{L_3} with decreasing collision energy is less sharp than predicted by the ECPSSR model. Experimental values of $2s_{\frac{1}{2}}$ state ionisation cross sections, although lying 5-10% above the ECPSSR values, exhibit a measure of agreement both with the ECPSSR and the PWBA theories. The energy dependence of σ_{L_1}, established experimentally, is reproduced quite accurately by the ECPSSR theory. The pronounced decrease of σ_{L_1} at $\eta_L \le 0.01$ ($E_p \le$ 1MeV, η_L = scaled energy), the origin of which was discussed in section 4.2, is verified by the experimental data. The disagreement between the ECPSSR values and experimental σ_{L_2} and σ_{L_3} is reflected in the total L shell ionisation cross sections (σ_{Lt}). Agreement with the ECPSSR theory is good for E_p > 2.2MeV.

The theoretical predictions can be tested further by comparing them with the ratios of experimental Li subhsell ionisation cross sections. These ratios are particular sensitive to the shape of the excitation function and highlight regions of disagreement not obvious from comparison with absolute values. Ionisation cross section ratios for proton impact on Dy are illustrated in figures 6.2 and 6.3 with increasing impact energy together with the values obtained by Jitschin et al (1982) in the energy range of interest. Theoretical predictions of $\sigma_{L_1}/\sigma_{L_2}$ agree with the present values for proton energies greater than 1.8MeV. At lower energies the experimental values lie below the theoretical curve. The $\sigma_{L_2}/\sigma_{L_3}$ ratios (figure 6.3) at lower proton energies lie above the values predicted by the theories. Assuming that any existing systematic discrepencies cancel the theory still deviates from the $\sigma_{L_2}/\sigma_{L_3}$ ratios by about 15% at lower E_p. These comparisons suggest that the ECPSSR significantly underestimate the L_2 subshell ionisation cross sections, particularly at lower proton energies. Better agreement is observed for the $\sigma_{L_1}/\sigma_{L_3}$ ratios implying that the theories reproduces σ_{L_1} and σ_{L_3} more closely than σ_{L_2}. The data of Jitschin et al (1982) follow the general trend exhibited by the present values and also agree quantitatively within the experimental uncertainties of 20%. Since the wave functions of $2p_{\frac{1}{2}}$ and $2p_{\frac{3}{2}}$ electrons are similar the ratio $\sigma_{L_2}/\sigma_{L_3}$ shows only slight variation with proton energy. The more distinct energy dependence for the $\sigma_{L_1}/\sigma_{L_2}$ and $\sigma_{L_1}/\sigma_{L_3}$ ratios is a direct consequency of the nodal structure in the 2s radial wave function. It is worthwhile noting that the PWBA and ECPSSR yield comparable values of the ratio since the corrections to the PWBA largely cancel out.

The measured L_ℓ, $L_{\alpha+\eta}$, $L_{\beta_{1346}}$, $L_{\beta_{2715}}$, $L_{\gamma_{15}}$ and $L_{\gamma_{23844'}}$ x-ray production cross sections are shown in figures 6.4 - 6.7. Present values are compared with PWBA and ECPSSR theories and with the data of Khan and Crumpton (1978) and the more recent data of Sokhi and Crumpton (1982) which formed a part of the preliminary measurements performed prior to the experiments described in this thesis. The present L_j x-ray production cross section, $\sigma^X_{L_j}$, in general lie systematically above the values of Khan and Crumpton (1978) by $\simeq$ 20%. Measurements by these authors were made on thick targets and this fact most probably explains much of these descrepencies since the precision of σ^X_{Lj} derived from thick target x-ray yields depends directly on the accuracy of energy loss values for protons and on the mass absorption coefficients. Typically uncertainties in the former are around 10% (Andersen and Zeigler 1977) and 3-10% in the latter (Storm and Israel 1970). The values of Sokhi and Crumpton (1982) are also systematically lower than the present values. The deviations are about 25% for $\sigma^X_{L\ell}$ and about 5-10% for the other cross sections. There was a time difference of about 2 years between the present and the preliminary measurements reported by Sokhi and Crumpton (1982). These initial measurements assumed the validity of theoretically calculated Si(Li) detector efficiency whereas the present values were corrected by experimentally determined Si(Li) efficiency (section 5.5). However, as pointed out in section 5.5 calculated efficiencies may not be reliable and may overestimate the true efficiency. Therefore the most likely explanation of the discrepencies is the further deterioration of the Si(Li) efficiency over the 2 years. As reported in section 5.5 differences of about 20% were noted between the measured and calculated efficiencies. Futhermore the initial experiments were conducted with nuclepore targets and thus low beam currents (≃ 3nA) had to be employed. In order to avoid long counting times data was accumulated for less charge compared to the present measurements which were made with carbon backed targets. Consequently the initial measurements were subject to relatively larger statistical uncertainties. This may also be regarded as a contributory cause of the observed differences in the two sets of measurements.

The σ_{Lj}^X values follow the trend exhibited by the relevant Li sub-shell ionisation cross sections. $\sigma_{L\ell}^X$, $\sigma_{L\alpha+\eta}^X$ and $\sigma_{L\beta_{2715}}^X$, which represent cross sections for L_j transitions to the L_3 subshell, are underestimated by the ECPSSR theory (figures 6.4 and 6.5) as was the case with σ_{L_3}

(figure 6.1). The contribution of the $L\eta$ x-rays to $\sigma^X_{L\alpha+\eta}$ is only about 1-2% and thus can be ignored for comparison purposes. $\sigma^X_{L\beta_{1346}}$ and $\sigma^X_{L\gamma_{15}}$, figures 6.5 and 6.6 respectively, mimic the response of σ_{L_2} since these x-ray transition are to the L_2 subshell. The major contribution to $\sigma^X_{L\gamma_{23844'}}$ comes from L_1 ionisation and is directly proportional to σ_{L_1}, through expression 5.27, and thus exhibits analogous behaviour to σ_{L_1}. The significant deviations in the partial L_{β_j} and $L_{\gamma_{15}}$ cross sections are reflected in the total $L\beta$ and $L\gamma$ x-ray production cross sections, as shown in figures 6.5 and 6.6 respectively. The underprediction of σ_{L_2} and σ_{L_3} by the ECPSSR theory is also evident in the total x-ray production cross sections (σ^X_{Lt}), shown in figure 6.7. The experimental values of Khan and Crumpton (1978) and Sokhi and Crumpton (1982) lie below the present data for reasons discussed earlier.

Figures 6.8 - 6.10 illustrate the variation of Lj x-ray production cross section ratios with proton energy. A major advantage of comparing these ratio with theoretical predictions is that the systematic uncertainties in the experimental procedure (subsection 5.7.4) are eliminated. Experimental values of $\sigma^X_{L\alpha+\eta}/\sigma^X_{L\ell}$ indicate an energy dependence in contrast to the constant value predicted by the ECPSSR theory. Such a marked energy dependence has also been noticed by Busch et al (1973), Tawara et al (1975) and Kamiya et al (1979) for light ion impact a high Z_2 elements. This dependence on the projectile energy may be explained in terms of $2p_{\frac{3}{2}}$ alignment effect as addressed in section 4.4. Kamiya et al (1979) have incorporated this effect into the PWBA theory and have obtained good agreement with measured data. The preliminary measurements (Sokhi and Crumpton 1982) indicate a trend opposite to that predicted by the present values. However, the $L\ell$ x-ray measurement were subject to high statistical deviations and since the ratios are very sensitive to the shape of the excitation functions large scatter in the ratio is not unexpected and thus cannot be relied upon to yield precise information. $\sigma^{x}_{L\ell}$ values reported in this work were measured with counting statistics of ≤ 5% and usually < 3% and hence are likely to be more trustworthy.

$\sigma^{x}_{L\alpha+\eta}/\sigma^{x}_{L\beta}$ ratios show reasonable qualitative agreement with the ECPSSR predictions (figure 6.9) and with measurements of Sokhi and Crumpton (1982). The values of Khan and Crumpton (1978), performed on thick targets, deviate considerably from the present measurements Similar behaviour was noticed in the case of $\sigma^{x}_{L\alpha+\eta}/\sigma^{x}_{L\gamma}$ and $\sigma^{x}_{L\beta}/\sigma^{x}_{L\gamma}$ ratios, illustrated in figure 6.10.

6.2.2 Deuteron impact measurements

L_i subshell ionisation cross sections for deuteron impact on Dy are shown in figure 6.11. The measured values are compared with the PWBA and ECPSSR theories. The structure in σ_{L_1} at deuteron energies $(E_d) \simeq$ 1MeV, due to the radial node in the $2_{s_{\frac{1}{2}}}$ wavefunctions, is clearly indicated by the measurements. The ECPSSR theory predicts the data well at E_d < 2.2MeV. At higher E_d the experimental values rise more steeply than the ECPSSR curve and converges towards the PWBA predictions. Unlike proton measurements where some agreement was observed at higher proton energies with ECPSSR theory, the experimental values of σ_{L_2} for deuter impact lie above the ECPSSR predictions by more than 30% throughout the energy range. The PWBA theory appears to reproduce the data well within experimental uncertainties. Disagreement is less for σ_{L_3} where the data deviates by about 12% from the ECPSSR curve. These descrepencies are transfered into the total L shell ionisation cross section, σ_{L_t}, also shown in figure 6.11.

L_i subshell ionisation cross section ratios are illustrated in figure 6.12. The structure in the σ_{L_1} causes a minimum in $\sigma_{L_1}/\sigma_{L_2}$ and $\sigma_{L_1}/\sigma_{L_3}$ ratios. Experimental values of $\sigma_{L_1}/\sigma_{L_2}$ are overestimated by the theories for $E_d \leq 2.2$MeV although the trend is reproduced quite well. Furthermore, the theories predicts a minimum at $\eta \simeq 0.01$ (E_d = 2MeV) whereas the data indicate a minimum at $\eta_L \simeq 0.008$ (E_d = 1.6MeV). Similar behaviour is exhibited by the $\sigma_{L_1}/\sigma_{L_3}$ ratio. This shift in the minimum implies that the plateau predicted by the PWBA in σ_{L_1} at $\eta_L \simeq 0.01$ occurs inreality at a lower η_L value. This was also noticed by Change et al (1975) and it suggests that the radial node in the $2s_{\frac{1}{2}}$ wave function occurs at a higher momentum value than predicted by hydrogenic nonrelativistic wave functions (Chang et al 1975). The failure of the ECPSSR to predict σ_{L_2} data is also highlighted in the comparison of σ_2/σ_{L_3} with theory (figure 6.12). The measured ratio follow the same pattern as σ_{L_2},in that they lie above the predicted values.

The measured absolute $\sigma_{L_j}^X$ are shown in figures 6.13 - 6.16. Since the L_α and L_ℓ transitions are to the L_3 subshell $\sigma_{L\ell}^X$ and $\sigma_{L\alpha+\eta}^X$ (figure 6.13) follow the trend of σ_{L_3} and numerically are underestimated by the ECPSSR theory. $\sigma_{L\ell}^X$, however, shows a larger deviation from the ECPSSR curve ($\sim$ 30%) than $\sigma_{L\alpha+\eta}^X$ (~ 14%). Partial $\sigma_{L\beta_j}^X$ and total $\sigma_{L\beta}^X$ (figure 6.14) exhibit agreement with the uncorrected PWBA theory. Similar behaviour is also expressed by the L_γ x-ray cross sections, shown in figure 6.15. Since $L_{\gamma_{2344'}}$ transitions occur to the $2s_{\frac{1}{2}}$ state $\sigma_{L_{\gamma_{23844'}}}^X$ data also reveals the structure of σ_{L_1}(figure 6.11) The total L x-ray production cross section, σ_{Lt}^X, illustrated in figure 6.16, depicts analogous behaviour to its individual components, $\sigma_{L_j}^X$, and differs from the ECPSSR values by as much as 18%.

The evidence for energy dependence of $\sigma_{L\alpha}^X/\sigma_{L\ell}^X$ provided by proton data (figure 6.8) is further reinforced by the measurements made with incident deuterons, and is shown in figure 6.17. With regard to the other ratios, illustrated in figures 6.18 and 6.19, agreement is noticed only with $\sigma^x_{L\beta}/\sigma^x_{L\gamma}$ whereas $\sigma^x_{L\alpha+\eta}/\sigma^x_{L\beta}$ and $\sigma^x_{L\alpha+\eta}/\sigma^x_{L\gamma}$ are overestimated by the theories. Since major components of L_β and L_γ x-rays arise from electronic transitions to the L_2 subshell this implies that much of the discrepencies noticed with σ_{L_2} values cancel when considering $\sigma_{L_\beta}/\sigma_{L_\gamma}$ ratios.

6.3 YTTERBUM (Z_2 = 70)

From the L x-ray spectra of ytterbium (Yb), obtained by proton, deuteron and alpha particle bombardment, L_ℓ, $L_{\alpha+\eta}$, $L_{\beta_{1346}}$, $L_{\gamma_{15}}$ and $L_{\gamma_{23844'}}$ x-ray transitions were analysed. As with Dy, contribution of the L_η x-rays to the L_α peak was taken into account when deriving σ_{L_3} cross sections from equation 5.29.

6.3.1 Proton Impact Measurements

The ECPSSR theory reproduces σ_{L_1} quite well and is illustrated in figure 6.20. At proton energies, E_p, less than 2 MeV the ECPSSR predictions deviate by about 20% below the measured value of σ_{L_2} (figure 6.20), describing similar behaviour to that noticed with proton bombardment of Dy (section 6.2.1). The experimental σ_{L_3} values lie below the ECPSSR prediction by 5-10%, just outside the experimental uncertainties of 4-6% in σ_{L_3}. Agreement of ECPSSR predictions with the total L shell ionisation cross section, σ_{L_t}, is remarkably good throughout the energy range of interest.

Experimental $\sigma_{L_1}/\sigma_{L_2}$ ratios, figure 6.21, are predicted by the theories qualitatively and quatitatively within experimental uncertainties. Data values, however, lie below the theoretical curves for $E_p < 2$ MeV and above the curves for higher E_p implying that the σ_{L_1} contribution relative to σ_{L_2} increases more sharply than indicated theoretically. The minimum at $E_p \simeq 1.2$ MeV predicted by theory is substantiated by the experimental measurements. The trend described by the measured $\sigma_{L_1}/\sigma_{L_2}$ is supported by $\sigma_{L_1}/\sigma_{L_3}$ ratios, shown in figure 6.22 where the experimental values depend more sharply on increasing Ep than the theoretical values. For the $\sigma_{L_2}/\sigma_{L_3}$ ratio the agreement with theory is poor at lower impact energies and also the data indicate a nearly constant value for the ratio, incontrast to theory, which predicts a slow increase in the σ_{L_2} contribution with increasing Ep relative to σ_{L_3}.

$\sigma_{L_j}^{x}$ for the appropriate L_j x-ray transition are illustrated in figures 6.23 - 6.26. $\sigma_{L\alpha+\eta}^{x}$ and $\sigma_{L\ell}^{x}$ follow the trend of σ_{L_3} and show reasonable correlation with ECPSSR predictions (figure 6.23). $\sigma_{L\beta_{2715}}^{x}$ describes similar behaviour since its main contributor is the L_{β_2} transition which occurs to the $2p_{\frac{3}{2}}$ state (figure 6.24). Since L_{β_1} x-rays originate from electronic transitions to the L_2 subshell, $\sigma_{L\beta_{1346}}^{x}$ describes a similar energy dependence to that of σ_{L_2}. The measured total L_β x-ray production cross sections, $\sigma_{L\beta}^{x}$, (figure 6.24) illustrate reasonable agreement with the ECPSSR values but lie above the theory by a few percent. $\sigma_{L\gamma_j}$ are shown in figure 6.25. Agreement of $\sigma_{L\gamma_{23844'}}$ is good with ECPSSR values unlike $\sigma_{L\gamma_{15}}$ which deviate from theory at low Ep by upto 23%. This discrepency is also visible in the total $L\gamma$ cross section, $\sigma_{L\gamma}^{x}$, illustrated in figure 6.25. The total L x-ray cross section, σ_{Lt}^{x}, shows very good agreement with the ECPSSR theory at all Ep values (figure 6.26).

Evidence for the energy dependence of $\sigma_{L\alpha}^{x}/\sigma_{L\ell}^{x}$ ratio is substantiated by the measurements, shown in figure 6.27. $\sigma_{L\beta}^{x}/\sigma_{L\gamma}^{x}$ ratio, figure 6.28, shows reasonable correlation with theory but deviations become significant at lower impact energies. The $\sigma_{L\alpha+\eta}^{x}/\sigma_{L\beta}^{x}$ ratio show only qualitative agreement with theory, except at intermediate energies (figure 6.28). The situation is similar in the case of $\sigma_{L\alpha+\eta}^{x}/\sigma_{L\gamma}^{x}$, shown in figure 6.29, but the data values depict a significantly less pronounced energy dependence than described by the theories. This is because the measured $\sigma_{L_1}/\sigma_{L_3}$ and $\sigma_{L_2}/\sigma_{L_3}$ ratio, presented in figure 6.22, suggests that the σ_{L_1} and σ_{L_2} contribute more to the total L shell ionisation relative to σ_{L_3} than is theoretically predicted. Consequently the ratio $\sigma^X_{L_{\alpha+\eta}}/\sigma^X_{L_\gamma}$ is smaller numerically than the predicted values. The less pronounced energy dependence at low E_p is explained by the experimental evidence, that σ_{L_2} is more important relative to σ_{L_3} at lower energies than is accounted for theoretically (figure 6.22).

6.3.2. Deuteron Impact Measurements

The measured σ_{L_1} values for deuteron impact on Yb show a more marked dependence on deuteron energy (Ed) than implied by both the theories (figure 6.30). The experimental σ_{L_1} values cross over the theoretical curves at $E_d \simeq 2.1$MeV. Such a behaviour was also noticed when considering Dy σ_{L_1} for incident deuterons and was shown in figure 6.11. The σ_{L_2} data repeat the trend demonstrated by the previously discussed measurements and exhibit closer agreement with the PWBA theory, as shown in figure 6.30. As with proton bombardment of Yb, σ_{L_3} for deuteron impact show reasonable agreement with the EPSSR theory although the latter does tend to overpredict the measured values. The total L shell ionisation cross sections, σ_{Lt}, illustrated in figure 6.30, are well reproduced by the ECPSSR theory. Figure 6.31 shows the variation of $\sigma_{L_1}/\sigma_{L_2}$ with E_d and highlights the large discrepencies between experimental data and theory for $E_d < 2$MeV. In this region the theory predicts values nearly twice the measured values. The shape of the experimental $\sigma_{L_1}/\sigma_{L_2}$ values also differs from that of the theories. This is due to the measured σ_{L_1} rising more steeply with Ed than the corresponding theoretical values whereas the energy depedence of the experimental and theoretical σ_{L_2} is very similar. This affect can again be observed for $\sigma_{L_1}/\sigma_{L_3}$ ratios, demonstrated in figure 6.32, where the data values show considerable deviations from the ECPSSR predictions at Ed > 2 MeV. The under-estimation of σ_{L_2} by the ECPSSR theory is strikingly obvious from the comparison of $\sigma_{L_2}/\sigma_{L_3}$ with theory, also shown in figure 6.32.

$\sigma^{X}_{L\alpha+\eta}$ and $\sigma^{X}_{L\ell}$, seen in figure 6.33 follow the behaviour of σ_{L_3} and exhibit close correlation with the predictions of the ECPSSR theory The case is similar for $\sigma^{X}_{L_{\beta_{2715}}}$ shown in figure 6.34. On the other hand $\sigma^{X}_{L_{\beta_{1346}}}$, and hence $\sigma^{X}_{L_\beta}$, lie systematically above the ECPSSR curve but show some quantitative similarities within experimental uncertainties (figure 6.34). $\sigma^{X}_{L_{\gamma_{23844'}}}$ exhibit analogous characteristics to that of σ_{L_3} since they are directly realted and $\sigma^{X}_{L_{\gamma_{15}}}$ follows the trend of σ_{L_2}. Since at Ed > 2 MeV $\sigma^{X}_{L_{\gamma_{22844'}}}$, as well as $\sigma^{X}_{L_{\gamma_{15}}}$, is under predicted by theory $\sigma^{X}_{L_\gamma}$ shows larger disagreement in this energy region with both the PWBA and ECPSSR predictions. The total x-ray production cross section, figure 6.36, is reproduced extremely well by the ECPSSR model.

The energy dependence of $\sigma^{X}_{L\alpha}/\sigma^{X}_{L\ell}$, not predicted by the theories, is again clearly reaffirmed by the measurements shown in figure 6.37. Smaller values of $\sigma^{X}_{L\alpha+\eta}/\sigma^{X}_{L_\beta}$ than those calculated with the ECPSSR model were obtained experimentally (figure 6.38). This also implies that the mechanism of $2p_{\frac{1}{2}}$ state ionisation by incident low energy charged particles is not fully accounted for by the ECPSSR model. Since L_γ x-rays contain a large component of $L_{\gamma_{15}}$ x-rays, a consequence of transitions to L_2 subshell, similar behaviour is demonstrated by $\sigma^{X}_{L\alpha+\eta}/\sigma^{X}_{L\gamma}$ ratio and is shown in figure 6.39. Some of the σ_{L_2} discrepencies are eliminated in the $\sigma^{X}_{L\beta}/\sigma^{X}_{L\gamma}$ ratio and as a result the disagreement between theory and experiment is markedly reduced (figure 6.39)

6.3.3 Alpha particle Impact

In contrast to proton and deuteron impact measurements the experimental σ_{L_1}, (figure 6.40) for alpha particles incident on Yb are overestimated by the ECPSSR theory by upto 30%. σ_{L_2} follows the trend encountered with the previously discussed measurements and lies systematically above the predictions of the ECPSSR model (figure 6.40). However, the discrepencies are much more serious and the values may disagree by a factor of 2. The ECPSSR theory is only able to explain σ_{L_3} and the total L shell ionisation cross section (σ_{Lt}) as shown in figure 6.41. The gross discrepencies observed for σ_{L_1} and σ_{L_2} are strikingly apparent when comparing $\sigma_{L_1}/\sigma_{L_2}$ ratio with the theories (figure 6.42). Disagreement by factors of 1.5 - 2.5 were noticed. Discrepencies are somewhat reduced for $\sigma_{L_1}/\sigma_{L_3}$ ratios (figure 6.43) but still is reproduced only by PWBA model. The highly inadequate explanation of the measured σ_{L_2} data by the ECPSSR theory is also sharply expressed by the $\sigma_{L_2}/\sigma_{L_3}$ ratios shown in 6.44.

$\sigma^{X}_{L\alpha+\eta}$, illustrated in figure 6.45, is reasonably explained by the ECPSSR model. The theory, however, deviates significantly from the $\sigma^{X}_{L\ell}$ data, also shown in figure 6.45. These deivations are probably caused by the anisotropy of $L\ell$ x-rays, an effect not taken into account by the theories. The total $L\beta$ and the partial L_{β_j} x-ray production cross sections are shown in figure 6.46. Close agreement with the predictions of the ECPSSR model is shown by the total and the partial cross sections. Figure 6.47 illustrates the x-ray production cross sections for the L_γ group. $\sigma^{X}_{L\gamma_{15}}$ and $\sigma^{X}_{L\gamma_{2384 4'}}$ exhibit similar behaviour to σ_{L_2} and σ_{L_1} respectively. Discrepencies between $\sigma^{X}_{L\gamma}$ and the ECPSSR theory tend to increase with alpha particle energy to about 25%. The total L shell x-ray production cross section, shown in figure 6.48, on the other hand is explained by the ECPSSR model extremely well.

The anisotropy of $L\ell$ x-rays, mentioned above, is also apparent in the $\sigma^{X}_{L\alpha+\eta}/\sigma^{X}_{L\ell}$ ratios (figure 6.49) which expresses an energy dependence not explained by theory. $\sigma^{X}_{L\alpha+\eta}/\sigma^{X}_{L\beta}$ ratios shown in figure 6.50, disagree significantly (7-15%) at the extremities of the energy range. Futhermore the energy dependence of the measured ratio at higher impact energies is less pronounced than indicated by theory. The ECPSSR model overestimates the experimental $\sigma^{X}_{L\alpha+\eta}/\sigma^{X}_{L\gamma}$ data (figure 6.51) by 20-35% with deviations increasing with increasing alpha particle energy. $\sigma^{X}_{L\beta}/\sigma^{X}_{L\gamma}$ data exhibits a similar qualitative behaviour to that of $\sigma^{X}_{L\alpha+\eta}/\sigma^{X}_{L\gamma}$ with deviations of 5-20% from the theory, as demonstrated in figure 6.51.

6.4 TUNGSTEN (Z_2 = 74)

$L\ell$, $L_{\alpha+\eta}$, $L_{\beta_{146}}$, $L_{\beta_{25715}}$, $L_{\gamma_{15}}$ and $L_{\gamma_{236844'}}$ x-ray lines were studied for proton, deuteron and alpha particle impact on tungsten (W). The Li subshell ionisation cross sections were obtained from $\sigma^{X}_{L\alpha+\eta}$, $\sigma^{X}_{L\gamma_{15}}$ and $\sigma^{X}_{L\gamma_{236844'}}$.

6.4.1 Proton Impact Measurements

The individual Li subshell (σ_{Li}) and total L shell (σ_{Lt}) ionisation cross section for proton impact on W are illustrated in figures 6.52 and 6.53 respectively. Comparison of the present data is made with the cross sections reported by Justiniano et al (1980) as well as with the PWBA and the ECPSSR theories. σ_{L_1} data generally lies a few percent above the ECPSSR curve but reporduces the predicted energy dependence. The values of Justiniano et al (1980), however, are markedly larger than the present values by nearly a factor of 2. The present σ_{L_2} values show close agreement with the PWBA theory and the data of Justiniano et al (1980). The ECPSSR theory predicts σ_{L_3} extremely well throughout the energy range of interest. Significant deviations of about 17%, however, occur from the values of Justiniano et al(1980) at lower Ep.

σ_{Lt}, shown in figure 6.53, exhibits close correlation with the ECPSSR theory except at intermediate Ep values. The data of Justiniano et al (1980) systematically lies above the present σ_{Lt} values by about 10%.

Experimental $\sigma_{L_1}/\sigma_{L_2}$ ratios, illustrated in figure 6.54, show good agreement with the theories except at Ep < 1.4 MeV. The measured values of Justiniano et al (1980), however, show considerable deviations from the present values and the theories, caused by their markedly larger σ_{L_1} values (figure 6.53). The same effect is observed with regard to the $\sigma_{L_1}/\sigma_{L_3}$ ratio shown in figure 6.55. The theoretical predictions exhibit a less sharp energy dependent than indicated by the present values. The underestimation of σ_{L_2} by the ECPSSR theory is also apparent in the case of $\sigma_{L_2}/\sigma_{L_3}$ ratios, figure 6.55, where the data consistently lies above the predicted values. The values of Justiniano et al (1980) closely follow the trend shown by the present measurements.

The Lj x-ray production cross section for incident protons on W are shown in figure 6.56 - 6.59. $\sigma^{x}_{L\alpha+\eta}$ and $\sigma^{x}_{L\ell}$ follow the trend of σ_{L_3} and show reasonable agreement with the ECPSSR predictions. The $\sigma^{x}_{L\alpha+\eta}$ values of Justiniano et al (1980) are higher than the present values by about 20%. $\sigma^{x}_{L\beta}$ and $\sigma^{x}_{L\beta_j}$, shown in figure 6.57, are underestimated by the ECPSSR theory and the deviations increase with decreasing Ep. Similar behaviour is observed in the cases of $\sigma^{x}_{L\gamma}$ and $\sigma^{x}_{L\gamma_{15}}$ whereas closer agreement with the ECPSSR model is seen for $\sigma^{x}_{L\gamma_{236844'}}$, figure 6.58. The ECPSSR model is also quite successful in explaining qualitatively and quatitatively the total L shell x-ray production cross section (figure 6.59).

In contrast to the ECPSSR predictions the present $\sigma_{L\alpha+\eta}/\sigma^{x}_{L\ell}$ values, shown in figure 6.60, clearly exhibit a dependence on energy, in line with observations noted for Dy and Yb,discussed earlier. In the case of $\sigma^{x}_{L\alpha+\eta}/\sigma^{x}_{L\beta}$ ratios (figure 6.61) the theories and data agree reasonably although the latter is systematically overestimated by the theories. The situation is very similar for $\sigma^{x}_{L\alpha+\eta}/\sigma^{x}_{L\gamma}$ and $\sigma^{x}_{L\beta}/\sigma^{x}_{L\gamma}$ ratios shown in figure 6.62 where the theories overpredict the experimental values significantly.

6.4.2 Deuteron Impact Measurements

For deuteron energies, E_d, greater than 2 MeV the ECPSSR model explains the σ_{L_1} data, illustrated in figure 6.63, within the experimental uncertainties. At low E_d values the present σ_{L_1} values deviate below the ECPSSR curve indicating a more pronounced plateau than predicted theoretically. The ECPSSR model reporduces the energy dependence of σ_{L_2}, figures 6.63, but falls short by about 20-80%. In contrast σ_{L_3} and σ_{Lt} are explained by the ECPSSR model extremely well, figure 6.64. The deviations observed for σ_{L_2} are stikingly apparent in the case of $\sigma_{L_i}/\sigma_{L_2}$ ratio, shown in figure 6.65, where discrepencies of upto 50% exist between experimental data and theory. The σ_{L_2} deviations are also observed for $\sigma_{L_2}/\sigma_{L_3}$ ratio, figure 6.66, where the data lies above the theories throughout the energy range. $\sigma_{L_1}/\sigma_{L_3}$ figure 6.66, however, is explained well for $E_d > 2.0$ MeV but agreement decreases for $E_d < 2.0$ MeV.

Very good agreement between experimental $\sigma^{x}_{L_{\alpha+\eta}}$ and $\sigma^{x}_{L\ell}$ values and the ECPSSR model is observed, figure 6.67. $\sigma^{x}_{L\beta}$ and $\sigma^{x}_{L\beta j}$ (figure 6.68) are reproduced reasonably well by the ECPSSR model although the measured values lie above the ECPSSR predictions. The behaviour of $\sigma^{x}_{L\gamma_{236844}}$, is analogous to that of σ_{L_1} and deviates from the ECPSSR curve only for $E_d < 2.0$ MeV. The present $\sigma^{x}_{L\gamma_{15}}$ values lie about 20% above the ECPSSR model. Agreement between experimental $\sigma^{x}_{L\gamma}$ and ECPSSR values deteriorates as E_d increases and disagreements of upto 16% are noticed, figure 6.69. Excellent agreement between σ^{x}_{Lt} and the ECPSSR theory is observed and is demonstrated in figure 6.70.

The energy dependence of $\sigma^X_{L\alpha+\eta}/\sigma^X_{L\ell}$ is indicated clearly by the experimental data, figure 6.71. Present $\sigma^X_{L\alpha+\eta}/\sigma^X_{L\beta}$ ratios lie below the ECPSSR curve, figure 6.72, but show a measure of agreement within the experimental uncertainties. $\sigma^X_{L\beta}/\sigma^X_{L\gamma}$ ratios, figure 6.73, exhibit similar behaviour whereas the discrepencies between the ECPSSR theory and $\sigma^X_{L\alpha+\eta}/\sigma^X_{L\gamma}$ are considerable at $E_d > 1.6$ MeV, figure 6.73.

6.4.3. Alpha Particle Impact Measurements

The ECPSSR model significantly overestimates the experimental σ_{L_1} values whereas σ_{L_2} is grossly underpredicted by upto 80%, figure 6.74. Discrepencies for σ_{L_3} and σ_{Lt} are much less but still nontrivial as illustrated in figure 6.75. Experimental $\sigma_{L_1}/\sigma_{L_2}$ ratio at low alpha particle energies (E_α) are overpredicted by the ECPSSR values by a factor of 2, although discrepenceis decrease as E_α increases (figure 6.76). $\sigma_{L_1}/\sigma_{L_3}$ exhibits closer agreement with the PWBA theory and differs by more than 35% at low E_α from the ECPSSR values. In the case of $\sigma_{L_2}/\sigma_{L_3}$ not only do the experimental and ECPSSR values differ numerically by as much as 50%, the energy dependence indicated by the data values is contradictory to that followed by the theory, in that the experimental $\sigma_{L_2}/\sigma_{L_3}$ ratios decrease and ECPSSR values increase with increasing E_α (figure 6.78). Similar behaviour was encountered for alpha particle impact on Yb (figure 6.44).

Very good agreement between the ECPSSR values and $\sigma^X_{L\alpha+\eta}$ (figure 6.79) is observed. The two values of Braziewicz et al (1984) lie significantly below the present data. For $\sigma^X_{L\ell}$ shown in figure 6.79, the experimental values are in general larger than the ECPSSR values by 10-20%. Discrepencies of nearly 50% are noticed between experimental $\sigma^X_{L\beta_{146}}$ and ECPSSR values (figure 6.80). $\sigma^X_{L\beta_{25715}}$ shows close agreement with the ECPSSR model for $E_\alpha > 2$ MeV. Below this energy the data and theory disagree by 50%. $\sigma^X_{L\beta}$ (figure 6.80) is predicted by the

ECPSSR theory quite well but differences of upto 18% exist. The data of Braziewicz et al (1984) are lower than the present $\sigma^X_{L\beta}$ values by about 10-15%. $\sigma^X_{L\gamma_{236844'}}$, shown in figure 6.81, follows the same trend as σ_{L_1} (figure 6.74). $\sigma^X_{L\gamma_{15}}$ data deviates from the ECPSSR predictions by as much as 50% where $\sigma^X_{L\gamma}$ shows reasonable agreement with the ECPSSR model except at $E_\alpha > 2.6$ MeV where the theory yields lower values (figure 6.81). The measured $\sigma^X_{L\gamma}$ values of Braziewicz et al (1984) lie significantly below the present data. σ^X_{Lt} is reproduced well by the ECPSSR approximation where as the data of Braziewicz et al (1984) disagree considerably (figure 6.82).

$\sigma^X_{L\alpha+\eta}/\sigma^X_{L\ell}$ data describes a less sharp variation with energy than observed for proton and deuteron impact data (figures 6.60 and 6.71 respectively) and is demonstrated in figure 6.83. The ECPSSR theory predicts $\sigma^X_{L\alpha+\eta}/\sigma^X_{L\beta}$ ratio quite well and agreement is also noticed with the values of Braziewicz et al (1984). The theory also explains reasonably well the $\sigma^X_{L\alpha+\eta}/\sigma^X_{L\gamma}$ ratio although the data lies below the theoretical curves (figure 6.85). Better agreement is observed with $\sigma^X_{L\beta}/\sigma^X_{L\gamma}$ ratio shown in figure 6.85.

6.5 GOLD(Z_2 = 79)

$L\ell$, $L\alpha$, $L\beta$, $L\gamma$, $L\gamma_{15}$ and $L\gamma_{236844'}$ x-ray production cross sections have been measured for protons, deuterons and alpha particles incident on gold (Au). L_i subshell ionisation cross section were determined from $\sigma^X_{L\alpha}$, $\sigma^X_{L\gamma_{15}}$ and $\sigma^X_{L\gamma_{236844'}}$.

6.5.1 Proton Impact Measurements

L_i subshell ionisation cross sections, σ_{Li}, for proton impact on Au are compared with the thin target measured values of Cohen (1980) and de Pinho (1982) as well as with the theories and are illustrated in figure 6.86. The present σ_{L_1} values show good agreement with the ECPSSR model for $E_p > 2.0$ MeV below which the data shows reasonable correlation with the PWBA theory. σ_{L_1} values of Cohen (1980) and de Pinho (1982) disagree markedly from the present data. Furthermore the measured values of Cohen (1980) do not indicate the presence of the plateau in σ_{L_1} at $E_p \simeq 1.1$ MeV unlike the present work. For σ_{L_2}, figure 6.86, values reported in this work are predicted better by the PWBA model and also exhibit very good agreement with the data of de Pinho (1982). The values of Cohen (1980) lie below the present data by about 10-20% but agree with in the experimental uncertainties of 20% quoted by Cohen (1980). In the case of σ_{L_3} the values measured in this study in general show close agreement with the vlaues of Cohen (1980) and de Pinho (1982) and with the ECPSSR theory, as demonstrated in figure 6.86. The discrepencies noticed for σ_{L_2} show themselves in σ_{Lt}, illustrated in figure 6.87, and the present data disagrees by upto 19% from the ECPSSR theory. The values of de Pihno (1982) are in closer agreement with the present data than the values of Cohen (1980) which lie below the measured data.

The minimum in $\sigma_{L_1}/\sigma_{L_2}$, caused by the plateau in σ_{L_i}, is reproduced well by the measured values and is shown in figure 6.88. The data of Jitschin et al (1982) also predicts the minimum reasonably well whereas the values of de Pinho (1982), and in particular the values of Cohen (1980), show large deviations at intermediate E_p values. The situation is very similar for $\sigma_{L_1}/\sigma_{L_3}$ ratios shown in figure 6.89. In the case of $\sigma_{L_2}/\sigma_{L_3}$ better agreement is observed with other measured values, figure 6.89, although all values lie significantly above the predicted curves.

Present values of $\sigma_{L\ell}^{X}$, figure 6.90, are predicted well by the ECPSSR model. The data of Tawara et al (1975) deviates by upto 30% at low E_p and converges with the values of Bhattacharya et al (1980). The preliminary measurements of $\sigma_{L\ell}^{X}$ on nuclepore targets (Sokhi and

Crumpton 1981) deviate significantly only at $E_p > 2.6$ MeV. $\sigma_{L\alpha}^{X}$ and $\sigma_{L\beta}^{X}$, shown in figure 6.91, exhibit good correlation with the other measured values except for those reported by Khan and Crumpton (1978) which lie systematically below the present values. The reasons for these deviations were considered in section 6.2.1. The PWBA theory tends to predict the $\sigma_{L\beta}^{X}$ values better than the ECPSSR model, as was the case with σ_{L_2} (figure 6.86). $\sigma_{L\gamma}^{X}$, figure 6.92, follows a very similar trend to that observed with $\sigma_{L\beta}$. $\sigma_{L\gamma_{15}}^{X}$ and $\sigma_{L\gamma_{236844'}}^{X}$, also illustrated in figure 6.92, show the same behaviour demonstrated by σ_{L_2} and σ_{L_1} respectively (figure 6.86). The present σ_{Lt}^{X} values and those reported by other authors, except by Khan and Crumpton (1978), agree reasonably well and are explained better by the PWBA model, figure 6.93.

The energy dependence of $\sigma_{L\alpha}^{X}/\sigma_{L\ell}^{X}$ ratio, figure 6.94, is observed to be much less than for targets discussed earlier. The present values show a measure of agreement with the values of Sokhi and Crumpton (1981), whereas the data of Tawara et al (1975) and Bhattacharya et al (1980) deviate considerably at low E_p. $\sigma_{L\alpha}^{X}/\sigma_{L\beta}^{X}$ ratios reported in this thesis and those of other workers, illustrated in figure 6.95, are overpredicted significantly by the theories and disagreement tends to increase to about 15% with decreasing E_p. $\sigma_{L\alpha}^{X}/\sigma_{L\gamma}^{X}$ ratios, figure 6.96, also show similar behaviour. However, the present values in contrast to the other measurements converge towards the predicted values. In the case of $\sigma_{L\beta}^{X}/\sigma_{L\gamma}^{X}$, also shown in figure 6.96, a very close agreement is observed with the theoretical approximations. The data reported by other authors, however, lie significantly below the present values.

6.5.2 Deuteron Impact Measurements

The energy dependence of the measured σ_{L_1} is reproduced well by the ECPSSR theory, as shown in figure 6.97, although quantitatively the data lies above the predictions by approximately 11%. σ_{L_2}, figure 6.97, is also reproduced qualitatively by the ECPSSR whereas numerically the PWBA model shows closer agreement. σ_{L_3} and σ_{Lt}, illustrated in figure 6.98, are explained quite well by the ECPSSR theory.

The theoretical predictions reproduce closely the measured $\sigma_{L_1}/\sigma_{L_2}$ ratios, figure 6.99. $\sigma_{L_1}/\sigma_{L_3}$, however, deviates increasingly from the theoretical values with decreasing E_d by upto 40% and $\sigma_{L_2}/\sigma_{L_3}$ ratios lie considerably above the ECPSSR curve, shown in figure 6.100.

$\sigma_{L\ell}^{x}$, $\sigma_{L\alpha}^{x}$ and $\sigma_{L\beta}^{x}$ are illustrated in figure 6.101. At $E_d > 2$ MeV $\sigma_{L\ell}^{x}$ data agrees very well with the ECPSSR values and tends towards the PWBA curve at lower energies. The ECPSSR predictions of $\sigma_{L\alpha}^{x}$ show very good correlation with the measured values. $\sigma_{L\beta}^{x}$, however, is systematically underestimated by the ECPSSR model by 10-20%. These deviations are in line with those observed for σ_{L_2}, figure 6.97. Similar discrepencies are noticed for $\sigma_{L\gamma}^{x}$ and $\sigma_{L\gamma_j}^{x}$, shown in figure 6.102, although the energy dependence is explained well by the theories. σ_{Lt}^{x}, figure 6.103, is reproduced very successfully by the ECPSSR approximation.

Energy dependence of the measured $\sigma_{L\alpha}^{x}/\sigma_{L\ell}^{x}$ ratios, figure 6.104, is more apparent than observed for proton impact measurements (figure 6.94) and the data converges towards the predicted value as E_d increases. $\sigma_{L\alpha}^{x}/\sigma_{L\beta}^{x}$ ratios are grossly overpredicted by the ECPSSR predictions, particularly at lower E_d values, shown in figure 6.105. Analogous behaviour is observed for $\sigma_{L\alpha}^{x}/\sigma_{L\gamma}^{x}$, figure 6.106. $\sigma_{L\beta}^{x}/\sigma_{L\gamma}^{x}$ ratios, also shown in figure 6.106, describe a much better agreement with the theories.

6.5.3 Alpha Particle Impact Measurements

Figure 6.107 illustrates the measured σ_{L_1} and σ_{L_2}, together with the values of Cohen (1981) and those predicted by the PWBA and ECPSSR approximations. σ_{L_1} values increasingly deviate from the ECPSSR model by about 46% as E_α decreases. The values reported by Cohen (1981) lie below the present data although agreement is observed within the experimental uncertainties of Cohen's (1981) values. σ_{L_2} exhibits much closer correlation with the PWBA model and the values of Cohen (1981) differ from the ECPSSR predictions even more, especially at lower impact energies. Agreement with the values predicted by the ECPSSR theory is much better for σ_{L_3} and σ_{Lt}, illustrated in figure 6.108. With regard to the values reported by Cohen (1981) correlation with the present data is seen only at intermediate energies.

Reasonable agreement is observed for $\sigma_{L_1}/\sigma_{L_2}$ with the theoretical predictions, figure 6.109. The data of Cohen (1981) deviates significantly below the present values by as much as 80%. Better agreement is observed for $\sigma_{L_1}/\sigma_{L_3}$ ratio with the theories and the values of Cohen (1981) except at $E_\alpha < 1.8$ MeV where the present data predict much higher values, figure 6.110. The measured $\sigma_{L_2}/\sigma_{L_3}$ ratios, figure 6.111, decrease with increasing E_α, in contrast to the theoretical models, and converge towards the theories at $E_\alpha > 2.6$ MeV. This circumstance is supported by the values of Cohen (1981) although these values show a less sharpe variation with E_α than indicated by the present data.

The σ_{Li} data of Bhattacharya et al (1982), for 0.9 - 1.8 MeV alpha particle impact on Au, came to the authors attention after the analysis of the data had been performed and, thus, was not included in figures 6.107 - 6.111. However, within the energy range of interest, the present values are larger than those of Bhattacharya et al (1982) by 25-50% for σ_{L_1}, 4-12% for σ_{L_2} and 80-180% for σ_{L_3}. In the case of σ_{Lt} the values differ by about a factor of 1.5. With regard to the ratios the data of Bhattacharya et al (1982) indicate similar trends to that of the present values, figure 6.109 - 6.111, but deviate numerically by 25-60%, $\sigma_{L_2}/\sigma_{L_3}$ showing the worst disagreement.

The ECPSSR theory predicts closely the $\sigma_{L\ell}^{X}$ data, figure 6.112, except at E_α < 2.0 MeV. For $\sigma_{L\alpha}^{X}$ deviations arise at E_α > 2.6 MeV, below which agreement with the ECPSSR theory is good, figure 6.112. Discrepencies are more pronounced for $\sigma_{L\beta}^{X}$ and increase with decreasing E_α to about 35%, also demonstrated in figure 6.112. $\sigma_{L\gamma_{236844'}}^{X}$ and $\sigma_{L\gamma_{15}}^{X}$, figure 6.113, exhibit similar behaviour to that of σ_{L_1} and σ_{L_2} respectively shown in figure 6.107. The large disagreements observed for $\sigma_{L\gamma_j}^{X}$ are reflected in $\sigma_{L\gamma}^{X}$, illustrated in figure 6.113, and are increasingly under-estimated by the ECPSSR theory as E_α decreases. σ_{Lt}^{X}, measured in this work, follow the general trend of the ECPSSR model but lie above the theory by 20%.

The measured $\sigma_{L\alpha}^{X}/\sigma_{L\ell}^{X}$ ratios show much more striking dependence on impact energy, figure 6.115, than was indicated by proton and deuteron measurements (figures 6.94 and 6.104 respectively). The measured values crossover the ECPSSR prediction at $E_\alpha \simeq$ 2.4 MeV. Large disagreement is noticed at E_α < 2.6 MeV for $\sigma_{L\alpha}^{X}/\sigma_{L\beta}^{X}$, as shown in figures 6.116. This behaviour is reprodcued by $\sigma_{L\alpha}^{X}/\sigma_{L\gamma}^{X}$, figure 6.117. Agreement with the theories is in general quite good for $\sigma_{L\beta}^{X}/\sigma_{L\gamma}^{X}$ ratio, since the large σ_{L_2} discrepencies cancel to a certain extent.

6.6 LEAD (Z_2 = 82)

L_ℓ, L_α, L_β, L_γ, $L_{\gamma_{15}}$ and $L_{\gamma_{236844'}}$ x-ray production cross sections were determined for protons, deuterons and alpha particles incident on lead (Pb). L_i subshell ionisation cross sections were deduced from $\sigma_{L\alpha}^{X}$, $\sigma_{L\gamma_{15}}^{X}$ and $\sigma_{L\gamma_{236844'}}^{X}$.

6.6.1 Proton Impact Measurements

Figures 6.118 and 6.119 illustrate L_i subshell and total L shell ionisation cross sections for proton impact on Pb. At E_p > 1.4 MeV

ECPSSR predictions and measured σ_{L_1} differ by upto 60% and much larger deviations are observed for the data Leite et al (1977) and Cohen (1980) from the theory. The thin target σ_{L_1} values of Cohen (1980) are larger than the present ones by nearly a factor of 2 in the region of the plateay at $E_p \simeq 1.2$ MeV. Agreement between the present σ_{L_2} values and those of Leite et al (1977) and Cohen (1980) is very good and all measured values exhibit better correlation with the PWBA model than the ECPSSR. With regard to σ_{L_3} and σ_{Lt} the present values in general show reasonable agreement with the ECPSSR model but differ significantly from the other measured data at $E_p < 2.0$ MeV.

The minimum in $\sigma_{L_1}/\sigma_{L_2}$ ratio, shown in figure 6.120, is reproduced well by the present data and that of Leite et al (1977) while the values of Cohen (1980) indicate a much less pronounced minimum. The under-prediction of σ_{L_1} and σ_{L_2} by the ECPSSR model is stikingly evident in $\sigma_{L_2}/\sigma_{L_3}$ and $\sigma_{L_2}/\sigma_{L_3}$ ratios, shown in figure 6.121, where the data consistently lies above the theoretical estimates. In the case of $\sigma_{L_2}/\sigma_{L_3}$ the present data indicate considerably larger discrepencies from the theories than implied by the other measured values.

The ECPSSR theory overpredicts the measured $\sigma_{L\ell}^{X}$ values at $E_p > 2.0$ MeV and this is supported by the data of Tawara et al (1974), figure 6.122. The initial measurements of $\sigma_{L\ell}^{X}$ (Sokhi and Crumpton 1982) show some disagreement with the present values at the extremities of the energy range (~ 18%). However, these differences are comparable to the uncertainties in the intial values. Furthermore the preliminary measurements were performed with low beam currents, typically 3 - 10nA, and consequently the problem of leakage current, discussed in subsection 5.4.1, can become significant. The present values of $\sigma_{L\alpha}^{X}$, and the other measured data of Tawara et al (1974), Leite et al (1977) and Sokhi and Crumpton (1982), describe very good agreement with the ECPSSR predictions whereas the $\sigma_{L\beta}^{x}$ values, although agreeing with each other, lie significantly above the theory, figure 6.123. $\sigma_{L\gamma_{15}}^{x}$ and $\sigma_{L\gamma_{236844'}}^{x}$, shown in figure 6.124, display large disagreement with the theories and these are reflected in $\sigma_{L\gamma}^{x}$ values, which are larger than the ECPSSR estimates by upto 35%. The other measured values of $\sigma_{L\gamma}^{x}$, figure 6.124, in general provide very close agreement with the present data. In the case of σ_{Lt}^{x}, figure 6.125, good agreement is found with the ECPSSR theory and with the values of other authors.

$\sigma_{L\alpha}^{x}/\sigma_{L\ell}^{x}$ data of Tawara et al (1974) support the energy dependence indicated by ratios measured in this study, figure 6.126. There is also a measure of agreement with the values of Sokhi and Crumpton (1982) except at higher energies. Since the experimental $\sigma_{L\beta}^{x}$ values are larger then predicted the $\sigma_{L\alpha}^{x}/\sigma_{L\beta}^{x}$ ratio yields values considerably smaller than those of the ECPSSR model, as demonstrated in figure 6.127. The other measured values exhibit similar trends. This effect is also apparent in the case of $\sigma_{L\alpha}^{x}/\sigma_{L\gamma}^{x}$ ratio and to a lesser extend in $\sigma_{L\beta}^{x}/\sigma_{L\gamma}^{x}$ shown in figure 6.128.

6.6.2 Deuteron Impact Measurements

Although the ECPSSR model describes the energy dependence of σ_{L_1} quite well it underestimates the measured values by upto 40% as illustrated in figure 6.129. A similar disagreement is observed for σ_{L_2}, also shown in figure 6.129. Measured values of σ_{L_3} show adequate correlation with the ECPSSR predictions and the agreement with theory is even better for σ_{Lt}, figure 6.130. The deviations encountered for σ_{L_1} and σ_{L_2}, figure 6.129, partly cancel in $\sigma_{L_1}/\sigma_{L_2}$ ratio and as a result the experimental data follows the ECPSSR curve quite well, figure 6.131. Underestimation of σ_{L_1} by the ECPSSR approximation is highlighted in $\sigma_{L_1}/\sigma_{L_3}$, shown in figure 6.132, where the data lies above the theory by about 25-50%. Disagreement with theory is even more striking in the case of $\sigma_{L_2}/\sigma_{L_3}$ ratio, figure 6.133.

In line with the trend of σ_{L_3}, figure 6.130, $\sigma_{L\ell}^{X}$ and $\sigma_{L\alpha}^{X}$ describe good agreement with the ECPSSR estimates, demonstrated in figure 6.134. The PWBA theory provides a better description of the measured $\sigma_{L\beta}^{X}$ values, figure 6.134. Energy variation of $\sigma_{L\gamma}^{X}$ and $\sigma_{L\gamma_j}^{X}$ is reproduced well by the ECPSSR model, figure 6.135, but the theory significantly underestimates the numerical values, unlike the case of σ_{Lt}^{X}, figure 6.136, where the theory provides an extremely good agreement.

The energy dependence of $\sigma_{L\alpha}^{X}/\sigma_{L\ell}^{X}$ observed for proton measurements figure 6.126, is supported by deuteron impact values, shown in figure 6.137. The theories grossly overpredict the $\sigma_{L\alpha}^{X}/\sigma_{L\beta}^{X}$ ratio, figure 6.138, although the energy variation is similar to that described by the data. The situation is analogous for $\sigma_{L\alpha}^{X}/\sigma_{L\gamma}^{X}$, figure 6.139. Overprediction of $\sigma_{L\beta}^{X}/\sigma_{L\gamma}^{X}$ by the theories, figure 6.139, is less marked but gains importance as E_d increases.

6.6.3 Alpha Particle Impact Measurements

The ECPSSR thoery describes the σ_{L_1} data well at $E_\alpha > 2.0$ MeV, figure 6.140, below which the data deviates by upto 24%. Devaitions of upto a factor of 3.5 are observed for σ_{L_2}, figure 6.140, in comparison with the ECPSSR theory. The measured values of Cohen (1981) disagree with the present σ_{L_1} values only at $E_\alpha < 1.8$ MeV and with σ_{L_2} at $E_\alpha > 2.2$ MeV. The present σ_{L_3} and σ_{Lt} values and those of Cohen (1981) show very good correlation with each other but deviate by upto 30% at low E_α from theory, figure 6.141.

$\sigma_{L_1}/\sigma_{L_2}$ ratio describe very large disagreements with the theories at lower energies. The measured values show a maximim at $E_\alpha \simeq 1.8$ MeV in stark contrast to the models. This appears to be verified by the thin target measurements of Cohen (1981), figure 6.142. In contrast $\sigma_{L_1}/\sigma_{L_3}$ ratios in general show good agreement with the ECPSSR theory. The data of Cohen (1981), however, disagrees with the presnt values considerably at $E_\alpha < 2.2$ MeV, as illustrated in figure 6.143. The present $\sigma_{L_2}/\sigma_{L_3}$ data and that a Cohen (1981) describe an energy dependence that is contradictory to the theoretically predicted variations and decreases with increases E_α, figure 6.144.

$\sigma_{L\alpha}^{x}$ and $\sigma_{L\ell}^{x}$ increasingly deviate from the ECPSSR curve as E_α decreases, as shown in figure 6.145, $\sigma_{L\ell}^{x}$, however, shows larger discrepencies than $\sigma_{L\alpha}^{x}$. Deviations of 15-65% are observed for $\sigma_{L\beta}^{x}$, figure 6.145, with larger deviations ocurring at low energies. $\sigma_{L\gamma_{236844'}}^{x}$ disagrees with the ECPSSR model significantly on at $E_\alpha < 2.0$ MeV. The large discrepencies noticed for σ_{L_2}, figure 6.140, are reflected in $\sigma_{L\gamma_{15}}^{x}$, and hence in $\sigma_{L\gamma}^{x}$, shown in figure 6.146. These differences and those observed for $\sigma_{L\beta}^{x}$ cause σ_{Lt}^{x} to disagree with the ECPSSR predictions by as much as 40% at low impact energies, figure 6.147.

Measured values of $\sigma_{L\alpha}^{x}/\sigma_{L\ell}^{x}$ for incident alpha particles provide further evidence for the ratio being energy dependent, demonstrated in figure 6.148. The gross σ_{L_2} discrepencies cause $\sigma_{L\alpha}^{x}/\sigma_{L\beta}^{x}$ ratio, figure 6.149, to be overestimated considerably by the ECPSSR model. The same is true for $\sigma_{L\alpha}^{x}/\sigma_{L\gamma}^{x}$ ratio shown in figure 6.150. σ_{L_2} deviations particularly cancel in the $\sigma_{L\beta}^{x}/\sigma_{L\gamma}^{x}$ ratios and consequently the experimental data provides a much better agreement with the ECPSSR theory, figure 6.151.

6.7 BISMUTH ($Z_2 = 83$)

Cross sections for $L\ell$, $L\alpha$, $L\beta$, $L\gamma$, $L\gamma_{15}$ and $L\gamma_{236844'}$ ($L\gamma_{2368}$ in the case of deuteron and alpha particle impact) have been measured for the three projectiles incident on Bi. σ_{Li}'s were determined from $\sigma_{L\gamma j}^{x}$ and $\sigma_{L\alpha}^{x}$.

6.7.1 Proton Impact Measurements

σ_{Li} and σ_{Lt} for incident protons are illustrated in figure 6.152. The structure in σ_{L_1}, as predicted by the theories at $Ep \simeq 1.8$ MeV, is not indicated by the present measured values. In this E_p region the data and the ECPSSR theory differ by upto 45%, below which the data converges towards the theory and may imply that the σ_{L_1} structure occurs at a lower E_p value than predicted by the theory. The sparse values of Leite et al (1977) are much larger than the present data but show agreement at lower energies. The measured σ_{L_2} values lie above the ECPSSR theory by about 20-50%. The values of Leite et al (1977) deviate from the present data only at high impact energies and show close correlation with the ECPSSR model. In general the present σ_{L_3} and σ_{Lt} are in good agreement with the ECPSSR theory and with the data of Leite et al (1977).

The ECPSSR model explains the present $\sigma_{L_1}/\sigma_{L_2}$ data at intermediate energies but deviates significantly at the extremities of the energy range, figure 6.153. Values measured by Leite et al (1977) show marked disagreement from the theories and from the present values. In the case of $\sigma_{L_1}/\sigma_{L_2}$, figure 6.154, the ECPSSR theory and the present values show good correlation only at low energies. As was the situation for $\sigma_{L_1}/\sigma_{L_2}$, $\sigma_{L_1}/\sigma_{L_3}$ values of Leite et al (1977) increasingly deviate from the results of this work as E_p increases. The $\sigma_{L_2}/\sigma_{L_3}$ ratios are consistently underestimated by the theoretical models by upto 50% in the case of the present values and by upto 27% for the values of Leite et al (1977), figure 6.154.

$\sigma_{L\ell}^{x}$ and $\sigma_{L\alpha}^{x}$, measured in this work and shown in figure 6.155, agree well with the ECPSSR model and with the measured data of Tawara et al (1975) and Leite et al (1977). The data of Bhattacharya et al (1980), however, lie significantly above the other values. With regard to the other experimental results the situation is similar for $\sigma_{L\beta}^{x}$, the ECPSSR model however, considerably underpredicts the measured data, figure 6.155. Large discrepencies between present $\sigma_{L\gamma}^{x}$ and $\sigma_{L\gamma_{15}}^{x}$ and the ECPSSR theory are also observed, figure 6.156. The other measured values of $\sigma_{L\gamma}^{x}$ describe larger deviations from the theory. $\sigma_{L\gamma_{236844}}^{x}$, figure 6.156, is also considerably underestimated by the ECPSSR theory and displays better agreement with the PWBA theory at low E_p. Agreement, however, is good between the present σ_{Lt}^{x} and the other measured data, except that of Bhattacharya et al (1980) which lie above the other values, figure 6.157. The ECPSSR model also offers a good description of the experimental values.

The present $\sigma_{L\alpha}^{x}/\sigma_{L\gamma}^{x}$ ratios and those of Tawara et al (1975) show very good agreement with each other and with thoretical predictions figure 6.158. The present data, however, suggests a slow variation with E_p. Values of Bhattacharya et al (1980) lie significantly below the values of this study. All the measured $\sigma_{L\alpha}^{x}/\sigma_{L\beta}^{x}$ ratios agree with each other quite well but lie considerably below the thories, as shown in figure 6.159. The situation is very similar for $\sigma_{L\alpha}^{x}/\sigma_{L\gamma}^{x}$ ratio, illustrated in figure 6.160. Comparison between the present $\sigma_{L\beta}^{x}/\sigma_{L\gamma}^{x}$ values, and of other authors, show a reasonable agreement with the theories, figure 6.160.

6.7.2 Deuteron Impact Measurements

Figure 6.161 shows σ_{L_i} and σ_{Lt} for deuteron impact on Bi. At Ep < 1.8 MeV the σ_{L_1} data is explained well by the ECPSSR model and at higher energies the data converges towards the PWBA theory. The σ_{L_2} data lies above the ECPSSR theory by as much as 60%. Agreement with the ECPSSR theory is very good for σ_{L_3} and σ_{Lt} except at low energies.

The σ_{L_2} discrepencies are clearly apparent in figure 6.162, which shows $\sigma_{L_1}/\sigma_{L_2}$, particularly at low impact energies. Agreement is much better for $\sigma_{L_1}/\sigma_{L_3}$, figure 6.163, throughout the energy range. The measured $\sigma_{L_2}/\sigma_{L_3}$ ratio lies systematically above the theory by about 40%, as shown in figure 6.164.

$\sigma^{x}_{L\ell}$ and $\sigma^{x}_{L\alpha}$, shown in figure 6.165, follow the trend of σ_{L_3} and deviate from the ECPSSR only at Ep < 1.8 MeV. The σ_{L_2} deviations, figure 6.161, are reflected in $\sigma^{x}_{L\beta}$ which lie considerably above the theories, figure 6.165. The ECPSSR model underestimates $\sigma^{x}_{L\gamma_{2368}}$ by upto 40% and $\sigma^{x}_{L\gamma}$ and $\sigma^{x}_{L\gamma_{15}}$ by upto 50%, figure 6.166. σ^{x}_{Lt}, shown in figure 6.167, is in general explained better by the PWBA model than the ECPSSR.

The energy variation described by the measured $\sigma^{x}_{L\alpha}/\sigma^{x}_{L\ell}$ ratio for deuteron impact, figure 6.168, is much more marked than was noticed for incident protons, figure 6.158. The $\sigma^{x}_{L\alpha}/\sigma^{x}_{L\beta}$ and $\sigma^{x}_{L\alpha}/\sigma^{x}_{L\gamma}$ ratios, measured in this study, are considerably overestimated by the theories, as demonstrated in figures 6.169 and 6.170 respectively. The σ_{L_2} deviations cancel to a certain extent in $\sigma^{x}_{L\beta}/\sigma^{x}_{L\gamma}$ ratio and consequently the ratio shows reasonable agreement with ECPSSR predictions.

6.7.3 Alpha Particle Impact Measurements

The present σ_{L_1} values for alpha particles incident on Bi, figure 6.171, exhibit good agreement with the ECPSSR model at intermediate energies. Values of Bhattacharya et al (1982) show reasonable agreement with the present data within the experimental uncertainties quoted by the author (15%). The present σ_{L_2} data, and that of Bhattacharya et al (1982), show much closer correlation with the PWBA theory than with the ECPSSR model, figure 6.171. In the case of σ_{L_3} and σ_{Lt}, shown in figure 6.172, they are explained well by the ECPSSR theory except at E_{α} < 2 MeV. Measurements of Bhattacharya et al (1982) show large deviations from the present data, particularly for σ_{L_3} where the deviations of upto a factor of 2.5 are observed.

$\sigma_{L_1}/\sigma_{L_2}$ ratio, measured in this work, lies considerably below the theories and show increasing disagreement as E_{α} decreases, figure 6.173. This is supported by the data of Bhattacharya et al (1982). Agreement with the theories is much better for the present $\sigma_{L_1}/\sigma_{L_3}$ values figure 6.174. Data of Bhattacharya et al (1982), however, depict very large discrepencies from the values of this study, particularly at lower impact energies. The situation is very similar for $\sigma_{L_2}/\sigma_{L_3}$, figure 6.175, with regard to the measured values of Bhattacharya et al (1982). The models underestimate the $\sigma_{L_2}/\sigma_{L_3}$ ratio considerably at all energies.

$\sigma_{L\ell}^{X}$ and $\sigma_{L\alpha}^{X}$, illustrated in figures 6.176 and 6.177, follow the trend of σ_{L_3} and show good correlation with the ECPSSR model for $E_\alpha > 2$ MeV. $\sigma_{L\beta}^{X}$, figure 6.177, disagree increasingly from the ECPSSR approximation as E_α decreases. $\sigma_{L\alpha}^{X}$ and $\sigma_{L\beta}^{X}$ values of Braziewicz et al (1984) lie significantly below the present values and disagree by as much as 80% at high E_α. The present $\sigma_{L\gamma_{2368}}^{X}$ values agree with the ECPSSR model at high energies but tend towards the PWBA curve as E_α decreases figure 6.178. $\sigma_{L\gamma_{15}}^{X}$ and $\sigma_{L\gamma}^{X}$, shown also in figure 6.178, are explained well by the uncorrected PWBA theory. The $\sigma_{L\gamma}^{X}$ values of Braziewicz et al (1984) lie below the present data. The same is true for σ_{Lt}^{X}, illustrated in figure 6.179. The ECPSSR model, however, reproduces σ_{Lt}^{X} quite well at $E_\alpha > 2.4$ MeV below which it underpredicts the data considerably.

The $\sigma_{L\alpha}^{X}/\sigma_{L\ell}^{X}$ ratio is observed to depend on E_α, in contrast to the ECPSSR theory, figure 6.180. The present $\sigma_{L\alpha}^{X}/\sigma_{L\beta}^{X}$ values, and those of Braziewicz et al (1984), shown in figure 6.181, are underpredicted by the ECPSSR model by upto 30%. Similar discrepencies are noticed for $\sigma_{L\alpha}^{X}/\sigma_{L\gamma}^{X}$ ratio, illustrated in figure 6.182. In the case of $\sigma_{L\beta}^{X}/\sigma_{L\gamma}^{X}$ ratio reasonable agreement with the ECPSSR theory is established only at low energies, figure 6.183. The data of Braziewicz et al (1984) agrees well with the present values.

6.8 THORIUM ($Z_2 = 90$)

$L\ell$, $L\alpha$, $L\beta$, $L\beta_{135}$, $L\beta_{24615}$, $L\gamma$, $L\gamma_{15}$ and $L\gamma_{2368}$ x-ray production cross sections have been determined for proton impact on Th. σ_{Li}

were deduced from $\sigma^{x}_{L\gamma_j}$ and $\sigma^{x}_{L\alpha}$.

The measured σ_{L_1} values, shown in figure 6.184 describe reasonable agreement with the ECPSSR theory except at E_p < 1.8 MeV. The data of Leite et al (1977) are considerably higher than the present data. Only qualitative agreement with the ECPSSR model is observed for σ_{L_2}, figure 6.184, and the present data and that of Leite et al (1977) are under-estimates markedly by the theory. In contrast, σ_{L_3} is explained well by the ECPSSR approximation and also shows good agreement with the values of Leite et al (1977) figure 6.185. σ_{Lt}, however, deviates significantly from the data of Leite et al (1977) and from the ECPSSR prediction at Ep > 2 MeV, also shown in figure 6.185.

The σ_{L_2} discrepencies are strikingly apparent in the case of $\sigma_{L_1}/\sigma_{L_2}$ ratio, illustrated in figure 6.186, where the data and the ECPSSR theory differ by upto a factor of 2. The data of Leite et al (1977) disagrees only at 3 MeV with the measurements of this study. Correlation between the present $\sigma_{L_1}/\sigma_{L_3}$ values and the ECPSSR theory is reasonable except at energies around 2.2 MeV, figure 6.187. Values of Leite et al exhibit large disagreements with the present data. The $\sigma_{L_2}/\sigma_{L_3}$ ratio is underestimated by the theories by about 70% and differs from the values of Leite et al (1977) at high Ep, as demonstrated in figure 6.188.

The present $\sigma^{x}_{L\ell}$ measurements show very good correlation with the ECPSSR model and the situation is similar for $\sigma^{x}_{L\alpha}$, figure 6.189. Agreement for $\sigma^{x}_{L\alpha}$ with the values of Leite et al (1977) is reasonable but rather poor with regard to the data of Bearse et al (1973) which are considerably below the present measurements. The nontrivial deviations observed for σ_{L_2}, figure 6.184, are reflected in $\sigma^{x}_{L\beta_{135}}$ and hence in $\sigma^{x}_{L\beta}$, shown in figure 6.190. The values of $\sigma^{x}_{L\beta_{24615}}$, figure 6.190, follow the behaviour of σ_{L_3} and describe satisfactory agreement with the ECPSSR model. $\sigma_{L\gamma}^{x}$ and $\sigma_{L\gamma_{15}}^{x}$, although agreeing qualitatively with the ECPSSR theory, are significantly underestimated by the theory, figure 6.191. Deviations between $\sigma_{L\gamma_{2368}}^{x}$ and the ECPSSR predictions increase with increasing Ep to about 45%, figure 6.191. The description of the measured σ_{Lt}^{x} data is quite good by the ECPSSR model except at Ep > 2 MeV, as shown in figure 6.192. Measurements of Leite et al (1977) disagree with the present data as Ep decreases.

$\sigma_{L\alpha}^{x}/\sigma_{L\ell}^{x}$ ratio, shown in figure 6.193, decreases at Ep < 2 Mev, unlike the theory which remains constant. Large differences between theory and present data are noticed for $\sigma_{L\alpha}^{x}/\sigma_{L\beta}^{x}$ and $\sigma_{L\alpha}^{x}/\sigma_{L\gamma}^{x}$ ratios, illustrated in figure 6.194 and 6.195 respectively. Much smaller deviations although still significant, are observed for $\sigma_{L\beta}^{x}/\sigma_{L\gamma}^{x}$ ratio, as shown in figure 6.196.

6.9 URANIUM (Z_2 = 92)

Proton induced L_ℓ, L_α, L_β, $L_{\beta_{135}}$, $L_{\beta_{24615}}$, L_γ, $L_{\gamma_{15}}$ and $L_{\gamma_{2368}}$ x-ray production cross sections have been measured for U. σ_{L_i} were determined from $\sigma_{L\gamma_j}^{x}$ and $\sigma_{L\alpha}^{x}$.

Figure 6.197 shows σ_{L_1} and σ_{L_2} measured in the present study. Disagreement for σ_{L_1} is observed from the ECPSSR values only at Ep around 2.2 MeV. The data of Leite et al (1977) shows good correlation with the present σ_{L_1} values except at 3 MeV. The present σ_{L_2} values, and those of Leite et al (1977), are underpredicted by the theories significantly. However, σ_{L_3} and σ_{Lt}, illustrated in figure 6.198, describe good agreement with the data of Leite et al (1977) and with the ECPSSR model.

The theories deviate increasingly from the present $\sigma_{L_1}/\sigma_{L_2}$ ratio at Ep < 2.2 MeV while the data of Leite et al (1977) show good correlation, figure 6.199. In the case of $\sigma_{L_1}/\sigma_{L_3}$, shown in figure 6.200, the theories underestimate the ratio at Ep > 2 MeV. The values of

Leite et al (1977) disagree only at 3 MeV. The present $\sigma_{L_2}/\sigma_{L_3}$ lie about 50% above the theories, the values of Leite et al (1977) describe even larger deviations, figure 6.201.

As was the case for σ_{L_3}, $\sigma^X_{L\ell}$ and $\sigma^X_{L\alpha}$ are described well by the ECPSSR model, figure 6.202. The other measured values of Tawara et al (1975), Leite et al (1977), and Bhattacharya et al (1980) show close agreement with the present values. The ECPSSR model explains $\sigma^X_{L\beta_{24615}}$ quite well but significantly underestimates $\sigma^X_{L\beta_{135}}$ and $\sigma^X_{L\beta}$, as shown in figure 6.203. The $\sigma^X_{L\beta}$ values of Tawara et al (1975) describe better agreement with the ECPSSR model at higher energies than the present data but agree with the present values, as do the data of Bhattacharya et al (1980), at lower energies. $\sigma^X_{L\gamma_{2368}}$ values measured in this work, follow the ECPSSR curve closely at Ep < 2 MeV but deviate above the theory at higher energies, figure 6.204. In the case of $\sigma^X_{L\gamma_{15}}$ and $\sigma^X_{L\gamma}$, shown also in figure 6.204, describe only the energy dependence predicted by the ECPSSR model and lie above the theory. The other experimental $\sigma^X_{L\gamma}$ values depict even larger descrepencies. Good agreement is observed for the present σ^X_{Lt} values with the ECPSSR predictions and with the other experimental data, as illustrated in figure 6.205.

Unlike the previous measurements, the $\sigma^X_{L\alpha}/\sigma^X_{L\ell}$ ratios for incident protons on U, figure 6.206, do not appear to depend on E_p noticibly and describe good correlation with the constant value predicted by the theory. The other measured data seems to support this observation. All the measured $\sigma^X_{L\alpha}/\sigma^X_{L\beta}$ values agree well with each other, figure 6.207, but lie considerably below the predicted curves. $\sigma^X_{L\alpha}/\sigma^X_{L\gamma}$ ratio of Bhattacharya et al (1980) shows better agreement with the values of this work than the data of Tawara et al (1975), figure 6.208. However, all values are overpredicted significantly by the theories. The present $\sigma^X_{L\beta}/\sigma^X_{L\gamma}$ ratios agree quite well with the ECPSSR model, in contrast to the values of other authors which lie considerably below the theories, particularly those of Tawara et al (1975).

6.10 TARGET ATOMIC NUMBER DEPENDENCE

To investigate the dependence of σ_{Li} and σ_{Lt} on target atomic number (Z_2) the appropriate cross sections were plotted versus Z_2 for 2 MeV incident ions. Figures 6.210-6.212 illustrate the Z_2 dependence for incident protons, deuterons and alpha particles respectively.

For incident protons the ECPSSR model predicts quite well the variation of σ_{L_1} with Z_2 except for Pb and Bi the values of which lie above the theoretical curve, figure 6.210. The PWBA theory yields the better agreement with the measured σ_{L_2} data for Dy, Yb, W, Au, Pb, and Bi. In the case of Th and U the model considerably underestimates the present values. σ_{L_3} and σ_{Lt} for all elements of interest are described well by the ECPSSR predictions, as shown in figure 6.210.

The flattening of the σ_{L_1} curve for incident 2 MeV deuterons at $Z_2 \simeq 80$, figure 6.211 , as predicted by the ECPSSR model, is reproduced quite reasonably by the present data. With regard to σ_{L_2} all values, except those for Pb and Bi, follow closely the trend described by the PWBA model. As with incident proton measurements σ_{L_3} and σ_{Lt}, shown in figure 6.211, show very good agreement with the ECPSSR model.

σ_{L_1}, σ_{L_3} and σ_{Lt} for 2 MeV incident alpha particles are explained reasonably by the ECPSSR theory whereas the PWBA theory exhibits better correlation with the σ_{L_2} data, as illustrated in figure 6.212.

6.11 GENERAL COMPARISON WITH THE ECPSSR THEORY

The ratio $R_i = \sigma_{Li}^{exp}/\sigma_{Li}^{ECPSSR}$ (exp = experimental), for the elements under study, has been plotted versus the corrected reduced velocity parameter, ξ_{Li}^{R}, defined by equation 4.54, for incident protons, deuterons and alpha particles. The resulting graphs indicate certain trends described by the measured data which are discussed below.

Figures 6.213-6.215 show R_i for L_1, L_2 and L_3 subshells for incident protons. R_1 clearly shows the large disagreement from the theory, upto 70%, for $\xi^R_{L_1} < 0.7$. Above this value of $\xi^R_{L_1}$ the ECPSSR model predicts the measured σ_{L_1} to within 15%. The considerable σ_{L_2} deviations noticed for the individual elements are dramatically displayed in the R_2 versus $\xi^R_{L_2}$ plot, shown in figure 6.214. The magnitude of this deviation appears to increase for heavier elements to about 60% for U. The theory reproduces the σ_{L_3} values for all elements of interest to within 20% although agreement improves as $\xi^R_{L_3}$ increases, as demonstrated in figure 6.215.

In the case of deuteron impact the σ_{L_1} data, represented by R_1 in figure 6.216, does not appear to depend on $\xi^R_{L_1}$ as clearly as did the proton data but deviations of nearly 50% are indicated by figure 6.216. With the exception of Dy σ_{L_1} values of the high Z_2 elements tend to be larger than the ECPSSR predictions at all values of $\xi^R_{L_1}$, whereas the lower Z_2 elements, Dy, Yb and W tend to yield values smaller than predicted. σ_{L_2} deviations, shown in figure 6.217, range from 10-60% above the theory with deviations tending to increase as $\xi^R_{L_2}$ decreases In contrast elements with intermediate Z_2 values appear to yield smaller σ_{L_3} than predicted by the ECPSSR model, as shown in figure 6.218. This plot of R_3 reveals the much better description of σ_{L_3} by the ECPSSR model than for σ_{L_1} and σ_{L_2}.

With regard to incident alpha particles disagreement for σ_{L_1} highlighted by the R_1 versus $\xi^R_{L_1}$ plot shown in figure 6.219, ranges upto nearly 50%. With the exception of Bi, σ_{L_1} data for higher Z_2 elements tend to be larger than the ECPSSR values and those of Yb and W are smaller at all $\xi^R_{L_1}$ values studied. Gross σ_{L_2} deviations are highlighted by figure 6.220, especially at $\xi^R_{L_2} < 0.4$ where experiment and ECPSSR theory differ by as much as a factor of 3.5. These particularly large discrepencies are displayed by Pb and Bi. Furthermore agreement between theory and experiments at best is only 25%. In general, σ_{L_3} is explained well by the ECPSSR model and deviation do not appear to exceed 30%, as demonstrated in figure 6.221. With the exception of Yb all other R_3 values appear to crossover the $R_3 = 1$ line at $\xi^R_{L_3} \simeq 0.4$.

Much of the above observations are supported by the recent works of Cohen (1983) and Mukoyama and Sarkadi (1983a, b) for proton and helium impact, although the present σ_{L_1} data indicate larger discrepencies than reported by these authors. A comparison of deuteron impact measurements does not appear to be available. The considerable deviations revealed by the present, and other measurements of σ_{Li} discussed in this thesis, clearly highlight the need for a more detail approach to the inner-shell ionisation phenomena. The possible reasons for these large disagreements, particularly for the L_2 subshell, are considered below. Firstly these disagreements may point directly at the approximate nature of the PWBA theory. More realistic atomic wave functions, instead of the hydrogenic type, would be desriable. Recently Mukoyama and Sarkadi (1983a, b) have employed relativistic, but still hydrogenic, wave functions and have noticed improvements in the calculated values of σ_{Li}. The relativistic Hartree-Fock type wave functions have been employed by Pauli et al (1978) in their impact-parameter-dependent treatment of inner-shell ionisations and they have observed significant improvements in σ_{Li} values. Secondly, the ECPSSR theory evaluates the Coulomb and binding energy correction by assuming the validity of the monopole approximation (Brandt and Lapicki 1979). As pointed out by Mukoyama and Sarkardi (1983b) dipole and quadrupole transitions may play an important role in the case of L_2 and L_3 subhsell ionisation. Sarkardi and Mukoyama (1981) have proposed a futher reason for these disagreements. They emphasise the need for taking into account collision-induced intra-shell transitions which will also affect σ_{Li}. Finally, the significant uncertainties in the atomic parameters, discussed in chapter 2, which are required to deduce σ_{Li} from σ_{Lj}^{x}, are also a source of concern and increase the difficulty in reaching precise conclusions regarding the actual reasons for the aforementioned discrepencies. Consequently, much more work is required in this field before the phenomena of inner-shell ionisation can be adequately understood and quantified.

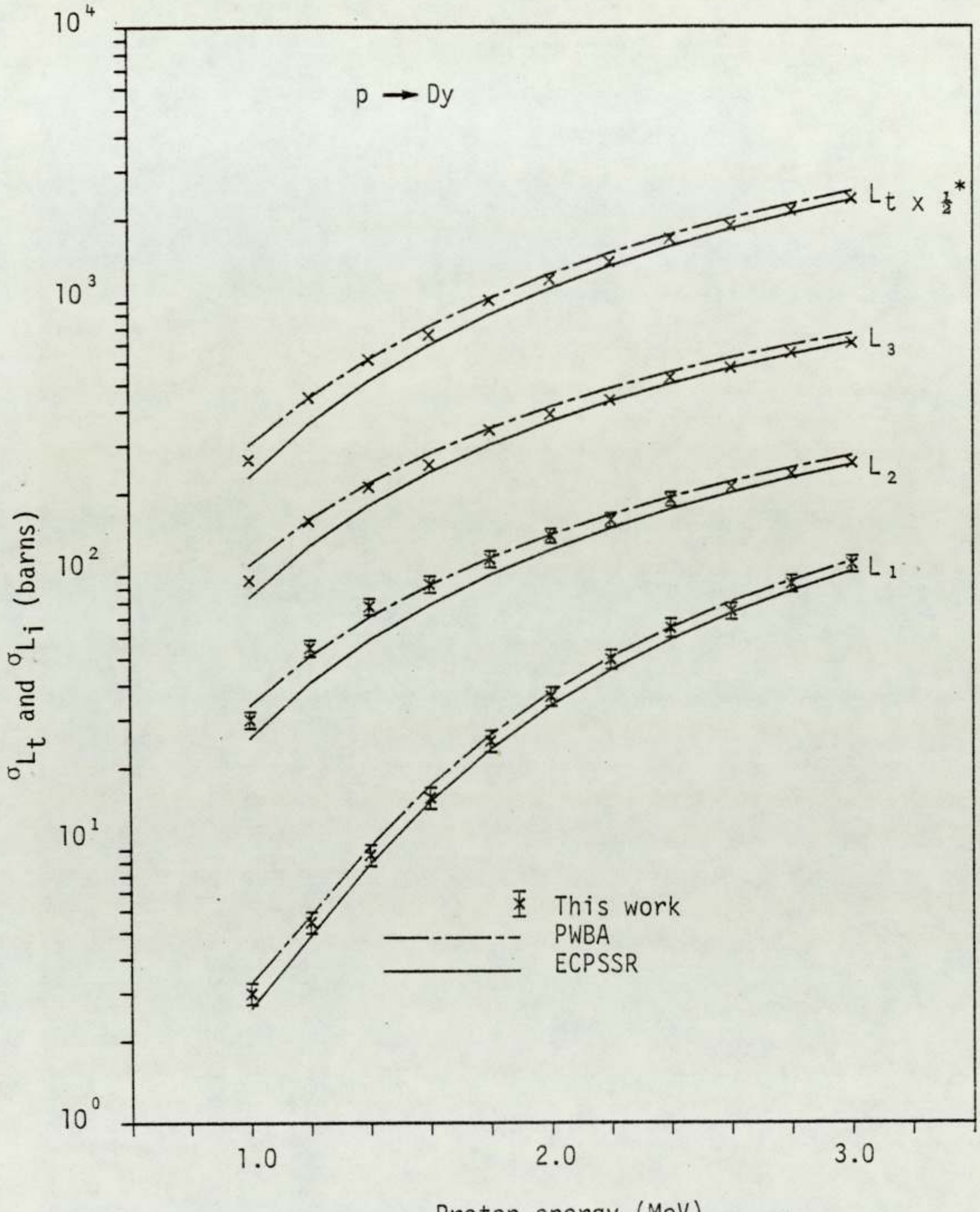

Figure 6.1. Experimental total (L_t) and individual L_i Subshell ionisation cross sections for proton impact on Dy.

* i To obtain the numerical values of the cross sections multiply by the factor indicated.

ii Error bars are omitted where they are too small to be seen clearly.

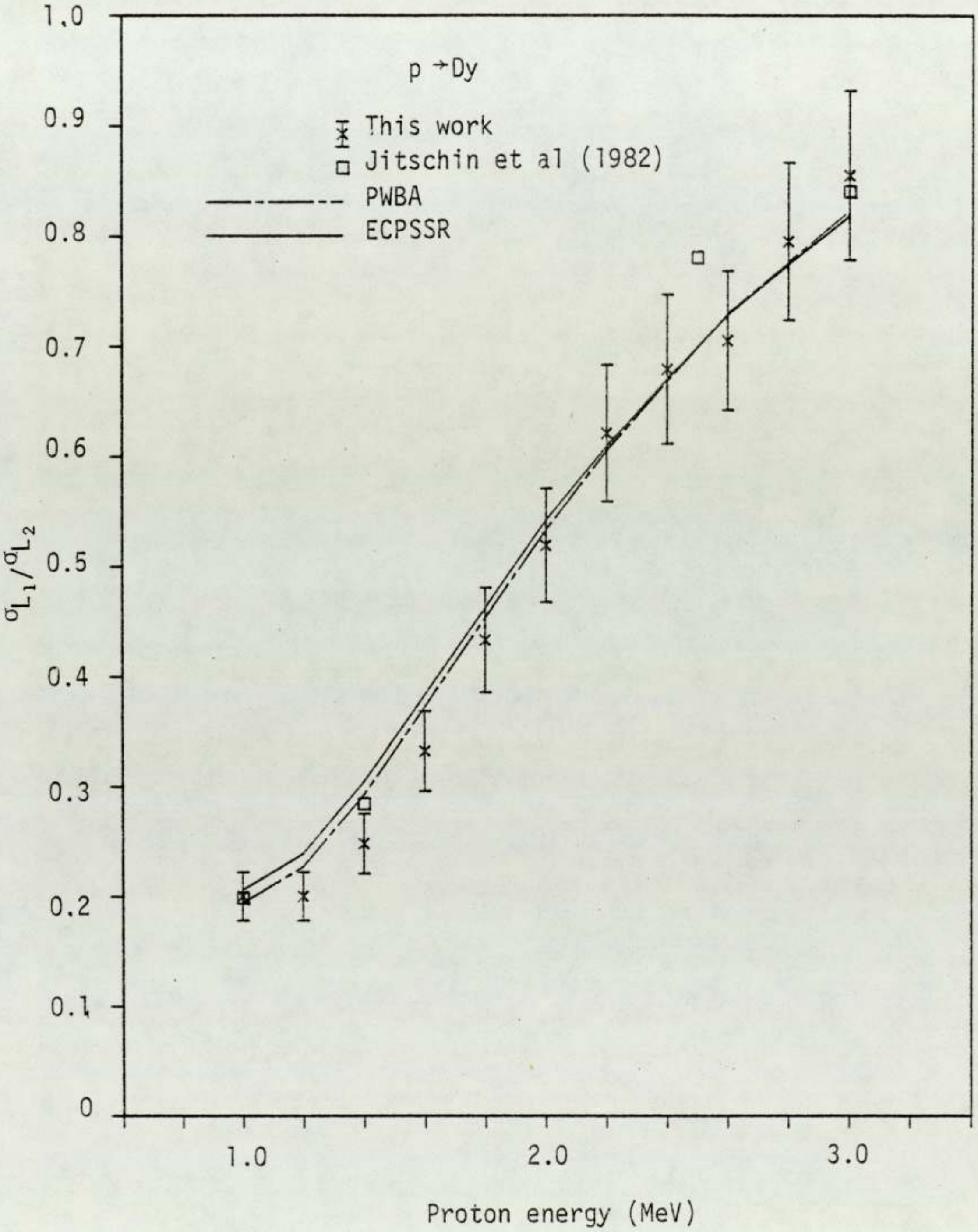

Figure 6.2. Experimental $\sigma_{L_1}/\sigma_{L_2}$ ratio for proton impact on Dy.

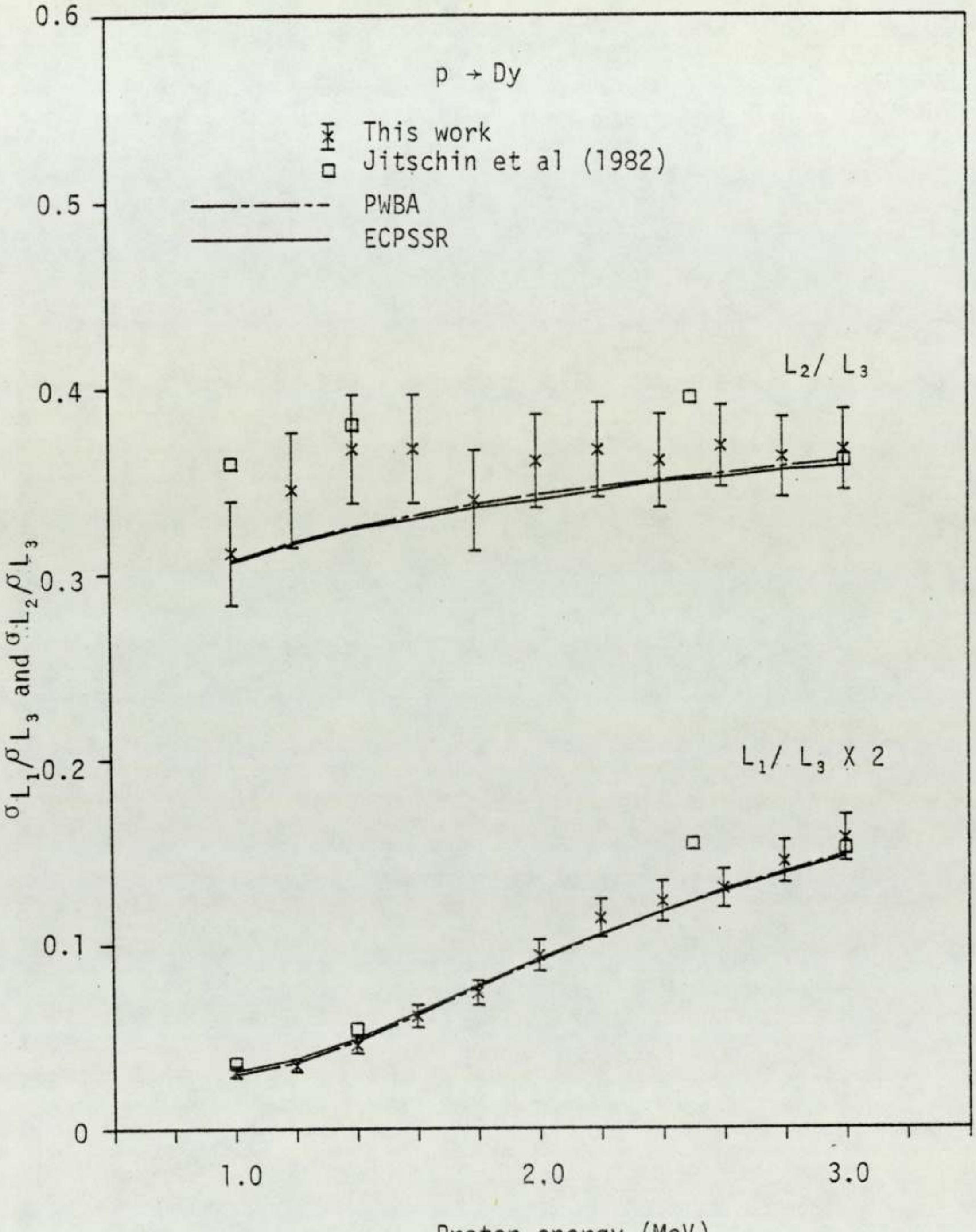

Figure 6.3. Experimental $\sigma L_1/\sigma L_3$ and $\sigma L_2/\sigma L_3$ ratios for proton impact on Dy.

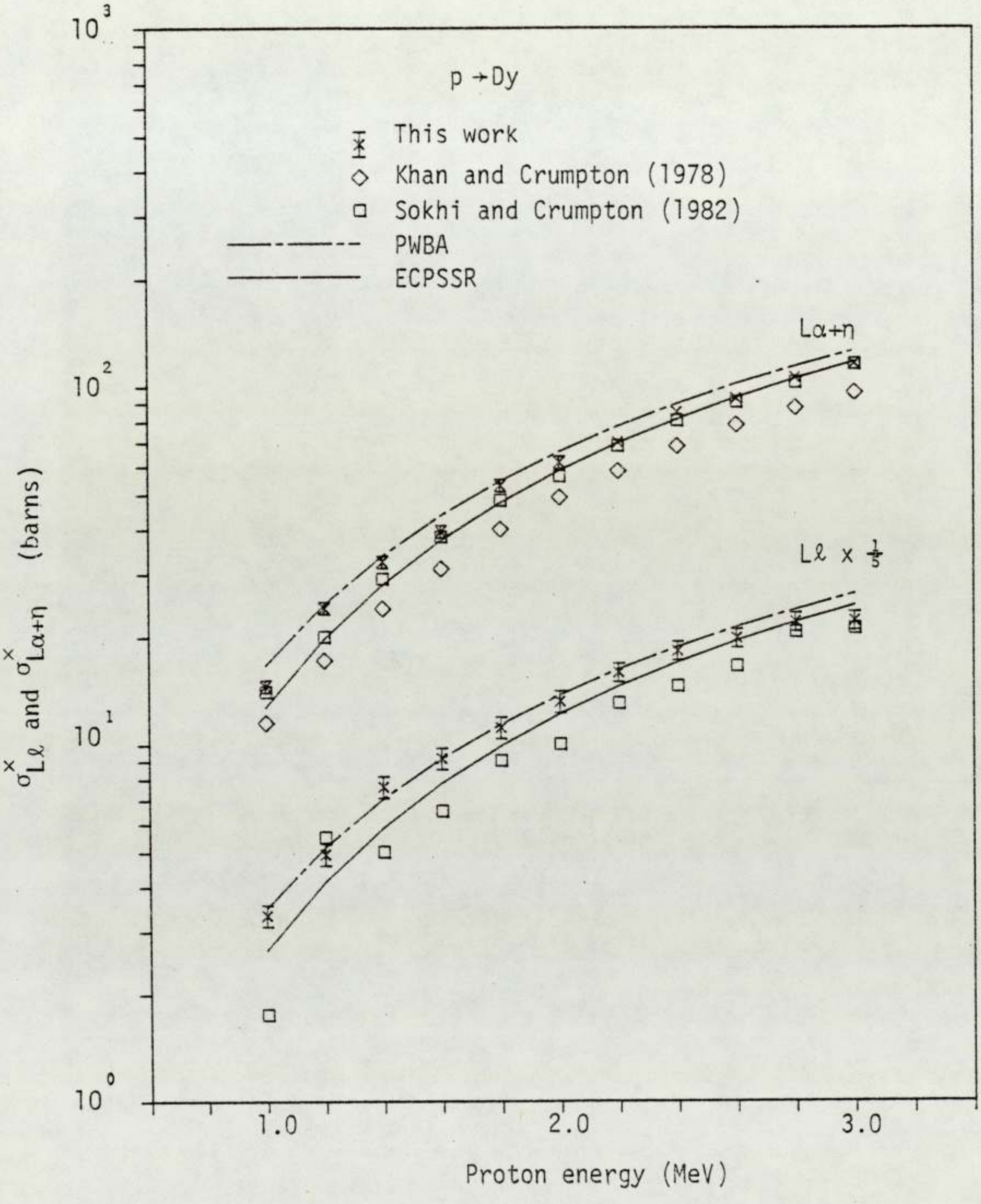

Figure 6.4. Experimental Lℓ and Lα+η x-ray production cross sections for proton impact on Dy.

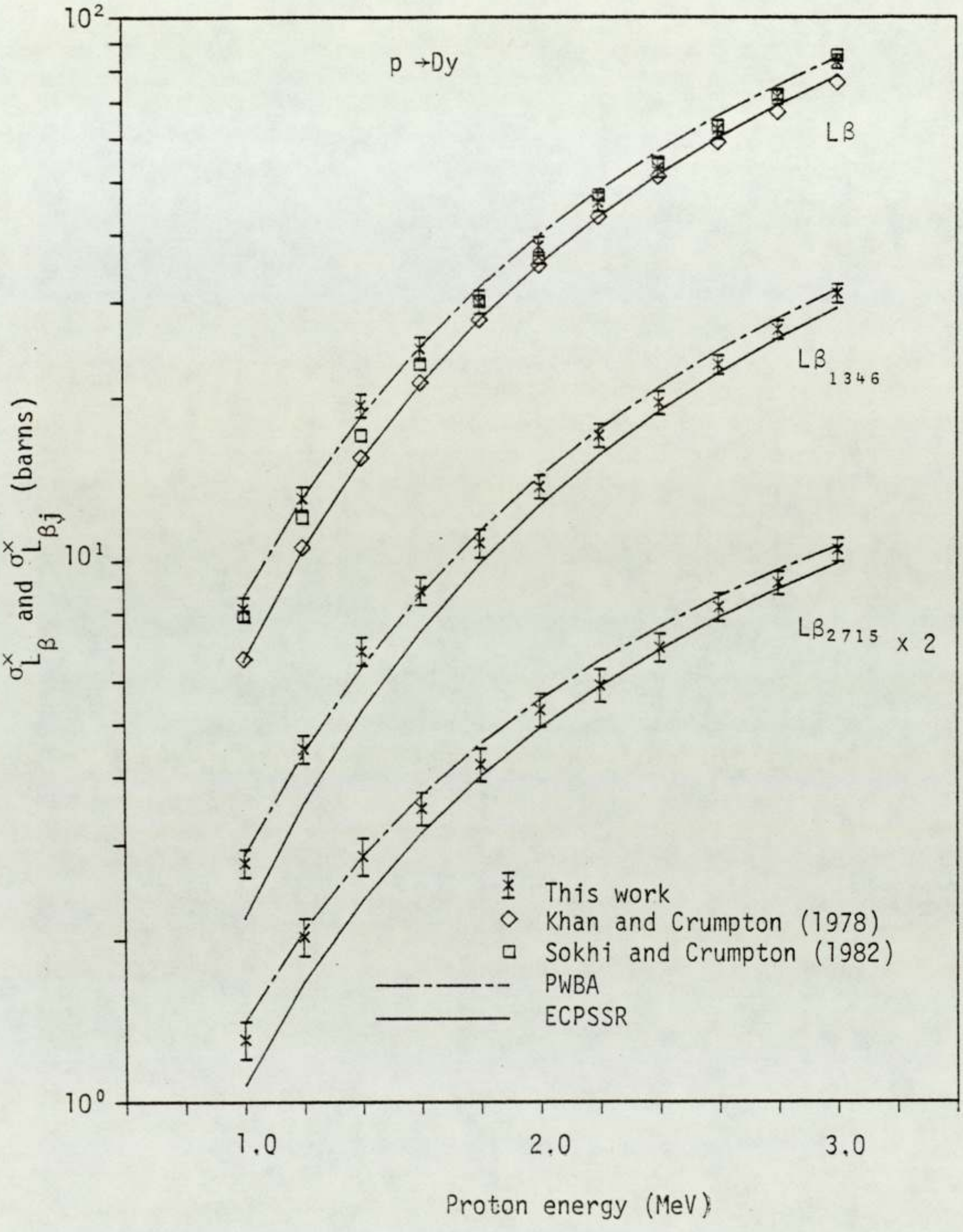

Figure 6.5. Experimental total Lβ and partial $L\beta_j$ x-ray production cross sections for proton impact on Dy.

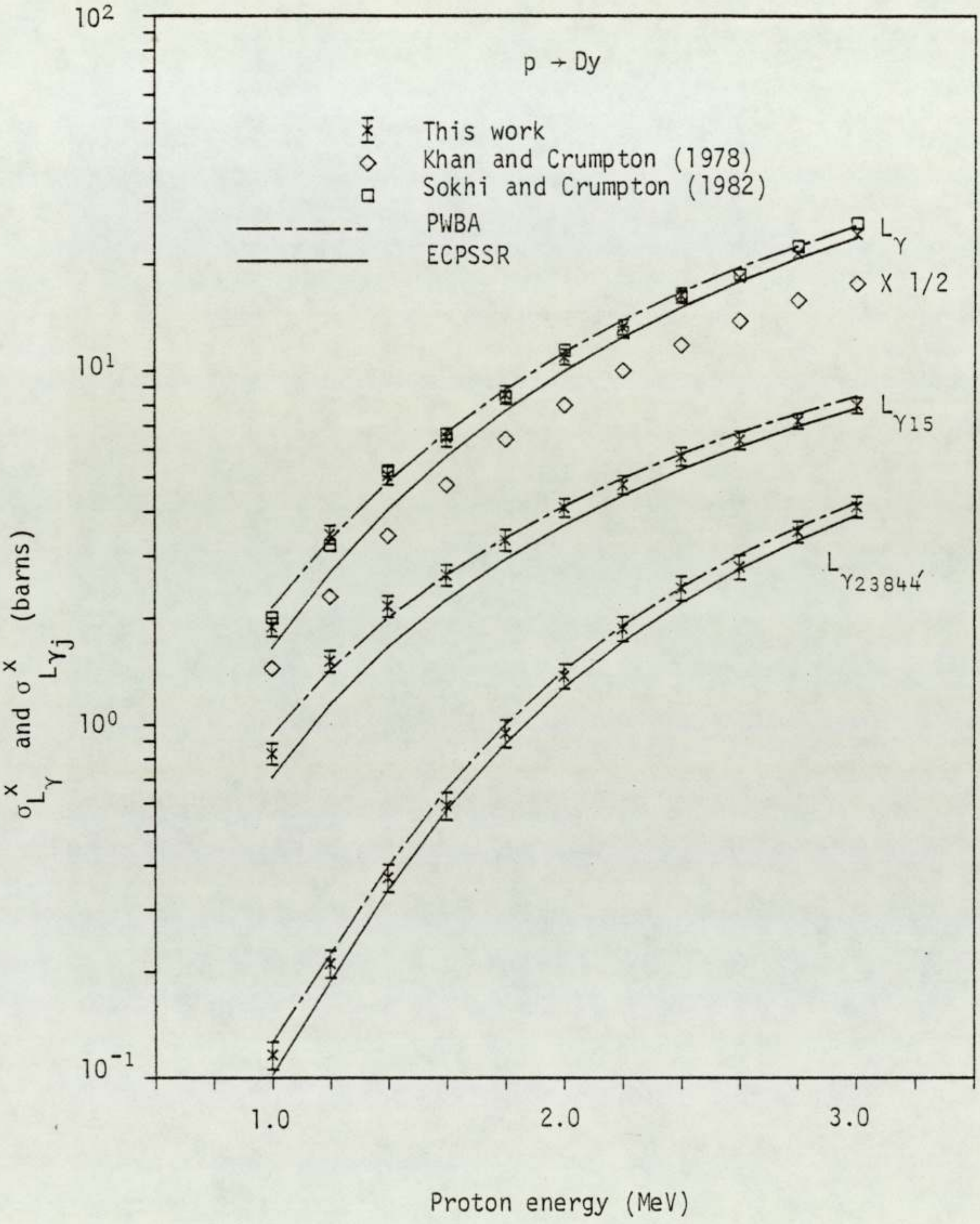

Figure 6.6. Experimental total L_γ and partial L_{γ_j} x-ray production cross-sections for proton impact on Dy.

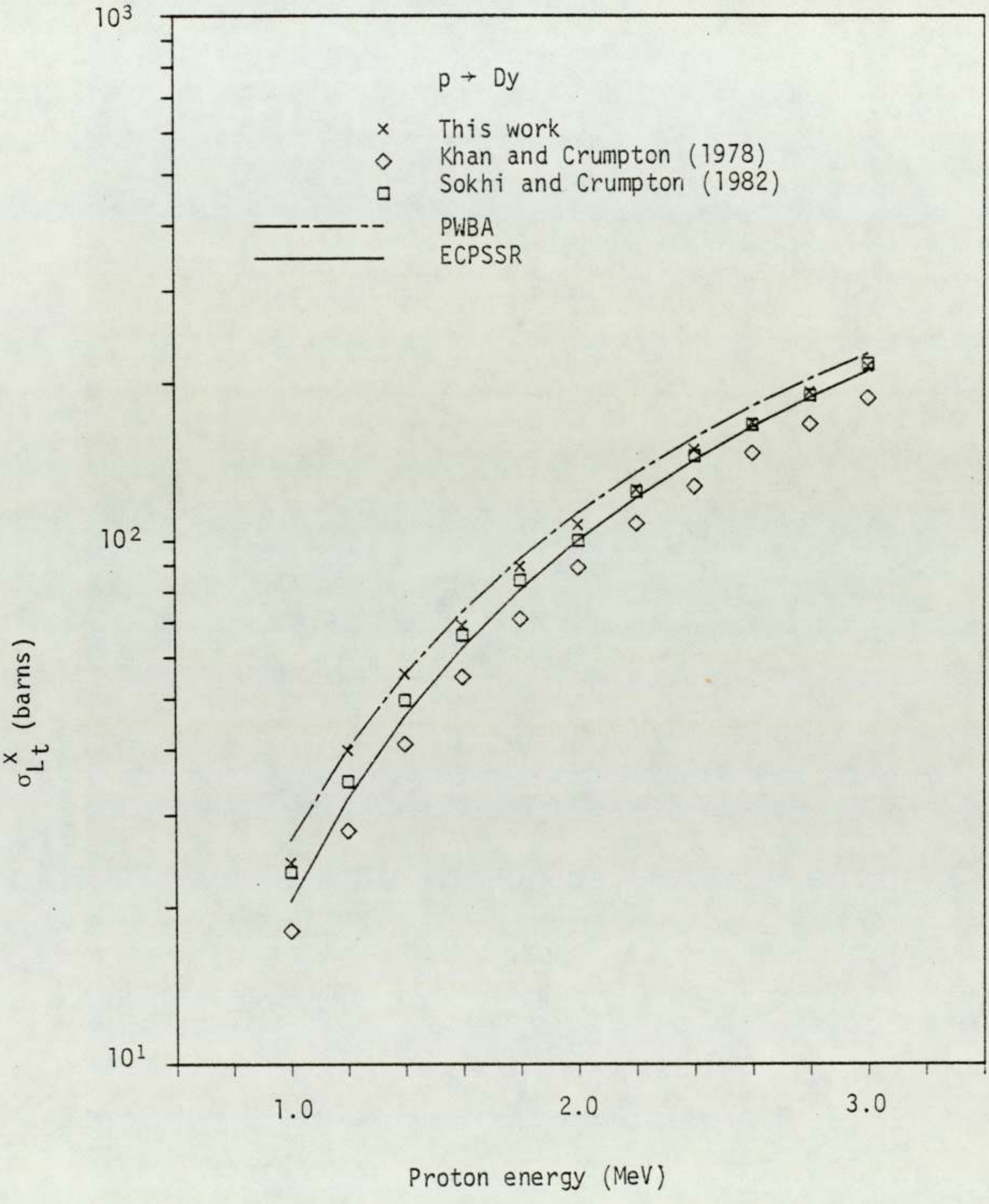

Figure 6.7. Experimental total L x-ray production cross-sections for proton impact on Dy.

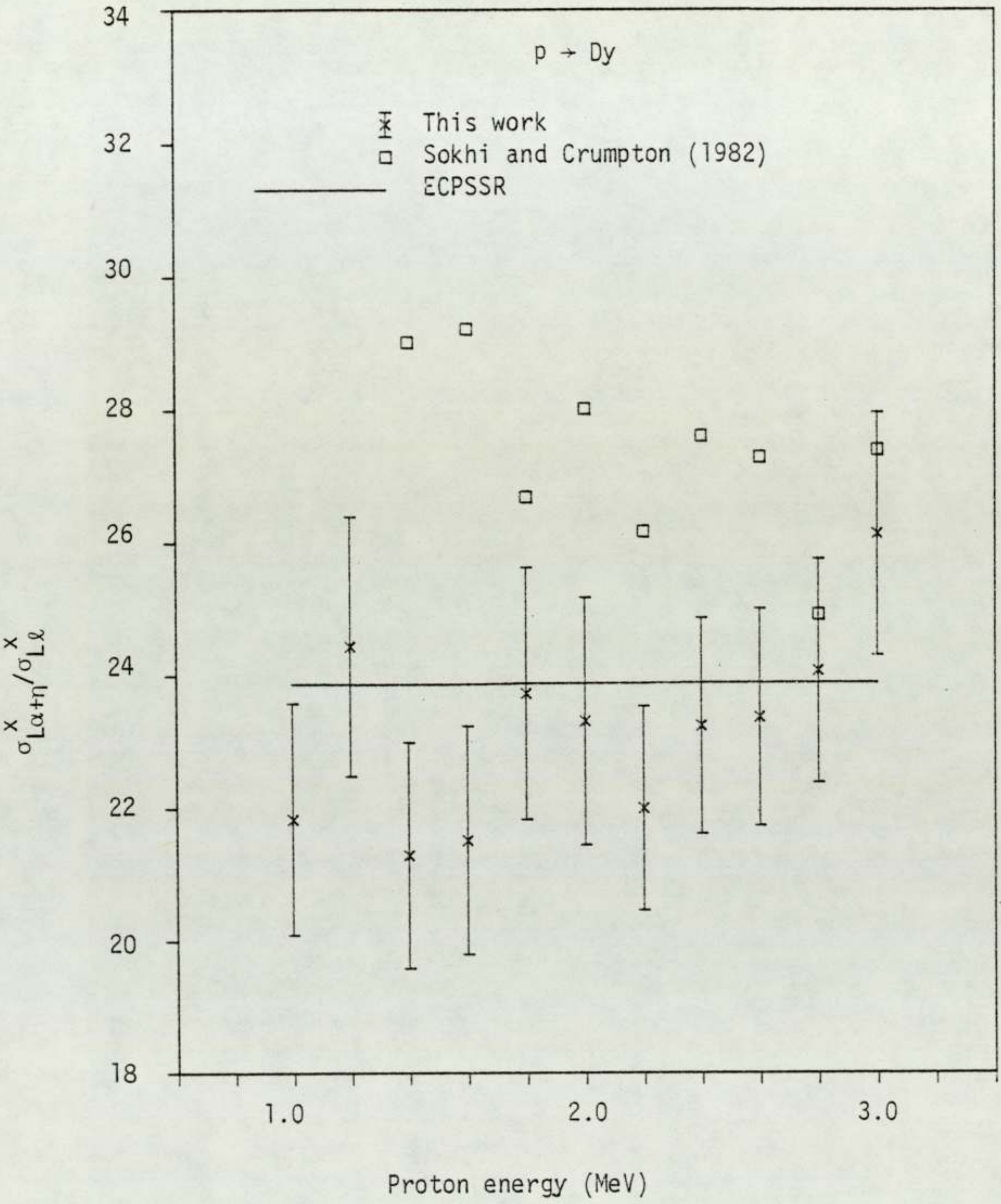

Figure 6.8. Experimental $\sigma^{x}_{L\alpha+\eta}/\sigma^{x}_{L\ell}$ ratio for proton impact on Dy.

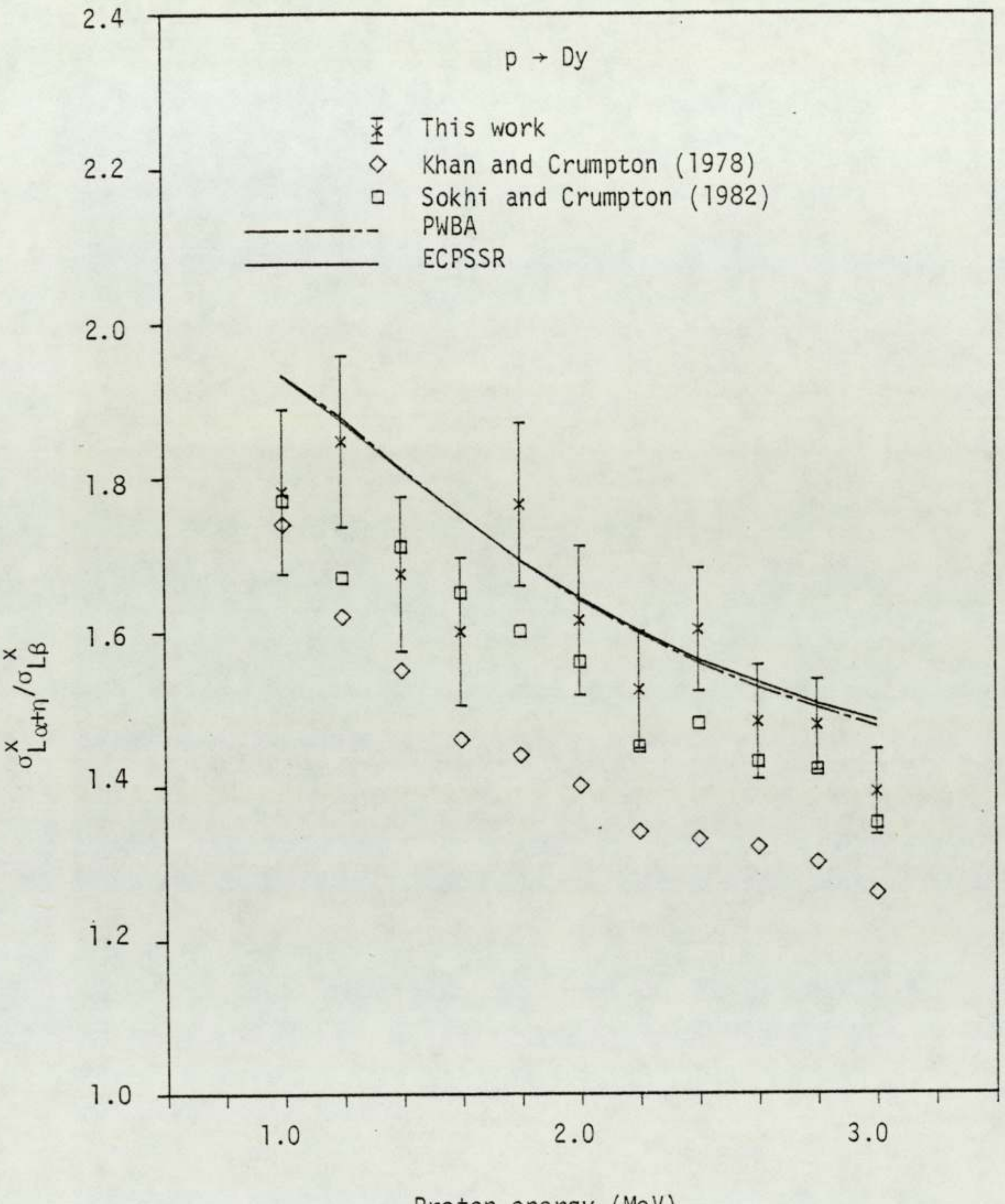

Figure 6.9. Experimental $\sigma^{x}_{L\alpha+\eta}/\sigma^{x}_{L\beta}$ ratio for proton impact on Dy.

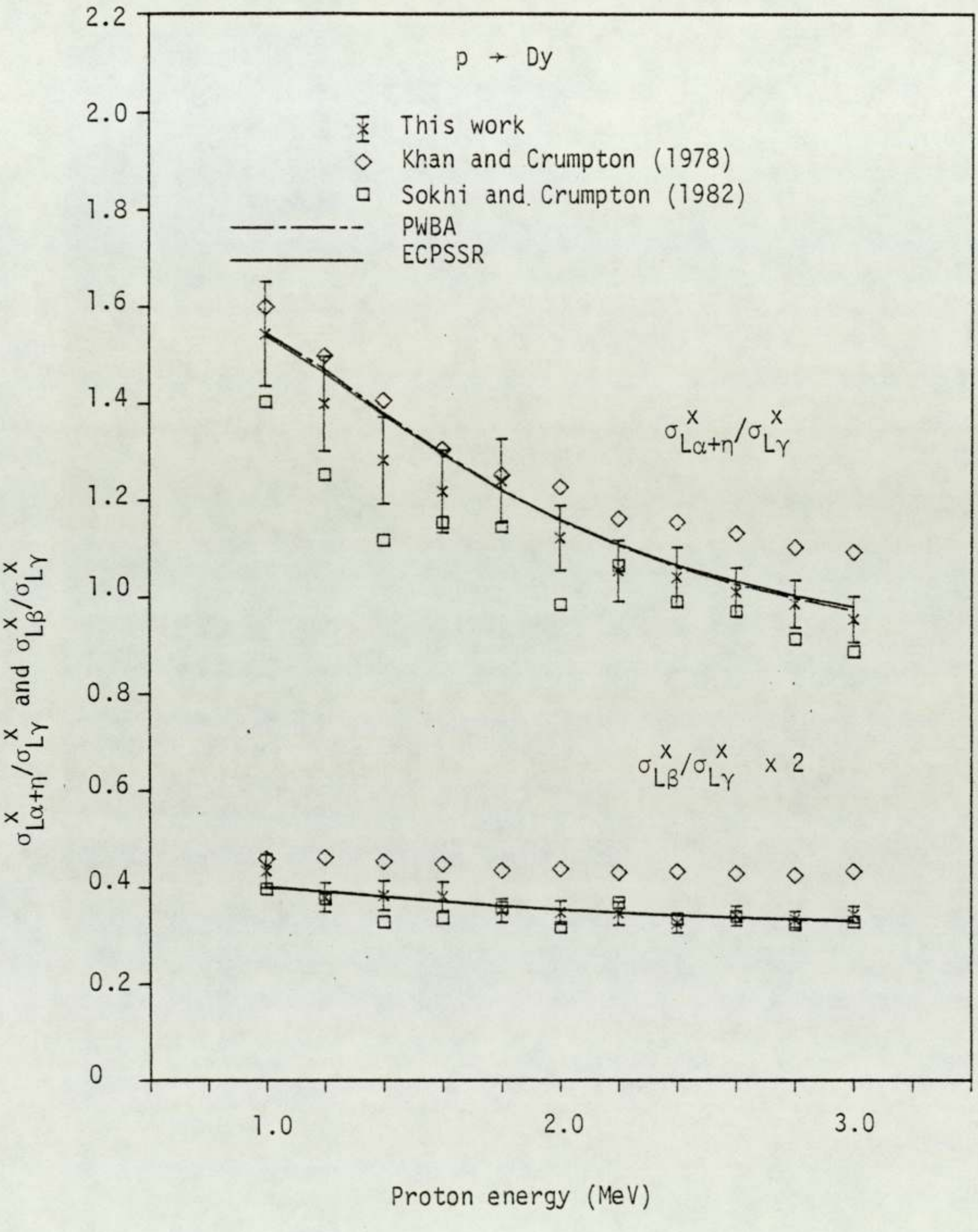

Figure 6.10. Experimental $\sigma^X_{L\alpha+\eta}/\sigma^X_{L\gamma}$ and $\sigma^X_{L\beta}/\sigma^X_{L\gamma}$ ratios for proton impact on Dy.

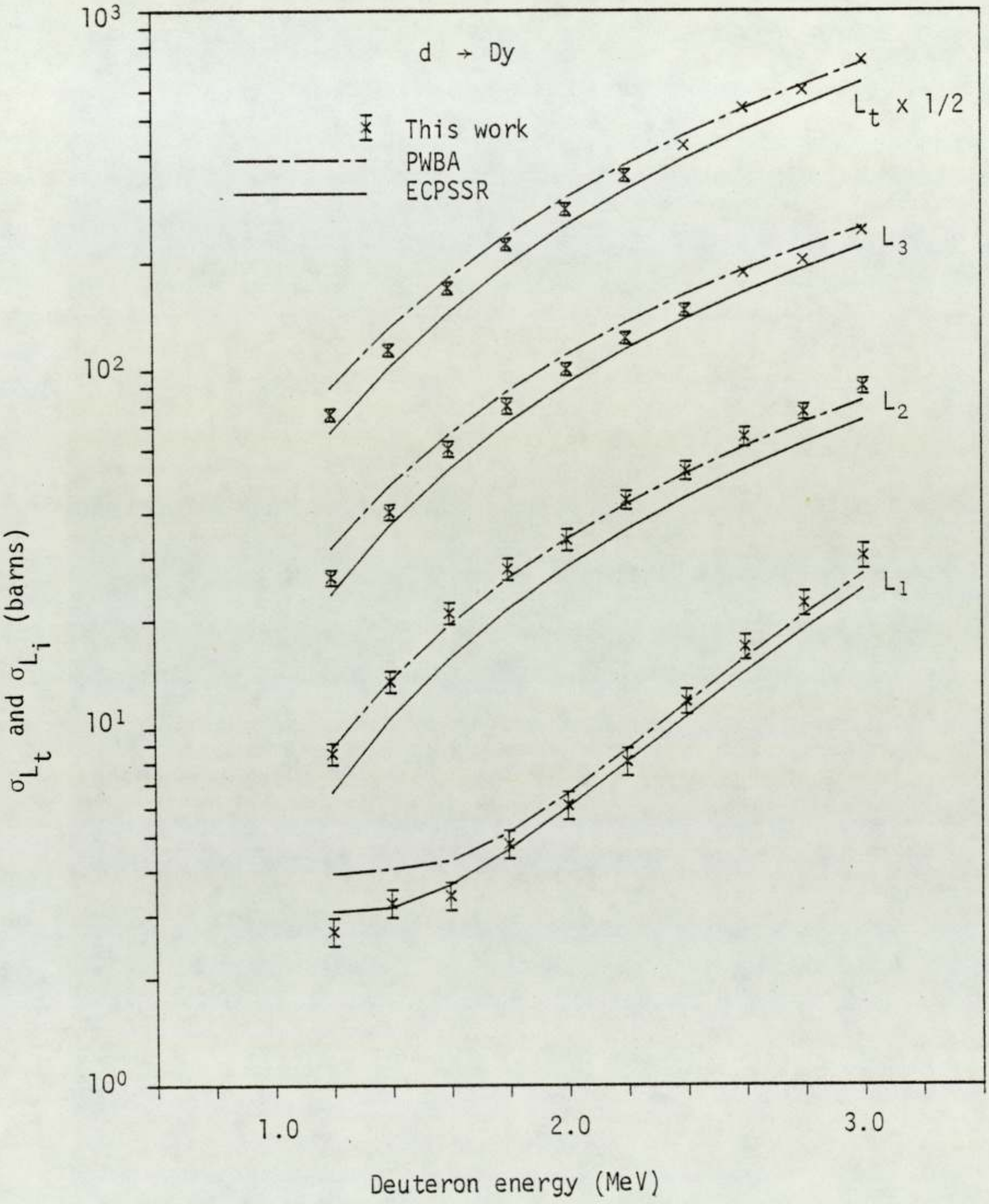

Figure 6.11. Experimental total (L_t) and individual L_i subshell ionisation cross sections for deuteron impact on Dy.

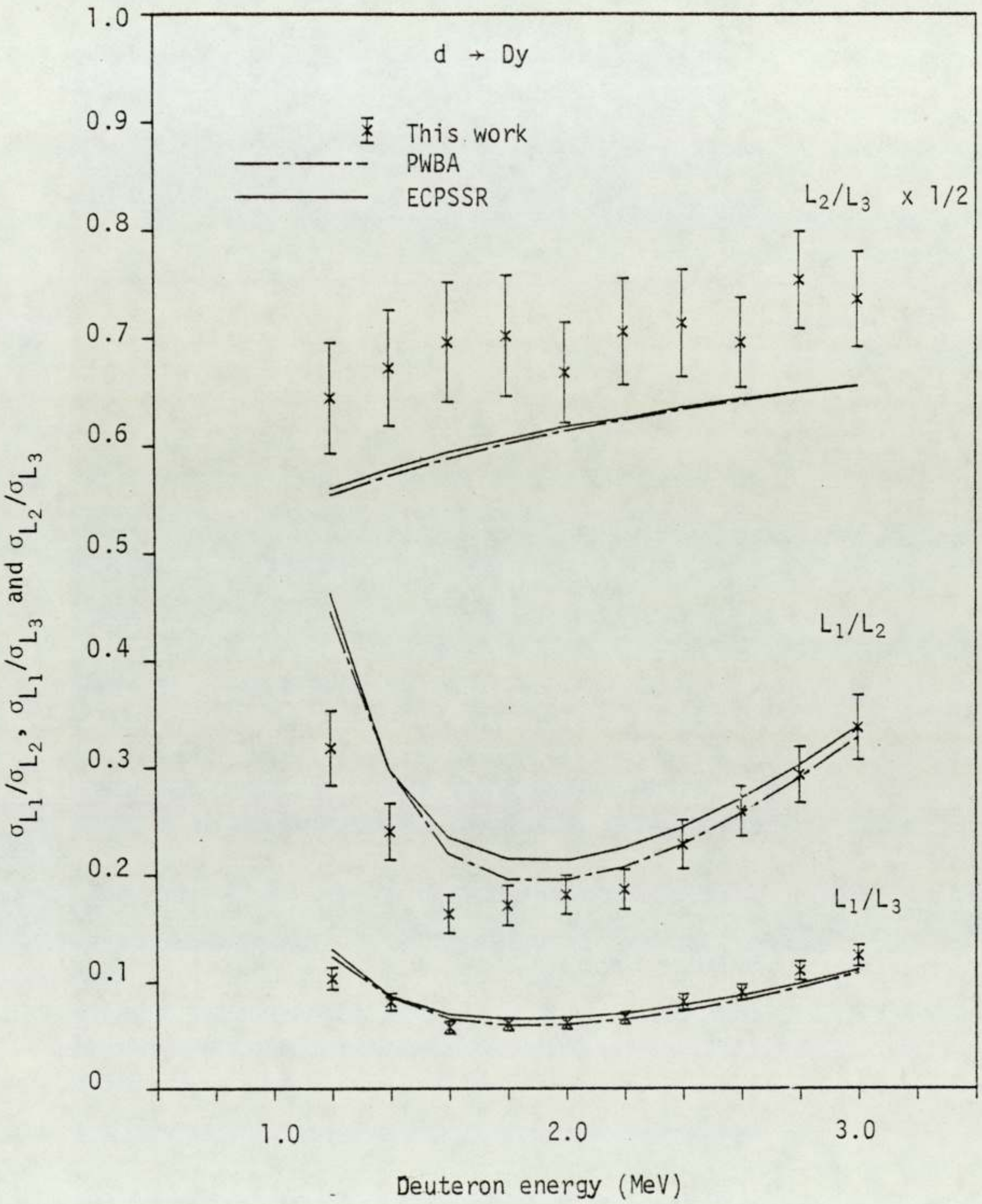

Figure 6.12. Experimental $\sigma_{L_1}/\sigma_{L_2}$, $\sigma_{L_1}/\sigma_{L_3}$ and $\sigma_{L_2}/\sigma_{L_3}$ ratios for deuteron impact on Dy.

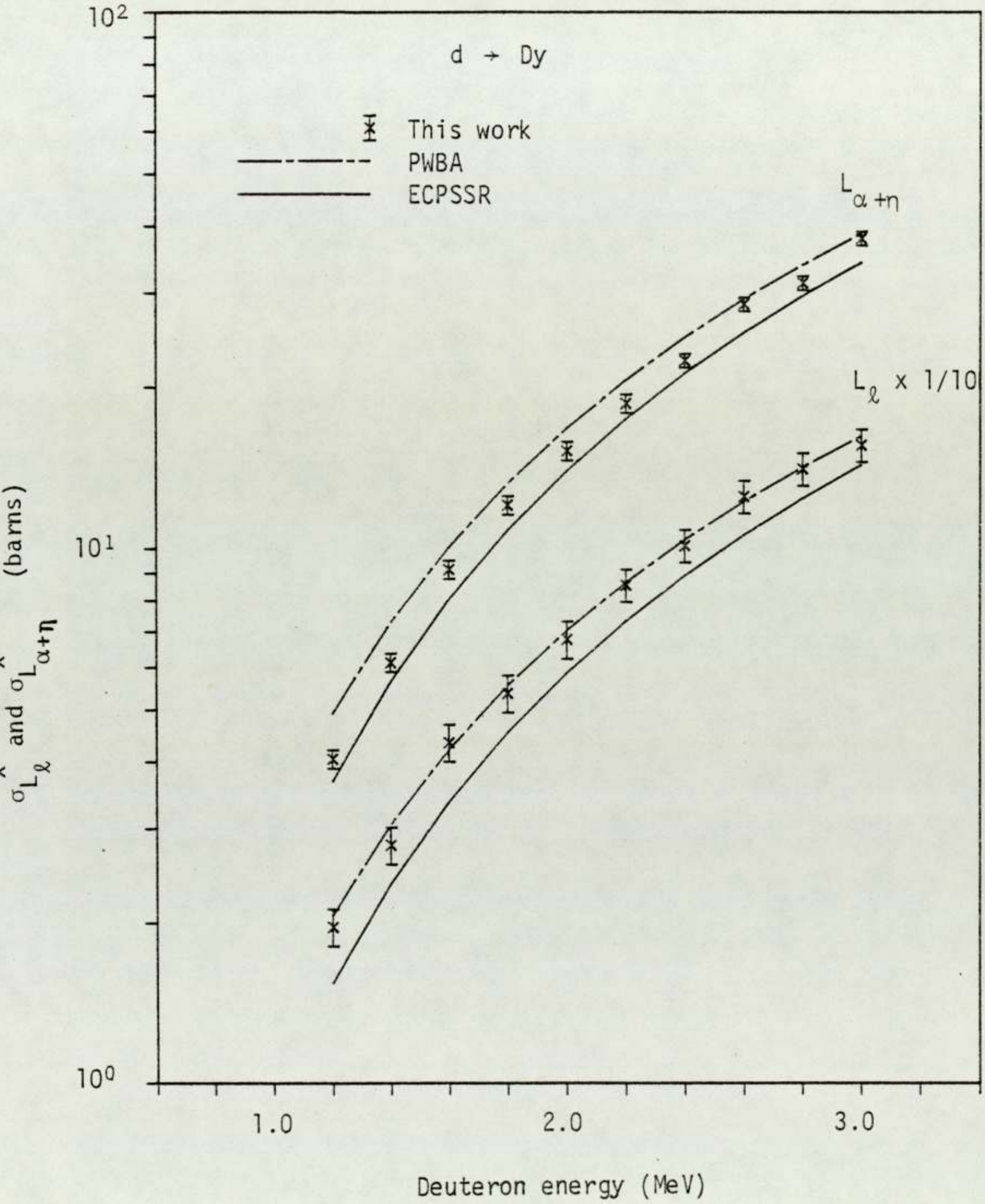

Figure 6.13. Experimental L_ℓ and $L_{\alpha+\eta}$ x-ray production cross sections for deuteron impact on Dy.

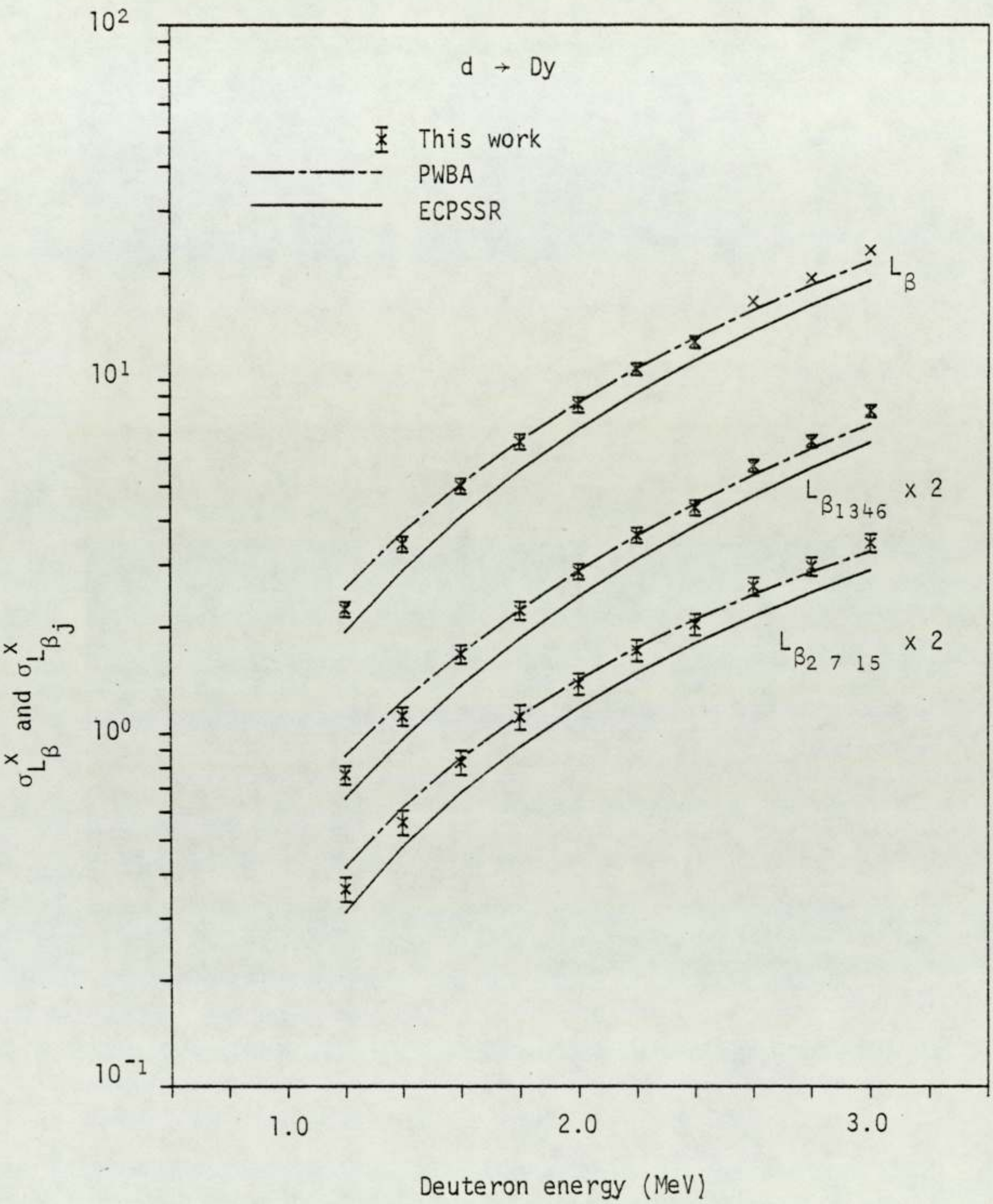

Figure 6.14. Experimental total L_β and partial L_{β_j} x-ray production cross sections for deuteron impact on Dy.

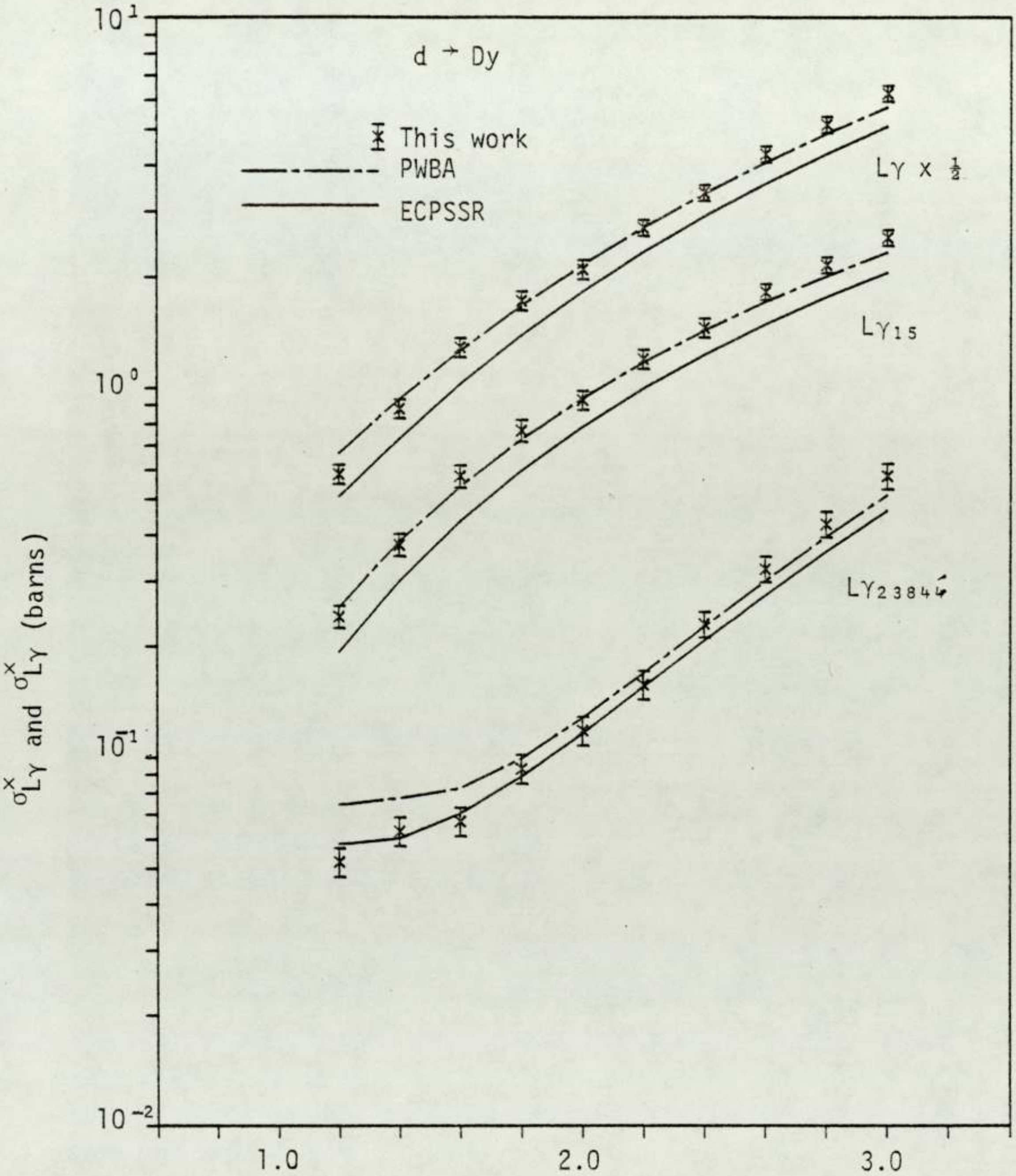

Figure 6.15. Experimental total Lγ and partial $L\gamma_j$ x-ray production cross sections for deuteron impact on Dy.

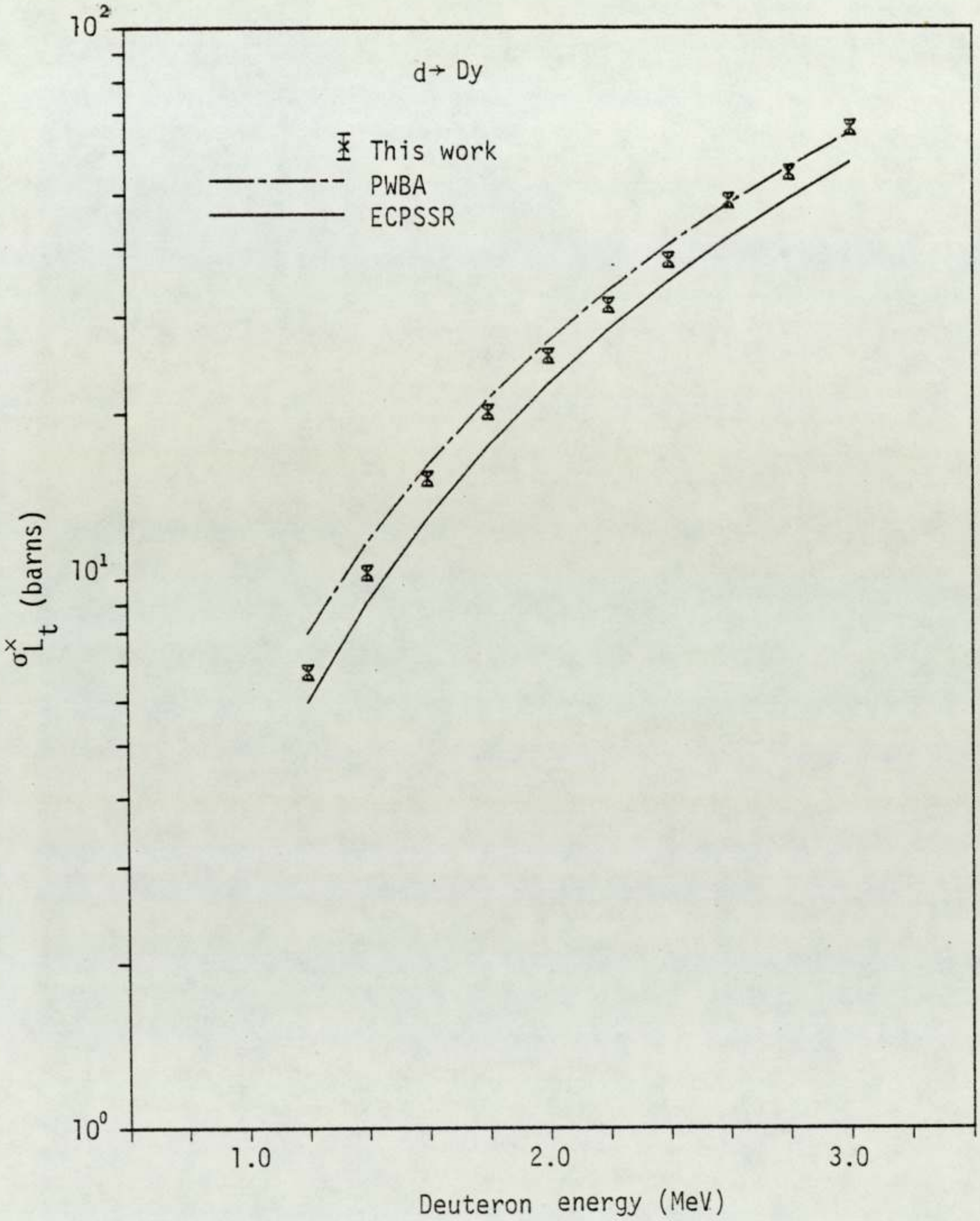

Figure 6.16. Experimental total L x-ray production cross sections for deuteron impact on Dy.

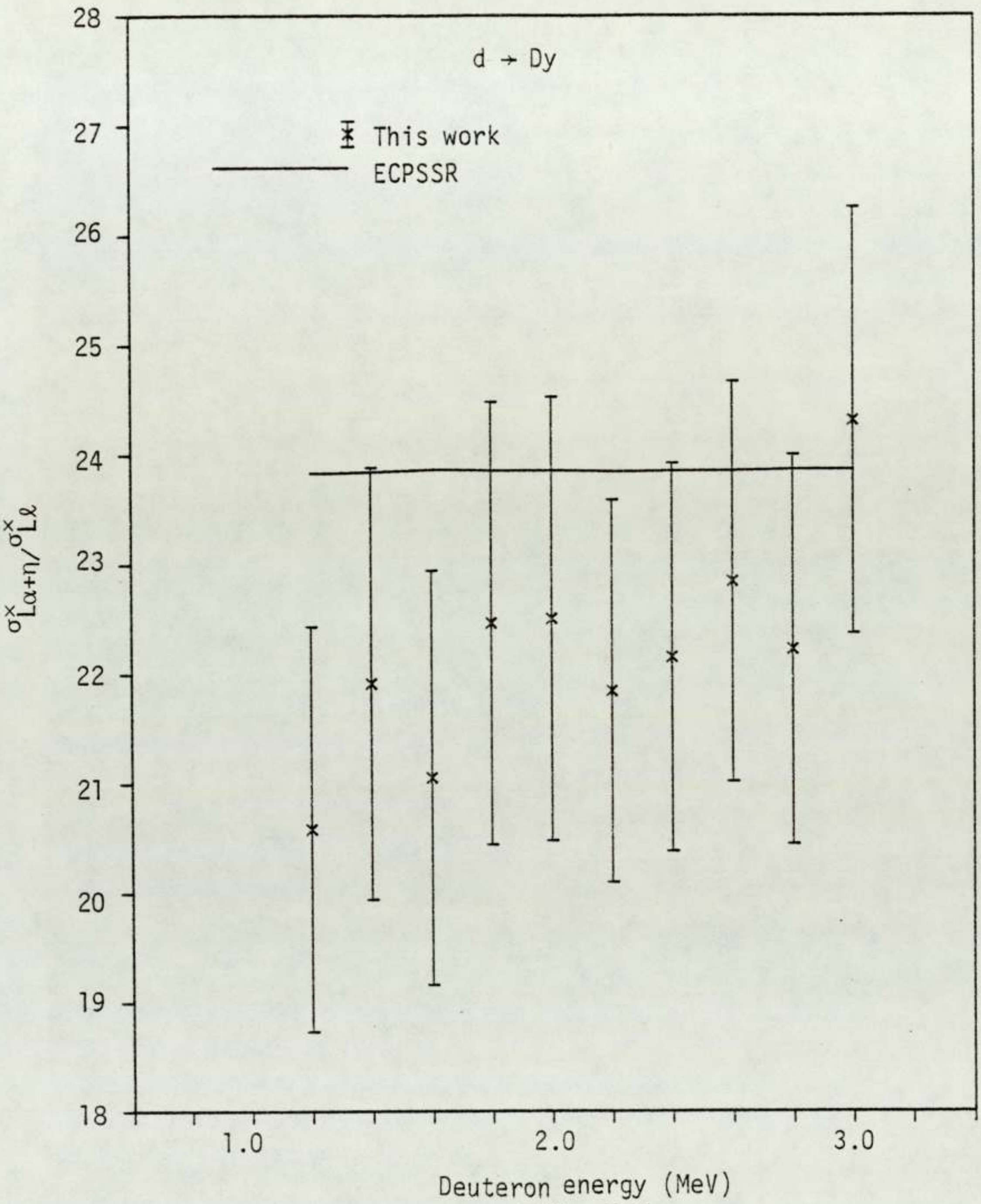

Figure 6.17. Experimental $\sigma^x_{L_{\alpha+\eta}}/\sigma^x_{L\ell}$ ratio for deuteron impact on Dy.

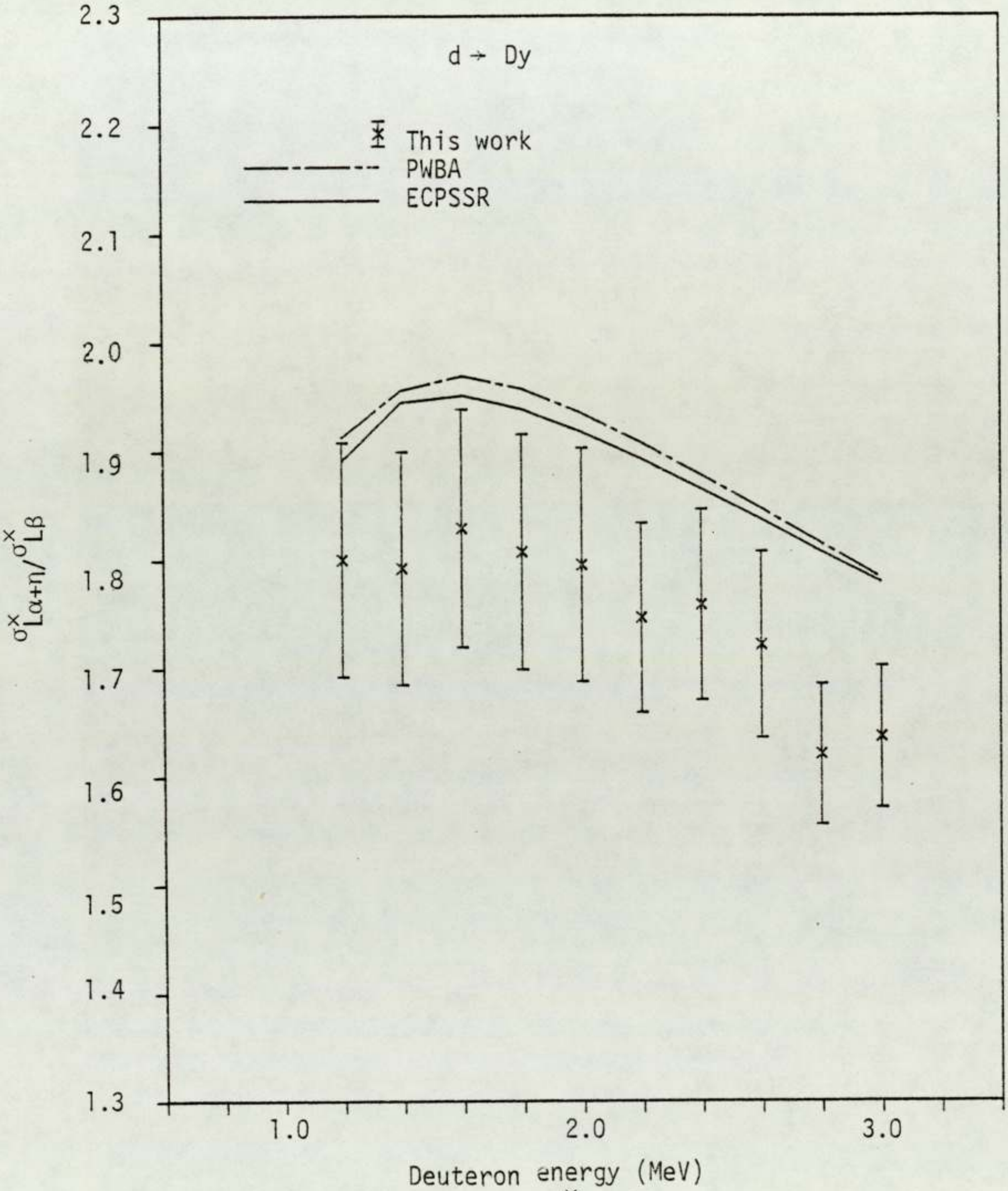

Figure 6.18. Experimental $\sigma^x_{L\alpha+\eta}/\gamma_{L\alpha+\eta}$ ratio for deuteron impact on Dy.

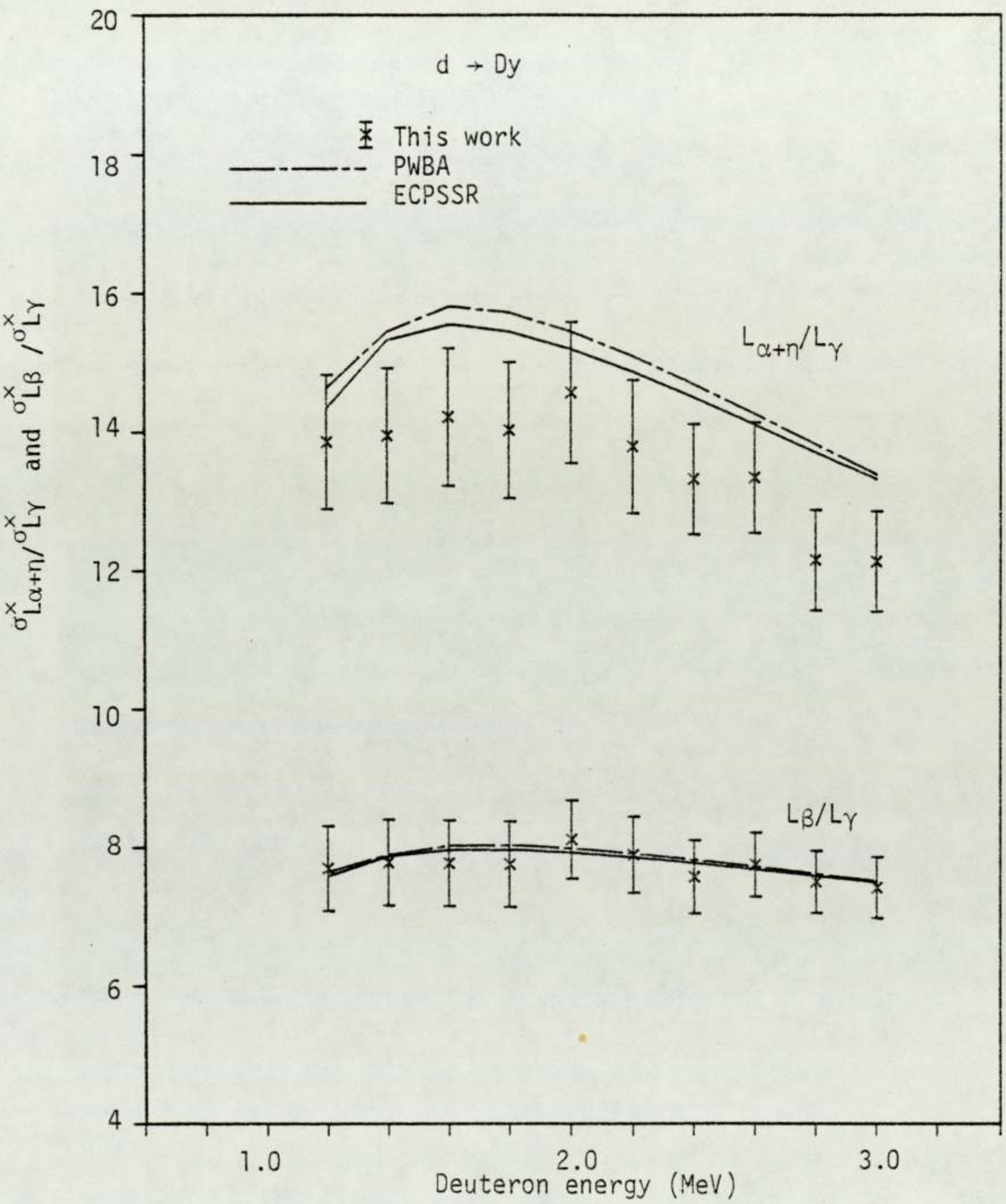

Figure 6.19. Experimental $\sigma^x_{L_{\alpha+\eta}}/\sigma^x_{L_\gamma}$ and $\sigma^x_{L\beta}/\sigma^x_{L\gamma}$ ratios for deuteron impact on Dy.

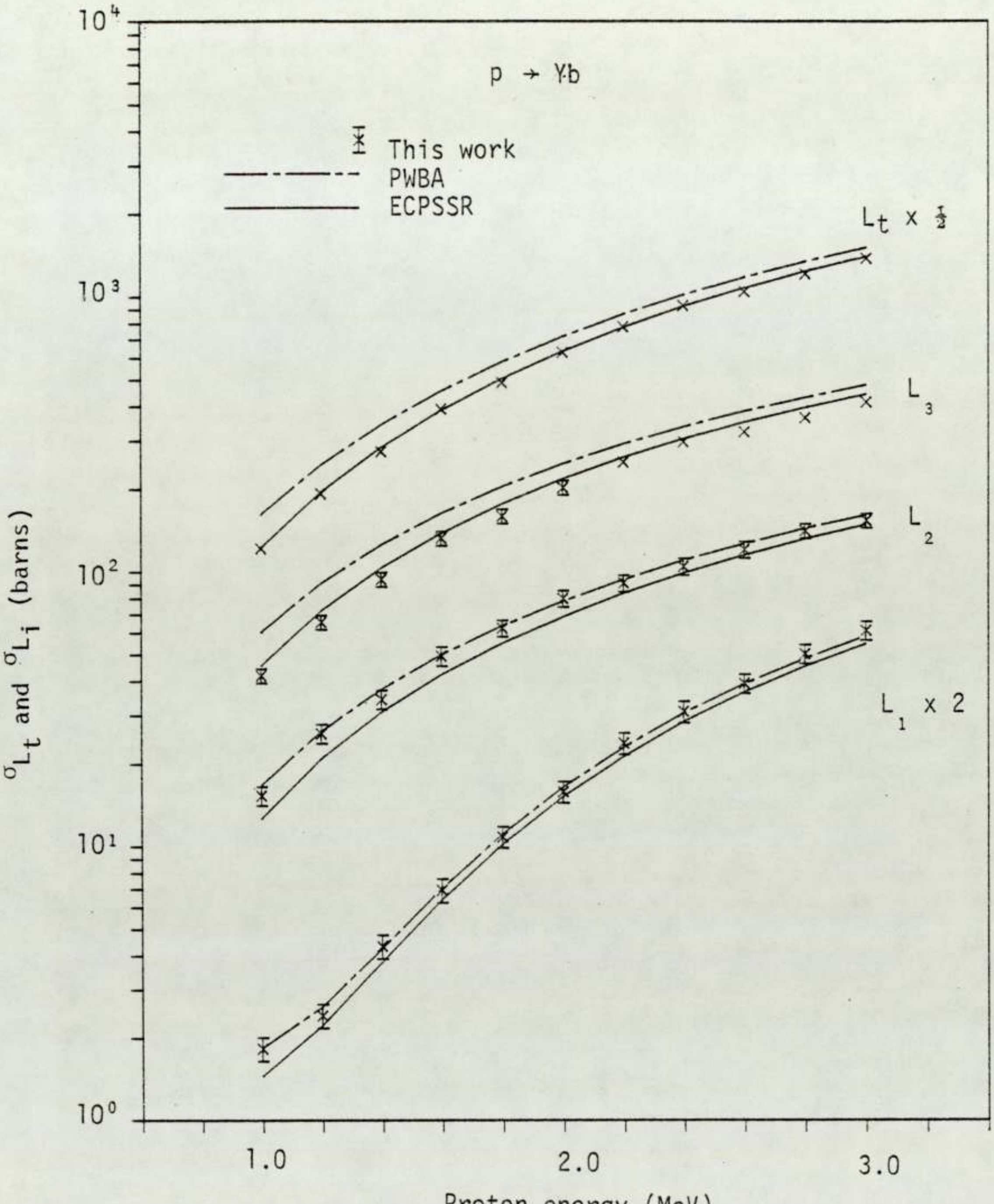

Figure 6.20. Experimental total and individual L_i subshell ionisation cross sections for proton impact on Yb.

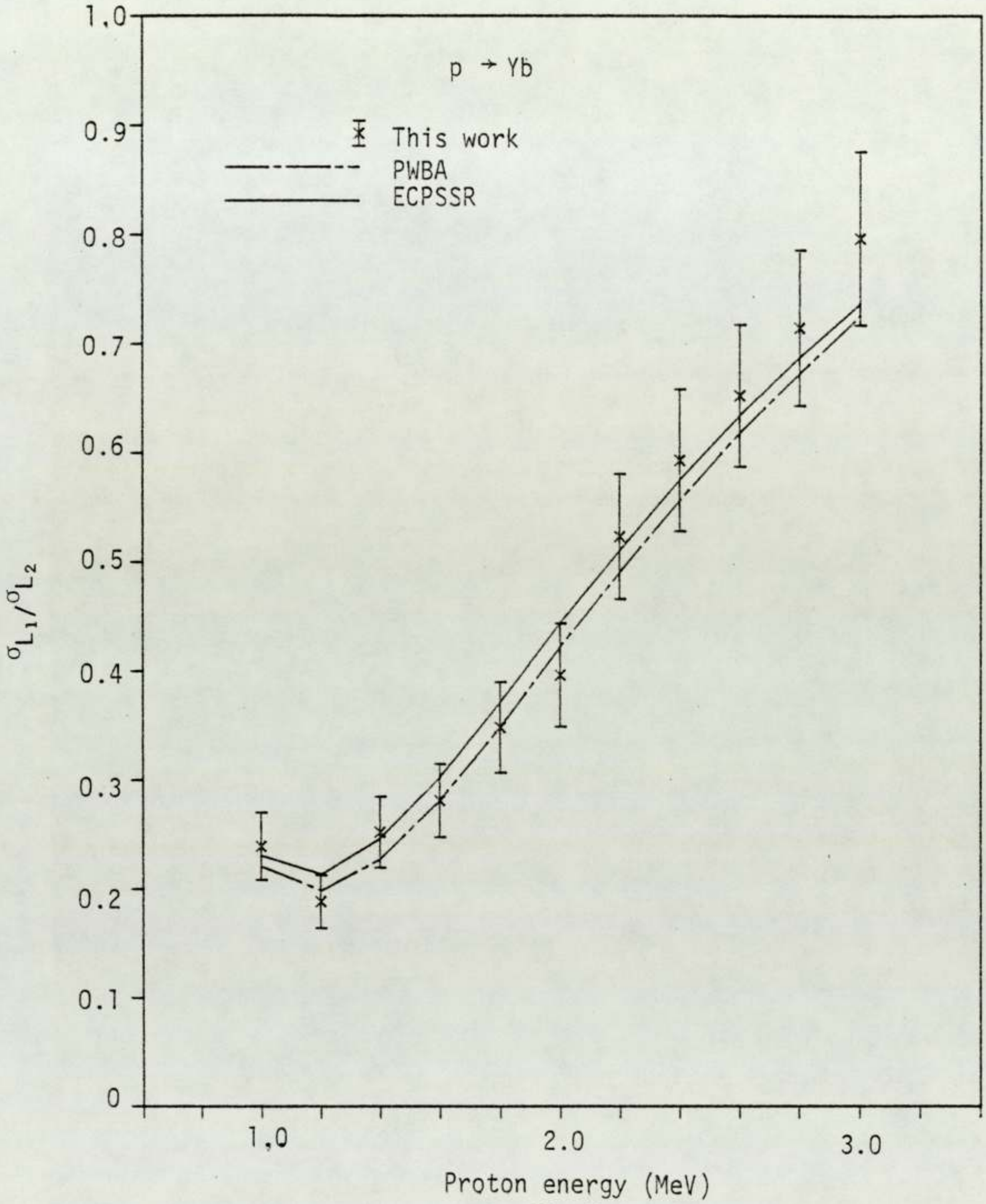

Figure 6.21. Experimental $\sigma_{L_1}/\sigma_{L_2}$ ratio for proton impact on Yb.

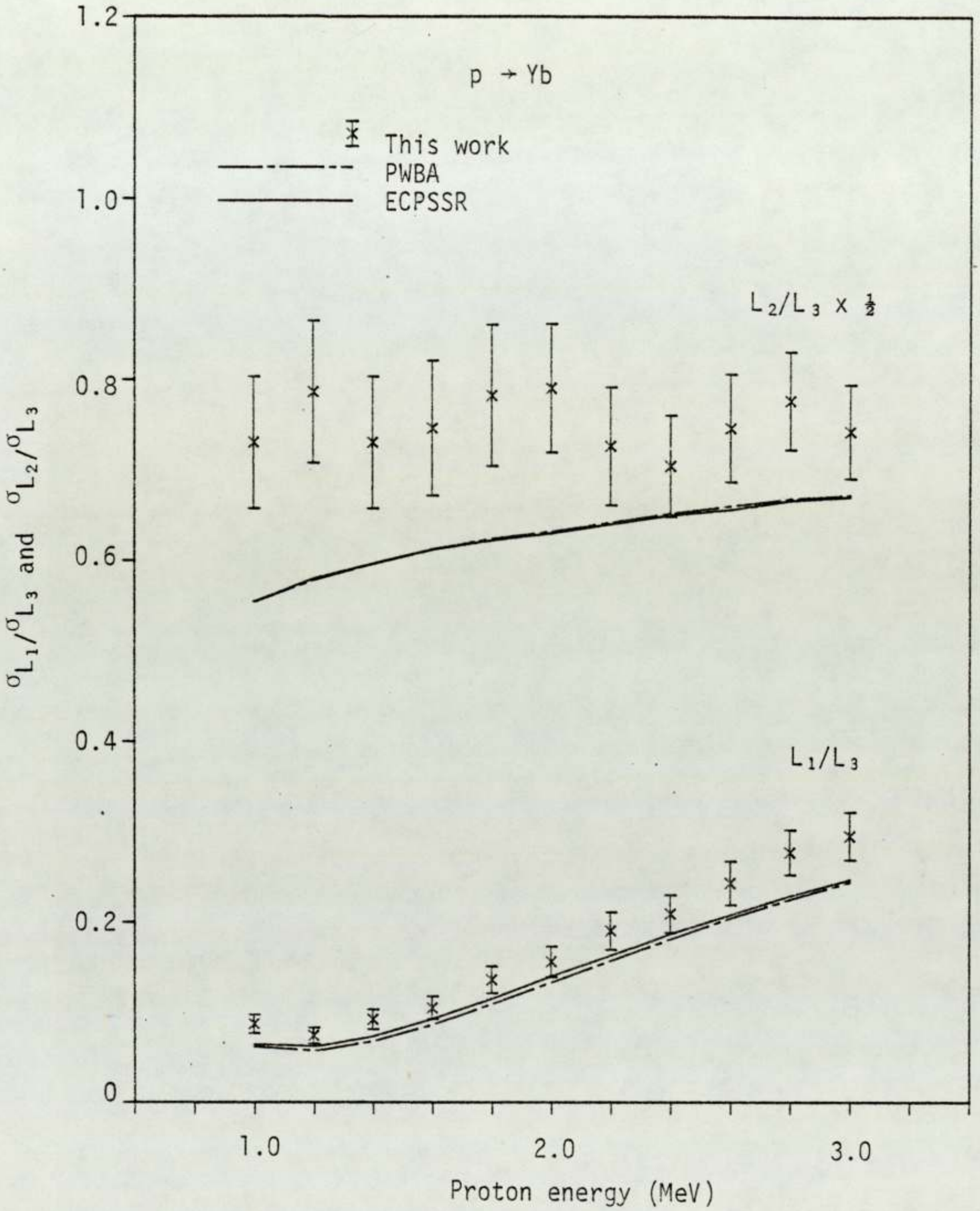

Figure 6.22. Experimental $\sigma_{L_1}/\sigma_{L_3}$ and $\sigma_{L_2}/\sigma_{L_3}$ ratios for proton impact on Yb.

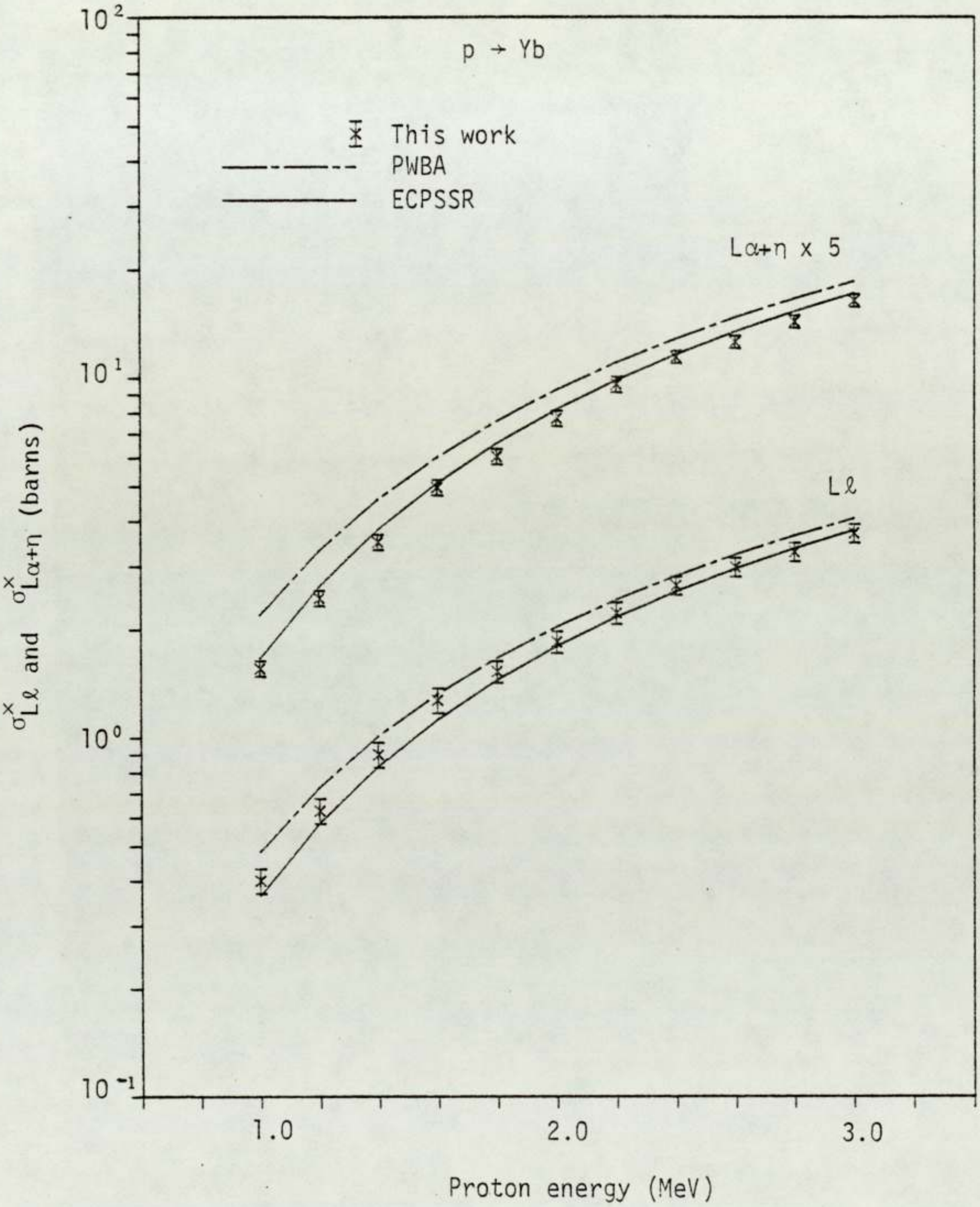

Figure 6.23. Experimental $L\ell$ and $L\alpha+\eta$ x-ray production cross sections for proton impact on Yb.

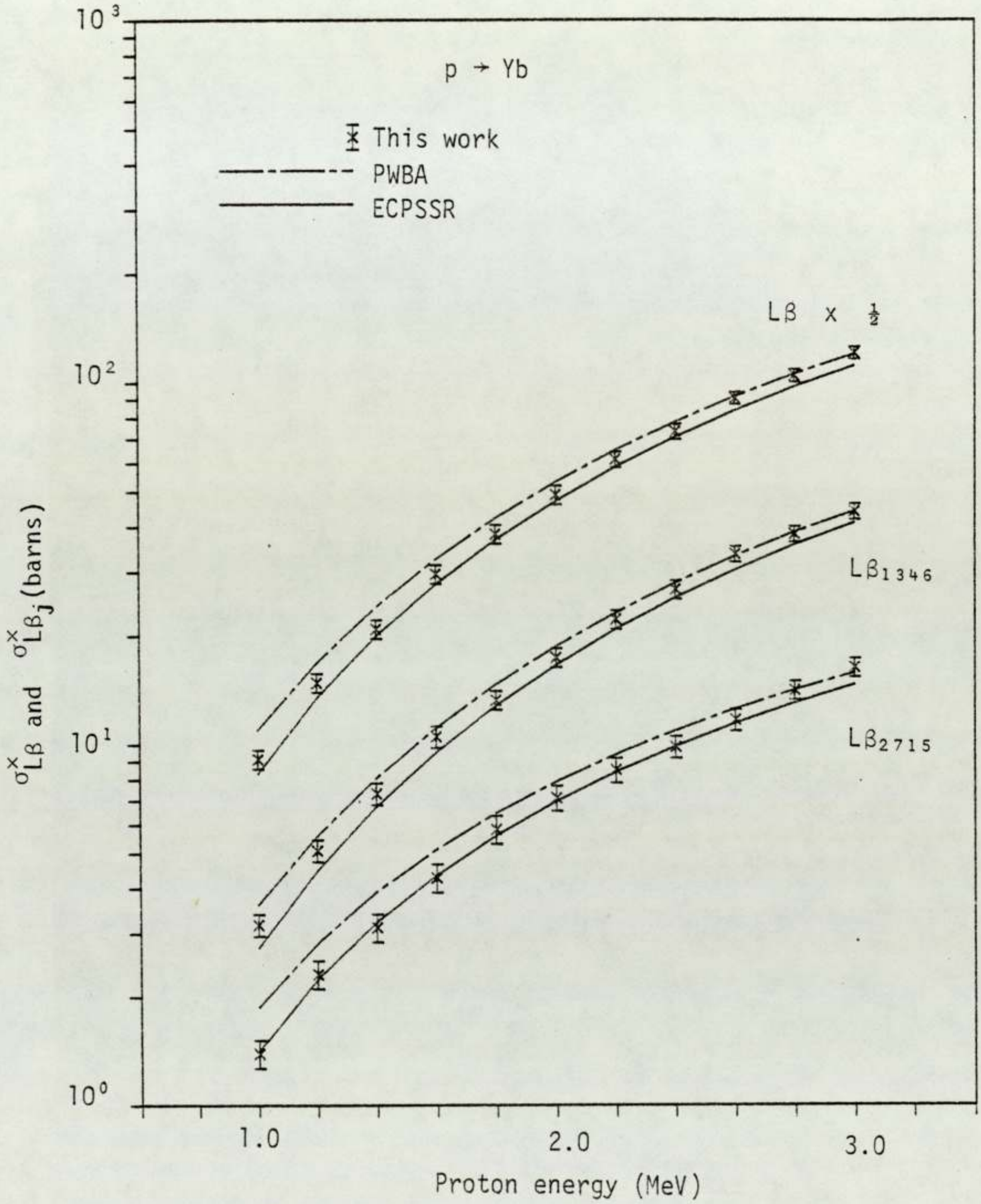

Figure 6.24. Experimental total L_β and partial $L\beta_j$ x-ray production cross sections for proton impact on Yb.

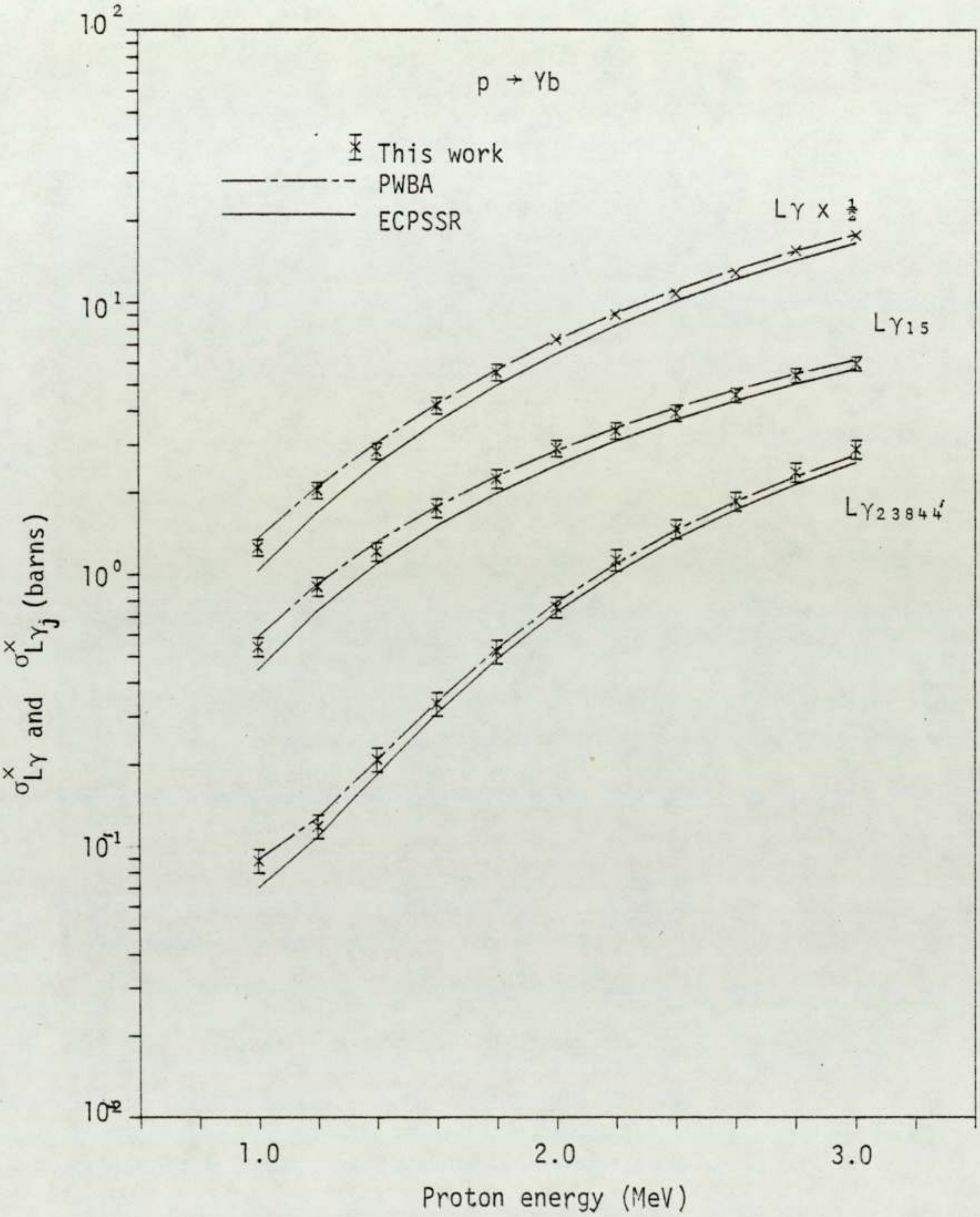

Figure 6.25. Experimental total Lγ and partial $L\gamma_j$ x-ray production cross sections for proton impact on Yb.

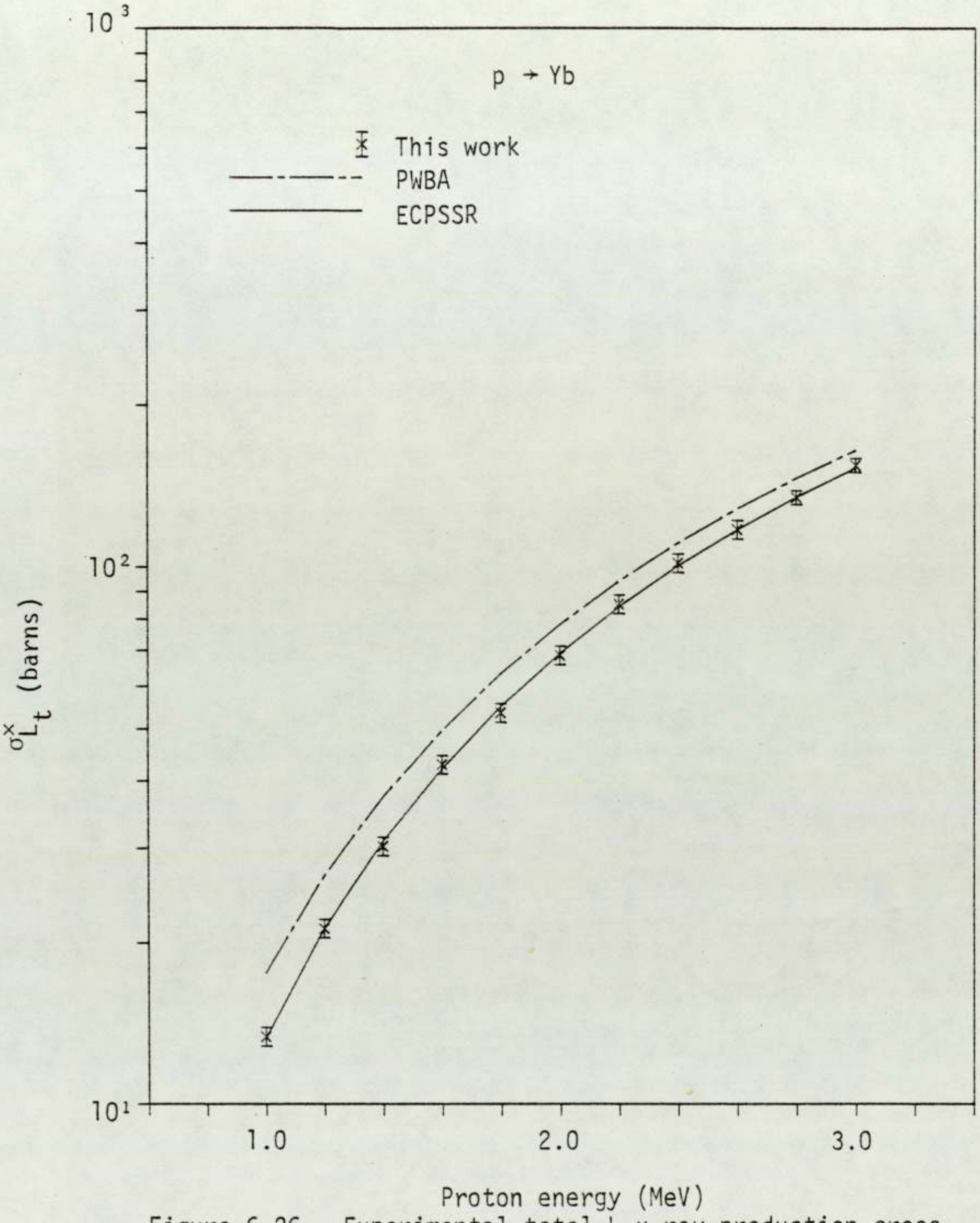

Figure 6.26. Experimental total L x-ray production cross sections, $\sigma^x_{L_t}$, for proton impact on Yb.

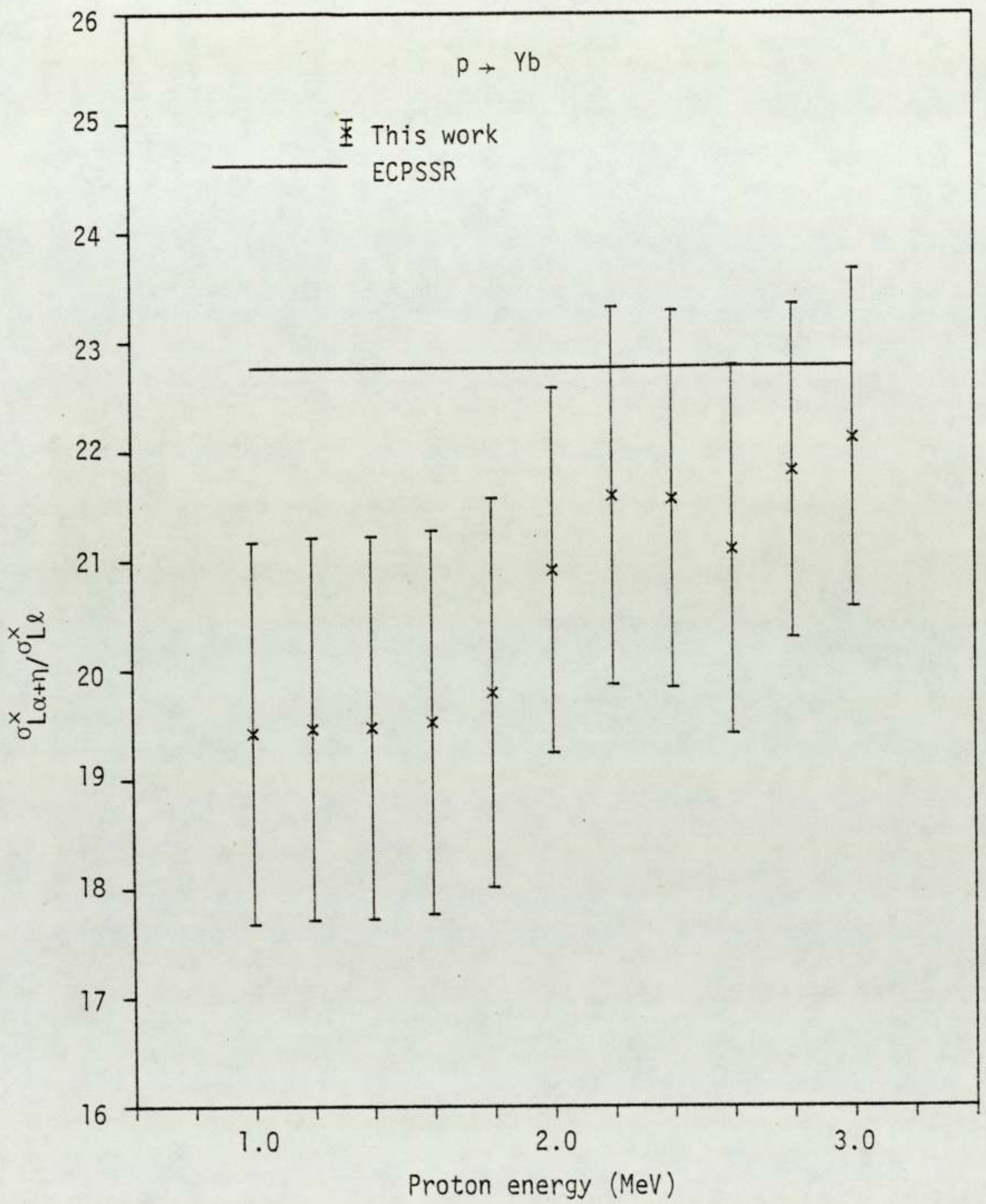

Figure 6.27. Experimental $\sigma^x_{L\alpha+\eta}/\sigma^x_{L\ell}$ ratio for proton impact on Yb.

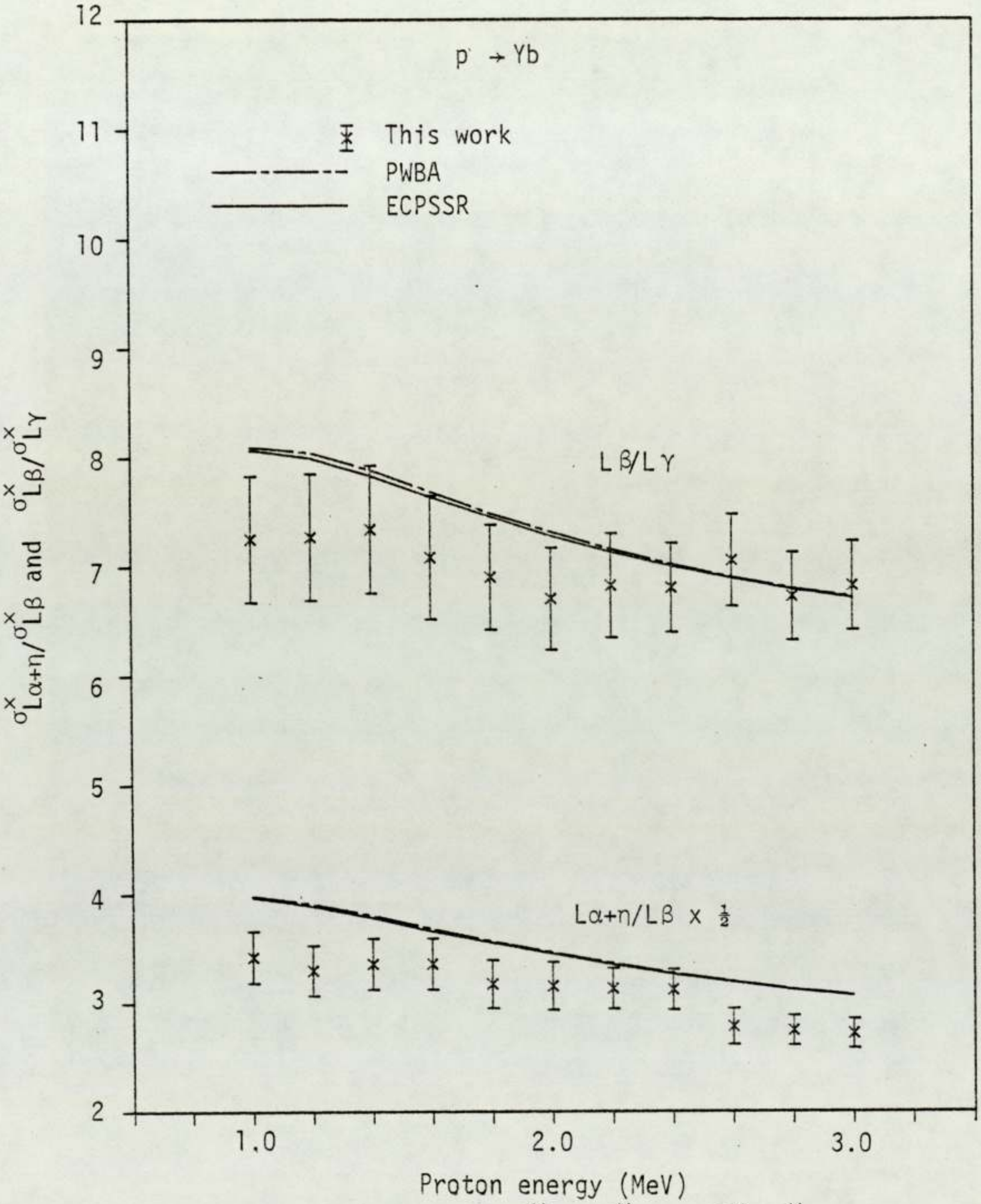

Figure 6.28. Experimental $\sigma^x_{L\alpha+\eta}/\sigma^x_{L\beta}$ and $\sigma^x_{L\beta}/\sigma^x_{L\gamma}$ ratios for proton impact on Yb.

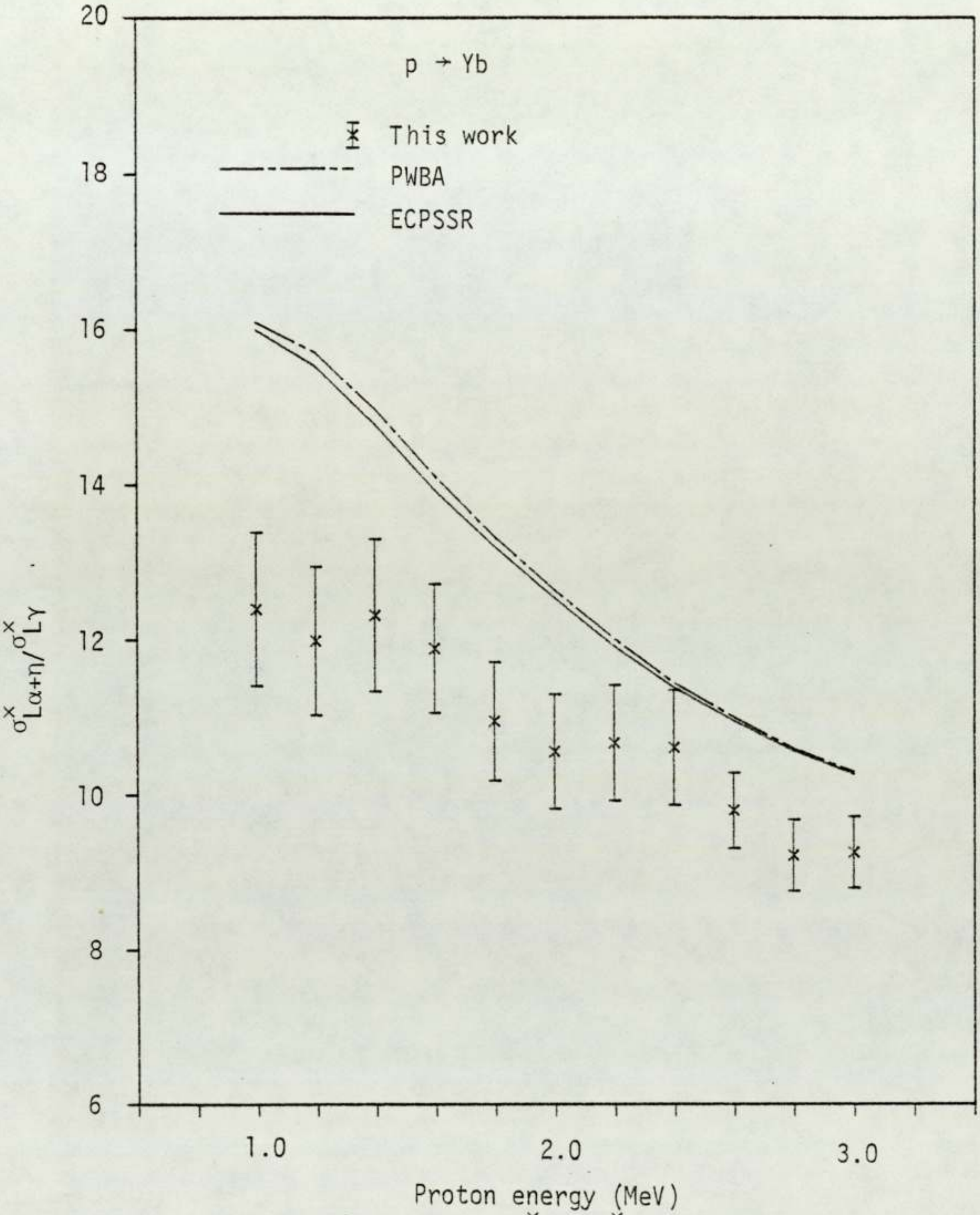

Figure 6.29. Experimental $\sigma^{x}_{L\alpha+\eta}/\sigma^{x}_{L\gamma}$ ratio for proton impact on Yb.

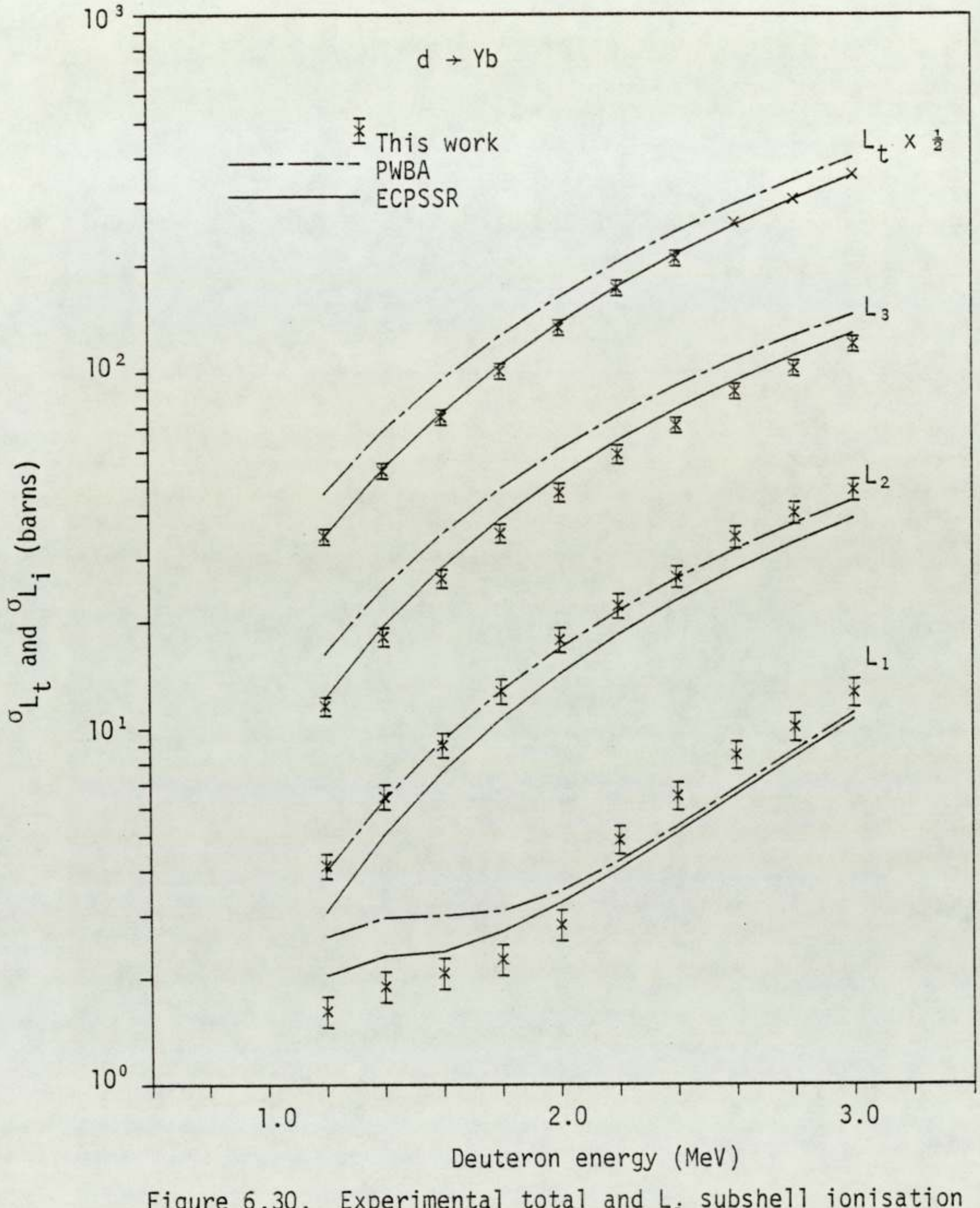

Figure 6.30. Experimental total and L_i subshell ionisation cross sections for deuteron impact on Yb.

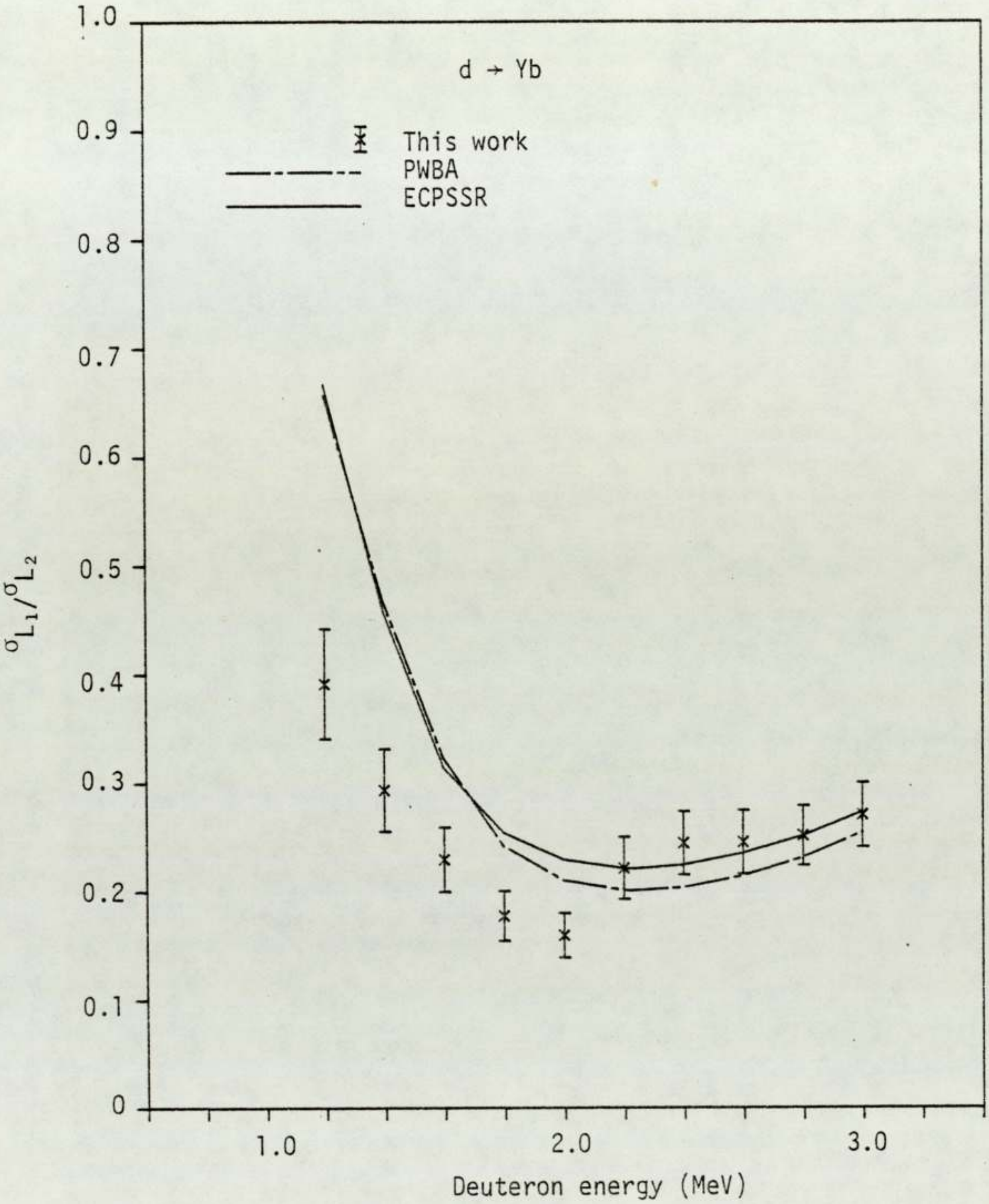

Figure 6.31. Experimental $\sigma_{L_1}/\sigma_{L_2}$ ratio for deuteron impact on Yb.

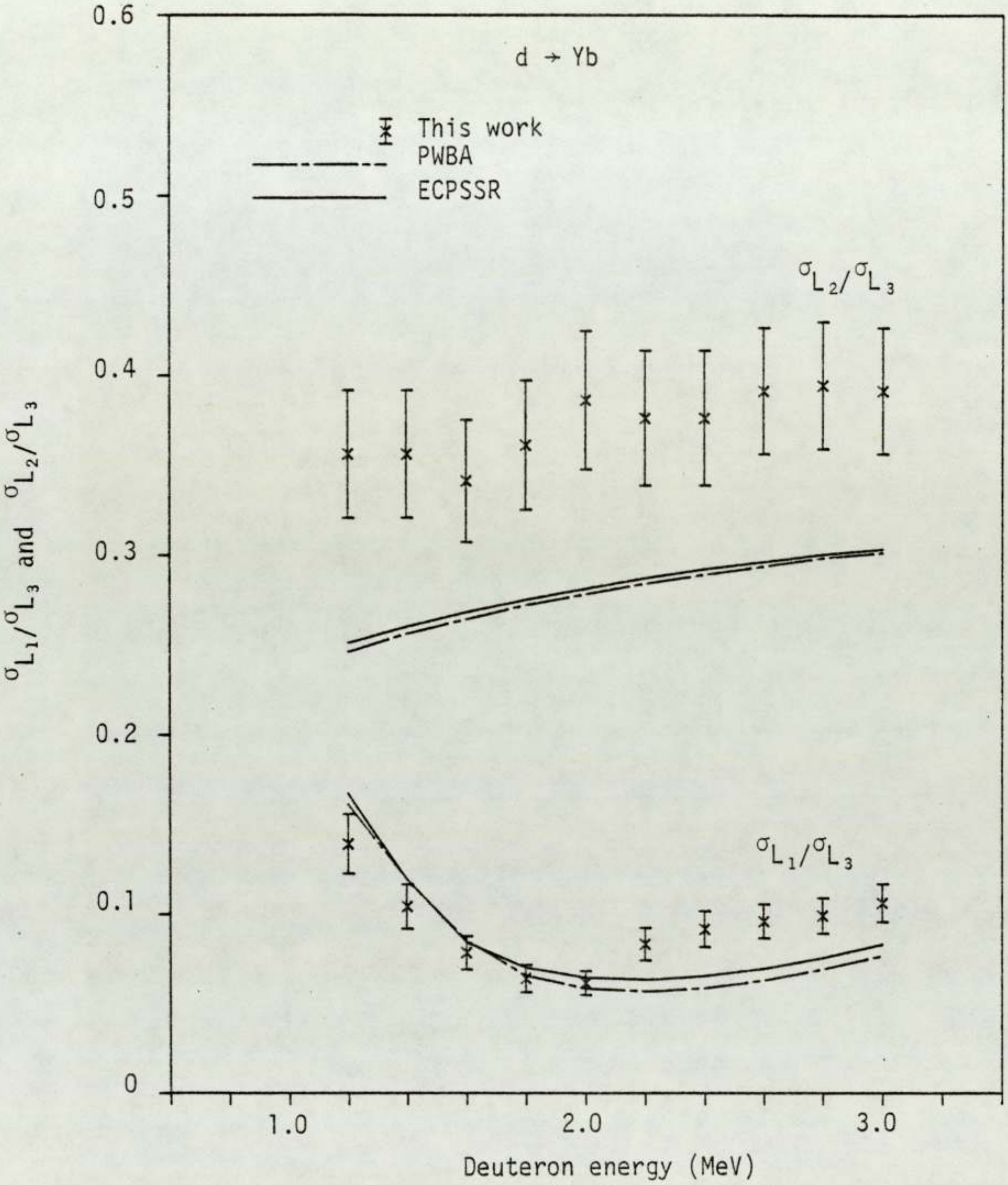

Figure 6.32. Experimental $\sigma_{L_1}/\sigma_{L_3}$ and $\sigma_{L_2}/\sigma_{L_3}$ ratios for deuteron impact on Yb.

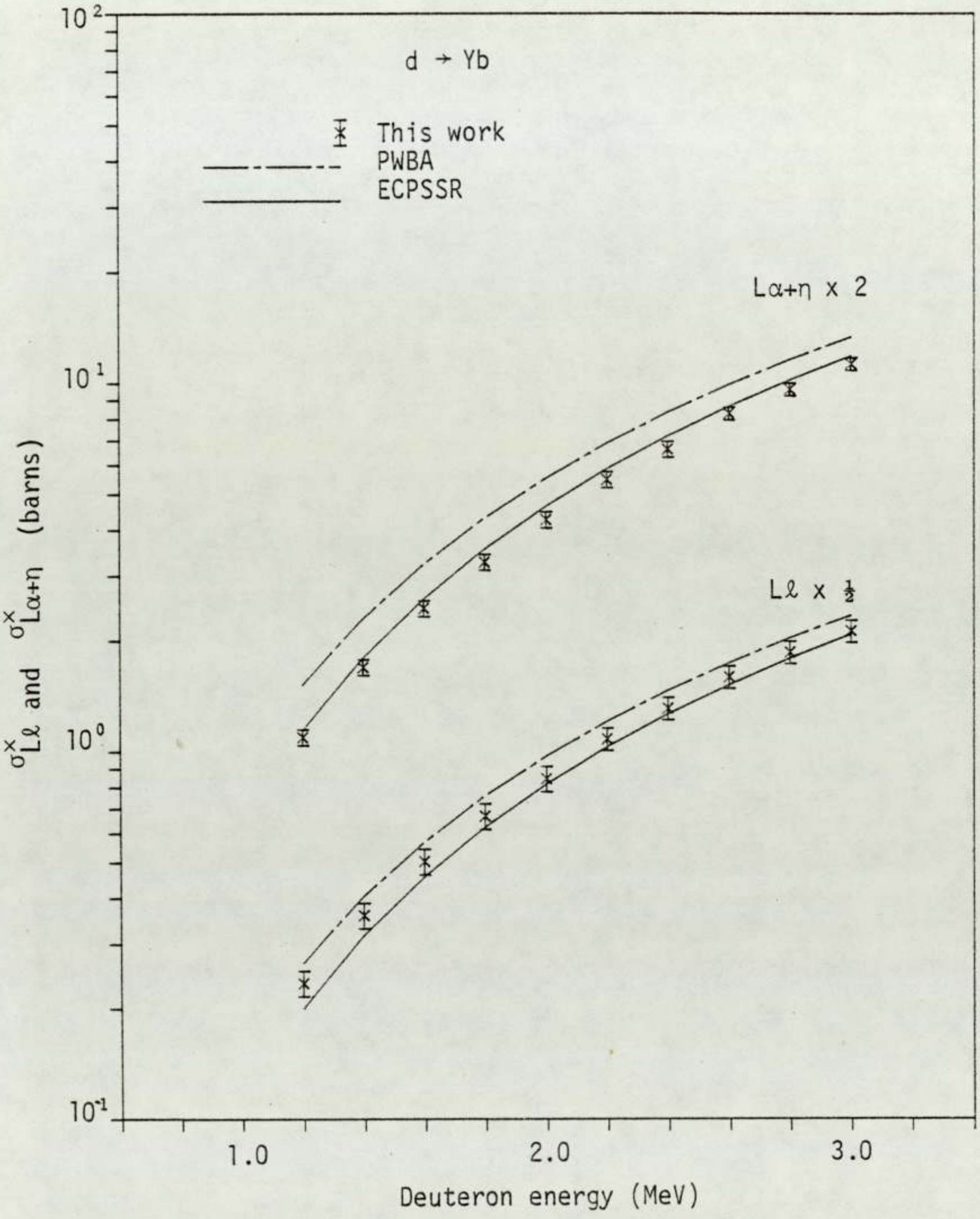

Figure 6.33. Experimental Lα+η and Lℓ x-ray production for deuteron impact on Yb.

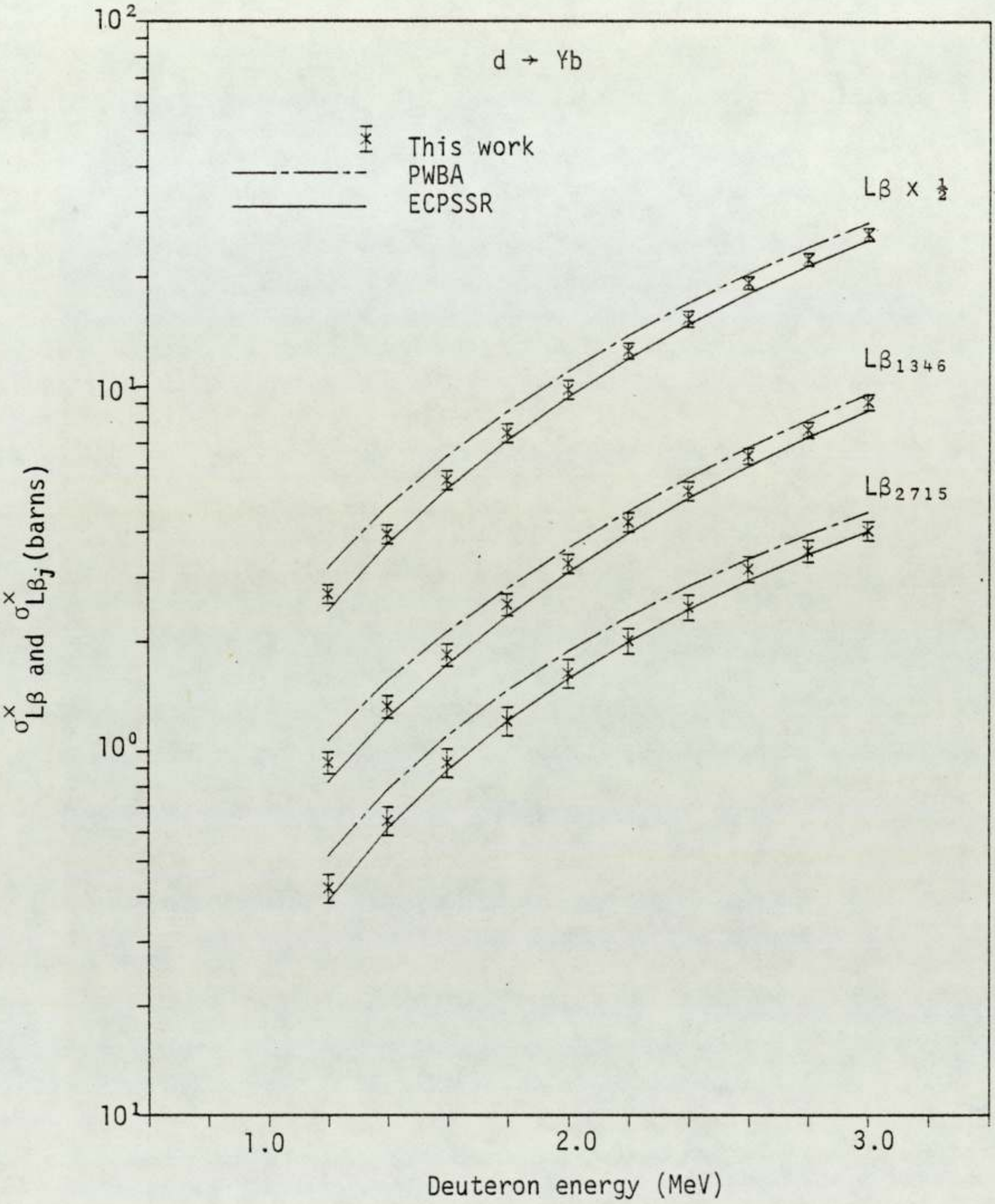

Figure 6.34. Experimental total Lβ and partial $L\beta_j$ x-ray production cross sections for deuteron impact on Yb.

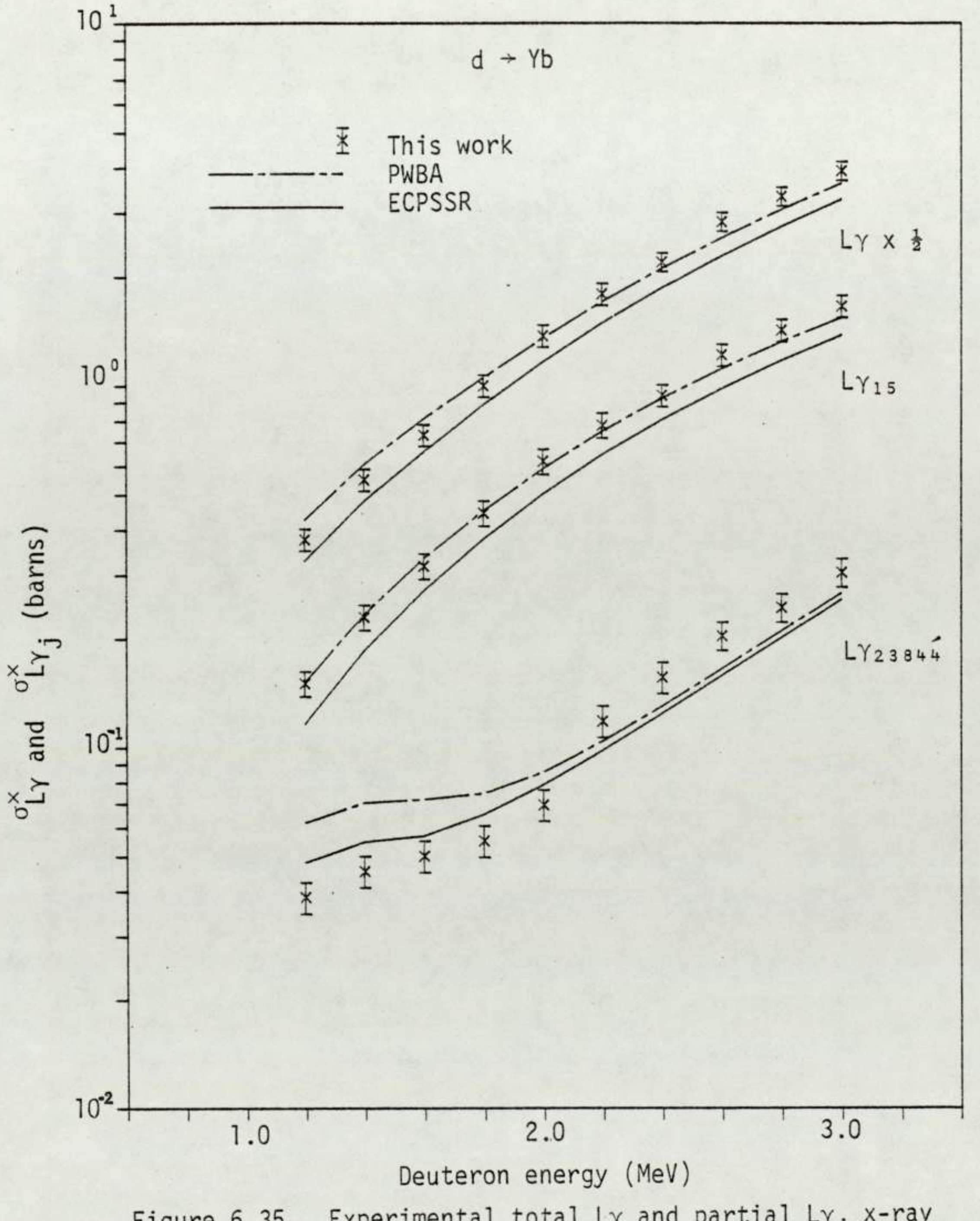

Figure 6.35. Experimental total Lγ and partial $L\gamma_j$ x-ray production cross sections for deuteron impact on Yb.

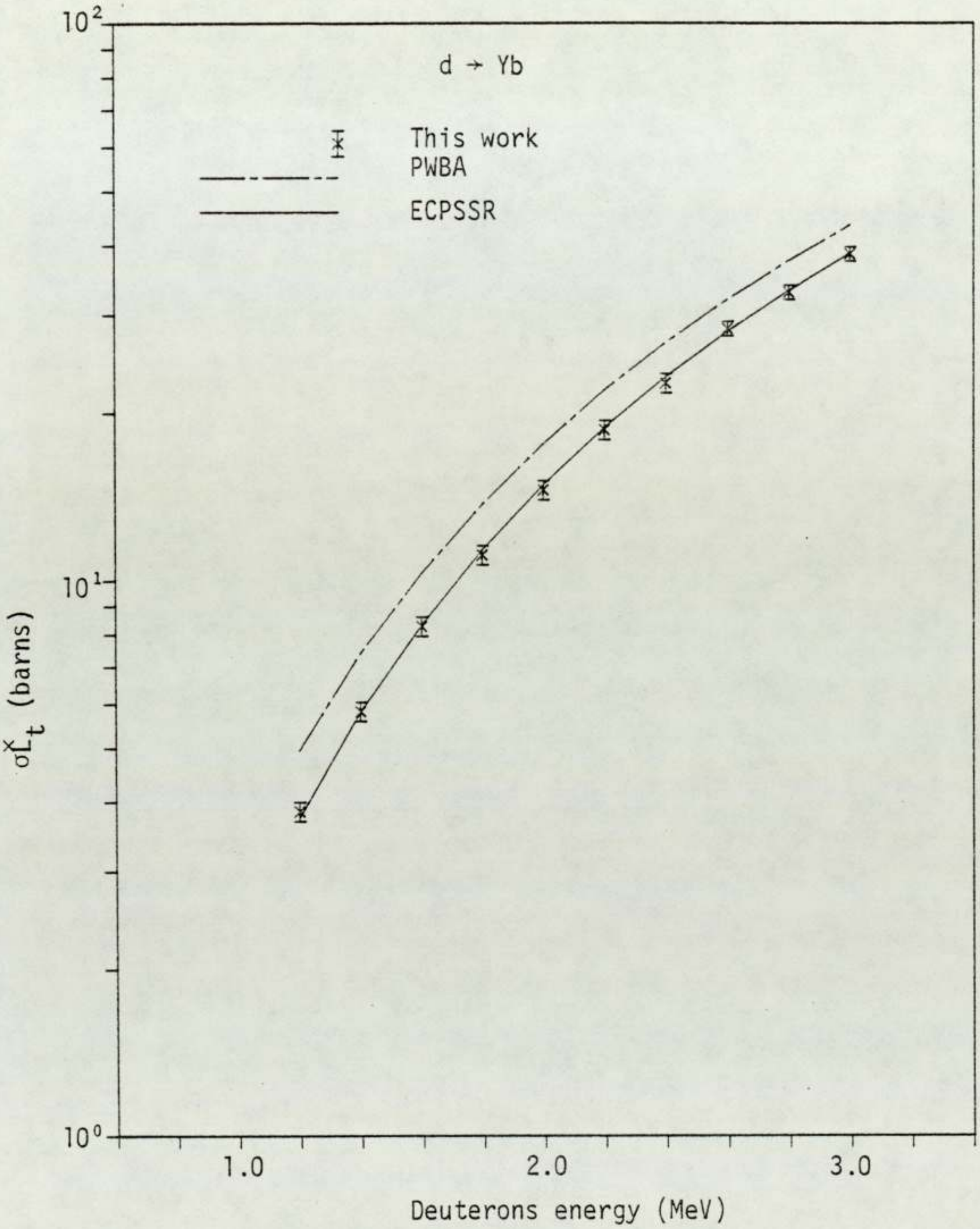

Figure 6.36. Experimental total L x-ray production cross sections for deuteron impact on Yb.

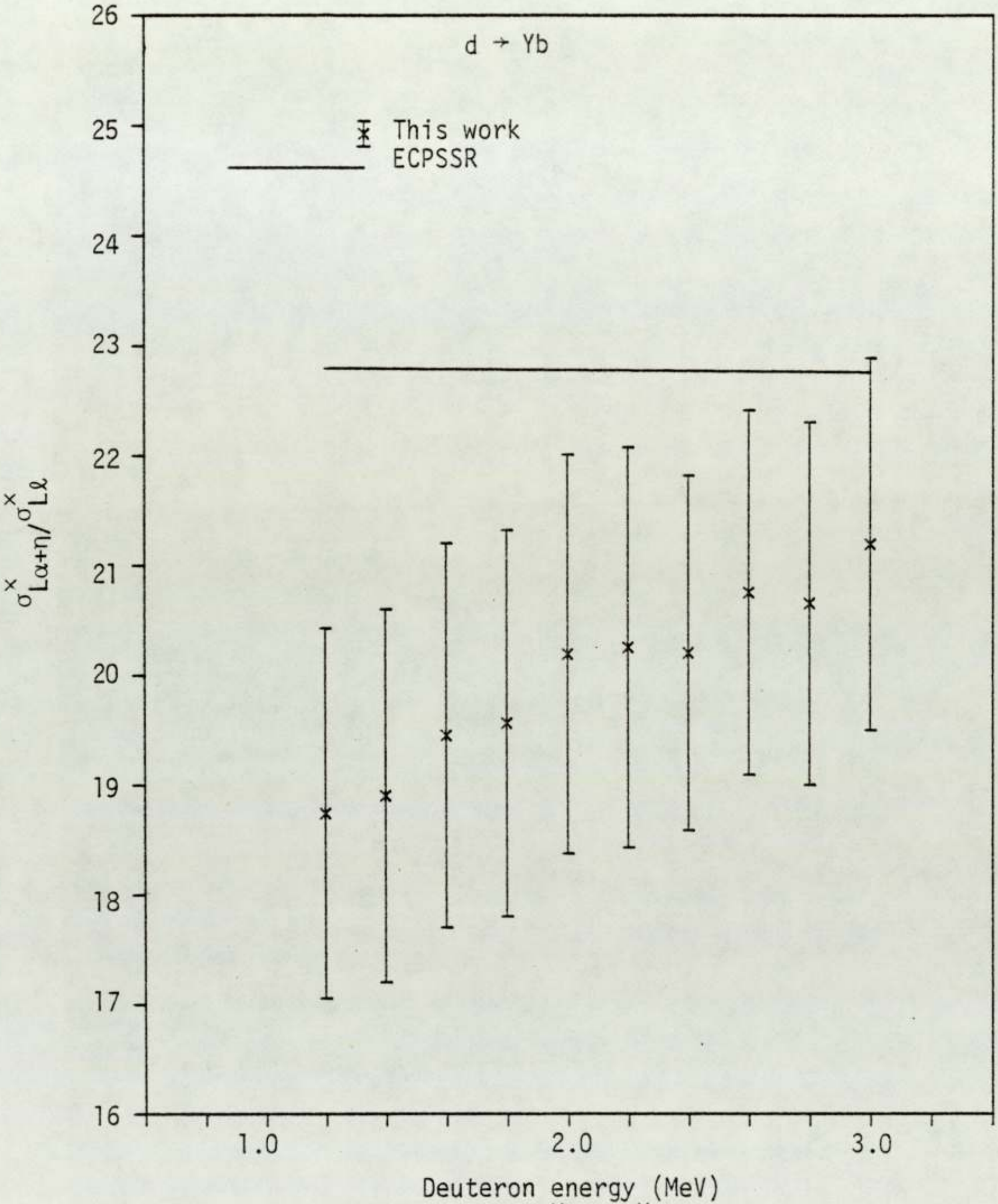

Figure 6.37. Experimental $\sigma^x_{L\alpha+\eta}/\sigma^x_{L\ell}$ ratio for deuteron impact on Yb.

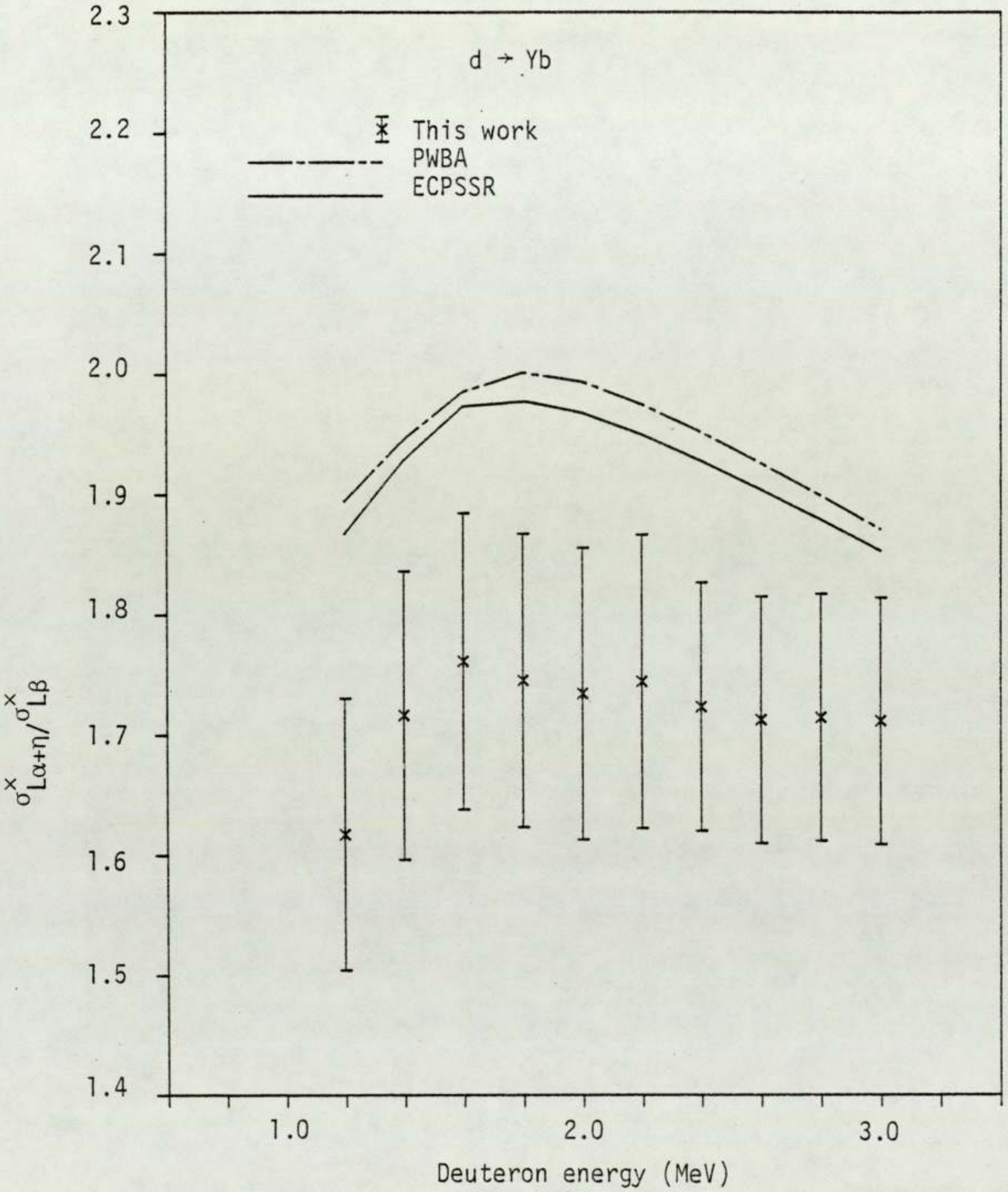

Figure 6.38. Experimental $\sigma^x_{L\alpha+\eta}/\sigma^x_{L\beta}$ ratio for deuteron impact on Yb.

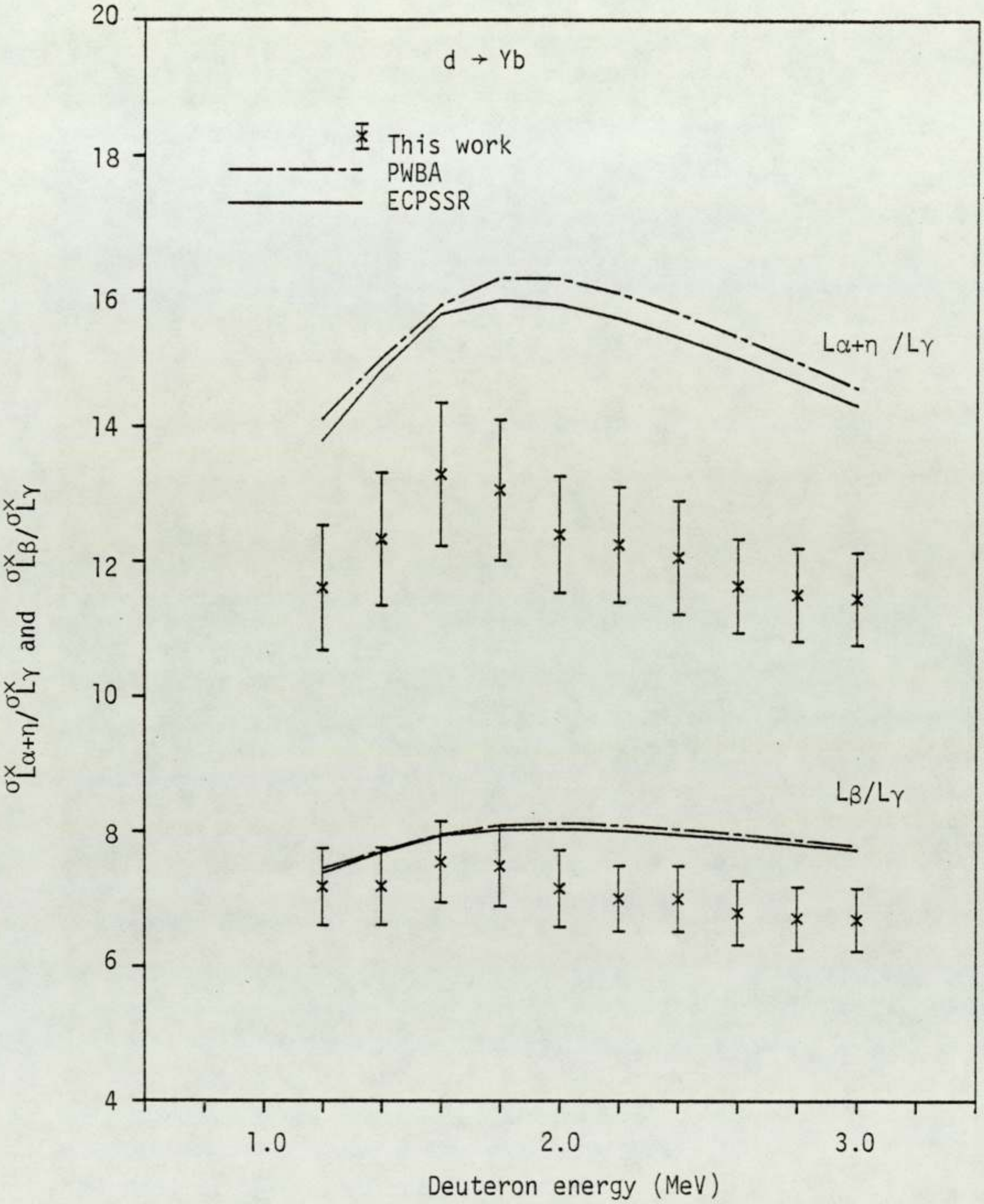

Figure 6.39. Experimental $\sigma^x_{L\alpha+\eta}/\sigma^x_{L\gamma}$ and $\sigma^x_{L\beta}/\sigma^x_{L\gamma}$ ratios for deuteron impact on Yb.

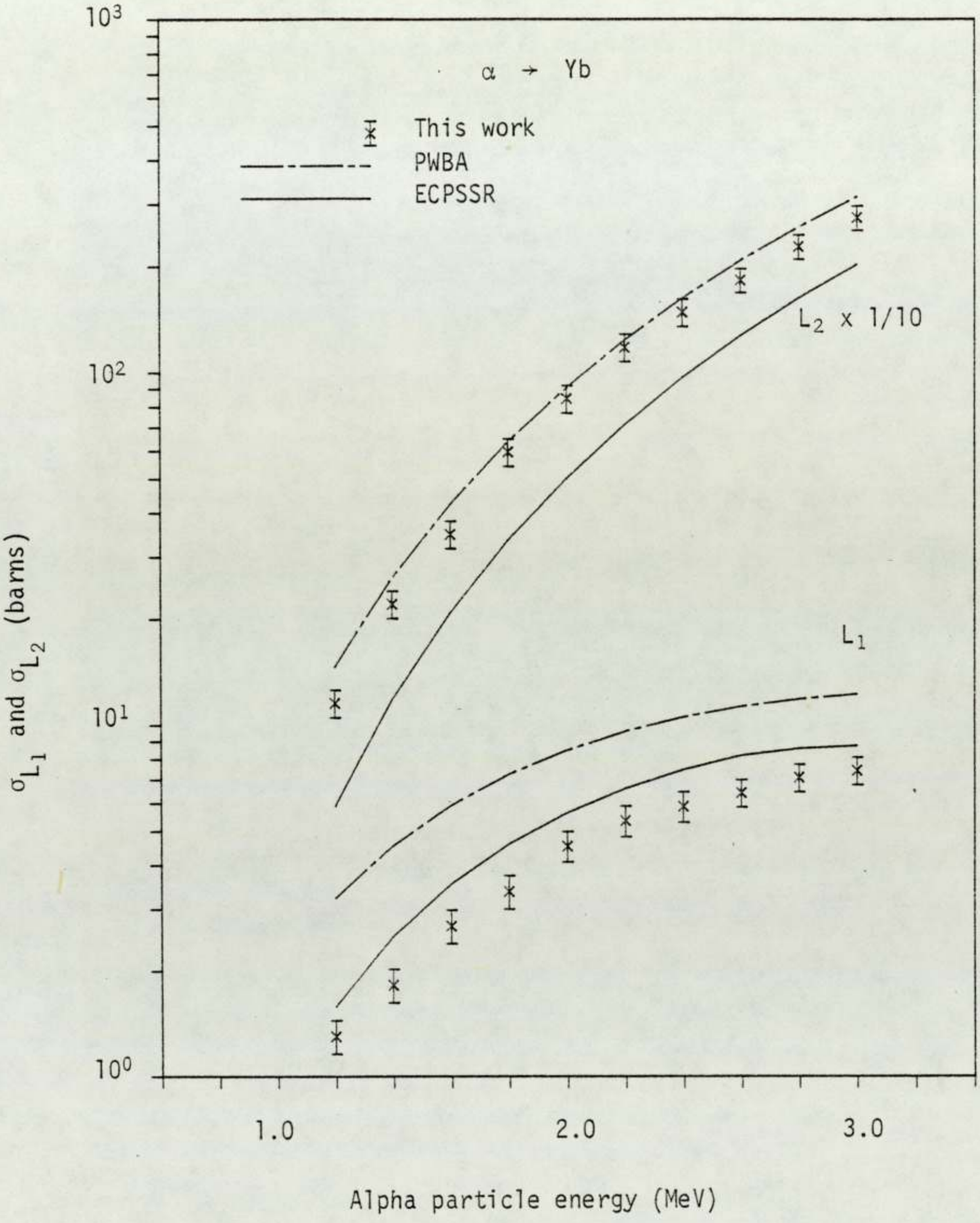

Figure 6.40. Experimental L_1 and L_2 subshell ionisation cross sections for alpha particle impact on Yb.

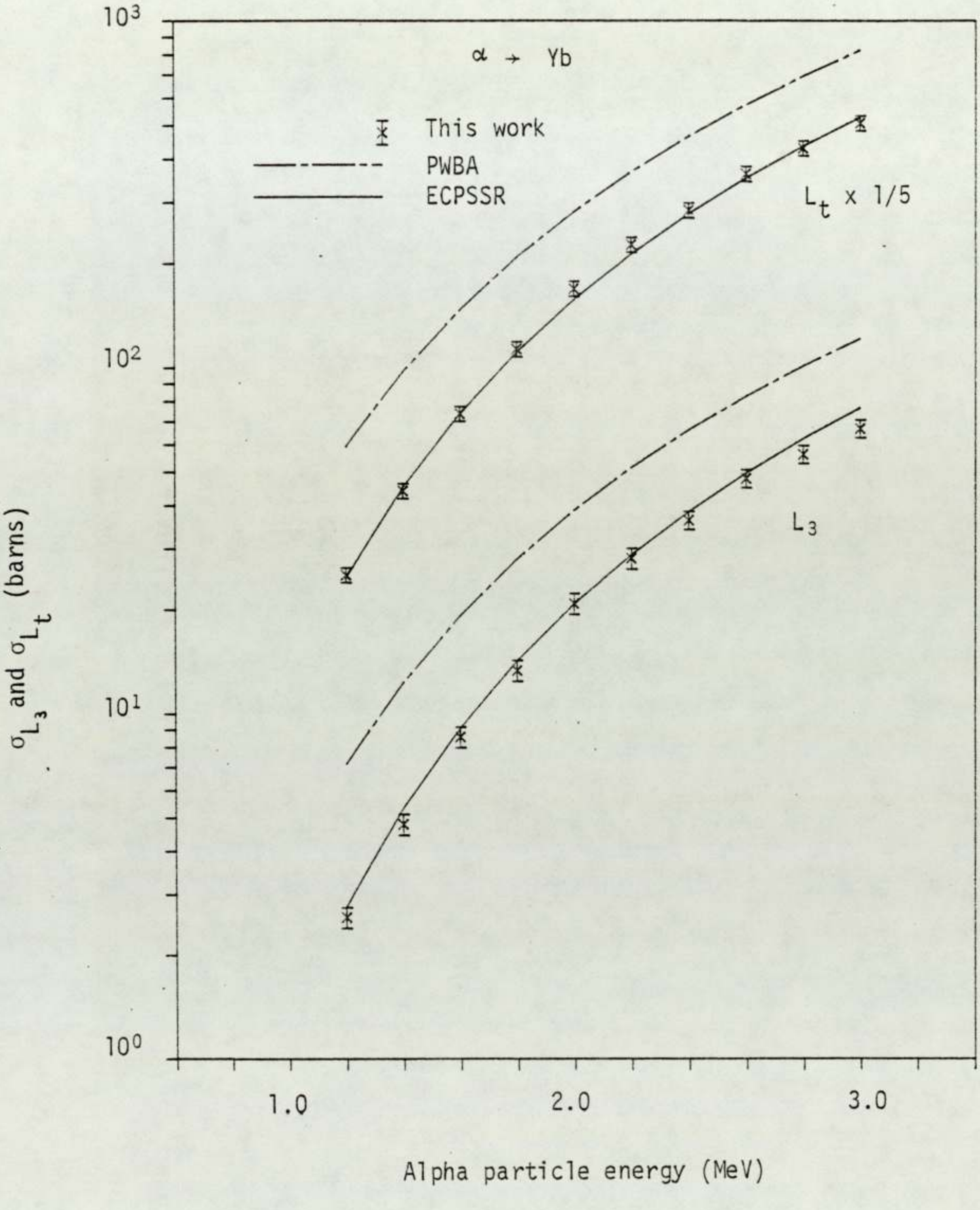

Figure 6.41. Experimental total L shell and L_3 subshell ionisation cross sections for alpha impact on Yb.

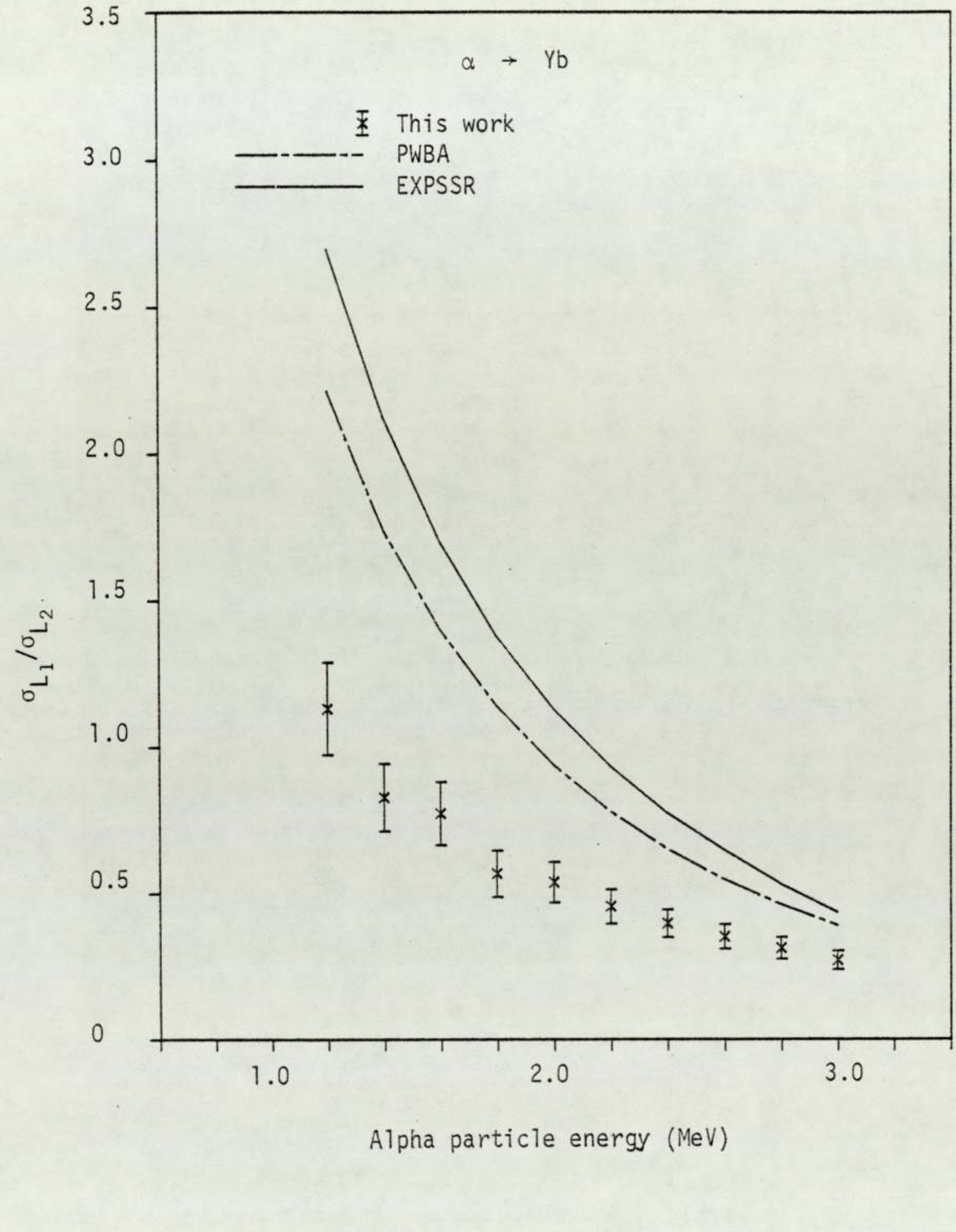

Figure 6.42. Experimental $\sigma_{L_1}/\sigma_{L_2}$ ratio for alpha particle impact on Yb.

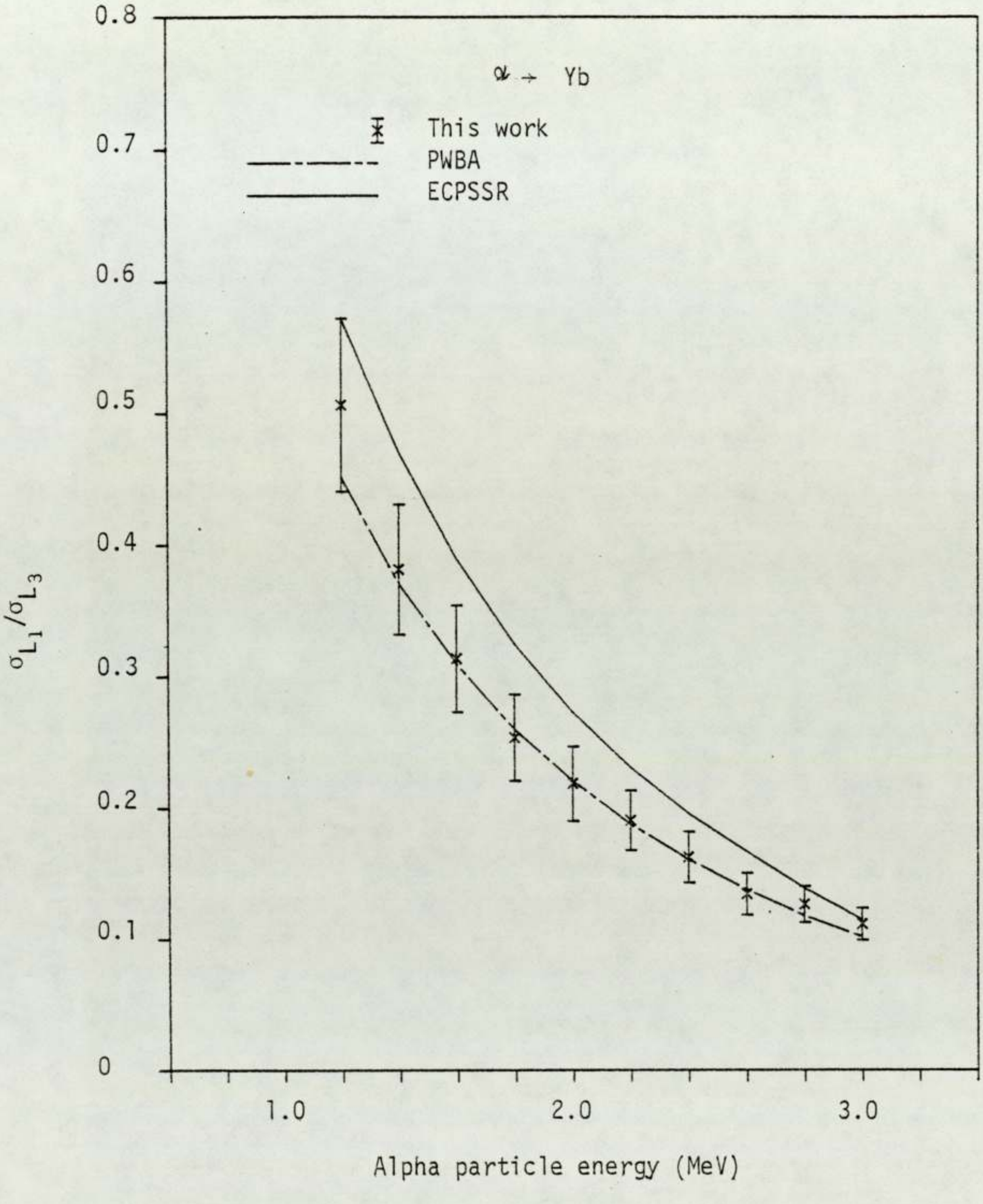

Figure 6.43. Experimental $\sigma_{L_1}/\sigma_{L_3}$ ratio for alpha particle impact on Yb.

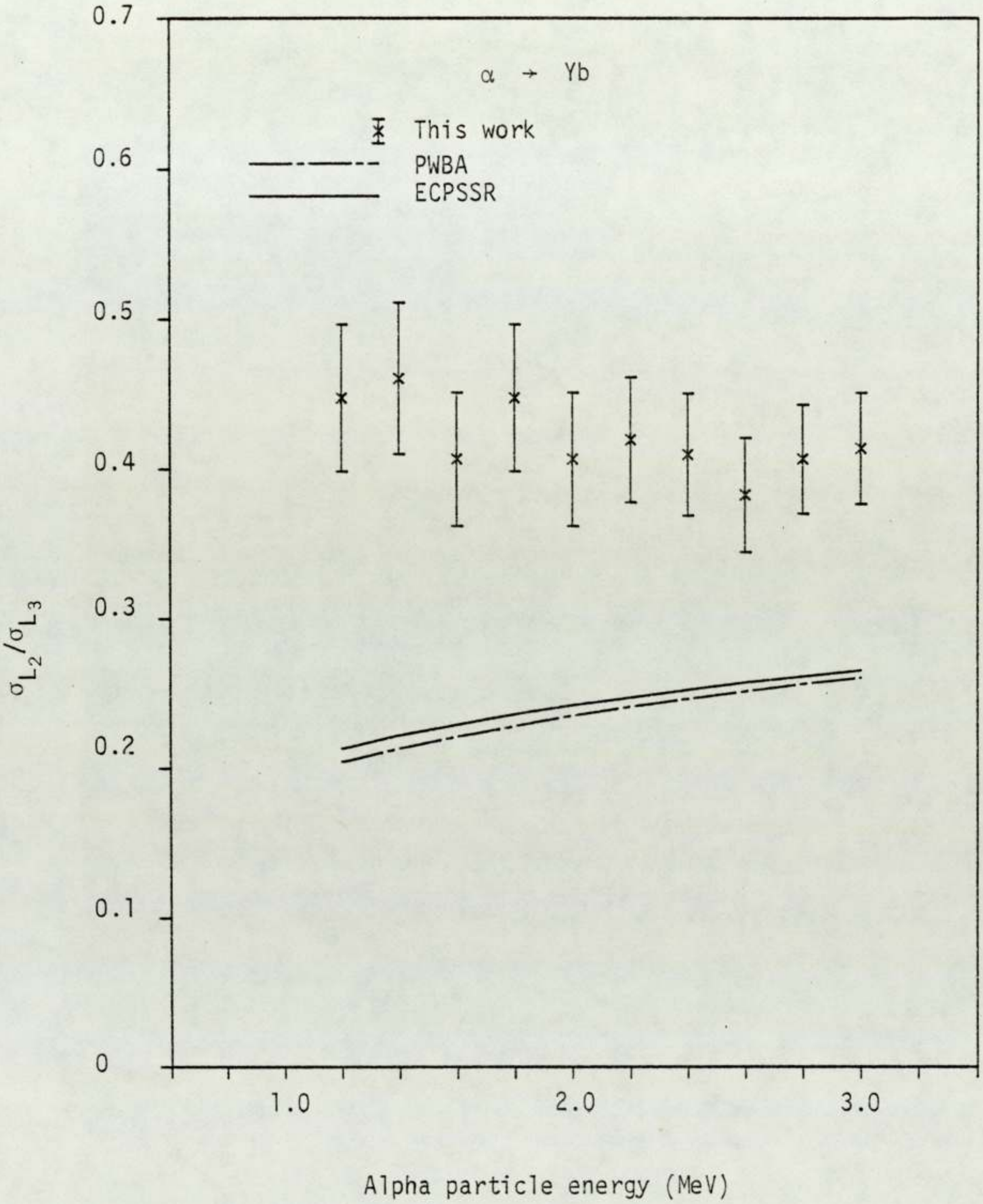

Figure 6.44. Experimental $\sigma_{L_2}/\sigma_{L_3}$ ratio for alpha particle impact on Yb.

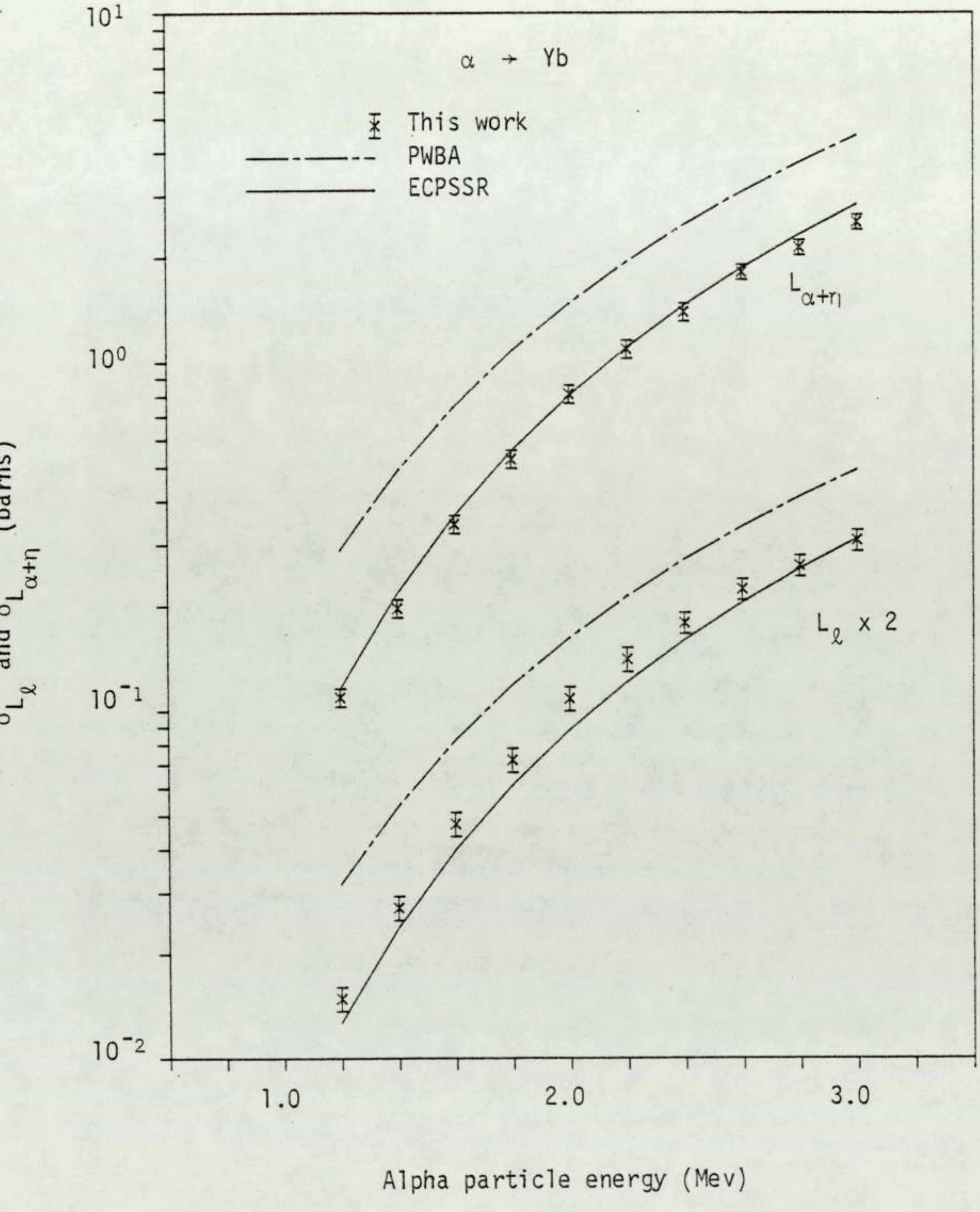

Figure 6.45. Experimental L_ℓ and $L_{\alpha+\eta}$ x-ray production cross sections for alpha particle impact on Yb.

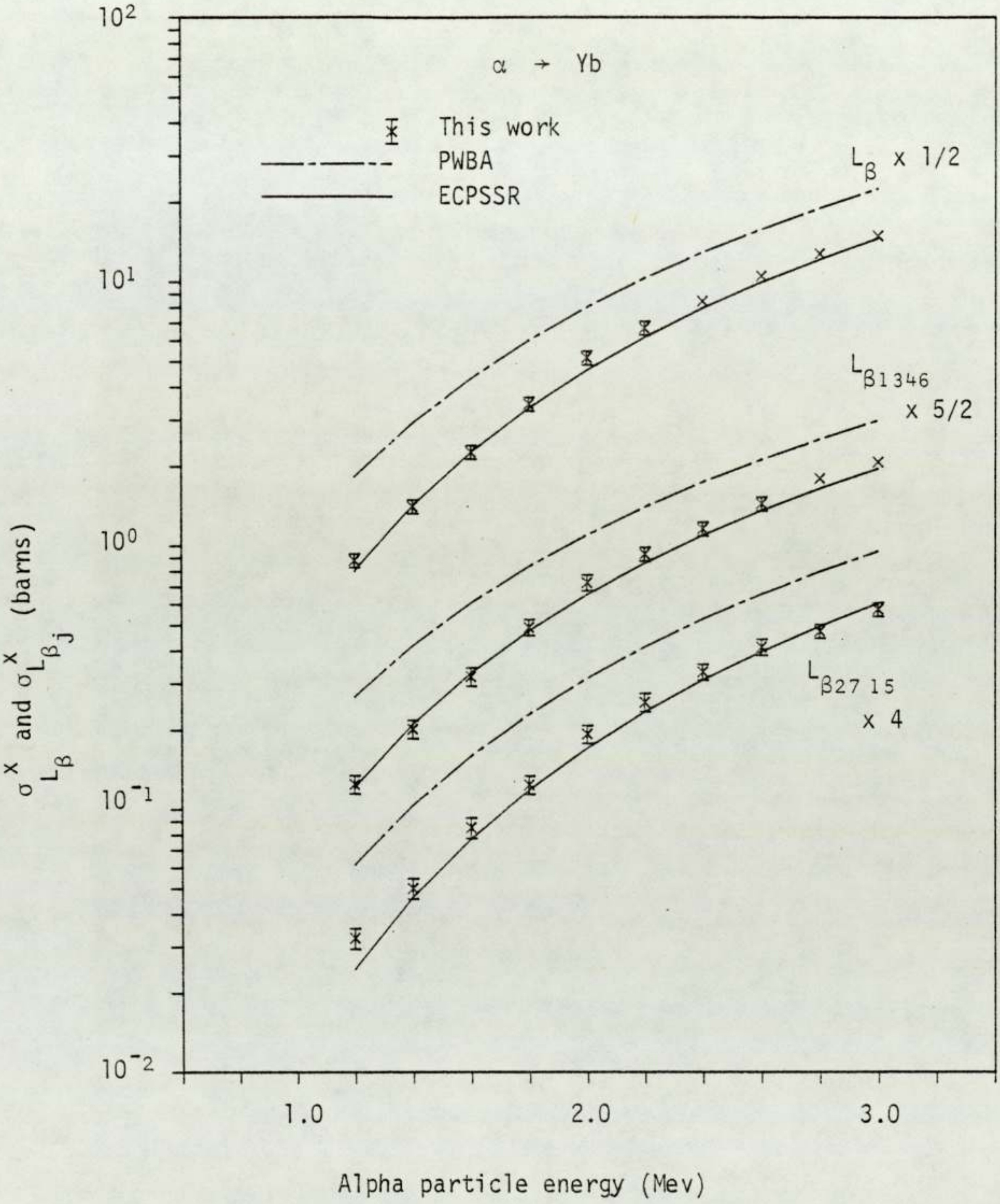

Figure 6.46. Experimental total L_β and partial L_{β_j} x-ray production cross sections alpha particle impact on Yb.

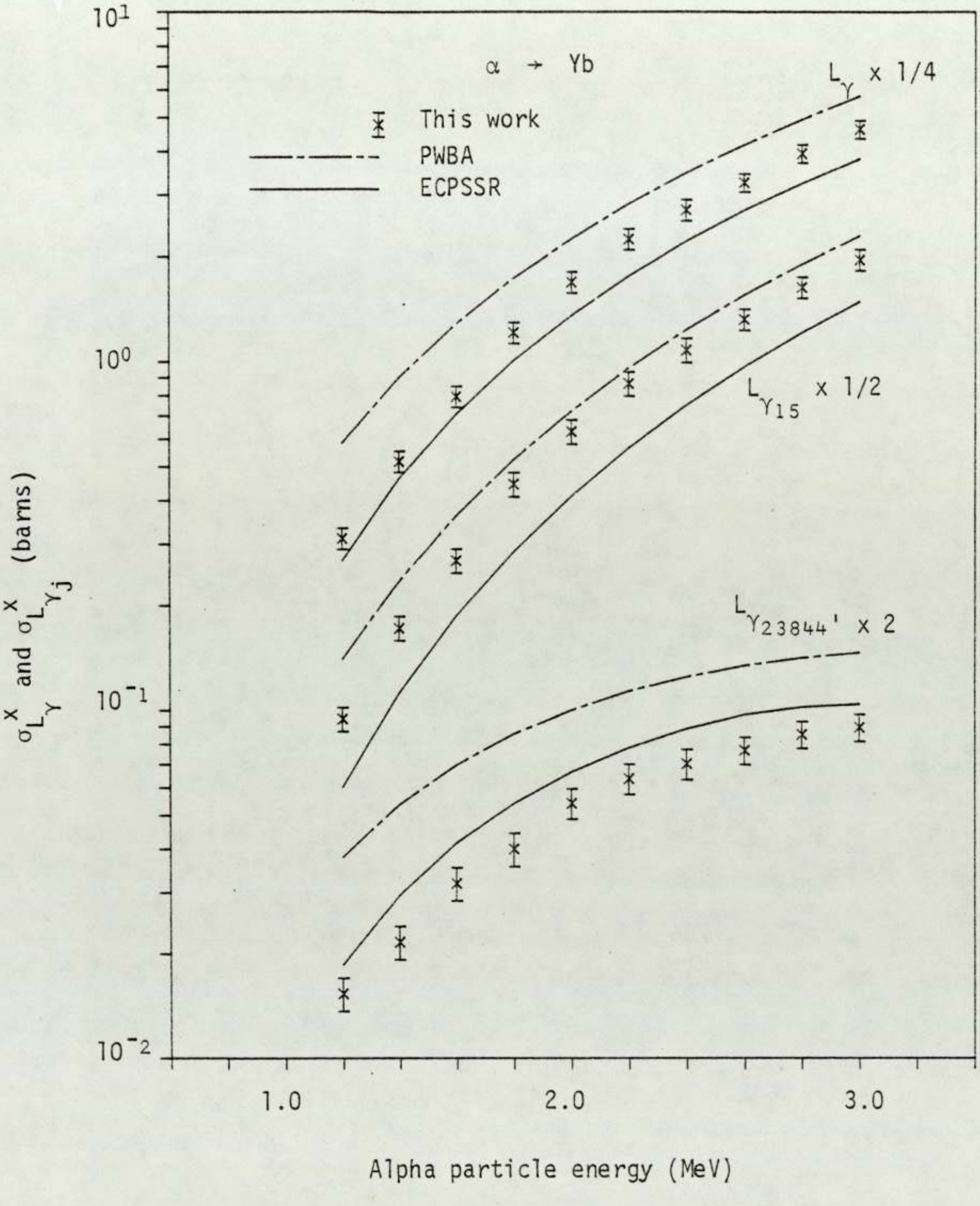

Figure 6.47. Experimental total $L\gamma$ and partial $L\gamma_j$ x-ray production cross sections for alpha particle impact on Yb.

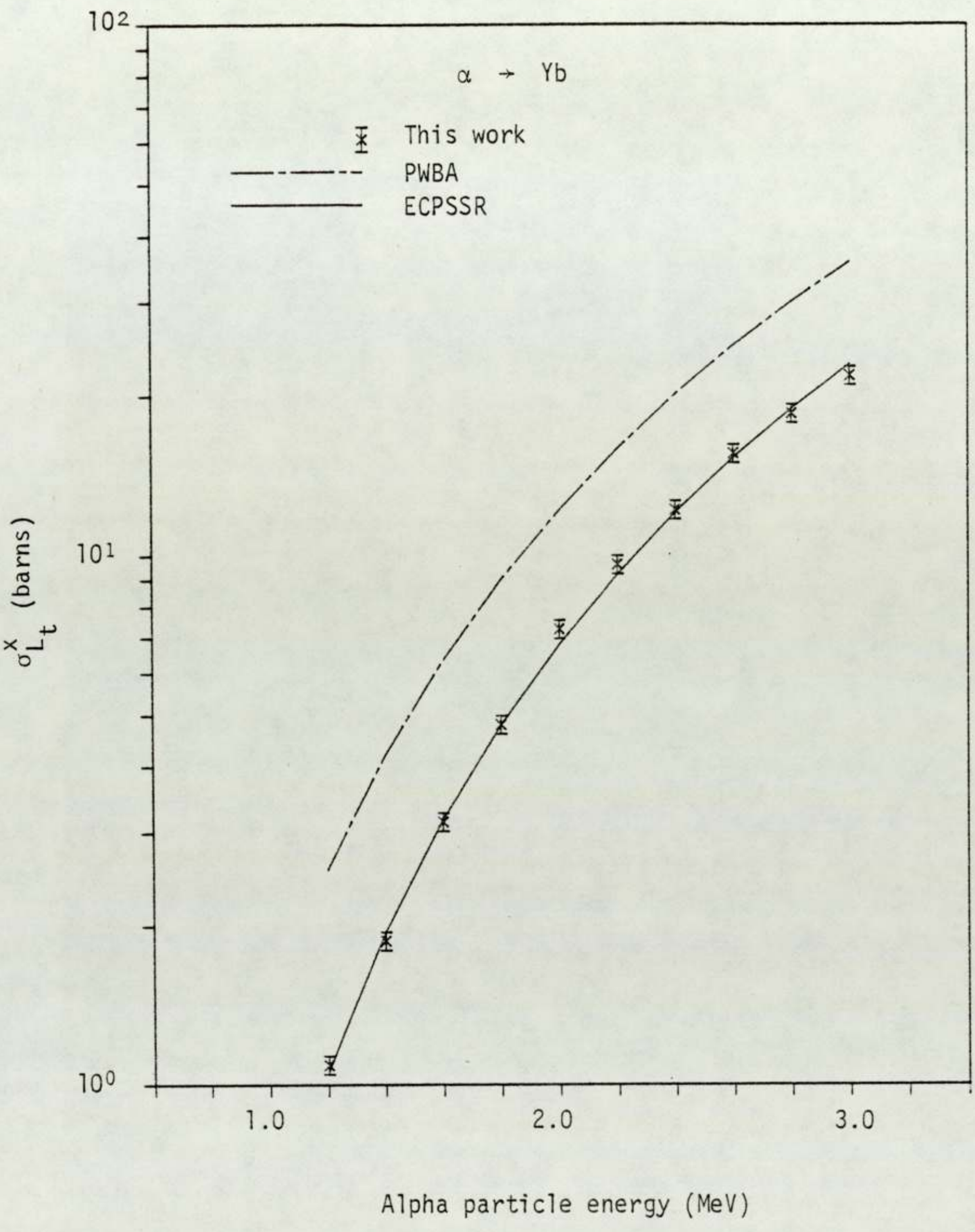

Figure 6.48. Experimental total L x-ray production cross section for alpha particle impact on Yb.

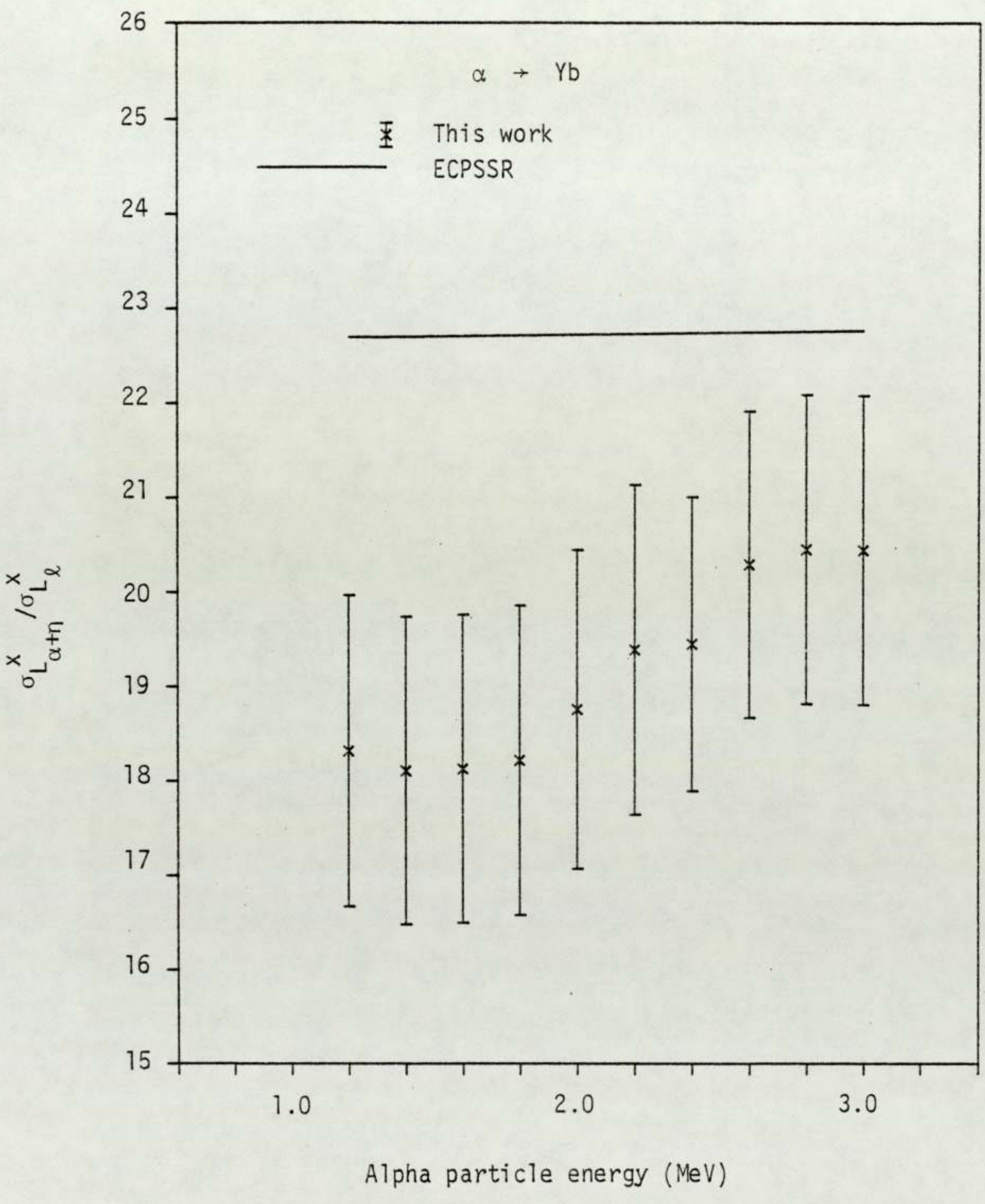

Figure 6.49. Experimental $\sigma^X_{L_{\alpha+\eta}}/\sigma^X_{L_\ell}$ ratio for alpha particle impact on Yb.

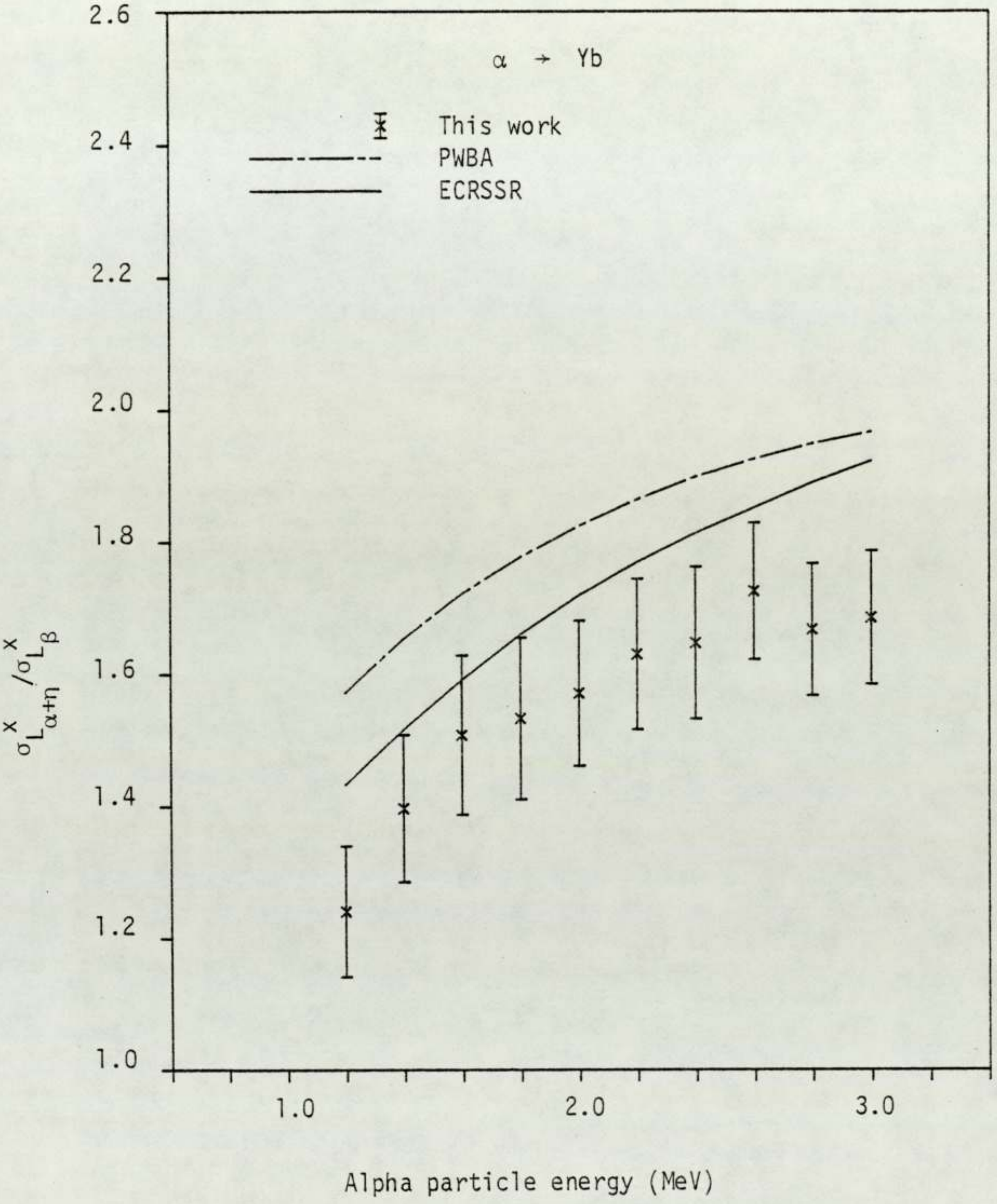

Figure 6.50. Experimental $\sigma^X_{L_{\alpha+\eta}} / \sigma^X_{L_\beta}$ ratio for alpha particle impact on Yb.

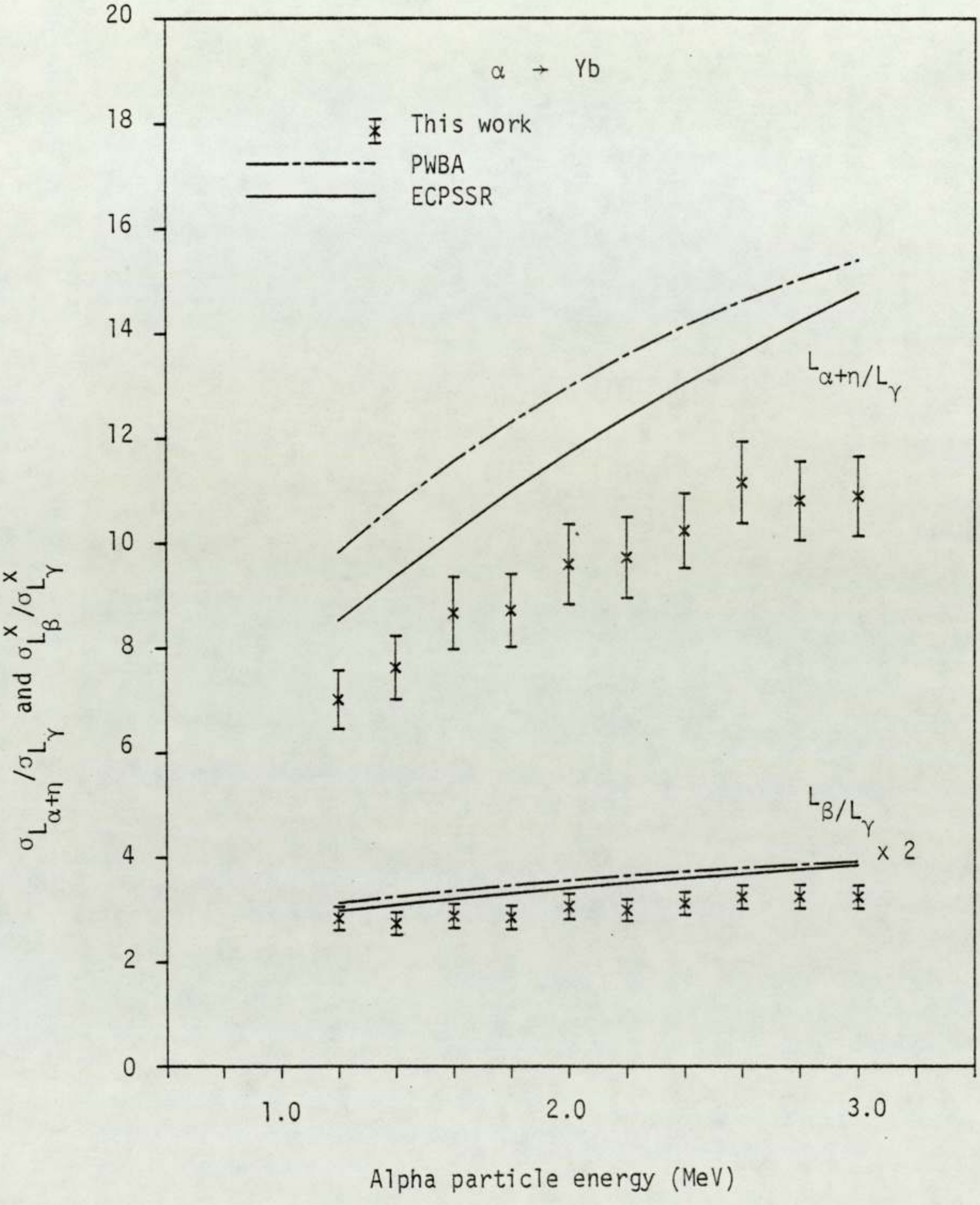

Figure 6.51. Experimental $\sigma^x_{L_{\alpha+\eta}}/\sigma^x_{L_\gamma}$ and $\sigma^x_{L_\beta}/\sigma^x_{L_\gamma}$ ratios for alpha particle impact on Yb.

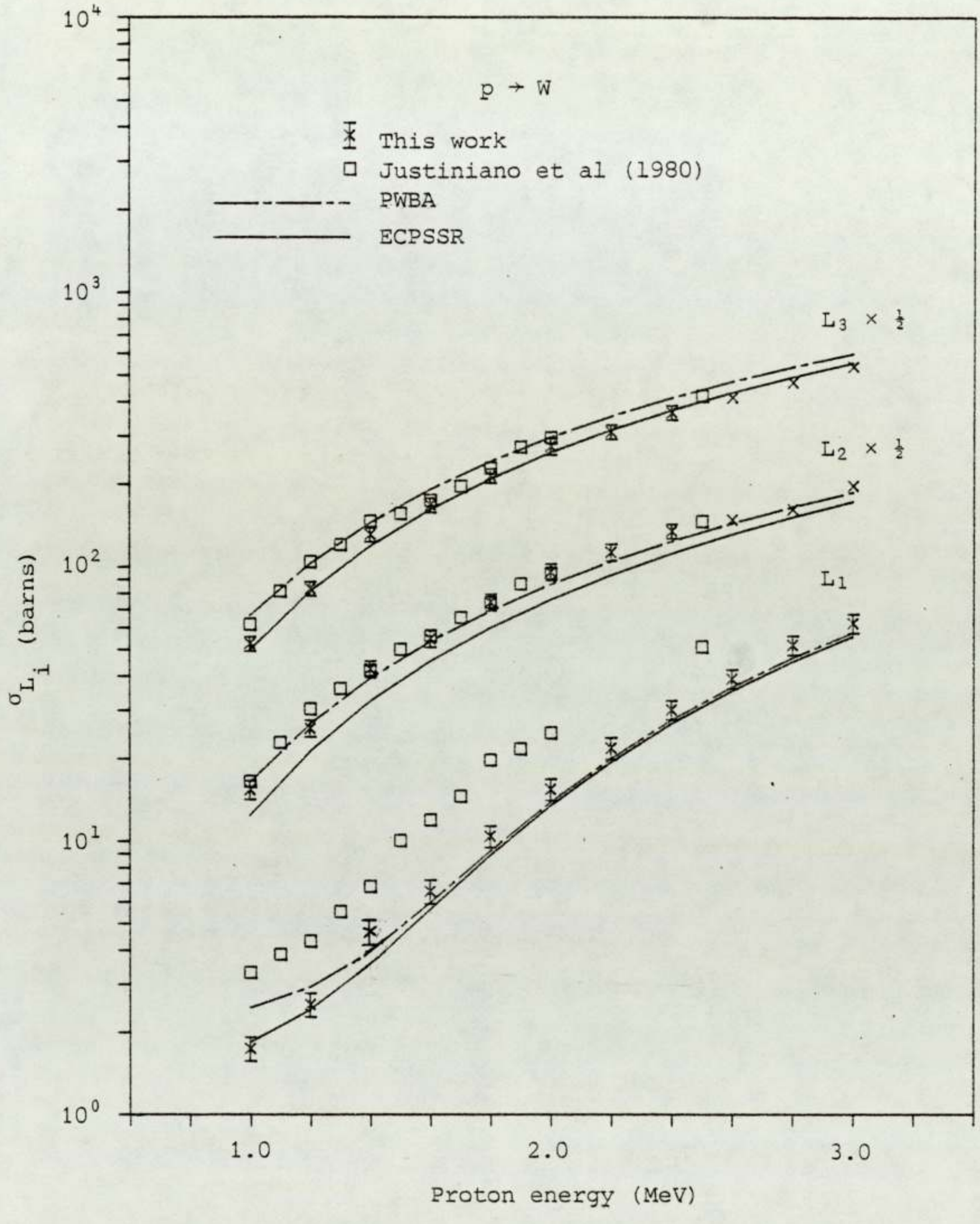

Figure 6.52. Experimental L_i subshell ionisation cross sections for proton impact on W.

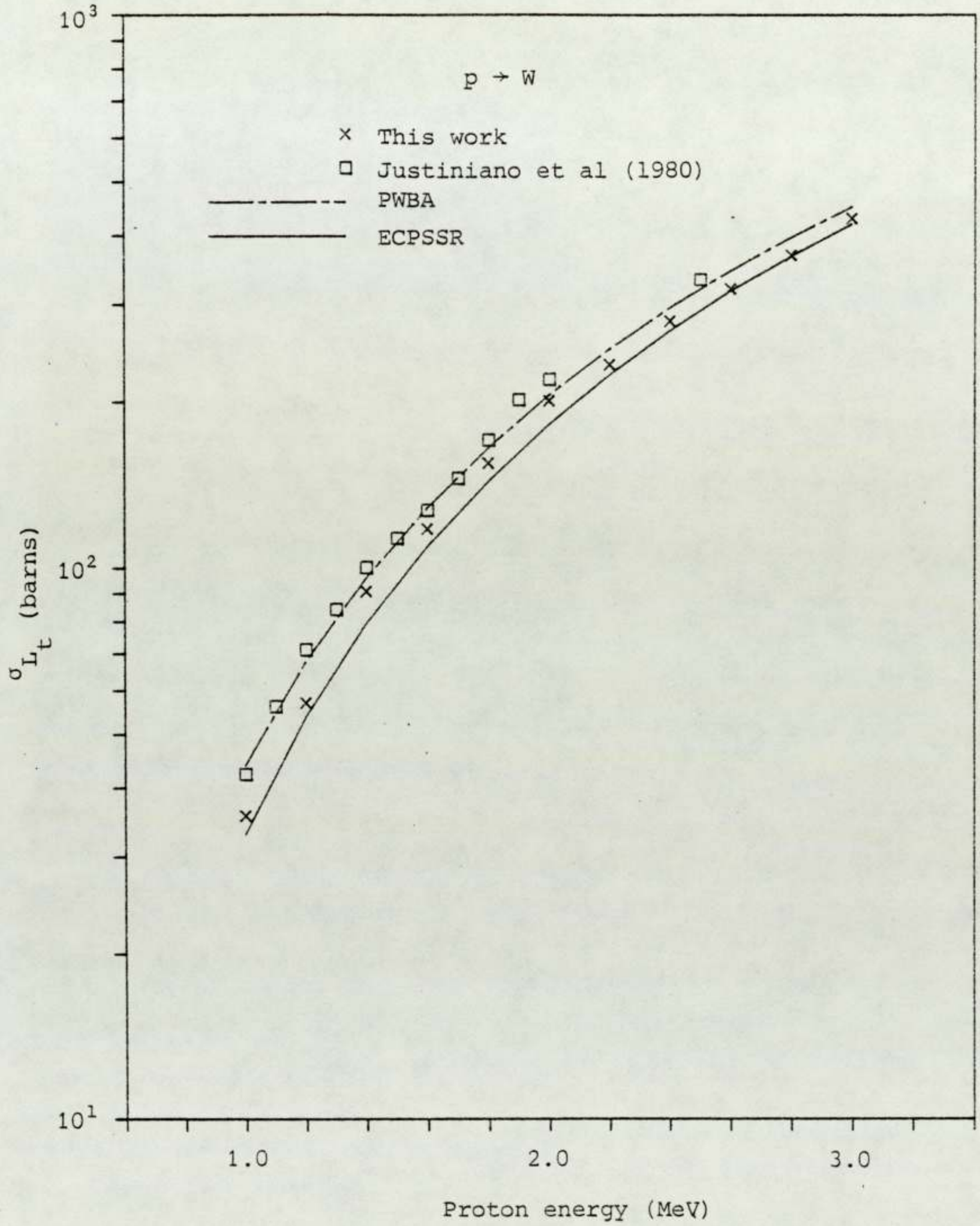

Figure 6.53. Experimental total L shell ionisation cross section for proton impact on W.

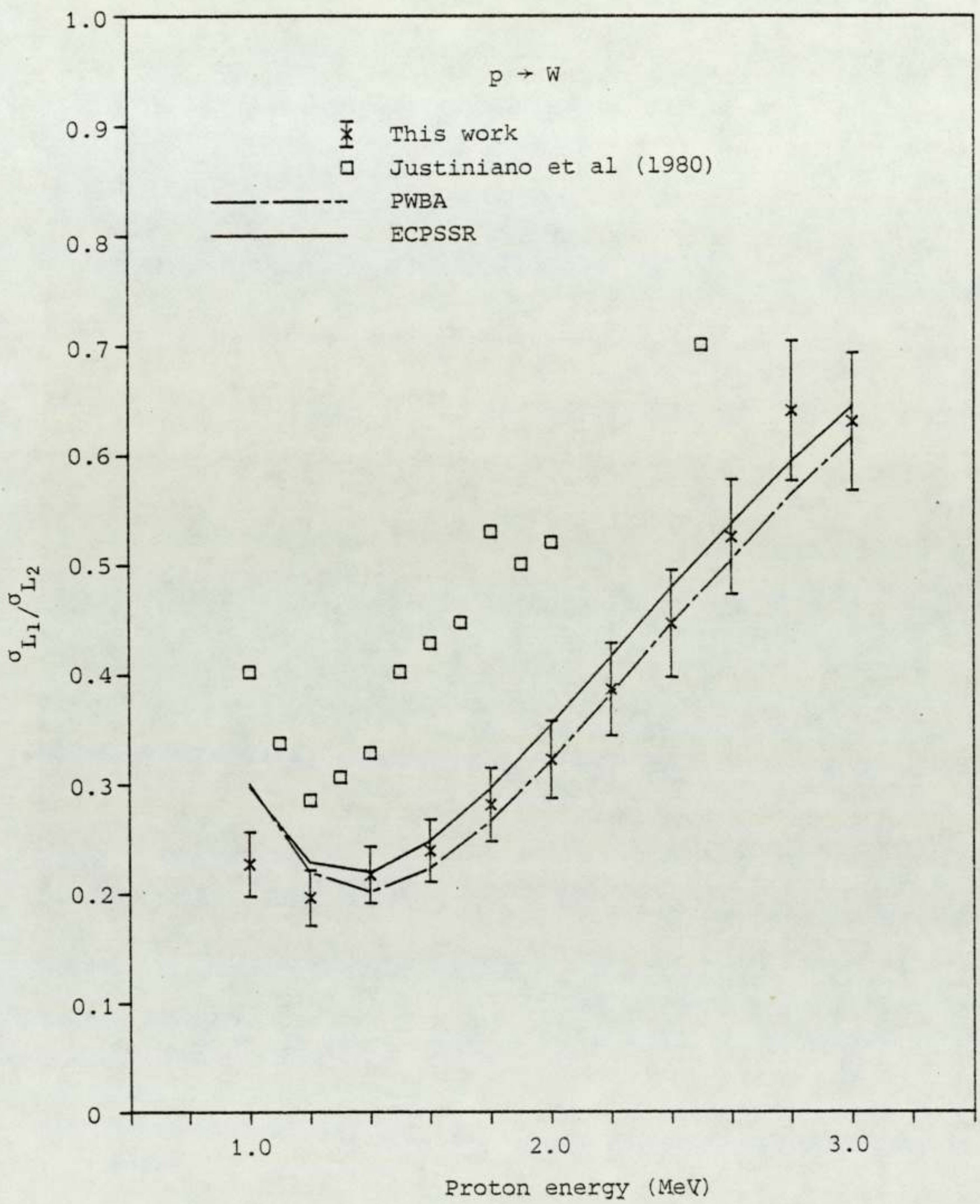

Figure 6.54. Experimental $\sigma_{L_1}/\sigma_{L_2}$ ratio for proton impact on W.

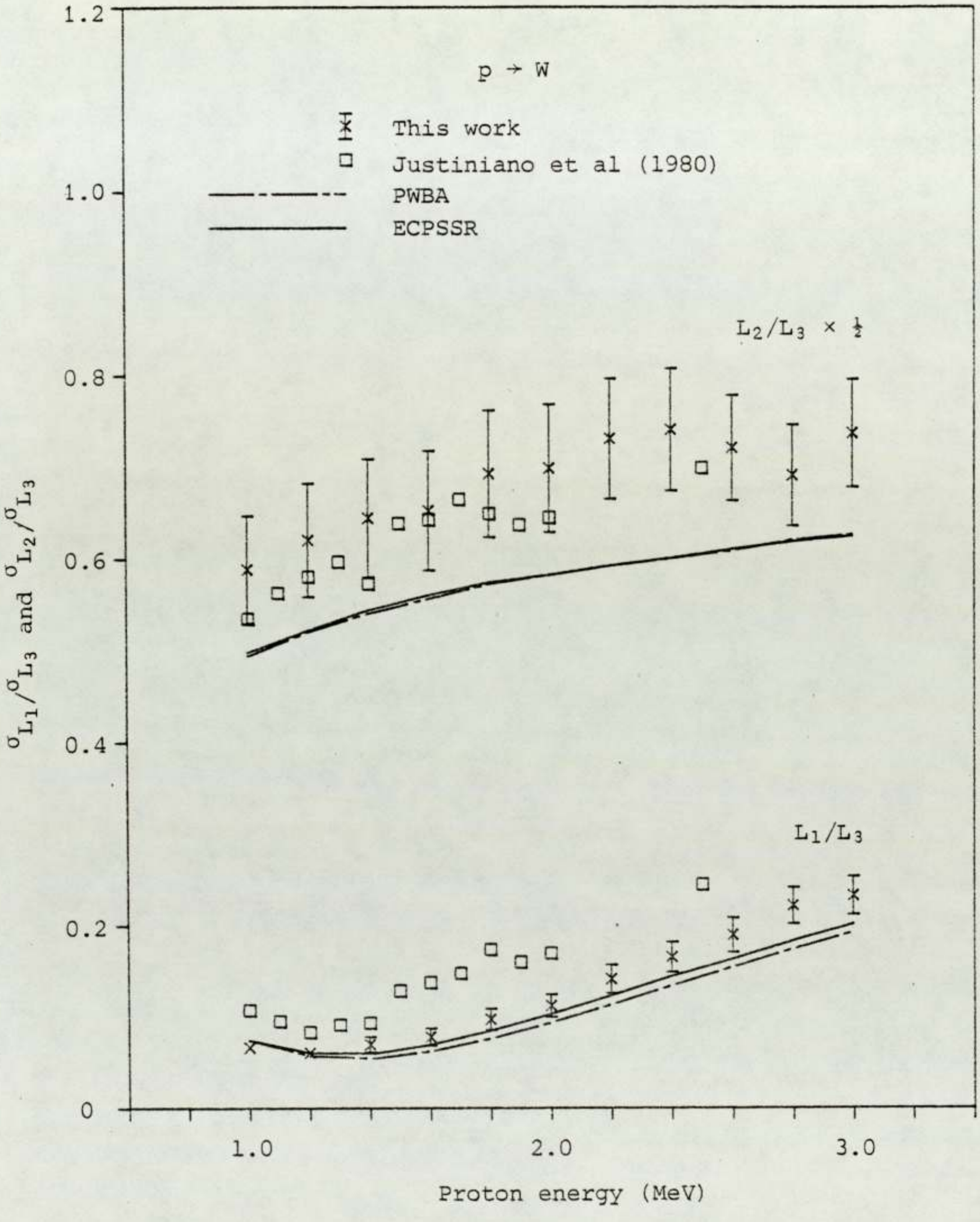

Figure 6.55. Experimental $\sigma_{L_1}/\sigma_{L_3}$ and $\sigma_{L_2}/\sigma_{L_3}$ ratios for proton impact on W.

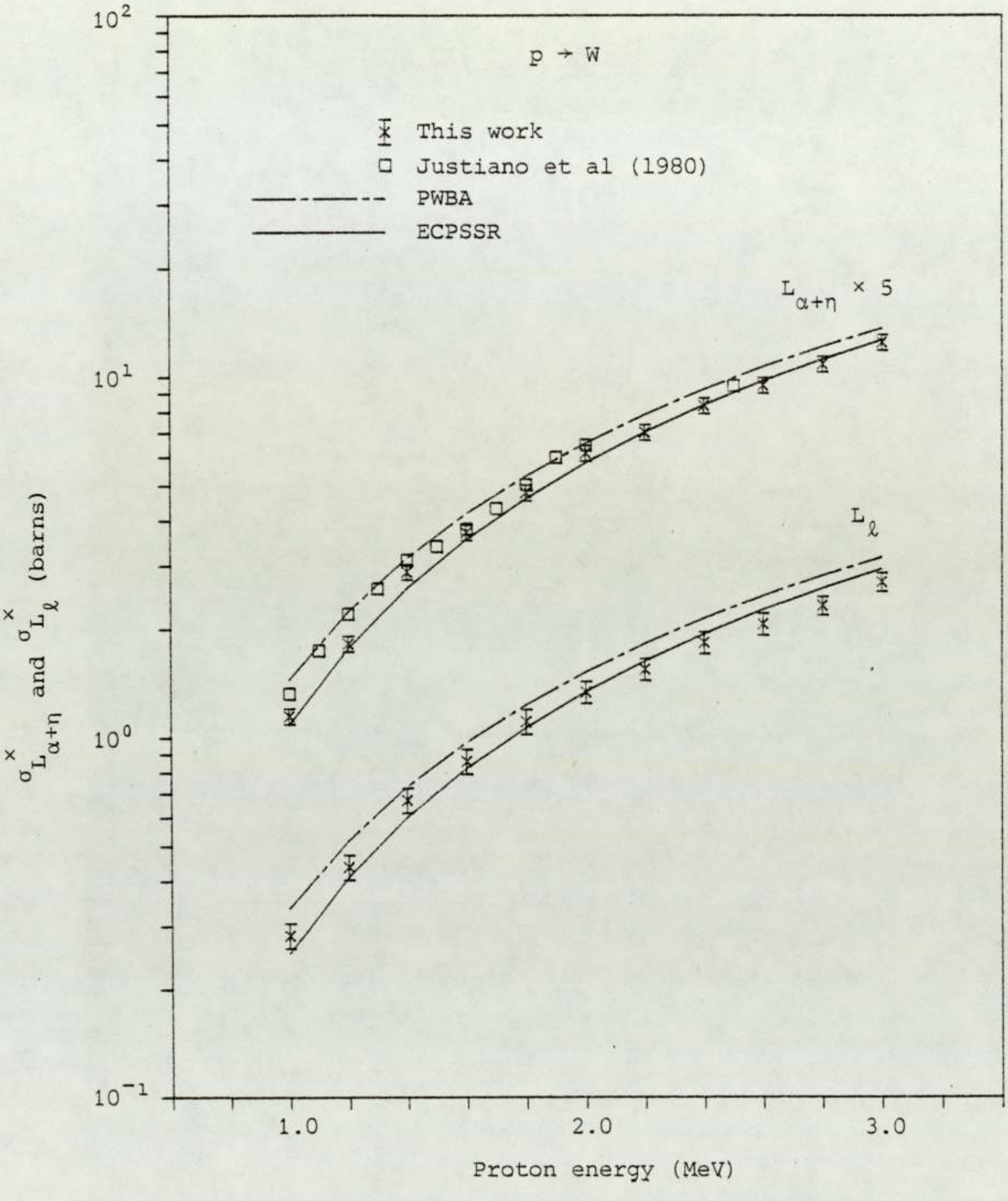

Figure 6.56. Experimental L_ℓ and $L_{\alpha+\eta}$ x-ray production cross sections for proton impact on W.

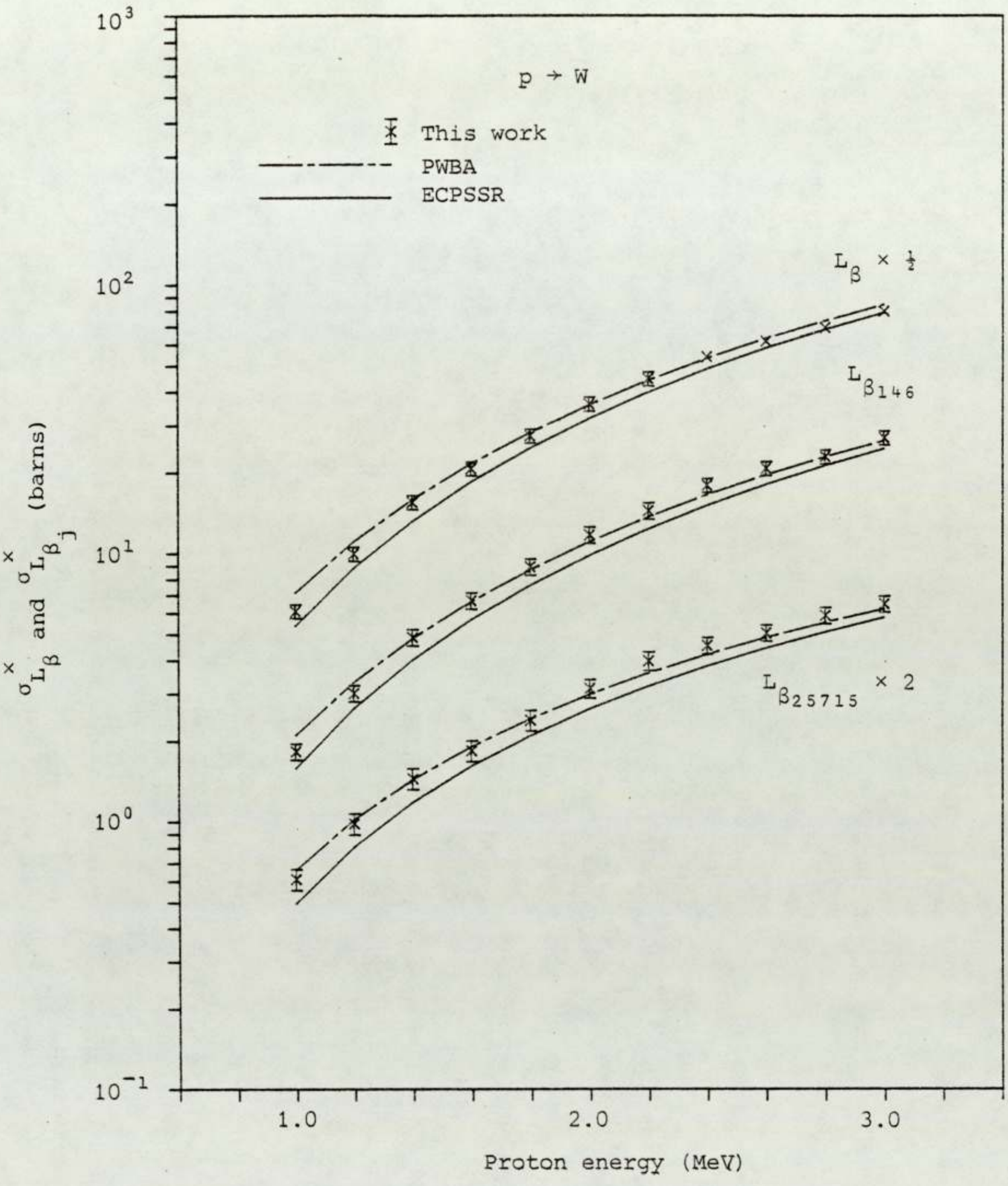

Figure 6.57. Experimental total L_β and partial L_{β_j} x-ray production cross sections for proton impact on W.

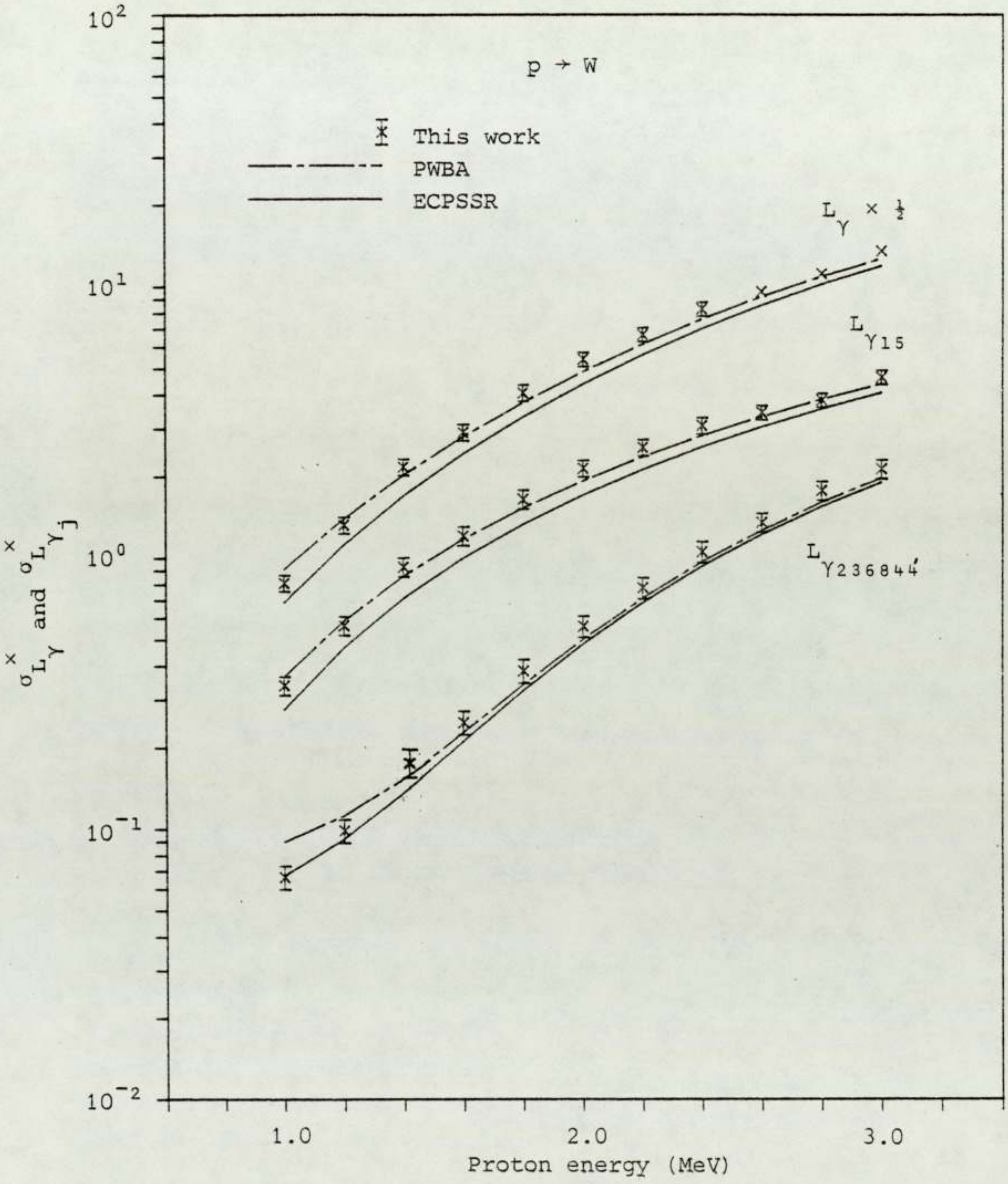

Figure 6.58. Experimental L_γ and L_{γ_j} x-ray production cross sections for proton impact on W.

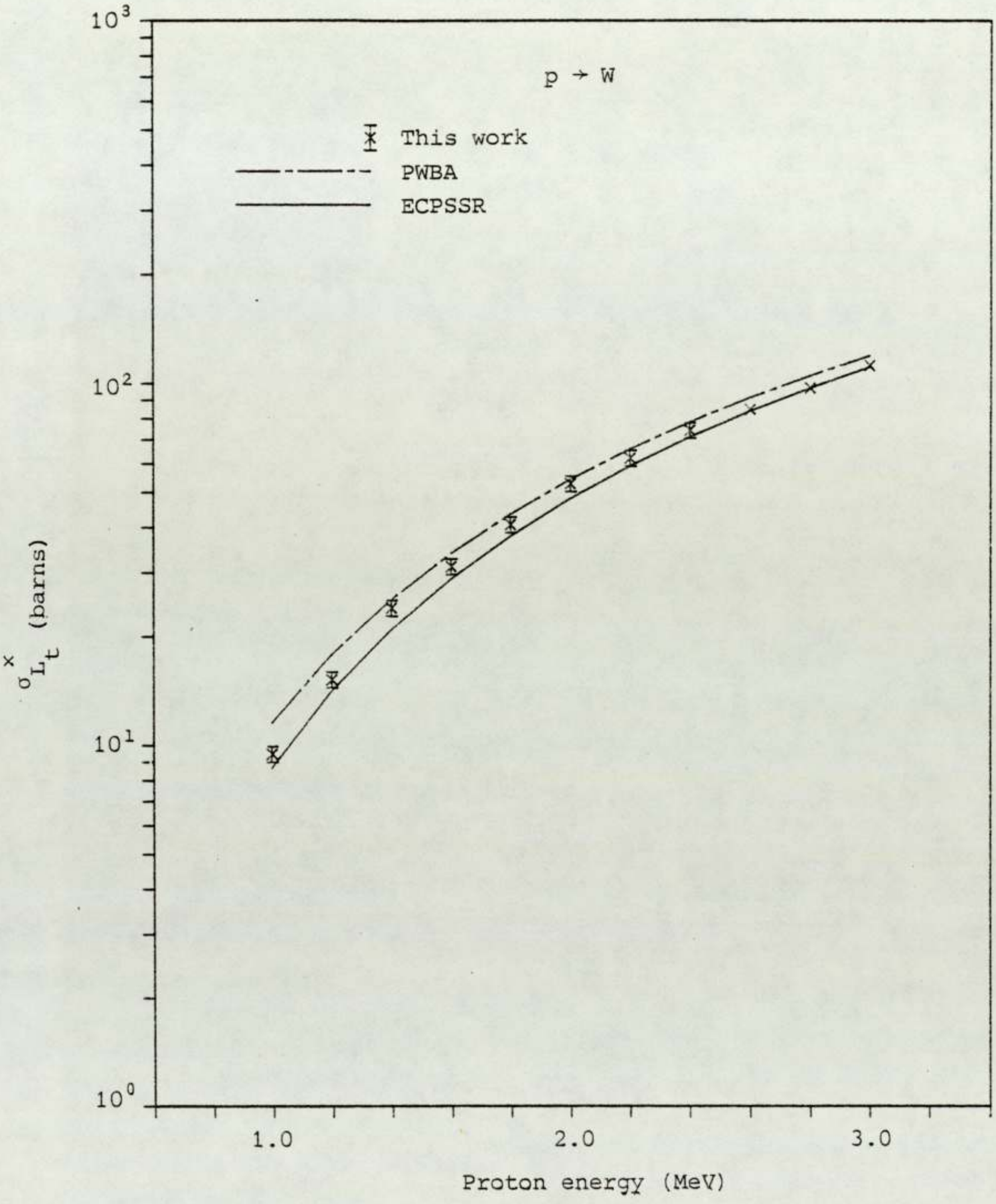

Figure 6.59. Experimental total L shell x-ray production cross section for proton impact on W.

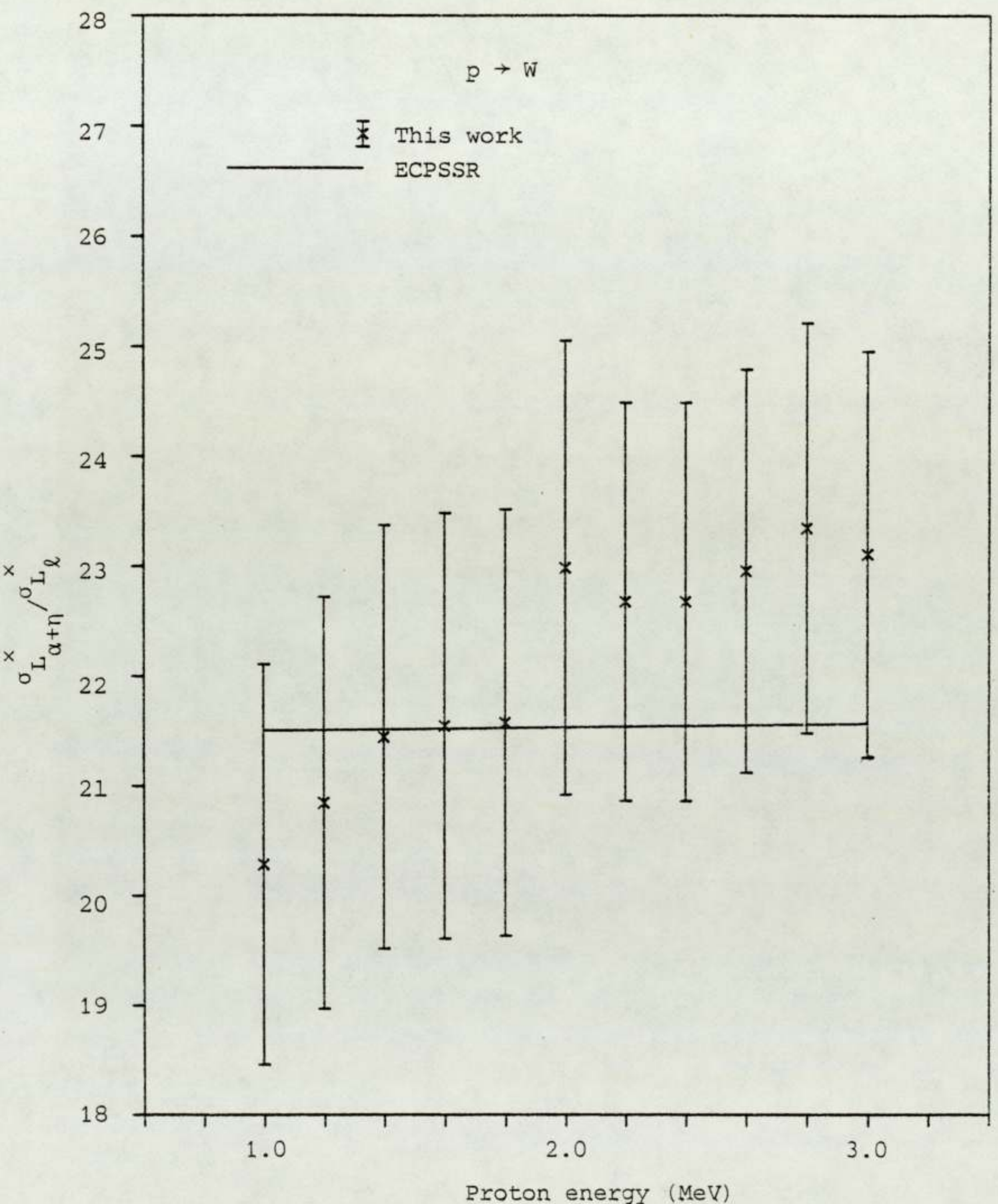

Figure 6.60. Experimental $\sigma^x_{L_{\alpha+\eta}}/\sigma^x_{L_\ell}$ ratio for proton impact on W.

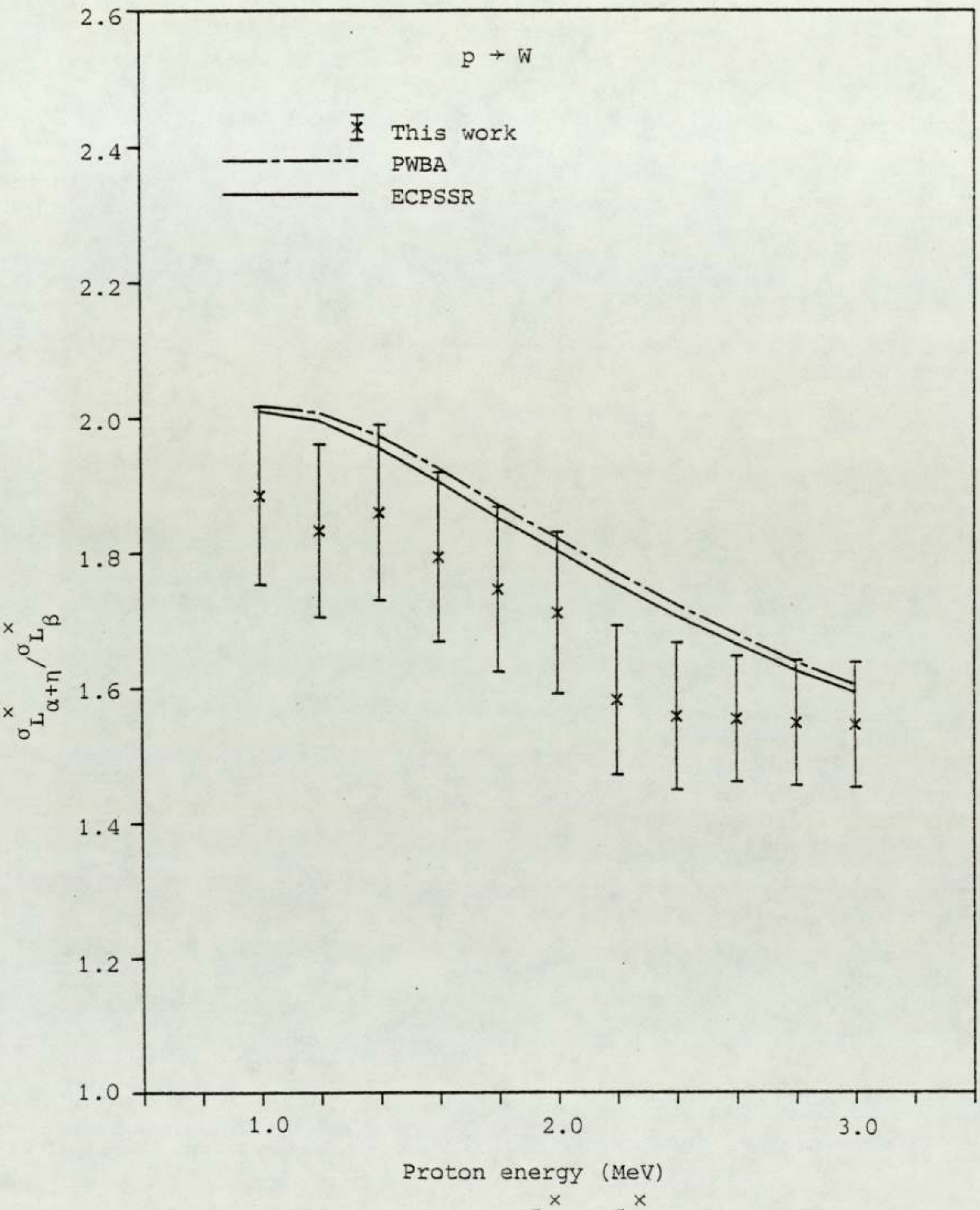

Figure 6.61. Experimental $\sigma^{x}_{L_{\alpha+\eta}}/\sigma^{x}_{L_{\beta}}$ ratio for proton impact on W.

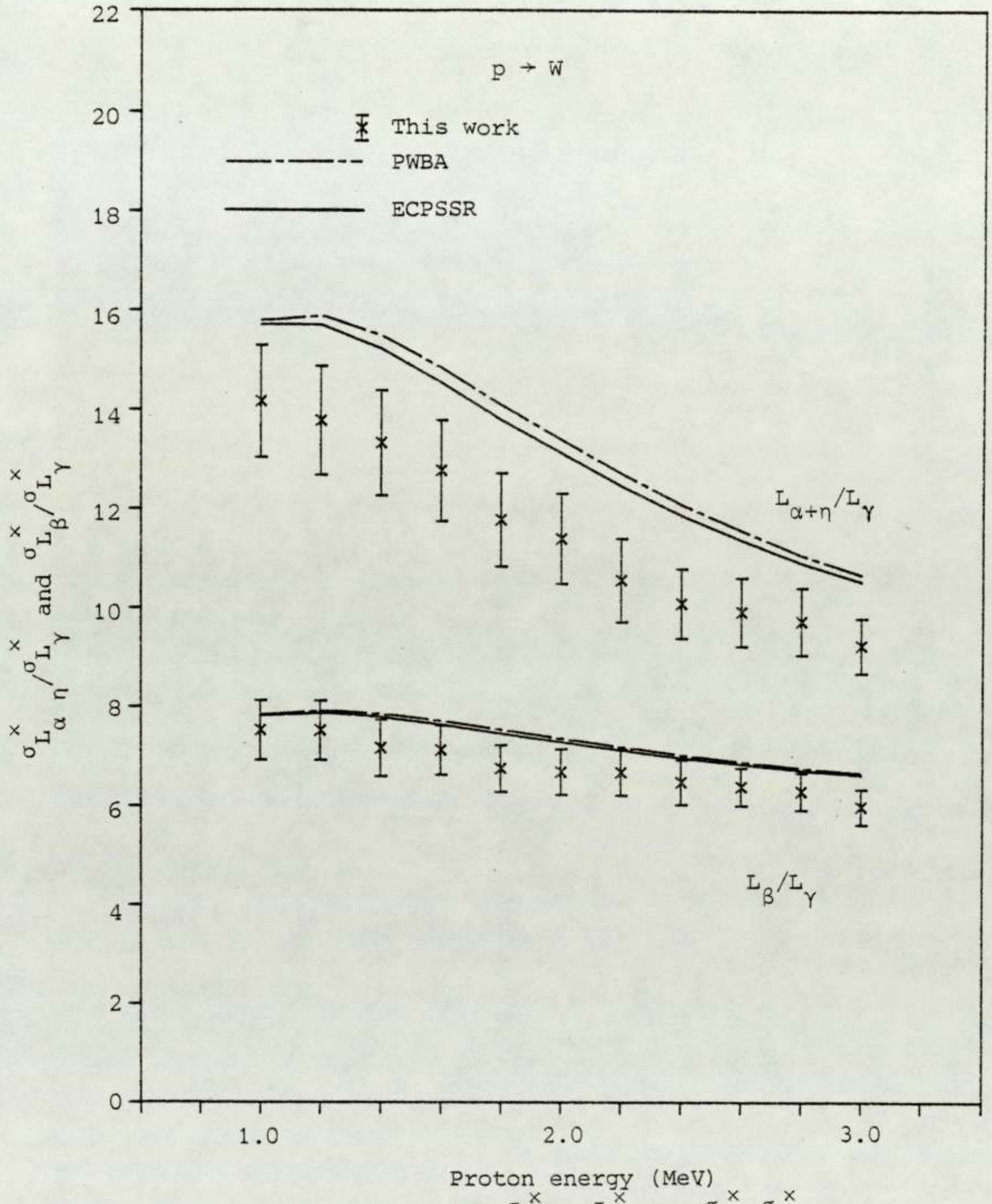

Figure 6.62. Experimental $\sigma^{x}_{L_{\alpha+\eta}}/\sigma^{x}_{L_{\gamma}}$ and $\sigma^{x}_{L_{\beta}}/\sigma^{x}_{L_{\gamma}}$ ratios for proton impact on W.

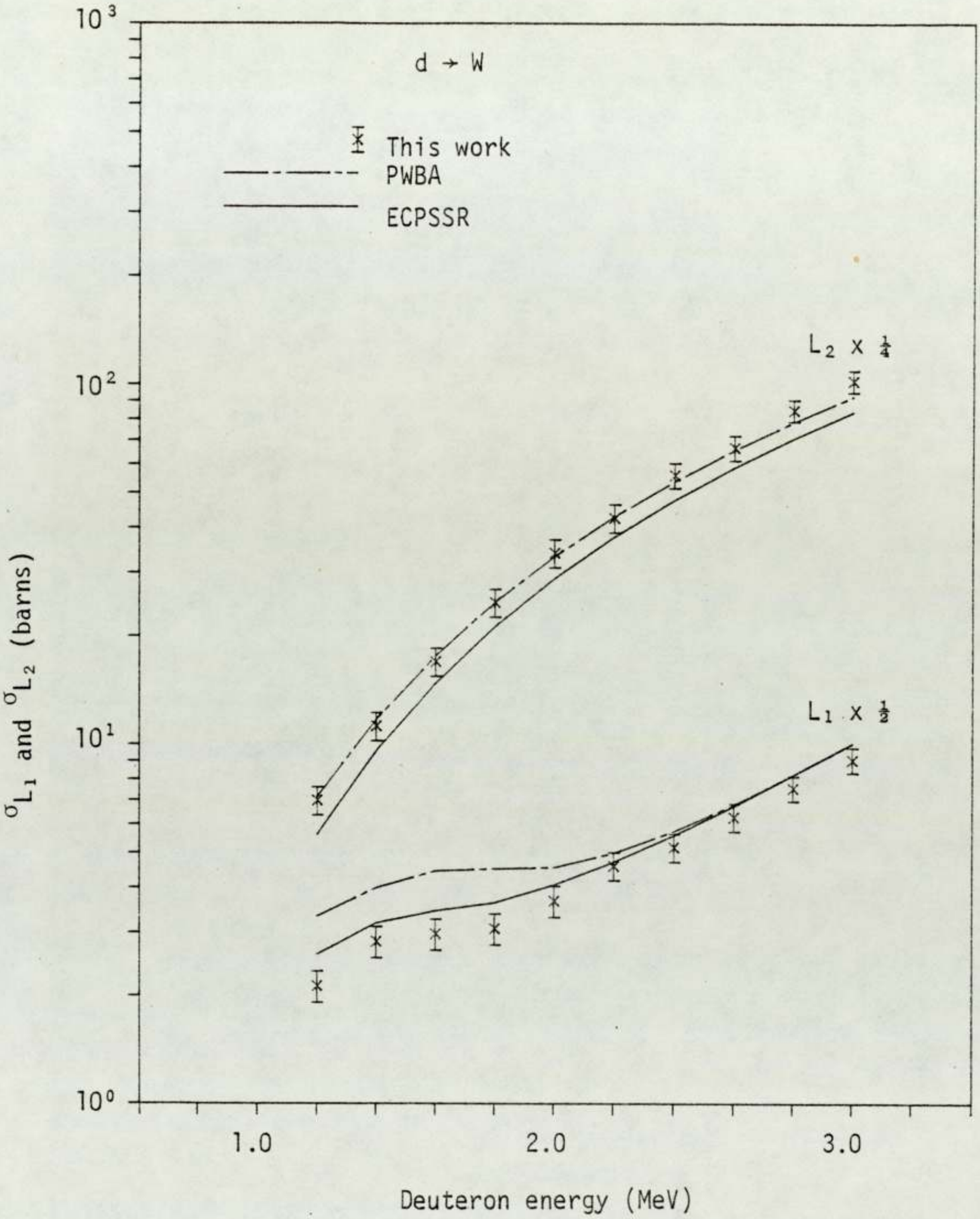

Figure 6.63. Experimental L_1 and L_2 subshell ionisation cross sections for deuteron impact on W.

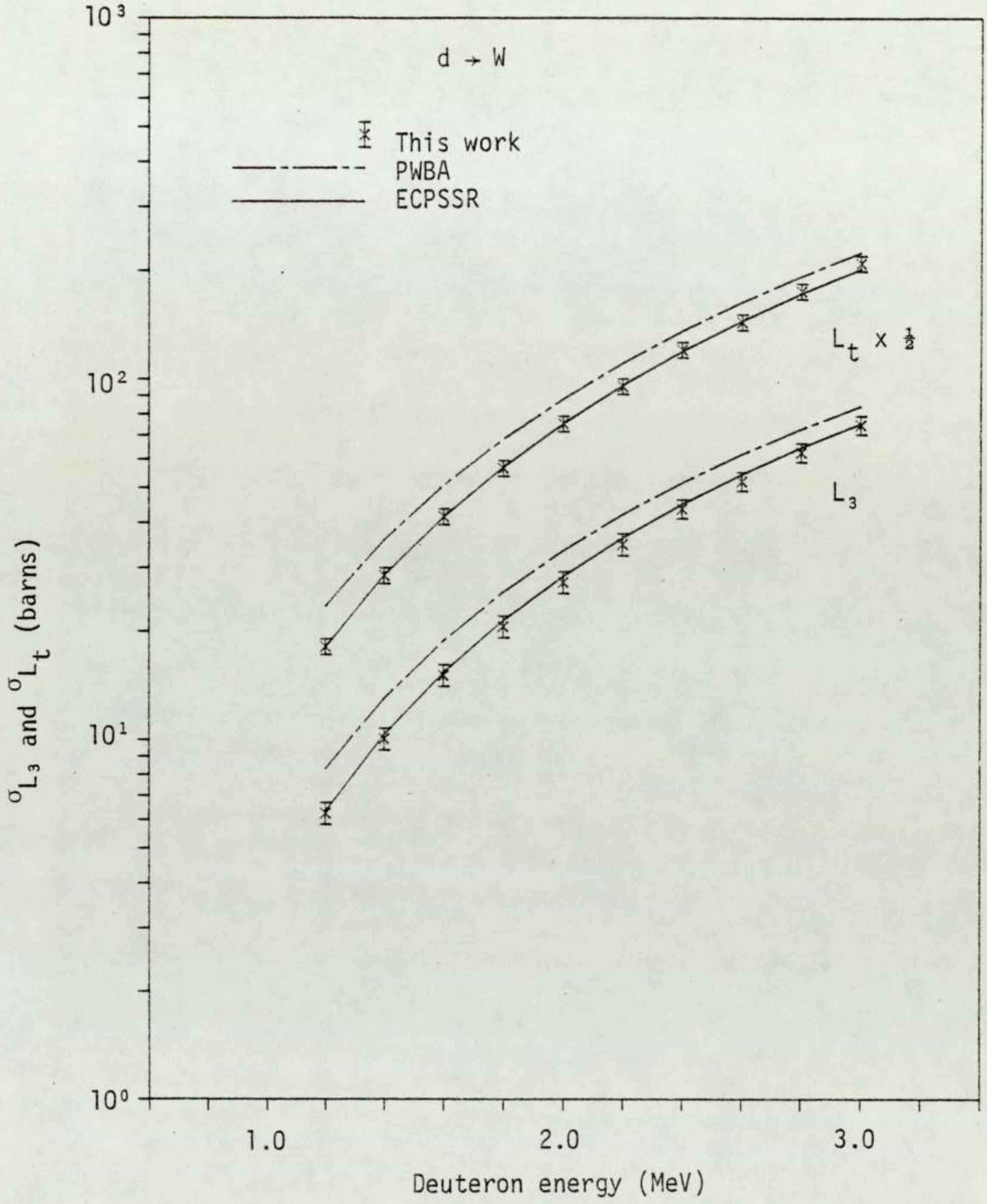

Figure 6.64. Experimental L_3 subshell and total L shell ionisation cross sections for deuteron impact on W.

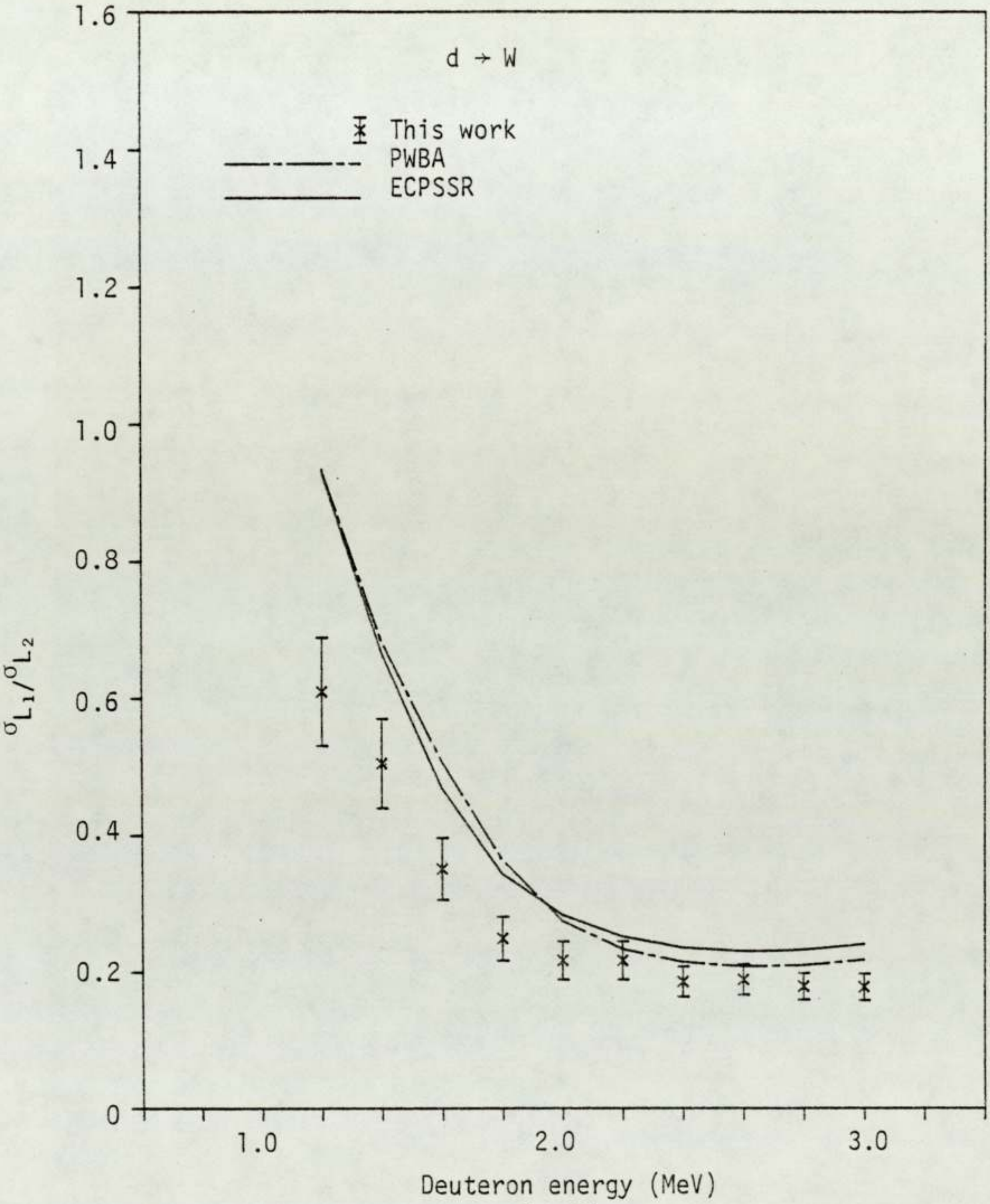

Figure 6.65. Experimental $\sigma_{L_1}/\sigma_{L_2}$ ratio for deuteron impact on W.

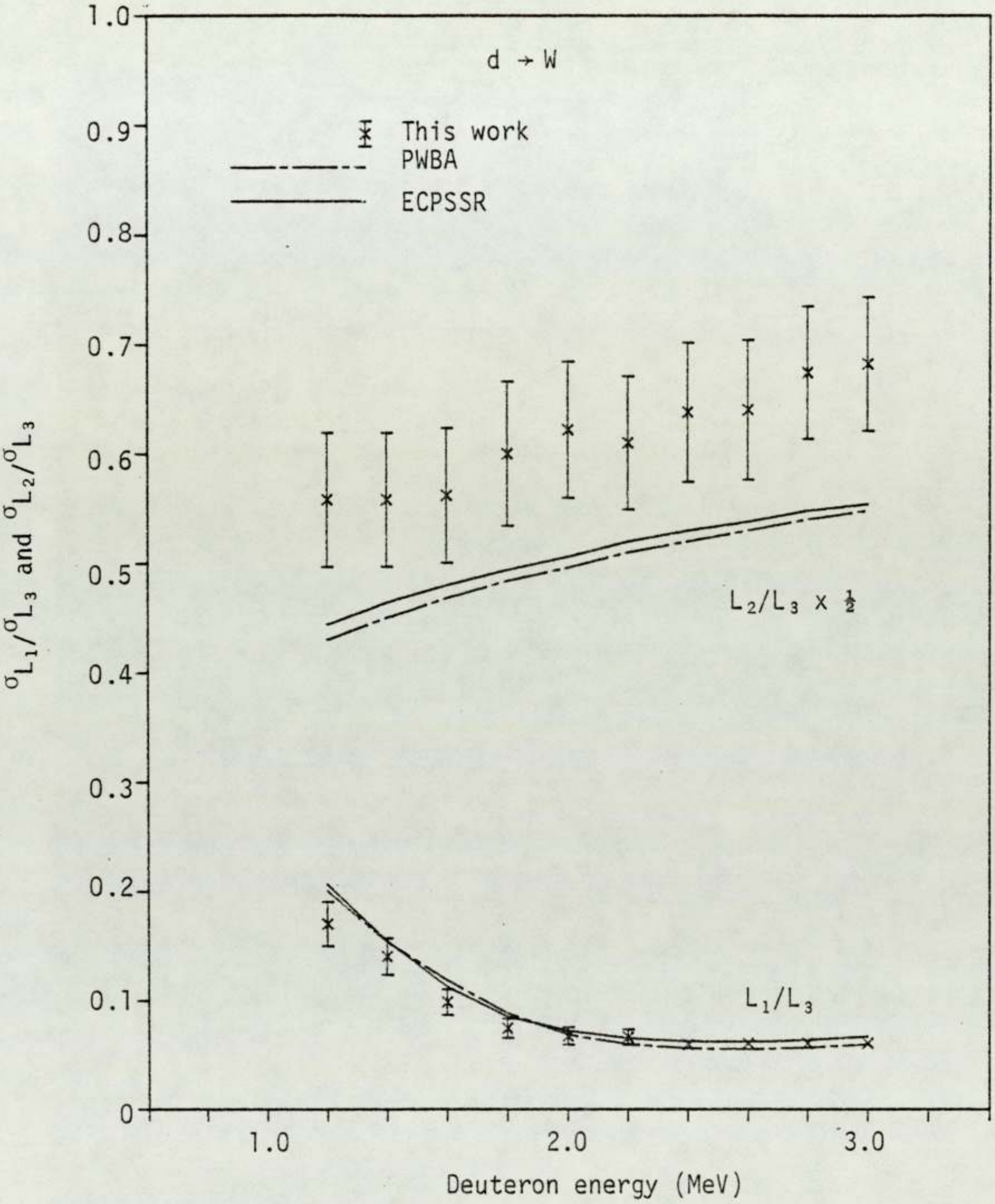

Figure 6.66. Experimental $\sigma_{L_1}/\sigma_{L_3}$ and $\sigma_{L_2}/\sigma_{L_3}$ ratios for deuteron impact on W.

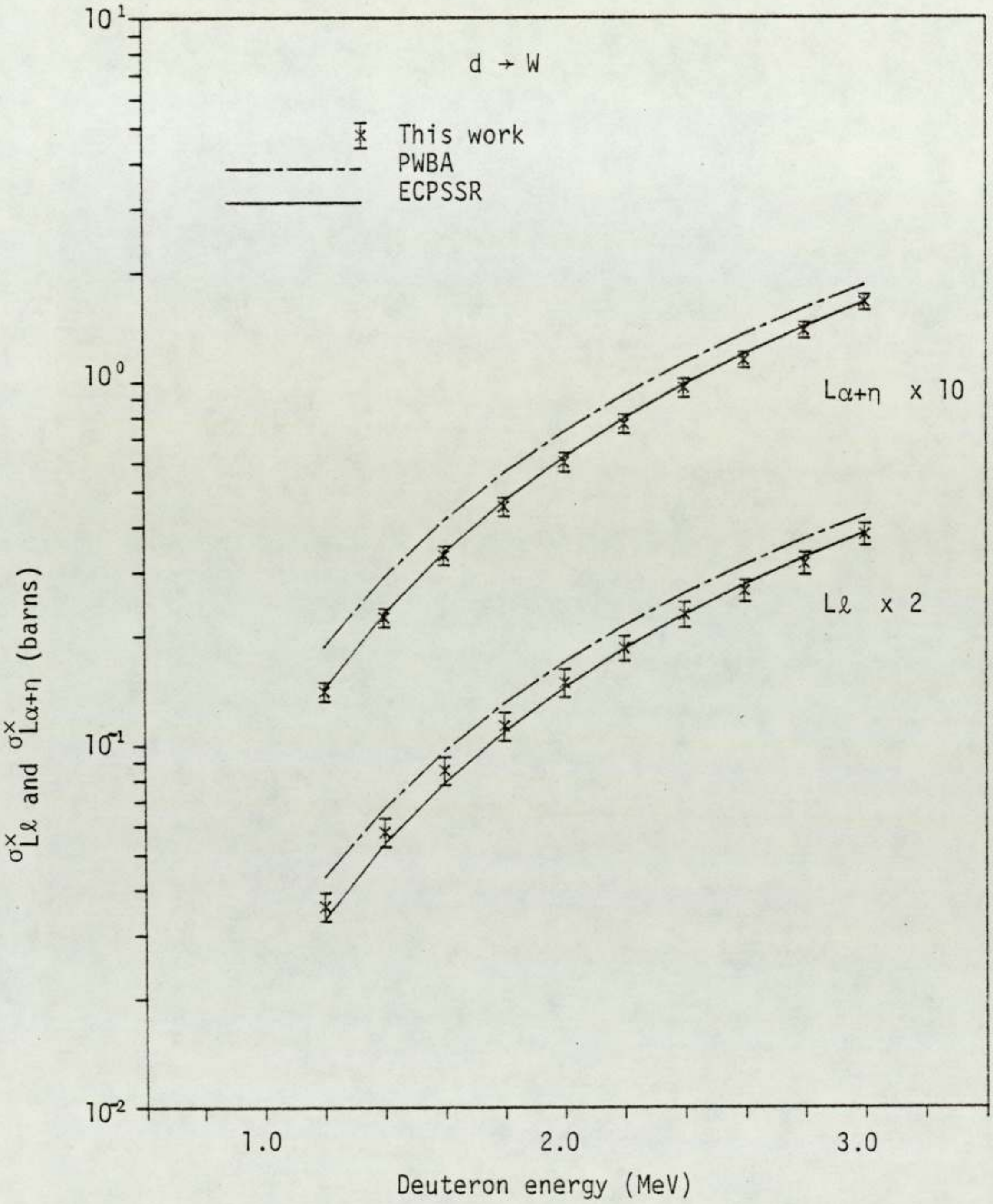

Figure 6.67. Experimental $L\ell$ and $L\alpha+\eta$ x-ray production cross sections for deuteron impact on W.

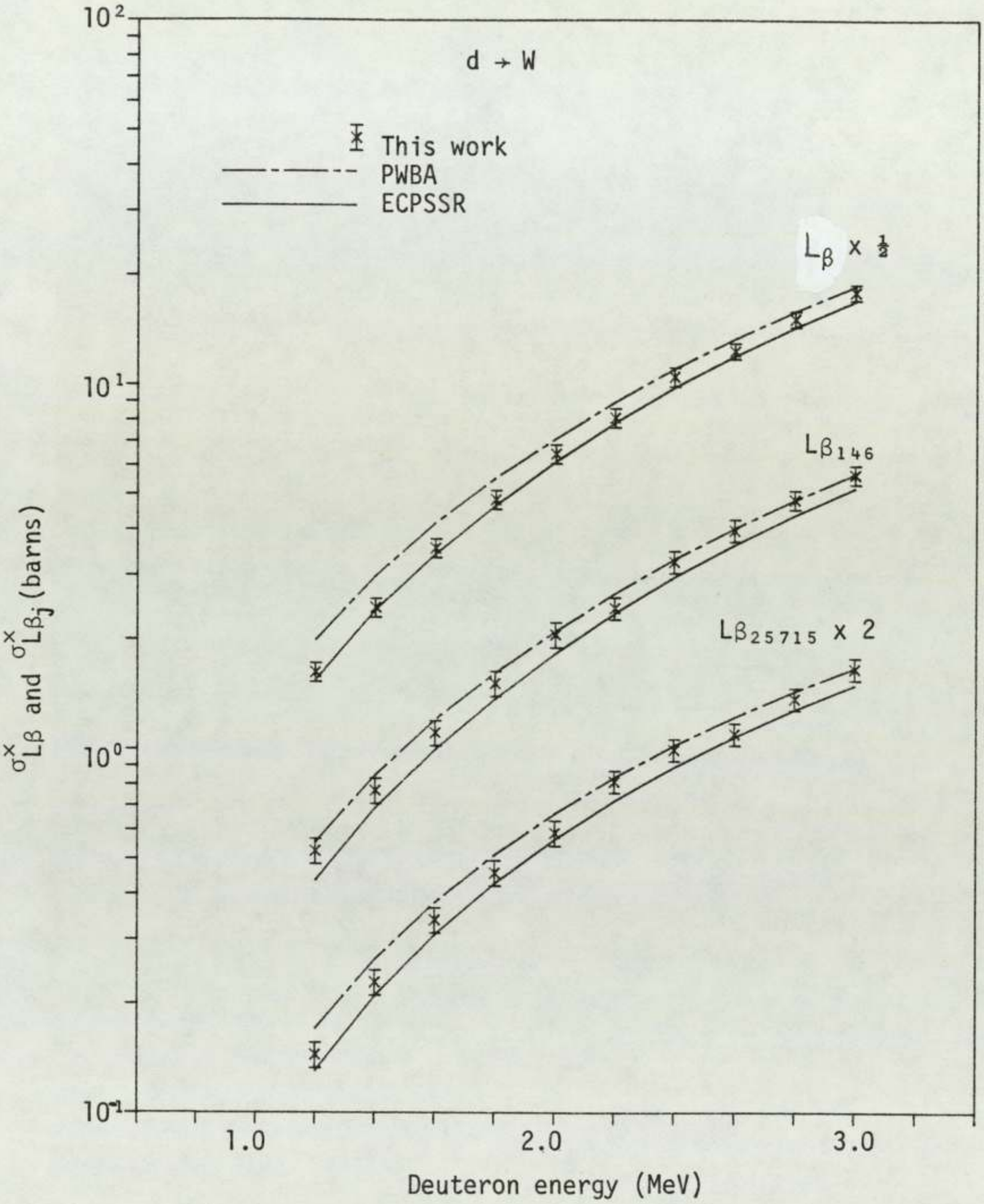

Figure 6.68. Experimental total $L\beta$ and partial $L\beta_j$ x-ray production cross sections for deuteron impact on W.

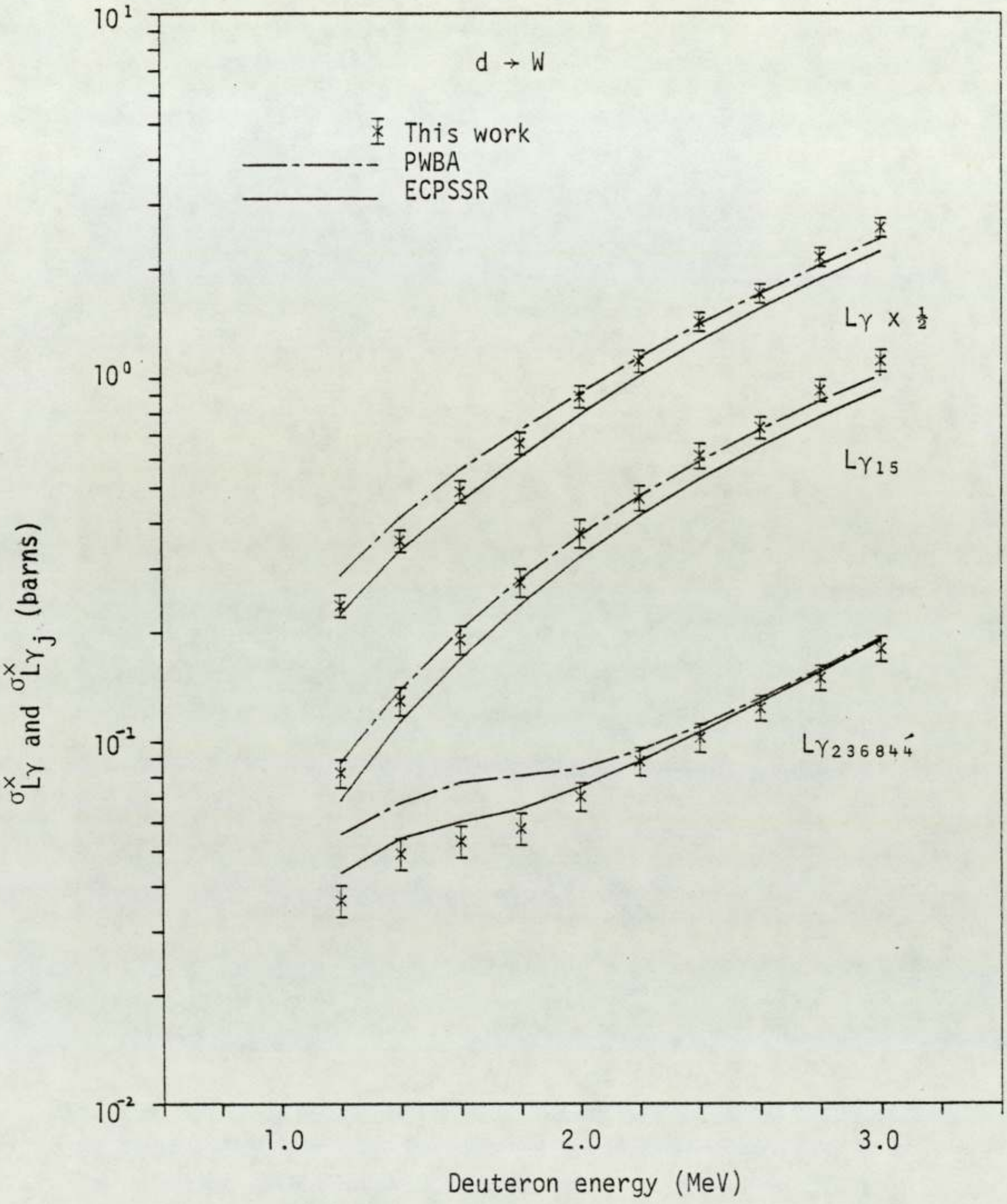

Figure 6.69. Experimental total Lγ and partial $L\gamma_j$ x-ray production cross sections for deuteron impact on W.

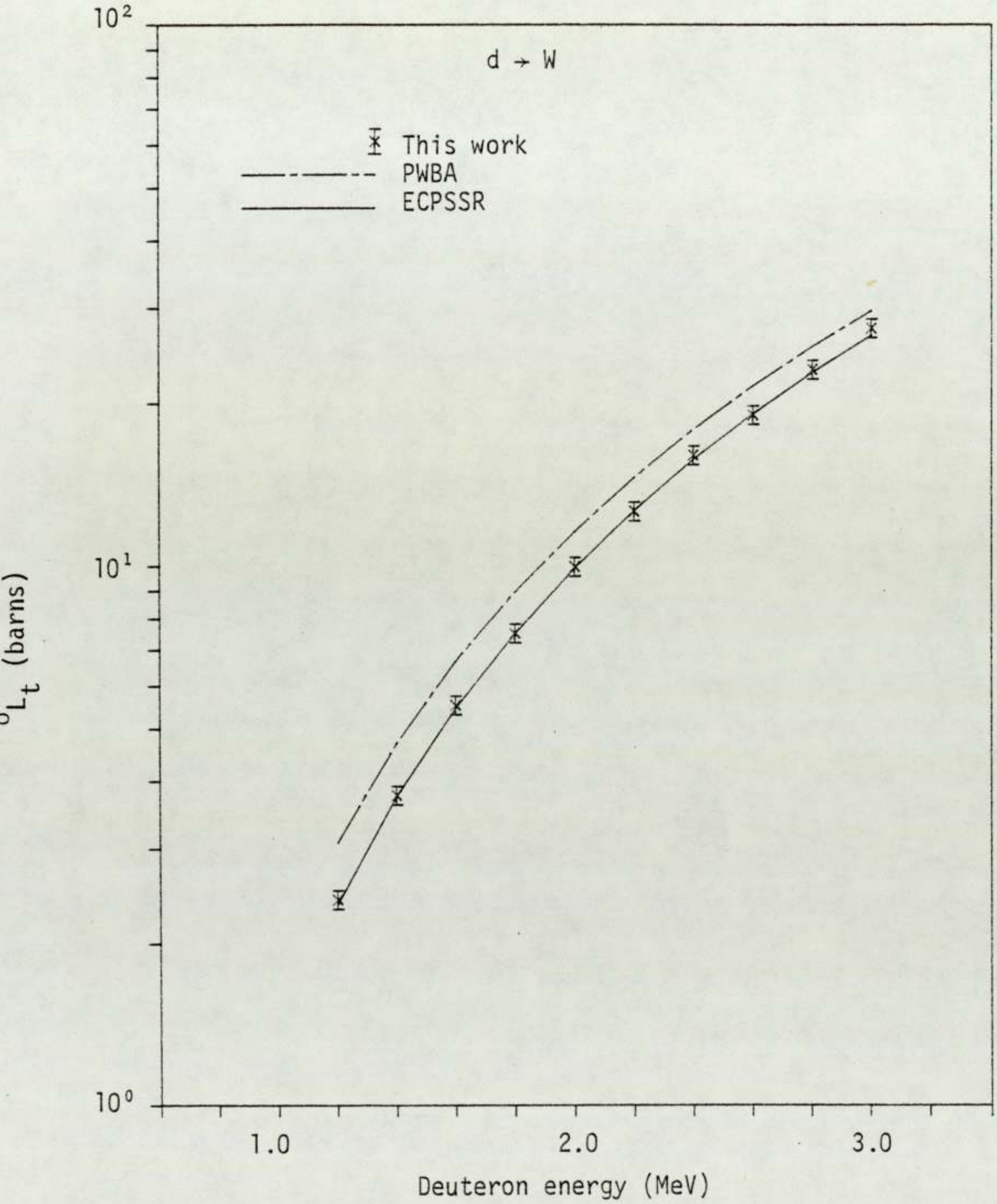

Figure 6.70. Experimental total L shell x-ray production cross section for deuteron impact on W.

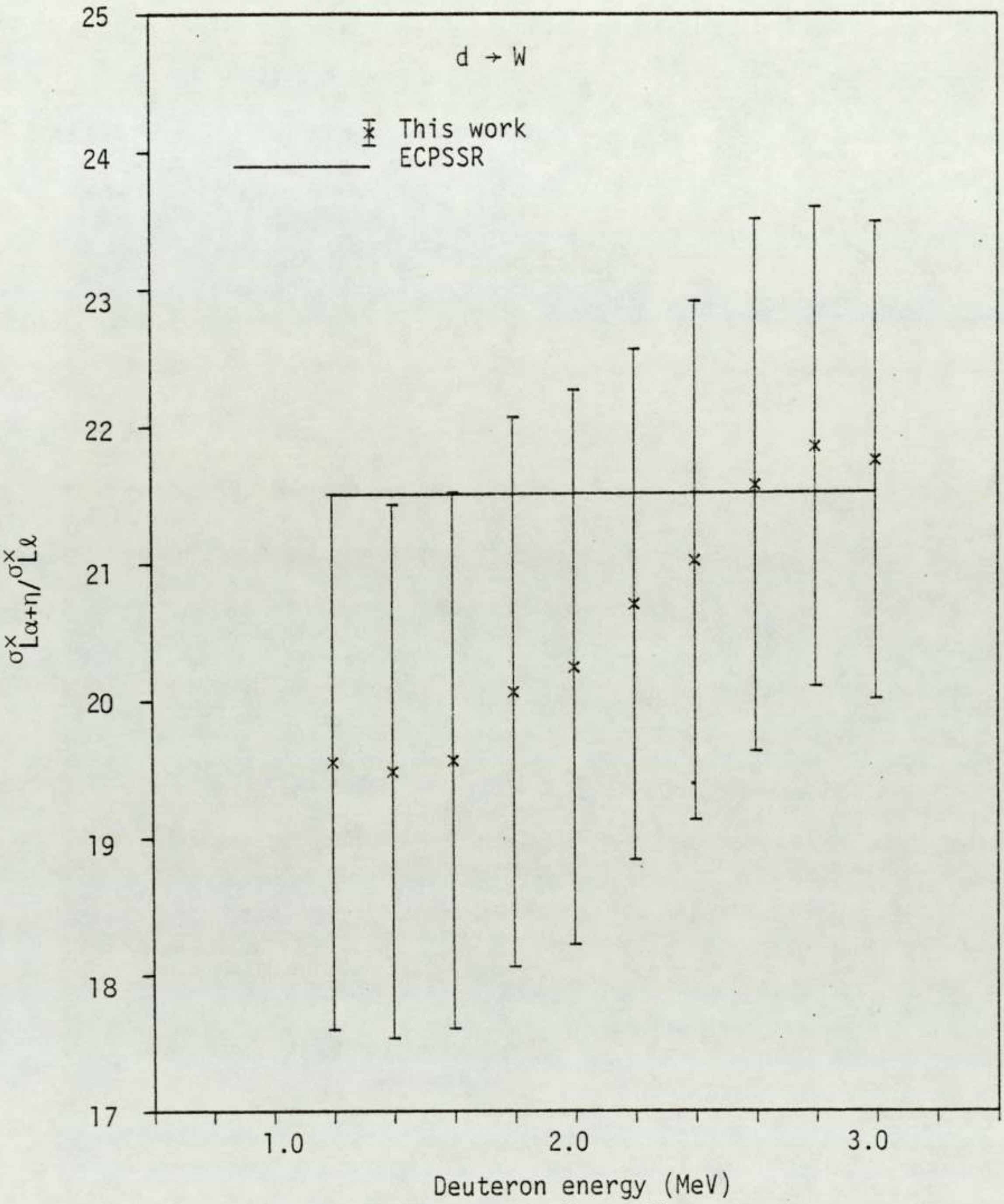

Figure 6.71. Experimental $\sigma^x_{L\alpha+\eta}/\sigma^x_{L\ell}$ ratio for deuteron impact on W.

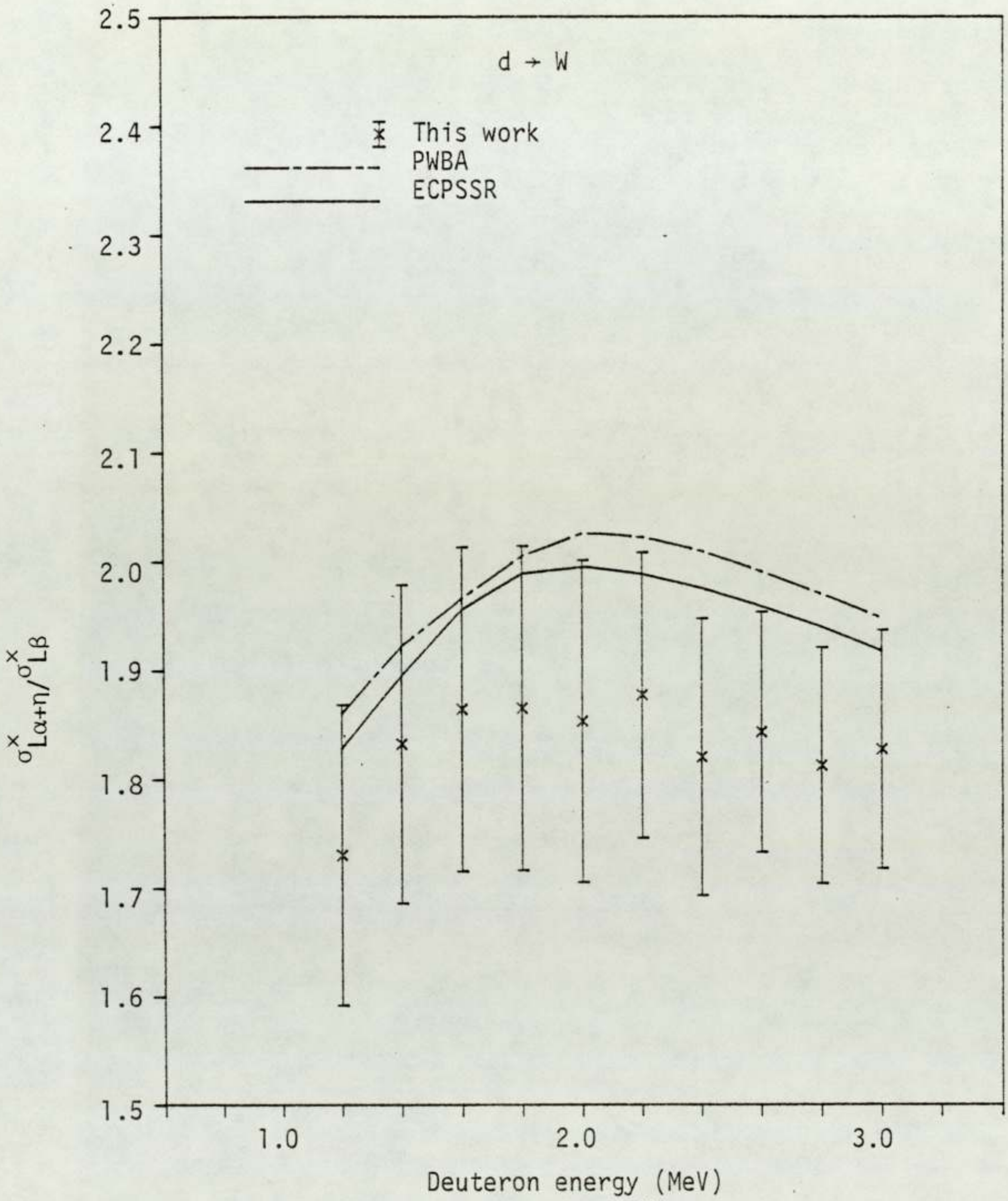

Figure 6.72. Experimental $\sigma^{x}_{L\alpha+\eta}/\sigma^{x}_{L\beta}$ ratio for deuteron impact on W.

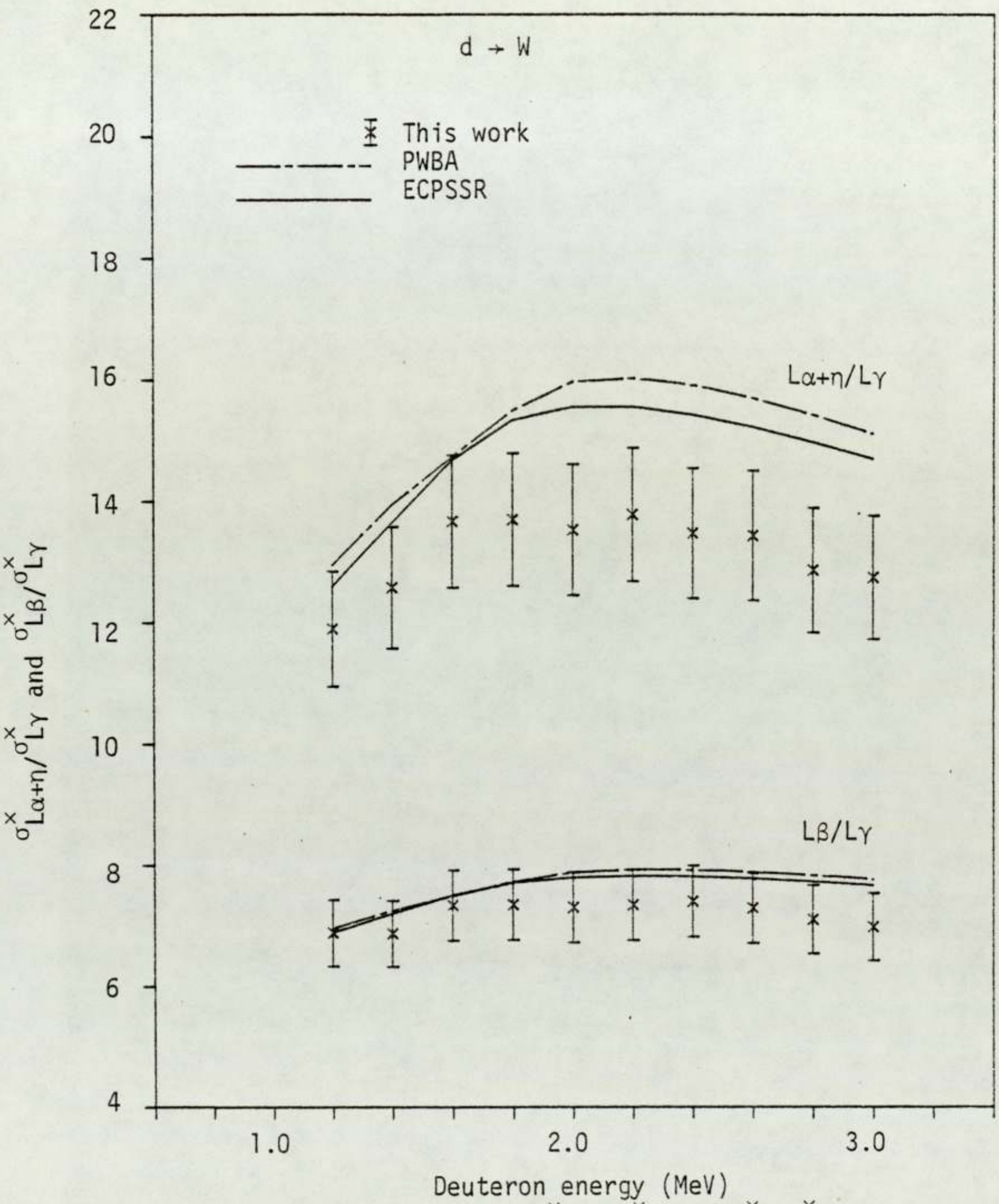

Figure 6.73. Experimental $\sigma^x_{L\alpha+\eta}/\sigma^x_{L\gamma}$ and $\sigma^x_{L\beta}/\sigma^x_{L\gamma}$ ratio for deuteron impact on W.

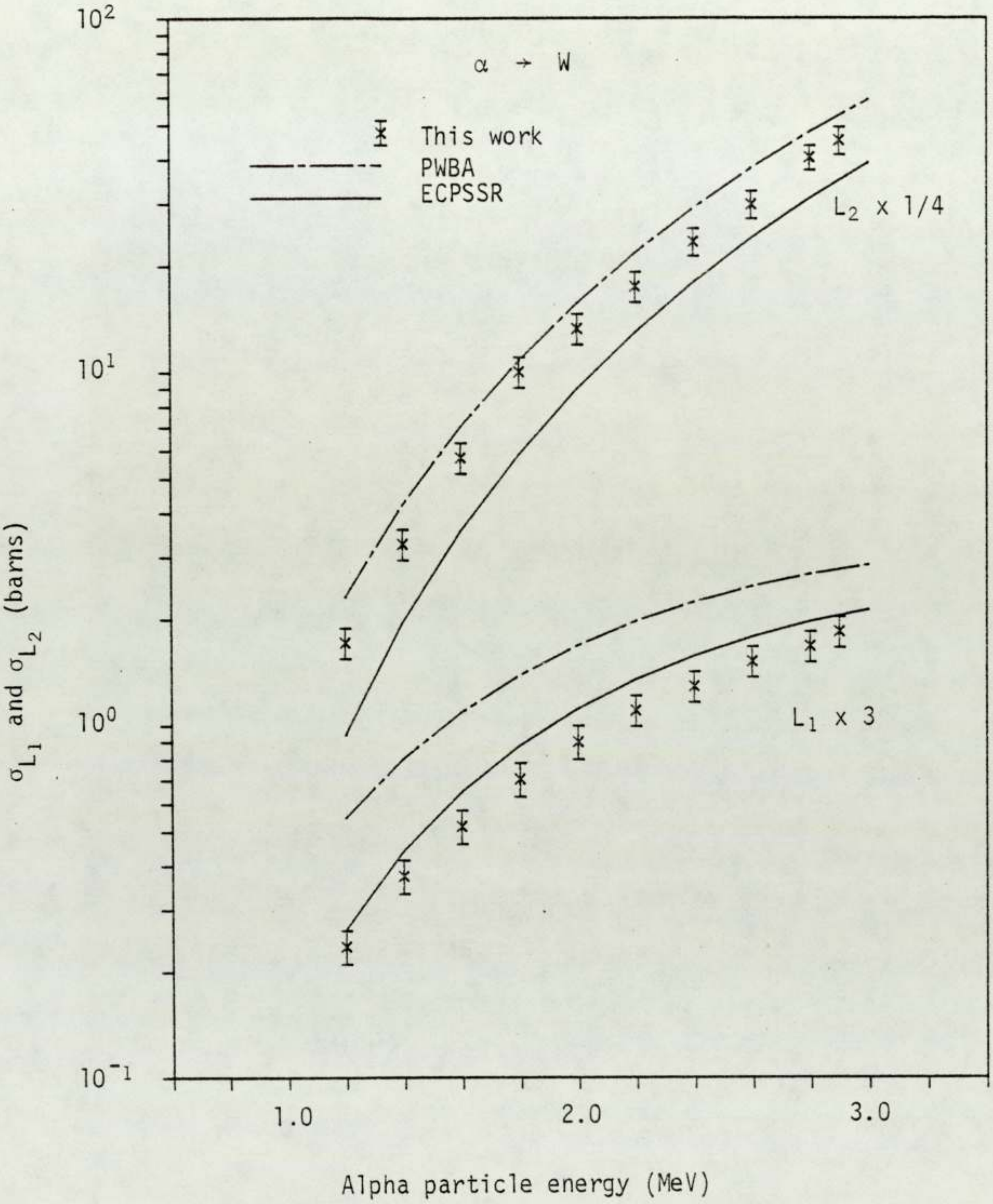

Figure 6.74. Experimental L_1 and L_2 subshell ionisation cross sections for alpha particle impact on W.

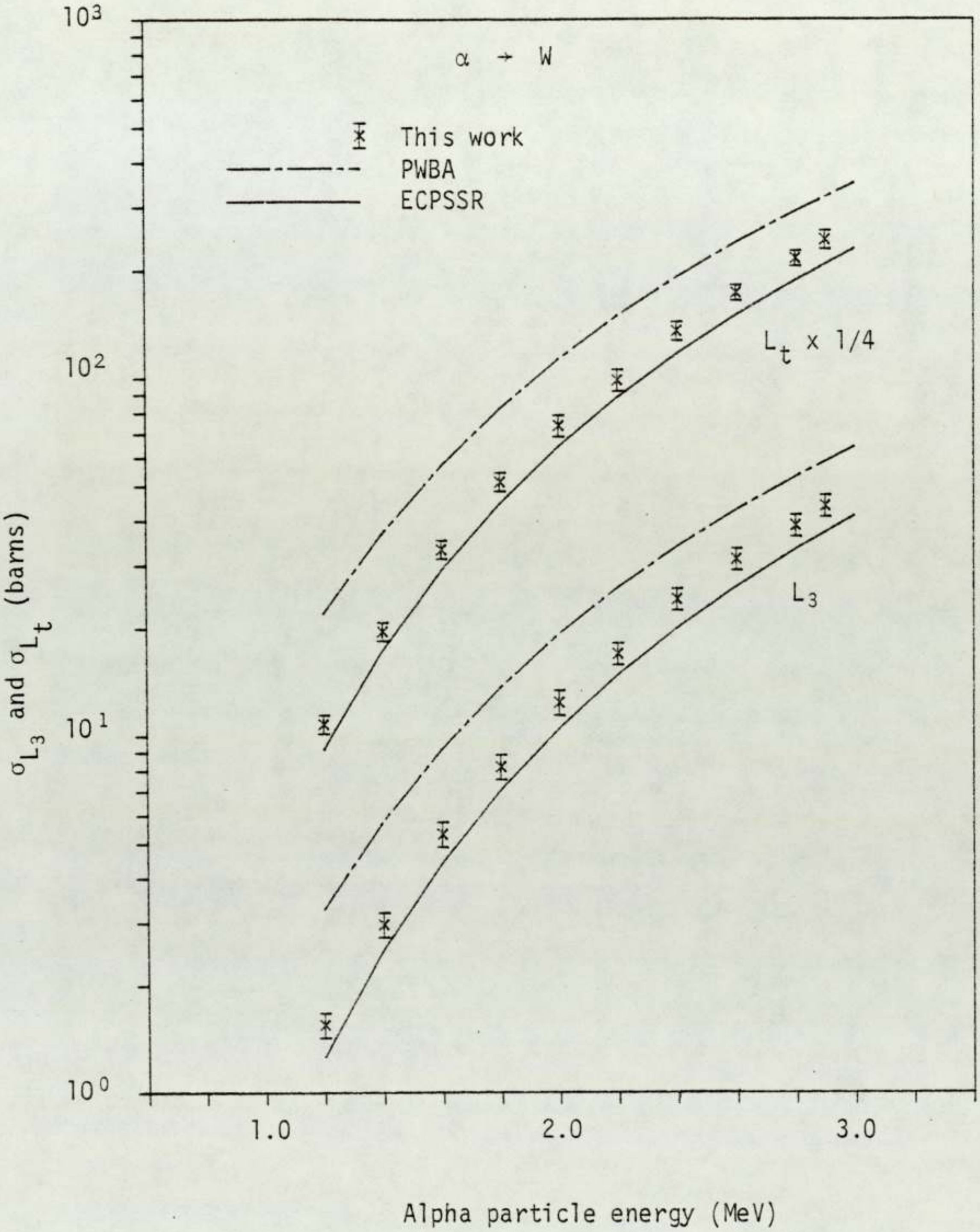

Figure 6.75. Experimental L_3 subshell and total L shell ionisation cross sections for alpha particle impact on W.

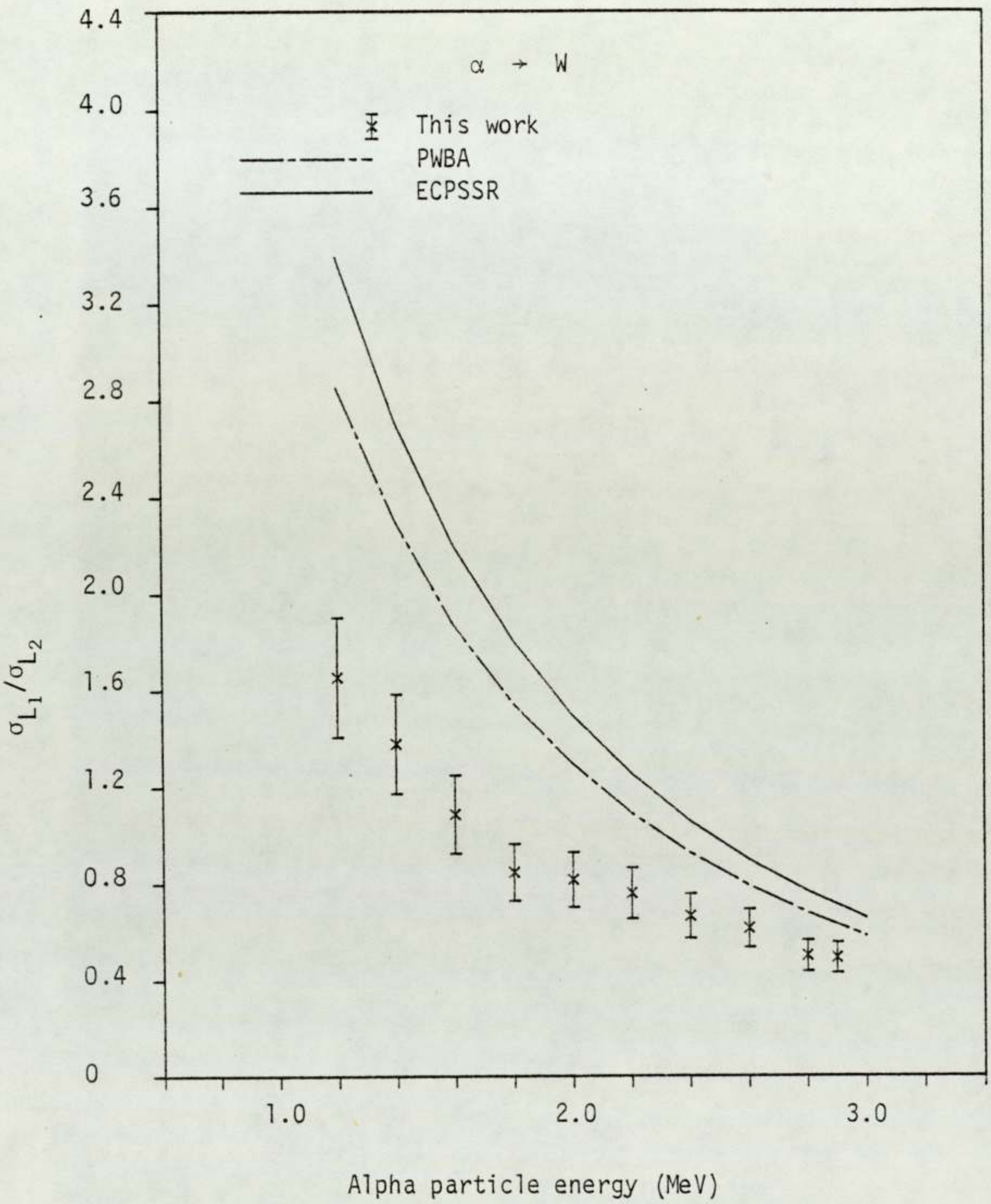

Figure 6.76. Experimental $\sigma_{L_1}/\sigma_{L_2}$ ratio for alpha particle impact on W.

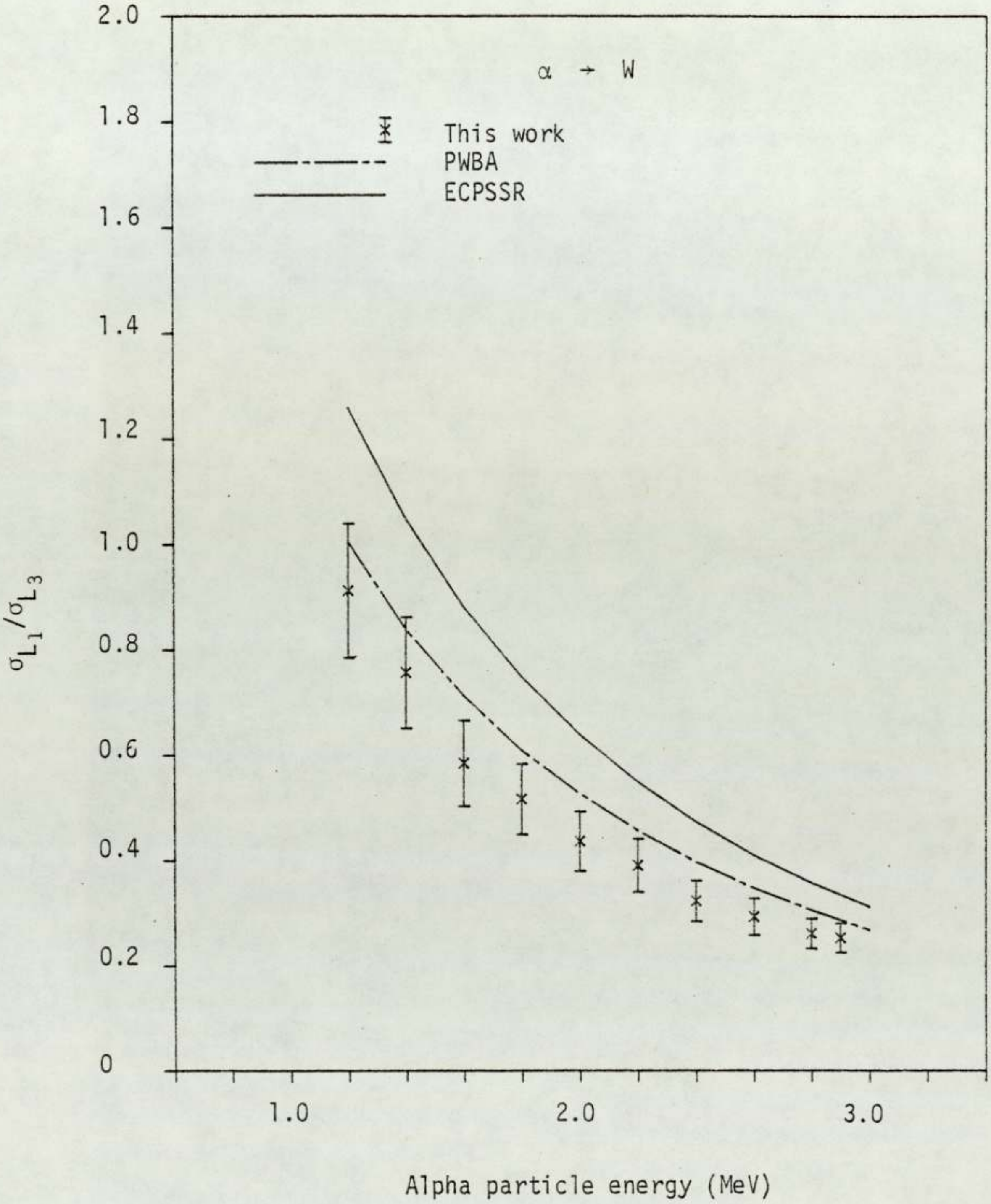

Figure 6.77. Experimental $\sigma_{L_1}/\sigma_{L_3}$ ratio for alpha particle impact on W.

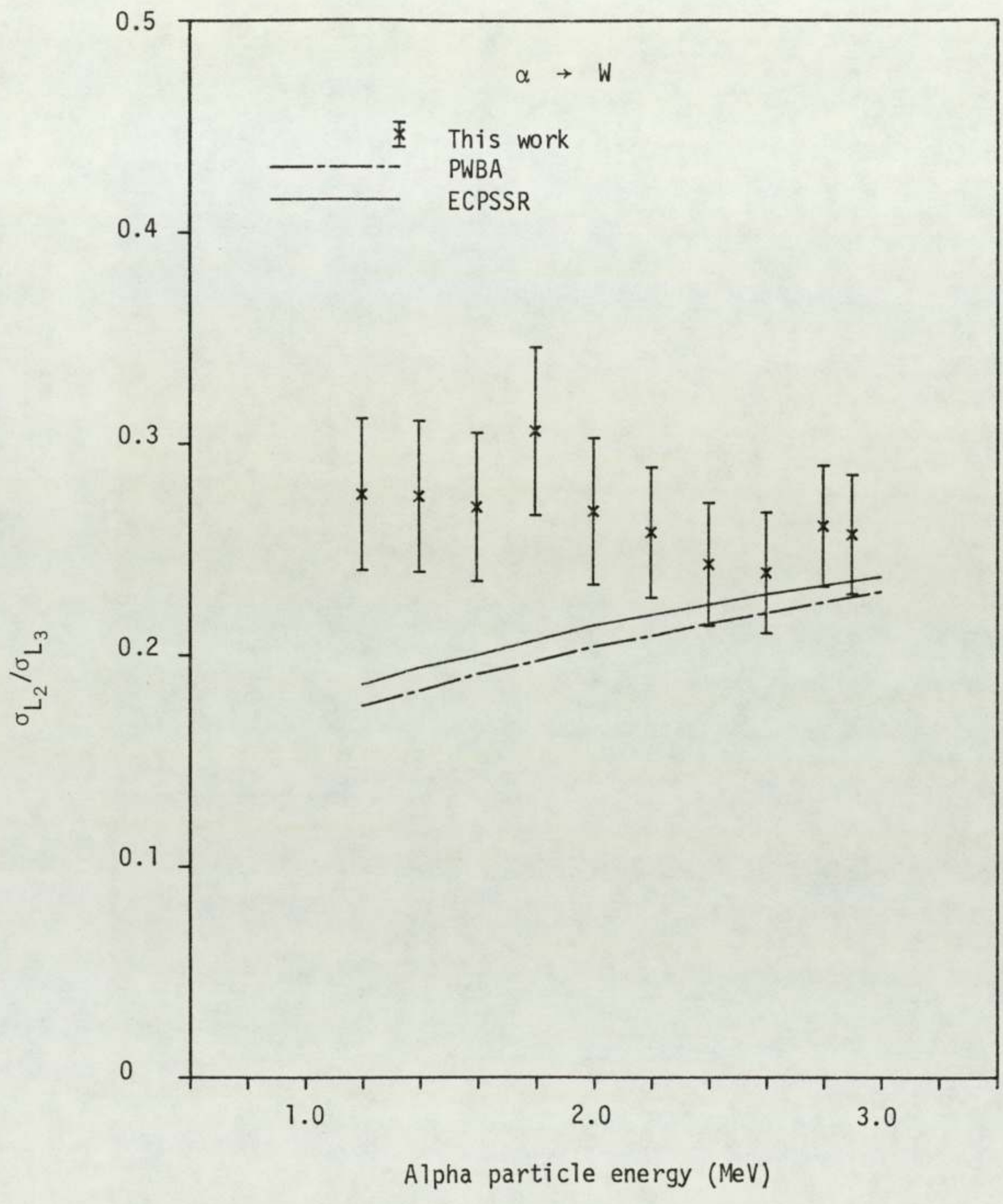

Figure 6.78. Experimental $\sigma_{L_2}/\sigma_{L_3}$ ratio for alpha particle impact on W.

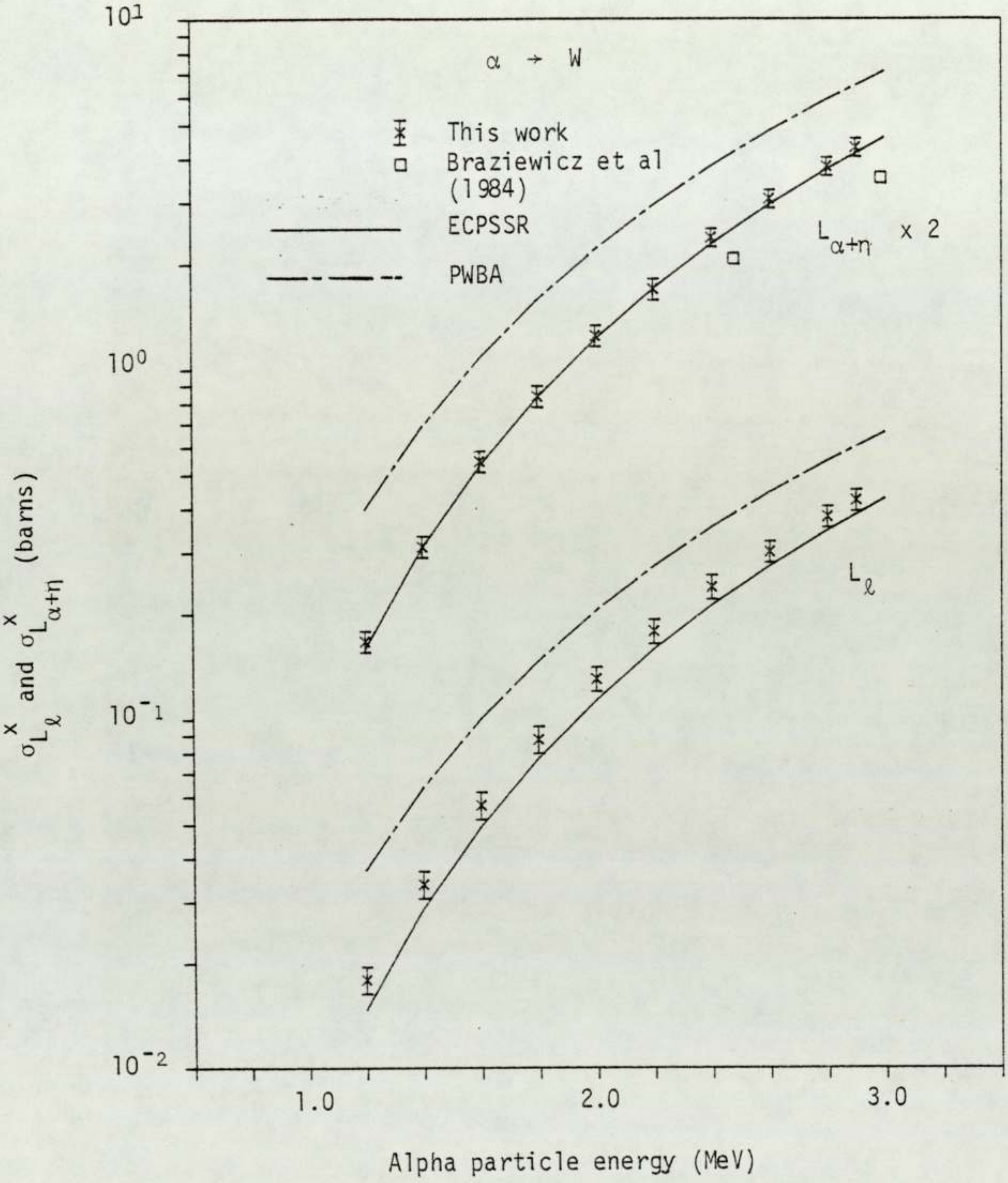

Figure 6.79. Experimental L_ℓ and $L_{\alpha+\eta}$ x-ray production ratios for alpha particle impact on W.

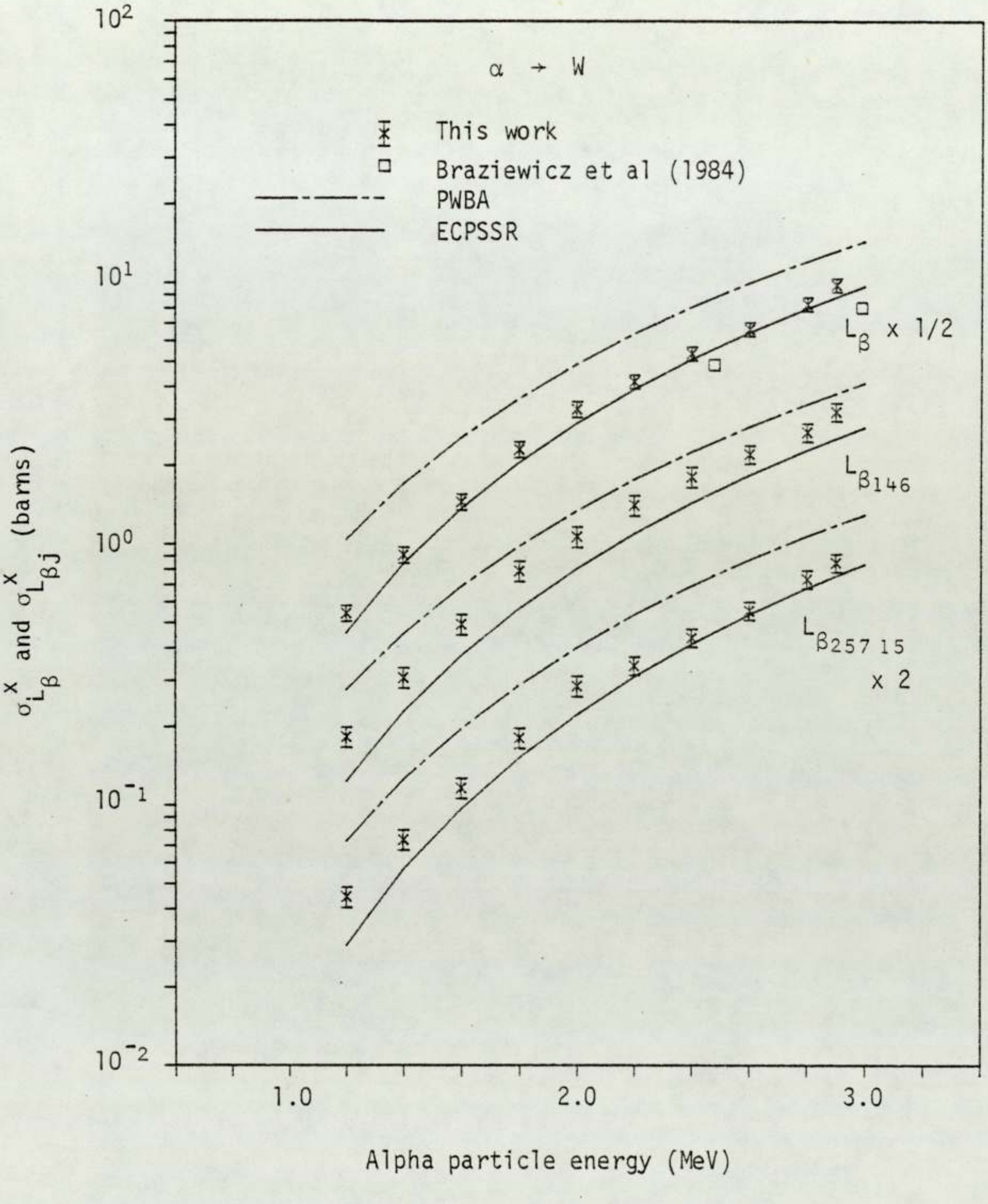

Figure 6.80. Experimental total L_β and partial L_{β_j} x-ray production cross sections for alpha particle impact on W.

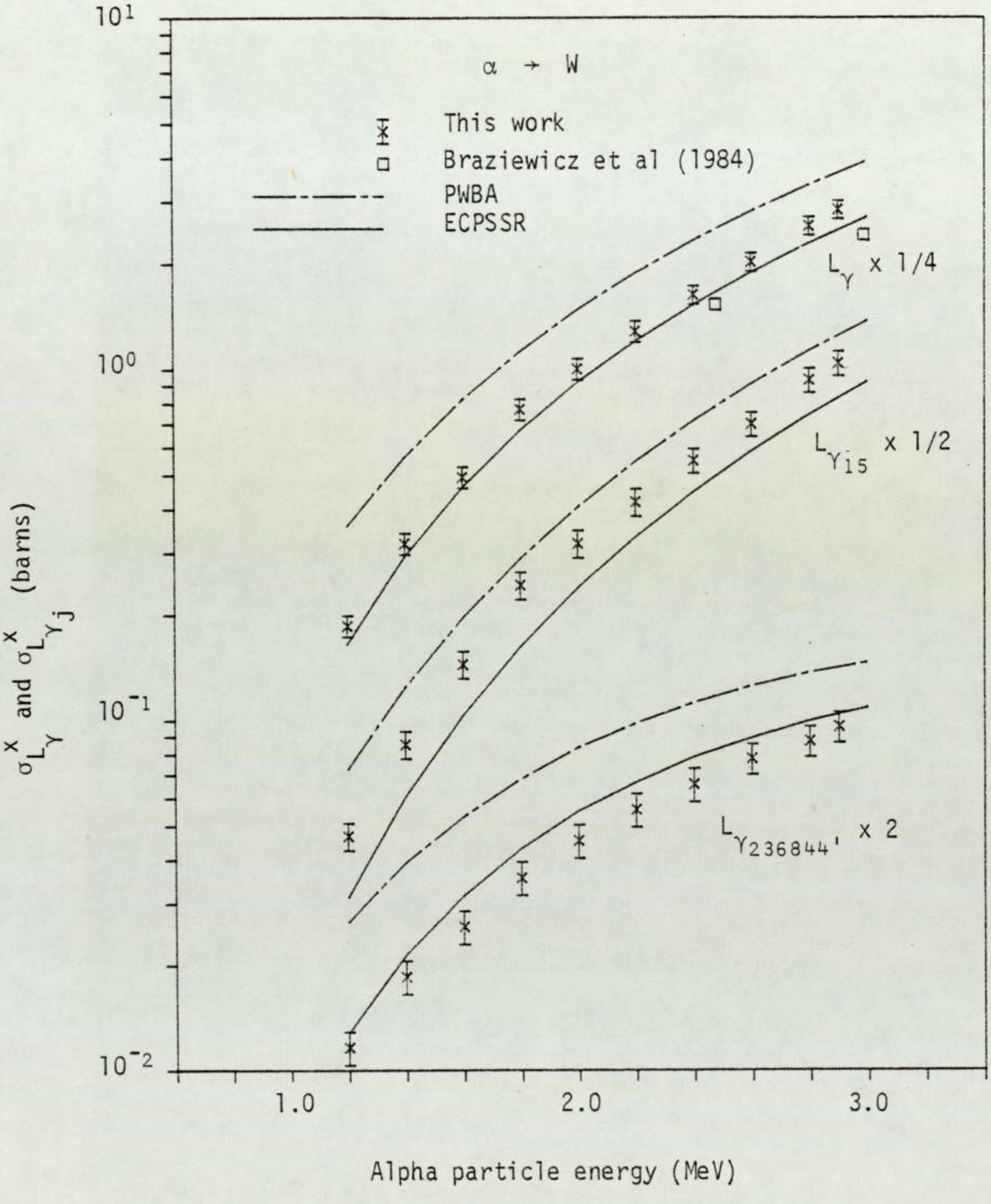

Figure 6.81. Experimental total L_γ and partial L_{γ_j} x-ray production cross sections for alpha particle impact on W.

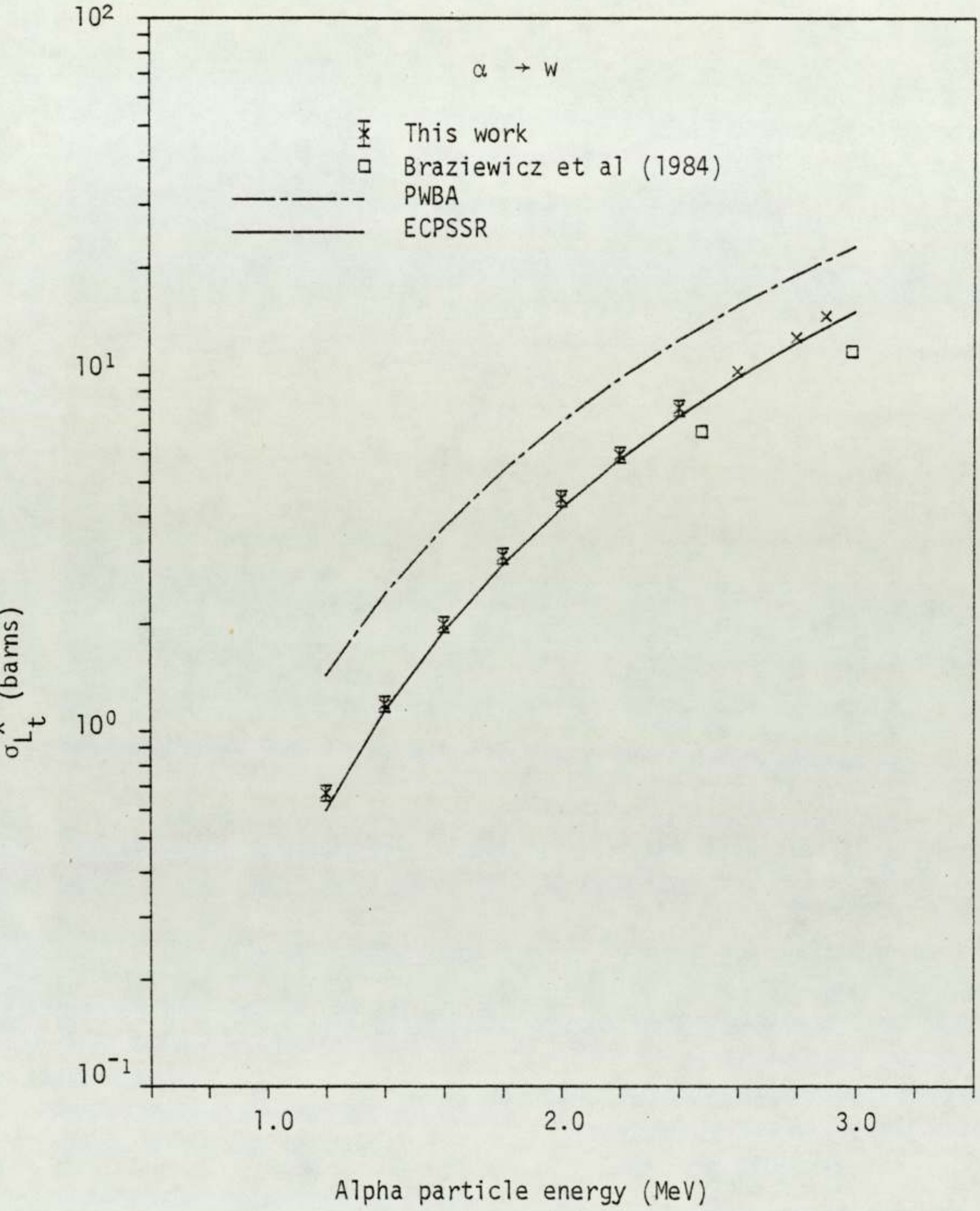

Figure 6.82. Experimental total L shell x-ray production cross section for alpha particle impact on W.

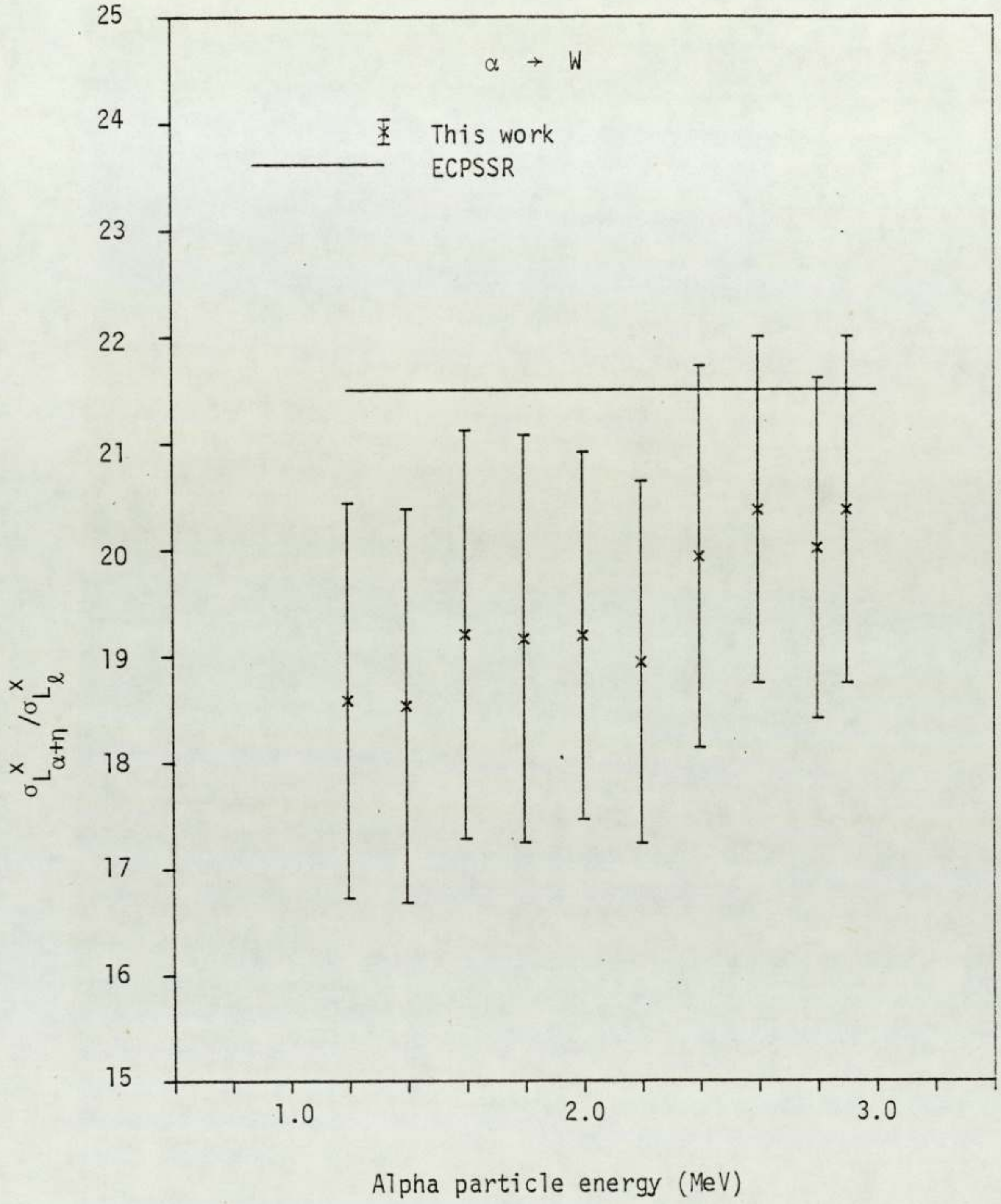

Figure 6.83. Experimental $\sigma_{L_{\alpha+\eta}}^{x}/\sigma_{L_{\ell}}^{x}$ ratio for alpha particle impact on W.

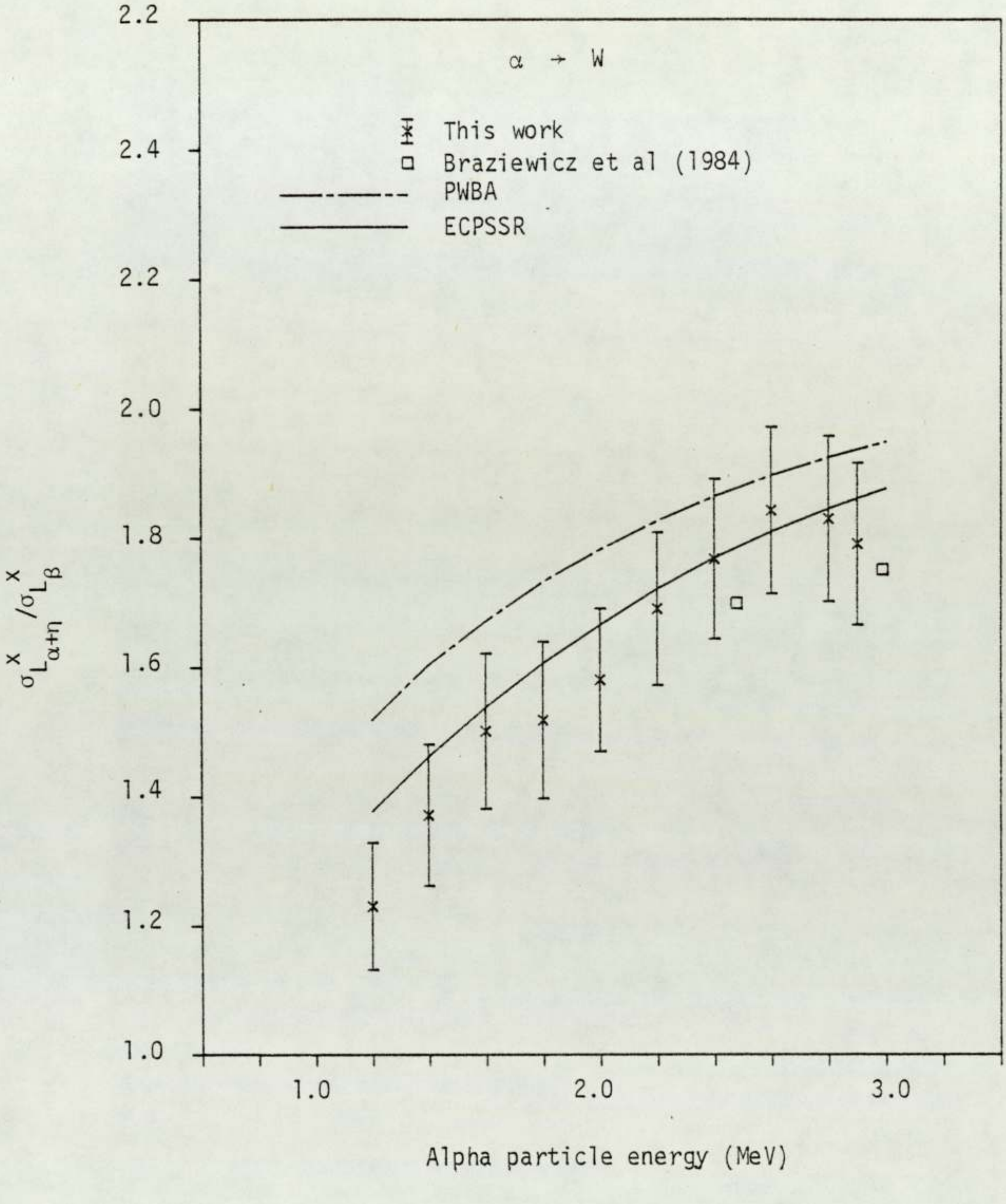

Figure 6.84. Experimental $\sigma^{x}_{L_{\alpha+\eta}}/\sigma^{x}_{L_{\beta}}$ ratio for alpha particle impact on W.

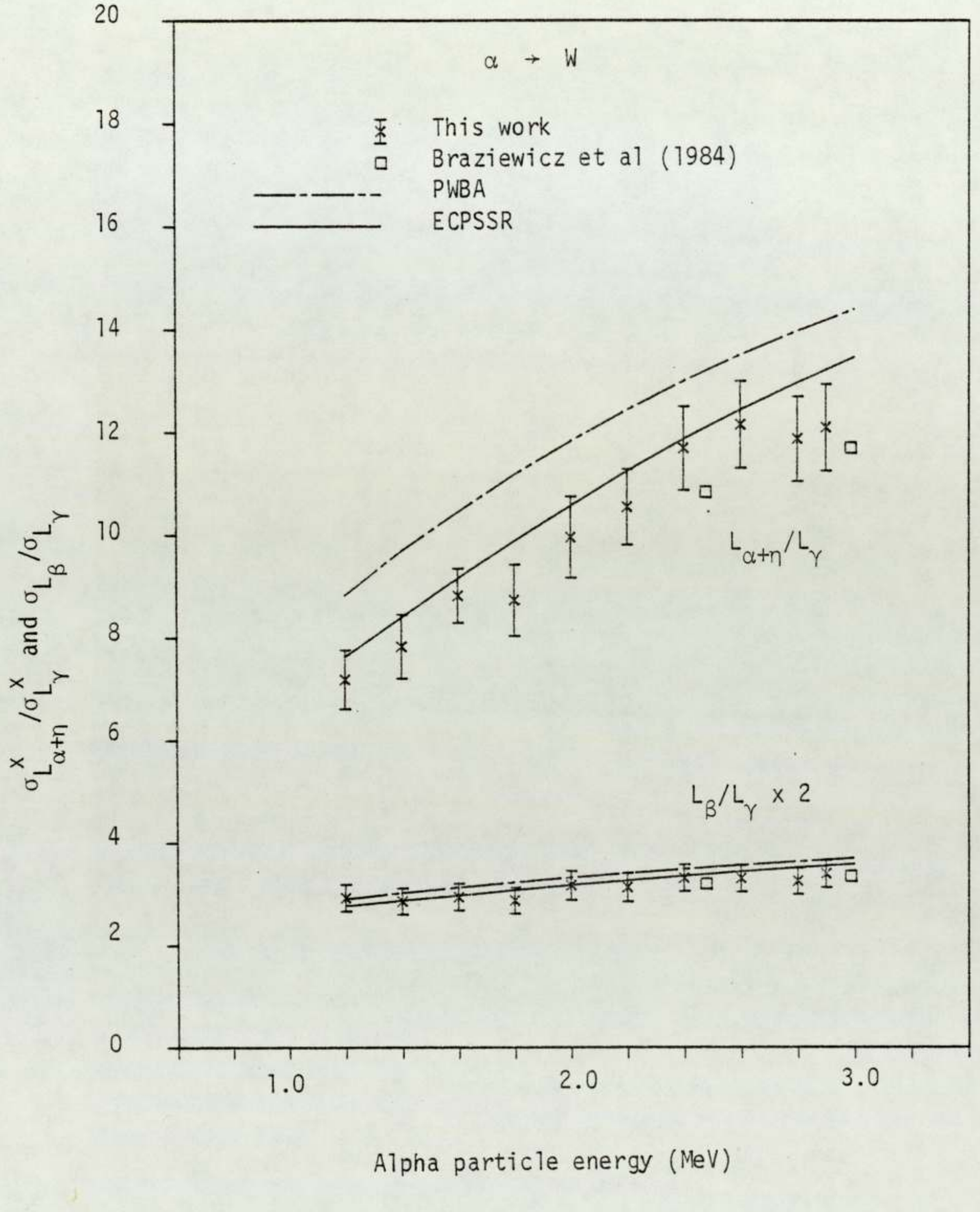

Figure 6.85. Experimental $\sigma^X_{L_{\alpha+\eta}}/\sigma^X_{L_\gamma}$ and $\sigma^X_{L_\beta}/\sigma^X_{L_\gamma}$ ratios for alpha particle impact on W.

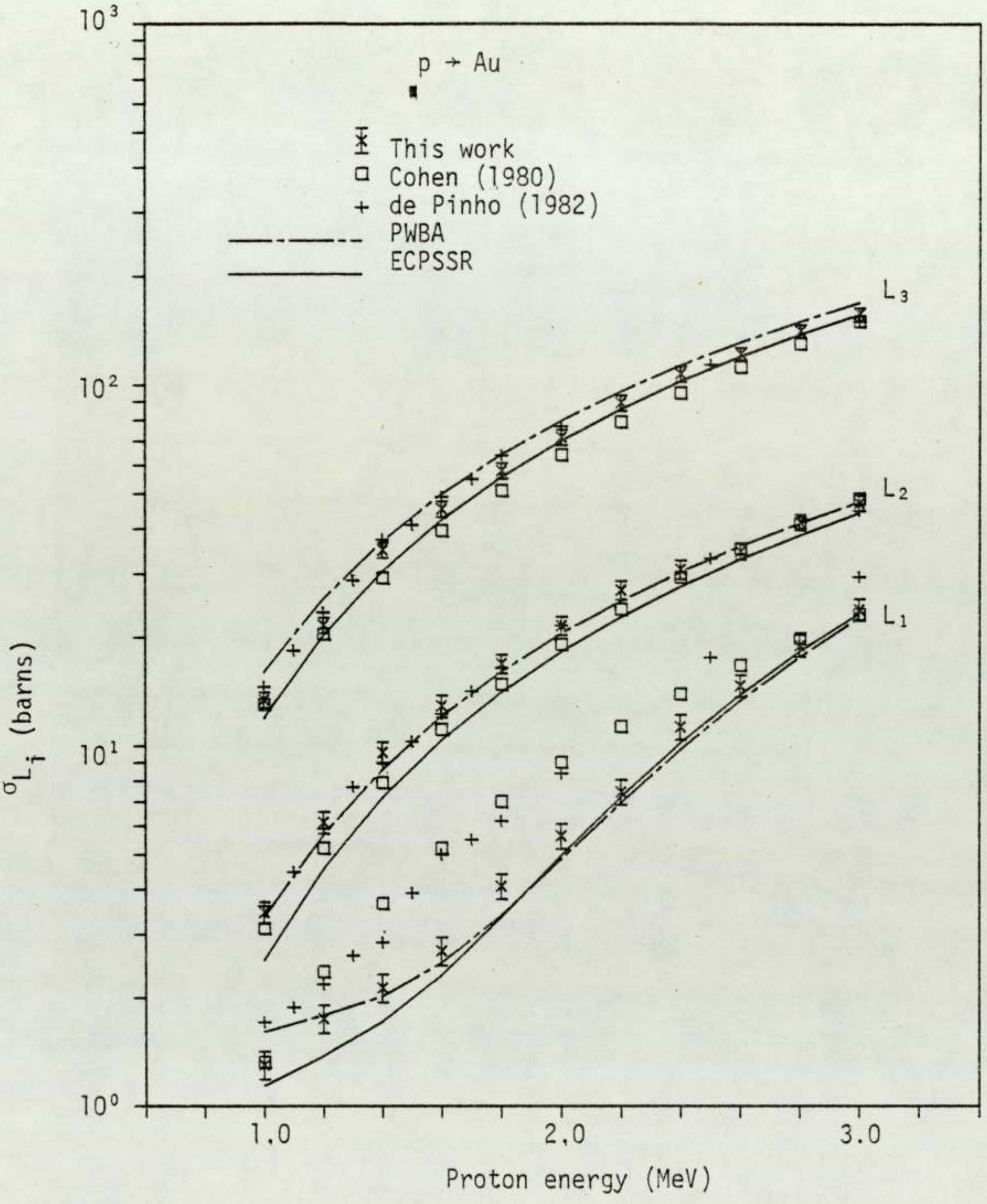

Figure 6.86. Experimental L_i subshell ionisation cross sections for proton impact on Au.

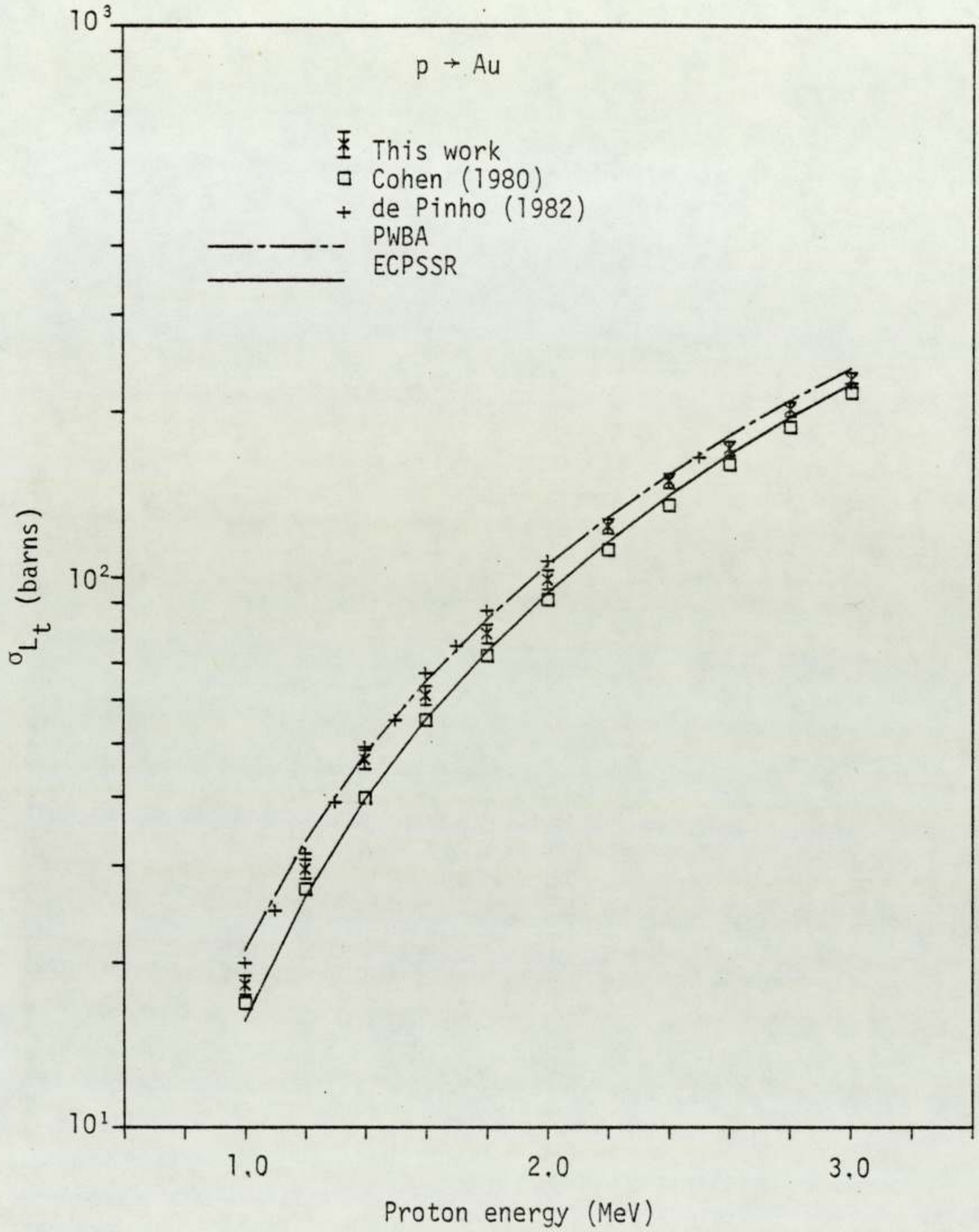

Figure 6.87. Experimental total L shell ionisation cross sections for proton impact on Au.

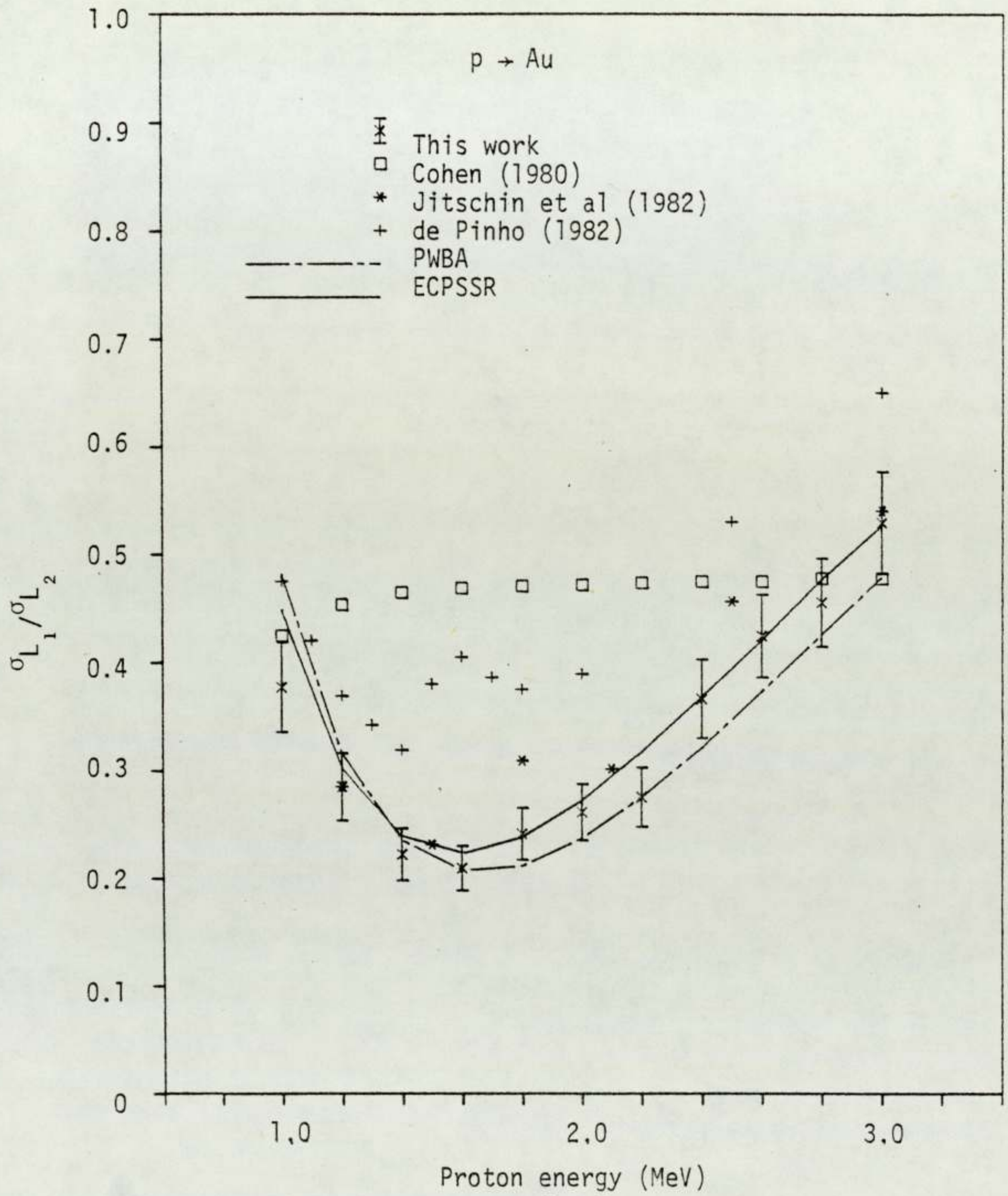

Figure 6.88. Experimental $\sigma_{L_1}/\sigma_{L_2}$ ratio for proton impact on Au.

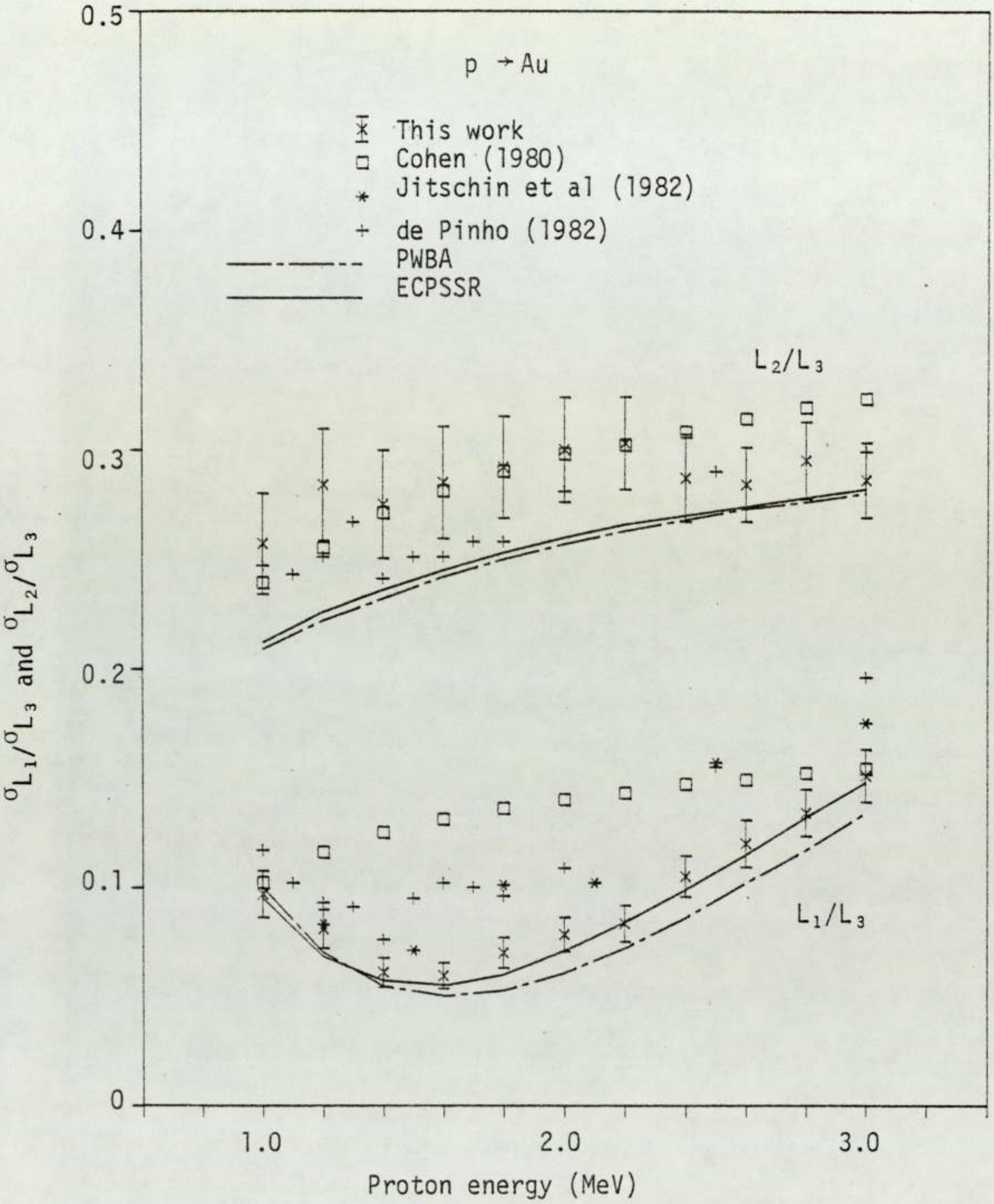

Figure 6.89. Experimental $\sigma_{L_1}/\sigma_{L_3}$ and $\sigma_{L_2}/\sigma_{L_3}$ ratios for proton impact on Au.

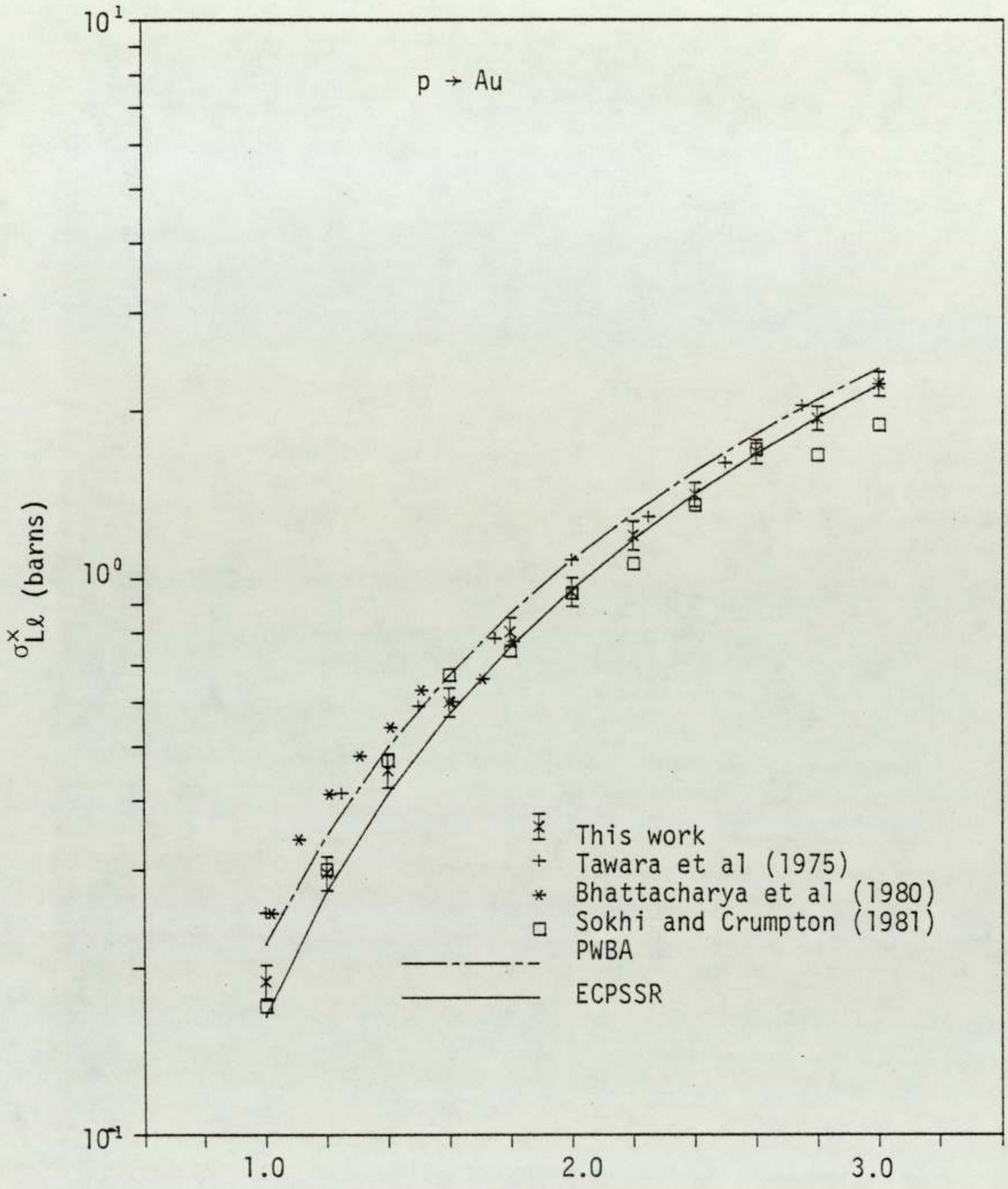

Figure 6.90. Experimental Lℓ x-ray production cross section for proton impact on Au.

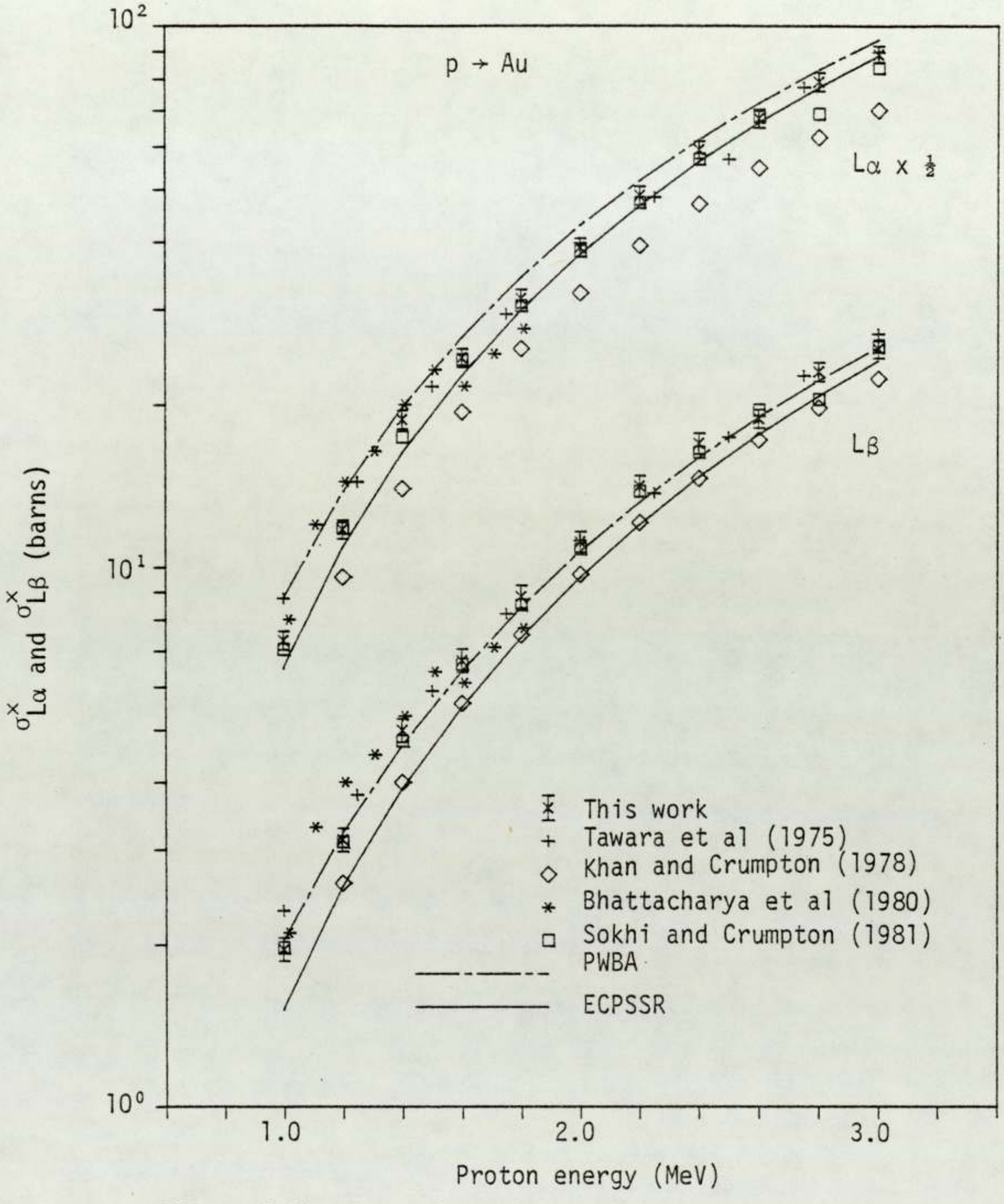

Figure 6.91. Experimental Lα and Lβ x-ray production cross sections for proton impact on Au.

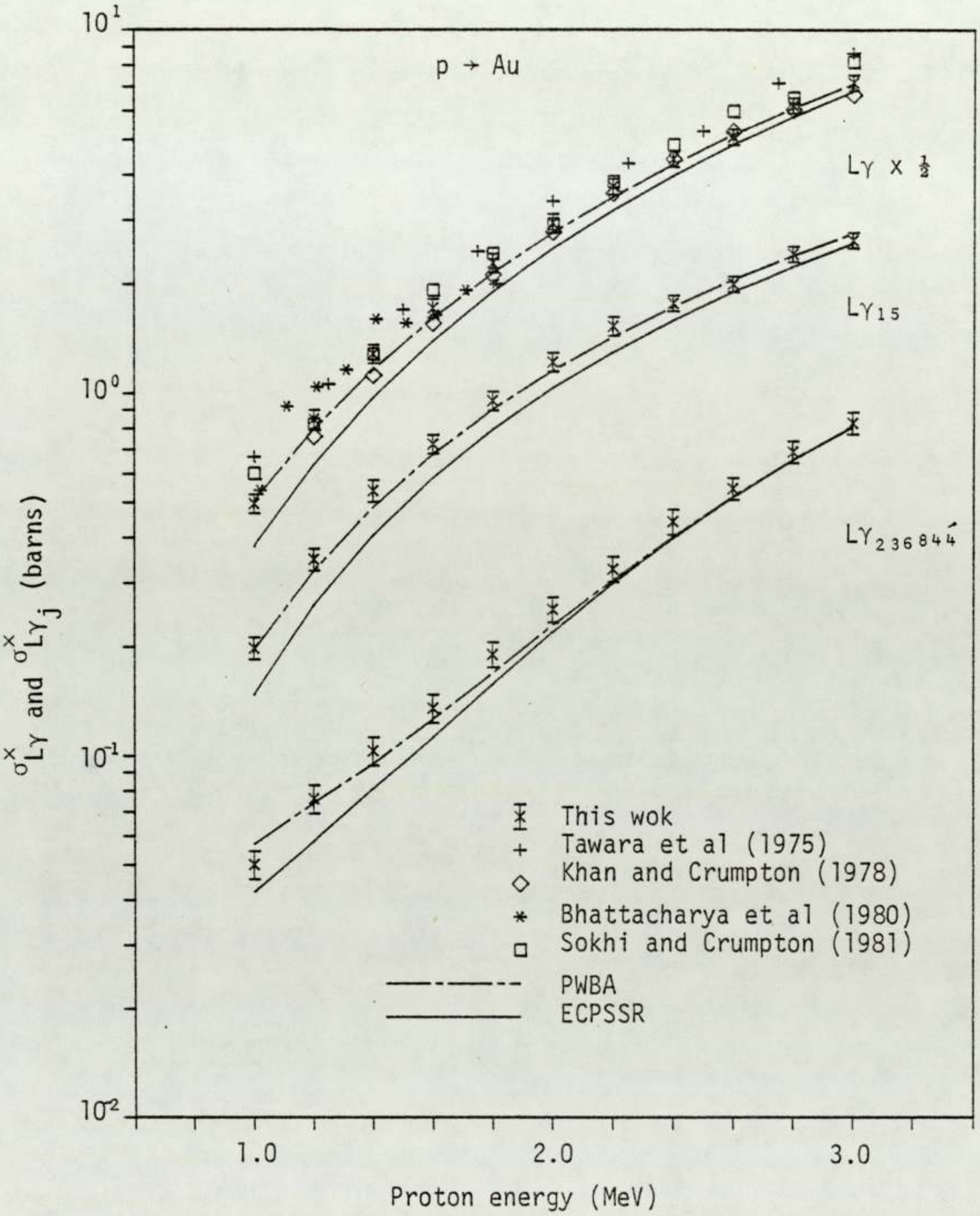

Figure 6.92. Experimental total Lγ and partial $L\gamma_j$ x-ray production cross sections for proton impact on Au.

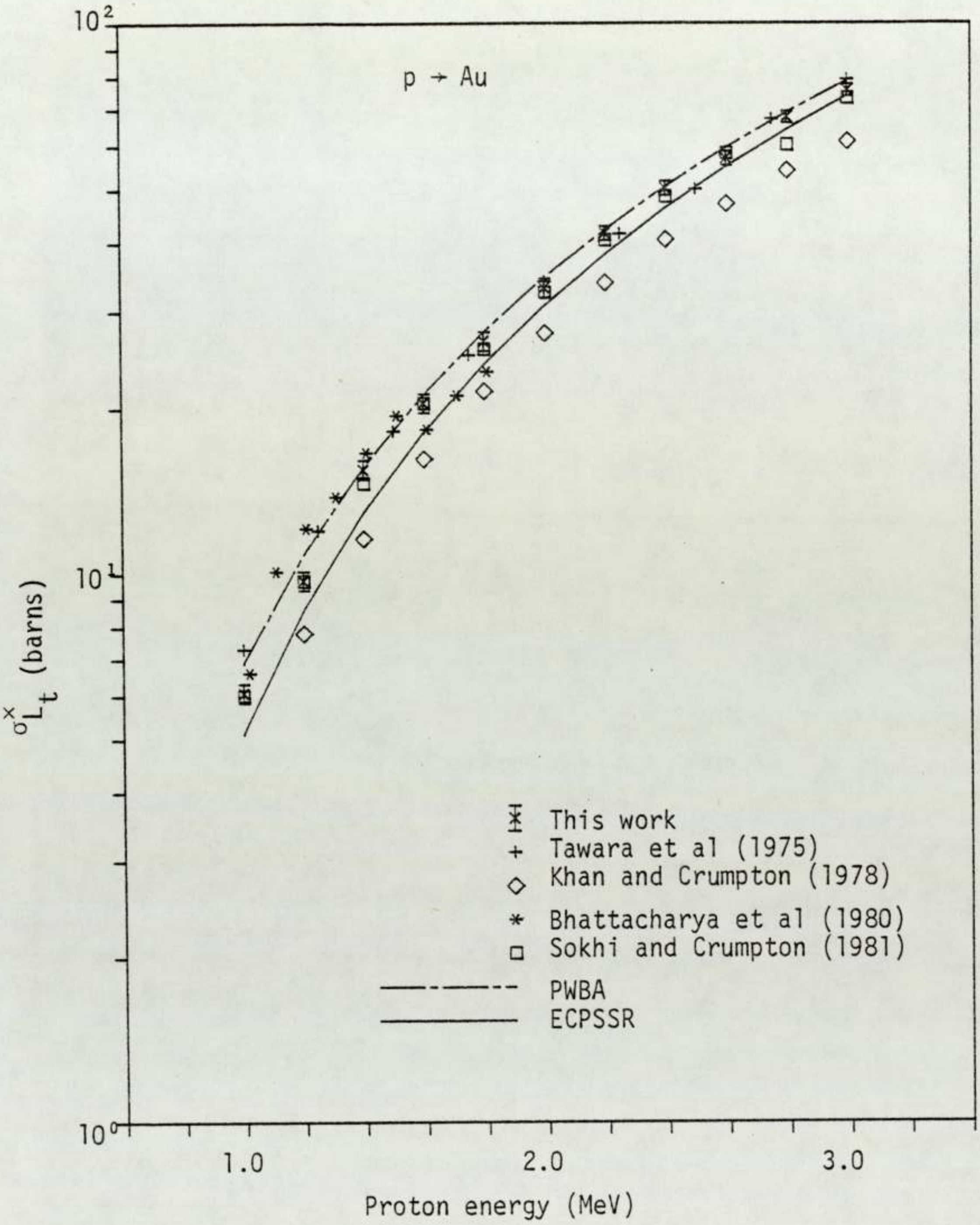

Figure 6.93. Experimental total L shell x-ray production cross section for proton impact on Au.

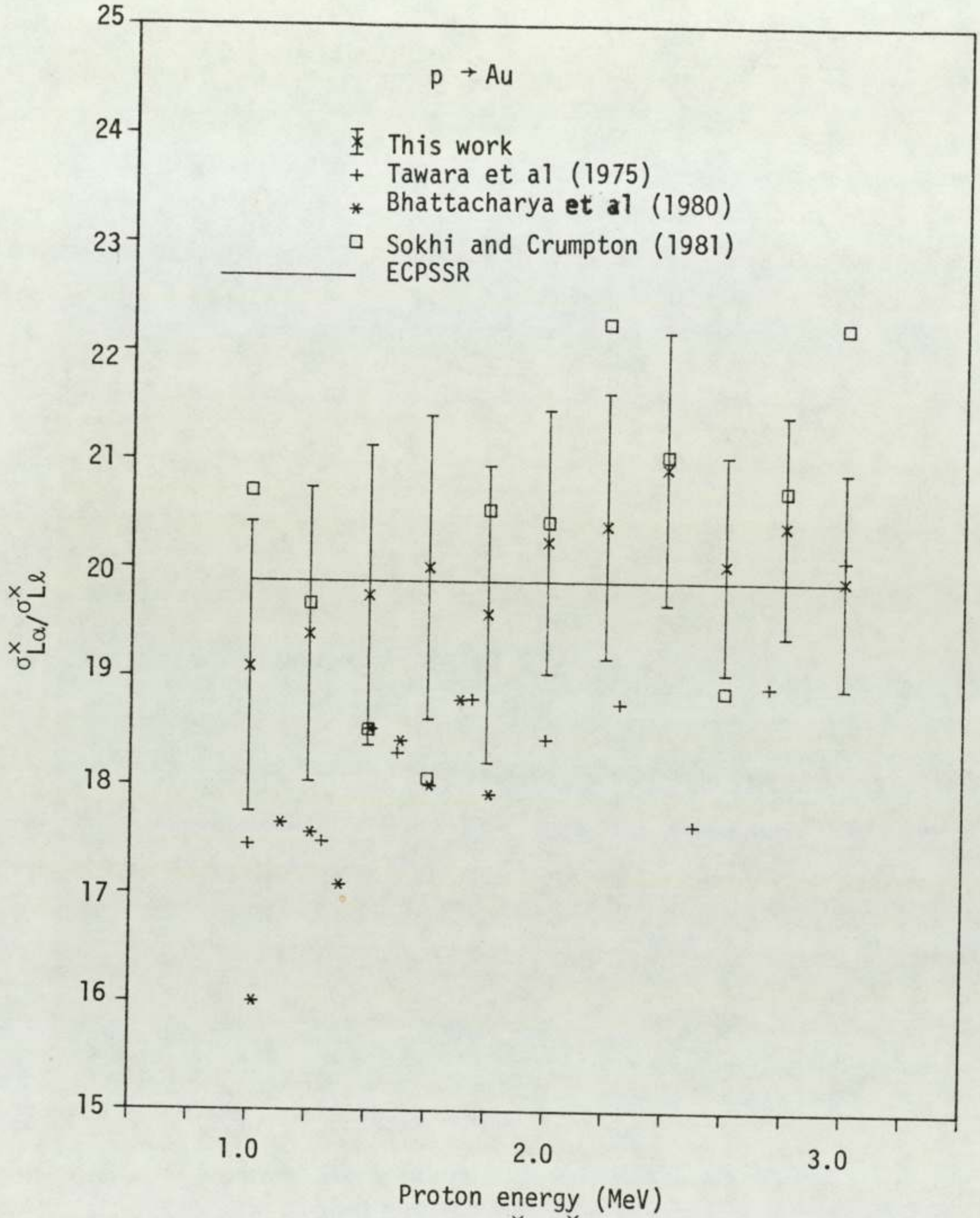

Figure 6.94. Experimental $\sigma^x_{L\alpha}/\sigma^x_{L\ell}$ ratio for proton impact on Au.

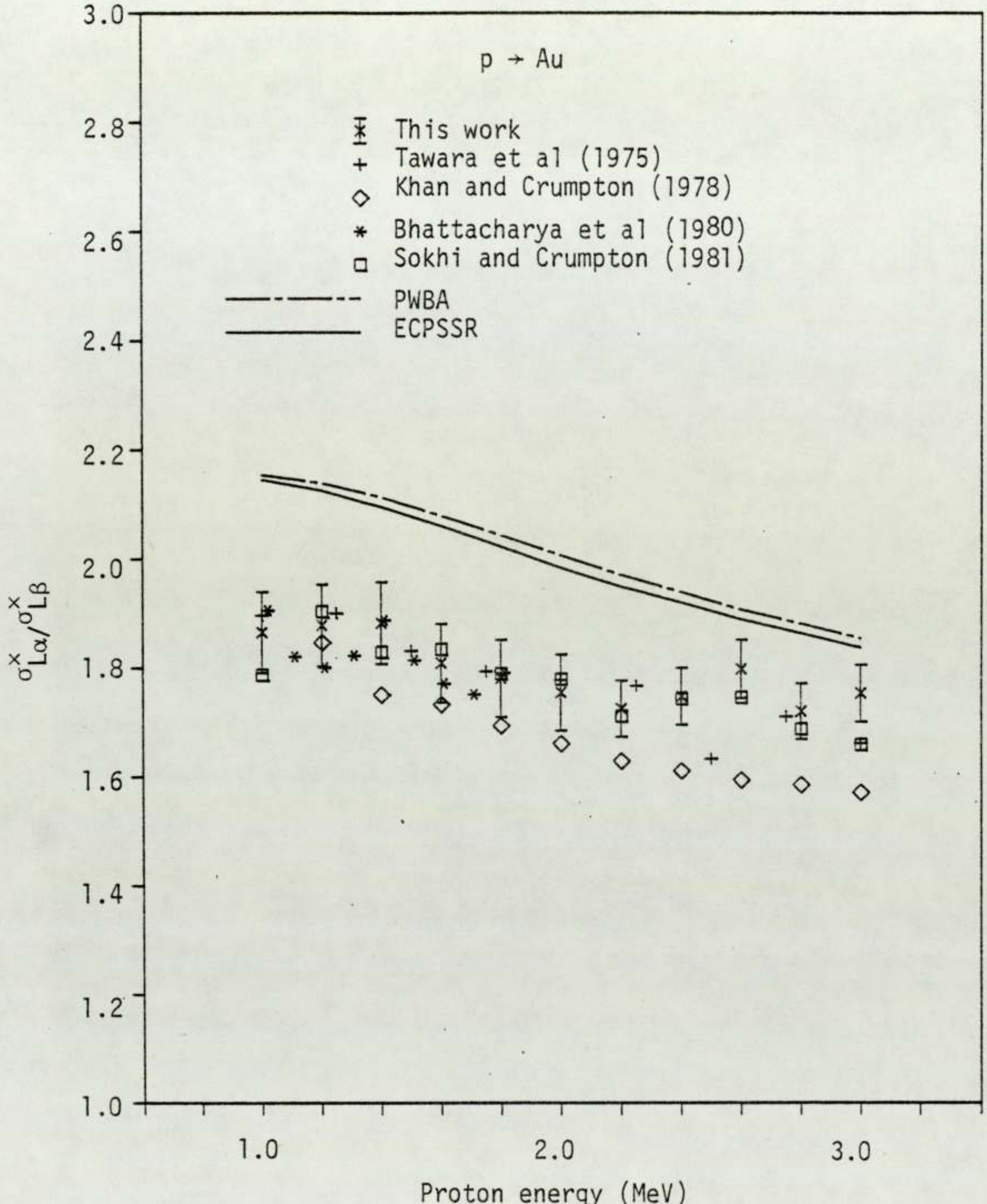

Figure 6.95. Experimental $\sigma^x_{L\alpha}/\sigma^x_{L\beta}$ ratio for proton impact on Au.

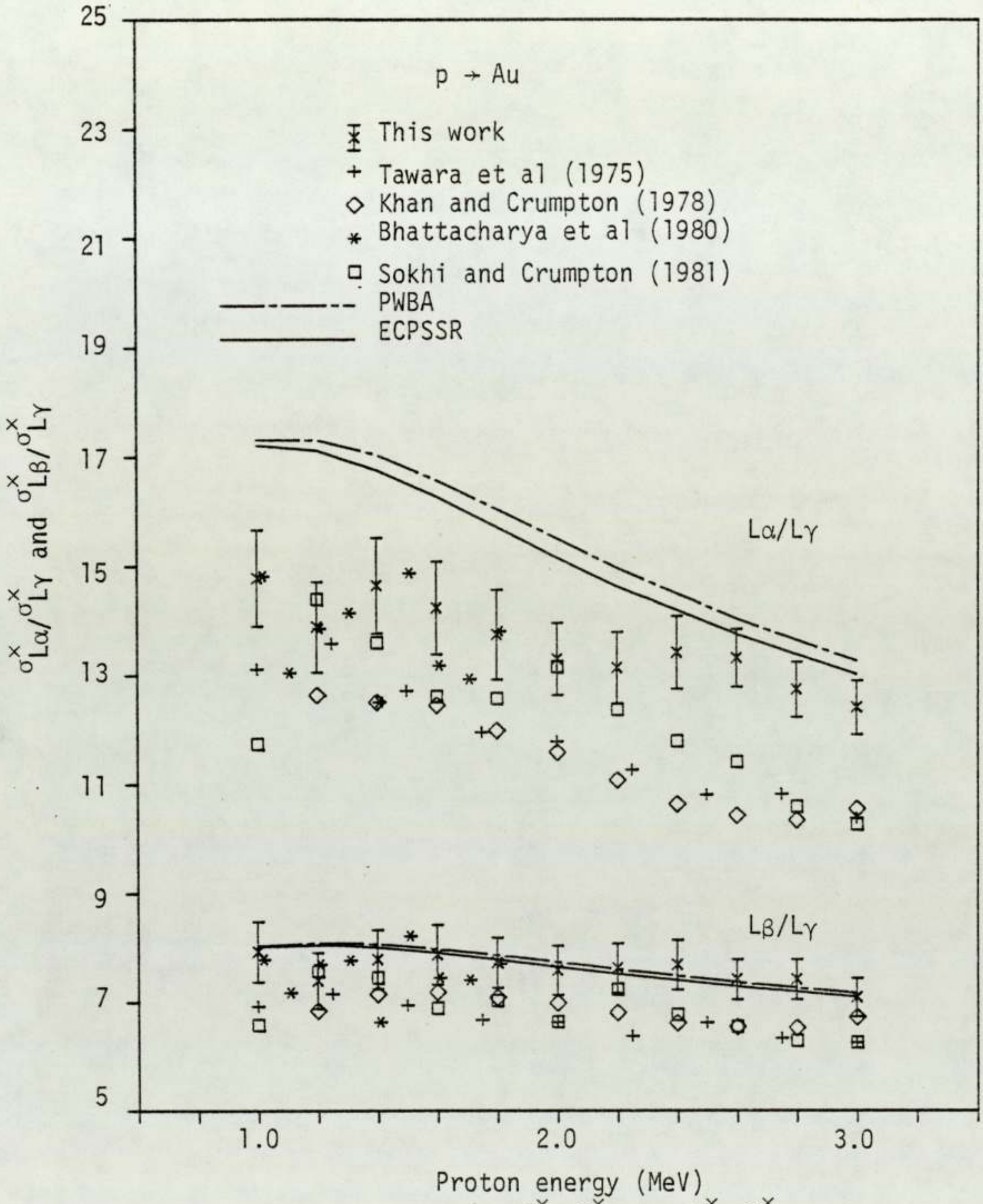

Figure 6.96. Experimental $\sigma^x_{L\alpha}/\sigma^x_{L\gamma}$ and $\sigma^x_{L\beta}/\sigma^x_{L\gamma}$ ratios for proton impact on Au.

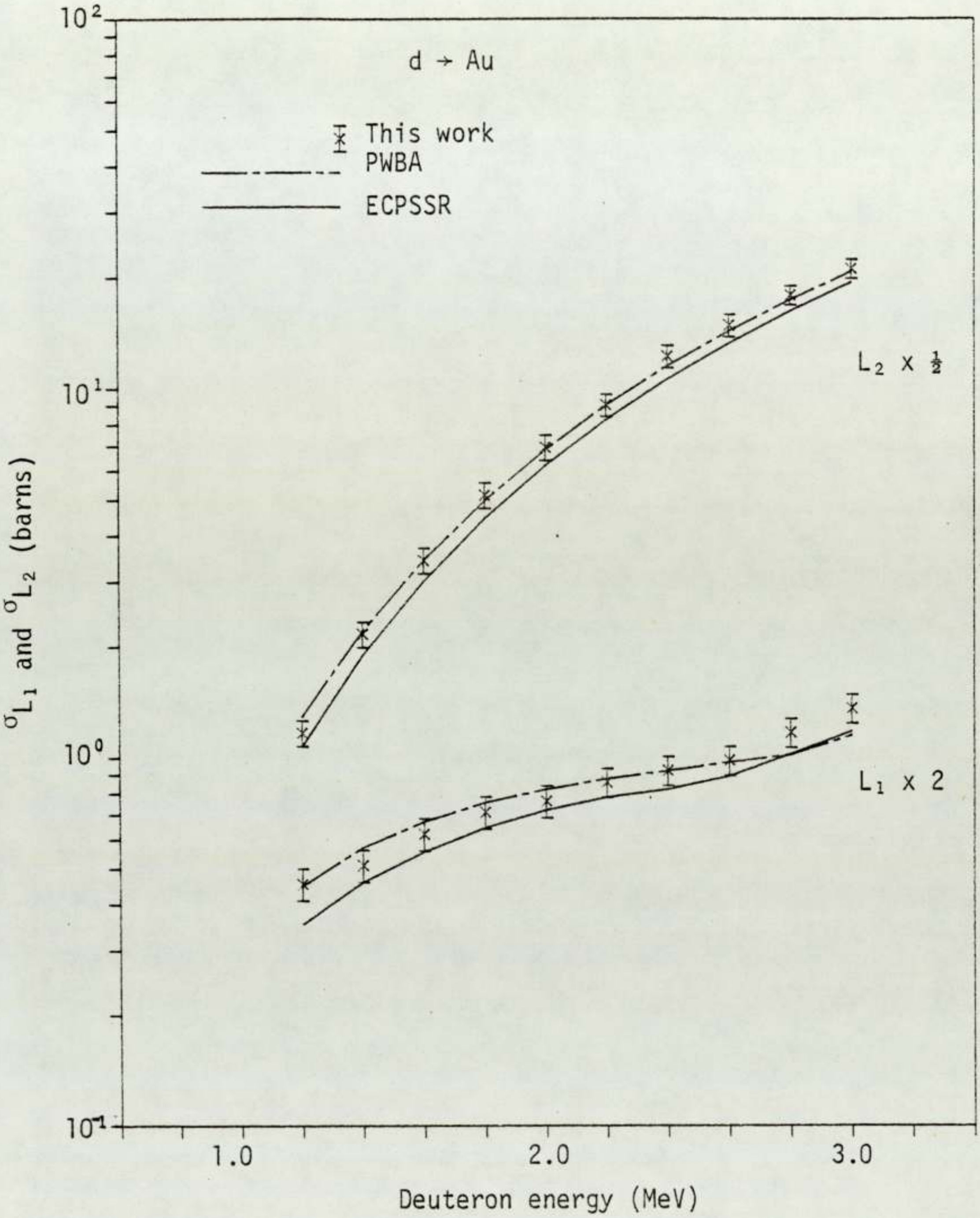

Figure 6.97. Experimental L_1 and L_3 subshell ionisation cross sections for deuteron impact on Au.

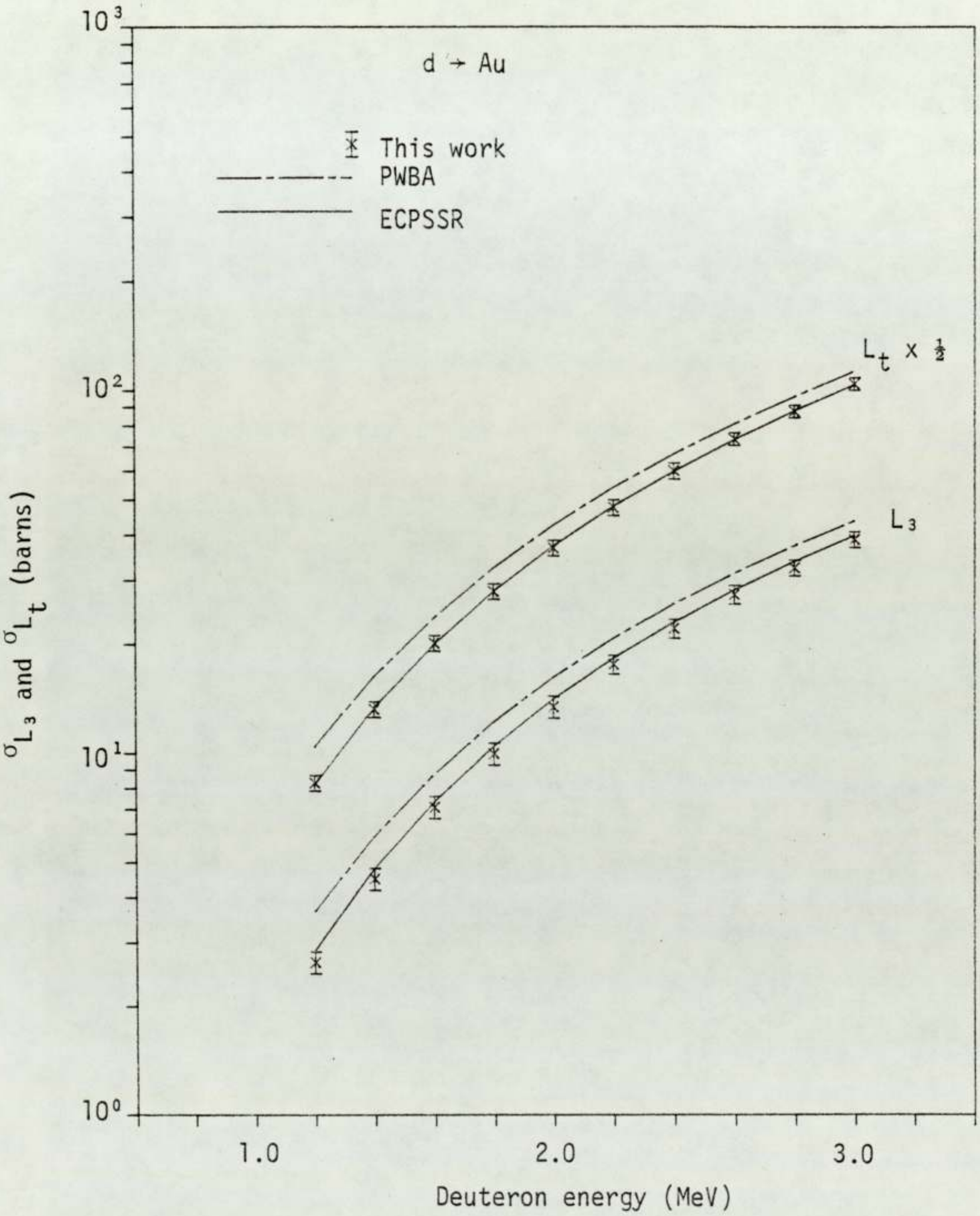

Figure 6.98. Experimental L_3 subshell and total L shell ionisation cross sections for deuteron impact on Au.

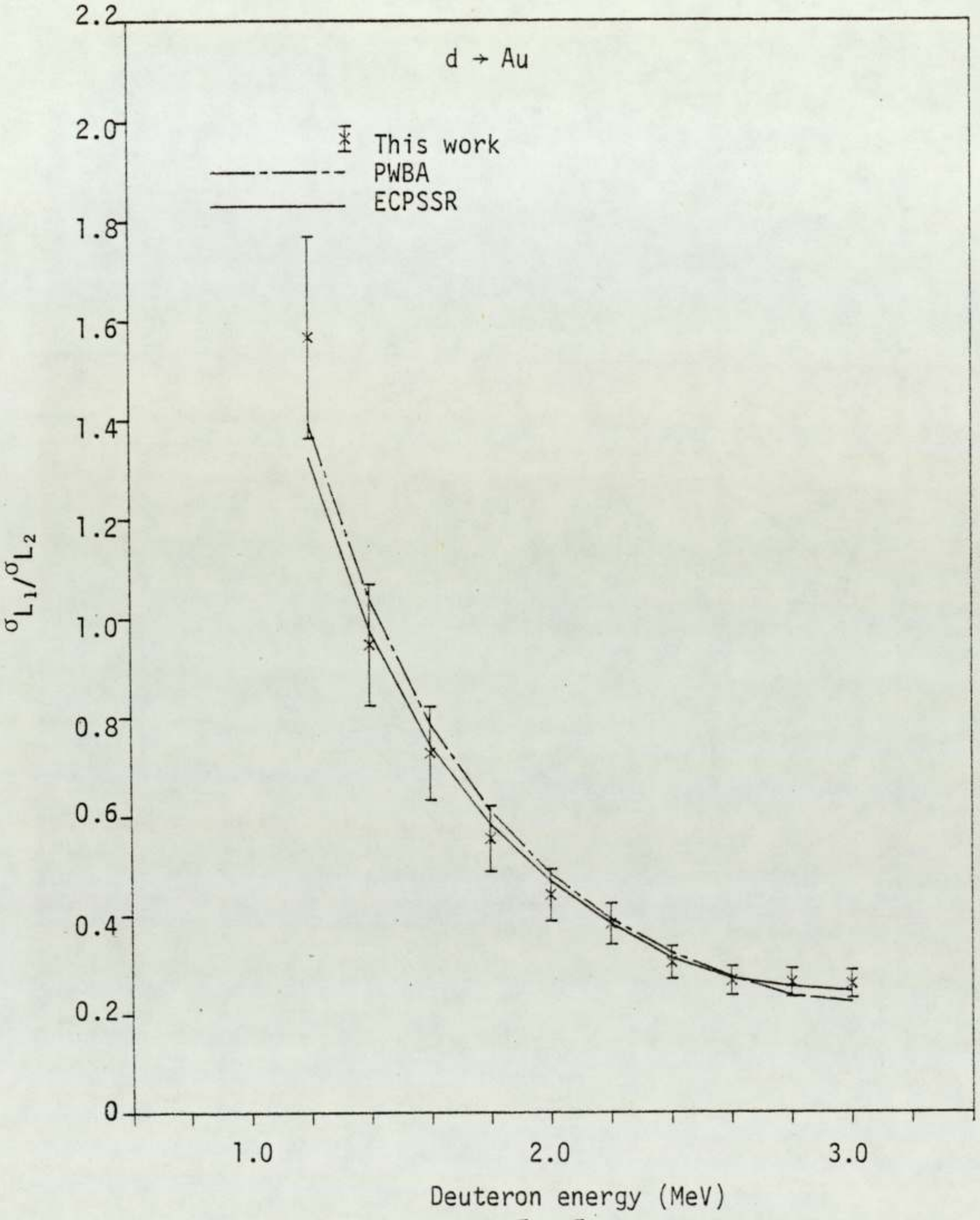

Figure 6.99. Experimental $\sigma_{L_1}/\sigma_{L_2}$ ratio for deuteron impact on Au.

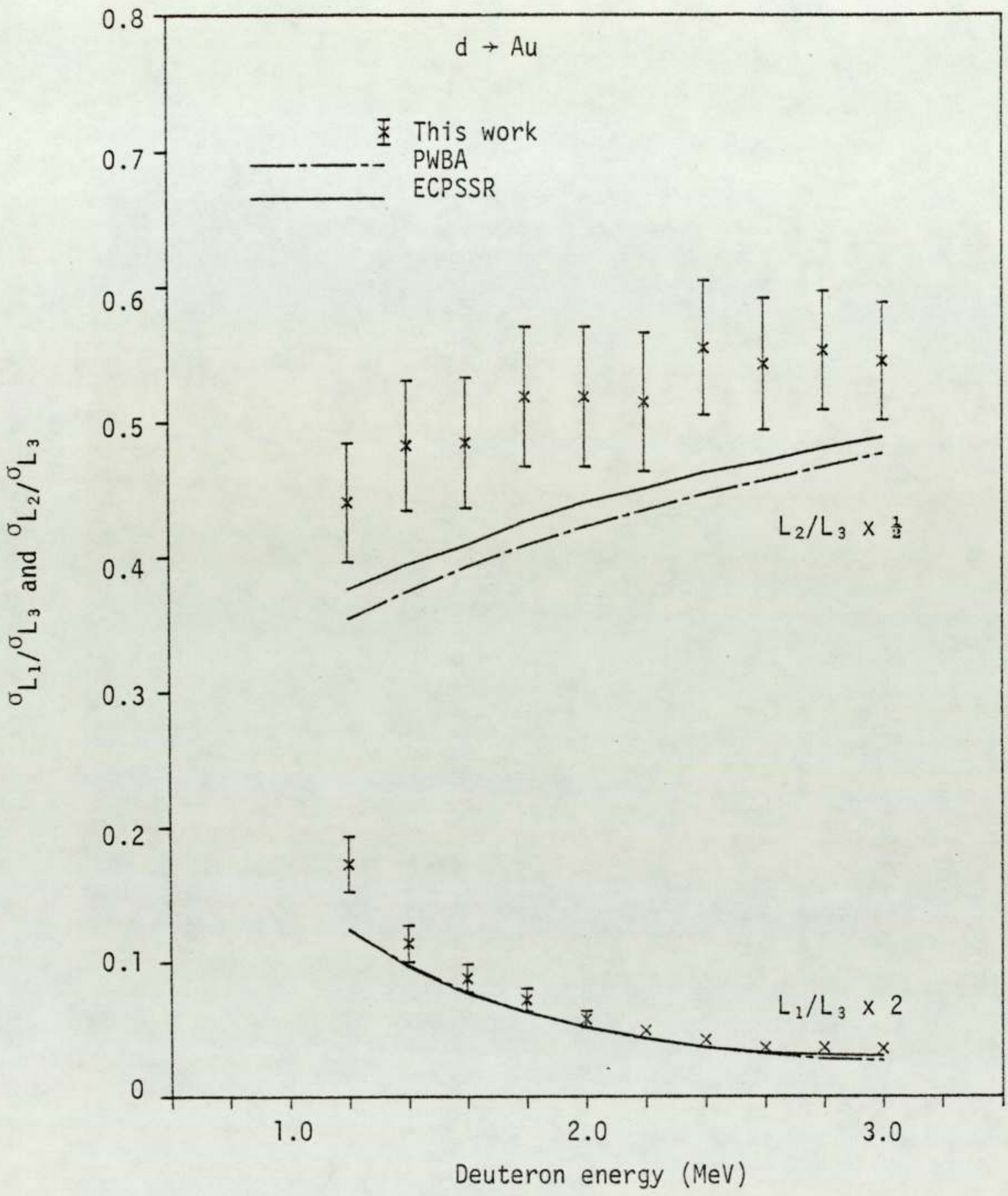

Figure 6.100. Experimental $\sigma_{L_1}/\sigma_{L_3}$ and $\sigma_{L_2}/\sigma_{L_3}$ ratios for deuteron impact on Ab.

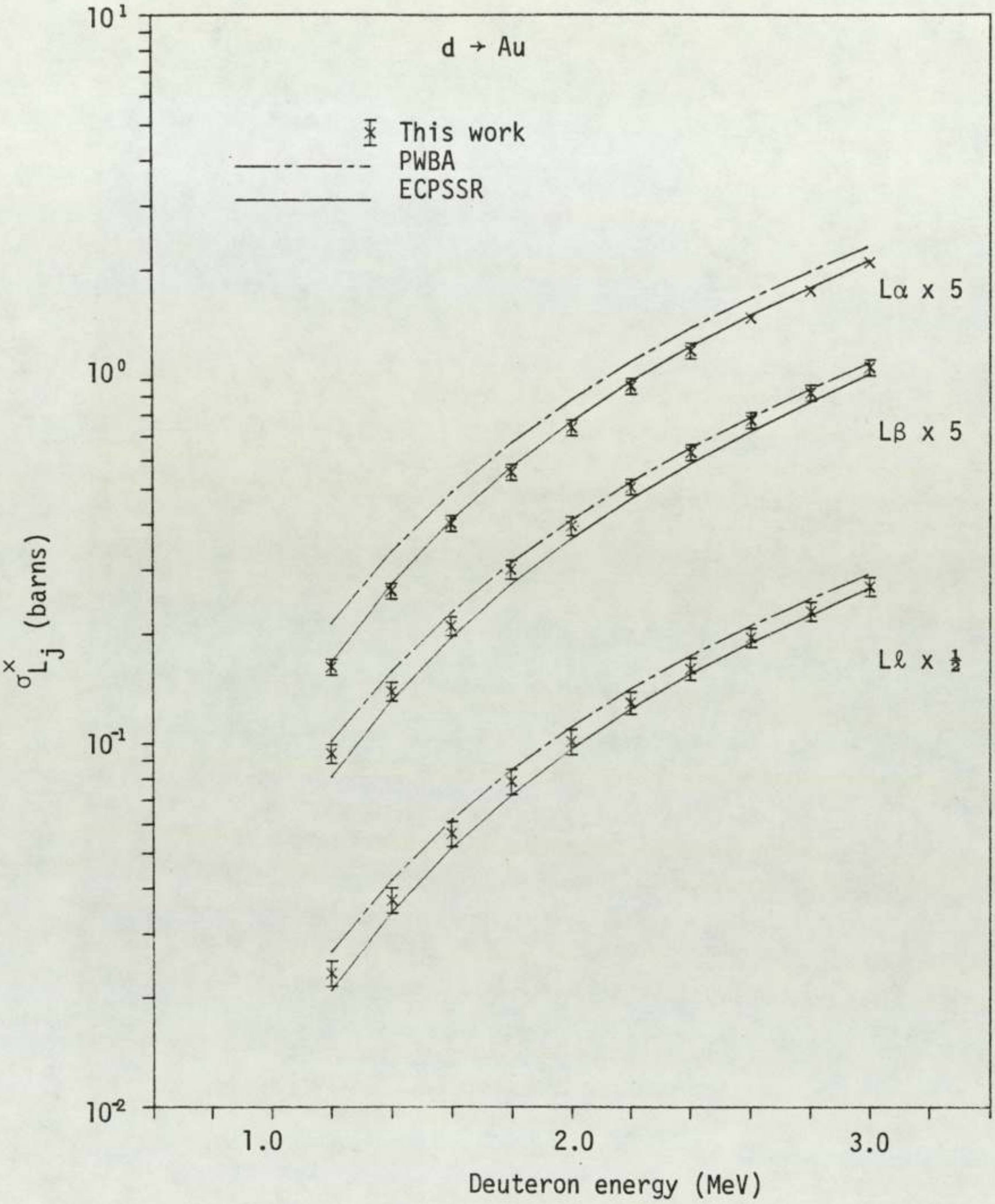

Figure 6.101. Experimental Lℓ, Lα and Lβ x-ray production cross sections for deuteron impact on Au.

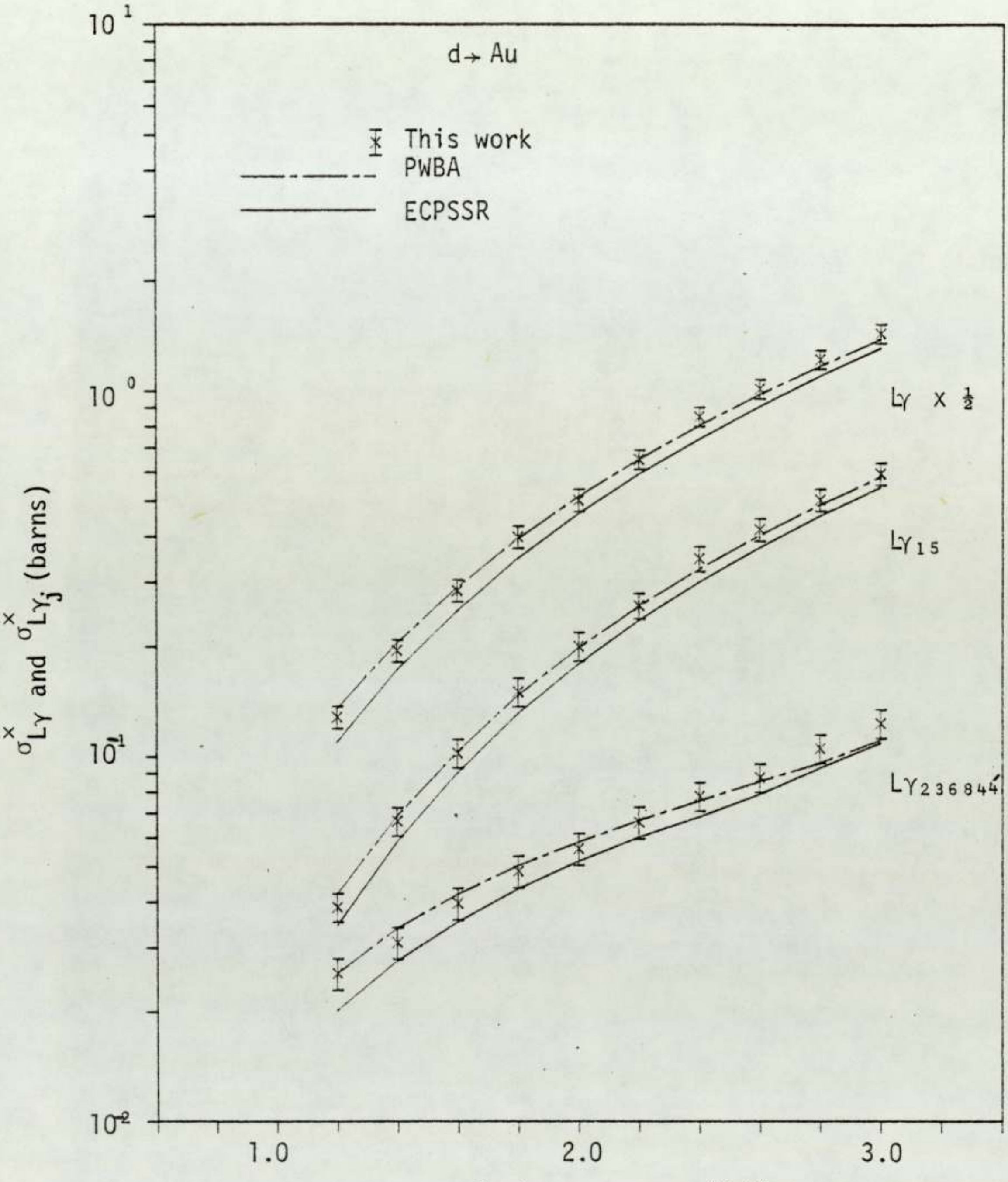

Figure 6.102. Experimental total Lγ and partial $L\gamma_j$ x-ray production cross sections for deuteron impact on Au.

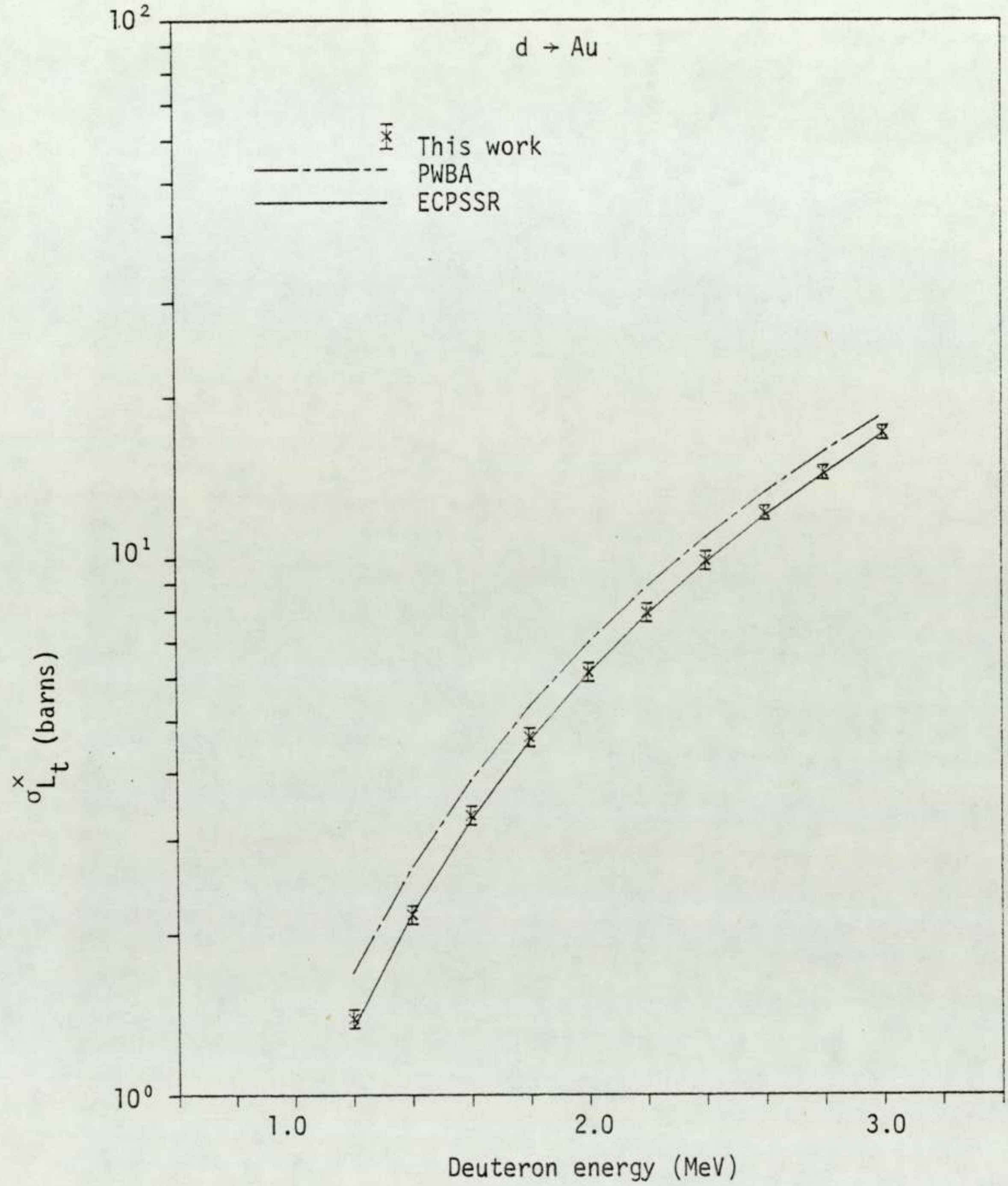

Figure 6.103. Experimental total L shell x-ray production cross section for deuteron impact on Au.

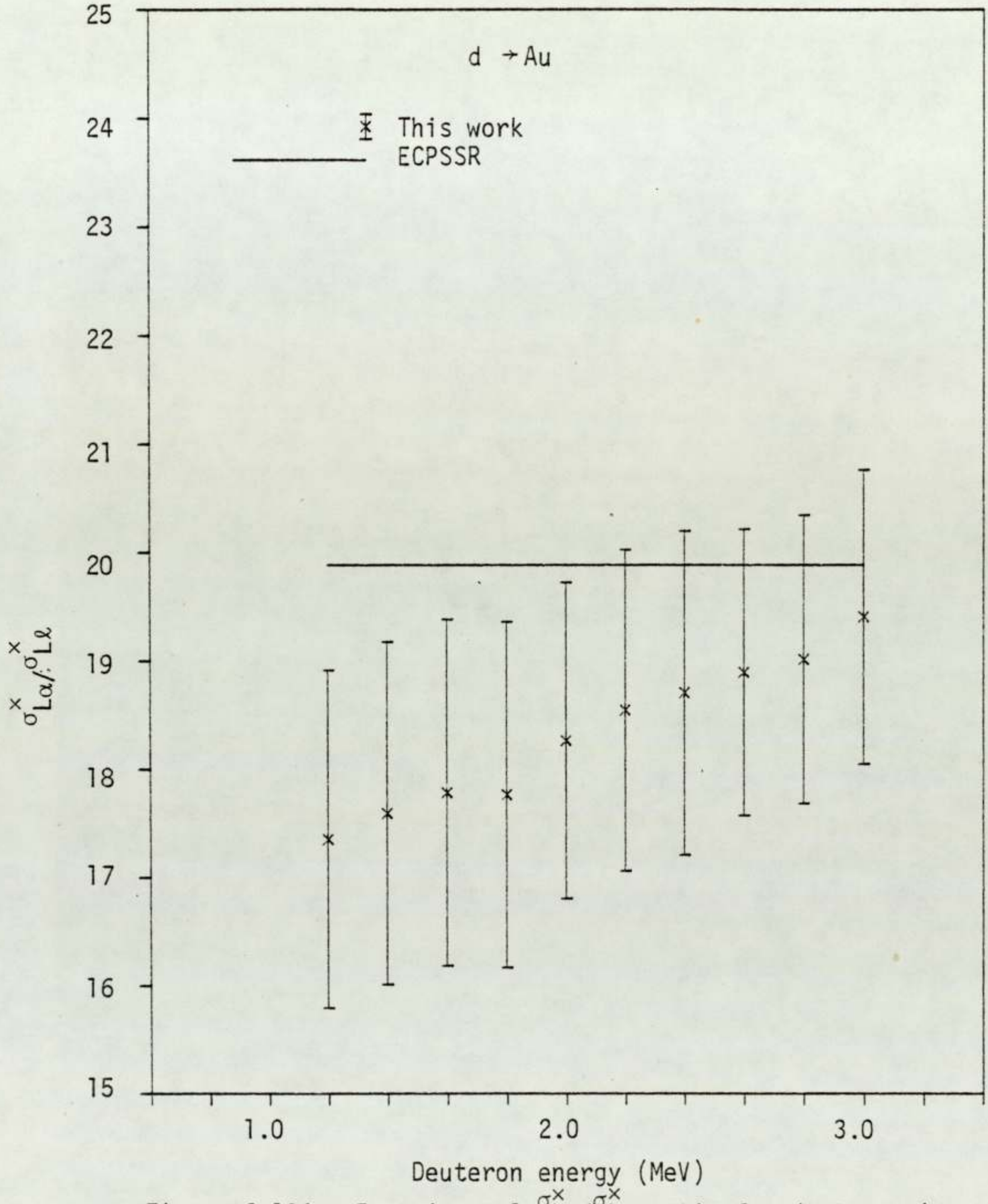

Figure 6.104. Experimental $\sigma^{x}_{L\alpha}/\sigma^{x}_{L\gamma}$ ratio for deuteron impact on Au.

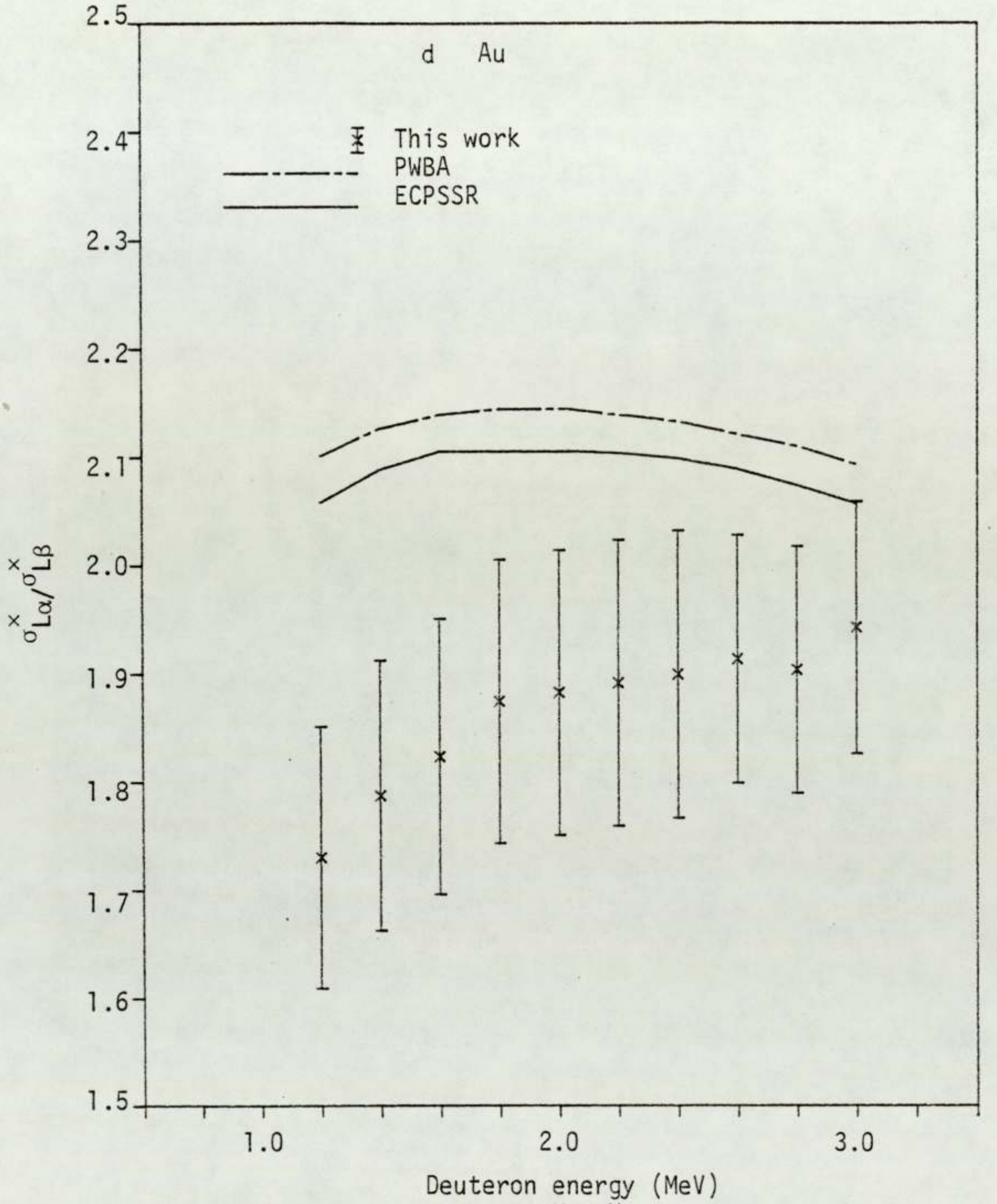

Figure 6.105. Experimental $\sigma^x_{L\alpha}/\sigma^x_{L\beta}$ ratio for deuteron impact on Au.

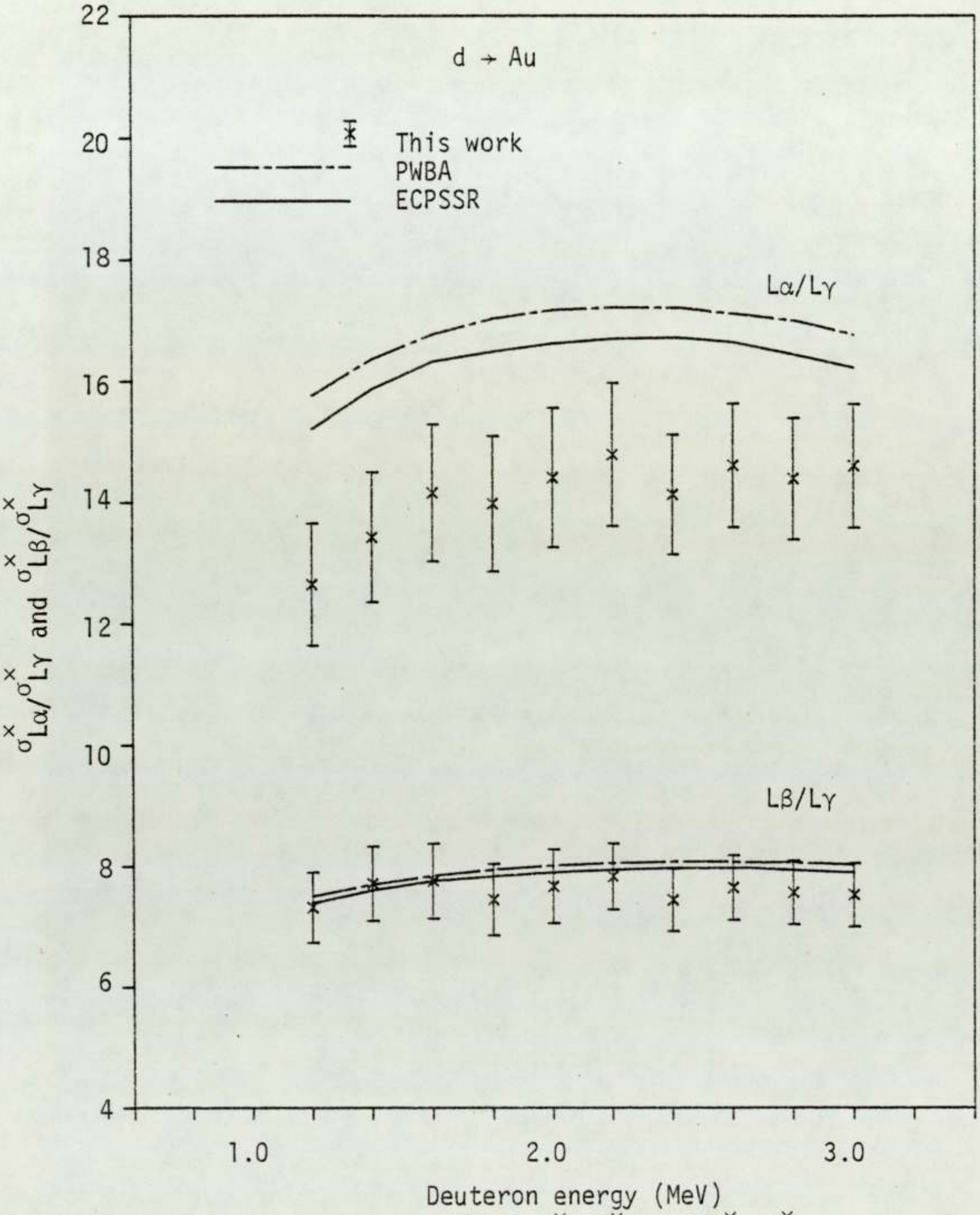

Figure 6.106. Experimental $\sigma^{x}_{L\alpha}/\sigma^{x}_{L\gamma}$ and $\sigma^{x}_{L\beta}/\sigma^{x}_{L\gamma}$ ratios for deuteron impact on Au.

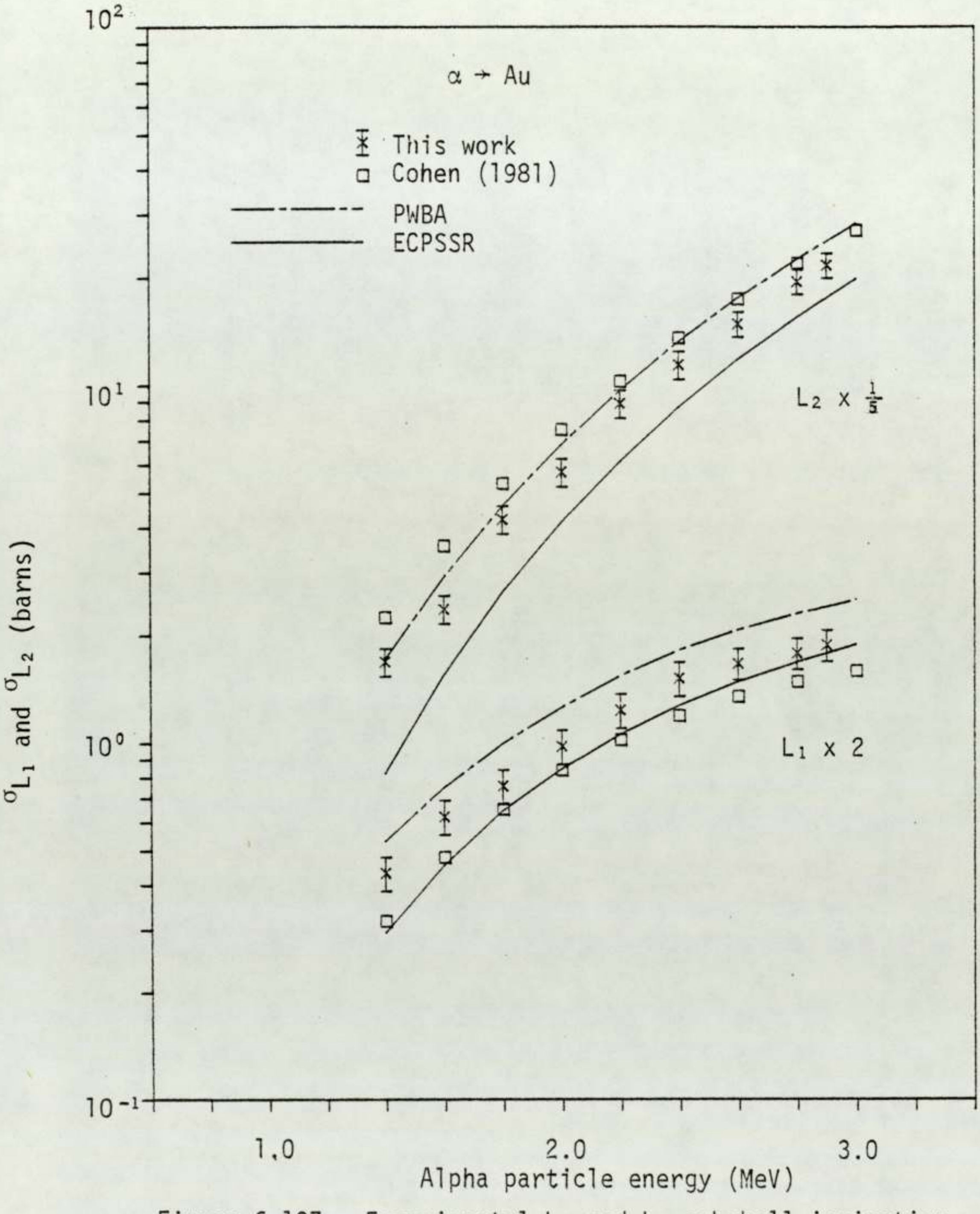

Figure 6.107. Experimental L_1 and L_2 subshell ionisation cross sections for alpha particle impact on Au.

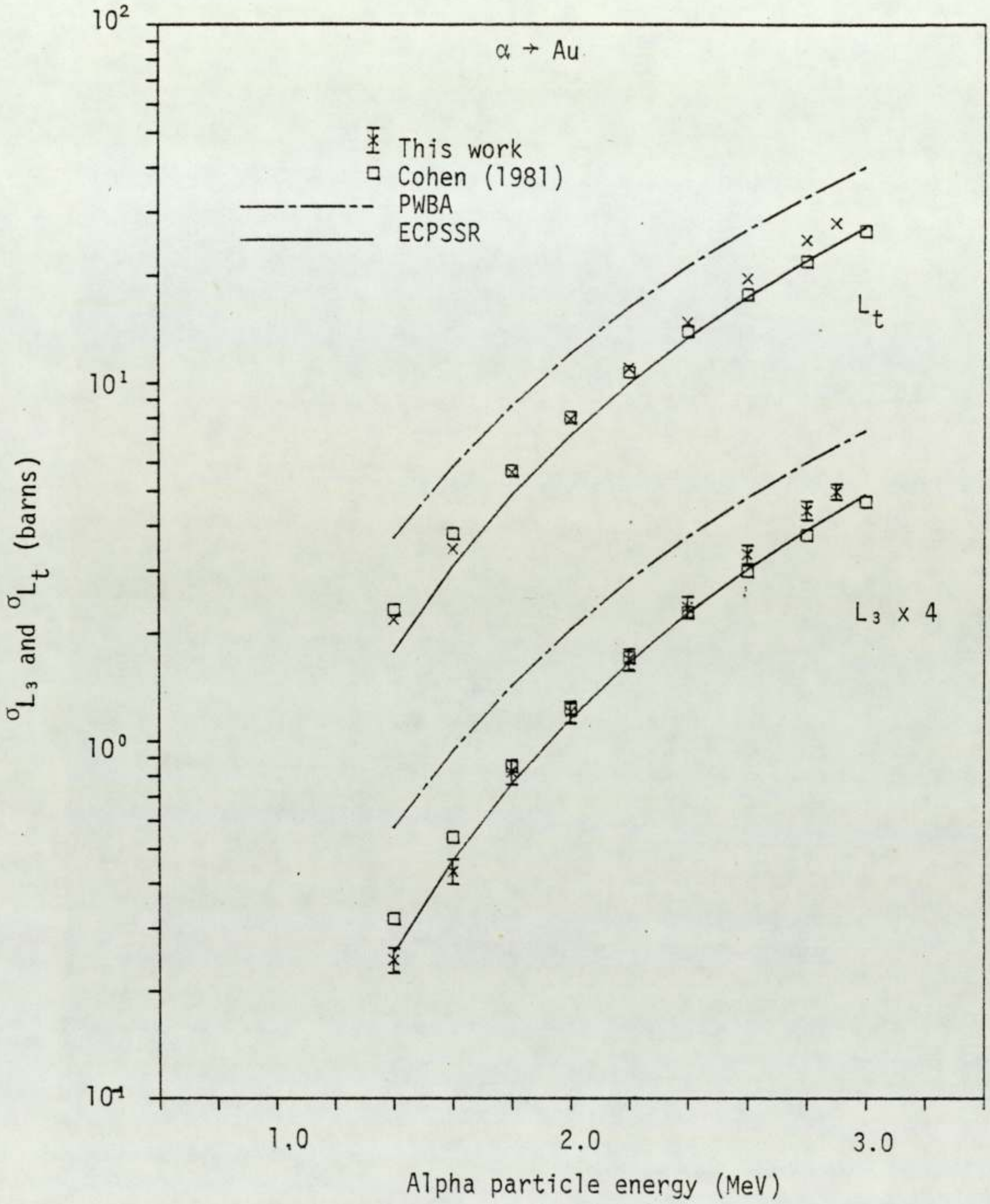

Figure 6.108. Experimental L_3 subshell and total L shell ionisation cross sections for alpha impact on Au.

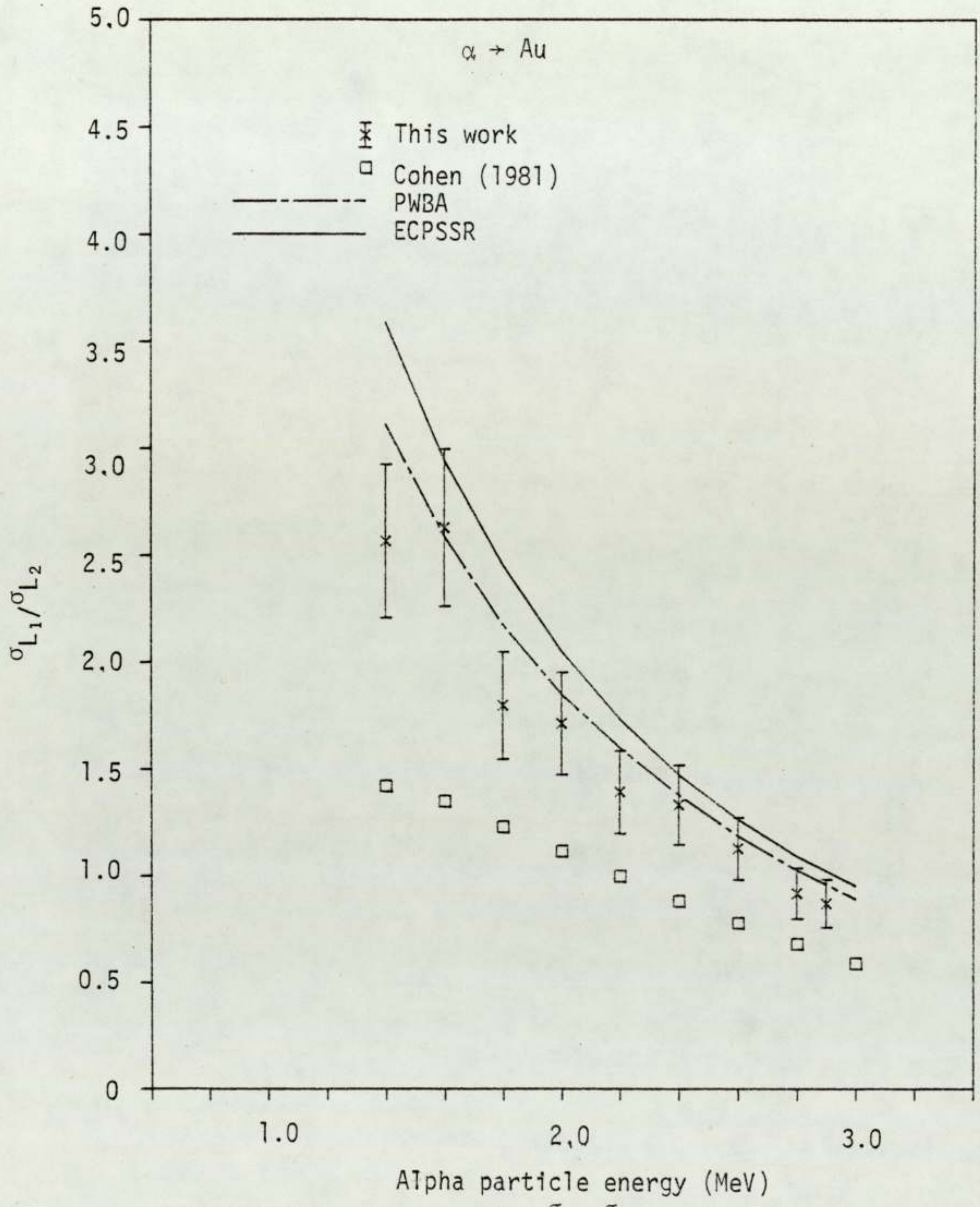

Figure 6.109. Experimental $\sigma_{L_1}/\sigma_{L_2}$ ratio for alpha particle impact on Au.

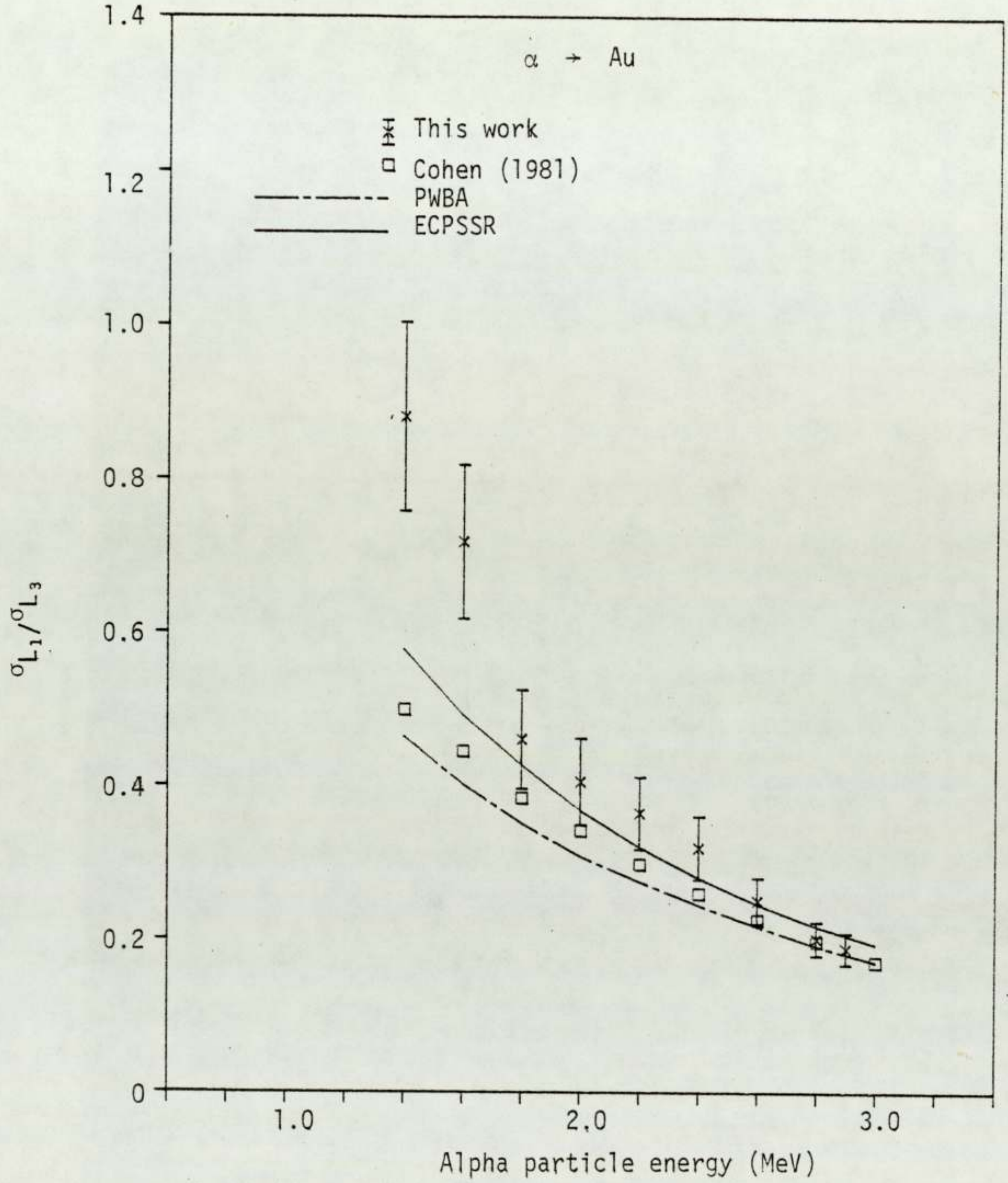

Figure 6.110. Experimental $\sigma_{L_1}/\sigma_{L_3}$ ratio for alpha particle impact on Au.

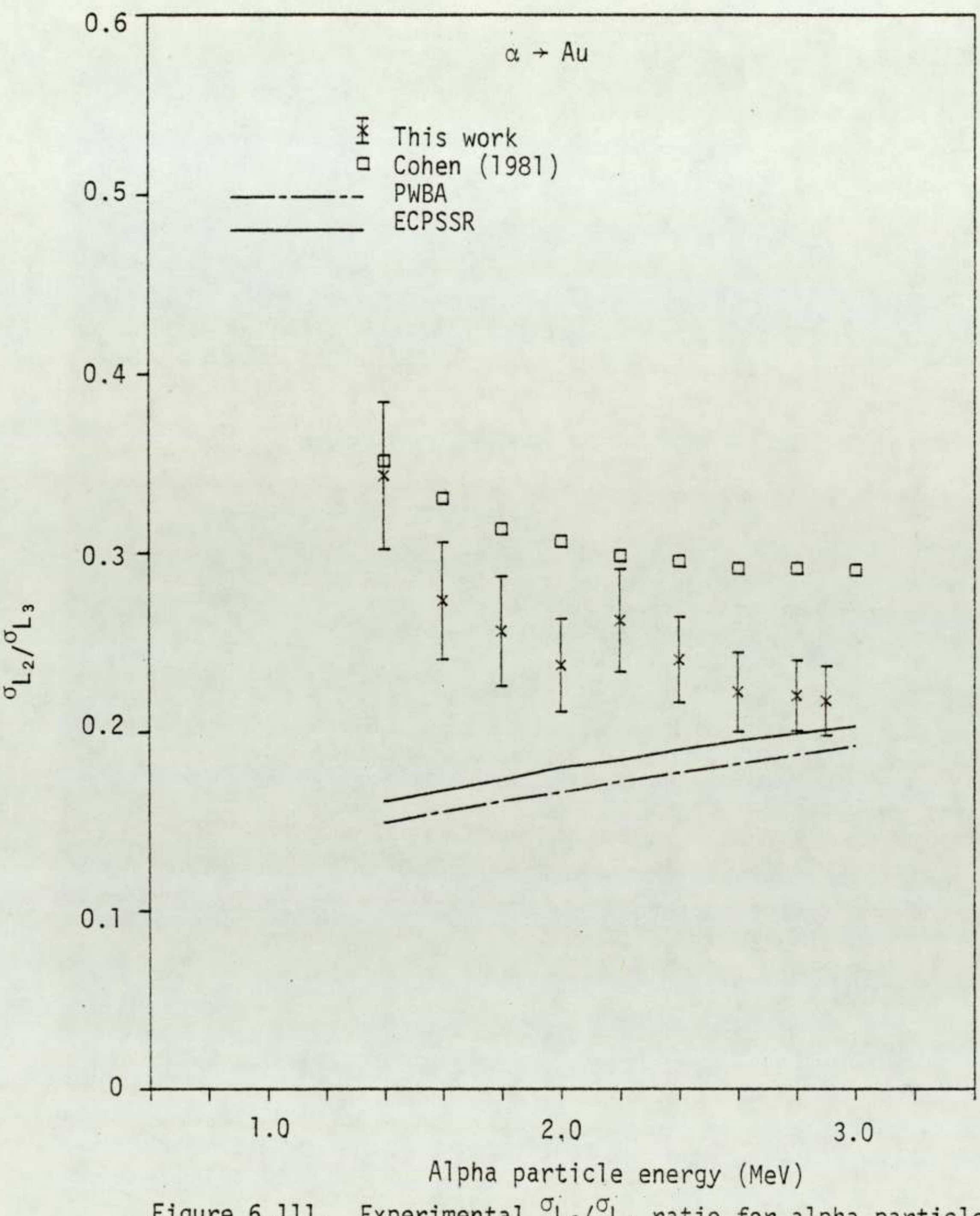

Figure 6.111. Experimental $\sigma_{L_2}/\sigma_{L_3}$ ratio for alpha particle impact on Au.

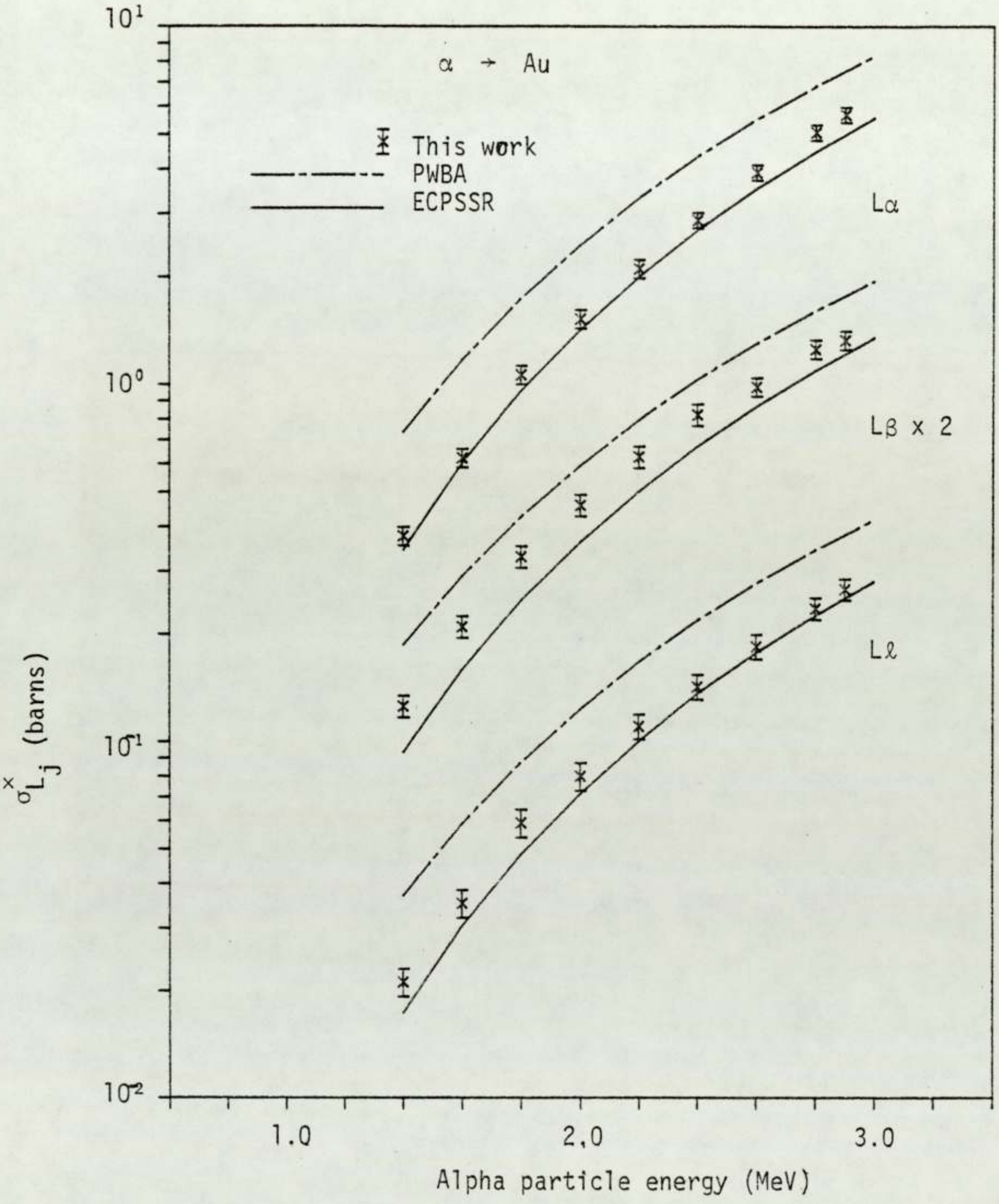

Figure 6.112. Experimental Lℓ, Lα and Lβ x-ray production cross sections for alpha particles impact on Au.

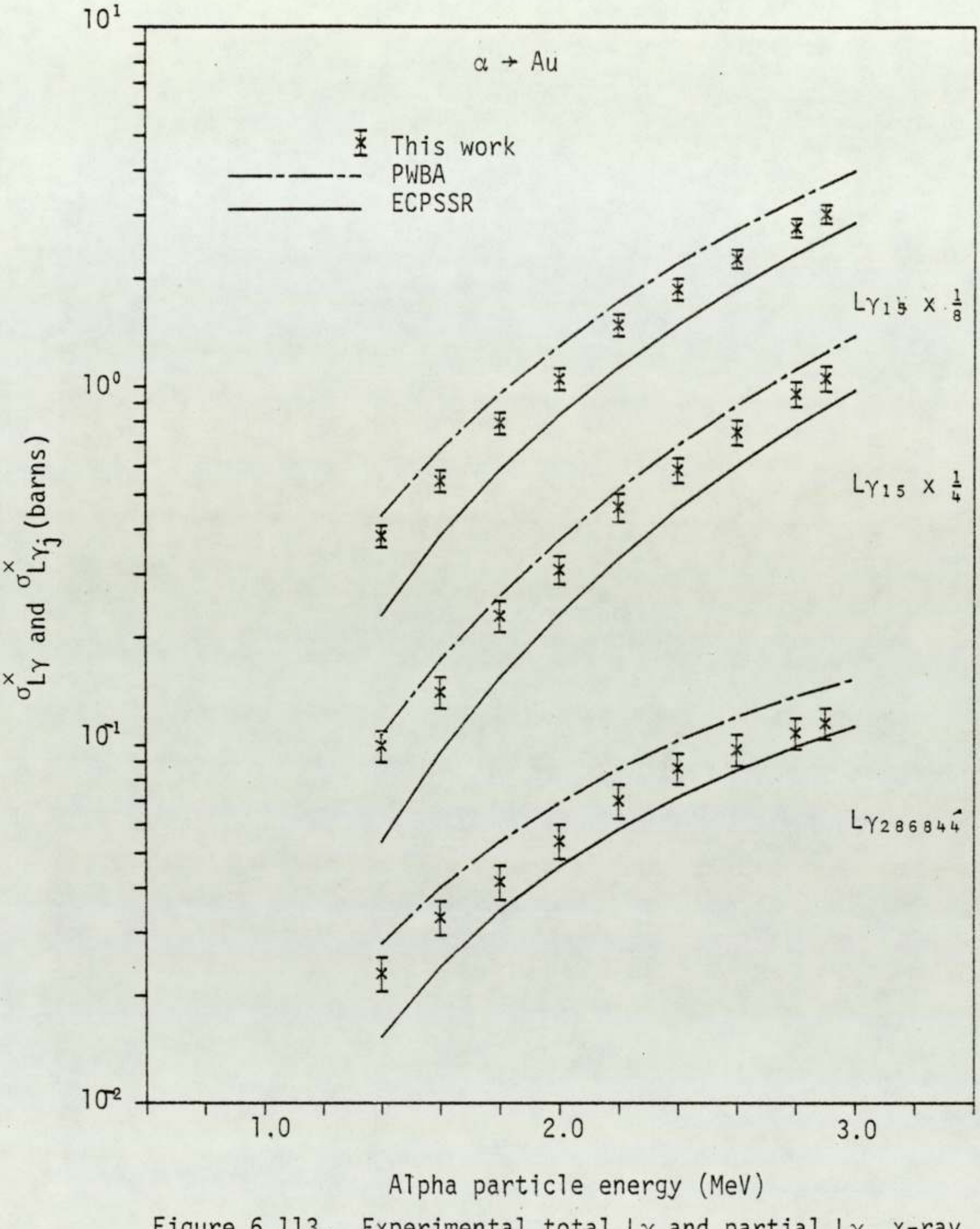

Figure 6.113. Experimental total Lγ and partial $L\gamma_j$ x-ray production cross sections for alpha particle impact on Au.

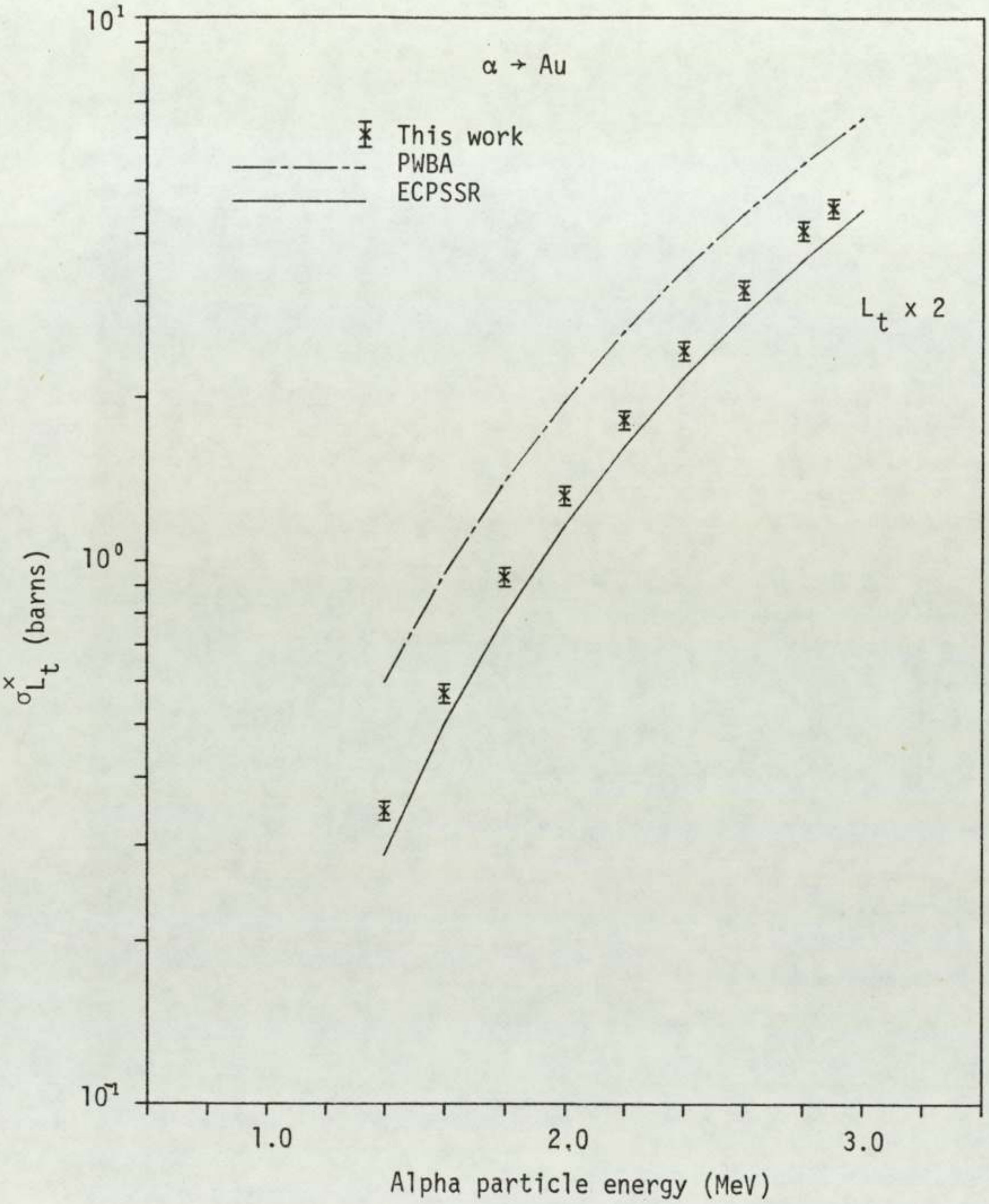

Figure 6.114. Experimental total L shell x-ray production cross section for alpha particle impact on Au.

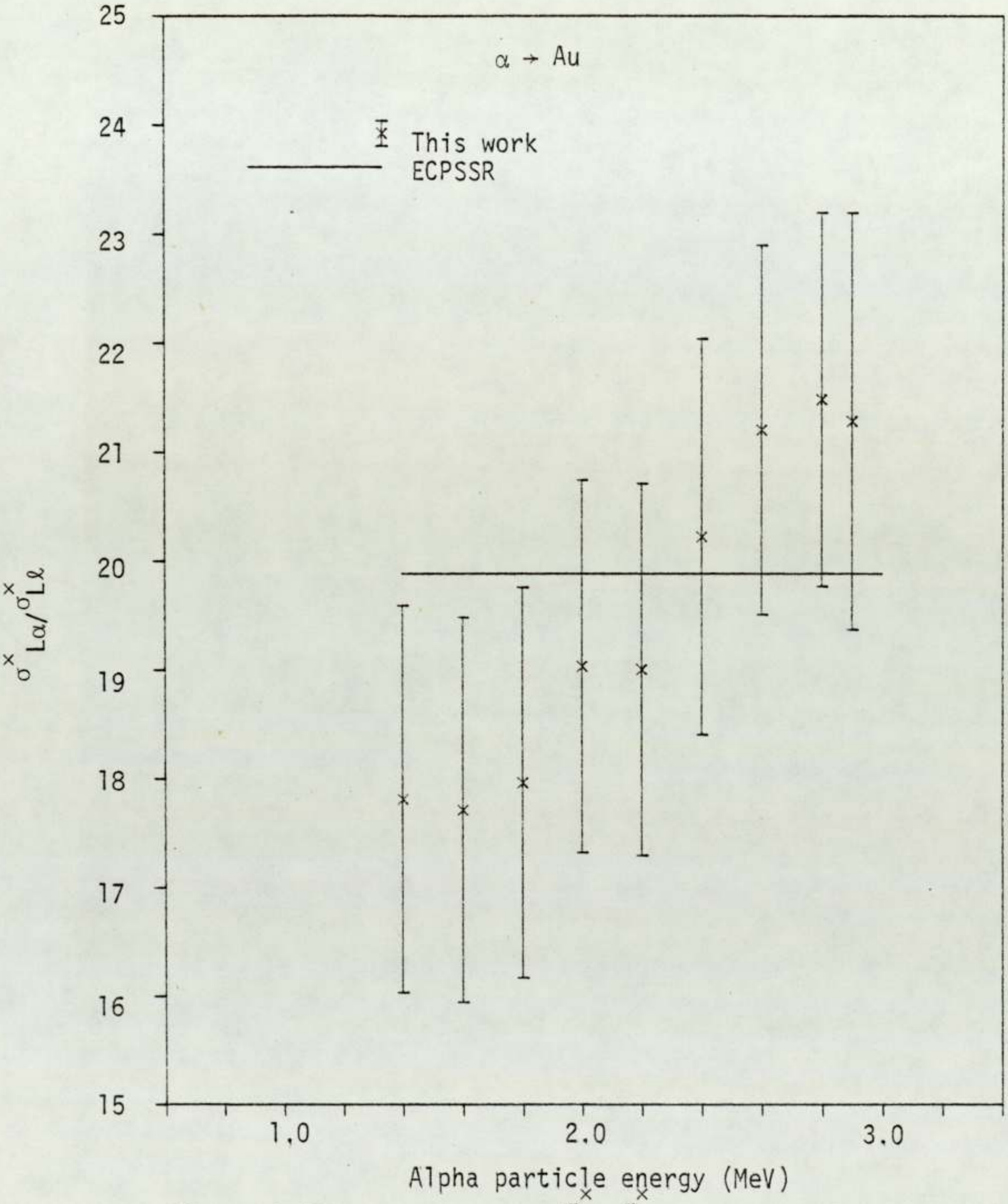

Figure 6.115. Experimental $\sigma^x_{L_\alpha}/\sigma^x_{L_\ell}$ ratio for alpha particle impact on Au.

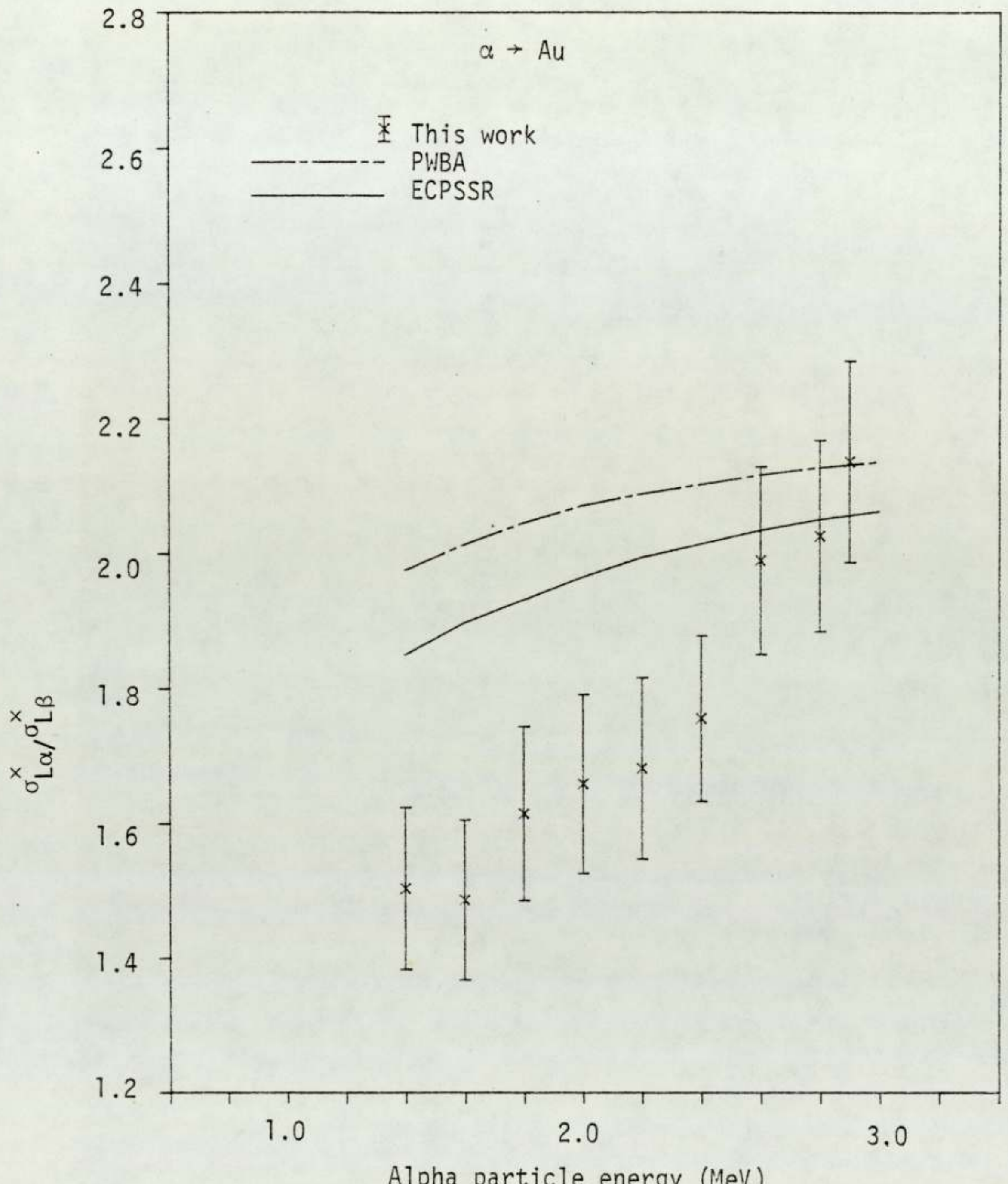

Figure 6.116. Experimental $\sigma^x_{L\alpha}/\sigma^x_{L\beta}$ ratio for alpha particle impact on Au.

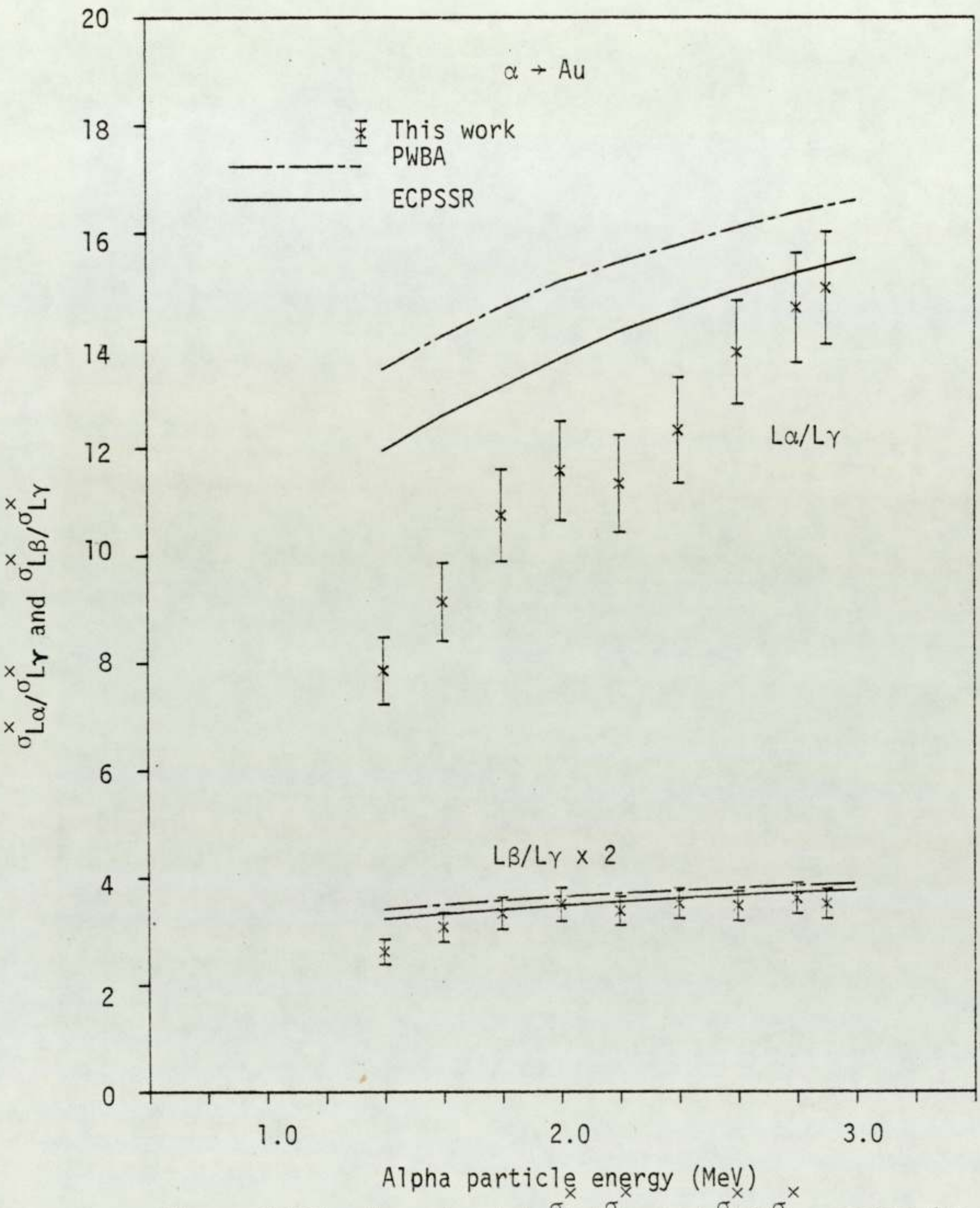

Figure 6.117. Experimental $\sigma^{x}_{L\alpha}/\sigma^{x}_{L\gamma}$ and $\sigma^{x}_{L\beta}/\sigma^{x}_{L\gamma}$ ratios for alpha particle impact on Au.

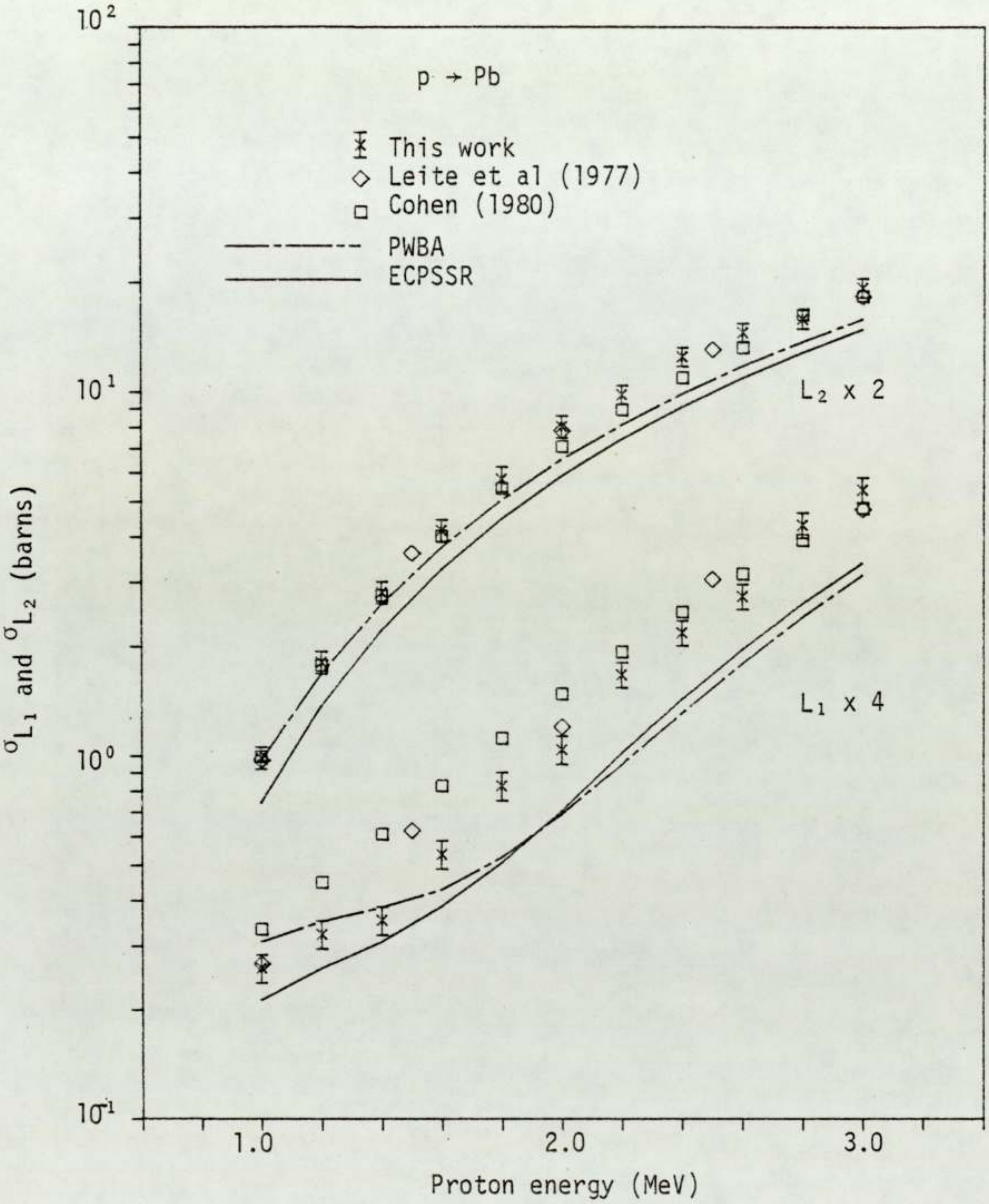

Figure 6.118. Experimental L_1 and L_2 subshell ionisation cross sections for proton impact on Pb.

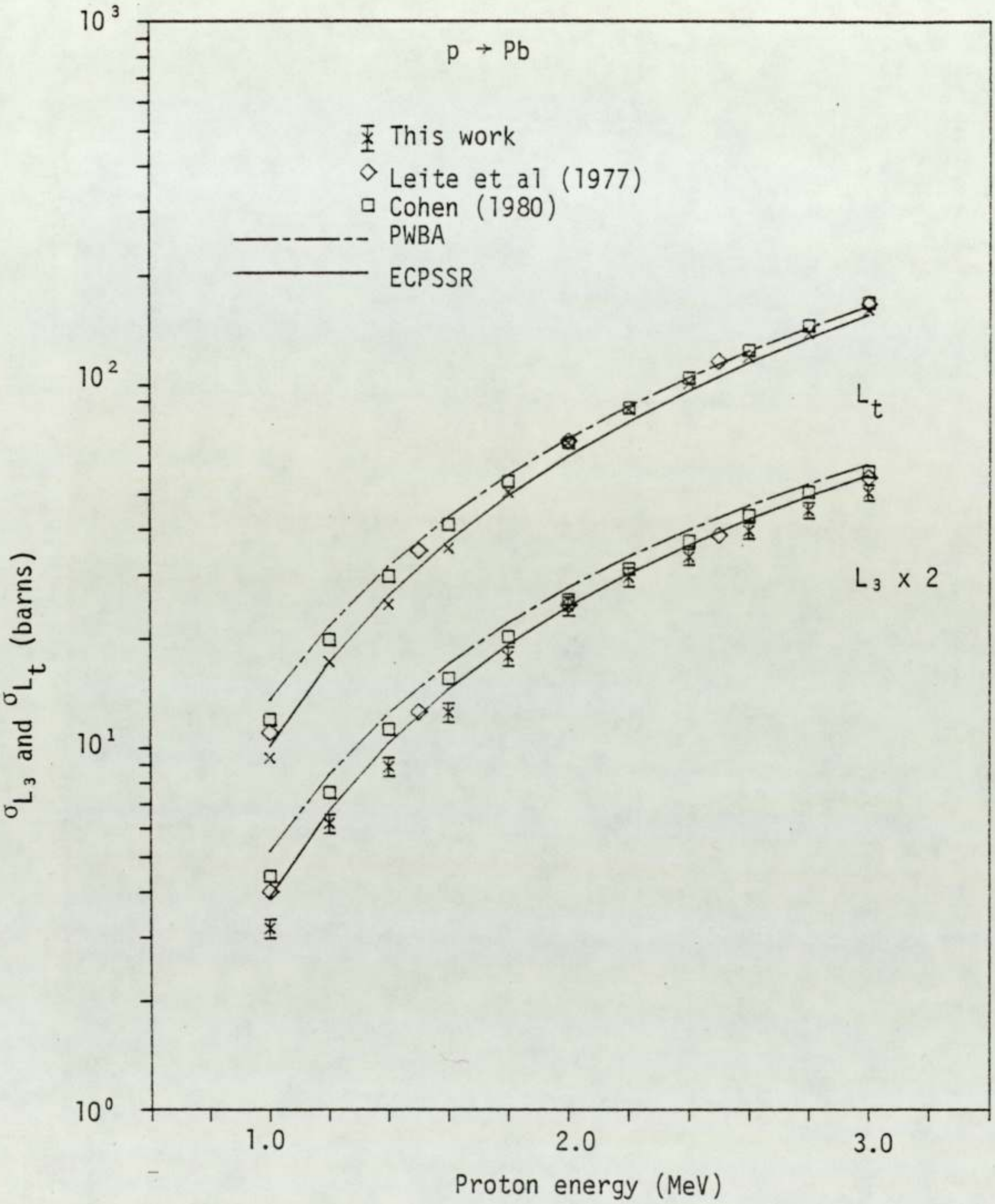

Figure 6.119. Experimental L_3 subshell and total L shell ionisation cross sections for proton impact on Pb.

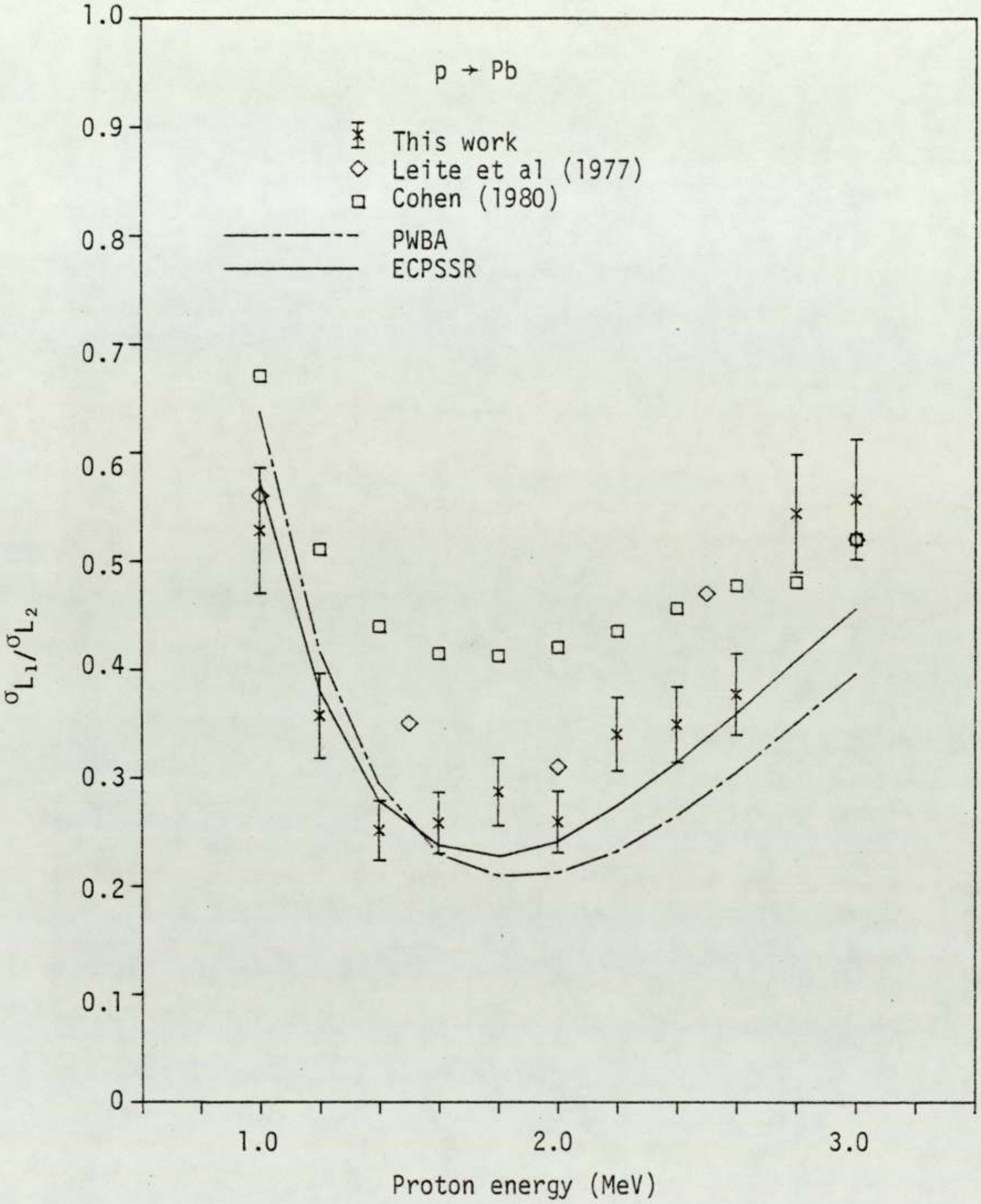

Figure 6.120. Experimental $\sigma_{L_1}/\sigma_{L_2}$ ratio for proton impact on Pb.

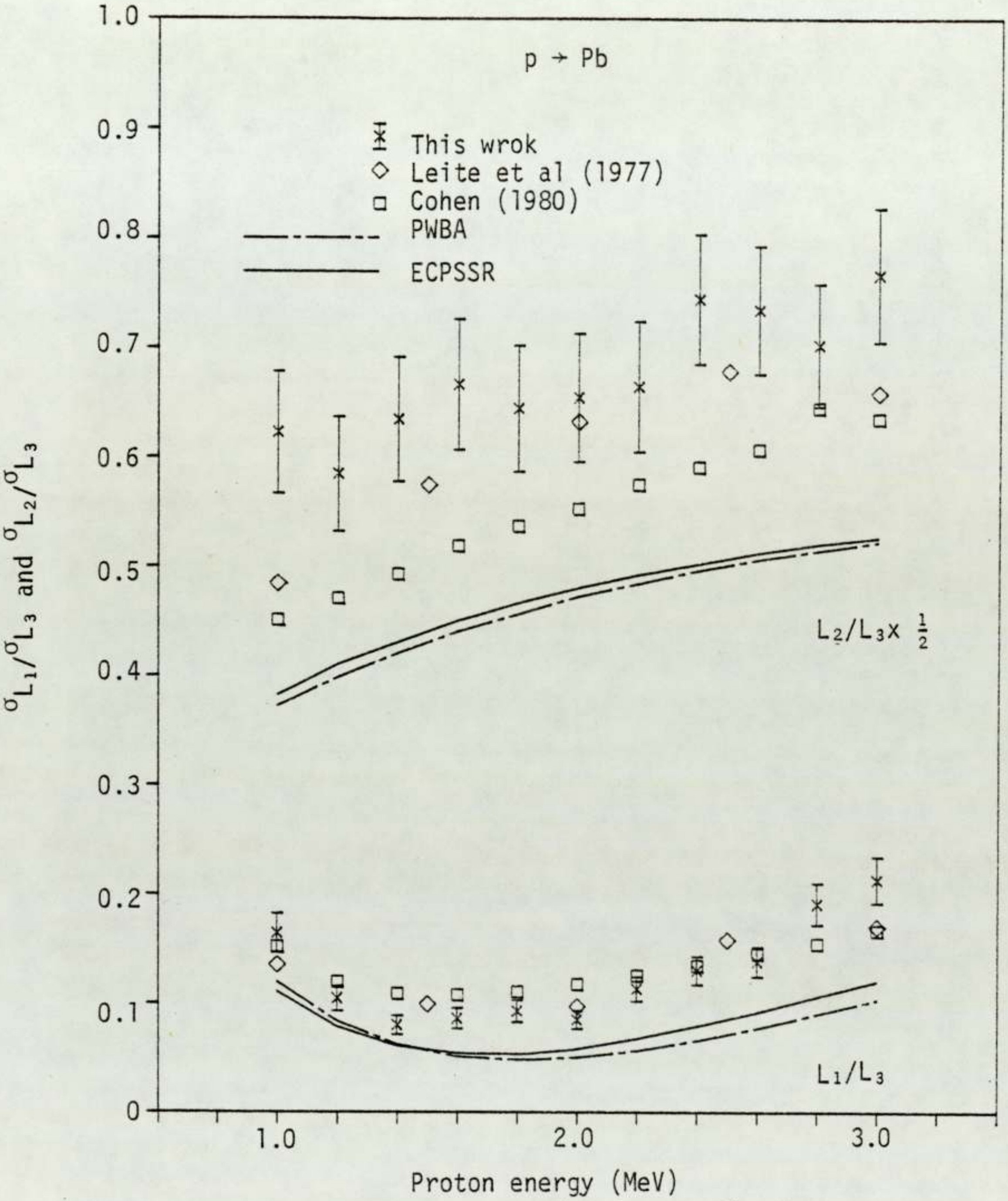

Figure 6.121. Experimental $\sigma_{L_1}/\sigma_{L_3}$ and $\sigma_{L_2}/\sigma_{L_3}$ ratio for proton impact on Pb.

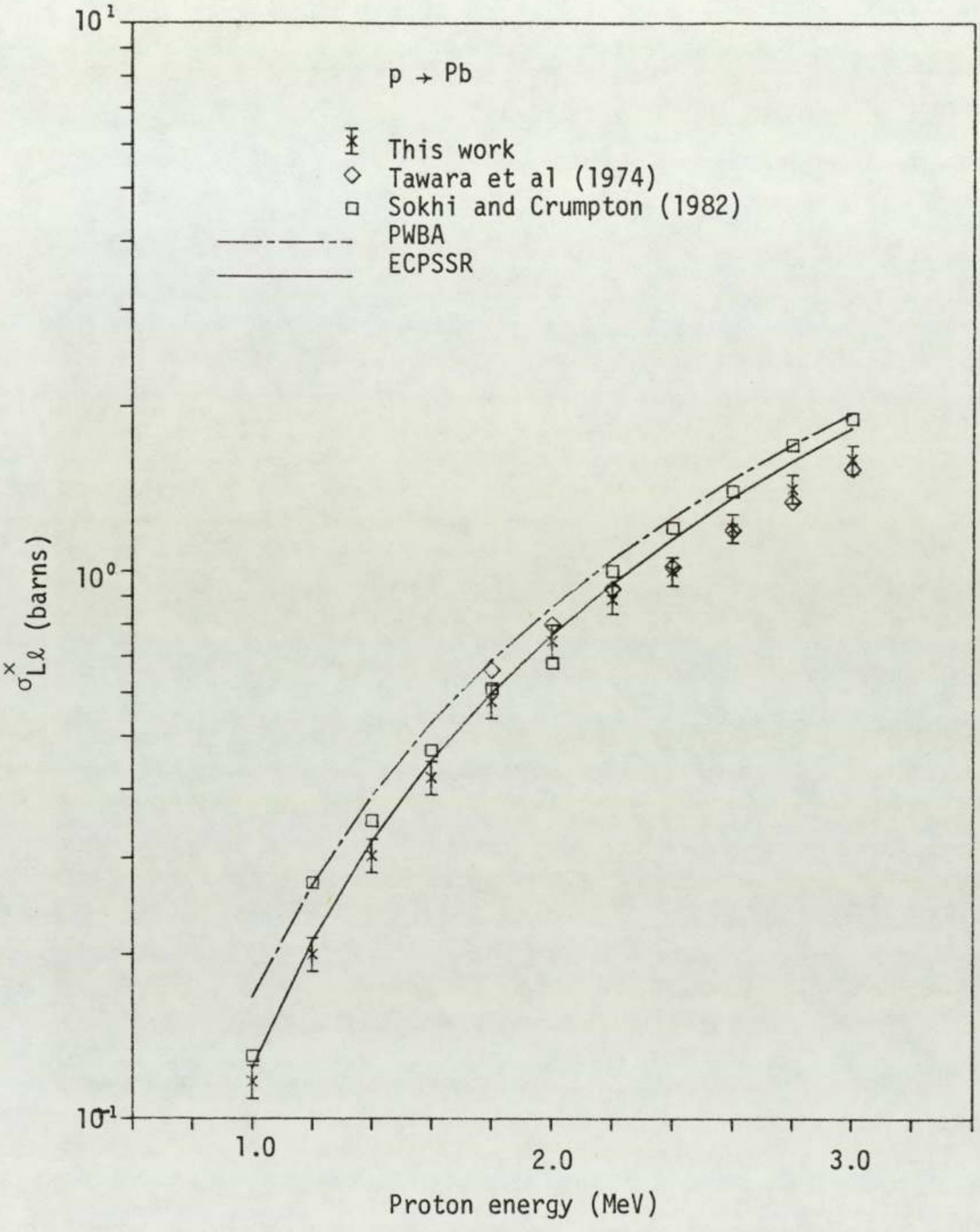

Figure 6.122. Experimental Lℓ x-ray production cross section for proton impact on Pb.

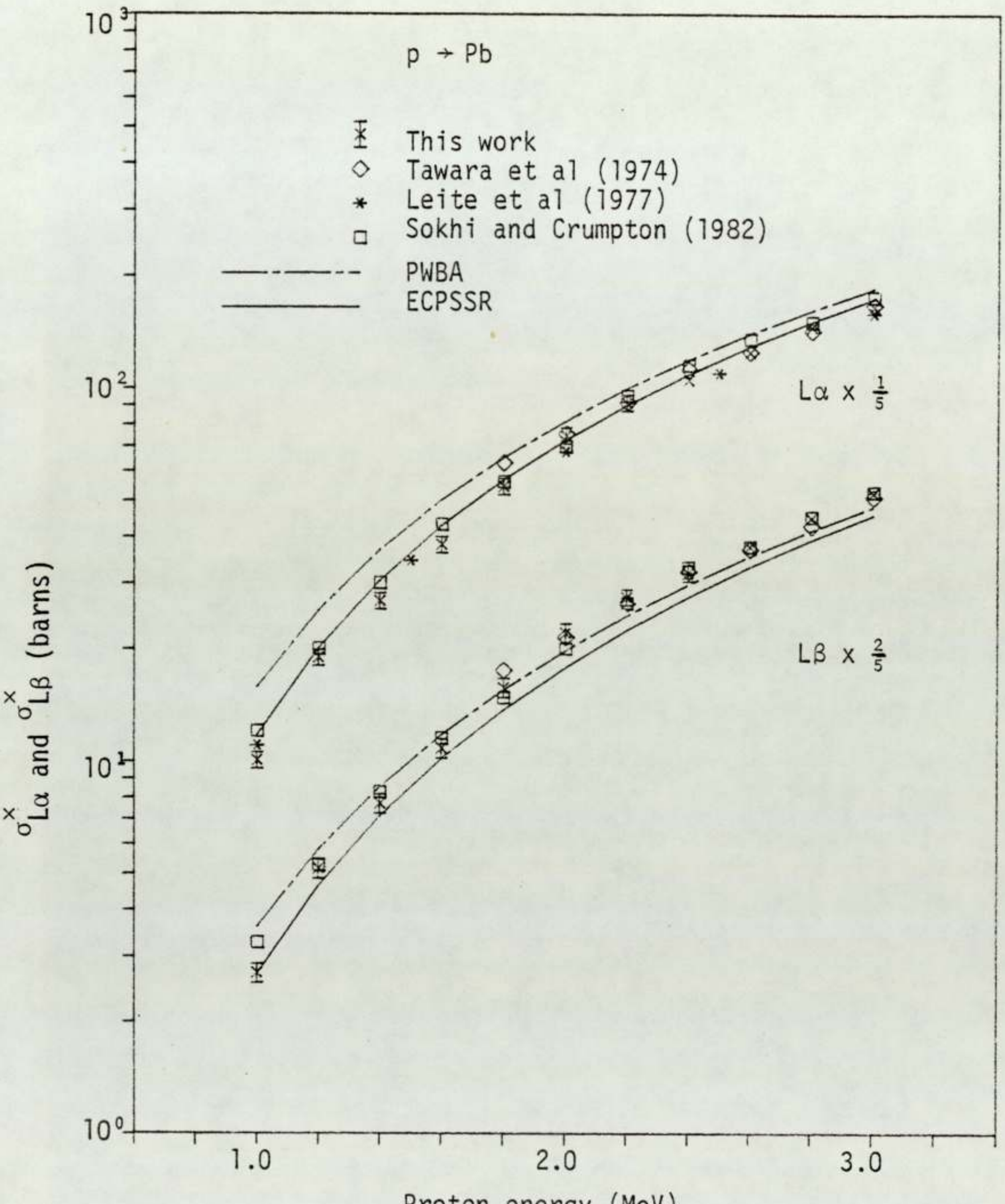

Figure 6.123. Experimental Lα and Lβ x-ray production cross sections for proton impact on Pb.

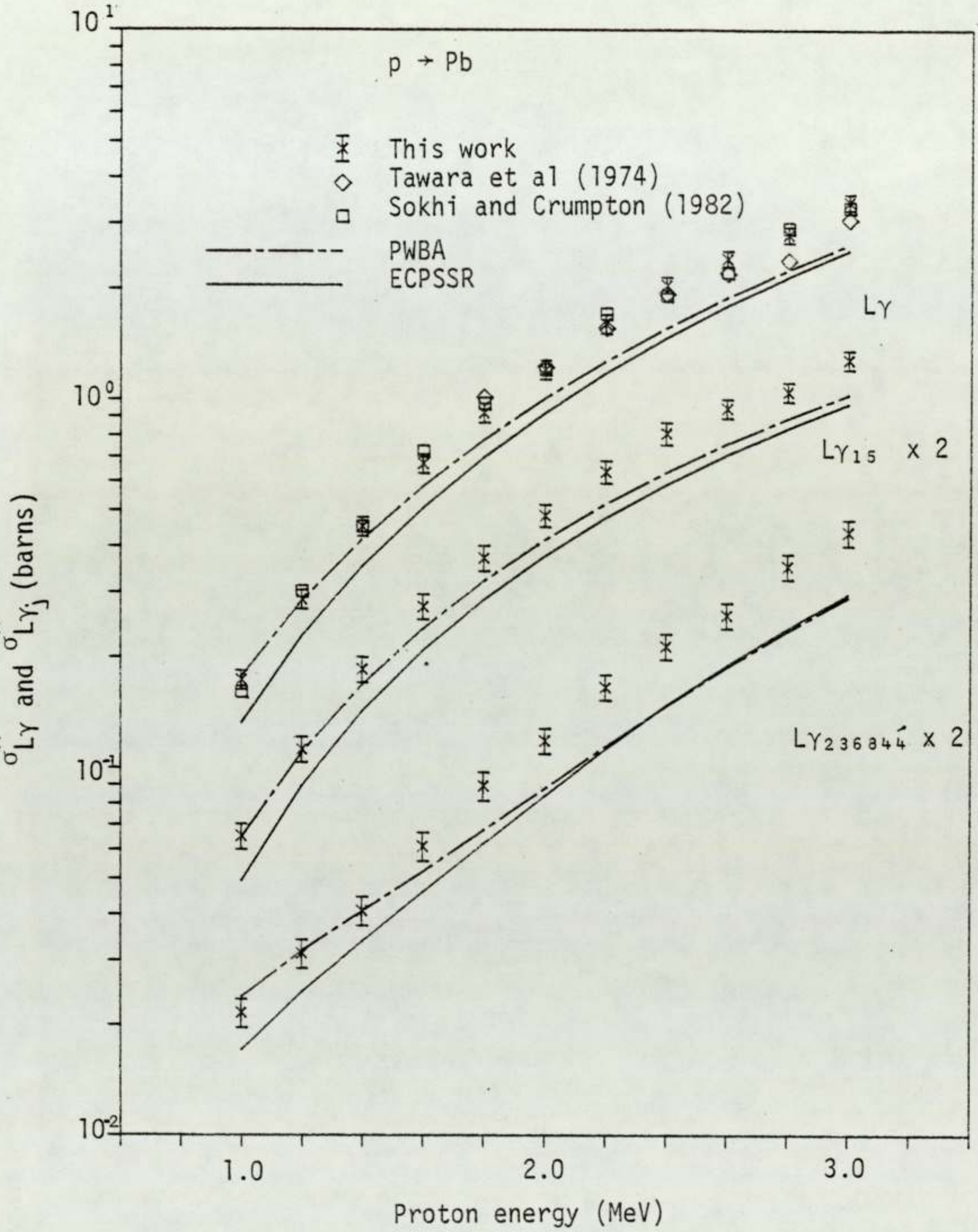

Figure 6.124. Experimental total Lγ and partial $L\gamma_j$ x-ray production cross sections for proton impact on Pb.

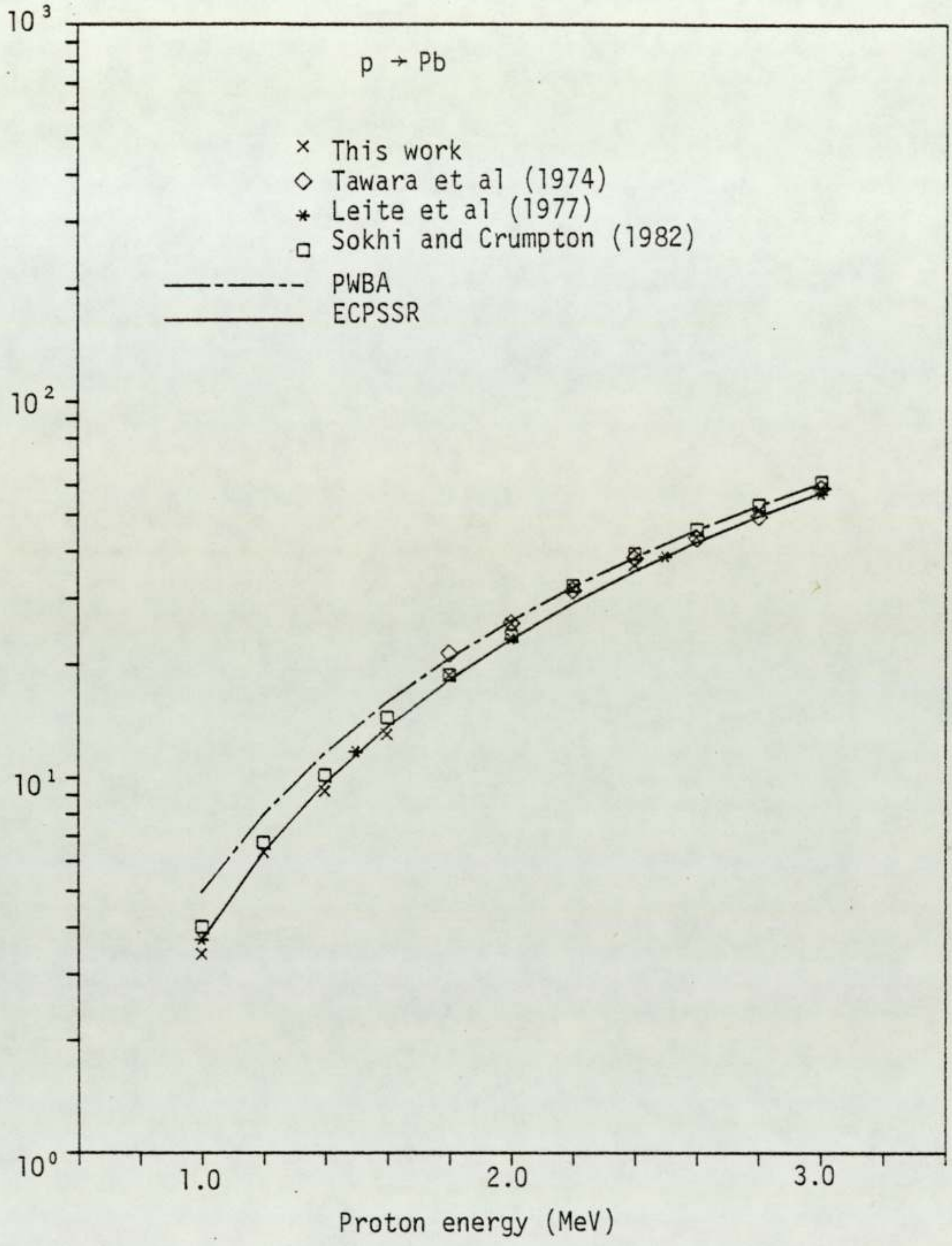

Figure 6.125. Experimental total L shell x-ray production cross section for proton impact on Pb.

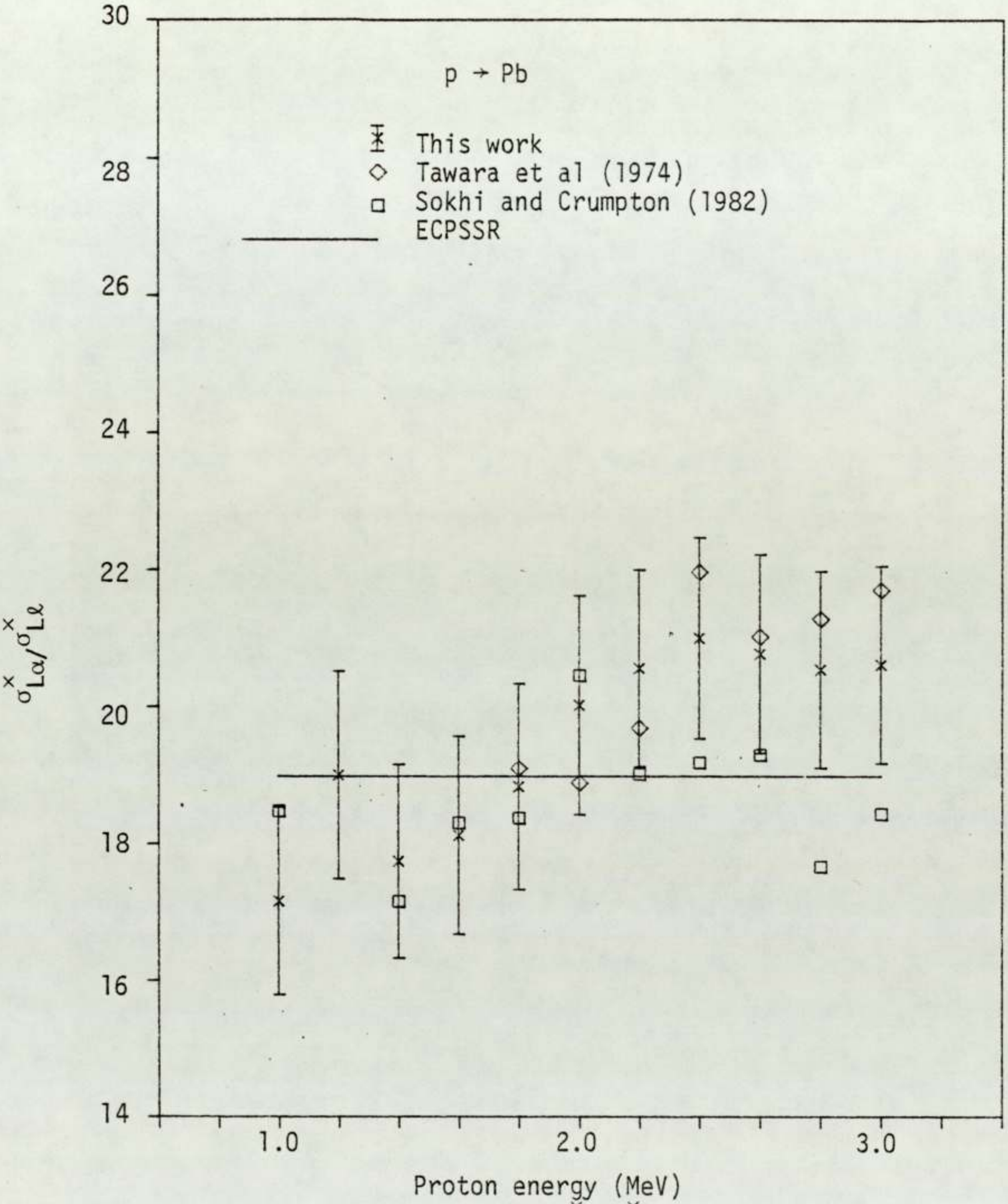

Figure 6.126. Experimental $\sigma^{x}_{L\alpha}/\sigma^{x}_{L\ell}$ ratio for proton impact on Pb.

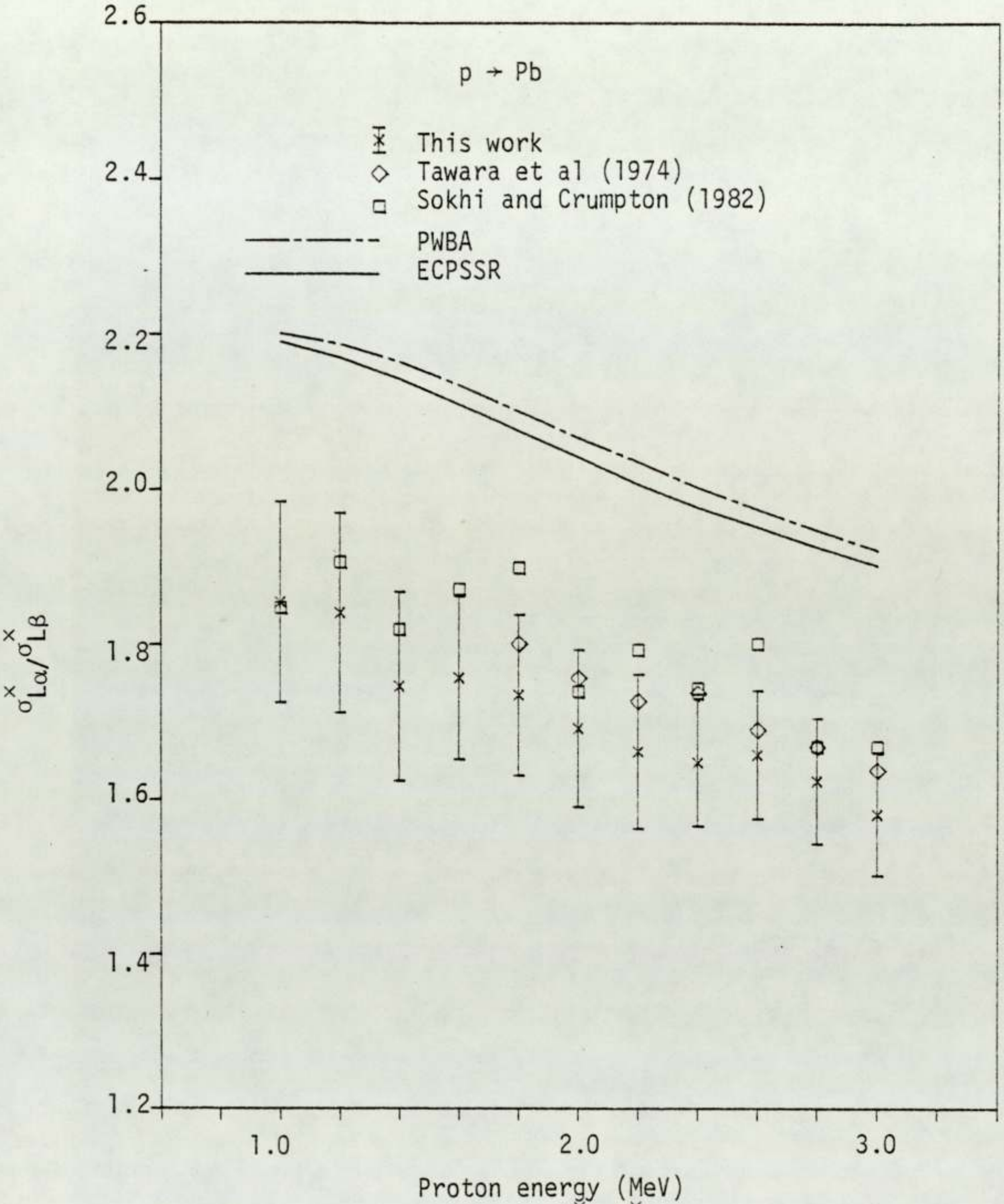

Figure 6.127. Experimental $\sigma^x_{L\alpha}/\sigma^x_{L\beta}$ ratio for proton impact on Pb.

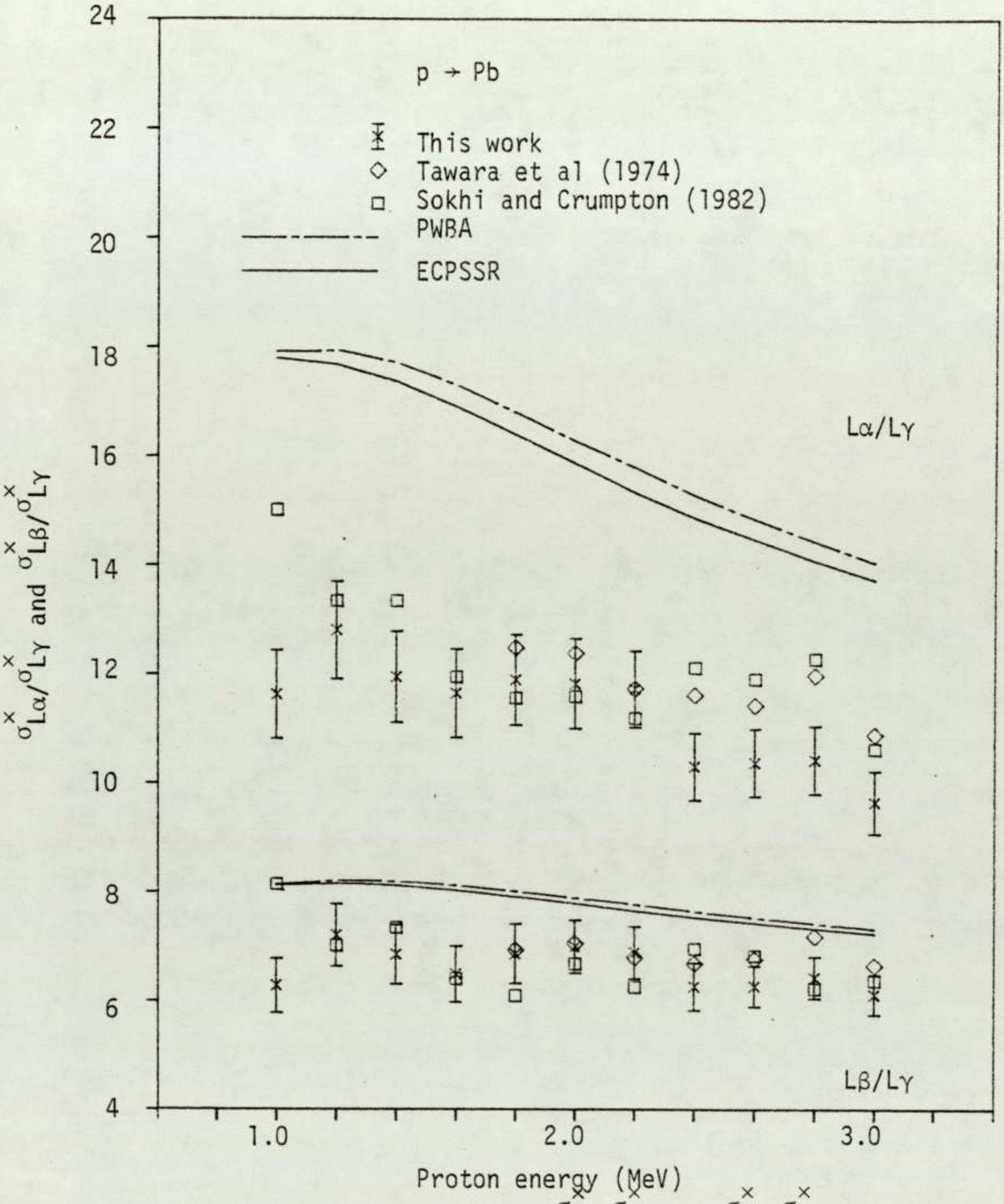

Figure 6.128. Experimental $\sigma^{x}_{L\alpha}/\sigma^{x}_{L\gamma}$ and $\sigma^{x}_{L\beta}/\sigma^{x}_{L\gamma}$ ratios for proton impact on Pb.

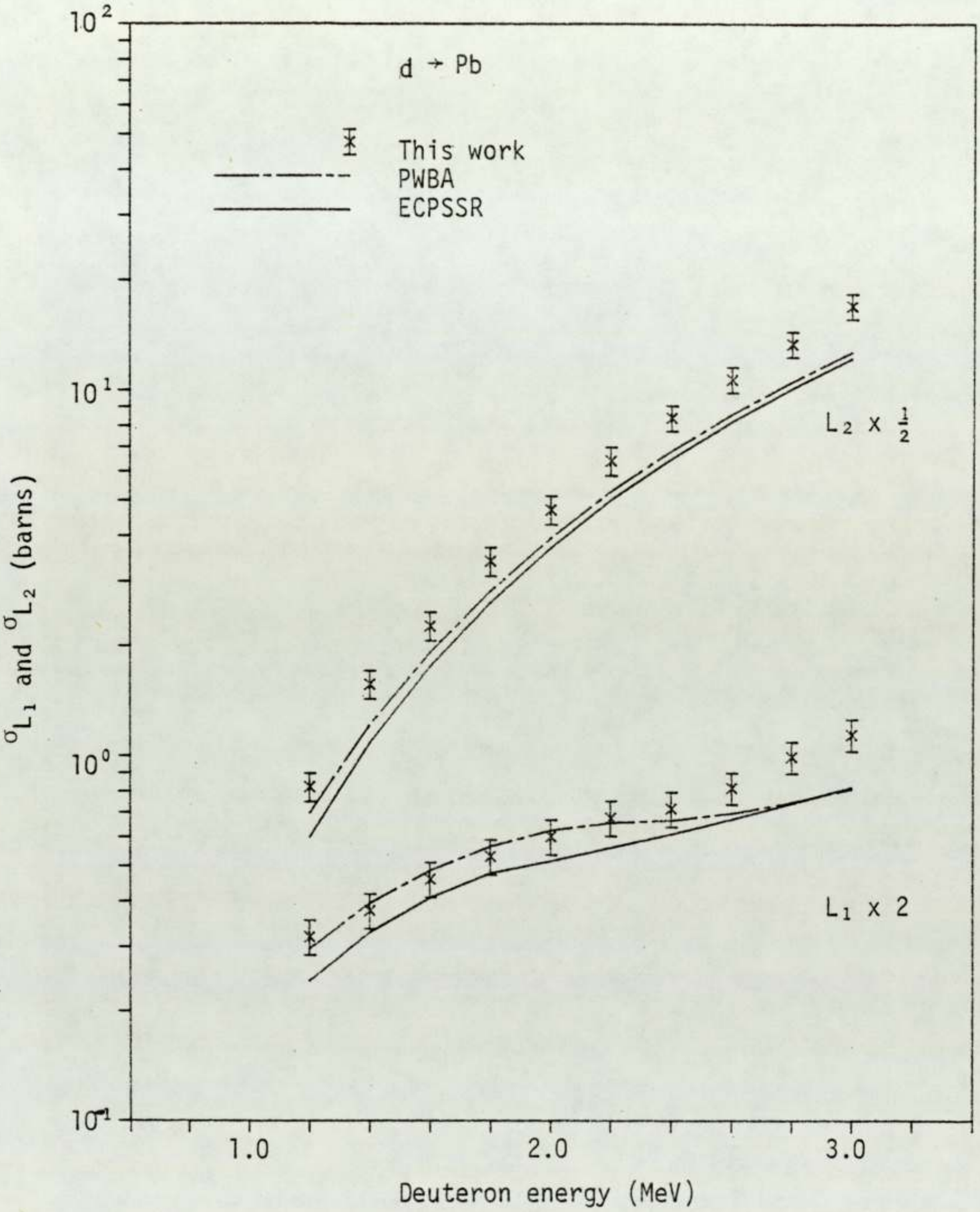

Figure 6.129. Experimental L_1 and L_2 subshell ionisation cross sections for deuteron impact on Pb.

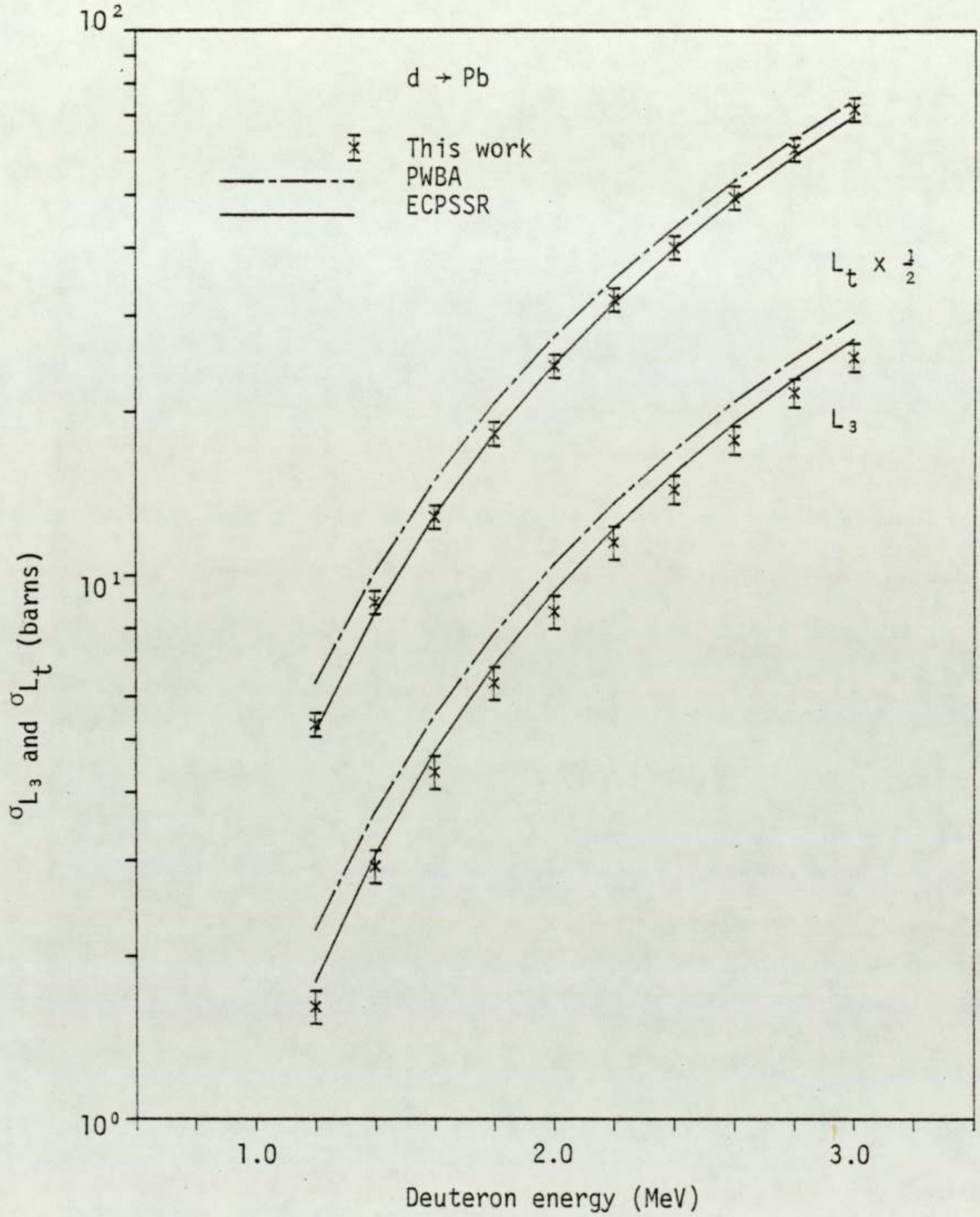

Figure 6.130. Experimental L_3 subshell and total L shell ionisation cross sections for deuteron impact on Pb.

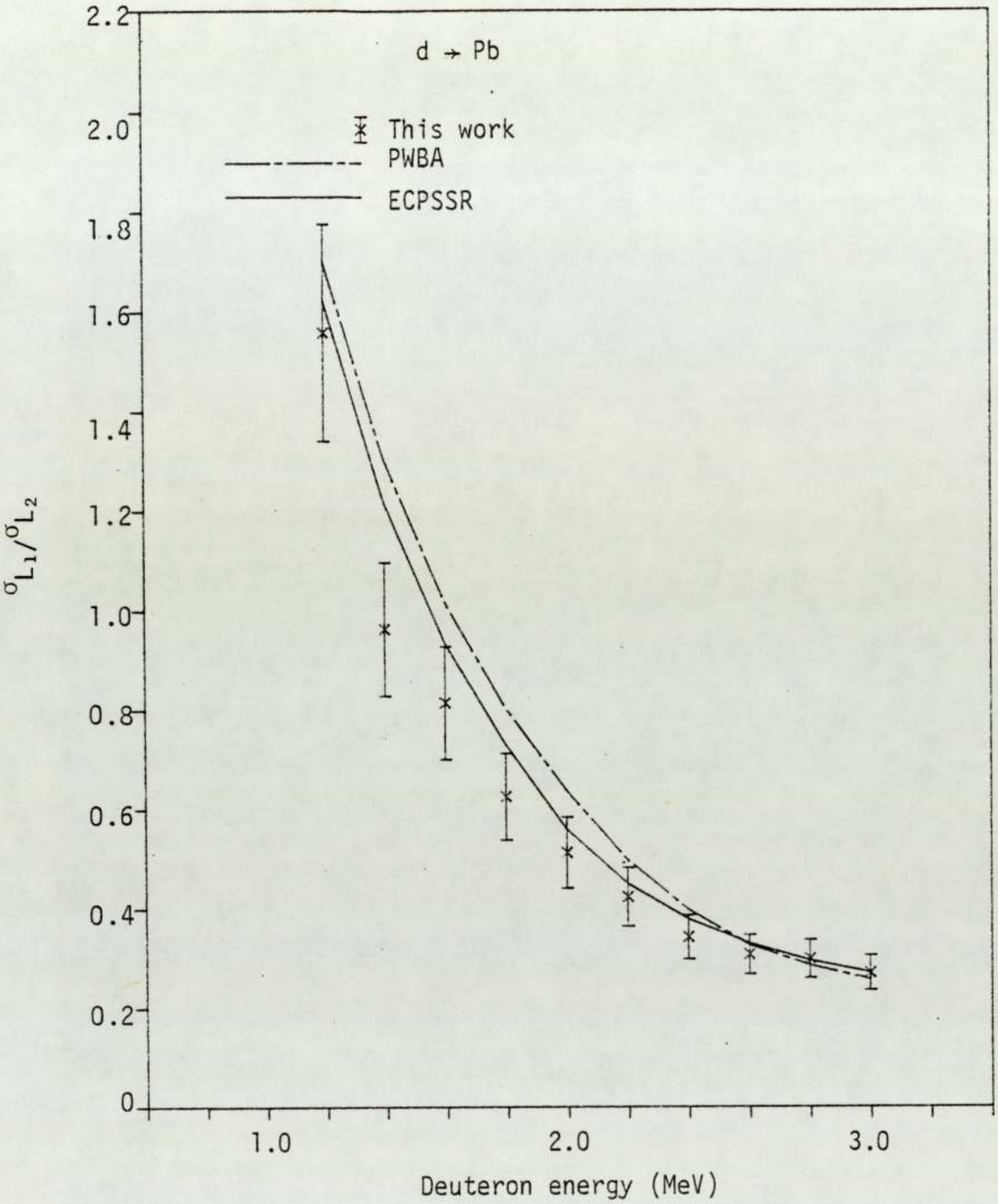

Figure 6.131. Experimental $\sigma_{L_1}/\sigma_{L_2}$ ratio for deuteron impact on Pb.

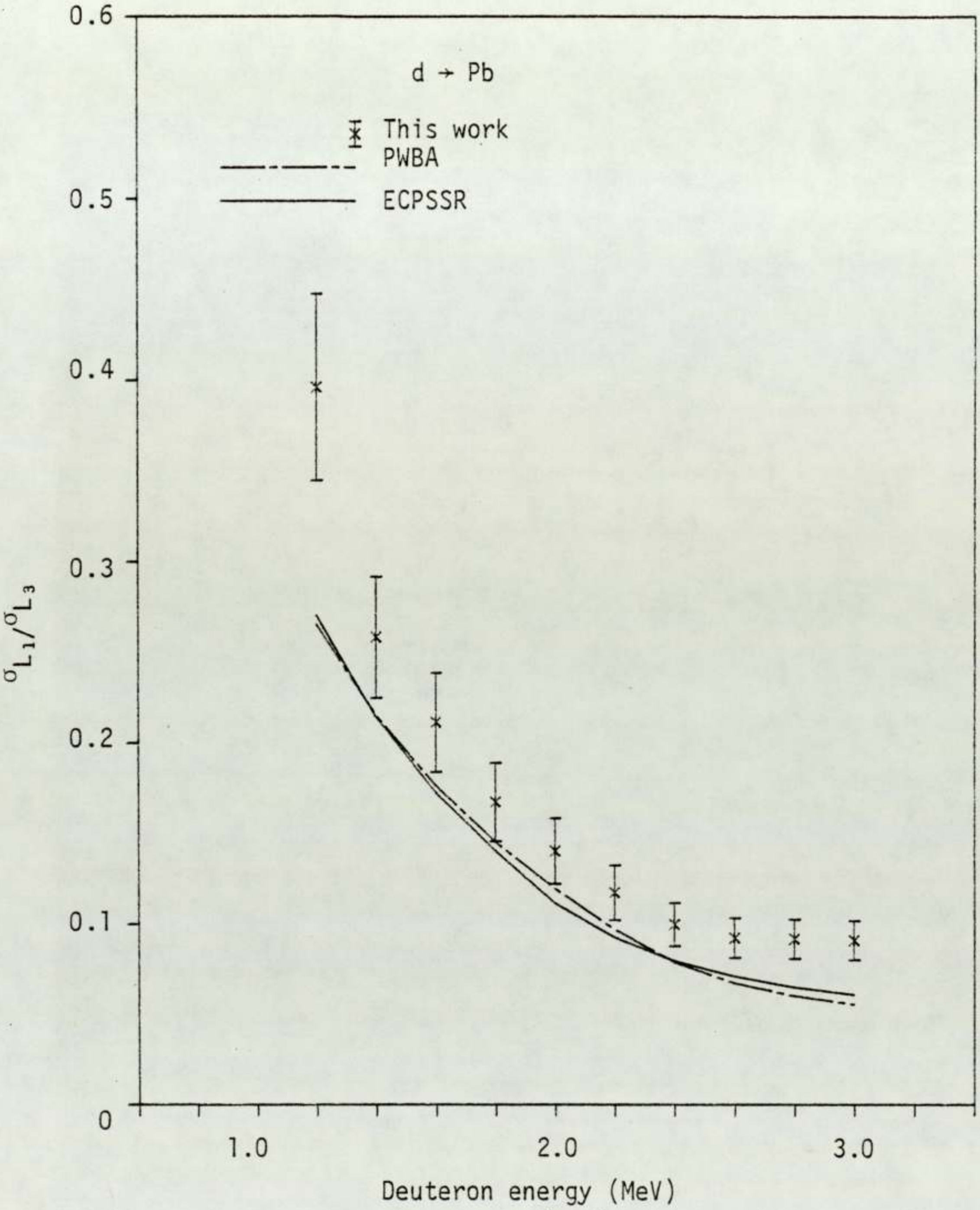

Figure 6.132. Experimental $\sigma_{L_1}/\sigma_{L_3}$ ratio for deuteron impact on Pb.

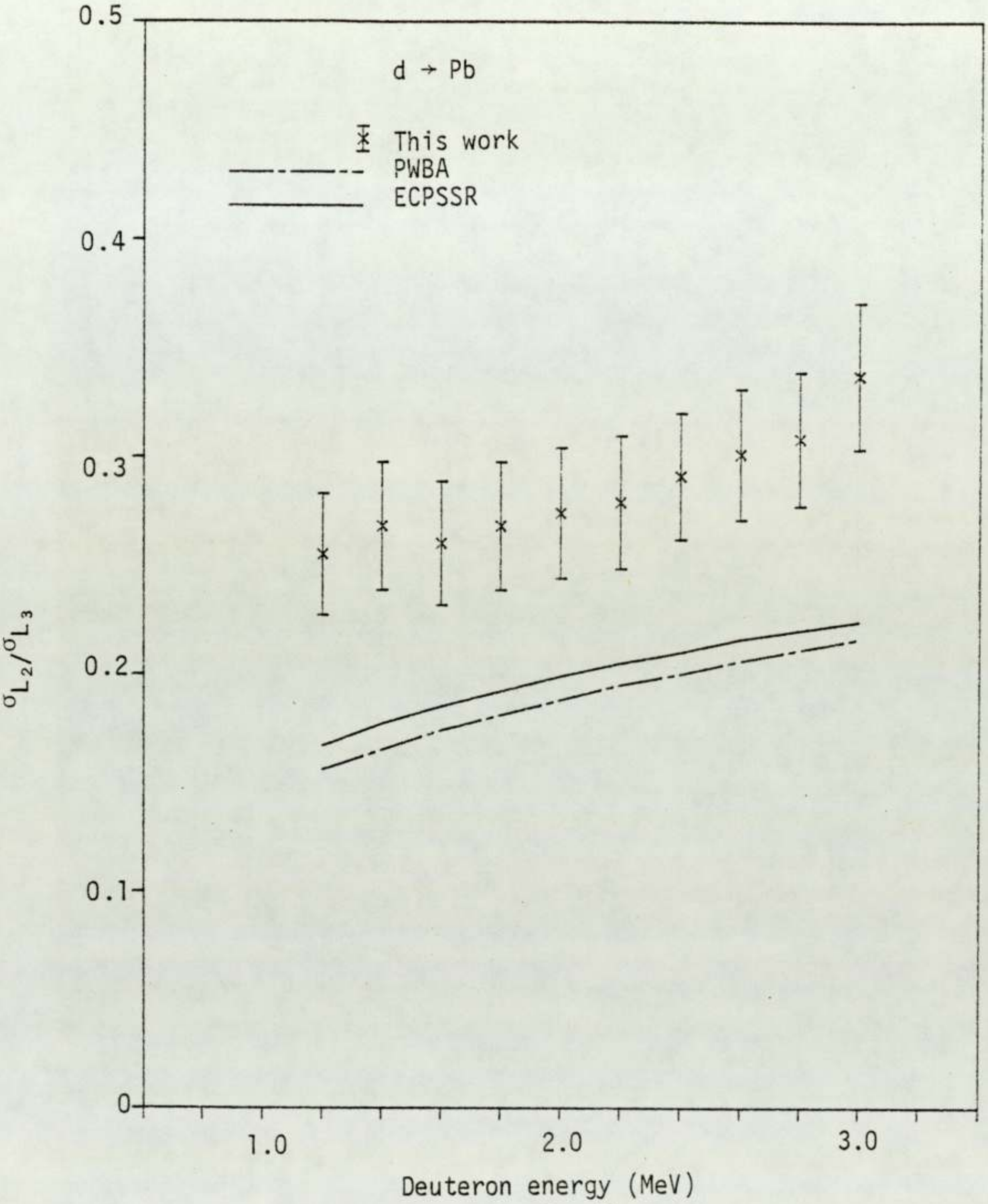

Figure 6.133. Experimental $\sigma_{L_2}/\sigma_{L_3}$ ratio for deuteron impact on Pb.

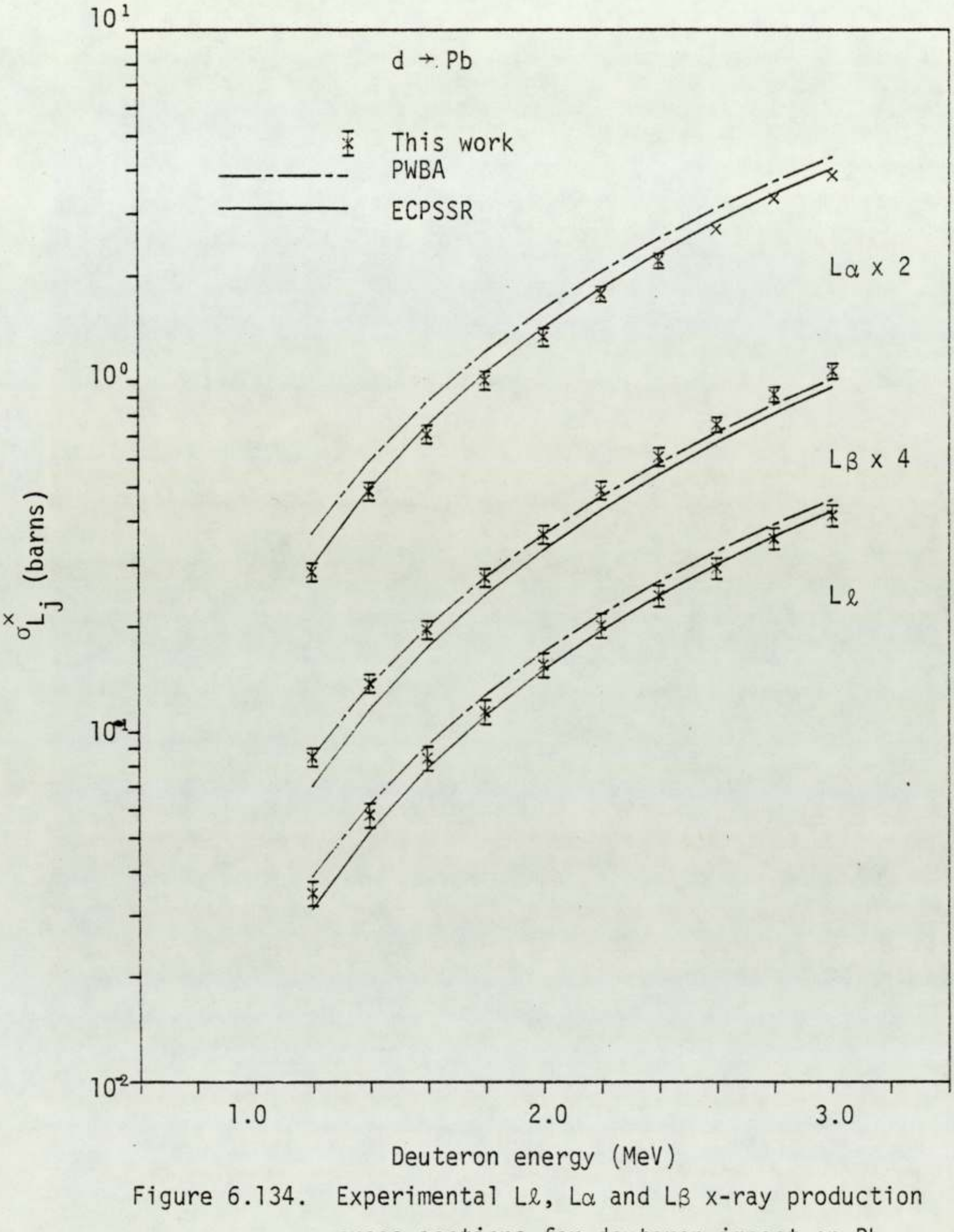

Figure 6.134. Experimental Lℓ, Lα and Lβ x-ray production cross sections for deuteron impact on Pb.

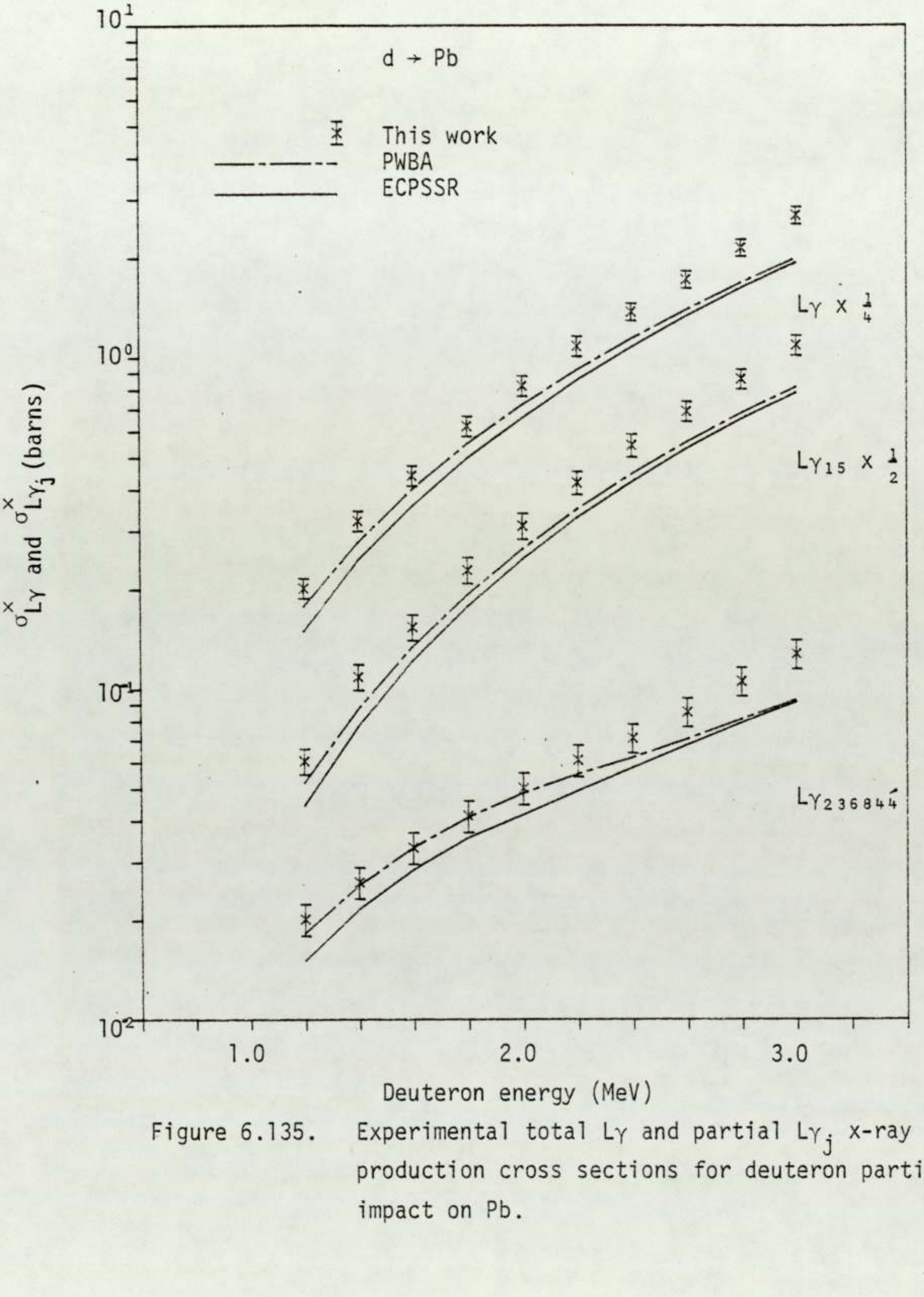

Figure 6.135. Experimental total Lγ and partial $L\gamma_j$ x-ray production cross sections for deuteron particle impact on Pb.

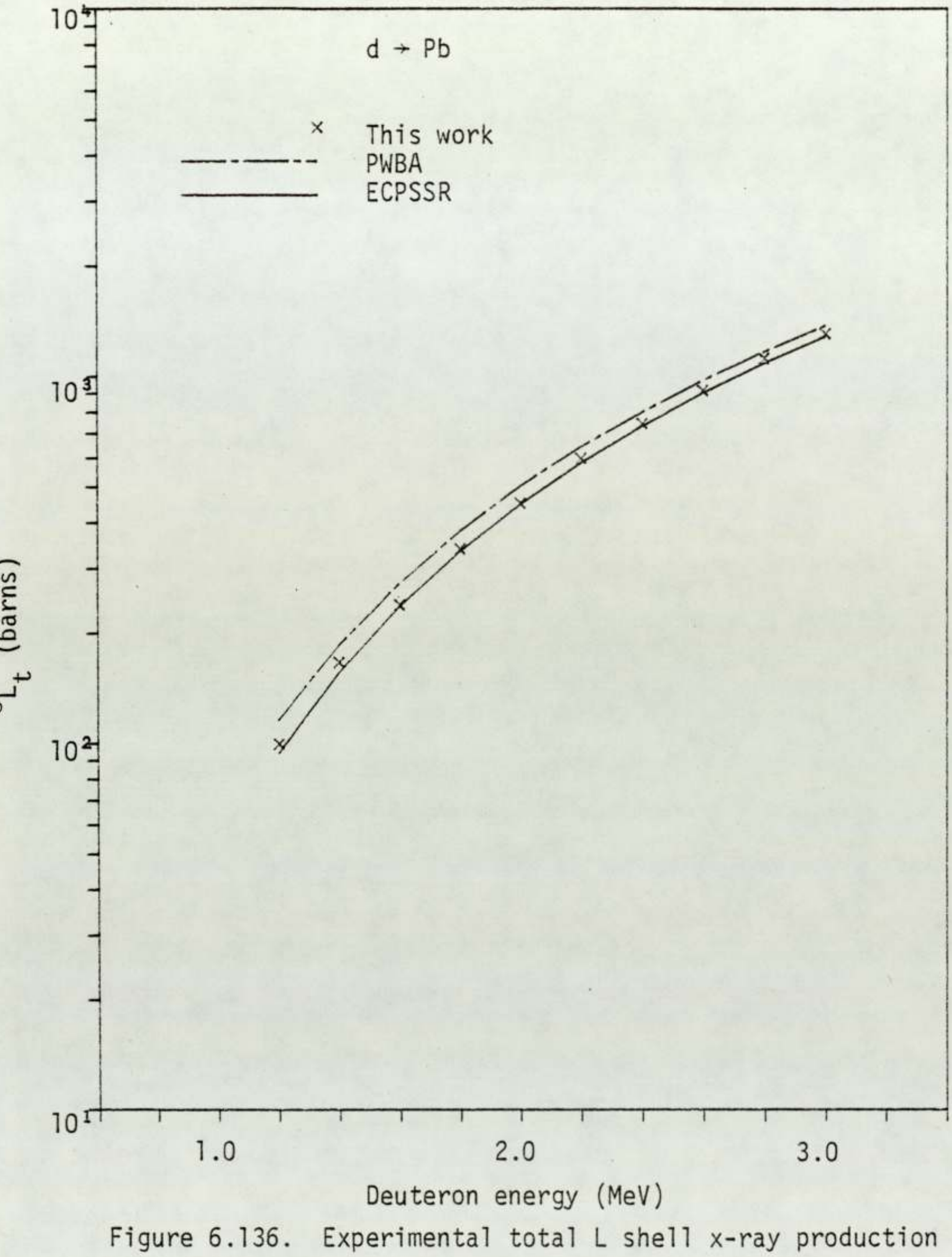

Figure 6.136. Experimental total L shell x-ray production cross section for deuteron impact on Pb.

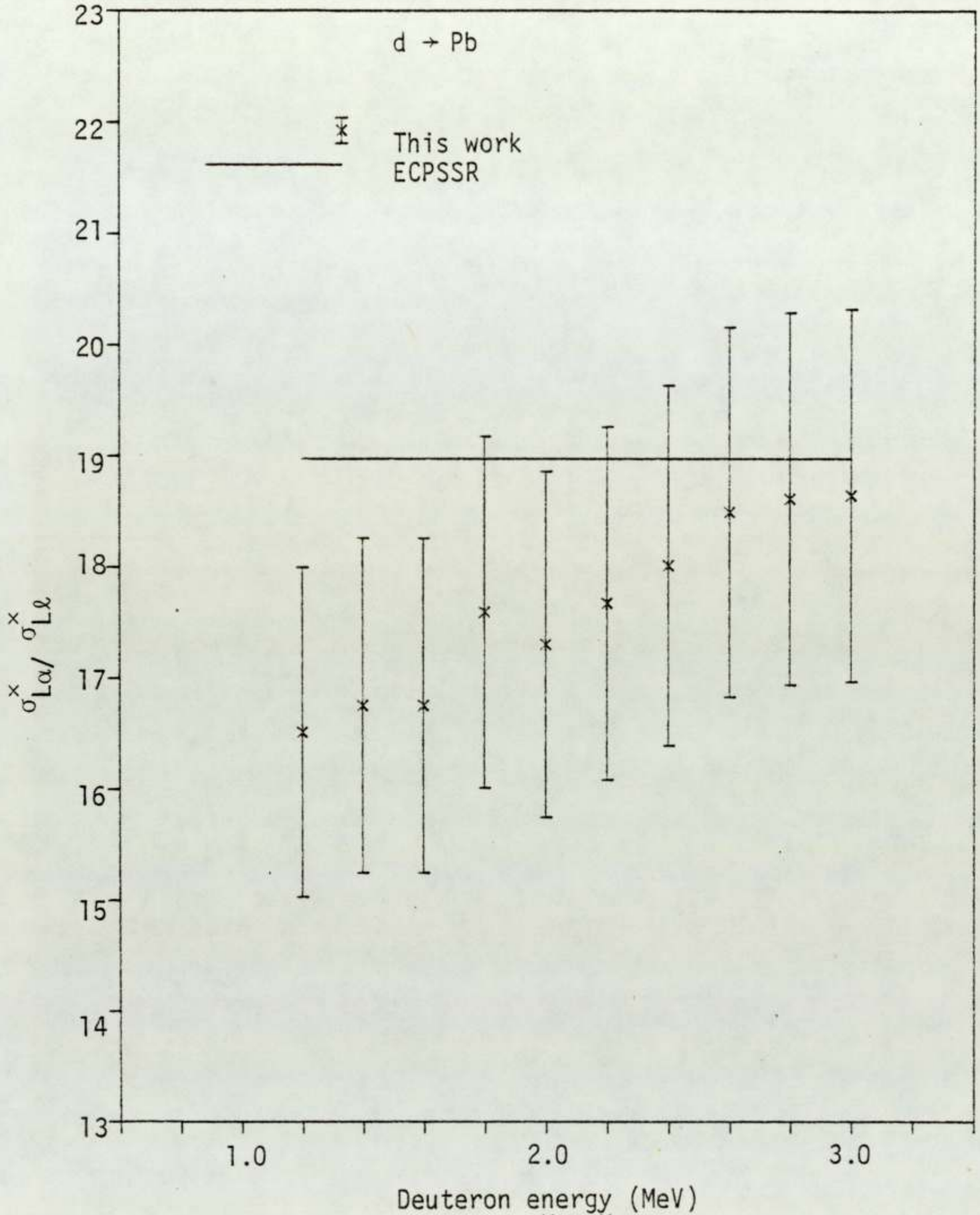

Figure 6.137. Experimental $\sigma^x_{L\alpha}/\sigma^x_{L\ell}$ ratio for deuteron impact on Pb.

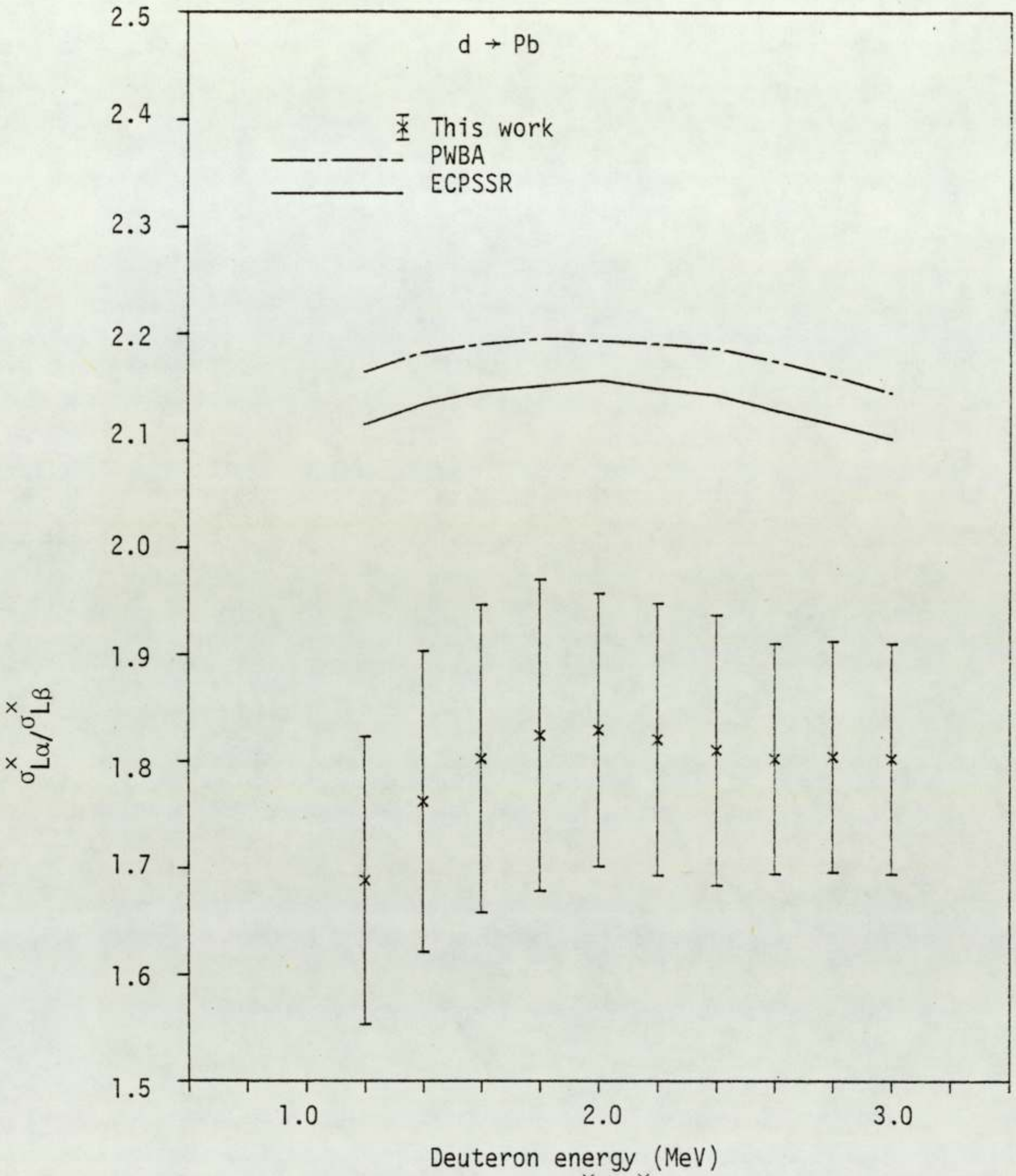

Figure 6.138. Experimental $\sigma^x_{L\alpha}/\sigma^x_{L\beta}$ ratio for deuteron impact on Pb.

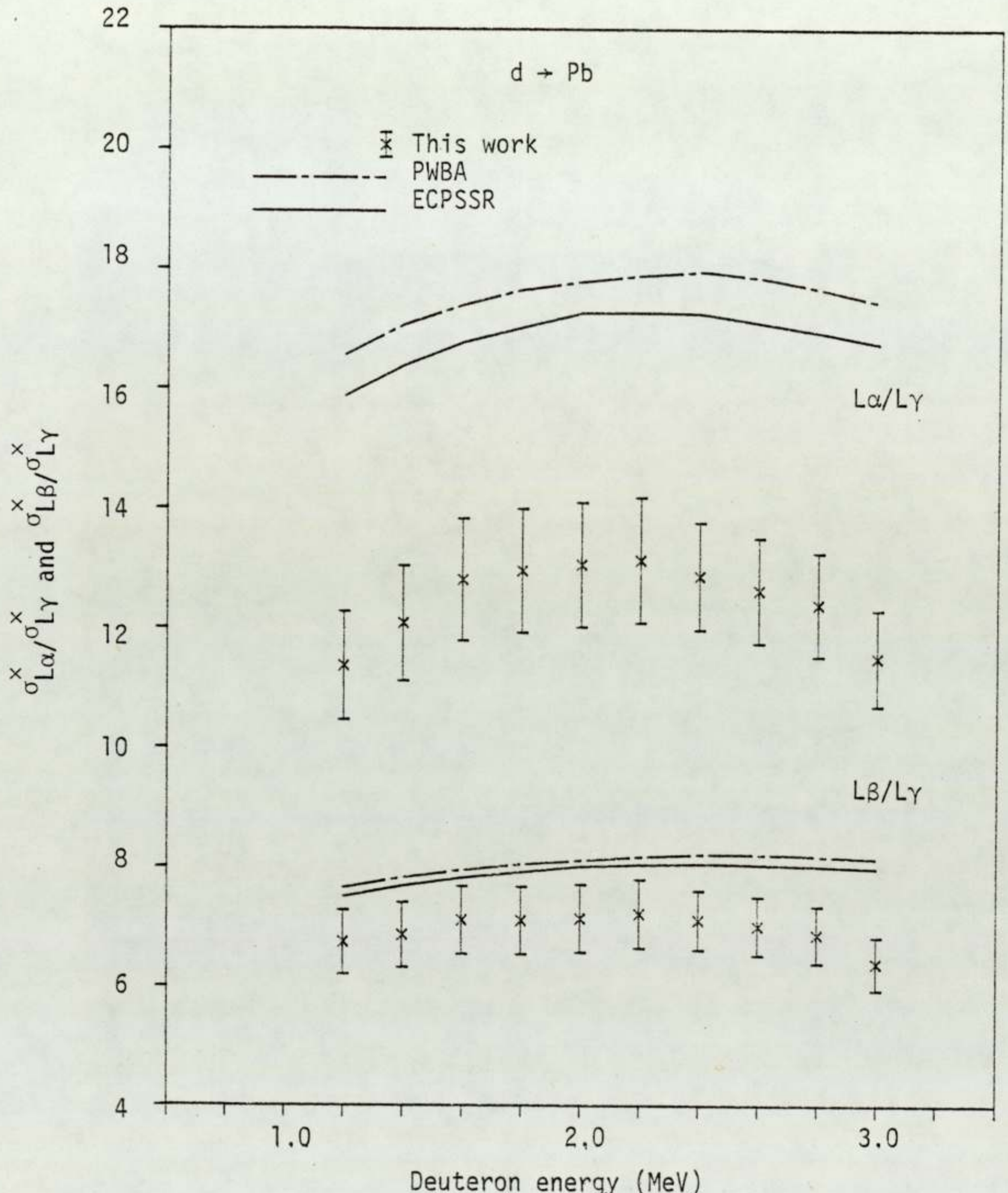

Figure 6.139. Experimental $\sigma^{x}_{L\alpha}/\sigma^{x}_{L\gamma}$ and $\sigma^{x}_{L\beta}/\sigma^{x}_{L\gamma}$ ratios for deuteron impact on Pb.

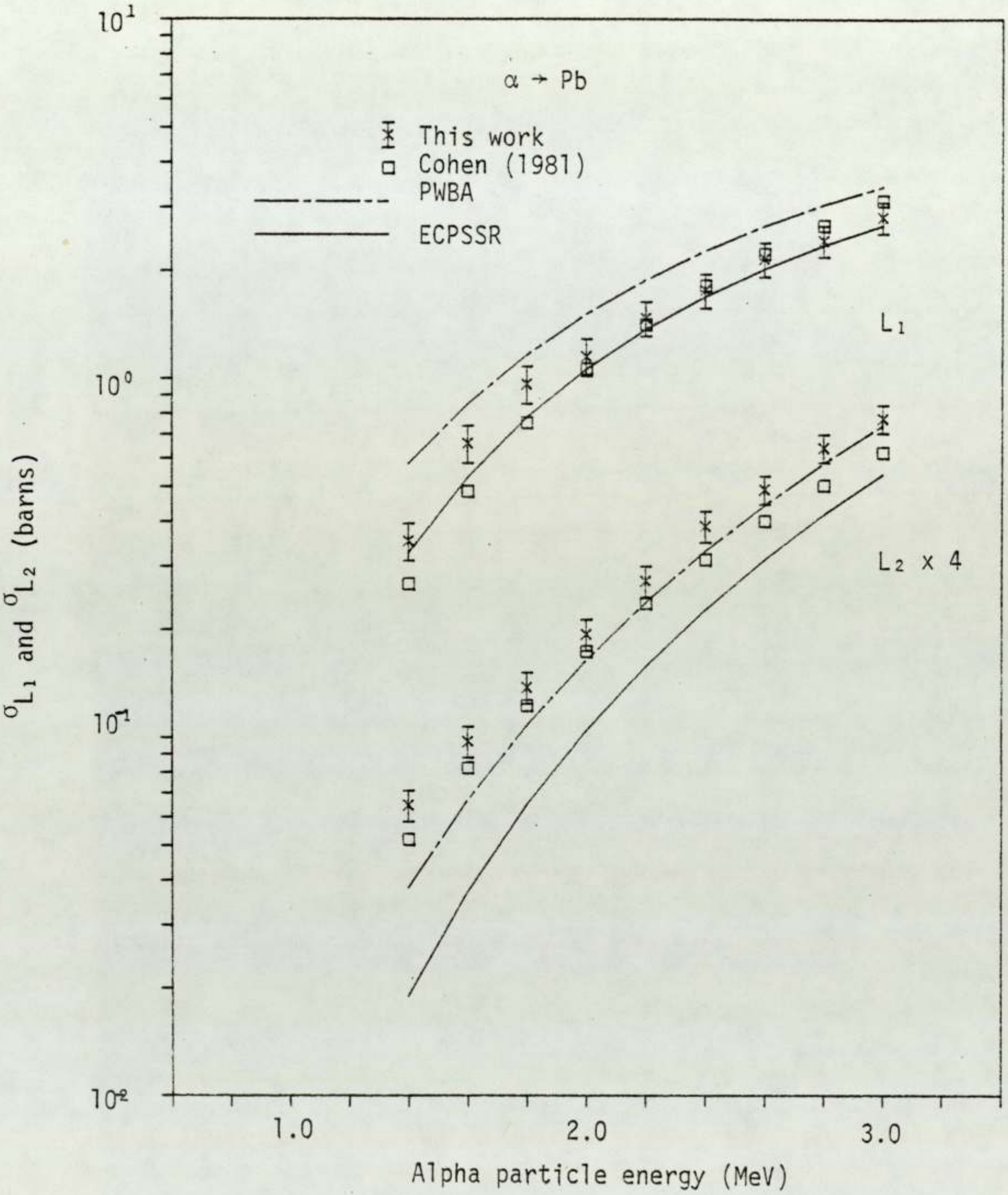

Figure 6.140. Experimental L_1 and L_2 subshell ionisation cross sections for alpha particle impact on Pb.

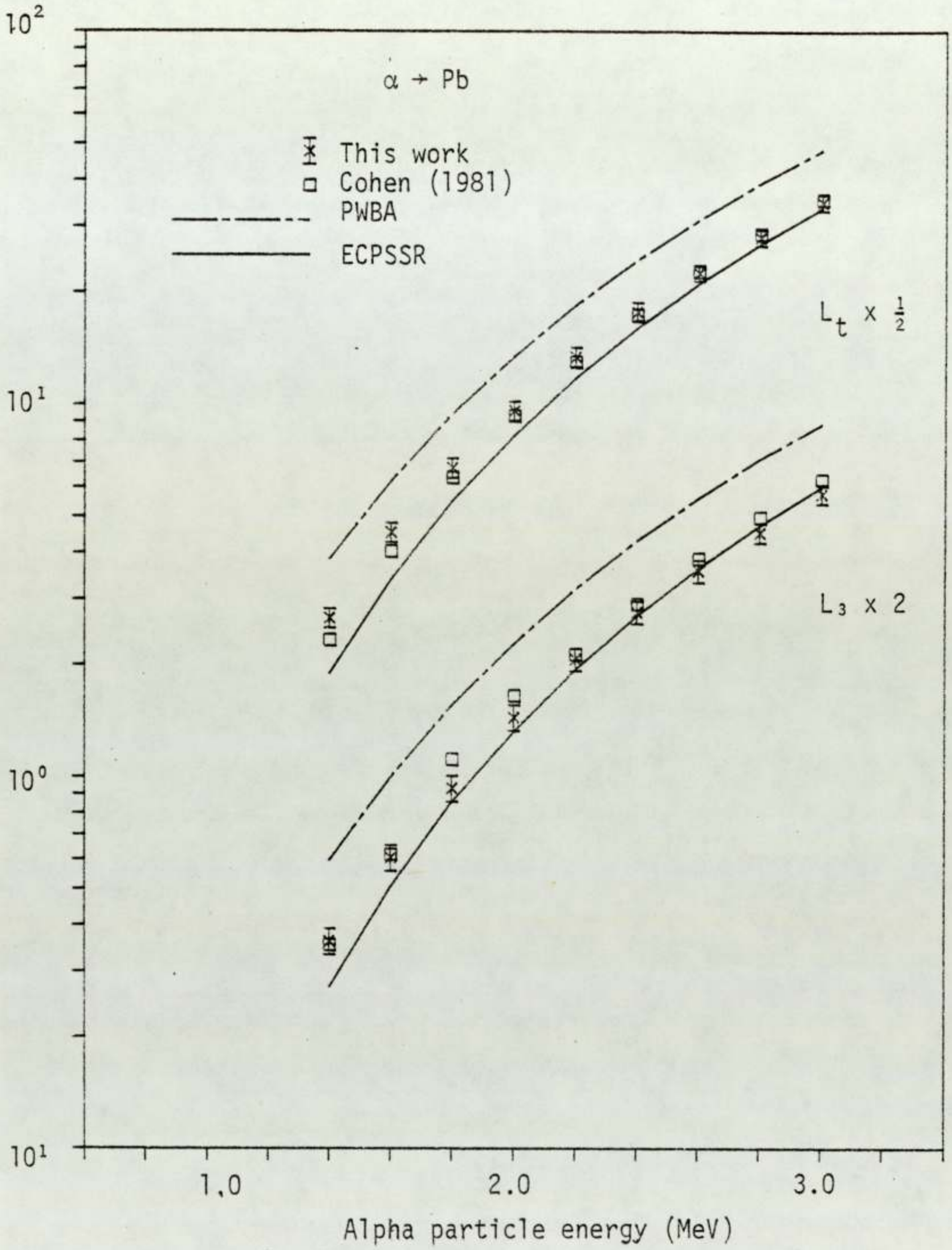

Figure 6.141. Experimental L_3 subshell and total L shell ionisation cross sections for alpha particle impact on Pb.

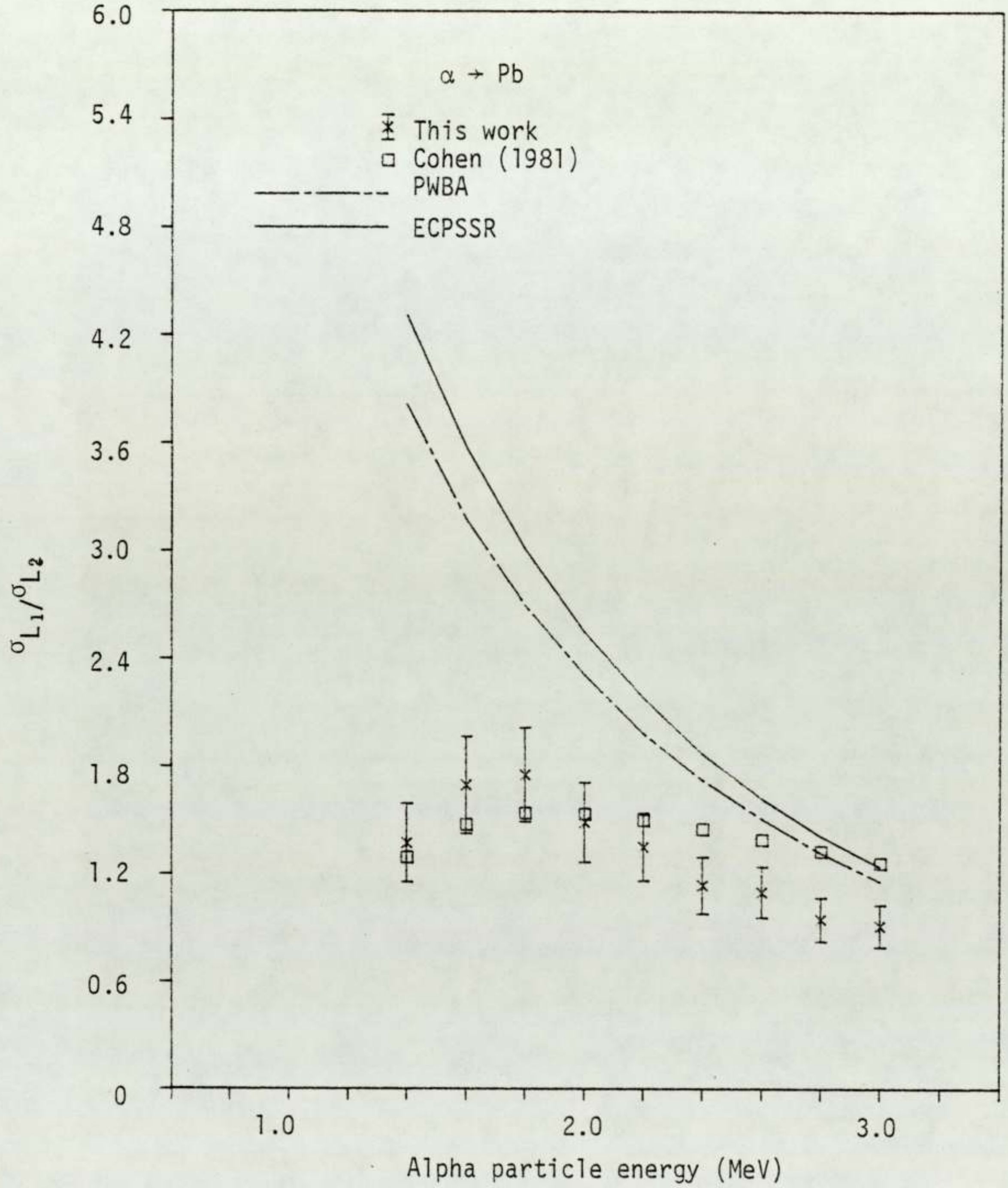

Figure 6.142. Experimental $\sigma_{L_1}/\sigma_{L_2}$ ratio for alpha particle impact on Pb.

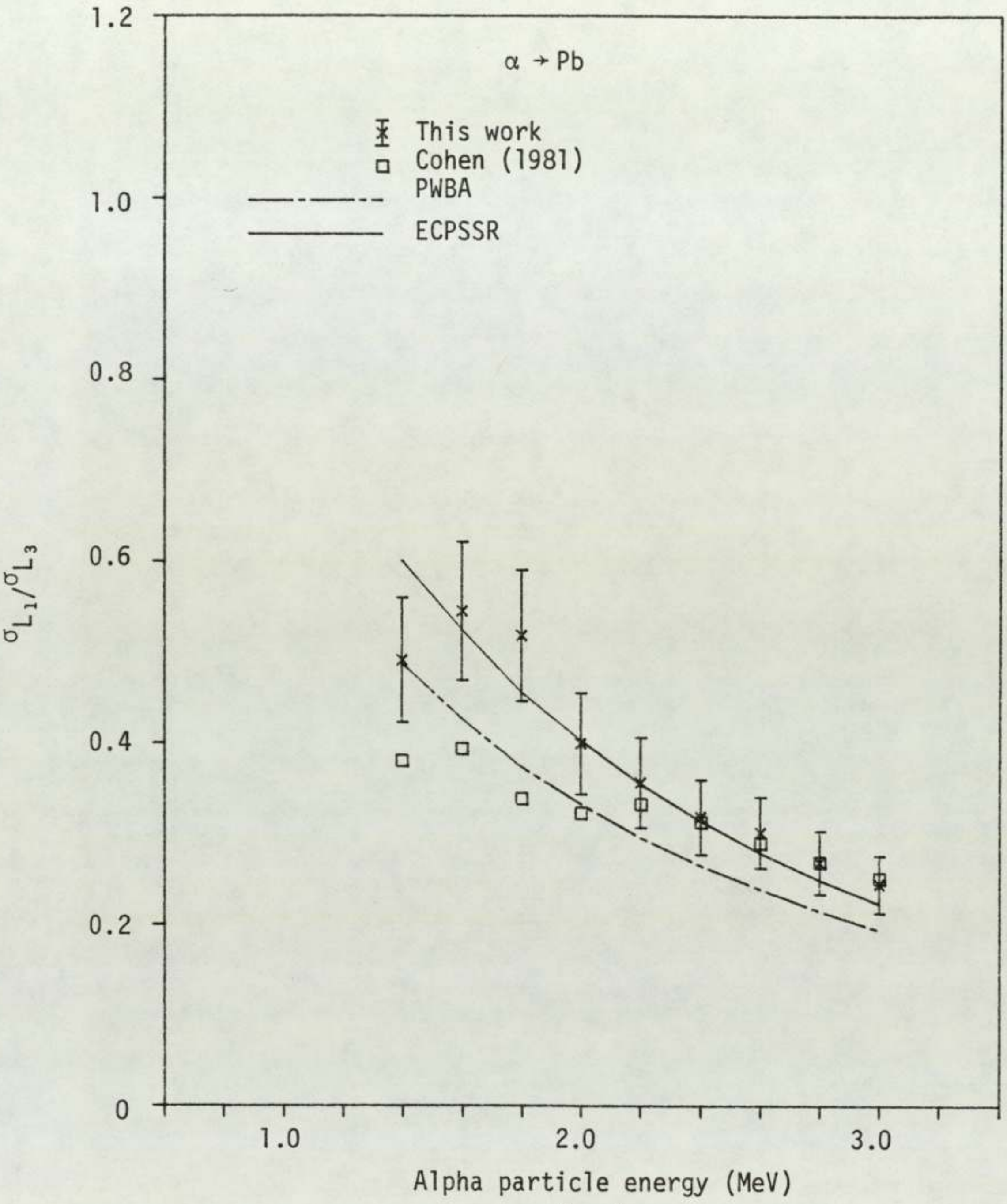

Figure 6.143. Experimental $\sigma_{L_1}/\sigma_{L_3}$ ratio for alpha particle impact on Pb

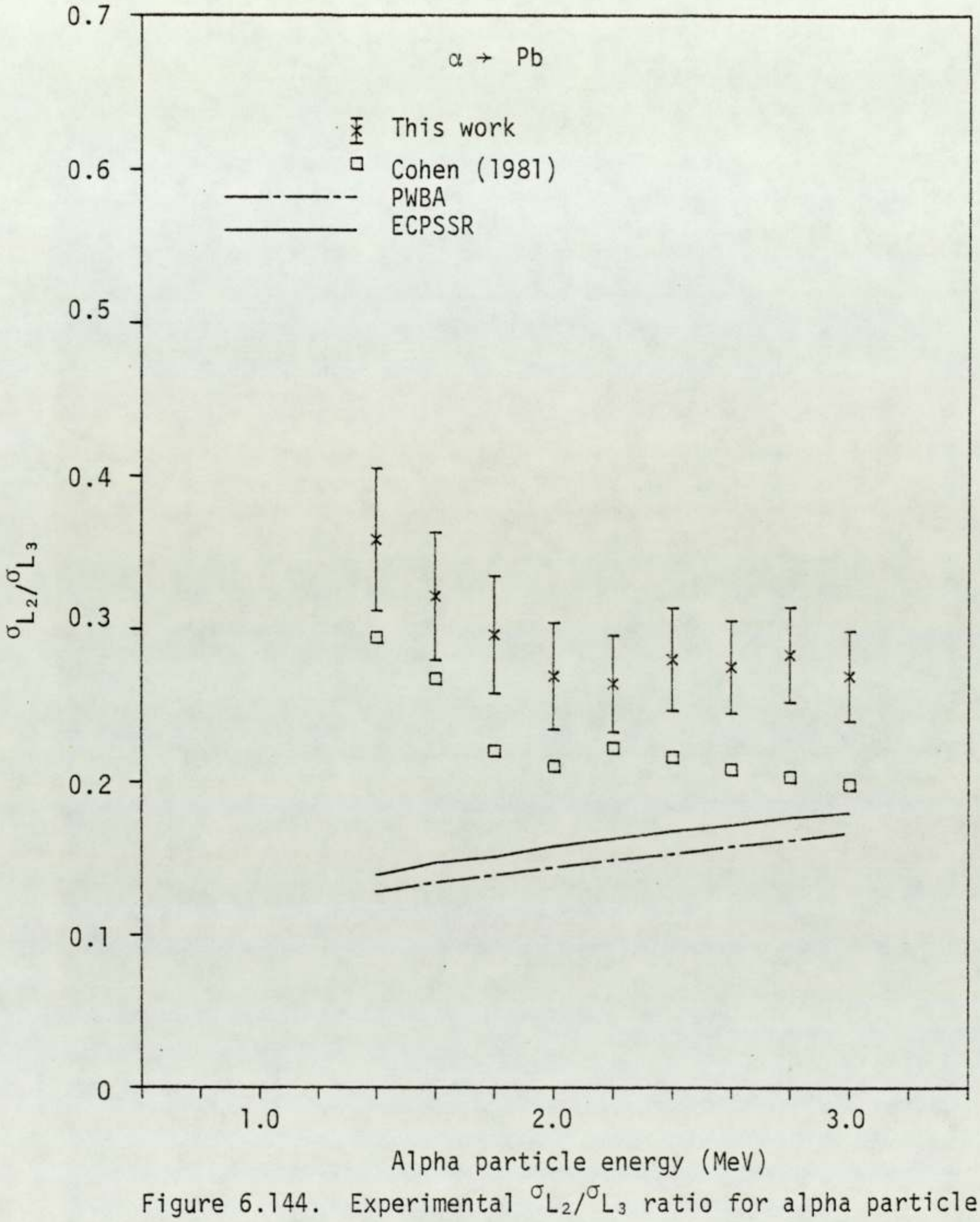

Figure 6.144. Experimental $\sigma_{L_2}/\sigma_{L_3}$ ratio for alpha particle impact on Pb.

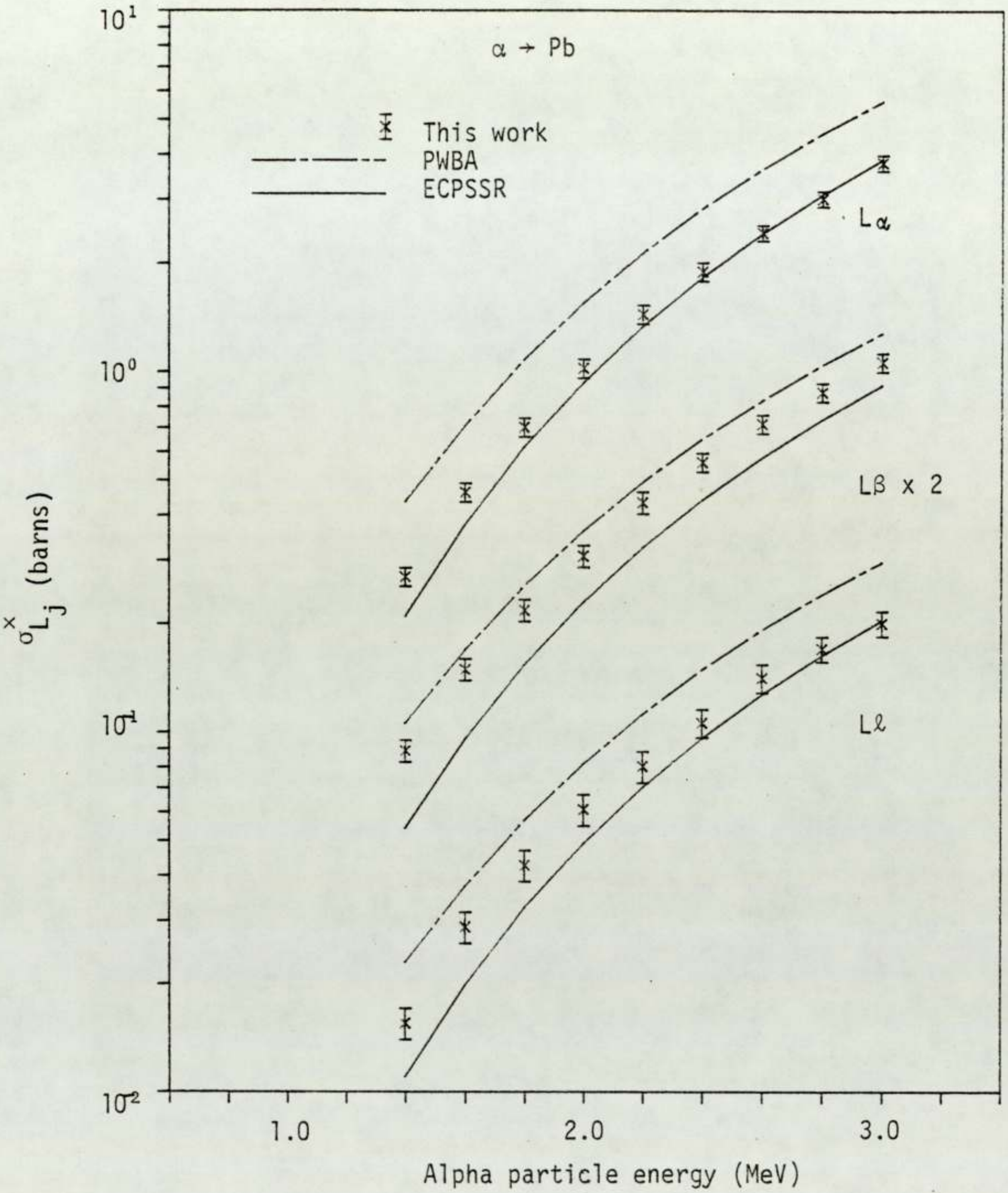

Figure 6.145. Experimental $L\ell$, $L\alpha$ and $L\beta$ x-ray production cross sections for alpha particle impact on Pb.

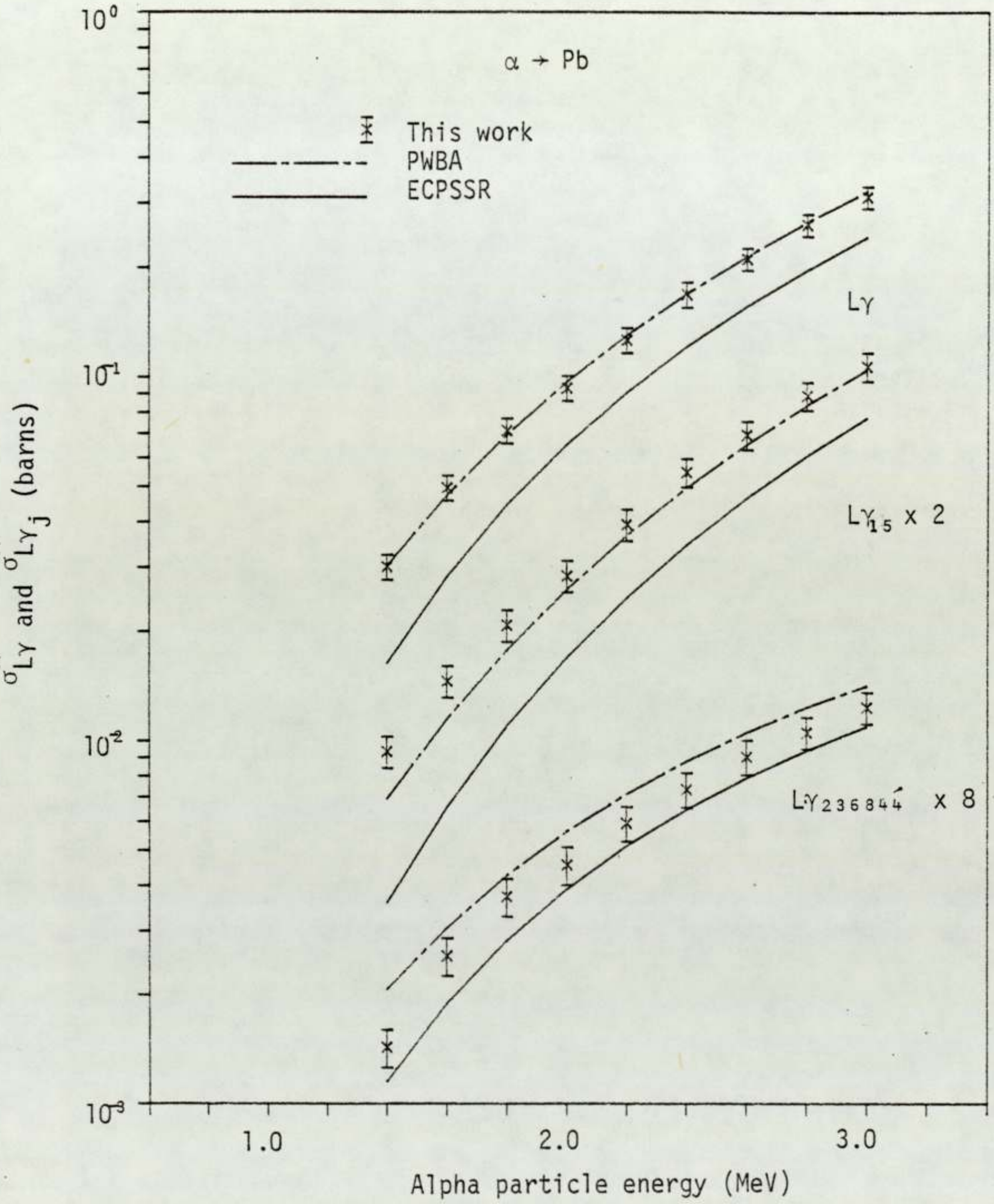

Figure 6.146. Experimental total $L\gamma$ and partial $L\gamma_j$ x-ray production cross sections for alpha particle impact on Pb.

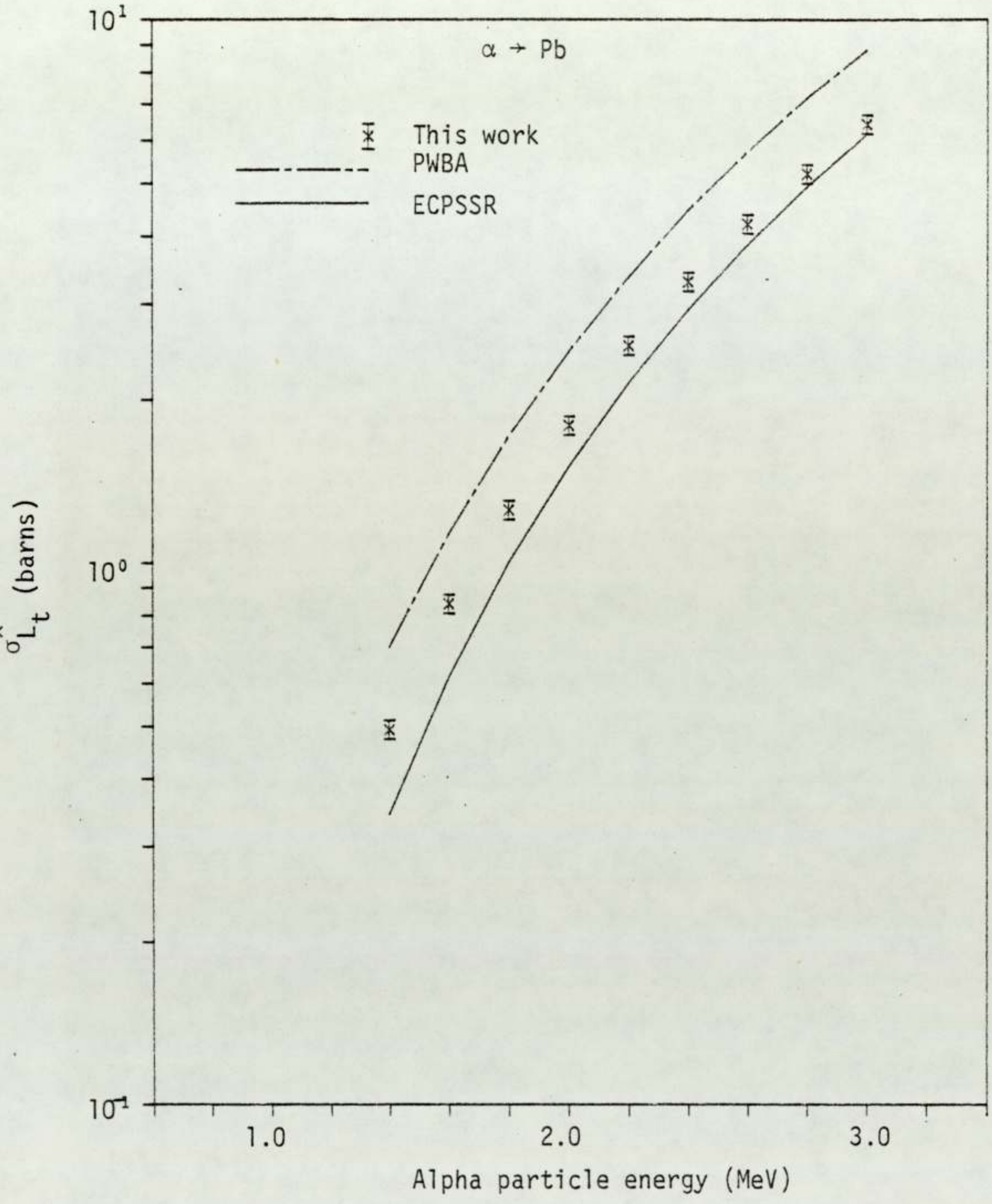

Figure 6.147. Experimental total L shell x-ray production cross section for alpha particle impact on Pb.

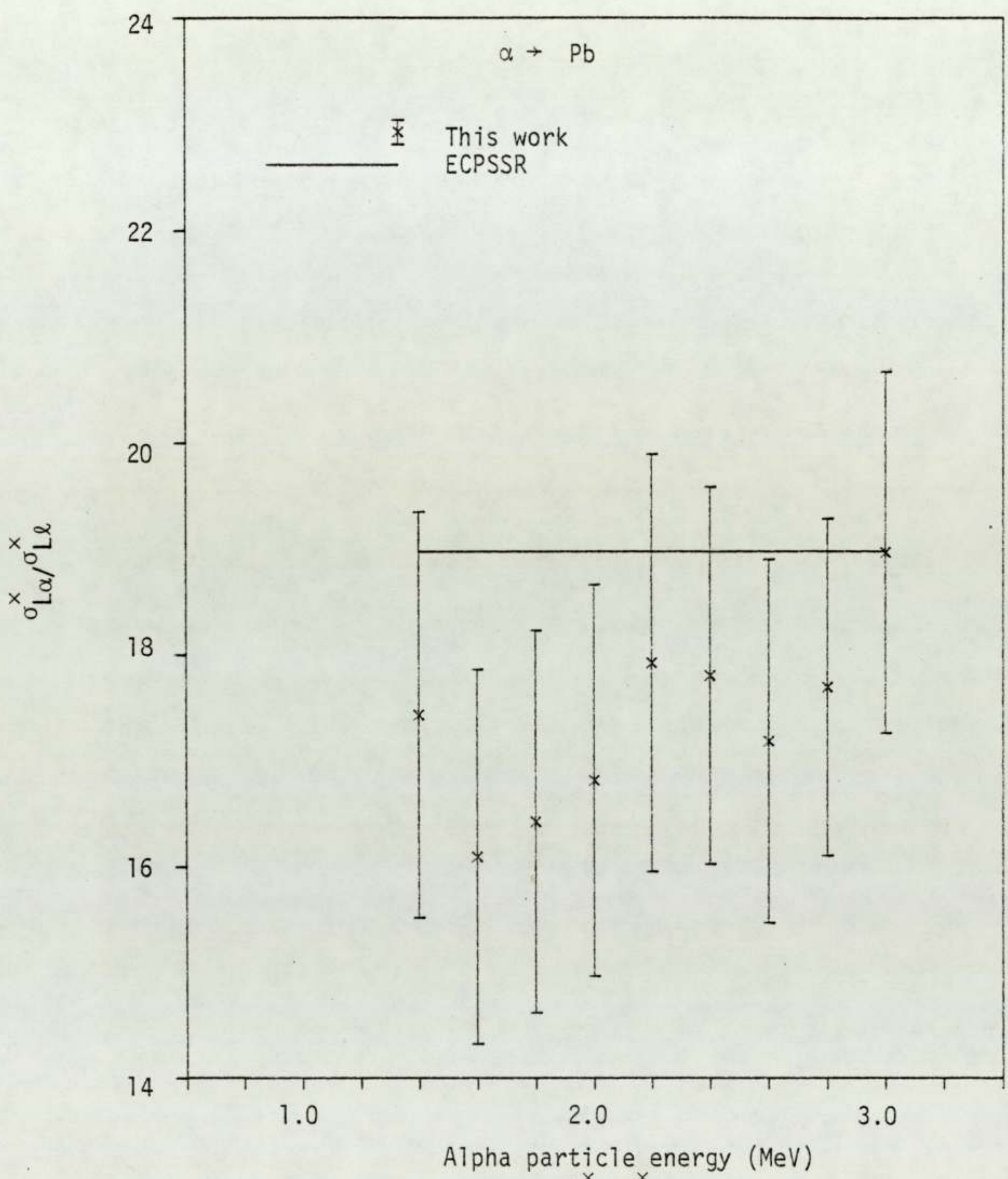

Figure 6.148. Experimental $\sigma^{x}_{L\alpha}/\sigma^{x}_{L\ell}$ ratio for alpha particle impact on Pb.

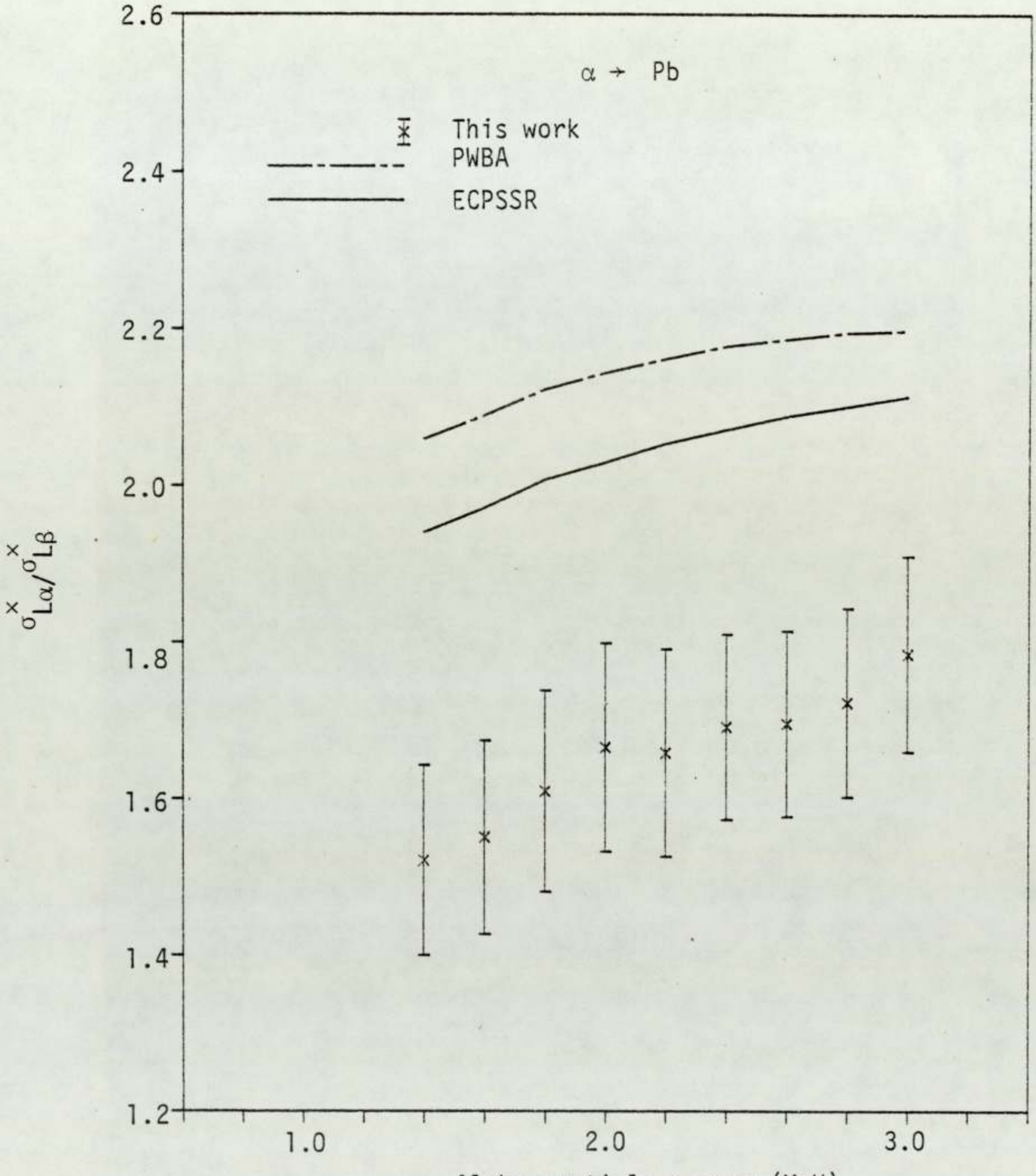

Figure 6.149. Experimental $\sigma^{x}_{L\alpha}/\sigma^{x}_{L\beta}$ ratio for alpha particle impact on Pb.

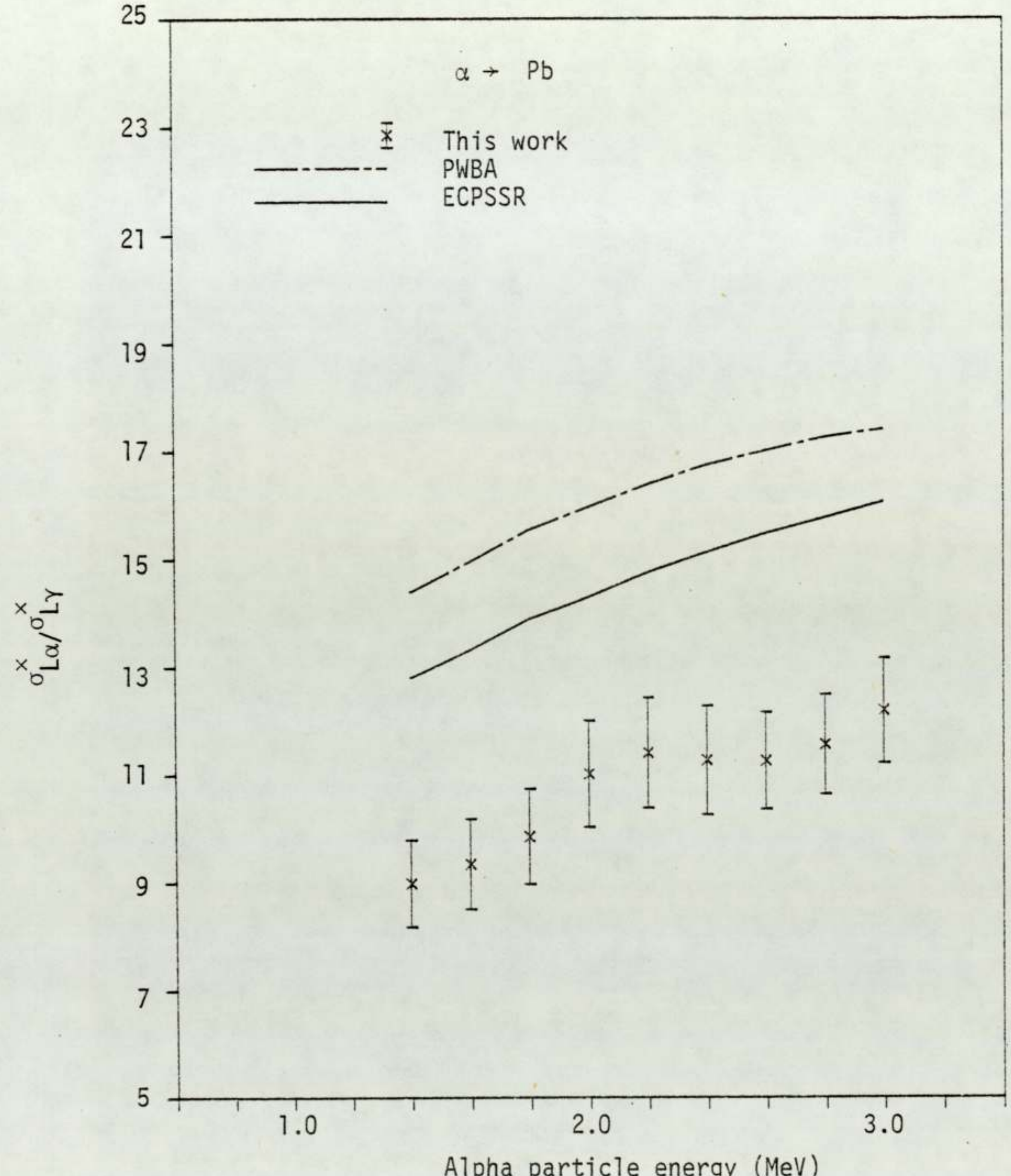

Figure 6.150. Experimental $\sigma^x_{L\alpha}/\sigma^x_{L\gamma}$ ratio for alpha particle impact on Pb.

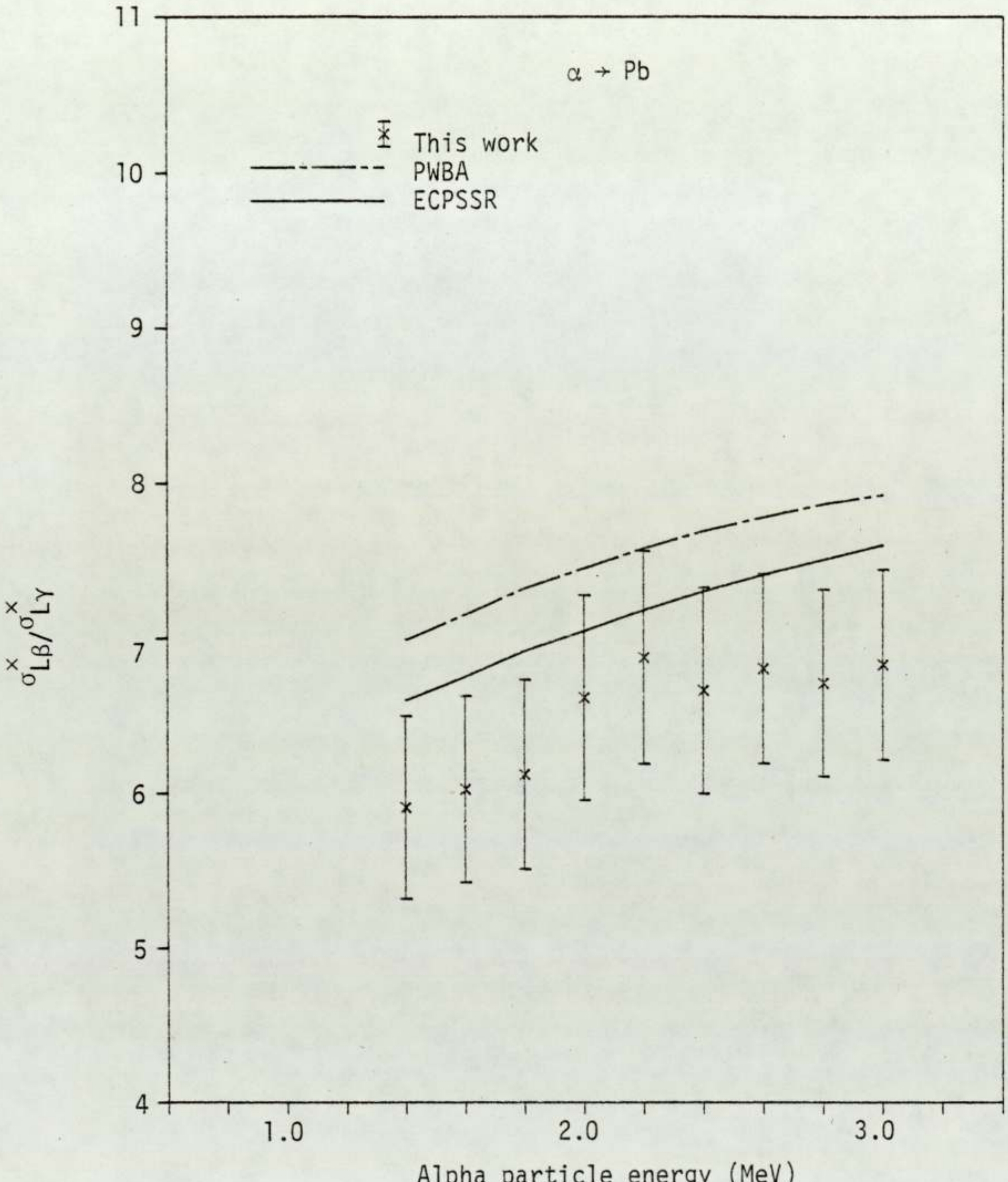

Figure 6.151. Experimental $\sigma^{x}_{L\beta}/\sigma^{x}_{L\gamma}$ ratio for alpha particle impact on Pb.

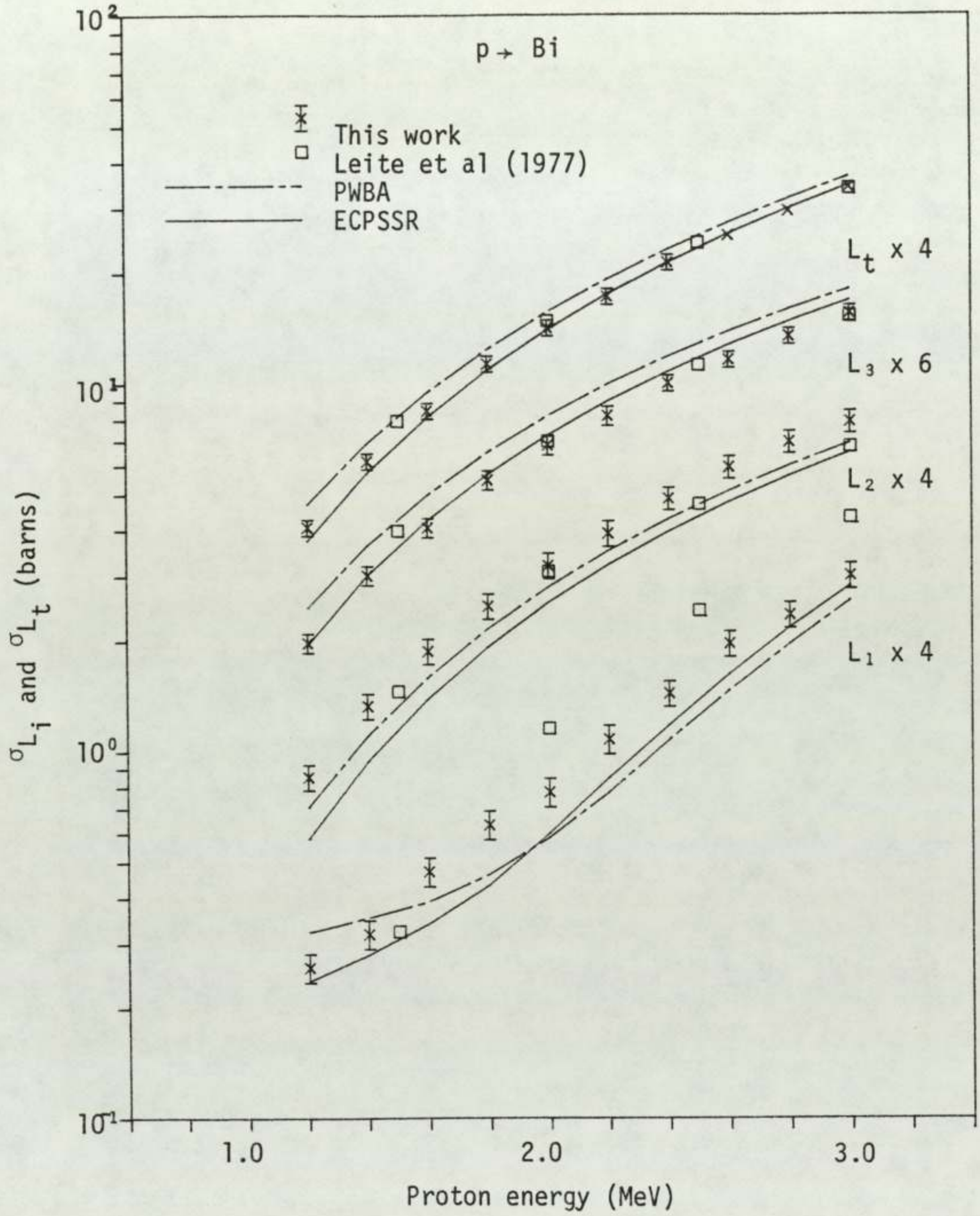

Figure 6.152. Experimental L_i subshell and total L shell ionisation cross sections for proton impact on Bi.

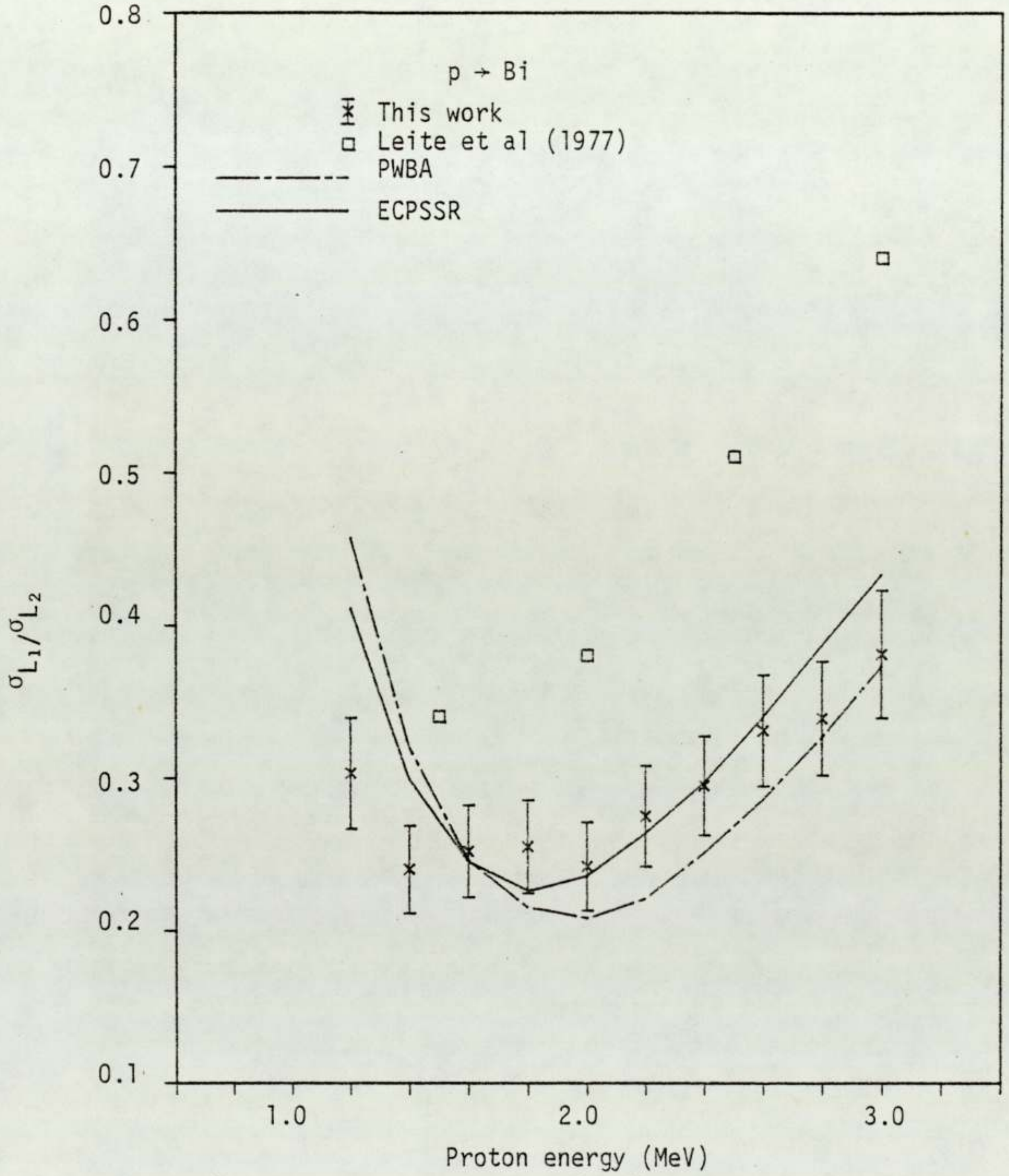

Figure 6.153. Experimental $\sigma_{L_1}/\sigma_{L_2}$ ratio for proton impact on Bi.

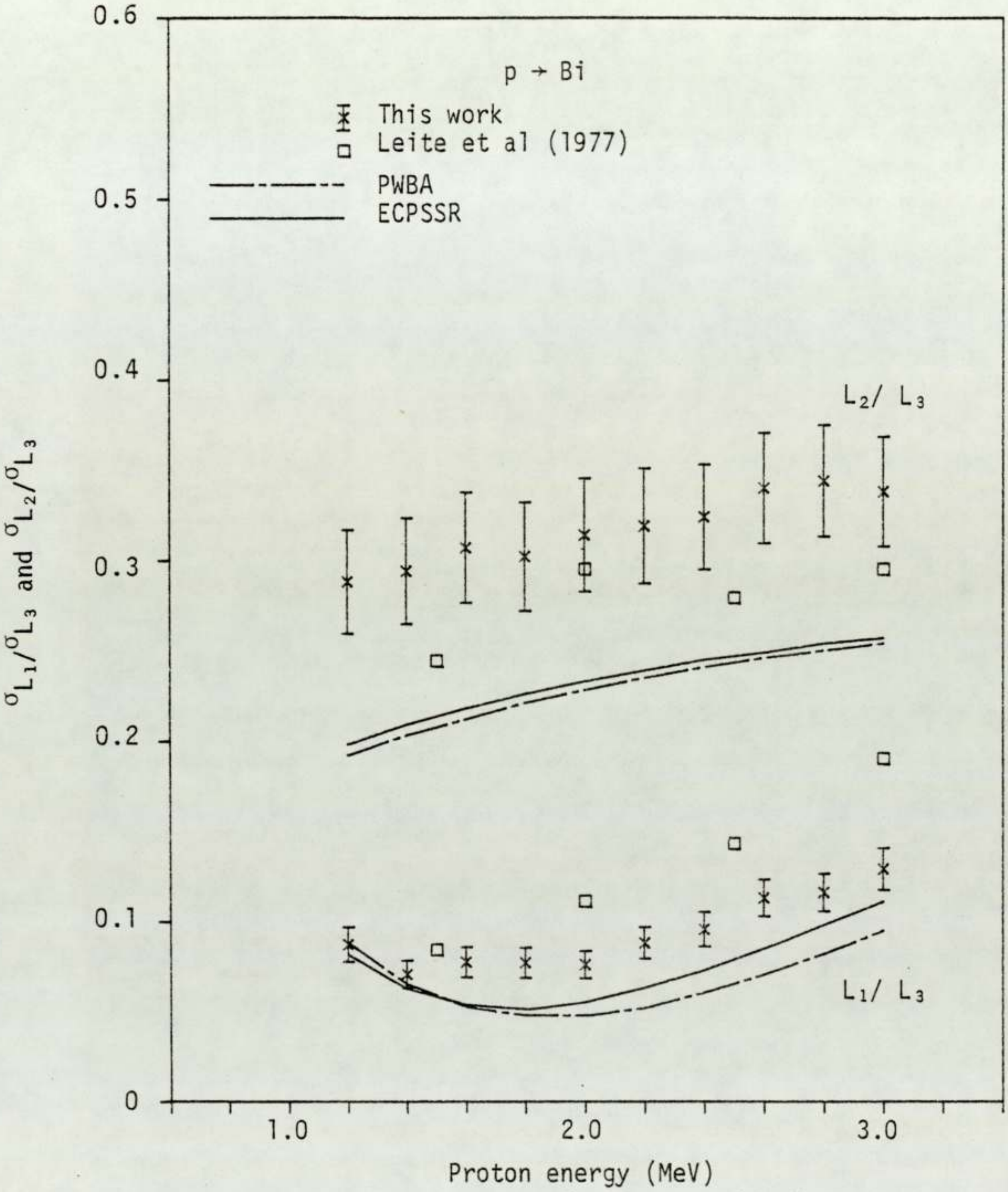

Figure 6.154. Experimental $\sigma_{L_1}/\sigma_{L_3}$ and $\sigma_{L_2}/\sigma_{L_3}$ ratios for proton impact on Bi.

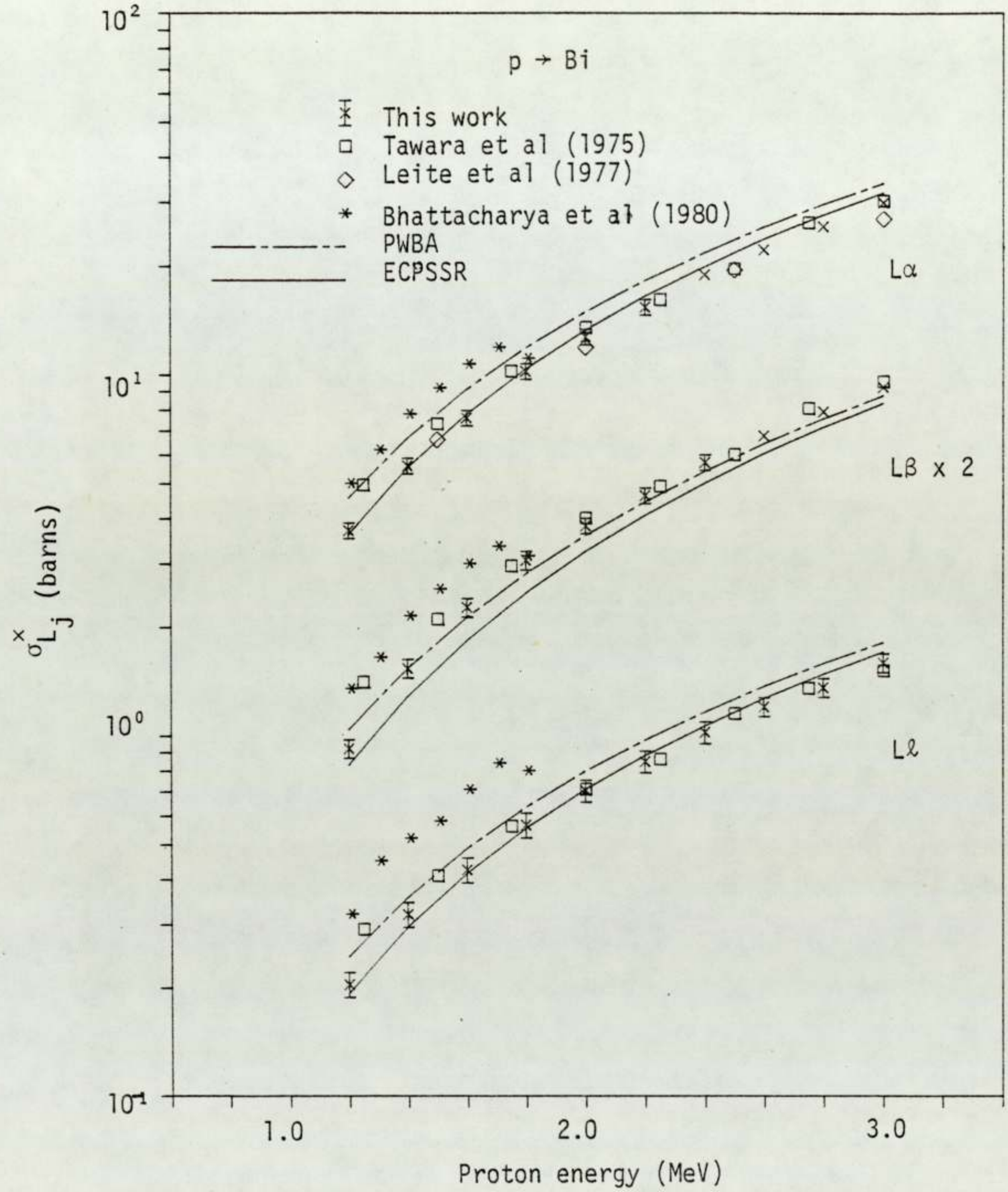

Figure 6.155. Experimental Lℓ, Lα and Lβ x-ray production cross sections for proton impact on Bi.

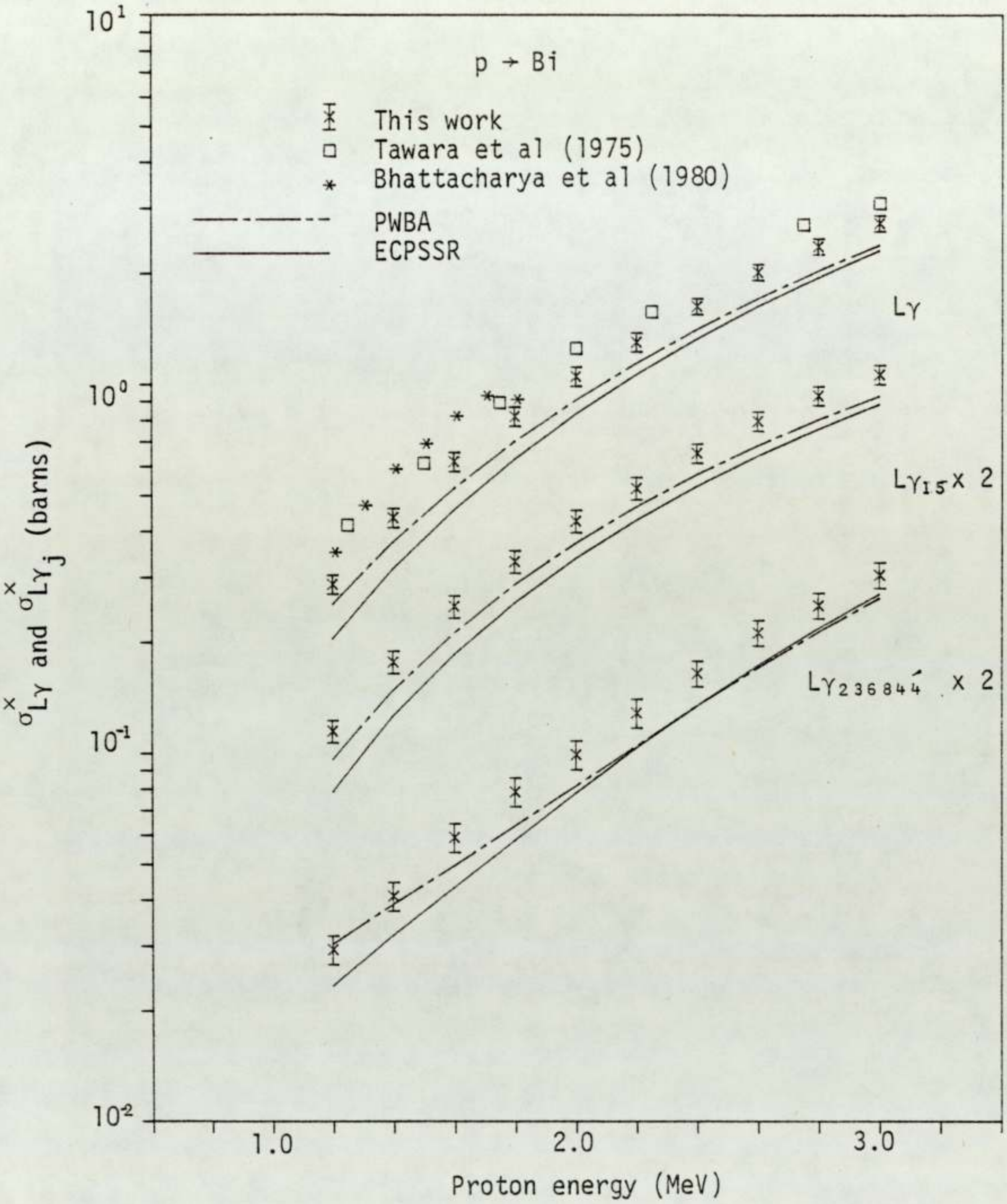

Figure 6.156. Experimental total Lγ and partial $L\gamma_j$ x-ray production cross sections for proton impact on Bi.

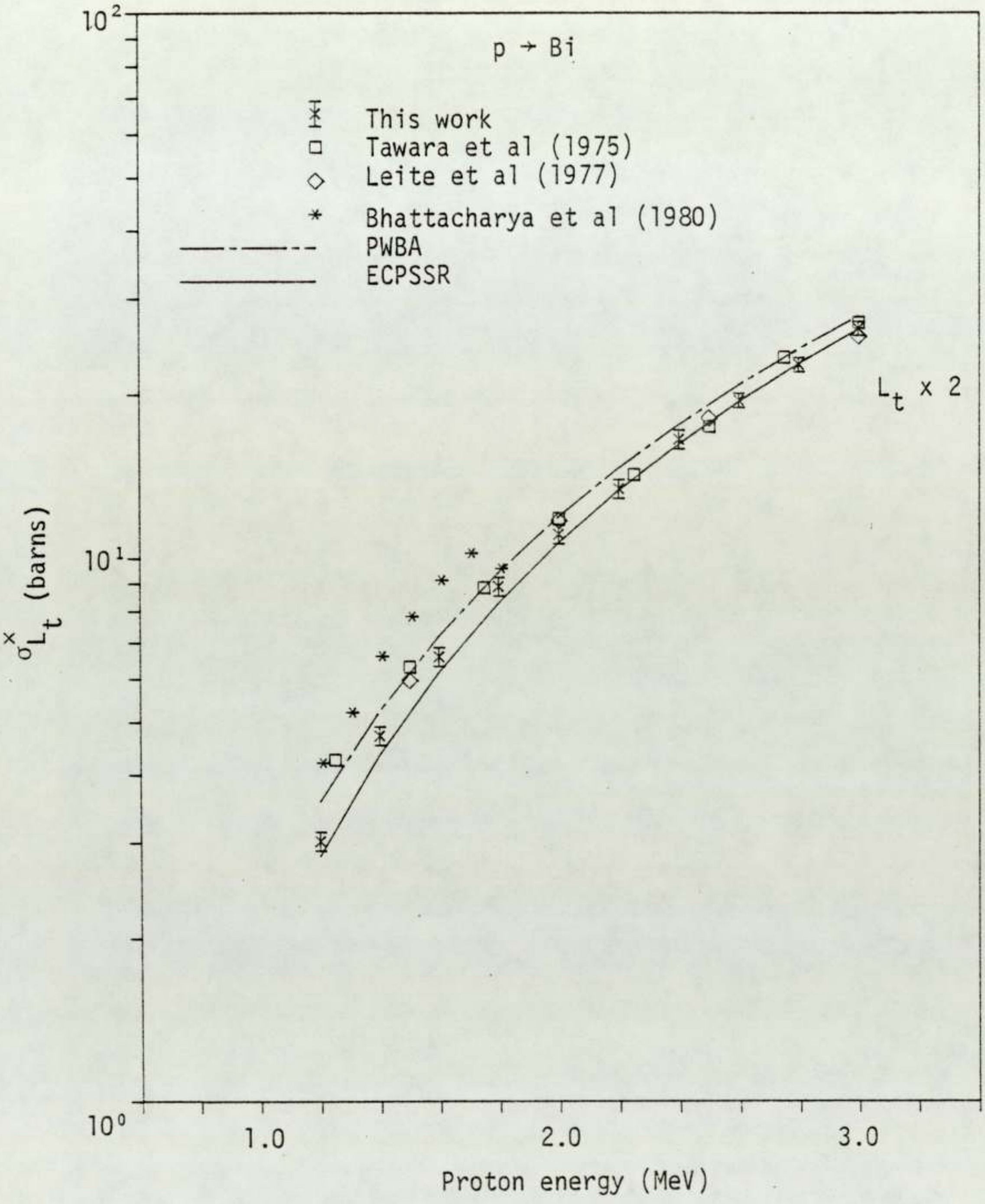

Figure 6.157. Experimental total L shell x-ray production cross section for proton impact on Bi.

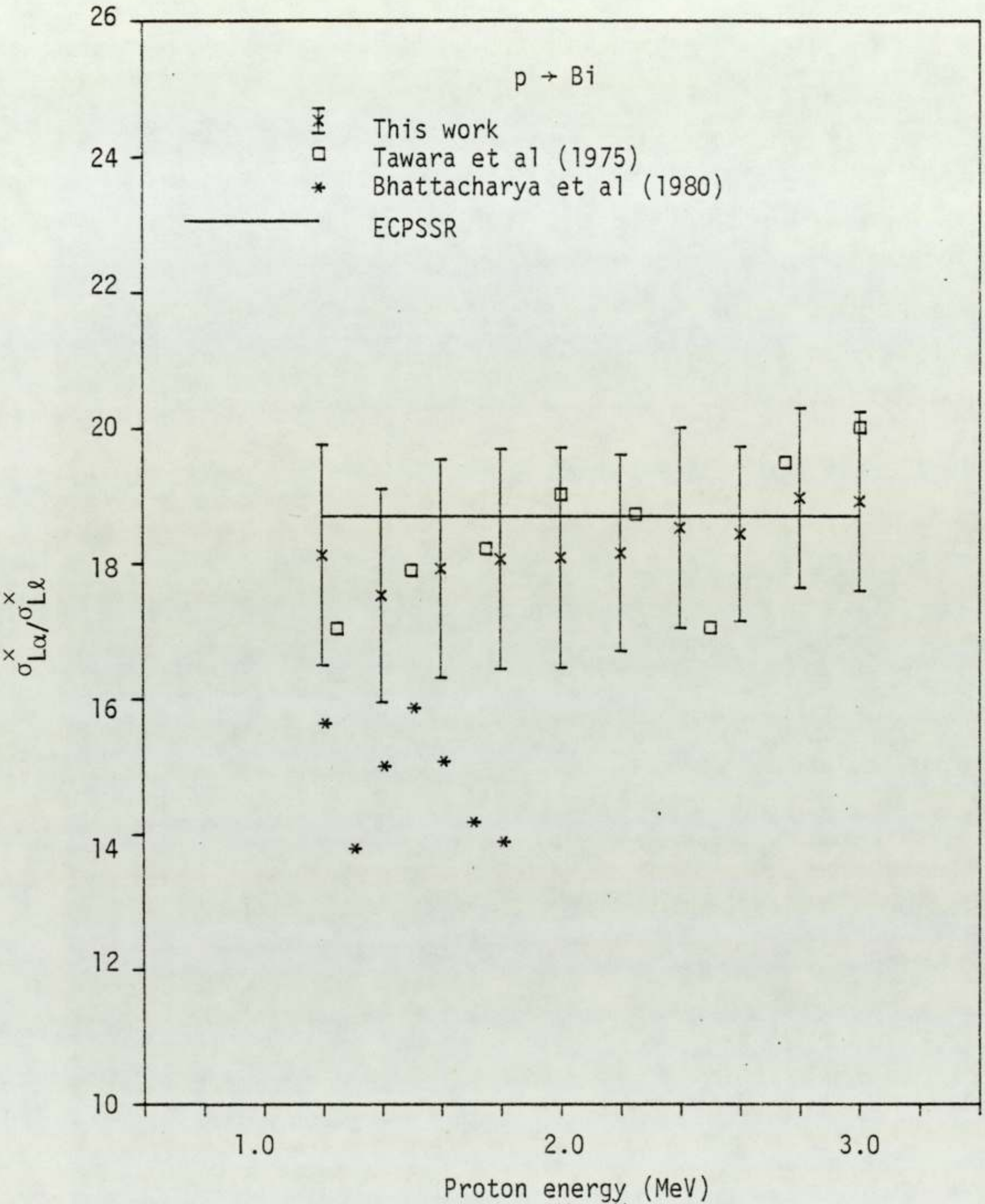

Figure 6.158. Experimental $\sigma^x_{L\alpha}/\sigma^x_{L\ell}$ ratio for proton impact on Bi.

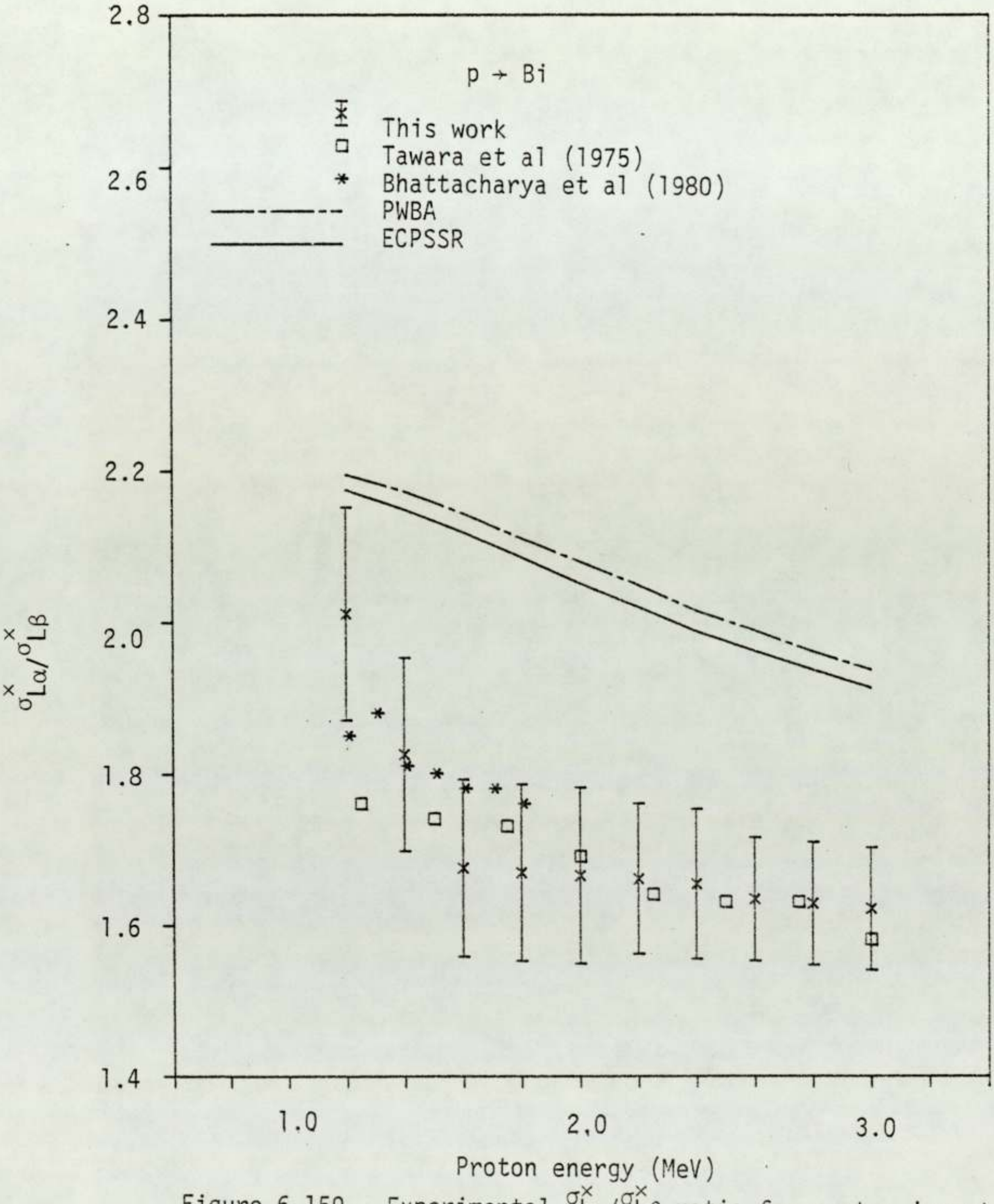

Figure 6.159. Experimental $\sigma^x_{L\alpha}/\sigma^x_{L\beta}$ ratio for proton impact on Bi.

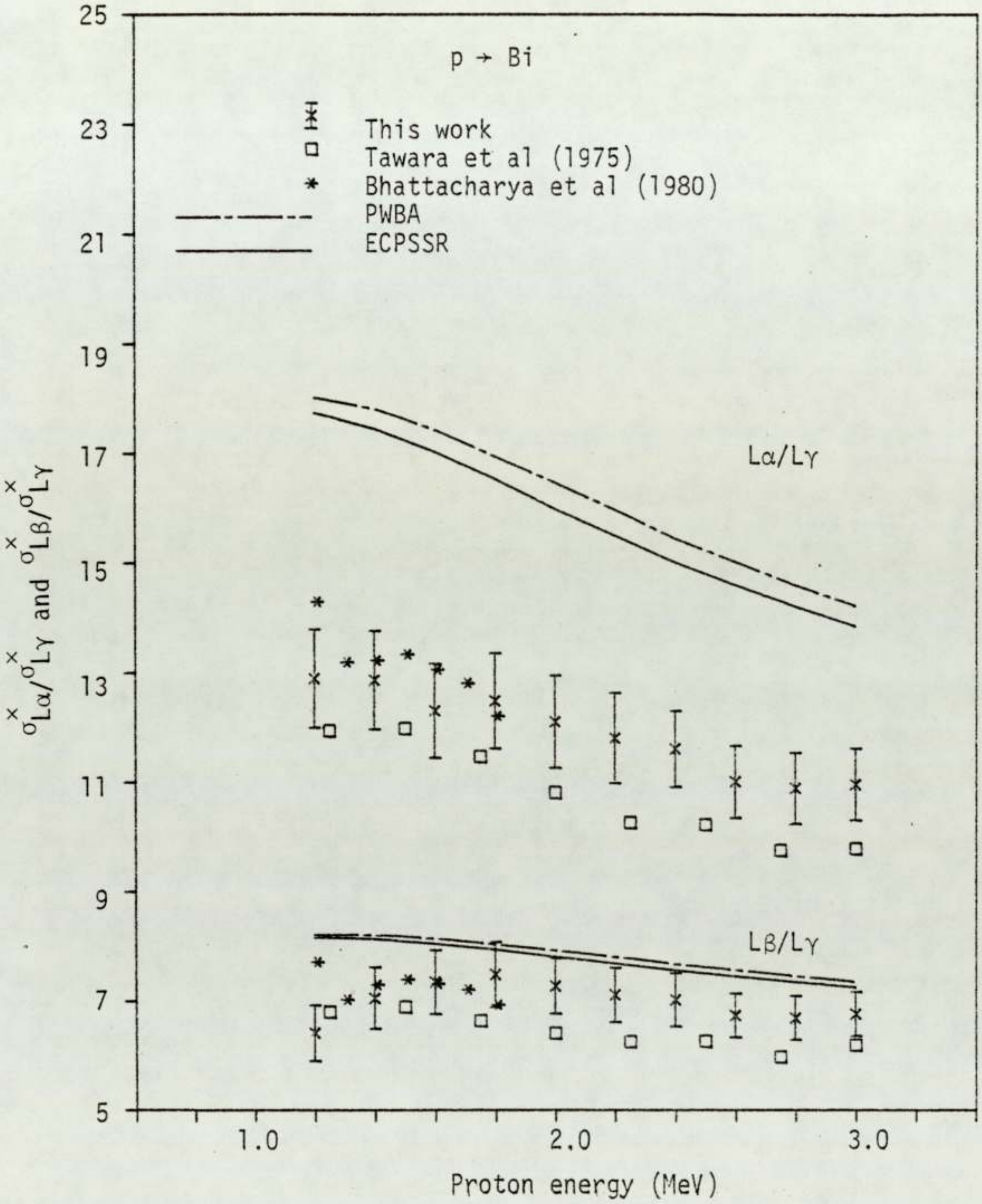

Figure 6.160. Experimental $\sigma^x_{L\alpha}/\sigma^x_{L\gamma}$ and $\sigma^x_{L\beta}/\sigma^x_{L\gamma}$ ratios for proton impact on Bi.

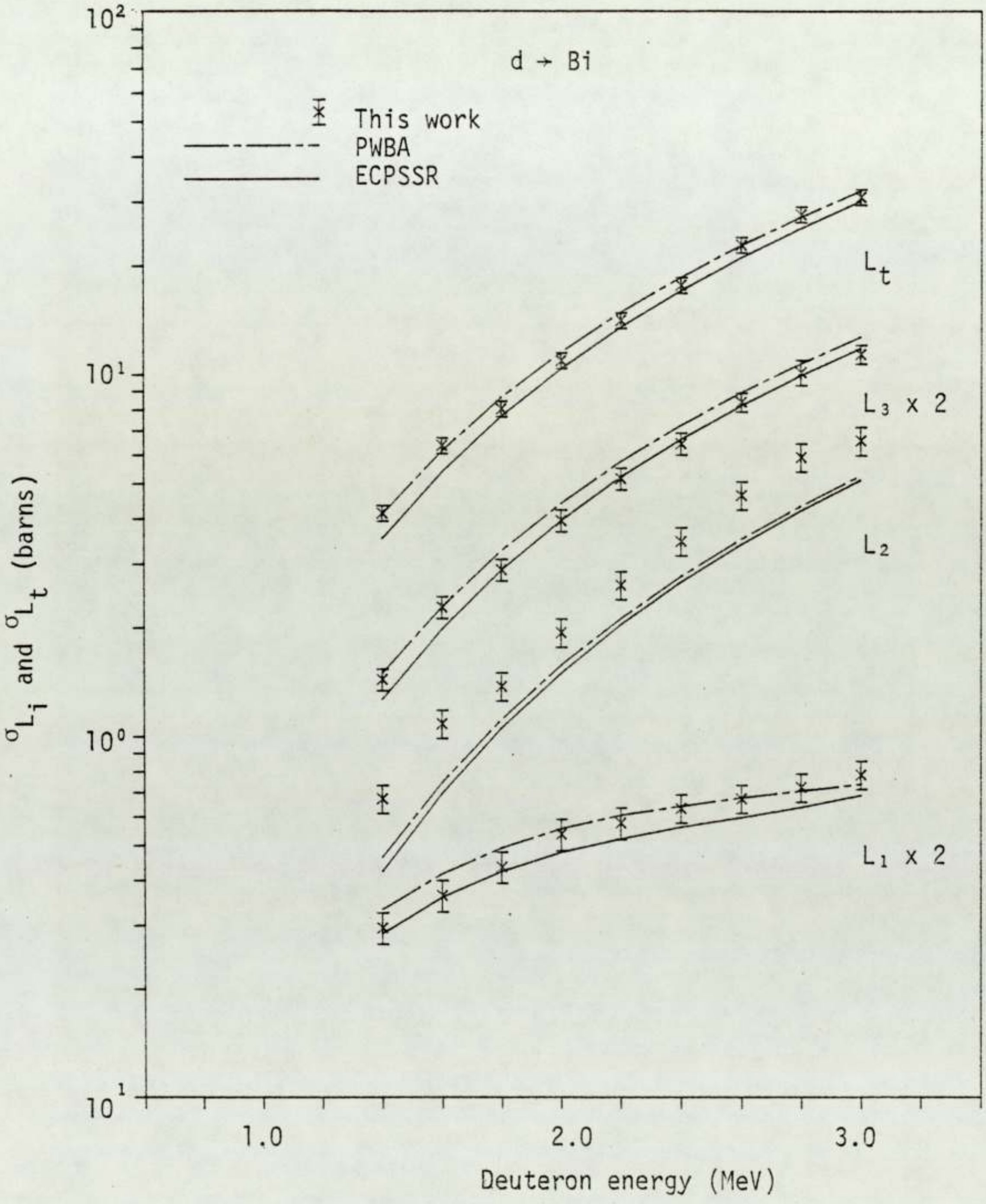

Figure 6.161. Experimental L_i subshell and total L shell ionisation cross sections for deuteron impact on Bi.

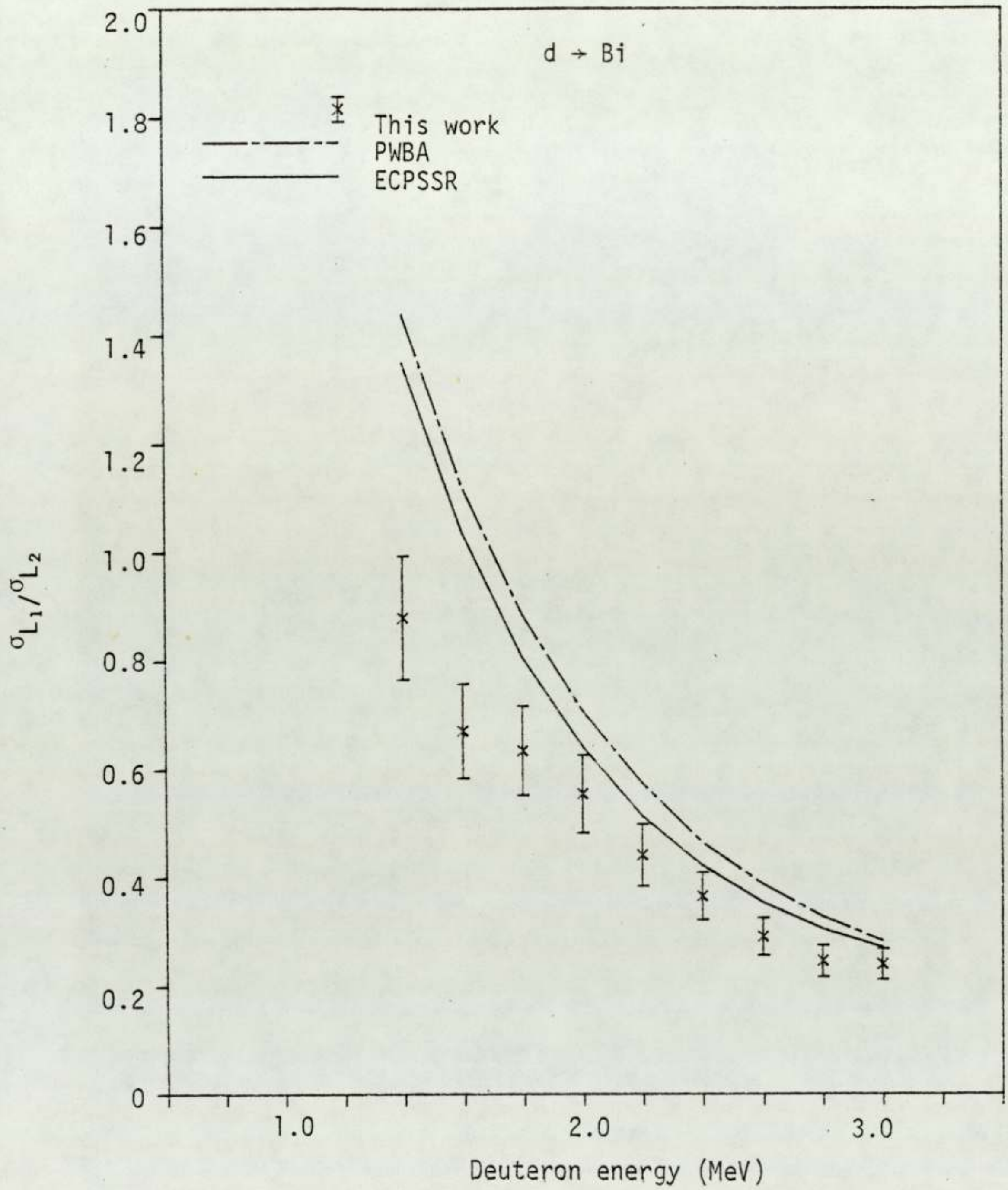

Figure 6.162. Experimental $\sigma_{L_1}/\sigma_{L_2}$ ratio for deuteron impact on Bi.

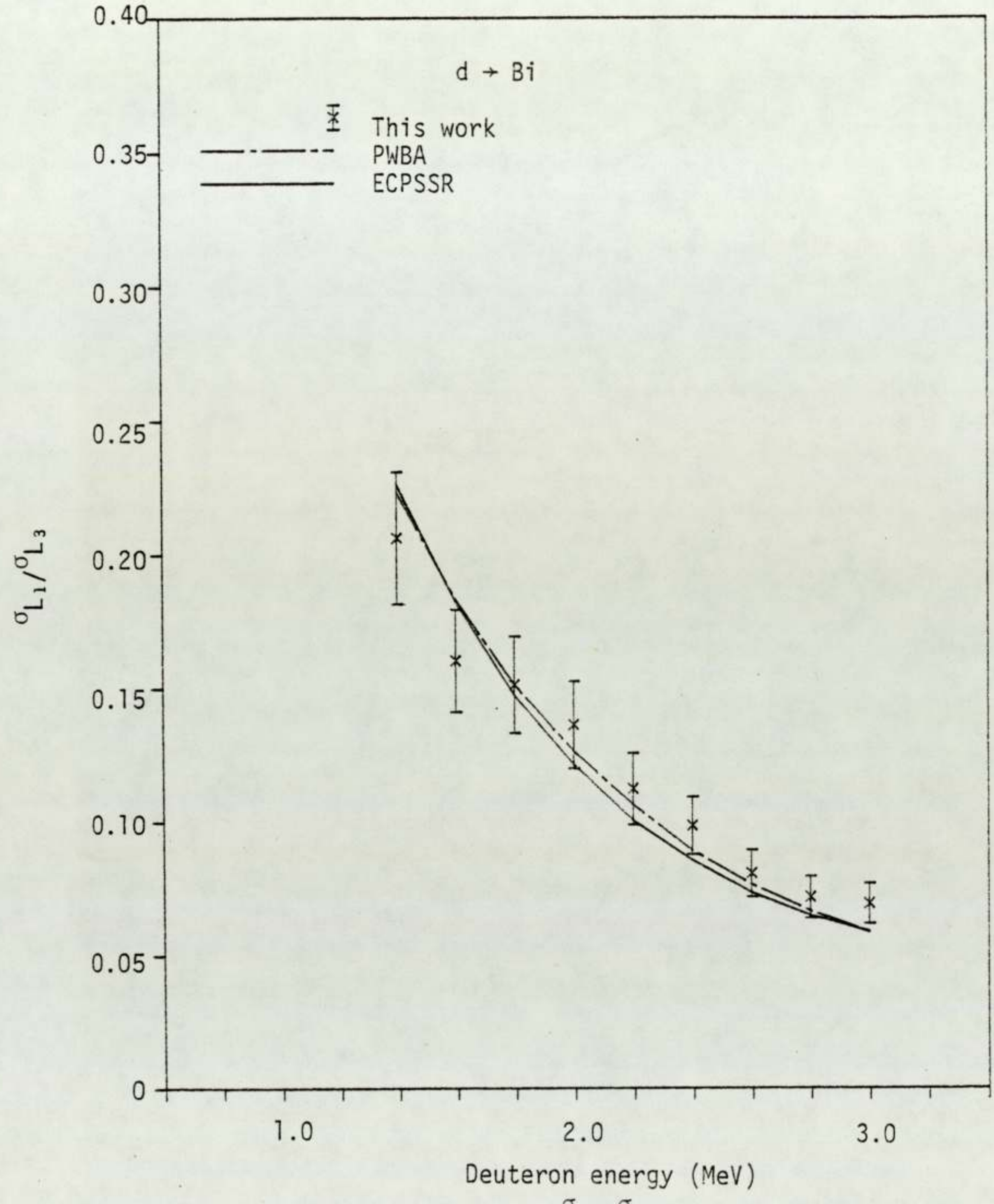

Figure 6.163. Experimental $\sigma_{L_1}/\sigma_{L_3}$ ratio for deuteron impact on Bi.

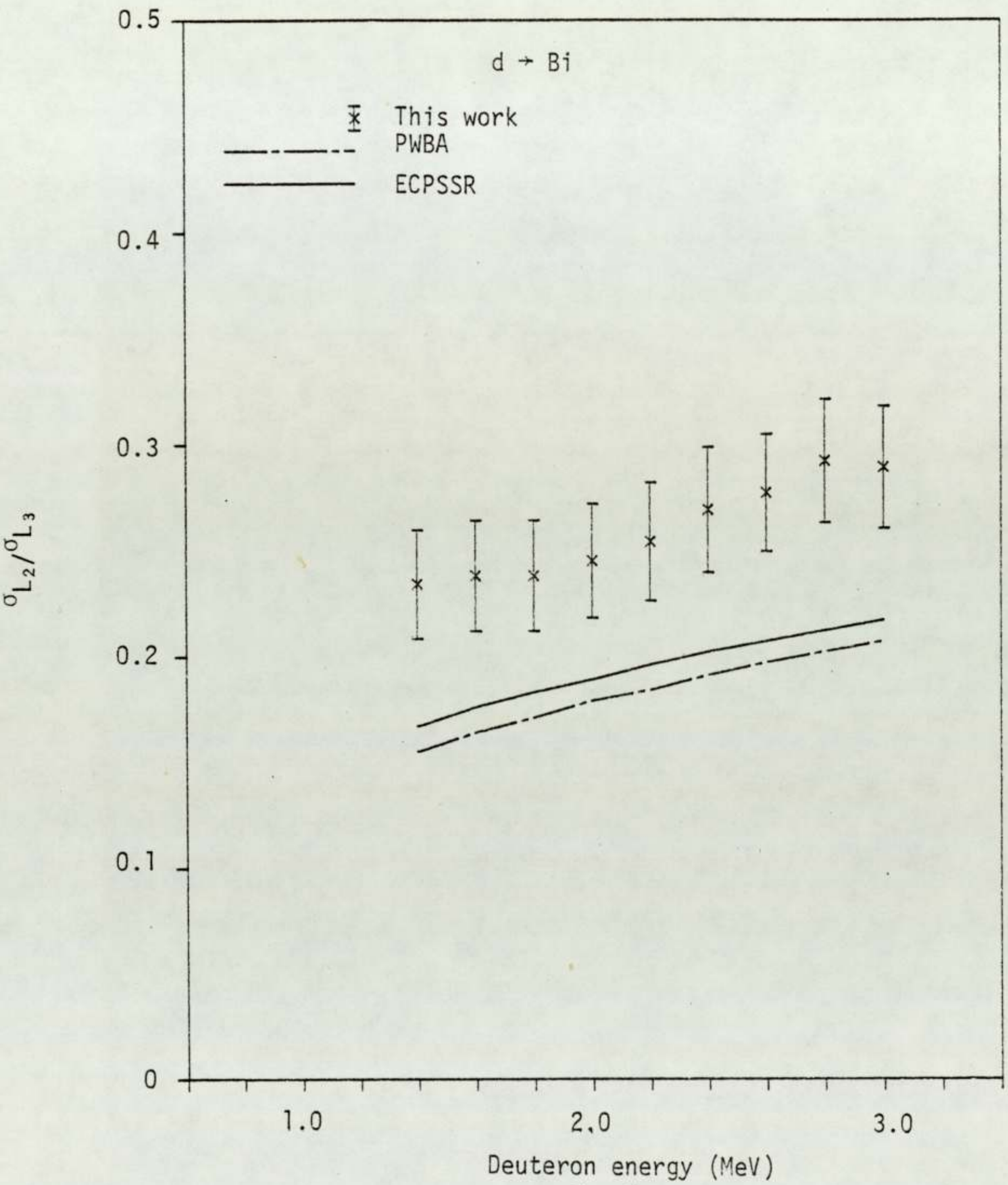

Figure 6.164. Experimental $\sigma_{L_2}/\sigma_{L_3}$ ratio for deuteron impact on Bi.

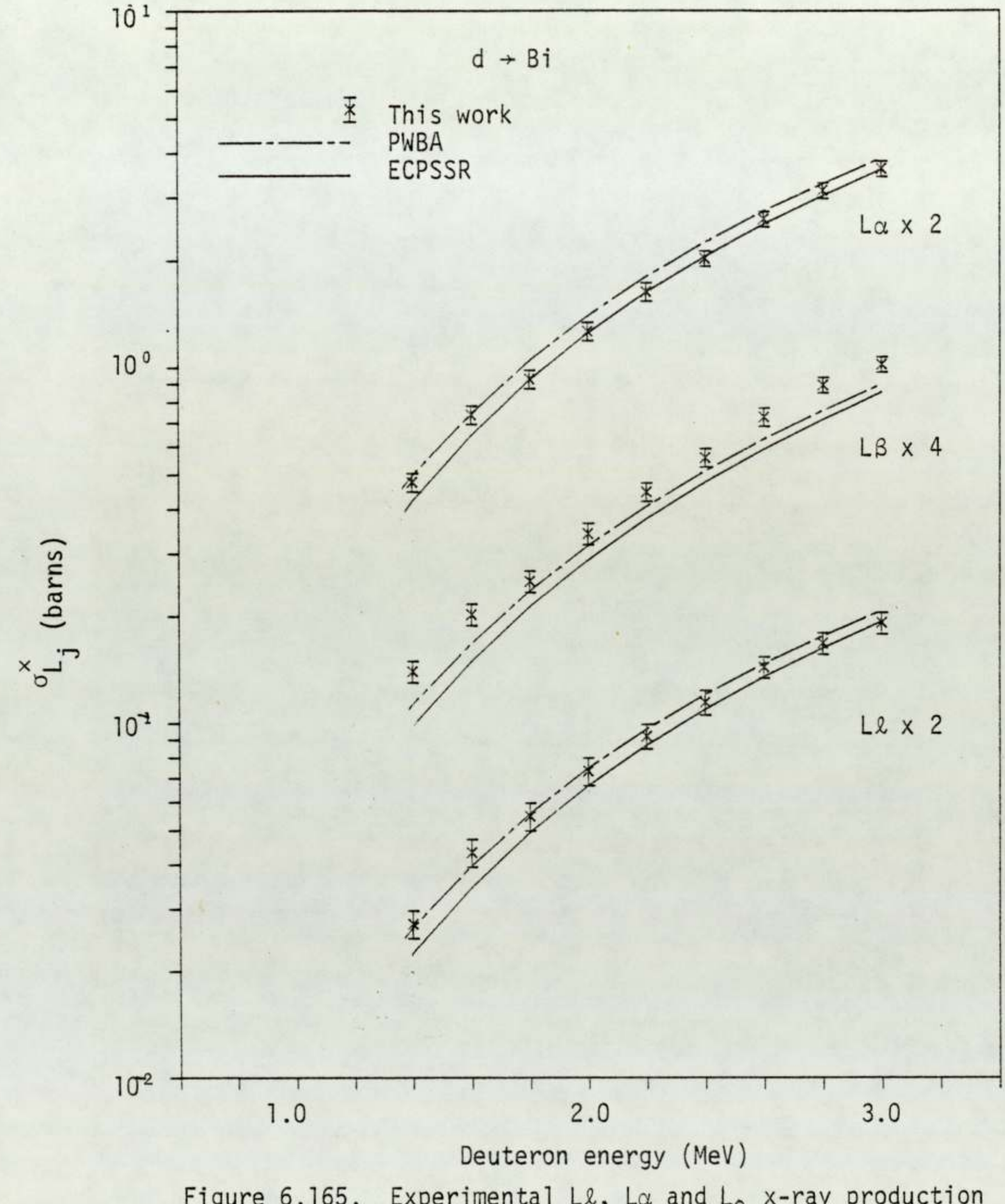

Figure 6.165. Experimental Lℓ, Lα and L_β x-ray production cross sections for deuteron impact on Bi.

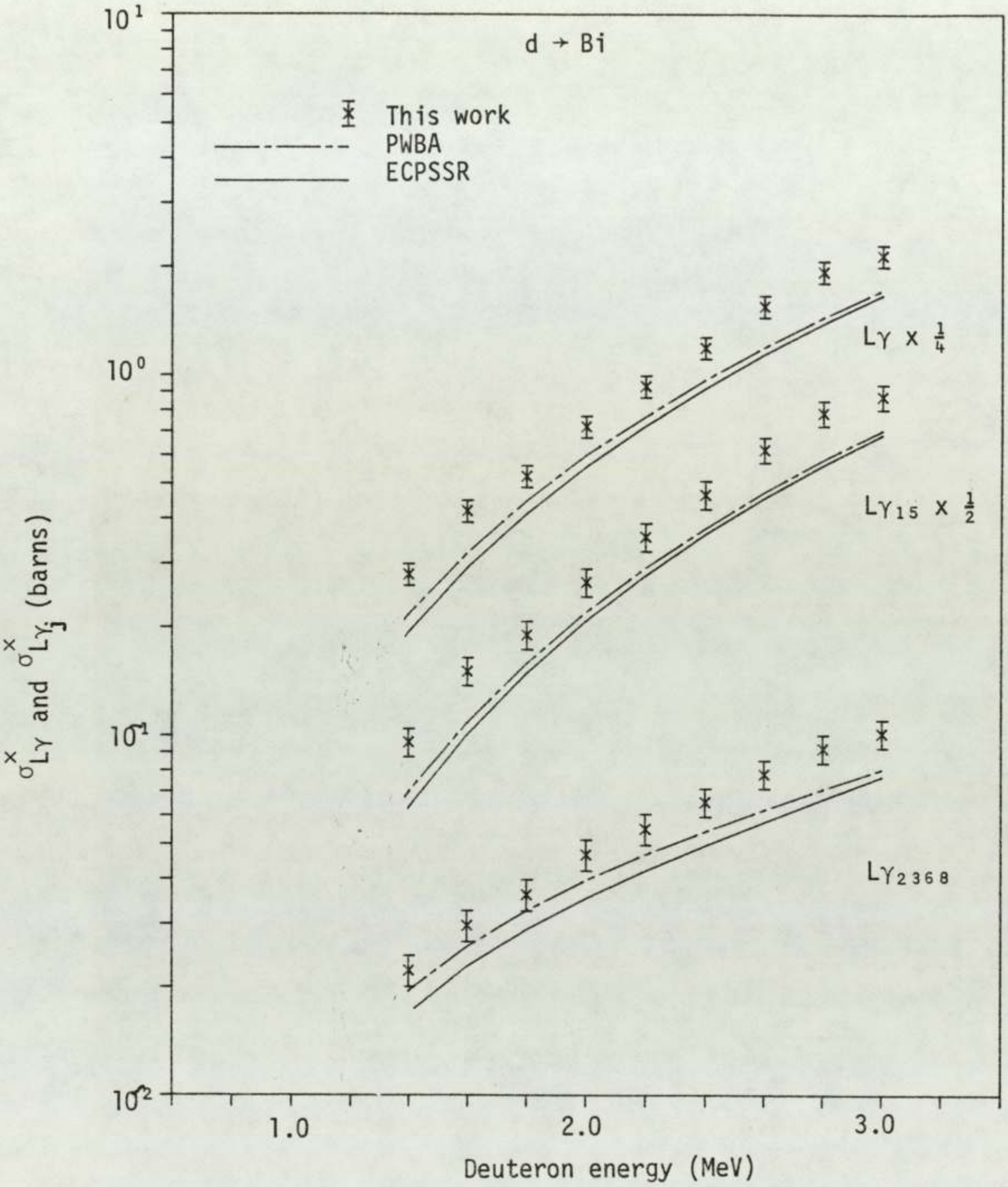

Figure 6.166. Experimental total Lγ and partial $L\gamma_j$ x-ray production cross sections for deuteron impact on Bi.

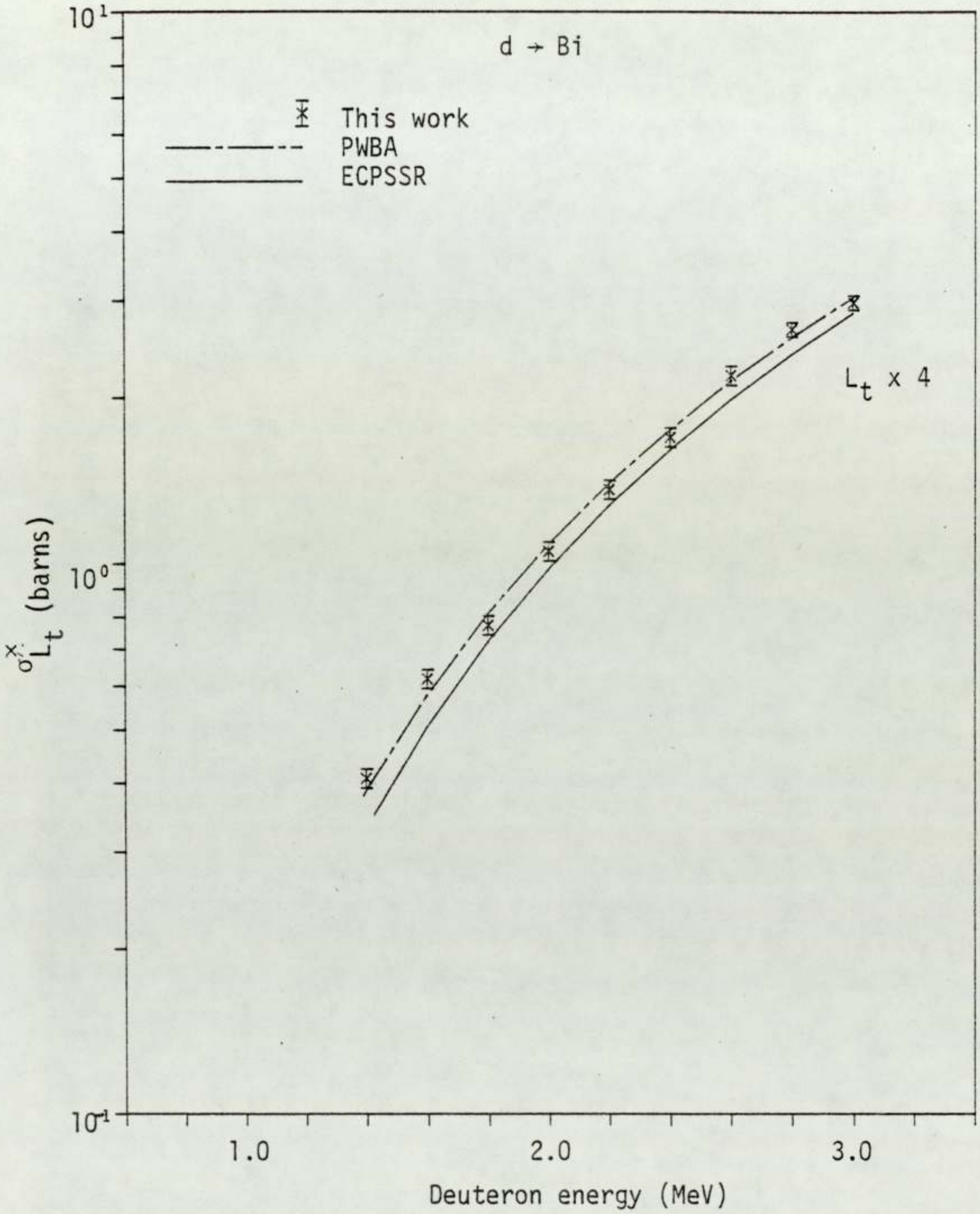

Figure 6.167. Experimental total L shell x-ray production cross section for deuteron impact on Bi.

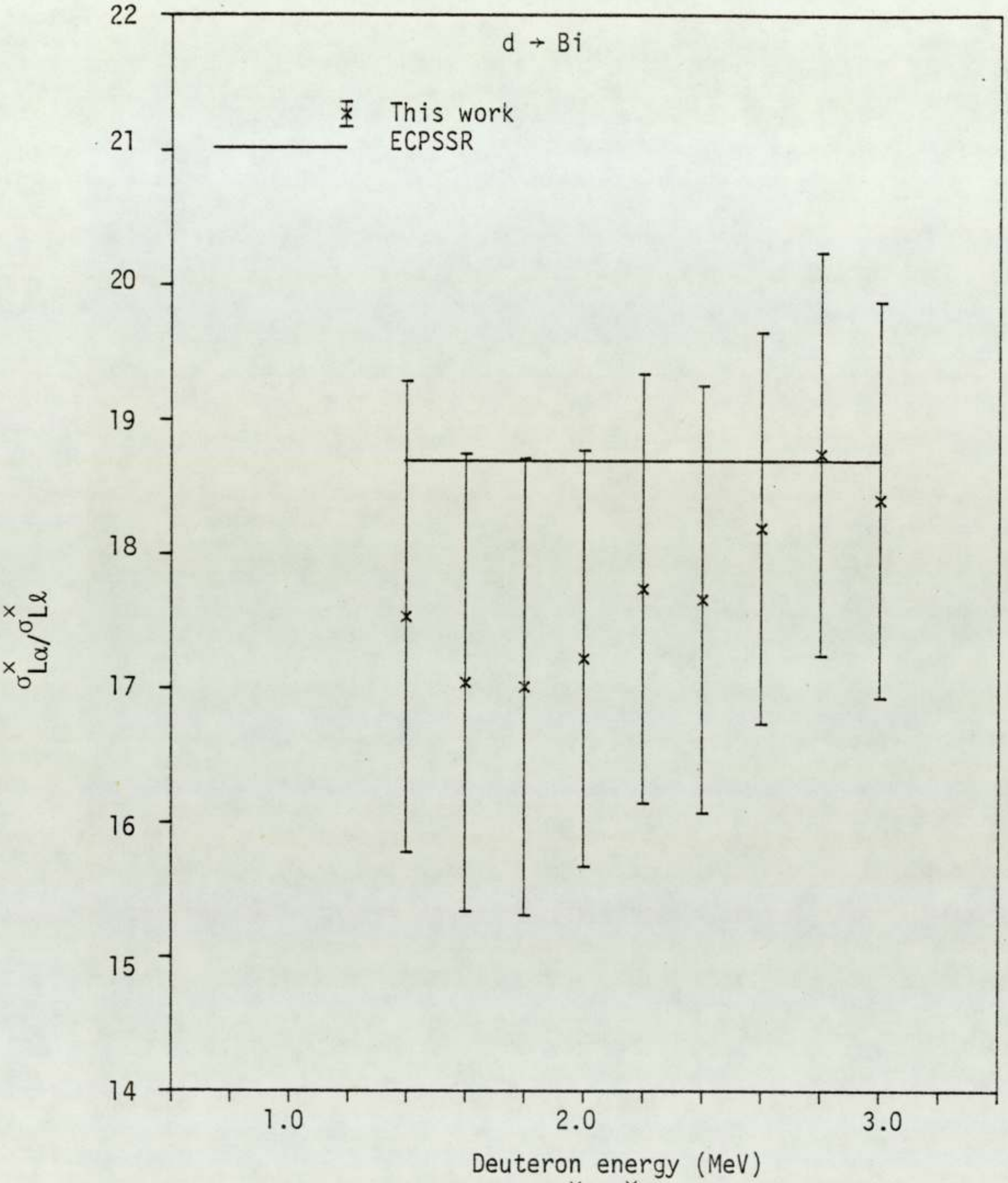

Figure 6.168. Experimental $\sigma^x_{L\alpha}/\sigma^x_{L\ell}$ ratio for deuteron impact on Bi.

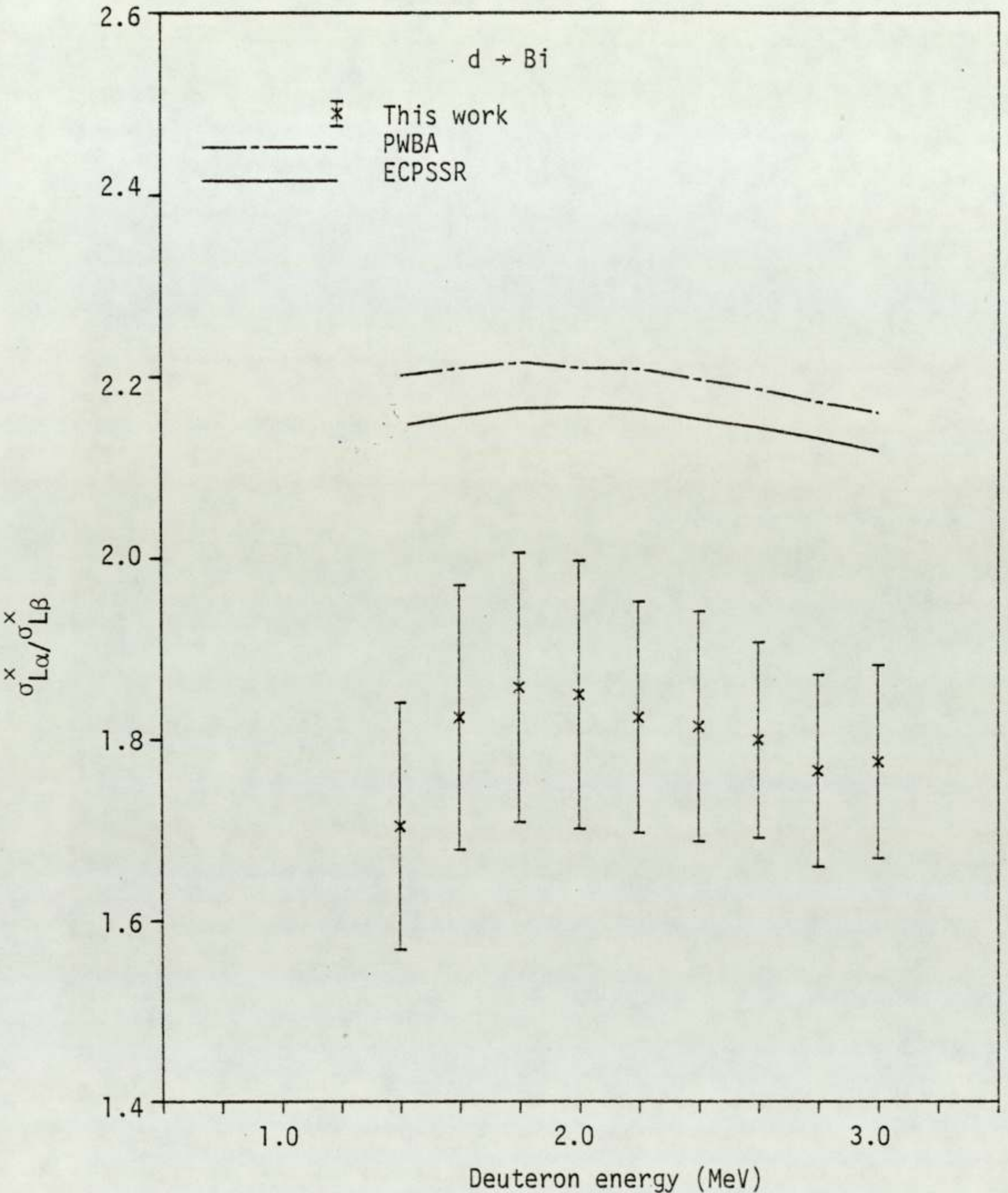

Figure 6.169. Experimental $\sigma^{x}_{L\alpha}/\sigma^{x}_{L\beta}$ ratio for deuteron impact on Bi.

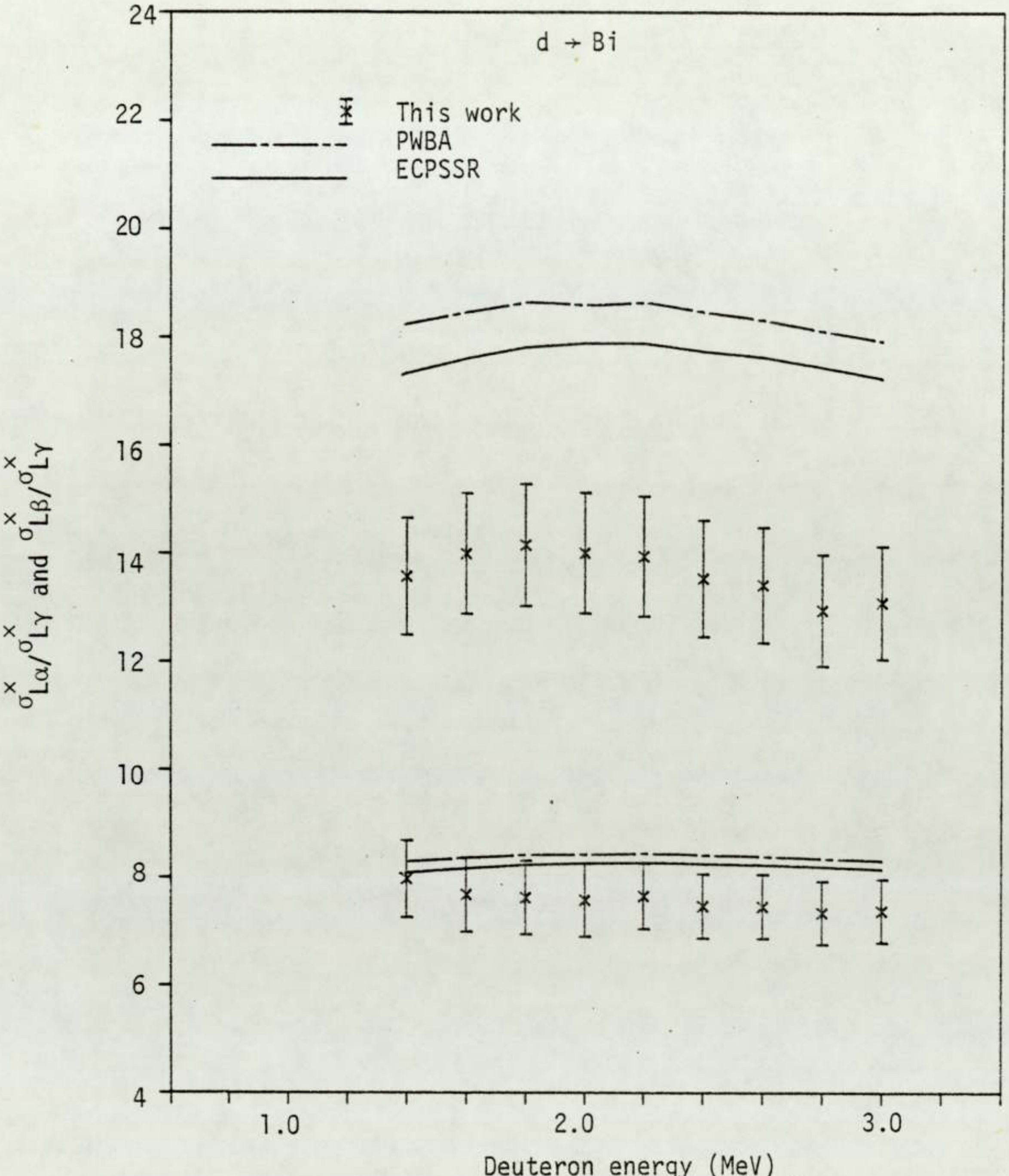

Figure 6.170. Experimental $\sigma^x_{L\alpha}/\sigma^x_{L\gamma}$ and $\sigma^x_{L\beta}/\sigma^x_{L\gamma}$ ratios for deuteron impact on Bi.

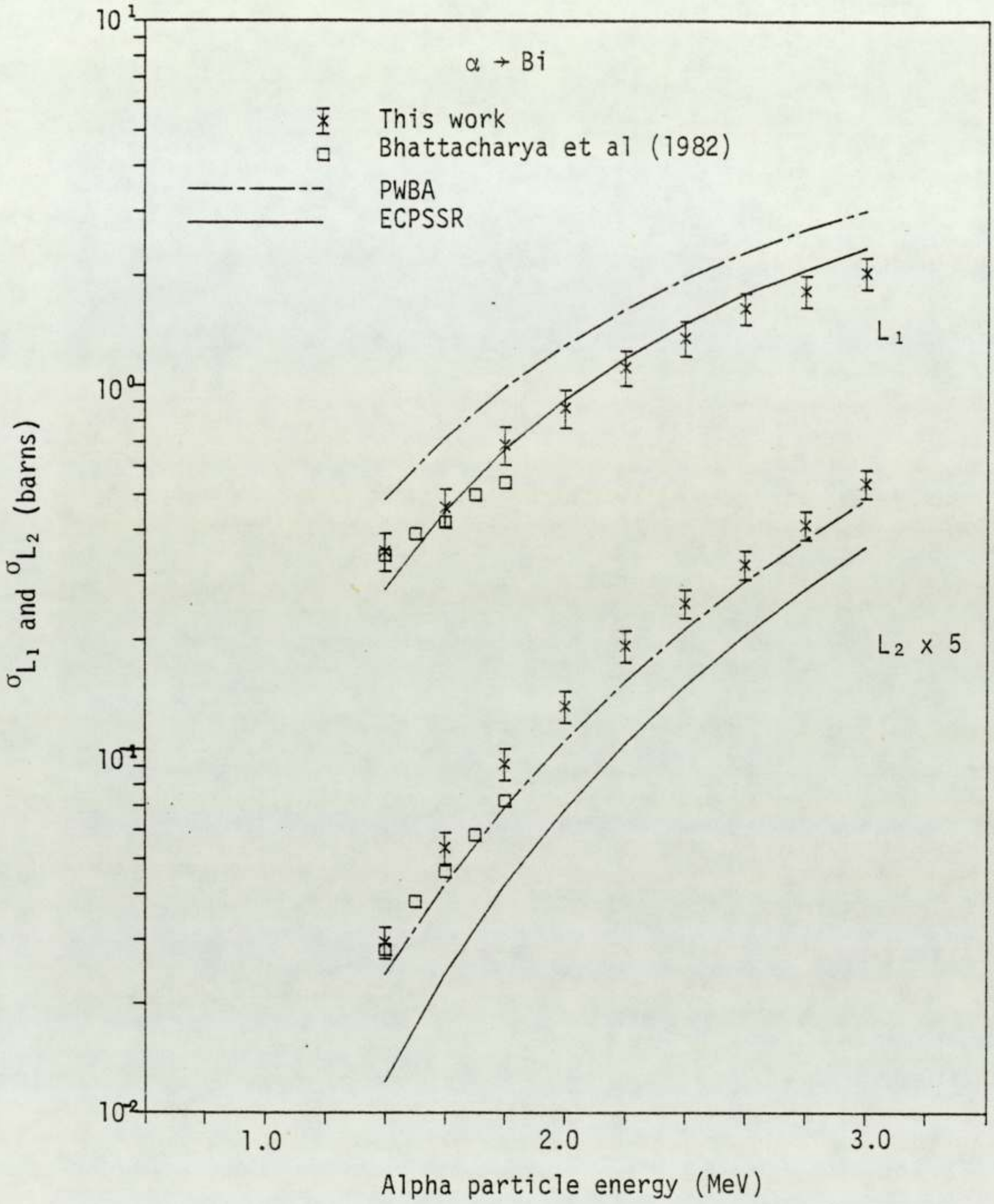

Figure 6.171. Experimental L_1 and L_2 subshell ionisation cross sections for alpha particle impact on Bi.

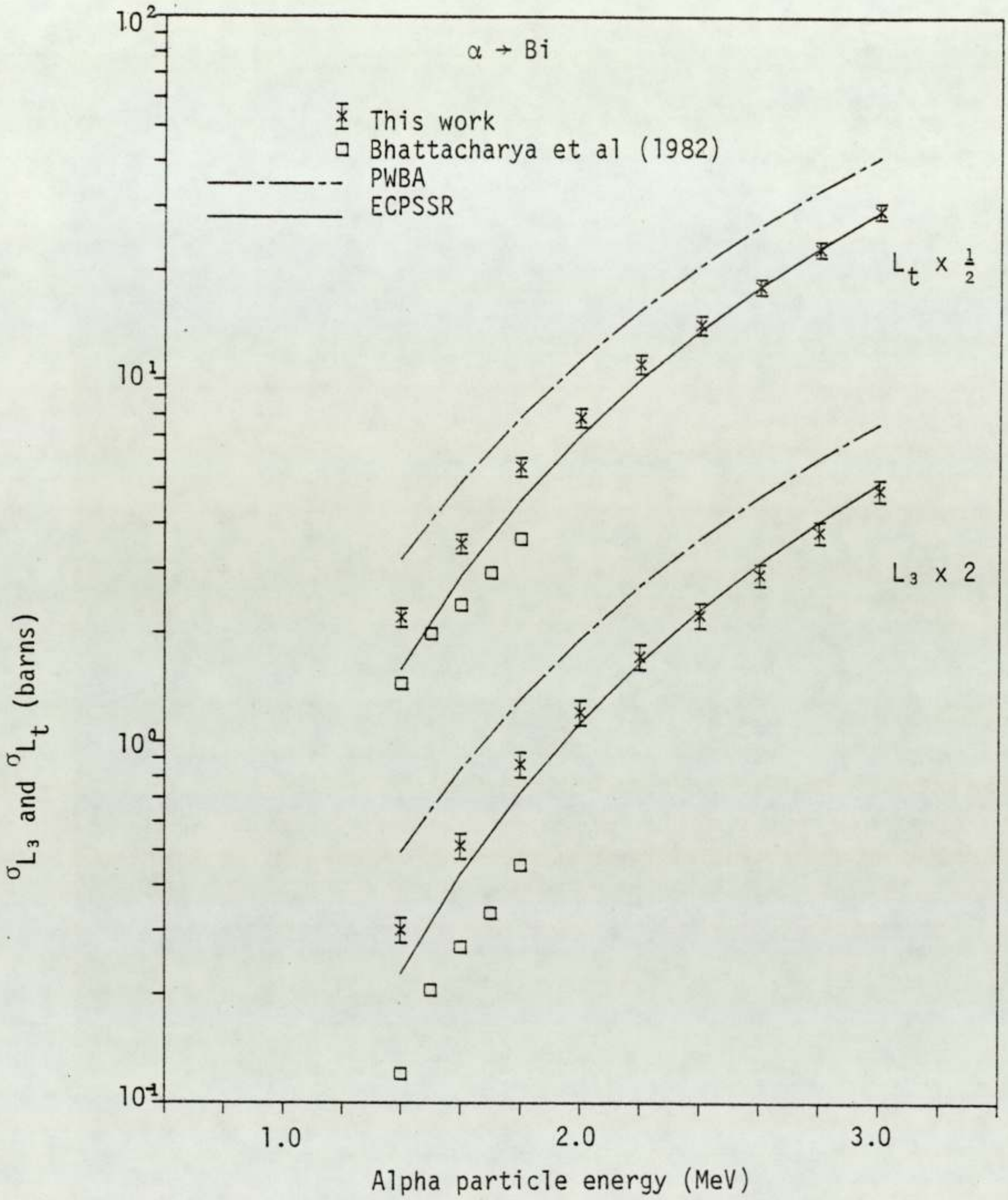

Figure 6.172. Experimental L_3 subshell and total L shell ionisation cross sections for alpha particle impact on Bi.

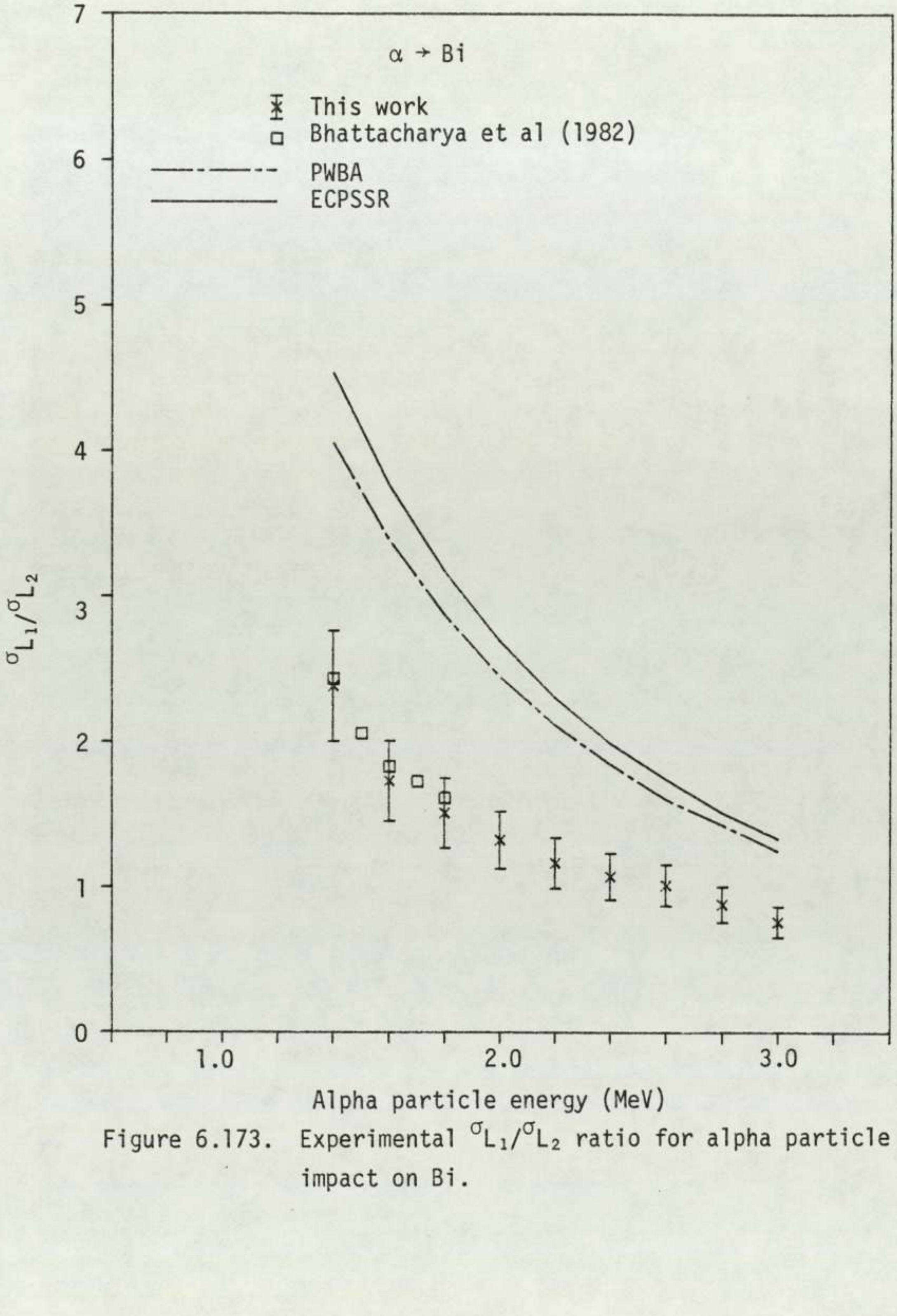

Figure 6.173. Experimental $\sigma_{L_1}/\sigma_{L_2}$ ratio for alpha particle impact on Bi.

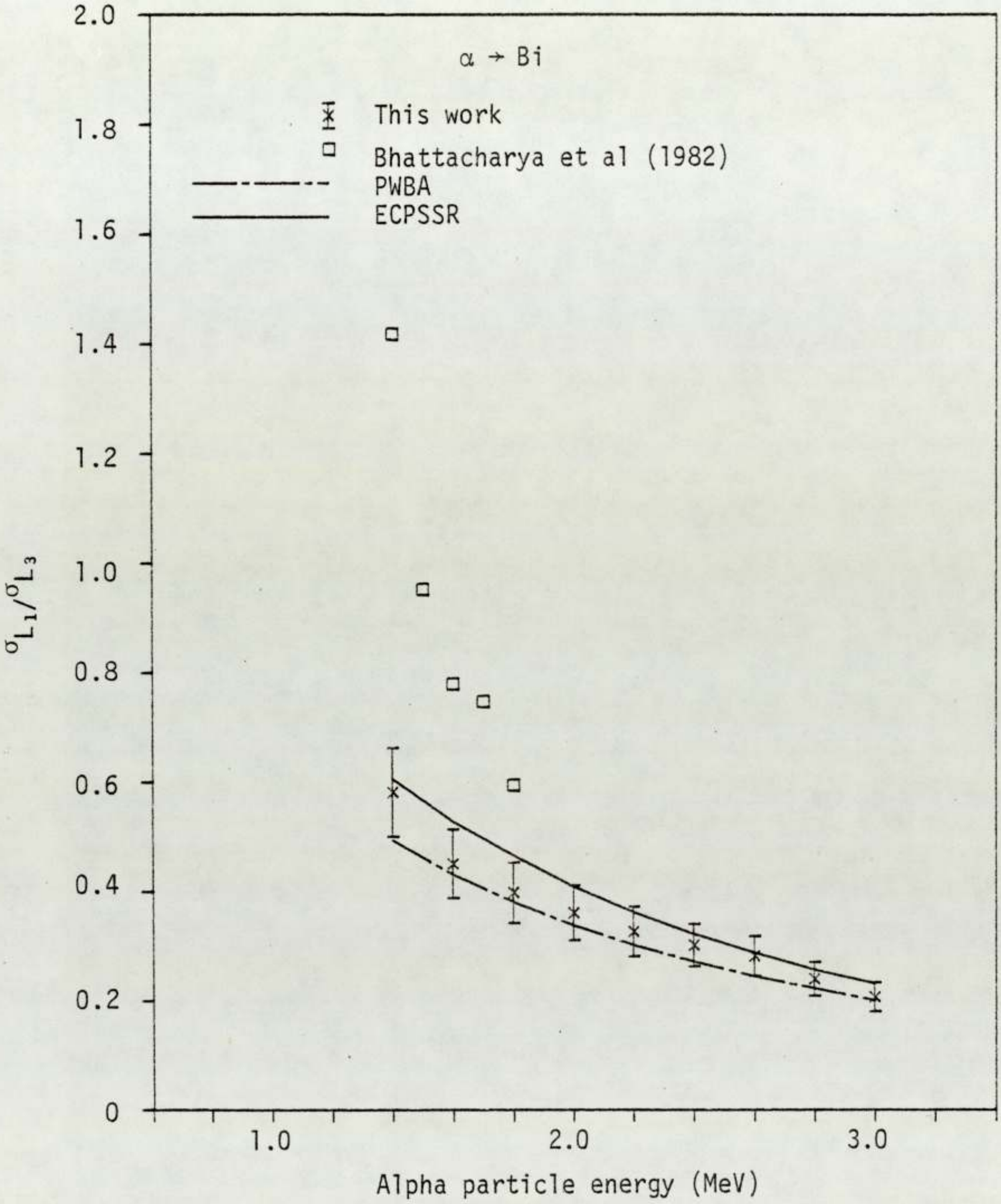

Figure 6.174. Experimental $\sigma_{L_1}/\sigma_{L_3}$ ratio for alpha particle impact on Bi.

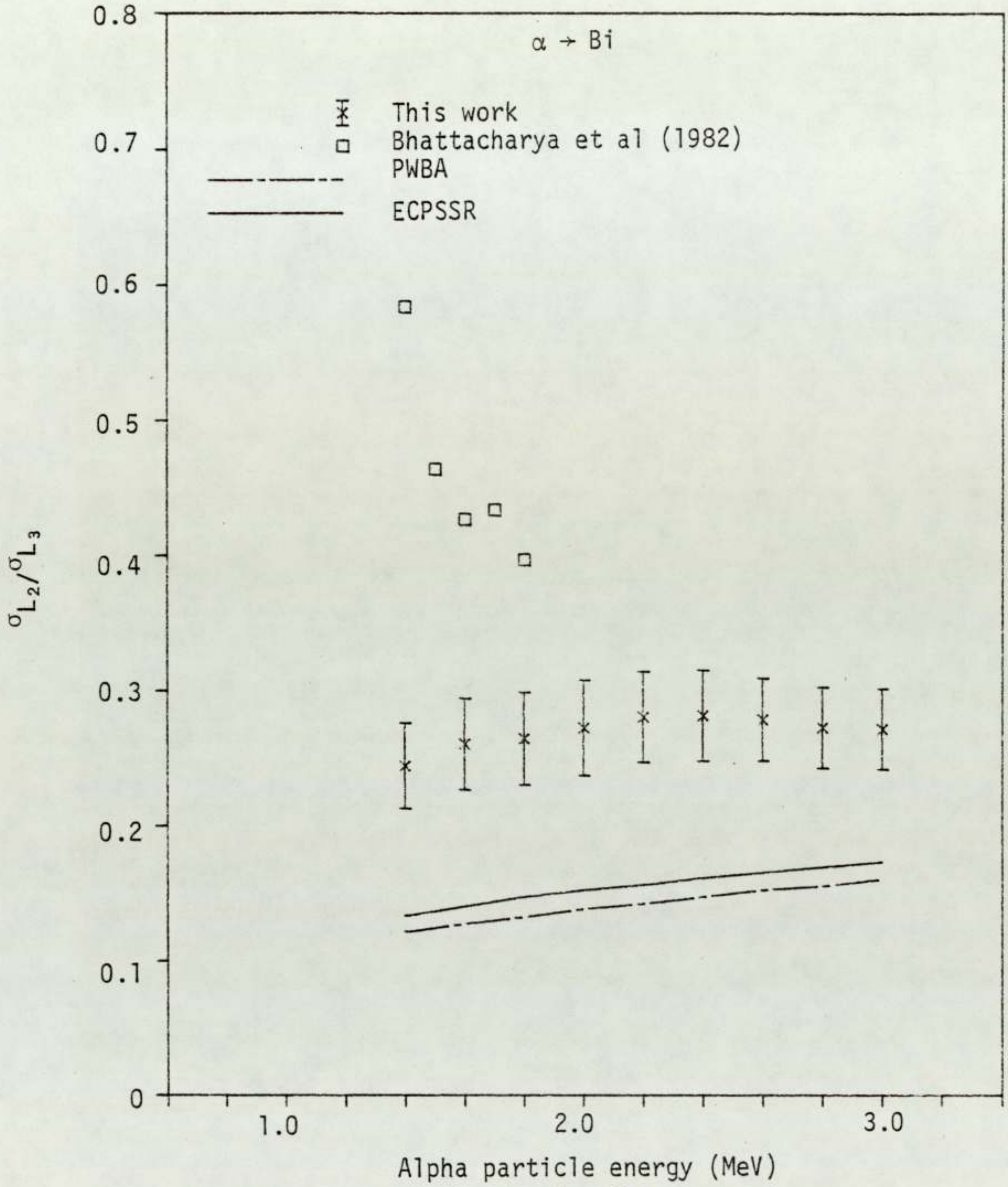

Figure 6.175. Experimental $\sigma_{L_2}/\sigma_{L_3}$ ratio for alpha particle impact on Bi.

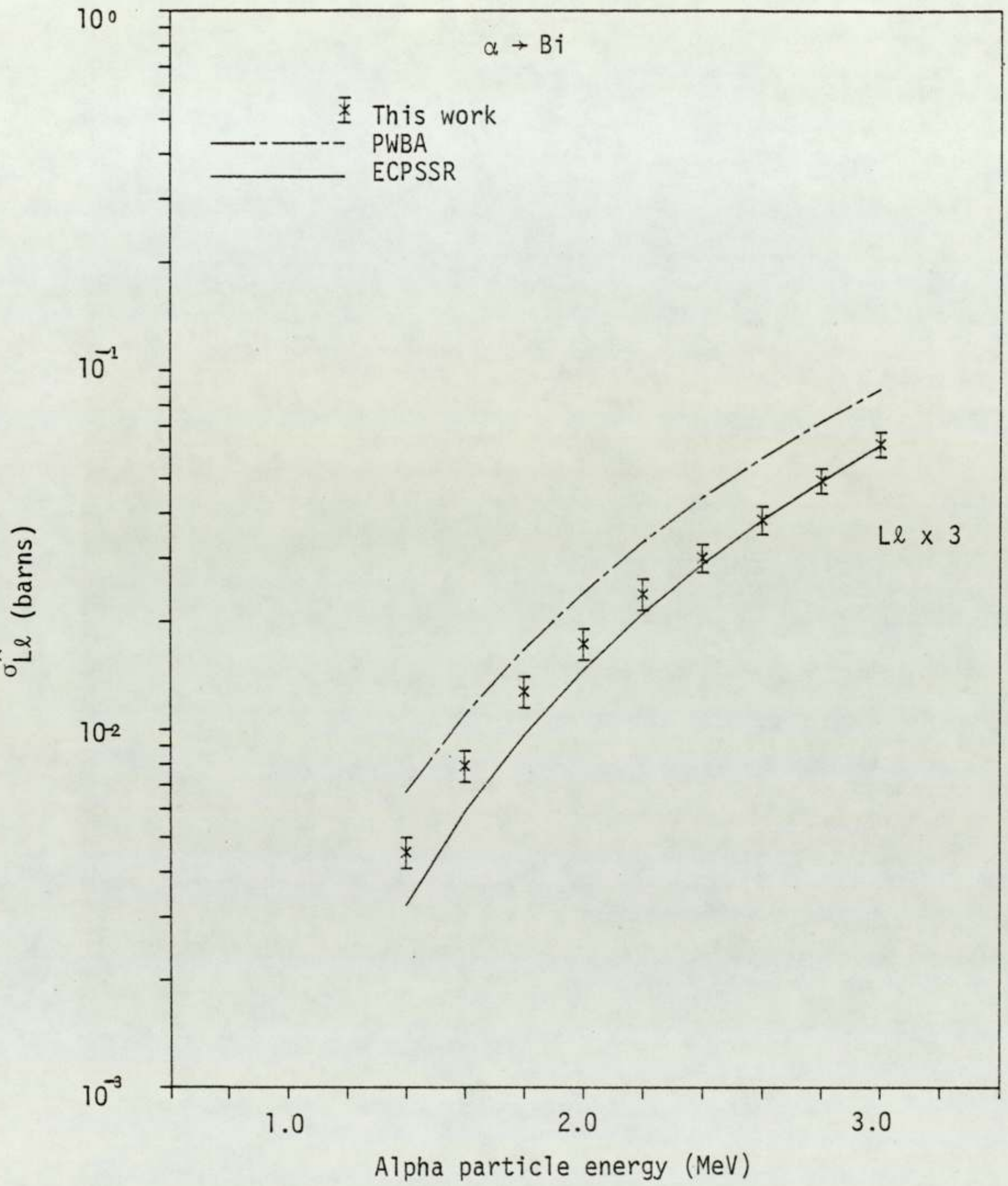

Figure 6.176. Experimental Lℓ x-ray production cross section for alpha particle impact on Bi.

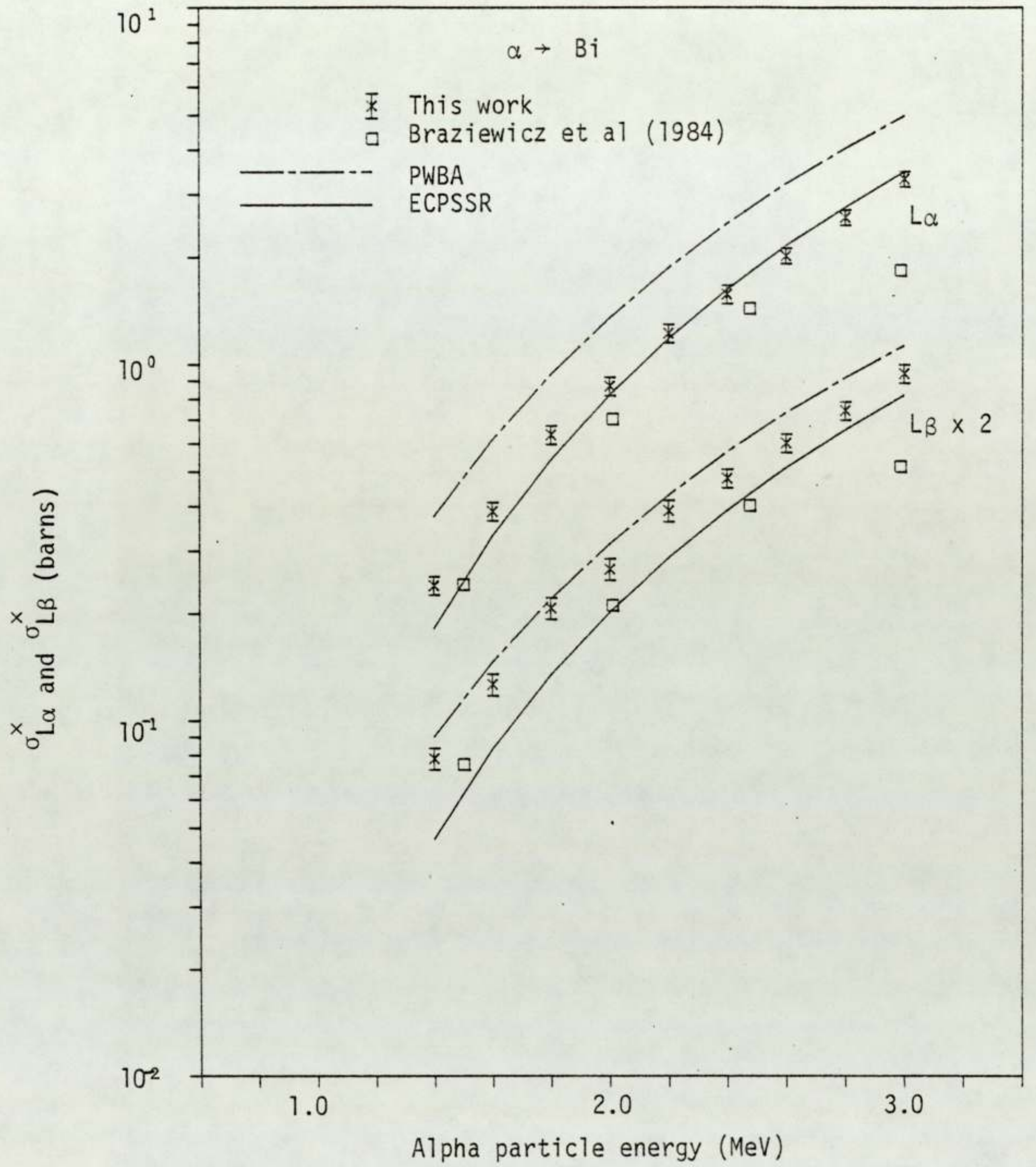

Figure 6.177. Experimental Lα and Lβ x-ray production cross sections for alpha particle impact on Bi.

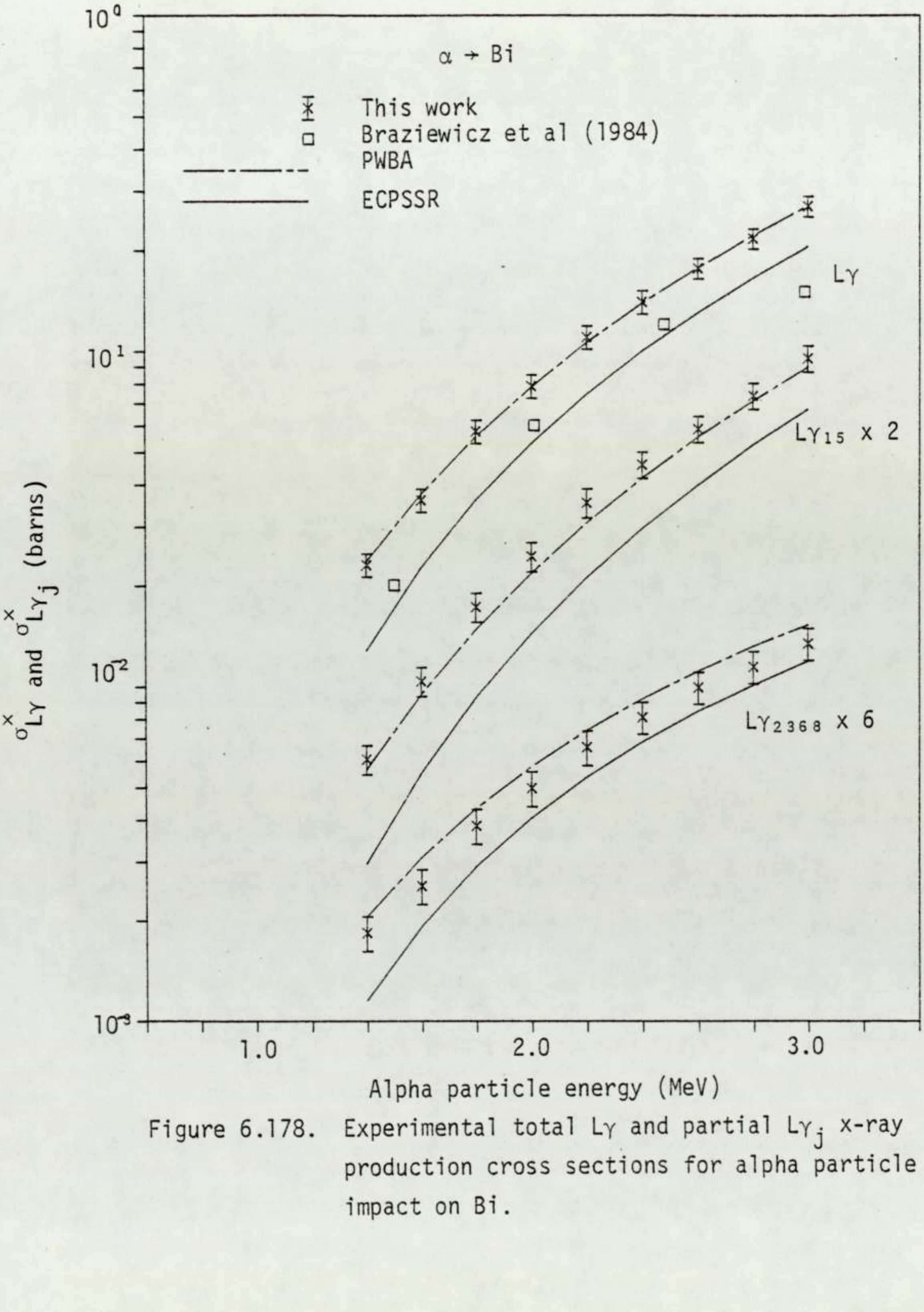

Figure 6.178. Experimental total $L\gamma$ and partial $L\gamma_j$ x-ray production cross sections for alpha particle impact on Bi.

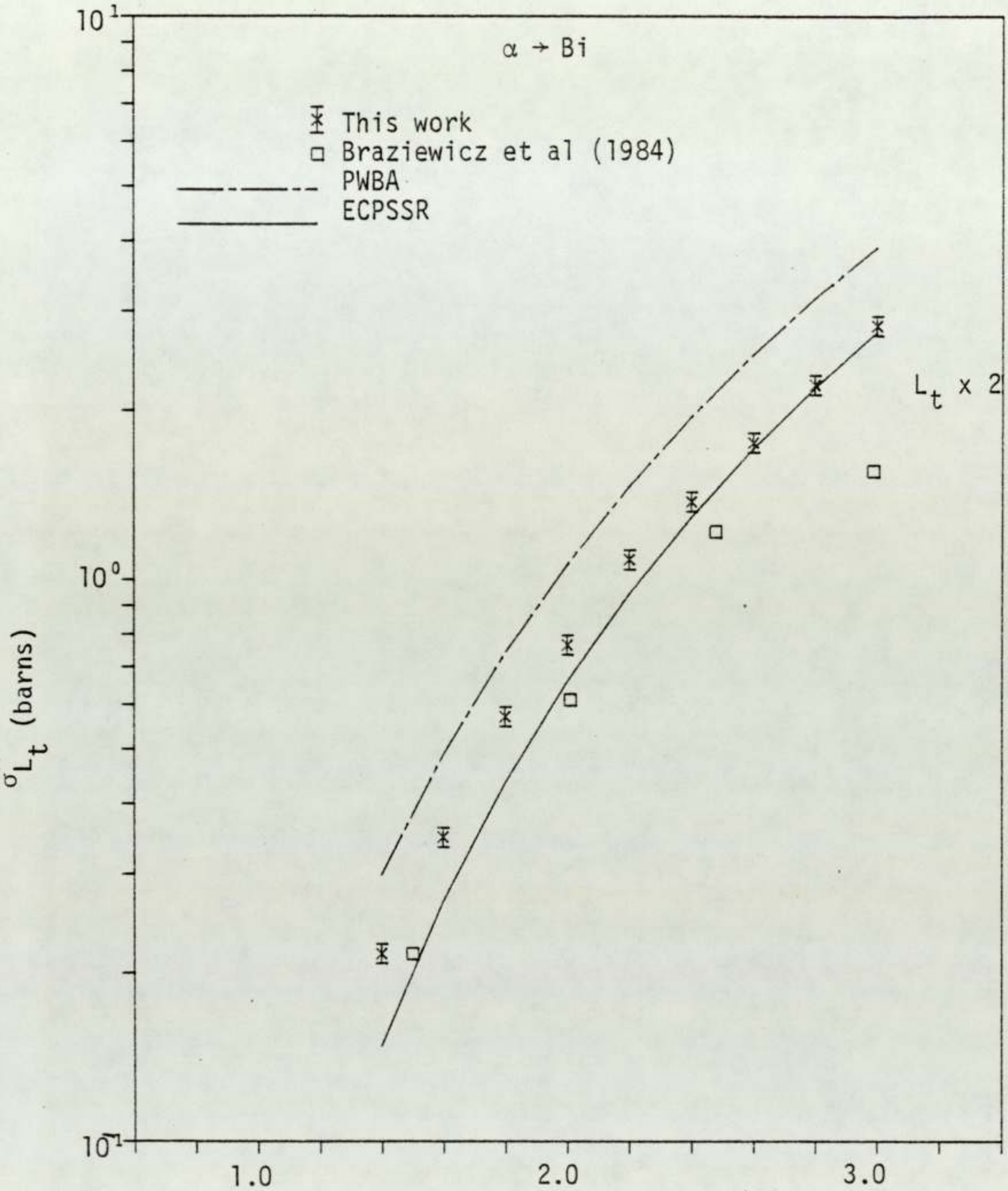

Alpha particle energy (MeV)

Figure 6.179. Experimental total L shell x-ray production cross section for alpha particle impact on Bi.

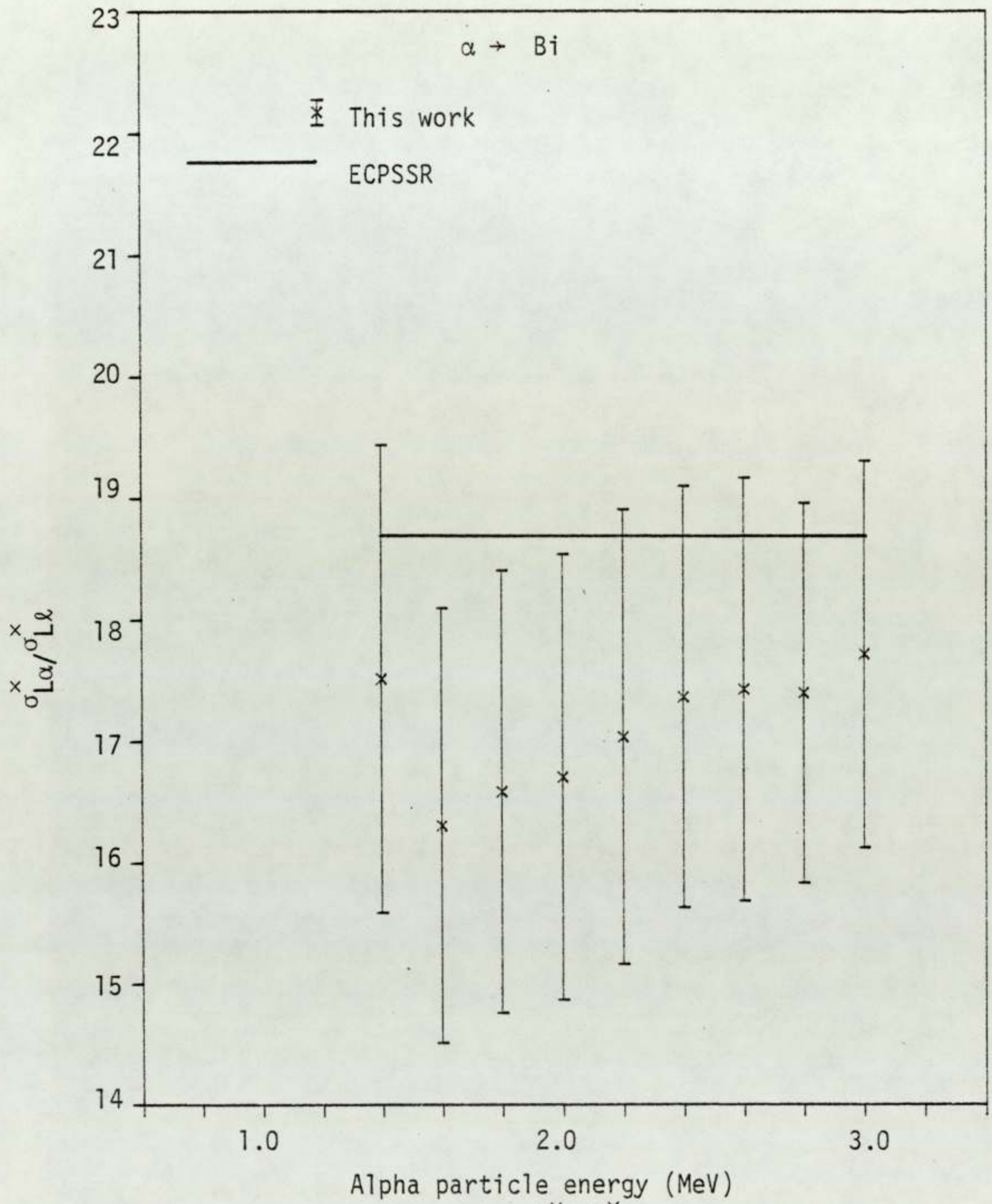

Figure 6.180. Experimental $\sigma^x_{L\alpha}/\sigma^x_{L\ell}$ ratio for alpha particle impact on Bi.

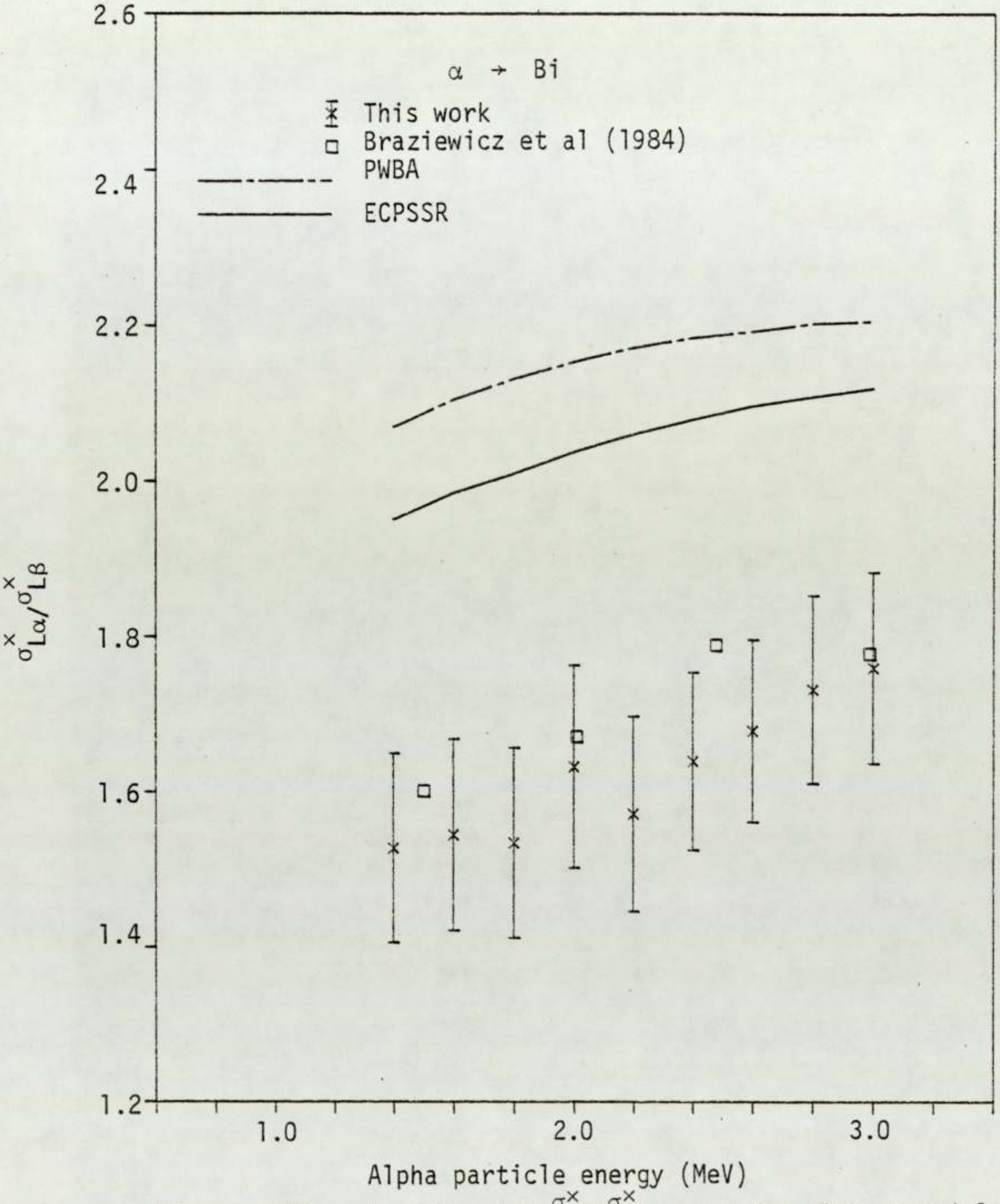

Figure 6.181. Experimental $\sigma^x_{L\alpha}/\sigma^x_{L\beta}$ ratio for alpha particle impact on Bi.

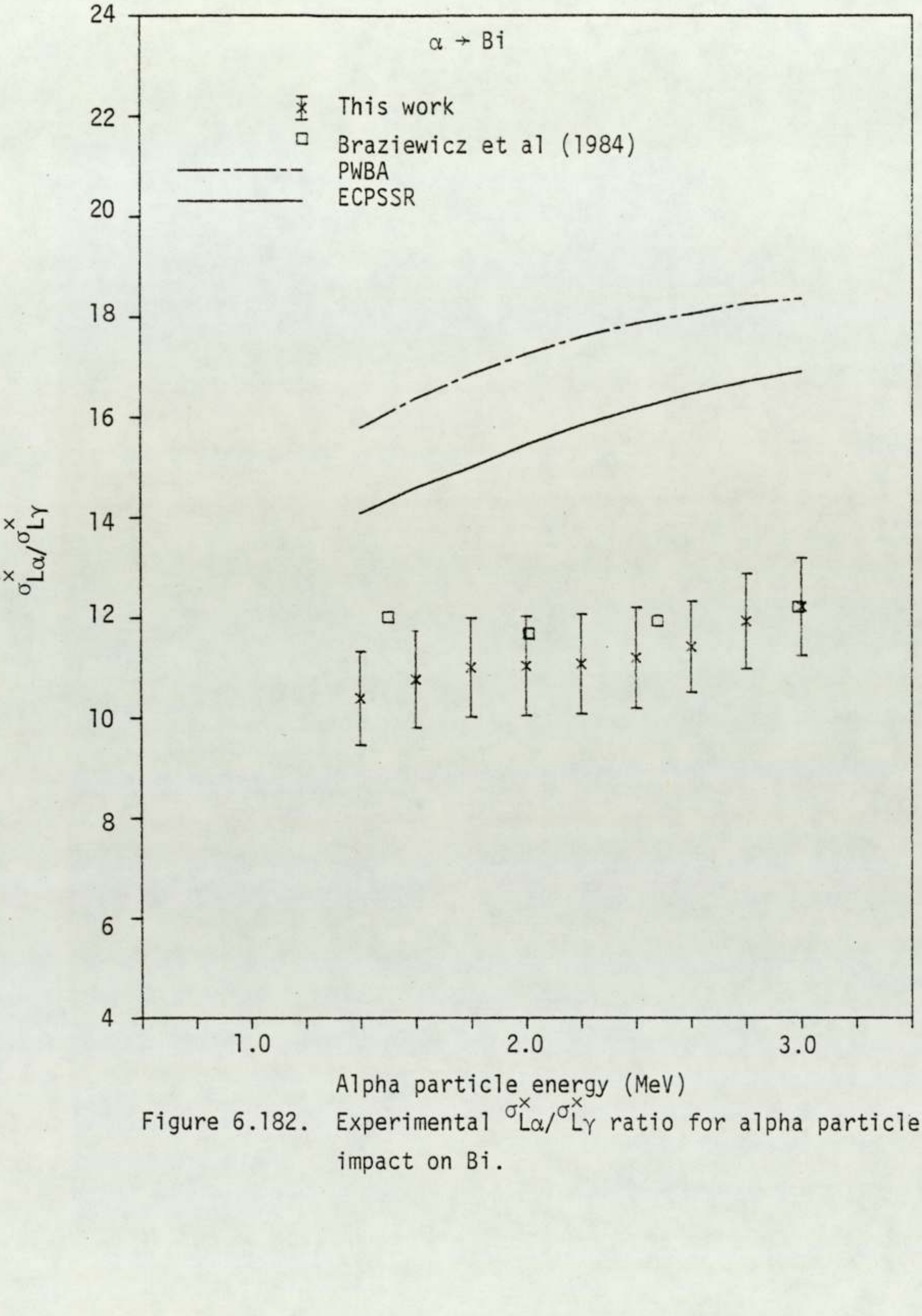

Figure 6.182. Experimental $\sigma^x_{L\alpha}/\sigma^x_{L\gamma}$ ratio for alpha particle impact on Bi.

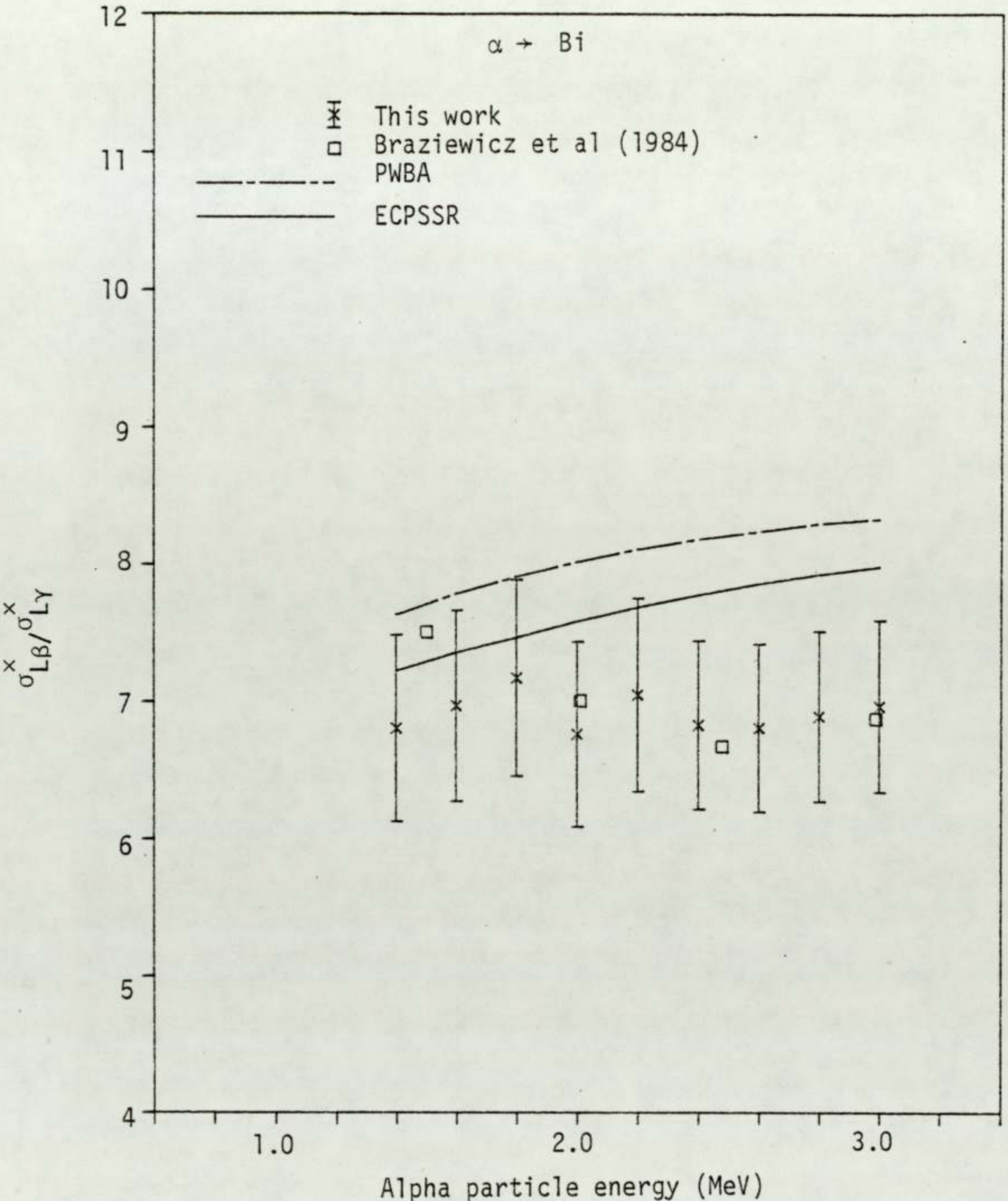

Figure 6.183. Experimental $\sigma^x_{L\beta}/\sigma^x_{L\gamma}$ ratio for alpha particle impact on Bi.

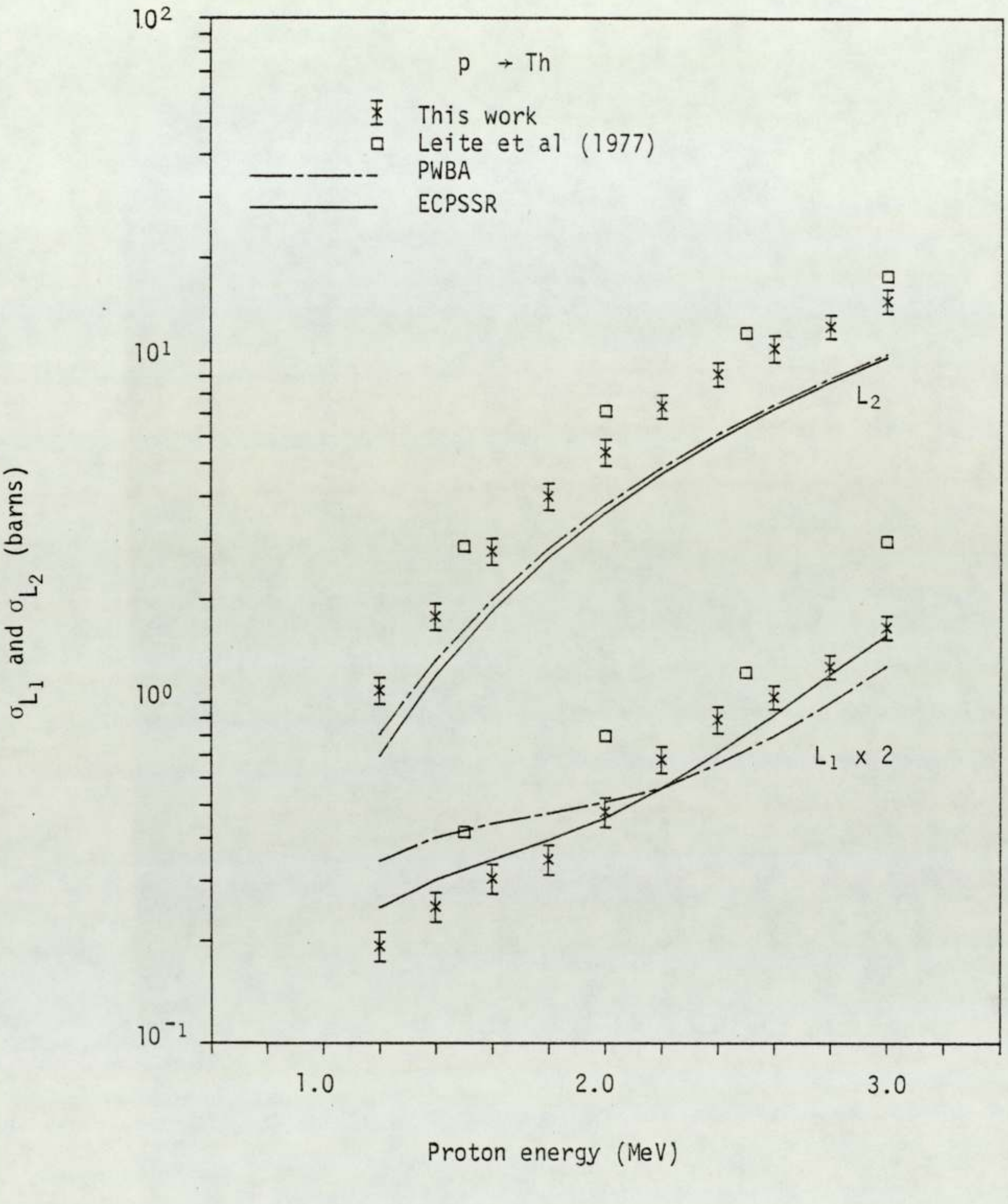

Figure 6.184. Experimental L_1 and L_2 subshell ionisation cross sections for proton impact on Th.

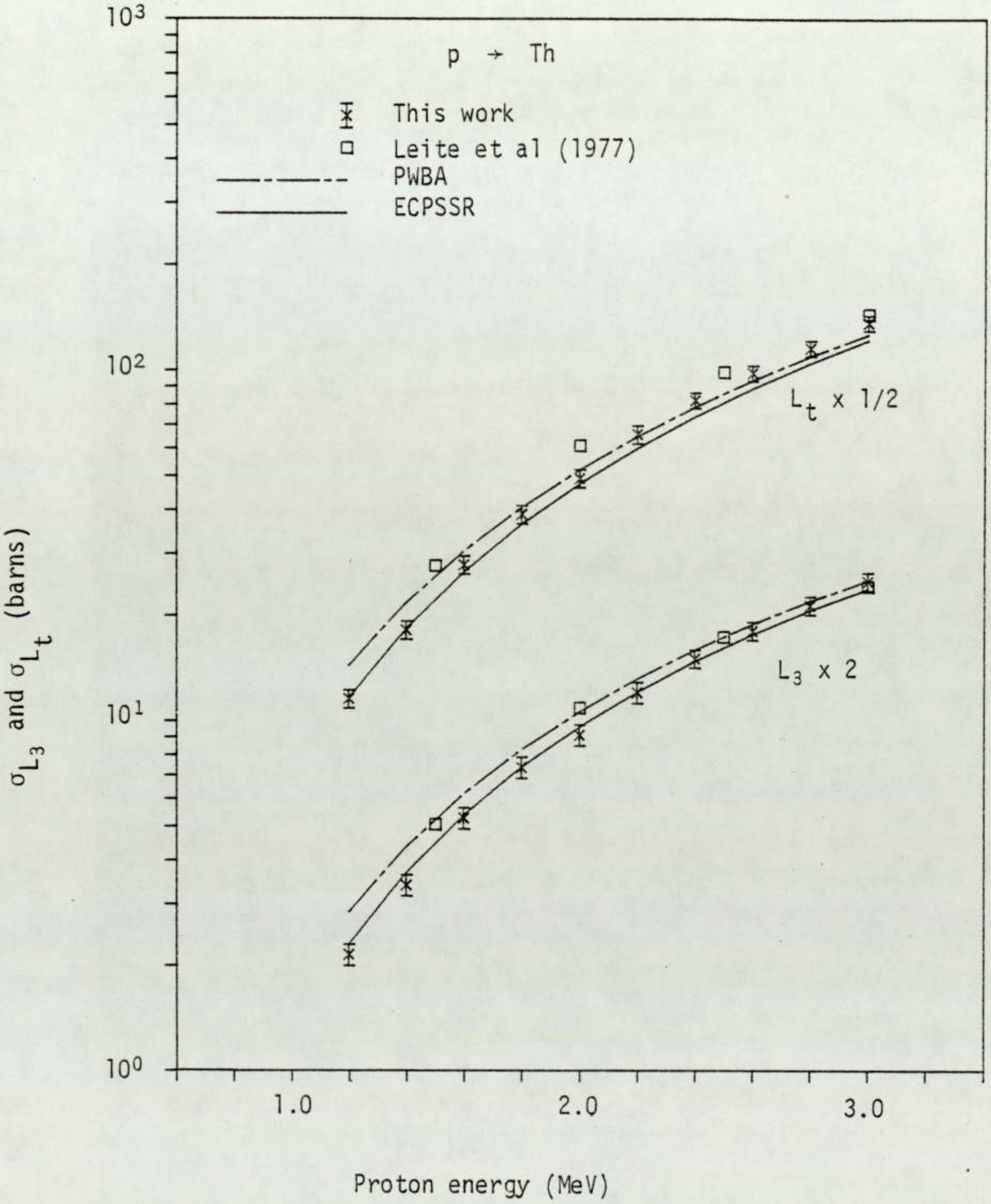

Figure 6.185. Experimental L_3 subshell and total L shell ionisation cross sections for proton impact on Th.

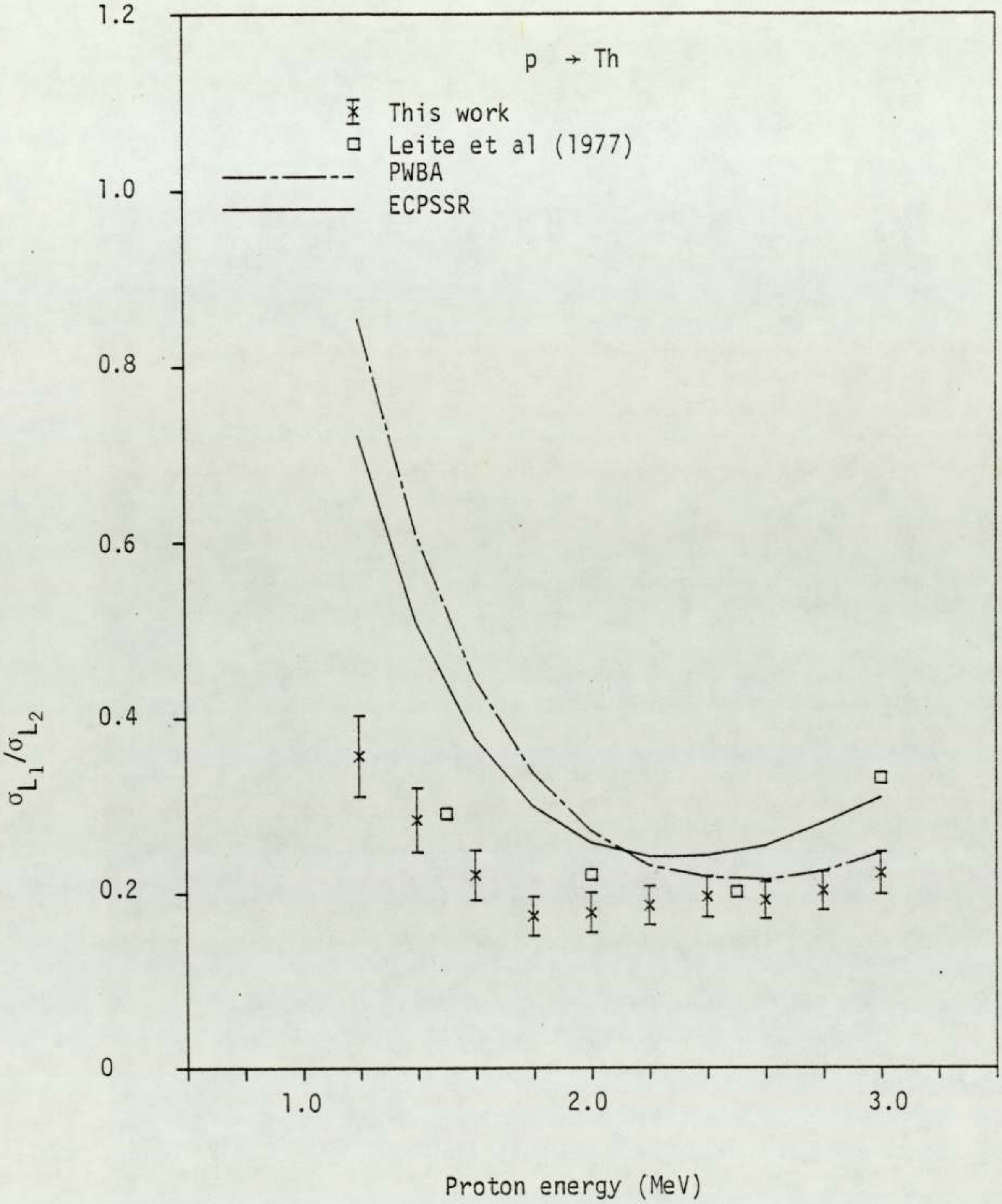

Figure 6.186. Experimental $\sigma_{L_1}/\sigma_{L_2}$ ratio for proton impact on Th.

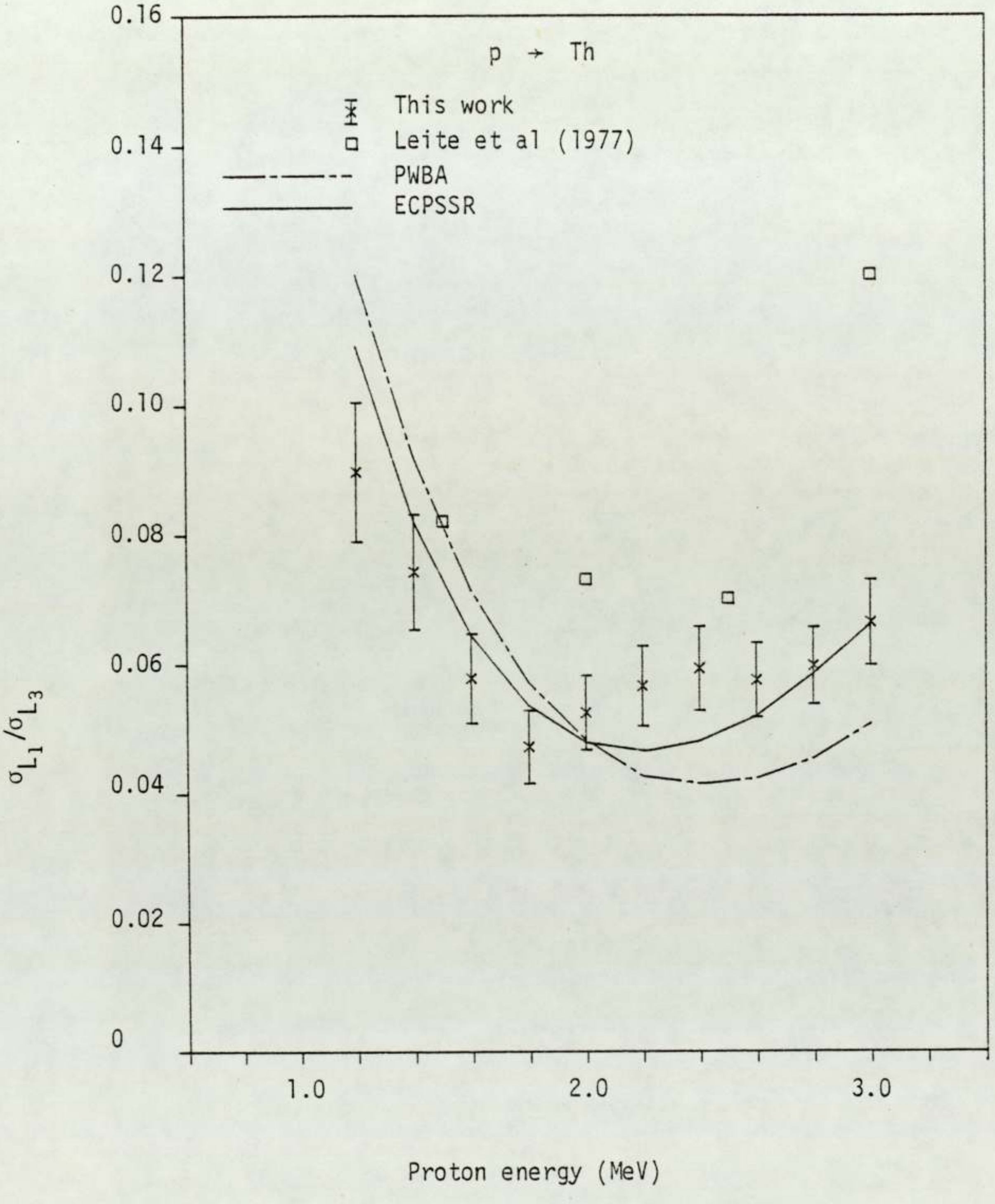

Figure 6.187. Experimental $\sigma_{L_1}/\sigma_{L_3}$ ratio for proton impact on Th.

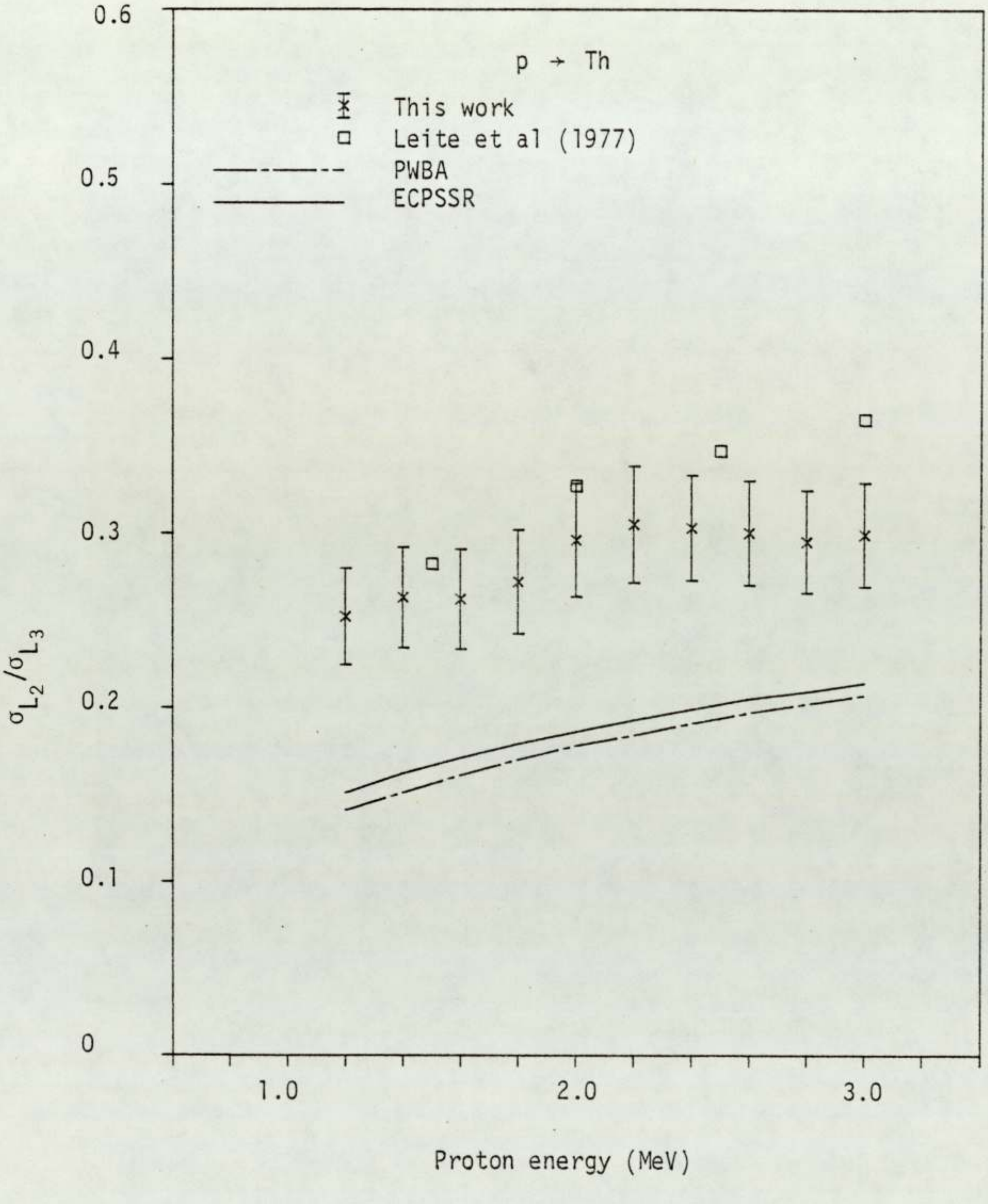

Figure 6.188. Experimental $\sigma_{L_2}/\sigma_{L_3}$ ratio for proton impact on Th.

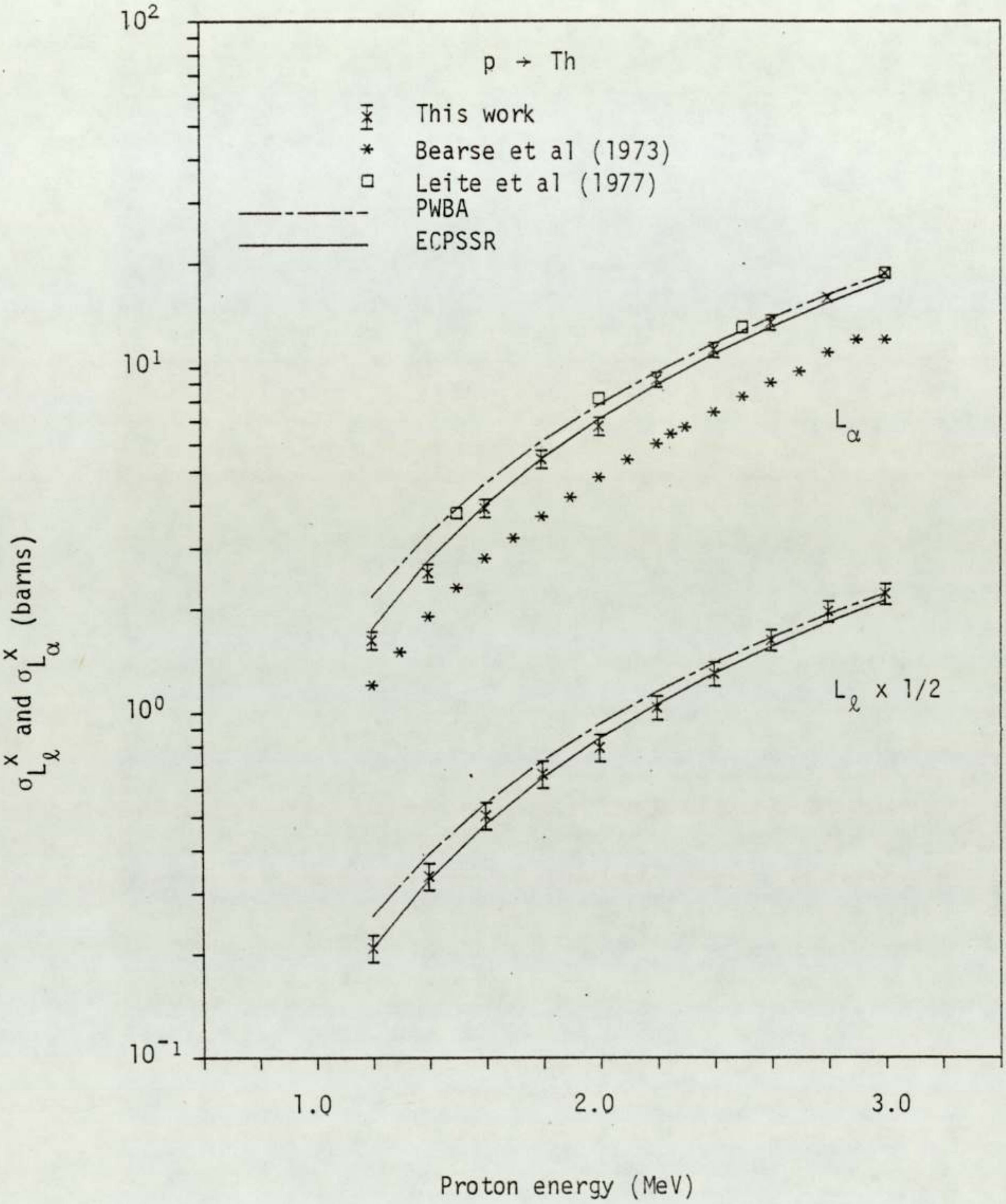

Figure 6.189. Experimental L_ℓ and L_α x-ray production cross sections for proton impact on Th.

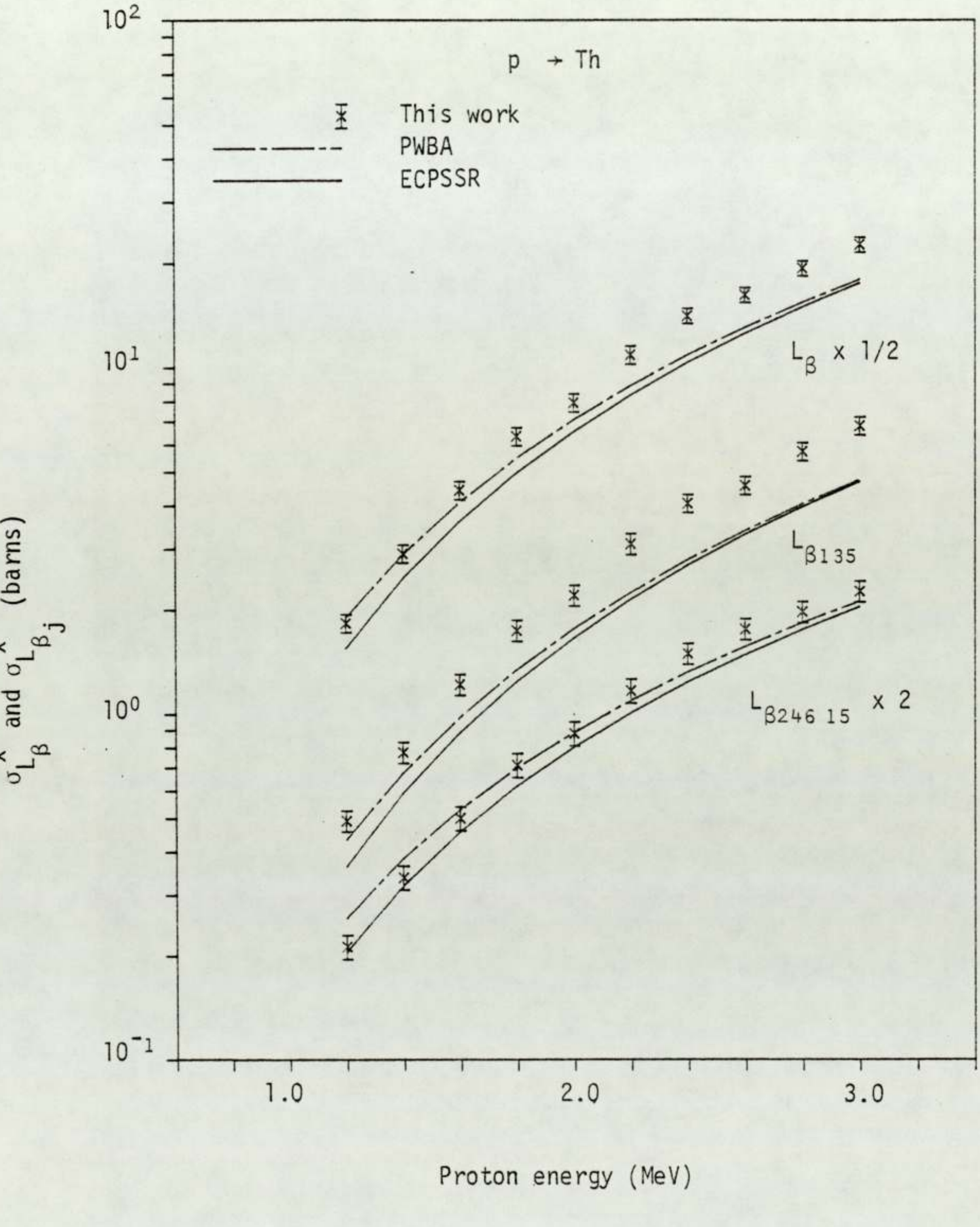

Figure 6.190. Experimental total L_β and partial L_{β_j} x-ray production cross sections for proton impact on Th.

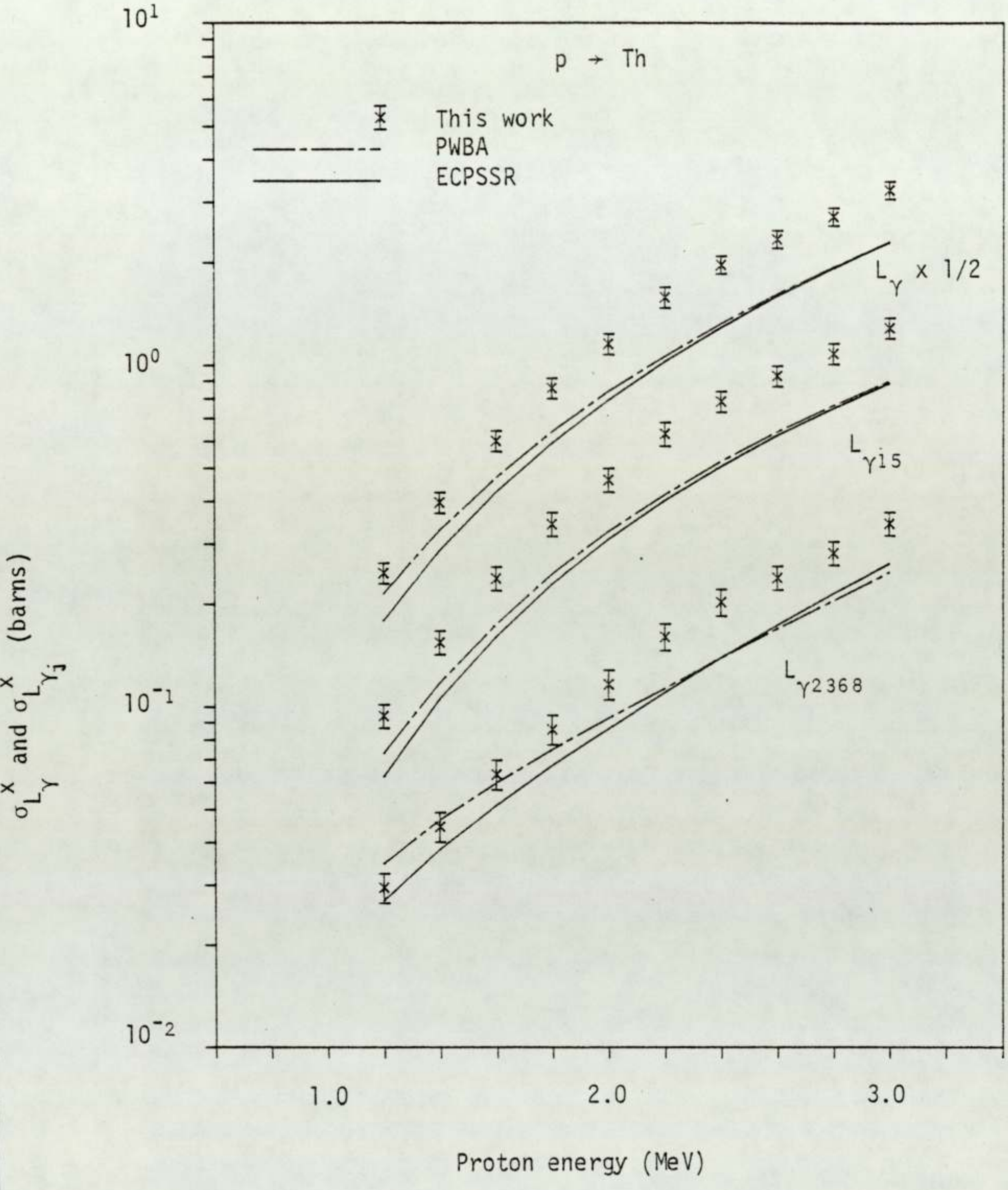

Figure 6.191. Experimental total L_γ and partial L_{γ_j} x-ray production cross sections for impact on Th.

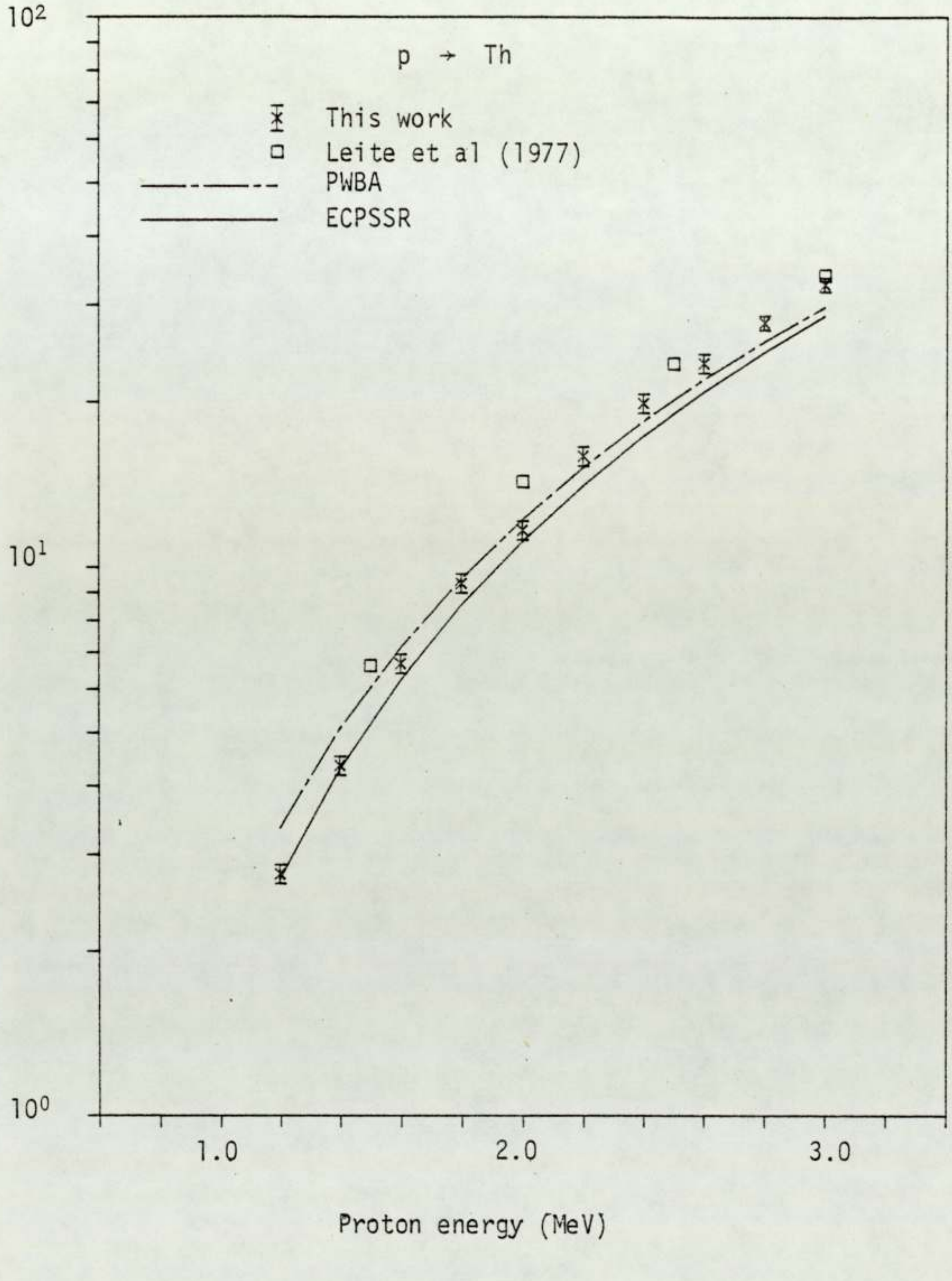

Figure 6.192. Experimental total L shell x-ray production cross section for proton impact on Th.

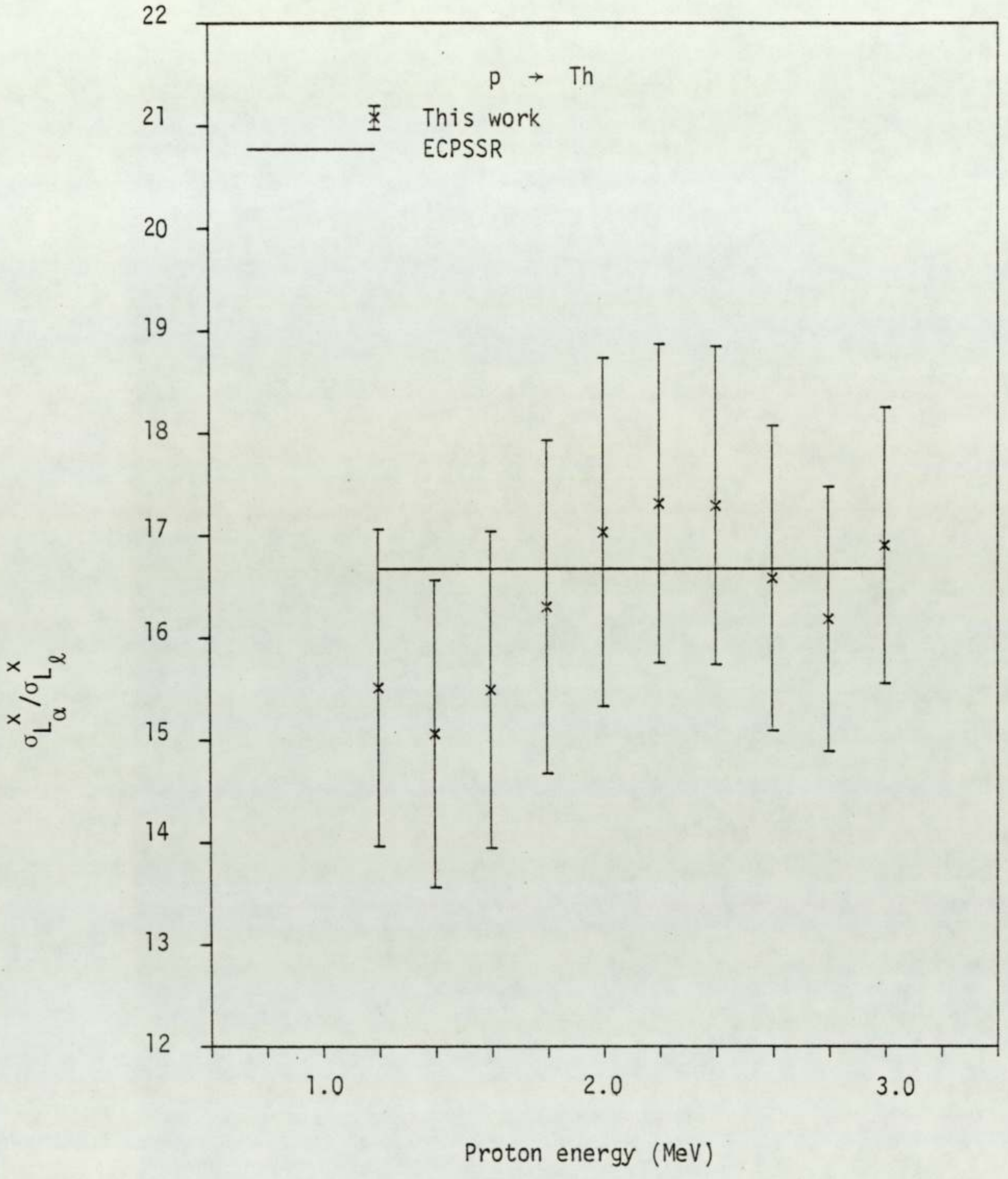

Figure 6.193. Experimental $\sigma_{L_\alpha}^X/\sigma_{L_\ell}^X$ ratio for proton impact on Th.

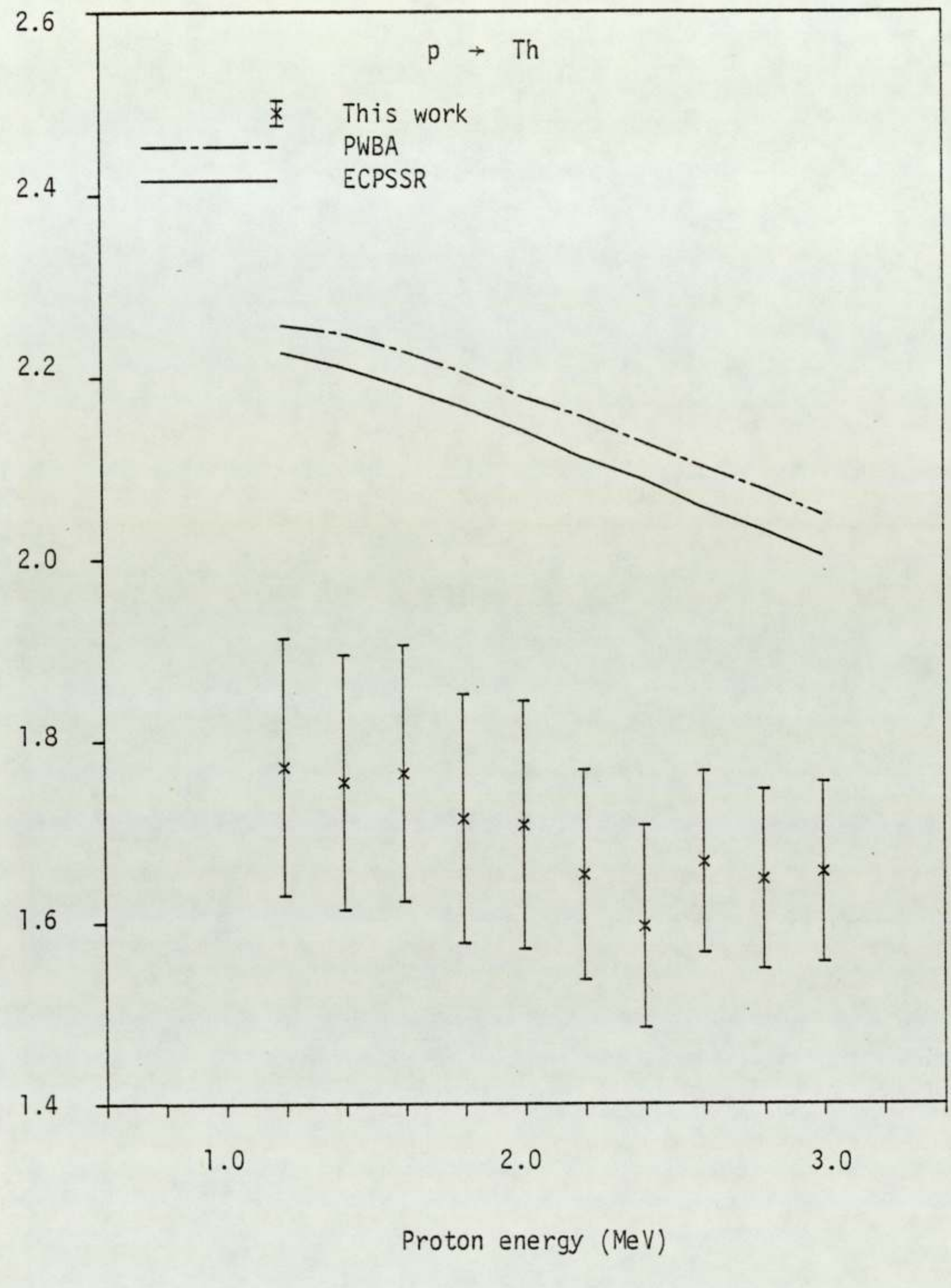

Figure 6.194. Experimental $\sigma_{L_\alpha}^{x}/\sigma_{L_\beta}^{x}$ ratio for proton impact on Th.

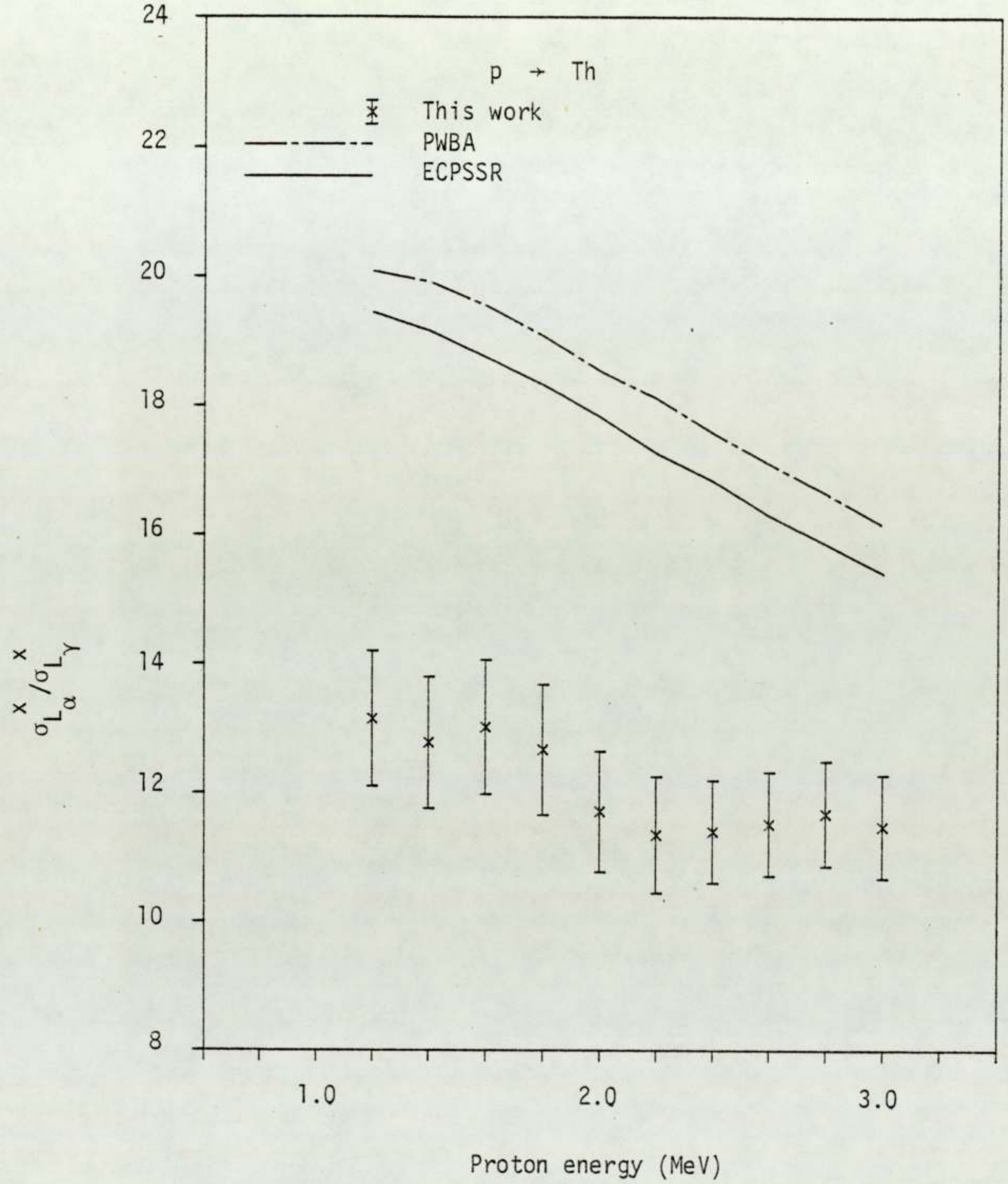

Figure 6.195. Experimental $\sigma_{L_\alpha}^{x}/\sigma_{L_\gamma}^{x}$ ratio for proton impact on Th.

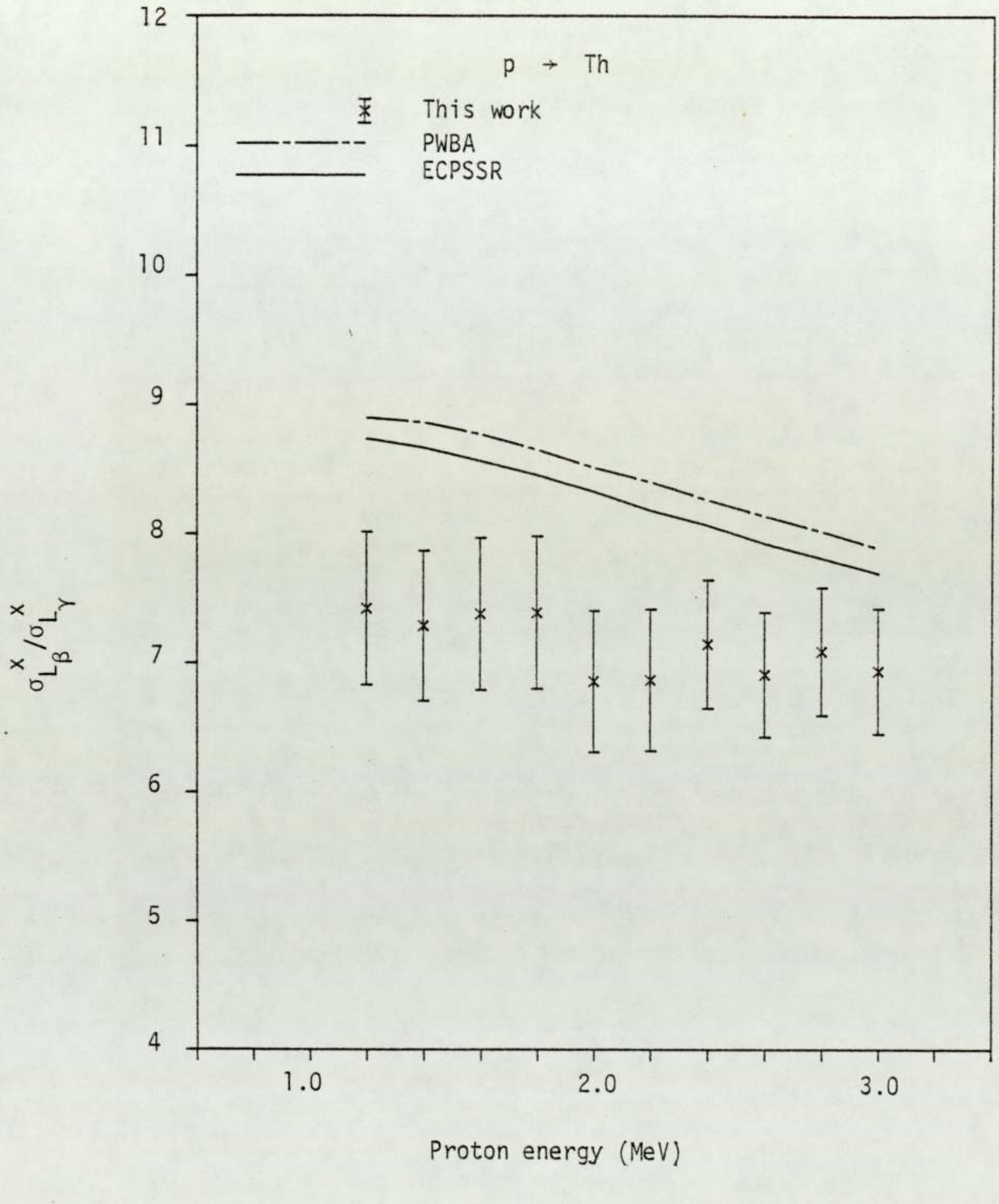

Figure 6.196. Experimental $\sigma^x_{L_\beta}/\sigma^x_{L_\gamma}$ ratio for proton impact on Th.

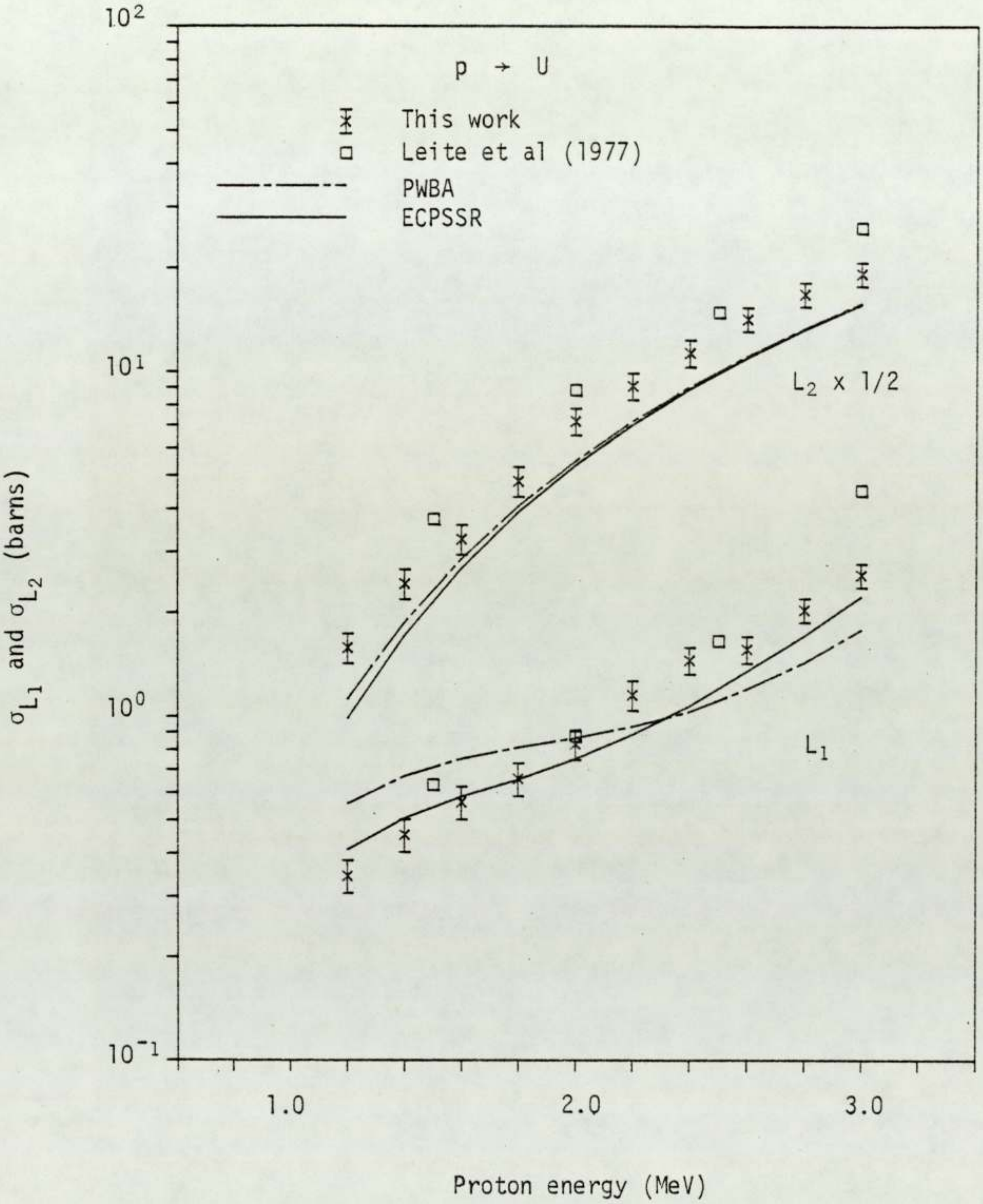

Figure 6.197. Experimental L_1 and L_2 subshell ionisation cross sections for proton on U.

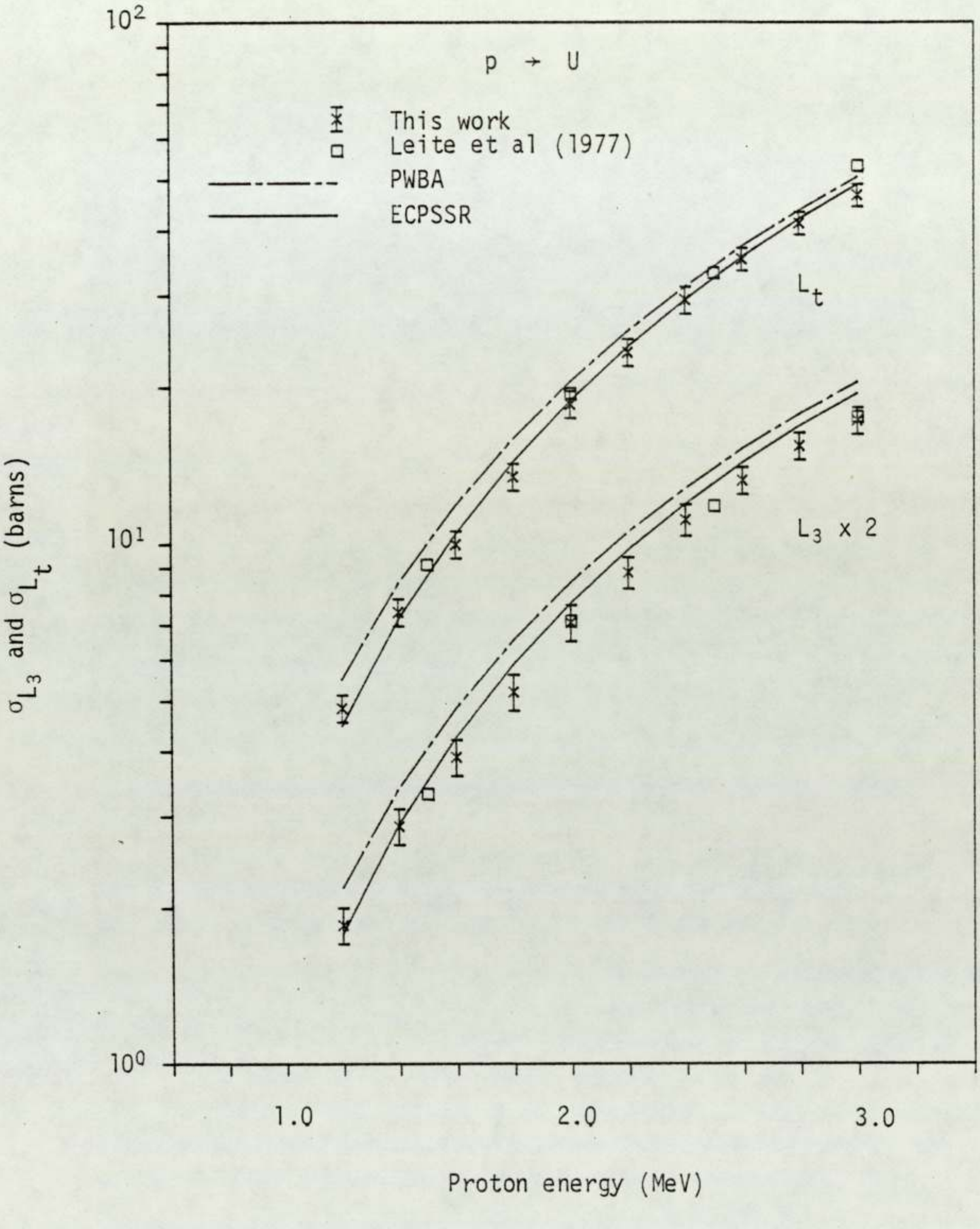

Figure 6.198. Experimental L_3 subshell and total L shell ionisation cross section for proton impact on U.

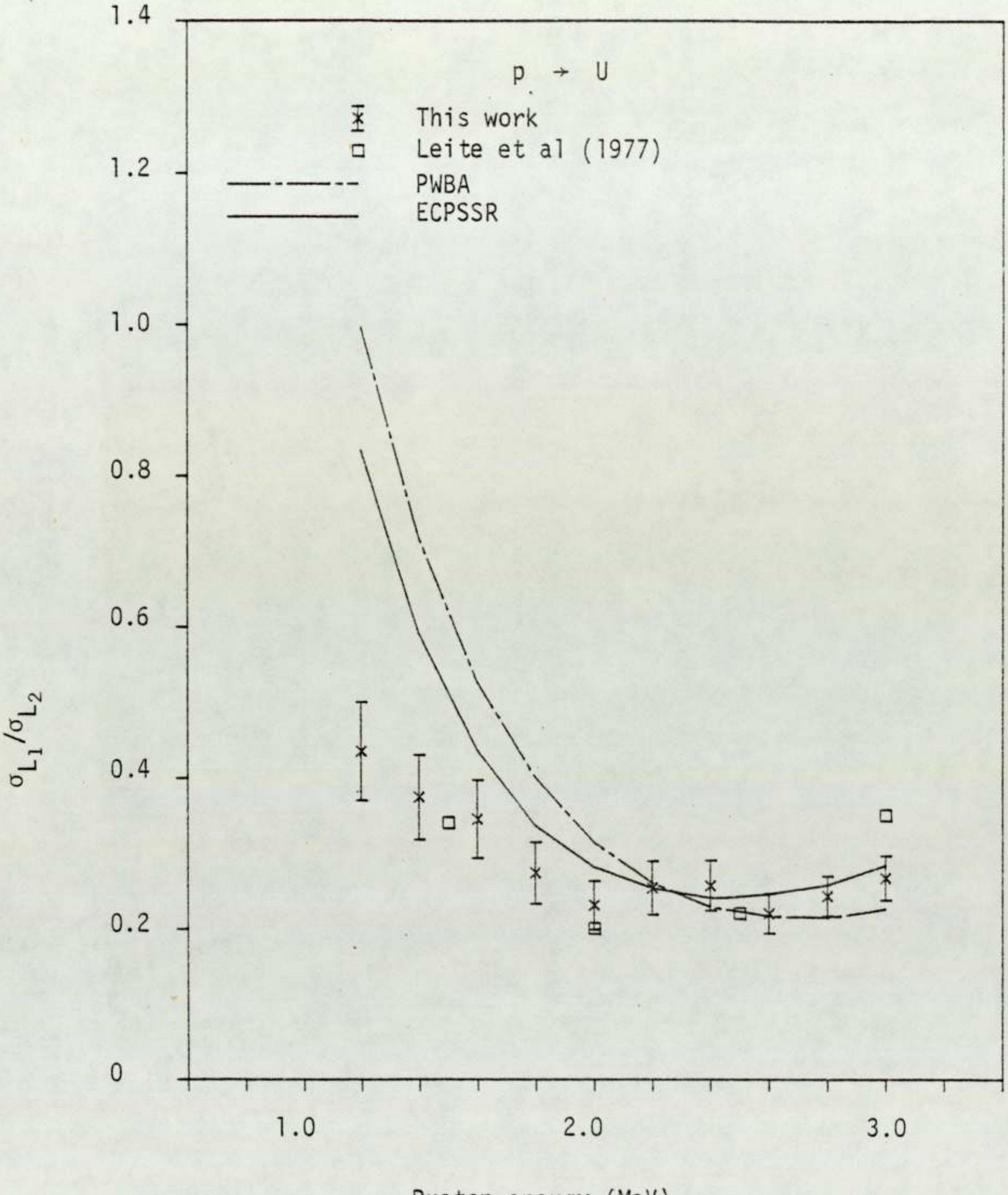

Figure 6.199. Experimental $\sigma_{L_1}/\sigma_{L_2}$ ratio for proton impact on U.

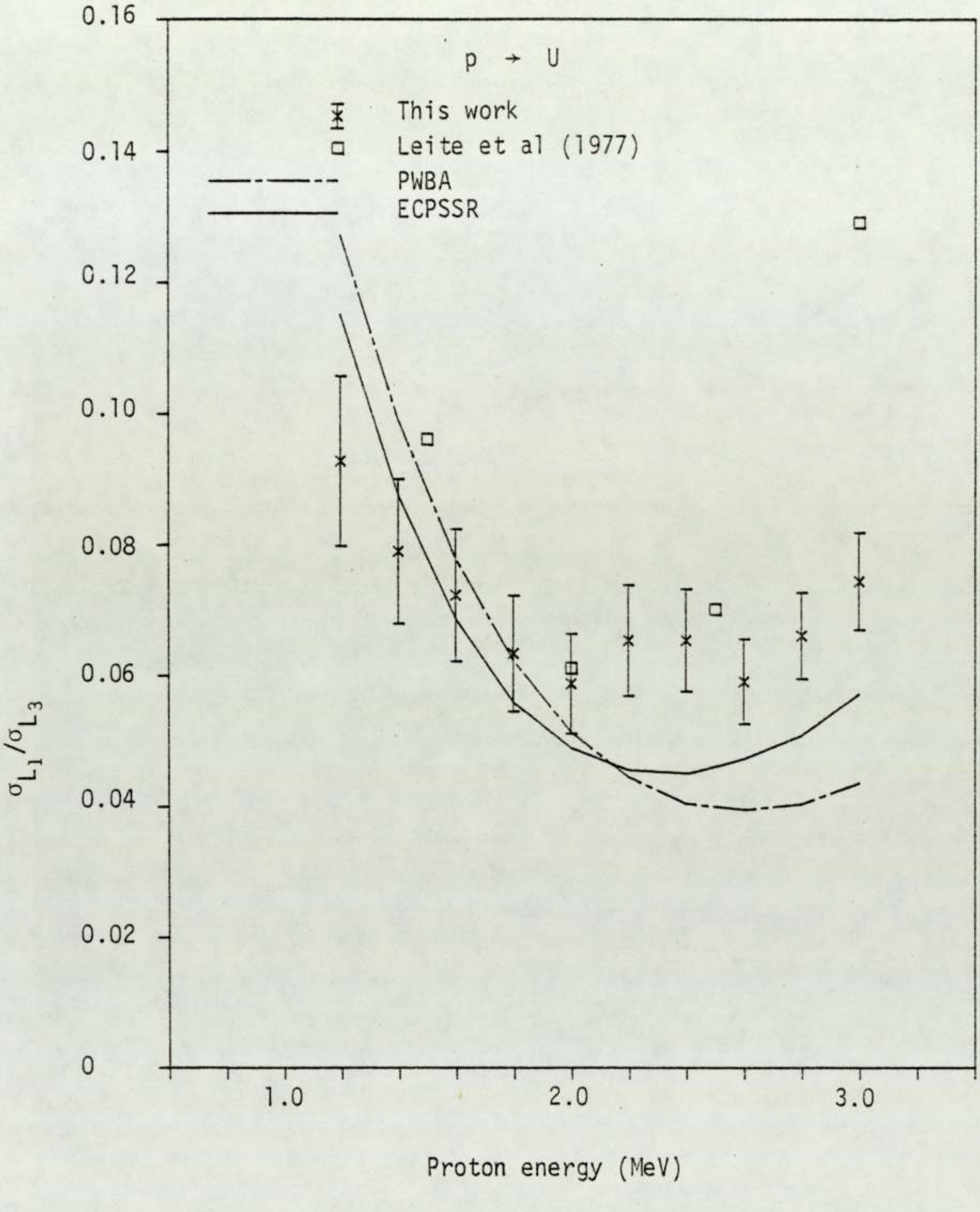

Figure 6.200. Experimental $\sigma_{L_1}/\sigma_{L_3}$ ratio for proton impact on U.

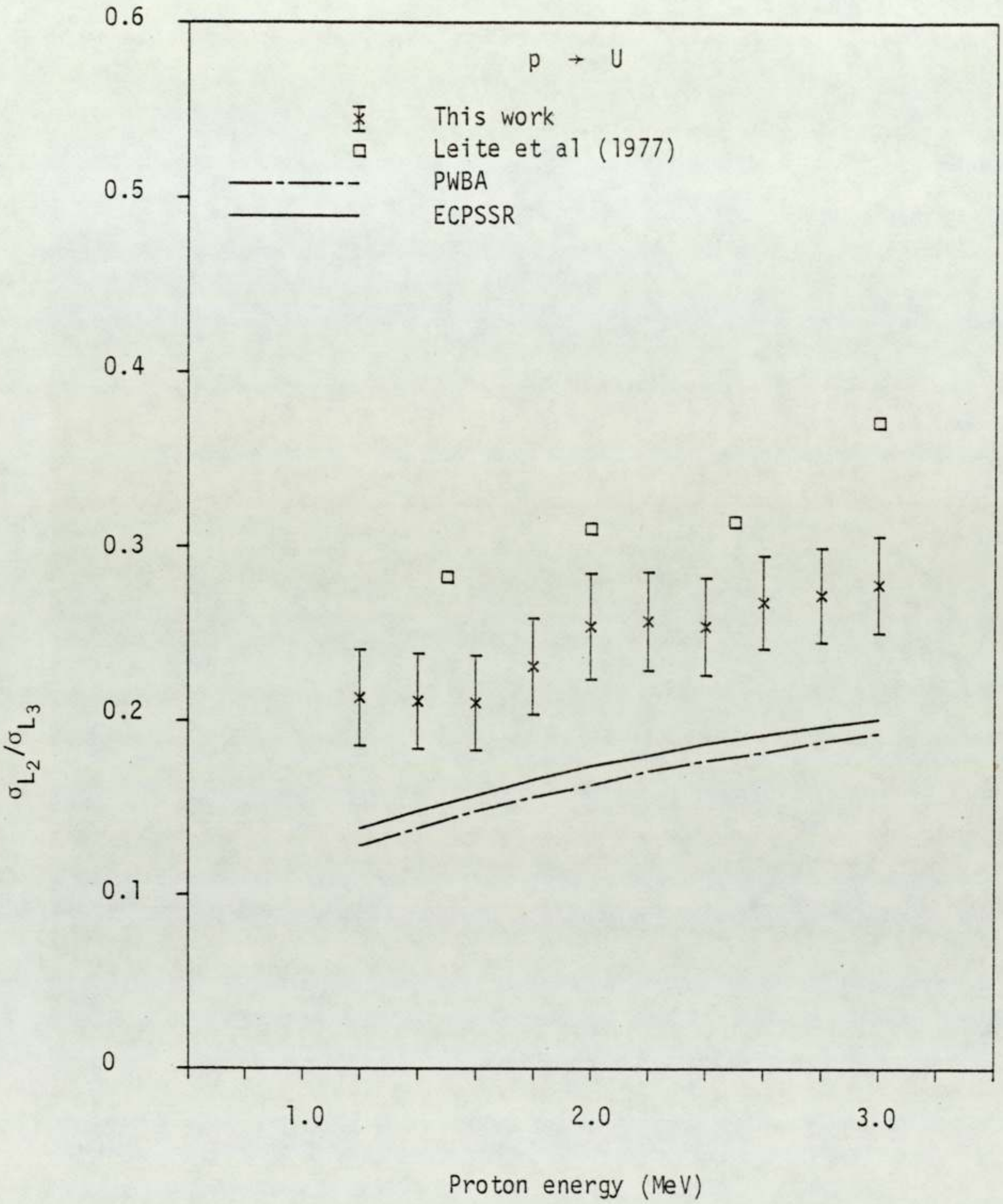

Figure 6.201. Experimental $\sigma_{L_2}/\sigma_{L_3}$ ratio for proton impact on U.

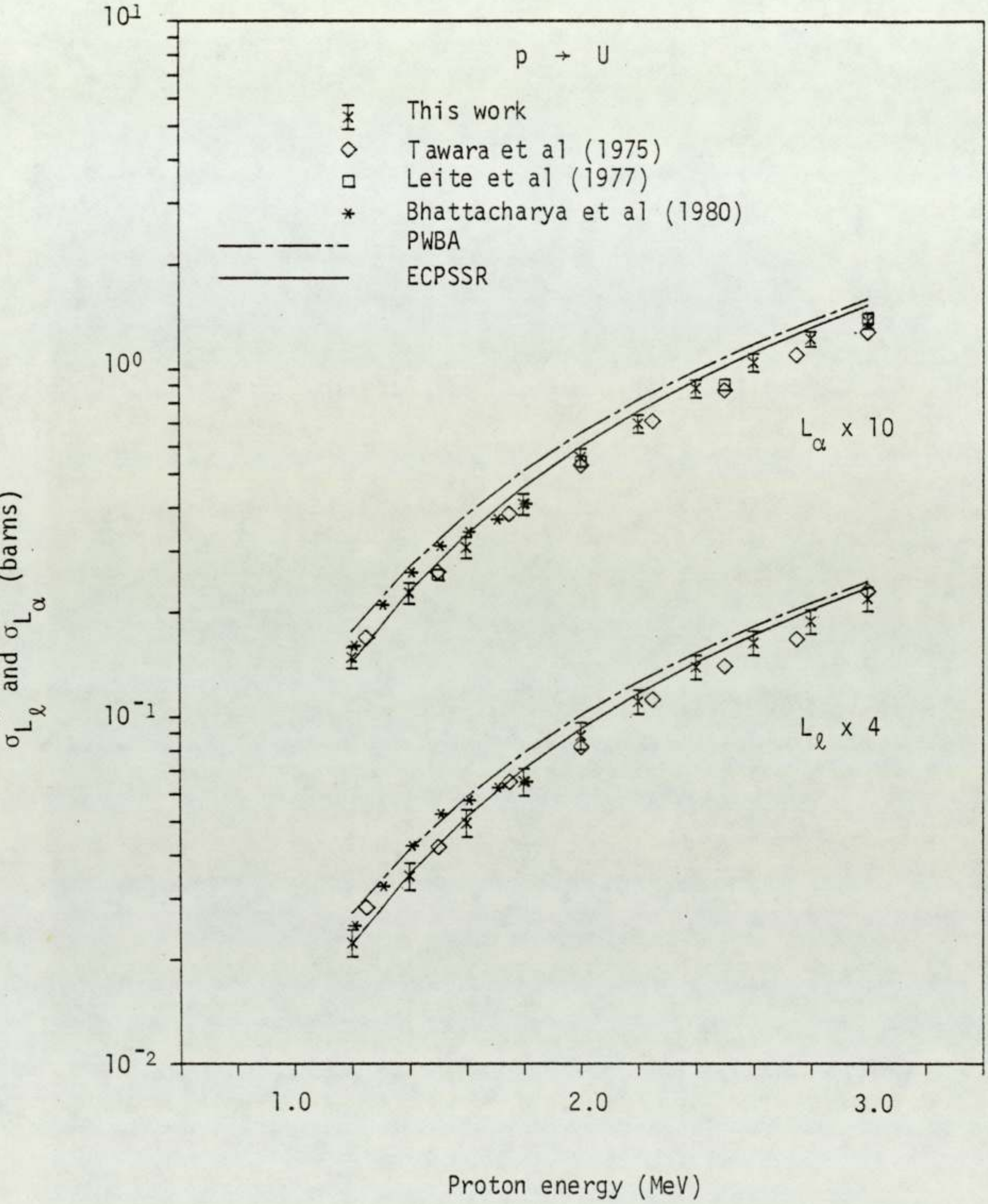

Figure 6.202. Experimental L_ℓ and L_α x-ray production cross sections for proton impact on U.

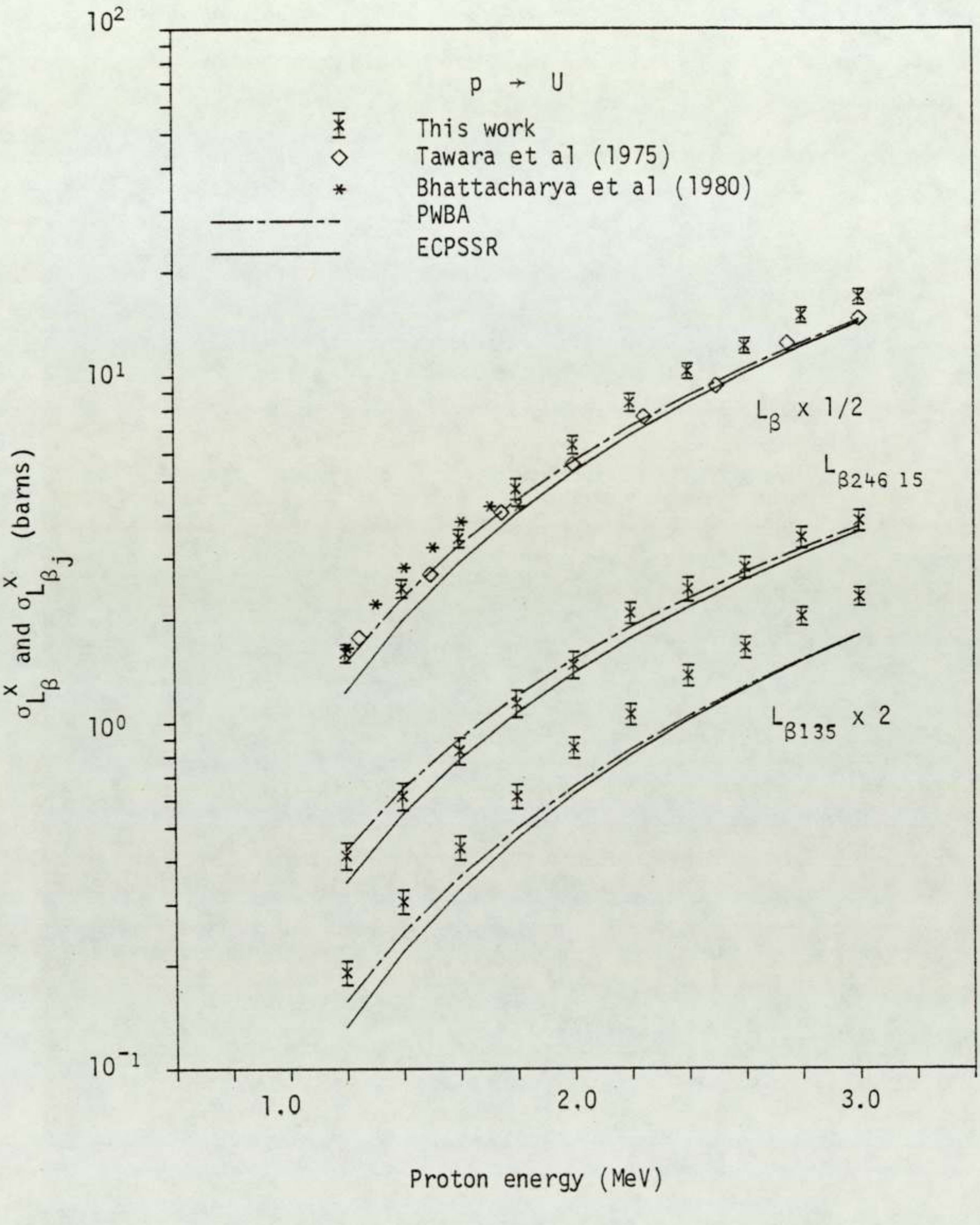

Figure 6.203. Experimental total L_β and partial L_{β_j} x-ray production cross sections for proton impact on U.

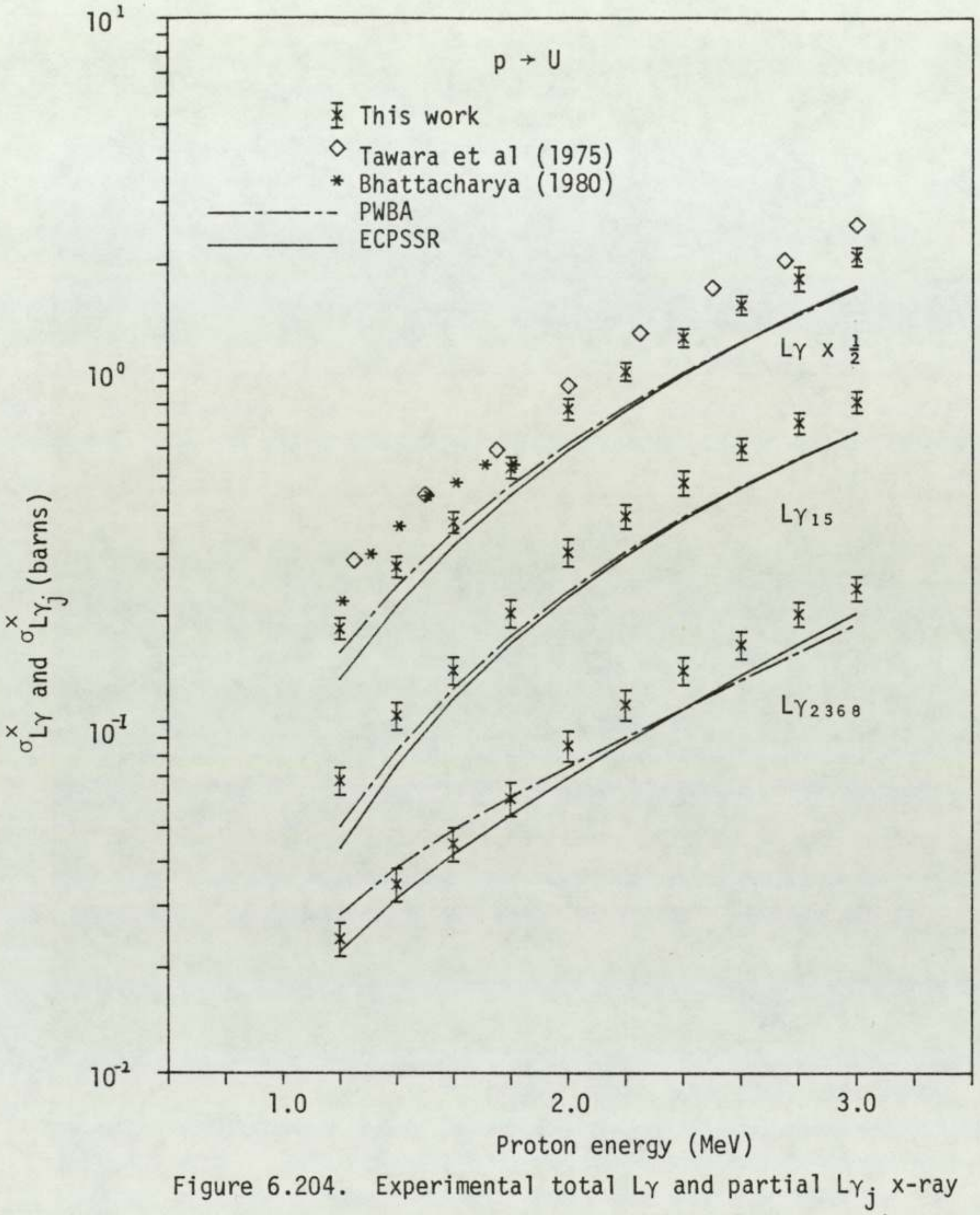

Figure 6.204. Experimental total Lγ and partial $L\gamma_j$ x-ray production cross sections for proton impact on U.

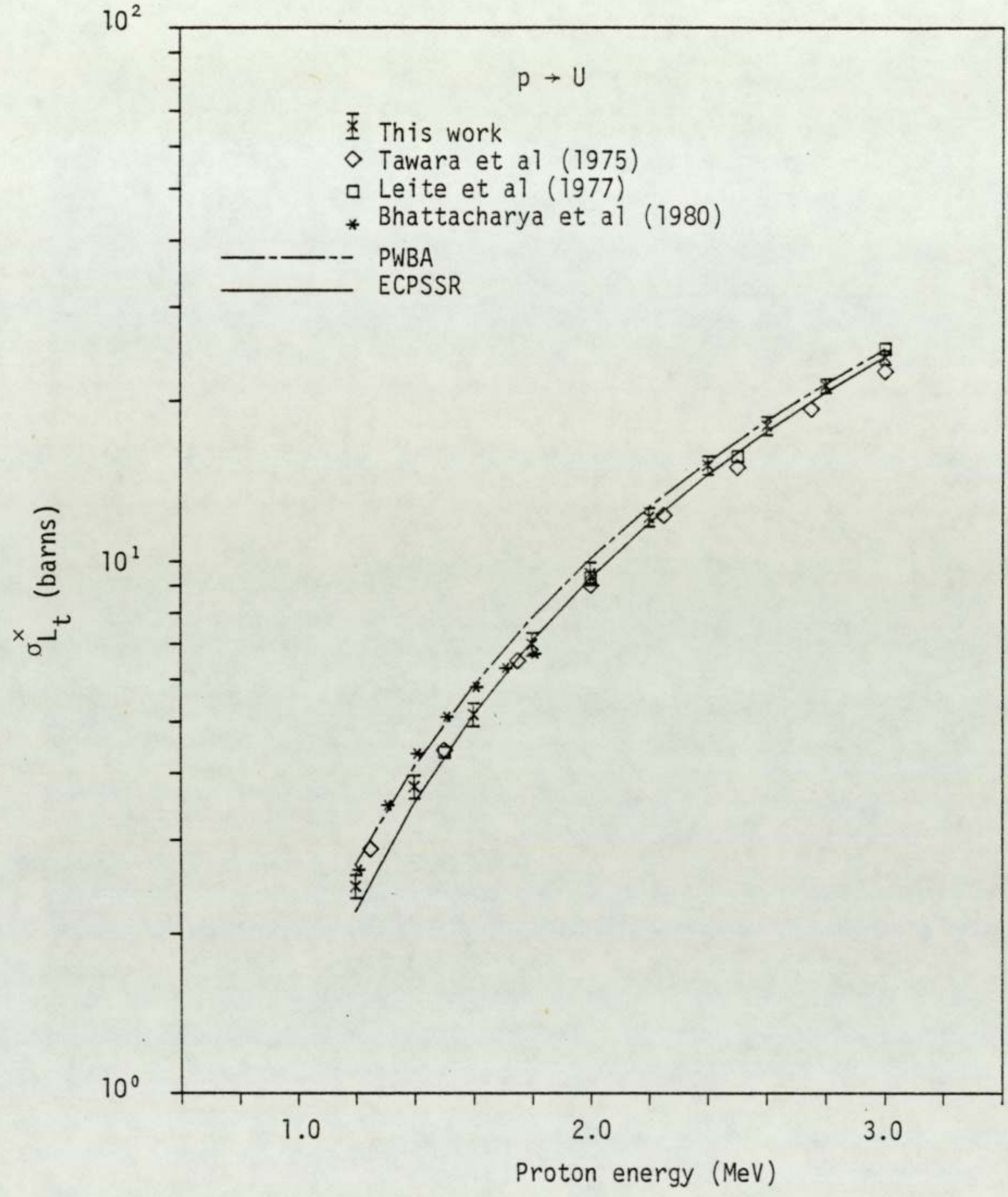

Figure 6.205. Experimental total L shell x-ray production cross section for proton impact on U.

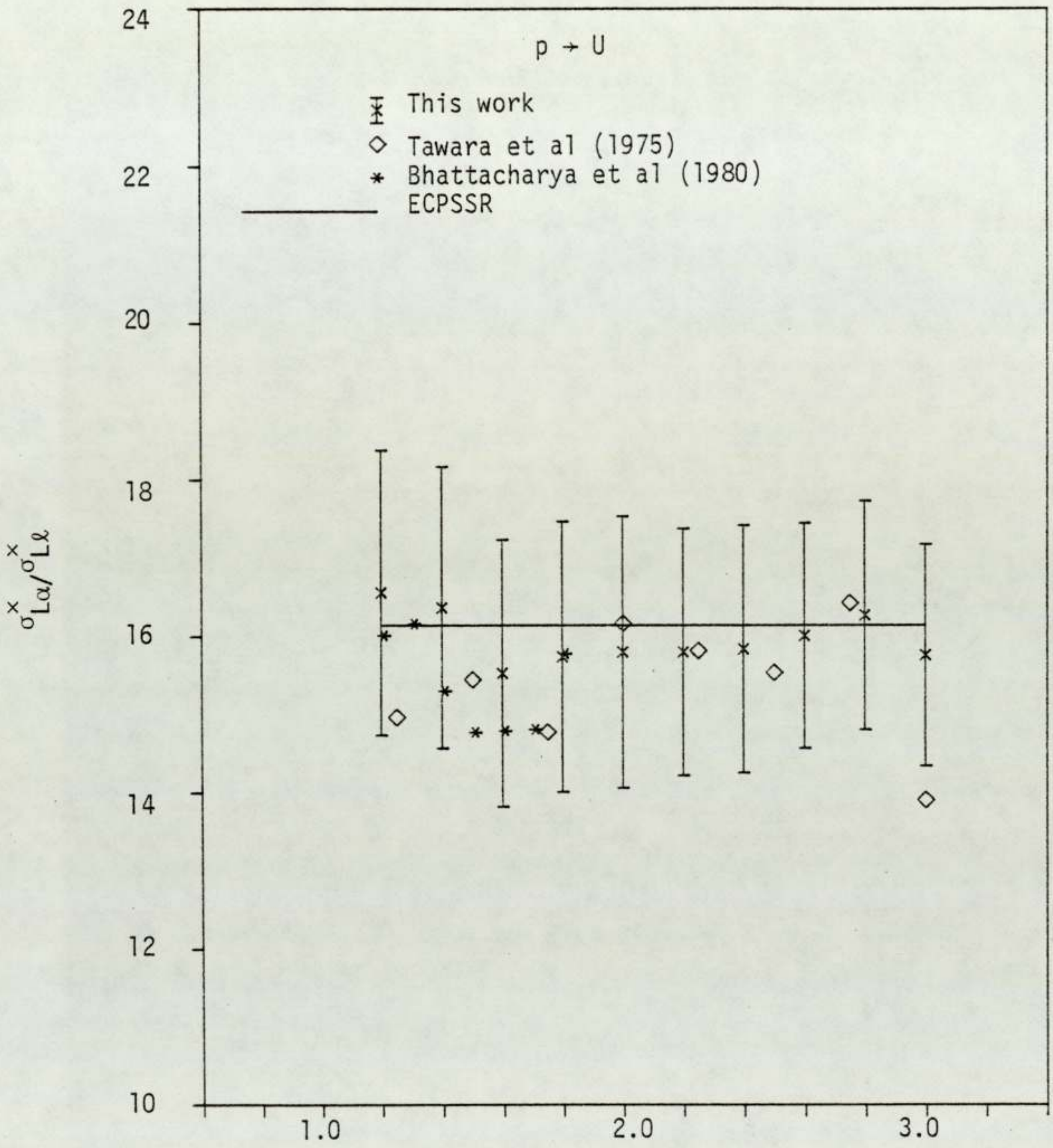

Figure 6.206. Experimental $\sigma^x_{L\alpha}/\sigma^x_{L\ell}$ ratio for proton impact on U.

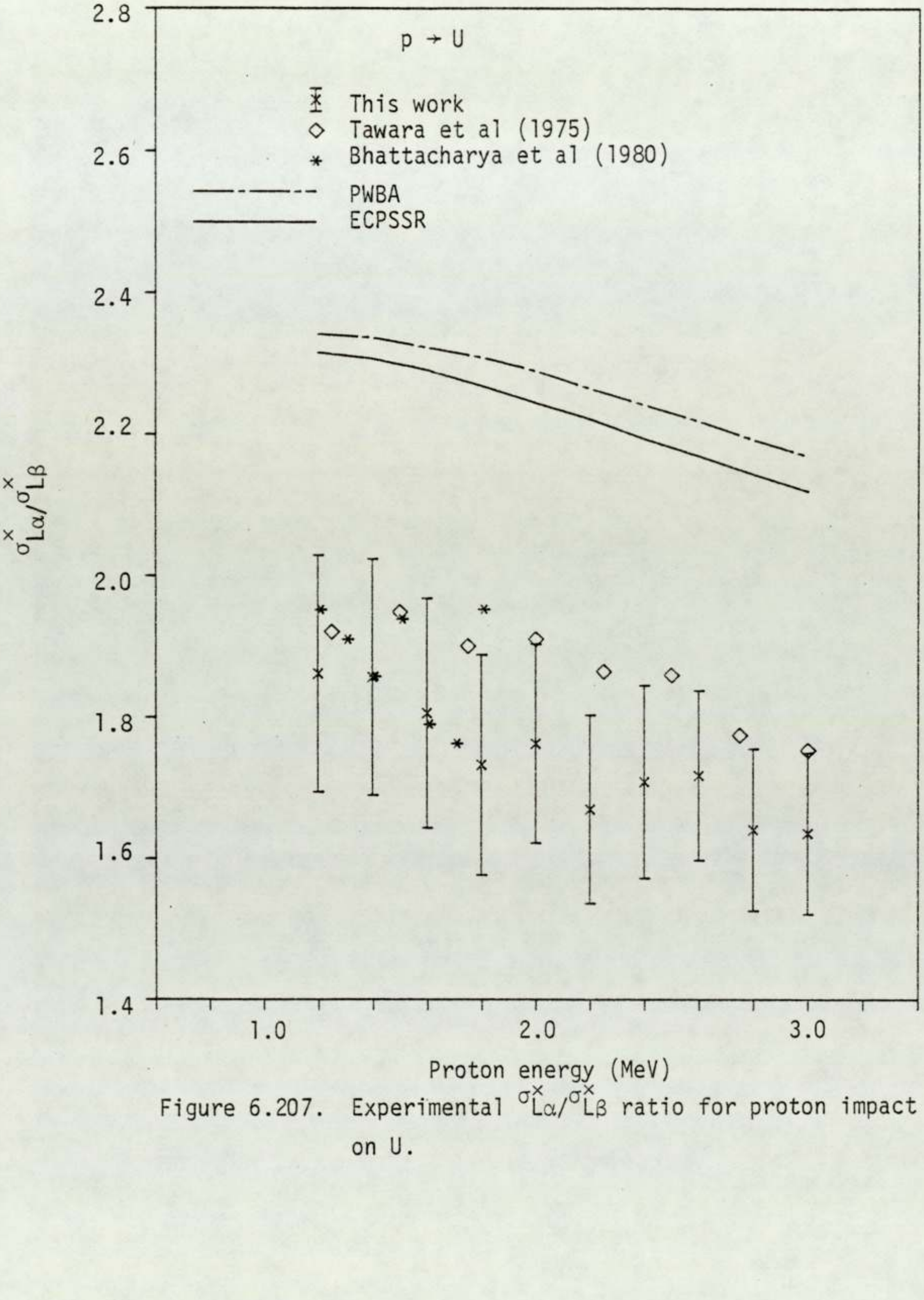

Figure 6.207. Experimental $\sigma^x_{L\alpha}/\sigma^x_{L\beta}$ ratio for proton impact on U.

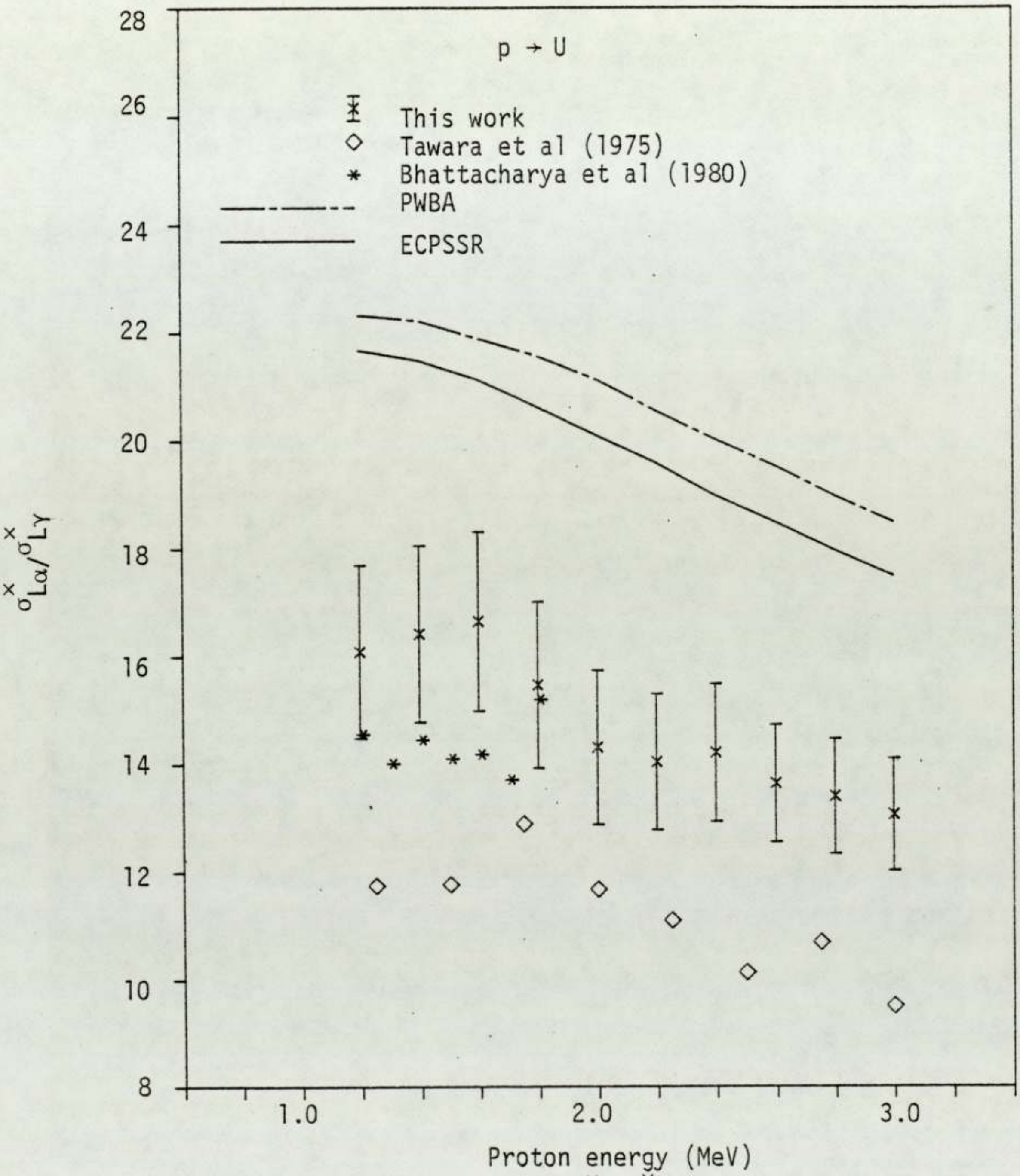

Figure 6.208. Experimental $\sigma^x_{L\alpha}/\sigma^x_{L\gamma}$ ratio for proton impact on U.

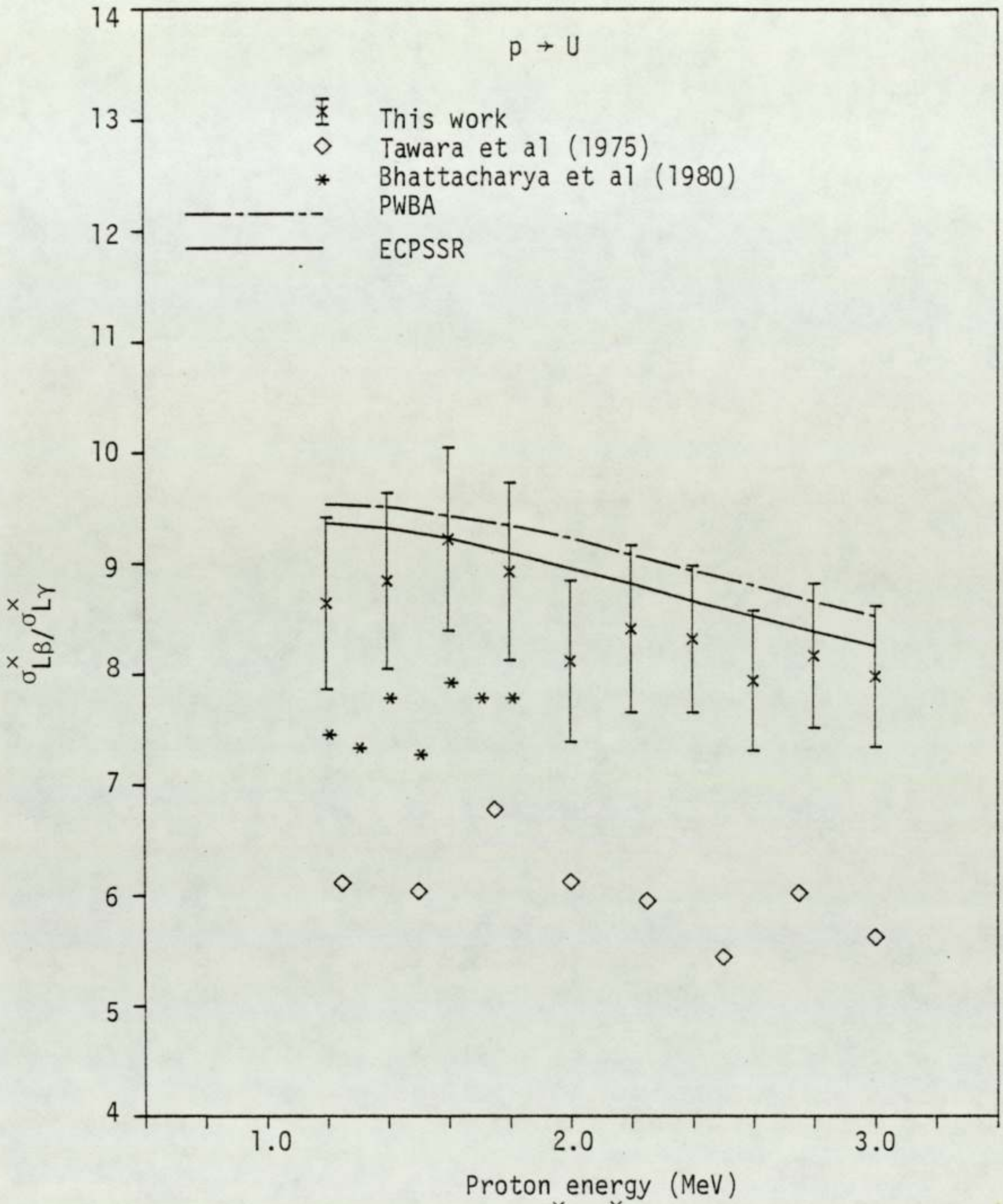

Figure 6.209. Experimental $\sigma^x_{L\beta}/\sigma^x_{L\gamma}$ ratio for proton impact on U.

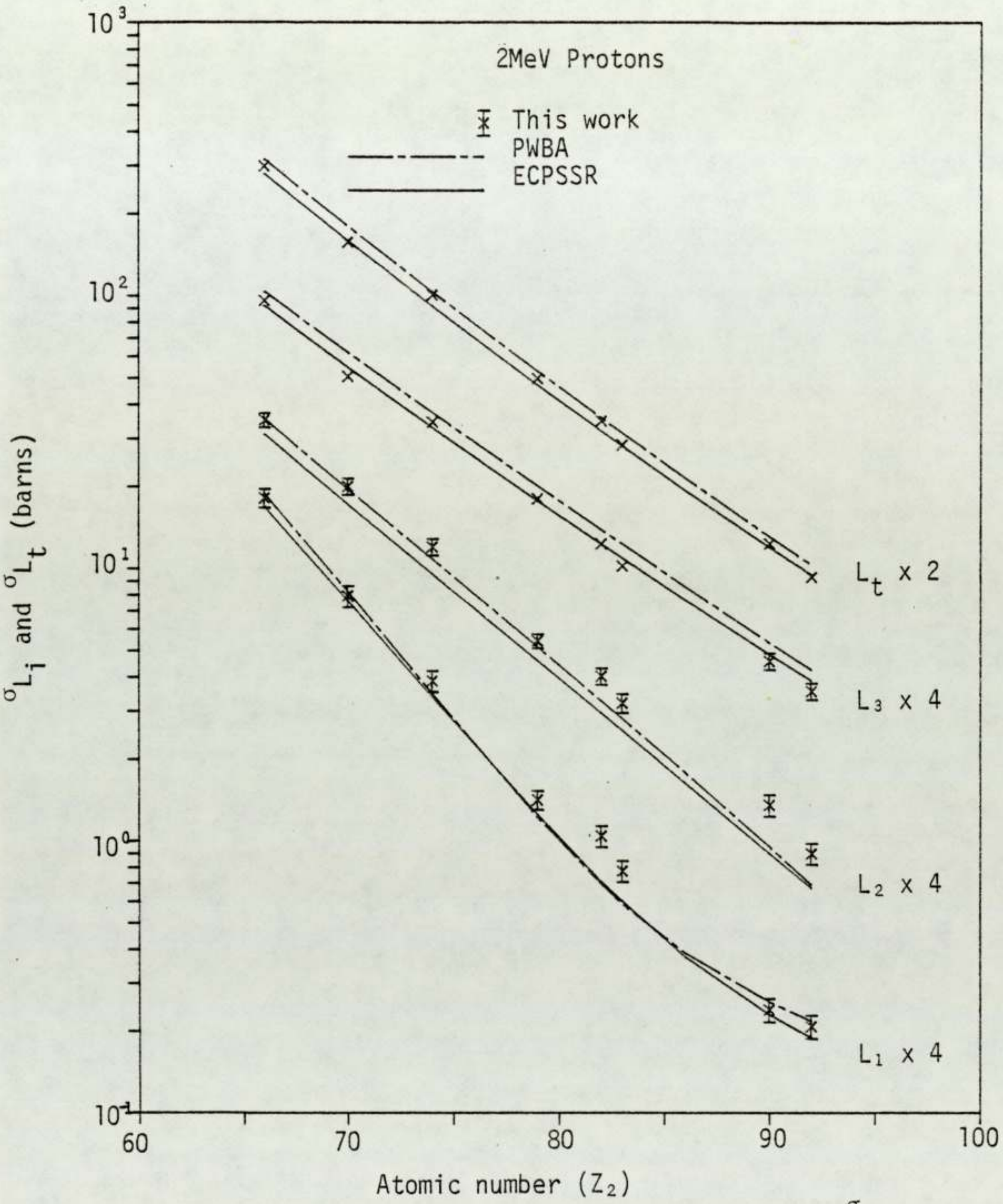

Figure 6.210. Target atomic number dependence of σ_{L_i} and σ_{L_t} for 2MeV incident protons

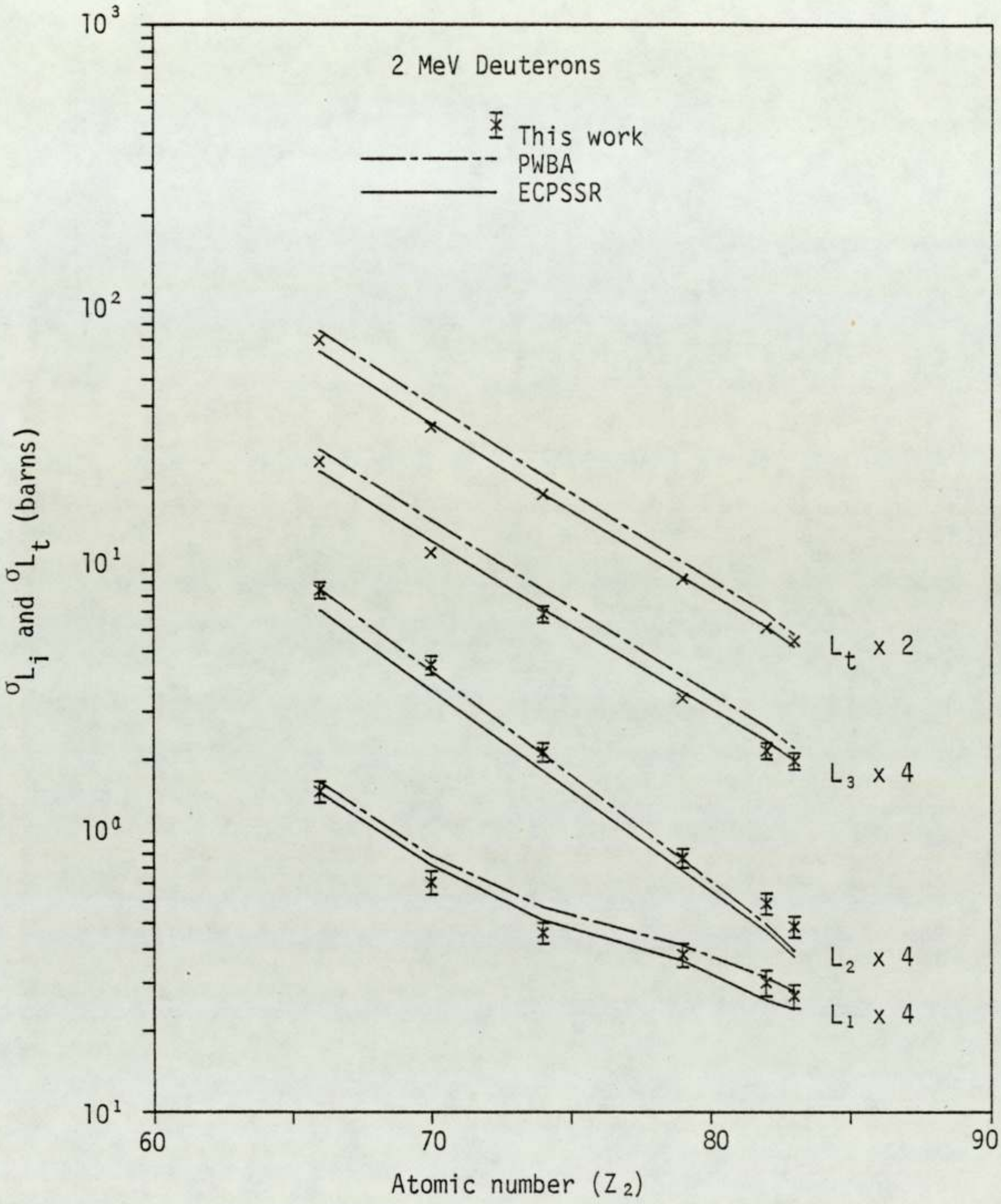

Figure 6.211. Target atomic number dependence of σ_{L_i} and σ_{L_t} for 2MeV incident deuterons.

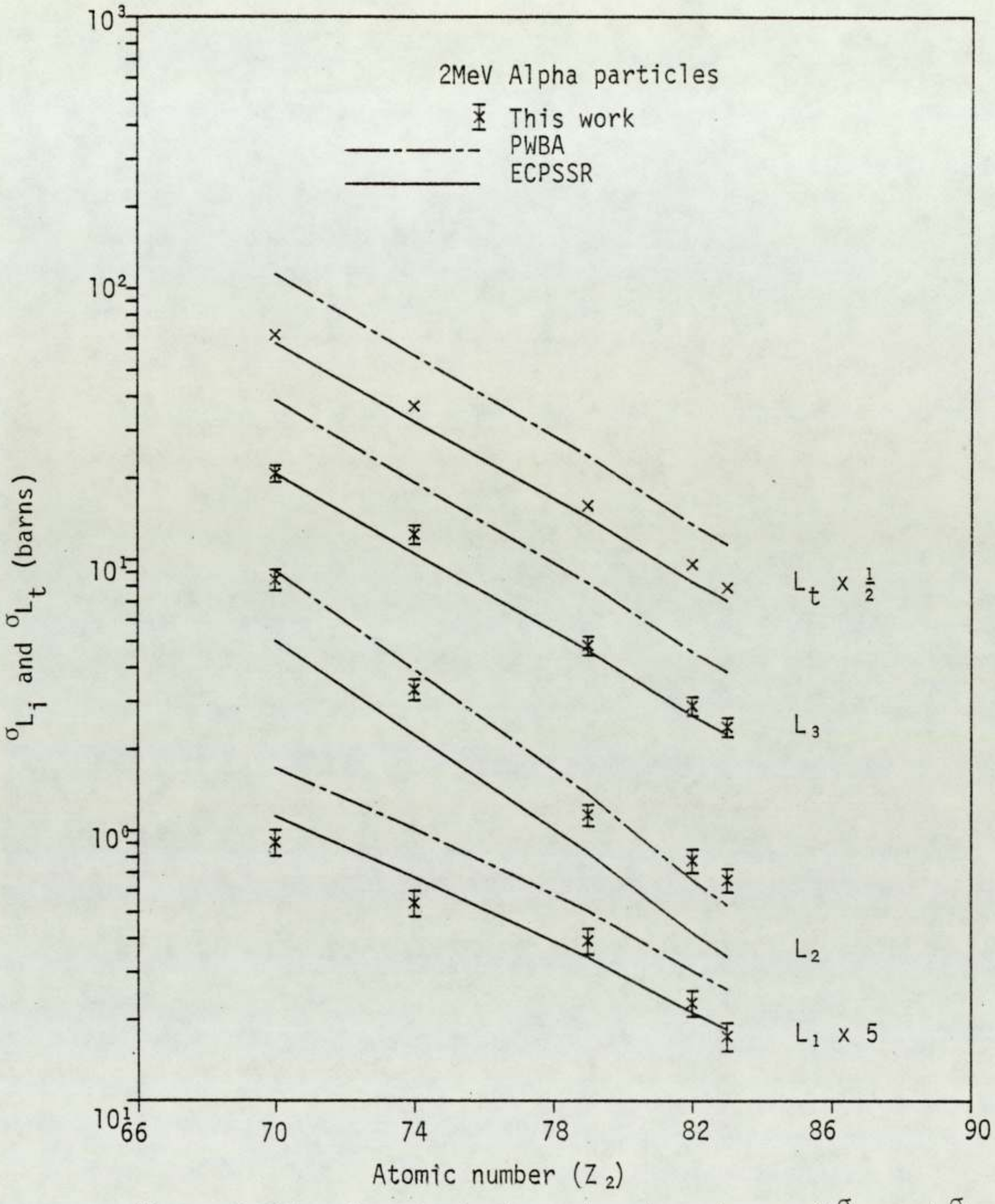

Figure 6.212. Target atomic number dependence of σ_{L_i} and σ_{L_t} for 2MeV incident alpha particles.

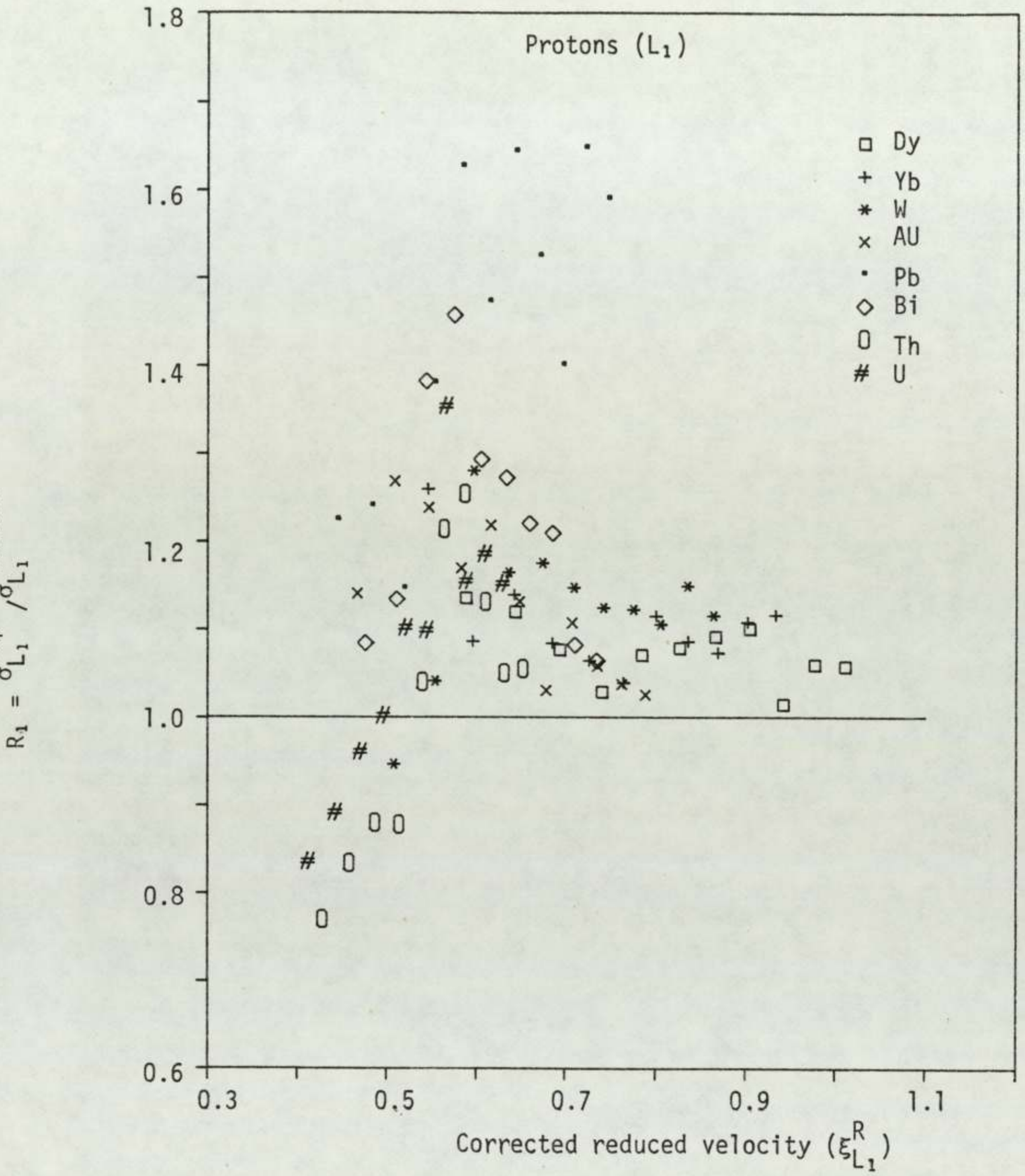

Figure 6.213. Comparison of the present σ_{L_1} values with the ECPSSR theory for incident protons.

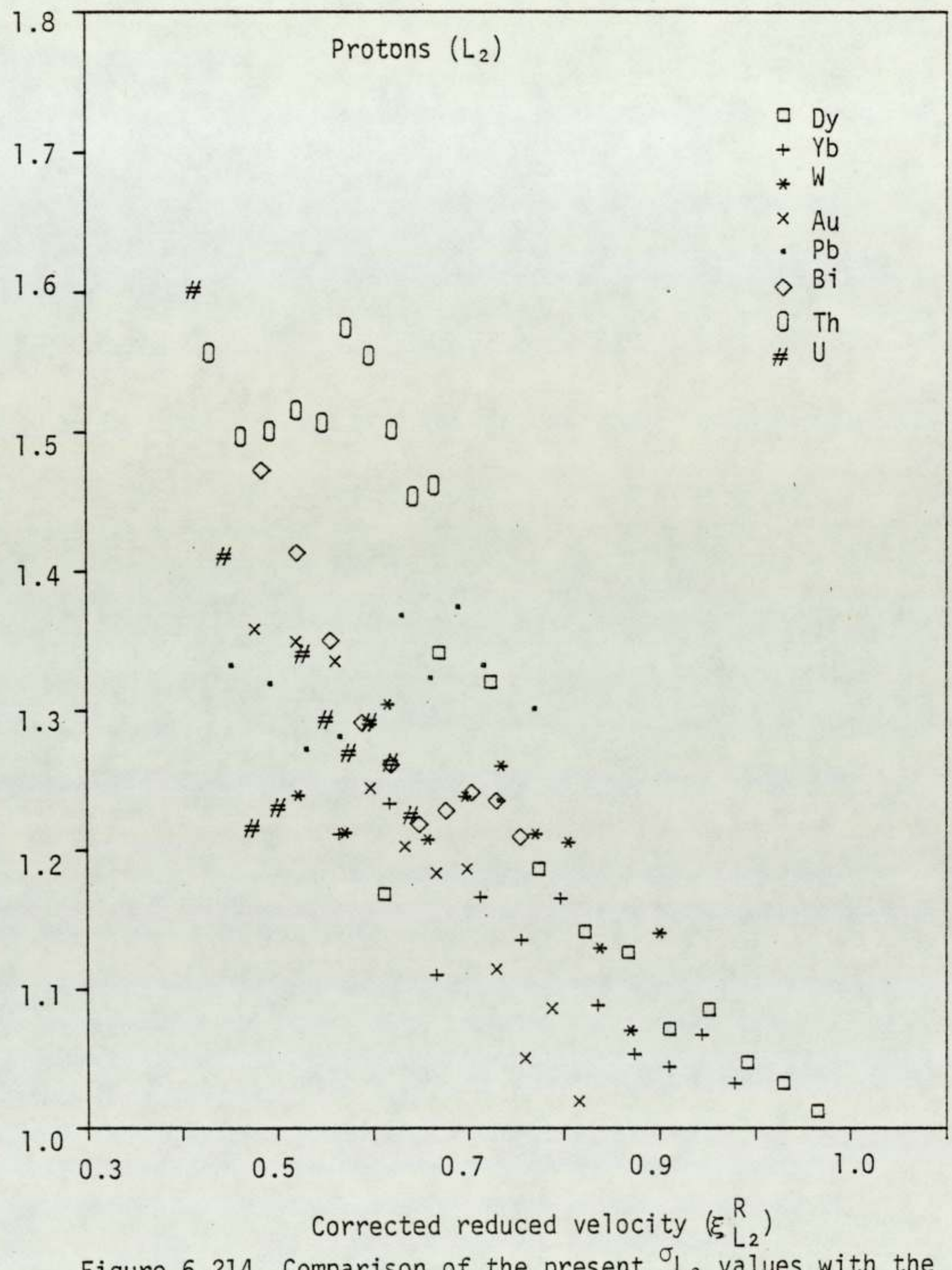

Figure 6.214 Comparison of the present σ_{L_2} values with the ECPSSR theory for incident protons.

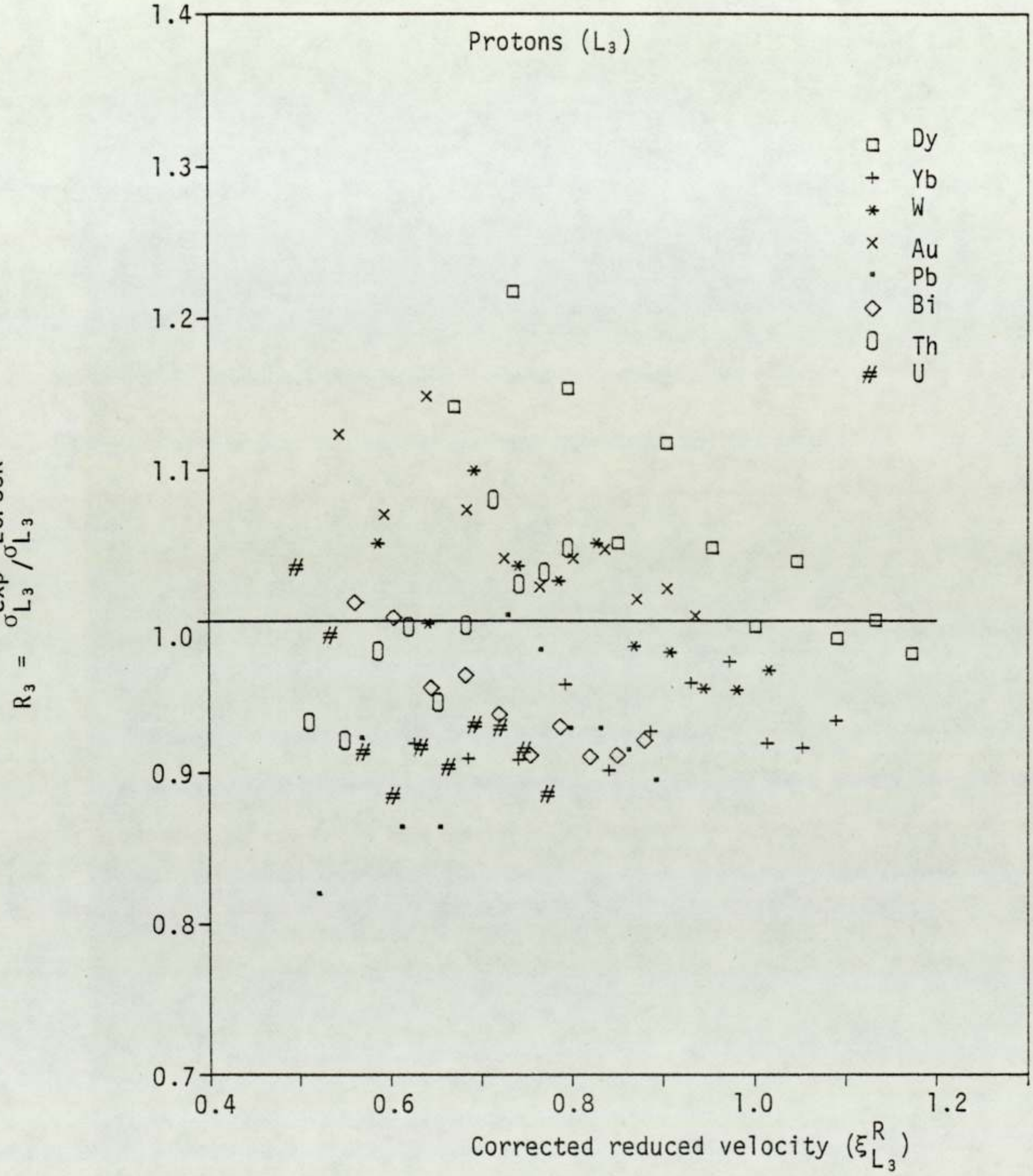

Figure 6.215. Comparison of the present σ_{L_3} values with the ECPSSR theory for incident protons.

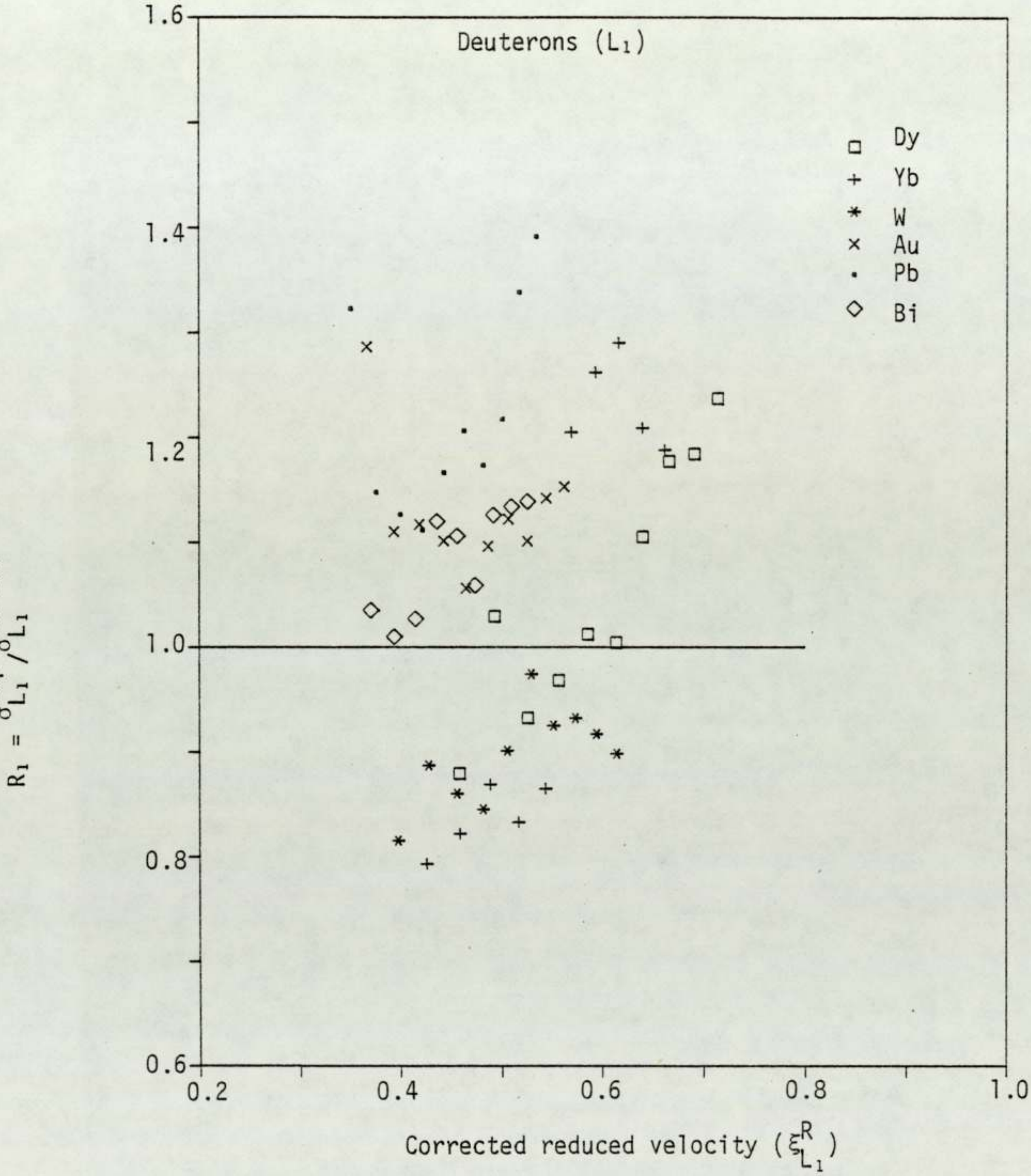

Figure 6.216. Comparison of the present σ_{L_1} values with the ECPSSR theory for incident deuterons.

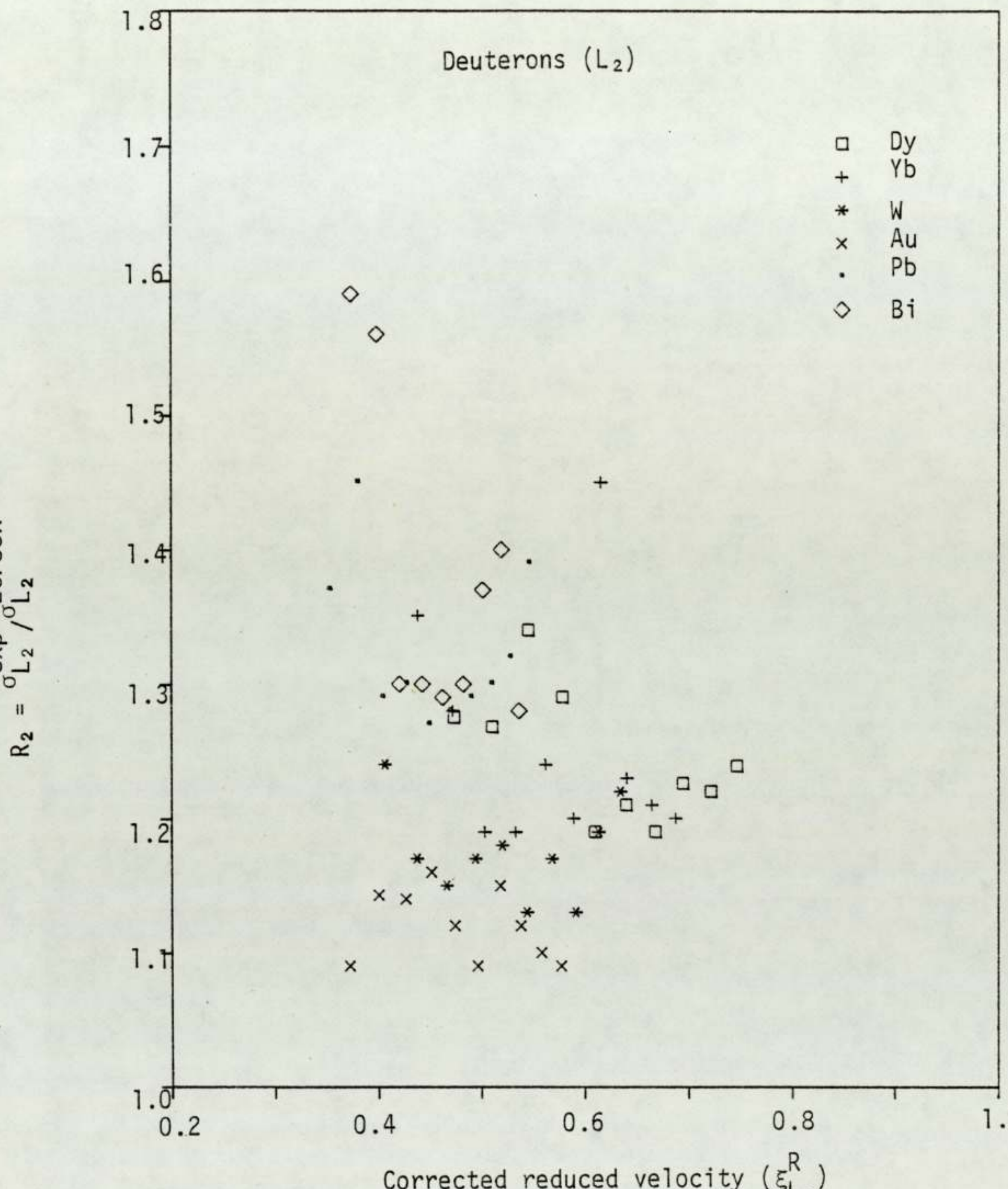

Figure 6.217. Comparison of the present σ_{L_2} values with the ECPSSR theory for incident deuterons.

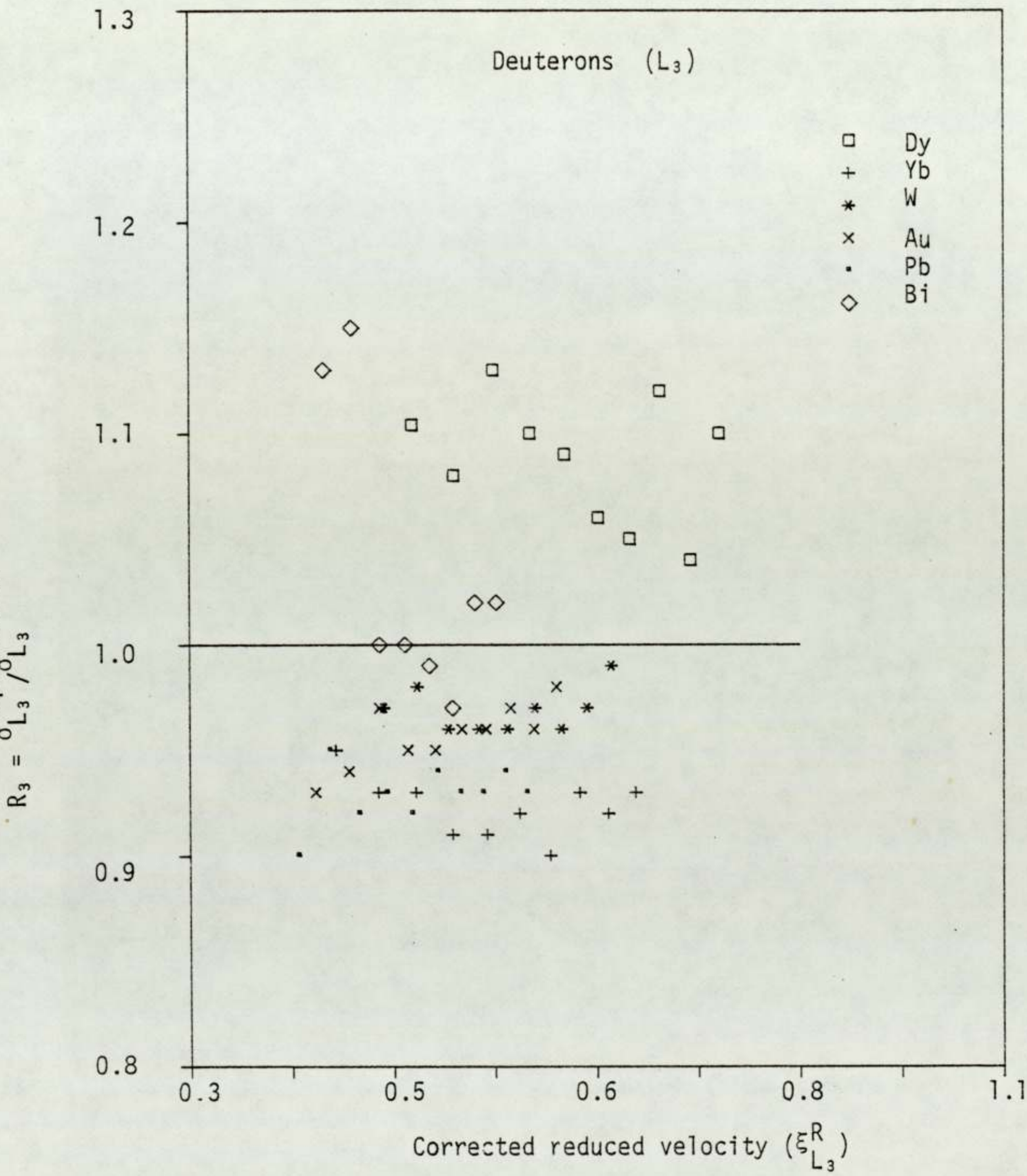

Figure 6.218. Comparison of the present σ_{L_3} values with the ECPSSR theory for incident deuterons.

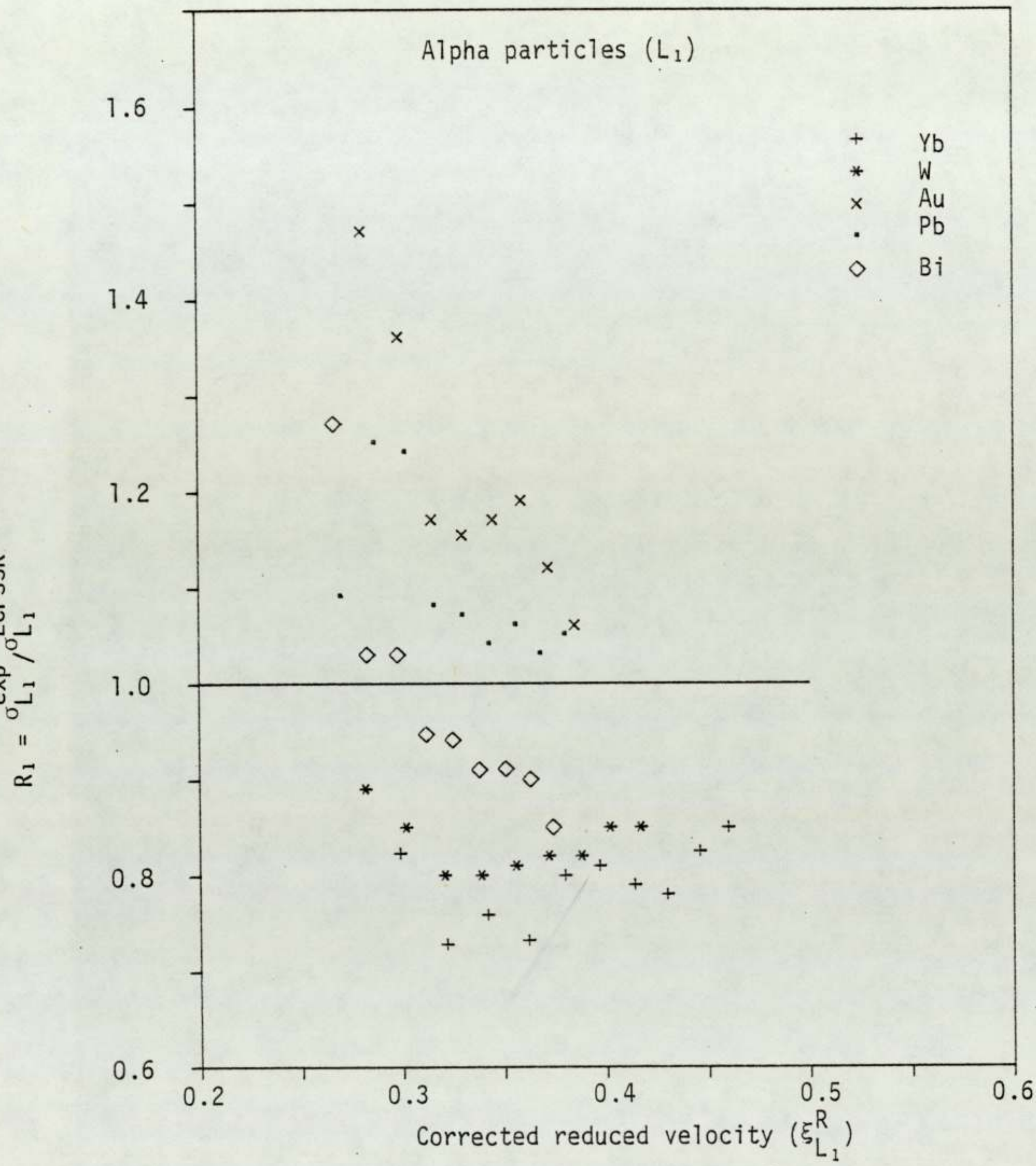

Figure 6.219. Comparison of the present σ_{L_1} values with the ECPSSR theory for incident alpha particles

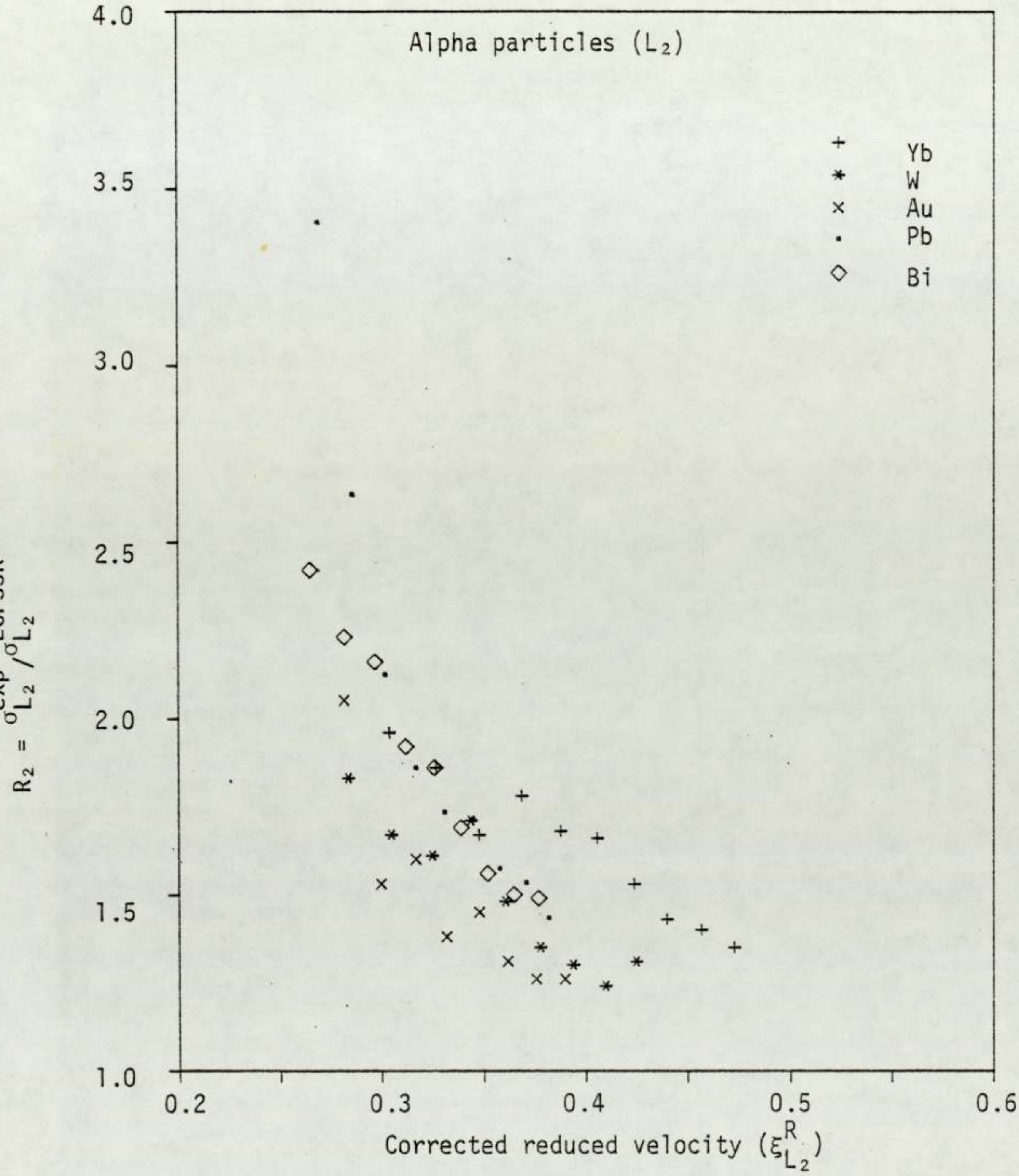

Figure 6.220. Comparison of the present σ_{L_2} values with the ECPSSR theory for incident alpha particles.

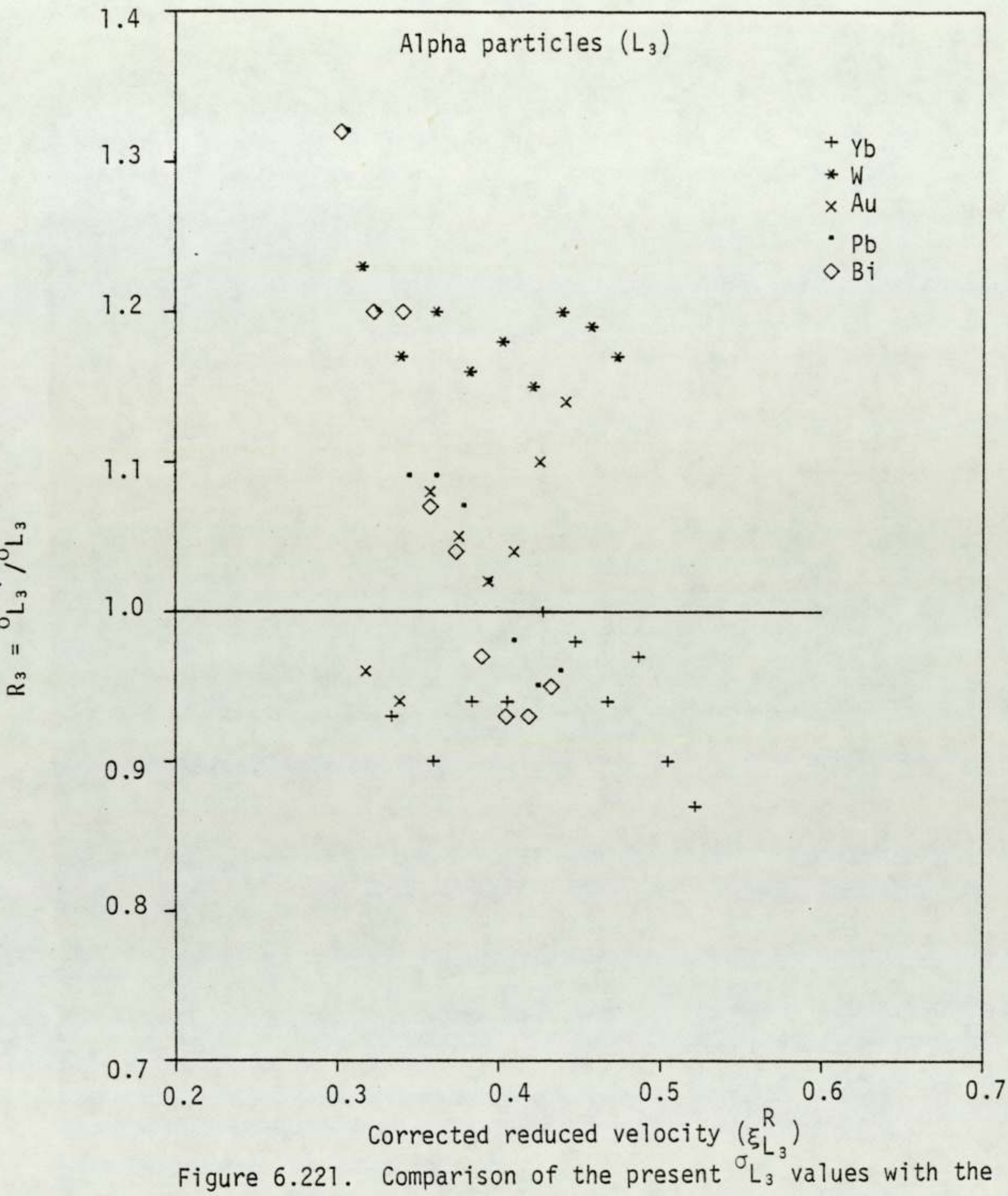

Figure 6.221. Comparison of the present σ_{L_3} values with the ECPSSR theory for incident alpha particles.

CHAPTER 7

CONCLUSIONS

A systematic study of L shell ionisation by incident protons (p) deuterons (d) and alpha particles (α) on selected medium to high atomic number elements has been performed. L shell x-ray production (σ^X_{Lj}) and ionisation (σ_{Li}) cross sections have been measured for p and d impact on Dy, p, d and α impact on Yb, W, Au, Pb and Bi and p impact on Th and U. To avoid any systematic uncertainties being introduced into σ^X_{Lj} and σ_{Li} by the Si(Li) detector efficiency and the target thickness these quantities were measured independently. In order to deduce σ_{Li} from σ^X_{Lj} a spectrum fitting programme has been written in Fortran 77 to extract the partially resolved components of L_γ.

Comparisons of σ^X_{Lj} and σ_{Li} have been made with the available recent data and with the PWBA and the ECPSSR theories for incident protons and alpha particles. In the case of deuteron impact there does not appear to be any available published data for the elements of interest and consequently comparison was performed only with the theories. A comprehensive compilation of all the available tabulated experimental data of σ^X_{Lj} and σ_{Li} for proton bombardment from 1975 to November 1982 has been prepared (Sokhi and Crumpton 1984 and see Appendix E). This greatly facilitated the comparison of proton impact measurements.

Large discrepencies between the present σ^X_{Lj} and σ_{Li} data and the ECPSSR model have been revealed. These disagreements are dramatically apparent when comparing the ratio $R_i = \sigma_{Li}^{exp}/\sigma_{Li}^{ECPSSR}$ (exp = experimental) versus the corrected reduced velocity parameter (ξ^R_{Li}) of the ECPSSR theory.

In the case of proton impact R_1 highlighted discrepencies of upto 70% at $\xi^R_{L_1} < 0.7$, above which deviations of about 15% were observed. The ECPSSR theory consistently underpredicts the σ_{L_2} data. Z_2

dependent discrepencies of upto 60% have been revealed by the R_2 plot. The ECPSSR theory, however, is successful to within 20% in explaining σ_{L_3}.

With regard to incident deuterons deviations of upto 50% are indicated by R_1 and 60% by R_2 whereas R_3 shows much better agreement with the ECPSSR predictions. For alpha particle impact R_1 reveals disagreements of upto 50% and upto 30% for R_3. In the case of R_2 the ECPSSR theory underestimates the experimental σ_{L_2} data by as much as a factor of 3.5, particularly for high Z_2 elements and at $\xi_{L_2}^R < 0.4$.

Similar observations have been reported by Cohen (1983) and Mukoyama and Sarkardi (1983a, b) for proton and helium impact. The present data, however, tends to indicate larger L_1 discrepencies than those found by these workers. Possible reasons for the considerable discrepencies highlighted by the present measurements have been discussed in section 6.11. Essentially a more realistic treatment for explaining inner-shell ionisation is required instead of the present theory which relies on the inadequate assumptions of the plane-wave Born approximation. This would probably entail a many-body approach to the inner-shell ionisation problem although such a treatment admittedly is very difficult. Much experimental work also needs to be conducted, not only in connection with absoluted Li subshell ionisation cross section measurements but also in allied research field such as impact-parameter-dependent cross section measurements. In addition investigation of the inner-shell alignment effect would provide further insight into the inner-shell ionisation mechanism. The $\sigma_{L\alpha}^X/\sigma_{L\ell}^X$ ratio measurements performed in this study indicate directly the need for incorporating this effect into the final theory.

In conclusion, this study has highlighted significant inadequacies in the ECPSSR theory when applied to the phenomena of L shell ionisation during highly asymmetric ion-atom collisions. Satisfactory explanation of L shell ionisation is obviously a prerequisite before ionisation mechanisms of higher and more complicated electronic shells can be understood and certainly before the advent of a unified theory of inner-shell ionisation can be envisaged. It is hoped that this study has provided useful information not only regarding the precise measurements of L shell x-ray production and ionisation cross sections but also regarding the future direction of research in this field.

APPENDIX A

SEMI-CLASSICAL AND BINARY ENCOUNTER APPROXIMATIONS

CONTENTS

A.1 INTRODUCTION

This appendix reviews the principles and developments of the semi-classical and the binary encounter approximations. Although these theories offer alternative interpretations of the inner-shell ionisation phenomena to that of the plane-wave Born approximation (PWBA), discussed in chapter 4, the fact that they can be related to the PWBA has been noted in this appendix.

Emphasis has been placed on discussing the main assumptions on which the two models are based and only the final expressions, required for calculating the ionisation cross sections, are quoted, although sources which offer greater detail have been referenced. As in Chapter 4 cgs units have been adopted.

A.2 SEMI-CLASSICAL APPROXIMATION

An approach which relies on a classical description of the projectile motion and a quantum mechanical description of the atomic inner-shell electron was introduced by Bang and Hansteen (1959) to study atomic Coulomb excitation. The applicability of this semi-classical approximation (SCA) rests on the Bohr's criterion (Bohr 1948) for a classical treatment of an incoming ionising charged particle being fulfilled, that is, the distance of closest approach (2d) in a head-on collision must be much greater than the de Broglie wavelength ($\lambda\!\!\!^-$) for the projectile, or

$$\kappa = \frac{2d}{\lambda\!\!\!^-} = \frac{2Z_1 Z_2 e^2}{\hbar\ v_1} >> 1 \qquad \text{A.1}$$

where $d = Z_1 Z_2 e^2/(M_1 v_1{}^2)$, Z_1 is the atomic number of the projectile of mass M_1 and velocity v_1 and Z_2 is the atomic number of the target atom. Provided that $Z_1 << Z_2$ and that the projectile is light and swift, the Coulomb interaction between the projectile and the inner-shell electron causing the latter to be ejected from the tightly bound inner-shell to the continuum can be treated as a time-dependent perturbation of the target atom, V(t), (Madison and Merzbacher 1975). This perturbing potential has the form

$$V(t) = \frac{Z_1 e^2}{|\underline{r} - \underline{R}(t)|} \qquad A.2$$

where $\underline{R}(t)$ represents the time-dependent position vector of the projectile and $\underline{r}$ the position vector of the atomic electron. In order to reduce computational difficulties associated with the SCA model the projectile is assumed to be moving with a uniform velocity in a straight line. This assumption is valid provided that (Madison and Merabacher 1975)

(i) the contribution of the elastic nuclear scattering to the inelastic collision at small impact parameters is negligible, and

(ii) the velocity of the incident particle does not change significantly as a consequence of the inelastic interaction.

The first condition requires that the radius of the Coulomb barrier be small compared with the radius of the inner-shell orbit and this is satisfied if Z_1 is small and if the incident particle energy is much greater than the relevent atomic ionisation potential. The minimum momentum transfer to the atom (q_{min}) is given by equation 4.2.4 provided that the energy lost (ε) by the projectile is much less than its initial energy. Thus, condition (ii) is fulfilled if

$$q_{min} << k_i \qquad A.3$$

where k_i is the initial momentum wave number of the motion (see equation 4.22) and, therefore, the deflection of the projectile may be neglected making the straight-line trajectory description of the projectile appropriate. The minimum momentum transfer is usually approximated as

$$\hbar q_{min} \simeq \frac{\varepsilon}{v_1} \qquad A.4$$

(provided ε << E) and where

$$\varepsilon = I_{Li} + E_f \qquad A.5$$

I_{Li} being the binding energy of the inner-shell electron, L-shell in the present context, and E_f the final energy of this electron after ejection.

As with the PWBA the electronic states are described by non-relativistic hydrogenic wave functions. The inner and outer screening effects are taken into account in the same fashion as for the PWBA. An important difference between the SCA and the PWBA is that the classical description of the incident particle introduces the impact parameter in the formulation of the SCA (Hansteen and Mosebekk 1973). Details of this formulation are given by Bang and Hansteen (1959), Hansteen (1975) and Madison and Merzbacher (1975) and only the final results are given here.

A coordinate system centred at the target nucleus is employed, the z-axis of which is in the direction of the incident particle moving in the y-z plane. For an incident particle with impact parameter, b, the differential Coulomb ionisation probability per energy interval dE_f of the ejected electron is given by (Hansteen and Mosebekk 1973)

$$\frac{dI_b}{dE_f} = \frac{1}{\hbar^2} \left| \int_{-\infty}^{\infty} e^{i\omega t} < f|V(t)| \; i > dt \right|^2 \qquad \text{A.6}$$

where i and f represent the initial and final states of the electron respectively and the frequency $\omega = \varepsilon/\hbar$ (ε is given by equation 4.70). Disregarding the Coulomb deflection of the projectile and assuming a straight-line trajectory equation A.6 may be rewritten as (Bang and Hansteen 1959)

$$\frac{dI_b}{dE_f} = \frac{2Z_1{}^2 M_1 e^4}{E\hbar^2} |M_b|^2 \qquad \text{A.7}$$

with

$$M_p = \int d\tau \; \psi_f^* \; \psi_i e^{iq_{min}z} K_0(q_{min}\rho) \qquad \text{A.8}$$

where M_p is the matrix element, $d\tau$ = dxdydz, ψ_i and ψ_f are the screened hydrogenic wave functions for the inital and final atomic electron states, $K_0(q_{min}\rho)$ is the modified Bessel function of the third kind and zeroth order with

$$q_{min} = \omega/v_1 \qquad \text{A.9}$$

and

$$\rho^2 = x^2 + (b - y)^2 \qquad \text{A.10}$$

The Coulomb ionisation probability is now given by (Hansteen et al 1975)

$$I_b = \int_0^\infty \left(\frac{dI_b}{dE_f}\right) dE_f \qquad A.11$$

and the total Coulomb ionisation cross section by

$$\sigma^{SCA} = 2\pi \int_0^\infty bdb\ I_b \qquad A.12$$

The matrix element M_p has been evaluated numerically by Hansteen et al (1975) with a maximum uncertainty of about 5%. These authors have expressed the straight-line SCA equations A.11 and A.12 in terms of special variables which allow the expressions to be scaled approximately for different target atoms. For a given subshell, belonging to the L-shell in the present case, characterised by hydrogenic quantum numbers n_L and ℓ_{Li}, the ionisation probability, I_{bLi}, can be expressed in terms of the generalised ionisation probability functions $G_{n\ell}$ (X_{Li}, B_{Li}),

$$I_{bLi} = \left(\frac{2j_{Li} + 1}{2\ell_{Li} + 1}\right) \frac{Z_1^2}{Z_{2L}^2 \theta_{Li}} G_{n_L \ell_{Li}} (X_{Li}, B_L) \qquad A.13$$

where $n_L = 2$, $\ell_{L_1} = 0$, $\ell_{L_2} = \ell_{L_3} = 1$,

$j_{L_1} = j_{L_2} = \frac{1}{2}$ and $j_{L_3} = 3/2$. The term in parenthesis is a statistical factor. The generalised ionisation probability functions in equation A.13 is a function of the quantities defined as

$$X_{Li} = \frac{Z_{2L}\theta_{Li}}{n_L E^{\frac{1}{2}}} \qquad A.14$$

where E is the projectile energy in MeV/amu and

$$B_L = \frac{b\ Z_{2L}}{n_L\ a_0}$$

where b is the impact parameter and a_0 is the Bohr radius = 5.29×10^{-9} cm. By substituting equation A.13 into A.12 and performing the integration the total cross section can be expressed as

$$\sigma_{Li}^{SCA} = \left(\frac{2j_{Li} + 1}{2\ell_{Li} + 1}\right) \frac{Z_1^2}{Z_{2L}^4 \theta_{Li}} F_{n_L \ell_{Li}} (X_{Li}) \qquad A.16$$

with

$$F_{n_L \ell_{Li}} (X_{Li}) = 2\pi a_0^2 n_L^2 \int B_L dB_L G_{n_L \ell_{Li}} (X_{Li}, B_L) \qquad A.17$$

where $F_{n_L \ell Li}$ is the generalised function for the total cross section and has the dimensions of length squared. The Z_2 - scaling relations A.13 and A.16 are valid only for $X_{Li} > 5$ (which holds for this work) but only to a few percent. For higher energies ($X_{Li} \lesssim 5$) Hansteen et al (1975) have determined a correction factor, $\mu n_L \ell_{Li}$, which is dependent on θ_{Li} and X_{Li}. For this energy range the corrected cross sections are obtained by multiplying expression A.16 by $\mu n_L \ell_{Li}$ (θ_{Li}, X_{Li}) tabulated by Hansteen et al (1975). For different projectiles the simple Z_1^2 - scaling law can be employed (as for the PWBA),

$$\sigma_{Li}^{SCA} (Z_1, v_1) = Z_1{}^2 \sigma_{Li}^{SCA} (Z_1 = 1, v_1) \qquad A.18$$

However, since the magnitude of the perturbation depends on Z_1 and that the SCA, like the PWBA, is based on the assumption that the perturbation is small, the above scaling law is applicable only for light charged particles, such as those considered in this work.

The following points should be noted in connection with the SCA model

(i) The straight line trajectory is only applicable in collisions where the ionisation process does not significantly effect the projectile path. This is justified when the energy of the projectile is much greater than the binding energy of the inner-shell in consideration (Madison and Merzbacher 1975).

(ii) The SCA model allows the ionisation cross sections to be calculated as a function of the impact parameter, thus making it possible to test the inequality A.1 (Hansteen and Mosebekk 1973).

(iii) The maximum contribution to inner-shell ionisation arises from impact parameters of a certain value denoted by b_{max}. For adiabatic collisions ($v_1 << v_{2_L}$) b_{max} lies deep inside the respective electron shell (Hansteen and Mosebekk 1970). As the collision loses its adiabaticity, that is, as the projectile energy increases, b_{max}, also increases and lies in the vicinity of the Bohr radius of the electron shell

(iv) In relation to the total L-shell ionisation cross section for gold Hansteen and Mosebekk (1973) have shown the relative contributions from the three L-subshells. In the extremities of the projectile energies the 2s state contributes the most to the total ionisation cross section where as in the intermediate energy region, which is studied here, the 2p states are the major contributors. This behaviour is a reflection of the relative, radial electron distributions for a hydrogen-like gold atom (Hansteen and Mosebekk 1973).

(v) Bearing in mind points (iii) and (iv) the plateau exhibited by the $2s_{\frac{1}{2}}$ ionisation cross section at low energies can be explained (Hansteen 1975). At low bombarding energies impact parameters comparable to or less than the adiabatic radius, r_{ad}, defined as

$$r_{ad} \simeq \frac{1}{q_{min}} = \frac{\hbar v_1}{\varepsilon} \qquad \text{A.19}$$

dominate in the ionisation process. Here the $2s_{\frac{1}{2}}$ electrons give the largest contributions to the cross section. As the projectile energy increases so does b_{max} and the $2s_{\frac{1}{2}}$ radial electron density distribution function exhibits a node while the 2p functions increase monotonically and become increasingly important. This node is reflected as a plateau in the $2s_{\frac{1}{2}}$ ionisation cross section whereas the 2p cross sections show a monotonic behaviour.

(vi) For total ionisation cross section the equivalence of the straight-line SCA and the PWBA has been established (Frame 1931, Bang and Hansteen 1959, Bethe and Jackiw 1968, Madison and Merzbacher 1975 and Taulbjerg 1977) provided that identical wave functions are chosen (Aashamar and Kochbach 1977 and Kocbach et al 1980). This, however, apparently leads to a paradox, in that the straight-line SCA which depends on $\kappa >> 1$ yields equivalent results as the PWBA which is based on the opposite condition $\kappa << 1$. However, the SCA condition requires that the deflection as well as the orbit of the projectile must be well-defined (Williams 1945) and therefore, if the scattering angle is not involved then the condition is no longer important (Hansteen 1975). In addition, in the region where $\kappa << 1$ the Coulomb ionisation cross sections originate predominantly from forward angle scattering and the contribution from other angles can be neglected. This imples that, provided that the projectile angle is not involved, the Coulomb ionisation cross sections may be predicted from the SCA model for all values of κ as long as $Z_1 << Z_2$ and $\varepsilon << E$ (Hansteen 1975) thus removing the contradictory nature of the validity conditions for total cross sections.

(vii) Examining equation A.16 and A.17 shows that the straight line SCA predicts a universal scaling relationship,

$$\left(\frac{2\ell_{Li} + 1}{2j_{Li} + 1}\right) \frac{\sigma_{Li}^{SCA} Z_{2L}^4 \theta_{Li}}{Z_1^2} = F_{n_L \ell_{Li}}(X_{Li}) \qquad A.20$$

Thus, plotting the left hand side factor versus X_{Li} yields a universal curve.

A.3 CORRECTIONS TO THE SEMI-CLASSICAL APPROXIMATION

When ε is not negligible compared to E the straight-line SCA model is no longer satisfactory. This situation arises at low projectile velocities and for inner-shells of heavy target atoms because (Madison and Merzbacher 1975)

(i) the Rutherford scattering from the target nucleus becomes appreciable, since the nuclear elastic scattering cross section is proportional to Z_2^2 (section 3.2.3), and as a result, the projectile suffers a deviation from its straight line path, and

(ii) for a given impact parameter the ionising collision itself may cause significant momentum transfers making the contributions to the ionisation cross section from all deflection angles appreciable.

Under the above circumstances the influence of the ionisation process on the incident particle cannot be neglected and the straight-line classical description of the projectile trajectory has to be reconsidered. Also the influence of the projectile on the atomic electron has to be taken into account through a quantum mechanical treatment (Madison and Merzbacher 1975). The possible corrections to the straight-line SCA model are considered below. It should be noted, however, that the collision circumstances that necessitate these corrections are similar to those already discussed in section 4.3.

A.3.1 Distortion of the Projectile Motion

In the adiabatic projectile energy region the assumption that the projectile travels in a straight-line with uniform velocity is not valid since the projectile suffers deviations from its initial path by the Coulomb field of the target nucleus. The decrease in the projectile velocity, resulting from these deviations, causes a reduction in the ionisation cross section (Kocbach et al 1980). This Coulomb deflection effect was first studied by Bang and Hansteen (1959) who proposed an approximate multiplicative correction for the K-shell,

$$C(q_{min}d) = \exp(-\pi q_{min}\, d) \qquad \text{A.21}$$

valid only for a limited projectile energy range. Bang and Hansteen (1959) arrived at this correction by employing hyperbolic trajectories for the projectile and a rather involved mathematical treatment. Anholt (1978) has proposed another Coulomb correction factor by comparing directly the straight-line and hyperbolic SCA calculation,

$$C(q_{min}d) = \left[0.22 + 0.78 \exp(1.9\pi q_{min}d)\right]^{-1} \qquad \text{A.22}$$

Several theoreticians involved in this field of ion-atom collisions have performed SCA calculations with hyperbolic trajectories to account for the deflection effect which have been reviewed by Kocbach et al (1980). Trautmann and Rosel (1980) have compared SCA cross section for hyperbolic trajectories and relativistic Hartree-Fock-Slater wave functions with experimental measurements of L-shell ionisation probability as a function of impact parameter and have observed very good agreement. Atomic ionisation has been recently considered by Montenegro and de Pinho (1982b) in the framework of hyperbolic semi-classical approximation who have derived an analytic expression for the Coulomb deflection factor which is in reasonable agreement with numerical calculations of Kocbach (1976).

A.3.2 Relativistic Improvements

The increase of the inner-shell ionisation cross section caused by the relativistic behaviour of the inner-shell electron was studied in the SCA model by Amundsen and Kocbach (1975). Further work on the relativistic description of the atomic electron has been summarised by Kocbach et al (1980). Amundsen et al (1976) have attempted to derive a multiplicative correction factor for the relativistic effect applied to K-shell ionisation but the accuracy of this factor is questionable when the magnitdue of the correction is high, as in the case of heavy target atoms (Kocbach et al 1980). Amundsen (1977b) has studied the relativistic effect for L-shell ionisation by light ions. This author has employed relativistic Coulomb wave functions in the SCA model and has noticed significant improvements in the agreement of theoretical (SCA) and experimental results at low projectile energies. The relativistic effect is explained in terms of an increase of high-momentum components of the electronic wave functions, thus making it easier to obtain sufficient momentum transfer for a given energy transfer in order for an electronic transition to occur. Amundsen (1977b) predicts that the relativistic effect for the $2s_{\frac{1}{2}}$ and $2p_{\frac{1}{2}}$ states will be of the same order but greater than the effect on the $2p_{3/2}$ state. This is explained by the circumstance that the relativistic effect reflects the change in the high-momentum part of the wave function and the magnitude of this change is of the same order for the $2s_{\frac{1}{2}}$ and $2p_{\frac{1}{2}}$ state. The relativistic effect has also been studied by Trautmann and Rosel (1980). They have accounted for Coulomb deflection effect by using hyperbolic trajectories, as mentioned in the previous section. By using Dirac wave functions an improvement of the ionisation probability predicted by the SCA has been achieved when comparing with experimental results, but a much greater degree of agreement has been attained by employing the more realistic relativistic Hartree-Fock-Slater wave functions.

A.3.3 Binding and Polarisation Effects

A perturbed stationary state approach has been used by Brandt and his colleagues to account for the binding effect (see subsection 4.3.2)(Basbas et al 1973b, Brandt and Lapicki 1974, 1979). A semi-classical approximation based on the first order time-dependent perturbation theory was used by these authors. The interaction potential V(t) is replaced by its instantaneous counterpart, V(0), that is, at the point of closest approach (t = 0). Similarly, the projectile velocity, the energy transfer and the initial and final atomic state wave functions, calculated for the instantaneous target-projectile configuration, are used (Madison and Merzbacher 1975). With these modification the binding effect has been taken into account (Brandt and Lapicki 1974). Trautmann and Rosel (1980) have employed a binding energy correction dependent on $\underline{R}$ to correct their relativistic SCA K-shell cross sections for alpha-particle impact on lead target and considerable improvement has been achieved. At higher velocities the polarisation effect gains significance and may be accounted for in terms of the second-order perturbation theory (Madison and Merzbacher 1975). Cross sections, which in the first order theory are propotional to Z_1^2, would now be expected to be increased by additive Z_1^3 - proportional terms. If 'distant' collisions are considered ($R \gg r$) then a multipole expansion of V(t) can be used in the second order perturbation calculations. Ashley et al (1972) and Hill and Merzbacher (1974) have used this method for a harmonic oscillator model of an atom. This approach was also adopted by Brandt and Lapicki (1979). These calculations have shown that the polarisation of the inner-shell electron is due to the quadruple component $\propto R^{-3}$ of the Coulomb interaction, that is, the electric dipole and quadrupole excitations collectively distort the atom during the collision and produce the Z_1^3 term (Madison and Merzbacher 1975 and Brandt and Lapicki 1979).

Trautmann and Rosel (1980) have highlighted three other effects which affect the ionisation probability and are now briefly mentioned.

A.3.4. Nuclear Distortion

As long as the projectile energy is below the Coulomb barrier, the Coulomb distortion by the target nucleus can be assumed to lead to hyperbolic trajectories in the semi-classical model. At energies where the projectile experiences only weak nuclear forces hyperbolic paths can still be used provided that the elastic scattering cross section of the projectile in the mean optical nuclear field of the target is accounted for. For higher energies a full quantum mechanical treatment would be required.

A.3.5 Influence of Screening Effect on Projectile Trajectory

At large impact parameters the trajectory of the projectile is influenced by the screeing effects of the target electrons. In this case, a trajectory due to a screened Coulomb potential has to be used. Trautmann and Rosel point out however, that his effect will only be small, even for shells higher than the K-shell.

A.3.6 Target Recoil Effect

In the SCA model the target mass is assumed to be infinitely heavy compared to the mass of the projectile ($M_2 >> M_1$). When this is not the case, that is, for a finite target mass, the Coulombic interaction term has to be modified,

$$V(\underline{r}, \underline{R}) \simeq \frac{-Z_1 e^2}{|\underline{r} - \underline{R}|} + \Delta V(\underline{r}, \underline{R}) \qquad \text{A.23}$$

$\Delta V(\underline{r}, \underline{R})$ leads to a dipole contribution ($\propto R^{-2}$) to the interaction and may make a correction to the ionisation probability necessary. The magnitude of such a correction, however, would be significant only for low-Z_2 target atoms when considering ionisation by light projectiles and may probably be neglected for the collision regimes under investigation in this work.

Trautmann et al (1983) have incorporated all these effects in their SCA model, based on a fully quantal approach, and, in general, have been successful in explaining the experimental data.

A.4 BINARY ENCOUNTER APPROXIMATION

The interest in a classical description of inner-shell ionisation by heavy charged particles was stimulated by the work of Gryzinski (1965) who developed a classical theory for calculating atomic collision cross sections. Following Gryzinski's procedure Garcia (1968 and 1970a,b) applied this classical theory to inner-shell ionisation phenomena. In this theory the dominant interaction, which causes an electronic transition to occur, is viewed as a direct energy exchange between the projectile and the bound atomic electron (impulse approximation)(Garcia 1970a). The nucleus and the other electrons of the target atom are, therefore, assumed to play only a passive role and simply help to establish the momentum distribution for the 'active' electron involved in the Coulombic collision and to ensure that the energy transferred to this electron exceeds the minimum energy required to ionise it in the field of the target atom. In other words, the energy transferred must be greater than the ionisation potential of the electron (Hansen 1973 and Briggs and Taulbjerg 1978). The collision is thus treated as a two-body interaction between an incident charged particle and a free electron, and as a result, this assumption is referred to as the 'Binary Encounter Approximation' (BEA). The differential cross section, $d\sigma/d\Delta E$, for an exchange of energy, ΔE, in the laboratory frame, between the incident particle and the bound electron is obtained by utilising the result that the classical and quantum mechanical differential cross sections in the centre-of-mass system are identical (Gerjouy 1966, Garcia 1970a). The cross section, $\sigma_i(v_1, v_2)$, for removal of an electron from subshell, i, with binding energy, u, (retaining Garcia's (1970a) notation) is obtained by integrating over all allowed energy exchanges from $\Delta E = u$ to $\Delta E = E_1$, where E_1 is the energy of the projectile with velocity v_1 and v_2 is the velocity of the electron.

$$\sigma_i(v_1, v_2) = \int_u^{E_1} \frac{d\sigma}{d\Delta E} \, d\Delta E \qquad \text{A.24}$$

The ionisation cross section, $\sigma^{BEA}(v_1)$, is arrived at by averaging over all speed distributions, $f_{n\ell}(v_2)$, of the atomic electrons and summing over all electrons in the subshell,

$$\sigma^{BEA}(v_1) = N_i \int_0^\infty \sigma_i \, (v_1, v_2) \, f_{n\ell} \, (v_2) dv_2 \qquad \text{A.25}$$

where n and ℓ denote the principal and the orbital quantum numbers respectively and N_i is the number of equivalent electrons with binding energy u. The expression for $f_{n\ell}$ (v_2) most commonly used is

$$f_{n\ell} \, (v_2) = \frac{32}{\pi} \, v_0^5 \left(\frac{v_2^2}{(v_2^2 \quad v_0^2)^4} \right) \qquad \text{A.26}$$

with $v_0 = (2u/m)^{\frac{1}{2}}$

and can be obtained classically or quantum mechanically for hydrogenic states (Garcia 1970a and Hansen 1973). It is assumed in the BEA calculations that $f_{n\ell}(v_2)$ remains unchanged as the projectile passes through the atom (static approximation) (McGuire and Richard 1973). The effects of nuclear repulsion on the projectile motion, namely the delfection and the reduction of its kinetic energy, have been incorporated into expression A.25 by assuming that the repulsion is due to a point charge Z' and evaluating the ionisation cross section at a reduced projectile energy of $E_1 - (2Z'/Z_2)u$ (for protons) (Thomas and Garcia 1969 and Garcia 1970a). For large Z_2 the point charge Z' has been replaced by Z_2 for K-shell ionisation (Garcia 1970a).

The following points should be noted in relation to the BEA model.

(i) Provided hydrogenic velocity distributions are used the cross sections for a given subshell obey the following scaling law (Garcia et al 1973)

$$\frac{u^2\sigma^{BEA}}{Z_1^2} = g\left(\frac{E_1}{\lambda u}, \lambda\right) \qquad A.27$$

where $\lambda = M_1/m$. Thus plotting the left-hand-side of A.27 versus $E_1/\lambda u$ yields a universal curve. Garcia et al (1973) have presented tabulated values of $u^2\sigma^{BEA}/Z_1^2$ versus $E_1/\lambda u$.

(ii) Several authors have demonstrated that the BEA total cross section can also be obtained from the PWBA model (Vriens 1970, Bates and McDonough 1970, 1972 and Madison and Merzbacher 1975). Taulbjerg (1976) has compared the two models under indentical condtions for the K and L-shell and has concluded that the PWBA, and its equivalent the straight-line SCA, are essentially identical as far as total ionisation cross sections are concerned. This has been substantiated for the BEA and the PWBA theories by Langenberg and van Eck (1978) who employed realistic velocity distributions for the target electron instead of the hydrogenic type and achieved agreement between the two models to within 20%.

(iii) Hansen (1973) has transformed the BEA model from its usual momentum space into configuration space. To do this a consistent relationship between the velocity of a bound electron and its distance from the nucleus has to be formulated (Gryzinski 1965). By reexpressing the BEA theory in the impact-parameter representation, Hansen (1973) has developed a model to describe the interaction between a bound electron and a particle of fixed trajectory, referred to as the Constrained Binary Encounter Approximation (CBEA). Cross sections calculated from this theory are usually smaller than those predicted by the BEA. Hansen (1973) points out that the prescription of assigning exactly one electron velocity for a given distance from the nucleus is idealised and would lead to an overestimation of the ionisation probability for close collisions and an underestimation for distant collisions.

(iv) The characteristic 'knee' in the $2s_{\frac{1}{2}}$ ionisation cross section is less pronounced in the CBEA description of Hansen (1973) than in the PWBA. The cross sections calculated from the two models in the vicinity of this 'knee' differ by nearly a factor of two (Taulbjerg 1976). The quantum mechanical description of the PWBA exhibits closer agreement with experimental measurements (Madison 1976). By using realistic electron velocity distributions Langenberg and van Eck (1978) have shown that the BEA can also duplicate qualitatively the behaviour of the $2s_{\frac{1}{2}}$ cross section.

A.5 CORRECTIONS TO THE BINARY ENCOUNTER APPROXIMATION

Several corrections have been proposed to improve agreement between the BEA predictions and experimentally measured ionisation cross sections. These are considered here briefly.

A.5.1 Nuclear Repulsion Effects

The loss of kinetic energy sufferred by the projectile during close collisions due to the Coulombic repulsion of the target nucleus can be accounted for by assuming that the projectile interacts at some average distance from the nucleus, namely at the adiabatic radius r_{ad}. The loss of energy experienced by the projectile, before causing ionisation, is $Z_1 Z_2 e^2/r_{ad}$. Magno et al (1979) have used an effective projectile energy by reducing the incident energy by the amount $Z_1(T + u)$ where T is the kinetic energy of the electron.

A.5.2 Relativistic Effect

In exact BEA calculations for medium and high Z_2 elements relativistic electronic wave functions should be used to generate the appropriate momentum distributions (Hansen 1973). An approximate correction has been proposed by Hansen (1973) which assumes that the kinetic energy of the electron can be correctly expressed in terms of the non-relativistic equation $T = \frac{1}{2}m_0 v_2{}^2$, where v_2 is the velocity of the electron. The relativistic velocity, v_{rel}, and mass m_{rel} of the electron can then be calculated from

$$v_{rel} = \left| \frac{R}{(1 + R)} \right|^{\frac{1}{2}} c \qquad A.28$$

and

$$m_{rel} = \frac{m_0}{(1 - \beta^2)^{\frac{1}{2}}} \qquad A.29$$

where $R = (T/m\,c^2)^2 + 2\,(T/m_0c^2)$ and $\beta = v_{rel}/c$, c being the velocity of light and m_0 the rest mass of the electron. These values can now be used in the cross section calculations. Recently Avaldi et al (1982) have derived the electron momentum distributions using relativistic wave functions to study K-shell ionisation of Ho and Au by proton impact. Reasonable agreement with experimental results is only achieved when corrections are made for the energy loss of the proton. As with the PWBA and the SCA scaling laws do not hold when these corrections are made.

A.5.3 Binding Energy Effect

This effect has been considered only qualitatively by Hansen (1973) and an expression for this correction has not been given. Magno et al (1979) in their study of K-shell ionisation have corrected the BEA for the binding effect on the basis of the work of Basbas et al (1973a).

A.5.4 Improvement of Electron Momentum Distribution

In the BEA model Zeff/n is replaced by $(u/R_\infty)^{\frac{1}{2}}$ in the electronic wave functions. Here Zeff is the effective atomic number of the target atom, n is the principal quantum number, u is the binding energy of the appropriate inner-shell and R_∞ is the Rydberg. A more plausible Z_{eff} is determined from simple semi-empirical screening procedures, such as reducing Z_2 by the Slater's constant for the particular shell (Hansen 1973). The importance of employing realistic electron momentum distributions has been demonstrated by the work of Langenberg and van Eck (1978) and Avaldi et al (1982).

APPENDIX B

PRESENT EXPERIMENTAL L SHELL

X-RAY PRODUCTION AND IONISATION

CROSS SECTIONS

CONTENTS Page

EXPLANATIONS

Tabulated experimental L shell x-ray production and ionisation cross sections measured in this study are presented in order of increasing atomic number

(1) L, BETA and GAMMA denote $\sigma_{L\ell}^{x}$, $\sigma_{L\beta}^{x}$ and $\sigma_{L\gamma}^{x}$ respectively.

(2) ALPHA denotes $\sigma_{L\alpha+\eta}^{x}$ for Dy, and Yb and W and $\sigma_{L\alpha}^{x}$ for Au, Pb, Bi, Th and U.

(3) BETA1 denotes $\sigma_{L\beta_{1346}}^{x}$ for Dy and Yb, $\sigma_{L\beta_{146}}^{x}$ for W and $\sigma_{L\beta_{135}}^{x}$ for Th and U.

(4) BETA2 denotes $\sigma_{L\beta_{2715}}^{x}$ for Dy and Yb, $\sigma_{L\beta_{25715}}^{x}$ for W and $\sigma_{L\beta_{24615}}^{x}$ for Th and U.

(5) BETA = BETA1 + BETA2 where appropriate.

(6) GAMMA1 denotes $\sigma_{L\gamma_{15}}^{x}$ for all elements.

(7) GAMMA2 denotes $\sigma_{L\gamma_{23844'}}^{x}$ for Dy and Yb, $\sigma_{L\gamma_{236844'}}^{x}$ for W, Au, Pb and Bi (protons only) and $\sigma_{L\gamma_{2368}}^{x}$ for Bi (deuterons and alpha particles), Th and U.

(8) GAMMA = GAMMA1 + GAMMA2 where appropriate

(9) TOTAL = L + ALPHA + BETA + GAMMA

(10) LA/LL, LA/LB, LA/LG and LB/LG denote $\sigma_{L\alpha}^{x}/\sigma_{L\ell}^{x}$, $\sigma_{L\alpha}^{x}/\sigma_{L\beta}^{x}$, $\sigma_{L\alpha}^{x}/\sigma_{L\gamma}^{x}$ and $\sigma_{L\beta}^{x}/\sigma_{L\gamma}^{x}$ ratios respectively.

(11) L1 and L2 and L3 denotes σ_{L_1}, σ_{L_2} and σ_{L_3} respectively.

(12) L1/L2, L1/L3 and L2/L3 denote $\sigma_{L_1}/\sigma_{L_2}$, $\sigma_{L_1}/\sigma_{L_3}$ and $\sigma_{L_2}/\sigma_{L_3}$ respectively.

(13) TOTAL = L1+ L2 + L3

(14) Percentage experimental uncertainties are shown in parenthesis. Wherever uncertainties are omitted the preceding value applies.

B.1 PROTON IMPACT

DYSPROSIUM(Z2=66)

EXPERIMENTAL L SHELL X-RAY PRODUCTION CROSS SECTIONS

FOR PROTON IMPACT

ENERGY MeV	L (BARNS)	ALPHA	BETA	GAMMA	GAMMA1	GAMMA2	TOTAL
1.0	.665(7)	14.53(4)	8.15(5)	.943(6)	.827 7	.116(9)	24.29(3)
1.2	.986	24.08	13.04	1.723	1.512	.211	39.82
1.4	1.521	32.37	19.32	2.528	2.160	.369	55.74
1.6	1.828	39.33	24.59	3.234	2.644	.590	68.98
1.8	2.228	52.85	29.95	4.270	3.324	.946	89.30
2.0	2.632	61.26	37.95	5.471	4.099	1.371	107.31
2.2	3.170	69.70	45.73	6.626	4.760	1.866	125.22
2.4	3.642	84.59	52.82	8.143	5.717	2.427	149.19
2.6	3.947(6)	92.22(3)	62.21(3)	9.148(4)	6.359 5	2.788(7)	167.52(2)
2.8	4.382	105.44	71.32	10.719	7.212	3.507	191.86
3.0	4.413	115.27	82.88	12.106	7.976	4.130	214.67

ENERGY MeV	BETA1 (BARNS)	BETA2	LA/LL	LA/LB	LA/LG	LB/LG
1.0	5.540(6)	2.613(8)	21.83(8)	1.782(6)	15.41(7)	8.650(8)
1.2	8.991	4.046	24.43	1.847	13.97	7.565
1.4	13.617	5.704	21.28	1.675	12.80	7.642
1.6	17.603	6.984	21.51	1.600	12.16	7.602
1.8	21.534	8.413	23.72	1.765	12.38	7.013
2.0	27.345	10.604	23.28	1.614	11.20	6.937
2.2	33.967	11.758	21.99	1.524	10.52	6.900
2.4	39.018	13.798	23.23	1.602	10.39	6.486
2.6	45.828(4)	16.380(5)	23.36(7)	1.482(4)	10.08(5)	6.800 (5)
2.8	53.174	18.145	24.06	1.478	9.84	6.654
3.0	61.984	20.900	26.12	1.391	9.52	6.847

EXPERIMENTAL L SUBSHELL IONISATION CROSS SECTIONS

FOR PROTON IMPACT

ENERGY MeV	L1 (BARNS)	L2	L3	L1/L2	L1/L3	L2/L3	TOTAL BARNS
1.0	5.97(9)	29.83(7)	95.15(5)	.200(11)	.063(10)	.314(9)	130.95 (4)
1.2	10.88	54.52	156.52	.200	.070	.348	221.92
1.4	19.14	77.19	208.29	.248	.092	.371	304.62
1.6	30.92	93.07	250.60	.332	.123	.371	374.59
1.8	49.83	114.95	335.76	.433	.148	.342	500.54
2.0	72.47	139.67	383.17	.519	.189	.365	595.31
2.2	98.89	159.35	430.41	.621	.230	.370	688.65
2.4	128.71	189.50	520.10	.679	.247	.364	838.31
2.6	147.96(7)	209.92(5)	563.90(3)	.705(9)	.262(8)	.372(6)	921.78(2.5)
2.8	186.37	234.51	639.89	.795	.291	.366	1060.77
3.0	219.63	256.79	694.18	.855	.316	.370	1170.60

YTTERBIUM(Z2=70)

EXPERIMENTAL L SHELL X-RAY PRODUCTION CROSS SECTIONS

FOR PROTON IMPACT

ENERGY	L	ALPHA	BETA	GAMMA	GAMMA1	GAMMA2	TOTAL
MeV				BARNS			
1.0	.400(8)	7.78(5)	4.55 (6)	.627(7)	.539(8)	.088(10)	13.35 (4)
1.2	.626	12.19	7.40	1.017	.899	.118	21.23
1.4	.897	17.46	10.41	1.418	1.210	.208	30.19
1.6	1.268	24.76	14.76	2.084	1.751	.333	42.86
1.8	1.524	30.16	19.03	2.758	2.240	.518	53.47
2.0	1.842	38.50	24.43	3.648	2.895	.754	68.42
2.2	2.216	47.85	30.60	4.490	3.364	1.126	85.16
2.4	2.642(6)	56.95(4)	36.52(4)	5.373(5)	3.909(6)	1.464(8)	101.49(3)
2.6	2.970	62.66	45.11	6.400	4.549	1.851	117.15
2.8	3.271	71.37	52.05	7.746	5.378	2.369	134.43
3.0	3.688	81.59	60.11	8.819	5.942	2.877	154.20

ENERGY	BETA1	BETA2	LA/LL	LA/LB	LA/LG	LB/LG
MeV	BARNS					
1.0	3.161(7)	1.389(9)	19.42(9)	1.709(7)	12.39(8)	7.253 (8)
1.2	5.080	2.316	19.46	1.648	11.98	7.270
1.4	7.301	3.108	19.47	1.678	12.31	7.339
1.6	10.484	4.272	19.52	1.678	11.88	7.082
1.8	13.220	5.806	19.79	1.585	10.94	6.899
2.0	17.345	7.087	20.91	1.576	10.55	6.697
2.2	22.121	8.477	21.59	1.564	10.66	6.815
2.4	26.719(5)	9.806(6)	21.56(7)	1.559(5)	10.60(5)	6.797(6)
2.6	33.458	11.656	21.10	1.389	9.79	7.049
2.8	38.003	14.047	21.82	1.371	9.21	6.719
3.0	43.860	16.248	22.12	1.357	9.25	6.816

EXPERIMENTAL L SUBSHELL IONISATION CROSS SECTIONS

FOR PROTON IMPACT

ENERGY	L1	L2	L3	L1/L2	L1/L3	L2/L3	TOTAL
MeV		BARNS					BARNS
1.0	3.65(10)	15.25(8)	41.73(6)	.239(13)	.087(12)	.365(10)	60.63 (5)
1.2	4.82	25.69	65.40	.188	.074	.393	95.91
1.4	8.62	34.16	93.59	.252	.092	.365	136.37
1.6	13.82	49.20	132.04	.281	.105	.373	195.06
1.8	21.62	62.19	158.94	.348	.136	.391	242.75
2.0	31.54	79.66	201.57	.396	.156	.395	312.77
2.2	47.34	90.57	249.32	.523	.190	.363	387.23
2.4	61.69(8)	103.96(6)	295.61(4)	.593(10)	.209(9)	.352(7)	461.26 (3)
2.6	78.07	119.80	321.08	.652	.243	.373	518.95
2.8	100.02	140.14	361.47	.714	.277	.388	601.63
3.0	121.61	152.76	412.14	.796	.295	.371	686.51

TUNGSTEN(Z2=74)

EXPERIMENTAL L SHELL X-RAY PRODUCTION CROSS SECTIONS

FOR PROTON IMPACT

ENERGY MeV	L	ALPHA	BETA	GAMMA	GAMMA1	GAMMA2	TOTAL
	BARNS						
1.0	.282(8)	5.72(5)	3.04(6)	.404(7)	.338(8)	.0663(10)	9.44(5)
1.2	.437	9.10	4.97	.662	.563	.0985	15.17
1.4	.670	14.38	7.73	1.100	.926	.175	23.88
1.6	.858	18.49	10.31	1.451	1.205	.247	31.11
1.8	1.105	23.83	13.66	2.028	1.645	.383	40.63
2.0	1.334	30.66	17.98	2.696	2.137	.559	52.68
2.2	1.543	34.99	22.13	3.324	2.550	.774	61.99
2.4	1.829	41.47	26.64	4.124	3.071	1.052	74.07
2.6	2.057(6)	47.21	30.40	4.775(5)	3.427(6)	1.348(8)	84.44(3)
2.8	2.315	54.03	34.93	5.568	3.803	1.765	96.84
3.0	2.687	62.09	40.21	6.743	4.624	2.119	111.73

ENERGY MeV	BETA1	BETA2	LA/LL	LA/LB	LA/LG	LB/LG
	BARNS					
1.0	1.821(7)	1.215(9)	20.28(9)	1.884(7)	14.14(8)	7.508(9)
1.2	3.006	1.962	20.84	1.832	13.75	7.504
1.4	4.849	2.885	21.44	1.859	13.07	7.031
1.6	6.643	3.669	21.54	1.793	12.74	7.106
1.8	8.894	4.766	21.57	1.745	11.75	6.736
2.0	11.737	6.248	22.98	1.705	11.37	6.671
2.2	14.206	7.922	22.67	1.581	10.53	6.658
2.4	17.705	8.934	22.67	1.557	10.06	6.460
2.6	20.446(6)	9.957(7)	22.95(8)	1.553(6)	9.89(6)	6.368(8)
2.8	23.557	11.372	23.34	1.547	9.70	6.273
3.0	27.312	12.901	23.10	1.544	9.21	5.964

EXPERIMENTAL L SUBSHELL IONISATION CROSS SECTIONS

FOR PROTON IMPACT

ENERGY MeV	L1	L2	L3	L1/L2	L1/L3	L2/L3	TOTAL BARNS
		BARNS					
1.0	1.74(10)	7.67(8)	26.13(6)	.227(13)	.0666(12)	.294(10)	35.54(5)
1.2	2.52	12.86	41.53	.196	.0607	.310	56.91
1.4	4.55	21.06	65.33	.216	.0696	.322	90.94
1.6	6.53	27.30	83.78	.239	.0779	.326	117.61
1.8	10.39	37.04	107.08	.281	.0970	.346	154.51
2.0	15.41	47.80	137.09	.322	.112	.349	200.30
2.2	21.78	56.46	154.86	.386	.141	.365	233.10
2.4	30.03	67.36	182.14	.446	.165	.370	279.53
2.6	38.99(8)	74.22(6)	206.22(5)	.525(10)	.189(9)	.360(8)	319.43(4)
2.8	51.76	80.92	234.48	.640	.221	.345	367.16
3.0	62.09	98.53	267.73	.630	.232	.368	428.35

GOLD(Z2=79)

EXPERIMENTAL L SHELL X-RAY PRODUCTION CROSS SECTIONS

FOR PROTON IMPACT

ENERGY MeV	L	ALPHA	BETA	GAMMA	GAMMA1	GAMMA2	TOTAL
				BARNS			
1.0	.192(7)	3.66(4)	1.96(5)	.248(6)	.198(7)	.0504(9)	6.07(4)
1.2	.303	5.88	3.13	.424	.348	.0758	9.74
1.4	.475	9.39	4.99	.642	.538	.103	15.50
1.6	.610	12.21	6.75	.859	.723	.135	20.43
1.8	.802	15.70	8.82	1.143	.952	.190	26.46
2.0	.965	19.53	11.14	1.470	1.217	.253	33.10
2.2	1.194	24.36	14.13	1.856	1.529	.327	41.54
2.4	1.414	29.60	16.94	2.208	1.767	.442	50.17
2.6	1.688(5)	33.82(3)	18.82(4)	2.541(5)	1.996(5)	.545(7)	56.87(3)
2.8	1.936	39.49	22.98	3.103	2.415	.688	67.50
3.0	2.232	44.40	25.34	3.463	2.637	.826	75.44

ENERGY MeV	LA/LL	LA/LB	LA/LG	LB/LG
1.0	19.09(7)	1.865(5)	14.78(6)	7.921(7)
1.2	19.39	1.878	13.87	7.384
1.4	19.75	1.882	14.63	7.771
1.6	20.01	1.808	14.22	7.861
1.8	19.58	1.780	13.73	7.717
2.0	20.25	1.754	13.29	7.575
2.2	20.40	1.724	13.13	7.612
2.4	20.93	1.747	13.41	7.674
2.6	20.04(5)	1.797(4)	13.31(5)	7.406(6)
2.8	20.40	1.719	12.73	7.405
3.0	19.90	1.752	12.82	7.319

EXPERIMENTAL L SUBSHELL IONISATION CROSS SECTIONS

FOR PROTON IMPACT

ENERGY MeV	L1	L2	L3	L1/L2	L1/L3	L2/L3	TOTAL
		BARNS					BARNS
1.0	1.30(9)	3.45(7)	13.41(5)	.377(11)	.0969(11)	.257(9)	18.16(4)
1.2	1.75	6.15	21.63	.285	.0809	.284	29.53
1.4	2.13	9.60	34.93	.222	.0610	.275	46.66
1.6	2.70	12.92	45.41	.209	.0595	.285	61.03
1.8	4.08	16.93	58.00	.241	.0703	.292	79.01
2.0	5.63	21.57	71.81	.261	.0784	.300	99.01
2.2	7.45	27.05	89.31	.275	.0834	.303	123.81
2.4	11.29	30.87	107.54	.366	.105	.287	149.70
2.6	14.68(7)	34.62(5)	121.96(4)	.424(9)	.120(8)	.284(6)	171.26(3)
2.8	18.98	41.71	141.23	.455	.134	.295	201.92
3.0	23.86	45.10	157.65	.529	.151	.286	226.61

LEAD(Z2=82)

EXPERIMENTAL L SHELL X-RAY PRODUCTION CROSS SECTIONS

FOR PROTON IMPACT

ENERGY MeV	L	ALPHA	BETA	GAMMA	GAMMA1	GAMMA2	TOTAL
			BARNS				
1.0	.117(7)	2.01(5)	1.08(6)	.173(6)	.130(7)	.0430(9)	3.39(4)
1.2	.200	3.79	2.06	.296	.234	.0624	6.34
1.4	.303	5.37	3.08	.441	.360	.0814	9.20
1.6	.420	7.61	4.33	.654	.532	.122	13.01
1.8	.579	10.90	6.29	.917	.740	.178	18.69
2.0	.746	14.92	8.82	1.262	1.026	.236	25.76
2.2	.889	18.27	11.00	1.599	1.269	.330	31.75
2.4	1.001	21.01	12.76	2.040	1.614	.426	36.81
2.6	1.200(6)	24.91(4)	15.03(4)	2.402(5)	1.885(5)	.517(8)	43.55(3)
2.8	1.417	29.10	17.93	2.793	2.091	.702	51.24
3.0	1.603	33.01	20.89	3.423	2.554	.869	58.92

ENERGY MeV	LA/LL	LA/LB	LA/LG	LB/LG
1.0	17.15(8)	1.854(7)	11.62(7)	6.269(8)
1.2	18.99	1.840	12.80	6.956
1.4	17.73	1.745	12.19	6.984
1.6	18.11	1.756	11.63	6.622
1.8	18.82	1.734	11.89	6.858
2.0	20.01	1.691	11.83	6.992
2.2	20.55	1.661	11.42	6.878
2.4	20.99	1.647	10.30	6.255
2.6	20.76(7)	1.657(5)	10.37(6)	6.259(6)
2.8	20.53	1.623	10.42	6.419
3.0	20.60	1.580	9.64	6.104

EXPERIMENTAL L SUBSHELL IONISATION CROSS SECTIONS

FOR PROTON IMPACT

ENERGY MeV	L1	L2	L3	L1/L2	L1/L3	L2/L3	TOTAL
		BARNS					BARNS
1.0	1.04(9)	1.97(7)	6.33(6)	.528(11)	.164(11)	.311(9)	9.34(4)
1.2	1.29	3.61	12.35	.357	.104	.292	17.25
1.4	1.41	5.62	17.71	.251	.0796	.317	24.74
1.6	2.14	8.31	24.94	.258	.0858	.333	35.39
1.8	3.30	11.50	35.66	.287	.0925	.322	50.46
2.0	4.15	16.02	48.99	.259	.0847	.327	69.16
2.2	6.67	19.61	59.02	.340	.113	.332	85.30
2.4	8.70	24.93	66.99	.349	.130	.372	100.62
2.6	10.95(8)	29.01(6)	79.12(5)	.377(10)	.138(9)	.367(8)	119.08
2.8	17.19	31.59	90.06	.544	.191	.351	138.84
3.0	21.47	38.52	100.65	.557	.213	.383	160.64

BISMUTH(Z2=83)

EXPERIMENTAL L SHELL X-RAY PRODUCTION CROSS SECTIONS FOR PROTON IMPACT

ENERGY MeV	L	ALPHA	BETA	GAMMA	GAMMA1	GAMMA2	TOTAL
				BARNS			
1.2	.204(8)	3.70 (5)	1.84 (6)	.287 (6)	.229 (7)	.0585 (9)	6.03 4
1.4	.319	5.59	3.07	.435	.353	.0818	9.42
1.6	.424	7.59	4.53	.617	.499	.118	13.16
1.8	.565	10.21	6.12	.818	.661	.157	17.71
2.0	.703	12.71	7.63	1.050	.851	.198	22.09
2.2	.847	15.36	9.25	1.302	1.045	.257	26.76
2.4	1.021	18.90	11.43	1.629	1.300	.329	32.98
2.6	1.200	22.12	13.53	2.011	1.587	.424	38.86
2.8	1.356(6)	25.70(4)	15.79(4)	2.363(5)	1.861(6)	.502(8)	45.21 (3)
3.0	1.590	29.91	18.45	2.731	2.123	.608	52.68

ENERGY MeV	LA/LL	LA/LB	LA/LG	LB/LG
1.2	18.12(9)	2.011 (7)	12.89 (7)	6.408 (8)
1.4	17.52	1.825	12.86	7.049
1.6	17.91	1.675	12.30	7.344
1.8	18.06	1.669	12.48	7.480
2.0	18.08	1.665	12.10	7.270
2.2	18.15	1.661	11.80	7.105
2.4	18.52	1.654	11.60	7.016
2.6	18.43	1.634	11.00	6.729
2.8	18.96 (7)	1.628 (5)	10.88 (6)	6.683 (6)
3.0	18.81	1.621	10.95	6.755

EXPERIMENTAL L SUBSHELL IONISATION CROSS SECTIONS FOR PROTON IMPACT

ENERGY MeV	L1	L2	L3	L1/L2	L1/L3	L2/L3	TOTAL BARNS
		BARNS					
1.2	1.03(9)	3.40(8)	11.81(6)	.303(12)	.0872(11)	.288(10)	16.24 (5)
1.4	1.27	5.30	18.02	.240	.0705	.294	24.59
1.6	1.88	7.47	24.32	.252	.0773	.307	33.67
1.8	2.52	9.90	32.74	.255	.0770	.302	45.16
2.0	3.09	12.77	40.72	.242	.0759	.314	56.58
2.2	4.30	15.61	48.87	.275	.0880	.319	68.78
2.4	5.72	19.38	59.86	.295	.0956	.324	84.96
2.6	7.81	23.56	69.27	.331	.113	.340	100.64
2.8	9.35(8)	27.61(7)	80.32 (5)	.339(11)	.116(9)	.344(9)	117.28(4)
3.0	11.96	31.36	92.90	.381	.129	.338	136.22

THORIUM(Z2=90)

EXPERIMENTAL L SHELL X-RAY PRODUCTION CROSS SECTIONS

FOR PROTON IMPACT

ENERGY MeV	L	ALPHA	BETA	GAMMA	GAMMA1	GAMMA2	TOTAL
	BARNS						
1.2	.104 (9)	1.62 (6)	.913 (6)	.123 (7)	.0937(8)	.0294(10)	2.76 (4)
1.4	.168	2.54	1.45	.198	.154	.0444	4.35
1.6	.252	3.91	2.21	.300	.237	.0632	6.67
1.8	.332	5.42	3.16	.428	.342	.0856	9.34
2.0	.396	6.74	3.95	.577	.461	.116	11.67
2.2	.517	8.95	5.42	.790	.629	.160	15.68
2.4	.648	11.20	7.02	.983	.782	.202	19.86
2.6	.810 (7)	13.42(4)	8.06 (5)	1.167 (6)	.928 (7)	.238(8)	23.45(3)
2.8	.981	15.86	9.63	1.359	1.079	.281	27.83
3.0	1.103	18.65	11.27	1.625	1.283	.343	32.65

ENERGY MeV	BETA1	BETA2	LA/LL	LA/LB	LA/LG	LB/LG
	BARNS					
1.2	.490 (7)	.424(8)	15.51(10)	1.771(8)	13.14(8)	7.419 (8)
1.4	.773	.673	15.06	1.754	12.77	7.284
1.6	1.215	.999	15.49	1.764	13.01	7.376
1.8	1.739	1.421	16.30	1.714	12.66	7.387
2.0	2.197	1.755	17.03	1.707	11.70	6.853
2.2	3.092	2.329	17.33	1.652	11.34	6.864
2.4	4.046	2.979	17.29	1.595	11.39	7.143
2.6	4.551(6)	3.505(7)	16.58(8)	1.666(6)	11.51(7)	6.906(7)
2.8	5.701	3.929	16.18	1.647	11.67	7.085
3.0	6.763	4.505	16.90	1.655	11.47	6.932

EXPERIMENTAL L SUBSHELL IONISATION CROSS SECTIONS

FOR PROTON IMPACT

ENERGY MeV	L1	L2	L3	L1/L2	L1/L3	L2/L3	TOTAL BARNS
	BARNS						
1.2	.385 (10)	1.08 (9)	4.29 (7)	.356 (13)	.0897(12)	.252 (11)	5.76 (6)
1.4	.503	1.78	6.78	.283	.0742	.263	9.06
1.6	.608	2.76	10.54	.220	.0577	.262	13.91
1.8	.692	4.00	14.69	.173	.0471	.272	19.38
2.0	.954	5.39	18.19	.177	.0524	.296	24.53
2.2	1.36	7.35	24.07	.185	.0565	.305	32.78
2.4	1.78	9.12	30.08	.195	.0592	.303	40.98
2.6	2.07(8)	10.84(8)	36.08(6)	.191(11)	.0574(10)	.300 (10)	48.99 (5)
2.8	2.54	12.57	42.62	.202	.0596	.295	57.73
3.0	3.31	14.92	49.90	.222	.0663	.299	68.13

URANIUM(Z2=92)

EXPERIMENTAL L SHELL X-RAY PRODUCTION CROSS SECTIONS FOR PROTON IMPACT

ENERGY	L	ALPHA	BETA	GAMMA	GAMMA1	GAMMA2	TOTAL
MeV				BARNS			
1.2	.0894(9)	1.48 (7)	.795 (6)	.0920(7)	.0679(9)	.0241 (11)	2.45 (5)
1.4	.139	2.27	1.22	.138	.104	.0345	3.77
1.6	.198	3.07	1.70	.185	.140	.0450(10)	5.15
1.8	.260	4.09	2.36	.265	.204	.0606	6.98
2.0	.353	5.57	3.16	.389	.304	.0856	9.47
2.2	.442	6.97	4.18	.497	.385	.112 (9)	12.09
2.4	.556	8.80	5.15	.620	.480	.140	15.13
2.6	.653 (8)	10.45 (5)	6.09 (5)	.767 (6)	.600 (7)	.166 (8)	17.96 (3)
2.8	.752	12.22	7.45	.913	.710	.203	21.34
3.0	.874	13.76	8.42	1.055	.815	.240	24.10

ENERGY	BETA1	BETA2	LA/LL	LA/LB	LA/LG	LB/LG
MeV	BARNS					
1.2	.380 (8)	.414 (9)	16.55(11)	1.861 (9)	16.08 (10)	8.640 (9)
1.4	.609	.614	16.36	1.856	16.41	8.842
1.6	.871	.830	15.52	1.805	16.64	9.219
1.8	1.227	1.136	15.73	1.732	15.46	8.927
2.0	1.693	1.467	15.79	1.762	14.30	8.115
2.2	2.111	2.068	15.79	1.669	14.03	8.409
2.4	2.730	2.423	15.83	1.708	14.20	8.316
2.6	3.289 (6)	2.799 (7)	16.00 (9)	1.717 (7)	13.63 (8)	7.939 (8)
2.8	4.039	3.413	16.26	1.640	13.39	8.165
3.0	4.599	3.816	15.75	1.635	13.05	7.978

EXPERIMENTAL L SUBSHELL IONISATION CROSS SECTIONS FOR PROTON IMPACT

ENERGY	L1	L2	L3	L1/L2	L1/L3	L2/L3	TOTAL
MeV		BARNS					BARNS
1.2	.343(11)	.788(10)	3.70 (8)	.435 (15)	.0927(14)	.213 (13)	4.83 (6)
1.4	.452	1.21	5.73	.374	.0789	.211	7.39
1.6	.562 (10)	1.63	7.78	.345(14)	.0722(13)	.210	9.97
1.8	.657	2.40	10.38	.274	.0633	.231	13.44
2.0	.828	3.58 (9)	14.11	.231	.0587	.254(12)	18.52
2.2	1.15 (9)	4.53	17.60	.254(13)	.0653(12)	.257	23.28
2.4	1.45	5.65	22.22	.257	.0653	.254	29.32
2.6	1.56 (8)	7.08 (8)	26.43 (6)	.220(11)	.0590(10)	.268 (10)	35.07 (5)
2.8	2.03	8.36	30.77	.243	.0660	.272	41.16
3.0	2.56	9.58	34.45	.267	.0743	.278	46.59

B.2 DEUTERON IMPACT

DYSPROSIUM(Z2=66)

EXPERIMENTAL L SHELL X-RAY PRODUCTION CROSS SECTIONS

FOR DEUTERON IMPACT

ENERGY	L	ALPHA	BETA	GAMMA	GAMMA1	GAMMA2	TOTAL
MeV				BARNS			
1.2	.196(8)	4.04(4)	2.24(5)	.291 (6)	.240 (7)	.052(9)	6.77 (3)
1.4	.279	6.12	3.42	.439	.376	.063	10.26
1.6	.434	9.13	4.99	.642	.576	.067	15.20
1.8	.536	12.04	6.66	.858	.766	.093	20.09
2.0	.676	15.20	8.47	1.043	.925	.118	25.39
2.2	.853	18.63	10.67	1.351	1.195	.157	31.51
2.4	1.011	22.38	12.73	1.680	1.451	.229	37.81
2.6	1.249(7)	28.53(3)	16.57(3)	2.137(5)	1.814(5)	.323(8)	48.49
2.8	1.406	31.24	19.28	2.570	2.143	.427	54.49
3.0	1.557	37.85	23.14	3.118	2.542	.576	65.67

ENERGY	BETA1	BETA2	LA/LL	LA/LB	LA/LG	LB/LG
MeV	BARNS					
1.2	1.521(6)	.723 (8)	20.58 (9)	1.800(6)	13.88(7)	7.713
1.4	2.299	1.117	21.91	1.792	13.94	7.781
1.6	3.339	1.653	21.05	1.829	14.22	7.777
1.8	4.439	2.222	22.46	1.807	14.03	7.763
2.0	5.716	2.754	22.50	1.795	14.57	8.121
2.2	7.247	3.423	21.84	1.746	13.79	7.898
2.4	8.668	4.063	22.15	1.758	13.32	7.578
2.6	11.386(4)	5.187 (6)	22.84(8)	1.721 (4)	13.35(6)	7.755 (8)
2.8	13.362	5.918	22.22	1.620	12.15	7.502
3.0	16.251	6.888	24.31	1.636	12.14	7.421

EXPERIMENTAL L SUBSHELL IONISATION CROSS SECTIONS

FOR DEUTERON IMPACT

ENERGY	L1	L2	L3	L1/L2	L1/L3	L2/L3	TOTAL
MeV		BARNS					BARNS
1.2	2.70(9)	8.45(7)	26.09(5)	.320(11)	.103(11)	.324(9)	37.24(4)
1.4	3.24	13.47	39.70	.241	.082	.339	56.41
1.6	3.40	20.89	59.56	.163	.057	.351	83.85
1.8	4.74	27.75	78.40	.171	.060	.354	110.89
2.0	6.08	33.45	99.25	.182	.061	.337	138.78
2.2	8.05	43.17	121.09	.186	.066	.357	172.31
2.4	11.86	52.05	144.70	.228	.082	.360	208.61
2.6	16.81(8)	64.70(5)	184.14(3)	.260(9)	.091(9)	.351(6)	265.65(2.5)
2.8	22.26	76.00	199.46	.293	.112	.381	297.72
3.0	30.16	89.42	241.10	.337	.125	.371	360.68

YTTERBIUM(Z2=70)

EXPERIMENTAL L SHELL X-RAY PRODUCTION CROSS SECTIONS FOR DEUTERON IMPACT

ENERGY MeV	L	ALPHA	BETA	GAMMA	GAMMA1	GAMMA2	TOTAL
	BARNS						
1.2	.117(8)	2.18(5)	1.35(6)	.188(7)	.150(8)	.0384(10)	3.84(4)
1.4	.179	3.38	1.97	.275	.229	.0454	5.81
1.6	.251	4.88	2.77	.367	.317	.0500	8.26
1.8	.333	6.52	3.73	.499	.444	.0551	11.08
2.0	.421	8.50	4.90	.686	.617	.0692	14.52
2.2	.539	10.92	6.26	.894	.776	.118	18.62
2.4	.653(7)	13.19(4)	7.65(4)	1.094(6)	.938(7)	.156(9)	22.59(3)
2.6	.794	16.46	9.61	1.416	1.213	.203	28.29
2.8	.926	19.13	11.16	1.663	1.420	.243	32.87
3.0	1.057	22.40	13.09	1.958	1.654	.304	38.51

ENERGY MeV	BETA1	BETA2	LA/LL	LA/LB	LA/LG	LB/LG
	BARNS					
1.2	.930(7)	.421(9)	18.74(9)	1.617(7)	11.60(8)	7.172(8)
1.4	1.326	.645	18.90	1.716	12.32	7.181
1.6	1.839	.930	19.45	1.761	13.28	7.543
1.8	2.525	1.210	19.56	1.745	13.05	7.481
2.0	3.269	1.636	20.19	1.734	12.39	7.147
2.2	4.253	2.009	20.25	1.744	12.21	7.001
2.4	5.172(5)	2.482(6)	20.20(8)	1.723(6)	12.05(6)	6.996(7)
2.6	6.453	3.161	20.75	1.712	11.63	6.789
2.8	7.612	3.545	20.65	1.714	11.50	6.708
3.0	9.065	4.027	21.19	1.711	11.44	6.686

EXPERIMENTAL L SUBSHELL IONISATION CROSS SECTIONS FOR DEUTERON IMPACT

ENERGY MeV	L1	L2	L3	L1/L2	L1/L3	L2/L3	TOTAL BARNS
	BARNS						
1.2	1.61(10)	4.12(8)	11.56(6)	.391(13)	.139(12)	.356(10)	17.29(5)
1.4	1.89	6.44	18.09	.293	.104	.356	26.42
1.6	2.06	8.99	26.34	.229	.0782	.341	37.39
1.8	2.25	12.71	35.25	.177	.0638	.361	50.21
2.0	2.81	17.72	45.85	.159	.0613	.386	66.38
2.2	4.87	22.04	58.60	.221	.0831	.376	85.51
2.4	6.46(9)	26.52(7)	70.59(5)	.244(11)	.0915(10)	.376(9)	103.57(4)
2.6	8.41	34.29	87.80	.245	.0958	.391	130.50
2.8	10.07	40.10	101.86	.251	.0989	.394	152.03
3.0	12.59	46.56	119.13	.270	.106	.391	178.28

TUNGSTEN(Z2=74)

EXPERIMENTAL L SHELL X-RAY PRODUCTION CROSS SECTIONS

FOR DEUTERON IMPACT

ENERGY	L	ALPHA	BETA	GAMMA	GAMMA1	GAMMA2	TOTAL
MeV				BARNS			
1.2	.0718(9)	1.40 (6)	.812 (6)	.118(7)	.0817(9)	.0364(10)	2.41 (4)
1.4	.115	2.24	1.22	.178	.129	.0490	3.76
1.6	.170	3.32	1.78	.243	.190	.0530	5.52
1.8	.225	4.52	2.42	.330	.273	.0575	7.50
2.0	.296	5.99	3.23	.443	.373	.0703	9.96
2.2	.368 (8)	7.62	4.06	.554	.466	.0879 (9)	12.60
2.4	.455	9.57	5.26	.711	.609	.102	15.99
2.6	.529	11.40	6.19	.850	.727	.123	18.97
2.8	.629 (7)	13.75 (5)	7.59 (5)	1.070	.920 (8)	.149 (8)	23.03
3.0	.755	16.42	8.39	1.290	1.111	.179	27.46

ENERGY	BETA1	BETA2	LA/LL	LA/LB	LA/LG	LB/LG
MeV	BARNS					
1.2	.524(8)	.288 (8)	19.55(10)	1.730 (8)	11.89(8)	6.873 (8)
1.4	.767	.456	19.48	1.832	12.57	6.862
1.6	1.106	.677	19.56	1.864	13.66	7.329
1.8	1.511	.912	20.06	1.865	13.69	7.340
2.0	2.059	1.174	20.24	1.853	13.52	7.294
2.2	2.435	1.626	20.70(9)	1.877	13.77	7.336
2.4	3.267	1.990	21.02	1.820	13.46	7.395
2.6	3.988	2.201	21.57	1.843	13.42	7.280
2.8	4.838 (6)	2.748(7)	21.85(8)	1.812 (6)	12.85	7.093
3.0	5.669	3.321	21.75	1.827	12.73	6.968

EXPERIMENTAL L SUBSHELL IONISATION CROSS SECTIONS

FOR DEUTERON IMPACT

ENERGY	L1	L2	L3	L1/L2	L1/L3	L2/L3	TOTAL
MeV		BARNS					BARNS
1.2	1.06(10)	1.74(9)	6.24(7)	.609(13)	.170 (12)	.279 (11)	9.04 (5)
1.4	1.41	2.80	10.04	.504	.140	.279	14.25
1.6	1.48	4.23	15.07	.350	.0982	.281	20.78
1.8	1.53	6.17	20.58	.248	.0743	.300	28.28
2.0	1.83	8.48	27.29	.216	.0671	.311	37.60
2.2	2.29 (9)	10.61(8)	34.77	.216(12)	.0659(11)	.305	47.67
2.4	2.58	13.94	43.64	.185	.0591	.319	60.16
2.6	3.13	16.62	51.99	.188	.0602	.320	71.74
2.8	3.76(8)	21.08(7)	62.50(6)	.178(11)	.0602(10)	.337(9)	87.34
3.0	4.51	25.43	74.61	.177	.0604	.341	104.55

GOLD(Z2=79)

EXPERIMENTAL L SHELL X-RAY PRODUCTION CROSS SECTIONS FOR DEUTERON IMPACT

ENERGY MeV	L	ALPHA	BETA	GAMMA	GAMMA1	GAMMA2	TOTAL
				BARNS			
1.2	.0466(8)	.809(5)	.468(6)	.0640(7)	.0386(8)	.0254(10)	1.39(4)
1.4	.0742	1.31	.730	.0973	.0664	.0309	2.21
1.6	.113	2.01	1.10	.142	.102	.0396	3.37
1.8	.157	2.78	1.48	.199	.150	.0485	4.62
2.0	.202	3.69	1.96	.256	.200	.0559	6.11
2.2	.258	4.79	2.53	.324	.258	.0660	7.91
2.4	.320(6)	5.99(4)	3.15(5)	.424(6)	.347(7)	.0777(9)	9.88(3)
2.6	.390	7.37	3.86	.505	.417	.0875	12.12
2.8	.460	8.74	4.59	.608	.503	.105	14.40
3.0	.538	10.45	5.38	.716	.593	.123	17.08

ENERGY MeV	LA/LL	LA/LB	LA/LG	LB/LG
1.2	17.35(9)	1.730(7)	12.64(8)	7.308(8)
1.4	17.59	1.787	13.42	7.507
1.6	17.78	1.823	14.15	7.761
1.8	17.76	1.874	13.97	7.455
2.0	18.26	1.882	14.40	7.656
2.2	18.54	1.891	14.78	7.819
2.4	18.70(7)	1.899(6)	14.12(7)	7.432(7)
2.6	18.89	1.913	14.60	7.634
2.8	19.01	1.903	14.38	7.554
3.0	19.40	1.942	14.59	7.512

EXPERIMENTAL L SUBSHELL IONISATION CROSS SECTIONS FOR DEUTERON IMPACT

ENERGY MeV	L1	L2	L3	L1/L2	L1/L3	L2/L3	TOTAL BARNS
		BARNS					
1.2	.908(10)	.582(8)	2.64(7)	1.560(13)	.344(12)	.220(10)	4.13(5)
1.4	1.02	1.08	4.49	.944	.227	.241	6.59
1.6	1.24	1.71	7.08	.725	.175	.242	10.03
1.8	1.42	2.57	9.94	.553	.143	.259	13.93
2.0	1.52	3.46	13.38	.439	.114	.259	18.36
2.2	1.71	4.50	17.53	.380	.0975	.257	23.74
2.4	1.84(9)	6.10(7)	22.01(5)	.302(11)	.0836(10)	.277(8)	29.95(4)
2.6	1.96	7.39	27.29	.265	.0718	.271	36.64
2.8	2.33	8.92	32.33	.261	.0721	.276	43.58
3.0	2.71	10.52	38.69	.258	.0700	.272	51.92

LEAD(Z2=82)

EXPERIMENTAL L SHELL X-RAY PRODUCTION CROSS SECTIONS

FOR DEUTERON IMPACT

ENERGY	L	ALPHA	BETA	GAMMA	GAMMA1	GAMMA2	TOTAL
MeV				BARNS			
1.2	.0346 (8)	.571 (5)	.339 (6)	.0503 (7)	.0302 (9)	.0201 (11)	.995 (4)
1.4	.0579	.970	.550	.0803	.0543	.0260	1.66
1.6	.0840	1.41	.781	.110	.0767	.0331	2.38
1.8	.114	2.01	1.10	.155	.114	.0413	3.38
2.0	.155	2.67	1.46	.205	.155	.0501	4.50
2.2	.201	3.54	1.95	.270	.209	.0608	5.96
2.4	.244	4.40	2.43	.342	.271	.0708	7.42
2.6	.292 (7)	5.40 (4)	3.00 (5)	.428 (6)	.343 (7)	.0849 (10)	9.12 (3)
2.8	.355	6.61	3.66	.534	.429	.105	11.16
3.0	.413	7.70	4.27	.670	.543	.127	13.05

ENERGY MeV	LA/LL	LA/LB	LA/LG	LB/LG
1.2	16.51 (9)	1.688 (8)	11.36 (8)	6.732 (8)
1.4	16.75	1.762	12.07	6.853
1.6	16.75	1.802	12.80	7.102
1.8	17.59	1.824	12.95	7.098
2.0	17.30	1.829	13.05	7.134
2.2	17.67	1.820	13.13	7.211
2.4	18.01	1.810	12.86	7.105
2.6	18.49	1.802 (6)	12.62 (7)	7.005 (7)
2.8	18.61	1.804	12.38	6.860
3.0	18.64	1.802	11.49	6.378

EXPERIMENTAL L SUBSHELL IONISATION CROSS SECTIONS

FOR DEUTERON IMPACT

ENERGY	L1	L2	L3	L1/L2	L1/L3	L2/L3	TOTAL
MeV		BARNS					BARNS
1.2	.638 (11)	.410 (9)	1.61 (7)	1.556 (14)	.396 (13)	.255 (11)	2.66 (5)
1.4	.752	.783	2.92	.960	.258	.268	4.46
1.6	.918	1.13	4.35	.812	.211	.260	6.40
1.8	1.06	1.70	6.34	.624	.167	.268	9.10
2.0	1.20	2.35	8.57	.511	.140	.274	12.12
2.2	1.35	3.20	11.49	.422	.117	.279	16.04
2.4	1.43	4.19	14.38	.341	.0994	.291	20.00
2.6	1.63 (10)	5.33 (8)	17.72 (6)	.306 (13)	.0920 (12)	.301 (10)	24.68
2.8	1.98	6.67	21.66	.297	.0914	.308	30.31
3.0	2.28	8.47	25.17	.269	.0906	.337	35.92

BISMUTH(Z2=83)

EXPERIMENTAL L SHELL X-RAY PRODUCTION CROSS SECTIONS FOR DEUTERON IMPACT

ENERGY MeV	L	ALPHA	BETA	GAMMA	GAMMA1	GAMMA2	TOTAL
	BARNS						
1.4	.0542 (9)	.950 (6)	.557 (7)	.0700 (7)	.0478 (9)	.0222 (10)	1.63 (4)
1.6	.0862	1.47	.806	.105	.0753	.0296	2.47
1.8	.109	1.85	.998	.131	.0950	.0361	3.09
2.0	.146	2.52	1.36	.180	.133	.0466	4.21
2.2	.183 (8)	3.25	1.78 (6)	.233	.178	.0550	5.45
2.4	.228	4.03	2.22	.298	.233	.0652	6.78
2.6	.286	5.20	2.89	.388	.310	.0780	8.77
2.8	.334 (7)	6.26 (5)	3.55 (5)	.484	.392 (8)	.0918 (9)	10.63 (3)
3.0	.381	7.01	3.95	.536	.435	.101	11.88

ENERGY MeV	LA/LL	LA/LB	LA/LG	LB/LG
1.4	17.53 (10)	1.704 (8)	13.57 (8)	7.963 (9)
1.6	17.04	1.824	13.99	7.672
1.8	17.01	1.857	14.15	7.618
2.0	17.22	1.849	14.00	7.571
2.2	17.74	1.824	13.94	7.644
2.4	17.66	1.814	13.53	7.460
2.6	18.19	1.799	13.41	7.452
2.8	18.74 (8)	1.765 (6)	12.94	7.334 (8)
3.0	18.40	1.775	13.08	7.368

EXPERIMENTAL L SUBSHELL IONISATION CROSS SECTIONS FOR DEUTERON IMPACT

ENERGY MeV	L1	L2	L3	L1/L2	L1/L3	L2/L3	TOTAL BARNS
	BARNS						
1.4	.589 (10)	.670 (9)	2.86 (7)	.879 (13)	.206 (12)	.234 (11)	4.12 (5)
1.6	.724	1.08	4.53	.670	.160	.238	6.33
1.8	.868	1.37	5.75	.634	.151	.238	7.99
2.0	1.07	1.93	7.87	.554	.136	.245	10.87
2.2	1.15	2.61	10.27	.441	.112	.254	14.03
2.4	1.26	3.45	12.83	.365	.0982	.269	17.54
2.6	1.34	4.62	16.69	.290	.0803	.277	22.65
2.8	1.44 (9)	5.88 (8)	20.16 (6)	.245 (12)	.0714 (11)	.292 (10)	27.48
3.0	1.56	6.53	22.61	.239	.0690	.289	30.70

B.3 ALPHA PARTICLE IMPACT

YTTERBIUM(Z2=70)

EXPERIMENTAL L SHELL X-RAY PRODUCTION CROSS SECTIONS

FOR ALPHA IMPACT

ENERGY	L	ALPHA	BETA	GAMMA	GAMMA1	GAMMA2	TOTAL
MeV				BARNS			
1.2	.0297(8)	.545 (6)	.439 (6)	.0777(7)	.0471(8)	.0306(11)	1.09 (4)
1.4	.0542	.982	.703	.129	.0858	.0431	1.87
1.6	.0944	1.71	1.13	.198	.134	.0635	3.14
1.8	.144	2.63	1.72	.302	.222	.0798	4.79
2.0	.216	4.04	2.57 (5)	.421	.314	.108	7.25
2.2	.280	5.43	3.33	.559	.431	.127	9.60
2.4	.356	6.93	4.21	.677	.537	.140	12.17
2.6	.445 (7)	9.03 (5)	5.24 (4)	.810 (6)	.657(7)	.153(9)	15.53
2.8	.519	10.61	6.37	.982	.812	.170	18.48
3.0	.614	12.55	7.45	1.152	.974	.178	21.77

ENERGY	BETA1	BETA2	LA/LL	LA/LB	LA/LG	LB/LG
MeV	BARNS					
1.2	.310(8)	.129(8)	18.31(9)	1.240(8)	7.01(8)	5.654(8)
1.4	.503	.200	18.10	1.396	7.62	5.455
1.6	.795	.340	18.12	1.507	8.66	5.744
1.8	1.221	.494	18.21	1.532	8.71	5.687
2.0	1.804(6)	.770(7)	18.75	1.570(7)	9.59	6.110
2.2	2.316	1.016	19.38	1.629	9.72	5.965
2.4	2.885	1.323	19.44	1.646	10.23	6.218
2.6	3.594(5)	1.645(6)	20.28(8)	1.724(6)	11.15(7)	6.465(7)
2.8	4.479	1.889	20.44	1.666	10.80	6.484
3.0	5.170	2.283	20.43	1.684	10.89	6.467

EXPERIMENTAL L SUBSHELL IONISATION CROSS SECTIONS

FOR ALPHA IMPACT

ENERGY	L1	L2	L3	L1/L2	L1/L3	L2/L3	TOTAL
MeV		BARNS					BARNS
1.2	1.30(11)	1.15(9)	2.57(7)	1.130(14)	.506(13)	.447(11)	5.02(5)
1.4	1.82	2.20	4.78	.827	.381	.460	8.80
1.6	2.68	3.47	8.55	.772	.313	.406	14.70
1.8	3.36	5.94	13.29	.566	.253	.447	22.59
2.0	4.52	8.42	20.76	.537	.218	.406	33.70
2.2	5.34	11.76	28.05	.454	.190	.419	45.15
2.4	5.86	14.78	36.12	.396	.162	.409	56.76
2.6	6.40(9)	18.21(8)	47.70(6)	.351(12)	.134(11)	.382(9)	72.31
2.8	7.07	22.69	55.94	.312	.126	.406	85.70
3.0	7.40	27.41	66.39	.270	.111	.413	101.20

TUNGSTEN(Z2=74)

EXPERIMENTAL L SHELL X-RAY PRODUCTION CROSS SECTIONS

FOR ALPHA IMPACT

ENERGY	L	ALPHA	BETA	GAMMA	GAMMA1	GAMMA2	TOTAL
MeV				BARNS			
1.2	.0179(9)	.333(6)	.271(7)	.0464(7)	.0233(9)	.0232(11)	.669(5)
1.4	.0336	.622	.454	.0796	.0426	.0370	1.19
1.6	.0566	1.09	.724	.123	.0720	.0514	1.99
1.8	.0873	1.67	1.10	.192	.121	.0709	3.05
2.0	.130	2.49	1.58	.250	.159	.0905	4.44
2.2	.178	3.38	2.00	.320	.209	.111	5.87
2.4	.238(7)	4.74(5)	2.68(6)	.406(6)	.274(8)	.131(10)	8.06(4)
2.6	.300	6.11	3.32	.503	.348	.155	10.22
2.8	.378	7.57	4.14	.638	.464	.174	12.72
2.9	.421	8.57	4.80	.709	.518	.191	14.50

ENERGY	BETA1	BETA2	LA/LL	LA/LB	LA/LG	LB/LG
MeV	BARNS					
1.2	.182(9)	.0886(9)	18.58(10)	1.230(8)	7.18(8)	5.838(9)
1.4	.307	.147	18.53	1.371	7.82	5.705
1.6	.492	.232	19.20	1.501	8.81	5.870
1.8	.758	.341	19.16	1.523	8.72	5.726
2.0	1.040	.540	19.19	1.574	9.95	6.322
2.2	1.340	.660	18.94	1.688	10.54	6.246
2.4	1.807(8)	.874(8)	19.93(8)	1.767(7)	11.68(7)	6.610(8)
2.6	2.206	1.109	20.37	1.842	12.14	6.592
2.8	2.674	1.465	20.01	1.829	11.86	6.486
2.9	3.104	1.693	20.37	1.786	12.08	6.763

EXPERIMENTAL L SUBSHELL IONISATION CROSS SECTIONS

FOR ALPHA IMPACT

ENERGY	L1	L2	L3	L1/L2	L1/L3	L2/L3	TOTAL
MeV		BARNS					BARNS
1.2	.707(11)	.428(10)	1.55(8)	1.652(15)	.456(14)	.276(13)	2.69(6)
1.4	1.12	.814	2.96	1.376	.378	.275	4.89
1.6	1.55	1.43	5.30	1.084	.292	.270	8.28
1.8	2.11	2.50	8.18	.844	.258	.306	12.79
2.0	2.69	3.31	12.36	.813	.218	.268	18.36
2.2	3.30	4.36	16.92	.757	.195	.258	24.58
2.4	3.86(10)	5.83(8)	24.03(7)	.662(13)	.161(12)	.243(11)	33.72(5)
2.6	4.54	7.43	31.12	.611	.146	.239	43.09
2.8	5.01	10.09	38.62	.497	.130	.261	53.72
2.9	5.51	11.27	43.81	.489	.126	.257	60.59

GOLD(Z2=79)

EXPERIMENTAL L SHELL X-RAY PRODUCTION CROSS SECTIONS

FOR ALPHA IMPACT

ENERGY MeV	L (BARNS)	ALPHA (BARNS)	BETA (BARNS)	GAMMA (BARNS)	GAMMA1 (BARNS)	GAMMA2 (BARNS)	TOTAL (BARNS)
1.4	.0211(9)	.375(6)	.250(7)	.0478(7)	.0248(9)	.0230(11)	.694(4)
1.6	.0351	.621	.418	.0681	.0351	.0330	1.14
1.8	.0590	1.06	.657	.0987	.0572	.0415	1.87
2.0	.0797	1.52	.915	.131	.0770	.0540	2.64
2.2	.110	2.10	1.25	.185	.115	.0699	3.64
2.4	.142	2.87	1.64	.233	.146	.0862	4.88
2.6	.184(7)	3.90(5)	1.96(6)	.283(6)	.186(8)	.0972(10)	6.32
2.8	.235	5.05	2.50	.346	.238	.108	8.13
2.9	.266	5.66	2.65	.378	.263	.115	8.95

ENERGY MeV	LA/LL	LA/LB	LA/LG	LB/LG
1.4	17.81(10)	1.503(8)	7.85(8)	5.224(9)
1.6	17.71	1.486	9.13	6.142
1.8	17.96	1.614	10.74	6.652
2.0	19.03	1.658	11.57	6.982
2.2	19.00	1.681	11.33	6.742
2.4	20.22	1.755	12.32	7.021
2.6	21.20(8)	1.989(7)	13.77(7)	6.921(8)
2.8	21.48	2.025	14.60	7.212
2.9	21.28	2.135	14.97	7.009

EXPERIMENTAL L SUBSHELL IONISATION CROSS SECTIONS

FOR ALPHA IMPACT

ENERGY MeV	L1 (BARNS)	L2 (BARNS)	L3 (BARNS)	L1/L2	L1/L3	L2/L3	TOTAL BARNS
1.4	.862(11)	.336(9)	.976(8)	2.565(14)	.883(14)	.344(12)	2.17(4)
1.6	1.24	.472	1.73	2.627	.717	.273	3.44
1.8	1.51	.841	3.28	1.795	.460	.256	5.63
2.0	1.95	1.14	4.81	1.711	.405	.237	7.90
2.2	2.46	1.77	6.75	1.390	.364	.262	10.98
2.4	3.02	2.27	9.46	1.330	.319	.240	14.75
2.6	3.32(10)	2.95(8)	13.29(6)	1.125(13)	.250(12)	.222(10)	19.56
2.8	3.55	3.88	17.63	.915	.201	.220	25.06
2.9	3.74	4.31	19.88	.868	.188	.217	27.93

LEAD(Z2=82)

EXPERIMENTAL L SHELL X-RAY PRODUCTION CROSS SECTIONS

FOR ALPHA IMPACT

ENERGY	L	ALPHA	BETA	GAMMA	GAMMA1	GAMMA2	TOTAL
MeV				BARNS			
1.4	.0155(10)	.269 (6)	.177(7)	.0300(8)	.0186(10)	.0114(12)	.492 (4)
1.6	.0287	.462	.298	.0495	.0291	.0204	.839
1.8	.0426	.700	.435	.0711	.0414	.0297	1.25
2.0	.0609	1.02	.615	.0930	.0566	.0363	1.79
2.2	.0802(9)	1.44	.866	.126	.0784	.0473(11)	2.51
2.4	.106	1.89	1.12	.168	.109	.0586	3.29
2.6	.141	2.42	1.43	.210	.138	.0721	4.20
2.8	.170 (8)	3.01(5)	1.75 (6)	.261(7)	.177 (9)	.0840(10)	5.20
3.0	.200	3.79	2.12	.311	.213	.0984	6.42

ENERGY MeV	LA/LL	LA/LB	LA/LG	LB/LG
1.4	17.43(11)	1.521 (8)	8.98 (9)	5.903 (10)
1.6	16.09	1.550	9.34	6.023
1.8	16.42	1.609	9.85	6.119
2.0	16.81	1.665	11.01	6.613
2.2	17.92(10)	1.658	11.40	6.873
2.4	17.80	1.691	11.26	6.659
2.6	17.18	1.695	11.52	6.800
2.8	17.69(9)	1.722 (7)	11.55 (8)	6.706(9)
3.0	18.96	1.784	12.18	6.825

EXPERIMENTAL L SUBSHELL IONISATION CROSS SECTIONS

FOR ALPHA IMPACT

ENERGY	L1	L2	L3	L1/L2	L1/L3	L2/L3	TOTAL
MeV		BARNS					BARNS
1.4	.354(12)	.258(10)	.721(8)	1.372(16)	.491(14)	.358 (13)	1.33 (6)
1.6	.659	.389	1.21	1.694	.545	.321	2.26
1.8	.963	.550	1.86	1.751	.518	.296	3.37
2.0	1.15	.774	2.88	1.486	.399	.269	4.80
2.2	1.47 (11)	1.09	4.13	1.349(15)	.356	.264	6.69
2.4	1.76	1.55	5.53	1.135	.318	.280	8.84
2.6	2.15	1.96	7.14	1.097	.301	.275	11.25
2.8	2.42 (10)	2.56(9)	9.03 (6)	.945(13)	.268(13)	.283(11)	14.01 (5)
3.0	2.81	3.09	11.50	.909	.244	.269	17.40

BISMUTH(Z2=83)

EXPERIMENTAL L SHELL X-RAY PRODUCTION CROSS SECTIONS

FOR ALPHA IMPACT

ENERGY MeV	L	ALPHA	BETA	GAMMA	GAMMA1	GAMMA2	TOTAL
	BARNS						
1.4	.0136 (10)	.239 (6)	.156 (7)	.0230 (8)	.0121 (10)	.0110 (12)	.432 (4)
1.6	.0237	.386	.250	.0359	.0207	.0152	.696
1.8	.0382	.633	.413	.0576	.0345	.0230	1.14
2.0	.0519	.867	.531	.0786	.0488	.0298	1.53
2.2	.0715	1.22	.775	.110	.0706	.0395	2.17
2.4	.0902	1.57	.956	.140	.0917	.0485	2.75
2.6	.115 (8)	2.01 (5)	1.20 (6)	.176 (7)	.117 (9)	.0595 (11)	3.50
2.8	.148	2.58	1.49	.216	.147	.0685	4.43
3.0	.187	3.31	1.88	.270	.190	.0804	5.64

ENERGY MeV	LA/LL	LA/LB	LA/LG	LB/LG
1.4	17.51 (11)	1.527 (8)	10.39 (9)	6.802 (10)
1.6	16.30	1.544	10.76	6.966
1.8	16.58	1.534	11.00	7.169
2.0	16.70	1.632	11.03	6.759
2.2	17.03	1.571	11.07	7.045
2.4	17.36	1.639	11.19	6.825
2.6	17.42 (9)	1.678 (7)	11.41 (8)	6.804 (9)
2.8	17.39	1.731	11.92	6.888
3.0	17.71	1.759	12.24	6.962

EXPERIMENTAL L SUBSHELL IONISATION CROSS SECTIONS

FOR ALPHA IMPACT

ENERGY MeV	L1	L2	L3	L1/L2	L1/L3	L2/L3	TOTAL BARNS
		BARNS					
1.4	.350 (12)	.147 (10)	.602 (8)	2.381 (16)	.581 (14)	.244 (13)	1.10 (6)
1.6	.463	.268	1.03	1.728	.450	.260	1.76
1.8	.687	.456	1.73	1.507	.397	.264	2.87
2.0	.867	.656	2.41	1.322	.360	.272	3.93
2.2	1.12	.962	3.44	1.164	.326	.280	5.52
2.4	1.35	1.26	4.48	1.071	.301	.281	7.09
2.6	1.63 (11)	1.61 (9)	5.80 (7)	1.012 (14)	.281 (13)	.278 (11)	9.04 (5)
2.8	1.82	2.07	7.60	.879	.239	.272	11.49
3.0	2.04	2.69	9.92	.758	.206	.271	14.65

APPENDIX C

THEORETICAL L SHELL X-RAY PRODUCTION AND IONISATION CROSS SECTIONS

CONTENTS Page

Theoretical L shell x-ray production and ionisation cross sections are presented for each element in order of increasing atomic number. See page 452 for explanations.

C.1 PROTON IMPACT

DYSPROSIUM(Z2=66)

PWBA L SHELL X-RAY PRODUCTION CROSS SECTIONS

FOR PROTON IMPACT

ENERGY	L	ALPHA	BETA	GAMMA	GAMMA1	GAMMA2	TOTAL
MeV				BARNS			
1.0	.698	16.653	8.543	1.057	.931	.126	26.813
1.2	1.032	24.620	12.996	1.642	1.420	.223	40.080
1.4	1.410	33.634	18.397	2.392	1.997	.396	55.537
1.6	1.829	43.640	24.637	3.303	2.648	.656	73.076
1.8	2.279	54.380	31.842	4.373	3.374	.999	92.375
2.0	2.751	65.667	39.657	5.574	4.152	1.422	113.035
2.2	3.242	77.394	47.989	6.876	4.971	1.905	134.765
2.4	3.736	89.215	56.694	8.258	5.824	2.435	157.041
2.6	4.251	101.510	65.828	9.724	6.699	3.025	180.321
2.8	4.754	113.530	74.943	11.193	7.583	3.611	203.297
3.0	5.264	125.725	84.363	12.731	8.483	4.248	226.826

ENERGY	BETA1	BETA2	LA/LB	LA/LG	LB/LG
MeV	BARNS				
1.0	5.725	2.818	1.933	15.618	8.079
1.2	8.830	4.164	1.878	14.862	7.913
1.4	12.708	5.688	1.812	13.935	7.690
1.6	17.317	7.378	1.751	13.092	7.476
1.8	22.649	9.192	1.692	12.321	7.282
2.0	28.557	11.098	1.640	11.670	7.114
2.2	34.909	13.078	1.597	11.149	6.980
2.4	41.618	15.074	1.558	10.699	6.865
2.6	48.677	17.149	1.527	10.337	6.770
2.8	55.762	19.177	1.500	10.042	6.695
3.0	63.124	21.235	1.475	9.777	6.627

ECPSSR L SHELL X-RAY PRODUCTION CROSS SECTIONS

FOR PROTON IMPACT

ENERGY	L	ALPHA	BETA	GAMMA	GAMMA1	GAMMA2	TOTAL
MeV				BARNS			
1.0	.533	12.718	6.532	.811	.709	.102	20.489
1.2	.827	19.721	10.437	1.323	1.136	.187	32.140
1.4	1.171	27.924	15.293	1.994	1.653	.340	46.136
1.6	1.559	37.200	21.059	2.821	2.249	.572	62.306
1.8	1.983	47.331	27.722	3.812	2.929	.883	80.414
2.0	2.436	58.137	35.046	4.927	3.657	1.271	100.005
2.2	2.904	69.326	42.912	6.147	4.436	1.711	120.632
2.4	3.388	80.894	51.294	7.467	5.260	2.207	142.264
2.6	3.888	92.837	59.978	8.845	6.098	2.748	164.646
2.8	4.387	104.761	68.920	10.280	6.967	3.313	187.315
3.0	4.895	116.907	78.024	11.746	7.839	3.908	210.412

ENERGY	BETA1	BETA2	LA/LB	LA/LG	LB/LG
MeV	BARNS				
1.0	4.380	2.152	1.931	15.555	8.056
1.2	7.100	3.336	1.873	14.774	7.886
1.4	10.570	4.722	1.810	13.883	7.671
1.6	14.768	6.290	1.751	13.066	7.464
1.8	19.720	8.001	1.692	12.303	7.272
2.0	25.218	9.826	1.643	11.689	7.113
2.2	31.195	11.715	1.600	11.172	6.981
2.4	37.624	13.668	1.562	10.729	6.870
2.6	44.292	15.685	1.533	10.393	6.781
2.8	51.220	17.697	1.505	10.091	6.705
3.0	58.275	19.747	1.483	9.854	6.642

DYSPROSIUM(Z2=66)

L SUBSHELL IONISATION CROSS SECTIONS FOR PROTON IMPACT

L 1 SUBSHELL

ENERGY MeV	PWBA	PWBAR	PSS	PSSR	CPSS	CPSSR	ECPSS	ECPSSR
	BARNS							
1.00	6.51	7.83	5.45	6.42	4.59	5.41	4.46	5.26
1.20	11.54	14.54	8.95	11.33	7.86	9.94	7.68	9.72
1.40	20.66	25.98	15.88	20.12	14.32	18.14	14.04	17.79
1.60	34.43	42.35	26.89	33.29	24.71	30.59	24.29	30.07
1.80	52.67	62.97	42.08	50.74	39.20	47.27	38.61	46.56
2.00	75.18	87.52	60.94	72.37	57.36	68.12	56.60	67.21
2.20	100.92	115.66	83.37	96.68	79.11	91.74	78.15	90.63
2.40	129.12	145.85	109.28	123.92	104.37	118.35	103.21	117.04
2.50	160.60	178.10	136.26	153.52	130.82	147.39	129.48	145.89
2.80	191.82	211.65	166.51	184.27	160.55	177.68	159.03	176.00
3.00	225.83	245.98	196.64	216.59	190.29	209.59	188.61	207.74

L 2 SUBSHELL

ENERGY MeV	PWBA	PWBAR	PSS	PSSR	CPSS	CPSSR	ECPSS	ECPSSR
	BARNS							
1.00	33.60	37.69	27.22	30.91	23.19	26.33	22.48	25.53
1.20	50.93	56.21	42.43	47.12	37.56	41.72	36.62	40.67
1.40	70.79	77.15	60.16	65.82	54.62	59.77	53.46	58.49
1.60	92.54	99.86	79.95	86.51	73.89	79.95	72.51	78.46
1.80	116.26	124.40	101.51	109.44	95.03	102.46	93.46	100.77
2.00	141.10	150.23	124.70	133.20	117.88	125.92	116.14	124.06
2.20	166.83	176.72	149.20	158.31	142.12	150.80	140.22	148.78
2.40	193.39	203.65	174.41	184.47	167.13	176.77	165.08	174.61
2.60	220.17	231.32	200.13	210.54	192.72	202.74	190.54	200.46
2.80	247.32	258.62	226.59	237.55	219.07	229.67	216.78	227.27
3.00	274.53	286.57	252.92	264.27	245.35	256.36	242.95	253.86

L 3 SUBSHELL

ENERGY MeV	PWBA	PWBAR	PSS	PSSR	CPSS	CPSSR	ECPSS	ECPSSR
	BARNS							
1.00	109.30	120.56	89.43	99.23	77.30	85.76	75.17	83.40
1.20	160.74	174.90	134.67	147.01	120.56	131.61	117.81	128.62
1.40	217.75	234.60	186.22	201.06	170.60	184.19	167.29	180.62
1.60	279.87	298.75	243.47	260.47	226.66	242.49	222.84	238.40
1.80	345.33	366.02	304.90	323.76	287.19	304.95	282.90	300.40
2.00	413.02	434.98	369.03	389.94	350.68	370.55	345.98	365.59
2.20	482.58	505.76	434.81	457.36	416.04	437.62	410.99	432.31
2.40	551.84	576.81	502.71	526.08	483.65	506.13	478.28	500.51
2.60	623.30	648.56	571.19	596.50	551.97	576.43	546.32	570.53
2.80	692.85	719.72	640.59	666.02	621.29	645.95	615.39	639.83
3.00	762.69	789.25	709.55	736.54	690.27	716.52	684.17	710.19

TOTAL ECPSSR L SHELL IONISATION CROSS SECTIONS AND SUBSHELL RATIOS FOR PROTON IMPACT

ENERGY MeV	TOTAL BARNS	L1/L2	L1/L3	L2/L3
1.00	114.19	.206	.063	.306
1.20	179.01	.239	.076	.316
1.40	256.90	.304	.098	.324
1.60	346.93	.383	.126	.329
1.80	447.73	.462	.155	.335
2.00	556.86	.542	.184	.339
2.20	671.71	.609	.210	.344
2.40	792.15	.670	.234	.349
2.60	916.87	.728	.256	.351
2.80	1043.09	.774	.275	.355
3.00	1171.79	.818	.293	.357

YTTERBIUM(Z2=70)

PWBA L SHELL X-RAY PRODUCTION CROSS SECTIONS

FOR PROTON IMPACT

ENERGY MeV	L	ALPHA	BETA	GAMMA	GAMMA1	GAMMA2	TOTAL
	BARNS						
1.0	.482	10.967	5.474	.677	.587	.0894	17.515
1.2	.727	16.529	8.399	1.045	.918	.127	26.566
1.4	1.009	22.950	11.983	1.521	1.314	.206	37.272
1.6	1.321	30.054	16.216	2.112	1.773	.338	49.446
1.8	1.665	37.882	21.102	2.820	2.288	.530	63.136
2.0	2.032	46.254	26.531	3.631	2.844	.785	78.035
2.2	2.417	55.030	32.488	4.543	3.451	1.090	93.977
2.4	2.812	64.031	38.885	5.548	4.096	1.450	110.680
2.6	3.223	73.400	45.620	6.617	4.763	1.851	128.167
2.8	3.635	82.785	52.645	7.750	5.462	2.285	146.021
3.0	4.062	92.527	59.851	8.916	6.161	2.751	164.459

ENERGY MeV	BETA1	BETA2	LA/LB	LA/LG	LB/LG
	BARNS				
1.0	3.602	1.872	1.988	16.080	8.088
1.2	5.579	2.820	1.952	15.689	8.037
1.4	8.069	3.914	1.899	14.965	7.879
1.6	11.092	5.125	1.837	14.110	7.679
1.8	14.644	6.458	1.779	13.317	7.484
2.0	18.647	7.884	1.728	12.626	7.307
2.2	23.110	9.378	1.678	12.002	7.151
2.4	27.975	10.910	1.631	11.434	7.009
2.6	33.116	12.505	1.594	10.988	6.894
2.8	38.544	14.101	1.557	10.579	6.793
3.0	44.092	15.759	1.531	10.278	6.713

ECPSSR L SHELL X-RAY PRODUCTION CROSS SECTIONS

FOR PROTON IMPACT

ENERGY MeV	L	ALPHA	BETA	GAMMA	GAMMA1	GAMMA2	TOTAL
	BARNS						
1.0	.364	8.286	4.148	.514	.444	.0703	13.248
1.2	.578	13.150	6.719	.841	.732	.108	21.182
1.4	.832	18.933	9.952	1.271	1.088	.183	30.830
1.6	1.120	25.478	13.841	1.814	1.507	.307	42.034
1.8	1.444	32.862	18.384	2.469	1.982	.486	54.871
2.0	1.794	40.823	23.500	3.230	2.505	.724	68.984
2.2	2.160	49.186	29.167	4.096	3.085	1.009	84.162
2.4	2.544	57.934	35.276	5.049	3.698	1.349	100.266
2.6	2.944	67.050	41.754	6.071	4.342	1.726	117.189
2.8	3.347	76.243	48.537	7.159	5.017	2.138	134.557
3.0	3.765	85.752	55.519	8.282	5.699	2.579	152.489

ENERGY MeV	BETA1	BETA2	LA/LB	LA/LG	LB/LG
	BARNS				
1.0	2.734	1.414	1.982	15.981	8.062
1.2	4.476	2.243	1.941	15.513	7.992
1.4	6.723	3.229	1.887	14.767	7.827
1.6	9.497	4.344	1.825	13.921	7.628
1.8	12.782	5.602	1.772	13.191	7.445
2.0	16.542	6.958	1.722	12.524	7.274
2.2	20.785	8.382	1.671	11.898	7.120
2.4	25.405	9.871	1.627	11.367	6.986
2.6	30.331	11.423	1.591	10.940	6.877
2.8	35.550	12.987	1.556	10.549	6.780
3.0	40.913	14.606	1.530	10.254	6.704

YTTERBIUM(Z2=70)

L SUBSHELL IONISATION CROSS SECTIONS FOR PROTON IMPACT

L 1 SUBSHELL

ENERGY MeV	PWBA	PWBAR	PSS	PSSR	CPSS	CPSSR	ECPSS	ECPSSR
				BARNS				
1.00	3.68	4.19	3.33	3.70	2.70	3.00	2.62	2.90
1.20	5.19	6.43	4.33	5.35	3.69	4.56	3.59	4.44
1.40	8.48	11.06	6.71	8.79	5.91	7.74	5.77	7.57
1.60	14.01	18.24	10.94	14.42	9.86	13.00	9.67	12.75
1.80	22.13	28.13	17.46	22.56	16.01	20.68	15.73	20.32
2.00	32.87	40.61	26.27	33.21	24.39	30.83	24.01	30.36
2.20	45.77	55.74	37.40	45.89	35.07	43.03	34.57	42.43
2.40	61.01	72.33	50.60	60.87	47.82	57.53	47.20	56.79
2.60	78.02	91.05	65.53	77.43	62.33	73.65	61.59	72.77
2.80	96.40	110.73	82.37	95.42	78.76	91.25	77.90	90.25
3.00	116.17	131.97	99.97	114.58	96.02	110.05	95.03	108.92

L 2 SUBSHELL

ENERGY MeV	PWBA	PWBAR	PSS	PSSR	CPSS	CPSSR	ECPSS	ECPSSR
				BARNS				
1.00	16.68	19.47	13.46	15.90	11.05	13.05	10.66	12.59
1.20	26.19	29.82	21.62	24.94	18.61	21.46	18.07	20.84
1.40	37.30	41.77	31.44	35.52	27.92	31.54	27.22	30.76
1.60	49.83	55.05	42.63	47.52	38.68	43.13	37.84	42.19
1.80	63.53	69.38	55.01	60.61	50.72	55.88	49.75	54.81
2.00	77.96	84.81	68.38	74.58	63.80	69.59	62.71	68.39
2.20	93.48	100.83	82.91	89.82	78.09	84.59	76.87	83.27
2.40	109.66	117.62	97.98	105.53	92.96	100.13	91.64	98.70
2.60	126.18	134.72	113.88	121.80	108.70	116.26	107.27	114.73
2.80	143.38	152.11	129.99	138.66	124.69	133.00	123.17	131.38
3.00	160.31	169.70	146.65	155.45	141.25	149.73	139.65	148.03

L 3 SUBSHELL

ENERGY MeV	PWBA	PWBAR	PSS	PSSR	CPSS	CPSSR	ECPSS	ECPSSR
				BARNS				
1.00	60.14	68.29	48.88	55.98	40.94	46.88	39.64	45.40
1.20	90.58	100.99	75.46	84.54	65.96	73.89	64.23	71.96
1.40	125.20	137.33	106.26	117.32	95.52	105.46	93.39	103.10
1.60	162.85	177.22	140.46	153.30	128.74	140.51	126.24	137.78
1.80	203.70	219.61	178.61	193.03	166.07	179.47	163.21	176.39
2.00	246.76	263.99	218.40	234.97	205.26	220.83	202.09	217.42
2.20	291.30	309.87	260.39	278.16	246.77	263.61	243.32	259.92
2.40	336.29	356.26	304.06	322.61	290.07	307.77	286.37	303.84
2.60	382.80	403.28	348.22	368.51	334.00	353.45	330.07	349.29
2.80	428.85	450.84	393.42	414.10	379.03	398.95	374.90	394.60
3.00	476.58	498.59	438.98	461.12	424.49	445.90	420.18	441.37

TOTAL ECPSSR L SHELL IONISATION CROSS SECTIONS AND SUBSHELL RATIOS FOR PROTON IMPACT

ENERGY MeV	TOTAL BARNS	L1/L2	L1/L3	L2/L3
1.00	60.88	.231	.064	.277
1.20	97.23	.213	.062	.290
1.40	141.43	.246	.073	.298
1.60	192.72	.302	.093	.306
1.80	251.52	.371	.115	.311
2.00	316.17	.444	.140	.315
2.20	385.63	.510	.163	.320
2.40	459.33	.575	.187	.325
2.60	536.80	.634	.208	.328
2.80	616.23	.687	.229	.333
3.00	698.32	.736	.247	.335

TUNGSTEN(Z2=74)

PWBA L SHELL X-RAY PRODUCTION CROSS SECTIONS

FOR PROTON IMPACT

ENERGY MeV	L	ALPHA	BETA	GAMMA	GAMMA1	GAMMA2	TOTAL
				BARNS			
1.0	.336	7.231	3.562	.455	.365	.0899	11.533
1.2	.518	11.148	5.515	.698	.586	.112	17.797
1.4	.731	15.726	7.916	1.010	.857	.153	25.263
1.6	.970	20.883	10.769	1.400	1.173	.227	33.859
1.8	1.231	26.515	14.063	1.872	1.530	.341	43.468
2.0	1.518	32.704	17.825	2.430	1.927	.502	54.208
2.2	1.821	39.230	21.992	3.070	2.360	.710	65.784
2.4	2.138	46.080	26.554	3.792	2.824	.968	78.170
2.6	2.471	53.250	31.457	4.581	3.319	1.261	91.296
2.8	2.806	60.489	36.649	5.440	3.838	1.601	104.849
3.0	3.155	68.020	42.077	6.342	4.375	1.966	118.984

ENERGY MeV	BETA1	BETA2	LA/LB	LA/LG	LB/LG
	BARNS				
1.0	2.094	1.319	2.016	15.767	7.822
1.2	3.305	2.034	2.006	15.853	7.901
1.4	4.811	2.868	1.972	15.453	7.838
1.6	6.604	3.808	1.924	14.800	7.693
1.8	8.677	4.834	1.870	14.052	7.513
2.0	11.030	5.961	1.820	13.349	7.336
2.2	13.640	7.149	1.769	12.669	7.163
2.4	16.494	8.396	1.721	12.047	7.002
2.6	19.564	9.701	1.678	11.522	6.866
2.8	22.825	11.018	1.636	11.021	6.737
3.0	26.223	12.388	1.602	10.630	6.635

ECPSSR L SHELL X-RAY PRODUCTION CROSS SECTIONS

FOR PROTON IMPACT

ENERGY MeV	L	ALPHA	BETA	GAMMA	GAMMA1	GAMMA2	TOTAL
				BARNS			
1.0	.252	5.417	2.678	.343	.276	.0674	8.652
1.2	.410	8.827	4.395	.559	.467	.0920	14.125
1.4	.601	12.941	6.572	.846	.710	.136	20.860
1.6	.821	17.683	9.213	1.210	.999	.211	28.788
1.8	1.065	22.948	12.305	1.656	1.332	.324	37.789
2.0	1.339	28.848	15.883	2.187	1.706	.482	48.019
2.2	1.628	35.068	19.863	2.801	2.117	.684	59.065
2.4	1.935	41.692	24.255	3.495	2.563	.932	71.020
2.6	2.258	48.663	29.005	4.259	3.041	1.218	83.761
2.8	2.586	55.731	34.026	5.086	3.541	1.544	96.934
3.0	2.928	63.130	39.325	5.964	4.065	1.897	110.780

ENERGY MeV	BETA1	BETA2	LA/LB	LA/LG	LB/LG
	BARNS				
1.0	1.579	.988	2.008	15.678	7.807
1.2	2.639	1.610	1.994	15.664	7.857
1.4	3.999	2.360	1.954	15.183	7.770
1.6	5.651	3.224	1.904	14.498	7.614
1.8	7.589	4.183	1.850	13.748	7.432
2.0	9.816	5.258	1.801	13.079	7.261
2.2	12.305	6.390	1.751	12.416	7.092
2.4	15.046	7.596	1.704	11.827	6.940
2.6	18.015	8.865	1.663	11.327	6.811
2.8	21.160	10.151	1.623	10.862	6.691
3.0	24.473	11.498	1.591	10.491	6.594

TUNGSTEN(Z2=74)

L SUBSHELL IONISATION CROSS SECTIONS FOR PROTON IMPACT

L 1 SUBSHELL

ENERGY MeV	PWBA	PWBAR	PSS	PSSR	CPSS	CPSSR	ECPSS	ECPSSR
	BARNS							
1.00	2.46	2.67	2.31	2.47	1.79	1.91	1.72	1.84
1.20	2.92	3.40	2.63	3.03	2.17	2.49	2.10	2.42
1.40	3.93	5.03	3.34	4.24	2.86	3.63	2.79	3.54
1.60	5.94	8.03	4.80	6.51	4.23	5.74	4.13	5.61
1.80	9.18	12.45	7.36	10.03	6.62	9.02	6.49	8.84
2.00	13.85	18.45	11.09	14.97	10.13	13.68	9.95	13.43
2.20	19.97	26.04	16.21	21.31	14.99	19.70	14.75	19.38
2.40	27.61	34.86	22.55	29.09	21.05	27.16	20.74	26.76
2.60	36.37	45.28	30.23	38.01	28.45	35.77	28.06	35.28
2.80	46.56	56.42	39.07	48.20	37.00	45.64	36.53	45.06
3.00	57.51	68.99	48.99	59.19	46.64	56.35	46.09	55.68

L 2 SUBSHELL

ENERGY MeV	PWBA	PWBAR	PSS	PSSR	CPSS	CPSSR	ECPSS	ECPSSR
	BARNS							
1.00	8.20	10.07	6.61	8.21	5.19	6.45	4.98	6.19
1.20	13.33	15.82	10.95	13.19	9.12	10.98	8.81	10.61
1.40	19.55	22.65	16.34	19.23	14.14	16.63	13.73	16.15
1.60	26.66	30.39	22.66	26.13	20.12	23.20	19.62	22.62
1.80	34.54	38.93	29.78	33.78	26.96	30.59	26.36	29.91
2.00	43.11	48.09	37.65	42.14	34.60	38.72	33.91	37.95
2.20	52.27	57.69	46.05	51.11	42.80	47.50	42.02	46.64
2.40	61.93	68.05	55.02	60.61	51.59	56.84	50.74	55.90
2.60	72.12	78.54	64.58	70.65	61.00	66.74	60.07	65.73
2.80	82.62	89.61	74.44	80.98	70.75	76.96	69.75	75.87
3.00	93.43	100.68	84.78	91.69	80.98	87.58	79.92	86.43

L 3 SUBSHELL

ENERGY MeV	PWBA	PWBAR	PSS	PSSR	CPSS	CPSSR	ECPSS	ECPSSR
	BARNS							
1.00	33.19	39.09	26.84	31.93	21.68	25.80	20.89	24.86
1.20	51.33	58.96	42.55	49.22	36.18	41.86	35.09	40.60
1.40	72.35	81.60	61.08	69.35	53.72	60.99	52.35	59.43
1.60	95.74	106.44	82.15	91.87	73.96	82.71	72:32	80.88
1.80	120.94	133.19	105.23	116.26	96.38	106.48	94.49	104.39
2.00	148.30	161.68	130.30	143.11	120.90	132.79	118.77	130.45
2.20	176.76	191.60	156.97	170.83	147.12	160.11	144.77	157.55
2.40	206.25	222.19	185.15	199.87	174.93	188.84	172.38	186.08
2.60	236.87	253.32	213.85	230.10	203.35	218.80	200.62	215.86
2.80	267.33	285.15	243.56	260.21	232.85	248.77	229.95	245.67
3.00	298.93	316.98	273.63	291.60	262.77	280.02	259.71	276.77

TOTAL ECPSSR L SHELL IONISATION CROSS SECTIONS AND SUBSHELL RATIOS FOR PROTON IMPACT

ENERGY MeV	TOTAL BARNS	L1/L2	L1/L3	L2/L3
1.00	32.88	.298	.074	.249
1.20	53.63	.228	.060	.261
1.40	79.12	.219	.059	.272
1.60	109.11	.248	.069	.280
1.80	143.14	.296	.085	.287
2.00	181.83	.354	.103	.291
2.20	223.57	.416	.123	.296
2.40	268.74	.479	.144	.300
2.60	316.87	.537	.163	.304
2.80	366.60	.594	.183	.309
3.00	418.88	.644	.201	.312

GOLD(Z2=79)

PWBA L SHELL X-RAY PRODUCTION CROSS SECTIONS

FOR PROTON IMPACT

ENERGY MeV	L	ALPHA	BETA	GAMMA	GAMMA1	GAMMA2	TOTAL
				BARNS			
1.0	.220	4.364	2.027	.252	.195	.0574	6.862
1.2	.345	6.863	3.210	.397	.322	.0741	10.815
1.4	.496	9.865	4.670	.579	.484	.0954	15.610
1.6	.669	13.308	6.404	.803	.677	.126	21.185
1.8	.864	17.169	8.410	1.071	.901	.169	27.513
2.0	1.079	21.444	10.694	1.384	1.155	.229	34.601
2.2	1.306	25.953	13.183	1.736	1.430	.305	42.177
2.4	1.555	30.904	15.953	2.134	1.731	.402	50.546
2.6	1.817	36.113	18.953	2.576	2.056	.519	59.459
2.8	2.091	41.569	22.127	3.050	2.394	.655	68.837
3.0	2.378	47.269	25.529	3.568	2.757	.810	78.744

ENERGY MeV	LA/LB	LA/LG	LB/LG
1.0	2.153	17.308	8.038
1.2	2.138	17.304	8.092
1.4	2.112	17.031	8.062
1.6	2.078	16.566	7.972
1.8	2.042	16.037	7.855
2.0	2.005	15.495	7.727
2.2	1.969	14.951	7.594
2.4	1.937	14.480	7.475
2.6	1.905	14.017	7.356
2.8	1.879	13.628	7.254
3.0	1.852	13.247	7.155

ECPSSR L SHELL X-RAY PRODUCTION CROSS SECTIONS

FOR PROTON IMPACT

ENERGY MeV	L	ALPHA	BETA	GAMMA	GAMMA1	GAMMA2	TOTAL
				BARNS			
1.0	.163	3.244	1.513	.189	.147	.0415	5.109
1.2	.273	5.425	2.554	.317	.259	.0582	8.568
1.4	.409	8.127	3.882	.485	.404	.0805	12.903
1.6	.569	11.302	5.490	.695	.583	.112	18.056
1.8	.751	14.926	7.387	.950	.793	.157	24.013
2.0	.953	18.952	9.560	1.252	1.032	.219	30.718
2.2	1.173	23.321	11.978	1.596	1.296	.299	38.068
2.4	1.416	28.145	14.676	1.985	1.586	.398	46.222
2.6	1.671	33.219	17.604	2.418	1.901	.516	54.912
2.8	1.940	38.574	20.726	2.886	2.231	.654	64.127
3.0	2.222	44.168	24.073	3.397	2.588	.807	73.860

ENERGY MeV	LA/LB	LA/LG	LB/LG
1.0	2.144	17.201	8.025
1.2	2.124	17.109	8.054
1.4	2.094	16.748	7.999
1.6	2.059	16.262	7.900
1.8	2.021	15.706	7.773
2.0	1.982	15.136	7.636
2.2	1.947	14.612	7.505
2.4	1.918	14.177	7.393
2.6	1.887	13.735	7.279
2.8	1.861	13.364	7.180
3.0	1.835	13.003	7.087

GOLD(Z2=79)

L SUBSHELL IONISATION CROSS SECTIONS FOR PROTON IMPACT

L 1 SUBSHELL

ENERGY MeV	PWBA	PWBAR	PSS	PSSR	CPSS	CPSSR	ECPSS	ECPSSR
				BARNS				
1.00	1.61	1.74	1.50	1.64	1.09	1.19	1.04	1.14
1.20	1.79	1.96	1.69	1.83	1.32	1.43	1.27	1.38
1.40	2.02	2.41	1.88	2.16	1.54	1.78	1.50	1.72
1.60	2.50	3.27	2.23	2.79	1.90	2.38	1.85	2.31
1.80	3.39	4.75	2.87	3.93	2.51	3.43	2.45	3.35
2.00	4.86	6.93	3.98	5.70	3.55	5.08	3.48	4.98
2.20	6.95	9.89	5.68	8.14	5.14	7.38	5.04	7.23
2.40	9.78	13.68	7.99	11.32	7.33	10.38	7.20	10.20
2.60	13.37	18.23	10.98	15.22	10.17	14.10	10.00	13.87
2.80	17.65	23.51	14.65	19.90	13.68	18.58	13.47	18.30
3.00	22.67	29.49	19.02	25.11	17.87	23.60	17.62	23.27

L 2 SUBSHELL

ENERGY MeV	PWBA	PWBAR	PSS	PSSR	CPSS	CPSSR	ECPSS	ECPSSR
				BARNS				
1.00	3.35	4.44	2.68	3.62	1.98	2.67	1.88	2.54
1.20	5.67	7.22	4.66	6.00	3.70	4.76	3.55	4.56
1.40	8.60	10.61	7.19	8.95	5.98	7.45	5.78	7.19
1.60	12.09	14.58	10.25	12.44	8.82	10.70	8.56	10.38
1.80	16.08	18.98	13.80	16.41	12.16	14.47	11.84	14.09
2.00	20.53	23.80	17.76	20.83	15.95	18.71	15.57	18.26
2.20	25.29	29.05	22.12	25.58	20.16	23.31	19.72	22.80
2.40	30.43	34.56	26.87	30.67	24.76	28.27	24.28	27.71
2.60	35.89	40.33	31.85	36.11	29.63	33.59	29.09	32.98
2.80	41.51	46.40	37.19	41.69	34.86	39.08	34.28	38.42
3.00	47.47	52.74	42.71	47.68	40.30	44.99	39.67	44.28

L 3 SUBSHELL

ENERGY MeV	PWBA	PWBAR	PSS	PSSR	CPSS	CPSSR	ECPSS	ECPSSR
				BARNS				
1.00	16.03	19.91	12.89	16.27	9.89	12.48	9.46	11.94
1.20	25.57	30.84	21.10	25.64	17.24	20.96	16.63	20.22
1.40	37.00	43.51	31.11	36.83	26.52	31.38	25.72	30.44
1.60	49.98	57.69	42.72	49.53	37.48	43.46	36.51	42.33
1.80	64.33	73.09	55.59	63.59	49.83	57.00	48.68	55.69
2.00	79.95	89.49	69.66	78.77	63.45	71.75	62.14	70.27
2.20	96.12	107.28	84.74	94.82	78.16	87.46	76.70	85.82
2.40	113.59	125.37	101.06	112.20	94.15	104.53	92.54	102.74
2.60	131.63	144.45	118.01	130.05	110.83	122.15	109.09	120.22
2.80	150.25	163.78	135.82	148.53	128.41	140.43	126.54	138.38
3.00	169.39	183.61	153.87	167.55	146.29	159.30	144.31	157.14

TOTAL ECPSSR L SHELL IONISATION CROSS SECTIONS AND SUBSHELL RATIOS

FOR PROTON IMPACT

ENERGY MeV	TOTAL BARNS	L1/L2	L1/L3	L2/L3
1.00	15.62	.448	.095	.212
1.20	26.16	.302	.068	.226
1.40	39.36	.239	.057	.236
1.60	55.02	.223	.055	.245
1.80	73.12	.238	.060	.253
2.00	93.51	.272	.071	.260
2.20	115.86	.317	.084	.266
2.40	140.65	.368	.099	.270
2.60	167.08	.420	.115	.274
2.80	195.10	.476	.132	.278
3.00	224.69	.526	.148	.282

LEAD(Z2=82)

PWBA L SHELL X-RAY PRODUCTION CROSS SECTIONS

FOR PROTON IMPACT

ENERGY MeV	L	ALPHA	BETA	GAMMA	GAMMA1	GAMMA2	TOTAL
				BARNS			
1.0	.167	3.164	1.438	.177	.129	.0476	4.946
1.2	.267	5.064	2.316	.283	.219	.0634	7.930
1.4	.388	7.370	3.407	.416	.335	.0814	11.582
1.6	.529	10.031	4.703	.580	.476	.104	15.843
1.8	.687	13.027	6.207	.776	.641	.135	20.696
2.0	.861	16.345	7.915	1.005	.830	.175	26.126
2.2	1.053	19.981	9.823	1.266	1.039	.228	32.123
2.4	1.254	23.789	11.888	1.558	1.265	.293	38.489
2.6	1.475	27.987	14.185	1.887	1.514	.374	45.535
2.8	1.704	32.322	16.607	2.242	1.774	.469	52.875
3.0	1.948	36.953	19.241	2.634	2.056	.579	60.776

ENERGY MeV	LA/LB	LA/LG	LB/LG
1.0	2.200	17.907	8.138
1.2	2.186	17.920	8.197
1.4	2.163	17.696	8.181
1.6	2.133	17.291	8.108
1.8	2.099	16.786	7.998
2.0	2.065	16.265	7.876
2.2	2.034	15.780	7.758
2.4	2.001	15.267	7.629
2.6	1.973	14.828	7.516
2.8	1.946	14.417	7.408
3.0	1.920	14.029	7.305

ECPSSR L SHELL X-RAY PRODUCTION CROSS SECTIONS

FOR PROTON IMPACT

ENERGY MeV	L	ALPHA	BETA	GAMMA	GAMMA1	GAMMA2	TOTAL
				BARNS			
1.0	.124	2.353	1.075	.132	.0983	.0341	3.685
1.2	.211	4.010	1.850	.227	.178	.0490	6.298
1.4	.321	6.091	2.846	.351	.284	.0673	9.609
1.6	.451	8.555	4.058	.506	.415	.0917	13.571
1.8	.599	11.366	5.480	.694	.570	.124	18.139
2.0	.766	14.524	7.120	.916	.749	.167	23.325
2.2	.949	18.009	8.980	1.176	.952	.224	29.113
2.4	1.146	21.750	11.011	1.464	1.171	.294	35.372
2.6	1.364	25.870	13.270	1.790	1.412	.378	42.293
2.8	1.589	30.153	15.675	2.145	1.668	.477	49.562
3.0	1.830	34.712	18.265	2.531	1.942	.590	57.338

ENERGY MeV	LA/LB	LA/LG	LB/LG
1.0	2.189	17.779	8.123
1.2	2.168	17.664	8.148
1.4	2.141	17.352	8.106
1.6	2.108	16.892	8.013
1.8	2.074	16.381	7.898
2.0	2.040	15.858	7,773
2.2	2.005	15.319	7.639
2.4	1.975	14.852	7.518
2.6	1.950	14.453	7.413
2.8	1.924	14.060	7.309
3.0	1.900	13.713	7.216

LEAD(Z2=82)

L SUBSHELL IONISATION CROSS SECTIONS FOR PROTON IMPACT

L 1 SUBSHELL

ENERGY MeV	PWBA	PWBAR	PSS	PSSR	CPSS	CPSSR	ECPSS	ECPSSR
				BARNS				
1.00	1.23	1.38	1.13	1.30	.782	.895	.743	.850
1.20	1.40	1.52	1.32	1.44	.995	1.08	.955	1.04
1.40	1.53	1.71	1.45	1.60	1.16	1.28	1.12	1.23
1.60	1.71	2.11	1.60	1.90	1.33	1.59	1.29	1.54
1.80	2.10	2.83	1.88	2.43	1.62	2.09	1.57	2.03
2.00	2.76	3.97	2.35	3.29	2.07	2.88	2.02	2.82
2.20	3.78	5.56	3.13	4.65	2.80	4.15	2.74	4.06
2.40	5.23	7.72	4.34	6.43	3.93	5.82	3.85	5.71
2.60	7.16	10.45	5.92	8.69	5.42	7.96	5.32	7.82
2.80	9.59	13.62	7.94	11.49	7.34	10.62	7.22	10.44
3.00	12.51	17.46	10.49	14.73	9.77	13.72	9.62	13.51

L 2 SUBSHELL

ENERGY MeV	PWBA	PWBAR	PSS	PSSR	CPSS	CPSSR	ECPSS	ECPSSR
				BARNS				
1.00	1.93	2.71	1.55	2.22	1.09	1.56	1.03	1.48
1.20	3.36	4.49	2.75	3.74	2.11	2.87	2.01	2.74
1.40	5.21	6.71	4.34	5.68	3.51	4.60	3.38	4.42
1.60	7.46	9.33	6.30	7.98	5.30	6.71	5.13	6.49
1.80	10.07	12.34	8.62	10.63	7.46	9.20	7.24	8.93
2.00	13.02	15.61	11.24	13.61	9.94	12.04	9.68	11.72
2.20	16.26	19.19	14.16	16.91	12.72	15.20	12.42	14.83
2.40	19.73	23.05	17.37	20.38	15.82	18.56	15.48	18.16
2.60	23.50	27.07	20.77	24.17	19.12	22.24	18.73	21.79
2.80	27.39	31.37	24.44	28.09	22.69	26.08	22.27	25.59
3.00	31.58	35.71	28.26	32.24	26.43	30.15	25.97	29.63

L 3 SUBSHELL

ENERGY MeV	PWBA	PWBAR	PSS	PSSR	CPSS	CPSSR	ECPSS	ECPSSR
				BARNS				
1.00	10.35	13.41	8.36	10.95	6.19	8.11	5.89	7.73
1.20	16.87	20.99	13.87	17.51	11.03	13.93	10.60	13.39
1.40	24.82	29.98	20.74	25.44	17.30	21.22	16.73	20.52
1.60	33.96	40.16	28.85	34.51	24.87	29.75	24.16	28.90
1.80	44.13	51.40	38.03	44.57	33.59	39.37	32.74	38.37
2.00	55.25	63.41	48.14	55.57	43.30	49.99	42.32	48.86
2.20	67.26	76.06	58.98	67.37	53.81	61.47	52.71	60.21
2.40	79.60	89.66	70.56	79.74	65.11	73.59	63.89	72.21
2.60	93.01	103.60	82.96	93.15	77.26	86.75	75.93	85.25
2.80	106.60	118.31	95.95	106.73	90.04	100.15	88.60	98.55
3.00	120.92	132.94	109.34	120.98	103.25	114.24	101.71	112.54

TOTAL ECPSSR L SHELL IONISATION CROSS SECTIONS AND SUBSHELL RATIOS FOR PROTON IMPACT

ENERGY MeV	TOTAL BARNS	L1/L2	L1/L3	L2/L3
1.00	10.05	.576	.110	.191
1.20	17.17	.380	.078	.205
1.40	26.18	.279	.060	.215
1.60	36.93	.237	.053	.225
1.80	49.34	.228	.053	.233
2.00	63.40	.240	.058	.240
2.20	79.11	.274	.067	.246
2.40	96.07	.314	.079	.251
2.60	114.86	.359	.092	.256
2.80	134.59	.408	.106	.260
3.00	155.67	.456	.120	.263

BISMUTH(Z2=83)

PWBA L SHELL X-RAY PRODUCTION CROSS SECTIONS

FOR PROTON IMPACT

ENERGY	L	ALPHA	BETA	GAMMA	GAMMA1	GAMMA2	TOTAL
MeV				BARNS			
1.0	.152	2.834	1.281	.157	.112	.0448	4.422
1.2	.244	4.556	2.077	.253	.192	.0606	7.130
1.4	.356	6.656	3.065	.374	.296	.0778	10.450
1.6	.487	9.098	4.246	.522	.423	.0991	14.353
1.8	.634	11.853	5.617	.700	.573	.127	18.804
2.0	.798	14.913	7.173	.906	.743	.163	23.790
2.2	.974	18.212	8.893	1.141	.932	.209	29.220
2.4	1.164	21.754	10.800	1.410	1.140	.269	35.127
2.6	1.369	25.587	12.874	1.705	1.364	.341	41.535
2.8	1.585	29.618	15.110	2.031	1.605	.426	48.344
3.0	1.813	33.882	17.504	2.386	1.859	.526	55.584

ENERGY MeV	LA/LB	LA/LG	LB/LG
1.0	2.213	18.080	8.170
1.2	2.194	18.007	8.209
1.4	2.172	17.805	8.198
1.6	2.143	17.423	8.131
1.8	2.110	16.937	8.026
2.0	2.079	16.456	7.915
2.2	2.048	15.964	7.796
2.4	2.014	15.433	7.662
2.6	1.988	15.009	7.551
2.8	1.960	14.583	7.440
3.0	1.936	14.202	7.337

ECPSSR L SHELL X-RAY PRODUCTION CROSS SECTIONS

FOR PROTON IMPACT

ENERGY	L	ALPHA	BETA	GAMMA	GAMMA1	GAMMA2	TOTAL
MeV				BARNS			
1.0	.113	2.105	.958	.118	.0854	.0322	3.293
1.2	.193	3.609	1.660	.204	.157	.0467	5.666
1.4	.295	5.507	2.564	.316	.252	.0641	8.682
1.6	.415	7.764	3.666	.456	.370	.0865	12.302
1.8	.554	10.352	4.965	.626	.511	.116	16.497
2.0	.710	13.275	6.476	.831	.675	.156	21.292
2.2	.882	16.479	8.161	1.064	.857	.207	26.585
2.4	1.065	19.911	10.019	1.328	1.059	.269	32.323
2.6	1.269	23.710	12.089	1.626	1.279	.346	38.694
2.8	1.480	27.673	14.297	1.950	1.514	.436	45.400
3.0	1.706	31.896	16.681	2.306	1.766	.540	52.589

ENERGY MeV	LA/LB	LA/LG	LB/LG
1.0	2.198	17.895	8.142
1.2	2.174	17.730	8.156
1.4	2.148	17.442	8.120
1.6	2.118	17.019	8.036
1.8	2.085	16.529	7.927
2.0	2.050	15.978	7.794
2.2	2.019	15.490	7.671
2.4	1.987	14.995	7.545
2.6	1.961	14.585	7.436
2.8	1.936	14.189	7.331
3.0	1.912	13.833	7.234

BISMUTH(Z2=83)

L SUBSHELL IONISATION CROSS SECTIONS FOR PROTON IMPACT

L 1 SUBSHELL

ENERGY MeV	PWBA	PWBAR	PSS	PSSR	CPSS	CPSSR	ECPSS	ECPSSR
				BARNS				
1.00	1.11	1.27	1.03	1.20	.699	.813	.663	.771
1.20	1.29	1.41	1.21	1.33	.903	.991	.865	.950
1.40	1.41	1.57	1.33	1.47	1.06	1.16	1.02	1.12
1.60	1.56	1.88	1.46	1.70	1.20	1.40	1.17	1.36
1.80	1.85	2.43	1.66	2.09	1.42	1.78	1.38	1.73
2.00	2.33	3.32	2.02	2.81	1.76	2.45	1.72	2.39
2.20	3.09	4.63	2.64	3.89	2.35	3.45	2.30	3.38
2.40	4.28	6.39	3.56	5.32	3.21	4.79	3.14	4.69
2.60	5.83	8.62	4.82	7.22	4.40	6.58	4.31	6.46
2.80	7.80	11.34	6.48	9.55	5.96	8.79	5.86	8.64
3.00	10.25	14.51	8.52	12.30	7.91	11.42	7.78	11.24

L 2 SUBSHELL

ENERGY MeV	PWBA	PWBAR	PSS	PSSR	CPSS	CPSSR	ECPSS	ECPSSR
				BARNS				
1.00	1.60	2.30	1.29	1.88	.892	1.31	.841	1.23
1.20	2.82	3.84	2.31	3.19	1.75	2.42	1.66	2.31
1.40	4.40	5.77	3.67	4.87	2.95	3.90	2.83	3.75
1.60	6.34	8.05	5.36	6.87	4.48	5.74	4.32	5.54
1.80	8.61	10.66	7.35	9.20	6.32	7.91	6.12	7.67
2.00	11.18	13.56	9.63	11.84	8.47	10.41	8.24	10.13
2.20	14.00	16.74	12.21	14.70	10.92	13.15	10.65	12.82
2.40	17.08	20.11	15.00	17.80	13.60	16.14	13.29	15.78
2.60	20.35	23.72	18.00	21.14	16.50	19.38	16.16	18.98
2.80	23.84	27.48	21.24	24.63	19.65	22.79	19.27	22.35
3.00	27.49	31.41	24.61	28.33	22.95	26.41	22.54	25.94

L 3 SUBSHELL

ENERGY MeV	PWBA	PWBAR	PSS	PSSR	CPSS	CPSSR	ECPSS	ECPSSR
				BARNS				
1.00	8.97	11.79	7.21	9.62	5.27	7.03	5.02	6.69
1.20	14.69	18.53	12.10	15.43	9.53	12.15	9.15	11.67
1.40	21.71	26.57	18.17	22.48	15.05	18.61	14.54	17.98
1.60	29.86	35.71	25.39	30.60	21.76	26.22	21.12	25.45
1.80	38.97	45.76	33.57	39.66	29.50	34.85	28.73	33.95
2.00	48.99	56.56	42.54	49.61	38.10	44.43	37.21	43.40
2.20	59.64	68.05	52.33	60.25	47.56	54.76	46.56	53.60
2.40	70.85	80.21	62.89	71.37	57.84	65.64	56.72	64.37
2.60	82.83	92.96	73.84	83.45	68.56	77.48	67.34	76.11
2.80	95.22	106.11	85.71	95.77	80.21	89.63	78.89	88.15
3.00	108.11	119.63	97.66	108.70	92.00	102.39	90.59	100.82

TOTAL ECPSSR L SHELL IONISATION CROSS SECTIONS AND SUBSHELL RATIOS FOR PROTON IMPACT

ENERGY MeV	TOTAL BARNS	L1/L2	L1/L3	L2/L3
1.00	8.69	.626	.115	.184
1.20	14.93	.412	.081	.198
1.40	22.85	.298	.062	.208
1.60	32.35	.245	.053	.218
1.80	43.35	.226	.051	.226
2.00	55.91	.236	.055	.233
2.20	69.80	.263	.063	.239
2.40	84.84	.298	.073	.245
2.60	101.54	.340	.085	.249
2.80	119.14	.387	.098	.254
3.00	138.00	.433	.111	.257

THORIUM(Z2=90)

PWBA L SHELL X-RAY PRODUCTION CROSS SECTIONS

FOR PROTON IMPACT

ENERGY MeV	L	ALPHA	BETA	GAMMA	GAMMA1	GAMMA2	TOTAL
				BARNS			
1.0	.0767	1.284	.562	.0639	.0402	.0236	1.986
1.2	.129	2.165	.947	.107	.0729	.0346	3.348
1.4	.195	3.274	1.439	.164	.117	.0465	5.070
1.6	.274	4.593	2.035	.234	.174	.0597	7.131
1.8	.364	6.103	2.732	.319	.244	.0747	9.511
2.0	.465	7.794	3.533	.419	.326	.0926	12.201
2.2	.576	9.656	4.422	.531	.418	.113	15.170
2.4	.697	11.686	5.422	.662	.523	.139	18.446
2.6	.825	13.839	6.501	.806	.637	.169	21.944
2.8	.964	16.164	7.686	.967	.762	.204	25.747
3.0	1.107	18.566	8.949	1.144	.897	.247	29.725

ENERGY MeV	BETA1	BETA2	LA/LB	LA/LG	LB/LG
	BARNS				
1.0	.250	.312	2.257	20.028	8.874
1.2	.433	.514	2.256	20.062	8.892
1.4	.674	.765	2.247	19.895	8.855
1.6	.976	1.059	2.228	19.526	8.764
1.8	1.339	1.394	2.205	19.057	8.644
2.0	1.764	1.769	2.177	18.514	8.505
2.2	2.238	2.184	2.155	18.091	8.395
2.4	2.782	2.640	2.127	17.555	8.255
2.6	3.373	3.128	2.100	17.076	8.130
2.8	4.026	3.660	2.075	16.621	8.010
3.0	4.731	4.218	2.047	16.130	7.881

ECPSSR L SHELL X-RAY PRODUCTION CROSS SECTIONS

FOR PROTON IMPACT

ENERGY MeV	L	ALPHA	BETA	GAMMA	GAMMA1	GAMMA2	TOTAL
				BARNS			
1.0	.0576	.965	.427	.0492	.0319	.0172	1.498
1.2	.104	1.741	.773	.0892	.0623	.0270	2.706
1.4	.164	2.749	1.228	.143	.105	.0381	4.281
1.6	.238	3.981	1.795	.212	.160	.0513	6.220
1.8	.324	5.435	2.476	.295	.228	.0671	8.523
2.0	.422	7.066	3.258	.395	.309	.0861	11.128
2.2	.529	8.876	4.151	.512	.402	.110	14.052
2.4	.649	10.886	5.150	.644	.505	.139	17.308
2.6	.776	13.017	6.249	.795	.622	.173	20.810
2.8	.913	15.319	7.446	.961	.747	.214	24.605
3.0	1.058	17.746	8.743	1.146	.884	.262	28.651

ENERGY MeV	BETA1	BETA2	LA/LB	LA/LG	LB/LG
	BARNS				
1.0	.194	.233	2.233	19.536	8.749
1.2	.362	.411	2.226	19.425	8.729
1.4	.590	.638	2.210	19.137	8.659
1.6	.882	.913	2.189	18.725	8.556
1.8	1.238	1.238	2.166	18.297	8.447
2.0	1.655	1.603	2.140	17.804	8.319
2.2	2.139	2.012	2.110	17.243	8.173
2.4	2.680	2.470	2.086	16.810	8.059
2.6	3.289	2.960	2.055	16.271	7.917
2.8	3.949	3.497	2.030	15.839	7.803
3.0	4.673	4.070	2.002	15.384	7.683

THORIUM(Z2=90)

L SUBSHELL IONISATION CROSS SECTIONS FOR PROTON IMPACT

L 1 SUBSHELL

ENERGY MeV	PWBA	PWBAR	PSS	PSSR	CPSS	CPSSR	ECPSS	ECPSSR
				BARNS				
1.00	.527	.715	.476	.663	.283	.394	.264	.368
1.20	.685	.830	.629	.786	.423	.528	.401	.500
1.40	.802	.907	.750	.866	.547	.632	.522	.603
1.60	.882	.971	.835	.930	.645	.719	.620	.691
1.80	.944	1.08	.898	1.01	.723	.816	.698	.788
2.00	1.02	1.25	.954	1.14	.794	.946	.763	.917
2.20	1.12	1.49	1.05	1.35	.895	1.15	.870	1.12
2.40	1.32	1.91	1.19	1.67	1.04	1.45	1.01	1.42
2.60	1.59	2.47	1.40	2.12	1.24	1.87	1.21	1.83
2.80	1.99	3.22	1.73	2.76	1.55	2.47	1.51	2.41
3.00	2.55	4.15	2.16	3.54	1.95	3.20	1.91	3.14

L 2 SUBSHELL

ENERGY MeV	PWBA	PWBAR	PSS	PSSR	CPSS	CPSSR	ECPSS	ECPSSR
				BARNS				
1.00	.430	.739	.346	.612	.211	.373	.196	.346
1.20	.803	1.28	.660	1.08	.453	.738	.426	.694
1.40	1.32	1.99	1.10	1.69	.816	1.25	.775	1.19
1.60	1.99	2.87	1.68	2.46	1.31	1.92	1.26	1.84
1.80	2.81	3.91	2.39	3.37	1.95	2.74	1.87	2.64
2.00	3.78	5.07	3.24	4.42	2.72	3.71	2.62	3.58
2.20	4.86	6.38	4.21	5.61	3.62	4.82	3.51	4.67
2.40	6.09	7.83	5.31	6.90	4.65	6.04	4.52	5.87
2.60	7.42	9.37	6.52	8.34	5.79	7.41	5.64	7.22
2.80	8.87	11.04	7.85	9.85	7.07	8.86	6.90	8.65
3.00	10.42	12.77	9.26	11.48	8.42	10.44	8.23	10.21

L 3 SUBSHELL

ENERGY MeV	PWBA	PWBAR	PSS	PSSR	CPSS	CPSSR	ECPSS	ECPSSR
				BARNS				
1.00	3.31	4.90	2.65	4.02	1.76	2.66	1.65	2.50
1.20	5.69	7.93	4.65	6.61	3.40	4.83	3.24	4.60
1.40	8.73	11.63	7.25	9.84	5.66	7.68	5.42	7.36
1.60	12.37	15.96	10.42	13.67	8.50	11.16	8.20	10.75
1.80	16.55	20.82	14.13	18.05	11.92	15.23	11.54	14.75
2.00	21.22	26.17	18.35	22.87	15.88	19.79	15.42	19.22
2.20	26.35	31.94	23.00	28.10	20.28	24.78	19.76	24.14
2.40	31.88	38.03	28.00	33.79	25.08	30.27	24.49	29.56
2.60	37.71	44.55	33.47	39.71	30.35	36.02	29.70	35.24
2.80	43.94	51.15	39.12	45.98	35.85	42.14	35.13	41.30
3.00	50.28	58.22	45.15	52.48	41.74	48.51	40.96	47.61

TOTAL ECPSSR L SHELL IONISATION CROSS SECTIONS AND SUBSHELL RATIOS FOR PROTON IMPACT

ENERGY MeV	TOTAL BARNS	L1/L2	L1/L3	L2/L3
1.00	3.22	1.063	.147	.138
1.20	5.79	.721	.109	.151
1.40	9.15	.507	.082	.162
1.60	13.29	.375	.064	.171
1.80	18.17	.299	.053	.179
2.00	23.72	.256	.048	.186
2.20	29.94	.240	.046	.193
2.40	36.85	.241	.048	.199
2.60	44.28	.253	.052	.205
2.80	52.36	.279	.058	.209
3.00	60.95	.307	.066	.214

URANIUM(Z2=92)

PWBA L SHELL X-RAY PRODUCTION CROSS SECTIONS

FOR PROTON IMPACT

ENERGY	L	ALPHA	BETA	GAMMA	GAMMA1	GAMMA2	TOTAL
MeV				BARNS			
1.0	.0637	1.032	.436	.0465	.0273	.0192	1.579
1.2	.109	1.762	.743	.0787	.0504	.0283	2.694
1.4	.166	2.693	1.138	.121	.0824	.0384	4.119
1.6	.235	3.808	1.619	.173	.124	.0493	5.836
1.8	.315	5.098	2.180	.236	.175	.0611	7.828
2.0	.405	6.564	2.830	.310	.235	.0746	10.106
2.2	.504	8.170	3.561	.396	.305	.0907	12.627
2.4	.611	9.902	4.361	.493	.383	.109	15.360
2.6	.728	11.804	5.251	.602	.470	.132	18.376
2.8	.850	13.776	6.201	.723	.565	.158	21.537
3.0	.982	15.928	7.247	.858	.668	.190	24.998

ENERGY	BETA1	BETA2	LA/LB	LA/LG	LB/LG
MeV	BARNS				
1.0	.179	.257	2.334	22.116	9.474
1.2	.314	.429	2.340	22.309	9.532
1.4	.494	.644	2.335	22.204	9.510
1.6	.720	.899	2.321	21.874	9.425
1.8	.989	1.191	2.307	21.549	9.341
2.0	1.307	1.522	2.288	21.116	9.227
2.2	1.675	1.886	2.263	20.535	9.073
2.4	2.082	2.279	2.240	20.005	8.931
2.6	2.537	2.715	2.217	19.505	8.798
2.8	3.031	3.170	2.191	18.952	8.649
3.0	3.575	3.672	2.168	18.465	8.518

ECPSSR L SHELL X-RAY PRODUCTION CROSS SECTIONS

FOR PROTON IMPACT

ENERGY	L	ALPHA	BETA	GAMMA	GAMMA1	GAMMA2	TOTAL
MeV				BARNS			
1.0	.0482	.781	.333	.0361	.0220	.0140	1.199
1.2	.0885	1.432	.611	.0659	.0437	.0222	2.198
1.4	.141	2.289	.980	.106	.0748	.0314	3.516
1.6	.206	3.340	1.440	.158	.116	.0420	5.143
1.8	.283	4.578	1.993	.221	.167	.0544	7.073
2.0	.370	5.988	2.633	.297	.227	.0694	9.284
2.2	.467	7.570	3.363	.385	.297	.0875	11.780
2.4	.573	9.287	4.179	.487	.378	.109	14.518
2.6	.688	11.161	5.078	.601	.466	.136	17.518
2.8	.812	13.163	6.062	.730	.563	.167	20.751
3.0	.942	15.283	7.119	.870	.666	.204	24.195

ENERGY	BETA1	BETA2	LA/LB	LA/LG	LB/LG
MeV	BARNS				
1.0	.140	.193	2.312	21.572	9.331
1.2	.265	.346	2.314	21.656	9.360
1.4	.436	.544	2.305	21.466	9.314
1.6	.656	.784	2.289	21.115	9.224
1.8	.927	1.065	2.267	20.606	9.090
2.0	1.247	1.386	2.243	20.076	8.949
2.2	1.615	1.748	2.220	19.568	8.813
2.4	2.036	2.143	2.192	18.963	8.651
2.6	2.499	2.580	2.168	18.463	8.517
2.8	3.012	3.049	2.142	17.943	8.377
3.0	3.564	3.554	2.118	17.467	8.249

URANIUM(Z2=92)

L SUBSHELL IONISATION CROSS SECTIONS FOR PROTON IMPACT

L 1 SUBSHELL

ENERGY MeV	PWBA	PWBAR	PSS	PSSR	CPSS	CPSSR	ECPSS	ECPSSR
				BARNS				
1.00	.418	.599	.374	.555	.212	.315	.198	.293
1.20	.557	.711	.513	.669	.334	.435	.314	.410
1.40	.670	.787	.627	.749	.446	.532	.424	.506
1.60	.752	.845	.714	.807	.539	.610	.517	.584
1.80	.811	.912	.773	.859	.611	.679	.589	.655
2.00	.864	1.00	.823	.949	.674	.776	.652	.751
2.20	.934	1.19	.877	1.08	.737	.911	.715	.884
2.40	1.03	1.43	.960	1.28	.825	1.10	.802	1.07
2.60	1.20	1.80	1.09	1.58	.954	1.38	.931	1.35
2.80	1.43	2.30	1.27	1.97	1.13	1.75	1.10	1.71
3.00	1.78	2.94	1.55	2.53	1.39	2.27	1.36	2.22

L 2 SUBSHELL

ENERGY MeV	PWBA	PWBAR	PSS	PSSR	CPSS	CPSSR	ECPSS	ECPSSR
				BARNS				
1.00	.294	.539	.238	.447	.139	.261	.128	.241
1.20	.560	.943	.459	.791	.305	.526	.285	.492
1.40	.936	1.48	.776	1.25	.561	.905	.531	.857
1.60	1.43	2.14	1.20	1.83	.918	1.41	.876	1.34
1.80	2.03	2.93	1.73	2.54	1.38	2.03	1.33	1.95
2.00	2.75	3.85	2.37	3.36	1.96	2.78	1.89	2.67
2.20	3.59	4.87	3.10	4.27	2.63	3.62	2.54	3.50
2.40	4.52	5.99	3.94	5.30	3.41	4.58	3.31	4.45
2.60	5.55	7.23	4.87	6.40	4.29	5.63	4.17	5.48
2.80	6.67	8.52	5.89	7.62	5.25	6.79	5.12	6.62
3.00	7.88	9.92	7.00	8.89	6.32	8.02	6.16	7.82

L 3 SUBSHELL

ENERGY MeV	PWBA	PWBAR	PSS	PSSR	CPSS	CPSSR	ECPSS	ECPSSR
				BARNS				
1.00	2.51	3.87	2.02	3.18	1.30	2.04	1.21	1.91
1.20	4.37	6.30	3.58	5.27	2.56	3.76	2.42	3.57
1.40	6.77	9.30	5.63	7.89	4.31	6.04	4.12	5.78
1.60	9.67	12.83	8.16	11.01	6.56	8.85	6.31	8.51
1.80	13.04	16.84	11.16	14.57	9.29	12.13	8.98	11.73
2.00	16.87	21.24	14.54	18.53	12.44	15.85	12.07	15.38
2.20	21.05	25.97	18.31	22.89	15.99	20.00	15.56	19.46
2.40	25.54	31.11	22.46	27.54	19.95	24.46	19.46	23.85
2.60	30.43	36.43	26.85	32.51	24.17	29.27	23.62	28.60
2.80	35.46	42.04	31.60	37.74	28.77	34.35	28.16	33.63
3.00	40.89	47.84	36.54	43.16	33.57	39.66	32.91	38.88

TOTAL ECPSSR L SHELL IONISATION CROSS SECTIONS AND SUBSHELL RATIOS FOR PROTON IMPACT

ENERGY MeV	TOTAL BARNS	L1/L2	L1/L3	L2/L3
1.00	2.45	1.216	.153	.126
1.20	4.47	.833	.115	.138
1.40	7.14	.591	.088	.148
1.60	10.44	.436	.069	.158
1.80	14.33	.336	.056	.166
2.00	18.80	.281	.049	.174
2.20	23.84	.253	.045	.180
2.40	29.37	.240	.045	.186
2.60	35.42	.246	.047	.192
2.80	41.96	.258	.051	.197
3.00	48.93	.284	.057	.201

C.2 DEUTERON IMPACT

DYSPROSIUM(Z2=66)

PWBA L SHELL X-RAY PRODUCTION CROSS SECTIONS

FOR DEUTERON IMPACT

ENERGY MeV	L	ALPHA	BETA	GAMMA	GAMMA1	GAMMA2	TOTAL
	BARNS						
1.0	.126	3.003	1.609	.217	.153	.0637	4.932
1.2	.206	4.912	2.547	.329	.255	.0744	7.957
1.4	.305	7.261	3.684	.461	.384	.0774	11.654
1.6	.421	10.035	5.056	.622	.540	.0824	16.055
1.8	.554	13.213	6.698	.824	.725	.0993	21.182
2.0	.703	16.750	8.589	1.063	.936	.128	26.967
2.2	.864	20.608	10.715	1.339	1.170	.169	33.354
2.4	1.038	24.756	13.074	1.653	1.428	.226	40.309
2.6	1.223	29.165	15.659	2.006	1.706	.300	47.800
2.8	1.417	33.813	18.472	2.400	2.005	.395	55.805
3.0	1.621	38.677	21.506	2.834	2.322	.512	64.295

ENERGY MeV	BETA1	BETA2	LA/LB	LA/LG	LB/LG
	BARNS				
1.0	1.100	.508	1.853	13.740	7.416
1.2	1.716	.832	1.913	14.795	7.733
1.4	2.455	1.229	1.956	15.627	7.991
1.6	3.357	1.698	1.969	15.995	8.123
1.8	4.462	2.236	1.957	15.906	8.129
2.0	5.755	2.834	1.934	15.626	8.079
2.2	7.228	3.486	1.907	15.261	8.002
2.4	8.886	4.187	1.877	14.847	7.908
2.6	10.726	4.933	1.846	14.411	7.805
2.8	12.753	5.718	1.814	13.965	7.697
3.0	14.965	6.540	1.782	13.524	7.587

ECPSSR L SHELL X-RAY PRODUCTION CROSS SECTIONS

FOR DEUTERON IMPACT

ENERGY MeV	L	ALPHA	BETA	GAMMA	GAMMA1	GAMMA2	TOTAL
	BARNS						
1.0	.0892	2.126	1.159	.158	.110	.0481	3.516
1.2	.154	3.666	1.924	.251	.193	.0582	5.967
1.4	.236	5.627	2.870	.360	.300	.0603	9.048
1.6	.336	8.017	4.076	.506	.435	.0704	12.871
1.8	.453	10.804	5.529	.686	.597	.0888	17.384
2.0	.585	13.952	7.217	.900	.784	.116	22.538
2.2	.731	17.429	9.134	1.150	.995	.155	28.295
2.4	.889	21.206	11.276	1.435	1.228	.207	34.625
2.6	1.059	25.259	13.641	1.757	1.483	.274	41.496
2.8	1.239	29.566	16.229	2.117	1.758	.360	48.891
3.0	1.432	34.172	19.050	2.518	2.052	.465	56.867

ENERGY MeV	BETA1	BETA2	LA/LB	LA/LG	LB/LG
	BARNS				
1.0	.799	.360	1.820	13.328	7.324
1.2	1.304	.621	1.891	14.496	7.668
1.4	1.917	.952	1.945	15.503	7.969
1.6	2.719	1.357	1.951	15.732	8.063
1.8	3.701	1.828	1.938	15.625	8.062
2.0	4.856	2.360	1.917	15.366	8.016
2.2	6.185	2.948	1.892	15.032	7.945
2.4	7.689	3.587	1.864	14.653	7.859
2.6	9.368	4.272	1.836	14.253	7.765
2.8	11.228	5.000	1.806	13.841	7.665
3.0	13.271	5.778	1.778	13.453	7.567

DYSPROSIUM(Z2=66)

L SUBSHELL IONISATION CROSS SECTIONS FOR DEUTERON IMPACT

L 1 SUBSHELL

ENERGY MeV	PWBA	PWBAR	PSS	PSSR	CPSS	CPSSR	ECPSS	ECPSSR
				BARNS				
1.00	3.38	3.70	3.01	3.35	2.35	2.62	2.29	2.55
1.20	3.92	4.09	3.58	3.78	2.97	3.14	2.90	3.07
1.40	4.04	4.09	3.74	3.73	3.22	3.21	3.16	3.15
1.60	4.26	4.75	3.83	4.19	3.40	3.71	3.34	3.65
1.80	5.11	6.05	4.45	5.16	4.02	4.66	3.96	4.59
2.00	6.57	8.05	5.52	6.65	5.06	6.10	4.99	6.01
2.20	8.72	10.88	7.11	8.75	6.59	8.12	6.51	8.02
2.40	11.69	14.70	9.30	11.59	8.70	10.85	8.61	10.73
2.60	15.62	19.64	12.20	15.30	11.51	14.43	11.39	14.28
2.80	20.63	25.81	15.95	20.00	15.14	18.98	15.00	18.80
3.00	26.83	33.27	20.66	25.80	19.71	24.62	19.54	24.39

L 2 SUBSHELL

ENERGY MeV	PWBA	PWBAR	PSS	PSSR	CPSS	CPSSR	ECPSS	ECPSSR
				BARNS				
1.00	5.09	6.31	3.74	4.73	2.97	3.75	2.88	3.64
1.20	8.80	10.57	6.65	8.11	5.58	6.81	5.44	6.63
1.40	13.59	15.95	10.50	12.48	9.14	10.86	8.94	10.62
1.60	19.40	22.36	15.27	17.80	13.63	15.89	13.37	15.59
1.80	26.15	29.72	20.92	24.01	19.03	21.84	18.71	21.47
2.00	33.76	37.92	27.40	31.04	25.27	28.63	24.89	28.20
2.20	42.13	46.87	34.63	38.83	32.29	36.20	31.85	35.70
2.40	51.20	56.50	42.56	47.29	40.02	44.47	39.52	43.92
2.60	60.87	66.71	51.12	56.38	48.41	53.39	47.85	52.77
2.80	71.10	77.45	60.26	66.01	57.39	62.88	56.78	62.20
3.00	81.80	88.65	69.91	76.15	66.90	72.88	66.24	72.16

L 3 SUBSHELL

ENERGY MeV	PWBA	PWBAR	PSS	PSSR	CPSS	CPSSR	ECPSS	ECPSSR
				BARNS				
1.00	19.14	22.93	14.06	17.12	11.40	13.88	11.08	13.49
1.20	31.76	37.04	24.02	28.40	20.48	24.22	20.00	23.65
1.40	47.44	54.26	36.75	42.53	32.39	37.48	31.75	36.74
1.60	65.90	74.26	52.10	59.29	46.99	53.47	46.18	52.55
1.80	86.83	96.68	69.85	78.44	64.07	71.95	63.09	70.85
2.00	109.94	121.22	89.77	99.73	83.40	92.65	82.25	91.38
2.20	134.95	147.60	111.64	122.92	104.75	115.33	103.45	113.90
2.40	161.60	175.55	135.25	147.80	127.90	139.77	126.45	138.18
2.60	189.67	204.85	160.40	174.16	152.65	165.75	151.06	164.01
2.80	218.97	235.30	186.91	201.82	178.82	193.08	177.08	191.21
3.00	249.31	266.73	215.07	231.09	206.67	222.07	204.80	220.06

TOTAL ECPSSR L SHELL IONISATION CROSS SECTIONS AND SUBSHELL RATIOS

FOR DEUTERON IMPACT

ENERGY MeV	TOTAL BARNS	L1/L2	L1/L3	L2/L3
1.00	19.68	.701	.189	.270
1.20	33.35	.462	.130	.280
1.40	50.51	.297	.086	.289
1.60	71.79	.234	.069	.297
1.80	96.91	.214	.065	.303
2.00	125.59	.213	.066	.309
2.20	157.62	.225	.070	.313
2.40	192.83	.244	.078	.318
2.60	231.07	.271	.087	.322
2.80	272.21	.302	.098	.325
3.00	316.61	.338	.111	.328

YTTERBIUM(Z2=70)

PWBA L SHELL X-RAY PRODUCTION CROSS SECTIONS

FOR DEUTERON IMPACT

ENERGY MeV	L	ALPHA	BETA	GAMMA	GAMMA1	GAMMA2	TOTAL
	BARNS						
1.0	.0793	1.801	.982	.138	.0885	.0496	2.988
1.2	.133	3.027	1.587	.213	.151	.0619	4.938
1.4	.202	4.581	2.338	.303	.233	.0703	7.390
1.6	.283	6.436	3.218	.405	.333	.0718	10.294
1.8	.378	8.587	4.258	.526	.451	.0746	13.684
2.0	.485	11.020	5.487	.676	.590	.0854	17.581
2.2	.603	13.708	6.891	.852	.748	.104	21.946
2.4	.731	16.626	8.455	1.053	.923	.130	26.731
2.6	.868	19.754	10.179	1.280	1.114	.165	31.919
2.8	1.014	23.075	12.057	1.532	1.321	.210	37.487
3.0	1.168	26.570	14.089	1.811	1.542	.267	43.413

ENERGY MeV	BETA1	BETA2	LA/LB	LA/LG	LB/LG
	BARNS				
1.0	.674	.308	1.821	12.947	7.109
1.2	1.070	.517	1.894	14.099	7.443
1.4	1.556	.782	1.945	14.998	7.712
1.6	2.120	1.099	1.985	15.786	7.953
1.8	2.793	1.466	2.001	16.191	8.091
2.0	3.606	1.880	1.993	16.172	8.116
2.2	4.552	2.339	1.974	15.954	8.084
2.4	5.619	2.836	1.951	15.657	8.027
2.6	6.809	3.370	1.925	15.309	7.954
2.8	8.122	3.936	1.898	14.937	7.871
3.0	9.558	4.531	1.870	14.551	7.782

ECPSSR L SHELL X-RAY PRODUCTION CROSS SECTIONS

FOR DEUTERON IMPACT

ENERGY MeV	L	ALPHA	BETA	GAMMA	GAMMA1	GAMMA2	TOTAL
	BARNS						
1.0	.0564	1.282	.713	.102	.0645	.0371	2.144
1.2	.100	2.279	1.212	.164	.116	.0481	3.739
1.4	.158	3.583	1.844	.240	.185	.0548	5.798
1.6	.228	5.180	2.606	.328	.271	.0569	8.303
1.8	.311	7.077	3.552	.443	.377	.0653	11.328
2.0	.407	9.252	4.668	.581	.502	.0788	14.835
2.2	.514	11.683	5.947	.744	.645	.0981	18.793
2.4	.631	14.347	7.386	.930	.805	.124	23.177
2.6	.757	17.229	8.977	1.139	.981	.158	27.960
2.8	.893	20.309	10.724	1.375	1.173	.201	33.130
3.0	1.036	23.574	12.623	1.635	1.379	.256	38.669

ENERGY MeV	BETA1	BETA2	LA/LB	LA/LG	LB/LG
	BARNS				
1.0	.494	.219	1.784	12.532	7.023
1.2	.823	.389	1.867	13.776	7.379
1.4	1.232	.612	1.928	14.820	7.685
1.6	1.722	.884	1.973	15.655	7.937
1.8	2.344	1.208	1.977	15.855	8.020
2.0	3.089	1.579	1.967	15.791	8.029
2.2	3.954	1.993	1.949	15.585	7.998
2.4	4.939	2.447	1.927	15.305	7.944
2.6	6.039	2.939	1.903	14.995	7.879
2.8	7.261	3.463	1.878	14.650	7.802
3.0	8.603	4.020	1.852	14.292	7.719

YTTERBIUM(Z2=70)

L SUBSHELL IONISATION CROSS SECTIONS FOR DEUTERON IMPACT

L 1 SUBSHELL

ENERGY MeV	PWBA	PWBAR	PSS	PSSR	CPSS	CPSSR	ECPSS	ECPSSR
				BARNS				
1.00	2.10	2.45	1.84	2.20	1.36	1.62	1.31	1.57
1.20	2.61	2.87	2.35	2.63	1.87	2.09	1.82	2.03
1.40	2.95	3.04	2.71	2.82	2.26	2.35	2.21	2.30
1.60	2.99	3.03	2.79	2.81	2.40	2.42	2.36	2.37
1.80	3.08	3.43	2.84	3.11	2.51	2.75	2.46	2.70
2.00	3.51	4.17	3.16	3.67	2.85	3.30	2.80	3.25
2.20	4.26	5.25	3.72	4.50	3.39	4.10	3.35	4.04
2.40	5.33	6.75	4.53	5.62	4.17	5.18	4.12	5.12
2.60	6.78	8.71	5.61	7.09	5.22	6.60	5.16	6.52
2.80	8.67	11.21	7.02	8.98	6.58	8.42	6.51	8.33
3.00	11.06	14.33	8.81	11.34	8.32	10.71	8.23	10.60

L 2 SUBSHELL

ENERGY MeV	PWBA	PWBAR	PSS	PSSR	CPSS	CPSSR	ECPSS	ECPSSR
				BARNS				
1.00	2.22	2.94	1.64	2.22	1.23	1.67	1.19	1.61
1.20	3.98	5.07	3.01	3.90	2.42	3.15	2.35	3.05
1.40	6.33	7.83	4.88	6.13	4.12	5.17	4.01	5.04
1.60	9.28	11.20	7.28	8.91	6.33	7.75	6.19	7.58
1.80	12.78	15.14	10.19	12.22	9.06	10.87	8.89	10.66
2.00	16.81	19.62	13.59	16.03	12.30	14.51	12.08	14.25
2.20	21.34	24.58	17.45	20.30	16.01	18.63	15.75	18.33
2.40	26.31	29.99	21.75	25.02	20.17	23.19	19.87	22.86
2.60	31.70	35.80	26.46	30.13	24.75	28.18	24.41	27.80
2.80	37.46	41.97	31.55	35.62	29.71	33.54	29.34	33.13
3.00	43.56	48.47	36.99	41.44	35.04	39.26	34.64	38.81

L 3 SUBSHELL

ENERGY MeV	PWBA	PWBAR	PSS	PSSR	CPSS	CPSSR	ECPSS	ECPSSR
				BARNS				
1.00	9.48	11.96	6.96	8.96	5.40	6.95	5.22	6.72
1.20	16.19	19.75	12.22	15.16	10.07	12.49	9.80	12.16
1.40	24.77	29.48	19.13	23.09	16.41	19.81	16.04	19.36
1.60	35.11	40.99	27.65	32.67	24.39	28.82	23.90	28.25
1.80	47.07	54.10	37.68	43.78	33.93	39.41	33.33	38.72
2.00	60.48	68.65	49.12	56.29	44.92	51.47	44.21	50.66
2.20	75.20	84.47	61.86	70.08	57.25	64.85	56.43	63.93
2.40	91.08	101.42	75.79	85.03	70.81	79.44	69.88	78.40
2.60	108.00	119.36	90.78	101.01	85.48	95.11	84.45	93.97
2.80	125.84	138.17	106.74	117.93	101.15	111.75	100.02	110.50
3.00	144.48	157.73	123.57	135.67	117.73	129.25	116.50	127.91

TOTAL ECPSSR L SHELL IONISATION CROSS SECTIONS AND SUBSHELL RATIOS FOR DEUTERON IMPACT

ENERGY MeV	TOTAL BARNS	L1/L2	L1/L3	L2/L3
1.00	9.90	.975	.234	.240
1.20	17.24	.666	.167	.251
1.40	26.70	.456	.119	.260
1.60	38.20	.313	.084	.268
1.80	52.08	.253	.070	.275
2.00	68.16	.228	.064	.281
2.20	86.30	.221	.063	.287
2.40	106.37	.224	.065	.292
2.60	128.29	.235	.069	.296
2.80	151.96	.251	.075	.300
3.00	177.31	.273	.083	.303

TUNGSTEN(Z2=74)

PWBA L SHELL X-RAY PRODUCTION CROSS SECTIONS

FOR DEUTERON IMPACT

ENERGY	L	ALPHA	BETA	GAMMA	GAMMA1	GAMMA2	TOTAL
MeV				BARNS			
1.0	.0501	1.077	.601	.0908	.0496	.0412	1.812
1.2	.0866	1.862	.994	.143	.0874	.0555	3.073
1.4	.134	2.886	1.491	.206	.138	.0676	4.697
1.6	.192	4.138	2.090	.279	.202	.0770	6.671
1.8	.260	5.601	2.774	.359	.279	.0804	8.956
2.0	.338	7.271	3.564	.452	.368	.0840	11.574
2.2	.425	9.146	4.491	.567	.472	.0944	14.563
2.4	.521	11.204	5.537	.700	.589	.110	17.879
2.6	.624	13.433	6.699	.850	.719	.131	21.506
2.8	.735	15.819	7.972	1.019	.861	.158	25.424
3.0	.852	18.346	9.352	1.206	1.014	.192	29.614

ENERGY	BETA1	BETA2	LA/LB	LA/LG	LB/LG
MeV	BARNS				
1.0	.329	.197	1.779	11.778	6.621
1.2	.554	.340	1.860	12.942	6.957
1.4	.845	.527	1.922	13.932	7.248
1.6	1.201	.755	1.966	14.724	7.490
1.8	1.616	1.022	2.005	15.489	7.724
2.0	2.101	1.327	2.026	15.962	7.880
2.2	2.672	1.669	2.022	16.018	7.923
2.4	3.321	2.044	2.009	15.897	7.915
2.6	4.044	2.450	1.990	15.678	7.877
2.8	4.840	2.885	1.969	15.403	7.821
3.0	5.704	3.346	1.947	15.096	7.755

ECPSSR L SHELL X-RAY PRODUCTION CROSS SECTIONS

FOR DEUTERON IMPACT

ENERGY	L	ALPHA	BETA	GAMMA	GAMMA1	GAMMA2	TOTAL
MeV				BARNS			
1.0	.0361	.776	.443	.0678	.0369	.0309	1.318
1.2	.0661	1.422	.773	.112	.0687	.0434	2.364
1.4	.107	2.291	1.201	.167	.113	.0541	3.750
1.6	.157	3.375	1.714	.228	.168	.0600	5.451
1.8	.217	4.672	2.332	.302	.237	.0651	7.491
2.0	.287	6.182	3.076	.395	.320	.0748	9.896
2.2	.367	7.891	3.939	.504	.416	.0881	12.643
2.4	.455	9.784	4.917	.630	.525	.106	15.714
2.6	.550	11.847	6.004	.773	.645	.128	19.084
2.8	.653	14.069	7.202	.933	.778	.155	22.749
3.0	.764	16.440	8.507	1.111	.922	.189	26.693

ENERGY	BETA1	BETA2	LA/LB	LA/LG	LB/LG
MeV	BARNS				
1.0	.245	.142	1.738	11.367	6.539
1.2	.435	.260	1.828	12.594	6.890
1.4	.687	.418	1.895	13.637	7.198
1.6	.994	.616	1.956	14.672	7.501
1.8	1.370	.853	1.989	15.337	7.709
2.0	1.826	1.128	1.995	15.548	7.793
2.2	2.358	1.439	1.988	15.540	7.816
2.4	2.965	1.785	1.975	15.407	7.802
2.6	3.641	2.161	1.958	15.208	7.767
2.8	4.389	2.566	1.939	14.957	7.716
3.0	5.207	2.998	1.917	14.679	7.655

TUNGSTEN(Z2=74)

L SUBSHELL IONISATION CROSS SECTIONS FOR DEUTERON IMPACT

L 1 SUBSHELL

ENERGY MeV	PWBA	PWBAR	PSS	PSSR	CPSS	CPSSR	ECPSS	ECPSSR
				BARNS				
1.00	1.25	1.59	1.08	1.40	.746	.974	.718	.936
1.20	1.66	1.96	1.47	1.77	1.11	1.34	1.08	1.30
1.40	1.99	2.21	1.80	2.04	1.44	1.63	1.40	1.59
1.60	2.22	2.25	2.04	2.11	1.71	1.76	1.67	1.72
1.80	2.25	2.28	2.11	2.15	1.82	1.85	1.78	1.81
2.00	2.27	2.52	2.14	2.35	1.88	2.06	1.85	2.03
2.20	2.49	2.93	2.31	2.67	2.07	2.39	2.03	2.35
2.40	2.86	3.52	2.60	3.12	2.36	2.83	2.32	2.79
2.60	3.39	4.31	3.01	3.72	2.75	3.41	2.72	3.36
2.80	4.10	5.33	3.54	4.49	3.27	4.15	3.23	4.10
3.00	5.01	6.60	4.22	5.45	3.93	5.08	3.89	5.02

L 2 SUBSHELL

ENERGY MeV	PWBA	PWBAR	PSS	PSSR	CPSS	CPSSR	ECPSS	ECPSSR
				BARNS				
1.00	.957	1.38	.710	1.05	.503	.744	.482	.712
1.20	1.78	2.44	1.35	1.89	1.04	1.45	1.00	1.40
1.40	2.92	3.85	2.25	3.03	1.83	2.46	1.78	2.39
1.60	4.39	5.62	3.44	4.48	2.90	3.78	2.83	3.68
1.80	6.19	7.73	4.92	6.24	4.27	5.41	4.17	5.29
2.00	8.30	10.16	6.69	8.30	5.92	7.35	5.80	7.20
2.20	10.72	12.91	8.73	10.65	7.86	9.59	7.72	9.41
2.40	13.42	15.94	11.05	13.27	10.08	12.10	9.91	11.90
2.60	16.39	19.24	13.62	16.15	12.55	14.88	12.36	14.65
2.80	19.61	22.78	16.44	19.27	15.28	17.91	15.06	17.65
3.00	23.06	26.54	19.48	22.62	18.24	21.17	17.99	20.89

L 3 SUBSHELL

ENERGY MeV	PWBA	PWBAR	PSS	PSSR	CPSS	CPSSR	ECPSS	ECPSSR
				BARNS				
1.00	4.71	6.33	3.46	4.77	2.55	3.51	2.46	3.38
1.20	8.28	10.68	6.25	8.22	4.95	6.51	4.80	6.31
1.40	12.99	16.22	10.01	12.72	8.33	10.58	8.11	10.30
1.60	18.79	22.90	14.75	18.25	12.69	15.69	12.40	15.34
1.80	25.63	30.63	20.44	24.76	18.02	21.82	17.66	21.38
2.00	33.43	39.32	27.04	32.18	24.28	28.89	23.84	28.37
2.20	42.12	48.89	34.49	40.46	31.42	36.85	30.91	36.25
2.40	51.61	59.24	42.74	49.52	39.38	45.63	38.79	44.95
2.60	61.84	70.30	51.72	59.29	48.10	55.15	47.44	54.39
2.80	72.74	82.00	61.37	69.73	57.52	65.35	56.79	64.52
3.00	84.23	94.27	71.65	80.76	67.58	76.18	66.78	75.28

TOTAL ECPSSR L SHELL IONISATION CROSS SECTIONS AND SUBSHELL RATIOS

FOR DEUTERON IMPACT

ENERGY MeV	TOTAL BARNS	L1/L2	L1/L3	L2/L3
1.00	5.03	1.315	.277	.211
1.20	9.01	.926	.206	.222
1.40	14.28	.666	.154	.232
1.60	20.74	.467	.112	.240
1.80	28.49	.343	.085	.247
2.00	37.60	.281	.071	.254
2.20	48.01	.250	.065	.260
2.40	59.63	.234	.062	.265
2.60	72.41	.230	.062	.269
2.80	86.27	.232	.064	.274
3.00	101.18	.240	.067	.278

GOLD(Z2=79)

PWBA L SHELL X-RAY PRODUCTION CROSS SECTIONS

FOR DEUTERON IMPACT

ENERGY MeV	L	ALPHA	BETA	GAMMA	GAMMA1	GAMMA2	TOTAL
				BARNS			
1.0	.0302	.600	.290	.0398	.0223	.0170	.960
1.2	.0535	1.064	.506	.0675	.0420	.0255	1.691
1.4	.0843	1.675	.788	.102	.0686	.0339	2.650
1.6	.123	2.437	1.139	.145	.103	.0420	3.845
1.8	.169	3.351	1.563	.197	.147	.0503	5.279
2.0	.222	4.405	2.055	.257	.198	.0584	6.939
2.2	.282	5.598	2.618	.325	.258	.0669	8.822
2.4	.348	6.920	3.246	.402	.326	.0757	10.917
2.6	.421	8.365	3.945	.489	.403	.0856	13.221
2.8	.499	9.924	4.705	.584	.488	.0960	15.713
3.0	.584	11.609	5.549	.693	.581	.111	18.435

ENERGY MeV	LA/LB	LA/LG	LB/LG
1.0	2.068	15.052	7.279
1.2	2.101	15.753	7.497
1.4	2.126	16.348	7.690
1.6	2.139	16.763	7.836
1.8	2.144	17.019	7.937
2.0	2.144	17.161	8.006
2.2	2.138	17.202	8.044
2.4	2.132	17.196	8.067
2.6	2.120	17.094	8.062
2.8	2.109	16.983	8.052
3.0	2.092	16.748	8.006

ECPSSR L SHELL X-RAY PRODUCTION CROSS SECTIONS

FOR DEUTERON IMPACT

ENERGY MeV	L	ALPHA	BETA	GAMMA	GAMMA1	GAMMA2	TOTAL
				BARNS			
1.0	.0224	.444	.220	.0309	.0177	.0131	.718
1.2	.0419	.832	.404	.0547	.0345	.0202	1.333
1.4	.0687	1.365	.654	.0861	.0584	.0276	2.174
1.6	.103	2.046	.972	.125	.0901	.0353	3.247
1.8	.144	2.872	1.364	.174	.131	.0435	4.555
2.0	.193	3.839	1.824	.231	.179	.0518	6.087
2.2	.248	4.940	2.349	.296	.236	.0602	7.833
2.4	.310	6.166	2.939	.369	.300	.0684	9.784
2.6	.378	7.523	3.602	.453	.373	.0789	11.957
2.8	.453	9.012	4.348	.549	.455	.0931	14.363
3.0	.534	10.614	5.161	.655	.545	.109	16.964

ENERGY MeV	LA/LB	LA/LG	LB/LG
1.0	2.017	14.393	7.137
1.2	2.058	15.206	7.389
1.4	2.088	15.860	7.597
1.6	2.105	16.314	7.749
1.8	2.105	16.478	7.827
2.0	2.105	16.609	7.890
2.2	2.103	16.690	7.936
2.4	2.098	16.706	7.964
2.6	2.088	16.625	7.961
2.8	2.073	16.423	7.923
3.0	2.056	16.204	7.879

GOLD(Z2=79)

L SUBSHELL IONISATION CROSS SECTIONS FOR DEUTERON IMPACT

L 1 SUBSHELL

ENERGY MeV	PWBA	PWBAR	PSS	PSSR	CPSS	CPSSR	ECPSS	ECPSSR
	BARNS							
1.00	.619	.907	.529	.795	.334	.501	.318	.478
1.20	.897	1.17	.778	1.04	.548	.733	.527	.706
1.40	1.14	1.38	1.01	1.25	.762	.949	.738	.919
1.60	1.34	1.55	1.21	1.43	.962	1.14	.935	1.11
1.80	1.51	1.68	1.38	1.60	1.14	1.32	1.11	1.29
2.00	1.64	1.79	1.54	1.74	1.30	1.47	1.28	1.44
2.20	1.75	1.89	1.68	1.83	1.46	1.59	1.43	1.56
2.40	1.84	1.99	1.79	1.89	1.58	1.67	1.55	1.64
2.60	1.94	2.18	1.86	2.03	1.66	1.81	1.64	1.78
2.80	2.03	2.52	1.91	2.28	1.73	2.07	1.70	2.04
3.00	2.29	2.94	2.10	2.60	1.92	2.38	1.89	2.35

L 2 SUBSHELL

ENERGY MeV	PWBA	PWBAR	PSS	PSSR	CPSS	CPSSR	ECPSS	ECPSSR
	BARNS							
1.00	.333	.547	.249	.422	.161	.273	.153	.259
1.20	.646	.993	.492	.777	.353	.558	.339	.535
1.40	1.10	1.61	.852	1.27	.655	.980	.632	.945
1.60	1.71	2.40	1.34	1.92	1.08	1.55	1.05	1.50
1.80	2.48	3.36	1.97	2.73	1.64	2.28	1.60	2.22
2.00	3.41	4.51	2.74	3.69	2.35	3.16	2.29	3.09
2.20	4.50	5.81	3.66	4.80	3.20	4.20	3.13	4.11
2.40	5.74	7.29	4.71	6.07	4.19	5.40	4.11	5.29
2.60	7.14	8.91	5.91	7.48	5.33	6.74	5.23	6.61
2.80	8.68	10.68	7.24	9.02	6.60	8.22	6.49	8.08
3.00	10.36	12.59	8.71	10.70	8.01	9.84	7.88	9.69

L 3 SUBSHELL

ENERGY MeV	PWBA	PWBAR	PSS	PSSR	CPSS	CPSSR	ECPSS	ECPSSR
	BARNS							
1.00	2.00	2.96	1.48	2.25	1.01	1.54	.966	1.47
1.20	3.65	5.11	2.75	3.95	2.06	2.96	1.99	2.85
1.40	5.89	7.92	4.54	6.23	3.61	4.95	3.50	4.80
1.60	8.73	11.37	6.84	9.08	5.67	7.53	5.52	7.33
1.80	12.17	15.44	9.68	12.49	8.27	10.67	8.08	10.42
2.00	16.17	20.09	13.04	16.44	11.40	14.38	11.16	14.07
2.20	20.71	25.28	16.89	20.90	15.04	18.61	14.76	18.25
2.40	25.76	30.98	21.23	25.84	19.18	23.34	18.84	22.93
2.60	31.27	37.13	26.02	31.24	23.78	28.54	23.39	28.08
2.80	37.22	43.70	31.23	37.05	28.81	34.18	28.39	33.67
3.00	43.56	50.65	36.85	43.25	34.26	40.22	33.79	39.66

TOTAL ECPSSR L SHELL IONISATION CROSS SECTIONS AND SUBSHELL RATIOS FOR DEUTERON IMPACT

ENERGY MeV	TOTAL BARNS	L1/L2	L1/L3	L2/L3
1.00	2.21	1.846	.325	.176
1.20	4.10	1.320	.247	.187
1.40	6.67	.972	.191	.197
1.60	9.94	.739	.152	.205
1.80	13.93	.582	.124	.213
2.00	18.60	.467	.102	.219
2.20	23.92	.378	.085	.225
2.40	29.86	.310	.071	.231
2.60	36.48	.270	.064	.236
2.80	43.79	.252	.060	.240
3.00	51.69	.242	.059	.244

LEAD(Z2=82)

PWBA L SHELL X-RAY PRODUCTION CROSS SECTIONS

FOR DEUTERON IMPACT

ENERGY MeV	L	ALPHA	BETA	GAMMA	GAMMA1	GAMMA2	TOTAL
				BARNS			
1.0	.0215	.408	.191	.0257	.0138	.0118	.646
1.2	.0387	.734	.339	.0443	.0260	.0183	1.156
1.4	.0621	1.178	.540	.0691	.0435	.0255	1.850
1.6	.0916	1.738	.794	.0999	.0668	.0331	2.723
1.8	.127	2.417	1.101	.137	.0960	.0409	3.783
2.0	.169	3.206	1.462	.180	.132	.0485	5.016
2.2	.216	4.099	1.872	.229	.174	.0553	6.416
2.4	.268	5.093	2.330	.284	.222	.0619	7.975
2.6	.327	6.198	2.850	.347	.277	.0704	9.722
2.8	.390	7.405	3.428	.419	.339	.0808	11.643
3.0	.459	8.704	4.060	.499	.407	.0927	13.722

ENERGY MeV	LA/LB	LA/LG	LB/LG
1.0	2.136	15.884	7.435
1.2	2.164	16.553	7.649
1.4	2.182	17.060	7.819
1.6	2.190	17.397	7.944
1.8	2.195	17.654	8.044
2.0	2.193	17.789	8.112
2.2	2.190	17.890	8.169
2.4	2.186	17.951	8.211
2.6	2.174	17.842	8.205
2.8	2.160	17.658	8.175
3.0	2.144	17.430	8.131

ECPSSR L SHELL X-RAY PRODUCTION CROSS SECTIONS

FOR DEUTERON IMPACT

ENERGY MeV	L	ALPHA	BETA	GAMMA	GAMMA1	GAMMA2	TOTAL
				BARNS			
1.0	.0162	.308	.148	.0204	.0111	9.31E-03	.493
1.2	.0312	.591	.280	.0373	.0222	.0151	.939
1.4	.0518	.984	.461	.0601	.0385	.0216	1.556
1.6	.0786	1.491	.695	.0889	.0605	.0284	2.354
1.8	.111	2.110	.981	.124	.0885	.0355	3.327
2.0	.150	2.837	1.316	.164	.123	.0417	4.468
2.2	.194	3.677	1.711	.213	.164	.0492	5.795
2.4	.244	4.624	2.159	.268	.210	.0577	7.295
2.6	.299	5.679	2.669	.332	.265	.0676	8.980
2.8	.360	6.833	3.231	.404	.325	.0788	10.829
3.0	.426	8.078	3.845	.483	.391	.0913	12.831

ENERGY MeV	LA/LB	LA/LG	LB/LG
1.0	2.081	15.114	7.263
1.2	2.115	15.868	7.501
1.4	2.134	16.376	7.675
1.6	2.146	16.770	7.814
1.8	2.151	17.023	7.914
2.0	2.156	17.265	8.009
2.2	2.148	17.269	8.038
2.4	2.142	17.248	8.053
2.6	2.128	17.088	8.031
2.8	2.115	16.931	8.004
3.0	2.101	16.741	7.968

LEAD(Z2=82)

L SUBSHELL IONISATION CROSS SECTIONS FOR DEUTERON IMPACT

L 1 SUBSHELL

ENERGY	PWBA	PWBAR	PSS	PSSR	CPSS	CPSSR	ECPSS	ECPSSR
MeV				BARNS				
1.00	.397	.633	.339	.555	.200	.328	.190	.311
1.20	.591	.848	.511	.753	.342	.504	.328	.483
1.40	.788	1.04	.691	.936	.502	.680	.484	.656
1.60	.971	1.20	.863	1.09	.665	.842	.645	.816
1.80	1.13	1.31	1.02	1.22	.819	.980	.797	.954
2.00	1.25	1.32	1.15	1.28	.955	1.06	.932	1.03
2.20	1.31	1.37	1.24	1.35	1.05	1.15	1.03	1.12
2.40	1.33	1.47	1.30	1.44	1.12	1.25	1.10	1.22
2.60	1.39	1.60	1.36	1.55	1.20	1.36	1.18	1.34
2.80	1.49	1.78	1.45	1.68	1.30	1.50	1.27	1.48
3.00	1.62	2.00	1.55	1.85	1.40	1.67	1.38	1.64

L 2 SUBSHELL

ENERGY	PWBA	PWBAR	PSS	PSSR	CPSS	CPSSR	ECPSS	ECPSSR
MeV				BARNS				
1.00	.175	.316	.132	.246	.08	.149	.0756	.141
1.20	.348	.582	.267	.459	.182	.314	.174	.299
1.40	.606	.954	.471	.761	.348	.563	.335	.541
1.60	.958	1.44	.755	1.16	.590	.907	.570	.876
1.80	1.41	2.04	1.13	1.66	.916	1.35	.888	1.31
2.00	1.97	2.76	1.59	2.27	1.33	1.90	1.30	1.85
2.20	2.64	3.60	2.15	2.98	1.84	2.56	1.80	2.50
2.40	3.41	4.55	2.80	3.79	2.45	3.32	2.39	3.24
2.60	4.29	5.61	3.55	4.71	3.15	4.18	3.09	4.10
2.80	5.27	6.77	4.39	5.72	3.95	5.15	3.87	5.05
3.00	6.35	8.03	5.33	6.83	4.84	6.21	4.75	6.10

L 3 SUBSHELL

ENERGY	PWBA	PWBAR	PSS	PSSR	CPSS	CPSSR	ECPSS	ECPSSR
MeV				BARNS				
1.00	1.20	1.90	.890	1.45	.579	.945	.551	.899
1.20	2.23	3.32	1.69	2.58	1.22	1.86	1.17	1.79
1.40	3.67	5.20	2.83	4.10	2.18	3.17	2.11	3.06
1.60	5.52	7.54	4.33	6.03	3.50	4.88	3.40	4.74
1.80	7.80	10.33	6.20	8.36	5.19	7.00	5.05	6.82
2.00	10.48	13.54	8.44	11.09	7.25	9.53	7.08	9.31
2.20	13.56	17.16	11.04	14.19	9.68	12.44	9.48	12.18
2.40	17.01	21.16	13.99	17.65	12.47	15.72	12.23	15.42
2.60	20.82	25.51	17.28	21.44	15.60	19.36	15.33	19.02
2.80	24.96	30.18	20.89	25.56	19.07	23.33	18.76	22.95
3.00	29.40	35.15	24.80	29.97	22.84	27.60	22.50	27.18

TOTAL ECPSSR L SHELL IONISATION CROSS SECTIONS AND SUBSHELL RATIOS

FOR DEUTERON IMPACT

ENERGY MeV	TOTAL BARNS	L1/L2	L1/L3	L2/L3
1.00	1.35	2.205	.345	.157
1.20	2.57	1.613	.270	.167
1.40	4.26	1.214	.214	.177
1.60	6.43	.932	.172	.185
1.80	9.09	.727	.140	.192
2.00	12.19	.559	.111	.199
2.20	15.80	.450	.092	.205
2.40	19.89	.377	.079	.210
2.60	24.45	.327	.070	.215
2.80	29.47	.293	.064	.220
3.00	34.92	.269	.060	.224

BISMUTH(Z2=83)

PWBA L SHELL X-RAY PRODUCTION CROSS SECTIONS

FOR DEUTERON IMPACT

ENERGY MeV	L	ALPHA	BETA	GAMMA	GAMMA1	GAMMA2	TOTAL
				BARNS			
1.0	.0176	.330	.153	.0192	.0107	8.52E-03	.520
1.2	.0324	.606	.278	.0340	.0204	.0136	.951
1.4	.0530	.990	.450	.0543	.0348	.0195	1.547
1.6	.0791	1.479	.669	.0801	.0542	.0259	2.307
1.8	.111	2.082	.940	.112	.0791	.0326	3.245
2.0	.149	2.781	1.259	.150	.110	.0396	4.338
2.2	.192	3.587	1.624	.192	.146	.0467	5.595
2.4	.240	4.477	2.039	.243	.188	.0541	6.999
2.6	.293	5.478	2.507	.299	.237	.0622	8.578
2.8	.350	6.546	3.015	.362	.291	.0709	10.273
3.0	.413	7.727	3.579	.431	.351	.0804	12.151

ENERGY MeV	LA/LB	LA/LG	LB/LG
1.0	2.150	17.198	8.000
1.2	2.181	17.818	8.168
1.4	2.201	18.244	8.288
1.6	2.209	18.458	8.357
1.8	2.215	18.639	8.415
2.0	2.209	18.590	8.417
2.2	2.208	18.634	8.438
2.4	2.196	18.459	8.407
2.6	2.185	18.303	8.378
2.8	2.171	18.101	8.336
3.0	2.159	17.914	8.297

ECPSSR L SHELL X-RAY PRODUCTION CROSS SECTIONS

FOR DEUTERON IMPACT

ENERGY MeV	L	ALPHA	BETA	GAMMA	GAMMA1	GAMMA2	TOTAL
				BARNS			
1.0	.0136	.254	.121	.0156	8.72E-03	6.88E-03	.405
1.2	.0266	.497	.234	.0294	.0178	.0115	.786
1.4	.0449	.839	.391	.0484	.0315	.0169	1.324
1.6	.0687	1.284	.595	.0729	.0502	.0228	2.021
1.8	.0983	1.837	.849	.103	.0743	.0289	2.887
2.0	.133	2.486	1.147	.139	.104	.0353	3.905
2.2	.173	3.243	1.499	.181	.139	.0421	5.097
2.4	.218	4.083	1.898	.230	.181	.0495	6.429
2.6	.269	5.031	2.347	.286	.228	.0575	7.933
2.8	.324	6.062	2.845	.348	.281	.0665	9.579
3.0	.385	7.188	3.395	.417	.341	.0767	11.385

ENERGY MeV	LA/LB	LA/LG	LB/LG
1.0	2.091	16.285	7.787
1.2	2.126	16.925	7.961
1.4	2.146	17.335	8.079
1.6	2.157	17.606	8.162
1.8	2.165	17.811	8.226
2.0	2.166	17.887	8.257
2.2	2.163	17.876	8.265
2.4	2.152	17.726	8.239
2.6	2.143	17.616	8.219
2.8	2.131	17.429	8.180
3.0	2.117	17.227	8.137

BISMUTH(Z2=83)

L SUBSHELL IONISATION CROSS SECTIONS FOR DEUTERON IMPACT

L 1 SUBSHELL

ENERGY MeV	PWBA	PWBAR	PSS	PSSR	CPSS	CPSSR	ECPSS	ECPSSR
				BARNS				
1.00	.318	.534	.270	.470	.155	.271	.147	.256
1.20	.486	.728	.419	.652	.275	.429	.263	.410
1.40	.664	.906	.581	.824	.416	.591	.401	.569
1.60	.832	1.06	.741	.972	.564	.740	.546	.717
1.80	.981	1.18	.890	1.09	.708	.870	.688	.845
2.00	1.11	1.27	1.02	1.19	.840	.980	.819	.955
2.20	1.21	1.34	1.12	1.27	.948	1.07	.926	1.04
2.40	1.28	1.40	1.21	1.33	1.04	1.14	1.02	1.12
2.60	1.35	1.47	1.27	1.39	1.12	1.21	1.10	1.19
2.80	1.41	1.56	1.33	1.46	1.18	1.29	1.16	1.27
3.00	1.47	1.67	1.38	1.55	1.25	1.39	1.22	1.37

L 2 SUBSHELL

ENERGY MeV	PWBA	PWBAR	PSS	PSSR	CPSS	CPSSR	ECPSS	ECPSSR
				BARNS				
1.00	.129	.243	.0969	.190	.0575	.113	.0541	.106
1.20	.261	.455	.200	.359	.134	.241	.128	.229
1.40	.462	.755	.359	.602	.262	.439	.251	.422
1.60	.743	1.15	.584	.929	.451	.718	.435	.693
1.80	1.11	1.65	.881	1.34	.710	1.08	.688	1.05
2.00	1.57	2.25	1.26	1.84	1.04	1.53	1.02	1.49
2.20	2.11	2.96	1.71	2.45	1.46	2.09	1.42	2.03
2.40	2.76	3.77	2.26	3.13	1.96	2.72	1.92	2.66
2.60	3.50	4.66	2.88	3.91	2.54	3.46	2.49	3.38
2.80	4.32	5.67	3.60	4.78	3.22	4.27	3.16	4.19
3.00	5.24	6.74	4.38	5.74	3.96	5.19	3.89	5.09

L 3 SUBSHELL

ENERGY MeV	PWBA	PWBAR	PSS	PSSR	CPSS	CPSSR	ECPSS	ECPSSR
				BARNS				
1.00	.938	1.54	.695	1.18	.444	.753	.422	.715
1.20	1.78	2.73	1.35	2.13	.959	1.51	.920	1.45
1.40	2.98	4.33	2.29	3.42	1.75	2.61	1.69	2.52
1.60	4.54	6.36	3.55	5.07	2.85	4.07	2.76	3.94
1.80	6.50	8.77	5.14	7.09	4.27	5.89	4.16	5.74
2.00	8.79	11.58	7.07	9.44	6.03	8.06	5.89	7.87
2.20	11.46	14.70	9.29	12.17	8.10	10.61	7.93	10.38
2.40	14.43	18.23	11.88	15.16	10.53	13.44	10.32	13.17
2.60	17.77	22.02	14.69	18.50	13.20	16.63	12.96	16.33
2.80	21.34	26.16	17.86	22.11	16.24	20.10	15.96	19.76
3.00	25.29	30.51	21.24	26.02	19.50	23.88	19.19	23.50

TOTAL ECPSSR L SHELL IONISATION CROSS SECTIONS AND SUBSHELL RATIOS FOR DEUTERON IMPACT

ENERGY MeV	TOTAL BARNS	L1/L2	L1/L3	L2/L3
1.00	1.08	2.419	.358	.148
1.20	2.09	1.788	.283	.158
1.40	3.51	1.350	.226	.167
1.60	5.35	1.034	.182	.176
1.80	7.63	.808	.147	.182
2.00	10.31	.641	.121	.189
2.20	13.46	.513	.101	.196
2.40	16.95	.421	.085	.202
2.60	20.90	.352	.073	.207
2.80	25.22	.304	.064	.212
3.00	29.97	.269	.058	.217

C.3 ALPHA PARTICLE IMPACT

YTTERBIUM(Z2=70)

PWBA L SHELL X-RAY PRODUCTION CROSS SECTIONS

FOR ALPHA IMPACT

ENERGY	L	ALPHA	BETA	GAMMA	GAMMA1	GAMMA2	TOTAL
MeV				BARNS			
1.0	.0334	.758	.512	.0856	.0374	.0481	1.384
1.2	.0634	1.441	.911	.146	.0700	.0757	2.551
1.4	.106	2.419	1.454	.224	.117	.107	4.186
1.6	.164	3.718	2.147	.320	.180	.139	6.321
1.8	.236	5.355	2.994	.432	.261	.171	8.979
2.0	.323	7.334	3.994	.561	.360	.200	12.159
2.2	.425	9.658	5.147	.706	.478	.227	15.866
2.4	.542	12.320	6.449	.865	.615	.249	20.086
2.6	.674	15.312	7.901	1.040	.772	.268	24.815
2.8	.820	18.627	9.499	1.230	.947	.282	30.038
3.0	.979	22.252	11.239	1.434	1.142	.292	35.738

ENERGY	BETA1	BETA2	LA/LB	LA/LG	LB/LG
MeV	BARNS				
1.0	.383	.129	1.469	8.797	5.987
1.2	.665	.246	1.571	9.821	6.251
1.4	1.041	.413	1.652	10.728	6.495
1.6	1.512	.635	1.720	11.553	6.719
1.8	2.080	.914	1.776	12.301	6.927
2.0	2.741	1.252	1.823	12.980	7.119
2.2	3.497	1.649	1.863	13.589	7.294
2.4	4.345	2.103	1.897	14.135	7.453
2.6	5.287	2.614	1.924	14.612	7.595
2.8	6.319	3.180	1.947	15.033	7.723
3.0	7.441	3.798	1.965	15.398	7.836

ECPSSR L SHELL X-RAY PRODUCTION CROSS SECTIONS

FOR ALPHA IMPACT

ENERGY	L	ALPHA	BETA	GAMMA	GAMMA1	GAMMA2	TOTAL
MeV				BARNS			
1.0	.0113	.257	.190	.0333	.0135	.0197	.490
1.2	.0254	.576	.400	.0671	.0300	.0371	1.064
1.4	.0476	1.082	.709	.115	.0559	.0588	1.945
1.6	.0795	1.806	1.127	.176	.0929	.0831	3.175
1.8	.122	2.772	1.658	.251	.142	.108	4.782
2.0	.176	3.992	2.307	.338	.205	.133	6.782
2.2	.241	5.477	3.075	.438	.282	.156	9.191
2.4	.318	7.237	3.964	.551	.374	.177	12.016
2.6	.408	9.269	4.973	.676	.481	.194	15.256
2.8	.509	11.563	6.079	.807	.603	.204	18.871
3.0	.621	14.126	7.296	.948	.739	.208	22.884

ENERGY	BETA1	BETA2	LA/LB	LA/LG	LB/LG
MeV	BARNS				
1.0	.147	.0438	1.339	7.666	5.726
1.2	.301	.0984	1.432	8.523	5.954
1.4	.524	.185	1.515	9.362	6.180
1.6	.819	.308	1.590	10.183	6.403
1.8	1.185	.473	1.659	10.981	6.621
2.0	1.625	.681	1.718	11.723	6.825
2.2	2.140	.935	1.768	12.404	7.016
2.4	2.729	1.235	1.812	13.036	7.195
2.6	3.391	1.582	1.850	13.614	7.360
2.8	4.106	1.974	1.888	14.219	7.533
3.0	4.885	2.411	1.921	14.786	7.695

YTTERBIUM(Z2=70)

L SUBSHELL IONISATION CROSS SECTIONS FOR ALPHA IMPACT

L 1 SUBSHELL

ENERGY MeV	PWBA	PWBAR	PSS	PSSR	CPSS	CPSSR	ECPSS	ECPSSR
				BARNS				
1.00	2.05	3.14	1.30	2.12	.534	.874	.513	.840
1.20	3.22	4.56	2.12	3.20	1.08	1.63	1.05	1.58
1.40	4.53	6.03	3.11	4.38	1.82	2.56	1.77	2.50
1.60	5.90	7.45	4.19	5.59	2.70	3.61	2.64	3.53
1.80	7.24	8.75	5.32	6.77	3.68	4.68	3.61	4.59
2.00	8.48	9.87	6.43	7.85	4.70	5.73	4.62	5.63
2.20	9.59	10.80	7.48	8.81	5.70	6.71	5.61	6.60
2.40	10.52	11.52	8.43	9.61	6.64	7.57	6.54	7.46
2.60	11.27	12.03	9.26	10.26	7.49	8.30	7.39	8.19
2.80	11.83	12.10	9.94	10.48	8.23	8.67	8.13	8.57
3.00	12.21	11.90	10.49	10.48	8.84	8.83	8.74	8.73

L 2 SUBSHELL

ENERGY MeV	PWBA	PWBAR	PSS	PSSR	CPSS	CPSSR	ECPSS	ECPSSR
				BARNS				
1.00	.718	1.16	.339	.584	.146	.252	.140	.241
1.20	1.46	2.23	.713	1.15	.376	.608	.363	.587
1.40	2.61	3.79	1.31	2.02	.791	1.21	.768	1.18
1.60	4.22	5.92	2.19	3.23	1.45	2.13	1.41	2.08
1.80	6.36	8.64	3.40	4.83	2.40	3.41	2.35	3.34
2.00	9.06	12.00	4.96	6.86	3.69	5.10	3.62	5.00
2.20	12.34	16.00	6.93	9.34	5.36	7.22	5.26	7.10
2.40	16.22	20.64	9.32	12.29	7.43	9.81	7.32	9.66
2.60	20.71	25.93	12.14	15.73	9.94	12.88	9.80	12.69
2.80	25.80	31.85	15.42	19.65	12.90	16.44	12.72	16.22
3.00	31.48	38.39	19.16	24.07	16.31	20.49	16.11	20.23

L 3 SUBSHELL

ENERGY MeV	PWBA	PWBAR	PSS	PSSR	CPSS	CPSSR	ECPSS	ECPSSR
				BARNS				
1.00	3.65	5.49	1.65	2.64	.772	1.23	.742	1.19
1.20	7.14	10.16	3.36	5.07	1.89	2.84	1.83	2.76
1.40	12.24	16.72	6.00	8.64	3.79	5.46	3.70	5.32
1.60	19.12	25.29	9.73	13.50	6.69	9.28	6.54	9.07
1.80	27.90	35.95	14.69	19.76	10.73	14.44	10.52	14.16
2.00	38.62	48.69	20.97	27.51	16.04	21.04	15.76	20.68
2.20	51.30	63.51	28.64	36.77	22.71	29.16	22.36	28.70
2.40	65.91	80.34	37.76	47.59	30.81	38.83	30.37	38.28
2.60	82.41	99.13	48.34	59.96	40.36	50.07	39.84	49.42
2.80	100.76	119.79	60.39	73.88	51.40	62.88	50.78	62.12
3.00	120.88	142.25	73.90	89.31	63.92	77.25	63.20	76.38

TOTAL ECPSSR L SHELL IONISATION CROSS SECTIONS AND SUBSHELL RATIOS FOR ALPHA IMPACT

ENERGY MeV	TOTAL BARNS	L1/L2	L1/L3	L2/L3
1.00	2.27	3.484	.707	.203
1.20	4.92	2.687	.572	.213
1.40	9.00	2.118	.469	.221
1.60	14.68	1.696	.389	.229
1.80	22.08	1.376	.324	.236
2.00	31.31	1.127	.273	.242
2.20	42.40	.930	.230	.247
2.40	55.40	.773	.195	.252
2.60	70.30	.645	.166	.257
2.80	86.91	.528	.138	.261
3.00	105.35	.432	.114	.265

TUNGSTEN(Z2=74)

PWBA L SHELL X-RAY PRODUCTION CROSS SECTIONS

FOR ALPHA IMPACT

ENERGY MeV	L	ALPHA	BETA	GAMMA	GAMMA1	GAMMA2	TOTAL
				BARNS			
1.0	.0189	.407	.287	.0516	.0190	.0326	.762
1.2	.0369	.794	.520	.0894	.0362	.0531	1.434
1.4	.0636	1.367	.847	.140	.0619	.0784	2.409
1.6	.0998	2.145	1.276	.204	.0977	.106	3.711
1.8	.146	3.149	1.807	.280	.144	.136	5.362
2.0	.204	4.388	2.446	.369	.202	.167	7.379
2.2	.273	5.868	3.193	.469	.273	.196	9.765
2.4	.353	7.586	4.043	.580	.356	.224	12.512
2.6	.444	9.547	5.001	.702	.453	.250	15.632
2.8	.546	11.743	6.063	.835	.563	.273	19.108
3.0	.659	14.171	7.226	.978	.686	.292	22.939

ENERGY MeV	BETA1	BETA2	LA/LB	LA/LG	LB/LG
	BARNS				
1.0	.152	.0744	1.411	7.845	5.559
1.2	.276	.145	1.518	8.821	5.812
1.4	.452	.250	1.603	9.680	6.039
1.6	.688	.392	1.671	10.437	6.248
1.8	.982	.575	1.732	11.167	6.448
2.0	1.341	.801	1.782	11.821	6.633
2.2	1.765	1.071	1.826	12.430	6.807
2.4	2.254	1.385	1.864	12.992	6.970
2.6	2.812	1.743	1.896	13.501	7.120
2.8	3.436	2.144	1.924	13.963	7.258
3.0	4.126	2.587	1.948	14.386	7.386

ECPSSR L SHELL X-RAY PRODUCTION CROSS SECTIONS

FOR ALPHA IMPACT

ENERGY MeV	L	ALPHA	BETA	GAMMA	GAMMA1	GAMMA2	TOTAL
				BARNS			
1.0	6.26E-03	.135	.104	.0195	6.71E-03	.0128	.263
1.2	.0147	.316	.228	.0412	.0156	.0256	.598
1.4	.0287	.617	.419	.0730	.0302	.0428	1.133
1.6	.0491	1.057	.682	.115	.0515	.0631	1.895
1.8	.0771	1.658	1.026	.167	.0808	.0860	2.917
2.0	.113	2.432	1.451	.229	.119	.110	4.208
2.2	.158	3.389	1.956	.300	.166	.133	5.779
2.4	.211	4.538	2.549	.380	.223	.157	7.647
2.6	.273	5.882	3.229	.470	.291	.178	9.814
2.8	.345	7.423	3.996	.569	.370	.199	12.281
3.0	.426	9.160	4.847	.676	.460	.217	15.045

ENERGY MeV	BETA1	BETA2	LA/LB	LA/LG	LB/LG
	BARNS				
1.0	.0554	.0246	1.289	6.871	5.331
1.2	.123	.0577	1.377	7.620	5.534
1.4	.227	.113	1.461	8.387	5.741
1.6	.373	.193	1.538	9.149	5.948
1.8	.565	.303	1.606	9.873	6.148
2.0	.805	.444	1.665	10.560	6.341
2.2	1.094	.619	1.721	11.238	6.529
2.4	1.436	.828	1.769	11.860	6.706
2.6	1.834	1.073	1.809	12.429	6.871
2.8	2.286	1.355	1.845	12.955	7.023
3.0	2.792	1.672	1.876	13.450	7.168

TUNGSTEN(Z2=74)

L SUBSHELL IONISATION CROSS SECTIONS FOR ALPHA IMPACT

L 1 SUBSHELL

ENERGY MeV	PWBA	PWBAR	PSS	PSSR	CPSS	CPSSR	ECPSS	ECPSSR
				BARNS				
1.00	1.01	1.76	.645	1.22	.220	.416	.210	.396
1.20	1.64	2.63	1.09	1.87	.481	.823	.463	.792
1.40	2.41	3.58	1.65	2.60	.860	1.36	.834	1.32
1.60	3.26	4.55	2.29	3.39	1.35	1.99	1.31	1.94
1.80	4.15	5.51	3.00	4.20	1.92	2.69	1.88	2.63
2.00	5.05	6.40	3.74	4.98	2.55	3.41	2.50	3.34
2.20	5.91	7.19	4.47	5.72	3.22	4.11	3.16	4.04
2.40	6.70	7.87	5.19	6.40	3.89	4.79	3.82	4.71
2.60	7.41	8.43	5.87	7.00	4.54	5.41	4.47	5.33
2.80	8.02	8.86	6.49	7.51	5.16	5.97	5.09	5.89
3.00	8.52	9.18	7.04	7.93	5.72	6.45	5.65	6.36

L 2 SUBSHELL

ENERGY MeV	PWBA	PWBAR	PSS	PSSR	CPSS	CPSSR	ECPSS	ECPSSR
				BARNS				
1.00	.276	.507	.136	.266	.049	.096	.046	.091
1.20	.576	.987	.290	.529	.133	.244	.128	.234
1.40	1.05	1.70	.543	.934	.294	.505	.284	.488
1.60	1.75	2.70	.924	1.51	.558	.913	.542	.886
1.80	2.69	4.00	1.46	2.29	.955	1.50	.931	1.46
2.00	3.91	5.63	2.17	3.28	1.51	2.29	1.48	2.24
2.20	5.43	7.61	3.07	4.51	2.25	3.30	2.20	3.23
2.40	7.26	9.94	4.19	5.99	3.19	4.56	3.13	4.47
2.60	9.42	12.64	5.54	7.74	4.35	6.07	4.27	5.97
2.80	11.91	15.69	7.13	9.75	5.74	7.85	5.65	7.73
3.00	14.73	19.10	8.96	12.04	7.37	9.90	7.26	9.76

L 3 SUBSHELL

ENERGY MeV	PWBA	PWBAR	PSS	PSSR	CPSS	CPSSR	ECPSS	ECPSSR
				BARNS				
1.00	1.63	2.72	.758	1.35	.305	.545	.292	.520
1.20	3.27	5.11	1.57	2.62	.787	1.31	.759	1.26
1.40	5.75	8.53	2.86	4.50	1.65	2.60	1.60	2.52
1.60	9.17	13.08	4.71	7.10	3.01	4.53	2.93	4.41
1.80	13.64	18.83	7.23	10.49	4.96	7.20	4.85	7.04
2.00	19.21	25.80	10.47	14.73	7.59	10.68	7.44	10.47
2.20	25.92	34.02	14.48	19.85	10.97	15.03	10.77	14.76
2.40	33.76	43.47	19.32	25.89	15.14	20.29	14.89	19.96
2.60	42.76	54.12	25.01	32.86	20.15	26.47	19.85	26.08
2.80	52.88	65.97	31.57	40.77	26.02	33.60	25.66	33.14
3.00	64.12	78.95	39.01	49.61	32.77	41.68	32.35	41.14

TOTAL ECPSSR L SHELL IONISATION CROSS SECTIONS AND SUBSHELL RATIOS

FOR ALPHA IMPACT

ENERGY MeV	TOTAL BARNS	L1/L2	L1/L3	L2/L3
1.00	1.01	4.340	.761	.175
1.20	2.29	3.390	.627	.185
1.40	4.33	2.703	.523	.193
1.60	7.24	2.190	.440	.201
1.80	11.12	1.798	.373	.207
2.00	16.04	1.492	.319	.214
2.20	22.03	1.249	.274	.219
2.40	29.14	1.053	.236	.224
2.60	37.38	.893	.204	.229
2.80	46.75	.762	.178	.233
3.00	57.27	.652	.155	.237

GOLD(Z2=79)

PWBA L SHELL X-RAY PRODUCTION CROSS SECTIONS

FOR ALPHA IMPACT

ENERGY MeV	L	ALPHA	BETA	GAMMA	GAMMA1	GAMMA2	TOTAL
				BARNS			
1.0	.0108	.214	.117	.0184	7.79E-03	.0106	.360
1.2	.0212	.422	.220	.0334	.0152	.0181	.697
1.4	.0369	.734	.372	.0545	.0266	.0279	1.197
1.6	.0587	1.168	.580	.0830	.0430	.0400	1.890
1.8	.0874	1.737	.850	.119	.0650	.0538	2.793
2.0	.123	2.448	1.182	.162	.0932	.0689	3.915
2.2	.167	3.315	1.588	.215	.129	.0860	5.284
2.4	.218	4.332	2.061	.275	.171	.103	6.886
2.6	.277	5.498	2.599	.342	.221	.120	8.715
2.8	.343	6.819	3.205	.416	.279	.137	10.784
3.0	.417	8.295	3.885	.499	.346	.153	13.097

ENERGY MeV	LA/LB	LA/LG	LB/LG
1.0	1.839	11.656	6.337
1.2	1.918	12.654	6.599
1.4	1.975	13.464	6.818
1.6	2.013	14.071	6.990
1.8	2.045	14.615	7.148
2.0	2.071	15.094	7.289
2.2	2.088	15.447	7.399
2.4	2.102	15.768	7.502
2.6	2.116	16.092	7.606
2.8	2.127	16.382	7.700
3.0	2.135	16.607	7.778

ECPSSR L SHELL X-RAY PRODUCTION CROSS SECTIONS

FOR ALPHA IMPACT

ENERGY MeV	L	ALPHA	BETA	GAMMA	GAMMA1	GAMMA2	TOTAL
				BARNS			
1.0	3.54E-03	.0703	.0402	6.59E-03	2.66E-03	3.93E-03	.121
1.2	8.66E-03	.172	.0954	.0152	6.60E-03	8.58E-03	.291
1.4	.0173	.343	.186	.0287	.0134	.0153	.575
1.6	.0303	.601	.317	.0478	.0237	.0240	.997
1.8	.0482	.958	.496	.0730	.0385	.0345	1.575
2.0	.0713	1.418	.722	.104	.0578	.0459	2.315
2.2	.100	1.995	1.000	.141	.0825	.0583	3.237
2.4	.136	2.695	1.338	.185	.114	.0716	4.353
2.6	.177	3.520	1.731	.236	.150	.0852	5.664
2.8	.225	4.470	2.180	.293	.194	.0990	7.168
3.0	.280	5.557	2.695	.358	.244	.113	8.889

ENERGY MeV	LA/LB	LA/LG	LB/LG
1.0	1.750	10.661	6.093
1.2	1.804	11.329	6.281
1.4	1.850	11.948	6.458
1.6	1.897	12.595	6.641
1.8	1.931	13.125	6.796
2.0	1.965	13.661	6.954
2.2	1.994	14.158	7.100
2.4	2.014	14.547	7.222
2.6	2.034	14.926	7.339
2.8	2.050	15.258	7.442
3.0	2.062	15.529	7.530

GOLD(Z2=79)

L SUBSHELL IONISATION CROSS SECTIONS FOR ALPHA IMPACT

L 1 SUBSHELL

ENERGY MeV	PWBA	PWBAR	PSS	PSSR	CPSS	CPSSR	ECPSS	ECPSSR
				BARNS				
1.00	.413	.879	.267	.629	.0692	.163	.0651	.154
1.20	.698	1.34	.471	.976	.168	.349	.161	.333
1.40	1.06	1.87	.738	1.38	.326	.611	.314	.588
1.60	1.50	2.44	1.06	1.83	.544	.939	.526	.909
1.80	1.99	3.07	1.43	2.32	.817	1.32	.795	1.29
2.00	2.51	3.67	1.84	2.80	1.14	1.73	1.11	1.69
2.20	3.08	4.21	2.27	3.27	1.50	2.16	1.47	2.11
2.40	3.63	4.71	2.71	3.72	1.88	2.59	1.85	2.54
2.60	4.13	5.15	3.14	4.16	2.28	3.01	2.24	2.96
2.80	4.59	5.55	3.57	4.57	2.67	3.42	2.63	3.36
3.00	5.02	5.90	3.97	4.95	3.06	3.82	3.01	3.76

L 2 SUBSHELL

ENERGY MeV	PWBA	PWBAR	PSS	PSSR	CPSS	CPSSR	ECPSS	ECPSSR
				BARNS				
1.00	.0853	.189	.0442	.105	.0123	.0291	.0115	.0273
1.20	.182	.370	.0955	.209	.0360	.0786	.0342	.0747
1.40	.341	.648	.182	.370	.0839	.171	.0805	.164
1.60	.580	1.04	.316	.604	.167	.320	.162	.309
1.80	.916	1.56	.508	.923	.298	.542	.289	.526
2.00	1.36	2.23	.769	1.34	.489	.849	.475	.826
2.20	1.93	3.06	1.11	1.86	.750	1.25	.732	1.22
2.40	2.64	4.05	1.54	2.49	1.09	1.77	1.07	1.73
2.60	3.49	5.22	2.07	3.25	1.53	2.39	1.50	2.35
2.80	4.49	6.55	2.71	4.14	2.06	3.15	2.02	3.09
3.00	5.65	8.07	3.46	5.16	2.70	4.03	2.65	3.96

L 3 SUBSHELL

ENERGY MeV	PWBA	PWBAR	PSS	PSSR	CPSS	CPSSR	ECPSS	ECPSSR
				BARNS				
1.00	.614	1.19	.297	.621	.0966	.202	.0914	.191
1.20	1.27	2.27	.628	1.21	.267	.513	.256	.491
1.40	2.29	3.84	1.16	2.09	.590	1.06	.569	1.02
1.60	3.74	5.97	1.95	3.32	1.12	1.91	1.09	1.85
1.80	5.69	8.70	3.05	4.95	1.91	3.11	1.86	3.03
2.00	8.17	12.08	4.49	7.01	3.02	4.71	2.95	4.60
2.20	11.23	16.11	6.31	9.54	4.47	6.76	4.38	6.61
2.40	14.88	20.81	8.54	12.54	6.31	9.27	6.19	9.09
2.60	19.13	26.18	11.20	16.04	8.57	12.27	8.42	12.06
2.80	24.00	32.21	14.32	20.05	11.27	15.78	11.08	15.52
3.00	29.48	38.90	17.89	24.58	14.42	19.80	14.20	19.51

TOTAL ECPSSR L SHELL IONISATION CROSS SECTIONS AND SUBSHELL RATIOS

FOR ALPHA IMPACT

ENERGY MeV	TOTAL BARNS	L1/L2	L1/L3	L2/L3
1.00	.372	5.622	.805	.143
1.20	.899	4.461	.679	.152
1.40	1.77	3.595	.576	.160
1.60	3.07	2.940	.492	.167
1.80	4.84	2.448	.425	.174
2.00	7.12	2.047	.368	.180
2.20	9.95	1.727	.319	.185
2.40	13.35	1.469	.279	.190
2.60	17.36	1.260	.245	.195
2.80	21.98	1.090	.217	.199
3.00	27.22	.949	.193	.203

LEAD(Z2=82)

PWBA L SHELL X-RAY PRODUCTION CROSS SECTIONS

FOR ALPHA IMPACT

ENERGY MeV	L	ALPHA	BETA	GAMMA	GAMMA1	GAMMA2	TOTAL
				BARNS			
1.0	6.19E-03	.117	.0603	9.24E-03	3.64E-03	5.59E-03	.193
1.2	.0127	.241	.120	.0177	7.55E-03	.0102	.391
1.4	.0229	.435	.211	.0302	.0138	.0165	.699
1.6	.0373	.707	.338	.0473	.0229	.0244	1.130
1.8	.0568	1.078	.508	.0694	.0354	.0340	1.712
2.0	.0815	1.547	.722	.0969	.0520	.0450	2.447
2.2	.112	2.130	.986	.130	.0731	.0570	3.358
2.4	.149	2.832	1.301	.169	.0990	.0702	4.451
2.6	.192	3.636	1.663	.214	.130	.0841	5.705
2.8	.241	4.581	2.088	.266	.167	.0987	7.176
3.0	.296	5.618	2.557	.323	.209	.113	8.794

ENERGY MeV	LA/LB	LA/LG	LB/LG
1.0	1.948	12.711	6.525
1.2	2.008	13.588	6.766
1.4	2.059	14.385	6.987
1.6	2.089	14.939	7.150
1.8	2.122	15.536	7.320
2.0	2.143	15.961	7.450
2.2	2.161	16.378	7.577
2.4	2.177	16.738	7.689
2.6	2.186	17.002	7.777
2.8	2.194	17.251	7.861
3.0	2.197	17.400	7.920

ECPSSR L SHELL X-RAY PRODUCTION CROSS SECTIONS

FOR ALPHA IMPACT

ENERGY MeV	L	ALPHA	BETA	GAMMA	GAMMA1	GAMMA2	TOTAL
				BARNS			
1.0	2.03E-03	.0385	.0207	3.31E-03	1.25E-03	2.05E-03	.0645
1.2	5.28E-03	.100	.0527	8.19E-03	3.34E-03	4.85E-03	.166
1.4	.0110	.209	.108	.0163	7.14E-03	9.19E-03	.344
1.6	.0198	.376	.191	.0282	.0131	.0151	.615
1.8	.0325	.617	.307	.0444	.0219	.0225	1.001
2.0	.0490	.929	.458	.0650	.0338	.0312	1.502
2.2	.0702	1.332	.649	.0904	.0493	.0411	2.142
2.4	.0961	1.823	.880	.121	.0689	.0517	2.920
2.6	.127	2.410	1.154	.156	.0927	.0631	3.847
2.8	.163	3.094	1.473	.196	.121	.0751	4.927
3.0	.204	3.877	1.835	.242	.154	.0874	6.158

ENERGY MeV	LA/LB	LA/LG	LB/LG
1.0	1.859	11.633	6.257
1.2	1.901	12.228	6.431
1.4	1.940	12.798	6.598
1.6	1.971	13.305	6.750
1.8	2.007	13.883	6.917
2.0	2.029	14.291	7.045
2.2	2.053	14.745	7.181
2.4	2.071	15.119	7.299
2.6	2.088	15.465	7.408
2.8	2.100	15.756	7.503
3.0	2.113	16.054	7.597

LEAD(Z2=82)

L SUBSHELL IONISATION CROSS SECTIONS FOR ALPHA IMPACT

L 1 SUBSHELL

ENERGY MeV	PWBA	PWBAR	PSS	PSSR	CPSS	CPSSR	ECPSS	ECPSSR
				BARNS				
1.00	.202	.527	.130	.373	.0279	.0799	.0260	.0746
1.20	.363	.826	.240	.595	.0743	.184	.0705	.174
1.40	.579	1.18	.392	.865	.154	.341	.148	.326
1.60	.847	1.58	.585	1.18	.273	.548	.263	.529
1.80	1.16	2.00	.818	1.52	.432	.803	.418	.778
2.00	1.51	2.43	1.09	1.88	.630	1.09	.613	1.06
2.20	1.88	2.87	1.38	2.25	.861	1.40	.840	1.37
2.40	2.27	3.28	1.70	2.62	1.12	1.73	1.09	1.69
2.60	2.66	3.69	2.03	2.98	1.41	2.06	1.38	2.02
2.80	3.05	4.04	2.36	3.33	1.70	2.40	1.67	2.35
3.00	3.42	4.39	2.71	3.65	2.01	2.71	1.98	2.67

L 2 SUBSHELL

ENERGY MeV	PWBA	PWBAR	PSS	PSSR	CPSS	CPSSR	ECPSS	ECPSSR
				BARNS				
1.00	.0344	.0917	.0179	.0521	4.13E-03	.0120	3.84E-03	.0112
1.20	.0779	.185	.0412	.106	.0135	.0349	.0128	.0329
1.40	.152	.331	.0819	.192	.0338	.0794	.0322	.0757
1.60	.267	.541	.146	.318	.0709	.154	.0681	.148
1.80	.431	.826	.241	.493	.131	.269	.127	.259
2.00	.655	1.19	.372	.722	.221	.430	.215	.417
2.20	.950	1.66	.547	1.01	.349	.647	.339	.629
2.40	1.32	2.22	.772	1.38	.520	.929	.508	.906
2.60	1.77	2.89	1.05	1.81	.741	1.28	.724	1.25
2.80	2.32	3.67	1.40	2.33	1.02	1.70	1.000	1.67
3.00	2.96	4.57	1.80	2.92	1.36	2.20	1.33	2.16

L 3 SUBSHELL

ENERGY MeV	PWBA	PWBAR	PSS	PSSR	CPSS	CPSSR	ECPSS	ECPSSR
				BARNS				
1.00	.295	.653	.143	.347	.0402	.0974	.0378	.0916
1.20	.635	1.27	.318	.690	.121	.263	.115	.250
1.40	1.19	2.20	.607	1.22	.282	.565	.271	.543
1.60	1.99	3.49	1.05	1.97	.559	1.05	.541	1.01
1.80	3.11	5.18	1.67	2.97	.987	1.76	.958	1.71
2.00	4.55	7.28	2.50	4.25	1.60	2.71	1.56	2.64
2.20	6.38	9.84	3.58	5.85	2.42	3.96	2.37	3.87
2.40	8.61	12.86	4.92	7.77	3.50	5.52	3.42	5.40
2.60	11.20	16.33	6.53	10.02	4.82	7.40	4.73	7.26
2.80	14.28	20.28	8.47	12.63	6.46	9.64	6.35	9.46
3.00	17.69	24.77	10.67	15.58	8.36	12.21	8.22	12.01

TOTAL ECPSSR L SHELL IONISATION CROSS SECTIONS AND SUBSHELL RATIOS

FOR ALPHA IMPACT

ENERGY MeV	TOTAL BARNS	L1/L2	L1/L3	L2/L3
1.00	.177	6.663	.814	.122
1.20	.457	5.297	.697	.132
1.40	.945	4.309	.601	.139
1.60	1.69	3.568	.521	.146
1.80	2.74	2.998	.456	.152
2.00	4.12	2.538	.400	.158
2.20	5.87	2.171	.353	.163
2.40	8.00	1.870	.313	.168
2.60	10.52	1.619	.278	.172
2.80	13.48	1.409	.248	.176
3.00	16.83	1.233	.222	.180

BISMUTH(Z2=83)

PWBA L SHELL X-RAY PRODUCTION CROSS SECTIONS

FOR ALPHA IMPACT

ENERGY MeV	L	ALPHA	BETA	GAMMA	GAMMA1	GAMMA2	TOTAL
				BARNS			
1.0	5.34E-03	.0998	.0509	7.06E-03	2.95E-03	4.12E-03	.163
1.2	.0110	.206	.102	.0137	6.16E-03	7.58E-03	.333
1.4	.0200	.373	.180	.0236	.0113	.0123	.597
1.6	.0328	.613	.291	.0374	.0189	.0185	.974
1.8	.0500	.935	.439	.0555	.0295	.0260	1.480
2.0	.0721	1.348	.626	.0781	.0435	.0346	2.125
2.2	.0997	1.863	.858	.106	.0615	.0444	2.927
2.4	.133	2.479	1.135	.139	.0836	.0552	3.886
2.6	.171	3.205	1.462	.177	.111	.0667	5.015
2.8	.216	4.039	1.834	.221	.142	.0791	6.311
3.0	.266	4.977	2.257	.271	.179	.0916	7.771

ENERGY MeV	LA/LB	LA/LG	LB/LG
1.0	1.959	14.128	7.210
1.2	2.019	15.004	7.431
1.4	2.069	15.790	7.630
1.6	2.104	16.371	7.781
1.8	2.131	16.852	7.907
2.0	2.153	17.253	8.014
2.2	2.171	17.599	8.107
2.4	2.184	17.862	8.180
2.6	2.192	18.057	8.236
2.8	2.202	18.262	8.293
3.0	2.205	18.362	8.327

ECPSSR L SHELL X-RAY PRODUCTION CROSS SECTIONS

FOR ALPHA IMPACT

ENERGY MeV	L	ALPHA	BETA	GAMMA	GAMMA1	GAMMA2	TOTAL
				BARNS			
1.0	1.74E-03	.0325	.0173	2.50E-03	1.00E-03	1.49E-03	.0540
1.2	4.59E-03	.0859	.0449	6.33E-03	2.73E-03	3.60E-03	.142
1.4	9.67E-03	.181	.0927	.0128	5.91E-03	6.92E-03	.296
1.6	.0176	.329	.166	.0226	.0110	.0115	.535
1.8	.0288	.538	.268	.0359	.0185	.0174	.870
2.0	.0438	.819	.402	.0530	.0287	.0243	1.317
2.2	.0630	1.178	.572	.0744	.0422	.0322	1.887
2.4	.0865	1.616	.777	.100	.0591	.0410	2.580
2.6	.115	2.147	1.024	.130	.0797	.0507	3.416
2.8	.147	2.757	1.307	.165	.105	.0605	4.377
3.0	.186	3.474	1.639	.205	.134	.0714	5.504

ENERGY MeV	LA/LB	LA/LG	LB/LG
1.0	1.874	13.002	6.938
1.2	1.915	13.567	7.085
1.4	1.950	14.084	7.221
1.6	1.984	14.590	7.354
1.8	2.009	14.995	7.463
2.0	2.037	15.449	7.582
2.2	2.060	15.835	7.686
2.4	2.079	16.161	7.774
2.6	2.096	16.465	7.856
2.8	2.108	16.705	7.923
3.0	2.119	16.909	7.980

BISMUTH(Z2=83)

L SUBSHELL IONISATION CROSS SECTIONS FOR ALPHA IMPACT

L 1 SUBSHELL

ENERGY MeV	PWBA	PWBAR	PSS	PSSR	CPSS	CPSSR	ECPSS	ECPSSR
				BARNS				
1.00	.167	.461	.108	.328	.0216	.0655	.0201	.0610
1.20	.303	.724	.201	.523	.0589	.153	.0557	.145
1.40	.486	1.04	.329	.762	.124	.288	.119	.275
1.60	.717	1.39	.495	1.04	.223	.469	.215	.451
1.80	.989	1.77	.697	1.35	.357	.691	.346	.668
2.00	1.29	2.16	.930	1.67	.526	.943	.511	.916
2.20	1.62	2.56	1.19	2.01	.724	1.23	.706	1.19
2.40	1.97	2.94	1.47	2.34	.953	1.52	.931	1.48
2.60	2.32	3.31	1.76	2.68	1.20	1.83	1.17	1.79
2.80	2.69	3.65	2.07	3.00	1.47	2.12	1.44	2.08
3.00	3.02	3.97	2.37	3.32	1.74	2.43	1.71	2.39

L 2 SUBSHELL

ENERGY MeV	PWBA	PWBAR	PSS	PSSR	CPSS	CPSSR	ECPSS	ECPSSR
				BARNS				
1.00	.0270	.0759	.0141	.0436	3.06E-03	9.43E-03	2.83E-03	8.74E-03
1.20	.0614	.153	.0328	.0889	.0102	.0277	9.63E-03	.0261
1.40	.120	.274	.0654	.161	.0259	.0638	.0247	.0607
1.60	.212	.449	.117	.267	.0550	.125	.0527	.120
1.80	.345	.686	.194	.413	.103	.219	.0990	.211
2.00	.528	.994	.301	.605	.175	.352	.169	.341
2.20	.768	1.39	.445	.852	.278	.533	.270	.518
2.40	1.07	1.86	.628	1.16	.416	.766	.405	.746
2.60	1.45	2.43	.859	1.53	.596	1.06	.582	1.03
2.80	1.89	3.08	1.14	1.96	.823	1.41	.805	1.38
3.00	2.43	3.85	1.48	2.47	1.10	1.84	1.08	1.80

L 3 SUBSHELL

ENERGY MeV	PWBA	PWBAR	PSS	PSSR	CPSS	CPSSR	ECPSS	ECPSSR
				BARNS				
1.00	.243	.559	.119	.300	.0316	.0801	.0297	.0751
1.20	.526	1.09	.264	.597	.0966	.218	.0919	.208
1.40	.988	1.89	.508	1.05	.229	.474	.219	.455
1.60	1.67	3.01	.880	1.71	.458	.887	.442	.857
1.80	2.61	4.46	1.41	2.57	.813	1.49	.788	1.44
2.00	3.84	6.29	2.12	3.69	1.32	2.31	1.29	2.25
2.20	5.40	8.54	3.04	5.09	2.03	3.39	1.98	3.31
2.40	7.29	11.14	4.18	6.76	2.93	4.73	2.86	4.63
2.60	9.55	14.21	5.57	8.74	4.06	6.38	3.98	6.25
2.80	12.17	17.64	7.22	11.01	5.45	8.31	5.35	8.15
3.00	15.16	21.63	9.15	13.64	7.09	10.58	6.97	10.40

TOTAL ECPSSR L SHELL IONISATION CROSS SECTIONS AND SUBSHELL RATIOS FOR ALPHA IMPACT

ENERGY MeV	TOTAL BARNS	L1/L2	L1/L3	L2/L3
1.00	.145	6.978	.812	.116
1.20	.379	5.559	.699	.126
1.40	.791	4.532	.605	.133
1.60	1.43	3.762	.527	.140
1.80	2.32	3.166	.463	.146
2.00	3.51	2.687	.407	.151
2.20	5.03	2.307	.360	.156
2.40	6.86	1.988	.320	.161
2.60	9.07	1.729	.286	.165
2.80	11.62	1.506	.256	.170
3.00	14.59	1.324	.230	.174

APPENDIX D

LISTING OF 'SPECTRUM' PACKAGE

```
FR
$MO $ADD=ON
SAUF77
      PROGRAM SPECTRUM
*     WRITTEN ON 26th MAY 1982
*     ---CONSTANTS---
      PARAMETER(PI=3.1415926)
*     ---VARIABLES---
      INTEGER INITIAL, FINAL, CH, PARA, REGION, J, CH1, J1, N, N1, NN, SK, P, G,
     :   P1, G1, G1, K, PEAKS, BGPARA, K1, ITER, CORREC, CPARA, LAM, FITER
       INTEGER GROUP, GROUPS
       REAL*6 D(1:70, 1:71), FIT(1:300),
     :   X1(1:70), S1(1:70), SD(1:70), DET,
     :         RESID(1:70), REFINEDX(1:70), PARAM1(1:70),
     :         XX, BGFIT, PFIT, POWER, CPFIT, LAMDA, NU, PARAM2(1:70),
     :    XTVI, XT, VI, MCOUNT, SUMSGREG, SUMSGM, MSUM, EX(1:20), SUMSG1,
     :         COUNT(1:300), RSG, PARAM, ERRORX, ECOUNT(1:300), SUMSG2,
     :      WNU, LAMDA1, SUMSG, KAPPA, RSG1, ALPHA, AREA(1:20)
       REAL*12 CHISG, CHISG1, CHISG2
       REAL*6 DF, RCHISG, PRECIS, JJJ
       REAL*6 U, D1, X, U1
       CHARACTER ELEMENT*25
       COMMON/MATRICES/XTVI(1:300, 1:300), XT(1:300, 1:300), VI(1:300, 1:300)
       COMMON/DERIVMAT/XX(1:300, 1:70), PARAM(1:70), ERRORX(1:70)
       COMMON/GAUSSMAT/U(1:70, 1:71), D1(1:70, 1:71), X(1:70)
        FITER=150
       READ(16, *)GROUPS, PRECIS
       FOR GROUP=1, GROUPS
       READ(16, *)ELEMENT
       READ(16, *)BGPARA, PEAKS, CORREC
       CPARA=CORREC*2
       PARA=BGPARA+PEAKS+CORREC
       N=PARA
       READ(16, *)INITIAL, FINAL
       REGION=FINAL-INITIAL
       DF=REGION-PEAKS*2-CPARA-BGPARA
       PRINT*, "ELEMENT=", ELEMENT, BGPARA+PEAKS*3+CPARA,
     :     "PARAMETER LEAST SQUARE FIT"
       PRINT*, "PEAKS=", PEAKS, "BGPARA=", BGPARA, "CORREC=", CORREC
     :        , "REGION=", REGION
       PRINT*, "DEGREES OF FREEDOM=", DF
       READ(16, *)(EX(K), K=1, PEAKS)
       J=BGPARA
       FOR K=1, PEAKS
        J=J+1
        PARAM(J+1)=(14.3442+24.523*EX(K))-INITIAL
        PARAM(J+2)=(1.5339+.4446*EX(K))*2.0
        PRINT*, "ENERGY=", EX(K), "CENTROID=", PARAM(J+1), "2SIGMA2=",
     : PARAM(J+2)
        J=J+2+CORREC
       END FOR
51     READ(16, *)(COUNT(CH), CH=1, REGION)
```

```
*     FOR CH=1,REGION
      IF(COUNT(CH).EQ.0)THEN
       COUNT(CH)=1
       ELSE
      ENDIF
       ECOUNT(CH)=COUNT(CH)
      END FOR
      MSUM=0
      FOR CH=1,REGION
       MSUM=MSUM+COUNT(CH)
      END FOR
      MCOUNT=MSUM/REGION
      PRINT*,"MEAN COUNT=",MCOUNT
*     ---MATRIX---
      FOR CH=1,REGION
       POWER=1.0
       XX(CH,1)=1
       FOR K1=2,BGPARA
        XX(CH,K1)=(CH*1.0)**POWER
       EXIT FOR IF(K1.EQ.BGPARA)
        POWER=POWER+1.0
       END FOR
      K1=0
       J=BGPARA
       FOR K=1,PEAKS
        J=J+1
       IF(CH.LT.PARAM(J+1))THEN
        ALPHA=0.0
        ELSE
        ALPHA=1.0
       ENDIF
        XX(CH,BGPARA+K+K1)=EXP(-((CH-PARAM(J+1))**2)/PARAM(J+2))
        IF(CORREC.EQ.0)THEN
        J=J+2
         GOTO 81
         ELSE
        PARAM(J+4)=PARAM(J+1)+SQRT(2*PARAM(J+2))
        ENDIF
       K1=K1+1
        XX(CH,BGPARA+K+K1)=EXP(-((CH-PARAM(J+4))**2)/PARAM(J+2))
        J=J+4
 81    END FOR
 401  END FOR
      ITER=0
      GOTO61
 400  PRINT'(3X,A,10X,A)',"COUNTS","*****MATRIX*****"
      FOR CH=1,REGION
       PRINT*,
     :   CH,COUNT(CH),(XX(CH,J),J=1,PARA)
       END FOR
 61    DO
       LAMDA1=1.0E-5
       LAMDA=LAMDA1
       NU=10
       WNU=0
       IF(ITER.EQ.0)THEN
        KAPPA=0
        ELSE IF(ITER.GE.1.AND.ITER.LE.10)THEN
        KAPPA=KAPPA+0.0010
         ELSE IF(ITER.GT.10.AND.(KAPPA+(ITER-10)/100.0).LT.1.0)THEN
```

```
          KAPPA=KAPPA+(ITER-10)/100.0
         ELSE IF(ITER.GT.10.AND.KAPPA.GE.1.0)THEN
          KAPPA=1.0
         ELSE
          KAPPA=1.0
        ENDIF
*       ---TRANSPOSE OF MATRIX---
        FOR CH=1,REGION
         FOR J=1,PARA
          VI(CH,J)=XX(CH,J)
          XT(J,CH)=XX(CH,J)
         END FOR
        END FOR
        FOR J=1,PARA
         FOR CH=1,REGION
          XTVI(J,CH)=0
         END FOR
        END FOR
        CALL XMATRIX(ECOUNT,PARA,REGION,PARA,J,CH,CH1)
        GOTO 23
*       ---PRINT ARGUMENT---
        FOR J=1,PARA
         PRINT*,(XTVI(J,CH1),CH1=1,PARA)
        END FOR
   23   FOR J=1,PARA
         XTVI(J,PARA+1)=0
        END FOR
        FOR J=1,PARA
         FOR CH=1,REGION
          XTVI(J,PARA+1)=XTVI(J,PARA+1)+XT(J,CH)*COUNT(CH)/ECOUNT(CH)
         END FOR
        END FOR
        GOTO 89
*       ---- SCALING THE AUGMENTED MATRIX ----
   90   IF(ITER.NE.0)THEN
        FOR J=1,PARA
         FOR CH1=1,PARA
          IF(J.NE.CH1)THEN
          XTVI(J,CH1)=XTVI(J,CH1)/SQRT(XTVI(J,J)*XTVI(CH1,CH1))
          ELSE
          ENDIF
         END FOR
         XTVI(J,PARA+1)=XTVI(J,PARA+1)/SQRT(XTVI(J,J))
        END FOR
        ELSE
        ENDIF
   89   LAM=0
*       ---PRINT AUGMENTED MATRIX---
   84   FOR J=1,N
         FOR CH1=1,N+1
          U(J,CH1)=XTVI(J,CH1)
         END FOR
        END FOR
*       ---- MARQUARDT'S ALGORITHM ----
        IF(ITER.NE.0)THEN
        FOR CH1=1,PARA
         U(CH1,CH1)=XTVI(CH1,CH1)+LAMDA
        END FOR
        ELSE
        ENDIF
```

```
$ADD REFINE
        IF(ITER.EQ.0)THEN
        GOTO 28
        ELSE
        FOR J=1,PEAKS*3+CPARA+BGPARA
         IF(LAM.EQ.0.AND.WNU.EQ.0)THEN
          PARAM1(J)=0
          PARAM1(J)=PARAM(J)
          ELSE
         ENDIF
         PARAM(J)=PARAM1(J)+REFINEDX(J)*KAPPA
         IF((J.EQ.1.OR.J.GT.BGPARA).AND.PARAM(J).LT.0)THEN
          PARAM(J)=(SQRT((PARAM(J)**2)))/10.0
          ELSE
         ENDIF
        END FOR
        END IF
        GOTO 29
*       ----INITIAL PARAMETERS----
   28   K=0
        FOR J=1,PEAKS+CORREC+BGPARA
         IF(BGPARA.EQ.1.AND.CORREC.NE.0.AND.(J/2.0).NE.INT(J/2.0).AND.J
     :   .GT.BGPARA+1)THEN
         K=K+2
         ELSE IF(BGPARA.EQ.1.AND.CORREC.NE.0.AND.(J/2.0).EQ.INT(J/2.0)
     :   .AND.J.GT.BGPARA+1)THEN
         K=K+1
         ELSE IF(CORREC.NE.0.AND.(J/2.0).EQ.INT(J/2.0).AND.J.GT.BGPARA+1
     :       .AND.BGPARA.GT.1)THEN
         K=K+2
         ELSE IF(CORREC.NE.0.AND.(J/2.0).NE.INT(J/2.0).AND.J.GT.BGPARA+1
     :     .AND.BGPARA.GT.1)THEN
         K=K+1
         ELSE IF(CORREC.EQ.0.AND.J.GT.BGPARA+1)THEN
         K=K+2
         ELSE
         K=0
         ENDIF
         PRINT*,"J=",J,"REF=",REFINEDX(J),"K=",K
         PARAM(J+K)=REFINEDX(J)
         IF((J.EQ.1.OR.J.GT.BGPARA).AND.PARAM(J+K).LT.0)THEN
          PARAM(J+K)=(SQRT(PARAM(J+K)**2))/10.0
          ELSE
         ENDIF
        END FOR
         PARAM(1)=PARAM(1)/1.0
         IF(BGPARA.EQ.2)THEN
          PARAM(2)=.1000
          ELSE
         ENDIF
        GOTO 29
        PRINT*,"PARAMETERS","ITER=",ITER,"LAM=",LAM,"LAMDA=",LAMDA
        PRINT*,(PARAM(J),J=1,PEAKS*3+CPARA+BGPARA)
   29   FOR CH=1,REGION
         FIT(CH)=0
         BGFIT=0
         PFIT=0
         CPFIT=0
         BGFIT=PARAM(1)
        POWER=1.0
```

```
      FOR K=2, BGPARA
      BGFIT=BGFIT+PARAM(K)*CH**POWER
      EXIT FOR IF(K. EQ. BGPARA)
      POWER=POWER+1. 0
      END FOR
       FOR J=BGPARA+1, PEAKS*3+CPARA+BGPARA
      IF(CH. LT. PARAM(J+1))THEN
       ALPHA=0. 0
       ELSE
       ALPHA=1. 0
      ENDIF
        PFIT=PFIT+PARAM(J)*EXP(-((CH-PARAM(J+1))**2)/PARAM(J+2))
       IF(CORREC. EQ. 0)THEN
       J=J+2
        CPFIT=0
        GOTO 82
        ELSE
       ENDIF
       CPFIT=PARAM(J+3)*EXP(-((CH-PARAM(J+4))**2)/PARAM(J+2))
       J=J+4
82      EXIT FOR IF(J. EQ. PEAKS*3+CPARA+BGPARA)
       END FOR
       FIT(CH)=BGFIT+PFIT+CPFIT
     END FOR
     SUMSQREG=0
     SUMSQM=0
     CHISQ=0
     SUMSQ=0
     FOR CH=1, REGION
      SUMSQREG=SUMSQREG+(FIT(CH)-MCOUNT)**2
      SUMSQM=SUMSQM+(ECOUNT(CH)-MCOUNT)**2
      SUMSQ=SUMSQ+((ECOUNT(CH)-FIT(CH))**2)
      CHISQ=CHISQ+((ECOUNT(CH)-FIT(CH))**2)/ECOUNT(CH)
     END FOR
     RSQ=SUMSQREG/SUMSQM
     IF(ITER. NE. 0)THEN
      EXIT DO IF(SQRT((CHISQ2-CHISQ)**2). LE. PRECIS. AND. ITER. GT. 10. OR.
   :    ITER. EQ. 150)
      IF(LAM. EQ. 0)THEN
       SUMSQ1=SUMSQ
       CHISQ1=CHISQ
       RSQ1=RSQ
       FOR J=1, PEAKS*3+CPARA+BGPARA
        PARAM2(J)=PARAM(J)
       END FOR
       LAMDA=LAMDA1/NU
       LAM=LAM+1
       GOTO 84
      ELSE IF(CHISQ. LE. CHISQ2)THEN
       LAMDA=LAMDA1/NU
       SUMSQ2=SUMSQ
      CHISQ2=CHISQ
       ELSE IF(CHISQ1. LE. CHISQ2)THEN
       LAMDA=LAMDA1
       SUMSQ2=SUMSQ1
       CHISQ2=CHISQ1
       RSQ=RSQ1
      FOR J=1, PEAKS*3+CPARA+BGPARA
       PARAM(J)=PARAM2(J)
      END FOR
```

```
      ELSE IF(CHISQ1.GT.CHISQ2.AND.CHISQ.GT.CHISQ2)THEN
       KAPPA=KAPPA*0.1
       WNU=WNU+2
       LAMDA1=LAMDA1*NU**2.0
       LAMDA=LAMDA1
      EXIT DO IF(LAMDA.GT.1.0E+10)
     GOTO 89
      ELSE
      ENDIF
      ELSE
      SUMSQ2=SUMSQ
     CHISQ2=CHISQ
     ENDIF
    RCHISQ=CHISQ/DF
    GOTO 91
    PRINT*,"**** ITER **** =",ITER
    PRINT*,"WNU=",WNU,"LAMDA=",LAMDA,"KAPPA=",KAPPA
     PRINT*,"BACKGROUND PARAMETERS"
     PRINT*,(PARAM(J),J=1,BGPARA)
     PRINT*,"PEAK PARAMETERS"
 91 FOR K=1,PEAKS
      AREA(K)=PARAM(BGPARA+1+(K-1)*3)*SQRT(2.0*PI)
   :    *SQRT(PARAM(BGPARA+1+(K-1)*3+2)/2.0)
    GOTO 68
    PRINT*,(PARAM(J),J=BGPARA+1+(K-1)*3,BGPARA+(K*3))
   :          ,"AREA",K,"=",AREA(K)
68   END FOR
    GOTO 52
    PRINT*,"COEFFICIENT OF REGRESSION=",RSQ
   :       ,"CHI SQUARED=",CHISQ
    PRINT*,"REDUCED CHISQ=",RCHISQ
52  CALL DERIV(PEAKS,BGPARA,CPARA,REGION,K,J,CH)
    FOR CH=1,REGION
     COUNT(CH)=0
     COUNT(CH)=ECOUNT(CH)-FIT(CH)
     IF(ITER.EQ.FITER)THEN
     PRINT'(3X,I3,3X,2(F10.3,3X),F10.3)',
   :   CH+INITIAL,ECOUNT(CH),FIT(CH),COUNT(CH)
     ELSE
     ENDIF
71  END FOR
    WRITE(3,*)ELEMENT,"ITER=",ITER
    WRITE(3,*)"CHISQ=",CHISQ,"RCHISQ=",RCHISQ
64  PARA=PEAKS*3+CPARA+BGPARA
    N=PARA
    ITER=ITER+1
    UNTIL(ITER.EQ.FITER+1)
     PRINT*,"***** ITER ***** =",ITER
    PRINT*,"WNU=",WNU,"LAMDA=",LAMDA,"KAPPA=",KAPPA
    PRINT*,"BACKGROUND PARAMATERS"
    PRINT*,(PARAM(J),J=1,BGPARA)
    PRINT*,"PEAK PARAMETERS"
    FOR K=1,PEAKS
     PRINT*,(PARAM(J),J=BGPARA+1+(K-1)*3,BGPARA+(K*3))
   :  ,"AREA",K,"=",AREA(K)
    END FOR
    PRINT*,"RSQ=",RSQ,"CHISQ=",CHISQ
    PRINT*,"SUMSQ=",SUMSQ,"RCHISQ=",RCHISQ
    PRINT*,"=========================================================
   :======="
```

```
      END FOR
      WRITE(3,*)"****** PROGRAM COMPLETE ******"
  100 END
      SUBROUTINE XMATRIX(ECOUNT,LIMIT1,LIMIT2,LIMIT3,S1,S2,S3)
      INTEGER LIMIT1,LIMIT2,LIMIT3,S1,S2,S3
      REAL*6 XMAT,MAT1,MAT2,ECOUNT(1:300)
      COMMON/MATRICES/XMAT(1:300,1:300),MAT1(1:300,1:300),
     :   MAT2(1:300,1:300)
      FOR S1=1,LIMIT1
       FOR S3=1,LIMIT3
        XMAT(S1,S3)=0
       END FOR
      END FOR
      FOR S1=1,LIMIT1
       FOR S3=1,LIMIT3
        FOR S2=1,LIMIT2
         XMAT(S1,S3)=XMAT(S1,S3)+MAT1(S1,S2)*MAT2(S2,S3)/ECOUNT(S2)
        END FOR
       END FOR
      GOTO 300
      PRINT*,"S1=",S1
       PRINT*,(XMAT(S1,S3),S3=1,LIMIT2)
  300 END FOR
      END
$ADD GAUSS
      SUBROUTINE DERIV(PEAKS,BGPARA,CPARA,REGION,K,J,CH)
      REAL*6 PARAM,ERRORX,ZO,ZSUM,ZSUMBG,ZSUMP,DELTA,
     :     POWERE,POWERP,ZSUMCP
      INTEGER PEAKS,REGION,K,J,CH,BGPARA,CPARA,K1
      COMMON/DERIVMAT/ZO(1:300,1:70),PARAM(1:70),ERRORX(1:70)
      FOR K=1,PEAKS*3+CPARA+BGPARA
       ERRORX(K)=0
       ERRORX(K)=PARAM(K)
      END FOR
      FOR CH=1,REGION
       FOR J=1,PEAKS*3+CPARA+BGPARA
        ZSUM=0
        ZSUMBG=0
        ZSUMP=0
        ZSUMCP=0
        DELTA=PARAM(J)/500.0
        ERRORX(J)=PARAM(J)+DELTA
       PARAM(J)=PARAM(J)-DELTA
       FOR K1=1,BGPARA
        ZSUMBG=ZSUMBG+ERRORX(K1)-PARAM(K1)
        EXIT FOR IF(K1.EQ.BGPARA)
      IF(BGPARA.EQ.2)THEN
      POWERE=1.0
      POWERP=1.0
      ELSE
       POWERE=ERRORX(K1+2)
       POWERP=PARAM(K1+2)
      ENDIF
       ZSUMBG=ZSUMBG+ERRORX(K1+1)*CH**POWERE
     :    -PARAM(K1+1)*CH**POWERP
       K1=K1+1
       EXIT FOR IF(K1.EQ.BGPARA)
      END FOR
      FOR K=BGPARA+1,PEAKS*3+CPARA+BGPARA
       IF(CH.LT.PARAM(K+1))THEN
```

```
          ALPHA=0.0
          ELSE
          ALPHA=1,0
        ENDIF
          ZSUMP=ZSUMP+ERRORX(K)*EXP(-((CH-ERRORX(K+1))**2)/ERRORX(K+2))
     :    -PARAM(K)*EXP(-((CH-PARAM(K+1))**2)/PARAM(K+2))
          IF(CPARA.EQ.0)THEN
          K=K+2
           ZSUMCP=0
           GOTO 83
           ELSE
          ENDIF
          ZSUMCP=ZSUMCP+ERRORX(K+3)*EXP(-((CH-ERRORX(K+4))**2)
     :    /ERRORX(K+2))
     :    -PARAM(K+3)*EXP(-((CH-PARAM(K+4))**2)/PARAM(K+2))
          K=K+4
   83     EXIT FOR IF(K.EQ.PEAKS*3+CPARA+BGPARA)
         END FOR
         ZSUM=ZSUMBG+ZSUMP+ZSUMCP
        PARAM(J)=PARAM(J)+DELTA
         ERRORX(J)=PARAM(J)
         ZO(CH,J)=ZSUM/(2.0*DELTA)
        END FOR
       END FOR
       END
$MO $ADD=OFF
$VU
LIB *LIBERY
BE
AS 6=*
AS 16=SPDATA
AS 17=SPECOUT
AS 6=*17
$RUN
EOF..
```

```
*     SUBPROGRAM IS CALLED 'REFINE'
*     THIS SUBPRODGRAM SOLVES SIMULTANEOUS EQUATIONS BY
*     THE GAUSSIAN ELIMINATION METHOD AND INCLUDES
*     ITERATIVE REFINEMENT
*     PIVOTAL CONDENSATION IS ALSO INCOPORATED
*     ---STORE MATRIX---
      DO 11 P=1,N
       DO 22 Q=1,N+1
        D(P,Q)=U(P,Q)
   22  CONTINUE
   11 CONTINUE
      SK=0
      N1=N+1
      CALL GAUSS(SK,N1,N,P,Q,P,NN)
*     ---RESTORE ORIGINAL MATRIX---
      DO 227 P=1,N
       X1(P)=X(P)
       DO 228 Q=1,N+1
        U(P,Q)=D(P,Q)
  228  CONTINUE
  227 CONTINUE
*     ---RESIDUAL CALCULATION---
      DO 331 P=1,N
       S1(P)=0
       DO 332 Q=1,N
        S1(P)=S1(P)+U(P,Q)*X1(Q)
  332  CONTINUE
       RESID(P)=U(P,N+1)-S1(P)
  331 CONTINUE
*     ---REPLACE U(N+1) COLUMN WITH RESIDUAL---
      DO 333 P=1,N
       U(P,N+1)=RESID(P)
  333 CONTINUE
*     ---REFINE SOLUTION---
      SK=0
      DO 334 P=1,N
       X(P)=0
  334 CONTINUE
      CALL GAUSS(SK,N1,N,P,Q,P,NN)
      GOTO 41
      PRINT'(1X,A,1X,A,2X,A)',"APPROX SOLUTION","REFINEMENT","SOLUTION"
   41 DO 335 P=1,N
       ERRORX(P)=X(P)
       REFINEDX(P)=X1(P)+ERRORX(P)
      GOTO 335
      PRINT*,X1(P),ERRORX(P),REFINEDX(P)
  335 CONTINUE
*     ---RESTORE MATRIX---
      DO 444 P=1,N
       DO 445,Q=1,N+1
        U(P,Q)=D(P,Q)
  445  CONTINUE
```

```
  444 CONTINUE
      GOTO 78
*     ---NORMALISED DETERMINANT---
      DO 336 P=1,N
       SD(P)=0
       DO 337 Q=1,N
        SD(P)=SD(P)+U(P,Q)**2
  337  CONTINUE
  336 CONTINUE
      DO 338 P=1,N
       DO 339 Q=1,N
        D1(P,Q)=U(P,Q)/SQRT(SD(P))
  339  CONTINUE
  338 CONTINUE
      DO 441 P=1,N
       DO 442 Q=1,N
        U(P,Q)=D1(P,Q)
  442  CONTINUE
  441 CONTINUE
      SK=1
      N1=N
      CALL GAUSS(SK,N1,N,P,Q,P,NN)
      DET=1
      DO 443 P=1,N
       DET=DET*U(P,P)
  443 CONTINUE
   78 DET=DET*(-1)**NN
```

```
      SUBROUTINE GAUSS(SK,N1,N,P,Q,P,NN)
      INTEGER N,N1,NN,SK,P,Q,P1,Q1,G1
      REAL*6 U,D1,X,U1,SP(1:70)
      COMMON/GAUSSMAT/U(1:70,1:71),D1(1:70,1:71),X(1:70)
*     ---INTERCHANGE ROWS---
      NN=0
      DO 44 Q1=1,N
       DO 55 P1=Q1+1,N
        IF (ABS(U(P1,Q1)).GT.ABS(U(Q1,Q1))) THEN
         NN=NN+1
         DO 66 Q=1,N1
          U1=U(Q1,Q)
          U(Q1,Q)=U(P1,Q)
          U(P1,Q)=U1
   66    CONTINUE
        ELSE
         ENDIF
   55  CONTINUE
       IF(SK.NE.1)THEN
*      ---DIAGONALISE & STORE MATRIX---
        DO 77 P=Q1,N
         DO 88 Q=Q1,N+1
          D1(P,Q)=U(P,Q)/U(P,Q1)
   88    CONTINUE
   77   CONTINUE
       ELSE
       DO 99 P=1,N
        DO 112 Q=1,N
         D1(P,Q)=U(P,Q)
  112   CONTINUE
   99 CONTINUE
       ENDIF
*      ---Q1ELIMINATIONS---
       DO 114 G1=Q1+1,N
        DO 115 Q=1,N1
         D1(G1,Q)=U(G1,Q)-U(Q1,Q)*U(G1,Q1)/U(Q1,Q1)
  115   CONTINUE
  114 CONTINUE
*      ---RESTORE MATRIX---
       DO 116 P=1,N
        DO 127 Q=1,N1
         U(P,Q)=D1(P,Q)
  127   CONTINUE
  116 CONTINUE
       GOTO 44
       PRINT*,"ELIMINATION=",Q1
       DO 113 P=1,N
        PRINT*,"P=",P
        PRINT*,(U(P,Q),Q=1,N1)
  113 CONTINUE
   44 CONTINUE
       IF(SK.NE.1)THEN
```

```
*       ---LU DECOMPOSITION---
        FOR P=1,N
         SP(P)=0
         X(P)=0
        END FOR
        FOR P=N,1,-1
         FOR G=N,1,-1
          SP(P)=SP(P)+U(P,G)*X(G)
         END FOR
         X(P)=U(P,N+1)-SP(P)
        END FOR
        GOTO 30
*       ---REDUCTION---
*       ---STORE MATRIX---
     24 DO 117 P=1,N
         DO 118 G=1,N1
         D1(P,G)=0
          D1(P,G)=U(P,G)
    118  CONTINUE
    117 CONTINUE
        DO 119 G1=1,N-1
         DO 221 P=1,N-G1
          DO 222 G=1,N+1
           D1(P,G)=U(P,G)-U(P,P+G1)*U(P+G1,G)
    222   CONTINUE
    221  CONTINUE
*       ---RESTORE MATRIX---
         DO 223 P=1,N
          DO 224 G=1,N1
         U(P,G)=0
           U(P,G)=D1(P,G)
    224   CONTINUE
         X(P)=U(P,N+1)
    223  CONTINUE
    119 CONTINUE
        GOTO 30
        PRINT*,"REDUCTION"
        DO 225 P=1,N
         PRINT*,"P=",P
         PRINT*,(U(P,G),G=1,N1)
    225 CONTINUE
        GOTO 30
        DO 226 P=1,N
         PRINT*,"X(P)=",X(P),"P=",P
    226 CONTINUE
        ELSE
     30 ENDIF
         RETURN
         END
EOF..
```

APPENDIX E

PUBLICATIONS

CONTENTS

Page

Nuclear Instruments and Methods 181 (1981) 5–9

THIN TARGET MEASUREMENTS OF PROTON INDUCED L-SHELL X-RAY CROSS-SECTIONS

R.S. SOKHI and D. CRUMPTON
Physics Department, University of Aston in Birmingham, Gosta Green, Birmingham, B4 7ET, England

Measurements have been made of the L X-ray production from Te, Dy, and Au. Thin targets have been employed and the L X-ray yields measured as a function of proton energy up to 3 MeV. From these measurements the total, and where appropriate the individual X-ray line cross-sections have been calculated and compared with the experimental results reported by other authors and with the plane-wave Born approximation with and without binding energy and Coulomb deflection corrections.

1. Introduction

The measurement of L-shell cross-sections is important for two main reasons. Firstly, there is a need for a reliable set of L-shell cross-section data for analytical work involving high atomic number elements, and secondly such measurements provide a means of testing the validity of current theories on inner-shell ionization by charged particles. These reasons have resulted in considerable work in this field [1–5]. Earlier work on thick target L-shell cross-section measurements performed at this laboratory has been reported in a previous publication [6]. The present paper reports on thin target measurements of L-shell production cross-sections for Te and Dy using protons of 0.6–3 MeV energy and for Au in the proton energy range of 1.1–3 MeV. Cross-section ratios $\sigma_{(L\alpha/L\beta)}$, $\sigma_{(L\alpha/L\gamma)}$ and $\sigma_{(L\alpha/Ll)}$ have also been determined for Dy and Au. The experimental data is compared with the PWBA theory, with and without binding energy and Coulomb deflection corrections, and with measurements reported by other authors. The need for an accurate set of related data, such as mass attenuation coefficients, fluorescence yields and Coster–Kronig transitions required for experimental and theoretical calculations is discussed.

2. Procedure

2.1. Experimental

A proton beam from the 3 MV Dynamitron accelerator at the Birmingham Radiation Centre was collimated to 1.5 mm diameter and directed on to thin targets placed at 45° to the beam axis. Target thicknesses typically 50 μg/cm² were employed in order to avoid self absorption corrections. A Si(Li) detector with a resolution of 164 eV at 5.898 keV was placed at 90° to the beam axis to detect the characteristic X-rays. The X-rays passed through a 50 μm thick melinex window, 3.2 cm air gap and 12.4 μm thick beryllium detector window before reaching the detector. Beam currents up to 10 nA were used and were measured using a Faraday cup and a Keithley electrometer. The signals from the detector were processed by a pulsed optical feedback preamplifier and then by a spectroscopy amplifier. The shaped pulses were then fed into a 200 MHz ADC of a Hewlett–Packard 5406A computer system which was employed for the data handling.

The L_α, L_β and L_γ lines were only resolved for Dy and Au and X-ray counts under the peaks were accumulated until the counts associated with the L_γ line, the least intense peak of the three, were 200 or more. The background counts under the L_α and L_β peaks were negligible compared with characteristic counts under the appropriate peak. For the L_γ peak the background was no more than 6% of the characteristic L_γ counts. X-ray yields in photons per proton, Y_{Li}, were measured for the individual lines for Dy and Au. The lines were unresolved for Te and hence the total of the characteristic counts was converted into X-ray yield. Measurements of the X-ray yield were performed in steps of 100 keV at the lower and higher energy region and every 200 keV in the middle energy region to establish the energy dependence accurately.

2.2. Theoretical

The individual L-shell production cross-sections, σ_{Li}, for Dy and Au were derived from the appropriate X-ray yields by employing the following expression:

$$\sigma_{Li} = \frac{Y_{Li} A\ 4\pi}{N C_i\ \mathrm{d}\Omega(\rho t)\ \epsilon_i}\ , \quad (i = \alpha, \beta, \gamma, l)\ , \qquad (4)$$

where A is the atomic weight of the target, N is Avogadro's number, $\mathrm{d}\Omega$ is the detector solid angle, (ρt) is the areal density of the target, ϵ_i is the intrinsic efficiency of the Si(Li) detector and C_i represents the total absorption correction factors for melinex, air and beryllium. Absorption corrections and the detector efficiency were weighted with the appropriate L X-ray relative intensities. These values and any additional data required for the calculation of C_i and ϵ_i were extracted from the tabulations by Storm and Israel [7]. The total L-shell production cross-section, σ_{Lx}, was obtained by summing the individual cross-sections, that is,

$$\sigma_{Lx} = \sigma_{L\alpha} + \sigma_{L\beta} + \sigma_{L\gamma} + \sigma_{Ll} . \qquad (2)$$

For Te, Y_{Li} represents the total X-ray yield in photons per proton and in this case expression (1) gives the total production cross-sections.

Theoretical values of the total and individual cross-sections for L_α, L_β, L_γ and L_l lines were determined by using the relationships given by Tawara et al. [8]. The values for fluorescence yields and Coster–Kronig transitions were taken from the tables published by Krause [9]. The values for radiative widths were extracted from the tabulation by Scofield [10]. The tabulation of the PWBA calculation by Benka and Kropf [11] was employed to derive the individual subshell ionization cross-sections. Binding energy and Coulomb deflection corrections were calculated from the expressions given by Brandt and Lapicki [12].

3. Experimental uncertainties

The sources of uncertainties associated with measured cross-sections are: (1) the counting statistics, 1–10%, (2) the target thickness, 5% (quoted by the manufacturers), (3) the solid angle, 2% (4) the current measurement, 1% and (5) the absorption corrections and detector efficiency calculations, 6–18%.

The errors in the counting statistics are only important for the L_γ and L_l peaks. The maximum background under the L_γ and L_l peaks was 6% and 8% of the characteristic counts respectively. This gives a maximum error of 7.5% and 11% in the counts associated with the L_γ and L_l peaks respectively. Factors (2), (3) and (4) appear in the calculations systematically and hence are eliminated in the calculation of the cross-section ratios. The errors in the absorption corrections were due to the uncertainties in the mass-absorption coefficients tabulated by Storm and Israel. They quote an error of 10% for X-ray energies less than 6 keV and 3% for higher enegies. The large uncertainty at the low X-ray region introduces an 18% error in the absorption correction for Te. In the case of Dy and Au this error is reduced to 6% since the X-ray energies are greater than 6 keV. A large error in the mass absorption coefficient, at low X-ray energies, however, introduces no significnat uncertainty in the detector efficiency. Also in this X-ray energy range (3.8–13.4 keV) variation in the silicon crystal thickness has negligible effect on the efficiency calculation.

The total experimental uncertainty in σ_{Lx} for Te was calculated to be 19% for the whole proton energy range. The combined error in σ_{Lx}, associated with eq. (2) varied from 16% for energies above 1 MeV for Dy and 1.4 MeV for Au, to 21% for lower energies. The total uncertainties in $\sigma_{L\alpha}$ and $\sigma_{L\beta}$ for both elements were about 8%. For $\sigma_{L\gamma}$ the total error was determined to be 8% for energies above 1 MeV for Dy and 1.4 MeV for Au. Below these energies the uncertainties increased to 11%. For the σ_{Ll} the final error was 9% but increased to 11% below 1 MeV for Dy and 1.6 MeV for Au.

The total uncertainty in the $\sigma_{(L\alpha/L\beta)}$ ratio remained 9% throughout the energy range. In the case of the $\sigma_{(L\alpha/L\beta)}$ ratio the uncertainty increased from 9% to 11% at energies below 1 MeV for Dy and 1.4 MeV for Au. The weighted mean of the $\sigma_{(L\alpha/Ll)}$ ratio was determined to a precision of 3% for both elements.

4. Theoretical discrepancies

The use of the tabulated data [9,11] employed in this study has not been reported recently by any other author. This would probably introduce discrepencies between the present PWBA calculations and those reported by other authors [4,6] using less up-to-date data [16,17]. The marked differences between the different sets of data is most obvious in the case of fluorescence yields and Coster–Kronig transitions. Krause [9] estimates the uncertainties in his tabulations to be from 3% to 20% in atomic number range of 50–80. Similar uncertainties are quoted by McGuire [16] in his data of fluorescence yields and Coster–Kronig transitions. McGuire also points out the gross differences in experimental and theoretical values. Apart from these internal discrepancies there are large differences between the two sets of data. In the case of Au, for example, the Coster–Kronig transitions differ by nearly 50%. Similar discrepancies occur in the case of other elements. Using the two sets of data independently in the PWBA calculations will obviously yield very different results for the cross-sections. This makes the comparison of experimental data with theoretical prediction more difficult. In light of these discrepancies much care has to be taken when comparing the extent of experimental to theoretical agreement with the work of other authors.

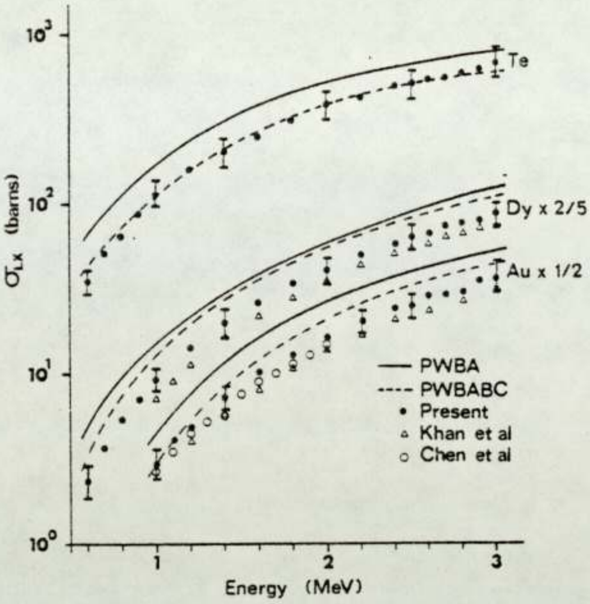

Fig. 1. Total L X-ray production cross-section as a function of proton energy. Bars represent typical uncertainties.

5. Results and discussion

The excitation functions for Te, Dy and Au are presented in fig. 1. For all three elements the experimental data generally lies below the theoretical predictions. For Te the difference between the experimental and the PWBA values increases from 17% at 3 MeV to nearly 90% at lower energies. The binding energy and the Coulomb deflection corrections (BC) greatly reduces the disagreement to below 12% for energies above 1.8 MeV and below 21% at lower proton energies. For Dy the BC correction is only about 3% at higher energies but increases to nearly 45% at lower enegies. The agreement with the PWBABC is not better than 25%. Similar characteristics are shown by Au where the BC correction is about 35% at lower energies and the difference between the experimental data and PWBABC varies from 13% to 35% at energies around 1.1 MeV. The present data for Dy and Au lies 18–25% above the data reported by Khan et al. [6] but agrees within experimental uncertainties with the data obtained by Chen et al. [14].

To eliminate systematic uncertainties the ratios $\sigma_{(L\alpha/L\beta)}$ and $\sigma_{(L\alpha/L\gamma)}$ were calculated and are presented in figs. 2 and 3 as a function of proton energy. The data for $\sigma_{(L\alpha/L\beta)}$ decreases slowly with increasing energy as predicted by the PWBA theory. The present data lies systematically higher than the data obtained by Khan et al. [6] by about 5% for Dy and Au. This difference, however, is within the experimental error. For Au, closer agreement is shown by the data published by Tawara et al. [4]. The BC corrections for Au are important throughout the energy range where as for Dy the corrections are negligible at energies above 1 MeV. The experimental $\sigma_{(L\alpha/L\gamma)}$ ratio for Dy shows a less sharp increase with decreasing energy than predicted by the PWBA. The predicted maximum for Dy at 0.75 MeV was not observed. The sparse data of Close et al. [13] is well within the experimental errors while the data obtained by Khan et al. [6] differs by up to 20%. The

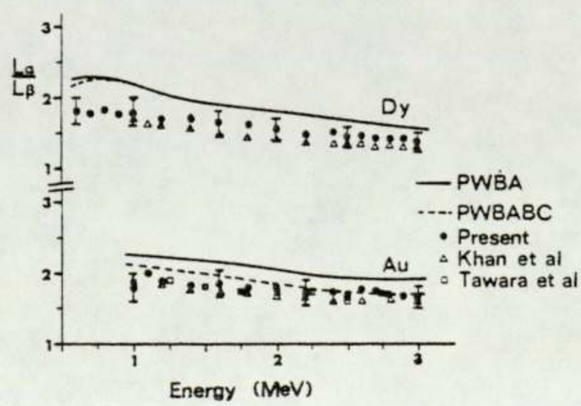

Fig. 2. $\sigma_{(L\alpha/L\beta)}$ ratio as a function of proton energy.

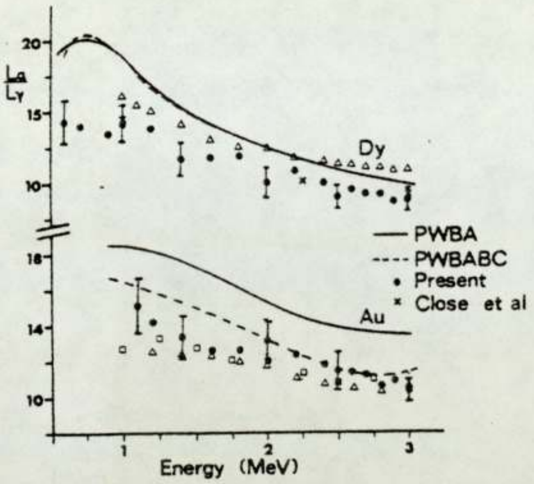

Fig. 3. $\sigma(L\alpha/L\gamma)$ ratio as a function of proton energy.

$\sigma_{(L\alpha/L\gamma)}$ ratio for Au remains in good agreement with the PWBABC till about 2 MeV, below which the experimental data deviates markedly. Generally the data by Khan et al. [6] and Tawara et al. [4] lie within the experimental errors but deviate at lower energies by about 20%.

The $\sigma_{(L\alpha/Ll)}$ ratios were also measured and are presented in table 1. The $\sigma_{(L\alpha/Ll)}$ ratios are independent of the proton energy because the L_α and L_l transitions are to the same subshell, L_{III}. The experimental values were also found to be constant throughout the energy range. The values for Dy differ from the predicted values by 12% but the predicted ratio for Au lies within the experimental uncertainty. The value for Dy agrees with that obtained by Khan et al. [6] but differs from the value quoted by Abrath [15] by 33%. Exact agreement is found for Au with the value obtained by Khan et al. [6]. The present value lies within the experimental uncertainties quoted by Tawara et al. [4] and Chen et al. [14].

Table 1

$\sigma(L\alpha/Ll)$ ratio. Numbers in ( ) represent % errors.

Element	Theory	Experimental			
		Present	Others		Ref.
Dy	23.7	26.7 (3)	27 (7)	Khan	6
			19 (14)	Abrath	15
Au	19.9	20.3 (3)	20.3 (3)	Khan	6
			18.9 (8)	Tawara	4
			19.7 (5)	Chen	14

6. Conclusion

Reasonable agreement was observed with the previous thick target results obtained by Khan et al. [6] at this laboratory. However, in some areas disagreements do exist.

Generally the differences between the theoretical and experimental values cannot be explained in terms of the experimental uncertainties alone. This highlights the need for more detailed experimental and theoretical studies.

Discrepancies also exist between fluorescence yields and Coster–Kronig transitions published by different authors [9,16].

Errors in the absorption corrections introduce serious uncertainties in the cross-section values. This is mainly due to the lack of reasonably accurate mass absorption coefficient data especially at low X-ray energies. Hubble et al. [18] have also reported serious systematic uncertainties in the absorption correction caused by the large errors in the mass absorption coefficients.

Because of the above problems the accuracy of the X-ray cross-section calculation suffers heavily. This makes detailed comparison of theoretical and experimental data very difficult.

We are most grateful to the staff at the Birmingham Radiation Centre for their assistance with the experimental work. One of us (R.S.S.) also wishes to thank the Science Research Council for supporting this work.

References

[1] Proc. Int. Conf. on Particle induced X-ray emission and its analytical applications, Nucl. Instr. and Meth. 142 (1977).
[2] C.E. Busch, A.B. Baskin, P.H. Nettles, S.M. Shafroth and A.W. Waltner, Phys. Rev. A7 (1973) 1601.
[3] T.J. Gray, G.M. Light, R.K. Gardner and F.D. McDanield, Phys. Rev. A12 (1975) 2393.
[4] H. Tawara, K. Ishii, S. Morita, H. Kaji and T. Shiokawa, Phys. Rev. A11 (1975) 1560.
[5] E.L.B. Justiniano, A.A.G. Nader, N.V. de Castro Faria, C.V. Barros Leite and A.G. de Pinho, Phys. Rev. A21 (1980) 73.
[6] Md R. Khan, A.G. Hopkins and D. Crumpton Z. Physik A288 (1978) 133.

[7] E. Storm and H.I. Israel, Nucl. Data Tables A7 (1970) 565.
[8] H. Tawara, K. Ishii, S. Morita, H. Kaji, C.N. Shu and T. Shiokawa, Phys. Rev. A9 (1974) 1617.
[9] M.O. Krause, J. Phys. Chem. Ref. Data 8 (1979) 307.
[10] J.H. Scofield, At. Data Nucl. Data Tables 14 (1974) 121.
[11] O. Benka and A. Kropf, 22 (1978) 219.
[12] W. Brandt and G. Lapicki, Phys. Rev. A10 (1974) 474.
[13] D.A. Close, R.C. Bearse, J.J. Malanify and C.J. Umbarger, Phys, Rev. A8 (1973) 1873.
[14] J.R. Chen, J.D. Reber, D.J. Ellis and T.E. Miller, Phys. Rev. A13 (1976) 941.
[15] F. Abrath and T.J. Gray, Phys. Rev. A9 (1974) 682.
[16] E.J. McGuire, Phys. Rev. A3 (1971) 587.
[17] B.H. Choi, E. Merzbacher and G.S. Khandelwal. At. Data 5 (1973) 291.
[18] J.H. Hubbie, W.H. McMaster, N. Ker Del Grande and J.H. Mallet, International tables for X-ray crystallography, Vol. 4 (1974) p. 47.

Nuclear Instruments and Methods 192 (1982) 121–127
North-Holland Publishing Company

MEASUREMENT OF PROTON-INDUCED L-SHELL X-RAY PRODUCTION CROSS-SECTIONS AND THEIR COMPARISON WITH THEORY

R.S. SOKHI and D. CRUMPTON
Department of Physics, University of Aston, Birmingham B4 7ET, England

Thin targets of Dy and Pb were bombarded by protons of energy up to 3 MeV and the L-shell X-rays observed were measured as a function of proton energy. The individual X-ray production cross-sections have been derived from these measurements. These, and the cross-section ratios, have been compared with the results reported by other workers and with the CPSSR theory.

1. Introduction

It is clear from the content and number of recent papers [1] on proton-induced X-ray emission (PIXE) analysis that the technique is making a significant contribution to the solution of many analytical problems in a variety of disciplines. Arising out of this has been an increasing requirement for a knowledge of accurate K and L shell proton-induced X-ray production cross-section data. Accurate data is also required for comparison with the predictions of current theories of inner-shell ionization by light ions, in which there is currently considerable interest [2].

In this paper we report on the measurements we have made on the L X-ray emission from thin targets of dysprosium and lead for protons in the energy range 0.6–3 MeV. From these yields the cross-sections $\sigma_{L\alpha}$, $\sigma_{L\beta}$, $\sigma_{L\gamma}$ and σ_{Ll} have been derived together with the cross-section ratios $(\sigma_{L\alpha}/\sigma_{L\beta})$, $(\sigma_{L\alpha}/\sigma_{L\gamma})$ and $(\sigma_{L\alpha}/\sigma_{Ll})$. These measurements were made as part of a comprehensive programme of K and L shell cross-section measurements undertaken at Aston over the last few years [3–5]. The results are compared with the CPSSR theory of Brandt and Lapicki [6].

2. Experimental arrangement

The details of the experimental arrangement have been briefly reported in a previous communication [7]. A beam of energetic protons from the Universities 3 MV Dynamitron accelerator was allowed to impinge on thin targets of dysprosium and lead mounted on a multiple target holder which positioned the targets sequentially at 45° to the incoming beam. Targets employed had areal densities of typically 50 μg/cm^2 and were deposited on polycarbonate backings of areal density 1 mg/cm^2. The diameter of the targets employed was 1 cm. The proton beam was collimated to give a beam spot of less than 1.5 mm diameter so that the geometry with respect to the X-ray detector could be accurately controlled. Beam currents employed were limited to a few nanoampere thus limiting the current density and preventing target damage. The target chamber was isolated and acted as a Faraday cup so that the current could be accurately measured using a Keithley electrometer. The measured currents were checked from time to time against a calibrated Ortec current digitizer.

The X-rays emerged from the target chamber at 90° to the beam direction and passed through a 50 μm thick melinex window, 3.2 cm air gap and a 12.4 μm thick beryllium detector window before reaching the detector. The Si(Li) detector employed had a working resolution of 164 eV at 5.898 keV and the output from the associated pulsed optical amplifier system was fed to a 200 MHz ADC of a Hewlett–Packard data acquisition and computer system.

An accurately defined aperture was positioned in front of the detector to define the detection solid angle and to ensure that the X-rays im-

0029-554X/82/0000–0000/$02.75

pinged only on the centre of the active area of the silicon crystal. The effective active area of the detector was obtained by scanning a highly collimated X-ray beam across the detector and recording the detector response. The active area was found to be in good agreement with the manufacturers quoted value. In selecting the aperture diameter to define the detection solid angle, due allowance was made for the fact that the detector was positioned several mm's behind the beryllium window. This distance was determined by recording the response of the detector to a point source of X-rays as a function of source–detector separation and then making a $1/r^2$ plot in the usual manner.

3. Measurements

Measurements of the X-ray yield were performed from 0.6 to 3 MeV for dysprosium and from 0.9 to 3 MeV for lead, in steps of 100 keV at the lower and higher energies and every 200 keV in the middle energy region to establish the energy dependence. The L_α, L_β, L_γ, and L_l lines were readily resolved as can be seen in fig. 1, which shows a typical lead spectrum generated by 3 MeV protons. The X-ray accumulation time was selected so that the areas under the L_γ peak in the spectrum was at least 200. The area under each peak was obtained using an appropriate software routine to remove the background and integrate the peaks. The background counts under the L_α and L_β peaks were negligible in comparison with the characteristic count. For the L_γ peak, backgrounds were typically 3% for lead and 6% for dysprosium.

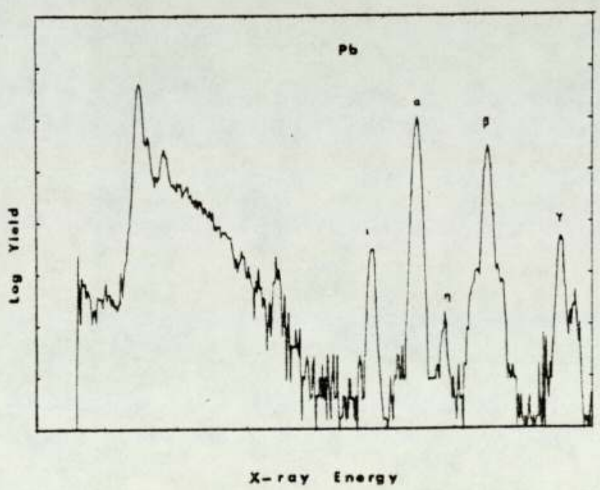

Fig. 1. Typical Pb L-shell X-ray spectrum produced by 3 MeV protons.

Assuming isotropic emission of the radiation the individual L-shell X-ray production cross-sections, σ_{Li}, were derived from the appropriate X-ray yield per proton, Y_{Li}, at a proton energy E using the relationship:

$$\underset{(i=\alpha,\beta,\gamma,l)}{\sigma_{Li}(E)} = \frac{Y_{Li}(E) A 4\pi}{N_A(\rho t)\,d\Omega C_i \varepsilon_i}, \qquad (1)$$

where A is the atomic weight of the target, N_A is Avogadro's number, $d\Omega$ is the detection solid angle, (ρt) is the areal density of the target, ε_i is the intrinsic efficiency of the Si(Li) detector and C_i represents the total absorption correction factors for melinex, air and beryllium. The mass absorption coefficients employed in the calculation of the absorption corrections and the detector efficiency for each Li X-ray peak were extracted from the tabulation by Storm and Israel [8]. As each of the Li peaks is composed of two or more X-ray lines the absorption coefficients were weighted by the appropriate relative L X-ray line intensities to allow for the hardening of the X-ray spectrum produced by absorption.

4. Experimental uncertainties

The uncertainties associated with each of the derived L-shell X-ray production cross-sections, σ_{Li}, are as follows:
(1) the counting statistics associated with the area of each X-ray peak, 1–10%; (2) the beam current measurement, 1%; (3) the detection solid angle, 2%; (4) the target thickness, 5%, as quoted by the suppliers; (5) the absorption corrections and detector efficiency calculations, 6%; and (6) the proton energy.

In the X-ray energy region of interest, 6.4–14.8 keV, the uncertainty in the mass absorption coefficients quoted by Storm and Israel [8] is 3%. This introduces no significant uncertainty in the intrinsic detector efficiency, neither does any variation in the silicon crystal thickness.

The energy calibration of the Dynamitron, which is performed regularly, is known to be better than 2 keV. This introduces an uncertainty of less than 1% even at low proton energies.

The uncertainties in the first two parameters are random. However, for a particular element although the errors in the parameters (3), (4) and (5) appear systematically in the σ_{L_l} calculations, the errors in these parameters are actually random in nature. The uncertainties were therefore, treated as random errors and hence combined quadratically. The total uncertainty in $\sigma_{L\alpha}$ and $\sigma_{L\beta}$ for both elements was 6–8%. For $\sigma_{L\gamma}$ and σ_{Ll} the uncertainties were estimated to be about 8% for energies above 1 MeV, and increasing to 12% below 1 MeV. In general the uncertainties for lead were lower than those for dysprosium by 1–2%.

In the determination of the cross-section ratios the beam current, target thickness and detection solid angle are eliminated together with their uncertainties. The uncertainty in the $(\sigma_{L\alpha}/\sigma_{L\beta})$ ratio was estimated to be about 8% for lead and 10% for dysprosium throughout the energy range employed. For the $(\sigma_{L\alpha}/\sigma_{L\gamma})$ and $(\sigma_{L\alpha}/\sigma_{Ll})$ ratios the uncertainties ranged from 9% and 10%, respectively at 3 MeV to 12–14% at energies below 1 MeV.

5. Results and discussion

The individual L-shell X-ray production cross-sections derived from the measurements are tabulated in table 1 and graphically presented in figs. 2 and 3 with the predictions of the CPSSR theory.

The theoretical values for the individual cross-sections $\sigma_{L\alpha}$, $\sigma_{L\beta}$, $\sigma_{L\gamma}$ and σ_{Ll} were determined by using the relationships given by Tawara et al. [9] relating the sub-shell ionization cross-sections σ_{LI}, σ_{LII} and σ_{LIII} to the production cross-sections, namely

$$\sigma_{L\alpha} = (\sigma_{LI}f_{13} + \sigma_{LI}f_{12}f_{23} + \sigma_{LII}f_{23} + \sigma_{LIII})\omega_3 F_{3\alpha}\ ; \quad (2)$$

$$\sigma_{L\beta} = \sigma_{LI}\omega_1 F_{1\beta} + (\sigma_{LI}f_{12} + \sigma_{LII})\omega_2 F_{2\beta} + (\sigma_{LI}f_{13} + \sigma_{LI}f_{12}f_{23} + \sigma_{LII}f_{23} + \sigma_{LIII})\omega_3 F_{3\beta}\ ; \quad (3)$$

$$\sigma_{L\gamma} = \sigma_{LI}\omega_1 F_{1\gamma} + (\sigma_{LI}f_{12} + \sigma_{LII})\omega_2 F_{2\gamma}\ ; \quad (4)$$

$$\sigma_{Ll} = (\sigma_{LI}f_{13} + \sigma_{LI}f_{12}f_{23} + \sigma_{LII}f_{23} + \sigma_{LIII})\omega_3 F_{3l}\ . \quad (5)$$

The values of sub-shell fluorescent yields ω_1, ω_2 and ω_3 and the Coster–Kronig yields f_{12}, f_{13} and

Table 1
L-shell X-ray production cross-sections in barns. Numbers in parenthesis represent % uncertainties, which also refer to the lines below, unless stated otherwise.

	Dy				Pb			
E (MeV)	L_α	L_β	L_γ	L_l	L_α	L_β	L_γ	L_l
0.6	3.6 (8)	2.0 (8)	0.25 (12)	0.11 (13)				
0.7	5.5	3.1	0.39	0.22				
0.8	8.0	4.4	0.78	0.34				
0.9	10.7	6.1	0.78	0.30	1.8 (6)	0.91 (6)	0.12 (10)	0.12 (12)
1.0	14	7.9	1.0 (8)	0.35 (9)	2.4	1.3	0.16	0.13
1.1	–	–	–	–	3.2	1.7	0.22	0.20
1.2	20	12	1.6	1.1	4.0	2.1	0.30	0.27
1.4	29	17	2.6	1.0	6.0	3.3	0.45 (7)	0.35 (9)
1.6	38	23	3.3	1.3	8.6	4.6	0.72	0.47
1.8	48	30	4.2	1.8	11.2	5.9	0.97	0.61
2.0	56	36	5.7	2.0	13.9	8.0	1.2	0.68
2.2	68	47	6.4	2.6	19	10.6	1.7	1.0
2.4	80	54	8.1	2.9	23	13.2	1.9	1.2
2.5	86	61	9.6	3.1	25	13.7	2.1	1.3
2.6	90	63	9.3	3.3	27	15	2.2	1.4
2.7	98	70	10.8	3.8	29	17	2.6	1.6
2.8	102	72	11.2	4.1	30	18	2.9	1.7
2.9	106	76	12	3.9	33	19	2.7	2.3
3.0	115	85	13	4.2	35	21	3.3	1.9

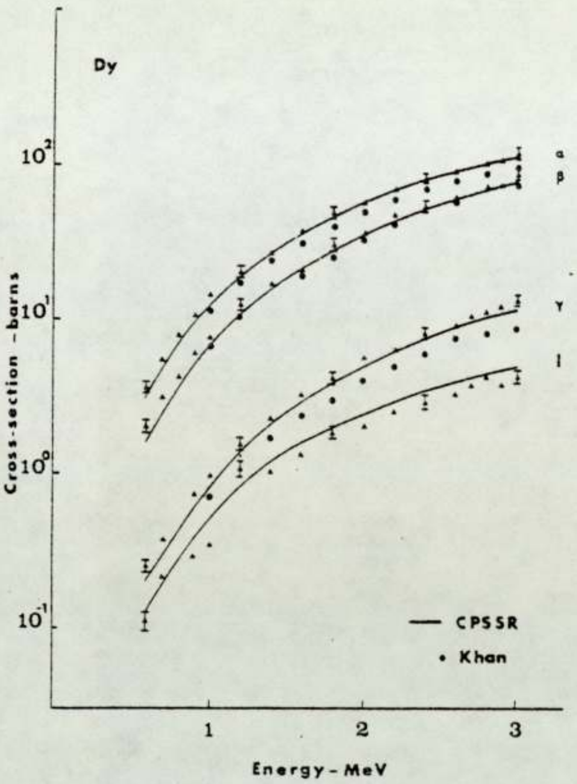

Fig. 2. L-shell X-ray production cross-sections for Dy as a function of proton energy. Bars represent typical uncertainties. Triangles: present work, circles: Khan [5] and solid line: CPSSR [6].

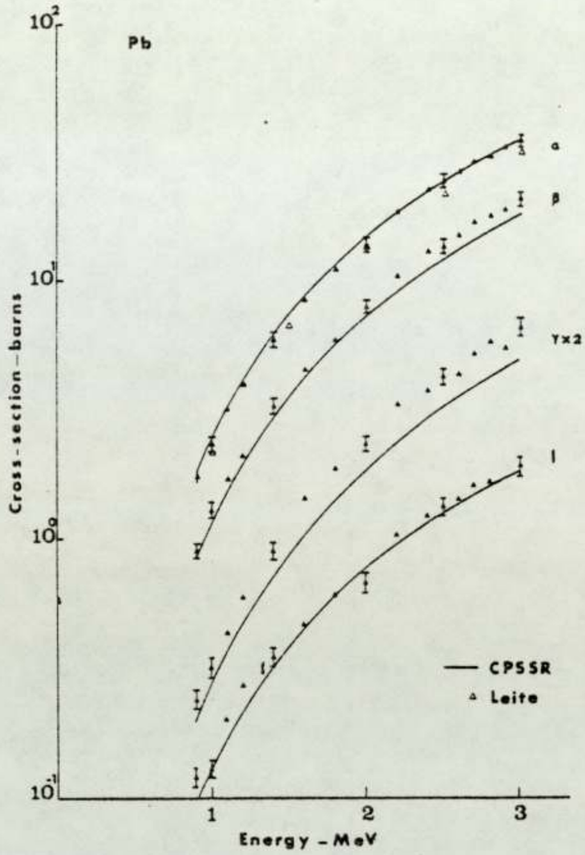

Fig. 3. L-shell X-ray production cross-sections for Pb as a function of proton energy. Solid triangles: present work, open triangles: Leite [14] and solid line: CPSSR [6].

f_{23} were taken from the internally consistent set of best values presented in the recent publication by Krause [10]. The relative radiative widths F were extracted from the compilation of Scofield [11]. The L-subhsell ionization cross-sections were obtained from the CPSSR theory in the manner described by Brandt and Lapicki [6] using the tabulations of Benka and Kropf [12]. Due to the discrepancies that exist in the fluorescent yields and Coster–Kronig yields care must be taken in making comparisons with the experimental work of other authors and theory, as previously discussed [7].

In the energy range 0.9–3 MeV the CPSSR predictions of $\sigma_{L\alpha}$ are in excellent agreement with the experimental data of both lead and dysprosium. In the case of dysprosium, however, below 1 MeV the data lie systematically above the predicted values. Also there is good agreement in the energy region 1.2–3 MeV between the $\sigma_{L\beta}$ data and theory and a measure of agreement in the 1.8–2.6 MeV region for the $\sigma_{L\gamma}$. The data for $\sigma_{L\beta}$ and $\sigma_{L\gamma}$ cross-sections for lead lie systematically above the predictions of the theory. In the case of the σ_{Ll} cross-sections there is reasonable agreement between the lead data and the theoretical predictions, the dysprosium data, however, lie below the predictions above 1.2 MeV by some 14%. Below 1.2 MeV the statistics associated with the data are rather poor and data is scattered above and below the predicted line.

The $\sigma_{L\alpha}$, $\sigma_{L\beta}$ and $\sigma_{L\gamma}$ data for dysprosium derived from a study of thick targets and reported previously by Khan et al. [5] lie systematically below the present data. This discrepancy may be related in a systematic way to the specific energy loss which is required for thick target measurements and clearly warrants further investigations.

For lead the graphical data of Gray et al. [13]

for $\sigma_{L\alpha}$ appears to be in agreement with the present data, while the tabulated data of Leite et al. [14] is lower than the present data at 3 MeV by 11% but agrees within experimental uncertainty at 1 and 2 MeV. Also included in the tabulation of Leite et al. [14] are the values at 1 and 3 MeV of Bearse et al. [15] and interpolated values at 2 and 3 MeV from the data of Tawara et al. [9]. The values of Bearse et al. [15] are about 25% below the present values while the data of Tawara is 6% higher at 2.0 MeV and 9% lower at 3 MeV.

The measured cross-section ratios $(\sigma_{L\alpha}/\sigma_{L\beta})$ are shown in fig. 4 together with theoretical predictions and the measurements of other authors. The ratios decrease slowly with increasing energy as predicted by the theory and are in agreement with other measurements. The data for lead are, however, 7–10% lower than predicted by the CPSSR theory.

The dysprosium and lead data for the cross-section ratios $(\sigma_{L\alpha}/\sigma_{L\gamma})$ follow the energy dependence predicted by the CPSSR as shown in fig. 5, but lie systematically below the predictions. The ratio obtained for dysprosium is in reasonable agreement with the sparse data of Close et al. [16] but is less than the data of Khan et al. [5]. The results of Close et al. [16], however, have only been presented graphically

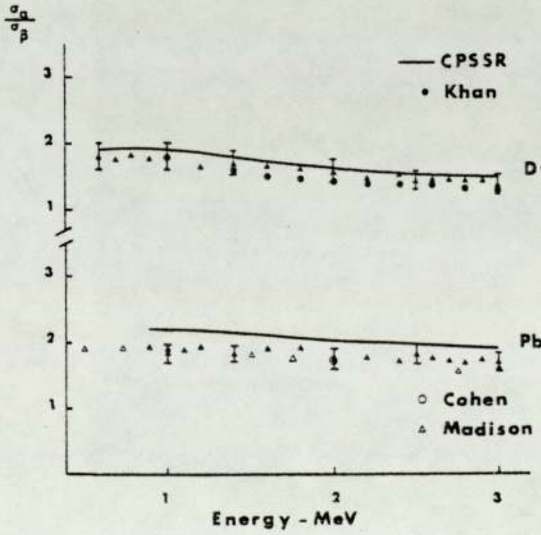

Fig. 4. $(\sigma_{L\alpha}/\sigma_{L\beta})$ ratio as a function of proton energy. Solid triangles: present work, open circles: Cohen [19], open triangles: Madison [18], solid line: CPSSR [6] and solid circles: Khan [5].

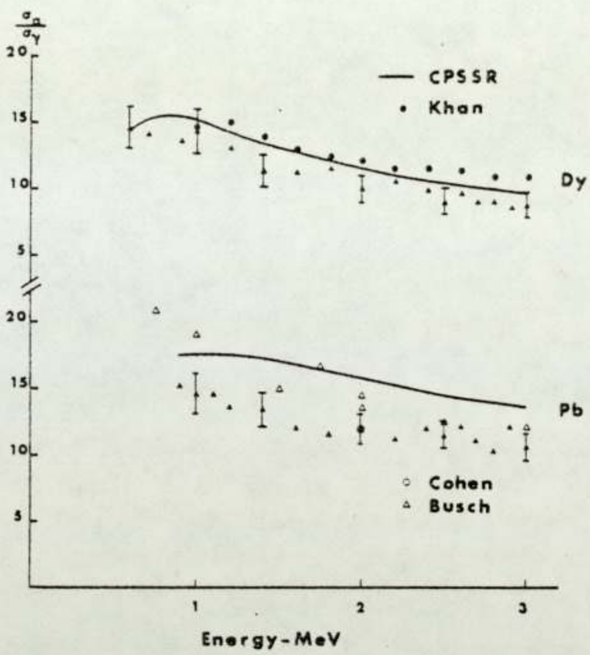

Fig. 5. $(\sigma_{L\alpha}/\sigma_{L\gamma})$ ratio as a function of proton energy. Solid triangles: present work, open circles: Cohen [19], open triangles: Busch [20], solid circles: Kahn [5] and solid line: CPSSR [6].

in their paper and hence have not been plotted in fig. 5. The precision of the present measurements was such that the theoretically predicted maximum at 0.75 MeV could not be confirmed. The values tabulated by Busch et al. [18] for lead are typically 10–30% higher than the present data, however, the value at 2 MeV reported by Cohen [19] agrees with the present data.

In the case of the $(\sigma_{L\alpha}/\sigma_{Ll})$ ratio a third order polynomial of the form

$$\ln(\sigma_{Ll}) = \sum_{i=0}^{3} K_i[\ln(E)]^i,$$

where K_i are constants and E is the proton energy, was fitted to the σ_{Ll} data for both elements. This was necessary because of the scatter in the σ_{Ll} data at low proton energies, due solely to the poor statistics. The ratios were calculated using the σ_{Ll} values predicted by the polynomials. Within experimental uncertainties the $(\sigma_{L\alpha}/\sigma_{Ll})$ ratios were found to be independent of energy as predicted by theory. The weighted mean values for $(\sigma_{L\alpha}/\sigma_{Ll})$ for dysprosium and lead are given in table 2 together with the results

Table 2
Cross-section ratio ($\sigma_{L\alpha}/\sigma_{LI}$).

Element	Theoretical	Experimental			
		Present	Others		Ref.
Dy	23.7	27.4 ± 0.8	19.0 ± 2.7	Abrath	17
			27 ± 1.9	Khan	5
Pb	18.95	17.3 ± 0.4	19.7 ± 1.0	Chen	21
			19.2 ± 0.1	Busch	20
			17.9 ± 0.1	Cohen	19
			20.9 ± 0.1 (thin)	Cohen	19

of other workers. The weighted average of the ($\sigma_{L\alpha}/\sigma_{LI}$) ratios for dysprosium was found to be 27.4 ± 0.8 in good agreement with the value obtained earlier, Khan et al. [5], but differs from the value quoted by Abrath [17] by 30%. The weighted average of ($\sigma_{L\alpha}/\sigma_{LI}$) for lead was found to be 17.3 ± 0.4 in good agreement with the value obtained by Cohen [19] using thick targets. The values reported by Cohen [19], from his thin target measurements, and Chen et al. [21] are respectively 21% and 14% higher than the present value. With the precision achieved in the present work there was no evidence of a minimum in the ratio between 0.5 and 2 MeV, as reported by Busch et al. [20]. Above 3 MeV the ratio was reported to be constant and equal to 19.2 ± 0.1. Cohen [19] and Chen et al. [21] both report that their data are consistent with a constant value for ($\sigma_{L\alpha}/\sigma_{LI}$).

6. Conclusions

It must be borne in mind that inherent in any procedure adopted for the comparison of theory with experiment is the difficulty that the theoretical predictions contain the uncertainties associated with the fluorescence yields and Coster–Kronig yields through the use of eqs. (2)–(5). An alternative approach is to derive from the experimental data values for the sub-shell ionization cross-sections σ_{LI}, σ_{LII} and σ_{LIII} which can then be compared directly with the theoretical predictions. This approach, however has an additional difficulty since the solution of eqs. (2)–(5) for σ_{LI}, σ_{LII} and σ_{LIII} invariably results in a set of ill-conditioned equations, in as much as small changes in the experimental data can produce large changes in the predicted values of the sub-shell ionization cross-sections, leading to physically unmeaningful results. A comparison of experimental data then becomes exceedingly difficult. Alternatively one has to employ semi-resolved peaks which are often of poor precision.

It clearly would be helpful if experimentalists would present their experimentally measured production cross-section data in addition to any other data they might wish to present. Discrepancies between experimental data could then be easily identified and an accurate set of data eventually established. A more realistic approach to the comparison of experiment and theory would eventually be possible.

We are most grateful to the staff at the Birmingham Radiation Centre for their assistance with the experimental work. One of us (R.S.S.) also wishes to thank the Science Research Council for supporting this work.

References

[1] Proc. 2nd Int. Conf. on PIXE and its analytical applications, Lund, Sweden, Nucl. Instr. and Meth. 181 (1981).
[2] Proc. 1st Int. Workshop on Inner shell ionization. Nucl. Instr. and Meth. 169 (1980) 249.
[3] M.R. Khan, D. Crumpton and P.E. Francois, J. Phys. B. 9 (1976) 445.
[4] M.R. Khan, A.G. Hopkins, D. Crumpton and P.E. Francois, X-Ray Spec. 6 (1977) 140.
[5] M.R. Khan, A.G. Hopkins and D. Crumpton, Z. Physik A288 (1978) 133.
[6] W. Brandt and G. Lapicki, Phys. Rev. A20 (1979) 465.
[7] R.S. Sokhi and D. Crumpton, Nucl. Instr. and Meth. 181 (1981) 5.
[8] E. Storm and H.I. Israel, Nucl. Data Tables A7 (1970) 565.
[9] H. Tawara, K. Ishii, S. Morita, H. Kaji, F.N, Shu and T. Shiokawa, Phys. Rev. A9 (1974) 1617.
[10] M.O. Krause, J. Phys. Chem. Ref. Data 8 (1979) 307.
[11] J.H. Scofield, At. Data Nucl. Data Tables 14 (1974) 121.
[12] O. Benka and A. Kropf, At. Data Nucl. Data Tables 22 (1978) 219.
[13] T.J. Gray, G.M. Light, R.K. Gardner and F.D. McDaniel, Phys. Rev. A12 (1975) 2393.
[14] C.V. Barros Leite, N.V. de Castro Faria and A.G. de Pinho, Phys. Rev. A15 (1977) 943.
[15] R.C. Bearse, D.A. Close, J.J. Malanify and C.J. Umbarger, Phys. Rev. A7 (1973) 1269.

[16] D.A. Close, R.C. Bearse, J.J. Malanify and C.J. Umbarger, Phys. Rev. A8 (1973) 1873.
[17] F. Abrath and T.J. Gray, Phys. Rev. A9 (1974) 682.
[18] D.H. Madison, A.B. Baskin, C.E. Busch and S.M. Shafroth, Phys. Rev. A9 (1974) 675.
[19] D.D. Cohen, J. Phys. B. 13 (1980) 2953.
[20] C.E. Busch, A.B. Baskin, P.H. Nettles, S.M. Shafroth and A.W. Waltner, Phys. Rev. A7 (1973) 1601.
[21] J.R. Chen, J.D. Reber, D.J. Ellis and T.E. Miller, Phys. Rev. A13 (1976) 941.

ATOMIC DATA AND NUCLEAR DATA TABLES 30, 49–124 (1984)

EXPERIMENTAL *L*-SHELL X-RAY PRODUCTION AND IONIZATION CROSS SECTIONS FOR PROTON IMPACT

R. S. SOKHI and D. CRUMPTON

Department of Physics, University of Aston
Birmingham B4 7ET, England

Cross sections for *L*-shell x-ray production and ionization by protons are tabulated according to target atomic number, target type, and incident proton energy. Cross sections for production of the individual *L*-shell component x-rays and for ionization of the three *L* subshells are presented separately. Ratios of $L\alpha$ to Ll x-ray production cross sections are also listed. Literature is covered from 1975 to November 1982. Experimental details pertaining to the cross-section measurements and the theoretical models employed by the experimenters for comparison with their data are included. It is intended that this information will help the reader to ascertain the most reliable cross-section values without recourse to the literature.

0092-640X/84 $3.00

CONTENTS

INTRODUCTION

General Remarks

Considerable effort has been directed in recent years to the study of inner-shell ionization of atoms by charged particles. Progress has been achieved not only in the realms of theoretical studies[1,2] but also in the field of applications of this phenomenon.[3] A substantial portion of this effort has been devoted to the application of x-rays resulting from inner-shell ionization by protons to trace elemental analysis, and consequently proton-induced x-ray emission analysis has become established as a versatile multitrace elemental analytic tool.[3,4]

As a result of this effort a considerable amount of *L*-shell x-ray production cross-section data for proton impact is now available in the literature. Several authors have also derived *L*-shell ionization cross sections from their x-ray production cross-section measurements. The procedures for achieving this require appropriate values for fluorescence yields, Coster–Kronig yields, and radiative rates for the *L* shell. The first two quantities have been tabulated by Bambynek et al.[5] and McGuire[6] and more recently by Krause.[7] The radiative rates have been tabulated by Scofield.[8]

This tabulation presents *L*-shell x-ray production and ionization cross sections separately according to target atomic number, target type, and incident proton energy. Tables containing experimental details have also been presented for each reference quoted. As far as we are aware all x-ray production and ionization cross-section data that are available in tabular form, either in the literature or directly from authors, from 1975 through November 1982 have been included.

Relation to Other Tables

Previous tabulations of inner-shell ionization and x-ray production cross sections for charged particle impact[9–11] have tended to quote total cross sections only, which are of limited value to the analyst and the theoretician. The present work contains, wherever possible, individual transition group x-ray production and ionization subshell cross sections. Experimental details, which have been sparse in previous works, have also been presented in the tables. The previous tabulation on *L*-shell x-ray production cross sections by Hardt and Watson[11] presented data for several charged particles; the present work however, concentrates solely on proton impact and consequently is more detailed. In general, references covered by Hardt and Watson[11] have been omitted from this work, although there is occasional overlap because in a small number of cases already referenced by Hardt and Watson,[11] individual transition group x-ray production cross sections became available. Since the above authors had frequently quoted only the total cross sections it was decided to include the individual cross sections in full.

Possible Users and General Policy

This tabulation is intended to be of use both to the analyst involved in the application of proton-induced x-ray emission analysis and to the theoretician studying light ion–atom collisions. To the theoretician both x-ray production and ionization cross sections are of importance, while to the analyst only the former is of interest. With these two requirements in mind the cross sections have been tabulated separately. The cross sections have also been segregated, wherever necessary, according to gas and solid targets; the latter is further subdivided into thin, semithick, and thick. This has been done because the data require stopping-power corrections to varying degrees depending on the type of target.

"Experimental details" tables have been presented not only to provide a source for comparison of procedures adopted by different laboratories but also as an aid to the reader in deciding the "best" cross-section values to use. As far as possible this compilation has been formulated to be self-explanatory for the most part; however, a comprehensive section, Explanation of Tables and Policies, has been included for completeness.

It is hoped that this tabulation will offer an overview of this field and be of some assistance in determining future research directions.

Data Sources and Presentation

References for the cross sections were obtained by computer and manual searches of the literature. An on-line information retrieval service was employed with the data base INSPEC[12] containing science abstracts. Tabular cross-section data were then collected from the literature or acquired by correspondence with the authors. Several attempts were made where contact had proven difficult. In the few instances where only graphical data were available the references were omitted. The combined experimental results for the *L*-shell x-ray production and ionization cross sections, respectively, are listed by element in Tables AII and BII.

Experimental details and the theories[13–33] used for comparison with the experimental results were extracted from each reference. They are given for each element in Tables AI and BI, immediately preceding the corresponding cross-section tables. In Table AIII we list the ratio $L\alpha/Ll$ for each experiment, if available. Where authors had not specifically quoted the $L\alpha/Ll$ cross-section ratios, they were computed from the individual $L\alpha$ and Ll cross sections.

Experimental errors on the cross sections are given in Tables AI and BI, respectively. In Tables AII and BII, experimental errors are not given directly. Instead, we have adopted the policy of indicating the typical uncertainty by restricting the number of significant figures as follows:

(i) For cross-section values $<0.5b$ three decimal places are quoted.

(ii) For values $\geqslant 0.5b$ and $<5.0b$ two decimal places are quoted.

(iii) For values $\geqslant 5.0b$ and $<50b$ one decimal place is quoted.

(iv) For values $\geqslant 50b$ no decimal places are quoted.

Acknowledgment

One of us (R.S.S.) wishes to thank the Science and Engineering Research Council for supporting this work.

References for Introduction

1. "Proceedings of the Workshop on Theories of Inner Shell Ionization by Heavy Particles," Nucl. Instrum. Methods **169**, 249 (1980)
2. "Proceedings of the Second Workshop on Inner Shell Ionization by Light Ions," Nucl. Instrum. Methods **192**, 1 (1982)
3. "Proceedings of the Second International Conference on Particle Induced X-ray Emission and Its Analytical Applications," Nucl. Instrum. Methods **181**, 1 (1981)
4. M. R. Khan and D. Crumpton, CRC Critical Reviews in Analytical Chemistry, Part I, **11**, 103 (1981); Part II, **11**, 161 (1981)
5. W. Bambynek, B. Crasemann, R. W. Fink, H. H. Freund, H. Mark, C. D. Swift, R. E. Price, and P. V. Rao, Rev. Mod. Phys. **44**, 716 (1972)
6. E. J. McGuire, Phys. Rev. A **3**, 587 (1971)
7. M. O. Krause, J. Phys. Chem. Ref. Data **8**, 307 (1979)
8. J. H. Scofield, ATOMIC DATA AND NUCLEAR DATA TABLES **14**, 121 (1974)
9. C. H. Rutledge and R. L. Watson, ATOMIC DATA AND NUCLEAR DATA TABLES **12**, 195 (1973)
10. R. K. Gardner and T. J. Gray, ATOMIC DATA AND NUCLEAR DATA TABLES **21**, 515 (1978); Erratum, **24**, 281 (1979)
11. T. L. Hardt and R. L. Watson, ATOMIC DATA AND NUCLEAR DATA TABLES **17**, 107 (1976)
12. Lockheed Information Systems, Code 52-08, Building 201, 3251 Hanover Street, Palo Alto, Calif., U. S. A.
13. J. D. Garcia, E. Gerjuoy, and J. E. Welker, Phys. Rev. **165**, 66 (1967)

14. J. D. Garcia, Phys. Rev. A **1**, 280 (1970)

15. J. D. Garcia, R. J. Fortner, and T. M. Kavanagh, Rev. Mod. Phys. **45**, 111 (1973)

16. J. D. Garcia, Phys. Rev. A **1**, 1 (1970)

17. L. Vriens and T. F. M. Bonsen, J. Phys. B **1**, 1123 (1968)

18. J. S. Hansen, Phys. Rev. A **8**, 822 (1973)

19. J. H. McGuire and K. Omidvar, Phys. Rev. A **10**, 182 (1974)

20. J. M. Hansteen and O. P. Mosebekk, Nucl. Phys. A **201**, 541 (1973)

21. J. M. Hansteen, O. M. Johnsen, and L. Kocbach, ATOMIC DATA AND NUCLEAR DATA TABLES **15**, 305 (1975)

22. P. A. Amundsen, J. Phys. B **10**, 1097 (1977)

23. E. Merzbacher and H. W. Lewis, in *Handbuch der Physik*, edited by S. Flügge (Springer-Verlag, Berlin 1958), Vol. 34, p. 166

24. G. S. Khandelwal, B. H. Choi, and E. Merzbacher, ATOMIC DATA **1**, 103 (1969)

25. B. H. Choi, E. Merzbacher, and G. S. Khandelwal, ATOMIC DATA **5**, 291 (1973)

26. O. Benka and A. Kropf, ATOMIC DATA AND NUCLEAR DATA TABLES **22**, 219 (1978)

27. G. H. Pepper, Ph.D. thesis, North Texas State University, 1974

28. W. Brandt and G. Lapicki, Phys. Rev. A **20**, 465 (1979)

29. W. Brandt and G. Lapicki, Phys. Rev. A **10**, 474 (1974)

30. K. Ishii, S. Morita, H. Tawara, H. Kaji, and T. Shiokawa, Phys. Rev. A **10**, 774 (1974)

31. T. Mukoyama and L. Sarkadi, Nucl. Instrum. Methods **190**, 619 (1981)

32. R. M. Wheeler, R. P. Chaturvedi, and S. Amey, IEEE Trans. Nucl. Sci., N.S. **26**, 1166 (1979)

33. W. Brandt and G. Lapicki, Phys. Rev. A **23**, 1717 (1981)

34. S. Datz, J. L. Duggan, L. C. Feldman, E. Laegsgaard, and J. U. Andersen, Phys. Rev. A **9**, 192 (1974) (referred to in Table BI for Au)

EXPLANATION OF TABLES AND POLICIES

TABLE A. Experimental *L*-Shell X-Ray Production Cross Sections for Proton Impact

TABLE AI	*Experimental Details*
REF	Publication reference
ENERGY RANGE	Incident proton beam energy range in MeV
AREAL DENSITY	Target areal density. E-6G/CMSQ is equivalent to μg/cm^2 and +− is equivalent to ±. Wherever the areal densities were not quoted by the experimenters, targets have been classified into GAS, THIN, SEMI-THICK, AND THICK.
BEAM CURRENT	Incident proton beam current in Amperes (A). Exponential notation is used: 10E-9 ≡ 10×10^{-9}.
BEAM COLL	(B) Incident proton beam diameter in mm. (C) Aperture size in mm of the final collimator. Aperture size is presented wherever the beam diameter was not available.
EXP ERROR	Percentage experimental uncertainties in the cross-section values. Wherever the uncertainty is not constant at different proton energies, the minimum and maximum percentage uncertainties have been shown.
LA, LB, LG, LL, LE, LT	$L\alpha$, $L\beta$, $L\gamma$, Ll, $L\eta$, and total *L*-shell x-ray production cross sections, respectively. LG 8-12 indicates an uncertainty of 8 to 12% in the $L\gamma$ cross sections.
LX	This notation is used wherever the experimenter has generalized the uncertainties in all the *L* transitions to a single value.
THEORIES	Theories employed by the experimenter for comparison with his measured data. Reference numbers refer to those given in the Introduction.
BEA	Binary-encounter approximation
BEA (G1)	Garcia et al., 1967[13]
BEA (G2)	Garcia, 1970[14]
BEA (G3)	Garcia et al., 1973[15]
BEA (G4)	Garcia, 1970[16]
BEA (V)	Vriens and Bonsen, 1968[17]
BEA (H)	Hansen, 1973[18]
BEA (M)	McGuire and Omidvar, 1974[19]
CBEA	Constrained binary-encounter approximation[18]
SCA	Semiclassical approximation
SCA1	Hansteen and Mosebekk, 1973[20]
SCA2	Hansteen et al., 1975[21]
RSCA	Amundsen, 1977[22]
PWBA	Plane wave Born approximation
PWBA1	Merzbacher and Lewis, 1958[23]
PWBA2	Khandelwal et al., 1969[24]
PWBA3	Choi et al., 1973[25]
PWBA4	Benka and Kropf, 1978[26]
PWBA5	Pepper, 1974[27]
PWBAR	PWBA with relativistic corrections[28]

PWBABC	PWBA with binding energy and Coulomb corrections[29]
PWBABTR	PWBA with binding energy, trajectory, and relativistic corrections[27]
IPWBAR	PWBA with relativistic corrections by Ishii et al.[30]
IPWBABCR	PWBA with binding energy, Coulomb, and relativistic corrections by Ishii et al.[30]
MPWBABCR	As above except by Merzbacher and Lewis[23]
PWBABCR	PWBA with binding energy, Coulomb, and relativistic corrections[28]
RPWBABC	As above, Mukoyama and Sarkadi[31]
PSS	Perturbed stationary state[29]
PSSR	PSS with relativistic corrections[32]
CPSSR	PSS with Coulomb and relativistic corrections[28]
ECPSSR	PSS with Coulomb, relativistic, and energy loss corrections[33]

COMMENTS	Comments in this column refer to the experimental setup and the procedure adopted by the experimenter. The comments are, in general, self-explanatory; however, a few less obvious ones are explained below:
RBS EMPLOYED	Rutherford backscattering spectrometry employed to determine the target thickness and/or to monitor the beam current
EFFICIENCY MEASURED/ CALCULATED	This indicates whether the efficiency of the x-ray detector was measured or calculated.
Si(Li)	Lithium-drifted silicon detector, mentioned only when other detectors were also used
BETA (2 + 15)	$L\beta_{2,15}$
GAMMA (1)	$L\gamma_1$

TABLE AII	*Experimental X-Ray Production Cross Sections*
	For many elements only the total *L*-shell cross sections were available. Cross sections, in barns, have been tabulated separately for GAS, THIN, SEMI-THICK and THICK targets.
ENERGY	Incident proton beam energy in MeV
ALPHA, BETA, GAMMA, L, ETA	*L*-shell x-ray production cross sections, in barns, for the $L\alpha$, $L\beta$, $L\gamma$, Ll, and $L\eta$ transitions. $L\alpha$, $L\beta$, and $L\gamma$ are transition groups and wherever the experimenter had quoted cross sections for individual transitions belonging to one group they were summed to give the total cross section for each group. For cross-section values less than 0.01 barn the following exponential notation is employed: $8.1\text{E-}03 \equiv 8.1 \times 10^{-3}$.
TOTAL	Total *L*-shell x-ray production cross section in barns. Wherever the total cross section was not specifically quoted it was obtained by summing the individual cross sections.
REF	Publication reference. Wherever the reference has been omitted the preceding reference applies.

TABLE AIII	*LALPHA/LL Ratios*
ENERGY RANGE	Incident proton energy range in MeV
TARGET	Targets classified as THIN or THICK
LA/LL	Ratio of $L\alpha$ to Ll x-ray production cross sections
REF	Publication reference

TABLE B. Experimental *L*-Shell Ionization Cross Sections for Proton Impact

Values of the ionization cross sections are taken directly as given in the respective references. In deriving *L*-shell ionization cross sections from x-ray production data, authors typically used atomic parameters from Refs. 5–8. Where Refs. 5–8 have not been employed, this is noted in the COMMENTS in BI.

TABLE BI	*Experimental Details*
REF	Publication reference
ENERGY RANGE	Incident proton beam energy range in MeV
AREAL DENSITY	Target areal density E-6G/CMSQ is equivalent to $\mu g/cm^2$ and +− is equivalent to ±. Wherever the areal densities were not quoted by the experimenters, targets have been classified as THIN and THICK.
BEAM CURRENT	Incident proton beam current in Amperes (A). Exponential notation is used: 10E-9 ≡ 10×10^{-9}.
BEAM COLL	(B) Incident proton beam diameter in mm. (C) Aperture size in mm of the final collimator. This has been presented wherever the beam diameter was not available.
EXP ERROR	Percentage experimental uncertainties in the cross section values and ratios. Wherever the uncertainty is not constant at different proton energies, the minimum and maximum percentage uncertainties have been shown.
L1, L2, L3, LT	$2s_{1/2}$, $2p_{1/2}$ and $2p_{3/2}$ *L*-subshell and total *L*-shell ionization cross sections, respectively
R1, R2	Ratios of $2s_{1/2}$ to $2p_{1/2}$ and of $2s_{1/2}$ to $2p_{3/2}$ subshell ionization cross sections, respectively. R1 22-28 therefore indicates a range of uncertainties of 22 to 28% in the ratio R1.
THEORIES	See Explanations for Table AI
COMMENTS	See Explanations for Table AI

TABLE BII	*Experimental Ionization Cross Sections*
	Total *L*-shell ionization cross sections have been tabulated wherever the subshell cross sections were not available. Cross section, in barns, have been tabulated separately for THIN and THICK targets.
L1, L2, L3	$2s_{1/2}$, $2p_{1/2}$ and $2p_{3/2}$ subshell ionization cross sections, in barns, respectively
L1/L2 L1/L3	Ratio of $2s_{1/2}$ to $2p_{1/2}$ and $2s_{1/2}$ to $2p_{3/2}$ subshell cross sections, respectively
TOTAL	Total *L*-shell ionization cross sections in barns. Wherever the total cross section was not specifically quoted it was obtained by summing the individual subshell cross sections.
REF	Publication reference. Wherever the reference has been omitted the preceding reference applies.

REFERENCES FOR TABLES

BADT78 T. Badica, C. Ciortea, A. Petrovici, and I. Popescu, Rev. Roum Phys. **23**, No. 9, 1019 (1978)

BAUC81 C. Bauer, H. Richter, P. Gippner, R. Mann, W. Ruddolph, B. Eckhardt, and K. O. Groeneveid, Z. Phys. A **303**, 13 (1981)

BEAR73 R. C. Bearse, D. A. Close, J. J. Malanify, and C. J. Umbarger, Phys. Rev. A **7**, 1269 (1973)

BHAD80 D. Bhattacharya, S. K. Bhattacherjee, and S. K. Mitra, J. Phys. B **13**, 967 (1980)

BONG78 G. Bonani, Ch. Stoller, M. Stöckli, M. Suter, and W. Wölfli, Helv. Phys. Acta **51**, 272 (1978)

CHAR75 R. P. Chaturvedi, R. M. Wheeler, R. B. Liebert, D. J. Miljanic, T. Zabel, and G. C. Phillips, Phys. Rev. A **12**, 52 (1975)

CHEJ76 J. R. Chen, J. D. Reber, D. J. Ellis, and T. E. Miller, Phys. Rev. A **13**, 941 (1976)

CHMJ81 J. H. Chmielewski, J. L. Flinner, F. W. Inman, B. Sollenberger, and N. V. Udeh, Phys. Rev. A **24**, 29 (1981)

COHD80 D. D. Cohen, J. Phys. B **13**, 2953 (1980)

CUZP81 P. Cuzzocrea, E. Perillo, E. Rosato, G. Spadaccini, N. De Cesare, and M. Vigilante, Nuovo Cimento Lett. **32**, 33 (1981)

FASS82 S. Fast, J. L. Flinner, A. Glick, F. W. Inman, L. Oolman, C. Pearson, and D. Wickelgren, Phys. Rev. A **26**, 2417 (1982)

ISHK74 K. Ishii, S. Morita, H. Tawara, H. Kaji, and T. Shiokawa, Phys. Rev. A **10**, 774 (1974)

JITW82 W. Jitschin, A. Kaschuba, R. Hippler, and H. O. Lutz, J. Phys. B **15**, 763 (1982)

JUSE80 E. L. B. Justiniano, A. A. G. Nader, N. V. de Castro Faria, C. V. Barros Leite, and A. G. de Pinho, Phys. Rev. A **21**, 73 (1980); and private communication for the x-ray production cross sections

KHAR78 M. R. Khan, A. G. Hopkins, and D. Crumpton, Z. Phys. A **288**, 133 (1978)

KROA82 A. Kropf, *Messung Protoneninduzierter L - Unterschalenröntgenwirkungsquer - schnitte für Elemente mit der Ordnungszahl zwischen 40 und 51* (Vienna, 1982); Dissertation der Johannes Kepler-Universität, Linz

LANA75 A. Langenberg, F. J. de Heer, and J. van Eck, J. Phys. B **8**, 2079 (1975)

LAPG80 G. Lapicki, R. Laubert, and W. Brandt, Phys. Rev. A **22**, 1889 (1980)

LEIC77 C. V. Barros Leite, N. V. de Castro Faria, and A. G. de Pinho, Phys. Rev. A **15**, 943 (1977)

LIER73 R. B. Liebert, T. Zabel, D. Miljanic, H. Larson, V. Valkovic, and G. C. Phillips, Phys. Rev. A **8**, 2336 (1973)

MILM76 M. Milazzo and G. Riccobono, Phys. Rev. A **13**, 578 (1976)

PETV80 V. P. Petukhov, E. A. Romanovskii, H. Kerkov, and G. Kreysch, Phys. Status Solidi (a) **60**, 79 (1980)

PINA82 A. G. de Pinho, private communication. The cross-section values for Au obtained from this reference are reported by the author to be more reliable than those published in LEIC77.

PONM79 M. Poncet and Ch. Engelmann, Nucl. Instrum. Methods **159**, 455 (1979)

SARL80 L. Sarkadi and T. Mukoyama, J. Phys. B **13**, 2255 (1980)

SARW81 W. Sarter, H. Mommsen, M. Sarkar, P. Schürkes, and A. Weller, J. Phys. B **14**, 2843 (1981)

SERK80 K. Sera, K. Ishii, A. Yamadera, A. Kuwoka, M. Kamiya, M. Sebata, S. Morita, and T. C. Chu, Phys. Rev. A **22**, 2536 (1980)

SOKR81 R. S. Sokhi and D. Crumpton, Nucl. Instrum. Methods **181**, 5 (1981)

SOKR82 R. S. Sokhi and D. Crumpton, Nucl. Instrum. Methods **192**, 121 (1982)

TAWH74 H. Tawara, K. Ishii, S. Morita, H. Kaji, C. N. Hsu, and T. Shiokawa, Phys. Rev. A **9**, 1617 (1974)

TAWH75 H. Tawara, K. Ishii, S. Morita, H. Kaji, and T. Shiokawa, Phys. Rev. A **11**, 1560 (1975)

UDEN81 N. V. Udeh, J. J. Chmielewski, J. L. Flinner, F. W. Inman, and B. Sollenberger, Phys. Rev. A **24**, 1746 (1981)

WHER79 R. M. Wheeler, R. P. Chaturvedi, and S. Amey, IEEE Trans. Nucl. Sci., N.S. **26**, 1166 (1979)

TABLE A. Experimental *L*-Shell X-Ray Production Cross Sections for Proton Impact

Z=18 ARGON(AR)

TABLE AI   EXPERIMENTAL DETAILS

REF	ENERGY RANGE MeV	AREAL DENSITY E-6G/CMSQ	BEAM CURRENT A	BEAM COLL mm	EXP ERROR %	THEORIES	COMMENTS
LANA75	.028-.5	GAS	10E-6	2.0(B)	LT 11	PWBA3 PWBABC	SQUARE BEAM. PROPORTIONAL COUNTER USED. EFFICIENCY MEASURED. L2 AND L3 SUBSHELL X-RAYS MEASURED. FLUORESCENCE YIELD MEASURED. e- H2+ He+ He2+ IMPACT STUDIED.

TABLE AII   EXPERIMENTAL X-RAY PRODUCTION CROSS SECTIONS

GAS TARGET

ENERGY MeV	TOTAL BARNS	REF	ENERGY MeV	TOTAL BARNS	REF
.0280	82	LANA75	.1250	823	LANA75
.0373	139		.1260	815	
.0483	222		.1350	860	
.0580	296		.1500	990	
.0676	365		.1700	1150	
.0773	427		.2000	1300	
.0870	498		.2500	1570	
.0966	561		.3000	1730	
.1060	650		.4000	2090	
.1160	740		.5000	2270	
.1200	764				

Z=28 NICKEL(NI)

TABLE AI   EXPERIMENTAL DETAILS

REF	ENERGY RANGE MeV	AREAL DENSITY E-6G/CMSQ	BEAM CURRENT A	BEAM COLL mm	EXP ERROR %	THEORIES	COMMENTS
PETV80	.07-.45	THICK	-	-	LT 25	PWBA1	PROPORTIONAL COUNTER USED. EFFICIENCY MEASURED.

TABLE A. Experimental *L*-Shell X-Ray Production Cross Sections for Proton Impact

Z=28 NICKEL(NI) CONTINUED

TABLE AII EXPERIMENTAL X-RAY PRODUCTION CROSS SECTIONS

THICK TARGET

ENERGY MeV	TOTAL BARNS	REF	ENERGY MeV	TOTAL BARNS	REF
.070	37.0	PETV80	.250	255	PETV80
.085	53		.300	345	
.100	71		.350	431	
.140	113		.400	504	
.165	159		.450	621	
.200	203				

Z=29 COPPER(CU)

TABLE AI EXPERIMENTAL DETAILS

REF	ENERGY RANGE MeV	AREAL DENSITY E-6G/CMSQ	BEAM CURRENT A	BEAM COLL mm	EXP ERROR %	THEORIES	COMMENTS
PETV80	.07-.45	THICK	-	-	LT 25	PWBA1	PROPORTIONAL COUNTER USED. EFFICIENCY MEASURED.

TABLE AII EXPERIMENTAL X-RAY PRODUCTION CROSS SECTIONS

THICK TARGET

ENERGY MeV	TOTAL BARNS	REF	ENERGY MeV	TOTAL BARNS	REF
.070	20.0	PETV80	.200	213	PETV80
.085	32.5		.250	276	
.100	50		.300	388	
.120	63		.350	497	
.140	105		.400	637	
.165	165		.450	769	

Z=30 ZINC(ZN)

TABLE AI EXPERIMENTAL DETAILS

REF	ENERGY RANGE MeV	AREAL DENSITY E-6G/CMSQ	BEAM CURRENT A	BEAM COLL mm	EXP ERROR %	THEORIES	COMMENTS
PETV80	.07-.45	THICK	-	-	LT 25	PWBA1	PROPORTIONAL COUNTER USED. EFFICIENCY MEASURED.

TABLE A. Experimental *L*-Shell X-Ray Production Cross Sections for Proton Impact

Z=30 ZINC(ZN) CONTINUED

TABLE AII EXPERIMENTAL X-RAY PRODUCTION CROSS SECTIONS

THICK TARGET

ENERGY MeV	TOTAL BARNS	REF	ENERGY MeV	TOTAL BARNS	REF
.070	17.4	PETV80	.200	241	PETV80
.085	27.1		.250	313	
.100	45.3		.300	460	
.120	64		.350	616	
.140	106		.400	787	
.165	163		.450	976	

Z=37 RUBIDIUM(RB)

TABLE AI EXPERIMENTAL DETAILS

REF	ENERGY RANGE MeV	AREAL DENSITY E-6G/CMSQ	BEAM CURRENT A	BEAM COLL mm	EXP ERROR %	THEORIES	COMMENTS
MILM76	.950	60	-	2.0(B)	LT 15	BEA(G3)	SQUARE BEAM. RBS EMPLOYED. EFFICIENCY CALCULATED. RbCl TARGET ON CARBON BACKING.

TABLE AII EXPERIMENTAL X-RAY PRODUCTION CROSS SECTIONS

THIN TARGET

ENERGY MeV	TOTAL BARNS	REF	ENERGY MeV	TOTAL BARNS	REF
.95	405	MILM76			

Z=38 STRONTIUM(SR)

TABLE AI EXPERIMENTAL DETAILS

REF	ENERGY RANGE MeV	AREAL DENSITY E-6G/CMSQ	BEAM CURRENT A	BEAM COLL mm	EXP ERROR %	THEORIES	COMMENTS
BONG78	3.0	THIN	-	-	LT 8	BEA(G3)	RBS EMPOLYED. EFFICIENCY MEASURED. K-SHELL STUDIED. METAL TARGET ON CARBON BACKING.

TABLE AII EXPERIMENTAL X-RAY PRODUCTION CROSS SECTIONS

THIN TARGET

ENERGY MeV	TOTAL BARNS	REF	ENERGY MeV	TOTAL BARNS	REF
3.00	1667	BONG78			

TABLE A. Experimental *L*-Shell X-Ray Production Cross Sections for Proton Impact

Z=39 YTTRIUM(Y)

TABLE AI EXPERIMENTAL DETAILS

REF	ENERGY RANGE MeV	AREAL DENSITY E-6G/CMSQ	BEAM CURRENT A	BEAM COLL mm	EXP ERROR %	THEORIES	COMMENTS
MILM76	.950	70	-	2.0(B)	LT 15	BEA(G3)	SQUARE BEAM. RBS EMPLOYED. EFFICIENCY CALCULATED. METAL TARGET ON CARBON BACKING.
SERK80	2.92-39.34	24	-	-	LT 12	BEA(V) PWBA3 PWBA4	RBS EMPLOYED. METAL TARGET ON MYLAR BACKING.

TABLE AII EXPERIMENTAL X-RAY PRODUCTION CROSS SECTIONS

THIN TARGET

ENERGY MeV	TOTAL BARNS	REF	ENERGY MeV	TOTAL BARNS	REF
.95	350	MILM76	18.12	937	SERK80
2.92	1410	SERK80	24.21	802	
3.97	1490		30.52	672	
6.13	1490		39.34	537	
12.31	1130				

Z=40 ZIRCONIUM(ZR)

TABLE AI EXPERIMENTAL DETAILS

REF	ENERGY RANGE MeV	AREAL DENSITY E-6G/CMSQ	BEAM CURRENT A	BEAM COLL mm	EXP ERROR %	THEORIES	COMMENTS
KROA82	.1015-.7422	110+-2 THICK	-	-	LT 16-18	CPSSR	CRYSTAL SPECTROMETER AND Si(Li) USED. RBS EMPLOYED. EFFICIENCY CALCULATED. METAL TARGET ON CARBON BACKING. ONLY LALPHA/LL RATIO AVAILABLE FOR THICK TARGET.

TABLE AII EXPERIMENTAL X-RAY PRODUCTION CROSS SECTIONS

THIN TARGET

ENERGY MeV	TOTAL BARNS	REF	ENERGY MeV	TOTAL BARNS	REF
.1015	1.69	KROA82	.3179	61	KROA82
.1334	5.7		.3991	104	
.1638	9.5		.4903	145	
.2051	19.3		.6011	223	
.2566	41.3		.7422	334	

TABLE A. Experimental *L*-Shell X-Ray Production Cross Sections for Proton Impact

Z=40 ZIRCONIUM(ZR) CONTINUED

TABLE AIII LALPHA/LL RATIO

ENERGY RANGE MeV	TARGET	LA/LL	REF	ENERGY RANGE MeV	TARGET	LA/LL	REF
0.5	THICK	24.4*	KROA82	0.5	THICK	25.4†	KROA82

* Si(Li) DETECTOR USED † CRYSTAL SPECTROMETER USED.

Z=41 NIOBIUM(NB)

TABLE AI EXPERIMENTAL DETAILS

REF	ENERGY RANGE MeV	AREAL DENSITY E-6G/CMSQ	BEAM CURRENT A	BEAM COLL mm	EXP ERROR %	THEORIES	COMMENTS
KROA82	.0916-.7459	55+-3 THICK	-	-	LT 15-17	CPSSR	CRYSTAL SPECTROMETER AND Si(Li) USED. RBS EMPLOYED. EFFICIENCY CALCULATED. METAL TARGET ON CARBON BACKING. ONLY LALPHA/LL RATIO AVAILABLE FOR THICK TARGET.

TABLE AII EXPERIMENTAL X-RAY PRODUCTION CROSS SECTIONS

THIN TARGET

ENERGY MeV	TOTAL BARNS	REF	ENERGY MeV	TOTAL BARNS	REF
.0916	.88	KROA82	.3239	46.6	KROA82
.1115	1.96		.4044	78	
.1417	4.58		.4951	121	
.1723	9.5		.6058	177	
.2129	17.1		.7459	258	
.2634	28.4				

TABLE AIII LALPHA/LL RATIO

ENERGY RANGE MeV	TARGET	LA/LL	REF	ENERGY RANGE MeV	TARGET	LA/LL	REF
0.5	THICK	47.2*	KROA82	0.5	THICK	25.2†	KROA82

* Si(Li) DETECTOR USED † CRYSTAL SPECTROMETER USED.

TABLE A. Experimental *L*-Shell X-Ray Production Cross Sections for Proton Impact

Z=42 MOLYBDENUM(MO)

TABLE AI EXPERIMENTAL DETAILS

REF	ENERGY RANGE MeV	AREAL DENSITY E-6G/CMSQ	BEAM CURRENT A	BEAM COLL mm	EXP ERROR %	THEORIES	COMMENTS
PETV80	.2-1.05	THICK	-	-	LT 25	PWBA1	PROPORTIONAL COUNTER USED. EFFICIENCY MEASURED.

TABLE AII EXPERIMENTAL X-RAY PRODUCTION CROSS SECTIONS

THICK TARGET

ENERGY MeV	TOTAL BARNS	REF	ENERGY MeV	TOTAL BARNS	REF
.20	7.4	PETV80	.55	95	PETV80
.25	13.5		.65	143	
.30	23.0		.75	194	
.35	34.0		.85	245	
.40	47.0		.95	316	
.45	59		1.05	347	

Z=45 RHODIUM(RH)

TABLE AI EXPERIMENTAL DETAILS

REF	ENERGY RANGE MeV	AREAL DENSITY E-6G/CMSQ	BEAM CURRENT A	BEAM COLL mm	EXP ERROR %	THEORIES	COMMENTS
PETV80	.2-.45	THICK	-	-	LT 25	PWBA1	PROPORTIONAL COUNTER USED. EFFICIENCY MEASURED.
KROA82	.09-.744	88+-5 THICK	-	-	LT 15-19	CPSSR	CRYSTAL SPECTROMETER AND Si(Li) USED. RBS EMPLOYED. EFFICIENCY CALCULATED. METAL TARGET ON CARBON BACKING. ONLY LALPHA/LL RATIO AVAILABLE FOR THICK TARGET.

TABLE AII EXPERIMENTAL X-RAY PRODUCTION CROSS SECTIONS

THIN TARGET

ENERGY MeV	TOTAL BARNS	REF	ENERGY MeV	TOTAL BARNS	REF
.0900	.247	KROA82	.3211	24.8	KROA82
.1096	.65		.4019	42.3	
.1393	1.78		.4925	69	
.1696	3.65		.6031	104	
.2100	7.8		.7440	156	
.2604	14.6				

TABLE A. Experimental *L*-Shell X-Ray Production Cross Sections for Proton Impact

Z=45 RHODIUM(RH) CONTINUED

TABLE AII EXPERIMENTAL X-RAY PRODUCTION CROSS SECTIONS CONTINUED

THICK TARGET

ENERGY MeV	TOTAL BARNS	REF	ENERGY MeV	TOTAL BARNS	REF
.20	4.48	PETV80	.35	18.9	PETV80
.25	7.8		.40	29.0	
.30	12.5		.45	45.4	

TABLE AIII LALPHA/LL RATIO

ENERGY RANGE MeV	TARGET	LA/LL	REF	ENERGY RANGE MeV	TARGET	LA/LL	REF
0.5	THICK	34.5*	KROA82	0.5	THIN	30.0+-2.1*	KROA82
0.5	THICK	25.0†					

* Si(Li) DETECTOR USED † CRYSTAL SPECTROMETER USED.

Z=46 PALLADIUM(PD)

TABLE AI EXPERIMENTAL DETAILS

REF	ENERGY RANGE MeV	AREAL DENSITY E-6G/CMSQ	BEAM CURRENT A	BEAM COLL mm	EXP ERROR %	THEORIES	COMMENTS
CHAR75	3-12	21+-2	-	-	LT 20	BEA(G3) PWBA3	RBS EMPLOYED. EFFICIENCY CALCULATED. O5+ IMPACT STUDIED. METAL TARGET ON CARBON BACKING.
PETV80	.2-.45	THICK	-	-	LT 25	PWBA1	PROPORTIONAL COUNTER USED. EFFICIENCY MEASURED.
KROA82	.09-.7438	99+-6 THICK	-	-	LT 15-20	CPSSR	CRYSTAL SPECTROMETER AND Si(Li) USED. RBS EMPLOYED. EFFICIENCY CALCULATED. METAL TARGET ON CARBON BACKING. ONLY LALPHA/LL RATIO AVAILABLE FOR THICK TARGET.

TABLE A. Experimental *L*-Shell X-Ray Production Cross Sections for Proton Impact

Z=46 PALLADIUM(PD) CONTINUED

TABLE AII EXPERIMENTAL X-RAY PRODUCTION CROSS SECTIONS

THIN TARGET

ENERGY MeV	TOTAL BARNS	REF	ENERGY MeV	TOTAL BARNS	REF
.0900	.192	KROA82	3.0000	1728	CHAR75
.1093	.52		4.0000	2208	
.1389	1.49		5.0000	2016	
.1692	3.02		6.0000	2496	
.2094	6.5		7.0000	2544	
.2601	12.3		8.0000	2640	
.3207	22.3		9.0000	2640	
.4015	37.8		10.0000	2688	
.4920	60		11.0000	2448	
.6026	94		12.0000	2208	
.7438	137				

THICK TARGET

ENERGY MeV	TOTAL BARNS	REF	ENERGY MeV	TOTAL BARNS	REF
.20	3.72	PETV80	.35	18.0	PETV80
.25	7.5		.40	28.0	
.30	12.1		.45	44.0	

TABLE AIII LALPHA/LL RATIO

ENERGY RANGE MeV	TARGET	LA/LL	REF	ENERGY RANGE MeV	TARGET	LA/LL	REF
0.5	THICK	31.1*	KROA82	0.5	THIN	32.2+-2.4*	KROA82
0.5	THICK	25.4†					

* Si(Li) DETECTOR USED † CRYSTAL SPECTROMETER USED.

Z=47 SILVER(AG)

TABLE AI EXPERIMENTAL DETAILS

REF	ENERGY RANGE MeV	AREAL DENSITY E-6G/CMSQ	BEAM CURRENT A	BEAM COLL mm	EXP ERROR %	THEORIES	COMMENTS
CHAR75	3-12	22+-2	-	-	LT 20	BEA(G3) PWBA3	RBS EMPLOYED. EFFICIENCY CALCULATED. O5+ IMPACT STUDIED. METAL TARGET ON CARBON BACKING.
MILM76	.950	70	-	2.0(B)	LT 10	BEA(G3)	SQUARE BEAM. RBS EMPLOYED. EFFICIENCY CALCULATED. AgCl TARGET ON CARBON BACKING.

TABLE A. Experimental L-Shell X-Ray Production Cross Sections for Proton Impact

Z=47 SILVER(AG) CONTINUED

TABLE AI EXPERIMENTAL DETAILS CONTINUED

REF	ENERGY RANGE MeV	AREAL DENSITY E-6G/CMSQ	BEAM CURRENT A	BEAM COLL mm	EXP ERROR %	THEORIES	COMMENTS
BADT78	4.0	66+-3	1-5E-9	-	LT 9	BEA(G3) PWBA2	EFFICIENCY MEASURED. K-SHELL STUDIED. METAL TARGET ON MYLAR BACKING.
BONG78	3.0	THIN	-	-	LT 7	BEA(G3)	RBS EMPOLYED. EFFICIENCY MEASURED. K-SHELL STUDIED. SELF-SUPPORTING METAL TARGET.
LAPG80	.035-.300	THICK	-	-	LT 25-50	PWBA ECPSSR	H2 AND He4 IMPACT STUDIED. K-SHELL STUDIED. COULOMB DEFLECTION FACTOR DEDUCED.
BAUC81	.3-4 .249-1.91	65+-5 THICK	.5-50E-9 2-500E-9	1.1(B)	LT 14 LT 25	CPSSR	RBS EMPLOYED. EFFICIENCY MEASURED. SELF-SUPPORTING METAL TARGET. He4 N2+ Ne3+ IMPACT STUDIED.
CUZP81	.611-3.85	THIN	-	-	LT 5-11	BEA(H) SCA2 PWBA3	EFFICIENCY MEASURED. AgIO3 TARGET ON CARBON BACKING. CROSS SECTIONS EVALUATED BY NORMALIZING TO K-SHELL DATA.
SARW81	.25-.40	100+-5 67+-3	3-100E-9	1.0(B)	LA 15 LT 15	PWBABC PWBABCR ECPSSR	RBS EMPLOYED. EFFICIENCY MEASURED. TWO TARGETS USED.
KROA82	.1397-.744	95+-3 THICK	-	-	LT 16	CPSSR	CRYSTAL SPECTROMETER AND Si(Li) USED. RBS EMPLOYED. EFFICIENCY CALCULATED. METAL TARGET ON CARBON BACKING. ONLY LALPHA/LL RATIO AVAILABLE FOR THICK TARGET.

TABLE AII EXPERIMENTAL X-RAY PRODUCTION CROSS SECTIONS

THIN TARGET

ENERGY MeV	ALPHA	BETA	GAMMA	L	ETA	TOTAL	REF
			BARNS				
.1397	-	-	-	-	-	1.13	KROA82
.1697	-	-	-	-	-	2.43	
.2102	-	-	-	-	-	5.3	

TABLE A. Experimental *L*-Shell X-Ray Production Cross Sections for Proton Impact

Z=47 SILVER(AG) CONTINUED

TABLE AII EXPERIMENTAL X-RAY PRODUCTION CROSS SECTIONS CONTINUED

THIN TARGET

ENERGY MeV	ALPHA	BETA	GAMMA	L	ETA	TOTAL	REF
			BARNS				
.2500	4.86	-	-	-	-	9.8	SARW81
.2608	-	-	-	-	-	10.3	KROA82
.3000	9.9	-	-	-	-	18.6	SARW81
.3000	-	-	-	-	-	9.2	BAUC81
.3214	-	-	-	-	-	18.0	KROA82
.3500	15.2	-	-	-	-	26.9	SARW81
.4000	19.2	-	-	-	-	36.8	
.4020	-	-	-	-	-	31.7	KROA82
.4925	-	-	-	-	-	54	
.5000	-	-	-	-	-	34.3	BAUC81
.6034	-	-	-	-	-	80	KROA82
.6110	-	-	-	-	-	158	CUZP81
.6500	-	-	-	-	-	74	BAUC81
.7440	-	-	-	-	-	126	KROA82
.8000	-	-	-	-	-	102	BAUC81
.8110	-	-	-	-	-	322	CUZP81
.9500	-	-	-	-	-	278	MILM76
1.0000	-	-	-	-	-	162	BAUC81
1.0190	-	-	-	-	-	468	CUZP81
1.2000	-	-	-	-	-	599	
1.4000	-	-	-	-	-	756	
1.6000	-	-	-	-	-	786	
1.8000	-	-	-	-	-	907	
2.0000	-	-	-	-	-	477	BAUC81
2.0000	-	-	-	-	-	1130	CUZP81
2.2000	-	-	-	-	-	1090	
2.4000	-	-	-	-	-	1200	
2.6000	-	-	-	-	-	1340	
2.8000	-	-	-	-	-	1580	
3.0000	-	-	-	-	-	1530	
3.0000	-	-	-	-	-	1620	CHAR75
3.0000	-	-	-	-	-	950	BONG78
3.2000	-	-	-	-	-	1670	CUZP81
3.4000	-	-	-	-	-	1690	
3.6000	-	-	-	-	-	1820	
3.8000	-	-	-	-	-	1810	
3.8500	-	-	-	-	-	1800	
4.0000	-	-	-	-	-	2160	CHAR75
4.0000	-	-	-	-	-	1666	BADT78
4.0000	-	-	-	-	-	690	BAUC81
5.0000	-	-	-	-	-	2376	CHAR75
6.0000	-	-	-	-	-	2646	
7.0000	-	-	-	-	-	2646	
8.0000	-	-	-	-	-	2484	
9.0000	-	-	-	-	-	2484	
10.0000	-	-	-	-	-	2484	
11.0000	-	-	-	-	-	2322	
12.0000	-	-	-	-	-	2160	

THICK TARGET

ENERGY MeV	ALPHA	BETA	GAMMA	L	ETA	TOTAL	REF
			BARNS				
.035	-	-	-	-	-	1.3E-05	LAPG80
.040	-	-	-	-	-	9.1E-05	
.045	-	-	-	-	-	4.4E-04	
.050	-	-	-	-	-	1.4E-03	
.055	-	-	-	-	-	3.4E-03	
.060	-	-	-	-	-	7.2E-03	
.070	-	-	-	-	-	.027	
.080	-	-	-	-	-	.059	
.090	-	-	-	-	-	.120	

TABLE A. Experimental *L*-Shell X-Ray Production Cross Sections for Proton Impact

Z=47 SILVER(AG) CONTINUED

TABLE AII   EXPERIMENTAL X-RAY PRODUCTION CROSS SECTIONS CONTINUED

THICK TARGET

ENERGY MeV	ALPHA	BETA	GAMMA	L	ETA	TOTAL	REF
			BARNS				
.100	-	-	-	-	-	.240	LAPG80
.110	-	-	-	-	-	.380	
.120	-	-	-	-	-	.59	
.130	-	-	-	-	-	.82	
.140	-	-	-	-	-	1.10	
.150	-	-	-	-	-	1.40	
.160	-	-	-	-	-	1.90	
.180	-	-	-	-	-	2.80	
.200	-	-	-	-	-	3.60	
.220	-	-	-	-	-	4.80	
.240	-	-	-	-	-	6.1	
.249	-	-	-	-	-	7.6	BAUC81
.260	-	-	-	-	-	7.2	LAPG80
.280	-	-	-	-	-	9.0	
.300	-	-	-	-	-	12.0	BAUC81
.300	-	-	-	-	-	11.1	LAPG80
.353	-	-	-	-	-	17.3	BAUC81
.403	-	-	-	-	-	22.8	
.484	-	-	-	-	-	33.6	
.552	-	-	-	-	-	44.2	
.635	-	-	-	-	-	59	
.720	-	-	-	-	-	77	
.810	-	-	-	-	-	100	
.900	-	-	-	-	-	125	
1.100	-	-	-	-	-	187	
1.300	-	-	-	-	-	242	
1.520	-	-	-	-	-	304	
1.720	-	-	-	-	-	350	
1.910	-	-	-	-	-	381	

TABLE AIII   LALPHA/LL RATIO

ENERGY RANGE MeV	TARGET	LA/LL	REF	ENERGY RANGE MeV	TARGET	LA/LL	REF
0.5	THICK	30.4*	KROA82	0.5	THIN	28.8+-2.0*	KROA82
0.5	THICK	25.1†					

* Si(Li) DETECTOR USED   † CRYSTAL SPECTROMETER USED.

Z=48 CADMIUM(CD)

TABLE AI   EXPERIMENTAL DETAILS

REF	ENERGY RANGE MeV	AREAL DENSITY E-6G/CMSQ	BEAM CURRENT A	BEAM COLL mm	EXP ERROR %	THEORIES	COMMENTS
BONG78	3.0	THIN	-	-	LT 8	BEA(G3)	RBS EMPLOYED. EFFICIENCY MEASURED. K-SHELL STUDIED. METAL TARGET ON CARBON BACKING.

TABLE A. Experimental L-Shell X-Ray Production Cross Sections for Proton Impact

Z=48 CADMIUM(CD) CONTINUED

TABLE AI EXPERIMENTAL DETAILS CONTINUED

REF	ENERGY RANGE MeV	AREAL DENSITY E-6G/CMSQ	BEAM CURRENT A	BEAM COLL mm	EXP ERROR %	THEORIES	COMMENTS
PETV80	.07-.45	THICK	-	-	LT 25	PWBA1	PROPORTIONAL COUNTER USED. EFFICIENCY MEASURED.
CHMJ81	.12-.42	32+-2 26+-2	-	-	LT 15-17	PWBA3 CPSSR	HP Ge DETECTOR USED. RBS EMPLOYED. EFFICIENCY MEASURED. TWO METAL TARGETS ON CARBON BACKING USED. ALPHA/BETA ALPHA/GAMMA AND BETA/GAMMA INTENSITY RATIOS PRESENTED.
SARW81	.25-.40	79+-4	3-100E-9	1.0(B)	LA 15 LT 15	PWBABC PWBABCR ECPSSR	RBS EMPLOYED. EFFICIENCY MEASURED.
KROA82	.1372-.7422	126+-4 THICK	-	-	LT 14-16	CPSSR	CRYSTAL SPECTROMETER AND Si(Li) USED. RBS EMPLOYED. EFFICIENCY CALCULATED. METAL TARGET ON VITRIOUS CARBON BACKING. ONLY LALPHA/LL RATIO AVAILABLE FOR THICK TARGET.

TABLE AII EXPERIMENTAL X-RAY PRODUCTION CROSS SECTIONS

THIN TARGET

ENERGY MeV	ALPHA	BETA	GAMMA	L	ETA	TOTAL	REF
			BARNS				
.1200	-	-	-	-	-	.262	CHMJ81
.1372	-	-	-	-	-	.79	KROA82
.1400	-	-	-	-	-	.53	CHMJ81
.1600	-	-	-	-	-	.83	
.1673	-	-	-	-	-	1.76	KROA82
.1800	-	-	-	-	-	1.49	CHMJ81
.2000	-	-	-	-	-	2.06	
.2076	-	-	-	-	-	3.85	KROA82
.2200	-	-	-	-	-	2.93	CHMJ81
.2400	-	-	-	-	-	4.11	
.2500	3.60	-	-	-	-	7.2	SARW81
.2581	-	-	-	-	-	7.8	KROA82
.2600	-	-	-	-	-	5.1	CHMJ81
.2800	-	-	-	-	-	6.2	
.3000	7.4	-	-	-	-	14.1	SARW81
.3000	-	-	-	-	-	7.4	CHMJ81
.3188	-	-	-	-	-	14.1	KROA82

TABLE A. Experimental L-Shell X-Ray Production Cross Sections for Proton Impact

Z=48 CADMIUM(CD) CONTINUED

TABLE AII   EXPERIMENTAL X-RAY PRODUCTION CROSS SECTIONS CONTINUED

THIN TARGET

ENERGY MeV	ALPHA	BETA	GAMMA	L	ETA	TOTAL	REF
			BARNS				
.3200	-	-	-	-	-	9.2	CHMJ81
.3400	-	-	-	-	-	11.2	
.3500	9.5	-	-	-	-	20.1	SARW81
.3600	-	-	-	-	-	13.2	CHMJ81
.3800	-	-	-	-	-	15.3	
.3997	-	-	-	-	-	25.4	KROA82
.4000	15.0	-	-	-	-	30.8	SARW81
.4000	-	-	-	-	-	17.6	CHMJ81
.4200	-	-	-	-	-	19.4	
.4906	-	-	-	-	-	42.6	KROA82
.6015	-	-	-	-	-	69	
.7422	-	-	-	-	-	110	
3.0000	-	-	-	-	-	916	BONG78

THICK TARGET

ENERGY MeV	ALPHA	BETA	GAMMA	L	ETA	TOTAL	REF
			BARNS				
.070	-	-	-	-	-	.060	PETV80
.085	-	-	-	-	-	.120	
.100	-	-	-	-	-	.235	
.120	-	-	-	-	-	.440	
.140	-	-	-	-	-	.66	
.165	-	-	-	-	-	1.05	
.200	-	-	-	-	-	2.20	
.250	-	-	-	-	-	4.68	
.300	-	-	-	-	-	8.8	
.350	-	-	-	-	-	14.0	
.400	-	-	-	-	-	18.2	
.450	-	-	-	-	-	21.3	

TABLE AIII   LALPHA/LL RATIO

ENERGY RANGE MeV	TARGET	LA/LL	REF	ENERGY RANGE MeV	TARGET	LA/LL	REF
0.5	THICK	29.2*	KROA82	0.5	THIN	27.0+-1.9*	KROA82
0.5	THICK	28.7†					

* Si(Li) DETECTOR USED   † CRYSTAL SPECTROMETER USED.

Z=49 INDIUM(IN)

TABLE AI   EXPERIMENTAL DETAILS

REF	ENERGY RANGE MeV	AREAL DENSITY E-6G/CMSQ	BEAM CURRENT A	BEAM COLL mm	EXP ERROR %	THEORIES	COMMENTS
KHAR78	1.0-3.0	THICK	-	1.0(C)	LT 14	BEA(G3) CBEA PWBA3	EFFICIENCY CALCULATED.

TABLE A. Experimental *L*-Shell X-Ray Production Cross Sections for Proton Impact

Z=49 INDIUM(IN) CONTINUED

TABLE AI   EXPERIMENTAL DETAILS CONTINUED

REF	ENERGY RANGE MeV	AREAL DENSITY E-6G/CMSQ	BEAM CURRENT A	BEAM COLL mm	EXP ERROR %	THEORIES	COMMENTS
FASS82	.118-.399	19+-1	-	-	LA 15 LB 15-18 LG 11-13 LT 14-15	CPSSR	HP Ge DETECTOR USED. RBS EMPLOYED. EFFICIENCY MEASURED. METAL TARGET ON CARBON BACKING. BETA(2+15) GAMMA(1) AND GAMMA(2+3) CROSS SECTIONS QUOTED.
KROA82	.1359-.7417	136+-8 THICK	-	-	LT 14-16	CPSSR	CRYSTAL SPECTROMETER AND Si(Li) USED. RBS EMPLOYED. EFFICIENCY CALCULATED. METAL TARGET ON VITRIOUS CARBON BACKING. ONLY LALPHA/LL RATIO AVAILABLE FOR THICK TARGET.

TABLE AII   EXPERIMENTAL X-RAY PRODUCTION CROSS SECTIONS

THIN TARGET

ENERGY MeV	ALPHA	BETA	GAMMA	L	ETA	TOTAL	REF
			BARNS				
.1180	.130	.068	.013	-	-	.220	FASS82
.1359	-	-	-	-	-	.61	KROA82
.1380	.360	.170	.029	-	-	.56	FASS82
.1580	.62	.270	.046	-	-	1.01	
.1661	-	-	-	-	-	1.43	KROA82
.1780	.91	.390	.079	-	-	1.47	FASS82
.1980	1.40	.56	.089	-	-	2.21	
.2066	-	-	-	-	-	3.17	KROA82
.2180	1.93	.77	.133	-	-	3.03	FASS82
.2380	2.54	1.01	.169	-	-	4.03	
.2573	-	-	-	-	-	6.6	KROA82
.2580	3.17	1.29	.198	-	-	4.96	FASS82
.2770	4.03	1.53	.258	-	-	6.5	
.2990	4.63	1.87	.302	-	-	7.6	
.3180	-	-	-	-	-	12.2	KROA82
.3190	5.9	2.21	.328	-	-	9.3	FASS82
.3390	6.9	2.70	.429	-	-	10.8	
.3590	8.1	3.08	.440	-	-	12.8	
.3790	9.4	3.51	.53	-	-	14.9	
.3989	-	-	-	-	-	22.3	KROA82
.3990	10.6	3.94	.58	-	-	16.7	FASS82
.4897	-	-	-	-	-	37.9	KROA82
.6006	-	-	-	-	-	60	
.7417	-	-	-	-	-	96	

TABLE A. Experimental L-Shell X-Ray Production Cross Sections for Proton Impact

Z=49 INDIUM(IN) CONTINUED

TABLE AII EXPERIMENTAL X-RAY PRODUCTION CROSS SECTIONS CONTINUED

THICK TARGET

ENERGY MeV	ALPHA	BETA	GAMMA	L	ETA	TOTAL	REF
	BARNS						
1.0000	-	-	-	-	-	180	KHAR78
1.2000	-	-	-	-	-	260	
1.4000	-	-	-	-	-	340	
1.6000	-	-	-	-	-	420	
1.8000	-	-	-	-	-	500	
2.0000	-	-	-	-	-	590	
2.2000	-	-	-	-	-	660	
2.4000	-	-	-	-	-	740	
2.6000	-	-	-	-	-	800	
2.8000	-	-	-	-	-	850	
3.0000	-	-	-	-	-	890	

TABLE AIII LALPHA/LL RATIO

ENERGY RANGE MeV	TARGET	LA/LL	REF	ENERGY RANGE MeV	TARGET	LA/LL	REF
0.5	THICK	29.0*	KROA82	0.5	THIN	27.4+-2.0*	KROA82
0.5	THICK	29.9†					

* Si(Li) DETECTOR USED † CRYSTAL SPECTROMETER USED.

Z=50 TIN(SN)

TABLE AI EXPERIMENTAL DETAILS

REF	ENERGY RANGE MeV	AREAL DENSITY E-6G/CMSQ	BEAM CURRENT A	BEAM COLL mm	EXP ERROR %	THEORIES	COMMENTS
CHAR75	3-12	29+-3	-	-	LT 20	BEA(G3) PWBA3	RBS EMPLOYED. EFFICIENCY CALCULATED. O5+ IMPACT STUDIED. METAL TARGET ON CARBON BACKING.
BONG78	3.0	THIN	-	-	LT 7	BEA(G3)	RBS EMPLOYED. EFFICIENCY MEASURED. K-SHELL STUDIED. SELF-SUPPORTING METAL TARGET.
KHAR78	1-3.0	THICK	-	1.0(C)	LT 13	BEA(G3) CBEA PWBA3	EFFICIENCY CALCULATED.
SERK80	2.92-39.34	339	-	-	LT 12	BEA(V) PWBA3 PWBA4	RBS EMPLOYED. SELF-SUPPORTING METAL TARGET.
SARW81	.30-.40	14.6+-.7	3-100E-9	1.0(B)	LA 15 LT 15-23	PWBABC PWBABCR ECPSSR	RBS EMPLOYED. EFFICIENCY MEASURED.

TABLE A. Experimental L-Shell X-Ray Production Cross Sections for Proton Impact

Z=50 TIN(SN) CONTINUED

TABLE AI EXPERIMENTAL DETAILS CONTINUED

REF	ENERGY RANGE MeV	AREAL DENSITY E-6G/CMSQ	BEAM CURRENT A	BEAM COLL mm	EXP ERROR %	THEORIES	COMMENTS
KROA82	.137-.743	115+-5 THICK	-	-	LT 14-17	CPSSR	CRYSTAL SPECTROMETER AND Si(Li) USED. RBS EMPLOYED. EFFICIENCY CALCULATED. METAL TARGET ON VITRIOUS CARBON BACKING. ONLY LALPHA/LL RATIO AVAILABLE FOR THICK TARGET.

TABLE AII EXPERIMENTAL X-RAY PRODUCTION CROSS SECTIONS

THIN TARGET

ENERGY MeV	ALPHA	BETA	GAMMA	L	ETA	TOTAL	REF
			BARNS				
.1370	-	-	-	-	-	.451	KROA82
.1678	-	-	-	-	-	1.10	
.2081	-	-	-	-	-	2.52	
.2591	-	-	-	-	-	5.1	
.3000	5.3	-	-	-	-	9.8	SARW81
.3199	-	-	-	-	-	9.7	KROA82
.3500	8.6	-	-	-	-	15.7	SARW81
.4000	11.5	-	-	-	-	21.0	
.4007	-	-	-	-	-	18.8	KROA82
.4915	-	-	-	-	-	32.2	
.6023	-	-	-	-	-	51	
.7430	-	-	-	-	-	81	
2.9200	-	-	-	-	-	868	SERK80
3.0000	-	-	-	-	-	1273	CHAR75
3.0000	-	-	-	-	-	800	BONG78
3.9700	-	-	-	-	-	1110	SERK80
4.0000	-	-	-	-	-	1541	CHAR75
5.0000	-	-	-	-	-	2010	
6.0000	-	-	-	-	-	2144	
6.1300	-	-	-	-	-	1370	SERK80
7.0000	-	-	-	-	-	2211	CHAR75
8.0000	-	-	-	-	-	2278	
9.0000	-	-	-	-	-	2345	
10.0000	-	-	-	-	-	2211	
11.0000	-	-	-	-	-	2017	
12.0000	-	-	-	-	-	2010	
12.3100	-	-	-	-	-	1420	SERK80
18.1200	-	-	-	-	-	1270	
24.2100	-	-	-	-	-	1100	
30.5200	-	-	-	-	-	961	
39.3400	-	-	-	-	-	827	

TABLE A. Experimental *L*-Shell X-Ray Production Cross Sections for Proton Impact

Z=50 TIN(SN) CONTINUED

TABLE AII EXPERIMENTAL X-RAY PRODUCTION CROSS SECTIONS CONTINUED

THICK TARGET

ENERGY MeV	ALPHA	BETA	GAMMA	L	ETA	TOTAL	REF
			BARNS				
1.00	-	-	-	-	-	160	KHAR78
1.20	-	-	-	-	-	230	
1.40	-	-	-	-	-	310	
1.60	-	-	-	-	-	390	
1.80	-	-	-	-	-	470	
2.00	-	-	-	-	-	550	
2.20	-	-	-	-	-	620	
2.40	-	-	-	-	-	690	
2.60	-	-	-	-	-	760	
2.80	-	-	-	-	-	810	
2.90	-	-	-	-	-	840	
3.00	-	-	-	-	-	860	

TABLE AIII LALPHA/LL RATIO

ENERGY RANGE MeV	TARGET	LA/LL	REF	ENERGY RANGE MeV	TARGET	LA/LL	REF
0.5	THICK	29.6*	KROA82	0.5	THIN	29.2+-2.1*	KROA82
0.5	THICK	26.7†					

* Si(Li) DETECTOR USED † CRYSTAL SPECTROMETER USED.

Z=51 ANTIMONY(SB)

TABLE AI EXPERIMENTAL DETAILS

REF	ENERGY RANGE MeV	AREAL DENSITY E-6G/CMSQ	BEAM CURRENT A	BEAM COLL mm	EXP ERROR %	THEORIES	COMMENTS
KROA82	.1399-.7433	106+-4 THICK	-	-	LT 15-17	CPSSR	CRYSTAL SPECTROMETER AND Si(Li) USED. RBS EMPLOYED. EFFICIENCY CALCULATED. METAL TARGET ON CARBON BACKING. ONLY LALPHA/LL RATIO AVAILABLE FOR THICK TARGET.

TABLE AII EXPERIMENTAL X-RAY PRODUCTION CROSS SECTIONS

THIN TARGET

ENERGY MeV	TOTAL BARNS	REF	ENERGY MeV	TOTAL BARNS	REF
.1399	.424	KROA82	.4017	17.3	KROA82
.1693	1.01		.4921	29.5	
.2096	2.29		.6028	46.4	
.2601	5.1		.7433	76	
.3206	9.7				

TABLE A. Experimental *L*-Shell X-Ray Production Cross Sections for Proton Impact

Z=51 ANTIMONY(SB) CONTINUED

TABLE AIII LALPHA/LL RATIO

ENERGY RANGE MeV	TARGET	LA/LL	REF	ENERGY RANGE MeV	TARGET	LA/LL	REF
0.5	THICK	29.8*	KROA82	0.5	THIN	28.2+-2.2*	KROA82
0.5	THICK	25.3†					

* Si(Li) DETECTOR USED † CRYSTAL SPECTROMETER USED.

Z=52 TELLURIUM(TE)

TABLE AI EXPERIMENTAL DETAILS

REF	ENERGY RANGE MeV	AREAL DENSITY E-6G/CMSQ	BEAM CURRENT A	BEAM COLL mm	EXP ERROR %	THEORIES	COMMENTS
SOKR81	.6-3.0	50+-5	1-10E-9	1.5(C)	LT 19	PWBA4 PWBABC	EFFICIENCY CALCULATED. METAL TARGET ON NUCLEPORE BACKING.

TABLE AII EXPERIMENTAL X-RAY PRODUCTION CROSS SECTIONS

THIN TARGET

ENERGY MeV	TOTAL BARNS	REF	ENERGY MeV	TOTAL BARNS	REF
.60	35.0	SOKR81	2.00	380	SOKR81
.70	52		2.20	416	
.80	64		2.40	489	
.90	89		2.50	514	
1.00	114		2.60	539	
1.20	160		2.70	556	
1.40	202		2.80	583	
1.60	251		2.90	616	
1.80	310		3.00	666	

Z=53 IODINE(I)

TABLE AI EXPERIMENTAL DETAILS

REF	ENERGY RANGE MeV	AREAL DENSITY E-6G/CMSQ	BEAM CURRENT A	BEAM COLL mm	EXP ERROR %	THEORIES	COMMENTS
BONG78	3.0-11.0	THIN	-	-	LT 8	BEA(G3)	RBS EMPLOYED. EFFICIENCY MEASURED. K-SHELL STUDIED. TARGET ON CARBON BACKING.

TABLE A. Experimental L-Shell X-Ray Production Cross Sections for Proton Impact

Z=53 IODINE(I) CONTINUED

TABLE AI   EXPERIMENTAL DETAILS CONTINUED

REF	ENERGY RANGE MeV	AREAL DENSITY E-6G/CMSQ	BEAM CURRENT A	BEAM COLL mm	EXP ERROR %	THEORIES	COMMENTS
CUZP81	.611-3.85	THIN	-	-	LT 5-10	BEA(H) SCA2 PWBA3	EFFICIENCY MEASURED. AgIO3 TARGET ON CARBON BACKING. CROSS SECTIONS EVALUATED BY NORMALIZING TO K-SHELL DATA.

TABLE AII   EXPERIMENTAL X-RAY PRODUCTION CROSS SECTIONS

THIN TARGET

ENERGY MeV	TOTAL BARNS	REF	ENERGY MeV	TOTAL BARNS	REF
.611	36.5	CUZP81	3.000	670	CUZP81
.811	81		3.000	630	BONG78
1.019	124		3.200	743	CUZP81
1.200	171		3.400	806	
1.400	229		3.600	881	
1.600	280		3.800	907	
1.800	328		3.850	916	
2.000	425		5.000	1004	BONG78
2.200	435		7.000	1203	
2.400	484		9.000	1220	
2.600	549		11.000	1181	
2.800	648				

Z=55 CESIUM(CS)

TABLE AI   EXPERIMENTAL DETAILS

REF	ENERGY RANGE MeV	AREAL DENSITY E-6G/CMSQ	BEAM CURRENT A	BEAM COLL mm	EXP ERROR %	THEORIES	COMMENTS
BADT78	4.0	47+-2	1-5E-9	-	LT 9	BEA(G3) PWBA2	EFFICIENCY MEASURED. K-SHELL STUDIED. CsBr TARGET ON MYLAR BACKING.

TABLE AII   EXPERIMENTAL X-RAY PRODUCTION CROSS SECTIONS

THIN TARGET

ENERGY MeV	TOTAL BARNS	REF	ENERGY MeV	TOTAL BARNS	REF
4.00	1117	BADT78			

TABLE A. Experimental *L*-Shell X-Ray Production Cross Sections for Proton Impact

Z=58 CERIUM(CE)

TABLE AI EXPERIMENTAL DETAILS

REF	ENERGY RANGE MeV	AREAL DENSITY E-6G/CMSQ	BEAM CURRENT A	BEAM COLL mm	EXP ERROR %	THEORIES	COMMENTS
BEAR73	1-3.0	129	-	-	LA 15	BEA(G4) PWBA2	RECTANGULAR BEAM. RBS EMPLOYED. EFFICIENCY MEASURED. Ce2O3 TARGET.

TABLE AII EXPERIMENTAL X-RAY PRODUCTION CROSS SECTIONS

THIN TARGET

ENERGY MeV	ALPHA (BARNS)	BETA	GAMMA	L	ETA	TOTAL	REF
1.00	23.0	-	-	-	-	-	BEAR73
2.25	97	-	-	-	-	-	
3.00	150	-	-	-	-	-	

Z=59 PRASEODYMIUM(PR)

TABLE AI EXPERIMENTAL DETAILS

REF	ENERGY RANGE MeV	AREAL DENSITY E-6G/CMSQ	BEAM CURRENT A	BEAM COLL mm	EXP ERROR %	THEORIES	COMMENTS
WHER79	.15-.40	THICK	-	2.0(B)	-	PSS PSSR PWBA3	EFFICIENCY MEASURED. GAMMA(1) AND GAMMA(2+3) CROSS SECTIONS QUOTED.

TABLE AII EXPERIMENTAL X-RAY PRODUCTION CROSS SECTIONS

THICK TARGET

ENERGY MeV	ALPHA (BARNS)	BETA	GAMMA	L	ETA	TOTAL	REF
.150	.035	-	3.7E-03	-	-	-	WHER79
.175	.087	-	8.7E-03	-	-	-	
.200	.180	-	.017	-	-	-	
.250	.55	-	.046	-	-	-	
.300	1.20	-	.094	-	-	-	
.350	2.20	-	.162	-	-	-	
.400	3.60	-	.246	-	-	-	

TABLE A. Experimental *L*-Shell X-Ray Production Cross Sections for Proton Impact

Z=60 NEODYMIUM(ND)

TABLE AI EXPERIMENTAL DETAILS

REF	ENERGY RANGE MeV	AREAL DENSITY E-6G/CMSQ	BEAM CURRENT A	BEAM COLL mm	EXP ERROR %	THEORIES	COMMENTS
KHAR78	1.0-3.0	THICK	-	1.0(C)	LA 7-10 LB 7-9 LT 8	BEA(G3) CBEA PWBA3	EFFICIENCY CALCULATED.

TABLE AII EXPERIMENTAL X-RAY PRODUCTION CROSS SECTIONS

THICK TARGET

ENERGY MeV	ALPHA	BETA	GAMMA	L	ETA	TOTAL	REF
			BARNS				
1.00	21.0	13.0	-	-	-	34.0	KHAR78
1.20	32.0	21.0	-	-	-	54	
1.40	45.0	30.0	-	-	-	79	
1.60	59	41.0	-	-	-	106	
1.80	74	54	-	-	-	137	
2.00	90	67	-	-	-	170	
2.20	110	81	-	-	-	200	
2.40	120	95	-	-	-	240	
2.60	140	108	-	-	-	270	
2.80	150	120	-	-	-	300	
3.00	170	130	-	-	-	330	

Z=62 SAMARIUM(SM)

TABLE AI EXPERIMENTAL DETAILS

REF	ENERGY RANGE MeV	AREAL DENSITY E-6G/CMSQ	BEAM CURRENT A	BEAM COLL mm	EXP ERROR %	THEORIES	COMMENTS
BEAR73	1.0-3.7	83	-	-	LA 15	BEA(G4) PWBA2	RECTANGULAR BEAM. RBS EMPLOYED. EFFICIENCY MEASURED.
MILM76	.950	100	-	2.0(B)	LX 10 LT 10	BEA(G3)	SQUARE BEAM. RBS EMPLOYED. EFFICIENCY CALCULATED. METAL TARGET ON CARBON BACKING.
WHER79	.15-.44	THICK	-	2.0(B)	-	PSS PSSR PWBA3	EFFICIENCY MEASURED. GAMMA(1) AND GAMMA(2+3) CROSS SECTIONS QUOTED.

TABLE A. Experimental *L*-Shell X-Ray Production Cross Sections for Proton Impact

Z=62 SAMARIUM(SM) CONTINUED

TABLE AII EXPERIMENTAL X-RAY PRODUCTION CROSS SECTIONS

THIN TARGET

ENERGY MeV	ALPHA	BETA	GAMMA	L	ETA	TOTAL	REF
			BARNS				
.95	13.8	8.4	1.20	-	-	23.4	MILM76
1.00	16.0	-	-	-	-	-	BEAR73
1.10	20.0	-	-	-	-	-	
1.20	24.0	-	-	-	-	-	
1.30	29.0	-	-	-	-	-	
1.40	34.0	-	-	-	-	-	
1.50	39.0	-	-	-	-	-	
1.60	45.0	-	-	-	-	-	
1.70	49.0	-	-	-	-	-	
1.80	55	-	-	-	-	-	
1.90	60	-	-	-	-	-	
2.00	69	-	-	-	-	-	
2.10	72	-	-	-	-	-	
2.20	77	-	-	-	-	-	
2.25	80	-	-	-	-	-	
2.30	83	-	-	-	-	-	
2.40	89	-	-	-	-	-	
2.50	94	-	-	-	-	-	
2.60	102	-	-	-	-	-	
2.70	107	-	-	-	-	-	
2.80	114	-	-	-	-	-	
2.90	119	-	-	-	-	-	
3.00	126	-	-	-	-	-	
3.10	132	-	-	-	-	-	
3.20	139	-	-	-	-	-	
3.30	142	-	-	-	-	-	
3.40	148	-	-	-	-	-	
3.50	152	-	-	-	-	-	
3.60	157	-	-	-	-	-	
3.70	163	-	-	-	-	-	

THICK TARGET

ENERGY MeV	ALPHA	BETA	GAMMA	L	ETA	TOTAL	REF
			BARNS				
.150	.014	-	1.5E-03	-	-	-	WHER79
.175	.038	-	3.9E-03	-	-	-	
.200	.083	-	8.3E-03	-	-	-	
.250	.270	-	.025	-	-	-	
.300	.64	-	.053	-	-	-	
.350	1.20	-	.091	-	-	-	
.400	1.90	-	.132	-	-	-	
.440	2.70	-	.176	-	-	-	

Z=64 GADOLINIUM(GD)

TABLE AI EXPERIMENTAL DETAILS

REF	ENERGY RANGE MeV	AREAL DENSITY E-6G/CMSQ	BEAM CURRENT A	BEAM COLL mm	EXP ERROR %	THEORIES	COMMENTS
MILM76	.950	100	-	2.0(B)	LX 10 LT 10	BEA(G3)	SQUARE BEAM. RBS EMPLOYED. EFFICIENCY CALCULATED. METAL TARGET ON CARBON BACKING.

TABLE A. Experimental L-Shell X-Ray Production Cross Sections for Proton Impact

Z=64 GADOLINIUM(GD) CONTINUED

TABLE AII EXPERIMENTAL X-RAY PRODUCTION CROSS SECTIONS

THIN TARGET

ENERGY MeV	ALPHA	BETA	GAMMA	L	ETA	TOTAL	REF
			BARNS				
.95	10.5	6.3	.86	-	-	17.6	MILM76

Z=65 TERBIUM(TB)

TABLE AI EXPERIMENTAL DETAILS

REF	ENERGY RANGE MeV	AREAL DENSITY E-6G/CMSQ	BEAM CURRENT A	BEAM COLL mm	EXP ERROR %	THEORIES	COMMENTS
WHER79	.15-.40	THICK	-	2.0(B)	-	PSS PSSR PWBA3	EFFICIENCY MEASURED. GAMMA(1) AND GAMMA(2+3) CROSS SECTIONS QUOTED.

TABLE AII EXPERIMENTAL X-RAY PRODUCTION CROSS SECTIONS

THICK TARGET

ENERGY MeV	ALPHA	BETA	GAMMA	L	ETA	TOTAL	REF
			BARNS				
.150	6.0E-03	-	7.5E-04	-	-	-	WHER79
.175	.017	-	2.1E-03	-	-	-	
.200	.039	-	4.7E-03	-	-	-	
.250	.140	-	.015	-	-	-	
.300	.370	-	.037	-	-	-	
.350	.77	-	.068	-	-	-	
.400	1.40	-	.111	-	-	-	

Z=66 DYSPROSIUM(DY)

TABLE AI EXPERIMENTAL DETAILS

REF	ENERGY RANGE MeV	AREAL DENSITY E-6G/CMSQ	BEAM CURRENT A	BEAM COLL mm	EXP ERROR %	THEORIES	COMMENTS
BEAR73	1.0-3.0	163	-	-	LA 15	BEA(G4) PWBA2	RECTANGULAR BEAM. RBS MEASURED. EFFICIENCY MEASURED.
KHAR78	1.0-3.0	THICK	-	1.0(C)	LA 4-6 LB 3-6 LG 4-6 LT 4-6	BEA(G3) CBEA PWBA3	EFFICIENCY CALCULATED.

TABLE A. Experimental *L*-Shell X-Ray Production Cross Sections for Proton Impact

Z=66 DYSPROSIUM(DY) CONTINUED

TABLE AI EXPERIMENTAL DETAILS CONTINUED

REF	ENERGY RANGE MeV	AREAL DENSITY E-6G/CMSQ	BEAM CURRENT A	BEAM COLL mm	EXP ERROR %	THEORIES	COMMENTS
SOKR82	.6-3.0	52+-3	1-10E-9	1.5(C)	LA 8 LB 8 LG 8-12 LL 9-13 LT 6	CPSSR	EFFICIENCY CALCULATED. METAL TARGET ON NUCLEPORE BACKING.

TABLE AII EXPERIMENTAL X-RAY PRODUCTION CROSS SECTIONS

THIN TARGET

ENERGY MeV	ALPHA	BETA	GAMMA	L	ETA	TOTAL	REF
			BARNS				
.60	3.60	2.00	.250	.110	-	6.0	SOKR82
.70	5.5	3.10	.390	.220	-	9.2	
.80	8.0	4.40	:78	.340	-	13.5	
.90	10.7	6.1	.78	.300	-	17.9	
1.00	12.0	-	-	-	-	-	BEAR73
1.00	14.0	7.9	1.00	.350	-	23.3	SOKR82
1.20	20.0	12.0	1.60	1.10	-	34.7	
1.40	29.0	17.0	2.60	1.00	-	49.6	
1.60	38.0	23.0	3.30	1.30	-	66	
1.80	48.0	30.0	4.20	1.80	-	84	
2.00	56	36.0	5.7	2.00	-	100	
2.20	68	47.0	6.4	2.60	-	124	
2.25	60	-	-	-	-	-	BEAR73
2.40	80	54	8.1	2.90	-	145	SOKR82
2.50	86	61	9.6	3.10	-	160	
2.60	90	63	9.3	3.30	-	166	
2.70	98	70	10.8	3.80	-	183	
2.80	102	72	11.2	4.10	-	189	
2.90	106	76	12.0	3.90	-	198	
3.00	94	-	-	-	-	-	BEAR73
3.00	115	85	13.0	4.20	-	217	SOKR82

THICK TARGET

ENERGY MeV	ALPHA	BETA	GAMMA	L	ETA	TOTAL	REF
			BARNS				
1.00	11.5	6.6	.72	-	-	18.0	KHAR78
1.10	14.2	8.5	.92	-	-	23.0	
1.20	17.2	10.6	1.15	-	-	28.0	
1.40	24.0	15.5	1.71	-	-	41.0	
1.60	31.0	21.3	2.38	-	-	55	
1.80	40.0	27.8	3.20	-	-	71	
2.00	49.0	35.0	4.00	-	-	89	
2.20	58	43.0	5.0	-	-	108	
2.40	68	51	5.9	-	-	127	
2.50	73	55	6.4	-	-	137	
2.60	78	59	6.9	-	-	147	
2.70	82	63	7.4	-	-	157	
2.80	87	67	7.9	-	-	167	
2.90	91	72	8.4	-	-	177	
3.00	96	76	8.8	-	-	187	

TABLE A. Experimental *L*-Shell X-Ray Production Cross Sections for Proton Impact

Z=66 DYSPROSIUM(DY) CONTINUED

TABLE AIII LALPHA/LL RATIO

ENERGY RANGE MeV	TARGET	LA/LL	REF	ENERGY RANGE MeV	TARGET	LA/LL	REF
1.0-3.0	THICK	27.0+-1.9	KHAR78	0.6-3.0	THIN	27.4+-0.8	SOKR82

Z=67 HOLMIUM(HO)

TABLE AI EXPERIMENTAL DETAILS

REF	ENERGY RANGE MeV	AREAL DENSITY E-6G/CMSQ	BEAM CURRENT A	BEAM COLL mm	EXP ERROR %	THEORIES	COMMENTS
WHER79	.15-.40	THICK	-	2.0(B)	-	PSS PSSR PWBA3	EFFICIENCY MEASURED. GGMMA(1) AND GAMMA(2+3) CROSS SECTIONS QUOTED.

TABLE AII EXPERIMENTAL X-RAY PRODUCTION CROSS SECTIONS

THICK TARGET

ENERGY MeV	ALPHA	BETA	GAMMA	L	ETA	TOTAL	REF
			BARNS				
.150	3.5E-03	-	4.0E-04	-	-	-	WHER79
.175	.013	-	1.6E-03	-	-	-	
.200	.035	-	4.3E-03	-	-	-	
.250	.140	-	.016	-	-	-	
.300	.320	-	.035	-	-	-	
.350	.56	-	.052	-	-	-	
.400	.77	-	.063	-	-	-	

Z=68 ERBIUM(ER)

TABLE AI EXPERIMENTAL DETAILS

REF	ENERGY RANGE MeV	AREAL DENSITY E-6G/CMSQ	BEAM CURRENT A	BEAM COLL mm	EXP ERROR %	THEORIES	COMMENTS
SARW81	.30-.40	15+-1.2	3-100E-9	1.0(B)	LA 10 LT 15	PWBABC PWBABCR ECPSSR	RBS EMPLOYED. EFFICIENCY MEASURED. SELF-SUPPORTING METAL TARGET.

TABLE A. Experimental *L*-Shell X-Ray Production Cross Sections for Proton Impact

Z=68 ERBIUM(ER) CONTINUED

TABLE AII EXPERIMENTAL X-RAY PRODUCTION CROSS SECTIONS

THIN TARGET

ENERGY MeV	ALPHA	BETA	GAMMA	L	ETA	TOTAL	REF
			BARNS				
.30	.169	-	-	-	-	.316	SARW81
.35	.316	-	-	-	-	.57	
.40	.59	-	-	-	-	1.03	

Z=69 THULIUM(TM)

TABLE AI EXPERIMENTAL DETAILS

REF	ENERGY RANGE MeV	AREAL DENSITY E-6G/CMSQ	BEAM CURRENT A	BEAM COLL mm	EXP ERROR %	THEORIES	COMMENTS
BEAR73	1.0-3.0	100	-	-	LA 15	BEA(G4) PWBA2	RECTANGULAR BEAM. RBS EMPLOYED. EFFICIENCY MEASURED.

TABLE AII EXPERIMENTAL X-RAY PRODUCTION CROSS SECTIONS

THIN TARGET

ENERGY MeV	ALPHA	BETA	GAMMA	L	ETA	TOTAL	REF
			BARNS				
1.00	7.9	-	-	-	-	-	BEAR73
2.25	45.0	-	-	-	-	-	
3.00	75	-	-	-	-	-	

Z=70 YTTERBIUM(YB)

TABLE AI EXPERIMENTAL DETAILS

REF	ENERGY RANGE MeV	AREAL DENSITY E-6G/CMSQ	BEAM CURRENT A	BEAM COLL mm	EXP ERROR %	THEORIES	COMMENTS
WHER79	.15-.40	THICK	-	2.0(B)	-	PSS PSSR PWBA3	EFFICIENCY MEASURED. GAMMA(1) AND GAMMA(2+3) CROSS SECTIONS QUOTED.
SARW81	.30-.40	93+-4	3-100E-9	1.0(B)	LA 9 LT 9	PWBABC PWBABCR ECPSSR	RBS EMPLOYED. EFFICIENCY MEASURED.

TABLE A. Experimental L-Shell X-Ray Production Cross Sections for Proton Impact

Z=70 YTTERBIUM(YB) CONTINUED

TABLE AII EXPERIMENTAL X-RAY PRODUCTION CROSS SECTIONS

THIN TARGET

ENERGY MeV	ALPHA	BETA	GAMMA	L	ETA	TOTAL	REF
			BARNS				
.30	.169	-	-	-	-	.317	SARW81
.35	.247	-	-	-	-	.441	
.40	.367	-	-	-	-	.65	

THICK TARGET

ENERGY MeV	ALPHA	BETA	GAMMA	L	ETA	TOTAL	REF
			BARNS				
.150	1.2E-03	-	1.1E-04	-	-	-	WHER79
.175	4.6E-03	-	5.2E-04	-	-	-	
.200	.013	-	1.7E-03	-	-	-	
.250	.058	-	7.7E-03	-	-	-	
.300	.160	-	.019	-	-	-	
.350	.310	-	.032	-	-	-	
.400	.51	-	.041	-	-	-	

Z=72 HAFNIUM(HF)

TABLE AI EXPERIMENTAL DETAILS

REF	ENERGY RANGE MeV	AREAL DENSITY E-6G/CMSQ	BEAM CURRENT A	BEAM COLL mm	EXP ERROR %	THEORIES	COMMENTS
JUSE80	.5-2.5	50	30-200E-9	-	LA 4-5	-	RBS EMPLOYED. EFFICIENCY MEASURED. METAL TARGET ON FORMVAR BACKING. He+ IMPACT STUDIED.
SARW81	.30-.40	155+-20	3-100E-9	1.0(B)	LA 14 LT 15	PWBABC PWBABCR ECPSSR	RBS EMPLOYED. EFFICIENCY MEASURED.

TABLE AII EXPERIMENTAL X-RAY PRODUCTION CROSS SECTIONS

THIN TARGET

ENERGY MeV	ALPHA	BETA	GAMMA	L	ETA	TOTAL	REF
			BARNS				
.30	.133	-	-	-	-	.240	SARW81
.35	.160	-	-	-	-	.286	
.40	.268	-	-	-	-	.470	
.50	1.00	-	-	-	-	-	JUSE80
.60	1.88	-	-	-	-	-	
.70	3.16	-	-	-	-	-	
.80	4.49	-	-	-	-	-	
.90	6.0	-	-	-	-	-	
1.00	7.5	-	-	-	-	-	
1.10	9.5	-	-	-	-	-	
1.20	12.0	-	-	-	-	-	

TABLE A. Experimental *L*-Shell X-Ray Production Cross Sections for Proton Impact

Z=72 HAFNIUM(HF) CONTINUED

TABLE AII EXPERIMENTAL X-RAY PRODUCTION CROSS SECTIONS CONTINUED

THIN TARGET

ENERGY MeV	ALPHA	BETA	GAMMA	L	ETA	TOTAL	REF
	BARNS						
1.30	15.1	-	-	-	-	-	JUSE80
1.40	17.6	-	-	-	-	-	
1.50	20.2	-	-	-	-	-	
1.60	22.8	-	-	-	-	-	
1.80	29.4	-	-	-	-	-	
2.00	35.1	-	-	-	-	-	
2.50	54	-	-	-	-	-	

Z=73 TANTALUM(TA)

TABLE AI EXPERIMENTAL DETAILS

REF	ENERGY RANGE MeV	AREAL DENSITY E-6G/CMSQ	BEAM CURRENT A	BEAM COLL mm	EXP ERROR %	THEORIES	COMMENTS
ISHK74	1.75-4.17	1340	-	3.0(C)	LA 15 LB 15 LG 17 LL 17 LT 10	BEA(G2) PWBA3 IPWBAR	RBS EMPLOYED. EFFICIENCY MEASURED. SELF-SUPPORTING SEMI-THICK METAL TARGET. LALPHA/LL RATIO FOUND TO BE ENERGY DEPENDENT.
CHEJ76	0.4-2.0	50-100	5-50E-9	3.2(B)	-	BEA(G1) CBEA PWBA3	RBS EMPLOYED. EFFICIENCY MEASURED. LALPHA/LL RATIO ONLY AVAILABLE. METAL TARGET ON CARBON BACKING.
JUSE80	0.6-2.5	50	30-200E-9	-	LA 4-11	-	RBS EMPLOYED. EFFICIENCY MEASURED. METAL TARGET ON FORMVAR BACKING. He+ IMPACT STUDIED.
BAUC81	.249-1.91	THICK	2-500E-9	1.1(B)	LT 25	CPSSR	RBS EMPLOYED. EFFICIENCY MEASURED. He4 IMPACT STUDIED.
UDEN81	.28-.40	20.5+-.7	-	-	LA 12 LG 9-15 LL 13-19 LT 11-14	CPSSR	HP Ge DETECTOR USED. RBS EMPLOYED. EFFICIENCY MEASURED. GAMMA(1) AND GAMMA(2+3) CROSS SECTIONS QUOTED.

TABLE A. Experimental L-Shell X-Ray Production Cross Sections for Proton Impact

Z=73 TANTALUM(TA) CONTINUED

TABLE AII   EXPERIMENTAL X-RAY PRODUCTION CROSS SECTIONS

THIN TARGET

ENERGY MeV	ALPHA	BETA	GAMMA	L	ETA	TOTAL	REF
			BARNS				
.28	.051	-	3.9E-03	3.1E-03	-	.084	UDEN81
.30	.068	-	4.5E-03	3.7E-03	-	.111	
.32	.092	-	6.9E-03	6.1E-03	-	.155	
.34	.136	-	.010	9.1E-03	-	.288	
.36	.172	-	.012	.011	-	.287	
.38	.229	-	.014	.015	-	.376	
.40	.294	-	.020	.018	-	.481	
.60	1.56	-	-	-	-	-	JUSE80
.80	3.78	-	-	-	-	-	
1.00	6.9	-	-	-	-	-	
1.20	11.0	-	-	-	-	-	
1.30	12.9	-	-	-	-	-	
1.40	15.5	-	-	-	-	-	
1.50	18.1	-	-	-	-	-	
1.60	20.8	-	-	-	-	-	
1.80	27.0	-	-	-	-	-	
2.00	36.0	-	-	-	-	-	
2.50	52	-	-	-	-	-	

SEMI-THICK TARGET

ENERGY MeV	ALPHA	BETA	GAMMA	L	ETA	TOTAL	REF
			BARNS				
1.75	22.0	13.4	1.74	1.10	-	38.2	ISHK74
1.95	26.5	16.9	2.15	-	-	46.6	
2.16	33.4	21.9	3.04	1.84	-	60	
2.36	43.2	25.0	3.82	2.48	-	75	
2.56	47.9	32.4	4.61	2.77	-	88	
2.76	50	32.5	4.68	2.88	-	90	
2.96	55	38.9	6.0	3.54	-	103	
3.57	77	56	8.3	4.12	-	147	
3.77	81	58	-	6.0	-	153	
3.97	95	70	11.0	6.1	-	182	
4.17	100	75	11.6	-	-	191	

THICK TARGET

ENERGY MeV	ALPHA	BETA	GAMMA	L	ETA	TOTAL	REF
			BARNS				
.249	-	-	-	-	-	.096	BAUC81
.300	-	-	-	-	-	.233	
.353	-	-	-	-	-	.460	
.403	-	-	-	-	-	.73	
.484	-	-	-	-	-	1.26	
.552	-	-	-	-	-	1.90	
.635	-	-	-	-	-	2.94	
.720	-	-	-	-	-	4.31	
.900	-	-	-	-	-	7.8	
1.100	-	-	-	-	-	12.8	
1.300	-	-	-	-	-	19.2	
1.520	-	-	-	-	-	26.6	
1.720	-	-	-	-	-	35.0	
1.910	-	-	-	-	-	46.3	

TABLE A. Experimental *L*-Shell X-Ray Production Cross Sections for Proton Impact

Z=73 TANTALUM(TA) CONTINUED

TABLE AIII LALPHA/LL RATIO

ENERGY RANGE MeV	TARGET	LA/LL	REF	ENERGY RANGE MeV	TARGET	LA/LL	REF
0.4-2.0	THIN	22.1+-1.2	CHEJ76	0.28-.40	THIN	15.8+-1.2	UDEN81

Z=74 TUNGSTEN(W)

TABLE AI EXPERIMENTAL DETAILS

REF	ENERGY RANGE MeV	AREAL DENSITY E-6G/CMSQ	BEAM CURRENT A	BEAM COLL mm	EXP ERROR %	THEORIES	COMMENTS
BEAR73	1.0-3.7	81	-	-	LA 15	BEA(G4) PWBA2	RECTANGULAR BEAM. RBS EMPLOYED. EFFICIENCY MEASURED. WO3 TARGET.
BADT78	4.0	99+-5	1-5E-9	-	LT 7	BEA(G3) PWBA2	EFFICIENCY MEASURED. K-SHELL STUDIED. WO3 TARGET ON MYLAR BACKING.
JUSE80	0.5-2.5	50	30-200E-9	-	LA 5-6	-	RBS EMPLOYED. EFFICIENCY MEASURED. METAL TARGET ON FORMVAR BACKING. He+ IMPACT STUDIED.
PETV80	.2-1.05	THICK	-	-	LT 25	PWBA1	PROPORTIONAL COUNTER USED. EFFICIENCY MEASURED.

TABLE AII EXPERIMENTAL X-RAY PRODUCTION CROSS SECTIONS

THIN TARGET

ENERGY MeV	ALPHA	BETA	GAMMA	L	ETA	TOTAL	REF
	BARNS						
.50	.72	-	-	-	-	-	
.70	2.20	-	-	-	-	-	JUSE80
.80	3.34	-	-	-	-	-	
.90	4.90	-	-	-	-	-	
1.00	6.6	-	-	-	-	-	
1.00	4.80	-	-	-	-	-	
1.10	8.7	-	-	-	-	-	BEAR73
1.10	6.0	-	-	-	-	-	JUSE80
1.20	11.0	-	-	-	-	-	BEAR73
1.20	7.4	-	-	-	-	-	JUSE80
		-	-	-	-	-	BEAR73

TABLE A. Experimental *L*-Shell X-Ray Production Cross Sections for Proton Impact

Z=74 TUNGSTEN(W) CONTINUED

TABLE AII EXPERIMENTAL X-RAY PRODUCTION CROSS SECTIONS CONTINUED

THIN TARGET

ENERGY MeV	ALPHA	BETA	GAMMA	L	ETA	TOTAL	REF
			BARNS				
1.30	12.9	-	-	-	-	-	JUSE80
1.30	8.9	-	-	-	-	-	BEAR73
1.40	15.5	-	-	-	-	-	JUSE80
1.40	11.0	-	-	-	-	-	BEAR73
1.50	16.9	-	-	-	-	-	JUSE80
1.50	13.0	-	-	-	-	-	BEAR73
1.60	18.9	-	-	-	-	-	JUSE80
1.60	14.0	-	-	-	-	-	BEAR73
1.70	21.5	-	-	-	-	-	JUSE80
1.70	17.0	-	-	-	-	-	BEAR73
1.80	25.0	-	-	-	-	-	JUSE80
1.80	19.0	-	-	-	-	-	BEAR73
1.90	29.8	-	-	-	-	-	JUSE80
1.90	21.0	-	-	-	-	-	BEAR73
2.00	32.2	-	-	-	-	-	JUSE80
2.00	23.0	-	-	-	-	-	BEAR73
2.10	26.0	-	-	-	-	-	
2.20	27.0	-	-	-	-	-	
2.25	29.0	-	-	-	-	-	
2.30	30.0	-	-	-	-	-	
2.40	33.0	-	-	-	-	-	
2.50	47.0	-	-	-	-	-	JUSE80
2.50	35.0	-	-	-	-	-	BEAR73
2.60	37.0	-	-	-	-	-	
2.70	41.0	-	-	-	-	-	
2.80	44.0	-	-	-	-	-	
2.90	46.0	-	-	-	-	-	
3.00	49.0	-	-	-	-	-	
3.10	52	-	-	-	-	-	
3.20	55	-	-	-	-	-	
3.30	58	-	-	-	-	-	
3.40	59	-	-	-	-	-	
3.50	63	-	-	-	-	-	
3.60	67	-	-	-	-	-	
3.70	70	-	-	-	-	-	
4.00	-	-	-	-	-	222	BADT78

THICK TARGET

ENERGY MeV	ALPHA	BETA	GAMMA	L	ETA	TOTAL	REF
			BARNS				
.20	-	-	-	-	-	.024	PETV80
.25	-	-	-	-	-	.046	
.30	-	-	-	-	-	.104	
.35	-	-	-	-	-	.208	
.40	-	-	-	-	-	.408	
.45	-	-	-	-	-	.83	
.55	-	-	-	-	-	1.71	
.65	-	-	-	-	-	3.04	
.75	-	-	-	-	-	4.75	
.85	-	-	-	-	-	7.2	
.95	-	-	-	-	-	11.9	
1.05	-	-	-	-	-	16.2	

TABLE A. Experimental *L*-Shell X-Ray Production Cross Sections for Proton Impact

Z=77 IRIDIUM(IR)

TABLE AI EXPERIMENTAL DETAILS

REF	ENERGY RANGE MeV	AREAL DENSITY E-6G/CMSQ	BEAM CURRENT A	BEAM COLL mm	EXP ERROR %	THEORIES	COMMENTS
JUSE80	0.6-2.5	50	30-200E-9	-	LA 4-5	-	RBS EMPLOYED. EFFICIENCY MEASURED. METAL TARGET ON FORMVAR BACKING.

TABLE AII EXPERIMENTAL X-RAY PRODUCTION CROSS SECTIONS

THIN TARGET

ENERGY MeV	ALPHA	BETA	GAMMA	L	ETA	TOTAL	REF
	BARNS						
.60	.80	-	-	-	-	-	JUSE80
.70	1.38	-	-	-	-	-	
.80	2.10	-	-	-	-	-	
.90	3.06	-	-	-	-	-	
1.00	4.10	-	-	-	-	-	
1.10	5.3	-	-	-	-	-	
1.20	6.6	-	-	-	-	-	
1.30	8.0	-	-	-	-	-	
1.40	9.7	-	-	-	-	-	
1.50	11.5	-	-	-	-	-	
1.60	13.2	-	-	-	-	-	
1.70	15.6	-	-	-	-	-	
1.80	17.6	-	-	-	-	-	
2.00	21.8	-	-	-	-	-	
2.50	33.8	-	-	-	-	-	

Z=78 PLATINUM(PT)

TABLE AI EXPERIMENTAL DETAILS

REF	ENERGY RANGE MeV	AREAL DENSITY E-6G/CMSQ	BEAM CURRENT A	BEAM COLL mm	EXP ERROR %	THEORIES	COMMENTS
CHEJ76	0.4-2.0	50-100	5-50E-9	3.2(B)	-	BEA(G1) CBEA PWBA3	RBS EMPLOYED. EFFICIENCY MEASURED. LALPHA/LL RATIO ONLY AVAILABLE. METAL TARGET ON CARBON BACKING.
KHAR78	1.0-3.0	THICK	-	1.0(C)	LA 3-5 LB 3-6 LG 3-5 LT 3-6	BEA(G3) CBEA PWBA3	EFFICIENCY CALCULATED.

TABLE A. Experimental *L*-Shell X-Ray Production Cross Sections for Proton Impact

Z=78 PLATINUM(PT) CONTINUED

TABLE AII EXPERIMENTAL X-RAY PRODUCTION CROSS SECTIONS

THICK TARGET

ENERGY MeV	ALPHA	BETA	GAMMA	L	ETA	TOTAL	REF
			BARNS				
1.00	3.50	1.86	.260	-	-	5.6	KHAR78
1.20	5.6	3.00	.430	-	-	9.0	
1.40	8.1	4.60	.65	-	-	13.2	
1.60	11.2	6.5	.92	-	-	18.4	
1.80	14.7	8.7	1.26	-	-	24.4	
2.00	18.8	11.2	1.65	-	-	31.2	
2.20	23.1	14.0	2.09	-	-	39.0	
2.40	27.7	17.0	2.57	-	-	47.0	
2.60	32.4	20.1	3.08	-	-	55	
2.80	37.0	23.3	3.60	-	-	63	
3.00	41.0	26.5	4.13	-	-	71	

TABLE AIII LALPHA/LL RATIO

ENERGY RANGE MeV	TARGET	LA/LL	REF	ENERGY RANGE MeV	TARGET	LA/LL	REF
0.4-2.0	THIN	19.6+-1.0	CHEJ76	1.0-3.0	THICK	21.1+-0.6	KHAR78

Z=79 GOLD(AU)

TABLE AI EXPERIMENTAL DETAILS

REF	ENERGY RANGE MeV	AREAL DENSITY E-6G/CMSQ	BEAM CURRENT A	BEAM COLL mm	EXP ERROR %	THEORIES	COMMENTS
BEAR73	1.0-3.0	124	-	-	LA 15	BEA(G4) PWBA2	RECTANGULAR BEAM. RBS EMPLOYED. EFFICIENCY MEASURED.
TAWH75	1-4.5	348+-35	-	3.0(C)	LA 15 LB 15 LG 15 LL 17 LE 50 LT 10	BEA(G2) BEA(H) PWBA3	RBS EMPLOYED. EFFICIENCY MEASURED. He3+ IMPACT STUDIED. METAL TARGET ON Al BACKING.
CHEJ76	.4-2.0	50-100	5-50E-9	3.2(B)	-	BEA(G1) CBEA PWBA3	RBS EMPLOYED. EFFICIENCY MEASURED. LALPHA/LL RATIO ONLY AVAILABLE. METAL TARGET ON CARBON BACKING.
BONG78	3.0-11.0	THIN	-	-	LT 8	BEA(G3) PWBA2	RBS EMPLOYED. EFFICIENCY MEASURED. SELF-SUPPORTING METAL TARGET.

TABLE A. Experimental *L*-Shell X-Ray Production Cross Sections for Proton Impact

Z=79 GOLD(AU) CONTINUED

TABLE AI EXPERIMENTAL DETAILS CONTINUED

REF	ENERGY RANGE MeV	AREAL DENSITY E-6G/CMSQ	BEAM CURRENT A	BEAM COLL mm	EXP ERROR %	THEORIES	COMMENTS
KHAR78	1.2-3.0	THICK	-	1.0(C)	LX 3-5 LT 3-5	BEA(G3) CBEA PWBA3	EFFICIENCY CALCULATED.
BHAD80	.33-1.81	200+-20	50-300E-9	1.0(C)	LX 15 LT 10	PWBA3 PWBABC IPWBABCR	RBS EMPLOYED. EFFICIENCY MEASURED. SELF-SUPPORTING METAL TARGET.
LAPG80	.14-.30	THICK	-	-	LT 25-50	-	COULOMB DEFLECTION FACTOR DEDUCED.
SARL80	2.0	THIN	-	-	LX 15 LT 15	PWBA1 PWBABC MPWBABCR	EFFICIENCY MEASURED. METAL TARGET ON CARBON BACKING. C12 N14 O16 IMPACT STUDIED.
SARW81	.30-.40	64+-3 49+-2	3-100E-9	1.0(B)	LA 8-9 LT 15	PWBABC PWBABCR ECPSSR	RBS EMPLOYED. EFFICIENCY MEASURED. TWO METAL TARGETS USED.
SOKR81	1-3.0	35+-2	1-10E-9	1.5(C)	LA 8 LB 8 LG 8-11 LL 9-11 LT 6	PWBA4 PWBABC	EFFICIENCY CALCULATED. METAL TARGET ON NUCLEPORE BACKING.
BAUC81	.5-4.0	225+-11	.5-50E-9	1.1(B)	LT 11	CPSSR	RBS EMPLOYED. EFFICIENCY MEASURED. He4 N2+ Ne3+ IMPACT STUDIED. SELF-SUPPORTING METAL TARGET.
PINA82	0.5-4.0	50	30-200E-9	-	LA 5-10	-	RBS EMPLOYED. EFFICIENCY MEASURED. SELF-SUPPORTING METAL TARGET. RADIATIVE DECAY BRANCHING RATIOS MEASURED.

TABLE AII EXPERIMENTAL X-RAY PRODUCTION CROSS SECTIONS

THIN TARGET

ENERGY MeV	ALPHA	BETA	GAMMA	L	ETA	TOTAL	REF
	BARNS						
.30	.022	-	-	-	-	.052	SARW81
.33	.090	.053	8.1E-03	-	-	.151	BHAD80
.35	.055	-	-	-	-	.109	SARW81
.37	.160	.095	.014	-	-	.269	BHAD80
.40	.107	-	-	-	-	.215	SARW81
.42	.270	.150	.021	.016	-	.457	BHAD80
.46	.390	.220	.031	.027	-	.67	

TABLE A. Experimental L-Shell X-Ray Production Cross Sections for Proton Impact

Z=79 GOLD(AU) CONTINUED

TABLE AII   EXPERIMENTAL X-RAY PRODUCTION CROSS SECTIONS CONTINUED

THIN TARGET

ENERGY	ALPHA	BETA	GAMMA	L	ETA	TOTAL	REF
MeV			BARNS				
.50	.400	-	-	-	-	-	PINA82
.50	-	-	-	-	-	.380	BAUC81
.52	.460	.260	.036	.030	-	.79	BHAD80
.56	.57	.310	.042	.036	-	.96	
.60	.80	-	-	-	-	-	PINA82
.61	.74	.410	.053	.046	-	1.25	BHAD80
.65	.97	.53	.069	.061	-	1.63	
.65	-	-	-	-	-	1.00	BAUC81
.70	1.17	-	-	-	-	-	PINA82
.70	1.20	.66	.088	.077	-	2.03	BHAD80
.74	1.50	.80	.110	.082	-	2.49	
.79	1.60	.88	.120	.094	-	2.69	
.80	1.86	-	-	-	-	-	PINA82
.80	-	-	-	-	-	1.80	BAUC81
.84	1.90	1.00	.130	.120	-	3.15	BHAD80
.87	2.60	1.40	.190	.150	-	4.34	
.90	2.68	-	-	-	-	-	PINA82
.91	3.10	1.60	.210	.180	-	5.1	BHAD80
1.00	2.70	-	-	-	-	-	BEAR73
1.00	4.38	2.31	.334	.251	.027	7.3	TAWH75
1.00	3.52	1.97	.300	.170	-	6.0	SOKR81
1.00	3.60	-	-	-	-	-	PINA82
1.00	-	-	-	-	-	4.50	BAUC81
1.02	4.00	2.10	.270	.250	-	6.6	BHAD80
1.10	5.0	2.50	.330	.240	-	8.1	SOKR81
1.10	4.50	-	-	-	-	-	PINA82
1.11	6.0	3.30	.460	.340	-	10.1	BHAD80
1.20	5.7	-	-	-	-	-	PINA82
1.20	5.9	3.10	.410	.300	-	9.7	SOKR81
1.21	7.2	4.00	.52	.410	-	12.1	BHAD80
1.25	7.2	3.79	.53	.412	.052	12.0	TAWH75
1.30	7.0	-	-	-	-	-	PINA82
1.31	8.2	4.50	.58	.480	-	13.8	BHAD80
1.40	9.0	-	-	-	-	-	PINA82
1.40	8.7	4.76	.64	.470	-	14.6	SOKR81
1.41	10.0	5.3	.80	.54	-	16.6	BHAD80
1.50	10.8	5.9	.85	.59	.079	18.2	TAWH75
1.50	10.0	-	-	-	-	-	PINA82
1.51	11.6	6.4	.78	.63	-	19.4	BHAD80
1.60	12.0	-	-	-	-	-	PINA82
1.60	12.1	6.6	.96	.67	-	20.4	SOKR81
1.61	10.8	6.1	.82	.60	-	18.3	BHAD80
1.70	13.4	-	-	-	-	-	PINA82
1.71	12.4	7.1	.96	.66	-	21.1	BHAD80
1.75	14.7	8.2	1.23	.78	.098	25.0	TAWH75
1.80	15.6	-	-	-	-	-	PINA82
1.80	15.2	8.5	1.21	.74	-	25.6	SOKR81
1.81	13.8	7.7	1.00	.77	-	23.3	BHAD80
2.00	19.0	-	-	-	-	-	PINA82
2.00	19.9	11.2	1.69	1.08	.130	34.0	TAWH75
2.00	19.2	10.8	1.46	.94	-	32.4	SOKR81
2.00	-	-	-	-	-	33.0	BAUC81
2.00	19.8	11.8	1.73	-	-	34.5	SARL80
2.20	23.6	13.8	1.91	1.06	-	40.4	SOKR81
2.25	24.2	13.7	2.15	1.29	.190	41.5	TAWH75
2.25	18.0	-	-	-	-	-	BEAR73
2.40	28.4	16.3	2.41	1.35	-	48.4	SOKR81
2.50	28.7	17.2	2.51	1.41	-	49.8	
2.50	28.4	17.4	2.63	1.61	.240	50	TAWH75
2.50	28.8	-	-	-	-	-	PINA82
2.60	34.0	19.5	2.98	1.81	-	58	SOKR81
2.70	34.6	20.0	3.08	1.70	-	59	
2.75	38.6	22.6	3.57	2.04	.270	67	TAWH75
2.80	34.4	20.4	3.25	1.66	-	60	SOKR81
2.90	41.1	24.8	3.76	1.71	-	71	
3.00	41.8	25.5	4.08	1.88	-	73	

TABLE A. Experimental *L*-Shell X-Ray Production Cross Sections for Proton Impact

Z=79 GOLD(AU) CONTINUED

TABLE AII EXPERIMENTAL X-RAY PRODUCTION CROSS SECTIONS CONTINUED

THIN TARGET

ENERGY MeV	ALPHA	BETA	GAMMA	L	ETA	TOTAL	REF
			BARNS				
3.00	-	-	-	-	-	65	BONG78
3.00	44.8	27.0	4.32	2.23	.330	79	TAWH75
3.00	32.0	-	-	-	-	-	BEAR73
3.00	38.8	-	-	-	-	-	PINA82
3.25	52	32.2	5.1	2.77	.53	93	TAWH75
3.50	49.0	-	-	-	-	-	PINA82
3.50	60	37.6	6.1	2.98	.61	108	TAWH75
3.75	72	45.4	7.2	3.64	.68	129	
4.00	60	-	-	-	-	-	PINA82
4.00	-	-	-	-	-	80	BAUC81
4.00	80	49.9	8.3	4.01	.80	143	TAWH75
4.25	90	57	9.5	4.76	.87	163	
4.50	97	62	10.3	4.82	.83	175	
5.00	-	-	-	-	-	169	BONG78
7.00	-	-	-	-	-	261	
9.00	-	-	-	-	-	357	
11.00	-	-	-	-	-	433	

THICK TARGET

ENERGY MeV	ALPHA	BETA	GAMMA	L	ETA	TOTAL	REF
			BARNS				
.140	-	-	-	-	-	4.6E-05	LAPG80
.150	-	-	-	-	-	1.1E-04	
.160	-	-	-	-	-	2.4E-04	
.170	-	-	-	-	-	4.9E-04	
.185	-	-	-	-	-	9.7E-04	
.200	-	-	-	-	-	2.1E-03	
.215	-	-	-	-	-	4.1E-03	
.230	-	-	-	-	-	6.9E-03	
.245	-	-	-	-	-	.011	
.260	-	-	-	-	-	.017	
.275	-	-	-	-	-	.026	
.300	-	-	-	-	-	.049	
1.200	4.80	2.60	.380	-	-	7.8	KHAR78
1.400	7.0	4.00	.56	-	-	11.6	
1.600	9.7	5.6	.78	-	-	16.2	
1.800	12.7	7.5	1.06	-	-	21.5	
2.000	16.1	9.7	1.39	-	-	27.4	
2.200	19.7	12.1	1.78	-	-	33.8	
2.400	23.5	14.6	2.21	-	-	40.5	
2.600	27.4	17.2	2.63	-	-	47.0	
2.800	31.2	19.7	3.02	-	-	54	
3.000	35.0	22.3	3.32	-	-	61	

TABLE AIII LALPHA/LL RATIO

ENERGY RANGE MeV	TARGET	LA/LL	REF	ENERGY RANGE MeV	TARGET	LA/LL	REF
1.0-4.5	THIN	18.9+-1.5	TAWH75	.33-1.81	THIN	16.8+-0.3	BHAD80
0.4-2.0	THIN	19.7+-1.0	CHEJ76	1.0-3.0	THIN	20.3+-0.6	SOKR81
1.2-3.0	THICK	20.3+-0.6	KHAR78				

TABLE A. Experimental *L*-Shell X-Ray Production Cross Sections for Proton Impact

Z=81 THALLIUM(TL)

TABLE AI EXPERIMENTAL DETAILS

REF	ENERGY RANGE MeV	AREAL DENSITY E-6G/CMSQ	BEAM CURRENT A	BEAM COLL mm	EXP ERROR %	THEORIES	COMMENTS
LEIC77	0.5-3.0	50	30-200E-9	-	LA 6-7 LT 7-8	-	RBS EMPLOYED. EFFICIENCY MEASURED. METAL TARGET ON FORMVAR BACKING. RADIATIVE DECAY BRANCHING RATIOS MEASURED.

TABLE AII EXPERIMENTAL X-RAY PRODUCTION CROSS SECTIONS

THIN TARGET

ENERGY MeV	ALPHA	BETA	GAMMA	L	ETA	TOTAL	REF
			BARNS				
.50	.330	-	-	-	-	.57	LEIC77
1.00	2.97	-	-	-	-	5.1	
1.50	9.7	-	-	-	-	16.6	
2.00	16.5	-	-	-	-	29.1	
2.50	27.0	-	-	-	-	48.1	
3.00	33.5	-	-	-	-	61	

Z=82 LEAD(PB)

TABLE AI EXPERIMENTAL DETAILS

REF	ENERGY RANGE MeV	AREAL DENSITY E-6G/CMSQ	BEAM CURRENT A	BEAM COLL mm	EXP ERROR %	THEORIES	COMMENTS
BEAR73	1.0-3.0	97	-	-	LA 15	BEA(G4) PWBA2	RECTANGULAR BEAM. RBS EMPLOYED. EFFICIENCY MEASURED.
LIER73	2.5-12	51+-2.6	-	-	LX 10 LT 17	BEA(G3) PWBA2	RBS EMPLOYED. EFFICIENCY MEASURED. K-SHELL STUDIED. METAL TARGET ON CARBON BACKING.
TAWH74	1.8-4.4	500+-50	-	3.0(C)	LA 15 LB 15 LG 17 LL 17 LE 20 LT 10	BEA(G2) PWBA2	RBS EMPLOYED. EFFICIENCY MEASURED. He3+ IMPACT STUDIED. SELF-SUPPORTING METAL TARGET.
CHEJ76	0.4-2.0	50-100	5-50E-9	3.2(B)	-	BEA(G1) CBEA PWBA3	RBS EMPLOYED. EFFICIENCY MEASURED. LALPHA/LL RATIO ONLY AVAILABLE. METAL TARGET ON CARBON BACKING.

TABLE A. Experimental *L*-Shell X-Ray Production Cross Sections for Proton Impact

Z=82 LEAD(PB) CONTINUED

TABLE AI EXPERIMENTAL DETAILS CONTINUED

REF	ENERGY RANGE MeV	AREAL DENSITY E-6G/CMSQ	BEAM CURRENT A	BEAM COLL mm	EXP ERROR %	THEORIES	COMMENTS
LEIC77	0.5-3.5	50	30-200E-9	-	LA 7-9 LT 7-8	-	RBS EMPLOYED. EFFICIENCY MEASURED. METAL TARGET ON FORMVAR BACKING. RADIATIVE DECAY BRANCHING RATIOS MEASURED.
BONG78	3.0	THIN	-	-	LT 5	BEA(G3)	RBS EMPLOYED. EFFICIENCY MEASURED. METAL TARGET ON CARBON BACKING.
SARW81	.30-.40	67+-3	3-100E-9	1.0(B)	LA 9 LT 9	PWBABC PWBABCR ECPSSR	RBS EMPLOYED. EFFICIENCY MEASURED.
SOKR82	.9-3.0	47+-2	1-10E-9	1.5(C)	LA 6 LB 6 LG 7-10 LL 9-12 LT 4	CPSSR	EFFICIENCY CALCULATED. METAL TARGET ON NUCLEPORE BACKING.

TABLE AII EXPERIMENTAL X-RAY PRODUCTION CROSS SECTIONS

THIN TARGET

ENERGY MeV	ALPHA	BETA	GAMMA	L	ETA	TOTAL	REF
			BARNS				
.30	.012	-	-	-	-	.019	SARW81
.35	.028	-	-	-	-	.046	
.40	.057	-	-	-	-	.095	
.50	.220	-	-	-	-	.370	LEIC77
.90	1.80	.91	.120	.120	-	2.95	SOKR82
1.00	1.80	-	-	-	-	-	BEAR73
1.00	2.20	-	-	-	-	3.70	LEIC77
1.00	2.40	1.30	.160	.130	-	3.99	SOKR82
1.10	3.20	1.70	.220	.200	-	5.3	
1.20	4.00	2.10	.300	.270	-	6.7	
1.40	6.0	3.30	.450	.350	-	10.1	
1.50	6.9	-	-	-	-	11.7	LEIC77
1.60	8.6	4.60	.72	.470	-	14.4	SOKR82
1.80	11.2	5.9	.97	.61	-	18.7	
1.80	12.6	7.0	1.01	.66	.087	21.4	TAWH74
2.00	13.9	8.0	1.20	.68	-	23.8	SOKR82
2.00	13.5	-	-	-	-	23.4	LEIC77
2.00	15.1	8.6	1.22	.80	.117	25.8	TAWH74
2.20	19.0	10.6	1.70	1.00	-	32.3	SOKR82
2.20	18.3	10.6	1.56	.93	.137	31.5	TAWH74
2.25	13.0	-	-	-	-	-	BEAR73
2.40	23.0	13.2	1.90	1.20	-	39.3	SOKR82
2.40	22.4	12.9	1.93	1.02	.158	38.4	TAWH74
2.50	21.9	-	-	-	-	38.7	LEIC77
2.50	25.0	13.7	2.10	1.30	-	42.1	SOKR82
2.50	22.2	13.1	1.81	-	-	37.1	LIER73
2.60	25.0	14.8	2.19	1.19	.176	43.4	TAWH74
2.60	27.0	15.0	2.20	1.40	-	45.6	SOKR82
2.70	29.0	17.0	2.60	1.60	-	50	
2.80	28.5	17.1	2.38	1.34	.182	49.5	TAWH74
2.80	30.0	18.0	2.90	1.70	-	53	SOKR82

TABLE A. Experimental *L*-Shell X-Ray Production Cross Sections for Proton Impact

Z=82 LEAD(PB) CONTINUED

TABLE AII EXPERIMENTAL X-RAY PRODUCTION CROSS SECTIONS CONTINUED

THIN TARGET

ENERGY MeV	ALPHA	BETA	GAMMA	L	ETA	TOTAL	REF
	BARNS						
2.90	33.0	19.0	2.70	2.30	-	57	SOKR82
3.00	35.0	21.0	3.30	1.90	-	61	
3.00	-	-	-	-	-	50	BONG78
3.00	31.7	-	-	-	-	57	LEIC77
3.00	33.4	20.4	3.07	1.54	.191	59	TAWH74
3.00	24.0	-	-	-	-	-	BEAR73
3.00	32.0	19.5	2.70	-	-	54	LIER73
3.20	35.9	22.3	3.36	1.62	.226	63	TAWH74
3.50	41.2	-	-	-	-	74	LEIC77
3.60	44.4	28.1	4.19	2.05	.312	79	TAWH74
3.80	51	32.8	4.89	2.50	.328	92	
4.00	58	37.4	5.8	2.91	.379	105	
4.00	52	32.7	4.72	-	-	89	LIER73
4.20	61	39.6	6.2	3.19	.400	111	TAWH74
4.30	62	39.9	6.3	3.08	.371	112	
4.40	65	42.2	6.6	3.30	.448	118	
4.50	64	40.7	6.0	-	-	111	LIER73
5.00	80	51	7.4	-	-	139	
6.00	97	65	9.4	-	-	171	
6.50	109	72	10.5	-	-	191	
7.00	136	88	12.6	-	-	237	
8.00	142	93	13.5	-	-	248	
8.50	157	106	15.7	-	-	279	
9.00	167	112	16.7	-	-	296	
10.00	187	122	17.7	-	-	327	
10.50	191	128	18.6	-	-	338	
11.00	201	132	19.0	-	-	352	
12.00	220	147	21.6	-	-	389	

TABLE AIII LALPHA/LL RATIO

ENERGY RANGE MeV	TARGET	LA/LL	REF	ENERGY RANGE MeV	TARGET	LA/LL	REF
1.8-4.4	THIN	20.4+-1.5	TAWH74	0.9-3.0	THIN	17.3+-0.4	SOKR82
0.4-2.0	THIN	19.7+-1.0	CHEJ76				

Z=83 BISMUTH(BI)

TABLE AI EXPERIMENTAL DETAILS

REF	ENERGY RANGE MeV	AREAL DENSITY E-6G/CMSQ	BEAM CURRENT A	BEAM COLL mm	EXP ERROR %	THEORIES	COMMENTS
BEAR73	1-3.0	100	-	-	LA 15	BEA(G4) PWBA2	RECTANGULAR BEAM. RBS EMPLOYED. EFFICIENCY MEASURED.
TAWH75	1-4.5	431+-43	-	3.0(C)	LA 15 LB 15 LG 15 LL 17 LE 35 LT 10	BEA(G2) BEA(H) PWBA3	RBS EMPLOYED. EFFICIENCY MEASURED. He3+ IMPACT STUDIED. METAL TARGET ON Al BACKING.

TABLE A. Experimental *L*-Shell X-Ray Production Cross Sections for Proton Impact

Z=83 BISMUTH(BI) CONTINUED

TABLE AI EXPERIMENTAL DETAILS CONTINUED

REF	ENERGY RANGE MeV	AREAL DENSITY E-6G/CMSQ	BEAM CURRENT A	BEAM COLL mm	EXP ERROR %	THEORIES	COMMENTS
LEIC77	0.5-3.0	50	30-200E-9	-	LA 6-7 LT 6-7	-	RBS EMPLOYED. EFFICIENCY MEASURED. METAL TARGET ON FORMVAR BACKING. RADIATIVE DECAY BRANCHING RATIOS MEASURED.
BHAD80	.33-1.81	80+-8	50-300E-9	1.0(C)	LX 15 LT 10	PWBA3 PWBABC IPWBABCR	RBS EMPLOYED. EFFICIENCY MEASURED. METAL TARGET ON CARBON BACKING.

TABLE AII EXPERIMENTAL X-RAY PRODUCTION CROSS SECTIONS

THIN TARGET

ENERGY MeV	ALPHA	BETA	GAMMA	L	ETA	TOTAL	REF
			BARNS				
.33	.012	6.5E-03	-	-	-	.019	BHAD80
.37	.031	.017	2.1E-03	2.0E-03	-	.052	
.42	.062	.034	4.4E-03	4.3E-03	-	.105	
.46	.110	.060	8.6E-03	7.2E-03	-	.186	
.50	.180	-	-	-	-	.321	LEIC77
.51	.140	.074	9.9E-03	9.0E-03	-	.233	BHAD80
.56	.210	.110	.015	.013	-	.348	
.60	.360	.190	.024	.025	-	.60	
.65	.65	.340	.044	.047	-	1.08	
.70	.78	.400	.053	.050	-	1.28	
.74	.98	.52	.070	.071	-	1.64	
.79	1.40	.73	.094	.098	-	2.32	
.84	1.60	.83	.110	.100	-	2.64	
.87	1.90	.96	.130	.140	-	3.13	
.91	2.40	1.30	.170	.150	-	4.02	
1.00	3.20	1.79	.253	.189	.022	5.5	TAWH75
1.00	2.40	-	-	-	-	4.33	LEIC77
1.00	1.60	-	-	-	-	-	BEAR73
1.02	3.40	1.80	.230	.220	-	5.7	BHAD80
1.11	4.40	2.30	.320	.280	-	7.3	
1.21	5.0	2.70	.350	.320	-	8.4	
1.25	4.94	2.81	.414	.290	.039	8.5	TAWH75
1.31	6.2	3.30	.470	.450	-	10.4	BHAD80
1.41	7.8	4.30	.59	.52	-	13.2	
1.50	7.3	4.20	.61	.408	.057	12.6	TAWH75
1.50	6.6	-	-	-	-	11.9	LEIC77
1.51	9.2	5.1	.69	.58	-	15.6	BHAD80
1.61	10.7	6.0	.82	.71	-	18.2	
1.71	11.9	6.7	.93	.84	-	20.4	
1.75	10.2	5.9	.89	.56	.067	17.6	TAWH75
1.81	11.1	6.3	.91	.80	-	19.1	BHAD80
2.00	13.5	8.0	1.25	.71	.094	23.6	TAWH75
2.00	11.9	-	-	-	-	23.4	LEIC77
2.25	16.1	9.8	1.57	.86	.120	28.4	TAWH75
2.25	12.0	-	-	-	-	-	BEAR73
2.50	19.6	12.0	1.92	1.15	.130	34.8	TAWH75
2.50	19.5	-	-	-	-	36.1	LEIC77
2.75	26.3	16.1	2.70	1.35	.170	46.6	TAWH75
3.00	30.2	19.1	3.09	1.51	.180	54	
3.00	27.0	-	-	-	-	51	LEIC77
3.00	22.0	-	-	-	-	-	BEAR73

TABLE A. Experimental *L*-Shell X-Ray Production Cross Sections for Proton Impact

Z=83 BISMUTH(BI) CONTINUED

TABLE AII EXPERIMENTAL X-RAY PRODUCTION CROSS SECTIONS CONTINUED

THIN TARGET

ENERGY MeV	ALPHA	BETA	GAMMA	L	ETA	TOTAL	REF
			BARNS				
3.25	37.0	23.5	3.89	1.87	.270	67	TAWH75
3.50	40.7	26.1	4.39	2.12	.270	74	
3.75	49.2	32.4	5.2	2.53	.380	90	
4.00	56	36.6	6.2	2.95	.450	102	
4.25	63	42.3	7.2	3.29	.480	117	
4.50	67	44.7	7.8	3.47	.51	124	

TABLE AIII LALPHA/LL RATIO

ENERGY RANGE MeV	TARGET	LA/LL	REF	ENERGY RANGE MeV	TARGET	LA/LL	REF
1.0-4.5	THIN	18.7+-1.5	TAWH75	.33-1.81	THIN	14.5+-0.2	BHAD80

Z=90 THORIUM(TH)

TABLE AI EXPERIMENTAL DETAILS

REF	ENERGY RANGE MeV	AREAL DENSITY E-6G/CMSQ	BEAM CURRENT A	BEAM COLL mm	EXP ERROR %	THEORIES	COMMENTS
BEAR73	1-3.7	168	-	-	LA 15	BEA(G4) PWBA2	RECTANGULAR BEAM. RBS EMPLOYED. EFFICIENCY MEASURED. ThF4 TARGET.
LEIC77	0.5-3.0	50	30-200E-9	-	LA 7 LT 6-7	-	RBS EMPLOYED. EFFICIENCY MEASURED. METAL TARGET ON Al BACKING. RADIATIVE DECAY BRANCHING RATIOS MEASURED.
SARW81	.40	19+-1	3-100E-9	1.0(B)	LA 29 LT 30	PWBABC PWBABCR ECPSSR	RBS EMPLOYED. EFFICIENCY MEASURED.

TABLE AII EXPERIMENTAL X-RAY PRODUCTION CROSS SECTIONS

THIN TARGET

ENERGY MeV	ALPHA	BETA	GAMMA	L	ETA	TOTAL	REF
			BARNS				
.40	6.8E-03	-	-	-	-	9.4E-03	SARW81
.50	.085	-	-	-	-	.160	LEIC77
1.00	1.07	-	-	-	-	1.88	
1.00	.72	-	-	-	-	-	BEAR73
1.10	.90	-	-	-	-	-	
1.20	1.20	-	-	-	-	-	
1.30	1.50	-	-	-	-	-	

TABLE A. Experimental *L*-Shell X-Ray Production Cross Sections for Proton Impact

Z=90 THORIUM(TH) CONTINUED

TABLE AII EXPERIMENTAL X-RAY PRODUCTION CROSS SECTIONS CONTINUED

THIN TARGET

ENERGY MeV	ALPHA	BETA	GAMMA	L	ETA	TOTAL	REF
			BARNS				
1.40	1.90	-	-	-	-	-	BEAR73
1.50	3.78	-	-	-	-	6.6	LEIC77
1.50	2.30	-	-	-	-	-	BEAR73
1.60	2.80	-	-	-	-	-	
1.70	3.20	-	-	-	-	-	
1.80	3.70	-	-	-	-	-	
1.90	4.20	-	-	-	-	-	
2.00	8.1	-	-	-	-	14.3	LEIC77
2.00	4.80	-	-	-	-	-	BEAR73
2.10	5.4	-	-	-	-	-	
2.20	6.0	-	-	-	-	-	
2.25	6.4	-	-	-	-	-	
2.30	6.7	-	-	-	-	-	
2.40	7.4	-	-	-	-	-	
2.50	13.0	-	-	-	-	23.4	LEIC77
2.50	8.2	-	-	-	-	-	BEAR73
2.60	9.0	-	-	-	-	-	
2.70	9.7	-	-	-	-	-	
2.80	11.0	-	-	-	-	-	
2.90	12.0	-	-	-	-	-	
3.00	18.7	-	-	-	-	33.9	LEIC77
3.00	12.0	-	-	-	-	-	BEAR73
3.10	13.0	-	-	-	-	-	
3.20	14.0	-	-	-	-	-	
3.30	15.0	-	-	-	-	-	
3.40	16.0	-	-	-	-	-	
3.50	17.0	-	-	-	-	-	
3.60	18.0	-	-	-	-	-	
3.70	19.0	-	-	-	-	-	

Z=92 URANIUM(U)

TABLE AI EXPERIMENTAL DETAILS

REF	ENERGY RANGE MeV	AREAL DENSITY E-6G/CMSQ	BEAM CURRENT A	BEAM COLL mm	EXP ERROR %	THEORIES	COMMENTS
BEAR73	1-3.0	122	-	-	LA 15	BEA(G4) PWBA2	RECTANGULAR BEAM. RBS EMPLOYED. EFFICIENCY MEASURED. UF4 TARGET.
TAWH75	1-4.5	291+-29	-	3.0(C)	LA 15 LB 15 LG 15 LL 17 LE 50 LT 10	BEA(G2) BEA(H) PWBA3	RBS EMPLOYED. EFFICIENCY MEASURED. He3+ IMPACT STUDIED. URANYLACETATE TARGET ON Al BACKING.
LEIC77	0.5-3.0	50	30-200E-9	-	LA 6-7 LT 6-7	-	RBS EMPLOYED. EFFICIENCY MEASURED. METAL TARGET ON Al BACKING. RADIATIVE DECAY BRANCHING RATIOS MEASURED.

TABLE A. Experimental *L*-Shell X-Ray Production Cross Sections for Proton Impact

Z=92 URANIUM(U) CONTINUED

TABLE AI   EXPERIMENTAL DETAILS CONTINUED

REF	ENERGY RANGE MeV	AREAL DENSITY E-6G/CMSQ	BEAM CURRENT A	BEAM COLL mm	EXP ERROR %	THEORIES	COMMENTS
BONG78	3.0	THIN	-	-	LT 5	BEA(G3) PWBA2	RBS EMPLOYED. EFFICIENCY MEASURED. METAL TARGET ON CARBON BACKING.
BHAD80	.43-1.81	4.0+-.4	50-300E-9	1.0(C)	LX 15 LT 10	PWBA3 PWBABC IPWBABCR	RBS EMPLOYED. EFFICIENCY MEASURED. UCl TARGET ON Al BACKING.
SARW81	.30-.40	132+-26	3-100E-9	1.0(B)	LA 30 LT 25	PWBABC PWBABCR ECPSSR	RBS EMPLOYED. EFFICIENCY MEASURED.

TABLE AII   EXPERIMENTAL X-RAY PRODUCTION CROSS SECTIONS

THIN TARGET

ENERGY MeV	ALPHA	BETA	GAMMA	L	ETA	TOTAL	REF
	BARNS						
.30	3.3E-04	-	-	-	-	3.9E-04	SARW81
.35	1.9E-03	-	-	-	-	2.8E-03	
.40	5.3E-03	-	-	-	-	7.7E-03	
.43	.020	.013	-	-	-	.033	BHAD80
.47	.043	.024	-	-	-	.067	
.50	.054	-	-	-	-	.094	LEIC77
.52	.072	.038	-	-	-	.110	BHAD80
.57	.120	.065	.011	-	-	.196	
.61	.160	.086	.012	.011	-	.269	
.65	.250	.130	.018	.018	-	.416	
.71	.300	.150	.024	.023	-	.497	
.76	.330	.160	.028	.024	-	.54	
.81	.440	.240	.033	.033	-	.75	
.85	.490	.280	.039	.032	-	.84	
.89	.56	.310	.043	.039	-	.95	
.91	.70	.370	.048	.053	-	1.17	
1.00	.69	-	-	-	-	1.17	LEIC77
1.00	.55	-	-	-	-	-	BEAR73
1.00	.91	.460	.078	.060	.024	1.53	TAWH75
1.01	1.10	.54	.064	.066	-	1.77	BHAD80
1.11	1.30	.65	.087	.081	-	2.12	
1.21	1.60	.82	.110	.100	-	2.63	
1.25	1.69	.88	.144	.113	.056	2.88	TAWH75
1.31	2.10	1.10	.150	.130	-	3.48	BHAD80
1.41	2.60	1.40	.180	.170	-	4.35	
1.50	2.61	1.34	.222	.169	.079	4.42	TAWH75
1.50	2.55	-	-	-	-	4.37	LEIC77
1.51	3.10	1.60	.220	.210	-	5.1	BHAD80
1.61	3.40	1.90	.240	.230	-	5.8	
1.71	3.70	2.10	.270	.250	-	6.3	
1.75	3.84	2.02	.298	.260	.110	6.5	TAWH75
1.81	4.10	2.10	.270	.260	-	6.7	BHAD80
2.00	5.3	2.78	.454	.328	.150	9.0	TAWH75
2.00	5.4	-	-	-	-	9.3	LEIC77

TABLE A. Experimental *L*-Shell X-Ray Production Cross Sections for Proton Impact

Z=92 URANIUM(U) CONTINUED

TABLE AII EXPERIMENTAL X-RAY PRODUCTION CROSS SECTIONS CONTINUED

THIN TARGET

ENERGY MeV	ALPHA	BETA	GAMMA	L	ETA	TOTAL	REF
			BARNS				
2.25	7.1	3.81	.64	.449	.230	12.2	TAWH75
2.25	5.4	-	-	-	-	-	BEAR73
2.50	8.7	4.68	.86	.56	.260	15.0	TAWH75
2.50	9.0	-	-	-	-	15.7	LEIC77
2.75	11.0	6.2	1.03	.67	.390	19.3	TAWH75
3.00	-	-	-	-	-	21.8	BONG78
3.00	14.0	-	-	-	-	25.0	LEIC77
3.00	12.8	7.3	1.30	.92	.390	22.7	TAWH75
3.00	10.0	-	-	-	-	-	BEAR73
3.25	15.8	9.1	1.64	1.00	.450	28.0	TAWH75
3.50	18.6	10.8	1.85	1.10	.57	32.9	
3.75	21.0	12.4	2.29	1.33	.63	37.6	
4.00	24.0	14.3	2.58	1.46	.71	43.1	
4.25	29.6	17.0	3.37	1.85	.88	53	
4.50	31.5	19.1	3..47	2.02	1.00	57	

TABLE AIII LALPHA/LL RATIO

ENERGY RANGE MeV	TARGET	LA/LL	REF	ENERGY RANGE MeV	TARGET	LA/LL	REF
1.0-4.5	THIN	15.6+-1.2	TAWH75	.43-1.81	THIN	14.7+-0.2	BHAD80

TABLE B. Experimental *L*-Shell Ionization Cross Sections for Proton Impact

Z=38 STRONTIUM(SR)

TABLE BI EXPERIMENTAL DETAILS

REF	ENERGY RANGE MeV	AREAL DENSITY E-6G/CMSQ	BEAM CURRENT A	BEAM COLL mm	EXP ERROR %	THEORIES	COMMENTS
BONG78	3.0	THIN	-	-	LT 14	BEA(G3)	RBS EMPLOYED. EFFICIENCY MEASURED. K-SHELL STUDIED. METAL TARGET ON CARBON BACKING.

TABLE BII EXPERIMENTAL IONIZATION CROSS SECTIONS

THIN TARGET

ENERGY MeV	TOTAL BARNS	REF	ENERGY MeV	TOTAL BARNS	REF
3.00	92611	BONG78			

Z=39 YTTRIUM(Y)

TABLE BI EXPERIMENTAL DETAILS

REF	ENERGY RANGE MeV	AREAL DENSITY E-6G/CMSQ	BEAM CURRENT A	BEAM COLL mm	EXP ERROR %	THEORIES	COMMENTS
PONM79	4.0-22.0	THIN	-	6.0(C)	-	BEA(G3) PWBA2 PWBA3	Ge(Li) AND Si(Li) DETECTOR USED. METAL TARGET ON MYLAR BACKING. He4 IMPACT STUDIED.

TABLE BII EXPERIMENTAL IONIZATION CROSS SECTIONS

THIN TARGET

ENERGY MeV	TOTAL BARNS	REF	ENERGY MeV	TOTAL BARNS	REF
4.00	57100	PONM79	14.00	47500	PONM79
6.00	61000		16.00	45500	
8.00	59000		18.00	41300	
10.00	53500		20.00	38600	
12.00	53100		22.00	36500	

TABLE B. Experimental *L*-Shell Ionization Cross Sections for Proton Impact

Z=40 ZIRCONIUM(ZR)

TABLE BI EXPERIMENTAL DETAILS

REF	ENERGY RANGE MeV	AREAL DENSITY E-6G/CMSQ	BEAM CURRENT A	BEAM COLL mm	EXP ERROR %	THEORIES	COMMENTS
KROA82	.1015-.7422	110+-2	-	-	LT 16-18	CPSSR	CRYSTAL SPECTROMETER AND Si(Li) USED. RBS EMPLOYED. EFFICIENCY CALCULATED. METAL TARGET ON CARBON BACKING.

TABLE BII EXPERIMENTAL IONIZATION CROSS SECTIONS

THIN TARGET

ENERGY MeV	TOTAL BARNS	REF	ENERGY MeV	TOTAL BARNS	REF
.1015	54	KROA82	.3179	1950	KROA82
.1334	183		.3991	3300	
.1638	303		.4903	4640	
.2051	616		.6011	7110	
.2566	1320		.7422	10700	

Z=41 NIOBIUM(NB)

TABLE BI EXPERIMENTAL DETAILS

REF	ENERGY RANGE MeV	AREAL DENSITY E-6G/CMSQ	BEAM CURRENT A	BEAM COLL mm	EXP ERROR %	THEORIES	COMMENTS
KROA82	.0916-.7459	55+-3	-	-	LT 15-17	CPSSR	CRYSTAL SPECTROMETER AND Si(Li) USED. RBS EMPLOYED. EFFICIENCY CALCULATED. METAL TARGET ON CARBON BACKING.

TABLE BII EXPERIMENTAL IONIZATION CROSS SECTIONS

THIN TARGET

ENERGY MeV	TOTAL BARNS	REF	ENERGY MeV	TOTAL BARNS	REF
.0916	25.7	KROA82	.3239	1350	KROA82
.1115	57		.4044	2260	
.1417	133		.4951	3510	
.1723	274		.6058	5150	
.2129	494		.7459	7500	
.2634	822				

TABLE B. Experimental *L*-Shell Ionization Cross Sections for Proton Impact

Z=45 RHODIUM(RH)

TABLE BI EXPERIMENTAL DETAILS

REF	ENERGY RANGE MeV	AREAL DENSITY E-6G/CMSQ	BEAM CURRENT A	BEAM COLL mm	EXP ERROR %	THEORIES	COMMENTS
KROA82	.09-.744	88+-5	-	-	L1 15-19 L2 15-20 L3 18-24 LT 15-19 R1 22-28 R2 23-31	CPSSR	CRYSTAL SPECTROMETER AND Si(Li) USED. RBS EMPLOYED. EFFICIENCY CALCULATED. METAL TARGET ON CARBON BACKING.

TABLE BII EXPERIMENTAL IONIZATION CROSS SECTIONS

THIN TARGET

ENERGY MeV	L1 (BARNS)	L2 (BARNS)	L3 (BARNS)	L1/L2	L1/L3	TOTAL BARNS	REF
.0900	1.08	1.32	2.86	.82	.379	5.3	KROA82
.1096	2.29	3.58	8.0	.64	.288	13.8	
.1393	4.39	10.4	23.1	.420	.190	38.0	
.1696	6.4	22.0	49.1	.289	.130	78	
.2100	9.2	48.5	108	.189	.085	166	
.2604	11.2	92	205	.122	.055	309	
.3211	17.0	159	350	.107	.049	525	
.4019	32.4	272	592	.119	.055	896	
.4925	86	436	937	.198	.092	1460	
.6031	191	641	1370	.299	.140	2200	
.7440	394	943	1980	.418	.199	3310	

Z=46 PALLADIUM(PD)

TABLE BI EXPERIMENTAL DETAILS

REF	ENERGY RANGE MeV	AREAL DENSITY E-6G/CMSQ	BEAM CURRENT A	BEAM COLL mm	EXP ERROR %	THEORIES	COMMENTS
CHAR75	3-12	21+-2	-	-	LT 20	BEA(G3) PWBA3	RBS EMPLOYED. EFFICIENCY CALCULATED. O5+ IMPACT STUDIED. METAL TARGET ON CARBON BACKING.
KROA82	.09-.7438	99+-6	-	-	L1 15-20 L2 15-22 L3 17-26 LT 14-20 R1 21-29 R2 23-33	CPSSR	CRYSTAL SPECTROMETER AND Si(Li) USED. RBS EMPLOYED. EFFICIENCY CALCULATED. METAL TARGET ON CARBON BACKING.

TABLE B. Experimental L-Shell Ionization Cross Sections for Proton Impact

Z=46 PALLADIUM(PD) CONTINUED

TABLE BII EXPERIMENTAL IONIZATION CROSS SECTIONS

THIN TARGET

ENERGY MeV	L1	L2 BARNS	L3	L1/L2	L1/L3	TOTAL BARNS	REF
.0900	.89	.90	2.03	.99	.438	3.81	KROA82
.1093	1.93	2.60	5.9	.74	.327	10.4	
.1389	4.13	7.7	17.6	.54	.234	29.5	
.1692	5.9	16.4	37.6	.361	.158	60	
.2094	8.8	36.1	83	.244	.106	128	
.2601	10.4	71	162	.147	.064	244	
.3207	16.7	129	294	.129	.057	440	
.4015	31.8	221	495	.144	.064	748	
.4920	69	350	776	.196	.088	1190	
.6026	153	534	1160	.287	.132	1850	
.7438	327	759	1630	.431	.201	2720	
3.0000	-	-	-	-	-	36000	CHAR75
4.0000	-	-	-	-	-	46000	
5.0000	-	-	-	-	-	42000	
6.0000	-	-	-	-	-	52000	
7.0000	-	-	-	-	-	53000	
8.0000	-	-	-	-	-	55000	
9.0000	-	-	-	-	-	55000	
10.0000	-	-	-	-	-	56000	
11.0000	-	-	-	-	-	51000	
12.0000	-	-	-	-	-	46000	

Z=47 SILVER(AG)

TABLE BI EXPERIMENTAL DETAILS

REF	ENERGY RANGE MeV	AREAL DENSITY E-6G/CMSQ	BEAM CURRENT A	BEAM COLL mm	EXP ERROR %	THEORIES	COMMENTS
CHAR75	3-12	22+-2	-	-	LT 20	BEA(G3) PWBA3	RBS EMPLOYED. EFFICIENCY CALCULATED. O5+ IMPACT STUDIED. METAL TARGET ON CARBON BACKING.
BONG78	3.0	THIN	-	-	LT 15	BEA(G3)	RBS EMPLOYED. EFFICIENCY MEASURED. K-SHELL STUDIED. SELF-SUPPORTING METAL TARGET.
CUZP81	.611-3.85	THIN	-	-	LT 5-11	BEA(H) SCA2 PWBA3	EFFICIENCY MEASURED. AgIO3 TARGET ON CARBON BACKING. CROSS SECTIONS EVALUATED BY NORMALIZING TO K-SHELL DATA.
KROA82	.1397-.744	95+-3	-	-	L1 15-16 L2 15-17 L3 17-20 LT 15-16 R1 21-24 R2 23-26	CPSSR	CRYSTAL SPECTROMETER AND Si(Li) USED. RBS EMPLOYED. EFFICIENCY CALCULATED. METAL TARGET ON CARBON BACKING.

TABLE B. Experimental *L*-Shell Ionization Cross Sections for Proton Impact

Z=47 SILVER(AG) CONTINUED

TABLE BII EXPERIMENTAL IONIZATION CROSS SECTIONS

THIN TARGET

ENERGY MeV	L1	L2 BARNS	L3	L1/L2	L1/L3	TOTAL BARNS	REF
.1397	3.35	5.3	12.4	.63	.270	21.1	KROA82
.1697	5.3	11.9	27.9	.448	.191	45.1	
.2102	8.3	26.7	63	.310	.130	98	
.2608	11.3	54	126	.211	.089	191	
.3214	14.1	95	224	.149	.063	333	
.4020	25.1	169	393	.149	.064	587	
.4925	56	288	661	.196	.085	1000	
.6034	119	419	948	.284	.125	1490	
.6110	-	-	-	-	-	2590	CUZP81
.7440	270	640	1430	.422	.189	2340	KROA82
.8110	-	-	-	-	-	5279	CUZP81
1.0190	-	-	-	-	-	7672	
1.2000	-	-	-	-	-	9820	
1.4000	-	-	-	-	-	12393	
1.6000	-	-	-	-	-	12885	
1.8000	-	-	-	-	-	14869	
2.0000	-	-	-	-	-	18525	
2.2000	-	-	-	-	-	17869	
2.4000	-	-	-	-	-	19672	
2.6000	-	-	-	-	-	21967	
2.8000	-	-	-	-	-	25902	
3.0000	-	-	-	-	-	25082	
3.0000	-	-	-	-	-	23750	BONG78
3.0000	-	-	-	-	-	30000	CHAR75
3.2000	-	-	-	-	-	27377	CUZP81
3.4000	-	-	-	-	-	27705	
3.6000	-	-	-	-	-	29836	
3.8000	-	-	-	-	-	29672	
3.8500	-	-	-	-	-	29508	
4.0000	-	-	-	-	-	40000	CHAR75
5.0000	-	-	-	-	-	44000	
6.0000	-	-	-	-	-	49000	
7.0000	-	-	-	-	-	49000	
8.0000	-	-	-	-	-	46000	
9.0000	-	-	-	-	-	46000	
10.0000	-	-	-	-	-	46000	
11.0000	-	-	-	-	-	43000	
12.0000	-	-	-	-	-	40000	

Z=48 CADMIUM(CD)

TABLE BI EXPERIMENTAL DETAILS

REF	ENERGY RANGE MeV	AREAL DENSITY E-6G/CMSQ	BEAM CURRENT A	BEAM COLL mm	EXP ERROR %	THEORIES	COMMENTS
BONG78	3.0	THIN	-	-	LT 12	BEA(G3)	RBS EMPLOYED. EFFICIENCY MEASURED. K-SHELL STUDIED. METAL TARGET ON CARBON BACKING.

TABLE B. Experimental *L*-Shell Ionization Cross Sections for Proton Impact

Z=48 CADMIUM(CD) CONTINUED

TABLE BI EXPERIMENTAL DETAILS CONTINUED

REF	ENERGY RANGE MeV	AREAL DENSITY E-6G/CMSQ	BEAM CURRENT A	BEAM COLL mm	EXP ERROR %	THEORIES	COMMENTS
KROA82	.1372-.7422	126+-4	-	-	L1 14-16 L2 15-17 L3 17-20 LT 14-16 R1 21-24 R2 22-26	CPSSR	CRYSTAL SPECTROMETER AND Si(Li) USED. RBS EMPLOYED. EFFICIENCY CALCULATED. METAL TARGET ON VITRIOUS CARBON BACKING.

TABLE BII EXPERIMENTAL IONIZATION CROSS SECTIONS

THIN TARGET

ENERGY MeV	L1 (BARNS)	L2 (BARNS)	L3 (BARNS)	L1/L2	L1/L3	TOTAL BARNS	REF
.1372	2.61	3.27	7.6	.80	.344	13.5	KROA82
.1673	4.48	7.6	18.0	.59	.249	30.1	
.2076	6.8	17.3	41.7	.394	.164	66	
.2581	9.2	36.2	88	.253	.104	133	
.3188	11.4	67	163	.171	.070	241	
.3997	19.7	122	293	.162	.067	435	
.4906	41.2	204	482	.202	.086	727	
.6015	93	329	760	.282	.122	1180	
.7422	214	509	1150	.420	.186	1870	
3.0000	-	-	-	-	-	19913	BONG78

Z=49 INDIUM(IN)

TABLE BI EXPERIMENTAL DETAILS

REF	ENERGY RANGE MeV	AREAL DENSITY E-6G/CMSQ	BEAM CURRENT A	BEAM COLL mm	EXP ERROR %	THEORIES	COMMENTS
KROA82	.1359-.7417	136+-8	-	-	L1 14-16 L2 15-18 L3 17-22 LT 14-16 R1 20-24 R2 22-28	CPSSR	CRYSTAL SPECTROMETER AND Si(Li) USED. RBS EMLPOYED. EFFICIENCY CALCULATED. METAL TARGET ON VITRIOUS CARBON BACKING.

TABLE BII EXPERIMENTAL IONIZATION CROSS SECTIONS

THIN TARGET

ENERGY MeV	L1 (BARNS)	L2 (BARNS)	L3 (BARNS)	L1/L2	L1/L3	TOTAL BARNS	REF
.1359	2.40	2.26	5.1	1.06	.472	9.7	KROA82
.1661	4.35	5.5	12.8	.79	.339	22.7	
.2066	6.9	12.8	30.7	.54	.224	50	

TABLE B. Experimental *L*-Shell Ionization Cross Sections for Proton Impact

Z=49 INDIUM(IN) CONTINUED

TABLE BII EXPERIMENTAL IONIZATION CROSS SECTIONS CONTINUED

THIN TARGET

ENERGY MeV	L1 (BARNS)	L2 (BARNS)	L3 (BARNS)	L1/L2	L1/L3	TOTAL BARNS	REF
.2573	9.3	27.4	67	.340	.138	104	KROA82
.3180	11.6	53	130	.220	.090	194	
.3989	17.5	98	239	.179	.073	353	
.4897	34.0	167	401	.204	.085	602	
.6006	75	262	618	.285	.121	955	
.7417	177	411	940	.430	.188	1530	

Z=50 TIN(SN)

TABLE BI EXPERIMENTAL DETAILS

REF	ENERGY RANGE MeV	AREAL DENSITY E-6G/CMSQ	BEAM CURRENT A	BEAM COLL mm	EXP ERROR %	THEORIES	COMMENTS
CHAR75	3-12	29+-3	-	-	LT 20	BEA(G3) PWBA3	RBS EMPLOYED. EFFICIENCY CALCULATED. O5+ IMPACT STUDIED. METAL TARGET ON CARBON BACKING.
BONG78	3.0	THIN	-	-	LT 12	BEA(G3)	RBS EMPLOYED. EFFICIENCY MEASURED. K-SHELL STUDIED. SELF-SUPPORTING METAL TARGET.
PONM79	4.0-22.0	THIN	-	6.0(C)	-	BEA(G3) PWBA2 PWBA3	Ge(Li) AND Si(Li) DETECTORS USED. METAL TARGET ON MYLAR BACKING. He4 IMPACT STUDIED.
KROA82	.137-.743	115+-5	-	-	L1 14-17 L2 15-19 L3 16-19 LT 14-17 R1 21-25 R2 21-25	CPSSR	CRYSTAL SPECTROMETER AND Si(Li) USED. RBS EMPLOYED. EFFICIENCY CALCULATED. METAL TARGET ON VITRIOUS CARBON BACKING.

TABLE BII EXPERIMENTAL IONIZATION CROSS SECTIONS

THIN TARGET

ENERGY MeV	L1 (BARNS)	L2 (BARNS)	L3 (BARNS)	L1/L2	L1/L3	TOTAL BARNS	REF
.1370	1.27	1.47	4.00	.86	.317	6.7	KROA82
.1678	2.45	3.78	10.2	.65	.240	16.4	
.2084	3.91	9.3	24.4	.423	.160	37.6	

TABLE B. Experimental *L*-Shell Ionization Cross Sections for Proton Impact

Z=50 TIN(SN) CONTINUED

TABLE BII EXPERIMENTAL IONIZATION CROSS SECTIONS CONTINUED

THIN TARGET

ENERGY MeV	L1 (BARNS)	L2 (BARNS)	L3 (BARNS)	L1/L2	L1/L3	TOTAL BARNS	REF
.2591	5.3	19.5	51	.273	.105	76	KROA82
.3199	7.1	38.1	99	.188	.072	144	
.4007	10.3	76	194	.136	.053	280	
.4915	19.2	130	330	.147	.058	479	
.6023	40.8	203	510	.201	.080	754	
.7430	95	318	791	.300	.121	1200	
3.0000	-	-	-	-	-	14815	BONG78
3.0000	-	-	-	-	-	19000	CHAR75
4.0000	-	-	-	-	-	23000	
4.0000	-	-	-	-	-	16100	PONM79
5.0000	-	-	-	-	-	30000	CHAR75
6.0000	-	-	-	-	-	32000	
6.0000	-	-	-	-	-	20000	PONM79
7.0000	-	-	-	-	-	33000	CHAR75
8.0000	-	-	-	-	-	34000	
8.0000	-	-	-	-	-	20300	PONM79
9.0000	-	-	-	-	-	35000	CHAR75
10.0000	-	-	-	-	-	33000	
10.0000	-	-	-	-	-	20000	PONM79
11.0000	-	-	-	-	-	31000	CHAR75
12.0000	-	-	-	-	-	30000	
12.0000	-	-	-	-	-	19100	PONM79
14.0000	-	-	-	-	-	18500	
16.0000	-	-	-	-	-	16700	
18.0000	-	-	-	-	-	16000	
20.0000	-	-	-	-	-	14700	
22.0000	-	-	-	-	-	13600	

Z=51 ANTIMONY(SB)

TABLE BI EXPERIMENTAL DETAILS

REF	ENERGY RANGE MeV	AREAL DENSITY E-6G/CMSQ	BEAM CURRENT A	BEAM COLL mm	EXP ERROR %	THEORIES	COMMENTS
KROA82	.1399-.7433	106+-4	-	-	L1 15-17 L2 15-20 L3 16-20 LT 15-17 R1 21-26 R2 22-26	CPSSR	CRYSTAL SPECTROMETER AND Si(Li) USED. RBS EMPLOYED. EFFICIENCY CALCULATED. METAL TARGET ON CARBON BACKING.

TABLE BII EXPERIMENTAL IONIZATION CROSS SECTIONS

THIN TARGET

ENERGY MeV	L1 (BARNS)	L2 (BARNS)	L3 (BARNS)	L1/L2	L1/L3	TOTAL BARNS	REF
.1399	1.29	1.28	3.33	1.01	.388	5.9	KROA82
.1693	2.47	3.18	8.3	.78	.297	14.0	
.2096	4.09	7.7	20.0	.53	.204	31.8	
.2601	6.3	18.0	46.4	.348	.135	71	
.3206	8.3	35.7	91	.232	.091	135	

TABLE B. Experimental *L*-Shell Ionization Cross Sections for Proton Impact

Z=51 ANTIMONY(SB) CONTINUED

TABLE BII EXPERIMENTAL IONIZATION CROSS SECTIONS CONTINUED

THIN TARGET

ENERGY MeV	L1	L2 BARNS	L3	L1/L2	L1/L3	TOTAL BARNS	REF
.4017	10.4	66	165	.158	.063	241	KROA82
.4921	17.7	112	279	.158	.063	409	
.6028	35.5	176	433	.202	.082	644	
.7433	84	284	688	.295	.122	1060	

Z=53 IODINE(I)

TABLE BI EXPERIMENTAL DETAILS

REF	ENERGY RANGE MeV	AREAL DENSITY E-6G/CMSQ	BEAM CURRENT A	BEAM COLL mm	EXP ERROR %	THEORIES	COMMENTS
BONG78	3.0-11.0	THIN	-	-	LT 10	BEA(G3)	RBS EMPLOYED. EFFICIENCY MEASURED. K-SHELL STUDIED. TARGET ON CARBON BACKING.
CUZP81	.611-3.85	THIN	-	-	LT 5-10	BEA(H) SCA2 PWBA3	EFFICIENCY MEASURED. AgIO3 TARGET ON CARBON BACKING. CROSS SECTIONS EVALUATED BY NORMALIZING TO K-SHELL DATA.

TABLE BII EXPERIMENTAL IONIZATION CROSS SECTIONS

THIN TARGET

ENERGY MeV	TOTAL BARNS	REF	ENERGY MeV	TOTAL BARNS	REF
.611	392	CUZP81	3.000	9403	BONG78
.811	874		3.000	7204	CUZP81
1.019	1333		3.200	7989	
1.200	1839		3.400	8667	
1.400	2462		3.600	9473	
1.600	3011		3.800	9753	
1.800	3527		3.850	9849	
2.000	4570		5.000	14985	BONG78
2.200	4677		7.000	17955	
2.400	5204		9.000	18209	
2.600	5903		11.000	17627	
2.800	6968				

TABLE B. Experimental *L*-Shell Ionization Cross Sections for Proton Impact

Z=55 CESIUM(CS)

TABLE BI EXPERIMENTAL DETAILS

REF	ENERGY RANGE MeV	AREAL DENSITY E-6G/CMSQ	BEAM CURRENT A	BEAM COLL mm	EXP ERROR %	THEORIES	COMMENTS
PONM79	4.0-22.0	THIN	-	6.0(C)	-	BEA(G3) PWBA2 PWBA3	Ge(Li) AND Si(Li) DETECTORS USED. METAL TARGET ON MYLAR BACKING. He4 IMPACT STUDIED.

TABLE BII EXPERIMENTAL IONIZATION CROSS SECTIONS

THIN TARGET

ENERGY MeV	TOTAL BARNS	REF	ENERGY MeV	TOTAL BARNS	REF
4.00	3680	PONM79	14.00	7050	PONM79
6.00	5850		16.00	6920	
8.00	6600		18.00	6650	
10.00	7380		20.00	6550	
12.00	7320		22.00	6340	

Z=58 CERIUM(CE)

TABLE BI EXPERIMENTAL DETAILS

REF	ENERGY RANGE MeV	AREAL DENSITY E-6G/CMSQ	BEAM CURRENT A	BEAM COLL mm	EXP ERROR %	THEORIES	COMMENTS
PONM79	4.0-22.0	THIN	-	6.0(C)	-	BEA(G3) PWBA2 PWBA3	Ge(Li) AND Si(Li) DETECTORS USED. METAL TARGET ON MYLAR BACKING. He4 IMPACT STUDIED.

TABLE BII EXPERIMENTAL IONIZATION CROSS SECTIONS

THIN TARGET

ENERGY MeV	TOTAL BARNS	REF	ENERGY MeV	TOTAL BARNS	REF
4.00	3350	PONM79	14.00	6540	PONM79
6.00	4670		16.00	6050	
8.00	5530		18.00	5870	
10.00	6610		20.00	5400	
12.00	7100		22.00	5150	

TABLE B. Experimental *L*-Shell Ionization Cross Sections for Proton Impact

Z=59 PRASEODYMIUM(PR)

TABLE BI   EXPERIMENTAL DETAILS

REF	ENERGY RANGE MeV	AREAL DENSITY E-6G/CMSQ	BEAM CURRENT A	BEAM COLL mm	EXP ERROR %	THEORIES	COMMENTS
WHER79	.15-.40	THICK	-	2.0(B)	L1 20 L2 20 L3 15	PSS PSSR PWBA3	EFFICIENCY MEASURED. GAMMA(1) AND GAMMA(2+3) CROSS SECTIONS QUOTED.

TABLE BII   EXPERIMENTAL IONIZATION CROSS SECTIONS

THICK TARGET

ENERGY MeV	L1	L2 (BARNS)	L3	L1/L2	L1/L3	TOTAL BARNS	REF
.150	.180	.044	.270	4.09	.67	.494	WHER79
.175	.390	.130	.68	3.00	.57	1.20	
.200	.71	.290	1.40	2.45	.51	2.40	
.250	1.60	1.10	4.50	1.45	.356	7.2	
.300	2.80	2.60	10.0	1.08	.280	15.4	
.350	4.00	5.3	19.0	.75	.211	28.3	
.400	5.0	9.1	31.0	.55	.161	45.1	

Z=62 SAMARIUM(SM)

TABLE BI   EXPERIMENTAL DETAILS

REF	ENERGY RANGE MeV	AREAL DENSITY E-6G/CMSQ	BEAM CURRENT A	BEAM COLL mm	EXP ERROR %	THEORIES	COMMENTS
PONM79	4.0-22.0	THIN	-	6.0(C)	-	BEA(G3) PWBA2 PWBA3	Ge(Li) AND Si(Li) DETECTORS USED. METAL TARGET ON MYLAR BACKING. He4 IMPACT STUDIED.
WHER79	.15-.44	THICK	-	2.0(B)	L1 20 L2 20 L3 15	PSS PSSR PWBA3	EFFICIENCY MEASURED. GAMMA(1) AND GAMMA(2+3) CROSS SECTIONS QUOTED.

TABLE BII   EXPERIMENTAL IONIZATION CROSS SECTIONS

THIN TARGET

ENERGY MeV	L1	L2 (BARNS)	L3	L1/L2	L1/L3	TOTAL BARNS	REF
4.00	-	-	-	-	-	3350	PONM79
6.00	-	-	-	-	-	4100	
8.00	-	-	-	-	-	5430	
10.00	-	-	-	-	-	5680	

TABLE B. Experimental *L*-Shell Ionization Cross Sections for Proton Impact

Z=62 SAMARIUM(SM) CONTINUED

TABLE BII EXPERIMENTAL IONIZATION CROSS SECTIONS CONTINUED

THIN TARGET

ENERGY MeV	L1 (BARNS)	L2 (BARNS)	L3 (BARNS)	L1/L2	L1/L3	TOTAL BARNS	REF
12.00	-	-	-	-	-	6340	PONM79
14.00	-	-	-	-	-	6600	
16.00	-	-	-	-	-	6420	
18.00	-	-	-	-	-	6240	
20.00	-	-	-	-	-	6040	
22.00	-	-	-	-	-	5850	

THICK TARGET

ENERGY MeV	L1 (BARNS)	L2 (BARNS)	L3 (BARNS)	L1/L2	L1/L3	TOTAL BARNS	REF
.150	.052	.021	.095	2.48	.55	.168	WHER79
.175	.130	.064	.259	2.03	.50	.453	
.200	.250	.150	.58	1.67	.431	.98	
.250	.64	.56	2.00	1.14	.320	3.20	
.300	1.10	1.40	4.70	.79	.234	7.2	
.350	1.60	2.70	8.9	.59	.180	13.2	
.400	2.00	4.50	15.0	.444	.133	21.5	
.440	2.30	6.1	20.0	.377	.115	28.4	

Z=65 TERBIUM(TB)

TABLE BI EXPERIMENTAL DETAILS

REF	ENERGY RANGE MeV	AREAL DENSITY E-6G/CMSQ	BEAM CURRENT A	BEAM COLL mm	EXP ERROR %	THEORIES	COMMENTS
WHER79	.15-.40	THICK	-	2.0(B)	L1 20 L2 20 L3 15	PSS PSSR PWBA3	EFFICIENCY MEASURED. GAMMA(1) AND GAMMA(2+3) CROSS SECTIONS QUOTED.

TABLE BII EXPERIMENTAL IONIZATION CROSS SECTIONS

THICK TARGET

ENERGY MeV	L1 (BARNS)	L2 (BARNS)	L3 (BARNS)	L1/L2	L1/L3	TOTAL BARNS	REF
.150	.021	9.0E-03	.032	2.33	.66	.062	WHER79
.175	.057	.027	.092	2.11	.62	.176	
.200	.120	.069	.220	1.74	.55	.409	
.250	.350	.270	.82	1.30	.427	1.44	
.300	.72	.73	2.20	.99	.327	3.65	
.350	1.20	1.50	4.60	.80	.261	7.3	
.400	1.70	2.80	8.4	.61	.202	12.9	

TABLE B. Experimental *L*-Shell Ionization Cross Sections for Proton Impact

Z=66 DYSPROSIUM(DY)

TABLE BI EXPERIMENTAL DETAILS

REF	ENERGY RANGE MeV	AREAL DENSITY E-6G/CMSQ	BEAM CURRENT A	BEAM COLL mm	EXP ERROR %	THEORIES	COMMENTS
JITW82	0.15-9.5	85	-	-	R1 20-30 R2 20-30	PWBA4 PWBABC RPWBABC CPSSR	BOTH SURFACES OF TARGET COVERD WITH THIN FILM OF CARBON. GAMMA(1)/ALPHA AND GAMMA(2+3)/ALPHA INTENSITY RATIOS PRESENTED.

TABLE BII EXPERIMENTAL IONIZATION CROSS SECTIONS

THIN TARGET

ENERGY MeV	L1 BARNS	L2	L3	L1/L2	L1/L3	TOTAL BARNS	REF
.150	-	-	-	3.01	.84	-	JITW82
.165	-	-	-	2.86	.83	-	
.175	-	-	-	2.77	.82	-	
.210	-	-	-	2.46	.77	-	
.240	-	-	-	2.22	.69	-	
.280	-	-	-	1.83	.55	-	
.300	-	-	-	1.61	.52	-	
.350	-	-	-	1.18	.384	-	
.500	-	-	-	.60	.194	-	
.700	-	-	-	.267	.091	-	
1.000	-	-	-	.198	.071	-	
1.400	-	-	-	.284	.108	-	
2.500	-	-	-	.78	.307	-	
3.000	-	-	-	.84	.302	-	
9.500	-	-	-	1.13	.432	-	

Z=67 HOLMIUM(HO)

TABLE BI EXPERIMENTAL DETAILS

REF	ENERGY RANGE MeV	AREAL DENSITY E-6G/CMSQ	BEAM CURRENT A	BEAM COLL mm	EXP ERROR %	THEORIES	COMMENTS
PONM79	4.0-22.0	THIN	-	6.0(C)	-	BEA(G3) PWBA2 PWBA3	Ge(Li) AND Si(Li) DETECTORS USED. METAL TARGET ON MYLAR BACKING. He4 IMPACT STUDIED.
WHER79	.15-.40	THICK	-	2.0(B)	L1 20 L2 20 L3 15	PSS PSSR PWBA3	EFFICIENCY MEASURED. GAMMA(1) AND GAMMA(2+3) CROSS SECTIONS QUOTED.

TABLE B. Experimental L-Shell Ionization Cross Sections for Proton Impact

Z=67 HOLMIUM(HO) CONTINUED

TABLE BII EXPERIMENTAL IONIZATION CROSS SECTIONS

THIN TARGET

ENERGY	L1	L2	L3	L1/L2	L1/L3	TOTAL	REF
MeV		BARNS				BARNS	
4.00	-	-	-	-	-	1720	PONM79
6.00	-	-	-	-	-	2540	
8.00	-	-	-	-	-	3570	
10.00	-	-	-	-	-	3950	
12.00	-	-	-	-	-	4180	
14.00	-	-	-	-	-	4450	
16.00	-	-	-	-	-	4660	
18.00	-	-	-	-	-	4730	
20.00	-	-	-	-	-	4560	
22.00	-	-	-	-	-	4350	

THICK TARGET

ENERGY	L1	L2	L3	L1/L2	L1/L3	TOTAL	REF
MeV		BARNS				BARNS	
.150	.012	3.4E-03	.017	3.53	.71	.032	WHER79
.175	.044	.015	.063	2.93	.70	.122	
.200	.120	.045	.170	2.67	.71	.335	
.250	.390	.210	.70	1.86	.56	1.30	
.300	.72	.55	1.70	1.31	.424	2.97	
.350	.93	.96	3.00	.97	.310	4.89	
.400	.94	1.30	4.30	.72	.219	6.5	

Z=70 YTTERBIUM(YB)

TABLE BI EXPERIMENTAL DETAILS

REF	ENERGY RANGE MeV	AREAL DENSITY E-6G/CMSQ	BEAM CURRENT A	BEAM COLL mm	EXP ERROR %	THEORIES	COMMENTS
WHER79	.15-.40	THICK	-	2.0(B)	L1 20 L2 20 L3 15	PSS PSSR PWBA3	EFFICIENCY MEASURED. GAMMA(1) AND GAMMA(2+3) CROSS SECTIONS QUOTED.

TABLE BII EXPERIMENTAL IONIZATION CROSS SECTIONS

THICK TARGET

ENERGY	L1	L2	L3	L1/L2	L1/L3	TOTAL	REF
MeV		BARNS				BARNS	
.150	3.3E-03	7.4E-04	5.5E-03	4.46	.60	9.5E-03	WHER79
.175	.014	4.2E-03	.020	3.33	.70	.038	
.200	.042	.015	.056	2.80	.75	.113	
.250	.180	.087	.250	2.07	.72	.52	
.300	.400	.240	.70	1.67	.57	1.34	
.350	.62	.440	1.50	1.41	.413	2.56	
.400	.76	.60	2.40	1.27	.317	3.76	

TABLE B. Experimental *L*-Shell Ionization Cross Sections for Proton Impact

Z=72 HAFNIUM(HF)

TABLE BI EXPERIMENTAL DETAILS

REF	ENERGY RANGE MeV	AREAL DENSITY E-6G/CMSQ	BEAM CURRENT A	BEAM COLL mm	EXP ERROR %	THEORIES	COMMENTS
JUSE80	0.5-2.5	50	30-200E-9	-	L1 7-9 L2 7-9 L3 6-9 LT 7-9 R1 10-12 R2 9-11	PWBA5 PWBABTR	RBS EMPLOYED. EFFICIENCY MEASURED. METAL TARGET ON FORMVAR BACKING. He+ IMPACT STUDIED.

TABLE BII EXPERIMENTAL IONIZATION CROSS SECTIONS

THIN TARGET

ENERGY MeV	L1 BARNS	L2 BARNS	L3 BARNS	L1/L2	L1/L3	TOTAL BARNS	REF
.50	1.38	1.22	5.2	1.13	.276	7.8	JUSE80
.60	1.90	2.32	9.9	.82	.192	14.1	
.70	2.48	4.40	16.7	.56	.149	23.5	
.80	3.00	6.5	23.8	.460	.126	33.0	
.90	3.24	8.8	32.1	.370	.101	44.0	
1.00	4.07	11.0	40.1	.370	.101	55	
1.10	4.31	14.3	51	.300	.085	69	
1.20	5.9	18.0	64	.330	.092	88	
1.30	7.7	22.7	80	.340	.095	111	
1.40	10.0	27.4	93	.370	.107	131	
1.50	11.7	31.2	107	.370	.109	150	
1.60	14.5	34.6	121	.420	.120	170	
1.80	24.0	49.0	154	.490	.156	227	
2.00	31.4	60	183	.53	.172	274	
2.50	69	95	273	.72	.253	437	

Z=73 TANTALUM(TA)

TABLE BI EXPERIMENTAL DETAILS

REF	ENERGY RANGE MeV	AREAL DENSITY E-6G/CMSQ	BEAM CURRENT A	BEAM COLL mm	EXP ERROR %	THEORIES	COMMENTS
JUSE80	0.6-2.5	50	30-200E-9	-	L1 11 L2 7-9 L3 8 LT 9 R1 10 R2 8	PWBA5 PWBABTR	RBS EMPLOYED. EFFICIENCY MEASURED. METAL TARGET ON FORMVAR BACKING. He+ IMPACT STUDIED.

TABLE B. Experimental L-Shell Ionization Cross Sections for Proton Impact

Z=73 TANTALUM(TA) CONTINUED

TABLE BII   EXPERIMENTAL IONIZATION CROSS SECTIONS

THIN TARGET

ENERGY MeV	L1 (BARNS)	L2 (BARNS)	L3 (BARNS)	L1/L2	L1/L3	TOTAL BARNS	REF
.60	1.70	2.20	7.3	.78	.240	11.3	JUSE80
.80	2.80	5.8	18.0	.480	.150	26.6	
1.00	3.50	11.0	33.1	.310	.100	47.6	
1.20	3.80	19.3	53	.200	.072	76	
1.30	4.90	22.9	62	.210	.078	90	
1.40	6.1	28.1	75	.220	.082	109	
1.50	7.8	33.1	87	.230	.089	128	
1.60	11.0	37.2	100	.300	.110	148	
1.80	19.0	48.2	128	.390	.150	195	
2.00	26.0	60	171	.430	.150	258	
2.50	57	97	238	.59	.240	391	

Z=74 TUNGSTEN(W)

TABLE BI   EXPERIMENTAL DETAILS

REF	ENERGY RANGE MeV	AREAL DENSITY E-6G/CMSQ	BEAM CURRENT A	BEAM COLL mm	EXP ERROR %	THEORIES	COMMENTS
PONM79	4.0-22.0	THIN	-	6.0(C)	-	BEA(G3) PWBA2 PWBA3	Ge(Li) AND Si(Li) DETECTORS USED. METAL TARGET ON MYLAR BACKING. He4 IMPACT STUDIED.
JUSE80	0.5-2.5	50	30-200E-9	-	L1 6-13 L2 7-9 L3 7-10 LT 8 R1 7-13 R2 7-14	PWBA5 PWBABTR	RBS EMPLOYED. EFFICIENCY MEASURED. METAL TARGET ON FORMVAR BACKING. He+ IMPACT STUDIED.

TABLE BII   EXPERIMENTAL IONIZATION CROSS SECTIONS

THIN TARGET

ENERGY MeV	L1 (BARNS)	L2 (BARNS)	L3 (BARNS)	L1/L2	L1/L3	TOTAL BARNS	REF
.50	1.19	.80	3.10	1.49	.384	5.1	JUSE80
.70	2.39	2.49	9.9	.96	.241	14.8	
.80	2.71	4.28	15.3	.63	.178	22.2	
.90	2.97	6.1	22.7	.489	.131	31.8	
1.00	3.29	8.2	30.7	.402	.107	42.2	
1.10	3.84	11.4	40.6	.337	.095	56	
1.20	4.29	15.1	52	.285	.083	71	
1.30	5.5	17.9	60	.306	.091	84	
1.40	6.8	20.9	73	.328	.093	100	
1.50	10.0	24.9	78	.402	.128	113	

TABLE B. Experimental *L*-Shell Ionization Cross Sections for Proton Impact

Z=74 TUNGSTEN(W) CONTINUED

TABLE BII EXPERIMENTAL IONIZATION CROSS SECTIONS CONTINUED

THIN TARGET

ENERGY MeV	L1 BARNS	L2 BARNS	L3 BARNS	L1/L2	L1/L3	TOTAL BARNS	REF
1.60	11.9	27.9	87	.428	.137	127	JUSE80
1.70	14.5	32.5	98	.447	.147	145	
1.80	19.7	36.9	114	.53	.173	170	
1.90	21.6	43.2	136	.50	.159	201	
2.00	24.7	47.3	147	.52	.169	219	
2.50	51	73	209	.70	.244	332	
4.00	-	-	-	-	-	530	PONM79
6.00	-	-	-	-	-	950	
8.00	-	-	-	-	-	1350	
10.00	-	-	-	-	-	1630	
12.00	-	-	-	-	-	1910	
14.00	-	-	-	-	-	2000	
16.00	-	-	-	-	-	2040	
18.00	-	-	-	-	-	2120	
20.00	-	-	-	-	-	2140	
22.00	-	-	-	-	-	2170	

Z=77 IRIDIUM(IR)

TABLE BI EXPERIMENTAL DETAILS

REF	ENERGY RANGE MeV	AREAL DENSITY E-6G/CMSQ	BEAM CURRENT A	BEAM COLL mm	EXP ERROR %	THEORIES	COMMENTS
JUSE80	0.6-2.5	50	30-200E-9	-	L1 7-9 L2 8 L3 8 LT 8 R1 9 R2 8	PWBA5 PWBABTR	RBS EMPLOYED. EFFICIENCY MEASURED. METAL TARGET ON FORMVAR BACKING.

TABLE BII EXPERIMENTAL IONIZATION CROSS SECTIONS

THIN TARGET

ENERGY MeV	L1 BARNS	L2 BARNS	L3 BARNS	L1/L2	L1/L3	TOTAL BARNS	REF
.60	1.41	.76	2.84	1.85	.496	5.0	JUSE80
.70	2.06	1.27	5.1	1.63	.404	8.4	
.80	2.12	2.46	8.2	.86	.260	12.7	
.90	2.44	3.57	12.2	.68	.200	18.2	
1.00	2.85	4.79	16.5	.60	.173	24.2	
1.10	3.00	6.1	21.7	.493	.138	30.8	
1.20	3.35	8.3	27.0	.405	.124	38.6	
1.30	3.53	11.5	32.9	.307	.107	47.9	
1.40	4.00	13.9	40.2	.287	.100	58	
1.50	5.8	15.3	47.1	.373	.122	68	
1.60	6.8	18.2	54	.372	.125	79	
1.70	8.5	22.1	63	.386	.134	94	
1.80	10.3	24.2	71	.426	.145	106	
2.00	13.9	31.4	88	.442	.159	133	
2.50	29.4	47.8	132	.62	.223	209	

TABLE B. Experimental L-Shell Ionization Cross Sections for Proton Impact

Z=79 GOLD(AU)

TABLE BI EXPERIMENTAL DETAILS

REF	ENERGY RANGE MeV	AREAL DENSITY E-6G/CMSQ	BEAM CURRENT A	BEAM COLL mm	EXP ERROR %	THEORIES	COMMENTS
BONG78	3.0-11.0	THIN	-	-	LT 7	BEA(G3) PWBA2	RBS EMPLOYED. EFFICIENCY MEASURED. SELF-SUPPORTING METAL TARGET.
PONM79	4.0-22.0	THIN	-	6.0(C)	-	BEA(G3) PWBA2 PWBA3	Ge(Li) AND Si(Li) DETECTORS USED. METAL TARGET ON MYLAR BACKING. He4 IMPACT STUDIED. M-SHELL STUDIED.
COHD80	1.0-3.0	7.5+-.2 THICK	15E-9	-	L1 23 L2 20 L3 11 LT 11	PWBA4 PWBAR CPSSR	RBS EMPLOYED. EFFICIENCY MEASURED. METAL TARGET ON CARBON BACKING.
SARL80	2.0	THIN	-	-	L1 19 L2 15 L3 15 LT 11	PWBA1 PWBABC MPWBABCR	EFFICIENCY MEASURED. METAL TARGET ON CARBON BACKING. C12 N14 O16 IMPACT STUDIED. USED ATOMIC PARAMETERS FROM REF(7+8)† AND REF(34)*.
JITW82	0.175-10.0	95	-	-	R1 20-30 R2 20-30	RSCA PWBA4 PWBABC RPWBABC CPSSR	SELF-SUPPORTING METAL TARGET. GAMMA(1)/ALPHA AND GAMMA(2+3+6)/ ALPHA INTENSITY RATIOS PRESENTED.
PINA82	0.5-4.0	50	30-200E-9	-	L1 9-11 L2 7-17 L3 6-9 LT 6-9 R1 11 R2 12	-	RBS EMPLOYED. EFFICIENCY MEASURED. SELF-SUPPORTING METAL TARGET. RADIATIVE DECAY BRANCHING RATIOS MEASURED.

TABLE BII EXPERIMENTAL IONIZATION CROSS SECTIONS

THIN TARGET

ENERGY MeV	L1 (BARNS)	L2 (BARNS)	L3 (BARNS)	L1/L2	L1/L3	TOTAL BARNS	REF
.175	-	-	-	4.90	.490	-	JITW82
.210	-	-	-	5.1	.63	-	
.250	-	-	-	4.94	.69	-	
.300	-	-	-	4.20	.69	-	
.350	-	-	-	3.47	.63	-	
.500	-	-	-	1.86	.398	-	
.500	.59	.195	1.43	3.02	.413	2.21	PINA82
.600	1.09	.53	2.88	2.07	.378	4.50	
.700	-	-	-	.89	.221	-	JITW82

TABLE B. Experimental L-Shell Ionization Cross Sections for Proton Impact

Z=79 GOLD(AU) CONTINUED

TABLE BII EXPERIMENTAL IONIZATION CROSS SECTIONS CONTINUED

THIN TARGET

ENERGY MeV	L1 (BARNS)	L2 (BARNS)	L3 (BARNS)	L1/L2	L1/L3	TOTAL BARNS	REF
.700	1.32	.82	4.36	1.62	.303	6.5	PINA82
.800	1.41	1.53	7.3	.92	.193	10.2	
.900	-	-	-	.492	.136	-	JITW82
.900	1.53	2.38	10.8	.64	.142	14.7	PINA82
1.000	1.32	3.11	13.0	.424	.102	16.8	COHD80
1.000	1.71	3.60	14.6	.475	.117	19.9	PINA82
1.100	1.88	4.48	18.4	.420	.102	24.8	
1.200	2.36	5.2	20.4	.453	.116	27.1	COHD80
1.200	-	-	-	.285	.083	-	JITW82
1.200	2.18	5.9	23.5	.369	.093	31.5	PINA82
1.300	2.62	7.7	28.8	.342	.091	39.0	
1.400	3.65	7.9	29.2	.464	.125	39.7	COHD80
1.400	2.85	9.0	37.4	.319	.076	49.2	PINA82
1.500	-	-	-	.231	.071	-	JITW82
1.500	3.91	10.3	41.1	.380	.095	55	PINA82
1.600	5.2	11.1	39.5	.468	.131	55	COHD80
1.600	5.0	12.3	49.1	.405	.102	67	PINA82
1.700	5.5	14.2	55	.386	.100	75	
1.800	7.0	14.8	51	.470	.136	72	COHD80
1.800	-	-	-	.309	.101	-	JITW82
1.800	6.2	16.5	64	.375	.096	87	PINA82
2.000	9.0	19.1	64	.471	.140	91	COHD80
2.000	7.7	23.8	72	.325	.108	103	SARL80†
2.000	6.6	21.2	70	.310	.094	98	SARL80*
2.000	8.4	21.6	77	.389	.109	107	PINA82
2.100	-	-	-	.305	.102	-	JITW82
2.200	11.3	23.9	79	.473	.143	112	COHD80
2.400	13.9	29.3	95	.474	.147	135	
2.500	-	-	-	.456	.157	-	JITW82
2.500	17.6	33.1	114	.53	.155	165	PINA82
2.600	16.7	35.2	112	.474	.149	160	COHD80
2.800	19.8	41.5	130	.477	.152	187	
3.000	-	-	-	-	-	190	BONG78
3.000	23.1	48.4	150	.477	.154	216	COHD80
3.000	-	-	-	.54	.175	-	JITW82
3.000	29.4	44.9	150	.65	.196	225	PINA82
3.500	40.0	54	189	.74	.212	283	
4.000	52	66	227	.78	.226	345	
4.000	-	-	-	-	-	260	PONM79
4.500	-	-	-	.86	.286	-	JITW82
5.000	-	-	-	-	-	497	BONG78
6.000	-	-	-	-	-	610	PONM79
6.700	-	-	-	1.17	.401	-	JITW82
7.000	-	-	-	-	-	768	BONG78
8.000	-	-	-	-	-	980	PONM79
9.000	-	-	-	-	-	1050	BONG78
10.000	-	-	-	1.22	.420	-	JITW82
10.000	-	-	-	-	-	1200	PONM79
11.000	-	-	-	-	-	1274	BONG78
12.000	-	-	-	-	-	1420	PONM79
14.000	-	-	-	-	-	1650	
16.000	-	-	-	-	-	1920	
18.000	-	-	-	-	-	1960	
20.000	-	-	-	-	-	2140	
22.000	-	-	-	-	-	2160	

TABLE B. Experimental *L*-Shell Ionization Cross Sections for Proton Impact

Z=79 GOLD(AU) CONTINUED

TABLE BII EXPERIMENTAL IONIZATION CROSS SECTIONS CONTINUED

THICK TARGET

ENERGY MeV	L1	L2 BARNS	L3	L1/L2	L1/L3	TOTAL BARNS	REF
1.00	2.03	3.20	14.3	.63	.142	18.9	COHD80
1.20	3.15	5.1	21.8	.62	.144	29.2	
1.40	4.68	7.5	30.8	.62	.152	41.7	
1.60	6.6	10.5	41.3	.63	.161	57	
1.80	9.0	14.1	53	.64	.169	74	
2.00	11.9	18.3	67	.65	.177	95	
2.20	15.2	23.3	83	.65	.184	118	
2.40	18.9	29.3	100	.65	.189	144	
2.60	23.1	36.1	119	.64	.194	174	
2.80	27.6	43.9	140	.63	.197	206	
3.00	32.5	53	162	.62	.201	242	

Z=81 THALLIUM(TL)

TABLE BI EXPERIMENTAL DETAILS

REF	ENERGY RANGE MeV	AREAL DENSITY E-6G/CMSQ	BEAM CURRENT A	BEAM COLL mm	EXP ERROR %	THEORIES	COMMENTS
LEIC77	0.5-3.0	50	30-200E-9	-	L1 8-11 L2 8-18 L3 8 LT 7-9 R1 8-11 R2 11	SCA1 PWBA5	RBS EMPLOYED. EFFICIENCY MEASURED. METAL TARGET ON FORMVAR BACKING. RADIATIVE DECAY BRANCHING RATIOS MEASURED.

TABLE BII EXPERIMENTAL IONIZATION CROSS SECTIONS

THIN TARGET

ENERGY MeV	L1	L2 BARNS	L3	L1/L2	L1/L3	TOTAL BARNS	REF
.50	.470	.170	1.06	2.82	.440	1.69	LEIC77
1.00	1.37	2.32	11.2	.59	.123	14.9	
1.50	2.08	8.8	37.6	.240	.055	48.4	
2.00	6.3	15.9	62	.400	.101	85	
2.50	13.4	26.7	100	.50	.134	140	
3.00	23.6	32.7	120	.72	.196	176	

TABLE B. Experimental *L*-Shell Ionization Cross Sections for Proton Impact

Z=82 LEAD(PB)

TABLE BI EXPERIMENTAL DETAILS

REF	ENERGY RANGE MeV	AREAL DENSITY E-6G/CMSQ	BEAM CURRENT A	BEAM COLL mm	EXP ERROR %	THEORIES	COMMENTS
LEIC77	0.5-3.5	50	30-200E-9	-	L1 8-11 L2 7-15 L3 7-9 LT 7 R1 11 R2 12	SCA1 PWBA5	RBS EMPLOYED. EFFICIENCY MEASURED. METAL TARGET ON FORMVAR BACKING. RADIATIVE DECAY BRANCHING RATIOS MEASURED.
BONG78	3.0	THIN	-	-	LT 7	BEA(G3)	RBS EMPLOYED. EFFICIENCY MEASURED. METAL TARGET ON CARBON BACKING.
COHD80	1-3	6.7+-.1 THICK	15E-9	-	L1 23 L2 20 L3 11 LT 11	PWBA4 PWBAR CPSSR	RBS EMPLOYED. EFFICIENCY MEASURED. METAL TARGET ON CARBON BACKING.

TABLE BII EXPERIMENTAL IONIZATION CROSS SECTIONS

THIN TARGET

ENERGY MeV	L1	L2 BARNS	L3	L1/L2	L1/L3	TOTAL BARNS	REF
.50	.370	.130	.64	2.79	.57	1.14	LEIC77
1.00	1.33	1.98	8.8	.67	.151	11.9	COHD80
1.00	1.07	1.94	8.0	.56	.135	11.0	LEIC77
1.20	1.79	3.53	15.0	.51	.119	19.8	COHD80
1.40	2.43	5.5	22.4	.439	.108	29.6	
1.50	2.49	7.2	25.1	.350	.099	34.9	LEIC77
1.60	3.30	8.0	30.9	.414	.107	41.1	COHD80
1.80	4.45	10.8	40.3	.412	.110	54	
2.00	5.9	14.1	51	.420	.117	69	
2.00	4.80	15.6	49.4	.310	.097	70	LEIC77
2.20	7.7	17.8	62	.435	.125	86	COHD80
2.40	9.9	21.8	74	.456	.134	104	
2.50	12.2	26.1	77	.470	.158	116	LEIC77
2.60	12.6	26.4	87	.477	.145	124	COHD80
2.80	15.6	32.5	101	.480	.154	145	
3.00	19.1	36.5	115	.52	.166	168	
3.00	-	-	-	-	-	126	BONG78
3.00	19.0	36.5	111	.52	.170	167	LEIC77
3.50	20.8	46.2	147	.450	.141	214	

THICK TARGET

ENERGY MeV	L1	L2 BARNS	L3	L1/L2	L1/L3	TOTAL BARNS	REF
1.00	1.03	2.06	9.3	.50	.110	12.1	COHD80
1.20	1.59	3.41	14.9	.466	.107	19.4	
1.40	2.41	5.1	21.6	.473	.112	28.3	
1.60	3.51	7.1	29.4	.492	.119	39.0	
1.80	4.80	9.6	38.6	.499	.124	52	
2.00	6.3	12.6	49.0	.50	.129	66	

TABLE B. Experimental *L*-Shell Ionization Cross Sections for Proton Impact

Z=82 LEAD(PB) CONTINUED

TABLE BII EXPERIMENTAL IONIZATION CROSS SECTIONS CONTINUED

THICK TARGET

ENERGY MeV	L1	L2 BARNS	L3	L1/L2	L1/L3	TOTAL BARNS	REF
2.20	8.1	16.1	61	.50	.133	83	COHD80
2.40	10.0	20.4	74	.488	.134	102	
2.60	12.0	25.2	89	.476	.135	123	
2.80	14.0	30.8	105	.455	.133	147	
3.00	16.2	37.3	123	.434	.132	173	

Z=83 BISMUTH(BI)

TABLE BI EXPERIMENTAL DETAILS

REF	ENERGY RANGE MeV	AREAL DENSITY E-6G/CMSQ	BEAM CURRENT A	BEAM COLL mm	EXP ERROR %	THEORIES	COMMENTS
LEIC77	0.5-3.0	50	30-200E-9	-	L1 8-12 L2 7-13 L3 7-10 LT 7-10 R1 10 R2 11	SCA1 PWBA5	RBS EMPLOYED. EFFICIENCY MEASURED. METAL TARGET ON FORMVAR BACKING. RADIATIVE DECAY BRANCHING RATIOS MEASURED.

TABLE BII EXPERIMENTAL IONIZATION CROSS SECTIONS

THIN TARGET

ENERGY MeV	L1	L2 BARNS	L3	L1/L2	L1/L3	TOTAL BARNS	REF
.50	.340	.075	.480	4.53	.71	.89	LEIC77
1.00	1.29	1.27	8.4	1.00	.153	10.9	
1.50	2.00	5.8	23.8	.340	.084	31.6	
2.00	4.60	12.3	41.7	.380	.111	59	
2.50	9.6	18.7	67	.51	.143	96	
3.00	17.2	26.8	91	.64	.190	135	

Z=90 THORIUM(TH)

TABLE BI EXPERIMENTAL DETAILS

REF	ENERGY RANGE MeV	AREAL DENSITY E-6G/CMSQ	BEAM CURRENT A	BEAM COLL mm	EXP ERROR %	THEORIES	COMMENTS
LEIC77	0.5-3.0	50	30-200E-9	-	L1 7-17 L2 8-11 L3 10-13 LT 9 R1 12 R2 8-12	SCA1 PWBA5	RBS EMPLOYED. EFFICIENCY MEASURED. METAL TARGET ON Al BACKING. RADIATIVE DECAY BRANCHING RATIOS MEASURED.

TABLE B. Experimental *L*-Shell Ionization Cross Sections for Proton Impact

Z=90 THORIUM(TH) CONTINUED

TABLE BII EXPERIMENTAL IONIZATION CROSS SECTIONS

THIN TARGET

ENERGY MeV	L1	L2 BARNS	L3	L1/L2	L1/L3	TOTAL BARNS	REF
.50	.120	.036	.160	3.30	.75	.320	LEIC77
1.00	.54	.70	2.67	.77	.200	3.91	
1.50	.83	2.85	10.1	.290	.082	13.8	
2.00	1.59	7.1	21.7	.220	.073	30.4	
2.50	2.44	12.0	34.6	.200	.070	49.2	
3.00	5.9	17.6	48.2	.330	.120	72	

Z=92 URANIUM(U)

TABLE BI EXPERIMENTAL DETAILS

REF	ENERGY RANGE MeV	AREAL DENSITY E-6G/CMSQ	BEAM CURRENT A	BEAM COLL mm	EXP ERROR %	THEORIES	COMMENTS
LEIC77	0.5-3.5	50	30-200E-9	-	L1 8-13 L2 8-12 L3 11 LT 10 R1 11-13 R2 10-12	BEA(M) SCA1 PWBA5 PWBABTR	RBS EMPLOYED. EFFICIENCY MEASURED. METAL TARGET ON Al BACKING. RADIATIVE DECAY BRANCHING RATIOS MEASURED.
BONG78	3.0	THIN	-	-	LT 9	BEA(G3)	RBS EMPLOYED. EFFICIENCY MEASURED. METAL TARGET ON CARBON BACKING.

TABLE BII EXPERIMENTAL IONIZATION CROSS SECTIONS

THIN TARGET

ENERGY MeV	L1	L2 BARNS	L3	L1/L2	L1/L3	TOTAL BARNS	REF
.50	.068	.025	.100	2.70	.66	.200	LEIC77
1.00	.320	.410	1.68	.79	.190	2.42	
1.50	.63	1.86	6.6	.340	.096	9.1	
2.00	.87	4.40	14.2	.200	.061	19.4	
2.50	1.65	7.4	23.6	.220	.070	33.0	
3.00	-	-	-	-	-	42.7	BONG78
3.00	4.50	13.0	35.0	.350	.129	53	LEIC77
3.50	7.7	24.3	48.0	.320	.162	80	

REFERENCES

Aashamar O. and Kocbach L.
Journal of Physics B : Atomic and Molecular Physics Vol 10, No. 5 (1977) pp 869-879.

Aberg T. and Utiainen J.
Physical Review Letters Vol 22 (1969) pp 1346-1348.

Aberg T.
'Two-Photon Emission, the Radiative Auger Effect and the Double Auger Process' in 'Ionization and Transition Probabilities' Vol 1 of 'Atomic Inner-Shell Processes'. Edited by B. Grasemann, chapter 9, pp 353-357, Academic Press (1975).

Afrosimov V.V., Gordeev Y.S., Zinoviev A.N., Rasulov D.H., and Shergin A.P.
in 'Inner Shell Ionization Phenomena'. Edited by W. Mehlhorn and R. Brenn. Freiburg University (1976).

Ahlberg M., Johansson G., and Malmquist K.
Nuclear Instruments and Methods. Vol. 131 (1975) pp 377-379.

Ahlberg M.S. and Adams F.C.
X-Ray Spectrometry Vol. 7 (1978) pp 73-80.

Ahlen S.P.
Physical Review A Vol 17 (1978) pp 1236-1239.

Ahlen S.P.
Reviews of Modern Physics Vol 52 (1980) pp 121-173.

Ahlen S.P.
Physical Review A Vol 25 (1982) pp 1856-1867.

Adler K. Bohr A., Huss T., Mottleson B. and Winther A.
Reviews of Modern Physics Vol 28 (1956) pp 432-542.

Amundsen P.A. and Kocbach L.
Journal of Physics B : Atomic and Molecular Physics Vol 8 (1975) L122-L126.

Amundsen P.A., Kochbach L and Hansteen J.M.
Journal of Physics B : Atomic and Molecular Physics Vol 9 (1976) L203-L206 and Corrigendum p 2755.

Amundsen P.A. (a).
Journal of Physics B : Atomic and Molecular Physics Vol 10 (1977) pp 2177-2187.

Amundsen P.A. (b).
Journal of Physics B : Atomic and Molecular Physics Vol 10 (1977) pp 1097-1112.

Andersen H.H., Simonsen H and Sorensen H.
Nuclear Physics A Vol 125 (1969) pp 171-175.

Andersen H.H.
'Biblography and Index of Experimental Range and Stopping Power Data' Vol 2 of 'The Stopping and Ranges of Ions in Matter' Pergamon Press (1977).

Andersen H.H., and Ziegler J.F. (a)
'Hydrogen Stopping Powers and Ranges in All Elements' Vol 3 of 'The Stopping and Ranges of Ions in Matter'. Pergamon Press (1977).

Andersen H.H. and Ziegler J.F. (b).
'Helium Stopping Powers and Ranges in All Elements' Vol 4 of 'The Stopping and Ranges of Ions in Matter'. Pergamon Press (1977).

Andersen H.H., Bak J.F., Knudsen H., and Nielsen B.R.
Physical Review A Vol 16 (1977) pp 1929-1940.

Andersen H.H., Bottiger J. and Knudsen H. (Editors).
Proceeding of the IVth Internation Conference on Ion Beam Analysis held at Aarhus, June 25-29 (1979) Nuclear Instruments and Methods Vol 168 (1980).

Anholt R. and Saylor T.K.
Physics Letters Vol 56A (1976) pp 455-457.

Anholt R.
Physical Review A Vol 17 (1978) pp 983-997.

Anthony J.M. and Lanford W.A.
Nuclear Instruments and Methods Vol 186 (1981) pp 647-654.

Ashley J.C., Ritchie R.H., and Brandt W.
Physical Review B. Vol 5 (1972) pp 2392-2397.

Auger P.
Journal of Physics, Radium, Vol 6 (1925) p 205.

Avaldi L., Lozarno G. and Milazzo M.
Journal of Physics B.: Atomic and Molecular Physics Vol 15 (1982) L129-133.

Azaroff L. (editor).
'X-Ray Spectrometry' McGraw-Hill (1974).

Badica T., Ciortea C., Dima S., Petrovici A. and Popescu I.
X-Ray Spectrometry Vol 6 No 2 (1977) pp 90-93.

Badica T., Ciortea C., Petrovici A. and Popescu I.
X-Ray Spectrometry Vol 8, No 4 (1979) pp 186-189.

Bambynek W., Crasemann B., Fink R.W., Freund H.U., Mark H., Swift C.D., Price R.E. and Rao P.V.
Review of Modern Physics Vol 44 (1972) pp 716-813.

Bang J. and Hansteen J.M.
Kgl. Danske Videnskab. Selskab, Mat. Fys. Medd 31, No. 13 (1959).

Baragiola R.A., Alonso E.V. and Raiti H.J.L.
Physical Review A Vol 25 (1982) pp 1969-1976.

Barfoot K.M., Mitchell I.V., Eschbach H.L. and Gilboy W.B.
Nuclear Instruments and Methods Vol 168 (1980) pp 131-138.

Barkas W.H., Dyer N.J. and Heckman H.H.
Physical Review Letters Vol 11 (1963) pp 26-28.

Barros Leite C.V., de Castro Faria N.V., Horowicz R.J., Montenegro E.C. and de Pinho A.G.
Physical Review A Vol 25 (1982) pp 1880-1886.

Basbas G., Brandt W. and Lauberts R. (a).
Physical Review A Vol 7 (1973) pp 983-1001.

Basbas G., Brandt W. and Ritchie R.H.(b).
Physical Review A Vol 7 (1973) pp 1971-1976.

Basbas G. Brandt W. and Laubert R.
Physical Review A Vol 17 (1978) pp 1655-1674.

Bastasz R. and Felter T.E.
Physical Review B Vol 26 (1982) pp 3529-3533.

Bates D.R. and McDonough W.R.
Journal of Physics B : Atomic and Molecular Physics Vol 3 (1970) pp L83-L88.

Bates D.R. and McDonough W.R.
Journal of Physics B : Atomic and Molecular Physics Vol 5 (1972) pp L107-L109.

Bauer C., Mann R. and Rudolph W.
Zeitschrift fur Physik A Vol 287 (1978) pp 27-32.

Bell F., Trollmann G., Bockl H. and Betz H.D.
Journal of Physics B : Atomic and Molecular Physics Vol 15 (1982) pp 1487-1497.

Benka O. and Kropf A.
Atomic Data and Nuclear Data Tables Vol 22 (1978) pp 219-233.

Benka O. and Geretschlager M.
Journal of Physics B : Atomic and Molecular Physics Vol 13 (1980) pp 3223-3233.

Berezhko E.G. and Kabachnik N.M.
Journal of Physics B : Atomic and Molecular Physics Vol 10 (1977) pp 2467-2477.

Beriende A., Deberth C., Neamu I., Protop C., Scinte M., Zoran V., Dost M. and Rohl S.
Journal of Physics B : Atomic and Molecular Physics Vol 11 (1978) pp 2875-2887.

Berry A.A. and Lawrence J.L.
Acta Crystallography A Vol 35 (1979) pp 316-318.

Bethe H.
Annalen der Physik, Leipzig, 5th series, Vol 5 (1930) pp 325-400.

Bethe H.A. and Ashkin J.A.
'Experimental Nuclear Physics'. Edited by E segre Vol 1. John Wiley and Sons, New York (1953).

Bethe H.A. and Salpeter E.E.
'Quantum Mechanics of One and Two electron Atoms'. Springer-Verlag, Berlin (1957).

Bethe H.A. and Jackin R.W.
'Intermediate Quantum Mechanics' 2nd edition. Benjamin, New York (1968).

Bevington P.R.
'Data Reduction and Error Analysis for Physical Sciences'. McGraw Hill (1969).

Bhattacharya D., Bhattacherjee S.K. and Mitra S.K.
Journal of Physics B : Atomic and Molecular Physics Vol 13 (1980) pp 967-979.

Bhattacharya D., Roy A., Bhattacherjee S.K. and Mitra S.K.
Journal of Physics B : Atomic and Molecular Physics Vol 15 (1982) pp 769-777.

Bischsel H. and Saxon R.P.
Physical Review A Vol 11 (1975) pp 1286-1296

Bird J.R. and Clark G.L.
'Proceedings of the Fifth International Conference on Ion Beam Analysis', Sydney , Australia, February 16-20 (1981). Nuclear Instruments and Methods Vol 191 (1981).

Bloch F.
Annalen der Physik, Leipzig Vol 16 (1933) pp 285.

Bohr N.
Philosophical Magazine Vol 25 (1913) pp 10-31.

Bohr N.
Philosophical Magazine Vol 30 (1915) pp 581-612.

Bohr N.
Kgl. Dansk. Vidensk. Selsk. Mat. Fys. Medd 18, No8 (1948).

Bonderup E. and Hvelplund P.
Physical Review A Vol 4 (1971) pp 562-569.

Bonsen R.F.M. and Vriens L.
Physica Vol 47 (1970) pp 307-319.

Born M.
Zeitschrift fur Physik Vol 37 (1926) pp 863 and Vol 38 (1926) pp 803.

Bottiger and Bosson F.
Radiation Effects Vol 2 (1969) pp 105.

Brandt W., Laubert R. and Sellin I.
Physical Review Vol 151 (1966) pp 56-59.

Brandt W. and Lapicki G.
Physical Review A Vol 10 (1974) pp 474-483.

Brandt W.
'Atomic Collisions in Solids' edited by S. Datz, B.R. Appleton and C.D. Moak.
Plenum Press, New York, Vol 1 (1975) pp 261.

Brandt W. and Lapicki G.
Physical Review A Vol 20 (1979) pp 465-480.

Brandt W.
Nuclear Instruments and Methods Vol 191 (1981) pp 453-461.

Brandt W. and Lapicki G.
Physical Review A. Vol 23 (1981) pp 1717-1729.

Braziewicz J., Braziewicz E., Ploskonka J., Pajek M. and Osteynski.
'L-Shell X-Ray Production Cross Sections by ^{4}He Ions Bombardment'.
To be published in Journal of Physics B (1984).

Briggs J.S. and Pathak A.P.
Solid State Physics Vol 7 (1974) pp 1929.

Briggs J.S. and Taulbjerg K.
'Theory of Inelastic Atom-Atom Collisions' in 'Structure and Collisions of Ions and Atoms' Vol 5 of 'Topics in Current Physics' edited by I.A. Sellin. Springer-Verlag (1978) pp 105-153.

Buckingham R.A.
'Numerical Methods' Pitman and Sons Ltd (1962).

Burcham W.E.
'Nuclear Physics - an Introduction', 2nd edition. Longmann (1973).

Burhop E.H.S.
'The Auger Effect and Other Radiationless Transitions'. Cambridge University Press (1952).

Burhop E.H.S. and Asaad W.N.
Advances in Atomic and Molecular Physics Vol 8 (1972) pp 163-284.

Burhop E.H.S.
Advances in Atomic and Molecular Physics Vol 15 (1979) pp 329-380.

Busch C.E., Baskin A.B., Nettles P.H. Shafroth S.M. and Waltner A.W.
Physical Review A Vol 7 (1973) pp 1601-1606.

Button T.M., Rice R.K., Duggan J.L. and McDaniel F.D.
Transactions in Nuclear Science Vol 26, No 2, part 2 (1979) pp 1150-1153.

Campbell J.L. and Jorch H.H.
Nuclear Instruments and Methods Vol 159 (1979) pp 163-170.

Chang C.N., Morgan J.F. and Blatt S.L.
Physical Review A Vol 11 (1975) pp 607-618.

Chattarji D.
'The Theory of Auger Transitions' Academic Press (1976).

Chaturvedi R.P., Wheeler R.M., Liebert R.B., Miljanic D.J., Zabel T and Phillips G.C.
Physical Review A Vol 12 (1975) pp 52-56

Chen J.R.
Nuclear Instruments and Methods Vol 142 (1977) pp 9-19.

Chen M.H., Crasemann B. and Mark H.
Physical Review A Vol 26 (1982) pp 1243-1251.

Chevallier P., Tavernier M. and Briand J.P.
Journal of Physics B : Atomic and Molecular Physics Vol 11 (1978) pp L171-L174.

Chevarier A., Chevarier N. and Chiodelli S.
Nuclear Instruments and Methods Vol 189 (1981) pp 525-531.

Choi B.H.
Physical Review A Vol 4 (1971) pp 1002-1008.

Choi B.H., Mercbacher E. and Khandelwal G.S.
Atomic Data Vol 5 (1973) pp 291-304.

Chu W.K. and Powers D.
Physics Letters Vol 40A (1972) pp 23-24.

Chu W.K.
'New Uses of Ion Accelerators' edited by J. Ziegler. Plenum Press (1975) pp 135-158.

Chu W.K.
Physical Review A Vol 13 (1976) pp 2057-2060.

Chu W.K., Mayer J.W. and Nicolet M.A.
'Backscattering Spectrometry'. Academic Press (1978).

Chu T.C., Ishii K., Yamadera A., Sebata M. and Morita S.
Physical Review A Vol 24 (1981) pp 1720-1725.

Cipolla S.J. and Hewitt M.T.
Nuclear Instruments and Methods Vol 136 (1976) pp 347-348.

Cleff B.
Acta Physica Polonica Vol A61 (1982) pp 285-319.

Cohen D.D.
Journal of Physics B : Atomic and Molecular Physics Vol 13 (1980 pp 2953-2964.

Cohen D.D.
Nuclear Instruments and Methods Vol 191 (1981) pp 551-557.

Cohen D.D.
Nuclear Instruments and Methods Vol 193 (1982) pp 15-19.

Cohen D.D.
Nuclear Instruments and Methods Vol 218 (1983) pp 795-798.

Compton A.H.
Physical Review Vol 21 (1923) pp 207 and pp 483-502.

Cooper J.W. and La Villa R.E.
Physical Review Letters Vol 25 (1970) pp 1745-1748.

Cooper M.
Advances in Physics Vol 20 (1971) pp 453-491.

Coster D. and Kronig R. De L.
Physica Vol 2 (1935) pp 13-24.

Cuevas J., Garcia-Munoz M., Torres P. and Allisons K.
Physical Review Vol 135 (1964) pp A335-A345.

Datz., Duggan J.L., Feldmann L.C., Laegsgaard E. and Andersen J.U.
Physical Review A Vol 9 (1974) pp 192-196.

Datz S.,
'Atomic Collisions in Solids' in 'Structure and Collisions of Ions and Atoms' edited by I.A. Sellin Vol 5 of 'Topics in Current Physics'. Springer-Verlag (1978) pp 309-345.

Davisson C.M.
'Interaction of γ-Radiation with Matter in Alpha-, Beta- And Gamma -Ray Spectroscopy' Vol 1 edited by K. Siegbahn. North-Holland Publishing Company (1965) pp 37-78.

Desclaux J.P.
Contemporary Physics Communcations Vol 9 (1975) pp 31.

Dias M.S. and Renner C.
Nuclear Instruments and Methods Vol 193 (1982) pp 91-93.

Doyle B.L. and Shafroth S.M.
Physical Review A Vol 19 (1979) pp 1433-1438.

Draper N. and Smith H.
'Applied Regression Analysis' 2nd edition. John Wiley and Sons, Inc. (1981).

Dyall K.G., and Larkins F.P.
Journal of Physics B : Atomic and Molecular Physics Vol 15 (1982) pp 1811-1829.

Dyson N.A.
'X-rays in Atomic and Nuclear Physics'.
Longmanns (1973).

Fano U.
Annual Review of Nuclear Science Vol 13 (1963) pp 1-66.

Foldy L.L.
Physical Review Vol 83 (1951) pp 397-399.

Folkmann F,, Gaarde C., Huss T. and Kemp K. (a)
Nuclear Instruments and Methods Vol 116 (1974) pp 487-499.

Folkmann F., Borggreen J. and Kjeldgaarde A. (b)
Nuclear Instruments and Methods Vol 119 (1974) pp 117-123.

Folkmann F.
Journal of Physics E : Scientific Instruments Vol 8 (1975) pp 429-444.

Folkmann F.
'Ion Beam Surface Layer Analysis' edited by O. Meyer, G. Linter and F. Kappeler. Plenum Press (1976) pp 695-718.

Forster J.S., Ward D., Andew H.R., Ball G.C., Costa G.J., Davis W.G. and Mitchell I.V.
Nuclear Instruments and Methods Vol 136 (1976) pp 349-359.

Foti G., Mayer J.W. and Rimini E.
'Backscattering Spectrometry' in 'Ion Beam Handbook for Material Analysis' edited by J.W. Mayer and E. Rimini. Academic Press (1977) pp 21-65.

Frame J.W.
Proceedings of the Cambridge Philisophical Society Vol 27 (1931) pp 511.

Friedland E.
Nuclear Instruments and Methods Vol 150 (1978) pp 301-304.

Friedland E. and Kotze C.P.
Nuclear Instruments and Methods Vol 191 (1981) pp 490-494.

Fukunda A.
Journal of Physics B : Atomic and Molecular Physics Vol 14 (1981) pp 4533-4544.

Gallagher W.J. and Gipolla S.J.
Nuclear Instruments and Methods Vol 122 (1974) pp 405-414

Garcia J.D., Gerjuoy E. and Welker J.E.
Physical Review Vol 165 (1968) pp 66-72.

Garcia J.D.(a).
Physical Review A Vol 1 (1970) pp 280-285.

Garcia J.D. (b).
Physical Review A Vol 1 (1970) pp 1402-1403

Garcia J.D., Fortrier R.J. and Kavanagh T.M.
Review of Modern Physics Vol 45 (1973) pp 111-177.

Gardner R.K. and Gray T.J.
Atomic Data and Nuclear Data Tables Vol 21 (1978(pp 515-536

Garibyan G.M.
Soviet Physics JETP, Vol 6(33), No 6 (1958) 1079-1085.

Gedcke D.A.
X-Ray Spectrometry Vol 1 (1972) pp 129-141.

Geiger H. and Marsden E.
Philosophical Magazine Vol 25 (1913) pp 604-623.

Gerald C.F.
'Applied Numerical Analysis' 2nd edition. Addison-Wesley Co (1978).

Geryuoy E.
Physical Review Vol 148 (1966) pp 54-59.

Gertner I., Merson M. and Rosner B.
Physical Review A Vol 21 (1980) pp 1191-1196.

Gerward L.
'Analytical Approximations for X-ray Attenuation Coefficients in the 5 to 25 and the 5 to 100 keV range' LTF III - Report No 27. The Technical Univesirty of Denmark, Lyngby (1980).

Gibb A., McKee J.S.S. and Wilk S.E.J.
Journal of Physics D : Applied Physics Vol 10 (1977) pp L203-L205.

Ginsburg V.L. and Frank I.M.
Zh. EKsp. Teor, Fiz. Vol 16 (1946) pp 15.

Gray T.J.
'Studies of L-Shell X-Ray Production for Fast Ions on Elements with $Z \geq 58$' in 'The Uses of Small Accelerators in Research and Teaching edited by J.L. Duggan and I.L. Morgan. Vol 1 (1974).

Gray T.J., Light G.M., Gardner R.K. and McDaniel F.D.
Physical Review A Vol 12 (1975) pp 2393-2398.

Greenburg J.S., Davis C.K. and Vincent P.
Physical Review Letters Vol 33 (1974) pp 473-476.

Gryzinski M.
Physical Review Vol 138 (1965) A305-A321, A322-A335 and A336-A358.

Gunnink R. and Niday J.B.
'Computerised Quantitative Analysis by Gamma-Ray Spectrometry' Vol 1 Lawrence Livermore Laboratory, California March 1 (1971).

Gunnink R.
Lawrence Livermore Laboratory, California, Report UCRL-74618 (1975).

Gyulai J.
Acta Physica Academiae Scientiarum Hungaricae, Tomus 49 (1980) pp 55-66.

Gyulai J.
'Rutherford Backscatteirng Spectrometry', Hugarian Academy of Science, Budapest, Central Research Institute for Physics, Report No KFKI - 1981-08, (1981)

Hall H.
Reviews of Modern Physics Vol 8 (1936) pp 358-397.

Hansen J.S.
Physical Review A Vol 8 (1973) pp 822-839.

Hansen J.S., McGeorge J.C., Nix D., Schmitt-Ott W.D., Unus I. and Fink R.W.
Nuclear Instruments and Methods Vol 106 (1973) pp 365-379.

Hansteen J.M. and Mosebekk O.P.
Zeitschrift fur Physik Vol 234 (1970) pp 281-292.

Hansteen J.M. and Mosebekk O.P.
Nuclear Physics A Vol 201 (1973) pp 541-560.

Hansteen J.M.
Advances in Atomic and Molecular Physics Vol 11 (1975) pp 299-329.

Hansteen J.M., Johnsen O.M. and Kocbach L.
Atomic Data and Nuclear Data Tables Vol 15 (1975) pp 305-317.

Hardt T.L. and Watson R.L.
Physical Review A Vol 7 (1973) pp 1917-1927.

Harris J.M. and Nicolet M.A.
Physical Review B Vol 11 (1975) pp 1013-1019 and Journal of Vaccum Science and Technology Vol 12 (1975) pp 439-443.

Hautala M. and Luomajarvi M.
Radiation Effects Vol. 45 (1980) pp 159-162.

Hawkes D.J. and Jackson D.F.
Physics in Medicine and Biology Vol 25 (1980) pp 1167-1171.

Henneberg W.
Zeitschrift fur Physik Vol 86 (1933) pp 592-604.

Hill K.W. and Merzbacher E.
Physical Review A Vol 9 (1974) pp 156.

Himmelblau D.M.
'Applied Nonlinear Programming' McGraw Hill and Co (1972).

Holmen G., Svensson B., Schou J. and Sigmund P.
Physical Review B Vol 20 (1979) pp 2247-2254.

Honl H.
Zeitschrift fur Physik Vol 84 (1933) pp1.

Hubbell J.H.
'Photon Cross Sections, Attenuation Coefficients and Energy Absorption Coefficients From 10keV to 100GeV'. National Standard Reference Data System, National Bureau of Standards 29, (1969) U.S. Department of Commerce.

Hubbell J.H.
Atomic Data Vol 3 (1971) pp 241-297.

Hubbell J.H., McMaster W.H., Kev Del Grande N. and Mallet I.H.
International Tables for X-ray Crystallography. Kynock Press, Birmingham Vol 4 (1974) pp 47.

Hubbell J.H., Veigele Wm.J., Briggs E.A., Brown R.T., Cromer D.T. and Howerton R.J.
Journal of Physical and Chemical Reference Data Vol 4 (1975) pp 471-538 and Errata Vol 6 (1977) pp 615.

Hubbell J.H. and Veigele Wm.J.
'Comparison of Theoretical and Experimental Photoeffect Data 0.1 keV to 1.5 keV'. National Bureau of Standards Technical Note 901 (1976) 43pp. U.S. Deparment of Commerce.

Hubbell J.H.(a)
Radiation Research Vol 70 (1977) pp 58-81.

Hubbell J.H.(b)
'Present Status of Photon Cross Section Data 100eV to 100Gev'. National Bureau of Standards (U.S.) Special Publication 461 (1977) pp 3-16.

Hubbell J.H.
International Journal of Applied Radiation and Isotopes Vol 33 (1982) pp 1269-1290.

Huda W.
Nuclear Instruments and Methods Vol 158 (1979) pp 587-594.

Huus J., Bjerregaarg J.H. and Elbek B.
Kgl.Dan.Vidensk.Selsk.Mat.Fys.Medd 30. No. 17 (1956).

Ingamells C.O. and Fox J.J.
X-Ray Spectrometry Vol 8 (1979) pp 79-84.

Inokuti M.
Reviews of Modern Physics Vol 43 (1971) pp 297-347.

Inokuti M., Dehmer J.L., Baer T and Hanson J.D.
Physical Review A Vol 23 (1981) pp 95.

Ishii K., Morita S. and Tawara H.
Physical Review A Vol 13 (1976) pp 131-138.

Jackson J.D.
Classical Electrodynamics. Second edition, John Wiley and Sons Inc (1975).

Jackson J.D. and McCarthy R.L.
Physical Review B Vol 6 (1972) pp 4131-4141.

Jackson D.F. and Hawkes D.J.
Physics Reports Vol 70 (1981) pp 169.

Jakubassa D.H. and Kleber M.
Zeitschrift fur Physik A Vol 273 (1975) pp 29-35.

Jamison K.A. and Richards P.
Physical Review Letters Vol 38 (1977) pp 484-487.

Jamnik D. and Zupancic C.
Kgl. Dansk. Vidensk. Selsk. Mat. Fys. Medd 31 No 2 (1957).

Jauncey G.E.M.
Physical Review Vol 25 (1925) pp 314-321 and pp 723-736.

Jenkins R., Gould R.W. and Gedcke D.
'Qualitative X-Ray Spectrometry'. Marcel Dekker Inc (1981).

Jitschin W., Kleinpoppen H., Hippler R. and Lutz H.O.
Journal of Physics B : Atomic and Molecular Physics Vol 21 (1979) pp 4077-4084.

Jitschin W., Kaschuba A., Kleinpoppen H. and Lutz H.O. (a)
Zeitschrift fur Physik A Vol 304 (1982) pp 69-73.

Jitschin W., Kaschuba A., Hippler R. and Lutz H.O.
Journal of Physics B : Atomic and Molecular Physics Vol 15 (1982) pp 763-768.

Johansson S.A.E. (editor)
'Proceedings of the 2nd International Conference on PIXE and its Analytical Applications'. Lund, Sweden, June 9-12, 1980. Nuclear Instruments and Methods Vol 181 (1981).

Johansson S.A.E. and Johansson T.B.
Nuclear Instruments and Methods Vol 137 (1976) pp 473-516.

Johnson G.A., Manson E.L., O'Foghludha J.R. and O'Foghludha F.
Nuclear Instruments and Methods Vol 151 (1978) pp 217-220.

Johnson D.E., Basbas G. and McDaniel F.D.
Atomic Data and Nuclear Data Tables Vol 24 (1979) pp 1-11.

Jorch H.H. and Campbell J.L.
Nuclear Instruments and Methods Vol 143 (1977 pp 551-559.

Justiniano E.L.B., Nader A.A.G., de Castro Faria N.V., Barros Leite C.V. and de Pinho A.G.
Physical Review A Vol 21 (1980) pp 73-78.

Kaji H., Shiokawa T. Ishii K., Morita S., Kamiya M., Sera K. and Tawara H.
Nuclear Instruments and Methods Vol 142 (1977) pp 21-26.

Kamiya M., Kinefuchi Y., Endo H., Kuwako A., Ishii K and Morita S.
Physical Review A Vol 20 (1979) pp 1820-1827.

Karttunen E., Freund H.U. and Fink R.W.
Physical Review A Vol 4 (1971) pp 1695-1705.

Keski-Rahkonen O. and Krause M.O.
Atomic Data and Nuclear Data Tables Vol 14 (1974) pp 139-146.

Khan M.R.
'Proton Induced X-Ray Analysis' Ph.D. thesis, University of Aston, England (1975) (unpublished).

Khan M.R., Hopkins A.G., Crumpton D. and Francois P.E.
X-Ray Spectrometry Vol 6 (1977) pp 140-143.

Khan M.R. and Crumpton D.
Applied Physics Vol 15 (1978) pp 335-339.

Khan M.R., Hopkins A.G. and Crumpton D.
Zeitschrift fur Physik A Vol 288 (1978) pp 133-137.

Khan M.R., Lodhi A.S. and Crumpton D.
Nuclear Instruments and Methods Vol 160 (1979) pp 127-129.

Khan M.R. and Crumpton D.
Critical Reviews in Analytical Chemistry Vol 11 (1981) pp 103-155 and Vol 12 (1981) pp 161-193.

Khandelwal G.S., Choi B.H. and Merzbacher E.
Atomic Data Vol 1 (1969) pp 103.

Kienle P. Kleber M., Povh B., Diamond R.M., Stephens F.S., Grosse E., Maier M.R. and Proetef D.
Physical Review Letters Vol 31 (1973) pp 1099-1102.

Kleber M. and Jakubassa D.H.
Nuclear Physics A Vol 252 (1975) pp 152.

Klein O. and Nishina Y.
Zeitschrift fur Physik Vol 52 (1929) pp 852-868.

Knoll G.F.
'Radiation Detection and Measurements'. John Wiley and Sons (1979).

Knudsen A.R., Burkhatter P.G. and Nagel D.J.
'Proceedings of the International Conference on Inner-Shell Ionisation Phenomena and future Applications'. Atlanta, 17-22 April 1972. U.S. Atomic Energy Commission Conference number - 72 0404. OakRidge, U.S.A. (1973).

Kocbach L., Hansteen J.M. and Gundersen R.
Nuclear Instruments and Methods Vol 169 (1980) pp 281-291.

Kodre A., Hribar M., Ajlec B. and Pahor J.
Zeitschrift fur Physic A Vol 303 (1981) pp 23-26.

Kojima H., Kobayashi N., Maeda N. and Sakisaka M.
Journal of the Physical Society of Japan Vol 46 (1979) pp 198-204.

Koopmans T.
Physica Vol 1 (1933) pp 104-113.

Kostrom V.O., Chen M.H. and Craseman B.
Physical Review A Vol 3 (1971) pp 533-545.

Kraft G., Mokler P.H. and Stein H.J.
Physical Review Letters Vol 33 (1974) pp 476-479.

Krause M.O.
Journal of Physical and Chemical Reference Data Vol 8 (1979) pp 307-327.

Kreussler S., Varelas C. and Brandt W.
Physical Review B Col 23 (1981) pp 82-84.

Land D.J., Simons D.G., Brennon J.G. and Brown M.D.
Physical Review A Vol 22 (1980) pp 68-75.

Landau L.D.
Journal of Physics Vol 8 (1944) pp 201.

Landau L.D. and Lifshitz E.M.
'Mechanics and Electrodynamics' Vol 1 of 'A Short Course of Theoretical Physics'. Pergamon Press (1972) pp 248-276.

Landau L.D. and Lfshitz E.M.
'Quantum Mechanics (Non-Relativistic Theory)', 3rd edition. Pergamon Press (1977).

Langenberg A. and Van Eck J.
Journal of Physics B : Atomic and Molecular Physics Vol 11 (1978) pp 1425-1434.

Lapicki G. and Losonsky W.
Physical Review A Vol 20 (1979) pp 481-490.

Lapp R. and Andrew H.L.
'Nuclear Radiation Physics', 4th edition. Prentice - Hall Inc (1972).

Lawrence J.R.
Acta Crystallographica A Vol 35 (1979) pp 845-848.

L'Ecuyer J., Davis J.A. and Matsunami N.
Nuclear Instruments and Methods Vol 160 (1979) pp 337-346.

Leite B.C.V., de Castro Faria N.V. and de Pinho A.G.
Physical Review A Vol 15 (1977) pp 943-955.

Lewis H.W.
Physical Review Vol 85 (1952) pp 20-24.

Lindhard J. and Scharaff M.
Kgl. Dansk. Vid. Selsk. Mat. Fys Medd 27 No 15 (1953).

Lindhard J. and Scharff M.
Physical Review Vol 124 (1961) pp 128-130.

Lindhard J.
Nuclear Instruments and Methods Vol 132 (1976) pp 1-5.

Livingston M.S. and Bethe H.
Reviews of Modern Physics Vol 9 (1937) pp 245-390.

Lopes J.S., Jesus A.P. and Ramos S.C.
Nuclear Instruments and Methods Vol 169 (1980) pp 311-317.

Madden R.P.
'Synchrotron Radiation and Applications' in 'X-Ray Spectroscopy' edited by L.V. Azaroff. McGraw Hill Book Co (1974) pp 338-378.

Madison D.H., Baskin A.B., Busch C.E. and Shafroth S.M.
Physical Review A Vol 9 (1974) pp 675-581.

Madison D.H. and Merzbacher E.
'Theory of Charged - Particle Excitation' in 'Ionisation and Transition Probabilities' Vol I of 'Atomic Inner-Shell Processes' edited by B. Crasemann. Academic Press (1975) pp 1-72.

Madison D.H.
'Inner Shell Ionisation By Simple Charged-Particles'. 'Proceedings of the Second International Conference on Inner-Shell Ionisation Phenomena', Freiburg. Edited by W. Mehlhorn and R. Brenn, (1976) pp 321-338.

Magno C., Milazzo M., Pizzi C., Porro F., Rota A. and Riccobono G.
Il Nuovo Gimento Vol 54A No 3 (1979) pp 277-304.

Malherbe J.B. and Alberts H.W.
Nuclear Instruments and Methods Vol 196 (1982) pp 499-503.

Mann A. and Brandt W.
Physical Review B Vol 24 (1981) pp 4999-5003.

Manson S.T. and Kennedy D.J.
Atomic Data and Nuclear Data Tables Vol 14 (1974) pp 111-120.

Marquardt D.W., Bennett R.G. and Burrell E.J.
Journal of Molecular Spectroscopy Vol 7 (1961) pp 269-279.

Marquardt D.W.
Journal of the Society of Industrial and Applied Mathematics Vol 11 No 2 (1963) pp431-441.

Mayer J.W. and Ziegler J.F.
'International Conference on Ion Beam Surface Layer Analysis'. IBM Research Laboratories June 18-20, 1973. Thin Solid Films (1973).

McDaniel F.D.
Nuclear Instruments and Methods Vol 214 (1983) pp 57-63.

McGuire E.J.
Physical Review A Vol 2 (1970) pp 273-278.

McGuire E.J.
Physical Review A Vol 3 (1971) pp 587-594.

McGuire E.J.
Physical Review A Vol 5 (1972) pp 1043-1047.

McGuire E.J.
'Auger and Coster-Kronig Transitions' in 'Ionisation and Transition Probabilities' Vol I of Atomic Inner-Shell Processes'.Edited by B. Crasemann, Academic Press (1975) pp 293-330.

McGuire J.H. and Richard P.
Physical Review A Vol 8 (1973) pp 1374-1384.

McGuire J.H. and Macdonald J.R.
Physical Review A Vol 11 (1975) pp 146-148.

McKnight R.H., Thornton S.T. and Karlowicz R.R.
Nuclear Instruments and Methods Vol 123 (1975) pp 1-4 .

McNelles L.A. and Campbell J.L.
Nuclear Instruments and Methods Vol 127 (1975) pp 73-81.

Mehlhorn W.
Physics Letters Vol 26A (1968) pp 166-167.

Merzbacher E. and Lewis H.W.
'X-Ray Production by Heavy Charged Particles'. Handbuch der Physik, edited by S. Flugge. Springer-Berlin Vol 34 (1958) pp 166-192.

Merzbacher E.
'Quantum Mechanics' second edition. John Wiley and Sons Inc (1970).

MicroMatter and Co
R.T.1 Box 72B, Eastsound, Seattle, WA, U.S.A. 98245.

Millar R.H. and Greening J.R. (a)
Journal of Physica B : Atomic and Molecular Physics Vol 7 (1974) pp 2332-2344.

Millar R.H. and Greening J.R. (b)
Journal of Physics B : Atomic and Molecular Physics Vol 7 (1974) pp 2345.

Mingay D.W. and Barnad E.
Nuclear Instruments and Methods Vol 157 (1978) pp 537-544.

Mokler P.H. and Folkmann F.
'X-Ray Production in Heavy Ion-Atom Collisions' in 'Structure and Collisions of Ions and Atoms' Vol 5 of 'Topics in Current Physics'. Edited by I.A. Sellin Springer-Verlag (1978) pp 201-271.

Montenegro E., Baptista G.B. and Duarte P.W.E.P.
Atomic Data and Nuclear Data Tables Vol 22 (1978) pp 131-177.

Montenegro E.C. and de Pinho A.G. (a)
Journal of Physics B : Atomic and Molecular Physics Vol 51 (1982) L1275-1279.

Montengro E.C. and de Pinho A.G. (b)
Journal of Physics B : Atomic and Molecular Physics Vol 15 (1982) pp 1521-1532.

Morgan S.H. and Eby P.B.
Nuclear Instruments and Methods Vol 106 (1973) pp 429-435.

Mott N.F.
Proceedings of the Cambridge Philosophical Society Vol 27 (1931) pp 553.

Mott N.F. and Massey H.S.W.
'The Theory of Atomic Collisions'. Oxford (1965).

Mukoyama T. and Sarkadi L.
Nuclear Instruments and Methods Vol 190 (1981) pp 619-626.

Mukoyama T. and Sarkadi L. (a).
Physical Review A Vol 25 (1982) pp 1411-1419.

Mukoyama T. and Sarkadi L.(b).
Journal of Physics B : Atomic and Molecular Physics Vol 15 (1982) L617-L621.

Mukoyama T. and Sarkardi L.(a).
Nuclear Instruments and Methods Vol 205 (1983) pp 341-346.

Mukoyama T. and Sarkadi L. (b)
Nuclear Instruments and Methods Vol 211 (1983) pp 525-528.

Muller P. and Ischenko G.
Journal of Applied Physics Vol 47 (1976) pp 2811-2820.

Nagel D.J. and Baun W.L.
'Bonding Effects in X-Ray Spectra' in 'X-Ray Spectroscopy' edited by L.V. Azaroff. McGraw Hill Book Co. (1974) pp 445-532.

Northcliffe L.C.
Annual Review of Nuclear Science Vol 13 (1963) pp 67-102.

Ogier W.T., Carlson R.D. and Knoche J.
Physical Review Vol 142 (1966) pp 50-52.

Palinkas J. and Schlenk B.
Nuclear Instruments and Methods Vol 169 (1980) pp 493-498.

Palinkas J., Sarkadi L. and Schlenk B.
Journal of Physics B : Atomic and Molecular Physics Vol 13 (1980) pp 3829-3834.

Palinkas J., Schlenk B. and Valek A.
Journal of Physics B : Atomic and Molecular Physics Vol 14 (1981) pp 1157-1159.

Papper C.S., Chaudhri M.A. and Rouse J.L.
Nuclear Instruments and Methods Vol 154 (1978) pp 219-221.

Park D.
'Introduction to The Quantum Theory' second edition. McGraw Hill Kogakusha Ltd (1974) pp 373-402.

Parratt L.G.
Reviews of Modern Physics Vol 31 (1959) pp 616-645.

Pattison P. and Weyrich W.
Journal of Physics and Chemistry Solids Vol 40 (1979) pp 213-222.

Pattison P., Hansen N.K. and Schneider J.R.
Zeitschrift fur Physik B Vol 46 (1982) pp 285-294.

Paul H.
Nuclear Instruments and Methods Vol 169 (1980) pp 249-258.

Paul H.
Nuclear Instruments and Methods Vol 192 (1982) pp 11-24.

Pauli M., Rosel F. and Trautmann D.
Physics Letters Vol 67A (1978) pp 28.

Petersson S., Tove P.A., Meyer O., Sundqvist B. and Johansson A.
Thin Solid Films Vol 19 (1973) pp 157-164.

Phillips G.W. and Marlow K.W.
Nuclear Instruments and Methods Vol 137 (1976) pp 525-536.

Pietsch W., Hauser U. and Neuwrith W.
Nuclear Instruments and Methods Vol 132 (1976) pp 79-87.

de Pinho A.G.
Private communication

Porter L.E. and Bryan S.R.
Nuclear Instruments and Methods Vol 178 (1980) pp 227-231.

Pratt R.H., Levee R.D., Pexton R.L. and Avon W.
Physical Review A Vol 134 (1964) pp 898-915.

Pratt R.H., Ron A. and Tseng H.K.
Reviews of Modern Physics Vol 45 (1973) pp 273-325.

Radiation Dynamics, Inc.
Technical Proposal for Dynamitron Accelerator Model RPEA 3.0.
Prepared for the University of Birmingham, RD1 No 65-11-1-155 (1967).

Raghava Rao A., Ramana Reddy S.V.S., Premchand K. Narasimham K.L.,
Parthasaradhi K. and Lakshminarayana V.
Pramana Vol 18 (1982) pp 271-278.

Rakavy G. and Ron A.
Physical Review Vol 159 (1967) pp 50-56.

Ramsay W.D. and McKee J.S.C.
Journal of Physics B : Atomic and Molecular Physics Vol 11 (1978)
pp L313-L315.

Rao P.V.
'Inner-Shell Transition Measurements with Radioactive Atoms' in
'Experimental Approaches and Application' Vol II of 'Atomic Inner-Shell Processes' edited by B. Crasemann (1975) pp 1-32.

Read F.H.
'Electromagnetic Radiation' John Wiley and Sons (1980).

Reinhardt J., Soff G. and Greiner W.
Zeitschrift fur Physik A Vol 276 (1976) pp 285-293.

Renan M.J.
X-Ray Spectrometry Vol 9 (1980) pp 90-94.

Rice R., Basbas G. and McDaniel F.D.
Atomic Data and Nuclear Data Tables Vol 20 (1977) pp 503-511.

Richard P.
'Ion-Atom Collisions' in 'Ionisation and Transtion Probabilities'
Vol I of 'Atomic Inner-Shell Processes' edited by B. Crasemann.
Academic Press (1975) pp 73-158.

Rindby A., Selin E., Berggren K.F. and Ribberfors R.
Nuclear Instruments and Methods Vol 196 (1982) pp 569-571.

Rooke G.A.
'Theory of Emission Spectra' in 'X-Ray Spectroscopy' edited by
L.V. Azaroff. McGraw Hill, Inc (1974) pp 173-225.

Rose. M.E. and Welton T.A.
Physical Review Vol 86 (1952) pp 432-433.

Rosel F., Trautmann D. and Baur G.
Zeitschrift fur Physik A Vol 304 (1982) pp 75-78.

Routti J.T. and Prussin S.G.
Nuclear Instruments and Methods Vol 72 (1969) pp 125-142.

Rutherford E.
Philosophical Magazine Vol 21 (1911) pp 669-688.

Saied S.O.
'The Development of a Proton Induced X-Ray Emission System for
Biomedical Analysis'. Ph.D thesis, Unviersity of Aston in Birmingham,
England (1981) (unpublished).

Salamon M.H., Ahlen S.P., Tarle G. and Crebbin K.C.
Physical Review A Vol 23 (1981) pp 73-76.

Salem S.I. and Leo P.L.
Physical Review A Vol 10 (1974) pp 2033-2036.

Salem S.I., Panossian S.L. and Krause R.A.
Atomic Data and Nuclear Data Tables Vol 14 (1974) pp 91-109.

Santry D.C. and Werner R.D.
Nuclear Instruments and Methods Vol 188 (1981) pp 211-216.

Saris F.W., Van der Weg W.F., Tawara H. and Laubert R.
Physical Review Letters Vol 28 (1972) pp 717-720.

Saris F.W. and Van der Weg W.F.
'Proceedings of the VIth International Conference on Atomic Collisions
in Solids', Amsterdam, September 22-26, 1975. Nuclear Instruments
and Methods Vol 132 (1976).

Sarkadi L. and Mukoyama T.
Journal of Physics B : Atomic and Molecular Physics Vol 14 (1981) pp L255 - L260.

Sarkadi L.
Nuclear Instruments and Methods Vol 214 (1983) pp 43-48.

Sarma K.S.R., Narasimhan K.L., Premchand K., Bhuloka Reddy S., Parthasaradhi K. and Lakshminarayana V.
Pramana Vol 18 (1982) pp 485-494.

Schamber F.H.
'Curve Fitting Techniques and the Application to the Analysis of Energy Dispersive Spectra'. 'Proceedings of the Workshop on Energy Dispersive X-Ray Spectrometry' held at NBS, Gaithersburg, Maryland, 23-25 April (1979). NBS special publication 604, Issued March 1981 pp 192-231.

Schiff L.I.
'Quantum Mechanics' 3rd edition. McGraw Hill Kogakusha (1968).

Schmidt W., Muller P., Bruckner V., Loffler F., Saemann-Ischenko G. and Schubert W.
Physical Review A Vol 24 (1981) pp 2420-2424.

Scheider D. and Stotterfoht N.
Physical Review A Vol 24 (1981) pp 2438-2444.

Schnopper H.W., Betz H.D., Dalvaille J.P., Kalata K., Sohval A.R., Jones K.W. and Wegner H.E.
Physical Review Letters Vol 29 (1972) pp 898.

Schnopper W., Delvaille J.F., Kalata K., Sohval A.R., Abdulwahab M., Jones K.W. and Wegner H.E.
Physics Letters Vol 47A (1974) pp 61-62.

Schulz F. and Brandt W.
Bulletine of American Physical Society Vol 26 (1981) pp 602.

Scofield J.H. (a).
Physical Review A Vol 10 (1974) pp 1507-1510 and Errata Physical Review A Vol 12 (1975) pp 345.

Scofield J.H. (b).
Atomic Data and Nuclear Data Tables Vol 14 (1974) pp 121-137.

Scofield J.H.
'Radiative Transitions' in 'Ionisation and Transition Probabilities' Vol I of 'Atomic and Inner-Shell Processes' edited by B. Crasemann Academic Press (1975) pp 265-292.

Segre E.
'Experimental Nuclear Physics'. John Wiley and Sons (1953).

Shabason L., Cohen B.1., Wedberg G.H. and Chan K.C.
Journal of Applied Physics Vol 44 (1973) pp 4749-4752.

Shima K., Makino I. and Sakisaka M.
Journal of Physical Society of Japan Vol 30 (1971) pp 611.

Shima K.
Nuclear Instruments and Methods Vol 165 (1979) pp 21-26.

Simons D.G., Crowe C.R. and Brown M.D.
Journal of Applied Physics Vol 53 (1982) pp 3900-3902.

Slater J.C.
Physical Review Vol 36 (1930) pp 57-64.

Sofield C.J., Cowern N.E.B. and Freeman J.M.
Nuclear Instruments and Methods Vol 191 (1981) pp 462-468.

Sohval A.R., Delvaille J.P., Kalata K. Kirby-Docken K. and Schnopper H.W.
Journal of Physics B ; Atomic and Molecular Physics Vol 9 (1976) pp L25-L29.

Sokhi R.S. and Crumpton D.
Nuclear Instruments and Methods Vol 181 (1981) pp 5-9.

Sokhi R.S. and Crumpton D.
Nuclear Instruments and Methods Vol 192 (1982) pp 121-127.

Sokhi R.S. and Crumpton D.
Atomic Data and Nuclear Data Tables Vol 30 (1984) pp 49-124.

Sorensen H. and Andersen H.H.
Physical Review B Vol 8 (1973) pp 1854-1863.

Spindler E., Betz H.D. and Bell F.
Journal of Physics B : Atomic and Molecular Physics Vol 10 (1977) pp L561-L564.

Sternglass E.J.
Physical Review Vol 108 (1957) pp 1-12.

Stoller C., Wolfli W., Bonani G., Stockli M. and Suter M.
Physical Review A Vol 15 (1977) pp 990

Stoller Ch, Anholt R. and Meyerhof W.E.
Zeitschrift fur Physik A Vol 302 (1981) pp 95-102.

Stolterfoht N.
'Excitation in Energetic Ion-Atom Collisions Accompanied by Electron Emission' in 'Structure and Collisions of Ions and Atoms' edited by I.A. Sellin. Springer-Verlag (1978) pp 155-199,

Stoquert J.P., Oberlin J.C., Heitz C., Cailleret J. and Lagarde G. (a).
Nuclear Instruments and Methods Vol 188 (1981) pp 249-251.

Stoquert J.P., Amokrane A., Beaumevielle H. and Oberlin J.C. (b).
Nuclear Instruments and Methods Vol 179 (1981) pp 343-347.

Storm E. and Israel H.I.
Nuclear Data Tables A Vol 7 (1970) pp 565-681.

Sullins R.T., Barros Leite C.V. and Schweikert E.A.
IEEE Transitions in Nuclear Science Vol N528 No 2 (1981)
pp 1831-1833.

Svensson B. and Holmen G.
Physical Review B. Vol 25 (1982) pp 3056-3062.

Taulbjerg K.
'Scaling Properties of Inner-Shell Excitation Cross Section'.
'Proceeding of the 2nd International Conference on Inner-Shell
Ionisation Phenomena', Freiburg (1976) edited by W. Mehlhorn and
R. Brenn.

Taulbjerg K.
Journal of Physics B : Atomic and Molecular Physics Vol 10 (1977)
pp L341-L346.

Tawara H., Ishii, K., Morita S., Kaji H., Hsu C.N. and Shiokawa T.
Physical Review A Vol 9 (1974) pp 1617-1625.

Tawara H., Ishii K., Morita S., Kaji H., and Shiokawa T.
Physical Review A Vol 11 (1975) pp 1560-1570.

Tawara H., Ishii K. and Morita S.
Nuclear Instruments and Methods Vol 132 (1976) pp 503-505.

Tawara H. and Richard P.
Nuclear Instruments and Methods Vol 205 (1983) pp 597-599.

Tennent R.M. (editor)
Science Data Book. Oliver and Boyd (1978).

Thoe R.S., Sellin I.A., Brown M.D., Forester J.P., Griffin P.M.,
Pegg D.J. and Peterson R.S.
Physical Review Letters Vol 34 (1975) pp 64-67.

Thomas B.K. and Garcia J.D.
Physical Review Vol 179 (1969) pp 94-101.

Thomas J.P., Cachard A., Fullavier M., Tardy J. Mars S. and Pivot J.
Revue de Physique Appliquee Vol 11 (1976) pp 65-72.

Tolson M.J. and Spyrou N.M.
Nuclear Instruments and Methods Vol 193 (1982) pp 99-103.

Tralli N. and Pomilla F.R.
'An Introduction to Wave Mechanics'. McGraw Hill (1969).

Trautmann D. and Rosel F.
Nuclear Instruments and Methods Vol 169 (1980) pp 259-272.

Trautmann D., Rosel F. and Baur G.
Nuclear Instruments and Methods Vol 214 (1983) pp 21-27.

Tschalar C.
Nuclear Instruments and Methods Vol 61 (1968) pp 141-156.

Veje E.
Nuclear Instruments and Methods Vol 194 (1982) pp 433-436.

Vollmer O.
Nuclear Instruments and Methods Vol 121 (1974) pp 373-377.

Vriens L.
Physica Vol 47 (1970) pp 267-276.

Walske M.C.
Physical Review Vol 88 (1952) pp 1283-1289.

Walske M.C.
Physical Review Vol 101 (1956) pp 940-944.

Watson R.L., McNeal C.J. and Jenson F.E.
Advances in X-Ray Analysis Vol 18 (1975) pp 288-298.

Weaver D.R.
Birmingham Radiation Centre Report No BRC - 76/ol (1976).

Weightman P.
Reports on Progress in Physics Vol 45 (1982) pp 753-814.

Wentzel G.
Zeitschrift fur Physik Vol 43 (1927) pp 524.

Wenzel W.A. and Whaling W.
Physical Review Vol 87 (1952) pp 499-503.

Wietschorke K.H. and Soff G.
Zeitschrift fur Physik A Vol 300 (1981) pp 273-276.

Wilken B. and Fritz T.A.
Nuclear Instruments and Methods Vol 138 (1976) pp 331-343.

Williams B. (editor)
'Compton Scattering' McGraw Hill Inc (1977).

Williams E.J.
Reviews of Modern Physics Vol 17 (1945) pp 217-226.

Yamadera A., Ishii K., Sera K. and Morita S. (a).
Nuclear Instruments and Methods Vol 181 (1981) pp 15-19.

Yamadera A., Ishii K., Sera K., Sebata M. and Morita S. (b).
Physical Review A Vol 23 (1981) pp 24-33.

Ziegler J.F. (editor)
'New Uses of Ion Accelerators'. Plenum Press (1975) pp 75-158.

Ziegler J.F.
Applied Physics Letters Vol31 (1977) pp 544-546.

Ziegler J.F.
'Handbook of Stopping Cross Sections for Energetic Ions in All Elements' Vol 5 of 'The Stopping and Ranges of Ions in Matter' edited by J.F. Ziegler. Pergamon Press (1980).

Ziegler J.F. and Chu W.K.
Atomic Data and Nuclear Data Tables Vol 13 (1974) pp 463-489.